THE 30TH EUROPEAN MODELING & SIMULATION SYMPOSIUM

SEPTEMBER 17-19, 2018
BUDAPEST, HUNGARY

EDITED BY
MICHAEL AFFENZELLER
AGOSTINO G. BRUZZONE
EMILIO JIMÉNEZ
FRANCESCO LONGO
YURI MERKURYEV
MIQUEL ANGEL PIERA

PRINTED IN RENDE (CS), ITALY, SEPTEMBER 2018

ISBN 978-88-85741-06-5 (Paperback)
ISBN 978-88-85741-03-4 (PDF)

THE 30TH EUROPEAN MODELING & SIMULATION SYMPOSIUM
SEPTEMBER 17 – 19, 2018
BUDAPEST, HUNGARY

ORGANIZED BY

DIME – UNIVERSITY OF GENOA

LIOPHANT SIMULATION

SIMULATION TEAM

IMCS – INTERNATIONAL MEDITERRANEAN & LATIN AMERICAN COUNCIL OF SIMULATION

DIMEG, UNIVERSITY OF CALABRIA

MSC-LES, MODELING & SIMULATION CENTER, LABORATORY OF ENTERPRISE SOLUTIONS

HUNGARIAN ACADEMY OF SCIENCES CENTRE FOR ENERGY RESEARCH

AUTONOMOUS UNIVERSITY OF BARCELONA

MODELING AND SIMULATION CENTER OF EXCELLENCE (MSCOE)

LATVIAN SIMULATION CENTER – RIGA TECHNICAL UNIVERSITY

LOGISIM

LSIS – LABORATOIRE DES SCIENCES DE L'INFORMATION ET DES SYSTEMES

MIMOS – MOVIMENTO ITALIANO MODELLAZIONE E SIMULAZIONE

MITIM PERUGIA CENTER – UNIVERSITY OF PERUGIA

BRASILIAN SIMULATION CENTER, LAMCE-COPPE-UFRJ

MITIM - MCLEOD INSTITUTE OF TECHNOLOGY AND INTEROPERABLE MODELING AND SIMULATION – GENOA CENTER

M&SNET - MCLEOD MODELING AND SIMULATION NETWORK

LATVIAN SIMULATION SOCIETY

ECOLE SUPERIEURE D'INGENIERIE EN SCIENCES APPLIQUEES

FACULTAD DE CIENCIAS EXACTAS. INGEGNERIA Y AGRIMENSURA

UNIVERSITY OF LA LAGUNA

CIFASIS: CONICET-UNR-UPCAM

INSTICC - INSTITUTE FOR SYSTEMS AND TECHNOLOGIES OF INFORMATION, CONTROL AND COMMUNICATION

NATIONAL RUSSIAN SIMULATION SOCIETY

CEA - IFAC

UNIVERSITY OF BORDEAUX

UNIVERSITY OF CYPRUS

DUTCH BENELUX SIMULATION SOCIETY

I3M 2018 INDUSTRIAL SPONSORS

CAL-TEK SRL

LIOTECH LTD

MAST SRL

SIM-4-FUTURE

I3M 2018 Media Partners

INDERSCIENCE PUBLISHERS – INTERNATIONAL JOURNAL OF SIMULATION AND PROCESS MODELING

INDERSCIENCE PUBLISHERS – INTERNATIONAL JOURNAL OF SERVICE AND COMPUTING ORIENTED MANUFACTURING

IGI GLOBAL – INTERNATIONAL JOURNAL OF PRIVACY AND HEALTH INFORMATION MANAGEMENT (IJPHIM)

HALLDALE MEDIA GROUP: THE MILITARY SIMULATION AND TRAINING MAGAZINE

HALLDALE MEDIA GROUP: THE JOURNAL FOR HEALTHCARE EDUCATION, SIMULATION AND TRAINING

SAGE
SIMULATION TRANSACTION OF SCS

DE GRUYTER
INTERNATIONAL JOURNAL OF FOOD ENGINEERING

MDPI - SUSTAINABILITY

EUROMERCI: THE ITALIAN MONTHLY LOGISTICS JOURNAL

EDITORS

MICHAEL AFFENZELLER
UNIVERSITY OF APPLIED SCIENCES, AUSTRIA
Michael.Affenzeller@fh-hagenberg.at

AGOSTINO G. BRUZZONE
MITIM-DIME, UNIVERSITY OF GENOA, ITALY
agostino@itim.unige.it

EMILIO JIMÉNEZ
UNIVERSITY OF LA RIOJA, SPAIN
emilio.jimenez@unirioja.es

FRANCESCO LONGO
DIMEG, UNIVERSITY OF CALABRIA, ITALY
f.longo@unical.it

YURI MERKURYEV
Riga Technical University, LATVIA
merkur@itl.rtu.lv

MIQUEL ANGEL PIERA
AUTONOMOUS UNIVERSITY OF BARCELONA, SPAIN
MiquelAngel.Piera@uab.cat

THE INTERNATIONAL MULTIDISCIPLINARY MODELING AND SIMULATION MULTICONFERENCE, I3M 2018

GENERAL CO-CHAIRS

AGOSTINO G. BRUZZONE, *DIME, UNIVERSITY OF GENOA, ITALY*
MIQUEL ANGEL PIERA, *AUTONOMOUS UNIVERSITY OF BARCELONA, SPAIN*

PROGRAM CO-CHAIRS

FRANCESCO LONGO, *DIMEG, UNIVERSITY OF CALABRIA, ITALY*
YURY MERKURYEV, *RIGA TECHNICAL UNIVERSITY, LATVIA*

THE 30TH EUROPEAN MODELING & SIMULATION SYMPOSIUM, EMSS 2018

GENERAL CO-CHAIRS

FRANCESCO LONGO, *DIMEG, UNIVERSITY OF CALABRIA ITALY*
EMILIO JIMÉNEZ *UNIVERSITY OF LA RIOJA, SPAIN*

PROGRAM CHAIR

MICHAEL AFFENZELLER, *UPPER AUSTRIA UNIVERSITY OF APPLIED SCIENCES, AUSTRIA*

EMSS 2018 International Program Committee

Michael Affenzeller, *Upper Austria UAS, Austria*
Rosa Maria Aguilar, *Universidad de La Laguna, Spain*
Joni A. Amorim, *University of Skövde, Sweden*
Maja Atanasijevic-Kunc, *University of Ljubljana, Slovenia*
Werner Backfrieder, *University of Applied Sciences Upper Austria, Austria*
Mikhail E. Belkin, *Moscow State Technological University (MIREA), Russia*
Ali Mili Mohamed Bettaz, *Philadelphia University, Jordan*
Marengle Biba, *University of New York Tirana, Albania*
Maria Valencia Betrán, *BSH Electrodomésticos, Spain*
Felix Breitenecker, *Technical University of Wien, Austria*
Agostino G. Bruzzone, *University of Genoa, Italy*
Eleonora Bottani, *University of Parma, Italy*
Alessandro Chiurco, *University of Calabria, Italy*
Zuhal Erden, *ATILIM University, Turkey*
Maria Pia Fanti, *Polytechnic University of Bari, Italy*
Idalia Flores, *University of Mexico, Mexico*
Sergio Gallo, *Univ. of Modena and Reggio Emilia, Italy*
Luis Gomes, UNL/UNINOVA, *Portugal*
Ricardo Gonçalves, *Universidade Nova de Lisboa, Portugal*
Manfred Gronalt, *Boku - University of Natural Resources and Life Sciences, Austria*
Samer Hassan, *Universidad Complutense de Madrid, Spain*
Xiaolin Hu, *Georgia State University*, USA
Witold Jacak, *Upper Austria UAS, Austria*
Emilio Jiménez, *University of La Rioja, Spain*
Hamdi Kavak, *Old Dominion University, Virginia USA*
Claudia Krull, *Otto-von-Guericke University*, Germany
Andreas Körner, *Vienna University of Technology*, Austria
Juan Ignacio Latorre Biel, Univ. Pública de Navarra, Spain
Francesco Longo, *MSC-LES, University of Calabria, Italy*
Edgar Alonso Lopez-Rojas, *Blekinge Institute of Technology, Sweden*
Louca Louca, *University of Cyprus, Cyprus*
Elena Manea, *National Institute for Research and Development in Microtechnologies - IMT Bucharest, Romania*
Moreno Marzolla, *University of Bologna, Italy*
Marina Massei, *Liophant Simulation, Italy*
Radek Matušu, *Tomas Bata University in Zlin, Czech Republic*
Riccardo Melloni, *Univ. of Modena and Reggio Emilia, Italy*
Yuri Merkuryev, Riga Technical University, Latvia
Galina Merkuryeva, *Riga Technical University, Latvia*
Saurabh Mittal, *Dunip Technologies, USA*
Miguel Mújica Mota, *Amsterdam University of Applied Sciences, Netherlands*
Gasper Music, *University of Ljubljana, Slovenia*
Nazmun Nahar, *University of Tartu, Finland*
Letizia Nicoletti, *Cal-Tek Srl, Italy*
Tuncer Ören, *University of Ottawa, Canada*
Alessandra Orsoni, *Kingston University, United Kingdom*
Antonio Padovano, *University of Calabria, Italy*
Catalin Pârvulescu, *National Institute for Research and Development in Microtechnologies - IMT Bucharest, Romania*
Eleonora Pantano, *Middlesex University, UK*
Carmelo Pina Gadea, *BSH Home Appliances, Spain*
Tomas Potuzak, *University of West Bohemia, Czech Republic*
Francesco Quaglia, *Sapienza Università di Roma, Italy*
Cristian Ravariu, *"Politehnica" University of Bucharest, Romania*
Jerzy Respondek, *Silesian University of Technology, Poland*
José Luis Risco Martín, *Universidad Complutense de Madrid, Spain*
Chumming Rong, *University of Stavanger, Norway*
Paolo Scala, *Amsterdam University of Applied Sciences, The Netherlands*
Jorge Sá Silva, *Warsaw Uiniversity of Tchnology, Poland*
Peer Olaf Siebers, *University of Nottingham, United Kingdom*
Alexander S. Sigov, *Moscow State Technological University (MIREA), Russia*
Boris Sokolov, *SPIIRAS and ITMO University, Russia*
Xiao Song, *Beihang University, China*
Giovanni Stea, *University of Pisa, Italy*

Chrysostomos Stylios, *Technological Educational Institute of Epirus, Greece*
Claudia Szabo, *The University of Adelaide, Australia*
Beatriz Sánchez Tabuenca, *Universidad Zaragoza, Spain*
Fei Tao, *Beihang University, China*
Halina Tarasiuk, *Warsaw Uiniversity of Tchnology, Poland*
Giuseppe A. Trunfio, *University of Sassari, Italy*
Walter Ukovich, *University of Trieste, Italy*
vignali
Ann Wellens, *University of Mexico, Mexico*
Thomas Wiedemann, *University of Applied Sciences at Dresden, Germany*
Richard Zaluski, *Center for Strategic Cyberspace + Security Science, United Kingdom*
František Zboril, *Faculty of Information Technology, Czech Republic*
Bernard P. Zeigler, *RTSync Corp, USA*
Jan Zenisek, *Upper Austria UAS, Austria*
Lin Zhang, *Beihang University, China*
Yu Zhang, *Trinity University, (USA)*

TRACKS AND WORKSHOP CHAIRS

ADVANCED IN DISCRETE AND COMBINED SIMULATION
CHAIRS: GASPER MUSIC, UNIVERSITY OF LJUBLJANA, SLOVENIA; THOMAS WIEDEMANN, HTW DRESDEN FB INFORMATIK, GERMANY

INDUSTRIAL PROCESSES MODELING & SIMULATION
CHAIR: AGOSTINO G. BRUZZONE, DIME, UNIVERSITY OF GENOA, ITALY

INDUSTRIAL ENGINEERING
CHAIR: FRANCESCO LONGO, MSC-LES, UNIVERSITY OF CALABRIA, ITALY

AGENT DIRECTED SIMULATION (ADS)
CHAIRS: YU ZHANG, TRINITY UNIVERSITY (USA); TUNCER ÖREN, UNIVERSITY OF OTTAWA, CANADA

PETRI NETS BASED MODELLING & SIMULATION
CHAIRS: EMILIO JIMÉNEZ, UNIVERSITY OF LA RIOJA, SPAIN; JUAN IGNACIO LATORRE, PUBLIC UNIVERSITY OF NAVARRE, SPAIN

WORKSHOP ON CLOUD MANUFACTURING
CHAIRS: PROF. LIN ZHANG, BEIHANG UNIVERSITY, CHINA; PROF. FEI TAO, BEIHANG UNIVERSITY, CHINA;

SIMULATION OPTIMIZATION APPROACHES IN INDUSTRY, AVIATION, SERVICES AND TRANSPORT
CHAIRS: IDALIA FLORES, UNIVERSITY OF MEXICO; MIGUEL MÚJICA MOTA, AMSTERDAM UNIVERSITY OF APPLIED SCIENCES, NETHERLANDS

HUMAN-CENTRED AND HUMAN-FOCUSED MODELLING AND SIMULATION
CHAIRS: AGOSTINO G. BRUZZONE, DIME, UNIVERSITY OF GENOA, ITALY; PEER OLAF SIEBERS, UNIVERSITY OF NOTTINGHAM, UK

WORKSHOP ON SOFT COMPUTING AND MODELLING & SIMULATION
CHAIRS: MICHAEL AFFENZELLER, UPPER AUSTRIAN UNIVERSITY OF APPLIED SCIENCES, AUSTRIA; WITOLD JACAK, UPPER AUSTRIAN UNIVERSITY OF APPLIED SCIENCES, AUSTRIA; STEFAN WAGNER, UPPER AUSTRIAN UNIVERSITY OF APPLIED SCIENCES (AUSTRIA);

WORKSHOP ON CLOUD COMPUTING
CHAIR: CHUNMING RONG, UNIVERSITY OF STAVANGER, NORWAY

ADVANCED SIMULATION FOR LOGISTICS SYSTEMS
CHAIRS: MARIA PIA FANTI, POLYTECHNIC OF BARI, ITALY; CHRYSOSTOMOS STYLIOS, TECHNOLOGICAL EDUCATIONAL INSTITUTE OF EPIRUS, GREECE; WALTER UKOVICH, UNIVERSITY OF TRIESTE, ITALY

MODELLING AND SIMULATION APPROACHES IN AND FOR EDUCATION
CHAIRS: MAJA ATANASIJEVIC-KUNC, UNIV. LJUBLJANA, SLOVENIA; ANDREAS KÖRNER, VIENNA UNIV. OF TECHNOLOGY, AUSTRIA

MODELLING AND SIMULATION IN PHYSIOLOGY AND MEDICINE (COMMON TRACK EMSS-IWISH)
CHAIRS: MAJA ATANASIJEVIC-KUNC, UNIV. LJUBLJANA, SLOVENIA; FELIX BREITENECKER, VIENNA UNIV. OF TECHNOLOGY, AUSTRIA

SIMULATION AND MODELLING FOR OCCUPATIONAL HEALTH AND SAFETY
CHAIRS: RICCARDO MELLONI, UNIV. OF MODENA AND REGGIO EMILIA, ITALY; SERGIO GALLO, UNIV. OF MODENA AND REGGIO EMILIA, ITALY

ADVANCED MODELS AND APPLICATIONS OF LOGISTICS & MANUFACTURING
CHAIRS: TERESA MURINO, UNIVERSITY OF NAPLES FEDERICO II ITALY; LIBERATINA C. SANTILLO, UNIVERSITY OF NAPLES FEDERICO II ITALY

RETAIL-ORIENTED SIMULATION
CHAIR: ELEONORA PANTANO, MIDDLESEX UNIVERSITY, UK

COMPUTER SIMULATION FOR SECURITY
CHAIRS: EDGAR ALONSO LOPEZ-ROJAS, BLEKINGE INSTITUTE OF TECHNOLOGY, SWEDEN, JONI A. AMORIM, UNIVERSITY OF SKÖVDE SWEDEN; RICHARD ZALUSKI, CENTER FOR STRATEGIC CYBERSPACE + SECURITY SCIENCE, UK

WORKSHOP ON MODEL ENGINEERING FOR SYSTEM OF SYSTEMS
CHAIRS: LIN ZHANG, BEIHANG UNIVERSITY, CHINA; PROF. BERNARD P. ZEIGLER, RTSYNC CORP, USA; DR. SAURABH MITTAL, DUNIP TECHNOLOGIES, USA

MODELLING, COMPUTER SIMULATION AND VISUALISATION OF HERITAGE
CHAIRS: GALINA MERKURYEVA, RIGA TECHNICAL UNIVERSITY; RICARDO GONÇALVES, UNIVERSIDADE NOVA DE LISBOA (UNINOVA)

MODELING AND SIMULATION IN PHOTONICS SCIENCE AND INDUSTRIAL TECHNOLOGIES
CHAIRS: ALEXANDER S. SIGOV, MOSCOW TECHNOLOGICAL UNIVERSITY (MIREA), (MOSCOW, RUSSIAN FEDERATION); MIKHAIL E. BELKIN, MOSCOW STATE TECHNOLOGICAL UNIVERSITY (MIREA), (MOSCOW, RUSSIAN FEDERATION)

WELCOME MESSAGE 2018

On behalf of the program committee, it is our pleasure to present the proceedings of the 30th anniversary edition of the European Modeling and Simulation Symposium – EMSS 2018.

The conference started under the name USER in Belgium in 1988, and has been continued as an annual event named European Simulation Symposium (ESS) between 1990 and 2005. Since 2006, when the event was held in Barcelona, the modeling aspect has been integrated into the conference name, resulting in the recent title EMSS. Over the years, imbedded in the International Multidisciplinary Modeling & Simulation Multiconference (I3M), EMSS has evolved into one of the most important simulation appointments in Europe. The organizational structure of EMSS 2018 is similar to other international scientific conferences. The backbone of the conference is the scientific program, which is complemented by workshops and open debates dedicated to special theoretical and application-oriented topics from the field of Modeling & Simulation (M&S) with a special focus on industrial applications. We are delighted to report that 56 papers from 17 different countries were selected by the program committee for presentation and discussion during the conference and subsequent publication in the conference proceedings. A breakdown by countries is given in the following table:

Country	Accepted papers	Country	Accepted papers
Austria	9	Germany	2
Czech Republic	6	Portugal	2
Italy	6	Finland	1
Russia	6	France	1
Spain	6	Netherlands	1
Mexico	4	Norway	1
Canada	3	Oman	1
China	3	Romania	1
United Kingdom	3		

All submissions were reviewed by an international panel of at least three expert referees. We highly acknowledge the invaluable assistance of the program committee and the international referees, who opted to provide detailed and insightful comments to the authors.

EMSS 2018 brings together fundamental and applied research contributions that reflect current trends and developments in Modeling and Simulation. We sincerely hope that the conference will encourage cross-fertilization between the different communities, bridging not only the gap between different fields but also, equally important, between different continents and cultures.

In closing, we would like to thank all authors for submitting their work, and all members of the program committee, who contributed greatly to make the conference a great success.

We wish you a fruitful and inspiring conference and a pleasant stay in Budapest.

Emilio Jiménez
La Rioja
University
Spain

Francesco Longo
DIMEG, University
of Calabria,
Italy

Michael Affenzeller
University of Applied
Sciences Upper
Austria,
Austria

Acknowledgements

The EMSS 2018 International Program Committee (IPC) has selected the papers for the Conference among many submissions; therefore, based on this effort, a very successful event is expected. The EMSS 2018 IPC would like to thank all the authors as well as the reviewers for their invaluable work.
A special thank goes to all the organizations, institutions and societies that have supported and technically sponsored the event.

I3M 2018 Internal Staff

This International Workshop is part of the I3M Multiconference: the Congress leading **Simulation around the World and Along the Years**

Index

INTEGRATING WEATHER IN MODELLING EARTHMOVING MINING OPERATION USING DISTRIBUTED SIMULATION WITH HLA STANDARDS

Mubarak AL-Alawi[a], Yasser Mohamed[b], Ahmed Bouferguene[c]

[a] Assistant Professor, Dept. of Civil and Architectural Engineering, Sultan Qaboos University, Oman
[b] Professor, Dept. of Civil and Environmental Engineering, University of Alberta, Canada
[c] Associate Professor, Dept. of Civil and Environmental Engineering, University of Alberta, Canada

[a]alawim@squ.edu.om, [b]yaly@ualberta.ca, [c]ahmed.bouferguene@ualberta.ca

ABSTRACT
Changes in weather conditions impact construction activities. The consideration of effects of changes in weather condition is important to better estimate the performance of construction resources. This paper demonstrates the integration of a weather generator to support modelling earthmoving operation using distribution simulation with high level architectural (HLA) standards. The modelled earthmoving operation is related to the oil sand mining. The weather effects on the breakdown and maintenance events of earthmoving resources (trucks and excavators) were analyzed under different weather testing scenarios and their results were reported accordingly.
Keywords: weather, distributed simulation, HLA, earthmoving

1. INTRODUCTION
Weather variables play different roles in estimating the performance of earthmoving operations. Earthmoving machinery is most affected. For instance, the rolling resistance factor is calculated based on the amount of tire penetration into the ground. Different soils have different tire interaction behavior. In the winter, snow cover or snow depth affects such interactions and varies the rolling resistance from two perspectives: first, if the snow cover is not packed, the tire penetration rate becomes higher, which results in a higher rolling resistance. Second, if the snow cover is packed, the rolling resistance is lower (Richmond, Shoop, and Blaisdell 1995). In the spring and summer, precipitation is the governing factor for rolling resistance. Precipitation increases the water content in the soil, which in turn increases the tire penetration rate. The increase in rolling resistance decreases hauling truck speed, which affects the productivity of the earthmoving cycle (Smith, Osborne, and Forde 1995). Furthermore, the increase in rolling resistance has a negative impact on a truck's fuel economy, which means that it has a direct relationship with fuel consumption (LaClair and Truemner 2005).
The low temperature in the winter season influences properties of soil, especially its strength. Wet soils are comprised of pores, water, and soil particles. When water in soil pores is subjected to a temperature below the freezing point, it results in changing the state of water from a liquid to solid state. This change gives the soil some ice characteristics like strength, increasing its strength by one or two orders of magnitude (Lindroth, Berglund, and Wingquist 1995). For example, a coarse-grained soil with a medium to high unit weight becomes very strong when water in the soil freezes. This change in soil strength has a direct effect on the excavation process (Orlando and Branko 2004). In contrast, an increase in temperature initiates the thawing process which reduces soil strength (Czurde 1983).
The variation in temperature from one season to another has a direct effect on a truck's operational cost, specifically breakdown repairs and maintenance costs. For example, a truck's performance depends on tire life, and the most significant environmental factor that affects tire life is temperature (Li, Liu, and Frimpong 2012). Li, Liu and Frimpong (2012) identified that dump truck tires are subjected to high stress and deformation when working under severe temperature conditions ranging from 40 to -40 ºC. As a result, tire failure may occur in earthmoving operations (Meech and Parreira 2013). Heavy rain and snow are also considered to be among the environmental factors affecting tires (GoodYear 2008). Temperature also has a negative effect on a wide range of equipment operations. For instance, low temperature has an adverse effect on engine performance; extreme low temperatures increase the number of engine failures and reduce fuel efficiency (Diemand and Lever 2004). Furthermore, low temperatures significantly change the brittleness of metals, resulting in an increase in vehicle breakdowns and machine part failures (Freitag and McFadden, 1997).
Based on the above discussion, weather variables can affect three processes of earth moving operations: (1) excavation, (2) loading, and (3) hauling. In the context of a simulation of an earthmoving operation, it is important to integrate such effects to create a realistic simulation environment. In each simulation run, weather variables should be generated carefully so that time dependency between weather variables is preserved. This way each weather variable generated for a certain earthmoving operation (e.g., excavation) will be correlated to other weather variables generated for other operations (e.g., hauling). Furthermore, all earthmoving operations should be controlled by a simulation time step (e.g., hourly or daily), allowing the simulation model to

preserve the operational dependency among all resources. Getting all earthmoving operations and a weather generator working in harmony based on a specified time step is a complex task. To accomplish this task, a high-level architecture (HLA) standard is one of the solutions offered in the field of simulation research. This study illustrates the integration of weather effects in earthmoving operations using a distributed simulation with HLA standards. The model underlying this study was developed for an earthmoving operation related to oil sand's mining and for which a non-parametric weather generation approach in the form of bootstrapping technique is employed. This contribution also focuses on demonstrating the effect of temperature on trucks in terms of their breakdowns repair durations. The effect of temperature on breakdown repair durations is analyzed using different weather scenarios generated by the embedded weather generator in the simulation model. The results are reported accordingly.

2. OVERVIEW OF DISTRIBUTED SIMULATION AND HLA STANDARDS

Distributed simulation or parallel/distributed simulation technology is defined as a technology that enables a program to be executed on a system composed of multiple computers (Fujimoto 1995, Fujimoto 2000). Fujimoto (2000) identified four principal benefits for applying distributed simulation: (1) reduced execution time, (2) geographical distribution of simulation or computer components, (3) integrating multiple simulators, and (4) fault tolerance. The first principal benefit, "reduced execution time," was the actual main objective of proposing the distributed simulation. Thus, a time effect technology to develop and execute large simulation programs was highly desired.

In real world applications, the flexibility requirements of the distributed simulation extend beyond the geographical distribution of simulation components and the integration of multiple simulators. An interaction between simulation components was of great interest. The US military initiated such a requirement because it wanted effective and economical ways to train personnel. The military's main objective was to develop a virtual environment capable of allowing interactions between geographically distributed hardware and personnel in a real-time framework (Fujimoto 1995). This led to a proposal for a Distributed Interactive Simulation (DIS). DIS is "an infrastructure that enables heterogeneous simulators to interoperate in a time and space coherent environment" (Cheung and Loper, 1994). Despite the ability of DIS to enable interaction between different simulation components, it was associated with challenges related to uncontrolled latencies and lack of time management services (Hakiri, Berthou, and Gayraud 2010). Furthermore, building simulation components in different environments limit the reusability of the simulation system. As a result, related to these challenges, an HLA standard was developed to improve the concept of standardization of simulation building and to improve data processing and acquisition through a time management infrastructure.

The HLA standard is a general purpose framework that supports the simulation of a system composed of multiple simulation components working independently (Cen and

Irene 2011). It was developed by the United States Department of National Defense with the main objectives to incorporate interoperability (the ability to integrate different simulation components created in different development environments), modularity (the standardization of the framework so it can be adopted in different applications), and reusability (the ability to use the simulation component in different scenarios or applications) into long-term simulation objectives (Department of Defence, 2000). It includes three core components: federation and federates rules, the federate object model (FOM), and HLA interface specification.

3. OIL SAND MINING PROCESS IN ALBERTA, CANADA

The oil sands regions, mainly located in the province of Alberta, Canada, are the fastest growing area in the world of developing petroleum resources (Paes and Throckmorton, 2008). Two main production processes are applied to oil extraction: (1) in-situ and (2) surface mining (SUNCOR, 2016). The in-situ technique uses a steam injection method to heat the oil, and after which it can be pumped out. Meanwhile, in surface mining, large shovels and trucks are used to extract oil sands from the surface. Open pit mining process is usually performed when the oil sand is located near the surface, which is the case in Alberta; 20 % of oil sands reserves are located less than 75 meters underground (Government of Canada 2016). The open-pit mining process used in the oil sand mining involves the following activities: (1) ore material collection, (2) material handling, (3) slurry conditioning and transfer, (4) extracting, (5) tailings, and (6) upgrading.

The ore material collection step involves an earthmoving operation; it uses shovels and trucks as the main resources. These resources are exposed to the environment which means that changes in weather conditions may affect their productivity. Therefore, this step has been selected to be modeled. In order to better understand the earthmoving operation in oil sand mining and its resources, and to clearly define the simulation components of the operation, a discussion was conducted with experts in this field.

4. THE DEVELOPMENT OF THE MINING EARTHMOVING OPERATION MODEL

The earthmoving process cycle, as per the discussion with experts, involves loading ore material into the hauling trucks using shovels/loaders. Trucks move the ore material from the excavation pit to the dump pit at the extraction facility, unload the ore material in the dump pit, and then return to the excavation pit. The experts agreed that the simulation model should contain three major components: excavators, trucks, and equipment breakdown and maintenance.

The earthmoving operation is comprised of resources integrated in such a way as to describe an earthmoving process cycle. Each resource has its own earthmoving operational cycle. For instance, hauling soil from an excavation pit to the dumping site and back again to excavation pit represents a full hauling cycle for a truck. On the other hand, excavators/shovels operate in two different locations, each with a different operational cycle. The first

cycle is located in the mining pit where excavators excavate oil sand and load it into the trucks. The second cycle is located at oil sand earth clumps where excavators/shovels move the oil sand to crushers. These earthmoving operational cycles are operated continuously by different types of trucks and loaders to maintain high productivity and lower operational cost. The major factor influencing the equipment performance is the unanticipated equipment's breakdown event. Therefore, the simulation model of the mining earthmoving operation should be allowed to test the operation under different resource scenarios.

The modeled mining operation is located in a cold, harsh environment; therefore, the experts asked to integrate a weather effect into the model of the mining earthmoving operation. Since weather can change dramatically throughout the day and the mining operation runs nonstop (i.e., for 24 hours), it was agreed that the simulation time step should represent a working hour and the weather generator should be developed in a way to provide hourly basis weather variables. Moreover, it was decided that all mining earthmoving operational cycles should run and interact with each other on an hourly basis. This was achieved by applying HLA standards to regulate the processing time. It was concluded from the discussion with experts that the simulation model should have six simulation components interacting with each other. These components along with the simulation structure are shown in Figure 1.

Each simulation component represents a federate in the mining earthmoving federation and is developed by a different team of researchers. The work description of each federate is as follows: (1) controller is responsible for initializing the simulation model, (2) mover is responsible for simulating hauler behaviour, (3) loader is responsible for simulating the loader behavior, (4) equipment breakdown and maintenance is responsible for simulating the trend of resources' breakdown and maintenance events, (5) weather is responsible for generating dynamic and realistic weather variables, and (6) 3D visualizer is responsible for animating the earthmoving operation.

After all federates of the mining earthmoving federation are identified, the simulation object model (SOM) for each federate is constructed so that the object class and its attribute, whether needed or provided by the federate, is clearly identified. Also, an investigation is conducted to determine which weather variables are affecting each federate and how. Once all SOM are created, they are all combined to create the mining earthmoving FOM. Table 1, below, shows a sample of the FOM containing weather variables as an interaction class called "CurrentWeather." This interaction class is published by the weather federate to provide others with a block containing all weather variables required in the simulation process.
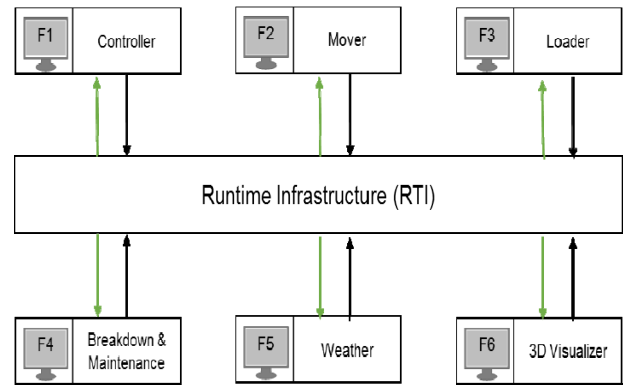
Figure 1: Earthmoving simulation structure

Table 1: Sample of "CurrentWeather" interaction class the FOM (S=subscribe, P=publish)

Attribute	Contr--ller	Mov--r	Load--er	Breakdow--n & Maintena--ce	Weath--er
Temper--ture	S	S	S	S	P

5. WEATHER FEDERATE

5.1. Historical weather database
The bootstrapping approach to randomly generate weather variables is integrated into the weather federate. The weather federate is linked to a historical weather database containing the location of operation. It reflects weather parameters to other federates. The location of the oil sand mining operation is Fort McMurray, Alberta, and the historical weather database is extracted from the Environment Canada website. The weather variables listed in the database are those requested by other federates and listed in the FOM. The weather variables are as follows:
- Temperature
- Wind speed
- Visibility
- Precipitation
- Snow depth

In the weather database, two tables were created to maintain hourly and daily weather variables. The daily weather forecast table classifies the temperature into three groups: maximum, minimum and average temperature of each day. Wind speed is classified into two groups: maximum and average. This classification of weather parameters is important to create different testing scenarios of weather conditions and to study their impact on the mining earthmoving operation.

5.2. The weather generation process
The weather generation in this study extracts real historical weather variables from the database for the purpose of preserving correlations and dependencies among meteorological variables. Hourly and daily forecast tables in the Fort McMurray weather database provide flexibility to generate different scenarios. In this stage of the research, the

weather federate provides other federates with weather parameters in the following three scenarios:

1. The first scenario (SC1) generates weather variables from the database based on the random selection of a year between 1961 and 2002. The hourly generated weather variables represent the daily average. This scenario is considered the conservative daily scenario.

2. The second scenario (SC2) is also based on generating weather variables from randomly selected years. However, the generated hourly weather variables represent the minimum daily values in winter and maximum daily values in summer. This scenario is considered the extreme daily scenario.

3. The third scenario (SC3) is based on generating weather variables from randomly selected years. The generated hourly weather variables in this scenario represent the actual values of weather variables which have been experienced at that particular hour. This scenario is considered the actual hourly scenario.

The weather generation process starts by first determining the location and the expected starting date of the operation. Then, the weather generator randomly selects the year of operation from the database and initializes the weather generation process based on the selected year, month, day, and location. All weather variables are provided on an hourly basis and in accordance with the selected testing scenario, except for snow depth and precipitation, because the measured records of those variables are normally presented in the form of accumulated amounts per day. Snow depth and precipitation are generated at hour 0 AM of each simulated day. The model assumes that the operation works for 24 hours, and each simulation run represents one minute. Therefore, the weather federate updates its weather interaction class values after the run time of every 60 simulation runs and moves to the second day forecast when a full day of operation is completed.

6. SIMULATION RUN AND TESTING SCENARIOS RESULTS

6.1. Simulation run

The simulation run of the operation is controlled and initiated by the controller federate. The controller federate is composed of two parts: (1) the interface and (2) the federate. The interface allows the user to enter the operation attributes such as project, road condition, truck types and their quantity, excavator types and their quantity, and the topological map of the site. This information is provided by the user and represents the attributes that are subscribed by the controller federate. These attributes are published by the controller to the other federates in the simulation model. The controller federate uses this information to start the simulation by populating the number of instances of each object class. For example, nine instances of object class "Truck" and three instances of object class "Excavator" are populated, each associated with their attributes such as the

truck model and its capacity to simulate the mining operation. Following the population stage of the resources class objects, the road section that hosts the hauling and returning routes of trucks is initiated. The road section is composed of multiple segments, each of which has different attributes such as road segment materials and layouts. The road section length used to haul and return trucks is equal to 2.2 km.

The trucks' breakdown and maintenance intervals and their repair times are shown in Table 2. The repair time for trucks is expected to increase by 20% depending on a pre-specified temperature threshold value (T). This percentage is experts-driven for a temperature less than or equal to -30 ºC. However, Koehn and Brown (Koehn and Brown 1985), in the context of labour productivity, identified -29 ºC as the temperature threshold value at which labors must stop work and at -18 ºC as the threshold value at which labour productivity starts deteriorating. Therefore, a sensitivity analysis which will apply a range of T from -18 ºC to -30 ºC will be used to study the effect of temperature on breakdown events.

The breakdown and maintenance federate subscribes temperature so that a temperature-based analysis can be performed. As previously described, the temperature is published within the interaction class called "CurrentWeather" that is provided by weather federate. The weather federate publishes the "CurrentWeather" interaction class based the three scenarios: (1) SC1 (the average daily temperature), (2) SC2 (the minimum daily temperature), and (2) SC3 (the actual daily temperature).

Table 2: Durations of expected trucks' breakdown and maintenance events

Event	Duration
Truck breakdown interval	Exponential (200)
Truck maintenance interval	Constant (400)
Truck repair time	Uniform (20,24)
Truck maintenance time	Triangular (18,21,24)
Time increase in truck repair due to a specified temperature threshold value (T)	20%

To analyze these scenarios combined with the temperature limit sensitivity analysis, a performance benchmark result for the trucks is generated based on the assumption that the working condition will not achieve any temperature threshold value. It was found that a given year is expected to have 8760 working hours which represent approximately 83% of the total yearly working hours and the breakdown and maintenance averages were found to be 10 % and 7 % respectively.

6.2. Scenarios' results

The mining earthmoving operation was tested under three different scenarios. The weather federate generated 10 randomly selected years, and an hourly based "CurrentWeather" interaction class was published to other federates. The effect of temperature on truck and excavator breakdown events was tested under different temperature

limit values ranging from -18 ºC to -30 ºC. The analysis was performed for each truck participating in the simulation. However, the results are summarized to reflect the overall breakdown repair duration expected for a truck. The result includes the minimum, average and maximum expected breakdown repair durations.

Figure 2 shows the breakdown repair durations for a truck. Figure 2-(a) shows the minimum breakdown repair duration expected for a truck. The results show that using the daily minimum temperature (SC2) generates on average a repair duration that is 1.2 % higher than SC1 and SC3, which is equivalent to 7.5 hours. Comparing SC1 (average daily temperature) to SC3 (actual hourly temperature), both scenarios provided the same breakdown repair durations when T was less than or equal to -21 ºC and SC3 generated a slightly higher repair duration when T was greater than -21 ºC. Comparing the total averages of the minimum expected repair duration of each scenario with the truck breakdown benchmark result (616.5 hrs) led to the following: (1) SC1 generated a 0.05% more repair duration, (2) SC2 generated a 1.32 % more repair duration, and (3) SC3 generated a 0.16% more repair duration.

Figure 2-(b) shows the average breakdown repair durations for a truck in the mining earthmoving operation. SC2 generates a 1.5 % more repair duration than SC1 and SC3, which is equivalent to 13.5 more repair hours. Both SC1 and SC3 generated the same breakdown repair duration, equal to 892 hours when tested against different T values. Comparing the total averages of the expected average breakdown repair duration with the truck breakdown benchmark result (876.7 hrs) led to the following: (1) SC1 generated a 1.7% more repair duration, (2) SC2 generates a 1.6 % more repair duration, and (3) SC3 generates a 3.1 % more repair duration. In the context of calculating the maximum expected breakdown repair duration, shown in Figure 2-(c), the results of SC1 and SC3 show different behavior: SC3 generates a slightly higher breakdown repair duration. The percentage of differences between SC2 and both SC1 and SC2 is 1.3% and the comparison with the truck breakdown benchmark result (1108.7 hrs) results in (1) SC1 and SC3 generating approximately 3.5% more breakdown repair duration, and (2) SC2 generating 4.8% more breakdown repair duration.

The conclusion results in this section are shown in Table 3. Based on calculating the expected breakdown repair duration with respect to different temperature limit values (*T*) and based on different temperature scenarios (SC1, SC2, and SC3), the expected contribution of each truck breakdown repair duration is between 7.04 % and 10.32 % in a one-year non-stop mining operation.
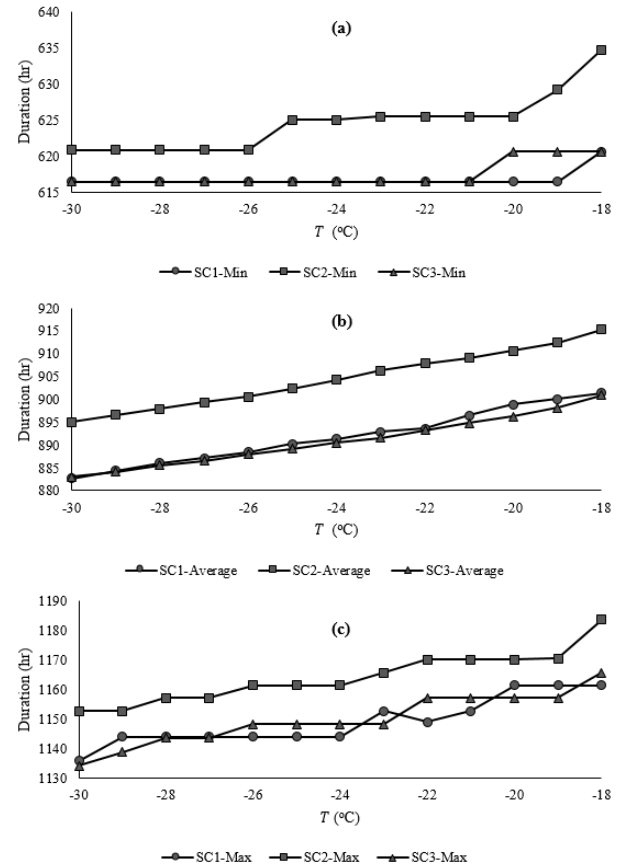
Figure 2: Truck breakdown repair durations under three testing scenarios (SC1, SC2, and SC3) and on different temperature limit values (T); (a) the expected minimum repair durations, (b) the expected average repair durations, and (c) the expected maximum repair durations.

Table 3: Expected percentages of breakdown repair durations for each scenario in the mining earthmoving operation

Scenar-io	% of Breakdown Repair Duration					
	Trucks			Excavators		
	Min	Average	Max	Min	Average	Max
SC1	7.04	10.18	13.12	8.54	9.71	11.90
SC2	7.13	10.32	13.29	8.63	9.82	12.03
SC3	7.05	10.17	13.13	8.54	9.71	11.88

7. CONCLUSION

A distributed simulation approach with HLA standards has been used to integrate weather in modelling the earthmoving operation of oil sand mining. The model was composed of different simulation components including trucks, excavators, breakdown and maintenance, and weather simulation components. The weather effect on trucks breakdowns was addressed and modeled. Furthermore, the weather generator provided different weather testing scenarios to analyze the trucks breakdown repair durations. It was found that the truck breakdown repair duration is

ranges between 7.04 % and 10.32 % in a one-year non-stop mining operation.

REFERENCES

Cen, N., & Irene, E. (2011). Adopting HLA standard for interdependency study. *Reliability Engineering and System Safety*, 149-159.

Cheung, S., & Loper, M. (1994). Synchronizing Simulations in Distributed Interactive Simulation. *Winter Simulation Conference* .

Czurde, K. A. (1983). Freezing Effects on Soils: Comprehensive Summary of the ISGF 82. *Cold Regions Science and Technology, 8*, 93-107.

Department of Defence. (2000). *High level architecture run-time programmers guide (ver 3.2).*

Diemand, D., & Lever, J. H. (2004). *Cold Regions Issues for Off-Road Autonomous Vehicles.* Engineer Research and Development Center-US Army Corps of Engineers.

Freitag, D. R., & McFadden, T. (1997). *Introduction to Cold Regions Engineering.* New York: ASCE PRESS.

Fujimoto, R. M. (1995). Parallel and Distributed Simulation . *Winter Simulation Conference* .

Fujimoto, R. M. (2000). *Parallel and Distributed Simulation Systems.* New York: John Wiley & Sons.

GoodYear. (2008). *Tire Maintenance Manual-Goodyear Off-The-Road (OTR).* Goodyear.

Government of Canada. (2016, 02 19). *Natural Resources Canada*. (Government of Canada) Retrieved 08 15, 2016, from http://www.nrcan.gc.ca/energy/oil-sands/18094

Hakiri, A., Berthou, P., & Gayraud, T. (2010). *Addressing the Challenge of Distributed Interactive Simulation With Data Distribution Service.* arXiv.org.

Koehn, E., & Brown, G. (1985). Climatic Effects on Construction . *Journal of Construction Engineering and Management, 111*(2), 129-137.

LaClair, T. J., & Truemner, R. (2005). *Modeling of Fuel Consumption for Heavy-Duty Trucks and the Impact of Tire Rolling Resistance.* Warrendale: SAE international.

Li, Y., Liu, W. Y., & Frimpong, S. (2012). Effect of ambient temperature on stress, deformation and temperature on dump truck tire. *Engineering Failure Analysis, 23*, 55-62.

Lindroth, D. P., Berglund, W. R., & Wingquist, C. F. (1995). Microwave Thawing of Frozen Soils and Gravels. *Journal of Cold Regions Engineering, 9*(2), 53-63.

Meech, J., & Parreira, J. (2013). Predicting Wear and Temperature of Autonomous Haulage Truck Tires. *16th IFAC Symposium on Automation in Mining, Mineral and Metal Processing.* San Diego.

Orlando, A., & Branko, L. (2004). *Frozen ground engineering.* Hoboken, New Jersey: John Wiley & Sons.

Paes, R., & Throckmorton, M. (2008). An overview of canadaian oil sand mega projects. *Petrolume and Chemical Industry Conferene* (pp. 1-9). Weimar: IEEE.

Richmond, P. W., Shoop, S. A., & Blaisdell, G. L. (1995). *Cold Regions Mobility Models.* Cold Regions Research & Engineering Laboratory- US Army Corps of Engineers.

Smith, S. D., Osborne , J. R., & Forde, M. C. (1995). Analysis of Earth-Moving Systems using Discrete-Events Simulation. *Journal of Construction Engineering and Management, 121*(4), 388-396.

SUNCOR. (2016, 08 15). *Getting oil from the oil sand* . (SUNCOR) Retrieved 08 16, 2016, from http://www.suncor.com/about-us/oil-sands/process

BEYOND SOI - THE NOI NANOTRANSISTOR - SIMULATIONS RESULTS AND NEW CHALLENGES

Cătălin Pârvulescu[a], Cristian Ravariu[b], Elena Manea[c], Florin Babarada[d], Alina Popescu[e]

[a],[c],[e] National Institute for Research and Development in Microtechnologies - IMT Bucharest, Romania
Street Erou Iancu Nicolae 126A, 077190, Voluntari, Ilfov
[b],[d] "Politehnica" University of Bucharest, Faculty of Electronics, Dept. of Electronic Devices Circuits and Architectures, Str. Splaiul Independentei 313, Sect.6, 060042, Bucharest, Romania

[a] catalin.parvulescu@imt.ro, [b] cristian.ravariu@upb.ro, [c] elena.manea@imt.ro,
[d] florin.babarada@upb.ro, [e] alina.popescu@imt.ro

ABSTRACT
For the beginning, this paper reconsiders the Nothing On Insulator transistor work principle. Then, some additional new studies are approached. Two directions are envisaged: (i) to change the source and drain composition or properties; (ii) to check if the vacuum from nanocavity can be replaced by oxide. The simulations proved excellent drain subthreshold slope of 45mV/dec for n^--V-p^+ NOI variant. Oxide sub-2nm allows similar tunneling conduction as in nVn NOI variant. Comparisons with experimental picked points from literature are available.

Keywords: SOI-NOI, nanodevices, thin film, tunneling

1. INTRODUCTION
The latest novelties in the electronic device development indicates an increased interest in tunnel devices, starting from Tunnel-FETs with oxide (Liu and Datta 2015), passing through Tunnel-pin-FETs with promising sub-threshold slope less than 60mV/dec - the MOSFET limit (Koswatta, Lundstrom, and Nikonov 2009), announcing in 2014 the vacuum transistor - a device made of Nothing (Han and Meyyappan 2014), ultimate vacuum tube (Armstrong 2015), gate insulated nanoscale vacuum channel transistor (Han, Oh, and Meyyappan 2012). The traditional vacuum devices, like vacuum triode or nanodiamond vacuum transistor (Subramanian, Kang, and Davidson 2008) posses different performances than the actual MOSFET: higher operation voltages, huge swing, high threshold voltages. In IEEE Spectrum Magazine, some NASA researchers claim that the transistors made by Nothing are the immediate future devices suitable for CMOS co-integration (Han and Meyyappan 2014).
On the other hand, Tunnel-FETs, provides better switch performances than a MOSFET (Boucart and Ionescu 2007).
Recent devices, composed by Semiconductor-Vacuum-Semiconductor On Insulator that combines different features of the previous NOI devices, are presented in this paper. The device is also named as Nothing On Insulator (NOI) transistor, due to the Vacuum On Insulator, as the device main body (Ravariu 2010).
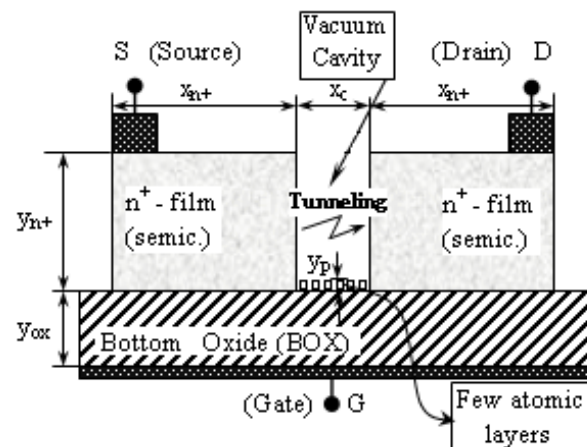
Figure 1: The evolution and state of the art of the NOI device.

A brief device history was frequently presented and there is drafted here. In a previous paper, a Silicon On Insulator SOI-MISFET, with a special "U" shape Si-film, was presented, (Ravariu and Babarada 2011). After a partial removal of the median p-semiconductor layer, the conduction simultaneously occurs by vacuum tunneling and by thinner p-type film. The median layer was thinned down, step by step, $y_p \rightarrow 0$, letting behind a vacuum cavity, fig. 1. When the region between source and drain completely becomes a "Nothing On Insulator" (NOI) space arises and the transistor works only by tunneling. This tunnel nano-transistor with a vacuum cavity between two electrodes was proposed in 2005 (Ravariu 2005) and timely updated.
The NOI device membership among the FET transistors is conditioned by the drain current modulation via the back-gate voltage, as in any SOI device. Hence, the NOI device simultaneously belongs to the vacuum devices, tunnel-FETs and SOI devices class, expressing their features, but keeping its distinct behavior. The first distinctive element of the NOI device is its main

conduction mechanism based on the electron tunneling thru a vacuum cavity with extremely low sizes.

Secondly, the NOI device differs from the standard vacuum devices by a fine modulation of the carriers concentration inside the source and drain islands, via the back-gate action. The carries modulation under a transversal electric field, from deep depletion up to strong accumulation, was recently demonstrated (Ravariu 2017).

Thirdly, it completely differs from a SOI-MOSFET or SON (Pretet, Monfray, Cristoloveanu, and Skotnicki 2004), with an inversion channel in a solid-state material and it is rather closer to a vacuum nanotransistor, based on the tunneling conduction. Unfortunately, the NOI device still has some poor performances, (Ravariu 2016). Therefore, the aim of this paper is to simulate new NOI structures with better parameters. In this scope, the neighbor source/drain regions, as the electron reservoirs, can be made both from n-type-Si offering the nVn succession or can change the doping in the source or drain region as n^-Vp^+ succession, searching for new effects. A second scope is to investigate if the oxide can replace the vacuum. In this case, rotating by 90^0 the NOI figure, a planar NOI variant, (p-NOI), is extremely closed to an experimental model. The p-NOI could be the first fabricated exponent of the entire NOI series and it is based on the insulator tunneling, too.

2. ASSIMETRICAL SOURCE/DRAIN ISLANDS

In this section, the device starts to be simulated by its minimum predicted sizes (Ravariu 2016): the height of the n^+ semiconductor islands of 10nm; the insulator thickness of 15nm; the cavity length of $x_c=2nm$; the semiconductor films length of 10nm; the doping in the semiconductor materials of $10^{19} \div 10^{21} cm^{-3}$, an interface charge of 3 x $10^{10} e/cm^2$; all aluminum electrodes. This is the reference nVn structure.
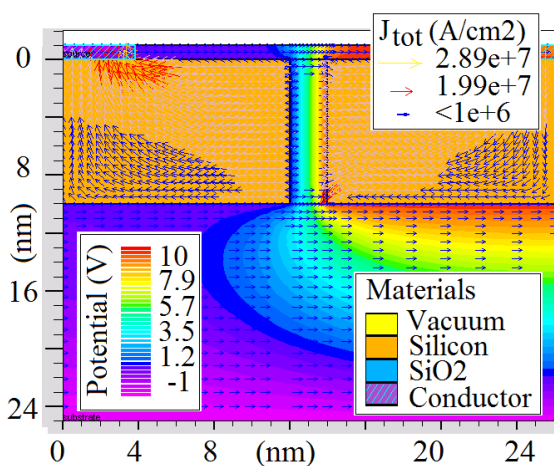
Figure 2: Simulation result of a NOI structure biased at $V_S=0V$, $V_D=10V$, $V_G=-1V$.

The model statement includes Fermi and BGN parameters in order to describe a Fermi carrier

distributions and Band Gap Narrowing in heavily doped source-drain regions.

Figure 2 presents a current flow inside a NOI structure with previous characteristics, at a relative high drain voltage that make sure the tunneling.

For the output characteristics analysis, I_D-V_{DS}, the drain voltage is ranged, while the gate voltage is kept constant.

The output characteristics are optimized after the semiconductor islands properties. At this stage, few parameters are already defined, like the *drain swing* (Sd), (Ravariu 2014), as the change in the drain voltage that creates a decade increasing in the output current. The output characteristic reveals negligible currents under a drain voltage, suggesting an *OFF drain state*, corresponding to I_{Dmin}. Let be the drain threshold voltage, V_{DST} that drain voltage that raises the drain current up to 1nA. The strong tunneling becomes prevalent for $V_{DS}>V_{DST}$, suggesting an *ON drain state*, corresponding to I_{DMax}.

In the first analysis, a maximum drain current spectrum is targeted, searching for an optimum concentration of the source and drain regions or optimum semiconductor material, when -8V<V_{DS}<8V, at V_{GS} = -5V. Changing the semiconductor properties, unanticipated capabilities occur. Different doping concentrations affect the carriers reservoir modulation in the semiconductor regions. Novel successions of semiconductor islands separated by vacuum, in comparison with a pin Tunnel-transistor, are comparatively simulated, fig. 3. For the pin device, usual features are adapted: (p-5×$10^{20}cm^{-3}$, i-5×$10^{18}cm^{-3}$, n-5×$10^{20}cm^{-3}$) ×50nm ×10nm-Si on 3nm-oxide.
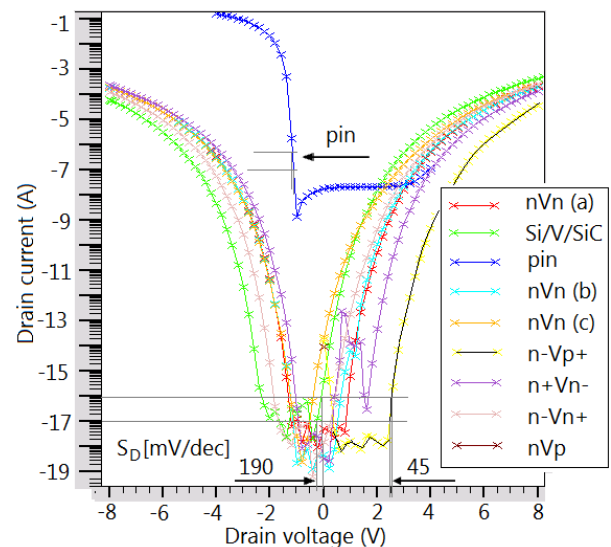
Figure 3: Output characteristics at V_G = -5V.

From the output characteristics, the maximum current excursion is offered by the Si/V/SiC structure with n-5×$10^{20}cm^{-3}$, providing the maximum ION current, but poorer drain slope Sd=190mV/dec. For the other NOI variants, Si is the semiconductor material used for

source and drain region, where n / p means $5 \times 10^{20} cm^{-3}$, n^- means $5 \times 10^{19} cm^{-3}$ and n^+ means $1 \times 10^{21} cm^{-3}$. Similar ION/IOFF ratio around 10^{14} occurs for all NOI variants higher than for pin. The minimum drain subthreshold slope of 45mV/dec, is similar to pin and occurs for the succession $n^- V p^+$, fig. 3. However, this swing is better than for a MOSFET. This behavior suggests possible applications of the NOI nano-device as pn-junction or multi-junctions implementation. The consumed area is reduced to a vacuum length of 2nm for the NOI case, instead a space charge region of 50nm for a pn junction, p zones can be replaced by n zones and the benefits of the exponential I-V dependence still exists.

The thermal regime simulations reveal a maximum heat power of $5 \times 10^{13} W/cm^3$, which produces a temperature increasing inside the NOI device from 290K to 299K, at $V_D=7V$ and $V_G=-1V$, fig. 4. So, the heat during a switch time of 100fs per a NOI device volume of $10^2 nm^3$ is $5 \times 10^{-19}J$ that is comparable with heat in TFET or MOSFET (Koswatta, Lundstrom, and Nikonov 2009).

In fig. 4 inset, a family of I_D-V_D curves of the nVn, $n^- Vn^+$, $n^- Vp^+$ and $n^+ Vn^-$, at linear scale are presented. Similar shapes of the I_D-V_D characteristics are encountered for a pnpn tunnel FET in the reverse mode, or in a vacuum SOI device. The strong tunneling regime for NOI is valuable, allowing superior currents excursions till 290μA for the $n^- Vn^+$ variant.
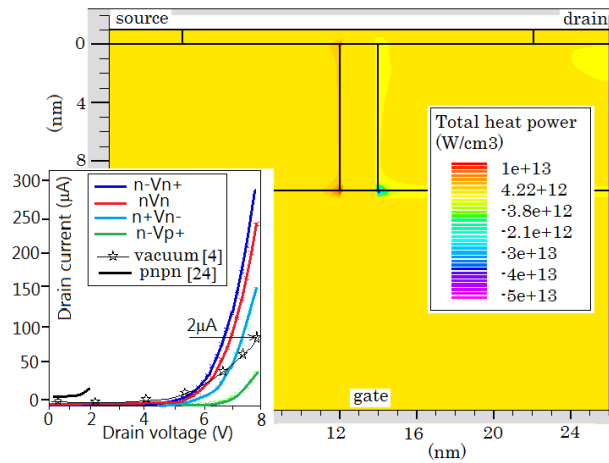
Figure 4: The I_D-V_D curves family at linear scale, at $V_D=7V$, $V_G=-1V$.

3. OXIDE VERSUS VACUUM

In our previous studies we have demonstrated by Atlas-Silvaco numerical simulations that NOI as nVn variant obeys to the Fowler-Nordheim FNORD model, offering exponential I_D-V_{DS} curves. Preliminary Atlas simulations suggest that oxide insulator can replace vacuum, as Si-n/Oxide/Si-n on insulator - the nOn variant. To validate this assertion, a NOI device with oxide instead vacuum is simulated by Atlas. The device nOn is biased at $V_{DS}=6V$, $V_{GS}=-4V$, fig. 5.

Figure 5 and Figure 6 proof the tunneling current across the oxide nano-cavity of 2nm, demonstrating a maximum current density $J_{tot}=2x10^8 A/cm^2$, as a I_{ON}

current $\approx 0.2mA$ in the device. The prior nVn device (Ravariu 2016) and actual nOn device have a similar behavior, in accordance with the theoretical Fowler-Nordheim conditions. A triangle barrier still arises in this case, at $V_{DS}=6V$, fig. 5.

Figure 6 presents a comparative analysis of the transfer characteristics among different Si-NOI structures with alternative successions: n-Vacuum-n (nVn), n^+-Vacuum-n^- ($n^+ Vn^-$), n-Vacuum-p (nVp), n-Oxide-n (nOn), n^+-Oxide-n^- ($n^+ On^-$) and n-Oxide-p (nOp). The doping is: $7 \times 10^{20} cm^{-3}$ for all the n or p-type regions, $10^{21} cm^{-3}$ for n^+ and $10^{20} cm^{-3}$ for n^-. For comparison with other classical devices, a pin-Tunnel transistor characteristic is simulated. The pin structure has similar sizes as NOI, excepting the intrinsic "i" region with 2nm length as the "Nothing" region and the dopings are extracted from the literature (Boucart and Ionescu 2007): Drain doping (n+) of $5 \times 10^{18} cm^{-3}$, source doping (p+) of $10^{20} cm^{-3}$ and Intrinsic p-doping (i) of $10^{17} cm^{-3}$.
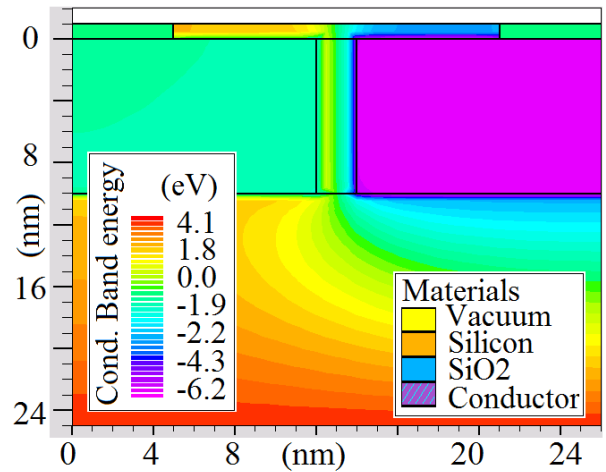
Figure 5: The conduction bang energies levels as colored contours, in the NOI transistor - the nOn variant, biased at $V_{DS}=6V$, $V_{GS}=-4V$.
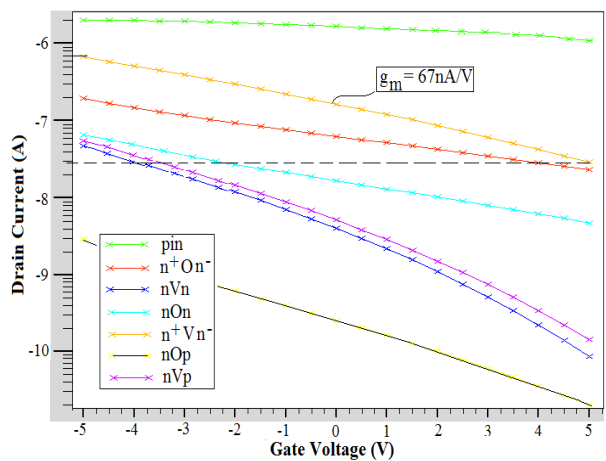
Figure 6: The transfer characteristics and extracted transconductance.

At a first inspection, an asymmetrical doping concentration - n^+Vn^- versus nVn, offers higher performances - maximum drain current $0.7\mu A$ versus $0.05\mu A$ and higher transconductance, $67nA/V$ versus $4.99nA/V$. The nVp variant has insignificant better performances as nVn. The nOp structure has the poorest performances: $I_{DMAX}=2nA$ and $g_m=0.2nA/V$.

Among the oxide structures, the n^+On^- variant presents the maximum performances, $I_{DMAX}=0.2\mu A$ and $g_m=17nA/V$, but poorer than the n^+Vn^- vacuum variant. The NOI results tend to become similar to the pin-Tunnel transistor simulated variant: $I_{DMAX}=1.9\mu A$ and $g_m=80nA/V$. The classical pin transistor with 50nm intrinsic region length has $I_{DMAX}=100\mu A$ and $g_m=90\mu A/V$ (Boucart and Ionescu 2007). So, the down-scaling of the pin transistor reduces their gains toward the NOI performances.

4. A PLANAR P-NOI DEMONSTRATOR

Previous results encourage us to search a planar Metal-Oxide-Semiconductor_n mOn variant as a p-NOI variant, instead of a vertical nOn variant, using the Si-planar technology.
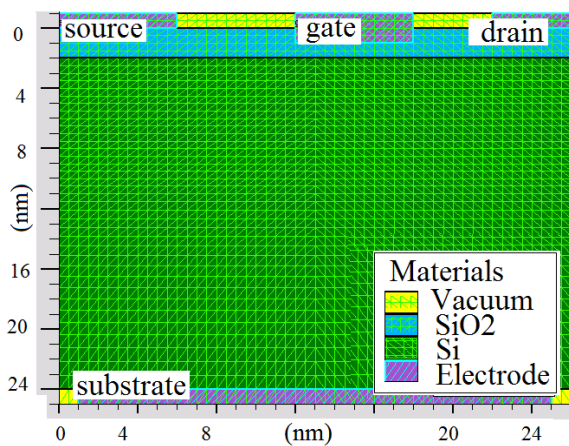
Figure 7: The proposed planar p-NOI device.
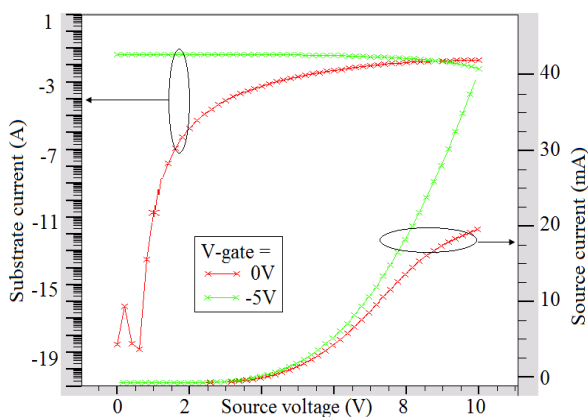
Figure 8: The simulated current-voltage characteristic of the proposed planar p-NOI device.

An ultrathin oxide can be grown onto a Si-wafer. Then n-poly-Si or metal can be deposited. The conduction occurs on the vertical direction in p-NOI, between the substrate and an upper contact, fig. 7, which simultaneously fulfills the role of more p-NOIs. Each upper electrode is different biased. The Substrate current, I_{SB}, becomes the current of the main interest.

The source and substrate current is extracted, while the source voltage rises from 0V to 10V. Each simulated characteristic obeys to the Fowler-Nordheim tunneling law, admitting an exponential current-voltage dependence, fig. 8.

5. INDIRECT EXPERIMENTAL SUPPORT

A first experimental proof is picked-up from the measurements of a vacuum transistor reported in 2012, (Han, Oh, and Meyyappan 2012). This experimental device is closest to the NOI transistor from this paper. It has high subthreshold slope, high operation voltages (SS=4V/dec, V_{DS}=20V), poor transconductance (g_m=0.2μS), but promising cut-off frequency (f_T=0.46THz), suggesting the future utility of these kind of vacuum nanodevices. The main experimental parameters are inferior versus our NOI simulated device (Ravariu 2016) with SS=650mV/dec. The slope is further improved in this paper for a drain subthreshold slope of Sd=45mV/dec.

A second experimental resource concerns the MOSFETs with ultra-thin gate oxide, that inherently includes a p-NOI parasitic device. The Fowler-Nordheim tunneling gate current reaches 1pA or a density of the current of $10^2 A/m^2$, through a MOSFET transistor with 1nm oxide/4nm HfO_2 biased at 3V (Basak, Maiti, and Mallik 2015). These experimental results are in accordance with the simulated I-V curves of the p-NOI device from fig. 8, indicating a null leakage current till 2V, and a suddenly current increasing over 2V.

The NOI transistor applications can be oriented on few directions: (a) high frequency circuits, using the source-drain voltage switching, due to its excellent low Sd parameter; (b) an important theoretical device able to offer information about the tunneling between two close adjacent Si-islands in ultra-large scale of integration circuits (Ravariu 2016), (c) planar p-NOI variant is an useful test device for the immediate next generations of MOSFET with sub-4nm oxide thickness.

6. CONCLUSIONS

The paper depicted new NOI variants with asymmetrical source/drain properties, reaching the best drain swing of 45mV/dec, which overpass the MOSFETs or vacuum devices, as simulation results. The nano-cavity with oxide instead vacuum offered similar behavior and open the door to a planar p-NOI device experimentation. The importance of the NOI devices understanding covers their main application areas: NOI as controlled or parasitic devices. Especially p-NOI devices can be co-integrated with MOSFETs

under a controlled mixed IC technology. Also, in the next ULSI circuits two semiconductors or two metallic traces will be separated by ultra-thin insulators, even vacuum, so that the NOI device becomes a main parasitic element.

ACKNOWLEDGMENTS

REFERENCES

Liu D.M., Datta S., 2015. Scaling Length Theory of Double-Gate Interband Tunnel Field-Effect Transistors. IEEE Trans. Electron Devices, 59 (4), 902–909.

Koswatta S.O., Lundstrom M.S., Nikonov D.E., 2009. Performance Comparison Between p-i-n Tunneling Transistors and Conventional MOSFETs. IEEE Trans. Electron Devices, 56 (3), 456–465.

Han J., Meyyappan M., 2014. Introducing the vacuum transistor: a device made of Nothing. IEEE Spectrum, 46 (6), 25–29.

Armstrong M., 2015. The quest for the ultimate vacuum tube, IEEE Spectrum, 47 (12), 29–35

Han J., Oh J., Meyyappan M., 2012. Vacuum nanoelectronics: Back to the future? Gate insulated nanoscale vacuum channel transistor. Applied Physics Letter, 100 (213505), 1–4.

Subramanian K., Kang W.P., Davidson J.L., 2008. A Monolithic Nanodiamond Lateral Field Emission Vacuum Transistor. IEEE Electron Device Letter, 29 (11), 1259-1261.

Boucart K., Ionescu A.M., 2007. Double-gate tunnel FET with high-kappa gate dielectric. IEEE Trans. Electron Devices, 54 (7), 1725–1733.

Ravariu C., 2010. The implementation methodology of the real effects in a NOI nanostructure aided by simulation and modelling. Elsevier Simulation Modeling Practice and Theory, 18, (9), 1274-1285.

Ravariu C., Babarada F., 2011. Modeling and simulation of special shaped SOI materials for the nanodevices implementation. Hindawi Journal of Nanomaterials, 792759 (6), 1–11.

Ravariu C., 2005. A NOI – nanotransistor. Proceedings of IEEE International Conference of Semiconductors, pp. 65–68, Oct. 11-14, Sinaia, (Europe, Romania).

Ravariu C., 2017. Gate Swing Improving for the Nothing On Insulator Transistor in Weak Tunneling. IEEE Transactions on Nanotechnology, 16 (6), 1115–1121.

Pretet J., Monfray S., Cristoloveanu S., Skotnicki T., 2004. Silicon-On-Nothing MOSFETs: performance, short channels effects and back gate coupling. IEEE Trans. Electron Devices, 51 (2), 240–245.

Ravariu C., 2016. Deeper Insights of the Conduction Mechanisms in a Vacuum SOI Nanotransistor. IEEE Transactions on Electron Devices, 63 (8), 3278–3283.

Ravariu C., 2014. Compact NOI Nano-Device Simulation. IEEE Transactions on Very Large Scale Integration (VLSI) Systems, 22 (8), 1841–1844.

Basak R., Maiti B., Mallik A., 2015. Analytical model of gate leakage current through bilayer oxide stack in advanced MOSFET. Superlattices and Microstructures, 80 (1), 20–31.

PARALLEL SIMULATION OF THE N-BODY PROBLEM USING QUAD-TREE HLPC

M. Rossainz-López[a], Manuel I. Capel[b], E. Álvarez Martínez[a], I. Pineda Torres[a]

[a] Faculty of Computer Science, Autonomous University of Puebla, San Claudio Avenue and South 14th Street, San Manuel, Puebla, Puebla, 72000, México
[b] Software Engineering Department, College of Informatics and Telecommunications ETSIIT, University of Granada, Daniel Saucedo Aranda s/n, Granada 18071, Spain

[a]rossainz@cs.buap.mx, [b]manuelcapel@ugr.es, [a]erialvam@gmail.com, [a]ipineda@cs.buap.mx

ABSTRACT

This work proposes the use of Parallel Objects using the model of High Level Parallel Compositions (HLPC) to implement a proposal for parallel simulation of the N-body Problem using the communication pattern between processes N-Tree under the HLPC Model. Particularly the implementation of the partitioning strategy divide and conquer as part of HLPC using the object orientation paradigm is shown. A HLPC comes from the composition of a set three object types: An object manager that represents the HLPC itself and makes an encapsulated abstraction out of it that hides the internal structure. The object manager controls a set of objects references, which address the object Collector and several Stage objects and represent the HLPC components whose parallel execution is coordinated by the object manager. With the strategy divide and conquer as HLPC the parallel processing technique N-Tree is used to parallelize sequential code that solve problems that can be partitioned by divide and conquer a N-ary Tree such the N-body problem that concerns with determining the effects of forces between "bodies". A case study of the N-body problem in terms of particles charged according to Coloumb's electrostatic law is shown, which is solved with the implementation of a new HLPC: the Quad-Tree HLPC. Finally the performance analysis of this implementation is shown comparing them with its corresponding sequential implementations to demonstrate their usefulness: programmability and performance.

Keywords: High Level Parallel Compositions, HLPC, N-ary Tree, N-body Problem, Divide and Conquer, Quad-Tree, Parallel Objects, Structured Parallel Programming.

1. INTRODUCTION

High Performance Computing or HPC has brought to reality the possibility of obtaining a great efficiency in data processing without a great rise in prices. Even though, open problems that motivate research in this area still exist. Some of these problems of parallel programming environments amount to the users' acceptance, which usually depends on whether they can offer complete expressions of the parallel programs behavior that are built with these environments (Corradi and Zambonelli, 1995). In OO application systems, the scientific community interested in the study of concurrency only accepts standards for programming environments based on Parallel Objects (POs). A first approach that tries to tackle this problem is to let the programmer to develop his programs according to a sequential programming style, then, he can automatically obtain the parallelized parts of the code with the help of a specific environment. However, intrinsic implementation difficulties exist mainly due to the difficult definition of programming languages formal semantics that refrain from the automatic (without user participation) sequential code parallelization, and thus the problem of generating parallelism in an automatic way for a general application continues unsolved. The so called structured parallelism has become a promising approach to solve the mentioned problem. In general, parallel applications follow predetermined patterns of execution. Communication patterns are rarely arbitrary and are not structured in their logic (Brinch Hansen 1993). We are interested, in parallel applications that use predetermined communication patterns, among other component–software. Even so, with this promising approach, at least the following ones have currently been identified as important open problems: The lack of acceptance structured parallel programming environments of use to develop applications, (Bacci 1999), The necessity to have patterns or High Level Parallel Compositions, the Determination of a complete set of patterns as well as of their semantics, (Corradi 1995), the adoption of an object-oriented approach, (Corradi 1991; Darlington 1993). HLPCs are parallel patterns defined and logically structured that, once identified in terms of their components and of their communication, can be adopted in the practice and be available as high level abstractions in user applications within an OO-programming environment. The process interconnection structures of parallel execution patterns such as trees can be built using HLPCs, within the work environment of POs that is the one used to detail the structure of a HLPC implementation. A structured approach to parallel programming is based on the use of communication/interaction patterns which are predefined structures of user's application processes. In such a situation, the structured parallelism approach provides the interaction-pattern abstraction and describes applications through HLPCs, which are able to implement the pattern mentioned already. The encapsulation of a HLPC should follow the modularity principle and it should provide a base to obtain an effective reusability of the parallel behavior to be

implemented. When there is the possibility of attaining this, a generic parallel pattern is built, which in its turn provides a possible implementation of the interaction structure between processes of the application, independently of the functionality of these. In addition, it is in line with the structured approach we have adopted that is the enrichment of traditional parallel environments with libraries of program skeletons (Darlington 1993) that concrete communication patterns represent. What it really means is a new design approach to parallel applications. Instead of programming a concurrent application from the beginning and controlling the creation of processes as well as the communications among them, the user simply identifies those HLPCs that can implement the adapted patterns to the communication needs of his application and uses them together with the sequential code that implements the computations that individually carry out their processes. Several significant and reusable parallel patterns of interconnection can be identified in multiple applications and parallel algorithms which has resulted in a wide library of communication patterns between concurrent processes such as HLPCs whose details are found in (Rossainz and Capel 2008; Rossainz and Capel 2014). In the present work we have implemented the partitioning strategy divide and conquer using N-Tree pattern as a generic HLPC and using the object orientation paradigm we have realized its concretion in one particular application: the solution of N-body particles, using for this one strategy for the parallel implementation as HLPCs of sequential algorithm of case study of the N-body problem in terms of particles charged according to Coulomb's electrostatic law (Devanshu and Munish 2014); particles of opposite charge are attracted and those of like charge are repelled. This concretion has led to the creation of a new HLPC: The Quad-Tree HLPC whose characteristics are shown in the following sections. In this way it is the user's own applications that specify the semantics of the N-Tree-Divide and Conquer according to the requirements of the software that was developed. Finally, we show an analysis of the performance in terms of acceleration Amdahl refers to the Quad-Tree HLPC for a restricted range of exclusive processors in a parallel computer.

2. HIGH LEVEL PARALLEL COMPOSITIONS (CPAN)

A HLPC comes from the composition of a set three object types: An object manager (Figure1) that represents the CPAN itself and makes an encapsulated abstraction out of it that hides the internal structure. The object manager controls a set of objects references, which address the object Collector and several Stage objects and represent the HLPC components whose parallel execution is coordinated by the object manager. The objects Stage (Figure 2) are objects of a specific purpose, in charge of encapsulating an client-server type interface that settles down between the manager and the

slave-objects. These objects do not actively participate in the composition of the CPAN but are considered external entities that contain the sequential algorithm that constitutes the solution of a given problem. Additionally, they provide the necessary interconnection to implement the semantics of the communication pattern which definition is sought. In other words, each stage should act a node of the graph representing the pattern that operates in parallel with the other nodes. Depending on the particular pattern that the implemented HLPC follows, any stage of it can be directly connected to the manager and/or to the other component stages. The Collector object (Figure 3) we can see an object in charge of storing the results received from the stage objects to which is connected, in parallel with other objects of HLPC. That is to say, during a service request the control flow within the stages of a HLPC depends on the implemented communication pattern. When the composition finishes its execution, the result does not return to the manager directly, but rather to an instance of the Collector class that is in charge of storing these results and sending them to the manager, which will finally send the results to the environment, which in its turn sends them to a collector object as soon as they arrive, without being necessary to wait for all the results that are being obtained.
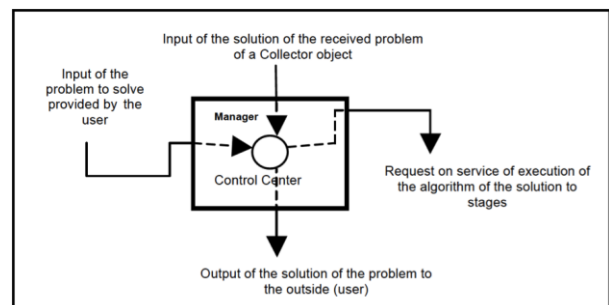
Figure 1: Component Manager of HLPC model
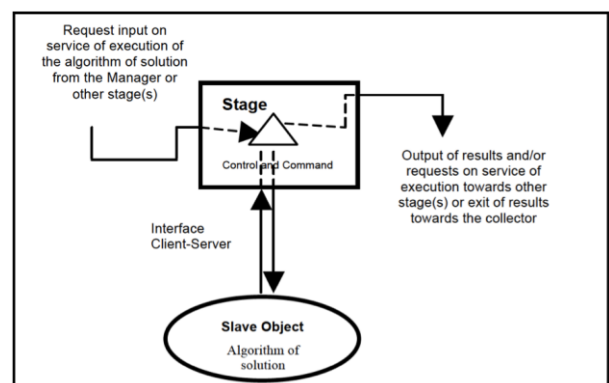
Figure 2: Component Stage of model CPAN and its associated slave object

In summary, a HLPC is composed of an object manager that represents the HLPC itself, some stage objects and an object of the class Collector, for each petition that should be managed within the HLPC.
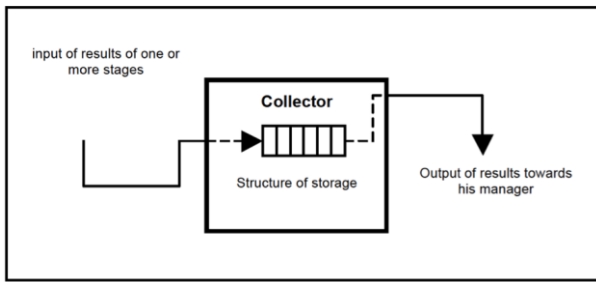
Figure 3: Component Collector of HLPC Model

Also, for each stage, a slave object will be in charge of implementing the necessary functionalities to solve the sequential version of the problem being solved (Figure 4). For details CPAN model, see see (Rossainz and Capel 2008).
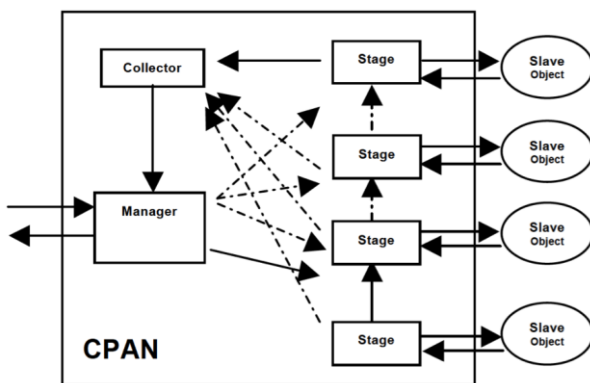
Figure 4: Internal structure of HLPC. Composition of its components

The (Figure 4) shows the pattern HLPC in general, without defining any explicit parallel communication pattern. The box that includes the components, represents the encapsulated HLPC, internal boxes represent compound objects (collector, manager and objects stages), as long as the circles are the objects slaves associated to the stages. The continuous lines within the HLPC suppose that at least a connection should exist between the manager and some of the component stages. Same thing happens between the stages and the collector. The dotted lines mean more than one connection among components of the HLPC.

2.1. The HLPC seen as composition of parallel objects

Manager, collector and stages are included in the definition of a Parallel Object (PO), (Corradi 1991). Parallel Objects are active objects, which is equivalent to say that these objects have intrinsic execution capability, (Corradi 1991). Applications that deploy the PO pattern can exploit the inter-object parallelism as much as the internal or intra-object parallelism. A PO-instance object has a similar structure to that of an object in Smalltalk, and additionally defines a scheduling politics, previously determined that specifies the way in which one or more operations carried out by the instance synchronize, (Corradi 1991; Danelutto and

Torquati 2014). Synchronization policies are expressed in terms of restrictions; for instance, mutual exclusion in reader/writer processes or the maximum parallelism allowed for writer processes. Thus, all the parallel objects derive from the classic definition of a class plus the synchronization restrictions (mutual exclusion and maximum parallelism), which are now included in that definition, (Birrel 1989). Objects of the same class share the specification contained in the class of which are instances. The inheritance allows objects to derive a new specification from the one that already exists in the super-class. Parallel objects support multiple inheritance in the HLPC model.

2.2. Communication types in the parallel objects of HLPC

Parallel objects define 3 communication modes: synchronous, asynchronous communication and synchronous future communication.

1. The synchronous communication mode stops the client activity until it receives the answer of its request from the active server object, (Andrews 2000).
2. The asynchronous communication does not delay the client activity. The client simply sends the request to the active object server and its execution continues afterwards. Its use in application programming is also easy, because it is only necessary to create a thread and start it to carry out the communication independently from the client, (Andrews 2000).
3. The asynchronous future will delay client activity when the method's result is reached in the client's code to evaluate an expression. The asynchronous futures also have a simple use, though its implementation requires of a special care to get a syntactical construct with the correct required semantics. For details see (Lavander y Kafura 1995).

The asynchronous and asynchronous future communication modes carry out the inter-objects parallelism by executing the client and server objects at the same time.

2.3. The base classes of any HLPC

As it has already been described, a HLPC comes from the composition of a set of objects of three types. In particular, each HLPC is made up of several objects: an object manager, some stage objects and a collector object for each request sent by client objects of the HLPC. Also, for each stage of the HLPC, a slave object will be in charge of implementing the sequential part of the computation that is sought and carried out in the application or in the distributed and parallel algorithm. In PO the necessary base classes to define the manager, collector, stages objects that compose a HLPC - the implementation details are in (Rossainz and Capel 2008) - are the next ones:

1. Abstract class ComponentManager: It defines the generic structure of the component manager of a

HLPC, from which will be derived all the manager instances depending on the parallel behavior that is assumed in the HLPC creation. All specific instances of a manager accept a list of n-associations as input. An association is a pair of elements, that is, an object slave and the name of the method that has to be executed by this object. The objects slaves are external entities that contain a sequential algorithm that have to be executed by one of their methods. Once the manager has obtained the list of n-associations, it will generate the concrete stages, one for each association and then each stage becomes responsible for an object slave together with its execution method. In turn, each stage is connected to each other, in accordance with the parallel pattern that has been implemented in the HLPC. Finally, the manager carries out a computation by the execution of one of its methods. To achieve the computation phase, it is necessary to pass on the input data that it requires to start to the method. The manager then generates a component collector and sends its reference to the stages, as well as the input data. The stages start processing the data according to the connection configuration that they keep to each other, results will be passed on as they become available. At the end the collector will gather the results sent by the stages to return them to the manager, which finally will transfer these results to the HLPC environment or to the code that uses them.

2. Abstract class ComponentStage: It defines the generic structure of the component stage of a HLPC, as well as their interconnections, from which will be derived all the concrete stages depending on the parallel behavior that is assumed in the creation of the HLPC. All specific instances of a stage accepts a list of associations slave-object/method as input to work with them, whether they are connected or not with the following stage of the list of associations and depending on the parallel pattern they are willing to implement. When the manager send in parallel a command to the stages, each one of them makes the object-slave to carry out the execution of its method, then the stage captures the results and sends them to the following stage or to the collector, depending on the implemented structure.

3. Concrete class ComponentCollector: It defines the concrete structure of the component collector of any HLPC. This component fundamentally implements a multi-item buffer, where it will store the results of stages that have the reference of this collector. This way one can obtain the result of the calculation initiated by the manager.

2.4. The Synchronization restrictions of a CPAN

It is necessary to have synchronization mechanisms available when parallel request of service take place in a HLPC, so that the objects that conform it can negotiate several execution flows concurrently and, at the same time, guarantee the consistency in the data that being processed. Within any HLPC the restrictions MAXPAR, MUTEX and SYNC can be used for correct programming of their methods.

1. MAXPAR: The maximum parallelism or MaxPar is the maximum number of processes that can be executed at the same time. That is to say the MAXPAR applied to a function represents the maximum number of processes that can execute that function concurrently. In the case of HLPC, the maximum parallelism is applied to the functions of the ComponentManager class and to the functions of the ComponentStage class.

2. MUTEX: The restriction of synchronization mutex carries out a mutual exclusion among processes that want to access to a shared object. The mutex preserves critical sections of code and obtains exclusive access to the resources. In the case of the HLPCs, the restriction mutex applied to a function represents the use of that function on the part of a process every time. In other words, the mutex allows that only one of the processes executes the function, blocking all the other processes trying to make use of the service until one of the ones that execute it finishes. The mutex within the HLPC is applied to the functions of an object collector.

3. SYNC: The restriction SYNC is not more than a producer/consumer type of synchronization; it is of use, for instance, for programming the methods of the ComponentCollector class. SYNC helps to synchronize these methods when accessing the shared resource at the same time, which in this case is a multi-item list.

The details of the algorithms and their implementation can be seen in (Rossainz and Capel 2008} and (Rossainz and Capel 2014}.

3. CONSTRUCTION OF A CPAN

With the base-classes of the PO model of programming, it is now possible to build concrete HLPCs. To build a HLPC, first it should have made clear the parallel behavior that the user application needs to implement, so that the HLPC becomes this pattern itself. Several parallel patterns of interaction have long been identified in Parallel Programming, such as farms, pipes, trees, cubes, meshes, a matrix of processes, etc. Once identified the parallel behavior, the second step consists of elaborating a graph of its representation, as an informal design of the objective system. This practice is also good for illustrating the general characteristics of the desired system and will allow us to define its representation with HLPCs later on, by following the pattern proposed in the previous section. When the model of a HLPC has already been made clear, it defines a specific parallel pattern; let's say, for example, a tree, or some other mentioned pattern, and then the following step will be to do its syntactic definition and specify its semantics. Finally, the syntactic definition prior to any programmed HLPC is transformed into the most appropriate programming environment, with the

objective of producing its parallel implementation. It must be verified that the resulting semantics is the correct one. To attain this, we use several different examples to demonstrate the generality and flexibility of the application HLPC-based design and the expected performance and quality as a software component. Some support from an integrated development environment (IDE) for Parallel Programming should be provided in order to validate the component satisfactorily. The parallel pattern worked in the present investigation has been the N-Tree to solve the N-body problem creating the Quad-Tree HLPC thats its a variant of the TreeDV HLPC which is shown in sections later.

4. THE TECHNIQUE OF DIVIDE AND CONQUER AS A HLPC

The programming technique is presented it Divide and Conquer as a CPAN, applicable to a wide range of problems that can be parallelizable within this scheme.

4.1. Divide and Conquer

The technique of it Divide and Conquer it is characterized by the division of a problem in sub-problems that have the same form that the complete problem (Brassard and Bartley 2000). The division of the problem in smaller sub-problems is carried out using the recursion. The method recursive continues dividing the problem until the parts divided can no longer follow dividing itself, and then they combine the partial results of each sub-problem to obtain at the end the solution to the initial problem (Brassard and Bartley 2000). In this technique the division of the problem is always made in two parts, therefore a formulation recursive of the method Divide and Conquer form a binary tree whose nodes will be processors, processes or threads. Remember that a binary tree is a 2-ary tree such that a child of a node is positioned at either the left or right of the node. A node in a binary tree may have a left but no right child. It may have a right but no left child. Positions of children of a node are an important property of a binary tree, (Liwu 2002). A complete binary tree construction showing the "divide" part of divide and conquer is shown in figure 5, with the final task at the bottom and the root at the top.
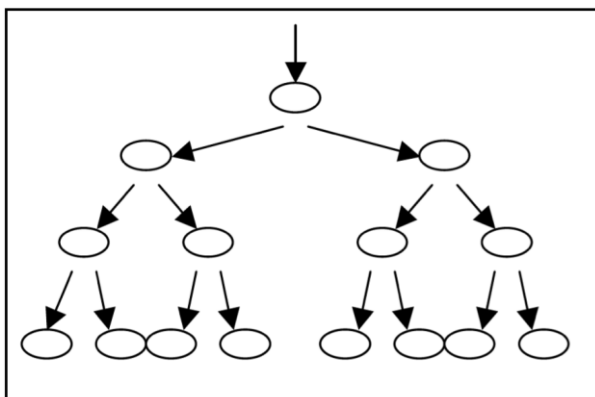
Figure 5: Binary Tree

This complete binary tree is a perfectly balanced tree with all bottom nodes at the same level. This occurs if the task can be divided into a number of parts that is a power of 2. If not a power of 2, one or more bottom nodes will be at one level higher than the others. The node root of the tree receives as input a complete problem that is divided in two parts. It is sent to the node left son, while the other is sent to the node that represents the right son (figure 5). This division process is repeated of recursive form until the lowest levels in the tree. Lapsed a certain time, all the nodes leaf receives as input a problem given by its node father; they solve it and the solutions (that are the exit of the node leaf) are again correspondents to its progenitor. Any node father in the tree will obtain his children's two partial solutions and it will combine them to provide an only solution that will be the node father's exit. Finally, the node root will give as exit the complete solution of the problem, (Brinch Hansen 1993). This way, while in a sequential implementation a single node of the tree can be executed or visited at the same time, in a parallel implementation, more than a node it can be executed at the same time in the different levels, it is, when dividing the problem in two sub-problems, both can be processed in a simultaneous way.

4.2. Representation of the Tree Divide and Conquer as a HLPC

The representation of the patron tree that defines the technique of it Divide and Conquer as HLPC has their model represented in figure 6. This parallel solution offers the prospect of traversing several parts of the tree simultaneously in the HLPC TreeDV. Once a division is made into two parts, both parts can be processed simultaneously executing the sequential algorithm contained in the slave object associated to the nodes of the tree. Though a recursive parallel solution could be formulated. One could simply assign one process o thread to each node in the tree. Contrary to the previous model, where the objects slaves were predetermined outside of the pattern HLPC, in this model an object slave is only predefined statically and associated to the first stage of the tree. The following objects slaves will be created internally by the own stages in a dynamic way, because the levels of the tree depend from the problem to solve and a priori the number of nodes that can have the tree is not known, neither its level of depth (see figure 6).

5. N-BODY PROBLEM

The N-Body problem is concerned with determining the effects of forces between bodies, for example, astronomical bodies that are attracted to each other through gravitational forces or charged particles are also influenced by each other according to electrostatic law (Wilkinson and Allen 1999; Devanshu and Munish 2014).
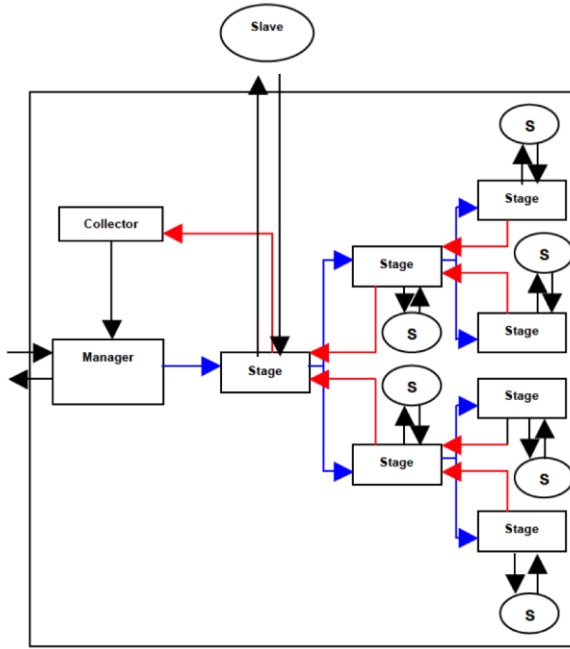
Figure 6: The Cpan of a TreeDV

The N-body problem appears in other areas like molecular dynamics and fluid dynamics (see Müller 2008; Bhatt, Chen, Lin and Liu 1992). We provide the basic equations to enable the application to be coded as a HLPC TreeDV using as a case study the N-Body problem in terms of particles charged according to Coloumb's electrostatic law; particles of opposite charge are attracted and those of like charge are repelled. Also charged particles may move away from each other. The objective is to find the positions and movements of the particles in the space that are subject to electrostatic forces from other particles using Coulomb laws.

For a computer simulation, we use values at particular times, t0; t1; t2, etc., the time intervals being as short as possible to achieve the most accurate solution. Let the t-time interval, then, for a particular particle of mass m, the force is given by:

$$F = \frac{m(v^{t+1} - v^t)}{\Delta t} \qquad (1)$$

and a new velocity by:

$$v^{t+1} = v^t + \frac{F\Delta t}{m} \qquad (2)$$

where v^{t+1} is the velocity of the particle at time $t+1$ and v^t is the velocity of the particle at time t. If a particle is moving at a velocity v over the t-time interval, its position changes by:

$$x^{t+1} - x^t = v\Delta t \qquad (3)$$

where x^t is position at time t. Once particles move to new positions, the forces change and the computation has to be repeated. The computation of the attraction or not of N-particles according to their electrostatic charge is described in the following algorithm:

```
for (t=0; t< tmax; t++)
    {
      for(i=0;i<N;i++)
        {
          f=force(i);
          v[i]_new = v[i]+f*dt/m;
          x[i]_new = x[i]+v[i]_new*dt;
        }
    }
for(i=0;i<nmax;i++)
    {
      x[i]=x[i]_new;
      v[i]=v[i]_new;
    }
```

For each time period t, for each particle i, compute force on i-th particle, compute new velocity and new position. For each particle i update velocity and position. Parallelizing this algorithm can use partitioning where by groups of particles are the responsibility of each process, and each force is carried in distinct messages between process (Carugati 2016). A large number of messages could result and it is not feasible if N is very large, (Wilkinson and Allen 1999; Greengard and Rokhijn 1997). The complexity can be reduced using the technique that a cluster of distant particles can be approximated as a single distant particle of the total mass of the cluster sited at the center of mass of the cluster (Carugati N. 2016), as illustrated in figure 7. This idea can be implemented as a HLPC by being applied recursively generating a m-ary tree, in particular way, a *quad-tree* (a tree in which each node of tree has four children) based on the Barnes-Hut algorithm, as you can see in (Roosta and Séller, 1999; Wilkinson and Allen 1999; D'Angelo A. 2016).
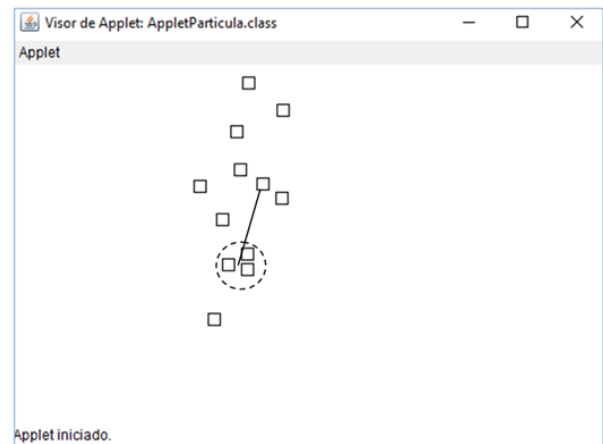
Figure 7: Clustering distant particles

A divide and Conquer formation to the problem using this clustering idea start for a two-dimensional space in which one square contains the particles. This square is

recursively divided into four sub-squares (see figure 8) creating a *quadtree*, ie a tree with up to four edges from each edge. If a sub-square contains no particles, the sub-square is deleted from further consideration. If a sub-square contains more than one particle, it is recursively divided until every sub-square contains one particle creates the *quadtree* (D'Angelo 2016). The tree will be unbalanced. The leaves represent cells each containing one particle. Figure 8 illustrates the decomposition for a two-dimensional space and the Figure 9 represents the resultant *quadtree* like a HLPC. In the "Cpan QuadTree Particle" of figure 9, the total mass and center of mass of the sub-square is stored at each node of tree. The force on each particle can be obtained by traversing the tree starting at the root, stopping at a node when the clustering approximation can be used for the particular particle, and otherwise continuing to traverse the tree downward.
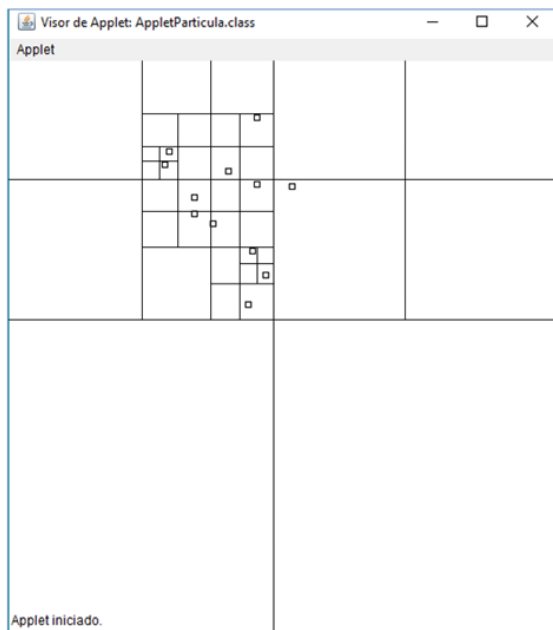
Figure 8: Particles. Recursive Subdivision of two-dimensional space
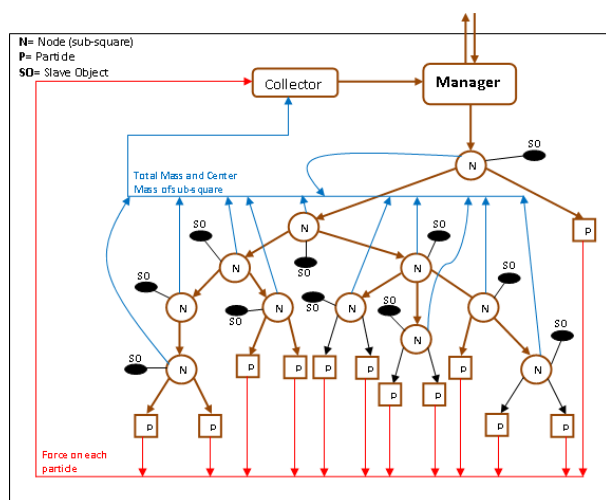
Figure 9: Cpan QuadTree Particle

After the tree has been constructed, the total mass and center of mass of the sub-square is stored at each node. The force on each body can be obtained by traversing the tree starting at the root, stopping at a node when the clustering approximation can be used for the particular body, and otherwise continuing to traverse the tree downward (Appel Andrew 1985; Wilkinson and Allen 1999).

5.1. Other Applications

Although we describe the problem in terms of particles bodies, the concept can be applied to other situations, for example, astronomical bodies are attracted to each other through gravitational forces (Alonso J. 2014). The objective is to find the positions and movements of the bodies in space (say planets) that are subject to gravitational forces from other bodies using Newtonian laws of physics.

A difference between the problem of the particles exposed in this work and astronomical bodies is that charged particles may move away from each other, whereas astronomical bodies are only attracted and hence will tend to cluster.

6. EXPERIMENTATION AND PERFORMANCE

Performance analysis of CPANS TreeDV for the N-Body Problem are shown. The aim is to show that the performances obtained are "good" based on the model of the HLPC. The HLPC TreeDV performance to solve the problem mentioned was carried out on a parallel computer with 64 processors, 8 GB of main memory, high-speed buses and distributed shared memory architecture. Performance measures obtained in implementing the HLPC TreeDV using Divide and Conquer Technique is carried out with the following restrictions execution: In the N-body problem, we work with a simulation of 50000 particles with electrostatic charge moving randomly in space. The calculations were: find the positions and movements of the particles in the space that are subject to electrostatic forces from other particles using Coulomb laws. For this, the HLPC QuadTree calculated with the sequential algorithms associated with the slave objects of the generated M-tree, the masses and the forces of each particle (see figure 9).

These execution conditions allow a sufficient load for the processors and show the good performance of the HLPC QuadTree when solving the problem. The execution was performed in 2, 4, 8, 16 and 32 exclusive processors and the results are shown in the figure 10 whose graph were obtained from the data shown in the table 1. In her show the series of measurements obtained including their corresponding sequential version for the HLPC QuadTree, magnitude speedup found and the upper bound on the magnitude of speedup using for that Amdahl's law, moreover the runtime execution in seconds of the program.

Table 1: HLPC QuadTree Particle Perfomance Management of 50000 random particles

HLPC QuadTree	CPU Seq	CPU Set2	CPU Set4	CPU Set8	CPU Set16	CPU Set32
RunTime Seconds	1810	1069.8	890	724.1	696.1	579.6
Speedup	1	1.69	2.03	2.50	2.60	3.12
Amdalh	1	1.74	2.76	3.90	4.92	5.66

Parallel executions of HLPC have a time shorter than the time used by its corresponding sequential versions, as expected. The execution times of its parallel version HLPC improve as the number of processors is increased, ie, as is increasing the number of processors with which HLPC is executed, its execution times are decreasing. A value of the magnitude called speedup is appreciated ever upward on improving execution time of parallel HLPC respect to its sequential counterpart, but always below the levels of Amdahl's Law calculated, obtaining "good" yields.
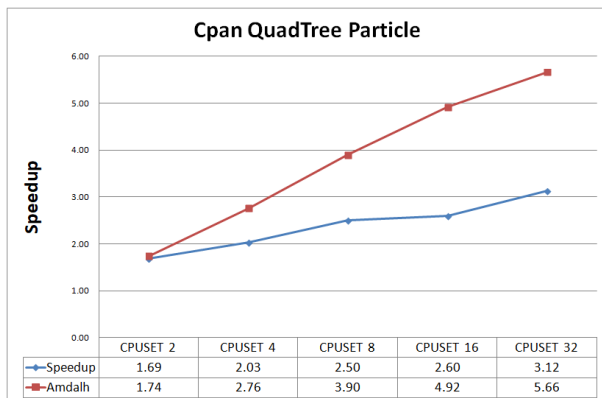
Fig. 10. Speedup scalability found for CpanQuadTree in solution of N-body problem for 2, 4, 8, 16 and 32 exclusive processors

7. CONCLUSIONS

We have presented a method for design of concurrent applications based on the construction of High Level Parallel Compositions or HLPC and which are usually used in different platforms, such as Java, C ++ and POSIX Threads. We discuss the implementation of HLPC treeDV as generic and reusable patterns of communication/interaction between processes which implements the algorithm design technique called divide and conquer making use of an N-tree as a pattern of communication associated, which can even be used by inexperienced parallel application programmers to obtain efficient code by only programming the sequential parts of their applications. The HLPC TreeDV has been reused in the communication/interaction between the processes of N-body (particles) problem. This problem have been included to show speedup and low execution times about their best sequential version of the algorithm that solve the problem. We have also obtained good

performance in their executions and speedup scalability compared to Amdahl's law on the number of processors used to obtain the solution.

REFERENCES

Alonso J. 2014. Fast methods for N-body problems. *CME342- Parallel Methods in Numerical Analysis. Lecture Notes* Springer. USA.

Andrews G.R., 2000. Foundations of Multithreaded, Parallel, and Distributed Programming, *Addison-Wesley*

Appel Andrew W. 1985. An Efficient Program for many-body simulation. *Society for Industrial and Applied Mathematics*. Volume 6, Number 1. SIAM.

Bacci, Danelutto, Pelagatti, Vaneschi, 1999. SklE: A Heterogeneous Environment for HPC Applications. *Parallel Computing 25*.

Bhatt S., Chen M, Lin C. Y. and Liu P., 1992. Abstractions for Parallel N-Body Simulations. *Proceeding of Scalable High Performance Computing Conference*. Pp:26-29.

Birrell A., 1989. An Introduction to Programming with Threads, *Digital Equipment Corporation, Systems Research Center*, Palo Alto California, USA.

Brassard G. and Bratley P., 2000. Fundamentals of Algorithmics, *Prentice-Hall*, USA.

Brinch Hansen, 1993. Model Programs for Computational Science: A programming methodology for multicomputers, *Concurrency: Practice and Experience*, Volume 5, Number 5.

Carugati N. 2016. The Parallelization and Optimization of the N-Body Problem using OpenMP and OpenMPI. *Gettysburg College*. Student Publications.422.http://cupola.gettysburg.edu/student_scholarship/422

Corradi A., Leonardi L., 1991. PO Constraints as tools to synchronize active objects. *Journal Object Oriented Programming* 10, pp. 42-53.

Corradi A, Leonardo L, Zambonelli F., 1995. Experiences toward an Object-Oriented Approach to Structured Parallel Programming. *DEIS technical* report no. DEIS-LIA-95-007.

Danelutto M. and Torquati M, 2014. Loop parallelism: a new skeleton perspective on data parallel patterns, *in Proc. of Intl. Euromicro PDP*: Parallel Distributed and Network-based Processing, Torino, Italy.

D'Angelo A. 2016. A Brief Introduction to Quadtrees and Their Applications. *Style file from the 28th Canadian Conference on Computational Geometry*. Canada.

Darlington et al., 1993, Parallel Programming Using Skeleton Functions. *Proceedings PARLE'93*, Munich (D).

Devanshu M. and Munish M., 2014. N-Body Simulation. *University at Buffalo*. The State University of New York.

Greengard L. and Rokhijn V. 1997. A Fast Algorithm for particle simulations. *Journal of Computational Phiysics*, Volume 135, Issue 2. pp:280-292

Lavander G.R., Kafura D.G. 1995. A Polimorphic Future and First-class Function Type for Concurrent Object-Oriented Programming. *Journal of Object-Oriented Systems*.

Liwu Li, 2002. Java Data Structures and Programming. *Springer Verlag*. Germany. ISBN: 3-540-63763X.

Müller M. 2008. CUDA Particle-based fluid simulation. *NVIDIA Corporation*.

Roosta, Séller, 1999. Parallel Processing and Parallel Algorithms. *Theory and Computation. Springer*.

Rossainz, M., Capel M., 2008. A Parallel Programming Methodology using Communication Patterns named CPANS or Composition of Parallel Object. *20TH European Modeling & Simulation* Symposium.Campora S. Giovanni. Italy.

Rossainz M., Capel M., 2014. Approach class library of high level parallel compositions to implements communication patterns using structured parallel programming. *26TH European Modeling & Simulation* Symposium. Campora Bordeaux, France.

Wilkinson B., Allen M., 1999. Parallel Programming Techniques and Applications Using Networked Workstations and Parallel Computers. *Prentice-Hall*. USA.

MORE THAN JUST CHOCOLATE: SUPPLY CHAIN MODEL OF PRODUCTION OF COCOA CROPS IN CÔTE D'IVOIRE

Miguel Mujica Mota [(a)], Abdel El Makhloufi[(b)], Nico De Bock[(c),], Paolo Scala[(d)]

[(a),(c),(d)]Aviation Academy, Amsterdam University of Applied Sciences, The Netherlands
[(b)] Research group Smart Mobility & Logistics, Amsterdam University of applied Sciences, The Netherlands

[(a)] m.mujica.mota@hva.nl, [(b)] a.el.makhloufi@hva.nl [(c)] n.de.bock@hva.nl, [(c)] p.m.scala@hva.nl

ABSTRACT

Côte d'Ivoire produces about 42 percent of the world's total Cocoa but processes only a very few amount of the production. A big part of the country depends on the commercial benefits of the Cocoa production and supply chain of it. For that reason, the World Bank asked the simulation group of the Amsterdam U. of Applied Sciences in collaboration with the Port of Amsterdam to develop a simulation model that allows the politicians assess the performance of the supply chain of the Cocoa in that region of the world. The simulation model gave light to the potential of improvement in the supply chain by identifying inefficiencies, bottlenecks and blockers that hinder the efficient transport of Cocoa in the chain with the consequence of low productivity. The most important results are presented in the article together with suggestions for improvement in order to increase the wellbeing of the farmers in that region of Africa.

Keywords: logistics modelling, Ivory Coast, developing countries, transport

1. INTRODUCTION

Côte d'Ivoire produces about 42,4 percent of the world's total Cocoa but processes only 0.51 million tons of Cocoa beans in the country (2015). The main importer of Cocoa from Côte d'Ivoire is the Netherlands. The last years, Côte d'Ivoire has gained a larger market share, both in production of Cocoa beans and grinding, respectively, from 36.7 percent in 2013 to 39.3 percent in 2015, and from 11.3 percent in 2013 to 12.6 percent in 2015 (Port of Amsterdam 2016). Seventy percent of the total Cocoa production in Côte d'Ivoire is obtained from the following production zones: Soubré, San Pedro, Dalao, Divo and Gagnoa.

There are many challenges facing the development of Cocoa sector and performance of the logistics system in Côte d'Ivoire. The organisation of the Cocoa's supply chain suffers from various problems such as limited traceability, poor quality and congested transport roads, increasing waste, lack of storage facilities/warehouses and time-consuming administrative processes. Furthermore, the market of Cocoa sector is highly concentrated in the sense that the bulk of trade and processing of the market of Cocoa is dominated by a limited number of foreign exporters. Because the multinational companies are strong in terms of capital and use of sophisticated technologies, barriers of entry are higher for local firms to enter the export market as economies of scale require large investments and volumes of export, especially in case of shipping Cocoa in liquid or solid forms.

Others main challenges that the Cocoa sector is facing are:

• The Cocoa supply chain in Côte d'Ivoire is dysfunctional and not favourable to the majority of Cocoa farmers that receive frequently low market prices. The supply chain is often too long and characterized by the proliferation of many stakeholders, with most operators not performing any marketing function that adds value to Cocoa beans, while taking a share of the market prices.

• Farmers often do not have access to market information and technology and their understanding of the quality requirements of the market is very limited. This translate into low productivity, low income and decreasing yield.

• A fragmented and inappropriate functioning of the market that results in a trading system in which quality is often compromised.

• The majority of Cocoa farmers sell their Cocoa beans individually to itinerant buyers (not necessarily retailers), which often operate in areas where it is difficult for farmers to transport the Cocoa themselves.

• A widespread practice of mixing good and bad quality Cocoa beans to meet minimum market quality standards.

• Limited access of farmers to productivity-enhancing inputs and resources such as fertilizers, agrochemicals, seedlings, farm tools and credits, which affect the productivity and competitiveness of the Cocoa sector.

Côte d'Ivoire has made significant progress in the development of roads, power and ICT networks during the 1990s. After 1999 this progress slowed down because of a lack of investments, and political turmoil. Spending on infrastructure was less than 5 percent of GDP in the mid-2000s, which is about half of what many neighbouring West African countries have been devoting to infrastructure in this period. Various empirical studies show that improvement of country's infrastructure

endowment, such as energy supply, roads networks, rail infrastructure and terminal capacity of ports and airports could rise growth at a rate of 2%.

Road network (82.000 km) is relatively well developed in Côte d'Ivoire and although of a low density, it provides sufficient connectivity to link the capital cities, secondary towns and international borders. In opposition, rail network is not developed. The country has only one rail link for transporting goods which connects Abidjan with the capital of Burkina Faso (Ouagadougou).

Besides low density and low quality of road network, there are several problems that have direct effect on transport and logistics sector in Côte d'Ivoire such as the increasing transport prices, high operational costs and unpredictable delays to the transport of goods due to the extraction of significant bribes from trucks along the roads by police. As result, transporters tend to overload their trucks to compensate for the costs of the bribes and other additional charges (for example, charge load per axle).

In order to develop and implement a wide logistics (supply) chains and network that capture various dimensions of performance at various levels in a consistent way, there is the need of using adequate and valuable tools (i.e. set of indicators) covering several levels; the strategic level, the tactical and the operational level together with novel techniques and methodologies that allow more transparency in the expected outcomes of policy processes.

Globally, the focus on the Cocoa's logistics chain and network in Côte d'Ivoire may be approached by looking at the following indicators dedicated to evaluate performance and trends in logistics practices:

• Physical state of road infrastructure and transport intensity (tonnes-km/total output).
• Freight volume through load capacity/factor of vehicle by mode (ton/vehicle).
• Distance by transport mode (km).
• Vehicle utilization (vehicle-km/ton-km).
• Freight movements and energy and emissions by supply chain link (energy consumed/vehicle-km).
• Energy consumption/emissions.
• Time (total time for transport and storage and related procedures, average and maximum number of hours/days).
• Cost (total costs of transport and storage and related procedures).
• Variability (total time of document processing hours/days).
• Complexity (total number of documents per trade transaction).
• Financial cost of logistics services and hidden costs (costs of delays and uncertainties). These costs include financial charges, obsolescence, and loss of damaged or stolen goods.

In addition, the domestic Cocoa supply chain is formed by approximately 800.000 farmers, 500 cooperative companies, 5400 traders (5000 pisteurs and 400 traitants), 50 exporters and about 6 local grinders and local processing firms (see Figure 1 below). What characterizes the Cocoa supply chain in Côte d'Ivoire is that farmers sells their crop to three different actors: to domestic processing firms through cooperatives, to traders (pisteurs and traiteurs) or market them through traders to exporters. The domestic processing firms sells processed Cocoa products directly on international market.

Due to the complex nature of the supply chain of Cocoa, the only approach that enabled to assess all the important aspects and the variability of the chain was Simulation. In the current work, we present a simulation model of the supply chain of Cocoa in Cote D'Ivoire which can be also used as a decision-support tool. The model represents the different relationships already mentioned, so that it enables the decision-makers with a wide-angle view for policy making.
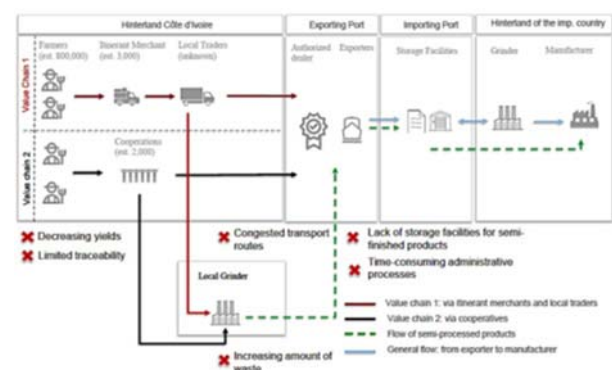
Figure 1: Conceptual Model of Supply Chain

2. STATE OF THE ART

Modelling and simulation is a technique that has been widely used for supply chain management (SCM), as it is mentioned in Longo (2011), it is "a powerful tool for analysis, investigation, examination, observation and evaluation of real-world industrial and logistics systems". In the work of Ingalls (1998), the author makes a review of the simulation technique applied to SCM where he outlines the advantages of using simulation. In his work he points out that simulation fits best for tactical planning, usually where the time horizon is long, and for supply chains affected by variance. Supply chain is usually modelled as a multi-agent and in a dynamic fashion (Swaminathan et al. 1998; Kahiara 2003) in order to be able to consider all the interactions between the different actors of the supply chain. Simulation models for SCM are usually based on agent-based simulation (ABS) and discrete-event simulation (DES), and even a combination of the two as it is proposed by Lee et al. (2002). Regarding ABS models we can find many of them in the literature, considering different policies and objectives. In the work of Gjerdrum et al. (2001) an ABS model was presented with the objective of simulating different demand-driven supply chains. They included an optimization model for the manufacturing component, with the objective of reducing operative costs and keeping a high level of customer order fulfilment. Albino et al. (2007), modelled a supply chain by focusing on

cooperation between supply chain actors in industrial district. The concept of industrial district consists of an area where many small and medium enterprises (SMEs) are located and work together in the supply chain; this concept has been also translated in the model proposed in this work by clustering the production sites. In other works we can find supply chain modelled using ABS focusing on different strategies such as: analysis of alternative production-sales policies (Amini et al. 2012) and different combined contract competition (Meng et al. 2017). DES models have been also widely exploited in the SCM, as it can be found in Longo and Mirabelli (2008), where they proposed a decision-making tool for different supply chain scenarios. Their scenarios were based on multiple performance measures and user-defined set of data input parameters. In the work of Mensah et al. (2017) another DES model was developed for a resilient supply chain with the aid of ICT implementation. The model follows a six sigma approach to improve the overall supply chain resiliency against disruption.

In the present work, a DES model has been implemented to describe and analyse the supply chain of Cocoa products from producers, distribution centre and final centre of collection and shipment. Because of the nature of the network and operations modelled and also the tactical nature of the analysis, DES was considered as a best approach by the authors. DES allowed us to make a scenario-based analysis based on different policies, and it enabled us to measure the performance of the supply chain based on different aspects (productivity, economic, and environment).

3. METHODOLOGICAL APPROACH

In this work, we simulated the different links of the supply chain, the main boundary is the Port of San Pedro where the exporting function is performed. The model was based on the supply chain mapping made by the Port of Amsterdam (Port of Amsterdam 2017). Figure 1 presents the description of the supply chain relationships that will be considered for the developed model.

The farmers produce the Cocoa beans which in turn are transported by a merchant or the production is concentrated by a cooperative of producers (Farmers) in warehouses. In the next link, the product is transported as raw material directly to the Port and some percentage is transported to the Grinders (30% of the production). In the grinder or refinery, the raw Cocoa is transformed into Cocoa butter and then transported as a higher-value product to the Port of San Pedro. The next link in the supply chain is the transport of either the raw material (beans) or the refined product (butter or oil) by sea to the destination Port, in our study the destination Port in Europe corresponds to the Port of Amsterdam. However, as mentioned before, the transport to the Port of Amsterdam will be out of the scope of the developed model.

3.1. Conceptual Modelling

The first modelling phase corresponds to the conceptual development in which the relationships between the main elements are identified based on public information and the discussion with subject-matter experts. The following table presents the elements that are included in the simulation model.

Table 1: Main elements of the conceptual model

Element	Description
Production quantities	The quantities of Cocoa beans produced in the specific region under study
Transport routes	The routes of transport that are used by the different transports
Grinder Facilities	Cocoa that is transported in the grinder facilities as well as the added value to the product for evaluating the impact of decisions
Transport trucks	The trucks that transport the products for being export at the Port. The speeds and capacities will be considered as well
Warehouses	The warehouses dwell time will be considered
Checkpoints along the transport routes.	These points will be considered since they hinder the smooth flow of trucks towards the Port.
State of roads and pavement	The quality of the road will be considered, since it has a direct impact in the transport time from the different locations in the region to the Port
Market value of the products	The market value of the modelled products will be considered
Emissions	In the model the green-house pollutants are considered, mainly CO_2 and NO_2

3.2. Production modelling

Some functionality is key for the correctness of the developed mode. Production is one of them, as it is appreciated in Figure 2, the production varies with the region of the country. Due to the objectives pursued, the production at an atomic level was not considered, instead, a high-level model was developed. The complexity of the production network was coped by developing clusters within the region under study (San Pedro Region), taking into consideration the production zones and the political boundaries.

The production of Cocoa in the model is generated in batches of 6 tons within the cluster and located randomly within the cluster. The model developed has stochastic, dynamic and flexible characteristics; the amount of entities is generated in such a way that they match the amount of production of the region within a year.
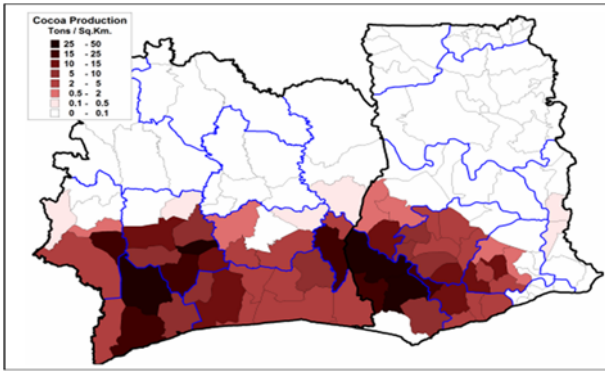
Figure 2: Production of Cocoa in Cote D'Ivoire

The production is modelled assuming a Poisson process where the main probability distribution is an exponential one with the average inter-arrival time of 3.33 minutes (1).

$$f(x) = \begin{cases} \dfrac{1}{\beta} e^{\frac{-x}{\beta}} & x \geq 0 \\ 0 & x < 0 \end{cases} \quad (1)$$

Assuming this inter-arrival time, the average production of a year will be 946 000 tons. It is important to mention that this production is stochastic meaning that every time the model is run, the production might vary, due to the interlinks and causal relationships present in the supply chain model. However, the average mean will be around 946 000 tons/yr.

3.3. Road Network Infrastructure
According with Openstreets (OpenStreets.org 2017), the road infrastructure of Côte d'Ivoire consists of 5 classifications of roads, however, for reducing the complexity, the model accounts with three types of roads:

- Primary Road (Paved). These roads are paved roads, with good maintenance, the achievable speeds of the trucks could get up to 100-120 km/hr. However, the maintenance of these roads is very scarce, thus, the roads are filled with potholes and stones making the vehicles reduce their speed and sometimes break their tires, decreasing drastically the average speed in the road. For the paved motorways we specified a stochastic speed following a Triangular distribution of T(40,50,60) km/hr.
- Secondary Road(s). The secondary roads are roads that are unpaved. In these roads, the average expected speed is also very uncertain. In this roads we assumed a stochastic speed following a triangular distribution of T (20,30,40) km/hr.
- Tertiary Road(s). These roads are also unpaved, and these types of roads are the ones used by the primary producers (individual and local

families), in these roads, the farmers can use small vehicles or even bicycles for the transport of Cocoa beans. For the modelling of these tertiary roads, we specified also a stochastic speed of T (10, 15, 20) km/hr.

The road infrastructure is modelled as a set of nodes and edges with two directions at a certain scale in which the edges correspond to the direction, sense and length of the actual roads. The links (edges of the network) in turn are placed over a GIS map from OpenStreet.org, then the entities modelling the production and the trucks transporting the product are placed over the GIS layer. Thus, two layers are used, one which is a GIS layer of the region under study and the second layer which is composed by the entities, nodes, edges and other objects like servers that model the performance of the production once it enters to a warehouse, location or to the Port (simulation layer). Figure 3 illustrates the layers used for constructing the scaled model of the regions of San Pedro.
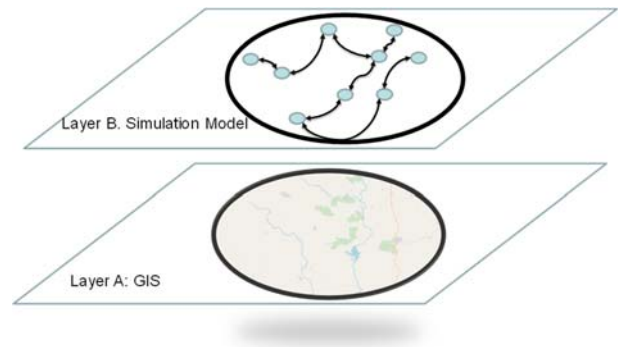
Figure 3: The GIS from OpenStreet.org for Côte d'Ivoire

The simulation layer has been developed using a discrete-event systems approach, using a commercial simulator called SIMIO (SIMIO 2018).We took the advantages of the functionalities of the simulator for making a more detailed model of the supply chain.

3.4. Grinders, warehouses and Ports
These elements are represented by functional nodes that are connected via the edges that model the roads, in addition, these nodes will have some functionalities. These functionalities, model characteristics such as capacity, delays of all the internal processes that the product undergo when they get to the node (e.g. grinding, loading, unloading, packing, unpacking, sorting, etc.). Figure 4 illustrates the network approach model of the supply chain under study.
The links or segments are geographically aligned with the GIS layer so that they have the right proportion and length that the vehicles need to traverse in order to go from one location to the other. Some of the nodes also have functionalities that are used to model operations performed in the locations of the GIS Map such as check

points, warehouses, grinding operations or check points along the road.
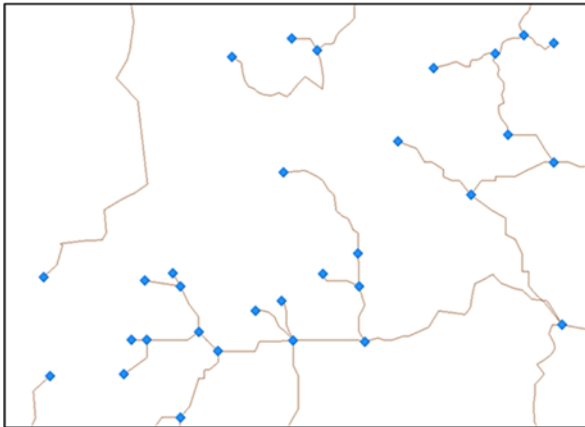
Figure 4: model of the road network

The warehouses and location nodes will have as main functions, the storage, transformation and transhipment of the product in the network layer. The processes related to those activities, consist of loading, unloading, processing, and storing. Table 2 illustrates the characteristics of these elements in the system.

Table 2: Characteristics of the Warehouses, Port and Grinders

Facility	Processing Time	Capacity
Warehouse	Triangular(5,6,7) days	Unlimited
Grinder	Uniform (12, 24) hrs.	Unlimited
Port	NULL	Unlimited

3.5. Vehicles
The production and transport of Cocoa is modelled using different entities, mainly two entities. One entity will represent the amount of 6 tons of Cocoa; the other vehicle will model the heavy trucks or trailers whose capacity is maximum of 60 tons. The entities will have other characteristics besides the capacity, such as speed, CO_2, NO_2 emissions and they will move through the edges of the network layer. Table 3 illustrates the characteristics of the different vehicles used in the model.

Table 3: Vehicle characteristics

Vehicle	Capacity	Speeds
Small Truck	6 ton (Fixed)	60 km/hr *
Trailer	[0..60] tons	Triangular (30, 45, 60) km/hr *

* Maximum speed, the model will be restricted by the roads limitations

The different types of vehicles are parameterized with the characteristics of the entities they represent. These parameters, will be used as variables that can be modified during the experimental design in order to compare the impact of different policies in the system.

In the warehouses, the entities are batched up to 60 ton (10 entities) and transported by another entity with similar characteristics but with a different representation. Figure 5 presents the entities used for modelling the transport and production of Cocoa with their characteristics.
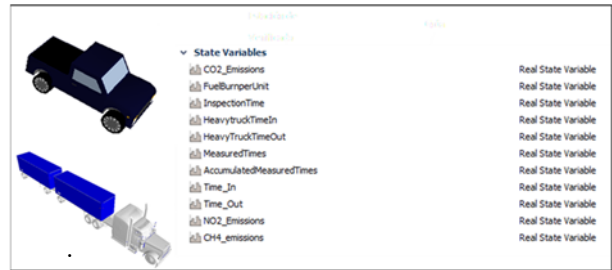
Figure 5: Vehicle characteristics

Inter-arrival time per Region
The amount of production per region was estimated based on the yearly production rate. In the case of San Pedro region, the production per year is approximately 946,000 tons/yr. In order to generate a stochastic approach for this production, it was assumed that the production follows a Poisson process where the production is modelled by an exponential distribution with an inter-arrival time with the correspondent mean. The matching value for the region under study is 3.33 min between entities for batches of 6 tons. The model assumes that during the year the number of tons is produced relatively evenly.

3.6. Check Point Implementations
The checkpoints at the roads are important elements to be considered in the model. Based on public information (World Bank, 2008), check points in the region of San Pedro have been located in the model, with a correspondent processing time and probability of being checked. The following figure illustrates the details of the check points in the road network.
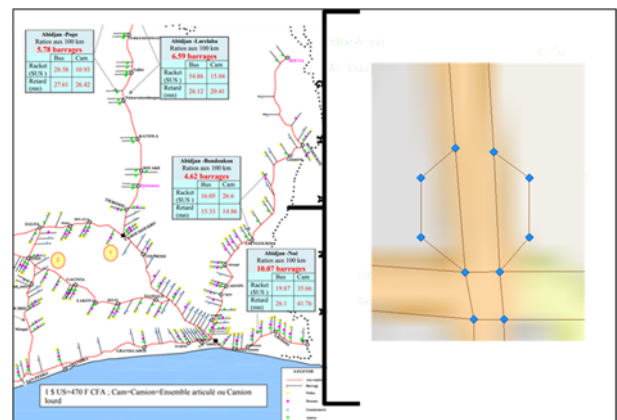
Figure 6: Check Point Implementation

For the implementation of the checkpoints, the network has a detour based on a probability for the vehicles to be checked. The checkpoint is composed by three segments

with functionality where the trucks are deviated from their original route to the Port. They have a specific probability of being checked, initially is 10%. In the experiments, the variation of this probability is used to evaluate the impact of the checkpoints in the lead time of the products. In this way, it also enables the decision makers to evaluate policies that reduce the hassle or inefficiencies that the checkpoints add to the supply chain. The following table presents the characteristics of the checkpoints in the supply chain model.

Table 4: check point characteristics

Element	Processing Time	Capacity	Initial Probability of Inspection
Checkpoint enter segment	Heavy Truck: Triangular (1,2,3) hrs.		
	Regular Truck : Triangular (5,10,15) mins	5 Entities	0.1
Checkpoint parking segment	NULL	Unlimited	n/a

3.7. Emissions

In the simulation model, the CO2, NO2 and CH4 emissions were considered. A lineal equation was used according to EPA factors and following the approach of different authors (Kenney et al. 2014). The emissions are dependent on the type, age and distance travelled by the vehicles. The formulas used for estimating the emissions of the trucks are the following ones:

$$E\_tot = (RL \times NV \times EF) \tag{2}$$

Where
E_tot : Total Gas Emissions
RL: route length
NV: Kilometres traversed
EF: Emission factor

Regarding the characteristics of the vehicles, Table 5 presents the values used for the vehicles in the model (EPA 2018).

Table 5: Vehicle emission characteristics

Type of Vehicle	Year Assumed	Emission Factor CO2	Emission Factor NO2	Emission Factor CH4
Regular Truck (Gasoline)	1973 – 1974	1.67 [kg/km]	0.31 [gr/km]	0.28 [gr/Km]
Heavy Truck (Gasoline)	1981	1.67 [kg/km]	0.31 [gr/km]	0.28 [gr/Km]

4. EXPERIMENTAL DESIGN

This section presents the scenarios that have been evaluated using the supply chain model. The evaluation started with a base-case scenario which simulates the status quo of the system under study. Then with the use of the other scenario, the impact of different policies are compared. The following table illustrates the different scenarios that can be possibly analysed by modifying the factors and levels. As it can be inferred, a full factorial design was not feasible since the number of combinations would be 216 scenarios, however, based on the authors experience, we selected the scenarios that were considered most relevant for illustrating the capabilities of the tool and that allowed to identify potential areas of improvement of the whole system to bring more productivity to the region.

Table 6: Design of Experiments for the Supply Chain Model

FACTOR	LEVELS		
Speed secondary road	Low speed	Medium speed	High speed
Speed tertiary road	Low speed	Medium speed	High speed
Probability of checkpoint	10%	5 %	0%
Check point times regular trucks	Long waiting times	Short waiting times	
Check Point times heavy trucks	Long waiting times	Short waiting times	
Grinder Percentage	30 %	50%	

Regarding the Performance indicators (PI) considered, the ones used for the study are the following:

- Cocoa Productivity (Ton/day): This PI measures the amount of Cocoa that is transported to the Port of San Pedro every day. By using this PI, we evaluate the impact of different infrastructure policies. The expectation is that if one policy has good impact in the system, the amount of Tons in the Port will increase, while if it has a negative effect, the amount in the Port will be reduced.

- Cocoa Butter Productivity (ton-day): This PI is similar to the one from Cocoa, and follows the same reasoning. The difference is that butter is a more valuable product, and with the simulation model it is possible to investigate when is more economically attractive to invest in the butter than just transporting the beans.
- Cocoa Market Value (USD/Day): With this indicator, we are able to evaluate and simulate the value of the produced Cocoa in the market. The value will be correlated with the productivity of Cocoa. For the simulation model it was assumed a constant value of 3.2 USD/KG.
- Butter Market Value (USD/Day): with this indicator, we are able to compare the value of butter versus the value of Cocoa and how the policies and decisions impact this indicator. For the simulation model the value was considered constant with a value of 7.78 USD/KG
- CO_2 emissions (Kg/day): This indicator is directly correlated with the distance travelled, age and type of trucks used to transport the Cocoa and the butter in the model. By using this indicator, it will be possible to measure the impact of some policies in the emissions of this pollutant.
- NO_2 emissions (kg/day): This pollutant is also measured in the model. The reasoning is the same as the CO_2.

The following section presents the description of the different scenarios evaluated and the explanation of why they were chosen.

4.1. Scenario I. Base Case Scenario

Every simulated scenario had 30 replications for a period of 14 weeks (3 months) in order to evaluate the performance of the considered PIs. The following table presents the main parameters and Table 8 the results obtained.

Table 7: Parameters of the base-case scenario

Parameter	Value
Speed Primary Road	Triangular(40,50,60) km/hr
Speed Secondary Road	Triangular(20,30,40) km/hr
Speed Tertiary Road	Triangular(10,15,20) km/hr
Checkpoint probability	0.1
Checkpoint times regular truck	Triangular(1 , 2 , 3) hrs
Checkpoint times heavy truck	Triangular(5 , 10 , 15) mins
Percentage of Grinding	30%

The following results are the average values out of all the 30 replications measured every day. The results mean that, for instance, the average productivity values

represent the measurement of 84 days (3 months) times 30 (number of replications) therefore it is an average of 2520 measurements of the productivity.

Table 8: Simulated Results for Base Case Scenario

Parameter	Average Value	Standard Distribution
Value Beans Production (USD/day)	2,278,031	171,884
Value Butter Production (USD/day)	826,915	84,008
Productivity Beans (Ton/day)	989	474
Productivity Butter (Ton/day)	146	69
Total CO2 Emission [KG](3 months)	802	9.8
Total NO2 Emission [KG] (3 months)	14	0.18

It was considered only intensive measures (measurement/day) in order to make the results not time-dependent. The only absolute values were the emissions which measure the total emissions after the 84 days for the 30 replications. Thus, the results can also be interpreted as intervals, for example in the case of the expected market value of the Beans: assuming a normal distribution one can expect that every day, in approximately 95% of the time, the market value productivity would be within and interval of [1 934 263, 2 621 799] USD/day, using a 2 standard deviation interval.

4.2. Scenario II. Impact of reducing the checkpoints on the roads

This scenario evaluates the impact of reducing the check points along the road. As it has been mentioned, the checkpoints produce inefficiencies in the supply chain, since it increases the lead time of the Cocoa. However, it is not known exactly how much is the impact in the potential of productivity of the system. The following results help to give light on this matter and on what impact would it have in the system if the government reduces the checkpoint frequency. This situation was modelled by reducing the checkpoint probability on 50% (from 10% to 5%). The other parameters of the model were left the same as the base-case scenario.

The results of the simulation are presented in the following table. In this scenario, the other parameters than checkpoint probability were left intact.

Table 9: Results of Scenario II

Parameter	Average Value	Standard Distribution
Value Beans Production (USD/day)	2,355,652	43,117
Value Butter Production (USD/day)	871,415	25,969
Productivity Beans (Ton/day)	1,289	231
Productivity Butter (Ton/day)	190	34
Total CO2 Emission [KG](3 months)	1057	13
Total NO2 Emission [KG] (3 months)	19.64	0.25

In comparison with the base case, the productivity of transported beans and butter increases around 30%, the value increases approximately 3% and 5% for Beans and Butter respectively. On the other hand, the pollution is increased with the increase of transport activity.

4.3. Scenario III. Impact of Improvement in Road infrastructure

This scenario evaluates the impact that the improvement in maintenance of the secondary and tertiary road might have. As it has been mentioned and illustrated, the road infrastructure is in a very bad shape in the country. This situation impacts directly the supply chain efficiency. This policy has been modelled by matching the speeds of the secondary and tertiary roads to the speed of the primary roads; Triangular(40,50,60) km/hr. Table 10 presents the results of this policies.

Table 10: Results of Scenario III

Parameter	Average Value	Standard Distribution
Value Beans Production (USD/day)	2,302,323	159,967
Value Butter Production (USD/day)	848,185	66,620
Productivity Beans (Ton/day)	1,083	424
Productivity Butter (Ton/day)	159	62
Total CO2 Emission [KG](3 months)	873	10
Total NO2 Emission [KG] (3 months)	16.21	0.20

It can be appreciated that the productivity of Beans and Butter is increased with 9.5% and 9% respectively, while the increase in value is only 1%. It is noticeable as well, that in this case the investment in secondary and tertiary roads does not have a big impact as with the previous scenario.

4.4. Scenario IV. Impact of Improvement in road infrastructure and check points

This scenario evaluates the impact of the combined effect of improving the road infrastructure and reducing the checkpoints at the same time. By having a combined policy of maintenance and more efficient flow of goods the expected impact is important as the following results illustrate.

Table11: Results of Scenario IV

Parameter	Average Value	Standard Distribution
Value Beans Production (USD/day)	2,353,241	54,509
Value Butter Production (USD/day)	869,877	21,440
Productivity Beans (Ton/day)	1,262	251
Productivity Butter (Ton/day)	186	36
Total CO2 Emission [KG](3 months)	1,036	13
Total NO2 Emission [KG] (3 months)	19.25	0.25

As it was expected, with this scenario, the values increased as well. However, it is noticeable that on the contrary as to what was expected, the combination of reducing the checkpoint values and investing in improving the secondary and tertiary roads does not produce a higher value than the one from only reducing the checkpoint probability. The standard distributions are also similar, thus, it is an interesting result that needs to be further investigated.

4.5. Scenario V. Impact of investment in producing more butter than Cocoa

The Cocoa butter has more value in the market than the Cocoa beans. For that reason, this scenario investigates what the impact would be if the butter percentage is increased by diverting more production to the grinders. For this scenario the percentage of beans that go to grinder is 50%, the other parameters are left the same as with the base-case scenario. This scenario also assumes that the grinders have enough capacity to process the beans and that 20% of the mass of the beans is transformed into butter. The characteristics and results are presented in the following tables.

The results show that since half of the beans now are converted to butter, the productivity of butter is increased. It is noticeable that beans productivity also increase a bit in comparison with the base case scenario. This is another interesting result that requires further investigation. The most remarkable result is that despite the butter value production is increased, the combined average productivity value (beans and butter) is decreased in comparison with the base case. This might be due to the market value of both products and also because in the simulation model other side products such as Cocoa oil or secondary products were not considered.

Table 12: Results of Scenario V

Parameter	Average Value	Standard Distribution
Value Beans Production (USD/day)	2,053,387	67,685
Value Butter Production (USD/day)	1,002,133	32,503
Productivity Beans (Ton/day)	1,021	290
Productivity Butter (Ton/day)	199	57
Total CO_2 Emission [KG](3 months)	956	11
Total NO_2 Emission [KG] (3 months)	17.75	0.21

4.6. Scenario VI. Impact of Investment in road infrastructure and Butter production

This scenario explores the situation of investing in improving the road infrastructure and increasing the butter production at the same time. This is simulated by modifying the speeds of the secondary and tertiary roads and increasing to 50% the percentage of beans that go to the grinders. This scenario again provides better results than the base-case scenario, but as the results show, it is not the best configuration for improving the PIs of the system.

Table 13: Results of Scenario VI

Parameter	Average Value	Standard Distribution
Value Beans Production (USD/day)	2,048,255	47562
Value Butter Production (USD/day)	999873	34182
Productivity Beans (Ton/day)	959	317
Productivity Butter (Ton/day)	189	62
Total CO_2 Emission [KG](3 months)	903	10
Total NO_2 Emission [KG] (3 months)	16.76	0.20

This final scenario illustrates that the change to producing more butter increases the productivity of butter but reduces the one of the beans, and the total sum of the average values of the combined production is less than the value for the base-case scenario. Furthermore, it illustrates that even though the productivity of butter is increased, the sum of the final market values do not, which means that for the improvement of the wellbeing of the population, probably the first policy impacts more than this one.

5. CONCLUSIONS

The current paper presents a novel approach of the analysis of the supply chain of the Cocoa in Côte d'Ivoire . The model presents an approach for modelling and simulating the evolution of production of the current system taking into consideration public information. The developed model considers the most important stakeholders of the system and it enables the evaluation of different policies for the current system. Several scenarios from the total combination are proposed in which different policies are analysed. They explore different policies like improving the road infrastructure, increasing the amount of production of butter or reducing the check in points in the road network. These policies are evaluated using different performance indicators. The following table summarizes the main findings of the study.

Table 14: Summary of results

Scenario	Comparison with current situation
Sc. II: Reducing check points on the roads	•Productivity increased by 30% •Value increased 3% and 5% of beans and Butter
Sc. III: Investing in improving secondary and tertiary roads	•Productivity increased by 9% •Value increased 1%
Sc. IV: Impact of Improvement in road infrastructure and checkpoints	•Productivity increased by 27% •Value increased by 3%
Sc. V: Increasing butter production	•Increase in productivity Beans by 3.2% and Butter by 36% •Value of Beans reduced by 10%, value of butter increase by 21%
Sc. VI: Investment in road infrastructure and butter production	•Reduction of productivity beans by 3%, increase by productivity in butter 29% •Value of Beans increased by 11%, value of butter increased by 21%
Pollution in all the cases increased, and the smallest contribution was achieved in scenario III followed by scenario VI	

Some results from the study were expected and other were counter-intuitive, for instance, the results suggest that by only decreasing the frequency of checkpoints by 50%, the productivity is increased by 30% and the monetary value at the Port by 5% in the case of the beans. This increase in value is translated into approximately 200,000 USD more per day of operation. The results also suggest that by investing in the least developed road infrastructure like secondary and tertiary roads will not have a big impact. This might be because there might be a bottleneck in the warehouses. On the other hand, by making the last link of the chain more efficient, which in this case is the transport to the Port, will have a big

impact. Another interesting result is that from the environmental point of view, the results suggest that the investment in secondary and tertiary roads will reduce the pollution, however, the increase in market value will not be high. This might be due to the amount of trucks that are required to take the product from the farms to the warehouses, which will be reduced once the investment takes place. Last but not least, with the current market values of butter and Cocoa, the investment in butter apparently does not increase the total value of the supply chain. However, in the model it was assumed that only 20% of the beans mass is transformed into butter taking out other products that might make the transformation to butter and other products more economically attractive. This should be further investigated.

As it can be perceived, the simulation model of the supply chain of Cocoa is a valuable tool that allows decision makers and analysts having more insight into the operation of the supply chain. The tool is flexible enough to incorporate new elements in addition to the variability of the system which plays a key role in the performance of it. With the inclusion of the variability factor in the different operations and links of the supply chain, it is possible to evaluate and reduce the risk of wrong, small-value or even dangerous decisions that might put at stake the wellbeing of the population that depends on the production of Cocoa. Moreover, the developed model of supply chain of Cocoa can be easily translated into the evaluation of another type of agro-logistic product. This approach can be used as a tool that allows to have more informed decisions with the consequence of reducing the risk of making wrong decisions on the management of public or private money.

ACKNOWLEDGMENT

REFERENCES

Albino, V., Carbonara, N., Giannoccaro, I., 2007. Supply chain cooperation in industrial districts: A simulation analysis. European Journal or Operational Research, 177 (2007), pp. 261-280.

Amini, M., Wakolbinger, T., Racer, M., Nejad, M. G., 2011. European Journal of Operational Research, 216 (2), pp.301-311.

Banks, J., Carson, J.S., Nelson, B., Nicol, D.M., 2010. Discrete-even System Simulation, fifth ed. Pearson.

Bogetic, Z., Espina, C, and Noer, J., 2007. Cote d'Ivoire: Competitiveness, Cocoa, and The Real Exchange Rate. Policy Research Working paper Nr. 4416 (WPS4416). The World Bank, November 2007. Washington DC.

Essoh, N.P.S., 2014. Cote d'Ivoire's Commodities Export and Shipping: Challenges for Port Traffic and Regional Market Size. American Journal of Industrial and Business Management, 4, 234-245. http://dx.doi.org/10.4236/ajibm.2014.45031

Gjerdrum, J., Shah, N., Papageorgiou, L. G., 2001. A combined optimization and agent-based approach to supply chain modelling and performance assessment. Production Planing & control, 12 (1), pp. 81-88.

Ingalls, R.,G., 1998. The value of simulation in modelling supply chains. Proceedings of the 1998 Winter Simulation Conference, pp. 1371-1375. December 13-16, Washington (DC, USA).

Kaihara, T., 2003. Multi-agent based supply chain modelling with dynamic environment. Int J. Production Economics 85 (2003), pp. 263-269.

Laven, A., Buunk, E and Ammerlaan, T., 2016. Market Concentration and Price Formation in the Global Cocoa Value Chain. SEO-report nr. 2016-79A. SEO Amsterdam Economics, Amsterdam.

Law A., Kelton W., 1991. Simulation Modelling and Analysis, McGraw-Hill, 2nd Ed.

Lee, Y. H., Cho, M. K., Kim, S. J., Kim, Y. B., 2002. Supply chain simulation with discrete-continuous combined modelling. Computers & Industrial Engineering, 43 (20002), pp. 375-392.

Longo, F., Mirabelli, G., 2008. An advanced supply chain management tool based on modelling and simulation. Computers & Industrial Engineering, 54 (2008), pp. 570-588.

Longo, F., (2011). Advances of modelling and simulation in supply chain and industry. Simulation: Transactions of the Society for Modeling and Simulation International, 87(8), 561-656. 10.1177/0037549711418033

Meng, Q., Li, Z., Liu, H., Chen, J., 2017. Agent-based simulation of competitive performance for supply chains based on combined contracts. International Journal of Production Economics, 193 (2017), pp. 663-676.

Mensah, P., Merkuryev, Y., Longo, F., 2015. Using ICT in developing a resilient supply chain strategy. Procedia Computer Science, 43 (2015), pp.101-108.

OpenStreets.org 2017 <www.openstreetmap.org>

Port of Amsterdam, 2017. Business Opportunities in d'Ivoire: Analysis of the Cocoa Sector. PoA International, Amsterdam.

SIMIO, 2018. Available from: https://www.simio.com/index.php [accessed 18 April 2018]

Swaminathan, J. M., Smith, S. F., Sadeh, N. M., 1998. Modeling supply chain dynamics: A multiagent approach. Decision Sciences, 29 (3) 607-632.

Weisfeld, M., 2009. The Object-Oriented Thought Process, 3rd ed., USA: Pearson Education.

World Bank, 2008. Etude du Racket sur les Routes en Cote D'ivoire, Technical report, May, 2018.

E-HEALTH BUBBLE: AN E-HEALTH SYSTEM FOR CAREGIVING SERVICES DEDICATED TO ELDERLY

M. Frascio[(a)], F. Mandolfino[(b)], M. Sguanci[(c)], F. Borasi[(d)], L. Bordignon[(e)] , G. Molinari[(f)]

[(a),(b),(c)]DiSC University of Genoa – School of Medicine
[(d),(e)]Technology For Edge Applications srl Genova
[(f)]Telemedico srl Telecardiology Center, Genova

[(a)] mfrascio@unige.it, [(b)] fcmandolfino@gmail.com, [(c)] marcosguanci@yahoo.it
[(d)]franco.borasi@gmail.com, [(e)]leo.bordignon@gmail.com, [(f)]C1339@unige.it

ABSTRACT

eHealth Bubble is an eHealth information and communication technology system whose aim is completing the tele health and tele caregiving services dedicated to elderly or affected by chronic disease patients.

eHealth Bubble integrates but does not substitute the existing telemedicine solutions: it makes available plug&play interfaces and easy connection systems, safe and solid to integrate and interface with more common and used medical tools; trough a complex sensors network, will permit to create a virtual space (eHealth bubble) around the patient able to control minute by minute every medical tool, drug and to follow him in all his clinically relevant activities without any kind of medical assistance.

The system has been thought both in a residential and in a mobile version.

Residential eHealth bubble (HB_R): to assist motionless or quite motionless patients

Mobile eHealth bubble (HB_M): to control autonomous patients

eHealth components are:

- Base station: a telematics station to connect eHealth bubble and the medical and paramedical units
- Sensors web: a sensors network wireless connected with the base station that define the virtual space landmarks
- Virtual space: is constantly related to the base station and integral with the patient

The project has been articulated in three phases:

1. High level pianification of functional peculiarities and selection of the technologies and informatics solutions more adequate to reach the telemedicine service goals (sensors, software applications and telecommunication networks)
2. Testing, engeenering and economics
3. Involving and cooperating with health experts.

It has been proposed in a service way for telemedicine companies.

Keywords: telemedicine, tele caregiving, medical sensors.

1. INTRODUCTION

The document describes the technological features of the eHealth Bubble technology system, whose goal is to make ICT technologies and platforms available to enable services to be developed innovations in telemedicine to improve the activities of staff in charge of care (in special way the family caregiver), to promote patient care and to improve its participation to social life, also by virtue of a better level of non-invasive control by the staff doctors (Fisk 1998, Ethical Frameworks for Telecare Technologies for older people at home 2011).

eHealth Bubble aims to promote the development of more integrated and integrated services effective for the patient, using telemedicine (May 2003) technologies, systems, products and services already available.(Stabilini 2013, Fornaro 2009, Fornaro 2008).

eHealth Bubble integrates and does not replace the telemedicine solutions already adopted by users: it makes available plug & play interfaces and simple, reliable and robust connection modes for medical instruments; through these connections a virtual space is created in which the patient is monitored and followed in all its clinically significant behavior (Health Expect 2015).

2. PROJECT ILLUSTRATION

The project of which eHealth Bubble is the cornerstone is these primary objectives:

• make available an eHealth solution for telemedicine services which, installed and configured at the patient's residence, can operate without the help of personnel doctor or paramedic present on site (Mort 2005).

• through a dedicated sensor network create a virtual space in which the medical instruments, medicines and people who assist the patient can be

hired at the eHealth Bubble entrance and then released during eHealth exit Bubble.

The eHealth Bubble platform will be in residential and mobile version:

- Residential eHealth Bubble (HB_R): for assistance to bed-ridden patients or generally little furniture and passing from bed to an armchair, however always inside one same environment or home (Bailey 2009, Sánchez Criado 2012).

- Mobile eHealth Bubble (HB_M): supplied to patients who live an active life without particular mobility constraints they need to be constantly monitored.

The project is divided into three macro phases:

1. High level design of the functional characteristics of the solution; contextual selection of information technologies and solutions (sensors, software applications and networks of telecommunication) considered consistent with the objectives of the telemedicine service.

2. Testing, engineering and economics:

a. evaluation of the cost of the engineered solution and identification of the price of the service, through the involvement of industry experts. Starting the business plan.

b. prototype testing through the selection of a set of medical instruments to be connected in plug & play mode (Willems 2010); verification of the adequacy of the health bubble solution by health operators and pilot users (Eccles A. 2010).

3. Involvement of operators in the sector for collaboration agreements.

The activities of the first and second phases aim to reach a version:

- technologically stable

- functionally adequate (not necessarily complete), at least for the part of the service plug & play

- tested with a significant user number

able to be proposed to the market (private companies, local administrations) and condidable to be patented.

3. DESCRIPTION OF THE ROLES AND SKILLS OF TEAM MEMBERS

The roles relevant to the development of eHealth Bubble are: the identification of a model of sustainable business, also evaluating the product / service alternative (while privileging the latter); the design and industrialization of the solution from a functional and technological point of view; there evaluation of the functional set on which to conduct the experimentation phase, in consideration of the primary target of patients to be served.

1. Business development

- Objective: to identify the most appropriate business model for the market introduction of eHealth Bubble telemedicine services; develop business relationship with operators in the sector telemedicine services;

engage public and private operators for the trial trials of the solution;

- Skills: account & key account management; business plan development; partnership development and definition of commercial and industrial agreements;

2. Realization of the solution

- Objective: to determine the functional set of eHealth Bubble; select technologies and sensors useful for the development of the solution; design and implement the software platform and services of telecommunication.

- Skills: design of technological systems composed of hardware, firmware and software. Capacity to identify and select technologies that are not directly related to the telemedicine sector.

3. Operational validation

- Objective: to support the solution development team in determining the functional set minimum and operational characteristics of the service offered; evaluate the consistency of eHealth Bubble with other telemedicine activities; identify the nucleus of experimenting patients

- Skills: since this is a very specific field of experimentation, linked to skills, rigorous and consolidated experiences and regulations, professionals in the sector are involved in the project health care that for some time also operate in telemedicine.

The skills are listed below:

• Physician surgeon specializing in cardiology, conducts scientific management of the cardiology telemedicine service for an important operator in the field of the telemedicine. He conducts specialist outpatient activities at the cardiology department for carrying out investigations of Cardiac Magnetic Resonance and Cardio-CT.

• Surgeon with assistance, teaching and research activities. He deals with physiology, pathophysiology, diagnosis and surgical treatment of diseases of the digestive system; he is an expert simulation in laparoscopic surgery; has conducted studies in clinical pharmacology. He takes care of teledidactic, telemedicine and medical informatics.

• Physician with specialization in Digestive System Surgery and Digestive Endoscopy Surgical. He worked as research fellow at the University of Genoa, School Engineering Polytechnic. He worked c / o the Department of Bioengineering, Robotics and Systems Engineering of the Genoese University

4. Service testing

In testing, an important partner will be involved, a national leader for telemedicine services: Telemedico has provided over 350,000 services and

teleconsultations over time, identifying numerous at-risk situations with over 15,000 acute coronary syndromes.

Since 2013 it has expanded its own services also evaluation of cardiac holter, holter pressers and cardio looper, to put a complete portfolio of professionals, health professionals and all citizens of products and solutions for the provision of cardiovascular disease prevention and treatment.

Description of the product / service and the needs to be met

I. The Components of eHealth Bubble

1. base station: a telematic station that allows the connection between the eHealth Bubble and the medical and paramedical operating units

2. sensors web: a network of sensors connected wirelessly with the base station and that defines the virtual space on the borders of which to carry out the operations of engagement and release of what goes through the (virtual) wall of eHealth Bubble.

In the HB_R version, the web sensor consists of a set of sensors positioned on rods rest on the floor; in the case of HB_M, the web sensor consists of a sensor network drowned in the fabric of a garment worn by the patient.

3. virtual space: conceptually similar to a microcella of a telecommunication network mobile. Inside is the patient. Virtual space is always connected to the base station and integral with the patient.

The architecture of the BdS

The following figure shows the structure of the HB_R version; is the solution for assistance to patients bedridden or generally not very mobile and passing from bed to an armchair, however always within the same environment or home:
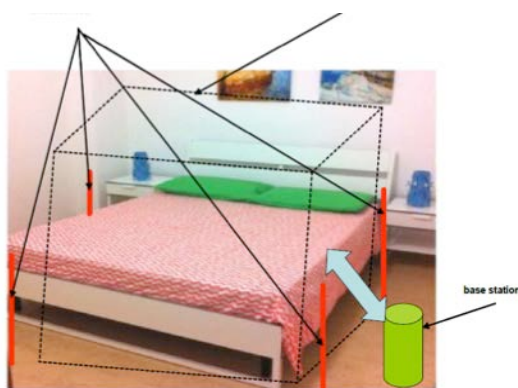
Figure 1: Structure of the HB

The following is the scheme of the mobile version HB_M; the typical prospect is the patient that though conducting an active life without particular constraints of mobility needs to be constantly monitored:

The sensors (inserted into the fabric of a garment that the patient wears), the bracelet and the smartphone they are worn by the patient.

4. HOW THE eHEALTH BUBBLE WORKS

The activation of the eHealth Bubble

In the residential version, HB_R provides for the preparation of the base station and the set of members inside the room that houses the patient, positioned in sight with respect to the bed and to the armchair; the activation of the system takes place with the connection between the base station and the sensors on auctions. In this way the virtual space within which the patient is located is determined.

In the mobile version, HB_M predicts that the patient is wearing the shirt with the sensors, the bracelet electronic and bring with you a smartphone with the eHealth Bubble car app installed. Activation of the system through the bracelet and the connection with the sensors that are industrially drowned of the worn mesh allows you to define the volume within which the patient is located.

The relationship between virtual space and the patient

The HB_R system, once determined the virtual space and the double relationship with patient and base station, is integral with both and reconfigures when moving the base station or patient (for example from bed to armchair and vice versa), maintaining the overall consistency.

The HB_M system is constantly integral with the patient's body.

The provision of telemedicine services

The preparation of a virtual space allows you to intercept any object or activity that cross the walls and then check which operations are performed on the patient; for both versions, HB_R and HB_M, it is also possible to constantly monitor the relevant parameters of the patient.

The objects and activities that can be engaged concern:

1. remote control of the patient's vital parameters through audio, video and specific instruments

2. verifying the correct administration of therapies (through, for example, the control of the type of therapy) medicinal product, after photographing the heel code or detecting the drowned RFID in the heel)

3. direct contact with the patient through audio and / or video telematic interaction In the HB_M version the services mainly concern points 1 and 2.

The functions of the eHealth Bubble solution

The product allows the provision of telemedicine services that do not require direct intervention by the authorized personnel, such as the registration and / or systematic transmission of data relating to the state of the patient, the visual inspection of the patient, the interview with the patient, the measurement of some vital parameters, interaction with the patient through requests from remote staff, verification of the correct sequence (also temporal) of drug intake.

In the HB_R version all audio and video connection services and for the use of medical devices they are activated through the drive in the base station of retractable panels (sliding shields) that make the required system is available (ex: Camera, Microphone, measures that, once the use is finished, they return to the original housing inside the base station).

In the HB_M version the available connections are always active and allow recording and, in the case of anomalies, transmit the patient's parameters to the operative center. The relationship, only audio, with the patient it can take place through the smartphone.

Description of the underlying technology

The main technologies used for the creation of eHealth Bubble are:

Wireless communication in many forms

Both short and long-range wireless communication technologies will be used. For the collection of local medical data will use Bluetooth, ZigBee and generic Wifi technologies.

For the communication of data extracted from the collection and processing of local data technologies will be used specifications (ADSL etc.) and mobile networks (3G, 4G and 5G).

Acquisition of images with radiometric infrared sensors

In the spectrum of electromagnetic radiation emitted or reflected by the surfaces that define the environment surrounding it is a band not visible to the human eye which is characterized by a length wave between 0.7 μm to about one millimeter.

These radiations are called infrared and are directly related to the temperature of the surfaces that emit them. There are both point and matrix sensors that are able to detect and measure these radiations operating in sub-bands of infrared radiation. For the project they will be used matrix sensors with medium definition and speed to collect radiation and form infrared images.

Given the type of application, the sensors operating in the infrared spectrum of 7 will be preferred and the 14 μm. This recovery band is particularly efficient in the radiometric measurement of temperatures around the epidermal temperature. In addition it allows to filter the solar radiation so as to be immune to measuring steps from any solar reflex. The observation of the patient by

means of one miniaturized infrared camera will allow a general assessment of the patient's state by measuring with a good approximation the patient's temperature in different points previously defined identified by an automatic processing of the image taken.

This type of observation will always be possible both at night and during the day in the presence or absence of lighting of the defined observation space (HB_R) and in particular cases also for the version HB_M.

Shooting images with a camera operating in the visible spectrum The spectrum of electromagnetic radiation perceived by the human eye is between 400 and 700 microns. Commercial cameras are sensitive to the band between 400 and 1000 μm. In the realiz -

The project will use high-definition cameras in both color and black and white.

The particular sensitivity of commercial sensors at frequencies equal to 800-900 nm will allow observations in the dark with the aid of invisible radiation led illuminators in order not to annoy the subjects under observation. The observation of the patient by means of a conventional camera will allow to a remote operator to define a general status of the patient.

An automatic processing of the images taken allows to define a state of activity and furniture - mean of the patient and the presence of respiratory movements. As previously mentioned a source of illumination infrared (not annoying because not felt by the patient) associated with the camera allows observation even in total lack of lighting. (HB_R)

Image processing

A variety of static or moving image processing techniques will be used. The elaborations static will allow to maintain the focus of the observation on the subject under examination or identification codes (bar codes on Bar Code or Dot Matrix placed on packs of medicines or prescriptions more or less generic).

The motion detection elaborations will allow instead to evaluate the general state of mobility and the pre - without and the evaluation of basic movements such as breathing.

Microphone monitoring

Microphones of various environmental types will be used, drowned in garments or in stationary furniture of the patient. Numerical filtering techniques will be used to isolate the rhythms and frequencies of reference. Microphonic type monitoring will allow the detection of many automatic vital activities such as heartbeat, respiratory movements and any rustling related to breathing.

The sensors can be integral with beds or armchairs that welcome the subject under observation (HB_R) or drowned in a garment worn by the patient himself

(HB_M). Sensors of this kind monitors are battery powered and communicate with wireless techniques (Bluetooth, ZigBee or simililari).

Measurement in transmission or reflection of electromagnetic radiation at specific frequencies

The use of electromagnetic radiation sources coupled with suitably tuned sensors allow the detection and measurement of parameters related to blood circulation.

Absorption or reflection by the patient's organic tissues under observation of the frequencies emitted measured by tuned sensors will allow relatively accurate measurements on variations of blood flow.

Differential measurements on different electromagnetic wavelengths will also be used. These technologies will allow the measurement of parameters related to cardiac pulsation, pressure and saturation blood with minimal patient involvement that should only introduce the hand into a predisposed slot of the totem (HB_R) or wear appropriate cuff (HB_M).

Processing of the collected data and remote alerting of the surveillance operator

It can be done voluntarily by means of a button or automatic when exceeding defined thresholds (maximum and minimum temperature, long-term immobility, reduction or absence of respiratory movements. (HB_R and HB_M)

Reading of BarCode, DotMatix or RFID

The reading of the BarCodes and of the DotMatrix will be carried out with system cameras or with the cameras of which are equipped with mobile phones. Electromagnetic RFID reading antennas will allow to achieve the communication and the consequent reading of the data contained in the electromagnetic TAGs glued or drowned in single or multiple packs of medicines.

These technologies allow the control and supervision of the correct administration sequence of medicines, by scanning the heels of the boxes containing the medicines prescribed for the sog -jet under observation (HB_R and HB_M).

5. CONCLUSION

The described project eHelath Bubble is now in the second of three phases. Overwhelmed indeed the step of the high level design of the functional charateristics, the Authors are engaged in the prototype testing. Through the selection of a set of medical instruments and verification of the adequacy of the health bubble solution by health operators and pilot users, the Authors aim to reach a version technologically stable and functionally adequate even not necessarily complete.

REFERENCES

1. Fisk M.J., 1998; J Telemed Telecare. Telecare at home: factors influencing technology choices and user acceptance. 4(2):80-3
2. Health Expect 2015. Ethical implications of home telecare for older people: a framework derived from a multisited participative study. Jun;18(3):438-49
3. May C, Mort M, Williams T, Mair F, Gask L. 2003 Health technology assessment in its local contexts: studies of telehealthcare. Social Science and Medicine; 57: 697–710
4. Eccles A. 2010 Ethical Considerations Around the Implementation of Telecare technologies. Journal of Technology in Human Services; 28: 44–59.
5. Mort M, Finch T. 2005; Generating Principles for Telehealthcare: a Citizens' Panel Perspective. Journal of Telemedicine and Telecare, 11: 1
6. Ethical Frameworks for Telecare Technologies for older people at home. 2011 Final Report of EC FP7 Science in Society project no 217797, 25
7. Bailey C, Sheehan C. Technology, older persons' perspectives and the anthropological ethnographic lens. ALTER. 2009 European Journal of Disability Research; 3: 179–197
8. Sánchez Criado T. Department. of Social Anthropology, Universidad Autónoma de Madrid, 2012 Las lógicas del telecuidado: La fabricación de la 'autonomía conectada' en la teleasistencia para personas mayores. PhD thesis.
9. Willems D. 2010 Varieties of goodness in high-tech home care In: Mol A, editor; , Moser I, editor; , Pols J, editor. (eds) Care in Practice. On Tinkering in Clinics, Homes and Farms. Bielefeld: Transcript verlag, 257–276
10. Willems D, Pols J. 2010 Goodness The empirical turn in health care ethics. Medische Antropologie/ Medical Anthropology; 22: 161–170
11. Stabilini C, Bracale U, Pignata G, Frascio M, Lazzara F, Gianetta E. 2013 Laparoscopic bridging vs. anatomic open reconstruction for midline abdominal hernia mesh repair [LABOR]: Single-blinded, multicenter, randomized, controlled trial on long-term functional results. Trials 14 (1),357
12. Fornaro, R., Frascio, M., Stabilini, C., Lazzara, F., Gianetta, E. 2009[Chron's disease and cancer]. Ann Ital Chir. Mar-Apr;80(2):119-25.
13. Fornaro, R., Frascio, M., Stabilini, C., Lazzara, F., Gianetta, E. 2008 [Crohn's disease surgery: problems of postoperative recurrence]. Chir Ital. 60(6):761-81.

MODEL-BASED IMAGE PROCESSING APPROACHES FOR AUTOMATED PERSON IDENTIFICATION AND AUTHENTICATION IN ONLINE BANKING

Andreas Pointner[a], Oliver Krauss[b], Georg Freilinger[c], Daniel Strieder[d], Gerald Zwettler[e]

[a],[b],[e]Research Group for Advanced Information Systems and Technology (AIST), Research and Development Department, University of Applied Sciences Upper Austria, Softwarepark 11, 4232 Hagenberg, AUSTRIA
[c],[d]Credi2 GmbH, Schottenfeldgasse 85/2, 1070 Wien, AUSTRIA
[e]School of Informatics, Communications and Media, University of Applied Sciences Upper Austria, Softwarepark 11, 4232 Hagenberg, AUSTRIA

[a]andreas.pointner@fh-hagenberg.at, [b]oliver.krauss@fh-hagenberg.at, [c]georg.freilinger@cashpresso.com, [d]daniel.strieder@cashpresso.com, [e]gerald.zwettler@fh-hagenberg.at

ABSTRACT
This research work covers the necessary image processing workflow to facilitate online person identification for financial authentication, to be carried out in a fully automated way. This brings the advantage of fewer errors due to human failures. Moreover, it reduces the cost of a single identification by quite a significant factor. The relevant authentication and validation steps are modelled in BPMN.
Validation and comparison of the person visible in the video stream is achieved utilizing a hybrid face recognition approach combined with OCR checking and model-derived individual instructions. To ensure authenticity of the identification card, security features like color-holograms are modelled for each version and supported country. The interconnection of the process sequence, which is individually and dynamically derived from the BPMN together with adaptive paradigms of human-computer-interaction, allow for a beyond the current state-of-the-art level of manipulation prevention and of user assistance.
The results show that the process of person identification and authentication can be automated when legal aspects are clarified, thus allowing for a state-of-the-art of precision on face recognition and hologram checking, at a competitive level with human staff.

Keywords: model-based hologram validation, face recognition, BPMN, human-computer-interaction

1. INTRODUCTION
In the last couple of years, e-commerce is on a significant economic upswing. Due to competitiveness in the banking sector, most of the provided services like money transfer, account management, stock trading or insurance administration are nowadays available for online use. While well-established traditional banking institutions had to follow the trends in e-banking, other recently founded online banking institutions no longer provide any of the services in physical customer branches (Meier 2012).

Due to competitiveness on the markets, the banking institutions nowadays focus on online customer acquisition. Therefore, the customer should be identified without ever having to go to a banking authority in person before. Service providers like *IDnow* (IDnow 2018a) offer online identification of potential customers for banking institutions, via video call, that fulfill legal specifications regarding money laundry in Germany and Austria. Thereby, identification of the customer is executed remotely and customer data like name, address, affiliation, photo and valid identification credentials (ID) are acquired by a human agent and transferred to the banking institution (IDnow 2018b). This kind of identification is a legal requirement for opening an account and opening a credit respectively (Finanzmarkt-Geldwäschegesetz 2017; Bundesfinanzministerium 2017).

Online identification services based on call-centers represent a significant cost factor in case of micro credits. Thus, any step towards (semi-)automation of this process step will lead to reduced costs and an advantage over competing companies. A law amendment in Financial-Money Laundering Act (i.G. Finanzmarkt-Geldwäschegesetz) (Finanzmarkt-Geldwäschegesetz 2017; Bundesfinanzministerium 2017) has prepared ground in Austria for fully-automated identification as long as the same level of reliability is preserved as for delivering an *RSa* letter (Zustellgesetz 2008), i.e. a government letter in Austria only the addressee may take delivery of. Future court ruling will clarify if this law amendment facilitates fully automated processing in user identification. Nevertheless, the legal basis for computer-based support in person analytics is provided (Finanzmarkt-Geldwäschegesetz 2017; Bundesfinanzministerium 2017).

Current online identification utilizing human agents shows some drawbacks. A received live video feed can

be of low quality, due to bandwidth restrictions, latency or can be affected by motion artefacts, thus complicating the identification process. Without technical support, it is a challenging task to compare the photo on a given ID with the person available in the video sequence, especially if the photo is outdated or the person has recently changed its appearance like wearing glasses, growing a beard and so on. Furthermore, it is challenging to check the security features of the ID as holograms need a certain exposure to the light by rotating the ID in horizontal and vertical direction and thus are only visible in a narrow range. Thus, the human agent can check if there are holograms present but may be unable to asses if they are at the right place or showing the expected morphology. Because of these challenges, a computer-based support in online user identification can help reduce the interview times and contribute to increased effectivity and accuracy in the identification process.

The automation of the online identification process necessitates a priori modelling of the ID, object detection in the live video feed, rectification and identification of hologram, text and portrait photo Region of Interest (ROI) as pre-processing for subsequent analysis utilizing optical character recognition (OCR), color segmentation and face recognition. Those aspects, especially the predefined reference images of the holograms, are used to calculate a confidence value for the security features.

1.1 State of the art

From a state-of-the-art point of view, several approaches for pattern retrieval, which is necessary to detect the ID, mostly in the form of a card or booklet, like a passport, are available. Frameworks like Vuforia (Vuforia 2018a) for Augmented or Mixed Reality (AR/MR) applications and OpenCV (OpenCV 2018a) for computer vision tasks offer robust functionality for visual template detection and tracking that also can be applied to IDs. The *Image Targets* provided by Vuforia are thereby a generic tracking approach for arbitrary images, not limited to binarization, specific geometry or encoded markers. Instead, natural image features are extracted from the reference and test images and utilized for tracking (Vuforia 2018b). The OpenCV template matching is designed as registration task, including affine transformations like translation, rotation, scale and shearing and utilizing local correlation as feature metric (OpenCV 2018b). To achieve a higher level of robustness regarding perspective distortion, OpenCV provides various feature detection approaches like SURF (Bay, Ess, Tuytelaars and Van Gool 2008), ORB (Rublee, Rabaud, Konolige and Bradski 2011), SIFT (Lowe 2004) or classic active appearance models (AAM) including color-pixel deviation besides shape and key features (Cootes, Edwards, and Taylor 1998). The mutable parts of the pattern, like personal data or the photo, should thereby be recessed from the reference ID document image to ensure higher accuracy.

Another approach to identify the rectangular shape of an ID is application of generalized Hough Transformation (GHT) (Ballard 1981) on line structures, covering orientation, translation and scale per dimension and providing robustness in case of partial occlusions.

In the field of face recognition, different approaches have been proposed the last 40 years. In the work of Kanade (Kanade 1973), face markers are assembled in feature vectors and compared according to Euclidean distance. This approach is robust to illumination and luminance but has an insufficient face recognition rate without providing additional input (Brunelli and Poggio 1992). The application of Eigenfaces and principal components analysis (PCA) allows for treating the face as holistic image (Turk and Pentland 1991). To allow for a higher level of robustness, the current approach is to analyze faces and compare them in small sections utilizing Local Binary Patterns (Ahonen, Hadid and Pietikainen 2004) as available in the OpenCV framework (OpenCV 2018c). State of the art face recognition like Microsoft Cognitive Services (Microsoft 2018), which emerged from the Oxford project, utilize various recognition approaches, such as artificial intelligence and machine learning as black box, not only allowing to detect and compare faces but also to quantitatively evaluate human emotion in facial expressions. To increase face recognition accuracy, several photos are grouped together as a profile. Such a profile, as well as acquisition via 3D camera or surface scanner, allow overcoming the planar limitation of plain photography (Bevilacqua, Caprioli, Cortellino, Giannini, Mastronardi and Santarcangelo 2010).

In the field of optical holographic template matching for security documents, several approaches have been presented in the past. The application of wavelet transforms (Burage-Lefebvre, Cotmellec, Lebrun, Ozkul 2000) and Wiener filter (Janucki and Owsik 2003) are applicable for individually modelled security ROIs while also common AR template matching approaches are highly applicable to this task (Hartl, Arth, Schmalsteig 2014; Pramila, Keskinarkaus, Rahtu, Seppänen 2011). The verification of holograms can be achieved by utilizing registration approaches combined with human-computer-interaction paradigms to make the watermarks visible via common cameras (Hartl, Grubert, Schmalstieg, and Reitmayr 2013).

Another necessary part in analyzing security documents is recognition of machine-readable text via OCR methods. Frameworks like Tesseract (Smith 2007; OpenCV 2018d) are applicable to this task, as the fonts, position and semantic content of the text is pre-determined (ICAO 2018).

1.2 Status Quo in Online User Identification

The status quo in online user identification as illustrated in Fig. 1 requires the user to fill their personal data in a web form. During the subsequent video call, a human agent compares the entered data to the data provided via ID. Additionally, the identity of the person is matched with the photo on the security document. In a final step,

the integrity of the security document itself is checked by verifying color-holograms and watermarks.
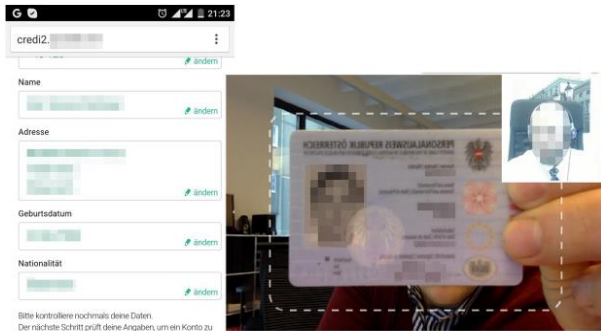
Figure 1: Illustration of the online identification process currently provided by credi2.

2. MATERIAL

In the following section, different ID types are evaluated. In general, the Austrian Passport and the German identity card are used. For some tests, the Austrian driving license was utilized, too. The main test data includes three different people, namely two males, aged *27* and *35* respectively and a female person aged *27* as well, acquiring several test videos. Out of this test data, a set of single frame images is extracted. All of the videos are in high, but heterogeneous resolution to test differences in runtime as well as in detection quality of results. Therefore, three different resolutions are used: *720p (1280x720)*, *1080p (1920x1080)* and *4k (3840x2160)*. All of the videos are recorded with a framerate of *30 fps*. In addition, additional data from other research employees is provided to test various different aspects, like wearing glasses, beards, long vs short hair, etc.

3. METHODOLOGY

The process described in section 1.1 is automated by executing various BPMN process definitions for the required analytics tasks like face detection, face recognition, OCR and a novel strategy to validate color holograms. Business Process Model and Notation (BPMN) is a graphical representation for a specific business process (OMG 2011). The BPMN also includes human-computer-interaction (HCI) feedback paradigms. The dynamic process model not only allows for adaption due to collected user feedback and reactions but also introduces a higher level of security due to stochastic elements. To facilitate security checks, automated face recognition and OCR analysis of machine-readable text, an a-priori model of a particular ID type has to be prepared in a semi-automated way. The following process steps and solutions represent an enhancement of the automated online identification concept delineated in (Pointner 2017).

3.1. Modelling the Identification Process in BPMN

To analyze the current human-driven process of online identification, a BPMN is modelled as seen in Fig. 2. The model is processed and executed by the Camunda

process engine (Camunda 2018). All of the process steps not related to the core identification process, shown in the boxed in section of Fig. 2, like online registration and filling the form with personal data, are achieved by arbitrary web applications providing the necessary input data, and are outside the scope of this publication.
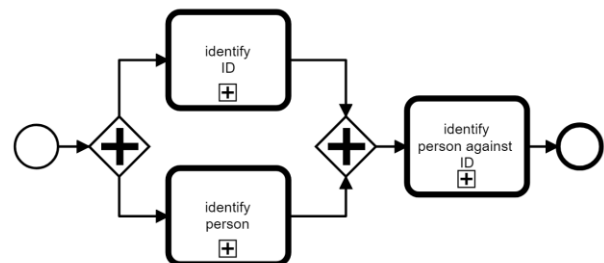
Figure 2: Main process for online user identification.

The sub-process of identifying and verifying a given ID comprises checking of the security features, of the ID type the ID corresponds with, such as watermarks or color-holograms. The user is instructed to vertically or horizontally flip the security document, allowing checking the features, see Fig. 3. The security features are thereby processed in a stochastic way, impeding fraud. Furthermore, as all process steps involve user-feedback in terms of human-computer-interaction, the process duration and number of necessary repetitions to achieve the desired process goals vary. Both aspects are explicitly claimed in the legal basis for automated online user identification (Finanzmarkt-Geldwäschegesetz 2017; Bundesfinanzministerium 2017).
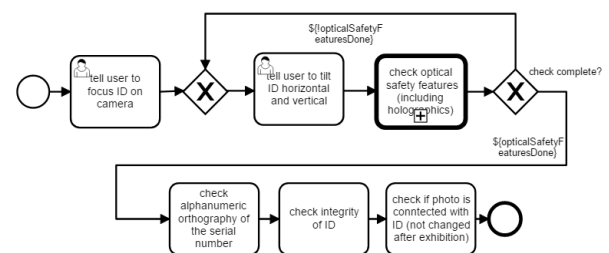
Figure 3: ID security document identification.

If a sufficient number of security features is confirmed according to a predefined confidence threshold, the text and photo on the ID are checked and the integrity of the ID is confirmed.

3.2. A priori Modelling of ID types

The relevant IDs, like passport or identity card, not only need to be discriminated according to the issuing country but also according to a specific version, as security features are modified in regular intervals.
For each ID type, the period of validity, and the physical features of the card including width, height and thickness and the geometry showing rounded corners, is

modelled. Furthermore, the placement of the photo visually identifying the person and the OCR text areas are defined.

According to the security features, additional information besides their position is required. For each of the color-holograms, the exact shape of the watermark is required at high resolution, thus allowing precise morphological matching of the hologram shape.

The security document areas are categorized as `ImageCharacteristic`, `TextCharacteristic` or `HologramCharacteristic`, all deriving from abstract base class `IDCharacteristic` and are configured via XML notation, Fig. 4 shows the classes mentioned above in an UML class diagram.

In the case of the `TextCharacteristic`, the model also comprises the font, font size and, in the case of hologram letters, the expected color setting.
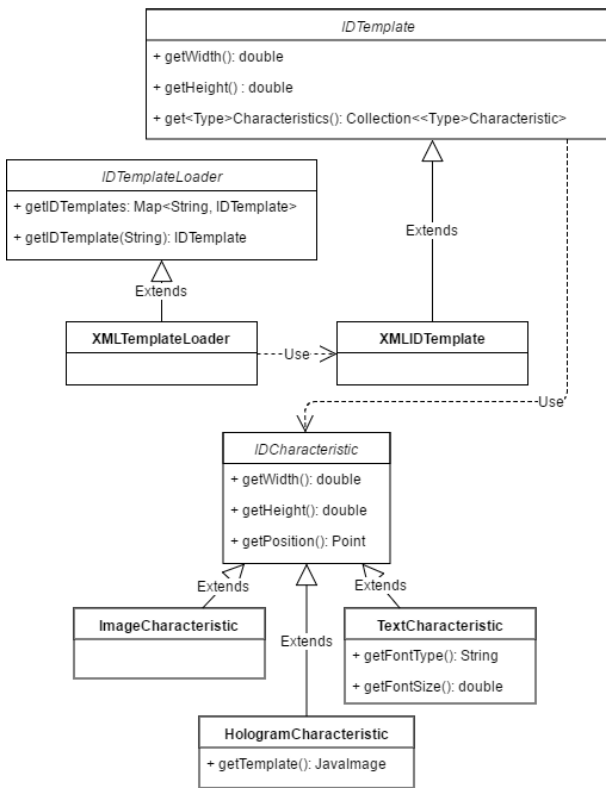
Figure 4: Security document feature categories.

Security features can be found on the a-trust Homepage (Atrust 2018).

Modelling of the hologram shape and the expected background texture within the relevant ROI necessitates a semi-automated segmentation approach. Therefore, the reference documents are captured at a camera angle best suited to let the color-holograms appear. Subsequently, for all pixels C_i with coordinates $<c_x, c_y>$ a probability metric $C_p(C_i)$, see Equ. 1, is evaluated, returning the probability of belonging to the color pixels (Jähne 2012; Meyer 1992) based on color channels k in each particular image denoted as I_j. To cover a wider range of chromacity, input images are transformed from RGB to HSV color space.

$$C_p(c_i) := \left| \max_{k=1..3}(I_j(c_i,k)) - \min_{k=1..3}(I_j(c_i,k)) \right| \quad (1)$$

The pixel coordinates showing $C_p(C_i)$ above a pre-determined threshold T_c are grouped together by applying Region Growing and then are morphologically post-processed utilizing opening and closing operators, thus lading to binary hologram shape mask R_h. Finally, borders of the segmented hologram region are derived by applying boundary tracing (Sonka, Hlavac and Boyle 2007).

The low-pass filtered background after removing black textual pixels $C_b(C_i)$ according to color-threshold T_b, see Equ. 2., is then cloned to the entire ROI-region by applying an iterative morphological dilation approach.

$$C_b(c_i) := \begin{cases} 1 & C_p(c_i) < T_b \\ 0 & else \end{cases} \quad (2)$$

3.3. Adapted Hough-Line Detection of ID Bounds

The generalized Hough Transform utilizing the R-table is not robust in case of partially occluded IDs as all four bordering lines need to be detected for security document rectification. Instead, the most dominant four lines in specific search sectors are searched, namely *[-30°;30°]* for vertical lines and *[60°;120°]* for horizontal lines. The search sectors are thereby defined in the outer half of the central crosshair coordinate system illustrated in red color in Fig. 5. The Hough-space thereby is composed at *0.1°* granularity, for preprocessing Sobel filtering is preferred over binary edge detection results achievable by Canny filtering.
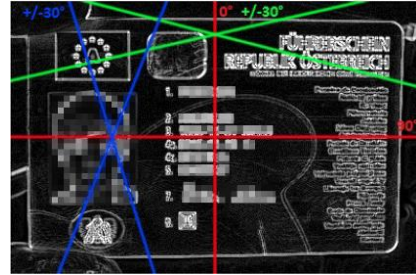
Figure 5: Restricted search sectors for the required four bordering lines of the ID (Austrian driving license).

The detected Hough-line candidates are then permutated to detect the representative of each sector that leads to the most plausible overall bounds with respect to affine characteristics and parallelism. Due to that validation, the correct lines can also be detected if the ID borders are partially occluded, e.g. by one or two fingers.

Based on the detected bordering lines of the security document, rectifications, such as perspective transform are performed, thus allowing the direct application of the modelled ROIs for images, holograms and text sections. Besides, the size-ratio of the four lines allows precise approximation of the current horizontal and vertical rotation angle as a necessary feedback

information in the sense of human-computer-interaction.

3.4. Face Detection and Face Recognition

Regarding the process of user identification via face recognition algorithms, a hybrid approach is implemented. A set of frames showing the face of the person is amplified and adjusted within the augmented face ROI and utilized to compare against the photo on the ID at a high level of confidence. This ensures that the person in the video and the ID document refer to the same identity. At a slightly lower confidence level, face recognition is applied to ensure that only the same person is visible in the video stream.

3.5. Analyzing Machine-Readable Parts with OCR

Machine Readable Zones (MRZ) are a highly relevant element in security documents, as the encoded information can be utilized to validate the personal data. As the MRZ is also part of the document modelling, the OCR can be restricted to the relevant ROI, thus increasing both, performance and robustness. The text in the particular ROI is binarized utilizing an Optimal Threshold implementation and then syntactically interpreted using the Tesseract framework.

Although Tesseract generally leads to text recognition results of state-of-the-art accuracy (Smith 2007) and the MRZ is designed for OCR analysis, the result character sequence will still show some errors or missing parts. Consequently, the OCR results per line are evaluated from different flipping angles and combined by applying approaches of bioinformatics genome sequencing. The standard (ICAO 2018) for Machine Readable Travel Document (MRTD) additionally defines checksum elements. These are used to validate the parsed and reconstructed data.

3.6. Validation of Color-Holograms

The validation of color holograms is comprised of different steps of validation. On the one hand, the template hologram regions are compared to the rectified ID, utilizing color pixel classification according to Equ. (1) and confidence-incorporating SSE thereby taking all false-positive and false-negative pixels into account. Thus, also colors appearing in the assumed background region are considered an error. The confidence weight w per pixel c_i thereby incorporates distance of the pixel with respect to the expected hologram borders derived from Euclidean distance map E, thus introducing robustness in case of spatial misalignment, see Equs. (3-5).

$$w(c_i) = 1.0 - \frac{\log(E(c_i))}{\log(\max(width(E), height(E)))} \quad (3)$$

$$ERR(c_i) := \begin{cases} 1 & \begin{array}{l}\left(R_h(c_i) \wedge \left(C_p(c_i) \leq T_c\right)\right) \vee \\ \left(\neg R_h(c_i) \wedge \left(C_p(c_i) \geq T_c\right)\right)\end{array} \\ 0 & else \end{cases} \quad (4)$$

$$SSE(I) = \prod_{\substack{x=1..width(I), \\ y=1..height(I)}} w(c_i) \cdot ERR(c_i) \quad (5)$$

Besides, in different viewing directions the hologram colors are expected to fade away. Thus, a hologram pixel is only classified, if it is assigned a background label in case of flat and steep flipping angles. Therefore, $C_p(C_i)$ is calculated at each pixel position for each of the frames sorted by the flip angles, thus leading to a line profile $P(C_i)$. Based on the line profile as shown in Fig. 6, a feature vector F <F_1, F_2, F_3, F_4> is calculated for features maximum gradient (F_1), variance (F_2), average value (F_3) and maximum value (F_4). Based on the feature vectors F_i statistical normal deviation profiles $N(\mu, \sigma)$ for both, hologram and non-hologram areas as N_h and N_b. Thus, hologram pixel classification is based on probability density function (PDF) to be evaluated for each particular feature vector F_{Ci} derived for pixel position C_i, see Equ. 6.

$$Err_h(c_i) := \sum_{m=1..4} \left(1.0 - \frac{pdf(c_i, F_m(c_i), N_h)}{pdf(c_i, F_m(c_i), N_h) + pdf(c_i, F_m(c_i), N_b)}\right)^2 \quad (6)$$

Figure 6: Line profile (red) for hologram features calculated per coordinate position for all sorted frames of varying viewing directions θ.

4. IMPLEMENTATION

The prototype is implemented in Java, utilizing Tesseract and wrapped OpenCV functionality. The core functionality for face recognition, hologram detection, OCR and the human-computer-interaction paradigms necessitated an analysis of user behavior and appropriate feedback. The functionality is encapsulated in modules, each module representing a specific BPMN task. These modules are scheduled by a workflow engine, which executes the entire BPM process. The tasks thereby are influenced according to their process life cycle allowing external process control.

As the client devices are heterogeneous smart phones with an arbitrary architecture and operating system, a generic design approach is required. Therefore, REST-interfaces (Adamczyk, Smith, Johnson and Hafiz 2011) are utilized to provide simple and clean interfaces for all of the services.

A high level of interchangeability of the particular services is achieved by consistent usage of Spring

(Gutierrez 2014), thus allowing the configuration and on-the-fly replacement of modules via a server-side XML configuration in the sense of plug-in design.

5. RESULTS
5.1 Adapted Hough-Line Detection of ID Bounds

The first part of the process is to detect the ID itself. In the following section, an Austrian Passport (censored for data protection) is used to visualize the functionality and show the achieved results.

The subsequent task is to crop out the ID itself. At first, the image is sharpened and the contrast is increased to create stronger borders, see Fig. 8(a).

The next step is to create a greyscale image and detect edges. For this a Sobel-Operator is applied, see Fig. 8 (b).

Figure 7: Raw image of an ID (Austrian Passport).

| (a) | (b) |

Figure 8: Image sharpened by contrast enhancement (a) and edge detection after (b) (Austrian Passport).

To detect the ID card, Hough-Lines are detected twice, once in horizontal and once in vertical direction. Each of those provides a result along one axis. Then the highest value in each sector represents the borderlines of the ID. The images are resized to 400 times 300 pixel to speed up the calculation. Figure 8 shows the results of the Hough-Line detection. On the x-Axis the pixel in either x or y-direction is labeled. On the y-Axis, the *strength* of the line is represented, logarithmically normalized to a value between 0 and 255.

| (a) | (b) |
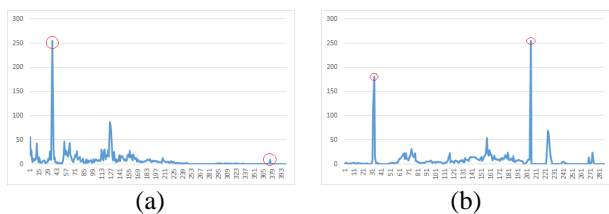
Figure 9: Hough Lines horizontally (a) and Lines vertically (b).

The lines marked with a red circle are those lines, which represent the borders of the ID, see Fig. 9 (a). Fig. 9 (b) shows the right border is hard to detect, as this side in the original image looks curved, see Fig. 8.

The last step is to crop out the ID. Therefore, the corner points are calculated. Those are then used to perform a

perspective transformation. The final result can be seen in Fig. 10 (b).

This analysis step is executed for every frame and is the base process for every other processing step. From now on, every consecutive step (OCR, Face Recognition, Hologram check) is executed on the rectified image as shown in Fig. 10 (b).

To test the detection rate, three scenarios are defined. In the first one, the ID lies on the table and the background is in a uniform color. For the second one, the user holds the ID in his hands, again with a uniform background color. In the last scenario the user holds the ID in his hands with confounders visible in the background, cf. Fig. 7.

| (a) | (b) |

Figure 10: ID borders (a) and Cropped out ID (b) (Austrian Passport).

The tests are executed with 30 images per scenario, where the 30 images split up in 10 images with three different ID types of three different persons.

Fig. 11 (a) shows the detection rate for the three different scenarios. While the detection rate is with around *90%*, for scenario #1 quite high, it drops down to under *30%* for scenario #2 and #3. Nevertheless, this is not a problem, because even if only every third frame can be detected, it is still sufficient for a security check.

The problem of the detection is that the finger, which is placed on the borderline of the ID, occludes the left edge. In Fig. 11 (b) can be seen, that the side, where the person holds the ID also strongly influences the detection rate. *60%* of the test images, where the person held the ID on the right side, where detected correctly, whereas only around *15%* of the tests, where the person held it on the left side.

The check, which IDs were detected correctly, was done manually.

| (a) | (b) |
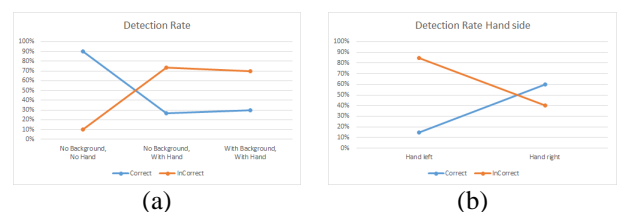
Figure 11 Detection Rate (a) and Detection Rate Hand side (b).

6.2 Results on Face Detection and Face Recognition

The next process step is the verification of the face. To perform face recognition two different implementations, OpenCV and Microsoft Cognitive Services Face API, are used. The reason for using two different

implementations is to increase the recognition confidence. For normal face-to-face comparison over multiple frames, OpenCV is used. To check if the photo on the ID matches the correct person, both systems are used to calculate an average confidence value. The recognition accuracy of Microsoft Face API is shown in Tab. 1. No negative match was predicted as positive. This implies a low error rate. In addition, with combining it with OpenCV face detection it prevents negative positive Matches and thus increases the reliability of the system.

		Predicted	
		Positive Matches	Negative Matches
Actual	Positive Matches	52	59
	Negative Matches	0	130

Table 1: Microsoft Cognitive Service Face API Confusion Matrix.

6.3 Analyzing Machine-Readable Parts with OCR

Another process step is the extraction of the MRZ, which exists on every MRTD. To analyze the MRZ it is necessary to read the single chars form the ID utilizing OCR. At first, the text over multiple frames is collected. Tesseract assigns a confidence for each letter, which can be used to calculate a better result. The letters at the same positions are compared and check which one is the most likely, which is then used for further operations. With this method, the recognition rate for correct letters is nearly 100%. As already mentioned, the standard for MRTD also defines some checksum fields inside the MRZ, with them, the correctness of the information can be validated.

6.4 Results on Validation of Color-Holograms

Finally, the process for verifying the correctness of the holograms is evaluated based on a-priori ID models. The procedure of preparing such a-priori hologram models is performed in a semi-automated way. With a sufficient amount of reference images from a given ID, it is possible to extract the relevant parts of the hologram by calculating difference images.

Multiple images showing the hologram in different states of visibility are thereby used as shown in Fig. 12 for Austrian passport, calculating reference masks. Based on the averaged reference image OpenCV contour detection and contour filling methods are applied resulting in a black and white image of the hologram, see Fig. 13 (a).

Figure 12: Example Hologram (Austrian Passport).

Figure 13: Hologram extracted (a) and Hologram Compare Image (b) (Austrian Passport).

After preparing the a priori model, the hologram is manually enhanced allowing for results of sufficient quality, see Fig. 13 (b).

The feature based hologram evaluation necessitates cropping of the modelled hologram ROI after ID rectification, shown in Fig. 14 (a), as well as preparing the background area by propagating the color pixels similar to region growing after applying significant low-pass filtering, shown in Fig. 14 (b). Subsequently, the color-differences at specific flipping angles of the frames is calculated and according to Equ. 1 and can be represented as difference image, see Fig. 15.

Figure 14: Hologram cropped (a) and Background recalculated (b) (Austrian Passport).
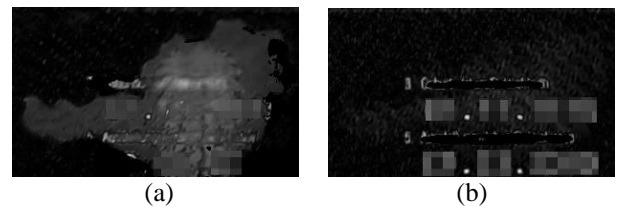
Figure 15: Difference in hologram (a) and difference calculated from background (b) (Austrian Passport).

The features are calculated from pixel-wise frame profiles and evaluated according to a priori estimated distributions N_h and N_b for hologram and background areas respectively, see Tab. 2 and Fig. 16.

	Hologram		No Hologram	
	Avg	Stdev	Avg	Stdev
AverageAbsoluteGradient	12.18	3.19	4.40	6.96
Average	67.61	20.94	25.12	30.27
AverageNegativeGradient	-14.16	4.44	-4.41	7.91
AveragePositiveGradient	6.48	5.52	4.16	7.46
MaxAbsoluteGradient	34.03	11.98	7.96	12.37
Max	147.03	50.44	31.77	38.88
MaxNegativeGradient	-33.36	12.99	-6.41	11.17
MaxPositiveGradient	14.60	11.98	5.76	10.14
Variance	2176.85	1541.87	84.10	307.87

Table 2: Evaluated features **F** $<F_1, F_2, F_3, F_4>$, namely maximum absolute gradient (F_1), variance (F_2), average (F_3) and max value (F_4) utilized to discriminate hologram N_h and plain background N_b respectively.

As presented in Equ. (3), a weighting function $w(c_i)$ derived from a Euclidean distance map as shown in Fig. 17 is utilized to sum up the pixel contributions as a cumulated confidence value. The results confirm that incorporation of the weighting function compensates marginal pixel mismatches analyzing the frame stack otherwise demanding for time consuming registration.

(a)   (b)

(c)   (d)
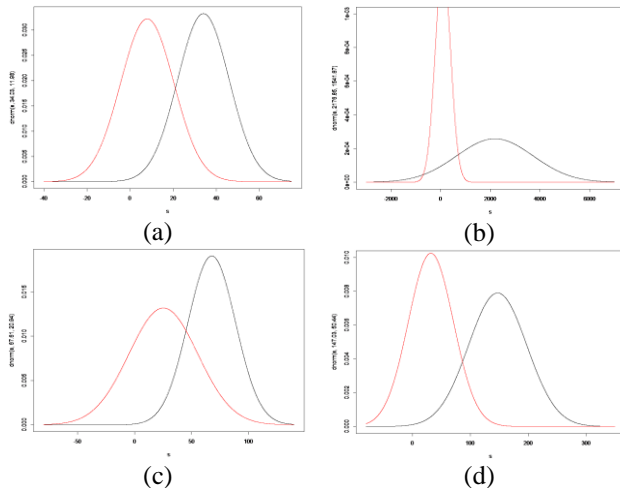
Figure 16: The four classification features - maximum absolute gradient (F_1) in (a), variance (F_2) in (b), average (F_3) in (c) and max value (F_4) in (d) showing low inter-feature correlation are selected to overall minimize Bayes Error.
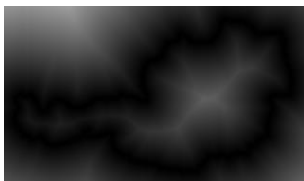
Figure 17: Weight map showing skeleton of the modelled hologram shape.

The cumulative quantitative result for hologram check allows a reliable discrimination of hologram and background. The resulting similarity range for holograms is defined as [0.7; 0.4] and therefore far above the confidence threshold $T_b=0.15$ for background and permanently colored emblems in case of a fraud attempt.

The main challenge with detecting the holograms is that some types are hardly visible on any frame, necessitating an extreme tilt to appear. Other hologram types in turn need specific illumination in general.

Thus, not every hologram can be checked during the identification process. This is not a disadvantage over the state of the art, because a trained person, who communicates over a live stream with the person, is also not able to check these holograms due to the technical limitations of the used smartphones (IDnow 2018a).

The overall assessment of the ID document is based on analysis results of several histograms. Thus, if some of the modelled holograms lead to a confidence below the pre-defined threshold, the entire integrity test still can succeed, if a sufficient number of the remaining security features is validated.

6.5 BPMN Process Controlled Analysis Application

All the process steps mentioned before, are called when a specific BPMN step is reached, see section 3.1. At the moment, an android demo app exists, where the process can be tested with respect to effectivity, efficiency and usability. As mentioned in chapter 4, the implementation utilizes a REST-Interface to communicate with the server. To establish this asynchronous connection, Service Tasks and User Tasks are used inside the BPMN processes. Service Tasks execute Java code, and are completed once the function call returns. Whereas User Tasks are active as long as a specific *complete* function is not called. During a User Tasks, the user has the possibility to send data to the server. This data is then assigned to the current active user task. This kind of implementation not only allows asynchronous communication, but it gives the possibility to check for a valid user behavior in a specific task.

6. DISCUSSION AND CONCLUSIONS

The results provide a high enough confidence to enable automated identification of a person. It already showed its power in the detection of the ID, as well as in the face recognition and OCR.

Nevertheless, a long-term test is required to check the full capabilities of the presented methods. Therefore, the system will be used beside the normal video identification process. Then the results of the software system will be compared to the video identification process. According to these results, the processes will then be revised to fit the adapted requirements.

In this work, it has been shown that the BPMN based modular identification process is highly applicable for automation of online user identification.

Future developments will incorporate automatic optimization of the process order and feedback strategies to be evaluated in a user study. In this context, relevant metrics are effectiveness, average time consumption for online identification and the number of process modules that have to be utilized to successfully guide a user through the identification process.

A very interesting aspect of high relevance is optimization of the applied human-computer-interaction paradigms. Thus, display annotations, textual directives and voice commands can be evaluated with respect to user cooperativeness. Besides, the tolerance intervals and the response are target of process optimization too.

7. OUTLOOK

The process has mainly been tested against cooperative and friendly users. Nevertheless, it is important to consider attacks on the system, since the research is conducted with a financial use case. Therefore, it is necessary to make the system tamper proof. In the next versions of the system, some additional security features have to be implemented. Moreover, in the field

of the hologram detection, there is still some work to do. Especially with different versions of IDs, it is necessary to extend the model, to be able to create models with different security features. For some holograms, new algorithms need to be implemented. For example, on some versions of the German ID, there is a hologram, which shows the face of the owner. In this case, it is not possible to create predefined comparison images, because the holograms are different on every ID.

The system consists of small process steps. These can be split up into even smaller sub-process steps, defining a more fine-granular process. By using non-deterministic sub-process-steps, it establishes the possibility to be tamper proof against prerecorded video inputs.

Another attack possibility would be that the attacker wears a mask of another person. A possible countermeasure would be to compare the confidence values of the face detection over multiple frames. A mask should lead to more homogenous confidence values than a real face. Moreover, Microsoft Face API could be used to receive additional information about the emotions as well as the face expressions of the person. If they are similar over multiple frames, it is an indication, that there is a manipulation attempt.

Finally, additional security checks for the ID could be implemented. For example, the flexibility, meaning if the document itself can be bent or shaped, of the ID can also be an additional information, which can be used to achieve even higher confidence.

ACKNOWLEDGMENTS

REFERENCES

Adamczyk P., Smith P.H., Johnson R.E., Hafiz M., 2011. REST and Web Services: In Theory and In Practice. In: *REST: From Research to Practice*, E. Wilde and C. Pautasso, Eds. Springer New York, 35–57. Available from: https://www.researchgate.net/publication/2652364 89_REST_and_Web_Services_In_Theory_and_in _Practice [accessed 26th March 2018].

Ahonen T., Hadid A., Pietikainen M., 2004. Face Recognition with Local Binary Patterns. In: T. Pajdla and Matas J. (Eds.): ECCV, *Lecture Notes in Computer Science LNCS* 3021:469-481, Springer Berlin Heidelberg (Germany).

Ballard D.H., 1981. Generalizing the Hough Transform to Detect Arbitrary Shapes. In *Pattern Recognition*, 13(2):111-122.

Bay H., Ess A., Tuytelaars T., Van Gool L., 2008. SURF – Speeded Up Robust Features. In *Computer Vision and Image Understanding* (CVIU), 110(3):346—359.

Bevilacqua V., Caprioli M., Cortellino M., Giannini M., Mastronardi G., Santarcangelo V., 2010. ACCURACY OF 3D FACE RECOGNITION FRAMEWORKS. In: Wagner W., Székely, B. (eds.): *ISPRS TC VII Symposium – 100 Years ISPRS*, Vienna, Austria, vol. 38, part 7B.

Bundesfinanzministerium, 2017. *Gesetz zur Umsetzung der Vierten EU-Geldwäscherichtlinie, zur Ausführung der EU-Geldtransferverordnung und zur Neuorganisation der Zentralstelle für Finanztransaktionsuntersuchungen*. Translation: Law for implementation of the fourth EU-Moneylaundering-Guideline for Execution of the EU-Moneytransfer-Ordinance and for reorganization of the central department for financial-transaction-investigation Available from https://www.bundesfinanzministerium.de/Content/ DE/Downloads/Gesetze/2017-06-24-G-z-Umsetzung-Vierte-Geldwaescherichtlinie.pdf [accessed 10th April 2018]

Burage-Lefebvre C., Cotmellec S., Lebrun D., Ozkul, C., 2000. Application of wavelet transform to hologram analysis: three-dimensional location of particles. In: *Optics and Lasers in Engineering*, 33(6):409– 421.

Brunelli R., Poggio T., 1992. *Face Recognition through Geometrical Features*. In: Proc. of the European Conference on Computer Vision (ECCV):792-800.

Camunda, 2018. *Camunda BPM Features*. Available from https://camunda.com/enterprise/ [accessed 26th March 2018].

Cootes, T.F., Edwards, G.J., Taylor, C.J., 1998. *Active Appearance Models*. In Proceedings of the 5th European Conference on Computer Vision, 484-498. June 2-6, Freiburg (Germany).

Gutierrez F., *2014. Introducing Spring Framework: A Primer*. Apress Berkely, (USA).

Hartl A., Grubert J., Schmalstieg D., Reitmayr G., 2013. *Mobile Interactive Hologram Verification*. In: Proc. of the IEEE International Symposium on Mixed and Augmented Reality (ISMAR, 75-82.

Hartl A., Arth C., Schmalstieg D., 2014. *AR-Based Hologram Detection on Security Documents Using a Mobile Phone*. In: Proc. of the 10th International Symposium ISVC 2014 on Advances in Visual Computing, Las Vegas (USA), 335-346.

ICAO, 2018. *Machine readable Travel Documents*. Available from https://www.icao.int/publications/pages/publicatio n.aspx?docnum=9303 [accessed 10th April 2018]

IDnow, 2018a. *IDnow Technology*. Available from https://www.idnow.de/technologie [accessed 26th March 2018].

IDnow, 2018b. *IDnow Video-Ident*. Available from https://www.idnow.de/produkte/video-identifizierung [accessed 26th March 2018].

Jähne B., 2012. *Digitale Bildverarbeitung und Bildgewinnung*. Berlin, Springer. Available from http://www.springer.com/de/book/9783642049514 [accessed 26th March 2018].

Janucki J., Owsik J., 2003. A Wiener filter based correlation method intended to evaluate

effectiveness of holographic security devices. In: *Optics Communications* 218:221-228.

Kanade T., 1973. *Picture Processing System by Computer Complex and Recognition of Human Faces*, Thesis (PhD.) Kyoto University, Japan.

Lowe D.G., 2004. Distinctive Image Features from Scale-Invariant Keypoints. In: *International Journal of Computer Vision* 60(2):91-110, Kluwer Academic Publishers Hingham, MA, USA.

Meier A., Stormer H., 2012. *eBusiness & eCommerce Management der digitalen Wertschöpfungskette*. Springer.

Microsoft 2018. *Microsoft Azure – Cognitive Services*. Available from https://azure.microsoft.com/en-us/services/cognitive-services/ [accessed 26th March 2018].

OMG, 2011. *Business Process Model And Notation Specification Version 2.0*. Available from https://www.omg.org/spec/BPMN/2.0 [accessed 26th June 2018]

OpenCV, 2018a. *OpenCV - Open Source Computer Vision Library*. Available from https://opencv.org/about.html [accessed 26th March 2018].

OpenCV, 2018b. *OpenCV - Template Matching*. Available from https://docs.opencv.org/2.4.13/doc/tutorials/imgproc/histograms/template_matching/template_matching.html [accessed 26th March 2018].

OpenCV, 2018c. *OpenCV – Face Recognition with OpenCV*. Available from: https://docs.opencv.org/2.4/modules/contrib/doc/facerec/facerec_tutorial.html [accessed 26th March 2018].

OpenCV, 2018d. *OpenCV – Scene Text Recognition*. https://docs.opencv.org/3.0-beta/modules/text/doc/ocr.html Available from: [accessed 26th March 2018].

Pointner A., 2017. *Bildverarbeitungsmethoden zur Personenidentifikation*. Thesis (BSc.). University of Applied Sciences Upper Austria.

Pramila A., Keskinarkaus A., Rahtu E., Seppänen T., 2011. Watermark Recovery from a Dual Layer Hologram with a Digital Camera. In: Heyden A., Kahl F. (eds) *Image Analysis. SCIA 2011. Lecture Notes in Computer Science* 6688. Springer, Berlin, Heidelberg (Germany).

Rublee E., Rabaud V., Konolige K., Bradski G.A., 2011. ORB – An efficient alternative to SIFT and SURF. In *IEEE International Conference on Computer Vision ICCV* 2011, 2564-2571.

Smith R., 2007. *An Overview of the Tesseract OCR Engine*. Available from https://github.com/tesseract-ocr/docs/blob/master/tesseracticdar2007.pdf [accessed 26th March 2018].

Sonka M., Hlavac V., Boyle R., 2007, *Image Processing, Analysis, and Machine Vision*. Thomson-Engineering, ISBN 049508252X.

Turk M., Pentland A., 1991. Eigenfaces for recognition. In: *Journal of Cognitive Neuroscience* 3:71-86.

Vuforia, 2018a. *Vuforia in Unity*. Available from https://www.vuforia.com/ [accessed 26th March 2018].

Vuforia, 2018b. *Vuforia - Optimizing Target Detection and Tracking Stability*. Available from https://library.vuforia.com/articles/Solution/Optimizing-Target-Detection-and-Tracking-Stability.html#natural [accessed 26th March 2018].

Zustellgesetz, 2008. *§17 Zustellung*. Available from https://www.jusline.at/gesetz/zustg/paragraf/17 [accessed 26th March 2018].

Meyer F., 1992. *Color image segmentation*. In: Proc. of the International Conference on Image Processing and its Applications.

AUTHORS BIOGRAPHY

Andreas M. Pointner was born in Wels, Austria and attends the University of Applied Sciences Upper Austria, Campus Hagenberg where he studied software engineering and graduated BSc. in 2017. In 2017, he started software engineering master. Since 2017, he is a research assistant in the research group AIST.

Oliver Krauss, born in Salzburg, Austria attended the University of Applied Sciences Upper Austria in the Software Engineering bachelor and master programs. He joined the research group AIST in 2012 as a research associate, and has been a lecturer in the Software Engineering and Medical and Bio-informatics programs since 2014. He is an active member of the Health Level 7 (medical data-exchange standardization organization) project on workflow management in medical data exchange. He is currently enrolled in the PhD program at the Faculty of Engineering & Natural Sciences at the Johannes Kepler University Linz, in the field of genetic improvement of performance in interpreters and compilers.

Gerald A. Zwettler was born in Wels, Austria and attended the University of Applied Sciences Upper Austria, Campus Hagenberg where he studied software engineering for medicine and graduated Dipl.-Ing.(FH) in 2005 and the follow up master studies in software engineering in 2009. In 2010 he has started his PhD studies at the University of Vienna at the Institute of Scientific Computing, where he received his degree in December 2014. Since 2005 he is working as researcher and lecturer at the Upper Austrian University of Applied Sciences at the school of informatics, communications and media at the Campus Hagenberg in the field of medical image analysis and software engineering with focus on computer-based diagnostics support and medical applications. Since 2017 he is associate professor at the software engineering department and since 2018 head of research group AIST in the field of advanced information systems and technology.

SURROGATE-ASSISTED HIGH-DIMENSIONAL OPTIMIZATION ON MICROSCOPIC TRAFFIC SIMULATORS

Bernhard Werth[a], Erik Pitzer[b], Gerald Ostermayer [c], Michael Affenzeller[d],

[a],[b],[d] Heuristic and Evolutionary Algorithms Laboratory, University of Applied Sciences Upper Austria, Hagenberg
[a],[d] Institute for Formal Models and Verification, Johannes Kepler University, Linz, Austria
[c] Research Group Networks and Mobility, University of Applied Sciences Upper Austria, Hagenberg

[a]bernhard.werth@fh-hagenberg.at, [b]erik.pitzer@fh-hagenberg.at,
[c]gerald.ostermayer@fh-hagenberg.at [d]michael.affenzeller@fh-hagenberg.at

ABSTRACT

Microscopic traffic simulation is able to capture many details of a traffic system, which makes it inherently interesting for simulation-based optimization. However, the considerable computational effort required for a single simulation run limits the use of standard heuristic optimization techniques and encourages the use of surrogate models to facilitate the search for an optimal solution. In this work, a grey-box surrogate model for microscopic traffic simulations is presented which allows the optimization of high-dimensional traffic optimization problems without relying on geographic or simulation-specific knowledge.

Keywords: traffic simulation, surrogate assisted optimization, evolutionary algorithms, noisy optimization

1. INTRODUCTION

With ever-increasing computing power, more and more complex and detailed simulations for traffic systems are created. Those simulations are generally divided in macroscopic and microscopic systems. While macroscopic simulators aim to capture traffic "en large", such simulations are computationally very efficient on a "per vehicle" basis, meaning that macroscopic simulations usually target road networks covering larger geographical areas and millions of vehicles participating in these networks (Geroliminis and Daganzo 2007). Microscopic traffic simulations, on the other hand, aim to capture intricate aspects of traffic, ranging from weather conditions (Samoili et al. 2011) and accidents to impacts of intelligent traffic light systems (Wiering et al 2004). As such, microscopic simulations are interesting for any number of optimization tasks, which could positively affect public and private transport. The simple fact that microscopic traffic simulation is a computationally expensive operation is a substantial hindrance for black-box optimization algorithms that require up to tens of millions of evaluations for a single optimization run. Surrogate-assisted optimization techniques are a common tool for alleviating some of the computational work. In surrogate-assisted optimization algorithms (SOAs), expensive computer experiments are approximated with a continuously updated generic regression model and only promising solution candidates are simulated.

A drawback of the classic surrogate optimization methods is that they quickly lose their performance with increasing problem dimensionality and dimensionality reduction techniques require specific decomposability properties (Werth et al. 2017, Shan and Wang 2010).

The pursuit of a type of surrogate model that allows heuristic optimization on microscopic traffic simulators, without being intrinsically tied to a specific type of simulator, is therefore a logical next step. In this paper, we present a general idea on how to construct gray-box surrogate models that require little knowledge of the traffic and logistics domain and compare variants thereof to classic surrogate-assisted optimization procedures.

The investigated optimization problem is the optimization of the departure times of 1000 vehicles traversing the northern part of the city of Linz, Austria, with the goal of minimizing the average travel time for all vehicles. This constitutes an optimization problem of high dimensionality. The microscopic traffic simulator, *TraffSim* (Backfrieder, Ostermayer and Mecklenbräuker 2015) was used, which enables the platform-independent and time-discrete simulation of vehicular traffic using a variety of configurable models.

The remainder of the paper is structured as follows: Section 2 presents related work on optimization in context of traffic simulation and surrogate-assisted optimization. In Section 3, the proposed method of surrogate model creation is described. Section 4 contains experimental results, concerning the accuracy and validity of the surrogate model with respect to the simulation and its applicability to optimization, while in Section 5, conclusions are drawn and future work is sketched out.

2. RELATED WORK

Generally speaking, there are two groups of optimization task of significant importance. In *model calibration* tasks, real-world data is gathered and heuristic optimization methods are employed to fine tune a microscopic simulator to most closely reflect and reproduce the data (Chiappone et al. 2016). The number of different algorithms proposed and used for this task is considerable, ranging from manual calibration (Moridpour et al. 2012) to multistart techniques (Ciuffo et al. 2008), neural networks (Otković et al. 2013) and many variants of genetic algorithms (Ma, Abdulhai, 2002; Sánchez-Medina et al. 2010; Qin et al. 2016; Cobos et al. 2016) and many more.

The second class of optimization tasks is the adjustment of some controllable traffic parameters (routes, traffic lights, traffic signs or even travel demands) with the goal to better utilize the real road network. Here, the simulation is used to estimate the effect of these adjustments as consecutive real tests would be unfeasible.

Macroscopic traffic simulators provide simulations for large numbers of vehicles for huge networks and/or long time horizons but are only suitable for optimization, if the parameter for which optimization is desired, is actually captured in the simulation. This might be a hindrance to some optimization tasks as macroscopic traffic simulators often have to calculate vehicular traffic as a flow of vehicle densities, which prohibits optimization on a per-vehicle or per-traffic-light basis. Microscopic traffic simulators like CORSIM (http://mctrans.ce.ufl.edu/featured/tsis/), VISSIM (www.vissim.de), PARAMICS (www.sias.com/paramics/) SUMO (http://sumo.dlr.de/index.html), or MITSIM (Yang, Koutsopoulos 1996), on the other hand try to capture the movement of each individual vehicle. An easy-to-read overview of the differences between macroscopic, microscopic and mesoscopic simulations, relevant models and techniques as well as the historical development can be found in (Miller et al. 2017).

In their effort to reflect reality as close as possible, microscopic traffic simulators are subject to a large number of demands. As stated in (Harri et al. 2009), accurate topological maps, precise and smooth acceleration and deceleration models, and models for intelligent driving patterns should be part of a microscopic traffic simulator. Furthermore, the simulator should be able to cope with obstacles for both driving and communication as well as attraction points and simulation time that give rise to non-random or only slightly non-deterministic vehicle distributions. Furthermore, traffic simulators are often used to gauge the effects of new technologies including but not limited to electric cars, automated driving, car-to-car- and car-to-vehicle-communication, intelligent traffic lights and variable speed limits.

In many cases of simulation-based optimization, the simulation serves as an *evaluation* function for the optimization process, that is trying to minimize or maximize a given *objective value*. The simple fact, that modern simulations usually provide no closed mathematical form for this objective value, much less a gradient thereof, requires the use of *heuristic* optimization approaches. Techniques like Genetic Algorithms (Holland 1992), Evolution Strategies (Bayer, Schwefel 2002), Simulated Annealing (Kirkpatrick, Gelatt, Vecchi 1983), Taboo Search (Gloyer, McMillan 1986) and Particle Swarm Optimization (Eberhart, Kennedy 1995) have proven time and time again, that they can provide satisfactory results given a certain computational budget. This budget usually encompasses several hundreds of thousands, if not millions of evaluations, which is justifiable only for problems that are fast to evauate like the Travelling Salesman (Applegate et al. 2006), Knapsack (Kellerer et al. 2004), Capacitated Vehicle Routing Problem (Toth, Vigo, 2014) or variations thereof. Simulations of complex systems, however, often require several minutes or even hours to calculate, quickly ruling out many heuristic algorithms. This predicament only worsens when facing higher-dimensional problems, where many parameters need to be optimized simultaneously, which in turn increases the required number of evaluations.

In order to enable heuristic optimization on more computationally expensive simulations, the use of surrogate models is a well-established method. Surrogate models are usually general regression models including Polynomial Regression (Gunst 1996), Regression Trees (Bajer, Pitra, Holeňa 2015), Gaussian Processes (Jones, Schonlau, Welch 1998), Artificial Neural Networks and Support Vector Machines. These models are faster to evaluate than full simulations and often describe the connection between parameters and objective function sufficiently to either find an optimal parameter setting directly or enhance an existing heuristic algorithm. A notable difference of surrogate models is their application as either *global* or *local* models (Zhou et al. 2007). Global models present the more straight forward way of utilizing all available previous evaluations as training data to create a regression model, spanning the entire search space. Local models, on the other hand, use fewer data points allowing to capture smaller structures and correlations in the vicinity of the restricted training data more clearly.

A significant restriction of surrogate-assisted heuristic optimization algorithms is their limitation to a comparatively low number of parameters (Werth et al. 2017, Shan and Wang 2010). Many potential optimizations in traffic systems incorporate large numbers of parameters and microscopic traffic simulations often require several minutes up to hours to finish. This requires specialized models and strategies to deal with these challenges in traffic optimization.

3. PROPOSED MODEL

Usually when applying surrogate-assisted optimization algorithms, the optimization problem is treated as a complete black box, where only input and output values are known, but no intermediate results. This requirement can be relaxed a bit to make optimization more feasible. Nevertheless, a surrogate model should keep a certain degree of genericity, so small code changes in the traffic simulator do not need to be reflected in the model. This also creates the benefit that the traffic simulator can be exchanged without creating new types of surrogate models. Therefore, only data that every microscopic traffic simulator is likely to be able to provide should be used in the construction of our surrogate model.

A minimum requirement for a microscopic traffic simulation is the availability of positions and vehicle IDs for each time step, thus, a reliance on the information which vehicle entered which road segment at which time should be enough. TraffSim has therefore been extended to return not only the cumulative driving time of all vehicles but also a list of additional pieces of information. Table 1 shows an example of this data.

Table 1: Routing data from a single simulation

VehicleID	SegmentID	ArrivalTime
V_1	S_2	13.4
V_2	S_1	15.3
V_1	S_1	16.8
…	…	…

Construction of the proposed surrogate model works by creating a directed graph of road segments (later called segments for simplicity) from the throughput data by first extracting consecutive routes (see Table 2) and inferring edges between segments from these routes. Also note, that in this graph, individual road segments are denoted by nodes, which makes the segment graph a *line graph* (Hararay and Norman 1960) in contrast to the more intuitive representation of a road network, where intersections are represented by nodes and streets are considered to be edges.

Table 2: Vehicle routes in terms of segments

VehicleID	Route
V_1	$S_2\ S_1\ S_3\ S_4$
V_2	$S_1\ S_3\ S_5$

The left side of Figure 1 depicts such a segment graph created from the two routes listed in Table 2, while the right side shows a simplified version where segments with a single connection are contracted into a single node. Please note that this graph was created using only the chronological ordering of road segments and no geographical information was required from the microscopic traffic simulator.

Each node of the graph is then associated with a regression model, that predicts the time required for a vehicle to traverse this segment. Disregarding what the actual inputs of these regression models are, one can derive two general schemes for inferring the arrival time of a vehicle:

1. The *naïve approach* where each vehicle is treated independently by summing over all times predicted by the node models. While this method ignores the effects of how different vehicles influence each other, the ability to optimize each vehicle separately, greatly alleviates difficulties for the optimization algorithms working with the surrogate. The surrogate problem becomes *linearly separable.*

2. The *parallel approach* tries to infer the arrival times of all vehicles simultaneously by taking into account the positions of all other vehicles, when predicting the time required to pass a certain segment. The practical implementation boils down to a very simplified version of discrete event simulation. Figure 2 presents a concrete example of how surrogate model evaluation would commence for the vehicles and routes from Table 2 on the simplified graph from Figure 1. The separability of the surrogate model is, of course, lost, but it should be noted that the parallel approach needs to perform exactly the same number of queries of the individual regression models as the naïve approach. The additional computational effort of maintaining the priority queue was negligible in preliminary experiments.
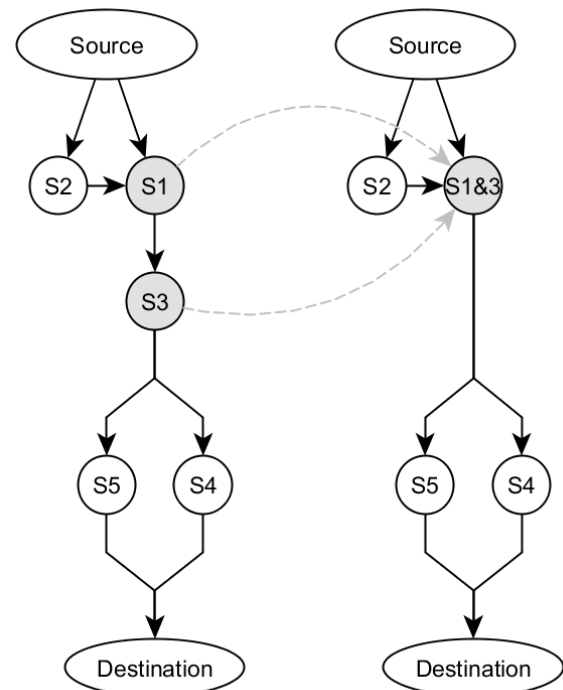
Figure 1: Segment graph and its simplification;
The nodes S_1 and S_3 are contracted into a new node $S_{1,3}$, preserving incoming and outgoing edges.

Vehicle: 1	Vehicle: 2
Segments: 2,(1&3),4	Segments: (1&3),5
Time: 00:00:18	Time: 00:00:25

Traversing
Segment 2:
22s

Vehicle: 2	Vehicle: 1
Segments: (1&3),5	Segments: (1&3),4
Time: 00:00:25	Time: 00:00:40

Traversing
Segment (1&3):
13s

Vehicle: 2	Vehicle: 1
Segments: 5	Segments: (1&3),4
Time: 00:00:38	Time: 00:00:40

Traversing
Segment 5:
24s

Vehicle: 1	Vehicle: 2
Segments: (1&3),4	Segments: []
Time: 00:00:40	Time: 00:01:02

Traversing
Segment (1&3):
13s

Vehicle: 1	Vehicle: 2
Segments: 4	Segments: []
Time: 00:00:53	Time: 00:01:02

Traversing
Segment 4:
19s

Vehicle: 2	Vehicle: 1
Segments: []	Segments: []
Time: 00:01:02	Time: 00:01:12

Arrival: Vehicle 2

Vehicle: 1
Segments: []
Time: 00:01:12

Arrival: Vehicle 1

Figure 2: Example of arrival time prediction

Finally, this leads to the question which features and regression models of the surrogate traffic model should be used as basis for the prediction of the traversal times of each segment. Sensible features that can be constructed without requiring knowledge of the road network itself or details about traffic lights, need to be

selected. Intuitive features would be the *current time* as well as the number of vehicles, currently traversing a given segment (here called the *density* of a node). While an argument can be made that any constructed feature should be included in the regression models as it would probably increase prediction accuracy, doing so, heavily impacts the time it requires to evaluate one potential vector of start times on the surrogate. Long evaluation times would in turn slow down the optimization process to the point of infeasibility. Evaluating which features and model types are suitable for start time optimization, as well as the analysis of the effects, different constellations create from an optimization point of view, is paramount to balancing accuracy, runtime and "optimizability" of the model.

4. EMPIRICAL EVALUATION

In order evaluate the viability of the proposed surrogate model, both its prediction capabilities and its usefulness for optimizations must be analyzed. There are several levels at which this model can be examined.

First, the difficulty of learning a regression model for a single road segment has to be assessed. In Figure 3 the times required to pass segment 2049 (an often congested segment leading to a major bridge) in reference to the arrival time (the time the vehicle arrives at the segment) of the vehicle trying to traverse is shown. As can be seen, segment 2049 undergoes three major phases. In the first phase, traversal times are distributed with significant variance, but the emerging congestion becomes apparent. In the second phase, most segments leading to the bridge are fully congested. And once the system stabilizes, distinct lines of arrival times develop. These lines are the results of lane merging before the bridge. In the last segment the congestion disperses. Learning this behavior is not trivial and is also subject to concerns of realism. Optimizing the departure time of a vehicle by a few seconds as to secure this vehicle a better spot in the merging might be possible in a simulation-based optimization scenario, but in real traffic, with hundreds of unknown influencing parameters, such an optimization would be hardly justified.

Second, an analysis of the predicted arrival times (the time, when a vehicle arrives at its destination) is in order. In Figure 4, a typical scatter plot of the predicted and simulated arrival times is shown. While the predicted and simulated arrival times for most vehicles correlate really well, a significant portion of vehicles with lower estimated arrival times achieve even lower simulated arrival times. This is an effect of the surrogate model assuming a fixed route for each vehicle while, much like in reality, vehicles in *TraffSim* have the ability to find alternative paths, if the planed route is perceived to take longer than expected.
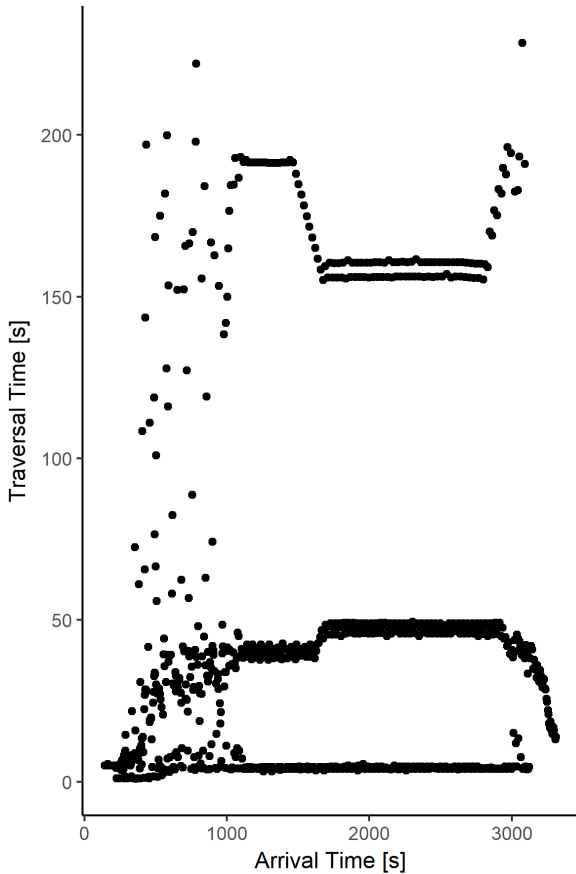
Figure 3: Simulated traversal times for a particularly crowded segment
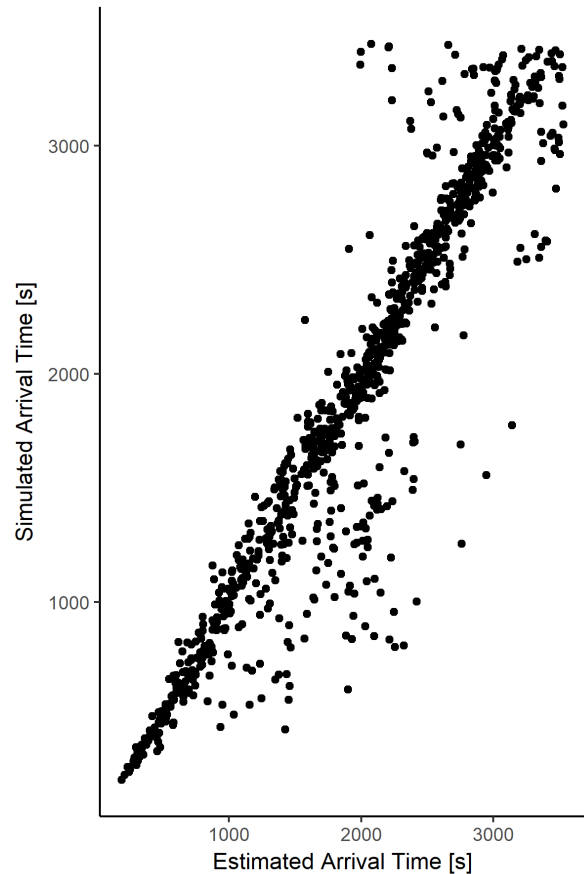
Figure 4: Predicted and simulated arrival times for all 1000 vehicles of one simulation

Third, the correlation between simulated and predicted arrival times over different departure time vectors that will later serve as solution candidates for the optimization is analyzed. In order to assess the capabilities of the model as a *local* surrogate, an *adaptive walk* (essentially a random search procedure with small search steps) was performed to gather data form multiple simulations concentrated in a small region of the search space. With this data, a model was built for every simulation and then used to predict the outcome of all other simulations. Figure 5 showcases the slow decay of simulation accuracy with increasing Euclidean distance between the departure time vectors as can be seen in the polynomial regression line (blue). While most predictions achieve accuracy rating above 0.75, a small number of times accuracy drops down to as low as 0.4, indicating widely different behavior between simulations or failures in building an adequate model.

Figure 6 compares the impact of density features on the arrival time prediction accuracy, with n specifying the "size" of the neighborhood for a segment model ($n = 0$ uses only the density of its own segment, $n = 1$ also uses the density of directly neighboring segments as features, $n = 2$ also includes the neighbors' neighbors and so on). Although faint, there is slight improvement in prediction quality for larger n. It has to be noted, that increasing n also increases the computational effort of building and evaluating a model up to a factor of ~15.
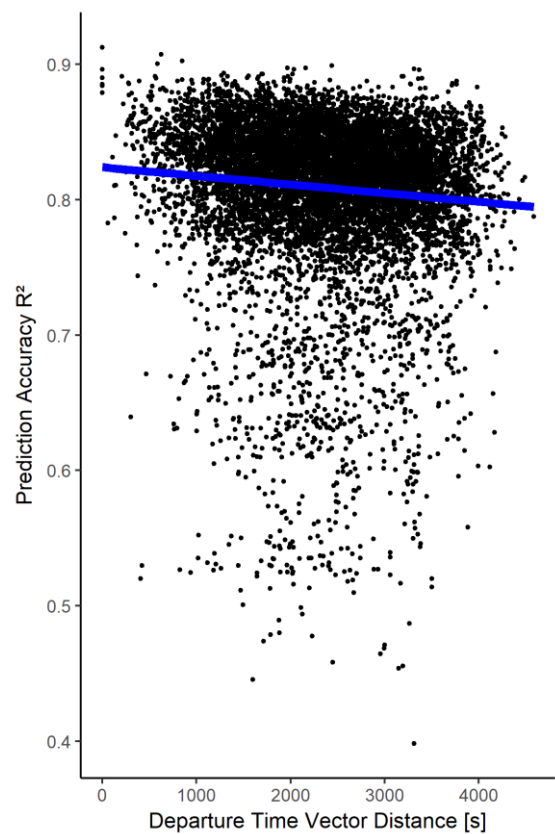
Figure 5: Decay of prediction accuracy with distance
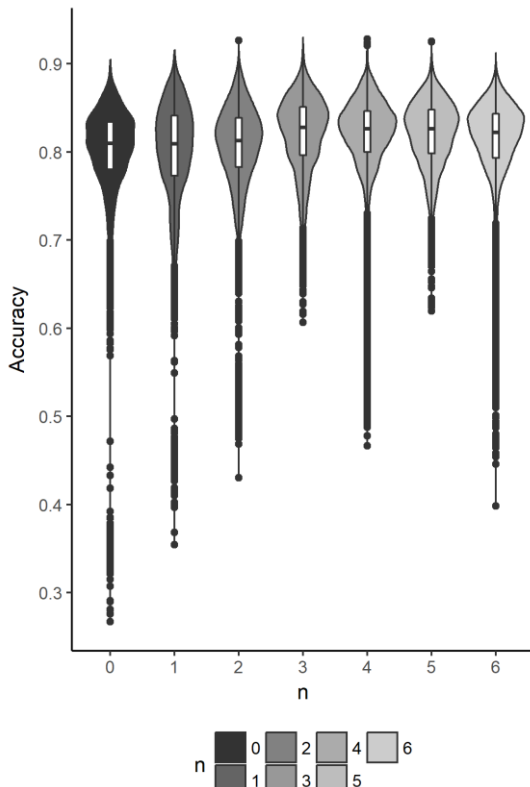
Figure 6: Predicted and simulated arrival times for all 1000 vehicles of one simulation

Last, to test the optimization potential, a simple *adaptive sampling* optimization scheme similar to the popular *efficient global optimization* algorithm (Jones, Schonlau, Welch 1998) is employed.

1. A random vector *r* of length 1000, representing the departure times of all vehicles, is created.

2. Vector *r* is evaluated on the microscopic traffic simulation and the throughput data from this simulation is collected.
3. A new surrogate model is constructed from the data collected in step 2.
4. 200 elements of *r* are selected at random and subjected to optimization using the surrogate model from step 3 and an offspring selection genetic algorithm (Affenzeller and Wagner 2005) is applied.
5. Vector *r* is updated with the optimized values. Go to 2 unless the computational budget (100 simulations) is exceeded.

Figure 7 shows the performance curves of an optimization run, where the regression models considered solely the time of entry for a segment and an optimization run, where the densities of each segment and directly neighboring segments were used as regression inputs. The time-based variant displays a pronounced periodic behavior alternating from very congested system states to states with lower overall driving time, while the density-based variant explores more continuously "good" regions of the search space.

As a reference point, the driving time for an (unachievable) "optimum" is given, where vehicles do not interact with each other in the microscopic simulation and can reach their destination via the shortest route with maximum allowed speed, completely unhindered by other traffic participants.

Please note that the initial selection for the starting times was chosen uniformly random from the given interval (30 minutes), which already constitutes a very good solution and both optimization runs managed to improve on that solution by approximately 10 %.
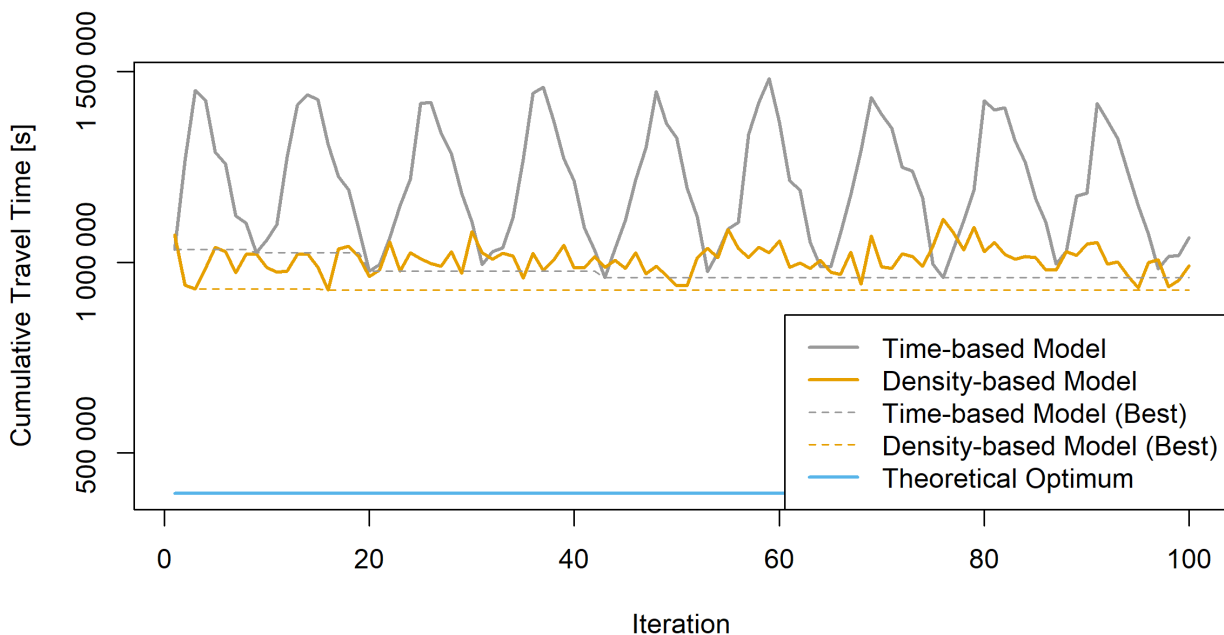
Figure 7: Performance graphs of optimization with time-based and density-based regression. Driving time is given in seconds

5. CONCLUSIONS

A new grey-box surrogate model for high-dimensional traffic optimization was proposed and analyzed on several levels. This grey-box approach allows to tackle a far more complex optimization task than standard surrogate-assisted black-box optimizers would.

Predicting the traversal time for individual segments is not easy, as segments display widely different behaviors, sometimes even with largely different phases during the simulation, as congestions build up and are resolved. It is, however, not required to accurately represent every such detail in the surrogate model, as effects over different segments can cancel themselves out. This allows for quite satisfying prediction accuracies for the arrival times of individual vehicles. An important lesson learned is that prediction accuracy is not the only metric with which a surrogate model needs to be measured. Different sets of features used in the model may lead to only insignificant differences in overall accuracy, but trigger widely different behavior under optimization. Furthermore, one has to be careful when optimizing traffic systems as not all influences and parameters can be controlled. Highly optimized solutions might not be favorable in the real world.

Future work will include mainly two major parts: First, the fact that surrogate models use the information from only one simulation and are not able to improve by incorporating new simulations is a disadvantage. Approaches to consolidate the information of multiple simulations into a single model could include the union of the datasets that serve as inputs for the individual segment models, the combination of those segment models to ensembles, by averaging or voting, or simply building multiple surrogate models and averaging their independent predictions. Second, the adaptive sampling scheme with the restriction of only optimizing a few vehicles per step is probably not the optimal choice for an optimization algorithm. More sophisticated algorithms, taking advantage of the locality of the model, like surrogate assisted genetic algorithms, might allow for even better optimization results.

REFERENCES

Affenzeller, M., & Wagner, S. (2005). Offspring selection: A new self-adaptive selection scheme for genetic algorithms. In Adaptive and Natural Computing Algorithms (pp. 218-221). Springer, Vienna.

Applegate, D. L., Bixby, R. E., Chvatal, V., & Cook, W. J. (2006). The traveling salesman problem: a computational study. Princeton university press.

Backfrieder, C., Ostermayer, G., & Mecklenbräuker, C. (2015). TraffSim—A traffic simulator for investigations of congestion minimization through dynamic vehicle rerouting. Int. J. Simul. Syst., Sci. Technol., 15(4), 38-47.

Bajer, L., Pitra, Z., & Holeňa, M. (2015, July). Benchmarking gaussian processes and random forests surrogate models on the BBOB noiseless testbed. In Proceedings of the Companion Publication of the 2015 Annual Conference on Genetic and Evolutionary Computation (pp. 1143-1150). ACM.

Beyer, H. G., & Schwefel, H. P. (2002). Evolution strategies–A comprehensive introduction. Natural computing, 1(1), 3-52.

Chiappone, S., Giuffrè, O., Granà, A., Mauro, R., & Sferlazza, A. (2016). Traffic simulation models calibration using speed–density relationship: an automated procedure based on genetic algorithm. Expert systems with applications, 44, 147-155.

Ciuffo, B., Punzo, V., & Torrieri, V. (2008). Comparison of simulation-based and model-based calibrations of traffic-flow microsimulation models. Transportation Research Record: Journal of the Transportation Research Board, (2088), 36-44.

Cobos, C., Daza, C., Martínez, C., Mendoza, M., Gaviria, C., Arteaga, C., & Paz, A. (2016, November). Calibration of Microscopic Traffic Flow Simulation Models Using a Memetic Algorithm with Solis and Wets Local Search Chaining (MA-SW-Chains). In Ibero-American Conference on Artificial Intelligence (pp. 365-375). Springer, Cham.

Eberhart, R., & Kennedy, J. (1995, October). A new optimizer using particle swarm theory. In Micro Machine and Human Science, 1995. MHS'95., Proceedings of the Sixth International Symposium on (pp. 39-43). IEEE.

Geroliminis, N., & Daganzo, C. F. (2007,). Macroscopic modeling of traffic in cities. In TRB 86th annual meeting (No. 07-0413)

Gloyer, F., & McMillan, C. (1986). The General Employee Scheduling Problem: an Integration of MS and AI. Computers & operations research, 13, 563-573.

Gunst, R. F. (1996). Response surface methodology: process and product optimization using designed experiments.

Harary, F., Norman, R. Z., (1960). Some properties of line digraphs. Rendiconti del Circolo Matematico di Palermo, 9(2), 161-168.

Harri, J., Filali, F., & Bonnet, C. (2009). Mobility models for vehicular ad hoc networks: a survey and taxonomy. IEEE Communications Surveys & Tutorials, 11(4).

Holland, J. H. (1992). Genetic algorithms. Scientific american, 267(1), 66-73.

Jones, D. R., Schonlau, M., & Welch, W. J. (1998). Efficient global optimization of expensive black-box functions. Journal of Global optimization, 13(4), 455-492.

Kellerer, H., Pferschy, U., & Pisinger, D. (2004). Introduction to NP-Completeness of knapsack problems. In Knapsack problems (pp. 483-493). Springer, Berlin, Heidelberg.

Kirkpatrick, S., Gelatt, C. D., & Vecchi, M. P. (1983). Optimization by simulated annealing. science, 220(4598), 671-680.

Ma, T., & Abdulhai, B. (2002). Genetic algorithm-based optimization approach and generic tool for calibrating traffic microscopic simulation parameters. Transportation Research Record: Journal of the Transportation Research Board, (1800), 6-15.

Miller, J. A., Peng, H., & Bowman, C. N. (2017, December). Advanced tutorial on microscopic discrete-event traffic simulation. In Simulation Conference (WSC), 2017 Winter (pp. 705-719). IEEE.

Moridpour, S., Sarvi, M., Rose, G., & Mazloumi, E. (2012). Lane-changing decision model for heavy vehicle drivers. Journal of Intelligent Transportation Systems, 16(1), 24-35.

Otković, I. I., Tollazzi, T., & Šraml, M. (2013). Calibration of microsimulation traffic model using neural network approach. Expert systems with applications, 40(15), 5965-5974.

Qin, Y., Dong, H., Zhang, Q., & Yang, Y. (2016, November). Parameter Calibration Method of Microscopic Traffic Flow Simulation Models based on Orthogonal Genetic Algorithm. In DMS (pp. 55-60).

Samoili, S., Bhaskar, A., Hai Pham, M., & Dumont, A. G. (2011). Considering weather in simulation traffic.

Sánchez-Medina, J. J., Galán-Moreno, M. J., & Rubio-Royo, E. (2010). Traffic signal optimization in "La Almozara" district in Saragossa under congestion conditions, using genetic algorithms, traffic microsimulation, and cluster computing. IEEE Transactions on Intelligent Transportation Systems, 11(1), 132-141.

Shan, S., & Wang, G. G. (2010). Survey of modeling and optimization strategies to solve high-dimensional design problems with computationally-expensive black-box functions. Structural and Multidisciplinary Optimization, 41(2), 219-241.

Toth, P., & Vigo, D. (Eds.). (2014). Vehicle routing: problems, methods, and applications. Society for Industrial and Applied Mathematics.

Werth, B., Pitzer, E., & Affenzeller, M. (2017, February). A Fair Performance Comparison of Different Surrogate Optimization Strategies. In International Conference on Computer Aided Systems Theory (pp. 408-415). Springer, Cham.

Wiering, M. A., Veenen, J. V., Vreeken, J., & Koopman, A. (2004). Intelligent traffic light control.

Yang, Q., & Koutsopoulos, H. N. (1996). A microscopic traffic simulator for evaluation of dynamic traffic management systems. Transportation Research-Part C Emerging Technologies, 4(3), 113-130.

Zhou, Z., Ong, Y. S., Nair, P. B., Keane, A. J., & Lum, K. Y. (2007). Combining global and local surrogate models to accelerate evolutionary optimization. IEEE Transactions On Systems, Man and Cybernetics-Part C, 37(1), 66-76.

A LUMPED PARAMETER MODEL OF AIRWAY/LUNG MECHANICS

Silvia Marconi[a], Claudio De Lazzari[b]

[a,b]Institute of Clinical Physiology, National Research Council, Rome
[b]National Institute for Cardiovascular Research, Bologna, Italy

[a]silvia.marconi@ifc.cnr.it, [b]claudio.delazzari@ifc.cnr.it

ABSTRACT

In this work we present a nonlinear lumped parameter model of the airway/lung mechanics. The model is able to reproduce the time evolution of the fundamental variables (pressure, flow and volume) within each compartment of the respiratory system during normal breathing. A particular attention is given to the pleural pressure that is the driving force of the system. Our purpose is to build a tool for a qualitative description of the lung/airway dynamics that is able to reproduce the physiological behavior of the main system variables. The aim of this work is to develop a model of the respiratory system and successively insert it into our numerical lumped parameter model of the cardiovascular system. In this way it will be possible to study the interactions between the cardiovascular, the respiratory system and the most used mechanical circulatory and ventilatory assist devices in terms of hemodynamic and energetic variables.

Keywords: airway/lung mechanics, nonlinear lumped parameter model, numerical simulation, normal breathing

1. INTRODUCTION

Human cardiovascular and respiratory systems are two complex systems interacting with each other. Zero-dimensional (0D) or lumped parameters models assume a uniform distribution of the fundamental variables (pressure, flow and volume) within each compartment of the respiratory and circulatory systems at any instant of time, thus reducing the complexity in their representation. Typically, a hydraulic and pneumatic electrical analogy is applied, so that the cardiovascular and respiratory systems can be represented by electrical circuits. Voltage and current correspond to pressure and flow (of blood or air); resistances and inductances correspond to friction and inertia (of blood in the vessels or air in the airways); capacitances correspond to elasticity properties or compliances (of cardiovascular or respiratory components such as vessels and lungs); Kirchhoff's laws correspond to mass and energy conservation laws. The governing equations of the model consist on a set of linear or nonlinear ordinary differential equations which has to be solved with proper initial conditions.

Many models can be found describing the respiratory system (Golden, Clark and Stevens 1973; Olender, Clark and Stevens 1976; Liu, Niranjan, Clark, San, Zwischenberger and Bidani 1998; Athanasiades, Ghorbel, Clark, Niranjan, Olansen, Zwischenberger and Bidani 2000; Masana 2015; Bersani, Bersani and De Lazzari 2017) and the cardiovascular system (Formaggia, Quarteroni and Veneziani 2009; Korakianitis and Shi 2006; Rideout and Snyder 1974; Shi 2007) but relatively few models can be found describing the interactions between them (Lu, Clark, Ghorbel, Ware and Bidani 2001; Hemalatha, Suganthi and Manivannan 2010).

A lumped parameter model for the cardiovascular system has been developed at Cardiovascular Numerical/Hybrid Modelling Lab (Institute of Clinical Physiology of the Italian National Research Council of Rome). This 0D model, named CARDIOSIM© (De Lazzari, Neglia, Ferrari, Bernini, Micalizzi, L'Abbate and Trivella, 2009; De Lazzari and Stalteri 2011; Capoccia, Marconi, Singh, Pisanelli and De Lazzari 2018), is made up of several modules describing the sections of the cardiovascular system. The software is a suitable and versatile environment to reproduce heart and circulation main features in both physiological and pathological conditions.

The final goal of this study is to develop a model of the respiratory system and insert it as a new modulus in CARDIOSIM©. In this way it will be possible to study the interactions between the cardiovascular, the respiratory system and the most used mechanical circulatory and ventilatory assist devices in terms of hemodynamic and energetic variables (De Lazzari, D'Ambrosi, Tufano, Fresiello, Garante, Sergiacomi, Stagnitti, Caldarera and Alessandri 2010; De Lazzari, Darowski, Ferrari, Pisanelli and Tosti 2006; De Lazzari, Darowski, Ferrari, Clemente and Guaragno, 2001; De Lazzari, Darowski, Ferrari and Clemente 1998; Colquitt, Colquhoun and Thiele 2011).

In this paper, we present the first results concerning only the airway/lung mechanics. Our purpose is to build a tool for a qualitative description of the lung/airway dynamics that is able to reproduce the physiological behavior of the

main system variables. In the future, the gas exchange will be added to complete the model. Once the model has been completed, the parameters will be properly set by fitting measured quantities and the model will be validated with clinical data.

A particular attention has been given to the pleural (or intra-thoracic) pressure which is the driving force of the model, as it is one of the principal factors that influence the cardio-pulmonary circulation. The model has been tested using some pleural pressure waveforms reproducing different kinds of normal breathing. Some preliminary results are presented.

The model has been implemented in MATLAB and solved in Simulink environment.

2. MATERIALS AND METHODS

2.1. Respiratory system

The model of the lung/airway mechanics considers the section of the respiratory system below the larynx, where the structures in which air flows divides into airways and alveoli. The lungs are considered as a unique alveolar region connected to the external environment through the airways which divide into the upper airway, the collapsible airway and the small, or peripheral, airways. The upper airway is considered as a rigid tubular structure; the collapsible airway is considered a tubular structure whose volume can change in time; the small airways are the ramified structures which lie in the lungs. Both alveolar region and most of the airways are surrounded by the pleural space. This space (containing the pleural fluid) separates the lungs visceral pleura from the internal parietal pleura of the chest wall (Bates 2009). The variables of the model are flow, pressures and volumes. The flow (F) of the air in the upper airway is the same as the airflow in the mouth. It is considered positive during expiration and negative during inspiration. The alveolar pressure (P_A), the collapsible airway pressure (P_C) and the pleural pressure (P_{pl}) are given with respect to environmental pressure (P_{ref}), which is set to zero. In our model the pressure at mouth (P_e) equals environmental pressure. Instead, the dynamic lung elastic recoil (P_{el}), or transpulmonary pressure, and the transmural pressure (P_{tm}) are referred to the pleural pressure. Thus we have:

$$P_A = P_{el} + P_{pl}, \qquad P_C = P_{tm} + P_{pl}. \tag{1}$$

Finally, we consider the alveolar volume (V_A) and the collapsible segment volume (V_C).

All these quantities vary in time. The spatially averaged pleural pressure is the driving pressure of the entire system. Its variation in time is caused by the contraction and relaxation of the respiratory muscles.

2.2. Model description

The electrical analogue of airway/lung mechanics is composed by four resistances, two capacitors and a generator (Fig. 1).
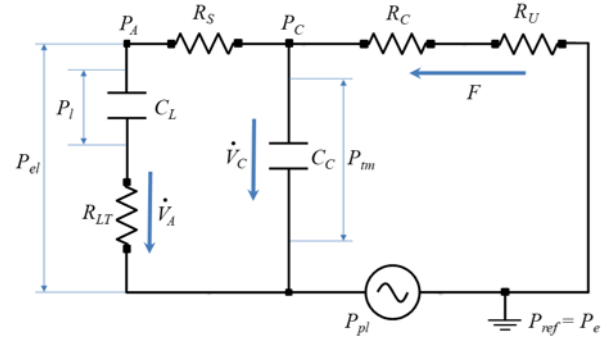
Figure 1: Electrical equivalent circuit of the airway/lung dynamics.

Each element characterizing each compartment of the respiratory system is defined as a function of the main variables (the flow F or the volumes V_A and V_C).

The resistive elements characterize the resistance of the corresponding compartment to the flow of air. The resistance of the upper airway (R_U) is given by:

$$R_U = A_u + K_u \,|\, F \,| \tag{2}$$

where A_u and K_u are positive constants.

The resistance of the collapsible airway (R_C) is given by:

$$R_C = K_c \left(\frac{V_{C\max}}{V_C} \right)^2 \tag{3}$$

where K_c is the value of the resistance when the volume reaches the maximum possible volume of the collapsible airway (V_{Cmax}).

The resistance of the small airways is given by:

$$R_S = A_s e^{-K_s \frac{V_A - V_R}{V^* - V_R}} + B_s \tag{4}$$

where A_s, K_s, B_s and V^* are positive constants and V_R is the residual volume that is the volume of air left in the lungs after a maximum expiratory effort.

Finally, the lung tissue viscous property is modelled by a constant resistance (R_{LT}).

The two capacitors simulate the compliance of the alveolar region and of the collapsible airway which expresses their elasticity (i.e. their ability to expand when a pressure change occurs). The currents passing through these elements are at any time the derivatives of the respective volumes and the pressure drop across them are the static lung elastic recoil (P_l) and the transmural pressure (P_{tm}), respectively. Their expressions are in Bersani, Bersani and De Lazzari (2017).

The generator simulates the pleural pressure (P_{pl}) which drives the respiratory process.

The electrical circuit is solved through Ohm's law and Kirchhoff's current and voltage laws:

$$\begin{cases} I = \dot{V}_A + \dot{V}_C \\ R_U I + R_C I + P_{tm} + P_{pl} = 0 \\ R_S \dot{V}_A + P_l + R_{LT} \dot{V}_A - P_{tm} = 0 \end{cases} \quad (5)$$

Substituting the first equation in the second, we obtain two nonlinear first order ordinary differential equations. V_A and V_C are the unknowns and P_{pl} is the input of the model.

The system in Eq. (5) has to be solved with proper initial conditions:

$$\begin{cases} V_A(0) = V_A^0 \\ V_C(0) = V_C^0 \end{cases} \quad (6)$$

The model has been implemented in MATLAB and solved in the Simulink environment through a variable time step Dormand-Prince method with a relative tolerance of 1×10^{-6}.

The parameters of the model are set as in Athanasiades, Ghorbel, Clark, Niranjan, Olansen, Zwischenberger and Bidani 2000 and Liu, Niranjan, Clark, San, Zwischenberger and Bidani 1998.

2.3. Pleural pressure

We tested the model response to three input pleural pressures simulating the regular breathing and two kinds of quiet breathing, respectively.

The respiratory frequency for the healthy adult at rest is about 12-18 breaths per minute and the pleural pressure keeps negative in a range of about -8 to -4 cmH_2O. In this work we consider a respiratory rate of 12 breaths per minute. Each respiratory act lasts 5 seconds. The pleural pressure oscillates in an overall range of -3.67 to -7.48 cmH_2O.

The pleural pressure of the regular breathing (P_{pl}^r) is taken from Bai, Zhang, Zhao, and Zhou (1998) (Fig. 2).

The pleural pressure waveform of the quiet breathing is inspired to those in Hemalatha and Manivannan (2010) and Lu, Clark, Ghorbel, Ware and Bidani (2001). These kinds of pleural pressure have been obtained applying a low-pass filter to a pulse generator. Setting the pulse amplitude, the duration of the pulse in each period and the values of the resistance and capacity, it is possible to change the waveform of the response, in order to obtain the desired final pleural pressure (Fig. 3).
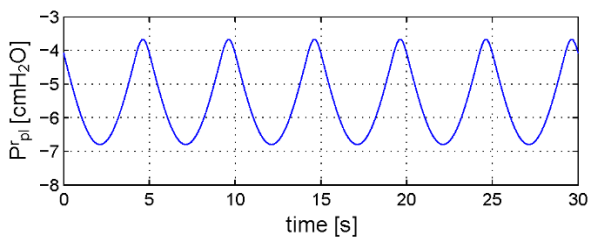
Figure 2: Pleural pressure of the regular breathing.
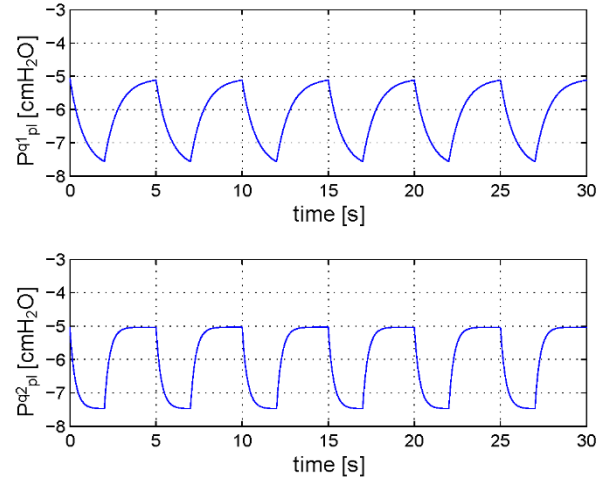
Figure 3: Two different pleural pressures (P_{pl}^{q1} and P_{pl}^{q2}) for the quiet breathing obtained from the RC circuit.

3. RESULTS

Figures 4 and 5 show the results when P_{pl}^r and P_{pl}^{q2} are applied as input of the model, respectively. In each figure, panel (A) shows the air flow at the mouth. Panel (B) shows the alveolar volume. Panel (C) shows the alveolar and the pleural pressures. Their difference at any instant of time is the dynamic elastic recoil. Panel (D) shows the flow-volume loop, where the volume is the total lung volume (V_L) referred to the residual volume (V_R). V_L is the sum of the alveolar volume, the collapsible volume and the death space (upper airway) volume (V_D):

$$V_L = V_A + V_C + V_D. \quad (7)$$

In normal breathing the difference $V_L - V_R$ keeps positive, since the lungs never collapse up to the residual volume. The loop is counterclockwise.

In regular breathing the pleural pressure keeps in a range of -6.80 to -3.67 [cmH_2O] while in quiet breathing it varies in a range of -7.48 to -5.03 [cmH_2O]. This causes the flow of air at mouth to be lower in regular breathing than in quiet breathing. In the first case the flow varies between -0.36 and 0.34 [l/s] (Fig. 4, panels A and D) while in the second it varies between -0.56 and 0.51 [l/s] (Fig. 5, panels A and D). Moreover, the flow waveforms show how fast or slow the air enters or exits the mouth in each respiratory cycle. This effect is highlighted in the differences in the flow-volume loops shape (Fig. 4 and 5, panel D).

Alveolar volume varies in a range of 3.10 to 3.59 [l] in the regular breathing and in a range of 3.32 to 3.69 [l] in the quiet breathing (Fig 4 and 5, panel B). The total lung volume varies accordingly, resulting in a horizontal shift of the flow-volume loops (Fig. 4 and 5, panel D).

The different waveforms of the pleural pressures are reflected also in the waveforms of alveolar pressure and elastic recoil (Fig. 4 and 5, panel C). The alveolar pressure varies between -0.55 and 0.54 [cmH_2O] in regular breathing and between -0.80 and 0.62 [cmH_2O] in quiet breathing.
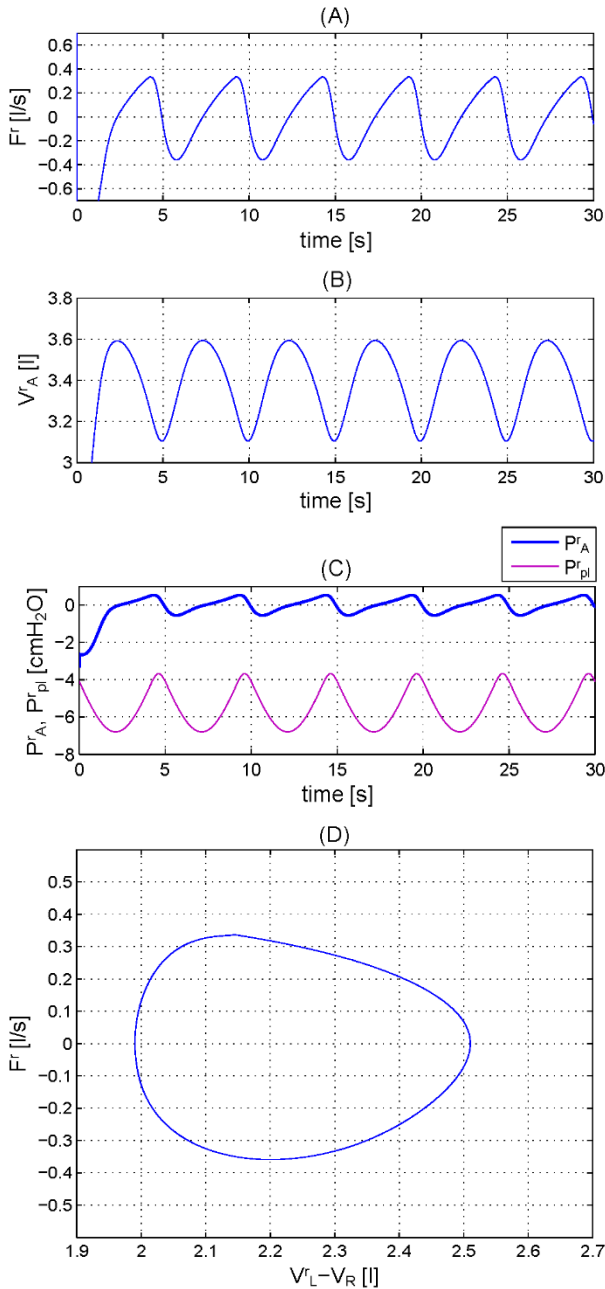
Figure 4: Simulation results: the pleural pressure of the regular breathing is applied as input in the model. (A) flow at the mouth; (B) alveolar volume; (C) alveolar pressure and pleural pressure; (D) flow-volume loop.

Figure 5: Simulation results: P^{q2}_{pl} is applied as input in the model. (A) flow at the mouth; (B) alveolar volume; (C) alveolar pressure and pleural pressure; (D) flow-volume loop.

These results are in agreement with data and simulations in the literature (Liu, Niranjan, Clark, San, Zwischenberger and Bidani 1998; Hemalatha, Suganthi and Manivannan 2010; Lu, Clark, Ghorbel, Ware and Bidani 2001; Masana 2015).

4. CONCLUSIONS

The nonlinear lumped parameter model of the airway/lung mechanics presented in this work is able to describe the time variation and the relations between the main variables of the respiratory system during normal breathing.

Our preliminary results regarding the flow-volume analysis are in accordance with data presented in literature.

We plan to test the model with other kinds of respiration and respiratory maneuvers. Also, increasing (emphysema) or decreasing (fibrosis) lung compliance and other lung diseases can be simulated using the presented model. A more in-depth study of the influence of the parameters on the model's response will come in the future as well as the proper setting of the parameters and the validation of the model by fitting measured data. Furthermore, gas exchange will be added to the model.

From the numerical point of view, suitable numerical schemes for the solution of the model will be considered to find out the most convenient and feasible way to make it dialogue with CARDIOSIM©, which is implemented using Visual Basic program language.

REFERENCES
Athanasiades A., Ghorbel F., Clark J.W. Jr., Niranjan S.C., Olansen J., Zwischenberger J.B. and Bidani A., 2000. Energy Analysis of a Nonlinear Model of the Normal Human Lung. Journal of Biological Systems, 8 (2), 115–139.

Bai J., Hongli L., Zhang J., Zhao B. and Zhou X., 1998. Optimization and mechanism of step-leap respiration exercise in treating of cor pulmonale. Computers in Biology and Medicine, 28, 289–307.

Bates J.H.T., 2009. Lung mechanics: an inverse modeling approach. Cambridge University Press.

Bersani A.M., Bersani E. and De Lazzari C., 2017. Interaction Between the Respiratory and Cardiovascular System: a Simplified 0-D Mathematical Model. In: De Lazzari C. and Pirckhalava M., eds. Cardiovascular and Pulmonary Artificial Organs: Educational Training Simulators. CNR Edizioni, 87–105.

Capoccia M., Marconi S., Singh S.A., Pisanelli D. and De Lazzari C., 2018. Simulation as a Preoperative Planning Approach in Advanced Heart Failure Patients. A Retrospective Clinical Analysis. BioMedical Engineering OnLine, 17, 52.

De Lazzari C., Stalteri D., 2011. CARDIOSIM© Cardiovascular Software Simulator National Research Council. Available from: http://cardiosim.dsb.cnr.it/Default.aspx.

De Lazzari C, D'Ambrosi A., Tufano F., Fresiello L., Garante M., Sergiacomi R., Stagnitti F., Caldarera, C.M., Alessandri N., 2010. Cardiac resynchronization therapy: could a numerical simulator be a useful tool in order to predict the response of the biventricular pacemaker synchronization? European Review for Medical and Pharmacological Science, 14 (11), 969–978.

De Lazzari C., Neglia D., Ferrari G., Bernini F., Micalizzi M., L'Abbate A., Trivella M.G., 2009. Computer simulation of coronary flow waveforms during caval occlusion. Methods of information in medicine, 48 (2), 113-122.

De Lazzari C., Darowski M., Ferrari G., Pisanelli D.M., Tosti G., 2006. Modelling in the study of interaction of Hemopump device and artificial ventilation. Computers in Biology and Medicine, 36 (11), 1235–1251.

De Lazzari C., Darowski M., Ferrari G., Clemente F., Guaragno M., 2001. Ventricular energetics during mechanical ventilation and intraaortic balloon pumping? computer simulation. Journal of medical engineering & technology, 25 (3), 103-111.

De Lazzari C., Darowski M., Ferrari G., Clemente F., 1998. The influence of left ventricle assist device and ventilatory support on energy-related cardiovascular variables. Medical Engineering and Physics, 20 (2), 83–91.

Colquitt R.B., Colquhoun D.A., Thiele R.H., 2011. In silico modelling of physiologic systems. Best Practice & Research Clinical Anaesthesiology, 25, 499–510.

Formaggia L., Quarteroni A. and Veneziani A., 2009. Cardiovascular Mathematics. Modeling and simulation of the circulatory system. Vol. 1. Springer-Verlag, Berlin, Heidelberg.

Golden J.F., Clark J.W. Jr. and Stevens P.M., 1973. Mathematical Modeling of Pulmonary Airway Dynamics. IEEE Transactions on Biomedical Engineering, BME-20 (6), 3247–3263.

Hemalatha K., Suganthi L. and Manivannan M., 2010. Hybrid Cardiopulmonary Model for Analysis of Valsalva Maneuver with Radial Artery Pulse. Annals of Biomedical Engineering, 38 (10), 3151–3161.

Liu C.H., Niranjan S.C., Clark J.W. Jr., San K.Y., Zwischenberger J.B. and Bidani A., 1998. Airway mechanics, gas exchange, and blood flow in a nonlinear model of the normal human lung. Journal of Applied Physiology, 84, 1447–1469.

Lu K., Clark J.W. Jr., Ghorbel F.H., Ware D.L. and Bidani A., 2001. A human cardiopulmonary system model applied to the analysis of the Valsalva maneuver. Americal Journal of Physiology-Heart and Circulatory Physiology, 281, H2661–H2679.

Masana F.N., 2015. Respiratory System Model Based on PSPICE. International Journal of Microelectronics and Computer Science, 6 (3), 102–109.

Olender M.F., Clark J.W. Jr and Stevens P.M., 1976. Analog Computer Simulation of Maximum Expiratory Flow Limitation. IEEE Transactions on Biomedical Engineering, BME-23 (6), 445–452.

Korakianitis T., Shi Y., 2006. A concentrated parameter model for the human cardiovascular system including heart valve dynamics and atrioventricular interaction. Medical Engineering & Physics, 28 (7), 613–628.

Rideout V.C., Snyder M.F., 1974. Computer simulation study of the cardiovascular and related physiological systems. Mathematics and Computers in Simulation, 16, 26–34.

Shi Y., 2007. Lumped-parameter cardiovascular model with Windkessel after-load. Auckland: CellML. Available from: http://models.cellml.org/exposure/ea64608ab564ee085bef7cde3ed1731e. Accessed on 2/7/12.

LOGIC-DYNAMIC MODEL AND ALGORITHMS OF OPERATION COMPLEX PLANNING OF ACTIVE MOBILE OBJECTS AUTOMATED CONTROL SYSTEM

Boris Sokolov[a], Aleksandr Kovalev[b], Vladimir Kalinin[c], Evgeniy Minakov[d], Dmitriy Petrovskiy[e]

[a], [b]SPIIRAS— St. Petersburg Institute of Informatics and Automation, Russian Academy of Sciences, 14th line 39, St. Petersburg, 199178, Russia
[c], [d]Military-space academy, Gdanovskaya str., 13, St. Petersburg, 197198, Russia
[e]NRUHSE(SPb) — National Research University Higher School of Economics (St. Petersburg), Kantemirovskaya Street 3A, St. Petersburg, 194100, Russia

[a]sokolov_boris@inbox.ru, [b] info@litsam.ru, [c]kvn.112@mail.ru
[d] ep.minakov12345@mail.ru, [e]inspectah28@gmail.com,

ABSTRACT
This article discusses the results of solving the problems of constructing an integrated schedule of active moving objects automatic control system (AMO ACS), which are based on proposed new approached to active mobile objects automated control system complex modeling. The main advantage of complex modeling (CM) is that the combined use of alternative models, methods and algorithms allows to compensate their objectively existing shortcomings and limitations while enhancing their positive qualities. In the paper, this advantage of CM is illustrated by the example of interconnection AMO ACS analytical logic-dynamic model for planning and scheduling with Petri net simulation model of possible scenarios for the implementation of the corresponding plans under conditions of various kinds of disturbing influences.

Keywords: complex modeling, active mobile objects, logic-dynamic models and algorithms for complex modeling, Petri nets

1. INTRODUCTION
At present, in order to increase the degree of forecasts validity and reliability for the development of existing and projected complex objects (CO) in such knowledge-intensive industries as ship-building, aerospace, fuel and energy and military-technical complexes, etc., a preemptive modeling and multivariate forecasting of various scenarios for realizing the life cycles of the objects under consideration.
In practice, for such situations, simulation modelling and corresponding models (SM) are most often used, (Chernousko and Lyubushin 1982; Choi, Yeung and Cheng 2013; Dejonckheere, Disney and Lambrecht 2004; Ye and Liu 2016). However, as analysis shows, at the present stage of the theory and technologies development of the CO simulation modelling, it is indispensable to considering the issues of its interaction with other theories and modeling technologies within the framework of an intensively developing concept of

complex (system) modeling (Aalst and Der 1992; Bozek and Wysocki 2015; Gubarev, Zakharov and Kovalenko 1988; Ivanov, Dolgui and Sokolov 2016a; Ivanov, Sokolov and Dolgui 2013; Ohtilev, Sokolov and Yusupov 2006).
This necessity is related to the following main features of existing and emerging CO: increased complexity and dimensionality, redundancy, multi-functionality, unification, homogeneity of the main elements, subsystems and connections of the CO; structural dynamics, nonlinearity and behavior unpredictability; hierarchical-network structure of the CO; non-equilibrium of CO functioning, uncertainty from choice of observer and it's interference for the CO; constant changes in the rules and technology of functioning, presence of both negative and positive feedback loops, leading to self-excitation modes activation (modes with exacerbation) of CO; along with deterministic and stochastic behavior, chaotic behavior of the CO is possible; no element has full information about the entire system; selective sensitivity to input effects (dynamic robustness and adaptation); the response time of the CO to changes caused by disturbing effects is greater than the time of manifestation of these changes consequences and, including, than the interval between these changes; absolute completeness and reliable information describing the real CO cannot be obtained in principle, with accordance to the Bremermann limit and Gödel's theorem (Harjunkoski, Maravelias and Bongers 2014; Ohtilev, Sokolov and Yusupov 2006; Pinedo 2008; Sotskov, Lai and Werner 2013).
Further, we will designate complex (system) modeling (CM) of complex objects (CO) of any nature CO (natural, artificial, real, and virtual, etc.) as the methodology and technologies of the specified objects model description, as well as the combined use of methods, algorithms and methodologies of multi-criterial analysis, synthesis and selection of the most preferable management decisions related to the creation, use and development of the objects under consideration under various conditions, the dynamically changing

external and internal environments (Ohtilev, Sokolov and Yusupov 2006).

The main advantage of CM is that the combined use of alternative models, methods and algorithms allows to compensate their objectively existing shortcomings and limitations while enhancing their positive qualities. The ideological side of the CM was laid by the great physicist N. Bohr when he formulated the principle of complementarity (Gubarev, Zakharov and Kovalenko 1988; Ohtilev, Sokolov and Yusupov 2006).

According to this principle, for a full description of quantum-mechanical phenomena it is necessary to apply two mutually exclusive ("additional") sets of classical concepts, aggregation of which provides exhaustive information about these phenomena as about holistic phenomena. The application of the principle of complementarity over time led to the creation of a concept of complementarity, encompassing not only physics, but also biology, psychology, cultural studies, and humanitarian knowledge in general.

It should be noted that the development and widespread implementation in practice in the last decade of such intelligent information technologies (IIT) as, for example, artificial neural net-works, multi-agent systems, fuzzy logic, evolutionary modeling technologies, etc., led to the appearance of yet another type of simulation — hybrid modeling (HM) (Giglio 2015; Harjunkoski, Maravelias and Bongers 2014; Hwanf, Fan and Erikson 1967; Ivanov, Dolgui and Sokolov 2016b; Ohtilev, Sokolov and Yusupov 2006; Sarimveis, Patrinos and Tarantilis 2008; Werner and Sotskov 2014).

These circumstances explain the particular relevance of the simulation modeling (SM) inter-action study with other types and modeling technologies (for example, analytical, logical-algebraic, logical-linguistic modeling and their combinations) within the framework of the CM concept of the investigated CO. In the proposed report, the main features of organization and carrying out of CO complex modeling are illustrated by the example of description and investigation of the complex planning processes of automated control systems (ACS) functioning by active mobile objects (AMO)(Kalinin V.N., 1981).

In this case, AMO, in general, is understood as a complex mobile system intended for information, energy or / and real interaction with the surrounding physical environment, (AMO of the 1st kind) or / and with other similar systems (AMO of the 2nd kind) (Kalinin and Sokolov 1985; Kalinin and Sokolov 1987). The process of AMO functioning could be described by four components: the movement of the AMO base in space (mechanical motion), the state changes of the on-board resource, the state changes of the instruments placed on its board, and, last but not least: the interaction of the AMO with the environment or with other AMO is target and the main attribute of the AMO.

2. MAJOR HEADINGS

Logical-dynamic interpretation of the implementation of the operation and resource allocation complexes, proposed earlier in (Ivanov, Sokolov and Dolgui 2013; Ivanov, Dolgui and Sokolov 2016b; Kalinin and Sokolov 1987; Ohtilev, Sokolov and Yusupov 2006) formed the basis for the developed poly-model description of the ACS AMO functioning. The following logical-dynamic models were included in the developed generalized model of its functioning (Kalinin and Sokolov 1985; Kalinin and Sokolov 1987; Ohtilev, Sokolov and Yusupov 2006): the dynamic model of motion control of ACS AMO; dynamic model of channel management in ACS AMO; Dynamic model of operations management conducted in ACS AMO; dynamic flow control model in ACS AMO; dynamic model of resource management in ACS AMO; dynamic model for controlling the parameters of operations conducted in the ACS AMO; Dynamic model of management of ACS AMO structural dynamics; a dynamic model of management of the ACS AMO auxiliary operations.

Let us represent a simplified version of the dynamic model of operations management conducted in the ACS AMO as the follows:

$$\Delta = \left\{ \mathbf{u} \mid \dot{x}_i = \sum_{j=1}^{m} u_{ij}; \sum_{i=1}^{n} u_{ij}(t) \leq 1; \right.$$
$$\sum_{j=1}^{m} u_{ij} \leq 1; u_{ij}(t) \in \{0,1\};$$
$$t \in (t_0, t_f] = T; \ x_i(t_0) = 0; x_i(t_f) = a_i; \quad (1)$$
$$\sum_{j=1}^{m} u_{ij} \left[\sum_{\alpha \in \Gamma_{1i}^-} (a_\alpha - x_\alpha(t)) + \prod_{\beta \in \Gamma_{i2}^-} (a_\beta - x_\beta(t)) \right] = 0;$$
$$\left. i = 1, ..., n; \ j = 1, ..., m \right\}$$

where $x_i(t)$ is the variable characterizing state of execution of interactional operation D_i, at time t; a_i - the specified amount of stated operation execution; $u_{ij}(t)$ is the control action that takes the value 1 if the interaction operation D_i is performed using the resource B_j of the ACS AMO, 0 in the opposite case; $\alpha \in \Gamma_{1i}^-$, $\beta \in \Gamma_{2i}^-$ are the sets of transaction numbers preceding and technologically related to the operation D_i with the logical operations "AND", "OR" (alternative "OR"), T - the time interval at which the operation of the ACS AMO is considered; t_0, t_f are the initial and final moments of time. In (Kalinin and Sokolov 1985; Kalinin and Sokolov 1987) possible variants of the detailed description of this model for different subject areas are considered.

Moreover, the above-mentioned poly-model complex was supplemented by a new modification of the computational G-model, previously developed by the authors, which is a dynamic alter-native system graph with a adaptive structure that is constructed on the basis

of combined use of the mathematical apparatus of Petri nets with the listed logical-dynamic models of program control.

In recent years Petri nets became widespread, first of all, as a convenient and intuitive tool for describing models of multi-level parallel, streaming, spatially-distributed processes and asynchronous transformation of information. Unlike traditional automata used in this case, Petri nets allows to formalize a set of different types of objects and processes occurring in them based on establishing local (distributed) relationships between components in the respective models and tracking local (distributed) state changes throughout the system of pre-education models and information processing.

The analysis of publications shows that by now a variety of tools have been developed and implemented for these models which are allow to perform automatic or automated transformation of networks, their construction and analysis. These transformations are based on normal representation of the subclass of Petri nets (regular networks) and their generalizations (structured networks), which are based, in turn, on the algebra of regular networks developed by V.Y. Kotov (Kotov V.Y. 1984.).

Previously performed studies show that use of Petri nets, make possible the integration such important classes of models of preparation and decision-making as: computational models used to describe operational control algorithms for modes of operation of these complex objects; expert models for describing the control activities of the specified objects dispatchers; and also dialogue models for the description of human-machine interaction in the systems under consideration. There-fore, a generalized description of objects under research was proposed, based on the imposition of the category of dynamic alternative system graphs with an adaptive structure (Ohtilev, Sokolov and Yusupov 2006).

Within of this description, it is possible to combine and interlink all the previously listed classes of dynamic models. This combination of models already opens up prospects for conducting interdisciplinary research, within of which it is possible to enrich the enumerated applied control theories with interesting scientific and practical results obtained in each of them.

As an example, let us represent a simplified version of the Petri net dynamic interpretation using a discrete dynamic system (DDS), which can be specified as follows for the problems of operations planning and allocating the resources of the ACS AMO. We assume that the value of each *i*-th component of the DDS state (the state of the ACS AMO) is of the form: $\mathbf{x}[l] = \left\| x_1[l], x_2[l], ..., x_n[l] \right\|^T$, $l = 1, ..., N$ (l is the current step number, the time instant) is numerically equal to the total number of tokens in the p_i position in the original Petri net, and to each t_j transition, the control action $u_j = [l] \in \{0, 1\}$ is matched, which takes the value 1, if t_j the transition is triggered at step l, 0 otherwise.

In addition, when every enabled transition is firing, moving tokens from one position to another is not instantaneous, but with a fixed duration (step). In this case, the equations describing the dynamics of the change of marking in the Petri net under consideration can be given in the form of the fol-lowing recurrence relations

$$x_i[l] = x_i[l-1] + \sum_{\beta \in \Gamma_i^-} k_\beta u_\beta[l] - \sum_{\alpha \in \Gamma_i^+} k_\alpha u_\alpha[l] , \qquad (2)$$

where k_β, k_α is the multiplicity of edges, which are connecting respectively t_β transitions with p_i position and p_i position with t_α transitions; $\Gamma_i^- (\Gamma_i^+)$ is the set of numbers of the input (output) transitions p_i of the position. Along with (1), it is necessary to set constraints in the DDS describing the structure of the Petri net, the logic of transitions triggering of (which correspond to spatiotemporal, technical and technological limitations associated with the functioning of the ACS AMO). These restrictions can be presented in the following form:

$$u_\alpha[l] \sum_{i \in I_\alpha} \prod_{\xi = k_i}^{s_i} (\xi - x_i[l-1]) = 0 , \qquad (3)$$

$$\sum_{\alpha \in \Gamma_i^+} k_\alpha u_\alpha[l] \le x_i[l-1] , \qquad (4)$$

$$u_\alpha[l] \sum_{v \in J_\alpha} x_v[l-1] = 0 , \qquad (5)$$

where $s_i = \max x_i[l]$, $l = 1, ..., N$ is the maximum possible number of tokens that can be in the p_i position; $I_\alpha(J_\alpha)$ is the set of the numbers of the input positions (output positions with restraining arcs) for the t_α transition. In addition to (2) - (5), the initial and final (required) Petri net marking $x[0]$, $x[N]$ had to be used; an indicator of functioning quality of complex objects $F = \sum_{l=1}^N g_l(\mathbf{x}[l-1], \mathbf{u}[l])$, where $g_l(.,.)$ are given functions.

It should be noted that the proposed approach to the formalization of the complex objects functioning processes is applicable in those cases where these processes are described by colored timed Petri nets. The main feature of the proposed dynamic interpretation of Petri nets is that, it is necessary to set the relations (2) - (5) in this way to ensure the values integrity of state vector components and controls in the constructed DDS at each step $l = 1, ..., N$. For this, constraints of the form (3) - (5) in terms of the theory of optimal control must satisfy the conditions of general position.

By now, a number of important scientific and applied problems have been solved on the basis of the proposed

dynamic interpretation of solving processes problems of planning and the corresponding dynamic interpretation of Petri nets functioning (Aalst and Der 1992; Desel and Reisig 2015; Jensen and Kristensen 2009; Ohtilev, Sokolov and Yusupov 2006).

The analysis shows that the developed algorithms for finding optimal schedules and corresponding plans for the functioning of the means can be used to search for optimal rules of firing transitions in Petri nets, estimating the reachability of a given Petri net marking (Kotov V.E. 1984). On the other hand, when solving a variety of problems in the theory of scheduling, the problems of the ACS AMO structure-functional synthesis, using the mathematical apparatus of Petri nets, it is possible to constructively evaluate the temporal and capacitive complexity of the corresponding optimization algorithms, search for dispatch plans (first approximations) in problems of optimal program control of operation complexes (Chernousko and Lyubushin 1982; Krylov and Chernousko 1972; Lyubushin 1979; Ohtilev, Sokolov and Yusupov 2006).

In addition, the proposed set of dynamic models can be used to evaluate and select best technologies for system modeling of a given AMO class. The considered dynamic interpretation of Petri nets can also be used to match the results obtained on mathematical and computational models.

One of the main advantages of the developed combined G-model of complex planning of the ACS AMO functioning is that it provides the correct coordination (at the conceptual, model-algorithmic, information and software levels of detail) of mathematical (in accordance with the homomorphism criteria of relations) analytical-simulation) models for controlling the structural dynamics of complex dynamic objects (active mobile objects (AMOs)) with their logical-algebraic and logical-linguistic analogs (models) based on intelligent information technologies (Ohtilev, Sokolov and Yusupov 2006).

At the same time, unlike the existing behavioral (scenario) ACS AMO models based on finite automaton and imitation descriptions, the proposed logical-dynamic approach allowed to solve constructively the tasks of operational structure-functional synthesis both in the shape of the ACS AMO and in the corresponding synthesis scenes of their behavior, program management operations;

To solve the problem of complex planning of the ACS AMO functioning, a generalized procedure was developed based on the authors' report on combined methods for solving problems of optimal proactive control of the structural dynamics of the complex organizational and technical systems under consideration, and includes the following stages (Ohtilev, Sokolov and Yusupov 2006): *adaptation of the parameters and structure of models, algorithms for planning and regulating the operation of ACS AMO with regard to the past and its current state, as well as the external state; dynamic structural and functional synthesis of the main elements and subsystems of the ACS AMO on the next cycle of its application; composition of various scheduling options for ACS AMO; simulation and multivariate forecasting generated scenarios for the implementation of the ACS AMO operation plans, taking into account various options for the situational response of its elements and subsystems to possible disturbances; adaptation (structural, parametric) of plans, models, algorithms of ACS AMO work scheduling to possible (predicted on imitation models) its states and states of the external environment.*

The main advantage of the given approach to the solution of the complex planning problem (Kalinin and Sokolov 1985; Kalinin and Sokolov 1987) lies in the fact that the solution of all particular problems of the structural dynamics control (SDC) of the ACS AMO is carried out on a single methodological and methodical basis, based on new scientific and practical results, obtained in modern control theory (Ohtilev, Sokolov and Yusupov 2006).

Based on the analyzed studies, it is possible to conclude that within the realization and application the proposed generalized procedure of complex planning (depending on the composition and structure of the initial data), it is expedient to use the following combined methods and algorithms for searching for solutions of nonlinear two-point (multipoint) problems: the method of successive approximations in the problems of searching for optimal controls in combination with Newton's method; the method of successive approximations in problems of searching for optimal controls in conjunction with the method of penalty functionals; the method of successive approximations in problems of searching for optimal controls in combination with a generalized subgradient method; method of successive approximations in problems of searching for optimal controls in combination with the method of "branches and boundaries".

These methods made it possible, in comparison with existing methods, to increase the operational efficiency and throughput of ACS of the AMO by an average of 10% -15% due to the optimal ordering of the operations performed in the implementation of the appropriate complexes of operations, as well as the best distribution of limited ACS AMO resources.

An important place in the organization of the complex planning processes of the CO (in our case, ACS AMO) functioning is given to simulations of possible scenarios for the implementation of the corresponding plans under conditions of various kinds of disturbing influences. We will consider as it is possible to use the mathematical apparatus of Petri nets for modeling and analysis of the processes of implementing the plans for the functioning of the AMO ACS in the conditions of disturbing influences.

Now, let us describe the Petri net more formally. In the general case, a simple Petri net is defined by a multiset

$P_n = \{p_1, p_2, p_3, ..., p_n\}$ - a set of positions, such that $P_n \subseteq \mathcal{C}^+$, thus set of position is defined on the set of all integers

$T_n = \{t_1, t_2, t_3, ..., t_n\}$ - A set of transitions, such that $T_n \subseteq \mathcal{C}^+$, thus set of transitions is defined on the set of all integers.

$I : (T_n \times P_n) \to \subseteq \yen^+$ – the input function, which mapping each position into a set of transitions, in other words, it is a set of input arcs.

$O : (P_n \times T_n) \to \subseteq \yen^+$ - the output function that maps each transition to a set of positions, in fact, the output function is the set of arcs emerging from the transition and entering the position.

$M_0 \subseteq \mathcal{C}^+$ - initial marking of the a net.

Further, let us introduce the notion of multiplicity for a position relative to a transition. The multiplicity of the input position p_i with respect to the transition t_i is the number of position appearances in the transition $\#(p_i, I(p_i))$ and, similarly, the multiplicity of the output position is the number of position appearances in the transition In other words, the multiplicity is the number of arcs emerging from the position in the transition, and the number of arcs that enter the same surveyed position from the transition.

Also, it is necessary to say that the transition can work if it is solved. In this case, the transition is allowed only if the number of tokens in the place is equal to the number of output arcs. Thus, when a transition is triggered, a new mark is formed $M_i = M_0 - \#(p_i, I(p_i)) + \#(p_i, O(t_i)), \forall i$.

It should be noted that the Petri nets have proven themselves in the following scenarios in the analysis of complex systems (Aalst and Der 1992; Desel and Reisig 2015; Jensen and Kristensen 2009; Ohtilev, Sokolov and Yusupov 2006):

- System design.
- Systems benchmarking.
- Monitoring of system parameters.

From the point of view of the analysis of the behavior of the ACS AMO, the following properties of the petri nets are of the greatest interest:

- Reachability.
- Liveness.

Reachability. The marking of a network is called reachable if there is such a transition t_i that $M_i = M_{i-1} - \#(p_i, I(p_i)) + \#(p_i, O(t_i)), \forall i$. Hence, it is possible to designate the property of potential reachability, consisting in the possibility of firing a series of transitions to achieve marking M_i, in other words, if there are many transitions whose firing leads to a marking M_i, then such a marking is called potentially reachable from the transition t_i.

Liveness. The Petri net is alive if $\forall t_i \in T_n | \exists M_j \in M | M_i = M_0 - \#(p_i, I(p_i)) + \#(p_i, O(t_i)),$

$\forall i$. I.e. for some reachable marking from the set of markings, there is at least one transition, whose firing is allowed.

When representing the ACS AMO in the form of a Petri net the analysis of the liveness network will characterize the presence of such a limiting state of the system upon which the state of the system at time t_{n+m} with $m \to \infty$ will not change. In the case that the network is alive for $\forall M_j \in M$, then such a limit state does not exist.

However, it is important that there can be many transitions, the firing of which can lead to the changeover of the system to the limiting state. The obtained markings, in this case, are called dead ends.

Therefore, when analyzing the behavior of ACS AMO, for the study of the network for the presence of deadlocks, it is necessary to construct a set of all reachable markings from M_0. Besides, this problem belongs to the class of np-complex (Jensen and Kristensen 2009). As a consequence, constructing the set of all possible states of the system is impossible in an acceptable time.

This leads to the impossibility of investigating the limiting states of the ACS AMO. However, the approach of complex modeling, proposed by the authors, alleviates this problem. If we represent the SP, in the form of a system of difference equations (that is, in the form of DDS). It becomes possible to perform an analysis of such a system and analytically find the values of the system parameters under which the occurrence of limit states of the ACS AMO is possible.

In conclusion, we give an example of the use of the proposed logical-dynamic model (2) - (5) and the corresponding scheduling algorithm for ACS AMO. Fig. 1 shows the structure of AMO automated control technology. In this figure, corresponding figures indicate the main processes associated with the processes of transmission, processing, storage of data and information, as well as the processes of control actions forming. In this case operations with numbers 1, 2, 3, 7, 8, 9, 21, 22, 23 are connected with subsequent operations by the logical condition "alternative or". Due to this condition, it is possible to select various options for AMO automated control technology. Fig. 2 shows possible architectures of the hardware-software complexes ACS AMO, on which AMO automated control technology is implemented. In Fig. 3 presents the results of solving two simultaneously (in parallel) solvable multi-criteria selection problems: the tasks of the operative structural and functional synthesis of the AMO automated control technology and the tasks of scheduling the work of the ACS AMO facilities.

When solving these problems, the following initial data were accepted: number of computing processes: 3, For each process: number of transactions: 30 basic and 8 subsidiary; number of logical links: 54; number of alternative technologies: 120; number of resources (computing devices): 3; the volume of the information flow of operations: from 1 to 6 GB; speed of information flow processing resources: from 1 to 3 GB

per minute; operation time: from 20 seconds to 6 minutes; average implementation time: 10 minutes. When solving these problems, two indicators of the quality of planning were optimized - energy consumption reduction, and reduction of time of execution. In Fig. 3 presents the results of the operational planning of the ACS operation with three AMO using the dynamic analog of the Petri net model (2) - (5). As a result, compared to the heuristic solutions used in practice for AMO management, the following improvements in the quality of planning were obtained - quality index of energy consumption reduction – on average for 21%; reduction of time of execution – on average for 6%, increase in uniformity of loading of resources – on average for 14%, improvement of the generalized indicator of quality of the plan – on average for 26%.

3. CONCLUSION

One of the main advantages of the proposed approach to solving the problem of complex planning of the ACS

AMO functioning and the corresponding combined methods for solving problems of optimal program control and mathematical programming is that during the formation of the program control vector (ACS AMO work plan) at the final moment of time, along with the optimal plan, the desired multi-structure macro state (or in another way the image of the ACS AMO), at the same time in which it can perform the tasks assigned to it in the developing (forecasted) environment in the planning period with the required degree of stability. To the present time, the proposed approach to the organization of integrated planning has received its practical implementation in solving a number of problems arising in the rocket and space industry and transport and logistics networks (Ohtilev, Sokolov and Yusupov 2006). More information on the implementation of the proposed approach is available on the website https://litsam.ru.

Fig. 1 Structure of AMO automated control technology

1. Data collecting.
2. Data preprocessing.
3. Main data processing.
4. Formation of control.
5. Implementation of control.
6. Transfer to the data processing century.
7. Data preprocessing.
8. Main data processing.
9. Formation of control.
10. Data processing century. Cloud.
11. Data processing century pf the cyber-physical system.
12. Data processing century. Cloud.
13. Data processing century pf the cyber-physical system.
14. Data processing century. Cloud.
15. Data processing century. Cloud.
16. Data processing century pf the cyber-physical system.
17. Data processing century pf the cyber-physical system.
18. Data processing century. Cloud.
19. Data processing century. Cloud.
20. Transfer to the cloud.
21. Data preprocessing.
22. Main data processing.
23. Formation of control.
24. Cloud of the data processing century.
25. Cloud of the cyber-physical system.
26. Cloud of the cyber-physical system.
27. Transfer to the cyber-physical system.
28. Cloud of the data processing century.
29. Cloud of the data processing century.
30. Transfer to the cyber-physical system.

Centralized architecture   Vague calculation   Cloud calculation

Fig. 2. Possible architectures of the hardware-software systems ACS AMO
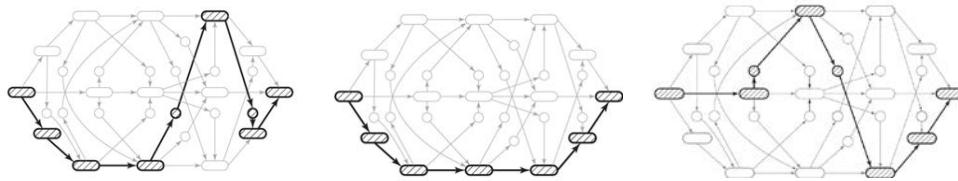
Рис. 3 Joint scheduling of three parallel processes

ACKNOWLEDGMENTS

REFERENCES

Aalst W. M. P. Van Der, 1992. Timed coloured Petri nets and their application to logistics. Thesis (PhD). Eindhoven University of Technology.

Athaus M., Falb P.L., 1966. Optimal control: An introduction to the theory and its applications. New York, San Francisco, CA, Sidney, NSW: McGraw-Hill.

Bożek A., M. Wysocki, 2015. Flexible Job Shop with Continuous Material Flow. International Journal of Production Research, 53(4), 1273–1290.

Chernousko F.L., Lyubushin A.A., 1982. Method of successive approximations for solution of optimal control problems. Optimal Control Applications and Methods, 3(2), 101–114.

Choi T.-M., Yeung W.-K., Cheng T.C.E., 2013. Scheduling and co-ordination of multi-suppliers single-warehouse-operator single-manufacturer supply chains with variable production rates and storage costs. International Journal of Production Research, 51(9), 2593–2601.

Dejonckheere J., Disney S.M., Lambrecht M.R., Towill D.R., 2004. The impact of information enrichment on the bullwhip effect in supply chains: A control engineering perspective. European Journal of Operational Research, 153(3), 727–750.

Desel J., Reisig W., 2015. The concepts of Petri nets. Software and Systems Modelling, 14(2), 669–683.

Disney S.M, Towill D.R, Warburton R.D.H., 2006. On the equivalence of control theoretic, differential, and difference equation approaches to modelling supply chains. International Journal of Production Economics, 101, 194-208.

Giglio D., 2015. Optimal control strategies for single-machine family scheduling with sequence-dependent batch setup and controllable processing times. Journal of Scheduling, 18(5), 525-543.

Gubarev V.A., Zakharov V.V., Kovalenko A.N., 1988. Introduction to systems analysis. Leningrad: LGU.

Harjunkoski I., Maravelias C.T., Bongers P., Castro P.M., Engell S., Grossmann I.E., Hooker J., Méndez C., Sand G., Wassick J., 2014. Scope for industrial applications of production scheduling models and solution methods. Computers and Chemical Engineering, 62, 161-193.

Hwang C.L., Fan L.T., Erikson L.E., 1967. Optimum production planning by the maximum principle. Management Science, 13(9), 751–755.

Hwang C.L., Fan L.T., Tillman F.A., Sharma R., 1969. Optimal production planning and inventory control. International Journal of Production Research, 8(1), 75-83.

Ivanov D., Dolgui A., Sokolov B., 2016a. Robust dynamic schedule coordination control in the supply chain. Computers and Industrial Engineering, 94(1), 18-31.

Ivanov, D., Dolgui A., Sokolov B., Werner F., 2016b. Schedule robustness analysis with the help of attainable sets in continuous flow problem under capacity disruptions, International Journal of Production Research, 54(1), 3397-3413.

Ivanov, D., Sokolov B., 2012. Dynamic supply chains scheduling, Journal of Scheduling, 15(2), 201-216.

Ivanov D., Sokolov B., Dolgui, A., 2013. Multi-stage supply chains scheduling in petrochemistry with non-preemptive operations and execution control, International Journal of Production Research, 52(13), 4059-4077.

Jensen K. and Kristensen L.M., 2009. Coloured Petri Nets. Modelling and Validation of Concurrent System. New York: Springer-Verlag Berlin Heidelberg.

Jungwattanakit J., Reodecha M., Chaovalitwongse P., & Werner F., 2009. A comparison of scheduling algorithms for flexible flow shop problems with unrelated parallel machines, setup times, and dual criteria. Computers & Operations Research, 36(2), 358–378.

Kalinin V.N., 1981. About the theory of management of active mobile objects. Instrumentation, 6. pp. 26–31. (In Russ.).

Kalinin V.N., Sokolov B.V., 1985. Optimal planning of the process of interaction of moving operating objects. International Journal of Difference Equations, 21(5), 502-506.

Kalinin V.N., Sokolov B.V., 1987. A dynamic model and an optimal scheduling algorithm for activities with bans of interrupts. Automation and Remote Control, 48(1-2), 88-94.

Kogan K., Khmelnitsky E., 2000. Scheduling: control-based theory and polynomial-time algorithms. Dordrecht: Kluwer

Kotov V.E. 1984. Petri nets – Moscow: Nauka. (in Russ.).

Krylov I.A., Chernousko F.L., 1972. An algorithm for the method of successive approximations in optimal control problems. Zh. Vychisl. Mat. Mat. Fiz., 12(1), 14–34.

Lee E.B., Markus L., 1967. Foundations of optimal control theory. New York: Wiley & Sons.

Lyubushin A.A., 1979. Modifications and convergence of successive approximations for optimal control problems. Zh. Vychisl. Mat. Mat. Fiz., 19(6), 1414–1421.

Ohtilev M.Yu., Sokolov B.V., and Yusupov R.M., 2006. Intellectual Technologies for Monitoring and Control of Structure-Dynamics of Complex Technical Objects. Moscow: Nauka. (in Russ.).

Pinedo M., 2008. Scheduling: Theory, Algorithms, and Systems. New York: Springer.

Sarimveis H., Patrinos P., Tarantilis C.D. & Kiranoudis C.T., 2008. Dynamic modeling and control of supply chains systems: A review. Computers & Operations Research, 35, 3530–3561.

Sethi S.P., Thompson G.L., 2000. Optimal Control Theory: Applications to Management Science and Economics, Second Edition. Berlin: Springer.

Sotskov Y. N., Lai T.-C. & Werner F., 2013. Measures of Problem Uncertainty for Scheduling with Interval Processing Times. OR Spectrum, 35(3), 659–689.

Werner F. & Sotskov Y. (Eds.), 2014. Sequencing and Scheduling with Inaccurate Data. Nova Publishers.

Ye H. and Liu R., 2016. A multiphase optimal control method for multi-train control and scheduling on railway lines. Transportation Research Part B: Methodological, 93 (Part A), 377-393.

Zimin I.N. & Ivanilov Yu.P., 1971. Solution of network planning problems by reducing them to optimal control problems. Zh. Vychisl. Mat. Mat. Fiz., 11(3), 632–641.

AUTHORS BIOGRAPHY

BORIS SOKOLOV is a Head of Laboratory of Information Technologies in System Analysis and Modelling of Saint Petersburg Institute of Informatics and Automation of the Russian Academy of Science. Professor Sokolov is the author of a new scientific lead: optimal control theory for structure dynamics of complex systems. Re-search interests: basic and applied research in mathematical modelling and mathematical methods in scientific research, optimal control theory, mathematical models and methods of support and decision making in complex organization-technical systems under uncertainties and multicriteria. He is the author and co-author of 9 books on systems and control theory and of more than 450 scientific papers. Professor B. Sokolov supervised more over 90 research and engineering projects. Web-page can be found at http://litsam.ru.

ALEXANDER KOVALEV — Doctor of Sciences (Tech), Prof., Honored scientist of Russian Federation; • Chief researcher, Laboratory for Information Technologies in Systems Analysis and Modeling, St. Petersburg Institute of Informatics and Automation of the RAS (SPIIRAS). Research interests: analyses of systems, reliability theory, mathematical models and methods of decision-making support in complex technical-organizational systems with the use of aerospace data. The number of publications: 170. info@litsam.ru, http://www.litsam.ru; office phone, +7(812) 328-0103.

VLADIMIR KALININ — Dr. Sc.in Technical Science, Prof., Honored Scientists of the Russian Federation; The full member of the Russian academy of astronautics of a name K.E. Tsiolkovsky, Professor of Military-space academy. Research interests – the theory of system researches, space cybernetics and computer science, the theory of optimum control of the dynamic systems, the automated control systems, preparation of the engineering staff and new information-didactic

technologies in higher education. Number of scientific publications – 170.

EVGENIY MINAKOV — Doctor of Sciences (Tech), Prof., Professor GCA name A.F. Mozhaisky. Area of scientific interests: System analysis, provision of ballistic spacecraft, effectiveness of space complexes and systems. Author of over 150 scientific papers. 50th St., 13.0, St Petersburg, RUSSIAN FEDERATION, 197082; r.t. +7 (812) 552-6341.

PETROVSKIY DMITRIY is a Ph. D. student at the department of the logistics and supply chain management, National Research University Higher School of Economics St. Petersburg – NRUHSE (SPb). Research interests: system analysis, modeling complex economic systems, operation research. The number of publication 5. Web-page can be found at https://www.hse.ru/org/persons/196156 641

INFLUENCE IN TONAL NOISE AND PRESSURE FLUCTUATION OF MECHANICAL COMPONENTS PLACED DOWNSTREAM OF A CENTRIFUGAL BLOWER IN THE REFRIGERATION SYSTEM OF AN INDUCTION COOKTOP

Maria Valencia Betrán[a], Carmelo Pina Gadea[a], Beatriz Sánchez Tabuenca[b], Cristian Albero Posac[b], Juan Lladó Paris[b]

[a] BSH Home Appliances Spain
[b] Universidad Zaragoza

[a]maria.valencia@bshg.com, [a]carmelo.pina@bshg.com, [b] bstb@unizar.es, [b] calbero@unizar.es, [b] juan.llado@unizar.es

ABSTRACT
In this work, a numerical and experimental investigation have been performed about the influence in the tonal noise-pressure level at the blade pass frequency of the additional components that are placed downstream a centrifugal blower in a refrigeration system of an induction cooktop. Four scenarios have been analysed by means of computational fluid dynamic software, evaluating the variation of pressure in time at the volute-tongue area and the results have been compared in a qualitative manner with the experimental acoustic measurements.

Keywords: refrigeration system noise, pressure fluctuation, CFD numerical simulation, acoustic measurements

1. INTRODUCTION
The inclusion of a blower in an induction cooktop means that a certain noise is introduced in the system. The tendency in last years is that customers complain about noisy environments. The objective for the industry is to manufacture appliances with lower noise level so that the degree of satisfaction of the customer is not affected. Although induction cooktop are not marked with noise labels, the noise criteria is already in the testing procedure of the product.

As stated in previous investigations, the tonal noise leads to higher levels of annoyance in comparison to broadband/overall noise (Evans and Cooper, 2015). In this work, the focus is also set in the tonal peak noise due to annoyance complaints that come from users.

The airborne noise generation mechanisms in rotating blades blowers are based in several acoustic analogies: Lighthill, Powell, Thompson & Hourigan, and Ffowcs Williams & Hawkins who solve an equation in which different acoustic mechanisms are identified which are linked to the movement of rigid surfaces: quadripole noise (associated to turbulent shear forces in the fluid), dipole noise (due to steady and non-steady forces exerted by surfaces to the fluid) and monopole noise (linked to the volume movement of the blade thickness) (Mathson, 2008). Among these noise mechanisms, the main noise generation mechanism is associated to forces on blades and volute wall due to the turbulent fluid in contact with them. Forces on blades can be periodic or random, therefore noise resultant may have discrete components and broadband component (Neise). Discrete components appear at blade pass frequency (BPF) and its harmonics. Variations of pressure in the volute tongue area and the distance between the blades and the tongue area are the main blower design factors to reduce the tonal noise (Velarde Suárez *et al.*, 2000) and (Suárez *et al.*, 2014)

Many recent investigations have been done in relation to design parameters of the blower construction with the objective to reduce the tonal noise in the source, such as distance between tongue and blades). An investigation has been done in relation to the influence of mechanical design of components sourrounding the blower area in an induction cooker (Wang, Y.S; Tang,X.L and Lee, C.M, 2011), without evaluating the effect of each component separately.

However, no deep research has been done in terms of how the different elements of the refrigeration system of an induction cooktop affect the tonal noise level of the blower.

The objective of the actual and future work is to analyse the effect in tonal peak noise of design modifications in the mechanical components which are assembled after a blower in a refrigeration system of an induction cooktop.

Therefore, to introduce an acoustic (tonal noise) criteria in the design of the refrigeration system, which up to now is designed only from thermal efficiency point of view.

This analysis will be performed by means of a hybrid numerical-experimental modelization of the system by means of Computational Fluid Dynamic software Fluent. In this article, the first step is performed by doing a qualitative comparison between the experimental noise measurements in terms of sound pressure and the aerodinamical pressure variation in the blower tongue area.

2. SYSTEM DESCRIPTION

The focus of this work is the analysis of the refrigeration system that is built inside an induction cooktop. Besides the inductors, inside an induction cooktop there are electronic boards, which include the power electronic devices. These devices (IGBTs and Diode Bridge) are very sensitive to temperature, which leads to the necessity of a refrigeration system inside the cooktop.

The refrigeration system consists of a centrifugal blower, a nozzle, a heatsink where the power devices are mounted and an outlet diffuser connected in series to create a flow path. When the power electronic components reach a certain temperature, the blower is activated. It suctions the air from the outside, and the rotation of the impeller increases both pressure and kinetic energy of the air. When the air is discharged from the blower, it continues its travel through the nozzle to the heatsink, leading to a force convection heat exchange reducing the temperature in the electronic components. Finally, the air leaves the system through an outlet diffuser.

2.1. Refrigeration system description

The refrigeration system is formed by the following components, which can be observed in Figure 1:

- Forward-curved 27 blades centrifugal blower. The blower is characterized by its P-Q curve at 24V.
- Nozzle: focus the airflow from the blower to the heatsink inlet section
- Aluminium heatsink with horizontal fins
- Final diffuser: focus the airflow going out of the heatsink to the outlet area of the cooktop.
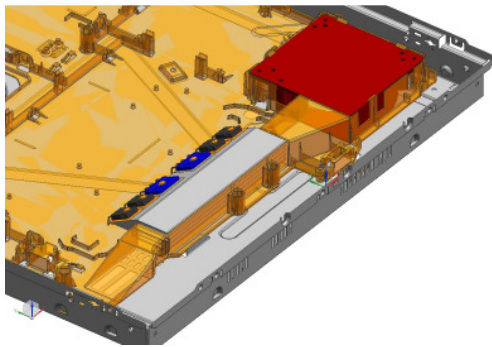
Figure 1: Refrigeration system.

3. EXPERIMENTAL MEASUREMENTS

Experimental measurements of the aerodynamic and acoustic performance of the refrigeration system are conducted: measurement of the flow velocity to validate the numerical aerodynamic results; and measurement of the sound pressure to know the contribution of each element of the refrigeration system to the tonal sound pressure, as well as to determine if there is any qualitative relationship between the pressure fluctuations at the volute tongue of the fan and the tonal noise. This experimental study also enables us to obtain

the boundary conditions for the aerodynamic simulation.

3.1. Aerodynamic measurements

Airspeed at the fan exit is determined from the dynamic pressure measured with a Pitot tube, Figure 2.
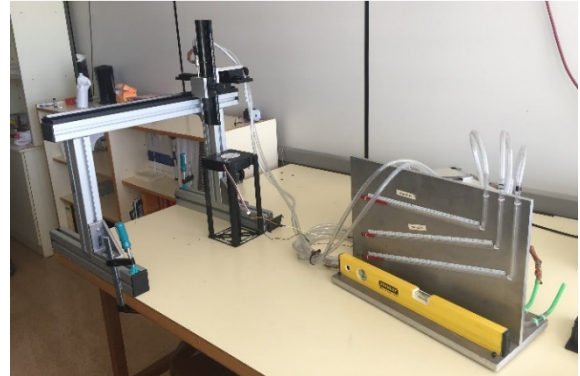
Figure 2: Pitot Tube measurement system

The tube is aligned with the flow velocity, and is moved in a 2mm mesh along the blower exit, about 400 measurement points, to obtain a velocity map that will be compared with the numerical results. The tests are performed twice, with the blower rotating at 2207 rpm.

3.2. Acoustic measurements

In order to achieve a low noise refrigeration system, first it is needed to know its acoustic performance. Although the blower is the driving force to generate flow and pressure within the refrigeration system, it is not the only contributor to the total aerodynamic noise.

The noise of centrifugal blowers has been extensively studied and, in a typical spectrum, it is mainly characterized by tonal components at multiples of the blade passing frequency, (BPF), produced by the pressure fluctuations at the volute tongue (Velarde 2008), that appear superimposed on a continuous range of broadband frequencies.

However, other elements of the refrigeration system can also affect the noise level. In order to know the contribution of each element of the refrigeration system to the tonal sound pressure, several configurations are tested in the following setup.

Measurements are made in a semianechoic room of 4.1 x 3.8x 2.4 m in size, with the refrigeration system positioned on an induction cooker base, placed in a cabinet against the reflecting wall. The sound pressure data are acquired with a Brüel and Kjær (B&K) Pulse multianalyzer, and a ½-inch B&K type 4189 microphone with matching preamplifier, located at 1,5 from ground level and 0,5 m from the cooker, in such a way as to approximate a user position.

In order to identify the effect of each element, the following scenarios have been defined:

- (B): Blower
- (B+N): Blower + Nozzle
- (B+N+H): Blower + Nozzle + Heatsink

- (B+N+H+D): Blower + Nozzle + Heatsink + Diffuser

The scenarios can be observed in Figure 3.
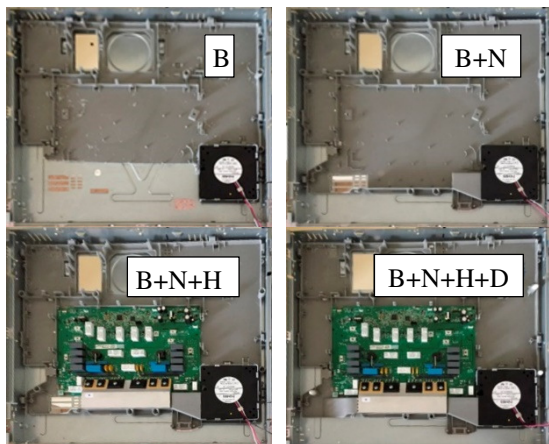
Figure 3. Analysed scenarios - Measurement

Initially the blower alone rotates at 2207 rpm, but this speed increases as the elements of the system are added. Table 1 shows the different rotational speeds of the blower obtained for each setting that will be used as input data for the aerodynamic simulations. In addition the Blade Pass Frequency (BPF) is calculated with formula $BPF = {n \cdot t}/{60}$ (1) where n is the angular velocity (rpm) and t is the blades number.

$$BPF = {n \cdot t}/{60} \qquad (1)$$

Table 1: Blower Operation point

RPM		BPF (Hz)
(B)	2207	997
(B+N)	2269	1021.5
(B+N+H)	2527	1137.15
(B+N+H+FD)	2520	1134.0

For each configuration, four different blowers are tested, and fifty sound pressure measurements are recorded during an interval of 10 s, each. FFT spectra are computed from 0 Hz to 6,4 KHz, as values above this limit are considered negligible. As example, Figure 4 shows the sound pressure spectrum of one measurement, where the dominant tonal noise can be noticed at the BPF.
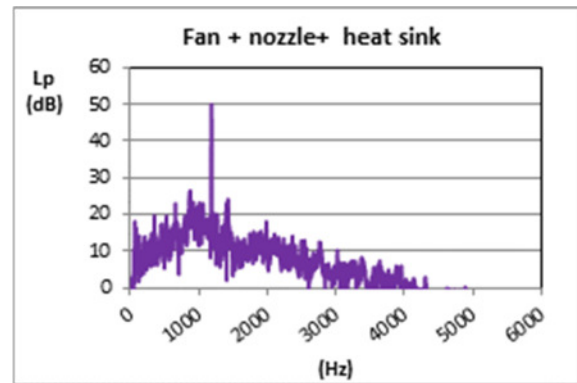
Figure 4: Sound pressure spectrum

4. NUMERICAL SIMULATION

A 3D numerical model has been developed to perform a transient simulation in order to capture the pressure fluctuations in the volute-tongue area of the blower.

In order to solve the steady and unsteady flow that occurs in a blower, the numerical model has been created by means of volume finite element method software Fluent. This software has been extensively used in simulations were pressure fluctuations are analysed for acoustic problems (Sjösvard, E. 2016), therefore the software is suitable choice for the current study.

The analysed scenarios correspond to scenarios defined in Table 1. In each simulation, the blower operation point has been defined according to experimental measurements included in the above mentioned table.

As expected, as additional components are placed downstream, the pressure drop increases for the blower, therefore the rotational speed of the blower increases.

In scenario (B), an additional air volume has been included in the outlet of the blower so that the boundary condition does not affect the fluid behaviour in that area.

In the inlet area an atmospheric pressure boundary condition has been defined. In the external surface of the additional geometry also an atmospheric static pressure boundary condition has been defined. The blower model consists of 2 volumes: the impeller, which contains the blades; and the volute.

The Rotating Frame Method (RFM) has been chosen to reproduce the behaviour of the blower during steady state phase. For transient phase, the Mesh Motion Technique has been chosen in order to take into account the blades passing effect in the tongue area. In both methods, an angular velocity has been defined in the impeller volume according to values enclosed in Table 1 for each scenario.

The fluid volumes have been meshed with tetrahedral non-structured mesh, as seen in Figure 5.
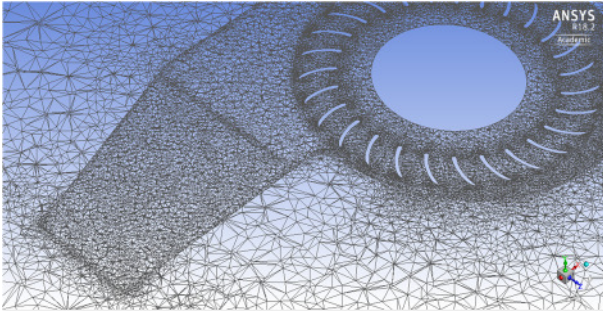
Figure 5: CFD Fluent Mesh

As a first step, a tetrahedral mesh is defined obtaining the following mesh characteristics in each scenario, Table 2. A skewness value below 0.7 has been selected to obtain a good quality mesh in all scenarios.

Table 2: Mesh characteristics

Elements / Nodes		
(B)	6.534.208	1.285.458
(B+N)	8.100.383	1.542.464
(B+N+H)	9.542.737	1.738.289
(B+N+H+FD)	11.319.347	2.105.332

Standard k-ε turbulence model has been chosen in the analyses performed for this work. It is based on model transport equations for turbulent kinetic energy (k) and the turbulence dissipation rate (ε), which are solved separately.

The rotation of the impeller in the simulation is characterised by means of the time step and the rotational speed. A time step of 9.26e-5sg has been defined for the definition of the transient simulation. After a hybrid initialization, 3150 time steps have been simulated, which means that 10 full rotations of the impeller have been simulated, therefore a blade passes approximately each 11 time-steps.

4.1. Numerical results

From the numerical simulation, the spatial and temporal variables of a fluid can be obtained. Therefore velocities (absolute and relative), see Figure 6, pressure (static and total), see Figure 7, can be extracted and post processed.
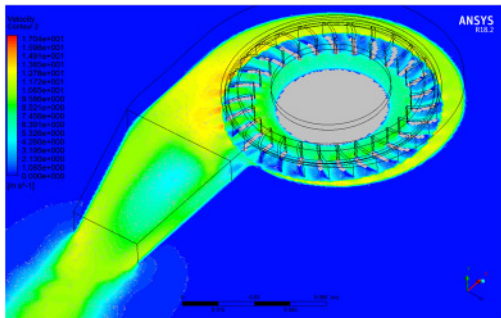
Figure 6. Velocity in Y plane in scenario B+N
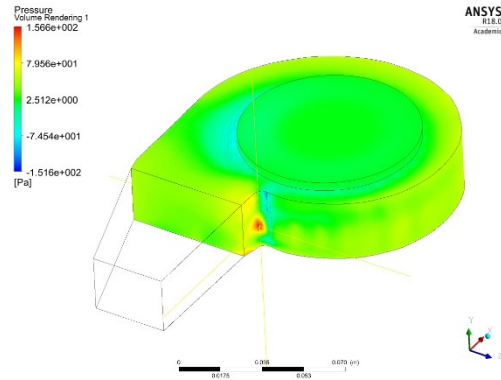
Figure 7: Pressure at the tongue area of blower volute in scenario B+N

In this work, the temporal variation of pressure in the volute tongue area is post processed in each scenario as shown in Figure 8, for scenario B+N.
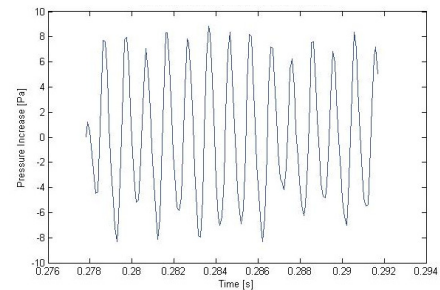
Figure 8: Evolution in time of Pressure variation.

A FFT algorithm has been applied to the pressure signal in order to obtain a pressure value that identifies the tonal peak in each scenario. In Figure 9, the FFT graph for the B+N scenario is shown.
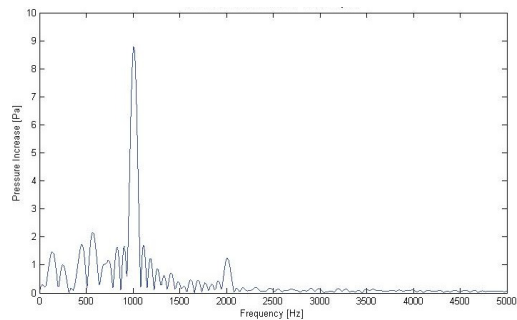
Figure 9. FFT pressure analysis

As it can be seen, a tonal peak appears at the BPF. The amplitude of this values varies as additional components are added to the blower as summarized in Table 3.

Table 3. Aerodynamic pressure (Pa) in tongue area at BPF

Pressure at tonal peak (Pa)			
B	B+N	B+N+H	B+N+H+N
27,5	11,0	8,8	9,4

If all the curves are compiled in a unique graph, as shown in Figure 10, it is observed that the amplitude of the pressure at the BPF decreases. As expected, the BPF at which the tonal peak appears is increased as a result of the higher angular velocity of the blower due to the downstream load of the blower.
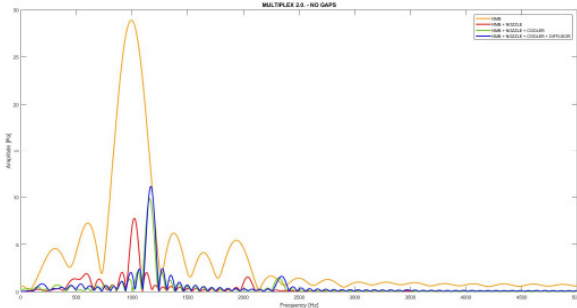
Figure 10. Evolution of tonal peak values at tongue area in all scenarios

5. RESULTS

A comparison between the experimental and the theoretical results has been performed.

5.1. Aero-dynamical measurements – CFD results

A comparison between the results obtained from experimental and numerical results from CFD, is performed in terms of velocity value and distribution.
For scenario (B), the velocity map measured at the outlet section can be seen in Figure 11.
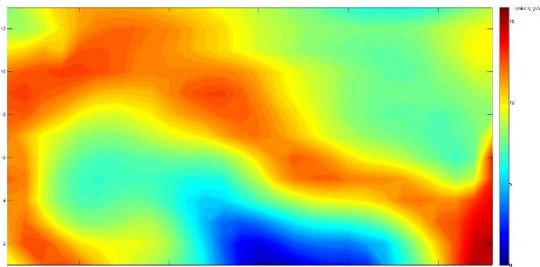
Figure 11. : Experimental velocity at blower outlet section

In Figure 12, the same variable result is extracted from the CFD model.
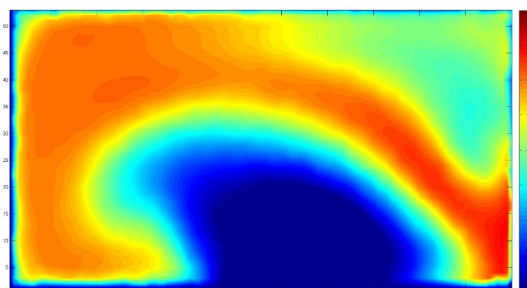
Figure 12. CFD Velocity at blower outlet section

As it can be observed, velocity maps show similar distributions, with localized maximum values, 15.30 m/s for the experimental measures and 16.34 m/s for the theoretical result, near the exterior of the blower volute and near the blower tongue area. Also a recirculation area at the bottom part of the outlet appears.

5.2. Acoustic measurements – Sound Power

The average aerodynamic tonal noise calculated from the experimental measurements performed for each case is shown in Table 4. The highest level is observed for the blower working alone, and the nozzle produces the higher decrement of the sound pressure level followed by the heat sink, however the diffusor increases slightly the level.

Table 4. Average sound pressure level (dB) at BPF

Test set up			
B	B+N	B+N+H	B+N+H+N
55.5	51.7	50.0	51.0

With the aim of doing a qualitative comparison of the numerical results with the experimental values, a transformation of the sound pressure level, Lp, is done from dB to sound pressure P, in Pa, by means of formula (2), where P0 is reference pressure of $20\mu Pa$.

$$Lp\,(dB) = 20 \cdot log_{10}\left(P/P_0\right) \quad (2)$$

The obtained values for the transformation have been enclosed in Table 5.

Table 5. Pressure in Pa at blower tongue area

Pressure at tonal peak Pa			
B	B+N	B+N+H	B+N+H+N
0.011913	0.007692	0.006325	0.007096
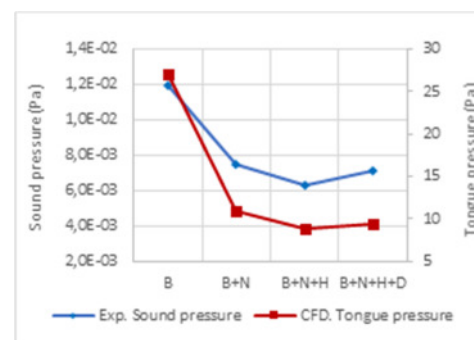
Figure 13. Comparison CFD pressure & Experimental sound pressure in Pa.

Figure 13 shows the comparison of the pressure at the volute tongue and the tonal sound pressure. It can be observed that numerical pressure changes qualitatively with the same tendency that the experimental values of sound pressure.

For the analysed construction, the nozzle geometry leads to a high reduction in the pressure level. When the heatsink is added the reduction is not so significant although the angular velocity increases the highest due to the significant reduction in air section area. When the diffuser is added, although the angular velocity increases slightly, the pressure is not reduced but increased slightly.

6. CONCLUSIONS

As a first step, a qualitative comparison has been performed between analytical model and experimental measurements of the evolution of the pressure values as additional components are added to the refrigeration system.

A model has been created that reproduces the tendency of peak tonal values at the blower tongue area, which is the primary noise source in centrifugal blowers. This tendency has been confirmed with the acoustical measurements.

These results lead the investigation to go deeper by introducing the CFD pressure results in specific software for acoustic simulation of the system. This step would lead to the possibility to predict in the future the effect of new mechanical designs in the sound level of the refrigeration system.

Additional research will be done in terms of the CFD model, in which boundary layer will be included in addition to more sophisticated turbulence models such as k-w SST, LES, etc.

ACKNOWLEDGMENTS

REFERENCES

Evans, T. and Cooper, J. (2015) 'a Comparison of Tonal Noise Regulations in Australia', pp. 1–12.

Wnag, Y.S., Tang X.L. abd Lee C.-M. (2011) 'A prediction of the acoustical properties of induction cookers based on a FVM-LES-acoustic analogy method.',

Mathson, T. (2008) 'Treatment of Tonal Sound in the Development of Fan Sound Ratings', (March).

Suárez, V. et al. (2000) 'Estudio de la generación aerodinámica de ruido tonal en un ventilador centrífugo industrial', (1992).

Sjösvard, E. (2016) 'Numerical estimation of the aerodynamic tones radiated from a centrifugal fan'.

Velarde Suárez, S. et al. (2014) 'Simulación numérica de la generación aerodinámica de ruido en un ventilador industrial'.

A MODEL VALIDATION METHOD WITH BOOTSTRAP APPROACH AND BAYES ESTIMATION FOR SMALL SAMPLE

Ting Song[a], Ping Ma[b], Yuchen Zhou[c], Ke Fang[d], Ming Yang[e]*

Control and Simulation Center, Harbin Institute of Technology
Harbin, P. R. China

[a] sting8259@163.com., [b] pingma@hit.edu.cn, [c] zhouyuchen-01@163.com,
[d] hitsim@163.com, [e] myang@ hit.edu.cn .

ABSTRACT

Generally, model validation is mainly based on statistical analysis. However, when the sample size of real system output is small, it is difficult to obtain accurate validation results with classical statistics theory. In such a situation, a model validation method based on improved Bootstrap approach and Bayes estimation is provided. First, Bootstrap method is used to enlarge observed samples size and obtain Bayes prior distribution information. Then, Bayes theory which combines prior information and small sample data is used to estimate the statistical characteristics of observed samples. Finally, single-sample hypothesis testing is used to evaluate the credibility of simulation model. Furthermore, an improved Bootstrap method is proposed, which raises the accuracy of parameter estimation and extends bootstrap samples range beyond the original data. The numerical experiment results reveal the effectiveness of validation method and improved Bootstrap method.

Keywords: model validation, small sample, improved Bootstrap method, Bayes estimation

1. INTRODUCTION

Model validation is realized by comparing the model output against experimental data (Li and Mahadevan 2016). In practical engineering applications, we can obtain sufficient simulation data through repeated numerical experiments. Nevertheless, due to the limitation of various factors such as expense, time-consuming and test conditions, etc, some physical tests are hard to repeat for many times or unrepeatable. Consequently, the samples obtained from real system output are limited, which brings difficulties for model validation. Statistical analysis is an important method for static data model validation (Sargent 2013). However, it is difficult to get accurate model validation results with classical statistics when the observed sample size is small. How to evaluate the credibility of simulation model with small observed samples and sufficient simulation samples is a practical problem to resolve.

One way to solve model validation problem for small sample is using suitable analysis methods like hypothesis testing for two samples. Oberkampf and Barone (2006) pointed out that both classical hypothesis testing and confidence intervals can be validation metrics to calculate for the difference between model prediction and observed data. Tang (2002) studied model validation method of static data in the case of small samples with nonparametric testing.

The other way to solve model validation problem for small sample is enlarging observed sample size and estimating statistical properties of observed samples, such as mean and variance; and then using hypothesis testing for single sample. Bayes estimation is a method combining the prior information with field test data, which provides an important theoretical support for small sample problem (Ahmed, Mohamed and Jaeyoung 2017). It can be used to estimate statistical properties of limited data. Dai (2014) utilized Bayes method and Monte-Carlo method to evaluate the reliability of protection system in the case of small sample failure data. Heydari, Miranda-Moreno, Lord and Fu (2014) offered a practical Bayes methodology to estimate and update Safety performance functions by making use of both data of limited samples and other parameters. However, the performance of Bayes methods vastly depends on the validity of the assumed prior distribution (Bunouf and Lecoutre 2006). In an early study, there are many approaches to obtain Bayes prior distribution, such as non-informative prior method (Meryem and Burak 2017), conjugate prior method and Bootstrap method, etc. This paper uses Bootstrap method to obtain Bayes prior distribution.

Bootstrap is a method based on resampling of the original random sample, which can provide more accurate inferences when the sample size is small (Klairung, Naratip and Mitchai 2017). However, the conventional Bootstrap method has disadvantages in generating resamples and limiting the bootstrap samples in the original data, which leading to a large deviation from the real sample distribution (Xiao, Gao, Ding and Han 2009). Thus, it is a problem worthy to study how to improve the quality of resample.

To solve the problems above, a model validation method based on Bootstrap approach and Bayes estimation for the similarity analysis between small observed samples and sufficient simulation samples is provided. Furthermore, an improved Bootstrap method which extends sample range and improves the quality of resample is proposed.

This paper is organized as follows. In section 2, a brief description of Bayes parameter estimation and Bootstrap method are given. In section 3, an improved Bootstrap method is proposed and a model validation method based on improved Bootstrap and Bayes theory is provided. Subsequently, Section 4 gives two numerical examples to test the effectiveness of proposed methods and Section 5 presents the conclusions.

2. RELATED WORK

In this section, the principle of Bayes estimation and Bootstrap method are described. First, we provide the sampling method of conventional Bootstrap method. Then, we take normal distribution as an example and give the detail process of Bayes posterior distribution.

2.1. Bayes Estimation

Bayes estimation is a special method for processing small sample problem, which could obtain relatively complete posterior information by effectively integrating various forms of prior information.

Bayes formula is defined as:

$$\pi(\theta \mid x) = \frac{f(x,\theta)}{m(x)} = \frac{\pi(\theta)p(x \mid \theta)}{\int_{\Theta} \pi(\theta)p(x \mid \theta)d\theta}, \quad (1)$$

where $\pi(\theta \mid x)$ is the posterior distribution when x is given, $f(x,\theta)$ is the joint probability density, $m(x)$ is marginal distribution density, $\pi(\theta)$ presents prior distribution of θ and $p(x \mid \theta)$ presents sample distribution. We take normal distribution as an example and describe the calculation process of the posterior distribution.

Suppose that observed samples $X_1, X_2, \cdots X_n$ follow normal distribution, which is denoted as $X \sim N(\theta, \sigma^2)$, where σ^2 is known and θ is unknown. The prior distribution of θ is stated as $\pi(\theta) \sim N(\mu, \tau^2)$, where μ and τ^2 are called hyperparameters. The posterior distribution of θ is described as $\pi(\theta \mid x)$ and the calculation procedure is as follows：

Define Conditional probability density function $f(x \mid \theta)$:

$$f(x \mid \theta) = (2\pi\sigma^2/n)^{-\frac{1}{2}} \exp\left\{-\frac{n(\overline{x}-\theta)^2}{2\sigma^2}\right\}$$
$$\propto \exp\left\{-\frac{n(\overline{x}-\theta)^2}{2\sigma^2}\right\}. \quad (2)$$

The prior distribution of θ can be written as:

$$\pi(\theta) = (2\pi\tau^2)^{-\frac{1}{2}} \exp\left\{-\frac{(\theta-\mu)}{2\tau^2}\right\} \propto \exp\left\{-\frac{(\theta-\mu)}{2\tau^2}\right\}. \quad (3)$$

Then the posterior distribution of θ can be written as:

$$\pi(\theta \mid x) = \frac{f(x,\theta)}{m(x)} \propto \exp\left\{-\frac{1}{2}\left[\frac{(\overline{x}-\theta)^2}{\sigma^2/n} + \frac{(\theta-\mu)^2}{\tau^2}\right]\right\}. \quad (4)$$

In that case, we define $\theta \sim N(\alpha, \beta^2)$, where σ and β are formed as follows:

$$\alpha = \frac{\sigma^2/n}{\sigma^2/n+\tau^2}\mu + \frac{\tau^2}{\sigma^2/n+\tau^2}\overline{x}. \quad (5)$$

$$\beta^2 = \frac{\sigma^2\tau^2/n}{\sigma^2/n+\tau^2}. \quad (6)$$

The key issue in Bayes theory is how to obtain prior distribution. This paper uses Bootstrap method to enlarge the observed samples size and obtain the hyperparameters of prior distribution.

2.2. Bootstrap Method

Bootstrap method was originally developed by Efron (1979), which is essentially a method applied to estimate the statistical characteristics of an unknown distribution estimator by using computer simulation (Kyselý 2010). The main idea of Bootstrap method is creating resamples by sampling with replacement from the original samples (Chihara and Hesterberg 2011); then calculating the statistic for each bootstrap sample; finally using the bootstrap distribution to represent the sampling distribution. It's mathematical description as follows:

Step1 Suppose $X = (x_1, \cdots x_n)$ is original sample with limited size and the distribution $F(x)$ of $x_i (i=1,2,\cdots,n)$ is completely unknown. Let $\theta = \theta(F)$ be some parameter of $F(x)$, such as mean and variance, etc. The empirical cumulative distribution function is defined as $F_n(x)$ and $\hat{\theta} = \hat{\theta}(F_n)$ is the estimator of θ. The estimation error is denoted as:

$$T_n = \hat{\theta}(F_n) - \theta(F). \quad (7)$$

Step2 Regenerate B groups samples from F_n, where B ($B>1000$) is the number of bootstrap samples, the sampling procedure of conventional Bootstrap is as follows：

- Generate n group random integer i over the interval $[1,n]$ with computer.

- Find sample x_i with corresponding index i as bootstrap sample, which is stated as $X^*(j) = (x_1^*, x_2^*, \cdots, x_n^*)$, where $j = 1, 2, \cdots n$.
- Repeat the above steps for N times and we can obtain N groups bootstrap samples.

Step3 Calculate Bootstrap statistics $R^*(X^*, F_n)$, it is defined as:

$$R^*(X^*, F_n) = \hat{\theta}(F_n^*) - \hat{\theta}(F_n) \triangleq R_n, \qquad (8)$$

where F_n^* is the empirical distribution function of bootstrap samples. It is difficult to calculate $\theta(F)$ when the sample size is small, so we replace $\theta(F)$ with $\hat{\theta}(F_n)$.

Step4 Approximate the distribution of T_n by the distribution of R_n. We can obtain B possible values of statistics $\theta(F)$, and then determine distribution and statistical properties of θ.

3. MODEL VALIDATION METHOD WITH IMPROVED BOOTSTRAP AND BAYES ESTIMATION FOR SMALL SAMPLE

During model validation process, due to the limitation of various factors, the observed samples obtained are limited. It is difficult to obtain accuracy validation results using statistical analysis method. This chapter we describe two schemes to solve model validation problem with small sample size. The first one is estimating statistical characteristics of observed samples and simulation samples, and then utilizing two-sample hypothesis testing to evaluate model credibility. The second one is enlarging observed sample size with improved Bootstrap method firstly, and then using Bayes method to estimate statistical properties of observed samples, finally utilizing single-sample hypothesis testing to evaluate model credibility. Our primary concern is the second model validation scheme. The core process is given in Figure 1.
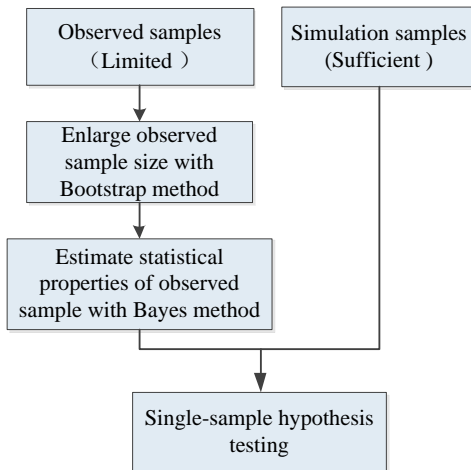
Figure 1: Model Validation Schemes with Small Sample Size

3.1. Improved Bootstrap Method

The sampling method of conventional Bootstrap utilizes empirical distribution function indirectly, which regenerates samples from the original data. The bootstrap samples don't increase any information beyond the original data. Especially in the case of small sample size, the probability distribution is concentrated in a few points after multiple sampling processes. It is difficult to obtain accurate parameter estimators due to large deviation from the real sample distribution (Zhang and Feng 2009).

We consider the limitations of conventional Bootstrap sampling method and propose an improved Bootstrap method. Assume $X_i (i = 1, 2, \cdots, n)$ are original samples, the improved Bootstrap sampling procedure is as follows:

- Generate arbitrary random λ follows uniform distribution over the interval [0,1] with computer, that is $\lambda \sim U(0,1)$.
- Let ζ be random variable and $\zeta = (n-1)\lambda$, denote $i = [\zeta] + 1$, where [.] is rounded down.
- Define the formula of bootstrap samples according to the value of i. If $i > [n/2]$, the bootstrap sample X^* can be stated as $X_{(i+1)} + (\zeta - i + 1)(X_{(i+1)} - X_{(i)})$; otherwise, X^* is stated as $X_{(i)} - (\zeta - i + 1)(X_{(i+1)} - X_{(i)})$.

Thus, we can obtain bootstrap sample X^* is defined as follow:

$$X^* = \begin{cases} X_{(i+1)} + (\zeta - i + 1)(X_{(i+1)} - X_{(i)}), i > [n/2] \\ X_{(i)} - (\zeta - i + 1)(X_{(i+1)} - X_{(i)}), i \leq [n/2] \end{cases}, \qquad (9)$$

where $X_{(i)}$ is the ith statistic of original data, and $X_{(1)} \leq X_{(2)} \leq \cdots \leq X_{(n)}$ is the order statistic and then we can obtain n groups bootstrap samples, $X_j^* = (X_{j1}^*, X_{j2}^*, \cdots, X_{jn}^*)$.

Repeat the above steps for N times and we can we get a matrix of N sets of Bootstrap samples which is defined as:

$$X^* = \begin{bmatrix} X_{11}^* & X_{12}^* & \cdots & X_{1n}^* \\ X_{21}^* & X_{22}^* & \cdots & X_{2n}^* \\ \vdots & \vdots & \ddots & \vdots \\ X_{N1}^* & X_{N2}^* & \cdots & X_{Nn}^* \end{bmatrix}_{N \times n} \qquad (10)$$

Under the equation given above, bootstrap sample X^* is a weighted average of the original data. When ζ is an integer, bootstrap samples contain original data, otherwise, bootstrap samples expand to non-observed data. We can get a larger or smaller bootstrap sample compared to the original data when i takes different

values, which increasing information of bootstrap samples. Consequently, the improved Bootstrap method extends bootstrap samples range and reduces the repetition of bootstrap sample and original data while keeping the distribution characteristics as consistent as possible.

3.2. Model Validation Method Based on Improved Bootstrap and Bayes Estimation

This chapter provides a model validation method for small sample combining the second model validation scheme and improved Bootstrap method above. The specific process is shown in Figure 2.
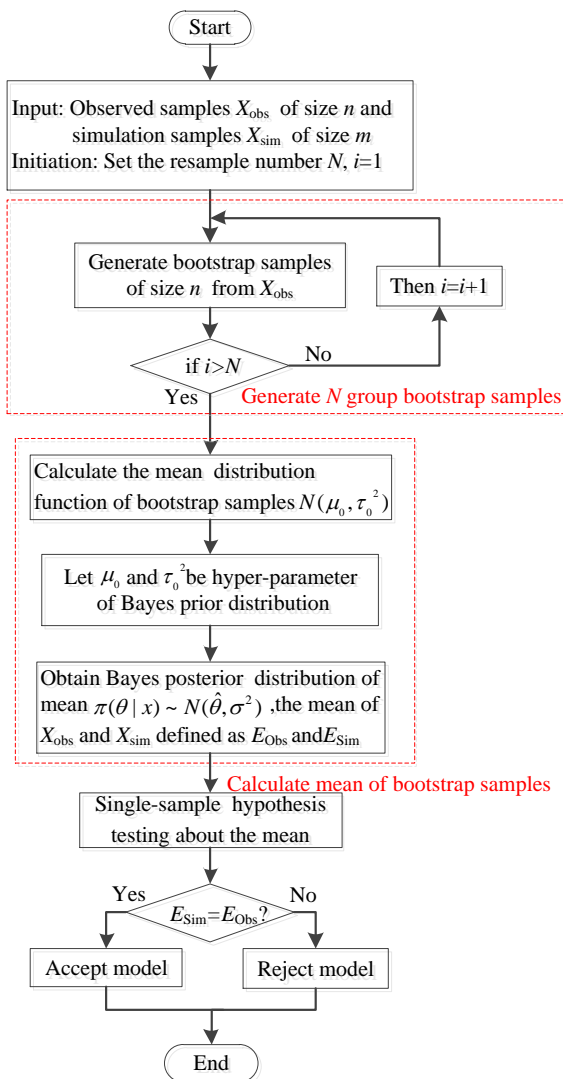
Figure 2: Validation Process Based on improved Bootstrap and Bayes Estimation

Step1 Give observed samples X_{obs} of size n and simulation samples X_{sim} of size m, where n is small and m is sufficient. Initialize the bootstrap samples number N and $i=1$.

Step2 Generate bootstrap samples from X_{obs} with Bootstrap method. Repeat above process for $i = 1, 2, \cdots N$, and then we can get N group bootstrap samples. By this way, the capacity of observed data is extended.

Step3 Calculate the mean distribution function of bootstrap samples, which is defined as $N(\mu_0, \tau_0^2)$.

Step4 Let parameters μ_0 and τ_0^2 replace the hyper-parameters of Bayes prior distribution $\pi(\theta) \sim N(\mu, \tau^2)$, which namely $\mu = \mu_0$ and $\tau^2 = \tau_0^2$.

Step5 Obtain the mean posterior distribution of observed samples with Bayes method, which is defined as $\pi(\theta \mid x) \sim N(\hat{\theta}, \sigma^2)$. Thus, we can obtain the mean estimator of observed samples which is defined as E_{Obs}. The mean of simulation samples is defined as E_{Sim}, and We take E_{Obs} as a known value.

Step6 Use single-sample hypothesis testing about the mean for the consistency analysis of observed samples and simulation samples.

Step7 Determine the similarity of E_{Obs} and E_{Sim}, if $E_{Obs} = E_{Sim}$, we accept simulation model and consider it is credible. Otherwise, we reject it.

4. CASE STUDY

This section gives two numerical examples to test the effectiveness of improved Bootstrap method and provided model validation method for small sample. The results of each example are given in the following two sub-sections.

4.1. Numerical Examples 1

We Generate a group of random sample X which follows normal distribution $N(1, 0.5)$ with computer, and the number of sample X is $n=10$.

X=0.2763, 1.7330, 0.1271, 0.6339, 1.1102, 0.3611, 0.6972, 0.7450, 0.4645, 0.3768.

Classical statistical method, conventional Bootstrap method and improved Bootstrap method are respectively used to estimate the mean value of sample X. We use conventional and improved Bootstrap method to generate N=10000 bootstrap samples respectively, and then estimate the mean value μ of bootstrap samples.
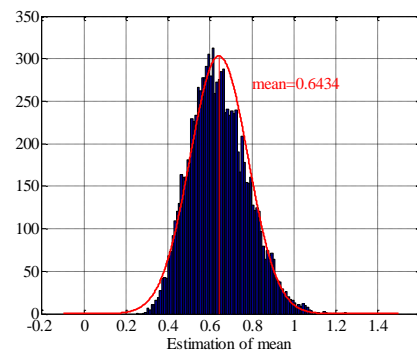
Figure 3: Distribution Histogram of Parameter μ from Conventional Bootstrap

Table 1: Parameter Estimation Results of Mean μ

Method	Mean Estimation			Improved Accuracy	Bootstrap Samples Range
	Estimator	Expected	Error		
Classical statistical	0.6325		0.3675	-	[0.1271, 1.7330]
Conventional Bootstrap	0.6434	1	0.3566	1.09%	
Improved Bootstrap	0.6856		0.3144	5.31%	[-0.0157, 2.4157]
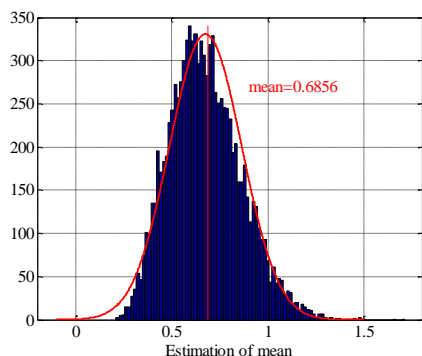
Figure 4: Distribution Histogram of Parameter μ from Improved Bootstrap

Figure 5: Box Plot of Bootstrap Samples mean μ

Figure 3 and Figure 4 respectively shows the distribution histogram of the mean for conventional Bootstrap and improved Bootstrap. We can see that the mean distributions of two methods approximately obey normal distribution. The red lines represent parameter estimators obtained from bootstrap samples, and the point estimators are respectively $\hat{\mu} = 0.6434$ and $\hat{\mu} = 0.6856$ with conventional and improved Bootstrap method. In order to prove the superiority of bootstrap method, the parameter estimation results from classical statistical method are also listed, which are shown in Table1.

The obtained mean estimation is $\hat{\mu} = 0.6325$ when using classical statistical method and the expected mean of sample X is 1. From results we can know, the advantages of classical statistical method are no longer obvious with limited sample, and it may bring a large estimation error. The accuracy of parameter estimation is raised 1.09% when using conventional Bootstrap method; and the accuracy obtained from improved Bootstrap method is raised 5.31%, which is higher compare to the conventional one. The mean μ obtained from improved Bootstrap method is closest to the true value with minimal error, which proves the improved Bootstrap method can get a better accuracy.

Moreover, the improved Bootstrap method extends the range of bootstrap samples from [0.1271, 1.7330] to [-0.0157, 2.4157], which can reflect the true distribution of original samples better. Figure 5 shows the boxplot of mean μ from conventional and improved Bootstrap samples. It is possible to see that the mean μ of improved bootstrap method is extended.

Overall, though the improvement of estimation accuracy is limited, it extends the range of resamples beyond the original data which can reflect the real distribution better.
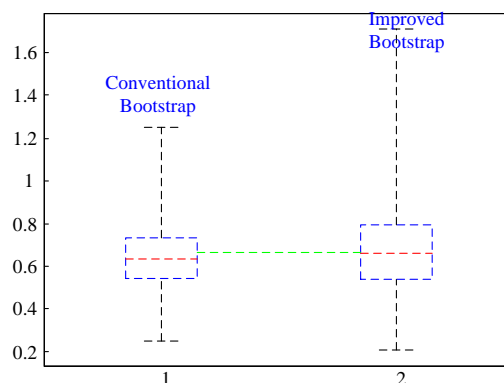
4.2. Numerical Examples 2

This section we use observed data and simulation data as an example to test the effectiveness of proposed model validation method. The observed sample X and simulation sample Y are given in Table 2, where the number of X and Y is $n=10$ and $n=1000$ respectively.

Table 2: Observed Samples and Simulation Samples

Observed Sample X	Simulation Sample Y
4.2268, 4.6096, 4.7890, 4.8821, 4.9283, 4.9499, 5.1543, 5.1656, 5.5389, 5.6459.	5.0971, 5.1488, 4.6449, 4.6562, 5.2864, 5.2226, 4.3370, 4.2501, 5.5080, ······ 5.5219, 4.9315, 4.5048, 5.5222, 5.9123, 5.3517, 4.5889, 4.7753, 5.3516.
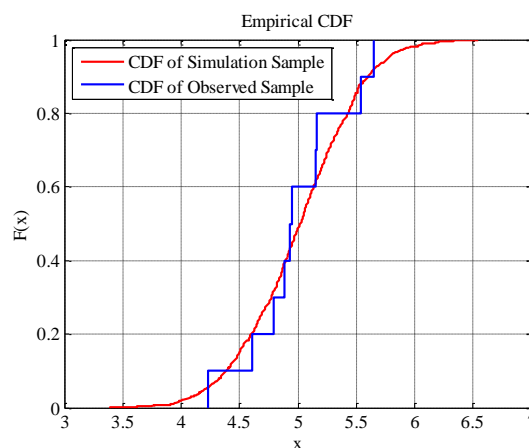
Figure 6: Cumulative Empirical Distribution Function Graph

Table 3: Comparison of Hypothesis Testing Results

Method	Bayes Prior $\pi(\theta)$	Bayes Posterior Estimator μ	Simulation Samples Mean μ	Error	Hypothesis Testing Results	
					p-value	h
Bayes Estimation (Conventional Bootstrap)	$N(4.9860, 0.0156)$	4.9875	5.0406	0.0531	0.1692	0(Accepted)
Bayes Estimation (Improved Bootstrap)	$N(4.9937, 0.0267)$	4.9914		0.0492	0.2640	0(Accepted)

Figure 6 shows the empirical cumulative distribution function graph of simulation samples and observed samples. We can observe that the distance between the two samples is close at the middle position; nevertheless, the difference between two samples is large at two ends. So we cannot determine whether the two samples come from the same normal distribution directly.

Thus, a model validation method based on Bootstrap method and Bayes estimation is applied for the consistency analysis between observed samples and simulation samples. Normality test is firstly carried through to verify whether the sample X and Y obey normal distribution. The Lilliefors test results can be obtained by using MATLAB, and the results reveal that both the sample X and Y follow normal distribution.

This chapter we take hypothesis testing about the mean as an example. Table 3 shows the testing results, where the mean of simulation samples is $\mu = 5.0406$, and Bayes posterior estimator of mean based on conventional Bootstrap and improved Bootstrap method are respectively $\mu = 4.9875$ and $\mu = 4.9914$. Obviously, the improved Bootstrap method can obtain less estimation error than the conventional one. We can draw the conclusion of accepting null hypothesis when using Bayes estimation based on conventional and improved Bootstrap method, in other words, the model is credible. Furthermore, we can get a larger p-value with improved Bootstrap method, which means there is a greater probability to accept the model.

From the numerical examples and analysis, we may draw the following conclusions. Firstly, compared to conventional Bootstrap method, the improved Bootstrap method can not only extends the range of resamples beyond the original data, but also raise the parameter estimation accuracy to some extent. Secondly, the provided model validation method based on improved bootstrap approach and Bayes estimation is effective for the similarity analysis between small observed samples and sufficient simulated samples.

5. CONCLUSIONS

This paper focuses on the model validation problem with limited observed samples. A method based on improved Bootstrap approach and Bayes estimation is provided. The model validation method, which combining Bootstrap approach, Bayes estimation and hypothesis testing for single sample, provides an effective solution for the similarity analysis between small observed samples and sufficient simulated samples. Furthermore, an improved Bootstrap method is proposed to raise the accuracy of parameter estimation and extend the resample range. The numerical examples reveal that the provided method can effectively solve the model validation problem with limited sample and the improved Bootstrap method can improve the quality of resample.

REFERENCES
Ahmed F., Mohamed A., Jaeyoung L., Naveen E., 2017. Application of Bayesian informative priors to enhance the transferability. Journal of Safety Research, 62, 155-161

Bunouf P., Lecoutre B., 2006. Bayesian priors in sequential binomial design. Comptes Rendus Mathematique, 343, 339-334.

Chihara L., Hesterberg T., 2011. Mathematical Statistics with Resampling and R. Hoboken, NJ, USA: Wiley.

Dai Z.H., Wang Z., Jiao Y., 2014. Bayes monte-carlo assessment method of protection systems reliability based on small failure sample data. IEEE Transactions on Power Delivery, 29(4), 1841-1848.

Efron B., 1979. Bootstrap methods: another look at the jackknife. Annals of Statistics, 7(1), 1-26.

Heydari S., Miranda-Moreno L., Lord D., Fu L., 2014. Bayesian methodology to estimate and update safety performance functions under limited data conditions: A sensitivity analysis. Accident Analysis and Prevention, 64, 41–51.

Kyselý J., 2010. Coverage probability of Bootstrap confidence intervals in heavy tailed frequency models, with application to precipitation data. Theoretical and Applied Climatology, 101(3-4), 345–361.

Li C.Z., Mahadevan S., 2016. Role of calibration, validation, and relevance in multi-level uncertainty integration. Reliability Engineering & System Safety, 148, 32-43.

Oberkampf W.L., Barone M.F., 2006. Measures of agreement between computation and experiment:

validation metrics. *Journal of Computational Physics*, 217(1), 5–36.

Sargent R.G., 2013. Verification and validation of simulation models. *Journal of Simulation*, 7(1), 12-24.

Samart K., Jansakul N., Chongcheawchamnan M., 2017. Exact bootstrap confidence intervals for regression coefficients in small samples. *Communication in Statistics-Simulation and Computation*. 1-7 (electronically published).

Tang X.M., 2002. Validation method of simulation model under small sample size. *Journal of System Simulation*, 14(10), 1263-1266.

Xiao Z.C., Gao H.M., Ding T., Han J.F., 2009. The application of self-help method in mean estimation of small sample data. *Journal of Naval Aeronautical Engineering Institute*, 24(5), 563-567.

Yalcinkaya M., Birgoren B., 2017. Confidence interval estimation of Weibull lower percentiles in small samples via Bayesian inference. *Journal of the European Ceramic Society*, 37, 2983-2990.

Zhang S.Y., Feng W.S., 2009. Study of sampled data creation for norm distribution on Bootstrap method. *Journal of Academy of Equipment Command & Technology*, 20(2), 97-100.

AUTHORS BIOGRAPHY

TING SONG is a M.S. candidate major in control science and engineering at Harbin Institute of Technology (HIT), Harbin, China. Her research interests include the system simulation, model validation. Her e-mail address is songting0928@outlook.com.

PING MA is a full professor with the Control and Simulation Center, HIT. She received the Ph.D. degree in control science and engineering from HIT, in 2003. Moreover, she serves as the standing director of China Simulation Federation (CSF). Her research interests include the complex system modeling & simulation, validation, validation & accreditation (VV&A). Her e-mail address is pingma@hit.edu.cn.

YUCHEN ZHOU is a Ph.D. candidate major in control science and engineering at HIT, Harbin, China. He received the M.S. degree in control science and engineering from HIT in 2014. His research interests include the complex system simulation, model validation, and experiment design. His e-mail address is zhouyuchen-01@163.com.

KE FANG is an associate professor with the Control and Simulation Center, HIT. He received the Ph.D. degree in control science and engineering from HIT, in 2007. He was at Arizona State University as a visiting scholar from 2014 to 2015. His research interests include complex system simulation, VV&A and credibility evaluation of complex simulation system. His e-mail address is hitsim@163.com.

MING YANG is the corresponding author. He is a full professor with the Control and Simulation Center, HIT. He received the Ph.D. degree in control science and engineering from HIT, in 1997. Moreover, he serves as vice president of China Simulation Federation. His research interests include the complex system simulation theory and advanced distributed simulation technology & application. His e-mail address is myang@hit.edu.cn.

STATE OF THE ART FOR THE OPTIMIZATION AND SIMULATION OF THE DISTRIBUTION OF HYDROCARBONS

Emilio Sampayo Trujillo[a], Idalia Flores De La Mota[b]

[a] PEMEX, Exploración y Producción [b] Faculty of Engineering, UNAM

[a]emilio.sampayo@pemex.com, [b]idalia@unam.mx

ABSTRACT
Hydrocarbons distribution networks are strategic for the oil industry. That is why the research being presented in this article focuses on thoroughly reviewing everything that has been developed on the subject in different parts of the world over the last fifteen years. The reviewed articles have been classified according to the models that were built, the methods used to solve said models and the approach that has been developed. Because of the characteristics of the problem in general, there is more research available that uses mathematical models and finds the solution with different optimization methods. Secondly, though no less important we found simulation models for studying some aspects that are differentiated from the optimization models.

Keywords: Hydrocarbons, distribution networks, optimization, simulation

1. INTRODUCTION

Petróleos Mexicanos is currently one of the 100 largest companies in the world. Its most profitable business is oil exploration and production which is done through Pemex Exploración y Producción (PEP), the only company in the Pemex Group with a special tax régime.

In 2004 PEP was the third biggest oil producer in the world with a yearly average of 3.4 million de barrels a day, of which 2.1 million came from Cantarell, one of the highest producing oil fields in the world. Since then, Cantarell has suffered a natural decline and nowadays only produces about 200 thousand barrels a day.

The challenge for Pemex Exploración y Producción is to replace the fall in Cantarell's production, stabilize production and eventually profitably, surely and sustainably increase the platform.

It also faces the challenge of adjusting the cost structure to a scenario of low prices and the historic opportunity to use all the tools provided by the Energy Reform, in other words, it can develop a similar operation to all the other oil companies in the world, which will allow it to share technical, technological and financial risks throughout the value chain.

To achieve this, Pemex put into operation its Business Plan, which it uses to encourage alliances to be created throughout Pemex's value chain as a mechanism for increasing its investments and efficiency. For example,

Petróleos Mexicanos and the Australian company, BHP Billiton, signed the license agreement for the development of the deepwater Trion block.

This is the first partnership for exploration and production via farm-out or partnership that Pemex has entered in all its history, taking advantage of the mechanisms and flexibility it is granted under the Energy Reform. The Trion block, discovered by Pemex in 2012, has total 3P reserves of 485 million barrels of equivalent crude oil, so there is certainty about its commercial viability.

However, it must be pointed out that oil acquires its true economic value on being sold, meaning that the hydrocarbons distribution process, which starts at the production complexes and ends at the points of sale, is particularly important.

Nowadays there is no tool or procedure that makes it possible to analyze the overall economic value that can be obtained through Pemex Exploración y Producción's hydrocarbons distribution, collection and treatment infrastructure, which it makes available to the Oil Concessions and new operators, if necessary.

This article gives the state of the art for the different techniques that have developed solutions over the last eighteen years for the distribution of gas main and, in some cases, crude oil. This bibliographic review basically deals with the optimization and simulation models used, which will allow us to frame the contribution to the optimization and simulation of PEMEX's Hydrocarbons Distribution System that we intend to set forth in a later article. Said model will allow us to generate higher economic value by optimizing mixtures.

The proposed methodological basis is based on optimization theories and techniques, mixed integer programming, which is suitable for the design of a large-scale complex networks model, and whose results support decision-making for adjusting the cost structure for the hydrocarbons distribution under a low-price scenario. Then, given the characteristics of the integer models, the simulation will be used to create scenarios.

Several systems have been put together to represent the operation of the hydrocarbons transportation and collection system, using virtual routes without taking into account the real routes, the installed capacity, and economy of hydrocarbons. These efforts have been very

valuable and have enabled us to see the importance of having more precise tools that include economic aspects. This article is organized as follows: Section 2 briefly describes the problem and its main characteristics. Section 3 presents a state of the art where the models and methods employed in the relevant literature are reviewed, with attention being paid to optimization, optimization-simulation and simulation models. Section 4 shows the most relevant lines of research and analyzes the literature. Finally, we give our conclusions and suggestions for future research.

2. DESCRIPTION OF THE PROBLEM

The hydrocarbons distribution, collection, and treatment system consist of hundreds of pipelines and facilities of various types and capacities that make up a highly complex network that, through multiple routes, connects the production complexes with the points of sale.

This complexity is multiplied by this system being used to distribute several products of varied qualities that are mixed with each other to obtain new products while being transported through the network.

Another particularity of the network is that the nodes can be associated with different processes, some of which specifically relate to transport, such as compression for gases or pumping for liquids, and others for the conditioning of the products, such as dehydration, desalination, and mixing, to name but a few.

Both the economic information for each pipeline and the prices associated with the products are preponderant for the programming of the economy that is implicit in the distribution, collection, and treatment system.

The problem to be solved consists of finding the routes that optimize the distribution of hydrocarbons from the production complexes to the points of sale, maximizing expected profits and giving customer satisfaction in terms of the quantity and quality of the product, in other words, the mixture that reaches the points of sale must meet the required quality.

Every transfer node that receives production from two or more nodes must have a process module for obtaining the quality of the outlet mixture. Routes generally have several transfer nodes.

In this regard, the problem can be identified as a maximum distribution problem in a network with minimum costs and with the following characteristics and restrictions.

This is a multimodal network as it considers two products: oil and gas, as well as having three types of pipelines: oil pipelines, gas pipelines and oil and gas pipelines. The methods to be employed for finding a solution may consider every product in the multimodal network, or else break the network down into layers in accordance with each product.

This problem consists of maximizing the profits obtained from the sale of the hydrocarbons that circulate in the system while at the same time considering the minimum cost. Some authors describe this problem as one of maximum flow at minimum cost. A minimum-cost maximum flow for a $G = (V, E)$ network is a maximum

flow with the lowest possible cost. This problem combines the maximum flow (obtaining the highest possible flow from the source node (or nodes) to the sink node (or nodes), with the lowest cost path from the source to the sink node.

There are several source nodes and several sink nodes.

What goes into the transfer nodes is the same as what comes out, as long as they are not transferred nodes that deal with mixtures or processes, in which case the products leave the node improved and differentiated by quality and other characteristics.

The pipelines have an installed capacity that depends on their diameters, length, intake and outlet pressures, while also considering chemical factors that are inherent to the product.

Costs per section (pipelines) are considered as is the volume that flows. It is a large-scale network as it has more than 300 nodes and 500 arcs.

The following figure 1 shows a part of the network in simplified form.
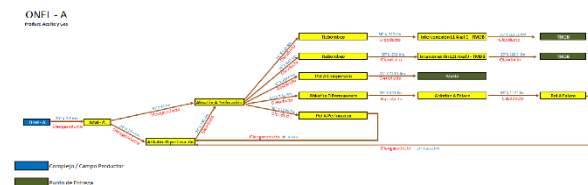
Fig.1 Simplified network of the problem

3. STATE OF THE ART

We will now review and describe a variety of articles published over the last few years. These articles are important for the definition of the models and tools to be used for solving the problem, however some of them were considered because of the problem's structure, such as a distribution network, even though in several of them the product is natural gas.

We will make a classification of the articles according to the type of problem being posed in the network or the approach for optimizing it, thus we get:

The products that go through chemical processes at certain nodes, as well as the characteristics inherent to said products.

Focus on the network's supply chain.

The above classification is framed around the models and their solution methods, which are basically optimization and simulation models.

The transport of hydrocarbons is a very important process for the oil and gas industry and, as such, needs to be performed with maximum efficiency. Pipeline systems are known to be the most economical, effective and safe means of transporting these products, but this literature review is required to support said assertion.

3.1. Optimization Models

Because of their relevance, since 2001 efforts have been made to optimize hydrocarbon transport networks. That

year, Jokic and Zavargo developed a nonlinear programming model (NLP) for optimizing a network for oil transport specified the volumes to be transported and considered the pressures at the intake and outlet from the pipelines, thus managing to minimize the operating cost. The model was solved using Mathead 2000 software.

Adeyanju and Oyekunle (2004) later developed a nonlinear optimization procedure NLP (objective function and nonlinear constraints), for a natural gas transportation network using an adaptation of the generalized reduced gradient algorithm, with which they determined the optimum economic conditions under which natural gas can be transported through a network of gas pipelines and compression stations.

MirHassani et al. (2008) presented an integer programming approach to oil derivative transportation scheduling. The system they reported is composed of an oil refinery, a multi-branch multi-product pipeline connected to several depots and local consumer markets that receive large quantities of refinery products. Batches of refined products and grades are pumped back-to-back in the pipeline, without any separation device between them. The sequence and length should be carefully selected for such pumping runs to meet market demands while, at the same time, satisfying a lot of pipeline operational constraints, such as minimum interfaces. The model was a MIP and was solved using CPLEX.

Selot (2009) analyzed short-term (2-12 weeks) supply chain management in upstream natural gas networks. A global optimization model (GO) is used for the production system, as it is a nonlinear mixed integer programming (MINLP) model. This paper included a model made up of two components: the infrastructure model, which is a physical model of the system (in other words, the wells, the pipelines and facilities) and the contractual model, which is a mathematical representation of the existing regulations.

It is important to explain the terms "upstream" and "downstream":

"Upstream" and "downstream" are general business terms referring to oil or Gas Company's location in the supply chain. The closer to the end user a function or firm is, the further downstream it is said to be. Raw material extraction and production are elements of the supply chain considered to be upstream. Upstream companies identify oil and natural gas deposits and engage in the extraction of these resources from underground. These firms are often called exploration and production companies. Refiners represent the downstream element of the oil and gas supply chain.

Midstream operations link the upstream and downstream entities. Midstream operations mostly include resource transportation and storage, such as pipelines and gathering systems.

Figure 2: Production and Gathering: Three Sectors
Source: https://www.psgdover.com/en/oil-and-gas/oil-gas-market-overview/oil-gas-upstream

Chebouba, et al. (2009) proposed a nonlinear integer model (NLIP) for which they designed an ant colony optimization algorithm for gas pipeline operations with a constant flow. This is a system consisting of connected compression stations. The decision variables are chosen to determine the number of turbochargers in operation and the discharge pressure for each compression station. The objective function is the power consumed by these stations in the system.

Analyzing the distribution of petroleum products in China, Huanchao et al. (2009) developed a logistics model for oil, based on the inventory-transportation integrated optimization problem - a linear problem (LP) using LINGO (Optimization Modeling Software for Linear, Nonlinear, and Integer Programming) software - to check and compare its results with traditional optimization methods and be able to prove its superiority. With the rise in global demand for energy, natural gas plays an increasingly important role in the energy market. To meet demand, optimization techniques, producing some promising results, have been widely used in the natural gas industry. In this vein Zheng et al. (2010) made a detailed analysis of optimization models in the natural gas industry, focusing on production, transport and the market. Thus, for the production problem, they proposed models for the production scheduling problem and the maximal recovery problem. For the gas transportation problem, the network design problems and the optimal fuel cost problem, and finally for the market problem, both regulated and deregulated market models are considered. The models used are nonlinear and non-convex so linearization is performed for their solution or the use of metaheuristics is proposed. Borraz-Sánchez (2010), in his doctoral dissertation, developed some models for solving the problem of optimizing gas pipelines. In this project, a multi-period model is proposed to tackle *the line-packing problem*. The model has nonlinear constraints and both continuous and integer decision variables, and qualities thus as such as a mixed-integer nonlinear programming (MINLP)

model. In the project, authors develop an extensive numerical experiment to evaluate the computability of the model. This experimental phase is based on a GAMS formulation for the MINLP model, while applying the global optimizer BARON. Exact methods and heuristics are used in the models that are presented.

Jin and Wojtanowicz (2010) developed a study aimed at optimizing the natural gas network to minimize its energy consumption and cost. They used four different optimization methods: the penalty function method; pattern search; implicit enumeration and non-sequential dynamic programming, to solve the problem. The results show that cost savings, because of global optimization, are reduced with increased throughput.

Domschke et al (2011) studied the technical optimization problem of a transient gas network, which can be considered a minimum-cost flow problem with a non-linear objective function and additional non-linear constraints on the network arcs. They solved it through a "combination of a novel mixed integer linear programming approach based on piecewise linearization and a classic sequential quadratic program applied for given combinatorial constraints".

Gupta and Grossmann (2012) presented an efficient strategic/tactical planning model for the problem of the development of offshore oilfields, which is generic and can be extended to include other complexities. The model, which is multi-period and mixed integer non-linear programming MINLP, is proposed for multi-field sites and includes three components (oil, water and gas) explicitly in the formulation. Aimed at maximizing the present total net value for the long-term planning horizon, the model involves decisions relating to the installation of FPSO (Floating Production Storage and Offloading), well drilling schedules and rates of production for the three components in each period. This model can be effectively solved using DICOPT (DIscrete and COntinuous OPTimizer) developed by Grossman and is useful for real cases as it gives good quality solutions.

Hübner y Haubrich (2012) proposed a method based on genetic algorithms for planning and optimizing natural gas distribution networks from a long-term planning perspective. The method can calculate network structures that are cost-efficient in terms of all the technical and economic conditions.

Babonneau et al. (2012) developed a multi-objective model to get around the difficulty represented by the operation of gas distribution networks, because of the total energy dissipated in the network. The two objectives posed in the model correspond to the

investment cost function and the energy that is required to transport the gas.

Borraz-Sánchez and Haugland (2013) approached the flow maximization problem in a natural gas transportation pipeline system. Their model incorporates the variation in pipeline flow capacities with the specific gravity of the gas and compressibility. Given that the proposed model is not convex and, therefore the global optimization can take a long time, they propose for their solution a heuristic method based on an iterative approach where a simpler NLP model solved in each iteration.

MohamadiBaghmolaei et al. (2014) carried out a study for minimizing the fuel consumption of a pipeline system that includes reinforcement units. For the analysis they used the steady-state non-isothermal natural gas flow. Due to the lack of information and difficulties in predicting gas turbine and compressor efficiency, intelligent systems may be used to find the relations between the parameters involved, including the Artificial Neural Network (ANN), the Adaptive Neuro-Fuzzy Inference System (ANFIS) and the Fuzzy Inference System (FIS), for predicting and optimizing the pipeline network from the IGAT 5 system that transports the natural gas from Asalouyeh (South Pars Energy Zone-IRAN) in order to injected into the oil wells. The results showed that ANN is slightly more precise than the other two predictive methods. Therefore, the ANN results were introduced into a Genetic Algorithm (GA) to determine the optimum speed for each compressor and its compression ratio.

For their part, Alinia et al. (2014) proposed a multi-objective approach to finding the optimum operating conditions for a natural gas network. For this purpose, they made a thermodynamic model of natural gas through the main elements of the network. Their aim is to find the optimum values of three objective functions: i) the maximum gas delivery flow; ii) the line pack and iii) the minimum operating cost. Here, a fast and elitist non-dominated sorting genetic-algorithm (NSGA-II) is applied by considering fourteen decision variables: the number of running turbo-compressors (TCs) and their rotational speed in compressor stations as well as the gas flow rate and pressure at injection points. The results of multi-objective optimization are obtained as a set of multiple optimum solutions, called 'the Pareto optimal solutions'. Furthermore, a set of typical constraints governing the pipeline operation is subjected to obtain more practical solutions.

Fabro et al. (2014) presented a model too assist in the operational decision-making of scheduling activities in a gas pipeline that transports heavy oil derivatives. The

approach they proposed develops a decomposition procedure that uses a sequence of mathematical and heuristic programming models (MILP), which were run on the CPLEX program to solve the problem.

Wu et al. (2014) built an MINLP optimization model for natural gas trunk pipelines for balancing the maximum operation benefit and the maximum transmission amount.

The sum of weight method was used to combine the two objective functions and, in this way, modeled a hybrid objective function. To weight each objective function, the Analytical Hierarchy Method (AHP) was used. Restrictions related to node pressure, flow rate and temperature were considered as restrictions of the model. The power and condition of the compressor, the pressure and temperature equations of the pipeline were also incorporated into the model. As the model is non-linear, the particle swarm optimization algorithm (PSO) was used to solve it, and the adaptive inertial weight adjustment method was adopted to improve the basic PSO for its premature defect. The IAPSO shows a faster convergence speed and better solution results than those of the other four PSO

Ribeiro de Lucerna et al. (2014) generated an optimization method for submarine pipeline routes, employed to carry the oil and gas from offshore platforms. Several methods associated with the modeling and solution of the optimization problem were addressed, including: the geometrical parameterization of the candidate routes; their encoding in the context of a genetic algorithm (GA) and the incorporation into the objective function of the several design criteria involved in the route evaluation.

Pfetsch et al. (2015) researched methods for solving gas transportation issues, particularly the validation of the nomination problem that takes as a given a gas transmission network consisting of passive pipelines, active, controllable elements and an amount of gas at every entry and exit point of the network; for which operational settings are sought for all the active elements in such a way that there is a network state that fulfills all the physical, technical, and legal constraints. The authors described a two-stage approach for solving the nonlinear feasibility problem; the first phase with four algorithms: the methods of mixed integer linear programming (MILP), mixed integer non-linear programming (MINLP), nonlinear reduced gradient (GRNL) and de complementarity constraints (CRP) for calculating the possible settings for discrete decisions; while the second phase employs a continuous nonlinear programming model of the gas network.

Chebouba (2015) addressed the management of the "GZ1 Hassi R'mell-Arzew" gas pipeline network. For this system, the decision-making on the line pack usually involves a delicate balance between the minimization of fuel consumption in the compression stations and the maximizing of the gas line pack. To select an acceptable pack considering these two aspects for the "GZ1 Hassi R'mell- Arzew" pipeline, the idea was introduced of multi-objective decision-making. The first step in the development of this procedure is the derivation of a numerical method to analyze the flow through the pipeline under transient isothermal conditions, for which the NSGA-II (Non-dominated Sorting Genetic Algorithm) algorithm of the mode FRONTIER (coupled with a Matlab program) was used to solve the multi-objective problem.

Kazemi et al. (2015) proposed a deterministic mixed integer linear programming (MILP) model for a downstream petroleum supply chain (PSC) network to determine the optimal distribution center (DC) locations, capacities, transportation modes, and transfer volumes. This model minimizes multi-echelon multi-product cost along the refineries, distribution centers, transportation modes and demand nodes.

Lui et al. (2015) analyzing the characteristics of oil–gas production process and the relationship between subsystems, a multi-objective optimization model is proposed with maximizing the overall oil production and minimizing the overall water production and comprehensive energy consumption for per-ton oil. And then the non-dominated sorting genetic algorithm-II (NSGA-II) is used to solve the model. To further improve the diversity and convergence of Pareto optimal solutions obtained by NSGA-II algorithm, an improved NSGA-II algorithm (I-NSGA-II) is proposed.

In recent years, a large amount of research has been conducted on problems in the natural gas industry and, specifically, in the optimization of the pipeline network. Ríos-Mercado and Borraz-Sánchez (2015) presented a review of the current state of the art. The authors focus on categories such as: short-term storage (line packing problems), gas quality satisfaction (grouping problems) and compressor station modeling (problems of fuel cost minimization). The optimization models were discussed, highlighting the modeling aspects and the most relevant solution approaches known to date.

Sedliak and Zácik (2016) designed a methodology for solving optimization tasks for gas transport in a pipeline system such as: finding of maximal outflow; minimization problems (e.g., finding minimal gas consumption under certain transport conditions), and multi-objective optimization (e.g., minimal energy consumption and prescribed line pack). To this end, they made modifications to the evolution strategy algorithm.

The proposed algorithm was implemented in C++ programming language as an embedded module in software MARTI Studio—a general tool for solving tasks in gas industry.

Zhou et al. (2017) described, in a document, the optimization problems of pipeline transport for multi-phase flows. This article established a route optimization model that combines the hydraulic calculations with optimization theory and adopt the general genetic algorithm (gGA) and the steady-state genetic algorithm (ssGA) for its solution. It also obtains the optimum route and discusses the influence of the parameters setting the result. This algorithm was applied to determining optimum pipeline routes in the methane collection and transportation system in the coal fields of Shanxi province, China. The result showed that the algorithm is feasible and improves the hydraulic properties by reducing the pressure drop along the line.

Zhang and Liu (2017) developed an optimal operation model based on an improved genetic algorithm for natural gas pipeline network. For its solution, they chose the maximum benefit and maximum flow as the objective function, and selected several conditions as the constraints including the input and output of gas, the input and output pressure of gas, the handling capacity of the compression station, the strength of the pipeline, the pressure drop in the pipeline, the compressor, the valve, and the flow balance of the node of the pipeline network. They also establish an optimal mathematical operation model for the natural gas pipeline network. For this, they propose an improved genetic algorithm as the possibility of the fitness value of an individual in the initial population is abnormal and the possibility of the probabilities of the crossover and the mutation are too high or too low.

Ye et al. (2017). They studied the programming and routing of the tramp shipment and the oil supply chain. With this objective they developed two models of whole programming (MILP) for the assignment between tasks, deposits and timing problems. The first model used a concept of a time interval in a continuous time representation, where they consider the limitations related to the allocation of vessels, capacity, time, demand and control of slack. The second model uses a discrete time representation with time allocation, portal count and inventory control restrictions.

The authors Zhang et al. (2017) developed a hybrid method for detailed programming of a pipeline with multiple pumping stations. They explain that a multi-product pipeline is the most effective way to transport refined products and is of vital importance in the energy supply chain. The essential task in the actual operation of the pipeline is to schedule the delivery and injection of numerous types of products. The article presents a nonlinear mixed integer programming model (MINLP) for ducts with a single source and multiple pumping stations. The model contains two parts and is solved by a hybrid computational approach, the ant colony optimization algorithm (ACO) and the simplex (SM) method.

Yea et al. (2017) the refined oil transportation problem investigated in this paper lies on the intersection of the scheduling and routing of tramp shipping and the petroleum supply chain, with unprecedented large-scale and complex rules. Two mixed-integer linear programming formulations MILP are developed for the assignment between tasks, vessels, and timing issues. The first model uses a time-slot concept under a continuous-time representation, where the constraints that deal with vessel assignment, capacity, timing, demand, and slack stock control are considered. The second model uses a discrete-time representation with time assignment, portal counting, and strict stock control constraints. Finally, the impact of the model parameters is analyzed under different optimization scenarios.

Chen et al. (2017) explained how to optimize the detailed schedules of a multi-product pipeline. They presented a MILPD mixed discrete time linear integer programming model, through an objective function that consists of the minimum sum of the pump speed variations in each pipe segment along a pipeline during a planning horizon. In addition to operational limitations, two sets of special restrictions are introduced into the model to improve the operability and viability of detailed schedules. It was concluded that the more stable the pumping speed of a pipe segment, the lower the friction loss for the pumping products. The proposed MILP model is successfully tested in two real-world multiproduct pipelines using CPLEX.

Mikolajková et al. (2017) presented a model of a pipeline network for gas distribution considering supply of gas, either from external gas networks or as injected biogas or gasified liquefied natural gas (LNG) at terminals. The model is based on mass and energy balance equations for the network nodes, equations of the pressure drop of a compressible gas in the pipes, as well as expressions of gas compression in compressor nodes. The model is applied within an optimization framework where the optimal supply of natural gas to the customers is studied under a multi-period mixed integer nonlinear programming (MINLP) formulation, considering possible extensions of the pipeline network to new sites as well as potential supply of the gas from LNG terminals. The natural gas network in Finland is used in a case study, which determines the network's size and operation conditions.

Zhang et al. (2018) explained in their paper that the optimization of multi-product pipeline scheduling is complicated due to multi-batch sequent transportation and multi-point delivery. Based on this fact authors considered batch interface migration and divided the

model into time nodes sequencing issue and a mixed-integer linear programming (MILP) model with the known time node sequence. And a self-learning approach is proposed through the combination of fuzzy clustering analysis and ant colony optimization (ACO). This algorithm is capable of self-learning, which greatly improves the calculation speed and efficiency. At last, a real pipeline case in China is presented as an example to illustrate the reliability and practicability of the proposed model.

3.2. Optimization and Simulation

Aalto (2008) pointed out that many pipeline systems are nonlinear, such as compression station shutdown or start-up. A dynamic, receding horizon optimization problem was defined, where the free response prediction of the pipeline was obtained from a pipeline simulator and the optimal values of the decision variables were obtained by solving an approximate quadratic programming (QP) problem, where the cost function is the energy consumption of the compression stations. The problem was broadened using discrete decision variables to represent the compressors' shutdown/start-up commands. A mixed logical dynamical system was defined, but the resulting mixed-integer quadratic programming problem was shown to be very high dimensional. Whereas, a sequence of these types of problems was defined that resulted in an optimization problem with a considerably smaller dimension. The receding horizon optimization was tested in a simulation environment and comparison with data from a true natural gas pipeline shows 5 to 8 % savings in compressor energy consumption

Rizwan et al. (2013) presented an approach adopted by Kuwait Oil Company to establish an integrated Crude Oil Export Pipeline simulation model in South & East Kuwait area to achieve increase in overall asset-wide production and to improve future Pipeline & Facilities Design.

The simulation used As-Built pipeline data along with field data to achieve the objectives of the study.

Accuracy of the pipeline model was verified by comparing simulation results of the existing pipelines and manifolds with the operating data to confirm that model results duplicated field measurements. The model developed in this study has the characteristics and the ability to predict the flows and pressures under wide range of conditions — including various operational modes and constraints.

The model accurately predicted the capacities and raised few flags which were solved within short time and subsequently the network was optimized. Hydraulics study revealed that no additional capacity or looping were required. Model was studied for reliability of supply under wide range of conditions subject to potential bottlenecks and constraints which were identified in the study.

Huang et al. (2015) analyzed underground oil pipelines, which are made from pressurized pipes, where, if there is any damage, consequences could be disastrous. Oil pipeline accidents caused by stress can be attributed to material corrosion, impractical design, manufacturing defect, environmental damage, and man-made destruction. In this study, by using the stress analysis software, CAESAR II, pipeline stress was analyzed under the same operating conditions and different piping technologies. Comparing the different simulation consequences of each technology, an optimized laying process was proposed to reduce the stress of underground oil pipelines in steep areas. This article uses simulation and optimization.

3.3. Simulation Methods

Herrán-González et al. (2009) performed the modeling and simulation of a gas distribution pipeline network. Gas ducts are the most important components of such kind of systems since they define the major dynamic characteristics. Isothermal, unidirectional flow is usually assumed when modeling the gas flow through a gas duct. This paper presents two simplified models derived from the set of partial differential equations governing the dynamics of the process. These models include the inclination term, neglected in most related papers. Moreover, two numerical schemes are presented for the integration of such models. Also, it is shown how the pressure drop along the pipe has a strong dependency with the inclination term. To solve the system dynamics through the proposed numerical schemes a based MATLAB-Simulink library was built.

Behbahani-Nejad et al. (2010) developed an efficient transient flow simulation for pipelines and networks. The proposed transient flow simulation is based on the transfer function models and MATLAB-Simulink. The transfer functions equivalent to the non-linear control equations were derived for different types of boundary conditions. Subsequently, a MATLAB-Simulink library was developed and proposed considering any border conditions. To verify the accuracy and computational efficiency of the proposed simulation, the results obtained were compared with the finite difference schemes. In the simulation, the effect of the inertia of the flow was incorporated. Efficiency is shown through several instances and it is verified that the proposed simulation is sufficiently accurate and computationally more efficient than other methods.

Woldeyohannes and Majid (2011a) discussed the use of a simulation model to analyze the effect of the age of pipes on the performance of a natural gas transmission system. The flow equations which govern the simulation were modified to consider the effect of the age of pipes. They evaluated and compared the performance of three

groups of pipelines and the results of the simulation analysis showed a 2.16 and 4.35% drop in the flow capacity for 10 and 20-year-old pipes, respectively.

Woldeyohannes and Majid (2011b) developed a simulation model for the analysis of transmission pipeline network system (TPNS) with detailed characteristics of compressor stations. The compressor station is the key element in the TPNS as it provides energy to keep the gas moving. The simulation model is used to create a system that simulates TPNS with different configurations to get pressure and flow parameters. The mathematical formulations for the TPNS simulation were derived from the principles of flow of fluid through pipe, mass balance and compressor characteristics. To determine the unknown pressure and flow parameters, a visual C++ code was developed based on Newton–Raphson solution technique.

Cernelev et al. (2014) focused their research on the problem of identifying and removing bottlenecks in a multi-terminal oil and gas pipeline network while achieving quality and delivery targets, which is a very real and complex problem. The most effective way to meet the above business objective was to develop a terminal network simulation model. This paper is a case study describing the approach in designing a complex multi-nodal pipeline network simulation model aimed at resolving a critical inter-company storage problem for a major refiner.

Costa et al. (2014) explained that oil refining companies and distributors often use pipelines to transport their products. In highly integrated, geographically challenging contexts, this may result in complex logistical systems. Pipelines which transport multiple products connect tanks, forming a, self-contained environment where distribution routes (called logistical channels), tactical inventory locations and operational criteria are defined to transfer, receive and deliver liquid oil derivatives. Authors describe a simulation model designed to represent such a regional pipeline network and includes a case study of a Brazilian region with refineries, a maritime terminal, a hub terminal and distribution bases.

Szoplik (2016) The objective of this study was to elaborate a relation between the pressure and the current of gas introduced in the gas network for which gas modeling results were used in the network, obtained for the existing gas network and with real data about the load of the network depending on the time of day and the air temperature, this author presents an example of application. Based on the results obtained, it was concluded that this approach allows reducing the amount of gas supplied to the network by 0.4% of the annual load.

Addo Pambour et al. (2016) This paper presents an integrated transient hydraulic model that describes the dynamic behavior of natural gas transport systems (GTS). The model includes sub models of the most important facilities comprising a GTS, such as pipelines, compressor stations, pressure reduction stations, underground gas storage facilities and LNG Terminals. The sub models are combined to an integrated network model and the algorithm for solving the resulting system of equations is detailed.

Corbet et al. (2018) described a dynamic flow model in networks, designed to inform analyses of disruptions in infrastructures and to help in the formulation of policies to design robust mitigations. They conceptualized the adaptive responses of infrastructure networks to perturbations as market transactions and business decisions of operators by means of simulation. They approximated commodity flows in these networks by a diffusion equation, with nonlinearities introduced to model capacity limits.

4. LINES OF RESEARCH
This state of the art shows the two main areas of research into the solution of problems involved with natural gas networks and hydrocarbon networks, in general. About optimization, models have been identified that, in their majority, are Mixed Integer Non-Linear Programming and the solution methods can be exact, using software such as CPLEX, among others, and heuristic methods particularly genetic, neural network and ant colony algorithms. The model varies depending on what the objective of the optimization is. Some articles only mention network optimization in respect of whether the flow being transported is gas or oil. Other articles consider the power, energy and fuel that are being consumed, either as the aim or as constraints of the model. Articles were also found that seek to optimize inventory and transport and production costs.

Another important characteristic is the focus, whether a supply chain, a scheduling and routing problem, maintenance and safeguarding problems or network design is being considered.

Some authors have approached the hydrocarbons transport network problem in general and use optimization and simulation where a short, medium and long-term planning horizon is realistically considered, and the infrastructure and its useful age are considered.

As for simulation, the literature is not quite so abundant. However, we found results that, just like the authors that used optimization and simulation, consider infrastructure, the market and major planning horizons. By using simulation, the idea that the problem is stochastic is taken as a given, which enables us to have an analytical tool that can act as a support for the optimization techniques.

5. CONCLUSIONS
The review of these articles shows that the problem, in general, of optimizing the management of hydrocarbons in a pipeline network is fundamental while the network's resilience and vulnerability are important factors whose

consideration should be included in future phases of the project.

A first phase consisted of reviewing and analyzing the articles published over the last few years on the subject. On this basis, the decision is made about which are the essential pieces for the development of the methodology, models and solution methods for solving the optimal routing problem. Afterwards more factors in the network are considered, such as the production processes, blends and market. Another aspect that we believe is important is sustainability, resilience and environmental impact.

Given the characteristics of PEMEX's hydrocarbons network, it is important to have analytical tools like simulation and optimization tools where different models can be constructed for solving linear integer and nonlinear integer and continuous problems.

Finally, it is important to consider the validation of the models and results that are obtained, together with their publication in international scientific media.

ACKNOWLEDGEMENTS

REFERENCES

Jokic A., Zavargo Z. 2001. Optimization of pipeline network for oil transport. Article in Hungarian Journal of Industrial Chemistry 29(2):113-117.

Adeyanju O.A., Oyekunle L.O. 2004. Optimization of Gas Natural Transportation in Pipeline. Petroleum and Gas Engineering Programme. Petroleum and Gas Engineering Programme, Department of Chemical Engineering, University of Lagos. Nigeria.

MirHassani S.A., Ghorbanalizadeh M. 2008. The multi-product pipeline scheduling system. Computers and Mathematics with Applications 56, 891–897.

Selot A. 2009. Short-Term Supply Chain Management in Upstream Natural Gas Systems. Thesis (PhD), Department of Chemical Engineering. Massachusetts Institute of Technology.

Chebouba A., Yalaoui F., Smati A., Amodeo L., Younsi K., Tairi A. 2009. Optimization of natural gas pipeline transportation using ant colony optimization. Computers and Operations Research, 36(6):1916–23.

Huanchao T., Lixin T., Lin J. 2009. Inventory-Transportation Integrated Optimization Problem: A Model of Product Oil Logistics. International Journal of Nonlinear Science, 1, 92-96.

Zheng QP., Rebennack S., Iliadis NA, Pardalos PM. 2010. Optimization Models in the Natural Gas Industry. Chapter in the Handbook of Power Systems I, 121-148. Rebennack, S., Pardalos, P.M., Pereira, M.V.F., Iliadis, N.A. Eds., Springer Verlag.

Borraz-Sánchez C. 2010. Optimization Methods for Pipeline Transportation of Gas Natural. Department

of Informatics. Thesis (PhD). University of Bergen, Norway.

Jin L., A. K. Wojtanowicz. 2010. Optimization on large gas pipeline network. A case study in China. Journal of Canadian Petroleum Technology, 49 (4):36-43.

Domschke P., Geißler B., Kolb O., Lang J., Martin A., Morsi A. 2011. Combination of Nonlinear and Linear Optimization of Transient Gas Networks. INFORMS Journal on Computing, 605-617.

Gupta V., Grossmann I. 2012. An Efficient Multiperiod MINLP Model for Optimal Planning of Offshore Oil and Gas Field Infrastructure. Department of Chemical Engineering, Carnegie Mellon University Pittsburgh. Ind. Eng. Chem. Res., 51 (19): 6823–6840

Hübner M, Haubrich H-J. 2012. Long-term pressure-stage comprehensive planning of natural gas networks. In: Sorokin A, Rebennack S, Pardalos PM, Iliadis NA, Pereira MVF, editors. Handbook of networks in power systems II. Energy systems. Berlin Heidelberg: Springer, 37–59.

Babonneau F, Nesterov Y, Vial J.P. 2012. Design and operations of gas transmission networks. Operations Research 60(1):34–47.

Borraz-Sánchez C, Haugland D. 2013. Optimization methods for pipeline transportation of natural gas with variable specific gravity and compressibility. TOP, 21(3):524–41.

MohamadiBaghmolaei M, Mahmoudy M, Jafari D, MohamadiBaghmolaei R, Tabkhi F. 2014. Assessing and optimization of pipeline system performance using intelligent systems. J Natural Gas Sci Eng., 18:64–76.

Alinia Kashani AH, Molaei R. 2014. Techno-economical and environmental optimization of natural gas network operation. Chem Eng Res Des, 92 (11):2106–22.

Fabro J., Stebel S., Rossato D., Polli H., Arruda L.V.R., Neves F., Ribas P., Barbosa-Póvoa A., Relvas S. A., 2014. MILP (mixed Integer Linear Programming) decomposition solution to the scheduling of heavy oil derivatives in a real-world pipeline. Computers and Chemical Engineering, 66 (4): 124-138.

Wu X, Li C, Jia W, He Y. 2014. Optimal operation of trunk natural gas pipelines via an inertia-adaptive particle swarm optimization algorithm. J Natural Gas Sci Eng., 21 (9):10.

Ribeiro de Lucerna R., Souza Baioco J., Souza Leite Pires de Lima B., Horst Albrecht C., Pinheiro Jacob B. 2014. Optimal design of submarine pipeline routes by genetic algorithm with different constraint handling techniques. Advances in Engineering Software, 76: 110-124.

Pfetsch ME, Fügenschuh A, Geißler B, Geißler N, Gollmer R, Hiller B. 2015. Validation of nominations in gas network optimization: models, methods, and solutions. Optim Methods Softw., 30(1):15–53.

Chebouba A. 2015. Multi objective optimization of line pack management of gas pipeline system. Journal of Physics: Conference Series 574 012114

Kazemi Y., Szmerekovsky J. 2015. Modeling downstream petroleum supply chain: The importance of multi-mode transportation to strategic planning. Transportation Research Part E 83, 111–125.

Liu T., Xianwen G., Wang L. 2015. Multi-objective optimization method using an improved NSGA-II algorithm for oil-gas production process. Journal of the Taiwan Institute of Chemical Engineers, 57, 42-53.

Ríos-Mercado R., Borraz-Sánchez C. 2015. Optimization Problems in Natural Gas Transportation Systems: A state-of-the-art review. Applied Energy, 147, 536–555.

Sedliak A., Zácik T. 2016. Tatra Mountains Mathematical Publications, 66 (1), 103–120.

Zhou J., Liang G., Deng T., Gong J. 2017. Route Optimization of Pipeline in Gas-Liquid Two-Phase Flow Based on Genetic Algorithm. International Journal of Chemical Engineering. Article ID 1640303, 9 pages, Hindawi.

Zhang Z., Liu X. 2017. Study on optimal operation of natural gas pipeline network based on improved genetic algorithm. Advances in Mechanical Engineering, 9(8):1–8.

Ye Y., Shengming L., Yushan Z. 2017. A mixed-integer linear programming-based scheduling model for refined-oil shipping. Computers and Chemical Engineering, 99, 106-116.

Zhang H., Liang Y., Liao Q., Wu M., Yan X. 2017. A hybrid computational approach for detailed scheduling of products in a pipeline with multiple pump stations. Energy 119, 612-628.

Yea Y., Lianga S., Zhua Y. 2017. A mixed-integer linear programming-based scheduling model for refined-oil shipping Computers and Chemical Engineering, 99,106–116

Chen H., Zuo L., Wu Ch., Wang L., Diao F., Chen J., Huang Y. 2017. Optimizing detailed schedules of a multiproduct pipeline by a monolithic MILP formulation Journal of Petroleum Science and Engineering, 159, 148–163

Mikolajková M., Haikarainen C., Saxén H., Pettersson F. 2017. Optimization of a natural gas distribution network with potential future extensions. Energy, 125, 848-859

Zhang H., Liang Y., Liao Q., Shen Y., Yan, X. 2018. A self-learning approach for optimal detailed scheduling of multi-product pipeline. Journal of Computational and Applied Mathematics, 327, 41–63.

Aalto H. 2008. Optimal Control of Natural Gas Pipeline Networks: A Real-Time, Model-Based, Receding Horizon Optimisation Approach. VDM Verlag, Saarbrücken Alemania.

Rizwan M., Al-Otaibi M., Al-Khaledi S. 2013. Crude Oil Network Modeling, Simulation and Optimization:

Novel Approach and Operational Benefits. Paper No. IOGPC2013-9853, pp. V001T02A007; 4 pages. ASME India Oil and Gas Pipeline Conference.

Huang K., Wu J., Hu M., Xiang H., Zhang Z. 2015. Optimization and Stress Analysis of Underground Oil Pipelines in High and Steep Slope Areas. The Open Civil Engineering Journal, 9, 477-483.

Herrán-González A., De La Cruz J.M., De Andrés-Toro B., Risco-Martín J.L. 2009. Modeling and simulation of a gas distribution pipeline network. Applied Mathematical Modeling, 33(3):1584–600.

Behbahani-Nejad M., Bagheri A. 2010. The accuracy and efficiency of a MATLAB-Simulink library for transient flow simulation of gas pipelines and networks. Journal of Petroleum Science and Engineering, 70, 256–265.

Woldeyohannes AD, Majid MAA. 2011a. Effect of Age of Pipes on Performance of Natural Gas Transmission Pipeline Network System. Journal of Applied Sciences, 11 (9): 1612-1617.

Woldeyohannes AD, Majid MAA. 2011b. Simulation model for natural gas transmission pipeline network system. Simul Model Pract Theory, 19(1):196–212.

Cernelev D., Chegus A., Lin F. 2014. Application of Multi-Nodal Network Simulation Models in The Debottlenecking of a Complex Pipeline Network. Proceedings of the Winter Simulation Conference A. Tolk, S. Y. Diallo, I. O. Ryzhov, L. Yilmaz, S. Buckley, and J. A. Miller, eds.

Costa R., Freitas A. Araujo C., Limoeiro C., Fuller D. 2014. Simulation model for regional oil derivatives pipeline networks considering batch scheduling and restricted storage capacity. Proceedings of the Winter Simulation Conference A. Tolk, S. Y. Diallo, I. O. Ryzhov, L. Yilmaz, S. Buckley, and J. A. Miller, eds.

Szoplik J. 2016. Improving the natural gas transporting based on the steady state simulation results. Energy, 109, 105-116

Addo Pambour K., Bolado-Lavin R., Dijkema G. 2016. An integrated transient model for simulating the operation of natural gas transport systems. Journal of Natural Gas Science and Engineering, 28, 672-690

Corbet T., Beyeler W., Wilson M., Flanagan T. 2018. A model for simulating adaptive, dynamic flows on networks: application to petroleum infrastructure. Reliability Engineering and System Safety, 169, 451-465.

DYNAMIC FINITE ELEMENT MODELING OF METAL SPINNING PROCESS WITH A STATIONARY MANDREL AND A ROTATING TOOL

Huy Hoan Nguyen[(a)], Henri Champliaud[(b)], Van Ngan Lê[(c)]

[(a),(b),(c)]Mechanical Engineering Department, École de Technologie Supérieure, Montréal, Québec, Canada

[(a)]huy-hoan.nguyen.1@ens.etsmtl.ca, [(b)]henri.champliaud@etsmtl.ca, [(c)]vanngan.le@etsmtl.ca

ABSTRACT

Metal spinning process has observed significant developments in recent years mostly by using finite element analysis. However, a long time-consuming computation is reported. In this paper, a simplified dynamic finite element model is proposed, which can be 4-time faster than a conventional model. The key configuration is a circular plate, the only deformable part, which is considered static but subjected to centripetal forces due to the constant angular velocity. Accordingly, the mandrel becomes a stationary rigid body. The roller, also rigid body, is the only dynamic part. It rotates around the axis of the mandrel and presses the plate in the axial direction. With this configuration, the explicit time scheme can be performed at a larger mass scaling factor or with larger time steps without losing the accuracy of the results. Descriptions for the conventional model and the proposed model and results comparisons are fully detailed in the paper.

Keywords: metal spinning process, finite element analysis, centripetal forces, stationary mandrel.

1. INTRODUCTION

Metal spinning is a process of forming a circular plate or disc into an axisymmetric part over a rotating mandrel. The elementary components of the process are a circular plate (Figure 1a) required to be formed, a rotating mandrel (Figure 1b), a tailstock for clamping the plate on the mandrel (Figure 1c), a forming tool or roller (Figure 1d). Simultaneous combination of roller path (Figure 1f) and mandrel rotational speed (Figure 1e) causes the initial flat plate to be formed into an axisymmetric shape over the mandrel (Figure 1g).

In the past decade, the numerical method based dynamic finite element (FE) analysis has been used to compute almost every output of the process thus enabling prediction stresses, strains, geometry and tool forces. However, the long computational time is required to obtain reasonable accuracy of these factors due to fine element mesh and small increment time steps. Many previous works have concentrated to reduce the computational time. One way of alleviating this issue is by constructing approximation models or surrogate models. The most popular type of this model

are kriging approach (Champliaud, Feng, Lê and Gholipour 2015; Champliaud, Feng, Provencher, Tousignant and Gholipour 2016). Another attempts are to use 2D axisymmetric model (Liu, Yang and Li 2002; Mori and Nonaka 2004) but these models gave inaccuracy results. This paper proposed a full 3D FE model of the process which modifies the kinematics and boundary conditions. Let analysis intensively this modification.

The FE models of this process have been developed so far, vary on the selections of time integration schemes: implicit and explicit, the type of elements: shell and solid element (Music, Allwood and Kawai 2010). However, they all considered that only the plate is deformable, and the remaining components are treated as rigid bodies. The deformable plate is rotated passively by the rotating mandrel and is deformed continuously by the roller applying contact pressure to it. In short, the metal spinning process can be considered as a combination of rotating disc problem and contact mechanics problem. The contact problem has been studied thoroughly in (Wriggers 2006), (Neto, Oliveira, Menezes and Alves 2016), (Zavarise and Wriggers 1998), (Popov 2010) and, it is not a focused topic in this paper. The remaining problem, the rotating disc, is investigated in the way that is suitable and efficient to model the metal spinning process using FE method.

Recent FE models of the metal spinning process (Awiszus and Härtel 2011; Härtel and Laue 2016; Liu 2007; Marghmaleki, Beni, Noghrehabadi, Kazemi and Abadyan 2011; Marghmaleki and Beni 2014; Zhan, Yang, Zhang, Xu and Ma 2007) defined the rotation of mandrel by means of boundary condition as a constant angular velocity over time. Then, the circular plate is driven to rotate by the pressure applied from the tailstock to the mandrel as in Figure 2a. This configuration has some drawbacks on performance due to its highly geometrical non-linear aspect. However, the standard and efficient approach to solve the rotating disc problem is to convert the original problem to the equivalent static problem subjected to the centrifugal forces described in Figure 2b. In this paper, the advantages of this configuration are used and adapted to the application of metal spinning process with an addition of explicit time integration scheme.

First, the paper presents the study of the rotating disc (initial plate) problems with specific boundary conditions encountered in the metal spinning process. Second, the equivalent kinematics for both roller and mandrel are presented. Finally, the results of the proposed model are compared with the conventional approach.
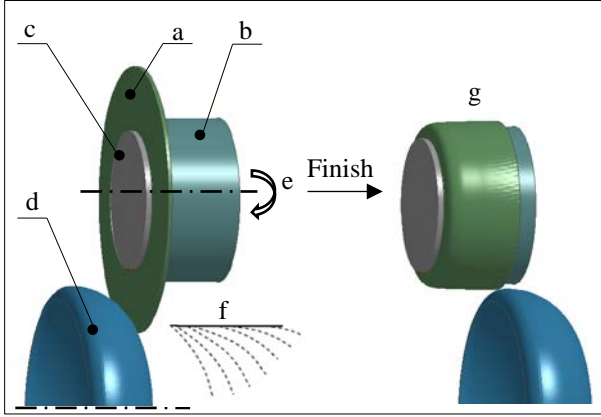
Figure 1. Metal spinning process, (a) a circular plate, (b) a mandrel, (c) a tailstock, (d) a roller, (e) mandrel rotation, (f) roller path, (g) final part.
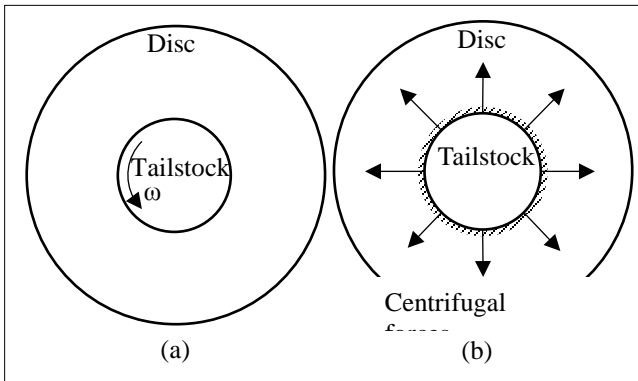
Figure 2. The rotating disc problem; (a) conventional configuration; (b) equivalent static configuration.

2. ANALYSIS OF ROTATING DISC PROBLEM

2.1. Analytical solution

The disc can be assumed as a plane stress problem due to a small ratio between thickness and the other dimensions. The material behavior is represented by Hooke's law. It is more convenient to study the rotating disc in the cylindrical coordinate system as in Figure 3. The stresses $\sigma_{rz}, \sigma_{\varphi z}, \sigma_{zz}$ are equal to zero in the plane stress assumption. The relation of stresses and strains in case of Hooke's law is

$$\begin{bmatrix} \epsilon_{rr} \\ \epsilon_{\varphi\varphi} \\ \gamma_{r\varphi} \end{bmatrix} = \frac{1}{E} \begin{bmatrix} 1 & -\nu & 0 \\ -\nu & 1 & 0 \\ 0 & 0 & 2(1+\nu) \end{bmatrix} \begin{bmatrix} \sigma_{rr} \\ \sigma_{\varphi\varphi} \\ \sigma_{r\varphi} \end{bmatrix} \qquad (1)$$

The constant angular velocity ω is converted to the centrifugal force or inertial force applied to the internal of the body.

$$F = \rho \omega^2 r \qquad (2)$$
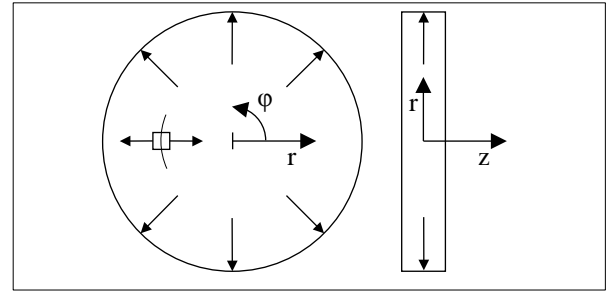
Figure 3. Plane stress problem in cylindrical coordinate system.

The tailstock can be neglected by introducing an equivalent boundary conditions assuming that zero deformation of material between the tailstock and mandrel thus the disc become a hollow geometry for the internal radius r_i is equal to the outer radius of the tailstock. With this boundary conditions, the radial stress of outer boundary and displacements of inner boundary are zero. The complete boundary conditions are illustrated in Figure 4.
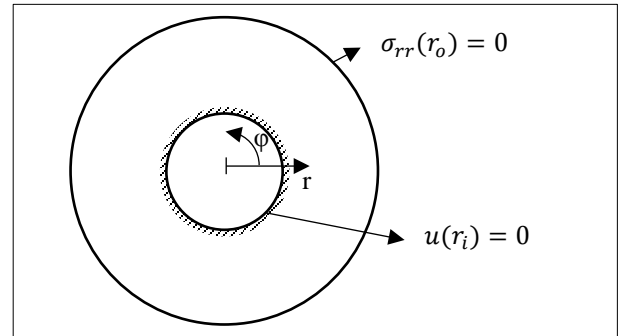
Figure 4. Boundary conditions of rotating disc problem. The analytical solution of this problem is given in (Bruhns 2003).

$$\sigma_{rr}(r) = \frac{c_1}{r^2} + 2c_2 - \frac{3+\nu}{8} \rho \omega^2 r^2 \qquad (3)$$

$$\sigma_{\varphi\varphi}(r) = -\frac{c_1}{r^2} + 2c_2 - \frac{1+3\nu}{8} \rho \omega^2 r^2 \qquad (4)$$

$$u(r) = \frac{1}{E} \left[-(1+\nu)\frac{c_1}{r} + 2(1-\nu)c_2 r \right. \\ \left. -\frac{1}{8}(1-\nu^2)\rho \omega^2 r^3 \right] \qquad (5)$$

With

ρ:	Density (g/mm^3)
ν:	Poisson's ratio
ω:	Angular velocity (rad/mm)
r:	Radius (mm)
σ:	Stresses (MPa)
c_1, c_2:	Parameters defined by boundary conditions

The parameters c_1 and c_2 can be found by applying two boundary conditions $\sigma_{rr}(r_o) = 0$ and $u(r_i) = 0$

$$c_1 = \frac{1}{8}(3+v)\rho\omega^2 r_o^4 - 2c_2 r_o^2 \tag{6}$$

$$c_2 = \left[\frac{(1+v)(3+v)\rho\omega^2 r_o^4}{8r_i} + \frac{(1-v^2)\rho\omega^2 r_i^3}{8}\right] / \left[\frac{(1+v)2r_o^2}{r_o} + 2(1-v)r_o\right] \tag{7}$$

2.2. Numerical solution

The numerical solution is carried out using the FE solver LS-Dyna. The one Gauss integration point solid element is used to model the disc since this is also the element type used for the metal spinning model presented in following sections. Meshes and boundary conditions of model are illustrated in Figure 5. The boundary conditions of nodes on the inner radius must assure a condition that is free movement in thickness direction as a plane stress property. The implicit time integration of one timestep of one millisecond is used for alternative of static solver. The elastic material is used for presenting Hooke's law.
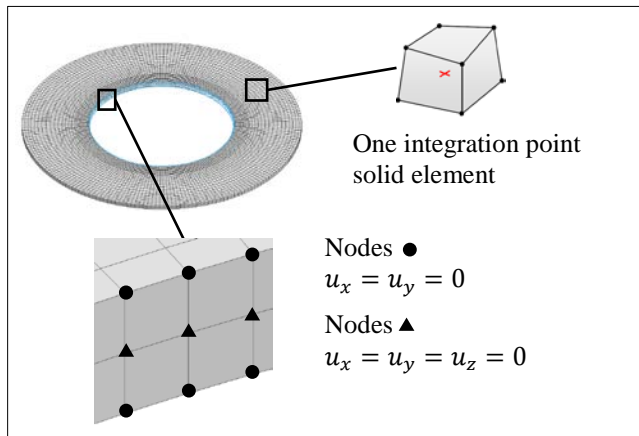
Figure 5. Mesh and boundary condition for solid element model.

2.3. Verification

Parameters are taken from a real metal spinning process setup. The angular speed of disc is 200 rpm or 20.94 rad/s. The aluminum A 1100-O has density of 2.7E-3 g/mm^3, Poisson ratio is 0.33. The inner and outer radius are 50 mm and 96 mm respectively.

The stresses distribution on the disc are showed in Figure 6. The maximum principle stress and second principle stress at Gauss points of elements are compared to the analytical solution described in a previous section. The trend of both radial and circumferential stresses of the analytical are displayed

in Figure 7. The radial stress obtains a maximum value at the inner boundary and decrease gradually to zero at the outer boundary. The circumferential stress peaks at the radius of 62.9 mm.
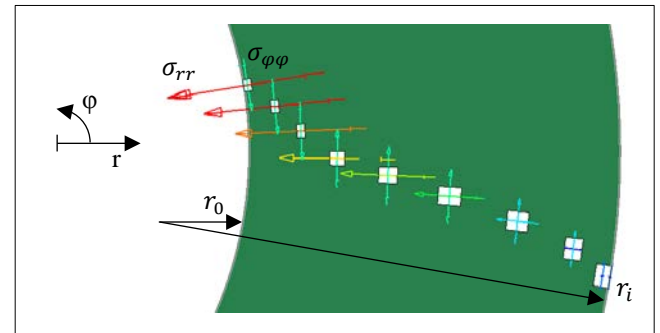
Figure 6. Stresses distribution on disc.

The maximum error between analytical and numerical solution is just 0.0167 percent thus it cannot be distinguished on the diagram. The Table 1 and Table 2 show the analytical, numerical and error value of radial and circumferential stresses at Gauss points. In conclusion, the numerical model can compute exactly results for the rotating disc problem.
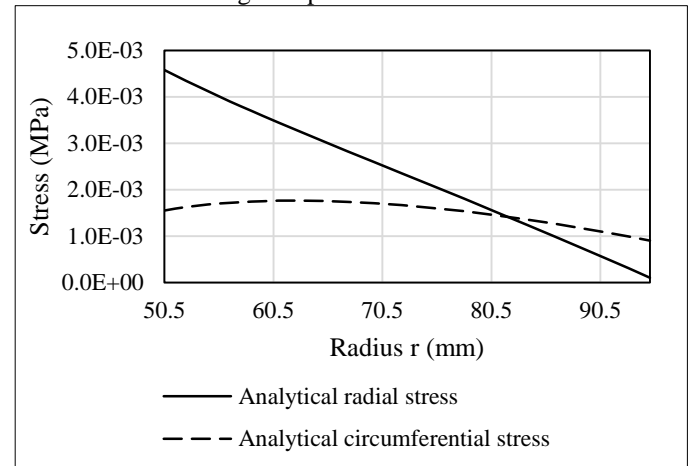
Figure 7. Stresses in rotating disc problems.

Table 1. Radial stresses of analytical and numerical solution measured at Gauss points.

r (mm)	Analytical σ_{rr} (MPa)	Numerical σ_{rr} (MPa)	Error (%)
50.5	4.58E-03	4.58E-03	1.67E-01
51.5	4.46E-03	4.47E-03	1.67E-01
52.5	4.34E-03	4.35E-03	1.66E-01
…	…	…	…
91.0	5.22E-04	5.22E-04	1.13E-01
93.1	3.05E-04	3.05E-04	8.54E-02
95.0	1.00E-04	9.99E-05	-5.09E-02

Table 2. Circumferential stresses of analytical and numerical solution measured at Gauss points.

r (mm)	Analytical $\sigma_{\varphi\varphi}$ (MPa)	Numerical $\sigma_{\varphi\varphi}$ (MPa)	Error (%)
50.5	1.55E-03	1.55E-03	1.8E-01
51.5	1.59E-03	1.59E-03	1.1E-01
52.5	1.62E-03	1.62E-03	1.6E-01
…	…	…	…
91.0	1.08E-03	1.08E-03	8.4E-02
93.1	9.90E-04	9.91E-04	1.3E-01
95.0	9.01E-04	9.02E-04	5.6E-02

The rotating disc problem can be used as a based finite element model to simulate a full metal spinning process by adding contact pressure of the roller on disc. The following section describe the kinematics of a revolving roller around a fixed mandrel.

3. EQUIVALENT KINEMATICS OF PROPOSED MODEL

The only dynamic part in the process is the roller whose movement can be divided into two components. The first component is the rotation ω about mandrel's axis with the same angular velocity as mandrel's speed. The second component is the movement of a roller path which is a combination of radial direction r on xy plane and stroked direction z. The velocity in z direction is the feed rate. The radial direction r is constant if the roller path is a straight line. The illustration of this kinematics is showed in Figure 8.
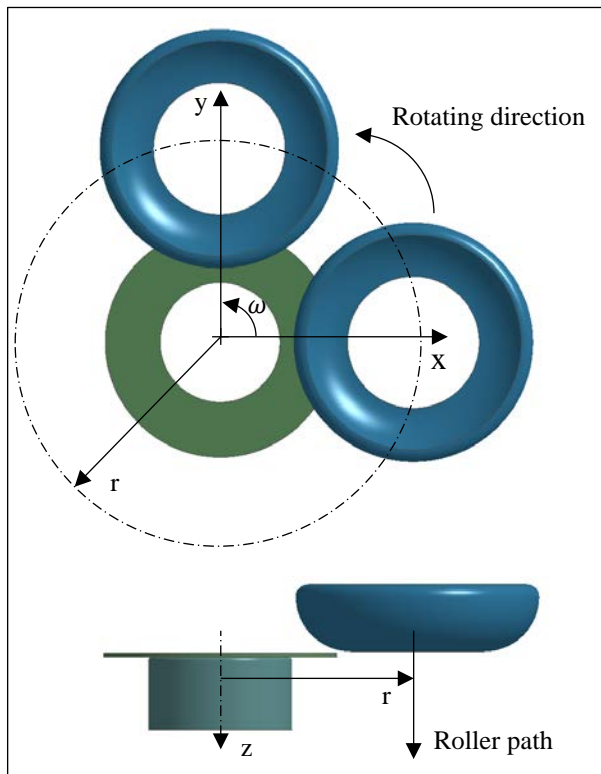
Figure 8. Equivalent kinematic of proposed model.

4. SIMULATION OF METAL SPINNING PROCESS BASED PROPOSED CONFIGURATION

The circular disc is made from the commercial pure aluminum A1100-O with properties taken from (Inc 2010) as in Table 3.

Table 3. Aluminum A1100-O properties.

Young modulus	E = 68.9 GPa
Yield offset	0.002
Yield strength at offset	σ_y = 345 MPa
Engineering ultimate tensile strength	EUTS = 896 MPa
Mass density	2.7E-6 kg/mm^3

The material model is isotropic elastoplastic using a power law hardening rule (see plot of Eq. (8) showed in Figure 10).

$$\sigma_t = K\epsilon_t^n \tag{8}$$

With

σ_t: True stress
ϵ_t: True strain
K: Strength coefficient
n: Strain hardening coefficient

Two parameters K and n can be found by using two conditions showed in Figure 9 that satisfy the yield engineering strength at offset and zero tangent slope of the engineering stress – strain curve at engineering ultimate strain. The values of K and n are 0.1636 and 0.2594 respectively.
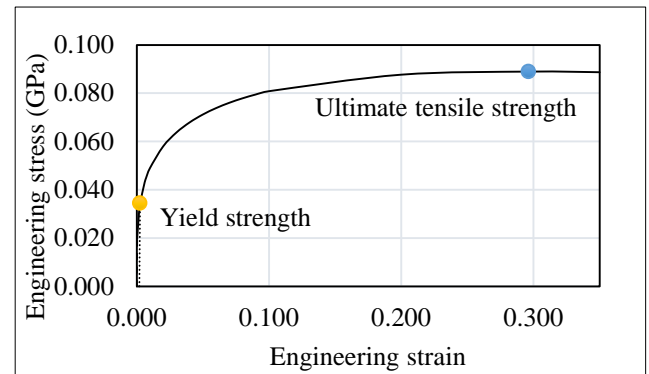
Figure 9. Engineering stress-strain curve A1100-O.
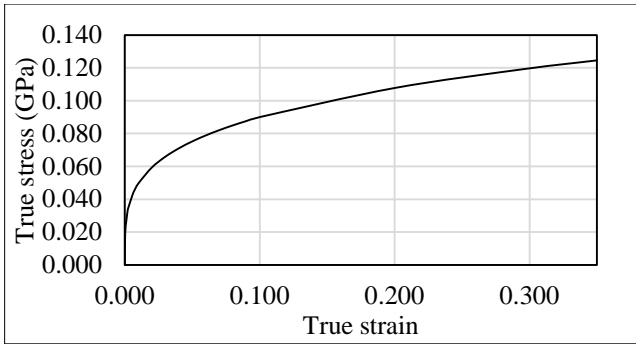
Figure 10. True stress-strain curve.

The contact one - way surface to surface is used for computing the contact pressure between the disc and mandrel as well as the disc and roller. This contact type assures the zero penetration one – way from slave surface to master surface. The disc is chosen for slave surface and the other are master surface.

The simulation uses explicit time integration scheme. Different time steps, 1E-3, 4E-3, 9E-3, 2E-2 millisecond, are studied to determine the convergence of maximum axial force. The results of conventional model and the proposed model are compared about the value of maximum axial force and run time.

The maximum axial forces of both models converged to the value of 2875N, but it comes from opposite directions, with the conventional model overestimating the axial force until it reaches the converged value and the proposed model underestimating it until convergence. A Figure 11 shows directions and speed of convergence for both models. It is clear that the proposed model got convergent value at time step 4E-3 ms, while the conventional model needs a time step of 1E-3 ms with the difference to the previous time step is about 1.63 percent. These values are presented in Table 4. Additionally, the computational time is nearly 4-time faster for a 4E-3 ms time step with 18h in comparison with 68h on a ZBook 15 core i7-4800MQ 2.7 GHz laptop.
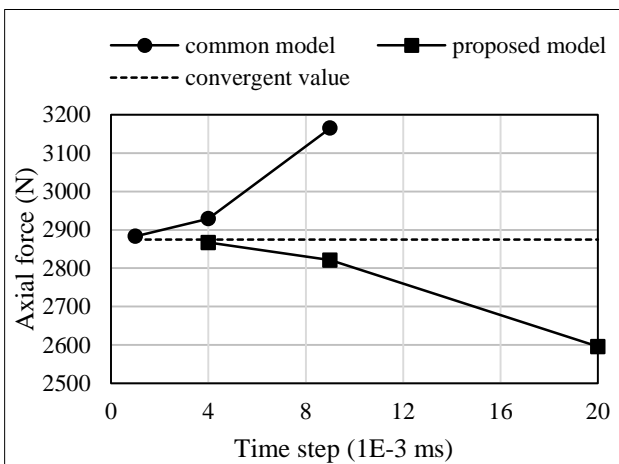
Figure 11. Time step convergence.

Table 4. Convergence of maximum axial force and runtime.

Δt	Conventional model; % change	Proposed model; % change	Runtime
1E-3	2883; -1.57%	N/A	68h16
4E-3	2929; -7.45%	2867; 1.63%	18h09
9E-3	3165	2821; 8.66%	8h27
2E-2	N/A	2596	3h43

The advantages of the proposed approach in case of metal spinning process is the displacement of deformable disc is almost in the z direction. On the other hand, the deformed part in conventional model includes additional displacement in xy plane due to rotation.

5. CONCLUSION

In this study, the dynamic finite element model of the metal spinning process with a revolving tool and a stationary deformed part is demonstrated thoroughly. The based model, a rotating disc problem, is solved by analytical solution as well as numerical solution. Equivalent kinematics are demonstrated. The simulation results of the proposed model gave a significant improvement of nearly 4-time faster in computational time in comparison to the conventional model while keeping the same level of accuracy.

Finally, this proposed model has the potential to provide quantitative computations of strains, stresses and geometry in metal spinning instead of only qualitative predictions, mainly due to a long solution time.

REFERENCES

Awiszus B., and Härtel S., 2011. Numerical simulation of non-circular spinning: A rotationally non-symmetric spinning process, *5*(6), 605–612.

Bruhns O.T., 2003. Plates and Shells (pp. 131–148). Berlin, Heidelberg: Springer Berlin Heidelberg.

Champliaud H., Feng Z., Lê N. Van, and Gholipour J., 2015. Line Heating Forming : Methodology and Application Using Kriging and Fifth Order Spline Formulations, *9*(9), 1664–1669.

Champliaud H., Feng Z., Provencher D., Tousignant D., and Gholipour J., 2016. Piecewise Fifth Order Spline Interpolation for Line Heating Forming Process (p. V002T02A029). ASME.

Härtel S., and Laue R., 2016. An optimization approach in non-circular spinning, *229*, 417–430.

Inc H.W. international, 2010. *Aluminium 1100-O properties*.

Liu C.-H., 2007. The simulation of the multi-pass and die-less spinning process, *192*, 518–524.

Liu, Yang H., and Li Y.Q., 2002. A study of the stress and strain distributions of first-pass conventional spinning under different roller-traces, *129*(1), 326–329.

Marghmaleki, Beni Y.T., Noghrehabadi A.R., Kazemi

A.S., and Abadyan M., 2011. Finite element simulation of thermomechanical spinning process, *10*, 3769–3774.

Marghmaleki I.S., and Beni Y.T., 2014. Thermo-Mechanical Investigation of Spinning Process, *39*(2), 1209–1217.

Mori K.-I., and Nonaka T., 2004. Simplified Three-Dimensional Finite Element Simulation of Shear Spinning Process Based on Axi-Symmetric Modeling, *45*(517), 34–38.

Music O., Allwood J.M., and Kawai K., 2010. A review of the mechanics of metal spinning, *210*(1), 3–23.

Neto D.M., Oliveira M.C., Menezes L.F., and Alves J.L., 2016. A contact smoothing method for arbitrary surface meshes using Nagata patches, *299*, 283–315.

Popov V.L., 2010. *Contact Mechanics and Friction*. Berlin, Heidelberg: Springer Berlin Heidelberg.

Wriggers P., 2006. *Computational contact mechanics*. Berlin, Heidelberg: Springer Berlin Heidelberg.

Zavarise G., and Wriggers P., 1998. A segment-to-segment contact strategy, *28*(4–8), 497–515.

Zhan M., Yang H., Zhang J.H., Xu Y.L., and Ma F., 2007. 3D FEM analysis of influence of roller feed rate on forming force and quality of cone spinning, *187–188*, 486–491.

AUTHORS BIOGRAPHY

Hoan Huy Nguyen is a PhD student in the Department of Mechanical Engineering, École de technologie supérieure (ÉTS), University of Québec (Canada). He obtained a bachelor's degree in mechanical engineering from Bach Khoa University (Vietnam) and master's degree in computational engineering from Ruhr University Bochum (Germany). His research interests are numerical method and optimization techniques applying to manufacturing process including metal forming.

Henri Champliaud is a professor at the Department of Mechanical Engineering, Ecole de technologie superieure (ETS), University of Quebec (Canada). He received a bachelor's degree from ÉTS, master's degree from Sherbrooke University and Ph.D in mechanical engineering from ETS in 1991, 1994 and 2000, respectively. He is specialized in the following fields: stress analysis (assemblies and mechanisms), theory and application of the finite element method (static and dynamic analysis in structural, numerical simulation of the nonlinear behavior of metals and rubber-like materials). His research interests are mainly FE simulation of manufacturing processes including forming and welding.

Van Ngan Lê is a retired and Associate professor in Mechanical Engineering Department, Ecole de technologie supérieure (ETS) since 2010 after being professor in the same department for more than 32 years. He obtained a B.Sc.A, M.Sc.A and D.Sc.A in Mechanical Engineering at École Polytechnique of Montreal in 1970, 1971 and 1977 respectively. He has more than 5 years of experience with industries as structure analyst of aircraft motors and pressure vessels. He is specialized in finite element analysis for structures, plasticity and creep behaviors of materials, stress analysis including fatigue, plastic collapse and buckling.

PROCESS MODEL FOR A SIMULATION-BASED EARLY WARNING SYSTEM USING ARTIFICIAL INTELLIGENCE

David Weigert[a], Tim Lippke[b], Tobias Reggelin[c], Michael Schenk[d]

[a],[b],[c], [d] Otto von Guericke University Magdeburg, Magdeburg (Germany)

[a]david.weigert@ovgu.de, [b]tim.lippke@st.ovgu.de, [c]tobias.reggelin@ovgu.de, [d]michael.schenk@ovgu.de

ABSTRACT

In the present paper a procedure model for forecasting component of an early warning system is developed. For this purpose, the simulation tool Siemens - Plant Simulation is combined with Artificial Intelligence (AI) in the form of neural networks. A prototypical production layout is used to calculate the system throughput under different parameter configurations (eg. processing times, buffer sizes). The simulation results are used to train a neural network, which then predicts the system throughput based on the current parameter configuration. The article should show the possibility and the benefits of the combination of simulation and AI. Two approaches have been developed. The first approach describes a general procedure for combining simulation and AI as an early warning system in production and logistics. The second approach describes a possible improvement of the prognosis and solution quality of the system. Here, commercial tools (Matlab, Excel) and open-source tools (TensorFlow, Kreas) were used.

Keywords: artificial intelligence, early warning system, neural networks, discrete event simulation

1. INTRODUCTION

Material flow simulations offer companies decisive advantages in today's global and highly competitive market situation in order to react flexibly to changing conditions and upcoming changes. The current and future development of entrepreneurial activities in production and logistics is characterized by ever shorter planning and development cycles as well as permanent restructuring in the company. With the help of simulation, process flows in production and logistics can be simulated in order to detect bottlenecks, under- or overcapacities at certain positions in the process or even disturbing influences. This allows the users of the simulation to make adjustments early in the process, which saves costs and time. With the rise of artificial intelligence in the field of forecasting in recent years, powerful new tools such as Support Vector Machines (SVM) or Artificial Neural Networks (ANN) have been added to the existing, relatively static forecasting tools. The current science and technology has made great progress here, so that these methods gradually improve the previously used forecasting methods. Currently, the methods are increasingly being applied to topics such as language and image recognition. Areas of application in production and logistics for forecasting, such as production and scheduling planning, are generally not taken into account. New solutions are required to master the increasing complexity and demanding customer requirements. More flexible supply chains, global sourcing, the increased use of just-in-time and just-in-sequence methods create individual customer products with the trend towards lot size 1. Increased application of the late-fit strategy creates a completely new range of requirements for today's production planning and control. Therefore, this article is dedicated to the development and subsequent optimization of a process model, which should combine simulation tools and artificial intelligence for the forecast. The process model is developed for the forecast component of a comprehensive early-warning system for production. It is designed to identify problems, review actions, and provide users with the best choices. The aim of the procedure model is to make the combination of simulation tool and artificial intelligence as simple and fast as possible, the application as user-friendly as possible and the predictive accuracy of artificial intelligence as high as possible.

2. STATE OF THE ART AND SCIENCE

Generally known logistic indicators such as throughput times, machine usage times, capital commitment costs and punitive costs for late or incorrect deliveries within the supply chain must be continuously kept in optimum operating state even under these conditions (Hausman et al. 2005). By mastering and forecasting predictable and random process fluctuations, the company can make its internal and external logistics processes robust and responsive to short-term changes (Hotz 2007, Li et al. 2010). Special challenges in existing logistics and production systems are complex dynamics triggered by loss of production resources such as equipment, vehicles and employees, unpredictable environmental factors and short-term dispatching of new customer orders and flexible release quantities. Already elaborated and retimed production orders and release quantities of

customers need to reschedule. This often can not happen in the desired requirement time (Timm, Lattner 2010). These challenges will hardly diminish in the future. On the contrary, the orientation of entrepreneurial activity in production and logistics will not only be faster in the future, but also much more individual (Gössler, Tiefenbrunner 2008). Today manufacturing reality shows that plan data and expected values are often not achieved. Machines and materials maybe not available, workers get sick and workpieces are damaged (Heuer 1997). The development of new approaches and the identification of optimization possibilities is not yet completed. For the use of a simulation-based early warning system, the decision aids to select Artifical Neural Networks (ANN) (s. Figure 1). The reason for this is the suitability of ANN for the pattern recognition and classification of system states based on predefined features (Weigert 2017a). Currently, the use of neural networks in combination with logistical systems is often selected only for the prognosis of individual key figures (Weigert, 2017b; Reggelin et al., 2017). These applications are simply pure classification tasks, which react relatively rigidly. If measures for the early warning are considered, usually only punctual processes are prognosticated. An issue of alternative courses of action due to past and current event data does not take place. Here usually the existing knowledge of the human logistics planner is used. In production planning, neural networks are mainly used for the prediction of operating times and production times. All of these reasons require a short-term response in order to react flexibly to these disruptions in a timely manner. The increase in computing power compared to the material flow simulation and the rapid innovation in the field of artificial intelligence creates significant benefit to the approach of simulation-based early warning by coupling discrete-event-simulation and artificial intelligence in use in the operational phase of new companies today. The detailed explanation of the individual features of the developed concept and prototype implementation should be the basis for this scientific elaboration. The contents are explained in more detail in the following chapters.
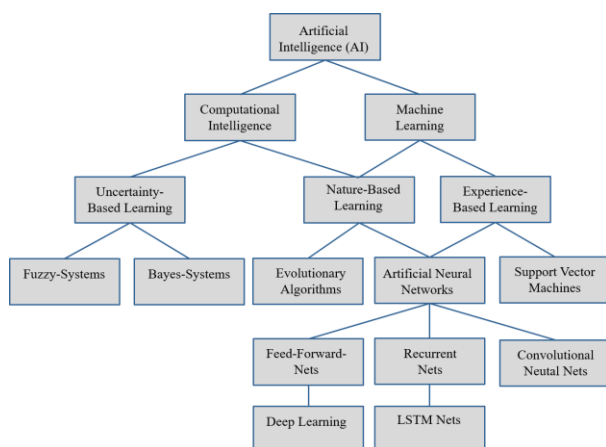
Figure 1 Systematics on terms of artificial intelligence

2.1. Data analysis and artificial intelligence

There is an increasing amount of data that includes part of the term big data (Bousonville, 2017; Hinton und Salakhutdinov, 2006; John Walker, 2015; Waller und Fawcett, 2013; Schoenherr und Speier-Pero, 2015). The data often contains large amounts of valuable knowledge. The raw data must first be broken up and analyzed before revealing the true added value (Lueth, K. L., Patsioura, C., Williams, Z. D., Kermani, Z. Z., 2016; Chen et al., 2012). This is one of the requirements of Digital Transformation and Industry 4.0. Modern methods for data analysis offer the field of artificial intelligence. By using them unknown patterns can be detected and evaluated without computationally intensive statistical calculations. The use of artificial intelligence captures the potential for applications in simulation and optimization. In the sense of this contribution the term optimization means an improvement of the simulation-based system, which results in a quicker and more accurate prognosis of system states. Artificial intelligence (AI) is to be understood as a generic term. There are strong and weak AI in theory, and there is a desire for both forms to simulate intelligent thinking and acting in particular fields of application (März et al. 2011). Further examples show that the use of neural networks in a closed problem works very well. Schmidt (2000) uses artificial neural networks as a forecasting tool for manufacturing in semiconductor manufacturing. Following Weber (1999) neural networks are used to predict production times for highly fluctuating products. Schulze and Marquardt (2000, 2003) uses recurrent neural networks to predict statements about the expected residence time in an operator station. Further assignments for neural networks can be found in the sequence planning, prognoses for the quality of the material deliveries, statements about possible damage to packing and work-pieces as well as scenario planning.

2.2. Material flow simulation as an early warning system

The focus of the work lies above all on the data supply of the simulation-based early warning system as well as the generation of action alternatives. Current research activities pursue the idea of handing over Enterprise Resource Planning (ERP) data to run-oriented simulation models, in order to use an established catalog of measures (eg increasing/ decreasing circulation inventory) to create an effective PPS configuration (Hanisch et al. 2003, Hanisch et al. 2005, Hotz et al. 2006) provides further derivation of early warning systems. Early warning systems have the task to detect emerging deviations from the nominal state and to warn people at risk as quickly and comprehensibly as possible. This should enable them to initiate appropriate countermeasures in good time. According to Hotz (2003), issuing countermeasures is not a necessary function of the early warning system, but should be available in order to increase user acceptance.

Classic early warning systems are based exclusively on historical and current measurement data, leading indicators, critical system states and potential threats. Simulations can be used to expand this spectrum. Simulation can also be used as a forecasting tool within the early warning. There are currently very few examples of simulation-based early-warning systems that can successfully introduced, and standardized methods have so far sought in vain in scientific papers. As one of the first in his field (Hotz et al., 2006; Hotz, 2007) deals explicitly with the topic of a simulation-based early-warning system to underpin operative production planning and control systems. Event-discrete simulation is used to predict future states of a real system (Faingloz and Tolujew 2017). The monitoring of process-relevant limit values ensures the identification of undesired status deviations. An application that meets these requirements has been described in VDI-Guideline 3633 (2013). This is where the concept of order monitoring can be found, in which the effects of disruptions are examined in order to initiate counter-measures at an early stage.

All in all, fault control is also an important part of PPS systems in practice (Schenk et al., 2014; Helmig, J., Schmidt, C., Kompa, S., 2012, 2012). The function of early warning systems can divided into three phases. In a first step, a prediction is made. If this prediction deviates from the nominal state, a warning will be issued. This in turn should lead to a reaction. In order to use an early warning system in the short-term operational level, real-time capability is required. This applies to the data provision as well as to the simulation result output. The faster the system reacts to faults and the new plans can be implemented, the more effectively it can be counteracted (Hausladen 2016). In terms of performance, it is also evident that high output speeds result in higher user acceptance. Practical simulation applications show that with a high levels of detail the systems reach their limits quickly (Rabe, M. und Hellingrath, B. 2001; Gruber et al., 2011). According to Hotz (2007) the most important features of early warning systems are:

- Performance (the faster the better)
- Reactive behavior (suggestions for action alternatives)
- Proactive behavior
- Scalability / Adaptability
- User friendliness
- Learning ability
- Standardization / Reusability / Automatism

Since a simulation model will never fully depict reality in any case, a quick approximation solution is more promising than lengthy optima. The simulation-based early warning is therefore proactive, with the task of the simulation being to evaluate and evaluate possible alternative courses of action.

Another possible area of application of simulation in the context of early warning is to simulate future system states with different parameter variations in order to identify bottlenecks and production problems for certain combinations at an early stage. This allows countermeasures for identified problems to be determined at an early stage. In this scenario, the simulation would also have the task of assessing the effectiveness of the countermeasures. Furthermore, it is possible to investigate previously unknown interference factors by means of a simulation. For this purpose, assumptions must be made with regard to these disturbing factors, which are then examined by several simulations for their effect on the production plant. Again, the simulation could be used to simulate possible countermeasures and to include promising countermeasures in the catalog of measures. In the course of this work, the simulation is used on the one hand to generate data, on the other hand, a review of the predictions of the ANN takes place. The simulation is thus used to check and validate the early detection and subsequent generation of action alternatives of the ANN.

3. DEVELOPMENT OF A PROCEDURE MODEL

After describing the current state of the art and describing existing systems, a new approach is developed in the following chapter to combine material flow simulations and neural networks. The aim is to use the system as an early-warning system at the operational level.

3.1. Concept and function

Figure 2 shows the functions of each software system in the overall system. The concept is based on the coupling of three software systems widely used in industry. The first subsystem represents the ERP system as well as measuring elements in production. This subsystem measure and transmit the actual real states of the system (1). The core of the concept is the created interface, which refers as "Control" (2). It is used as an evaluation and control tool. It automatically generates action alternatives, referred below as "Scenario") (3-4). Furthermore, the "Control" is used to generate the learning patterns for the neural network in the material flow simulation. The second element is the "Neural Network". It will make rapid predictions during the usage phase. It is trained by input and associated output data (5-6). Subsequently, the results are compared by logistical key figures and evaluated on the cost side. The selected scenarios are prepared for the simulation model (7-8). The last subsystem describes the simulation model. Here, the data and scenarios in the learning and use phase are prepared and evaluated (9-10). In the final step, the alternative courses of action are evaluated and presented to the logistics planner. Here, among other things, a manual intervention can be made (11).Since fictitious data is generated in the framework of this paper, the possibilities and characteristics of these systems will not discussed in detail here.
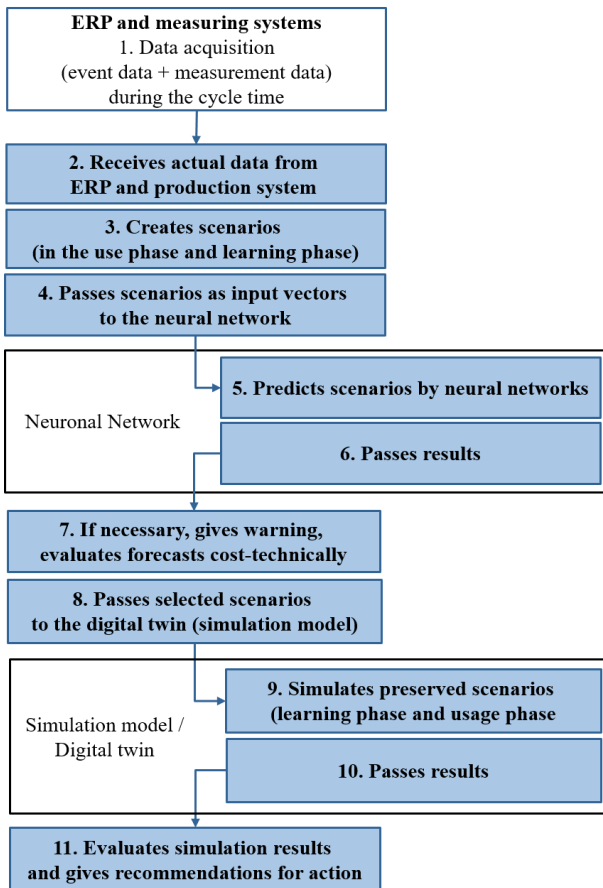
Figure 2 Concept description and function
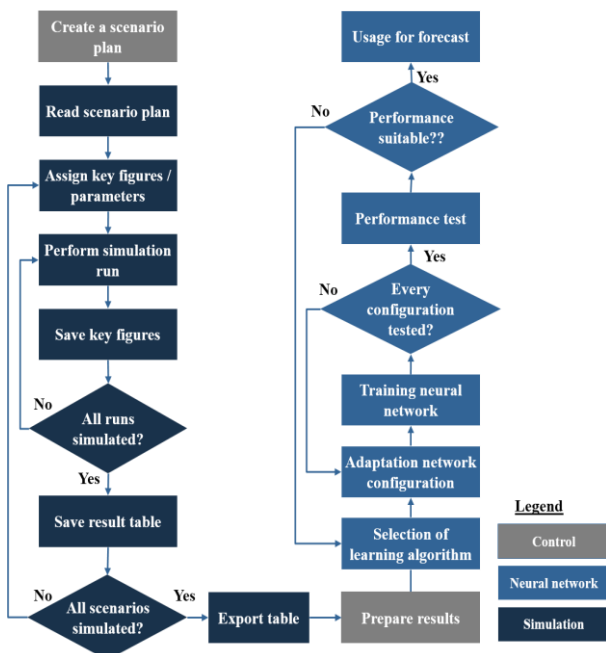
Figure 3 Structure of the subfunctions

3.2. Description of the system components

The aim is to generate as soon as possible good alternatives of action in case of deviations from the target state. The goal is to use the adaptability and speed of the neural network. The functions described result in the flowchart of alternative action generation, which overall represents an intelligent machine control taking costs into account. In the first step, the actual states of the real system are captured and transferred to the controller. This creates further scenarios depending on variable parameters. In the next step, the created scenarios are transferred to the neural network, which provides forecasts for the individual scenarios in a short time. These are confirmed to the controller and evaluated by means of cost evaluation. Subsequently, the cost-optimal scenarios are checked for their quality by the material flow simulation. The now secured result is presented to the decision maker so that he can make adjustments in the real system. Figure 3 summarizes the procedure. In the first step, scenarios are created in the control unit. The scenarios are transferred to the simulation and individually simulated 100 times. The results of the simulation are prepared and provided for the learning phase of the neural networks. A neural network measured must be found at the forecast quality continues to run through a trail-and-error process. Therefore, many networks trained and selected the highest quality.

4. APPLICATION EXAMPLE

The resulting model is a fictitious example. Nevertheless, some tasks must be fulfilled by the system. The primary goal for the learning phase of the neural network is to generate output data. Simulation experiments must be carried out in a targeted manner and the results be transferred to the controller. There must be an interface to the controller in the connected usage phase of the overall system. This is necessary in order to check the results of the action alternatives handed over by the control module. In addition, the system is kept simple for initial experiments, so that a neural network should understand the relationships within the system. In summary, the following prerequisites are set for the planned model:

1. Simulation requirements
   - Stochastic processing times
   - Different products
   - Different working times
2. Alternatives
   - Increase processing time
   - Minimize processing time
3. Manageable number of input parameters
   - To keep the learning record as low as possible
   - Minimize the simulation time of a run
4. Controllable from the controller (import and export of data)

4.1. System description

In the course of system analysis, the conceptual model emerges. In the considered case it is a flow production. The procedure is a bottom-up approach, in which the detail is synthesized step by step as the formation proceeds. The system consists of a three-stage production line delimited by a source and sink (Figure 4, Figure 5). The source produces three different products (black, blue, red).
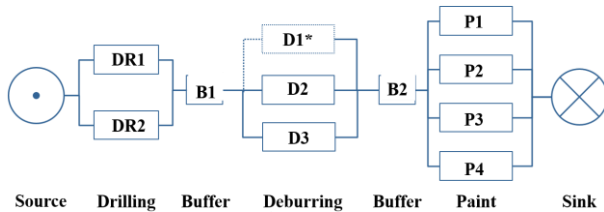
Figure 4 Conception model
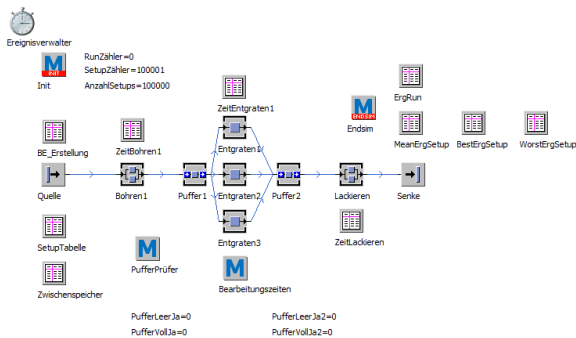
Figure 5 Simulation model

All products must go through each of the three machine levels. They are drilled on the first level, deburred on the second and painted on the last level. Buffers are installed between the levels. The first machine level consists of two production stations, the second level of three deburring machines, the third is considered as cold redundancy (reserve machine). The processing times are described by triangular distribution de-pending on the parameter "C". In the last production stage, there are four machine. The first-in-first-out (FIFO) rule is followed in the buffer. They are provided with a limited capacity, which will lead to possible blockages of individual machines during operation. The processing times of individual machines represent the control variables of the system.

5. EXPERIMENTS

5.1. Scenario development via the control interface

The „Control" generates the scenarios that are used for the learning phase. Therefore, the scenario generation should be designed in a way that it can be used in the subsequent usage phase. The severity limits and the step size are described as a percentage of design capacity. These are defined as working speed in processing machines and maximum buffer capacity in the buffers. If necessary additional parameters can be added easily in

future applications. Two different sets of scenarios are created for the learning phase of the neural network. The first set "Fixed Step Sizes" now consists of fixed, relatively large step sizes. At the machining speeds, this is 10%, for the buffers 25%. In a first step, all possible configurations are generated. In a second step, redundant scenarios deleted. In the last step, random scenarios are taken from the comprehensive overall plan. The second set "Random Percent" results from purely random configurations of the percentage utilization. 10,000 scenarios are generated for the first experiment. In addition to the learning sets, test data is generated. These are used to examine the neural networks for their forecasting quality.

5.2. Selection and description of datasets

The data sets are the learning data of the neural networks. The sets are transferred as input parameters to the material flow simulation. The input data consists of five processing times and the two buffer levels. They represent the actual state of the material flow system and are used for model initialization. Each data set is simulated 100 times. The simulation time is limited to 60 minutes and thus reflects the time window to forecast. The time window should not be too large because it assumed that the processing times of the machines com-ply with the time interval of the specified triangular distributions. The larger the interval chosen, the less likely this assumption will be. Due to the fictitious actual state, the simulation calculates the output, the relative buffer occupancy and other buffer characteristics. Based on these, the individual scenarios can evaluated cost-technically in the usage phase. In addition, three different scenarios are generated the best case – Set1 (1st decile), worse case – Set2 (9th quintile) and average case – Set3 (median). For the following experiments, two learning sets as well as test data generated with the scenario generator. The basic idea of Set1 is that the neural net-work should have the widest possible range of possible system states. If 10% increments are chosen for the machines and 25% intervals for the buffers, there are a number of scenarios of 4.03 million. If all the scenarios are simulated 100 times, this far exceeds the computational capacity for this simple system. Furthermore, it should be considered that as the number of learning data increases. Therefore, the large number is limited by three steps:

1. The step size of the third deburring machine is increased to 25% (omission of 1.2 million scenarios)
2. The deburring machines 2 and 3 are assumed equivalent in processing time (distribution function in processing). Deleting identical states if $ab = ba$ and $a <> b$ (reduction by 830,000 scenarios)
3. Random selection of 10,000 scenarios

The random selection of 10,000 scenarios will made, since the calculation is kept to a manageable size. At the same time, it is risked that the entire result horizon is no longer included in the learning quantities. In summary, the following brief description results.

- Set1: Fixed intervals of processing times (10% increment) and buffer states (25% increment) as well as random selection of 10,000 scenarios out of nearly one million possible scenarios

- Set2: Random percentages of processing time and buffer states. The learning set consists of 10,000 random data sets. For this, a random number between 0 and 1 is generated, which describes the percentage value with which the de-sign value is multiplied

- Testdata: Random percentages of processing time and buffer states. The test data do not affect the learning phase of the neural network. They are used for the evaluation of the configured network. In order to be able to evaluate the individual networks that are configured using the learning set, the same test data are always used.

5.3. Experiment description and evaluation

The goal of the experiments is to generate high-quality neural networks with the simplest possible means. The quality of the networks is measured in a first step on the forecast accuracy based on the Mean-Square-Error (MSE) test data. The task is a fitting problem because the exact number of outputs or the exact buffer conditions should be predicted. For this purpose, a Feedforward Multilayer Perceptron (MLP) network with a hidden layer is chosen. These are suitable for these applications. It is limited to one layer, since according to common doctrine a hidden layer can approximate every nonlinear function. The network is teached using the Levenberg-Marquardt algorithm. These are backpropagation methods and can therefore be assigned to supervise learning. The data is divided into training data, validation data and test data using the Divide-block function.

The default setting of the algorithm will terminate the learning phase if either 1,000 iterations are exceeded, or six times no improvement in the validation data is achieved. At the beginning of the learning phase, the initial configuration (weights and bias) is set at random. This will mean that the results will be different even with the same number of neurons and the same data input. Each network configuration is learned several times and the results are compared. Then the networks with the best results are used to set up an expert system. Figure 6 shows the median of the results of the MSE.
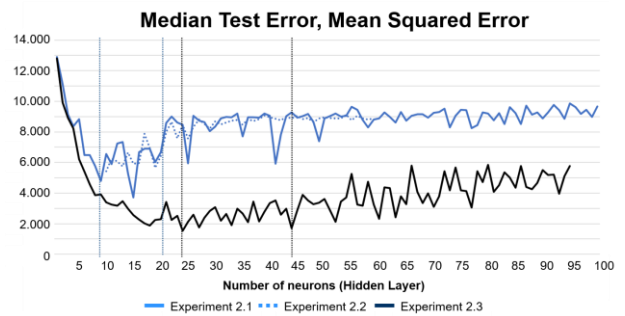
Figure 6 Median Test Error and Mean Squared Error

Figure 7 shows the best nets related to the quadratic error in the respective neuron configuration.
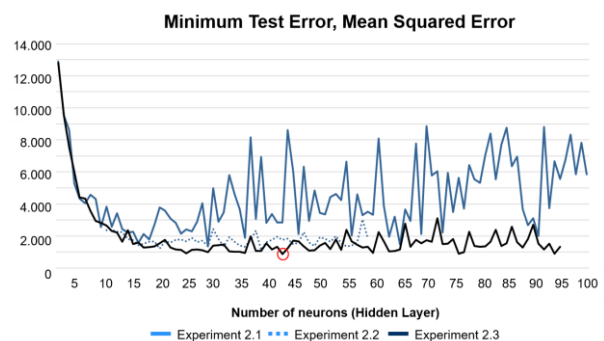
Figure 7 Minimum Test Error and Mean Squared Error

How these results are composed by different experiments will be explained in more detail in the following chapters.

5.4. Experiments

Fixed increments of the parameters in the scenarios seem less appropriate than random variable data (Table 1).

Table 1 Experiment 1 – Data Composition

Data type	Data set	Number of scenarios
Training data	Set1 (fixed intervals)	8,800
Validation data	Set1 (fixed intervals)	1,200
Test data	Test data	2,000

Since there is no connection to these increments, further testing can be carried out in future applications. It should be checked whether the number of parameters used for the prognosis could be increased. For the first experiment, the following statements are made:

- Extreme difference in the forecasting quality of training and test data
- System is unable to approximate the intermediate steps
- System not considered further in the next iteration.

Table 2 Experiment 2.1 – Data Composition

Data type	Data set	Number of scenarios
Training data	Set2 (random intervals)	8,800
Validation data	Set2 (random intervals)	1,200
Test data	Test data (random intervals)	2,000

Due to the strong fluctuations and good results in this learning set, further experiments are performed. For the first experiment, the following statements are made:

- Overall, good results are achieved with strong fluctuations
- In a first step, the number of nets per neuron number increased to 100. The learning set itself is retained and the first 10 experiments of the neuron configuration from Experiment 2.1 (Table 2) are integrated

Table 3 Experiment 2.2 – Data Composition

Data type	Data set	Number of scenarios
Training data	Set2 (random intervals)	17,600
Validation data	Set2 (random intervals)	2,400
Test data	Test data (random intervals)	4,000

In another experiment (Table 3), the relationship between the numbers of learning scenarios is examined. For this purpose, all scenarios of the data type extended. The three courses reflect the experiments 2.1 to 2.3. Experiment 2.1 shows good results from a neuron count >10 neurons. The result is a range of good results between 10 and 20 neurons in the hidden layer. With higher numbers of neurons worse results are achieved, which are at an MSE of about 9,000. Overall, due to the small number of 10 attempts, large fluctuations result. In addition, it is concluded that the results are heavily dependent on the starting weights of the network. Since these are generated randomly before each learning phase, further possible good configurations are to be expected. This has been checked by experiment 2.2. Experiment 2.2 shows a strong smoothing of the course in a similar course. Experiment 2.3 generates much better results. The range of good results shifts to a higher number of neurons (24-44). The fluctuation of the results is still close to the low number of runs. Here, as in the case of the median, an improvement of the results to 17 neurons can be recognized. The results of experiment 2.1 are expected to vary greatly and can be smoothed by further experiments (Experiment 2.2). By the further 90 attempts per neuron number, apart from number $= 29$ with each configuration a better result is obtained. In comparison the results of experiment 2.3 are relatively constant. The best result with an MSE of 882 has been achieved by experiment 2.3 in 43 neurons. The training of networks is relatively time-consuming and varies in the example, depending on the number of iterations and number of neurons between a few seconds and about ten minutes. A higher number of learning scenarios should therefore be sought in this case. Considering Figure 9, it stated that due to the median rarer good results are expected with a high number of neurons. Taking into account that a larger network structure is associated with a longer learning phase, in Experiment 2.3 the search range should be limited to 25-50 neurons. In another experiment (Table 4), the learning set 1 is mixed with the learning set 2. The training data from the first learning set is selected and the validation data from the learning set 2 is compiled.

Table 4 Experiment 3 – Data Composition

Data type	Data set	Number of scenarios
Training data	Set1 (fixed intervals)	8,800
Validation data	Set2 (random intervals)	1,200
Test data	Test data (random intervals)	2,000

The results of this configuration are significantly worse than the results from Experiment 1 and therefore will not be considered further. In next experiments an attempt is made to further minimize the MSE. For this the learning data are normalized. Furthermore, the number of covered layer can be increased. In addition, it should be checked whether a cross validation is necessary. The overall system depends on the predictive quality of the neural networks used. The aim of this work, however, is to develop a working concept. Therefore, subsequent investigations should focus on this point.

Table 5 Summary results expert system

Prognosis net	RMSE	Experts / Best Network	MAD	Experts / Best Network	Mean absolute deviation
Expert System Out	1,65	101,6%	1,17	98,3	-0,19
Best network Out	1,63		1,19		-0,20
Expert System Buffer A	0,28%	86,1%	0,19%	81,2%	-0,05%
Best network Buffer A	0,32%		0,23%		-0,05%
Expert System Buffer B	0,31%	86,0%	0,21%	81,5%	-0,05%
Best network Buffer B	0,36%		0,26%		-0,06%

5.5. Results

Better results related to the test error are achieved by coupling several neural networks. For this, the five best nets are combined into one expert system. From their forecasts, the mean values are calculated as the actual forecast value. They forecast 100,000 independent data generated using Scenario Manager. The parameters are randomly generated in the range 0-100 percent and checked for duplicates. Table 5 shows the Mean-Absolute-Deviation (MAD) and Root-Mean-Square Error (RMSE) of the individual experiments and compares in columns 3 and 5 the expert system with the respective best individual network. If the value is <1, the expert system achieves better results, relative to the characteristic value. A value> 1 means that the best mesh produces better results. The mean absolute deviation (column 6) shows that the forecasts of all systems are slightly shifted to the negative. All sample pairs consist of seven input parameters, five machine processing times and stocks in two buffers. Each input configuration is simulated 100 times to generate the nine output parameters. These include the production quantity and the relative occupancy states of both buffers for the best, worst and average case. These pairs of patterns are grouped into two different sets of 20,000 pairs of patterns. In addition, 4,000 test pattern pairs are created. With the learning sets experiments are carried out to generate neural networks with simple means. The reduction of the data set is possible, but leads to somewhat poorer results, based on the test error. At the same time the learning time decreases rapidly. In this article, it is decided to use the 20,000 pattern pairs to train the ANN. In the last experiment it is shown that expert systems consisting of several nets provide better prognoses for the buffer states. With regard to the accuracy of the forecast, it can be stated that the average case can be forecast most accurately. Another method for combining large amounts of data, machine learning and simulation-based analysis describes the Ensamble Modeling (EM). This approach will be considered forward-looking. One goal may be to supplement the results obtained with this method and thus obtain secure and robust results.

5.6. Outlook for improving the forecasting and solution quality of the system

Here, the second approach complements the previously described approach for implementing a procedure model for the coupling of simulation and artificial intelligence. This time, the scenario plan was created using the Python programming language, representing the different scenarios in production over varying processing times and buffer states at the beginning of the simulation. The simulation has then been optimized to assign the input data from the scenario plan to the appropriate processing stations, run the simulation for a fixed amount of time, store the results in a table. Then rerun the next record from the scenario plan is initialized. Due to this loop structure, the simulation runs fully automatically for all incoming scenarios. The simulation data thus obtained

are then used for training first, then for testing an ANN, which was created by the machine learning program package TensorFlow. First, the calculation speed of the simulation is improved by using special simulation methods within the tool. For this purpose, the model is recreated with the high-level API Keras, which has extended functionality compared to the underlying TensorFlow. In the further course, the performance of the ANN with regard to forecasting speed and forecasting quality is improved by sensitivity analyzes of the individual network parameters. First results show that the calculated values for the forecast quality can be classified as very good results by the present multi-linear regression problem with peak accuracies of 99.84%. The true quality of the statements is, however, clear only when compared with conventional methods for regression analysis (Table 6). Therefore, in the following a comparison of the prognosis results of the NN with prognosis results of classical methods for the multiple linear regression is made.

Table 6 Comparison of forecast results with other methods for solving multi-linear regression problems with stochastic processing times

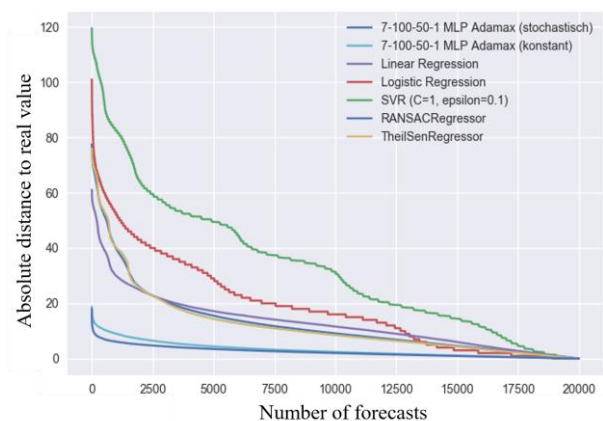| Method	Highest individual deviation	Share forecasts deviation > 1%	Ø-Error test data
7-100-50-1 MLP (stochastically)	18,01	12,76%	2,43
7-100-50-1 MLP (constant)	18,78	22,63%	3,16
Linear Regression	61,12	79,86%	12,95
Logistics Regression	101	70,84%	18,79
SVR (C=1, epsilon=0,1)	119,56	87,42%	32,90
RANSAC Regressor	77,53	74,39%	12,47
TheilSen Regressor	76,03	72,99%	12,08

Figure 8 Comparison of the prediction quality of different methods for regression analysis in stochastic processing times

The comparison methods were implemented using the statics and ML module scikit-learn in Python. The results are shown in Figure 8. It is noticeable that the previous step form of many linear regressors deviates from a weaker and more continuous slope. However, the forecast accuracy of the other methods hardly changes. The predictions were made for the stochastic data. The graph shows that the performance difference is low. This is due to the fact that for the training of an ANN on training data generated with stochastic processing times significantly more training data sets are needed for a prognosis quality close to the training data generated with constant processing times. In a study carried out for this purpose, a 2.75-fold increased training data amount was not sufficient to significantly reduce the forecasting error. Therefore, for stochastic problems the use of a deep ANN is recommended, which should be trained with at least five times the amount of data. Due to this focus on forecasting quality and speed of calculation, further functionalities could not be developed. Therefore, the first starting point for future work in the field of embedding in an early warning system (with variant comparison and catalog of measures) can be seen. To do this, several NN with forecasting levels above a specified limit (e.g. 99.5%) should be used together to make forecasts. The various forecasts can then transmit to be more resistant to various false predictions.

6. CONCLUSION AND OUTLOOK

For the first time, this article describes an innovation to reach short-term forecasts in the context of Industry 4.0 through the coupling of material flow simulation (discrete event simulation) and artificial intelligence (neural networks). By coupling both systems with a self-designed middleware, the strengths of the systems is used very well. The article showed that the simulation removed the existing black-box properties of neural networks. Another necessary development for the application of the methodology in the production environment is the use of real machine data through the connection to an ERP system or another reliable data source. In principle, however, no comprehensive changes should be necessary. For the future development a certain flexibility should be made possible here, so that the data can be drawn directly from a database or transmitted via sensors from the machines to the ANN. In very large production plants, it is possible to forecast individual subareas of the plant via a separate ANN. This makes the complexity much easier to control than in a large ANN for the entire production plant. These ANN make independent forecasts for the respective subareas such as goods receipt, goods issue, picking, final production etc. At the interfaces between the areas, the expected throughput per hour can then be given as a value. In this way, the system is robust against outliers in the use of a single ANN for the entire production forecast. The design of the information transfer at the interfaces as well as the effect on the quality of the prognoses represent further open research questions for future work.

REFERENCES

Bousonville, T.: Logistik 4.0: Die digitale Transformation der Wertschöpfungskette. Wiesbaden: Springer Gabler 2017.

Chen, H.; Chiang, R.H.; Storey, V.C.: Business intelligence and analytics. Management information systems : mis quarterly 36 (2012) 4, S. 1165–1188.

Faingloz, L.; Tolujew, J.: Simulation Modelling Application in Real-time Service Systems. Procedia Engineering 178 (2017), S. 200–205.

Gössler, G., Tiefenbrunner, M.: Selbstlernende Analyse-, Planungs- und Optimierungs-Modelle für reale und virtuelle SCM-Netzwerke. In: Engelhardt-Nowitzki, C.; Krenn, B.; Nowitzki, O. (Hrsg.): Management komplexer Materialflüsse mittels Simulation. s.l.: Gabler Verlag 2008, S. 147–162.

Gruber, M.; Rinner, M.; Löscher, T.; Almeder, C.; Hartl, R.; Katzensteiner, S.: Vorausschauende Produktionsregelung durch simulationsbasierte heuristische Optimierung. In: März, L.; Krug, W.; Rose, O.; Weigert, G. (Hrsg.): Simulation und Optimierung in Produktion und Logistik. Berlin, Heidelberg: Springer-Verlag Berlin Heidelberg 2011, S. 65–77.

Hanisch, A.; Tolujew, J.; Richter, K.; Schulze, T.: Online simulation of pedestrian flow in public buildings. In: Chick, S.E. (Hrsg.): Proceedings of the 2003 Winter Simulation Conference, New Orleans, LA, USA, 7-10 Dec. 2003, 2003, S. 1635–1641.

Hanisch, A.; Tolujew, J.; Schulze, T.: Initialization of Online Simulation Models. In: Kuhl, M.E. (Hrsg.): Proceedings of the 2005 Winter Simulation Conference, Orlando, FL. USA, Dec. 4, 2005, 2005, S. 1795–1803.

Hausladen, I.: IT-gestützte Logistik: Systeme - Prozesse - Anwendungen. Wiesbaden: Springer Gabler 2016.

Hausman, W.H.; Lee, H.; Subramanian, U.: Global Logistics Indicators, Supply Chain Metrics, and Bilateral Trade Patterns. SSRN Electronic Journal (2005).

Helmig, J., Schmidt, C., Kompa, S.: Zeitdynamische Simulation in der Produktion. In: Schuh, G.; Stich, V. (Hrsg.): Produktionsplanung und -steuerung 2. Berlin: Springer 2012, S. 195–231.

Heuer, J.: Neuronale Netze in der Industrie: Einführung - Analyse - Einsatzmöglichkeiten. Wiesbaden: Deutscher Universitätsverlag 1997.

Hinton, G.E.; Salakhutdinov, R.R.: Reducing the dimensionality of data with neural networks. Science (New York, N.Y.) 313 (2006) 5786, S. 504–507.

Hotz, I.: Simulationsbasierte Frühwarnsysteme zur Unterstützung der operativen Produktionssteuerung und -planung in der Automobilindustrie. Magdeburg, Otto-von-Guericke Universität, Dissertation, 2007.

Hotz, I.; Hanisch, A.; Schulze, T.: Simulation-Based Early Warning Systems as a Practical Approach for the Automotive Industry. In: Proceedings of the 38th conference on Winter simulation, Monterey, CA, USA, 3/12/2006 - 6/12/2006, 2006, S. 1962–1970.

John Walker, S.: Big Data. International Journal of Advertising 33 (2015) 1, S. 181–183.

Li, Y.; Kramer, M.R.; Beulens, A.J.M.; van der Vorst, J.G.A.J.: A framework for early warning and proactive control systems in food supply chain networks. Computers in Industry 61 (2010) 9, S. 852–862.

Lueth, K. L., Patsioura, C., Williams, Z. D., Kermani, Z. Z., 2016: Industrial Analytics 2016/2017: The current state of data analytics usage in industrial companies. Hg. v. IOT Analytics, Digital Analytics Association Germany.

Markwardt, U., Schulze, F.: Neuronale Netze als Meta-Modelle in der Materialfluss-Simulation. In: Hohmann, R. (Hrsg.): Simulationstechnik, Magdeburg, 16.09.2003, 2003, S. 397–402.

März, L.; Krug, W.; Rose, O.; Weigert, G. (Hrsg.): Simulation und Optimierung in Produktion und Logistik: Praxisorientierter Leitfaden mit Fallbeispielen. Berlin, Heidelberg: Springer-Verlag Berlin Heidelberg 2011.

Rabe, M.; Hellingrath, B. (Hrsg.): Handlungsanleitung Simulation in Produktion und Logistik: Ein Leitfaden mit Beispielen für kleinere und mittlere Unternehmen. Erlangen, San Diego, Calif.: SCS European Publ. House; SCS International 2001.

Reggelin, T.; Schauf, C.; Lang, S.; Weigert, D.: Application of discrete-rate based mesoscopic simulation models for production and logistics planning. In: The 19th International Conference on Harbor, Maritime and Multimodal Logistics Modelling and Simulation (HMS 2017): Barcelona, Spain, September 18-20, 2017. Genova: DIME Università 2017, S. 141–147.

Schenk, M.; Wirth, S.; Müller, E.: Fabrikplanung und Fabrikbetrieb: Methoden für die wandlungsfähige, vernetzte und ressourceneffiziente Fabrik. Berlin: Springer Vieweg 2014.

Schmidt, T.: Grobplanung mit künstlichen neuronalen Netzwerken für die Halbleiterfertigung. Heimsheim: Jost-Jetter 2000.

Schoenherr, T.; Speier-Pero, C.: Data Science, Predictive Analytics, and Big Data in Supply Chain Management. Journal of Business Logistics 36 (2015) 1, S. 120–132.

Schulze, F., Marquardt, H.-G: Neuronale Netze in der Materialflußsimulation. In: Mertins, K. (Hrsg.): The new simulation in production and logistics: prospects, views and attitudes. Berlin: IPK Eigenverl. 2000, S. 473–482.

Timm, I. J., Lattner, A.D.: Künstliche Intelligenz in der Logistik. KI - Künstliche Intelligenz 24 (2010) 2, S. 99–103.

VDI 3633: Simulation of systems in materials handling, logistics and production. Berlin, Düsseldorf: Beuth 2013.

Waller, M.A.; Fawcett, S.E.: Data Science, Predictive Analytics, and Big Data. Journal of Business Logistics 34 (2013) 2, S. 77–84.

Weber, M.: Vorgageermittlung mit künstlichen neuronalen netzen für die variantenreiche kleinserienfertigung. Heinsheim: Jost Jetter Verlag 1999.

Weigert, D.: Development of an early warning system in production and logistics through the combination of artificial intelligence and material flow simulation. In: 10th International Doctoral Students Workshop on Logistics, June 20, 2017, Magdeburg. OvGU 2017, S. 57–62.

Weigert, D.: Prozessbegleitende Simulation, Analyse, Planung und Steuerung logistischer Systeme. Ressourceneffiziente Produktion und Logistik : 18. Forschungskolloquium am Fraunhofer IFF (2017b), S. 19–28.

AUTHORS BIOGRAPHY

DAVID WEIGERT studied Industrial Engineering with specialization in Logistics at the Otto-von-Guericke-University Magdeburg. He became a research associate at the Chair Logistical Systems at the Otto von Guericke University Magdeburg and scientific project assistant at the Fraunhofer Institut for Factory Operation and Automation IFF. His areas of competence are the analysis and optimization of logistics processes, as well as modelling, simulation and optimization of logistics systems.

TIM LIPPKE studied Industrial Engineering with specialization in Logistics at the Otto von Guericke University Magdeburg. His research interests are applied science of artificial intelligence in logistics.

TOBIAS REGGELIN is a research and project manager at Otto von Guericke University Magdeburg and the Fraunhofer Institute for Factory Operation and Automation IFF. He received a doctoral degree in engineering from Otto von Guericke University Magdeburg. His research interests include the development and application of new modeling and simulation methodologies.

MICHAEL SCHENK after studying mathematics and various industrial activities, he received his doctorate in 1983 in the field of factory planning. 1988 Habilitation. 1989 lecturer for production process control in the University of Magdeburg. Since 1994 Director of the Fraunhofer Institute for Factory Operation and Automation IFF in Magdeburg and since 2003 professor at the department Logistic Systems at the Otto-von-Guericke University Magdeburg.

DISTRIBUTED SIMULATION EXECUTION ON A HIGH-PERFORMANCE CLUSTER USING HEURISTICLAB HIVE

Johannes Karder[(a)], Andreas Beham[(b)], Stefan Wagner[(c)], Michael Affenzeller[(d)]

[(a),(b),(c),(d)]Heuristic and Evolutionary Algorithms Laboratory
University of Applied Sciences Upper Austria, Softwarepark 11, 4232 Hagenberg, Austria
[(a),(b),(d)]Institute for Formal Models and Verification
Johannes Kepler University, Altenberger Straße 69, 4040 Linz, Austria

[(a)]johannes.karder@fh-hagenberg.at, [(b)]andreas.beham@fh-hagenberg.at,
[(c)]stefan.wagner@fh-hagenberg.at, [(d)]michael.affenzeller@fh-hagenberg.at

ABSTRACT
This paper presents a generic way of distributing simulation executions. The proposed method can be applied on high performance clusters in order to execute many simulation runs simultaneously and gather respective results. These results can then be collected into datasets, which one can use for data analysis and examination of different properties of the implemented simulation model and the underlying simulated process, e.g. production plants or logistics systems. The approach is showcased using a concrete simulation of a production process controlled by different disposition parameters. After executing 30 000 simulation runs, we are able to create respective datasets in order to further analyse the properties of the production process and build surrogate models of the simulation model, which in turn can be used in surrogate-assisted parameter optimization.

Keywords: distributed simulation execution, high-performance cluster, software architecture, HeuristicLab

1. INTRODUCTION

Data analysis is a useful tool that enables researchers and others to gain more insights into different kinds of production and logistics systems. In order to apply data analysis and machine learning methods, appropriate data has to be gathered beforehand. Data can e.g. be collected by observing production cycles over weeks or months. If no such data is available, or different scenarios of a current production process should be explored, implementing a simulation model is necessary. If such simulation models exist, a certain amount of data, i.e. many different simulation parameters (input parameters) and corresponding simulation results (output parameters), has to be generated in order to gain useful insights into the production process. However, such simulation models, e.g. from production plants or logistics systems, can be computationally very expensive. To generate a significant amount of data, thousands of simulation runs have to be executed, which, depending on the level and complexity of the simulation model, can take up to days or even weeks. Furthermore,

such simulations are often of stochastic nature, meaning that many repetitions of a single simulation configuration have to be executed in order to achieve statistical significance. If the speed of the simulation itself cannot be improved and hardware is at its limits, the only way overcome the tremendous runtime costs and to shorten the overall execution time of the experiment is to increase the degree of parallelism within the experimental setup.

In this paper, we introduce a generic way of executing many simulation runs in a massively parallel fashion on a high performance cluster. A simulation model of a real-world production plant is used, where lot sizes and planned lead times for a set of materials are input parameters and numerous results, including e.g. inventory and tardiness costs are generated during the simulation run. The simulated results are then collected to form datasets and can be evaluated to gain more insights into the production process. Using such a dataset, we also explore the possibility to create a surrogate model for the actual simulation model, which can be used to optimize the input parameters to e.g. minimize the production plant's inventory and tardiness costs. The paper concludes with possible improvements and future work.

The paper is outlined as follows. Related work is presented in Section 2 and Section 3 quickly introduces the reader to the used simulation model. Section 4 constitutes the main part of the paper, explaining how the generic distribution of simulation runs has been implemented and datasets are created. Experiments and results are presented in Sections 5. Finally, the paper is concluded by raising potential for improvement and giving an outlook on planned future work in the final Section 6.

2. RELATED WORK

Simulation is a prominent tool used in various research fields in order to transfer real-world systems into computational models. Simulations have been used for a broad spectrum of tasks, e.g. disaster risk assessment (Latcharote et al. 2018), logistics case studies (Crainic et

al. 2018), simulation-based design (Mefteh 2018), simulation-based optimization (Gosavi 2015, Affenzeller et al. 2015), training tasks (Bruzzone and Longo 2013) or weather prediction (Lynch 2008).

Simulations can get expensive in runtime depending on their level of detail and the complexity of the simulated system. In order to shorten the time that is required to execute runtime-expensive simulation runs, researchers try to parallelize the simulations themselves or distribute workloads amongst multiple workers and calculate parts of the simulation or whole simulation runs in parallel. Parallel and distributed simulation (Fujimoto 2000) is a relevant topic within today's research fields, e.g. in operational research (Taylor 2018). Furthermore, there exist specific standards and frameworks for creating parallel and distributed simulations, e.g. the high-level architecture (Kuhl 1999, Law 2015, Falcone et al. 2017). However, to the best of our knowledge, no work in this area has been published where HeuristicLab Hive (Scheibenpflug et al. 2012) has been extended to distribute and execute many simulation runs in parallel.

3. SIMULATION MODEL

The used simulation model represents a production process of a real-world company, where different materials and low-level codes exist. All in all, there are 53 materials and for each material, its lot size and planned lead time have to be specified. These 53 * 2 = 106 parameters affect the overall production process, which is simulated. The results yielded by a single simulation run include, but are not limited to:

- buffer properties
- inventory and tardiness costs
- service level
- utilization

In addition to the 106 input parameters, the simulation receives many more scenario parameters from a database model. These parameters allow to configure the actual production plant, e.g. by specifying the number of machines that are used in the production process, the probability of machine breakdowns, etc. A single simulation run takes around 5.5 minutes to complete.

The simulation model was implemented in AnyLogic. This allows it to be exported as a standalone Java application. Furthermore, the required database model is built upon an H2 database, which also requires no installation and can be deployed in a portable way. The AnyLogic simulation can access the database through a H2 connector. These are important considerations when distributing simulations. This way, one only has to ensure that the target machines that will execute the single simulation runs have a Java runtime installed. No additional installations, e.g. large database servers or the like, have to be done.

4. DISTRIBUTED SIMULATION EXECUTION

This section constitutes the main part of the paper. First, insights into existing computing infrastructure, namely HeuristicLab Hive, are given. We then proceed with the detailed explanations of how simulation runs are distributed using Hive. Finally, the proposed approach is summarized.

4.1. HeuristicLab Hive

The generic approach has been implemented for HeuristcLab Hive, a grid computing system that is developed as part of HeuristicLab (HL) (Wagner et al. 2014), a paradigm-independent and extensible environment for heuristic optimization. Both run on top of Microsoft's .NET framework and are implemented in C#. The source code is freely and openly available for everyone at https://dev.heuristiclab.com. The general Hive infrastructure is shown in Figure 1.
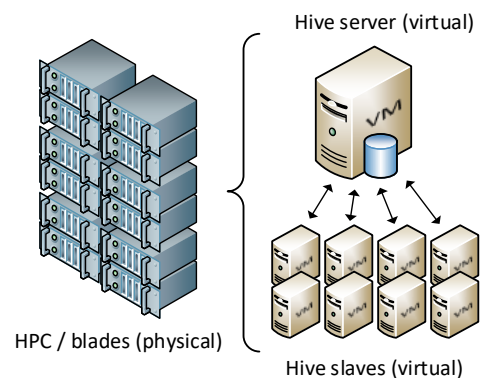
Figure 1: The Hive infrastructure. A physical blade hosts a virtual machine that acts as a Hive server and many smaller virtual machines that act as Hive slaves.

The physical high performance cluster (HPC) used in this study consists of 16 blade systems, each of which has the following specifications:

- 8 Intel Xeon E5420 @ 2.50 GHz
- 32 GB RAM
- 60 GB HDD

The HPC hosts multiple virtual machines, one of them having the function of the Hive server. The server is responsible for distributing calculation tasks, also called Hive tasks, between virtual machines that actually process them, called Hive slaves. HeuristicLab users are able to upload Hive jobs that consist of many different tasks to the Hive server and download optimization results as soon as the tasks have been processed by the slaves.

Figure 2 shows how clients, server and slaves interact with each other. A HL client uploads jobs (large boxes) which contain one or more (calculation) tasks to the Hive server. Hive slaves fetch the tasks (small boxes) of these jobs from the server, calculate them, and store results within. Finished tasks are sent back to the server. The jobs, and therefore their calculated tasks with respective results, can then be downloaded again by the client.
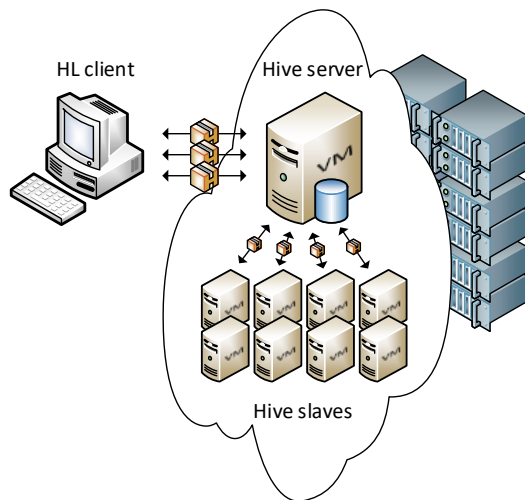
Figure 2: Transmission of jobs and tasks between HL client, Hive server and Hive slaves.

Usually, a slave calculates one task on one CPU core, meaning that a Hive slave which runs on a quad core machine will calculate at most 4 tasks at once. However, the amount of tasks one slave should calculate at a time is configurable. Furthermore, heartbeats are sent by every slave to inform the server about the current condition of the slave. A heartbeat includes information such as the currently calculating tasks and calculation time, CPU utilization, etc. This allows the server to detect if any slave goes offline while calculating a task, e.g. because the host machine was shut down. If a slave fetched tasks from the server, but does not send any heartbeats anymore, the server will detect the slave as being offline and reschedule the tasks which had been assigned to the slave.

4.2. EvaluationAlgorithm

For the proposed distribution of simulation runs, a special type of algorithm, namely the EvaluationAlgorithm, has been implemented, which can be executed within HeuristicLab. Usually, the user is responsible for uploading jobs/tasks onto the Hive server and for retrieving the results. The EvaluationAlgorithm has been implemented to automatically create respective jobs/tasks for all parameter configurations that should be simulated on the HPC, as shown in Figure 3. All distributed simulation runs will be downloaded after completion and the results will be added to a dataset.

	P_1	P_2	P_3	
PC_1	68	21	74	...
PC_2	12	91	43	...
PC_3	81	36	17	...
	⋮	⋮	⋮	
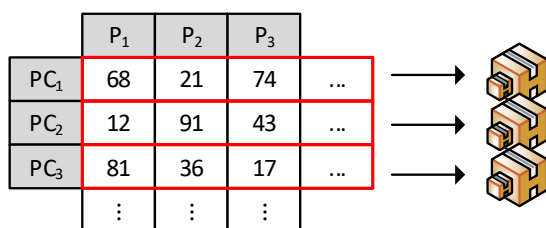
Figure 3: For each set of parameters (P_n), i.e. parameter configuration (PC_m), that should be simulated, a single Hive job that contains a single Hive task is created.

The user can define the configuration parameters that should be simulated in form of comma-separated values (CSV). The number of simulations that should be executed concurrently is configurable, as is the maximum duration of a simulation run and the number of replications that should be created for each parameter configuration. A maximum simulation time is necessary in order to e.g. abort hanging simulations and free up cores of Hive slaves.

4.3. PayloadAlgorithm

To enable a generic approach for distributed simulation execution, some precautions had to be made. The basic idea is to distribute jobs in form of isolated simulation packages. In the example of our production plant simulation, and in any other example, this package must contain all information required to execute a simulation run. Therefore, the following steps have to be taken:

1. Create an entity that can be executed by a Hive slave
2. Define the parameter configuration to be simulated within this entity
3. Package the actual simulation, including eventual dependencies such as a database, together with helper scripts and attach it to this entity
4. Upload this entity to the Hive server

The entities that are usually executed by Hive slaves are some kind of metaheuristic optimization algorithms, e.g. population-based algorithms such as genetic algorithms, evolution strategies or particle swarm optimization or trajectory-based ones such as local search or simulated annealing. These algorithms then return e.g. best found solutions, number of evaluated solutions, quality histories, etc. In our case, we had to implement an entity, i.e. an algorithm, whose sole task is to execute a simulation model and return the simulation results. In order to distribute the simulation model and additional dependencies, we introduced a PayloadAlgorithm which is able to transport a payload in form of a binary serialized ZIP archive and extract it on the Hive slave. In order to set up the payload on a Hive slave, some additional steps might be required. Therefore, a generic approach enables users to configure this payload setup by including PowerShell scripts into the payload itself. The PayloadAlgorithm, once run, will extract the payload and execute the helper scripts. Four different scripts can be specified:

1. Before – gets executed before the actual task; useful to setup the simulation environment, and eventual dependencies such as databases
2. After – gets executed after the actual task
3. Catch – gets executed in case the actual task threw an exception
4. Finally – gets executed in any case after the actual task finished or an error occurred; useful to clean up after the actual task

4.4. TaskAlgorithm

We then derived a TaskAlgorithm from the PayloadAlgorithm. It specifies some more properties necessary for the simulation execution, e.g. the parameter configuration that should be simulated, the replication number and an evaluation timeout after which a simulation run is considered to have failed (i.e. a maximum simulation time limit). The TaskAlgorithm's actual task is to execute a simulation run, i.e. pass the parameters to the running simulation application, wait for completion of the simulation and collect the simulation results.

As mentioned before, a payload, i.e. a package in form of a ZIP archive, has to be created that contains specific files, depending on the simulation that should be executed. In our case, we included the production plant simulation, the portable database containing the scenario parameters, as well as two helper scripts that are responsible for setting up the simulation and cleaning up afterwards. This resulted in a ZIP archive which contents are shown in Figure 4.
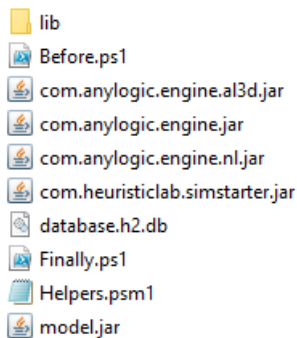

Figure 4: The contents of the ZIP archive. It includes the simulation application, the database file and server, as well as some other required libraries.

The most important files are as follows:
- Before.ps1 – the helper script responsible for setting up the simulation environment
- Finally.ps1 – the helper script responsible for cleaning up after the simulation; Clean up involves stopping the simulation application and shutting down the portable database server
- model.jar – the simulation model
- database.h2.db – the H2 database file

HeuristicLab offers features for sending and receiving objects to and from external applications using Google's Protocol Buffers (https://developers.google.com/protocol-buffers/). This concept is used within the TaskAlgorithm to send parameter configurations to the simulation application. The TaskAlgorithm's actual task now is to 1) set up a connection to the simulation application, 2) send the parameter configuration to the simulation application and 3) extract the simulation results after the simulation finishes. As mentioned before, executing the actual task, i.e. the simulation, might require additional steps. The Before.ps1 script first starts the database server on a randomly assigned TCP

port. Then the simulation application is started on a randomly assigned TCP port as well (needed for Protocol Buffer communication). After the database server and simulation application have been set up, the TaskAlgorithm can continue with its actual task. The simulation application waits for incoming messages, i.e. parameter configurations that should be simulated. When the TaskAlgorithm sends its parameter configuration to the simulation application, the simulation is started. Once the simulation finishes, the simulation application will notify the TaskAlgorithm, which in turn will extract the simulation results. Then the Finally.ps1 script is executed which will kill the simulation and database processes. After the clean-up has been performed, the extracted payload contents will be removed from the Hive slave's file system. Pseudo code that represents the logic of a Payload-/TaskAlgorithm is shown in Algorithm 1.

```
// the algorithm's entry point
procedure Run()
  try
    ExtractPayload()

    ExecuteBeforeScript()
    Work()
    ExecuteAfterScript()
  catch Exception e
    ExecuteCatchScript(e)
  finally
    ExecuteFinallyScript()

    DeletePayload()
end procedure


// the algorithm's actual task
procedure Work()
  // configure connection to simulation app
  ConfigureConnection()

  // establish connection to simulation app
  // and send parameters
  // returns quality when simulation finishes
  quality ← Evaluate(properties.params)

  // extract and store results
  results.quality ← quality
  results.simResults ← ExtractSimResults()
  properties.results ← results
end procedure
```

Algorithm 1: Pseudo code expressing the logic that gets executed by a Payload-/TaskAlgorithm.

A PowerShell module provides functions to start and stop processes, as well as retrieving TCP ports bound by a process. Listing 1 shows the contents of the Helpers.psm1 script.

```
Function StartProcess($command, $arguments) {
  $process = Start-Process
    -WindowStyle Hidden
    -PassThru $command $arguments
  $process.Id;
}

Function StopProcess($processId) {
  Stop-Process -Id $processId;
}
```

```
Function GetPort($processId) {
  $connections = @(Get-NetTCPConnection | Where {
    $_.OwningProcess -eq $processId -and
    $_.State -eq "Listen"
  });
  While ($connections.Count -le 0) {
    $connections = @(Get-NetTCPConnection | Where {
      $_.OwningProcess -eq $processId -and
      $_.State -eq "Listen"
    });
  }
  $connections[0].LocalPort;
}
```
Listing 1: The contents of Helpers.psm1.

The contents of the Before.ps1 script, which will start the database server, as well as the simulation, are shown in Listing 2.

```
# properties
$dbName = "simgen";

# start database
$processId = StartProcess java
  "-cp ""lib\h2-1.3.173.jar""
  org.h2.tools.Console
  -tcp
  -tcpPort 0";
Set-Content db.pid $processId -NoNewline;
$port = GetPort($processId);
Set-Content db.port $port -NoNewline;
Set-Content db.name $dbName -NoNewline;

# start simulation
$processId = StartProcess java
  "-cp "".;*;lib\*;lib\database\querydsl\*""
  com.heuristiclab.simgenopt.SimStarter
  -hlPort 0
  -dbPort $port
  -dbPath /file:$dbName";
Set-Content sim.pid $processId -NoNewline;
$port = GetPort($processId);
Set-Content sim.port $port -NoNewline;

Start-Sleep 2
```
Listing 2: The contents of Before.ps1.
```
Import-Module .\Helpers.psm1
```

After the simulation finishes, the Finally.ps1 script shuts down the simulation and the database server, as shown in Listing 3.

```
# kill simulation
$processId = Get-Content sim.pid;
StopProcess $processId;

# kill database
$processId = Get-Content db.pid;
StopProcess $processId;

Start-Sleep 2
```
Listing 3: The contents of Finally.ps1.
```
Import-Module .\Helpers.psm1
```

The communication between the TaskAlgorithm and the simulation app is established using HL's external evaluation API, which builds upon Google's Protocol Buffers. A new EvaluationServiceClient is created, which will connect to the local machine via a TCP evaluation channel using the port that was automatically allocated by the system ("-hlPort 0") when the simulation app was started in the Before.ps1 script. The simulation app itself will listen to incoming connections on this port. Furthermore, a solution message is created which contains the parameters, as well as the replication number. This solution message is sent to the simulation app, which use the replication number to seed its random number generator and then starts a simulation run. After the simulation finishes, the simulation app creates a quality message which contains the objective value of the simulated parameters. This message is sent back to the TaskAlgorithm via the same TCP channel.

In addition to the objective value specified in the quality message, the simulation also outputs much more information for a particular simulation run. This data is written to the H2 database file. Once the TaskAlgorithm receives a response from the simulation app, meaning that the simulation run finished, it can retrieve further information about the run by reading the database.

4.5. Summary
The generic simulation distribution can be summarized as follows:

- An EvaluationAlgorithm is created and, amongst other parameters, the configuration parameters that should be simulated are provided in form of a CSV file
- For each set of configuration parameters, the EvaluationTask uploads *n* Hive jobs that contain a single TaskAlgorithm as task to the Hive server, where *n* is the number of replications that should be simulated; The maximum number of jobs (i.e. tasks) that are concurrently created is limited; The EvaluationTask also polls the Hive server for completed jobs
- A Hive slave fetches one task per core and executes the TaskAlgorithm
- The TaskAlgorithm extracts its payload and executes the specified helper scripts (e.g. to start a simulation)
- Once the setup of the payload is done, the TaskAlgorithm sends the parameter configuration to the running simulation application via Protocol Buffers
- When the simulation finishes, the TaskAlgorithm stores the simulation results; Furthermore, the simulation application, as well as the database server are killed and the extracted payload removed from the Hive slave
- The Hive slave updates the TaskAlgorithm (which now includes the results) on the Hive server and fetches a new available task via the next heartbeat
- The EvaluationAlgorithm notices the finished job and downloads it; The simulated configuration parameters, together with the
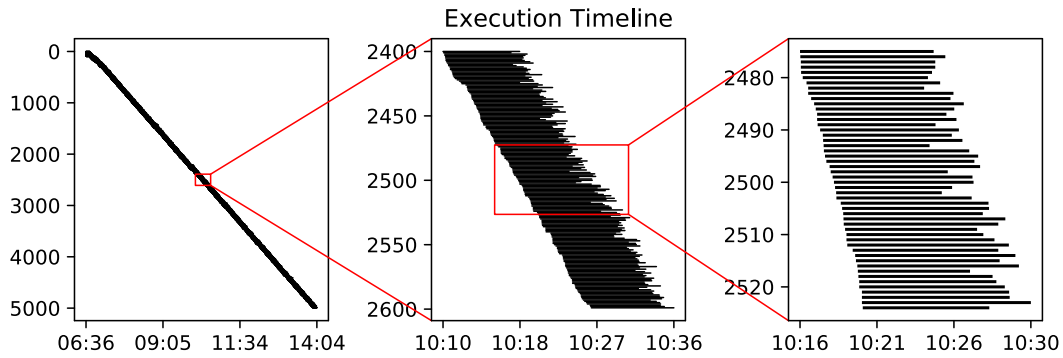
Figure 5: The execution timeline of experiment #1.

5. EXPERIMENTS & RESULTS

For our initial experiments, we used a total of 32 virtual machines, each of which running a single Hive slave, with the following specifications: 4 CPU cores, 13.5 GB RAM, 15 GB HDD. This results in a total of 128 CPU cores, 432 GB RAM and 480 GB HDD. The created ZIP archive ha a total file size of less than 10 MB. The EvaluationAlgorithms were configured to create TaskAlgorithms with an evaluation timeout of 10 minutes, which includes a safety margin to the average simulation time of 5.5 minutes.

The goal was to simulate a number of different parameter configurations to be able to apply data analysis methods on the generated data, e.g. to create surrogate models for the simulation model. To test the distribution of simulation executions, we initially started with 100 randomly generated parameter configurations, each of which should be simulated 10 times in order to generate 1 000 data points for our dataset. We repeated the process five times to generate a total of 6 000 data points. We then decided to increase the batch size of parameter configurations up to 400 in order to generate 4 000 data points and reach 10 000 in total. Finally, four more batches for 500 parameter configurations each were launched. In the end, we had simulated 3 000 parameter configurations with 10 repetitions, which should result in a total of 30 000 data points. However, in 113 out of 30 000 runs (0.38 %), errors occurred, reducing the number of available data points to 29 887. Out of these, three data points were deemed invalid since negative inventory costs were reported by the simulation. This left us with a dataset containing a total of 29 884 data points. This dataset was then used to build surrogate models which predict the inventory and tardiness costs that occur within the production plant. With the created models, we conducted surrogate-based optimization of the material planning parameters (i.e. lot sizes and planned lead times). Following the optimizations, the best found parameter configurations were simulated in order to get simulation results for the inventory and tardiness costs. The costs predicted by the surrogate models were quite accurate, which indicates that the data generated by the proposed approach can successfully be used to create good surrogate models, which again can be used for surrogate-based optimization.

Finally, we conducted four more experiments to measure execution times and calculate the speedup that is achieved when using the distributed approach. The EvaluationAlgorithms were executed with the following experimental settings shown in Table 1:

Table 1: Settings used for the runtime experiments.

Parameter	Value
Number of Parameters	500
Number of Repetitions per Parameter	10
Max. Parallel Jobs	100
Max. Parallel Job Up-/Downloads	4
Max. Simulation Time	10 [min]
Job Polling Interval	20 [sec]
Heartbeat Interval	90 [sec]
Available Cores	120

All of the four experiments took around 7.5 hours to complete. The average execution time of the simulation runs was around 5.5 minutes. Sequentially evaluating 20 000 parameter configurations would have resulted in an execution time of around 20 000 * 5.5 = 110 000 minutes, i.e. 1 833.33 hours. Using this configuration, we therefore achieved a 61.11x speedup. Table 2 shows more detailed statistics for all four experiments. The evaluation time is the time it took to finish a task after its creation. It includes the execution time, which is the time it took for a slave to execute the TaskAlgorithm, more precisely the time it took to execute the helper scripts and the simulation. A plot of the execution timeline of one experiment is depicted in Figure 5.

Table 2: The experiments' duration (Δ) as well as the average evaluation time (α) and the average execution time (β) of each job.

Exp.	Δ [h]	α [min]	β [min]
#1	7.460	7.825	5.488
#2	7.565	7.765	5.493
#3	7.559	8.152	5.673
#4	7.409	7.928	5.589

6. CONCLUSION & OUTLOOK

In this paper, a method for distributing simulations on a high performance cluster was proposed in order to generate simulation results for a set of predefined simulation parameters. Hive tasks are created for every parameter configuration that should be simulated and all tasks are then distributed among the Hive slaves. Tasks contain all the necessary information for the slaves to be able to execute the simulation in form of a payload. The payload, a ZIP archive, can be enriched as required and helper scripts can be used to e.g. set up the simulation environment and clean up after the simulation has been executed.

By conducting many simulation runs in parallel, the overall simulation time can be drastically lowered and speedups of up to 61.11 are observed. Some overhead costs caused by the polling for finished jobs and the maximum number of parallel up- and downloads can be observed. By optimizing these polling intervals and increasing the number of concurrent job transfers, we expect to observe even higher speedups. The approach should then also scale with the number of slaves that are present on the given HPC infrastructure.

In the future, more simulation models should be executed using the proposed infrastructure. The tested simulation model, including some required libraries and a database, was just about 10 MB in size. It would be interesting to distribute heavier simulations models that are hundreds of MB in size. Furthermore, measures should be taken to minimize the communication overhead due to heartbeat intervals and polling. Slaves will only fetch new tasks at certain intervals and finished jobs are only downloaded at certain intervals. Both timings could be improved to take the average simulation duration into account, thus providing better usage of available resources and minimizing idle times. Another usage of distributed simulation execution would be to find one possible high quality solution using surrogate-based optimization and then try to improve this solution using optimization algorithms. This further optimization should be done by executing simulations on the HPC and thus using the simulated results instead of the surrogate model predictions.

REFERENCES

Affenzeller M., Beham A., Vonolfen S., Pitzer E., Winkler S., Hutterer S., Kommenda M., Kofler M., Kronberger G., Wagner S., 2015. Simulation-Based Optimization with HeuristicLab: Practical Guidelines and Real-World Applications. In: Mujica Mota, M., De La Mota, I., Guimarans Serrano, D., eds. Applied Simulation and Optimization. Cham:Springer, 3–38.

Bruzzone A., Longo F., 2013. 3D simulation as training tool in container terminals: The TRAINPORTS simulator. Journal of Manufacturing Systems 32: 85–98.

Crainic T., Perboli G., Rosano M., 2018. Simulation of intermodal freight transportation systems: a taxonomy. European Journal of Operational Research 270:401–418.

Falcone A., Garro A., Anagnostou A., Taylor S., 2017. An Introduction to Developing Federations with the High Level Architecture (HLA). Proceedings of the 2017 Winter Simulation Conference, 262–291. December 3–9, Las Vegas, USA.

Fujimoto R., 2000. Parallel and Distributed Simulation Systems. New York:Wiley.

Gosavi A., 2015. Simulation-Based Optimization. Boston:Springer.

Kuhl F., Dahmann J., Weatherly R., 1999. Creating Computer Simulation Systems: An Introduction to the High Level Architecture. New Jersey:Prentice Hall.

Latcharote P., Terada K., Hori M., Imamura F., 2018. A Prototype Seismic Loss Assessment Tool Using Integrated Earthquake Simulation. International Journal of Disaster Risk Reduction [in press, corrected proof].

Law A.M., 2015. Simulation Modeling and Analysis. New York:McGraw-Hill.

Lynch P., 2008. The origins of computer weather prediction and climate modeling. Journal of Computational Physics 227:3431–3444.

Mefteh W., 2018. Simulation-Based Design: Overview about related works. Mathematics and Computers in Simulation 152:81–97.

Scheibenpflug A., Wagner S., Kronberger G., Affenzeller M., 2012. HeuristicLab Hive - An Open Source Environment for Parallel and Distributed Execution of Heuristic Optimization Algorithms. Proceedings of the APCast'12 Conference, 63–65. February 6–8, Sydney, Australia.

Taylor S., 2018. Distributed simulation: state-of-the-art and potential for operational research. European Journal of Operational Research [in press, corrected proof].

Wagner S., Kronberger G., Beham A., Kommenda M., Scheibenpflug A., Pitzer E., Vonolfen S., Kofler M., Winkler S., Dorfer V., Affenzeller M., 2014. Architecture and Design of the HeuristicLab Optimization Environment. In: Klempous, R., Nikodem, J., Jacak, W., Chaczko, Z., eds. Advanced Methods and Applications in Computational Intelligence. Heidelberg:Springer, 197-261.

AUTHORS BIOGRAPHY

JOHANNES KARDER received his master's degree in software engineering in 2014 from the University of Applied Sciences Upper Austria and is a research associate in the Heuristic and Evolutionary Algorithms Laboratory at the research center in Hagenberg. His research interests include algorithm theory and development, simulation-based optimization and optimization networks. He is a member of the HeuristicLab architects team.

ANDREAS BEHAM received his master's degree in computer science in 2007 from the Johannes Kepler University in Linz, Austria, and is a research associate in the Heuristic and Evolutionary Algorithms Laboratory at the research center in Hagenberg. His research interests include metaheuristic methods applied to combinatorial and simulation-based problems. He is a member of the HeuristicLab architects team.

STEFAN WAGNER received his PhD in technical sciences in 2009 from the Johannes Kepler University in Linz, Austria. He is a professor at the University of Applied Sciences Upper Austria, member of the Heuristic and Evolutionary Algorithms Laboratory and head developer of the HeuristicLab optimization environment.

MICHAEL AFFENZELLER has published several papers, journal articles and books dealing with theoretical and practical aspects of evolutionary computation, genetic algorithms, and metaheuristics in general. In 2001 he received his PhD in engineering sciences and in 2004 he received his habilitation in applied systems engineering, both from the Johannes Kepler University in Linz, Austria. He is a professor at University of Applied Sciences Upper Austria and head of the Heuristic and Evolutionary Algorithms Laboratory.

COMPARING MACHINE LEARNING METHODS
ON CONCEPT DRIFT DETECTION FOR PREDICTIVE MAINTENANCE

Jan Zenisek[a], Josef Wolfartsberger[b], Christoph Sievi[c], Michael Affenzeller[d]

[a],[b],[c],[d] University of Applied Sciences Upper Austria, Hagenberg
[a],[d] Institute for Formal Models and Verification, Johannes Kepler University Linz, Austria

[a]jan.zenisek@fh-hagenberg.at, [b]josef.wolfartsberger@fh-steyr.at,
[c]christoph.sievi@fh-wels.at, [d]michael.affenzeller@fh-hagenberg.at

ABSTRACT

In this work we present a comparison of various machine learning algorithms with the objective of detecting concept drifts in data streams characteristical for condition monitoring of industrial production plants. Although there is a fair number of contributions employing machine learning algorithms in related fields such as traditional time series forecasting or concept drift learning, data sets with sensor streams from a production plant are rarely covered. This work aims at shedding some light on the matter of how efficient the depicted algorithms perform on concept drift detection to pave the way for Predictive Maintenance (PdM) and which intermediate data processing steps therefore might be beneficial.

Keywords: machine learning, predictive maintenance, concept drift detection, time series regression

1. INTRODUCTION

The motivation for this study originates from the trending concept of Predictive Maintenance (PdM), one of the key topics in the ongoing Industry 4.0 movement (Lee et al. 2014). In contrast to corrective maintenance and the established fixed-interval based preventive maintenance, PdM takes it one step forward and aims at preventing breakdowns of production plants by taking a plant's current and previous condition into account. The implementation of Predictive Maintenance requires collecting operational data and hence, to attach sensor equipment to the plant in order to keep track of its condition over the time. Downstream analysis and reasoning systems continuously evaluate the sensed time series in order to detect factual need for maintenance and subsequently determine a proper time slot to trigger correcting actions. Besides reducing the chance for total outages, such a real-time acting strategy also prevents unnecessary overhauls, which leads to improved predictability and higher productivity.

For the data analysis part frequently machine learning models such as Random Forests, Linear Regression, Bayesian Networks (Mattes et al. 2012), Markov-Models (Cartella et al. 2015), or Support Vector Machines (Widodo and Yang 2007) are applied. Regarding the underlying problem of time series forecasting Ahmed et al. 2010 provides a comparison of eight standard models on several macroscopic, economic data series. In recent work of Graff et al. 2017 also the forecasting capabilities of Genetic Programming are compared to Auto Regressive Moving Average (ARMA) models. Krawczyk et al. 2017 surveys the characteristics of non-stationary data streams before discussing several ensemble learning approaches for classification and regression tasks. Also Winkler et al. 2015 investigates data streams with changing behaviour and adapts a Genetic Programming based learning technique to detect such drifts during the model training phase.

This study differs from the stated literature in a way that it aims to combine several of the mentioned aspects by asking the specific question how efficient different machine learning techniques are at detecting changing behaviour in sensor time series. Since one can assume that the detection of such unexpected drifts might give a good indicator for necessary checks on the real plant, i.e. the time series streaming source, this methodological comparison aims to be a valuable contribution to the currently intensively investigated topic of Predictive Maintenance.

In Section 2 of this work we present synthetically generated data sets, which have been created following a reverse modelling approach in order to obtain realistic sensor time series. This includes a method to introduce concept drifts representing characteristic deterioration of plant conditions. Further on, Section 3 outlines a general strategy for data preprocessing, training of various machine learning regression models and their online evaluation on the generated time series in order to compare their competitiveness regarding drift detection. The potential of each algorithm for the specified task is analysed based on experiments in Section 4. Herein, results of the conducted tests are illustrated and the actual comparison is performed. Conclusively, Section 5 provides a brief summary of the presented content and some ideas for successive work, which might enhance this study regarding both the presented methods and application scenarios.

2. EXPERIMENT SETUP

Generating reasonable time series for industrial condition monitoring is a non-trivial task because there is generally only little high quality real-world data available to orient to and even less which was authorized for publication. However, such synthetic data sets are necessary for algorithm development, since they guarantee reproducibility and controllability, which was our motivation for proposing following synthesizing method.

2.1. Reverse Data Modelling
In most of the real-world sensor data sets, which we received from our partners in production industry, we observed some sort of cyclic behaviour (e.g. production of one unit), stationarity (e.g. regulated climatic conditions), seasonal effects (e.g. light conditions), trend (e.g. wear and tear) and noise (i.e. measurement deviation), all of which and many more aspects to consider when generating synthetic streams. Based on these observations, we developed a methodology to reproduce realistic uni- and multivariate time series and implemented it in form of a publicly available software application (https://github.com/smartfactorylab/dsg). Further details concerning the functionality of the application can be found in Zenisek et al. 2018. The goal of this approach is to enable the reuse of mathematical models – e.g. results from applying the Box-Jenkins method (Box and Jenkins 1970) or computing Fourier series by harmonic analysis (Stein 1993) on real-world time series – in order to produce new synthetic time series with the characteristics of the original data. In the following, the modelling approach is briefly summarized on the basis of an example.

Within the scope of this work we consider a sinusoid formula (1) as representation of a production plant's periodic behaviour, similar to what we obtained from a real-world data set.

$$cy_t = 10 + 2 * \left(\sin\left(\frac{t}{5}\right) + \frac{\sin\left(\frac{t}{2.5}\right)}{2} + \frac{\sin(t)}{7} \right) \qquad (1)$$

In (1) t refers to an integer counter variable which starts at *1* and increases by *1* for each generated value. Starting from this basic signal, arbitrary time series may be derived in order to receive more or less correlated features. However, in the context of this work we initially consider a univariate problem and hence, derive only one series. The subsequent definition (2) of an exemplary autoregressive moving-average (ARMA, cf. Box and Jenkins 1970) model represents a sensor attached to the previously conceptualized plant and therefore, depends on the defined cycle to some extent.

$$s_t = c + \varepsilon + P + Q + C \qquad (2)$$

with $c = 5.0$, $\varepsilon \sim N(0, 0.2)$, $P = [0.35, 0.2, 0.1]$,
$Q = [0.2, 0.15]$, $C = [0.75, 0.35, 0.1]$

Equation (2) illustrates the definition of an ARMA model with a constant value c, a normal distributed error term ε and the weighting vectors P for the autoregressive and Q for the moving-average part, which determine the impact of past values and error terms. In line with this, we add the cyclic series' (1) last *3* values with the respecting weights in vector C to the model. Moreover, we introduce two additional time series, both same configured as the series in Equation (2), but with an increased error term, simulating higher noise levels: $\varepsilon \sim N(0, 0.35)$ and $\varepsilon \sim N(0, 0.5)$. Short sample segments for all three versions of the cycle derived series (cf. *s0.2, s0.35, s0.5*) are depicted in Figure 1, together with the cyclic series *cy* itself.
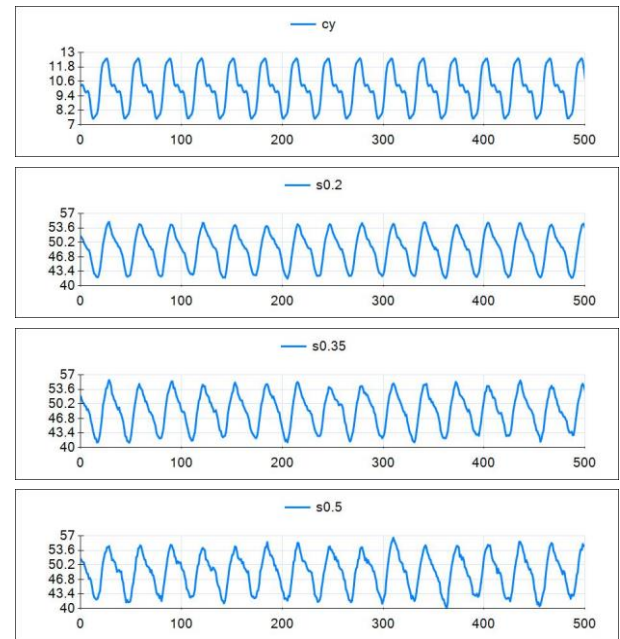
Figure 1: Basic plant cycle *cy* and the derived ARMA series *s0.2*, *s0.35* and *s0.5*

The described procedure is related to the approach of modelling ARMA models with exogenous parts (cf. ARMAX, Bauer 2009). However, instead of fitting a model to existing time series, we reverse the process and use synthetic or previously built models to produce new, reasonable series. The shown models are inspired by those that we modelled based on a real-world sensor signal. Due to the dependencies of a time series' current value to its own predecessors and values from exogenous series, it might take several sample generations to reach a stationary level. Therefore, we perform a burn-in phase and pre-generate values, which are not exported to the subsequently considered data stream.

2.2. Introducing Concept Drifts
In the context of PdM, a concept drift means an unwanted change regarding the behaviour of a monitored plant, caused by expectable gradual deterioration and hard-to-predict abrupt fractures. Despite this, usual definitions also refer to change of seasonality, which e.g. might affect climate related time series, as concept change

(Tsymbal 2004). In this work, wear and tear are conceived as long-term trend in recorded data, while damage caused by rather abrupt fatigue failure might be indicated by a short-term trend. Concerning the degradation course, most commonly models with exponential or logistic behaviour have been found to suit well for describing the so-called *run-to-failure*. While Ryll and Freund (2010) illustrate a macroscopic model with a sigmoid form for describing increasing wear, Saxena et al. surveys several mathematical models with exponential characteristics for damage propagation. However, also more linear progression might fit for some cases, as for instance considering friction linings, which degrade in a constant fashion when stressed.

Based on these considerations, we developed two functions representing one gradual (3) and one more abrupt (4) increase of wear.

$$d1_t = \frac{\tanh\left(\frac{t-150}{50} - 3.5\right)}{2} + 0.5 \qquad (3)$$

$$d2_t = \frac{\tanh\left(\frac{t-150}{20} - 3.5\right)}{2} + 0.5 \qquad (4)$$

Both functions are dependent to the same counter variable t as the functions cy and s, and generate values from 0 to 1 with logistic behaviour (cf. Figure 2). However, the first 150 values of series $d1$ and $d2$ are set to 0.0 in order to indicate normal behaviour in the beginning and the functions are only used to produce values after $t=150$.
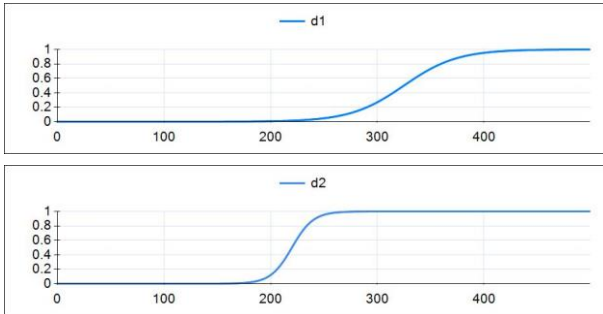
Figure 2: Deterioration signals *d1* and *d2*

In order to simulate the growing effect of deterioration in the data stream, we modified the presented basic plant cycle signal (1).

In Equation (5) we adapted the second and third sinusoid term of the plant cycle by including the current value of the deterioration series *d1*. By this means the impact of the second term is slowly reduced, while the impact of the third term increases.

$$cy_t = 10 + 2 * \left(\sin\left(\frac{t}{5}\right) + \frac{\sin\left(\frac{t}{2.5}\right)}{2 + d1_t * 0.5} + \frac{\sin(t)}{7 - d1_t * 5} \right) \qquad (5)$$

As illustrated in Figure 3, the resulting signals' progression appeal noisier than their pristine ancestors (cf. Figure 1). While the drift is visually still clearly

recognizable for signal *s0.2 (d1)*, it is almost swallowed by the larger noise in *s0.5(d1)*.
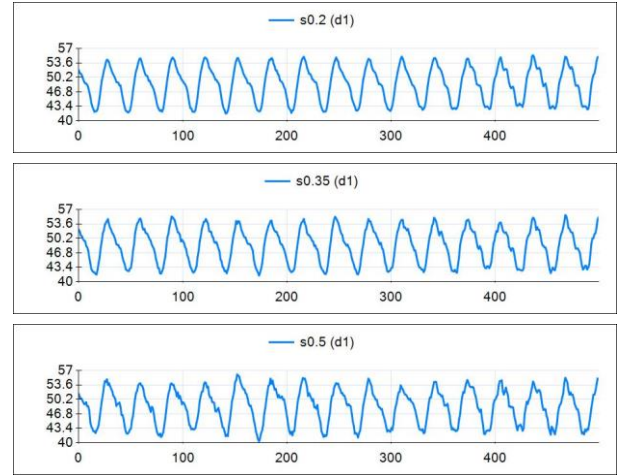
Figure 3: Gradually drifting cycle-derived series

The more abruptly increasing deterioration signal *d2* modifies the cycle by introducing an additional sinusoid term as depicted in Equation (6).

$$cy_t = 10 + 2 * \left(\sin\left(\frac{t}{5}\right) + \frac{\sin\left(\frac{t}{2.5}\right)}{2} + \frac{\sin(t)}{7} - d2_t * \frac{\sin\left(\frac{i}{3.5}\right)}{5} \right) \qquad (6)$$

The introduction of this new harmonic is motivated by the consideration of real-world failures which might bring a system "out of beat" rapidly, e.g. due to a deposition.
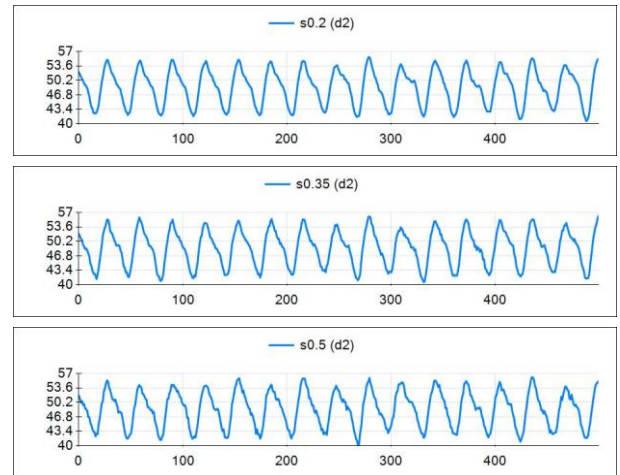
Figure 4: Abruptly drifting cycle-derived series

A similar approach to change a synthetic system's behaviour over time has been used by Winkler et al. 2015 for linear concept drifts. However, the various characteristics of the drifting series presented in this work (gradual/abrupt, noise level, type of change) provide a more realistic testbed for the subsequently described methods.

3. METHOD

The goal of the subsequently proposed strategy, regardless of the employed machine learning algorithm, is to model the state of a plant in which it is allegedly working "normal" even under varying ambient terms. Eventually, the strategy enables to alert if this concept (cf. "normal") starts to drift towards an "erroneous" or "unknown" state. There are basically two approaches for detecting drifting behaviour in time series.

- Classifying time series either as "normal" or "erroneous" based on models such as decision trees or instance-based comparison algorithms.
- Forecasting values of a series in an *n-step-ahead* fashion with regression algorithms and comparing predicted values with actually sensed ones; Herein, an increasing prediction error indicates a drifting concept.

Training these models, or respectively, building proper instance pools, requires data sets with correctly classified sample series. In this work we focus on the second approach, since we see more potential in reasoning on the base of the real-valued prediction error. The predictions are initially performed in a *1-step-ahead* fashion, meaning that the prediction error is calculated as difference between the algorithm forecast and the next value in the original series, which has not yet been available to the algorithm. However, we also consider *n-step-ahead* forecasting with varying *n* in a smaller experiment sequence in Section 4.3. The employed algorithms are trained on data streams without drifting concept and tested against streams with one. In Figure 5 the overall methodological approach of this comparison is illustrated. The subsequent Sections elaborate on the depicted system components.

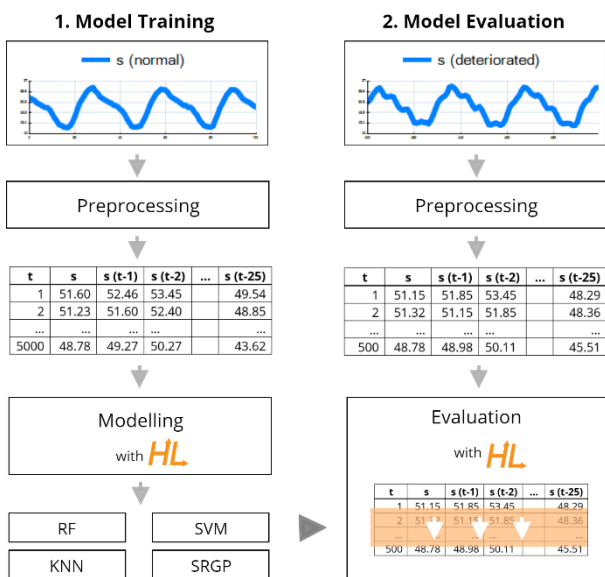
Figure 5: From model training to evaluation

3.1. Preprocessing

The success of machine learning algorithms heavily depends on the quality and form of the available data. Since solely synthetic data is used for this comparison, usually necessary tasks like handling missing values, outliers or time-related irregularities are no issue. Nevertheless, especially when dealing with time series, most algorithms such as those we employed for this study require transforming the data in some way beforehand, or otherwise they will not be able to build prediction models at all.

Among the most frequently applied preprocessing techniques on time series is their decomposition into parts for season, cycle, trend and noise, e.g. by using local regression based *STL* (Cleveland et al. 1990). Such transformations are well studied on economic data, however, require exact parametrization e.g. regarding seasonality – the periodic plant cycle in the context of this study – and therefore, further intermediate steps and tests. Instead, this work aims for comparing the algorithms' capabilities of modelling exactly such characteristics without preliminary investigation. In case they are not capable to do so automatically, it might be interesting if these algorithms can compensate by using other data transformations. Furthermore, any decomposition causes additional time-consumption, since more series emerge. This might hamper the already time-sensitive online condition monitoring situation, where new data arrives at least every second. Nevertheless, we plan to investigate opportunities with decomposition techniques in future work.

Similar to the strategy Ahmed et al. (2010) proposed for the related purpose of plain time series forecasting, we focus on the applicability of using time lagged values and performing series differencing as preprocessing, but for concept drift detection. Herein, time lagged values are extracted by simply transposing the historically seen last *n* values in a series to a new feature vector, which is subsequently provided to the machine learning algorithm. In analogy, a similar lagged-value vector may be built by computing the differences between the last *n+1* values. Accordingly, machine learning models built with a differentiated input vector forecast the next gradient instead of the upcoming real value. For this preprocessing step we performed the *5-point-stencil* (cf. Equation (7)), which is a more sophisticated and robust variant for numerical differentiation. The stencil is used to approximate the first derivative for the function of the real-valued series *s* at the time *t* by using four neighbouring points of *t* in *s*.

$$s_t' = \frac{-s_{t-2} + 8*s_{t-1} - 8*s_{t+1} + s_{t+2}}{12} \qquad (7)$$

For all the experiments we performed, the time lag maximum of unprocessed and differentiated series was set to *n=25*. Considering a series with 5000 events, this results with a matrix consisting of 5000 rows and 26 columns (i.e. $s, s_{t-1}, s_{t-2}, \ldots s_{t-25}$).

3.2. Machine Learning Algorithms

For this comparison a small set of prominent machine learning algorithms, which either train models (e.g. trees), or use training instances (e.g. by averaging samples) to perform time series regression has been compiled. For more details regarding the algorithms, the reader is referred to the stated literature.

- K-Nearest-Neighbor Regression (KNN), instance-based, Altman (1992)
- Support Vector Machine Regression (SVM), meta-instance-based, Cortes and Vapnik (1995)
- Random Forest Regression (RF), model-based, Breiman (2001)
- Symbolic Regression by Genetic Programming (SRGP), model-based, Koza (1992), Affenzeller et al. (2009)

All experiments have been performed with the open source framework HeuristicLab (Wagner et al. 2014, https://heuristiclab.com). Although the utilized algorithm implementations correspond to the state of the art, there exist many variants, strongly adapted for specific problem domains. However, this study employs basic forms in order to allow more general statements regarding the capabilities of each algorithm type and to ease reproducibility. For similar reasons, this work also does not concentrate on tuning algorithm parameters extensively.

3.3. Evaluation

The algorithms we used for this comparison are among the most popular ones for time series forecasting (cf. Ahmed et al. 2010, Affenzeller et al. 2009) and learning under the influence of concept drifts (cf. Krawczyk et al. 2017, Winkler et al. 2015). This study aims to shed light on how efficiently they can be applied on the task of the detection of concept drifts. To a large extent, this depends on how these algorithms are evaluated on a constantly updated data stream.

As mentioned at the beginning of this section, we monitor the relation between the model forecasts and the factual values. If the prediction error increases for a certain period, models do not fit the current data anymore, which might indicate a concept drift. For a fair comparison, this obviously requires that all models were capable of performing forecasts with high accuracy in the first place, i.e. on training data which is qualified as normal behaviour. In order to mitigate being prone to outliers or short-term anomalies and to make the general trend more visible, we use a sliding window evaluation schema. This way, the last m forecasts are compared to the actually sensed values and the Pearson Correlation Coefficient PR^2 is computed and averaged. For all experiments we performed, the window size was set to $m=25$ and the window movement step size to 1.

Depending on the accuracy results achieved on the training data, a properly set lower-bound threshold might be reasonable to determine the "point of failure" in case of the threshold's transgression. The algorithm comparison could be performed by measuring the timestamp for this transgression regarding each model and the factual start of deterioration in series d. Another way to accomplish the algorithm detection capability comparison we aim for is to check against the entire actual drift function, which is available in such a synthetic scenario. Therefore, we compute the correlation of the prediction quality progress and the deterioration series d. By this means, high negative correlation values indicate good algorithm performance in the presence of a drifting time series.

4. EXPERIMENTS AND RESULTS

In the following section the conducted experiments are documented and the collected results are discussed.

4.1. Model Training

For the determination of reasonable algorithm settings we performed a parameter grid search by creating experiments using HeuristicLab. The scope of this search orients on comparisons in the work of Ahmed et al. 2010 and Winkler et al. 2015 and is listed in Table 1.

Table 1: Settings of the parameter grid search

KNN	K: 2 … 100
SVM	γ: 0.5, 0.75, 1, 1.25, 1.5; ϵ: 0.05, 0.1, 0.25, 0.5, 1, 2, 4; C: 1, Degree: 3; Nu: 0.5; RBF Kernel
RF	Trees: 100, 250, 500, 1000; R: 0.2, 0.3 … 0.8, M: 0.4, 0.5 … 0.8
SRGP	Tree Length/Depth: 25, 35, 50/50; Symbols: +, -, *, /, sin, cos, exp, log; PopSize: 100; Generations: 1000; MutRate: 15%; CrossRate: 100%; Proportional Selector; Offspring Selection; SelPressure: 100

Each individual configuration has been tested by performing 10 repetitions, with exception of the KNN algorithm, as it does not base on any kind of stochasticity. The search has been performed on each of the produced non-deteriorated data sets (cf. *s0.2*, *s0.35* and *s0.5*) independently and the most accurate models have been picked for the subsequent evaluation. Genetic Programming tends to be more prone to stochastic effects due to its evolutionary process for model creation. Hence, we also provide the average model accuracy of GP's top 10 models (cf. øSRGP) which is a common practice and known as ensemble modelling.

The forecasting accuracies of the best models on data sets processed by building time lagged value vectors are listed in Table 2. Although, there is a slight decrease of accuracy aligned to the level of noise in the used data set, all of the algorithms accomplished creating very accurate models.

Table 2: Algorithm forecasting accuracy as PR^2 on data sets with time lagged input vector

PR^2	KNN	SVM	RF	SRGP	øSRGP
s0.2	0.9961	**0.9972**	0.9970	0.9963	0.9954
s0.35	0.9891	**0.9918**	0.9917	0.9907	0.9889
s0.5	0.9740	0.9809	0.9809	**0.9810**	0.9793

In Table 3 the accuracies for models trained on the differentiated series are presented. The decrease of accuracy linked to noise is herein significantly higher, however, still good models could have been developed.

Table 3: Algorithm forecasting accuracy as PR^2 on data sets with differentiated time lagged input vector

PR^2	KNN	SVM	RF	SRGP	øSRGP
s0.2	0.9711	**0.9746**	0.9711	0.9649	0.9546
s0.35	0.9186	**0.9287**	0.9200	0.9054	0.8837
s0.5	0.8455	**0.8622**	0.8481	0.8239	0.8050

Overall, the SVM algorithm created the most accurate models, although, the performance of the others is on the same level, since the quality difference is only marginal in terms of real numbers. All of the listed values originate from the evaluation of solely the test partitions (34 %) of the compiled 5000-event long data series with no concept drift present.

4.2. Simulation-Based Evaluation

In order to perform the described evaluation process, we implemented a simulation environment on the base of HeuristicLab, which is now publicly available. Within a run of this simulation, a prepared data set is replayed value by value such that the preliminary trained models are evaluated on a continuously progressing stream, as they would be in a real online scenario. In this course, the previously mentioned evaluation criterion as well as several plots and statistics for further investigation are constantly updated (cf. Figure 6, 7, 8). The reader is referred to Figure 5, where the overall process from model training to stream-wise evaluation is depicted.

We tested the algorithms on a drifting stream (cf. Equations (5) and (6)) with 500 events. Further on, we computed the correlation of prediction quality and deterioration (cf. *PR*) as proposed in Section 3.3. Again, all of the tested algorithms obtained good results, which means that they are all capable of detecting the introduced drift – their prediction quality negatively correlates with the course of the drift. Figure 6 visually supports this inference, since the decay of prediction quality can be clearly observed.

Table 4 lists the correlation values of the decreasing model accuracy and the increasing drift on data sets with different noise level (cf. *s0.2*, *s0.35* and *s0.5*), preprocessed by building lagged value vectors and most importantly, including two kinds of concept drifts (cf. *d1* and *d2*). Table 5 solely differs in the preprocessing method applied on the data set. The results in both tables show that overall, each of the employed algorithms is capable of achieving sufficiently high prediction accuracy in most of the data sets.

Table 4: Algorithm concept drift detection performance on data sets with time lagged input vector

PR	KNN	SVM	RF	SRGP	øSRGP
s0.2$_{d1}$	-0.8519	**-0.8587**	-0.8066	-0.774	-0.7564
s0.35$_{d1}$	**-0.8476**	-0.8362	-0.8401	-0.7695	-0.7596
s0.5$_{d1}$	-0.7139	-0.6717	**-0.7226**	-0.2009	-0.5452
s0.2$_{d2}$	**-0.6342**	-0.554	-0.6199	-0.4835	-0.3426
s0.35$_{d2}$	**-0.5548**	-0.4964	-0.4643	-0.4402	-0.3769
s0.5$_{d2}$	**-0.4813**	-0.2998	-0.2516	-0.0485	-0.0378

In line with decreasing model training accuracy on noisy data sets, also the concept drift detection performance decays, but much faster. Furthermore, the abrupt concept drift *d2* seems to be much harder to detect than the gradual *d1*. The best detector is KNN, whereas SRGP is the worst, especially on the noisy, *d2*-influenced data sets, where a detection is almost not possible anymore. The values of Table 4 are also visually presented in Figure 6.

Table 5: Algorithm concept drift detection performance on data sets with differentiated time lagged input vector

PR	KNN	SVM	RF	SRGP	øSRGP
s0.2$_{d1}$	-0.8422	-0.8235	**-0.8458**	-0.0346	-0.6083
s0.35$_{d1}$	-0.8338	-0.8439	**-0.8478**	-0.5850	-0.6573
s0.5$_{d1}$	**-0.7077**	-0.5991	-0.6267	-0.1321	-0.2326
s0.2$_{d2}$	-0.3948	**-0.4044**	-0.4021	-0.1802	-0.0844
s0.35$_{d2}$	-0.2444	**-0.2563**	-0.2454	-0.1286	-0.1599
s0.5$_{d2}$	-0.2068	-0.2238	**-0.2395**	-0.0927	-0.1149

In Table 5 one can observe similar detection behaviour for the differentiated series. However, this time RF, SVM and KNN perform on the same level, while SRGP trails behind.
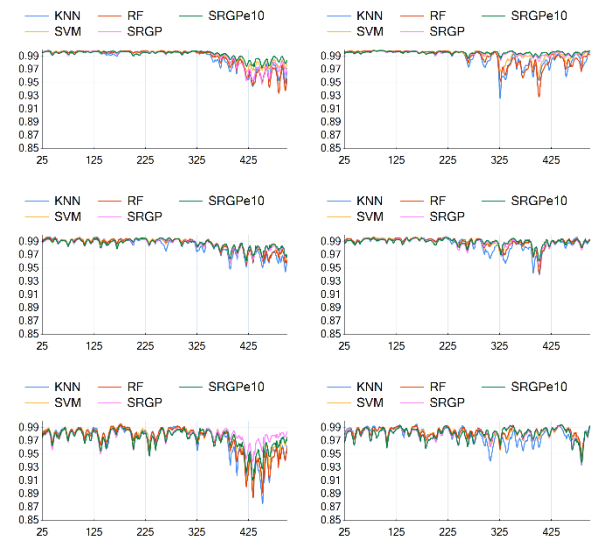
Figure 6: Progress of PR^2 received from model evaluation in a sliding window (size *m=25*) fashion; The charts visualize the results from Table 4 with *d1* left- and *d2* right-hand-side.

4.3. N-Step-Lookahead

In a smaller experiment setup we tested how the algorithms perform with a larger forecasting horizon. Therefore, we prepared the *s0.5* data set with a larger offset between the target value and the lagged input vector and trained new prediction models. The accuracy of these new models slowly decays with increasing forecasting horizon, however, still very accurate models

with all tested machine learning algorithms could be developed (cf. Tables 6 and 7). The reason for this might be the strong periodic behaviour of the trained signal and only minor influence of noise.

Table 6: Algorithm forecasting accuracy as PR^2 on data set *s0.5 (d1)* with time lagged input variables and increasing lookahead horizon (1 to 25 – see first column)

PR^2	KNN	SVM	RF	SRGP	øSRGP
1	0.9740	0.9809	0.9809	**0.9810**	0.9793
5	0.9664	**0.9676**	0.9664	0.9557	0.9454
10	**0.9641**	0.9631	0.9632	0.9557	0.9520
15	**0.9652**	0.9650	0.9639	0.9564	0.9514
20	**0.9627**	0.9623	**0.9627**	0.9541	0.9512
25	**0.9618**	0.9612	0.9621	0.9535	0.9509

Table 7: Algorithm forecasting accuracy as Average Relative Error (ARE) in percentage on data set *s0.5 (d1)* with time lagged input variables and increasing lookahead horizon (1 to 25)

ARE (%)	KNN	SVM	RF	SRGP	øSRGP
1	1.085	**0.924**	0.925	0.927	0.972
5	1.249	**1.215**	1.236	1.429	1.571
10	**1.284**	1.298	1.299	1.399	1.472
15	1.280	**1.273**	1.288	1.447	1.516
20	1.298	1.308	**1.297**	1.455	1.486
25	1.357	1.386	**1.352**	1.479	1.531

Interestingly, the detection quality decays quite fast with increasing lookahead horizon (cf. Table 8), while the trained model accuracy remained rather stable (cf. Tables 6, 7). Finding reasons for this requires successive investigation, which will be part of future work.

Table 8: Algorithm concept drift detection performance on data sets with time lagged input variables

PR	KNN	SVM	RF	SRGP	øSRGP
1	-0.711	-0.6706	**-0.7239**	-0.215	-0.5451
5	-0.702	-0.7137	**-0.7201**	-0.4311	-0.6377
10	-0.5824	**-0.596**	-0.576	-0.3171	-0.1047
15	**-0.6214**	-0.5674	-0.4734	-0.2589	-0.0742
20	-0.5998	**-0.6402**	-0.594	-0.3087	-0.1939
25	-0.5778	**-0.6201**	-0.4905	-0.1041	-0.0471

The main advantage of an increased forecasting horizon is that the point of finding concept drifts may be earlier (cf. Figure 7), which is possible according to our tests. However, this is not in the focus of this study. Future work might also deal with the trade-off between forecasting horizon and detection quality.
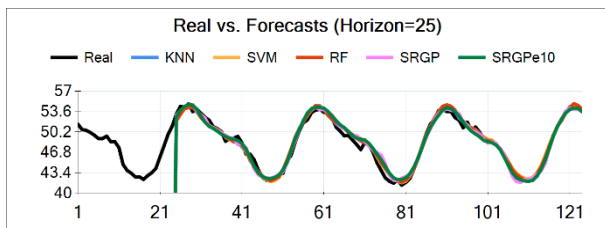

Figure 7: Real signal vs. 25-step-lookahead forecasts

4.4. Algorithm Comparison

After further investigating the simulation statistics and plots, we conclude that although all employed algorithms proved to be good detectors, their microscopic prediction behaviour differs to some extent. While KNN, SVM and RF naturally tend to produce rather "smooth" progressions, the symbolic regression model is more sensitive to changing points in the signal. In Figure 8, one can observe that the models do not change this behaviour when the concept drift is introduced. GP utilizes a symbolic vocabulary (variables, constants, trigonometric functions etc.) to build mathematical functions. With a similar vocabulary we generated the synthetic time series. Although GP supposedly has the power to capture the series' characteristics best due to this similarity, it is neither the first ranked predictor nor detector. It seems that the model adapts its prediction behaviour to the introduced drift and anticipates the drift in a lagged fashion. Since this behaviour is in fact not intended, we are looking forward to investigate how GP in particular and the other algorithms react to other training settings and differently preprocessed series in future work.
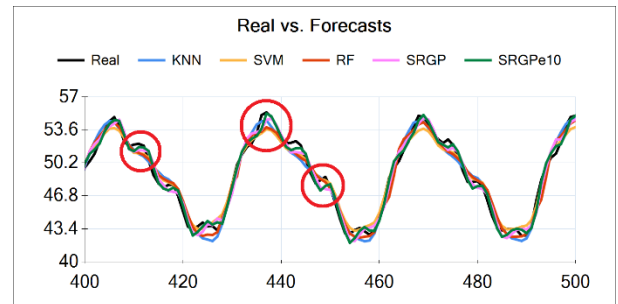
Figure 8: Real vs. forecasted values with introduced drift

In terms of runtime performance, SVM and RF are faster in training than SRGP by far. For KNN there is no training at all, since it performs distance comparisons during evaluation time. This becomes an important detail when considering the necessity for iteratively training models in online situations. Despite this, the evaluation of symbolic regression models is quite fast, since it requires solely computing a single mathematical function. In contrast, the runtime for KNN increases dramatically with additional dimensions, larger instance pool and a higher number *k* of samples to consider.

5. CONCLUSION AND OUTLOOK

In the first part of this study we presented an approach to synthesize time series with and without drifting concepts. On the basis of these data sets machine learning models have been trained and a methodology to test and compare the trained models capabilities for concept drift detection has been depicted. Subsequently, the results of the conducted experiments have been discussed. The main contribution of this work is the developed and implemented evaluation methodology in form of a simulation, which might be of value as a testbed for upcoming *what-if* scenario experiments. Furthermore,

we have shown, that all employed algorithms are able to produce models, which may serve as quite good concept drift detectors. However, their performance decays rapidly with increasing noise, the speed of the drift and the forecasting horizon.

Based on these promising results and initial algorithm assessments, we plan to perform further larger scaled and differently configured experiments in a subsequent study. In this scope we aim for additional insights regarding the strengths and weaknesses of one or another algorithm and preprocessing method on more complex problem instances. Future work might also tackle the following issues:

- Dealing with multivariate time series
- Testing against real-world data
- Enlarging the comparison regarding the utilized machine learning algorithms
- Applying decomposition techniques as additional preprocessing step
- Employing ensemble models for more robust forecasting and new evaluation possibilities
- Testing *rolling* horizon evaluation

ACKNOWLEDGMENTS

REFERENCES

Affenzeller M., Wagner S., Winkler S. and Beham A., 2009. Genetic Algorithms and Genetic Programming: Modern Concepts and Practical Applications. Chapman & Hall / CRC Press.

Ahmed N. K., Atiya A. F., Gayar N. E. and El-Shishiny H., 2010. An empirical comparison of machine learning models for time series forecasting. Econometric Reviews, 29 (5-6), 594-621.

Altman N. S., 1992. An introduction to kernel and nearest-neighbor nonparametric regression. The American Statistician, 46 (3), 175-185.

Bauer D., 2009. Estimating ARMAX systems for multivariate time series using the state approach to subspace algorithms. Journal of Multivariate Analysis, 100 (3), 397-421.

Box G. E. and Jenkins G. M., 1970. Time series analysis: forecasting and control. Holden-Day, San Francisco, CA.

Breiman L., 2001. Random forests. Machine Learning, 45 (1), 5-32.

Cartella F., Lemeire J., Dimiccoli L. and Sahli, H., 2015. Hidden semi-Markov models for predictive maintenance. Mathematical Problems in Engineering, 2015.

Cleveland R. B., Cleveland W. S. and Terpenning I., 1990. STL: A seasonal-trend decomposition procedure based on loess. Journal of Official Statistics, 6 (1), 3.

Cortes C. and Vapnik V., 1995. Support-vector networks. Machine Learning, 20 (3), 273-297.

Graff M., Escalante H. J., Ornelas-Tellez F. and Tellez E. S., 2017. Time series forecasting with genetic programming. Natural Computing, 16 (1), 165-174.

Koza J., 1992. Genetic Programming: On the Programming of Computers by Means of Natural Selection. MIT Press, Cambridge, MA, 1992.

Krawczyk B., Minku L. L., Gama J., Stefanowski J. and Woźniak, M., 2017. Ensemble learning for data stream analysis: A survey. Information Fusion, 37, 132-156.

Lee J., Kao H. A., and Yang S., 2014. Service Innovation and Smart Analytics for Industry 4.0 and Big Data Environment. Procedia Cirp, 16, 3-8.

Mattes A., Schöpka U., Schellenberger M., Scheibelhofer P. and Leditzky G., 2012. Virtual equipment for benchmarking predictive maintenance algorithms. In Simulation Conference (WSC), Proceedings of the 2012 Winter, pp. 1-12. IEEE.

Ryll F., and Freund C., 2010. Grundlagen der Instandhaltung. In Instandhaltung technischer Systeme, 23-101. Springer, Berlin, Heidelberg.

Saxena A., Goebel K., Simon D. and Eklund N., 2008. Damage Propagation Modeling for Aircraft Engine Run-To-Failure Simulation. Prognostics and Health Management, 2008. Proceedings of 2008 IEEE International Conference on PHM, 1-9.

Stein E. M., 1993. Harmonic Analysis: Real-Variable Methods, Orthogonality, and Oscillatory Integrals. Princeton University Press.

Tsymbal A., 2004. The problem of concept drift: definitions and related work. Computer Science Department, Trinity College Dublin, 106 (2).

Wagner S., Kronberger G., Beham A., Kommenda M., Scheibenpflug A., Pitzer E., ... and Affenzeller M., 2014. Architecture and Design of the HeuristicLab Optimization Environment. In Advanced Methods and Applications in Computational Intelligence, pp. 197-261. Springer, Heidelberg.

Winkler S.M., Affenzeller M., Kronberger G., Kommenda M., Burlacu B. and Wagner S., 2015. Sliding window symbolic regression for detecting changes of system dynamics. Genetic Programming Theory and Practice XII. Springer 91-107.

Widodo A., and Yang B. S., 2007. Support vector machine in machine condition monitoring and fault diagnosis. Mechanical systems and signal processing, 21 (6), 2560-2574.

Zenisek J., Wolfartsberger J., Sievi C. and Affenzeller M., 2018. Streaming Synthetic Time Series for Simulated Condition Monitoring. IFAC-PapersOnLine, 51, pp. 6.

COMPLEX NETWORKS OF THE AIR PASSENGER TRAFFIC IN CULIACAN´S AIRPORT

Olivia Sashiko Shirai Reyna[(a)], Idalia Flores de la Mota[(b)]

[(a),(b)] Posgrado en Ingeniería de Sistemas - Maestría en Investigación de Operaciones
Facultad de Ingeniería, Edificio Bernardo Quintana 3er, Piso, Departamento de Sistemas, UNAM, Cd. Universitaria, Del. Coyoacán, C.P. 04510, México C.D.M.X.

[(a)] sashikosr@outlook.com, [(b)]idalia@unam.com

ABSTRACT
Nowadays, the air passenger traffic has been increasing, becoming an excellent, viable and reachable option for many people. This causes that airports may require an efficient organization to serve both, the companies that use the facilities and the passengers. In addition, it is important to consider that the amount of information that is generated may not be easy to analyze, sometimes because the managers don´t know all the information that they have, or they don´t know how much this information can help the business or what they can do with all this data. Therefore, in this work, we perform an analysis of the information obtained from Culiacan´s airport (domestic and international passengers), using the methodology of Complex Networks and simulation to validate the forecast. Also, with the results obtained, we will seek to put forward improvements in the service of this type of facilities, and the infrastructure.

Keywords: Air passengers, complex networks; visibility; time series, forecast.

1. INTRODUCTION
Since 2000, a record of all the passengers that arrive and depart at Mexican airports from domestic and international flights have been kept and have not been analyzed because some of these data are not open data. Some of the data that may concern will be the number of airlines that operate in Mexican airports, the number of passengers, the number of routes, the number of available and occupied seats, delays on the flights and more information at domestic and international flights.

The main problem is that the strengths and weaknesses of Mexican airports as a whole system are not known or identified, causing, among other things, losses in business opportunities and system saturation. For this reason, it is important to perform an initial diagnosis. Then according to the results of this analysis we model the system. Then we built mathematical models of the real data using complex networks, in order to put forward improvements for market strategies.

In order to improve overall business strategies, it is necessary to apply statistical models and mathematical models to analyze, find patterns and predict data behavior. In this work, we will use different mathematical techniques such as network theory, complex networks, statistics, simulation and time series.

Mexico is the third country with the highest number of airports, aerodromes and flight tracks with a total of 1714, according to data published by the CIA (Central Intelligence Agency) World Factbook in 2013. So, it is important to perform a study of what is happening in Mexican airports, how the flow of passengers in these airports behaves and the problems they have. And therefore, propose alternatives to improve both, its operations and its infrastructure. For this reason, we focused the study on one of the most important airports in Mexico, the Culiacan´s airport. Culiacan is the economic and political capital of Sinaloa, with advanced infrastructure and a full range of services. The Culiacan Airport ranks as OMA's (Grupo Aeroportuario Centro Norte) second busier airport.

2. METHOLODOGY
For this study we focused on the analysis of national, international and total passengers served by the Culiacan, so, we have the monthly information of the air passenger traffic in Culiacan´s airports from January 2000 to December 2017. So, with this information the first step was to analyze the data with statistical techniques, the second step was to work with all this information as time series, we did a decomposition of the time series, we obtained the ACF (Auto Correlation Function), PACF (Partial Auto Correlation Function) and we computed the differences, so, then with the results we modelled our time series as an ARIMA (Auto Regressive Integrated Moving Average) model. Finally, with this model we were able to do some forecast of the air passenger traffic for the next two years to analyze the strengths and the weaknesses of all the system in the future.

As a third step, after the time series analysis, we used the visibility algorithm to transform the time series into a complex network. Once this network is obtained we used the methodology of complex networks, specially to analyze the topology or structure of the networks, for example, the clustering, the closeness, betweenness, assortativity, and more metrics of complex networks. Also, we can have the degree distribution of the networks and we can have a good approach of the networks behavior.

With all these results we were able to analyze and compare the national, international and total passenger networks, in addition, we could analyze the topology of these networks, which concludes what type of network model they belong to and what specific characteristics and properties they share.

For all this statistical analysis, we used the R software, which is an open source programming language and software environment for statistical computing and graphics. For this work, we used specific R software packages, such as, igraph, networks, tkrplot, sand, sna, forecast, TimeSeries, TSA and others, this software allow us to generate graphs/networks, compute different network metrics like clustering or transitivity, different centrality metrics, plot networks, create mathematical models, forecast data and more functions.

First, we used all the data that we had, so, we plot this information as a time series. The next figures show the different time series for domestic, international, and total passengers of Culiacan´s Airport (respectively).
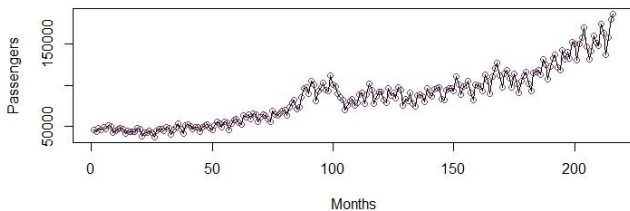
Figure 1 Time Series Domestic Passengers Culiacan´s Airport

Figure 2 Time Serie of International Passengers at Culiacan´s Airport

Figure 3 Time Serie of Total Passengers at Culiacan´s Airport

Now, once we have the plots of the time series we use a technique to transform these time series into complex networks, so the best way to do this transformation is with the visibility algorithm (Lacasa L. et al 2008).

The main goal of this algorithm is to map a time series into a complex network, so, we want to study and analyze the complex networks with all the techniques and properties of network theory, so it will be a more complete analysis not only the study of the time series with all their properties. Another important thing is that this network inherits several properties of the time series.

The criterion of this algorithm is to set up two arbitrary data values (t_a, y_a) and (t_b, y_b) that will have visibility, and consequently will become two connected nodes of the associated graph, if any other data (t_c, y_c) placed between them fulfills:

$$y_c < y_b + (y_a - y_b)\frac{t_b - t_c}{t_b - t_a}$$

(1)

So, we apply this algorithm to our time series and we obtain the next graphs.
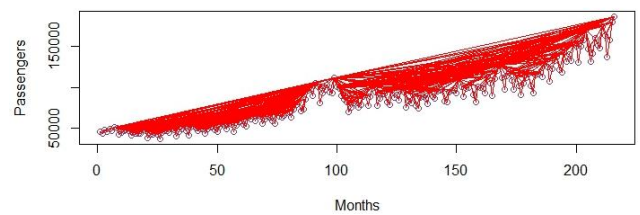
Figure 4 Visibility Domestic Passengers Culiacan´s Airport
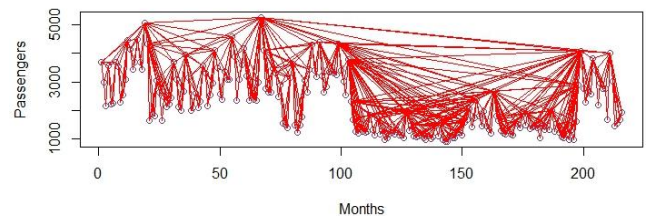
Figure 5 Visibility International Passengers Culiacan´s Airport
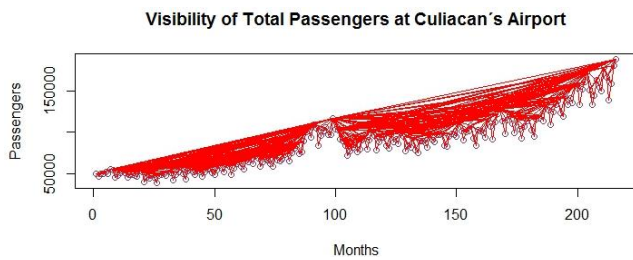
Figure 6 Visibility Total Passengers Culiacan´s Airport

We can easily check that by means of the present algorithm, the associated graph extracted from a time series is always:

- Connected: each node sees at least its nearest neighbours (left and right), the first and the last one at least sees one.

- Undirected: the way the algorithm is built up, there is no direction defined in the links.

- Invariant under affine transformations of the series data: the visibility criterion is invariant under rescaling of both horizontal and vertical axes, and under horizontal and vertical translations.

After, we applied the visibility algorithm, we can obtain the visibility graph, then we plot the time series as complex networks to compute specific network metrics to study the topology, that is what we will see in the next figures.
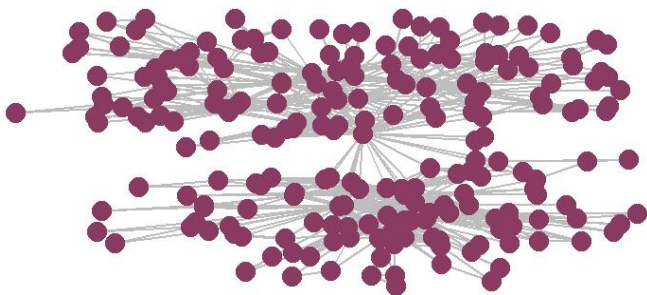
Figure 7 Complex Network Domestic Passengers Culiacan´s Airport
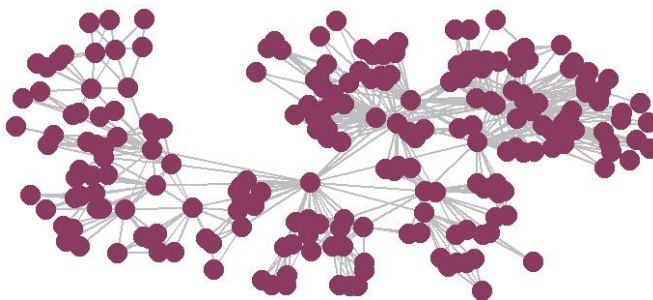
Figure 8 Complex Network International Passengers Culiacan´s Airport
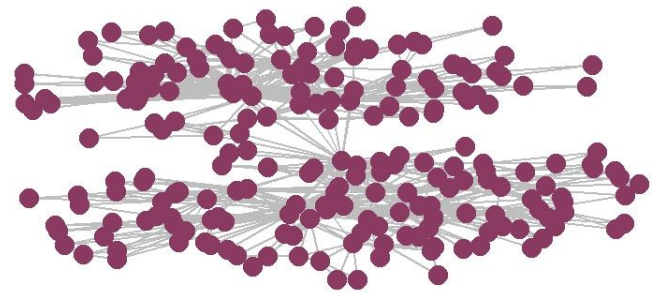
Figure 9 Complex Network Total Passengers Culiacan´s Airport

Now, with the graphs above we are going to give some important definitions. A complex network is a graph or network with non-trivial topological features, with patterns of connection between their elements that are neither purely regular nor purely random. Such features include a heavy tail in the degree distribution, a high clustering coefficient, assortativity or disassortativity among vertices, community structure, and hierarchical structure. that do not occur in simple networks such as lattices or random graphs but often occur in graphs modelling of real systems (Newman, 2010).

After we have our data as networks we can compute the different network´s metrics. We compute and compare metrics of our three networks, such as the number of edges, minimum, maximum and mean degree, diameter, mean distance, the number of cliques, the density of the network, if its assortativity or disassortativity among nodes, the global clustering of the network, the mean local clustering, closeness centrality, degree centrality and betweenness centrality. We compute these metrics to study the topology of the networks and to understand and identify different patterns and to classify the networks in the different complex networks models that we have (Random networks, Scale-free networks and Small World networks).

Table 1 Metric Results

Results	Domestic	International	Total
Nodes	216	216	216
Edges	898	782	825
Max. Degree	48	38	43
Min. Degree	2	2	3
Mean Degree	8.314815	7.240741	7.638889
Diameter	6	7	7
Mean Distance	3.406761	3.615202	3.500818
Cliques	10	8	9
Density	0.0386735	0.03367786	0.0355297
Assortativity	0.1426983	0.09158975	0.142267
Global Clustering	0.4189869	0.4224797	0.4103618
Mean Local Clustering	0.7280571	0.7698117	0.7322579
Closeness Centrality	0.4001511	0.3529065	0.3835342
Degree Centrality	0.1845823	0.1430663	0.1644703
Betweenness Centrality	0.5480585	0.549588	0.5474317

First, we need to understand the numbers that we have in the Table 1. We notice that there is a lot of difference between the minimum, maximum and the mean degree, which is because there are just few nodes with a lot of links and there are many nodes with just a few links. The diameter is similar in the three networks. The mean distance is small that means that we can go from any node from the network to another node in a few steps, in this case approximately 3 steps. The number of cliques in the network tells us the number of complete subgraphs in our network. The network density describes the portion of potential connections in a network that are actual connected, so that means that our networks don´t have a lot of actual connections.

To continue with our analysis, our three networks are assortative so that means that there is a preference for a network´s nodes to attach to others that are similar in some way, so assortativity is often operationalized as a correlation between nodes. The global clustering coefficient is based on triplets of nodes and the local clustering coefficient of a node in a network quantifies how close its neighbors are to be a clique (Bollobás, 1998). In our networks, the global clustering and the mean local clustering are not so high approximately 0.4 but we have a high mean local clustering in the cases of the for international and total passengers.

We also computed the centrality metrics, the closeness centrality of a node is a measure of centrality in a network, calculated as the sum of the length of the shortest paths between the node and all other nodes in the network. Thus, the more central a node is, the closer it is to all other nodes, so, in our networks the closeness centrality is not so high only for the domestic passengers we have a high closeness centrality (Caldarelli et. al. 2012). The degree centrality is defined as the number of links incident upon a node (i.e., the number of ties that a node has), in our case, the networks have a low degree centrality (Newman, 2010). The betweenness centrality is a measure of centrality in a network based on shortest paths. For every pair of vertices in a connected network, there exists at least one shortest path between the vertices such that either the number of edges that the path passes through so, the betweenness centrality for each node is the number of these shortest paths that pass through the node; in our networks, we have betweenness centrality among .54 that is not to low but not so high (Caldarelli et. al. 2012).
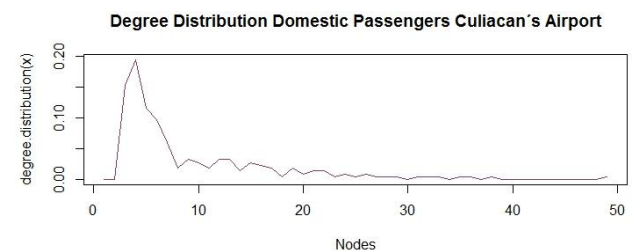
Figure 10 Degree Distribution Domestic Passengers Culiacan´s Airport
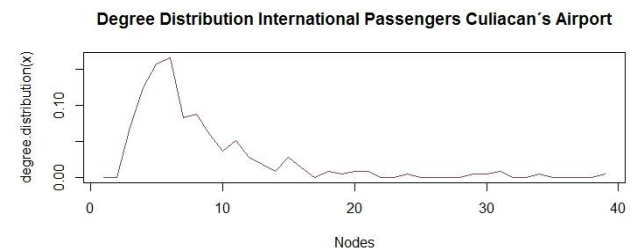
Figure 11 Degree Distribution International Passengers Culiacan´s Airport
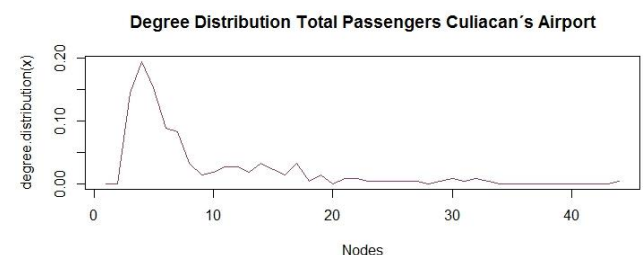
Figure 12 Degree Distribution Total Passengers Culiacan´s Airport

With the degree distribution graphs above we notice that it seems that our networks have a power law distribution. Maybe, it is not so clear but there are a few nodes with a high degree and it decays fast, so, there are a lot of nodes with a low degree.

As part of the statistical analysis, we create mathematical models (ARIMA – Auto Regressive Integrated Moving Average models) to forecast the time series so we can

have an idea of how is going to be the pattern of growth, the tendency and cycle of our passengers in the next 24 months, also we have a confidence interval of 80% and 95%.
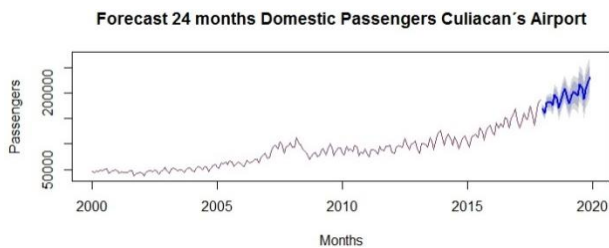
Figure 13 Forecast 24 Months Domestic Passengers Culiacan´s Airport
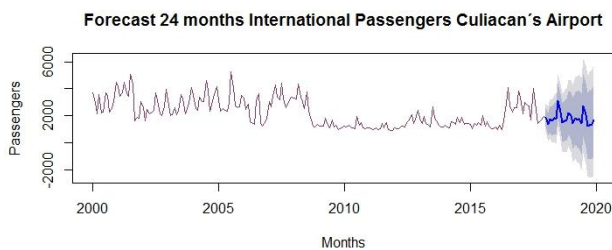
Figure 14 Forecast 24 Months International Passengers Culiacan´s Airport
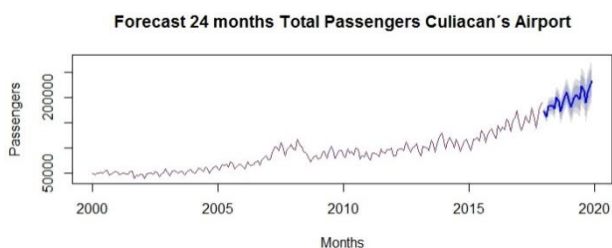
Figure 15 Forecast 24 Months Total Passengers Culiacan´s Airport

During the last eight years, the airport has had an average annual growth of 9.5% in passengers. To provide an efficient service, this airport has a new terminal building, more spacious, comfortable and modern. In 2012, the expansion and modernization of the main building began.

Since February 2012, the airport began the work of extending the terminal building. The work consists of improving the functioning, airport functionality and passenger comfort, with an extension of 3,000 m², which includes: a new lobby and the growth of the external consultation, the remodeling of 2,500 m² for passengers, the reconfiguration of the documentation point in the upper level with 3 simultaneous registration lines, the construction of a vertical circulation core in the front face that includes a panoramic lift, the growth of the waiting area, the redesign of the commercial area and a projection of an image of modernity in its front and inside it.

3. CONCLUSIONS
With all these results, we can conclude that our networks follow a scale-free model. The most notable

characteristic in a scale-free network is the relative commonness of nodes with a degree that greatly exceeds the average. The scale-free property strongly correlates with the network's robustness to failure. It turns out that the major hubs are closely followed by smaller ones. This implies that the low-degree nodes belong to very dense sub-networks and those sub-networks are connected to each other through hubs (Barabási et. al. 2003). For the time series and forecast analysis, we have a growth in the passengers but it´s supposed that the tendency and cycle will be the same as the have seen in the last years the only thing is that we need to have an action plan when there´s a high number of passengers because of the capacity of the airport.

REFERENCES
Barabási A.-L., Albert R., 1999. Emergence of scaling in random networks. Science 286 (5439): 509-512.

Barabási A.-L., Bonabeau E., 2003. Scale-Free Networks. Scientific American. 50-59.

Boccaletti S., Latora V., Moreno Y., Chavez., Hwang D.-U., 2006. Complex networks: Structure and dynamics. Physics Reports. 424. 175-308.

Bollobás B., 1998. Modern Graph Theory. Springer.

Buchanan M., 2002. Nexus: Small Worlds and the Groundbreaking Science of Networks. New York, N.Y.: W.W. Norton.

Caldarelli G., Catanzaro M., 2012. Networks: A Very Short Introduction. Oxford University Press, Oxford.

Caldarelli G., Vespignani A.,2007. Large Scale Structure and Dynamics of Complex Networks: From Information Technology to Finance and Natural Science. World Scientific Publishing Co., Inc., USA.

Dalgaard P., 2008. Introductory Statistics with R. Springer.

Dorogovtsev S.N., 2010. Lectures on Complex Networks. Oxford University Press, Inc. New York, NY, USA.

Kolaczyk E.D., Csárdi G., 2014. Statistical Analysis of Network Data with R. Springer, New York, USA.

Lacasa L., Luque B., Ballesteros F., Luque J., Nuño J.C., 2008. From time series to complex networks: The visibility graph. PNAS. Vol. 5. No, 13. 4972-4975.

Lacasa, L. et al., 2015. Network structure of multivariate time series. Sci. Rep. 5, 15508; doi: 10.1038/srep15508.

Lütkepohl H., 2005. New Introduction to Multiple Time Series Analysis. Springer.

Newman M.E.J., 2010. Networks: An Introduction. Oxford University Press, Oxford.

Newman M.E.J., 2003. The Structure and Function of Complex Networks. SIAM Review 45,167-256.

Newman M.E.J., Barabási A.-L., Watts D.J., 2006. The Structure and Dynamics of Networks. Princeton University Press, Princeton, NJ, USA.

Newman M.E.J., Peixoto T.P., 2015. Generalized Communities in Networks. Physical Review Letters 115, 08870. American Physical Society.

Wei W. W. S., 2006. Time Series Analysis Univariate and Multivariate Analysis. Pearson.

Zanin M., Lacasa L., Cea M., Crístobal S., 2009. A dynamical model for the air transportation network. Proceedings 23rd European Conference on Modelling and Simulation.

Zanin M., Lillo F., 2013. Eur. Phys. J. Spec. Top. 215:5. doi:10.1140/epist/e2013-01711-9

AUTHORS BIOGRAPHY

Sashiko Shirai obtained her bachelor in Actuarial Science in the Faculty of Science of the UNAM. She is studying her Master in Operations Research in the Faculty of Engineering of the UNAM. She is an assistant professor at the Faculty of Engineering and the Faculty of Science. Her research interests lie in complex networks, statistics and operational research.

Idalia Flores received a Master with honors, being awarded with the Gabino Barreda Medal for the best average of her generation, in the Faculty of Engineering of the UNAM, where she also obtained her Ph.D. in Operations Research. Dr. Flores is a referee and a member of various Academic Committees at CONACYT as well as being a referee for journals such as Journal of Applied Research and Technology, the Center of Applied Sciences and Technological Development, UNAM and the Transactions of the Society for Modeling and Simulation International. She is a full-time professor at the Postgraduate Program at UNAM and her research interests lie in simulation and optimization of production and service systems, based on this research she has been editor of two books edited by Springer.

OPTIMIZATION OF ORDER PICKING ACTIVITIES IN A WHOLESALE FOOD COMPANY

Eleonora BOTTANI[a], Andrea PANCIROLI[b], Roberto MONTANARI[c], Andrea VOLPI[d]

[a],[b],[c],[d]Department of Engineering and Architecture, University of Parma, Viale delle Scienze 181/A

[a]eleonora.bottani@unipr.it, [b]andrea.panciroli8@gmail.com, [c]roberto.montanari@unipr.it, [d]andrea.volpi@unipr.it

ABSTRACT

This paper focuses on the optimization of the picking process in a real refrigerated warehouse of a food wholesaler operating in the UK. The warehouse layout is unusual, as the warehouse has only one cross-aisle at the front of the shelves and no cross-aisles at the end of the rack, which, instead, ends in a blind wall. Because of this layout, traditional routing policies (e.g. the S-shape or largest gap policies) are not applicable. The current policy adopted for order preparation is batch picking & sorting. By means of an *ad hoc* simulation model, developed in Microsoft Excel^TM, we reproduced the warehouse layout and tested 48 alternative picking configurations, with the aim of enhancing the performance of the current order preparation process. Because routing cannot the varied so much, the analysis carried out focuses on the allocation of product in the warehouse, the use of classes for grouping products, and on an alternative picking policy, called "area batch picking". From the results obtained through simulation, a configuration deserves particular attention for a practical application, as it allows the total picking time to be decreased by approx. 223 minutes per day.

Keywords: warehouse management; picking; simulation model; optimization.

1. INTRODUCTION

Warehouse operation and management is an essential part of manufacturing and service operations (Zhang & Lai, 2006). The efficiency and effectiveness of logistics activities is in fact largely determined by the way warehouses operate. The logistics cost relating to warehouse processes, including receiving, storage, order picking and shipping, is often high (Rouwenhorst et al., 2000). Order picking, i.e. the process of selecting a set of items, retrieving them from their storage locations and transporting them to a sorting/consolidation process for order fulfilment (Rouwenhorst et al., 2000), is generally recognized as a particularly expensive activity, because it is either very labour intensive or capital intensive (Frazelle, 2002). In the case of a manual process, it is estimated that picking operations account for more than 55% of the total cost of warehouse operations (Coyle et al., 1996; Tompkins et al., 1996; Bottani et al., 2015). This is the main reason why researchers and logistics managers consider order picking as a promising area for productivity improvement (de Koster et al., 2007).

Most of the times, the high cost of picking is due to the so called "travel time", i.e. the time spent by pickers when travelling (unproductively) in the warehouse. This quota accounts for approximately 50% of the total order picking time (Tompkins et al., 1996). Obviously, the travel time is an increasing function of the travel distance the picker should cover to retrieve the pick the items requested in a customer's order. Therefore, minimizing this distance is typically suggested by many authors as potential leverage for optimising the total picking time of warehouses (Jarvis & McDowell, 1991; Hall, 1993; Petersen, 1999; Roodbergen & de Koster, 2001a; Petersen & Aase, 2004).

Researchers (e.g. Gu et al., 2007 or de Koster et al., 2007) agree that several factors affect travel distance in an order picking system. These factors include:

1. the overall structure of the warehouse in terms of size and layout (Roodbergen & Vis, 2006; Parikh & Meller, 2010);
2. the operational strategy, e.g. order picking vs. batch picking (Van Nieuwenhuyse & de Koster, 2009; Le-Duc & de Koster, 2007; Henn, 2012; Hong et al., 2012);
3. the storage assignment policy (Petersen & Schmenner, 1999; Webster et al., 2012; Bottani et al. 2012; Jane & Laih, 2005);
4. the use of zone picking (de Koster et al. 2012; Petersen, 2002);
5. the routing policy (Petersen & Aase, 2004; Kulak et al., 2012; De Santis et al., 2018);
6. the use of narrow aisles and the consequent risk of congestions among the pickers (Pan & Wu, 2012; Chen et al., 2013, 2016; Mowrey & Parikh, 2014).

Although all the factors listed above contributes, to various extent, to the efficiency of an order picking system, it is hard to take into account all these elements simultaneously when trying to optimize the picking process. The typical approach followed in literature is to focus on a specific topic to be analysed and optimised (de Koster et al., 2007; Bottani et al., 2012, 2015), fixing the remaining factors and keeping them unchanged in the optimization.

In this paper, we propose a different approach, whose aim is to evaluate more than one design factor in the optimization of the picking process. To be more precise, the factors taken into account in this study are:

- the *storage assignment policy* of items in the warehouse, and in particular the number of classes in which the picking items should be classified in a class-based storage;
- the *storage allocation*, i.e. the way the picking items, once classified, should be distributed in the different storage locations;
- the *classification criterion* used to group the picking items in different classes; and
- the *operational strategy*, and in particular the use of batch picking & sorting vs. the use of order picking.

A simulation model was developed using Visual basic for applications (VBA) in Microsoft Excel^{TM}, as an effective tool to model the different elements listed above and allow their reproduction (singularly or in combination) in the picking process. Statistical analyses were made on the simulation outcomes to evaluate whether the effect of the design factors was statistically significant. The whole analysis was carried out in a real context, referring to the warehouse of a food retailer located in the UK, and is therefore proposed in the form of a case study.

The reminder of the paper is organized as follows. The next section provides a brief overview of those studies that have taken into account more than one design factor in the optimization of the picking process, to highlight the newness of this study compared to the published literature. Section 3 describes the case study carried out in this paper. Section 4 discusses the main findings of this study and highlights the relating practical implications. Section 5 concludes by summarizing the contribution of this work and suggesting future research directions.

2. LITERATURE ANALYSIS

Routing policies for pickers in manual warehouses range from simple heuristics to optimal procedures. Optimal routing policies typically approach the routing problem as a travelling salesman problem (TSP) and try to find the exact solution to this problem. Such policies obviously result in shorter travel times, but can be effectively applied only if routes in the warehouse can be defined with full flexibility. Minimizing the travel distance has a direct impact on the warehouse performance in terms of cost and delivery lead-time, and consequently affects the performance of the whole supply chain. The faster items are picked from the warehouse, the less time is spent on order fulfilment; the lead-time required for delivering the product to the final customer thus decreases correspondingly. As detailed in the introduction, the main factors that affect the efficiency of the picking process are the overall structure of the warehouse, the use of order picking vs. batch picking, the storage assignment policy and the use of zone picking.

Parikh & Meller (2010) developed an analytical model to estimate the throughput of a manual warehouse based on probability models and order statistics results assuming random storage. The model is intended for person-onboard order picking systems. The authors illustrate the use of their travel-time model by incorporating it into a simple, cost-based optimization model to recommend the height of a one-pallet-deep storage system. They analysed several operational aspects of the warehouse, where a key one is determining the optimal storage system configuration (the number, length, and height of the storage aisles). As per the routing, however, since the warehouse configuration is already determined in the case under examination, physical changes to the warehouse structure are not allowed and only operational factors can be improved.

Order picking is the process of selecting a set of items, retrieving them from their storage locations and transporting them to a sorting/consolidation process for order fulfilment and shipment, in response to a customer's request (Rouwenhorst et al., 2000). On the contrary, batch picking generates a unique picking list, (and thus only one picking task) by consolidating the product/quantities of more orders. As a consequence, after picking, a further process (i.e. sorting) is required to split again the products in accordance with the customer's orders. Batch picking is usually more efficient than order picking, but it needs a sorting activity, while order picking takes more time but doesn't require further processes.

In this work, taking inspiration from the case study described in section 3, we evaluated a different picking policy (called area batch picking) as an alternative to batch picking & sorting. When varying the picking policy, the critical point is to simultaneously reduce the cost and increase the speed of the order picking activity, as studied by Petersen & Schmenner (1999). These authors evaluated various routing heuristics and an optimal routing in a volume-based and random storage environment and compared the performance of volume-based storage to that of random storage. The experimental results show that the solution gap between routing heuristics and optimal routing is highly dependent on the travel speed and picking rate, the storage policy, and the size of the picking list.

The study by Petersen & Schmenner (1999) is an example of existing literature that evaluates the impact of a combination of two or three factors on order picking performance. Typically, the approach followed by the researchers is to explore one factor at a time, to that relationships with more factors remain completely unexplored. The results available in literature therefore do not allow managers to fully determine the relative importance of different factors on picking performance (Petersen & Aase, 2004).

3. THE CASE STUDY (AP)

3.1. Company overview

The company under examination is a food retailer operating in the United Kingdom. The product portfolio consists mainly of sweet frozen products such as cakes, desserts and snacks. Distribution logistics exploits three different channels: (i) National Accounts, including batches of products sold to large catering chains; (ii) Wholesalers, for products on which it has exclusive rights on other distributors in the United Kingdom; and (iii) Direct Distribution, encompassing small product quantities delivered to individual direct resellers in the London area. The typical customer is a food business that buys from the company any time it runs out of stock (or is about to). Channel (iii), i.e. the Direct Distribution, is the focus of this study. In fact, Direct Distribution requires an intense logistics flow to provide its customers with a large product catalogue and volumes and serve them in short delivery lead times, ensuring that the product is shipped and received by the day following the order. In better serve the them, customers have been divided into four geographical areas of London, each of which served by one or more dedicated transport means. The company has three separated warehouses where the product is stored at different temperature; among them the main one consists of 851 pallet locations at -35° C.

3.2. The AS IS picking process

To ensure on time delivery of goods to customers of Direct Distribution, the company defined the following order fulfilment process: 1. The order cut-off time is set at 19:00 for deliveries in the next day. 2. The orders received are aggregated and a single common picking list is prepared. 3. The product picking in the warehouse is carried out by two employees equipped with an electric fork lift truck and an order picker for high-level picking. 4. During the Sorting activity, products are divided according to the delivery area, thereby preparing the loads for the various means. 5. The loading activity ends early in the morning and then products are delivered to the customer during the day.

Because of the limitation in the applicable routing policies, other factors affecting the total time of picking and sorting activities have been evaluated in the study.

Focusing on the picking and sorting operations, the initial configuration of the main (frozen) warehouse is analysed. Pallet locations of this warehouse are divided into three categories, i.e.: Picking locations – used for picking activities; Bulk locations – for storage and replenishment of picking locations; and General storage locations – for other departments of the company delivering high quantities to big customers.

Picking locations are obviously the most easily accessible storage locations, but as a matter of facts there is not a rigorous policy for product allocation; in fact, location is determined empirically by the warehouse manager. This random storage policy for storage and picking locations leads to a uniform distribution of the products in the warehouse, which does not take into account the characteristics of the product to be picked.

On the basis of this consideration, the company was interested in analysing the current processes to identify alternative configurations that would optimize the order fulfilment process in terms of total time. In particular, the company asked to evaluate whether a different approach to the product picking, with the use of areas (the so-called area batch picking) would be more suitable compared to the current picking policy (i.e. batch picking & sorting). Area batch picking would avoid the downstream sorting activity, since the products would already be sorted according to the delivery area when they leave the warehouse.

Splitting the products ordered in more picking lists may bring important inefficiencies to the activities; in fact, this would cause some picking locations being visited several times during the day, leading thus an inhomogeneous picking activity in the storage area. These inefficiencies may cause, for the same orders, an increase in the total picking time compared to the order picking scenario; it is thus paramount to quantify this inefficiency in order to be able to compare it with the time saved thanks to the avoided sorting activity, which is no longer required in case of zone picking. Moreover, this analysis should be carried out taking into account the allocation policy of products in stock. In particular, the results have to be computed considering a reorganization of the allocation of products to the warehouse. In particular, the adoption of a class-based policy could be evaluated, as in this policy items would be assigned to specific classes that would occupy a dedicated space in the warehouse that would reflect the characteristics of the references that compose it.

3.3. Methodology

The objective of the study is the identification of the warehouse configuration that would optimize the picking process. A Microsoft Excel™ tool has been developed and used to compare the different scenarios resulting when including or excluding the sorting activity. The total time required for picking and sorting activities was identified as the main performance indicator for the evaluation of the different configurations.

The tool should also take into account several input variables, namely:

- picking policy (area batch picking vs. batch picking and sorting);
- number of classes of the class-based storage policy, used to divide the picking locations;
- the distribution layout of the classes in the warehouse;
- the reference index for the assignment of products to the classes.

The routing policy instead, was not included among the variables to be investigated. Indeed, the warehouse configuration under examination instead does not allow to apply so many different routing policies; in fact, the warehouse has a single corridor facing the head of the

shelves and no cross-aisles; hence, the picker is forced to follow a defined route for each picking mission, as shown in figure 1. To be more precise, the only feasible route is visiting sequentially all the locations, as shown in the same figure.
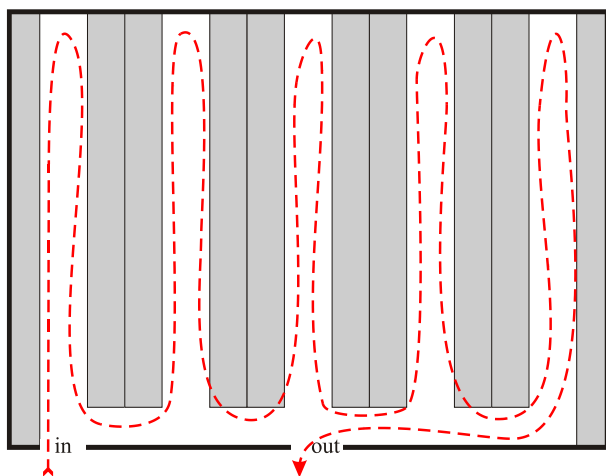

Figure 1: warehouse configuration.

For each factor analysed, we discussed with the company which were the most significant values to include in the simulation.

Concerning the number of classes in the warehouse, we may first expect an increase in performance as the number of classes increases. In fact, performance may increase as each reference is more likely assigned to a location that reflects the features of the specific class. On the other hand, however, a high number of classes causes difficulties in its management, as it decreases the flexibility of the allocation system. After some evaluations arranged with the company, the maximum number of classes was set at 5, obtaining therefore 4 values for the first factor (2, 3, 4, 5 classes).

With respect to the layout of the picking area, the first criterion used is called "within-aisle". The locations were then sorted first by the aisle number (in ascending order from 1 to 5) and, for the same aisle, by the location depth. The second criterion is the one called "cross-aisle". In this case, the locations are ordered first by absolute shelf depth and then by line numbering. In both cases the sorting is first applied on all the location on the ground floor and then on the locations at height B. The reason has to be found in the statement that picking on the ground is always more efficient, despite the location depth, than picking at higher locations.

The third parameter is the criterion used for sorting the references and assigning them to classes. Literature reports (Guerriero et al, 2013) that the most frequently used indexes are Inventory turnover index (ITI), Popularity (POP), Order Index Cube (COI), Pick Density (PD). In our case it was suggested to neglect COI and Pick Density; in fact, such criteria consider the product volume, based on the average stock, in order to make "denser" the areas with privileged picking positions. In other words, references with a high popularity rate and reduced volume are preferred, so

they occupy the minimum "privileged" space. In our case, however, this approach would not lead to improvements as all the locations are assigned to a single product, each location occupies the same volume, and each product can be assigned only one picking location.

As far as the picking policy is concerned, there were two choices to simulate: the first, currently adopted, is the batch picking policy, aggregating all the orders and creating a single picking list. The second is the area batch picking and creates as many picking lists as the areas (London area) to be visited the next day, avoiding the sorting phase.

The combinations of picking policy and three variables defines the different TO BE criterion (Figure 2).

Figure 2: Factors adopted in the simulation.

Finally, the tool should have the flexibility to be reused in the future in case of changes in the warehouse.

Taking into account these aspects, the most suitable tool for our objective is discreet events simulation. A simulation model was developed and implemented in Microsoft Excel™ in combination with the programming of macros in VBA language. Microsoft Excel™ is an excellent tool for entering data, manipulate it and finally carrying out results analysis. *Ad hoc* developed macros guarantee a good level of automation of the computational procedure and is expected to encourage the use of the tool in the future by the operators of the warehouse. Finally, the framework based on different modules gives the flexibility to be used and adapted in case of different conditions.

The model is divided into two main modules: the first one defines the allocation of references within the warehouse based on values of selected variables (Figure 3). The second deals with the simulation considering the factors defined by the locations assigned in the first module and the picking policy.

A random order generator (Figure 4) is developed on the basis of the orders history, and it allows the simulation of a specific configuration for many times. It should be noted that the historical data does not show seasonality within the year, but highlight a very different trend within the days of the week. For this reason, different orders are generated in different days of the week. At this point, an algorithm calculates the total time of the picking process on the basis of the picking list, the route followed by the operators, the type of locations and equipment used, the amount of product picked, the capacity of the collection pallet and other minor parameters.

Before running the simulations, the model was validated. A sample week was identified to this end and the total time of operations measured throughout the week. Then, the simulation model was launched using the same orders processed in the real scenario. The first results showed that the real picking time was much higher than the simulated one (about +20%). The gap was greater on weekdays with higher order quantities, which could be justified taking into account two main factors. The first one refers to the difficulty for the operator to position properly the new references on the pallet as the number of boxes increases, thus requiring more time than expected. The second one refers to volume of the same product greater than 10 boxes; under this circumstance the operator has to compact and stabilize the picked boxes once they have been placed on the pallet before moving on to the next location. These manual activities have been considered in the model by increasing the unloading time of the full pallet (for boxes consolidation) and all the picking time of products boxes greater than 10. The trend of the gap between the days of the week have stabilized but still remains around 15%. Thus, a general inefficiency factor for the exaction of operations was introduced and set to 85%. After having computed and introduced these corrective parameters, two new sample weeks were used to compare the simulated and real scenarios, returning acceptable gap values (about 1%). Thus, the picking model could be considered as validated. A similar validation procedure, although much simpler because of the lower number of factors, was followed for sorting operations.

After validation, the simulation model was launched to reproduce the 48 variable combinations (scenarios) and derive the performance of each scenario.
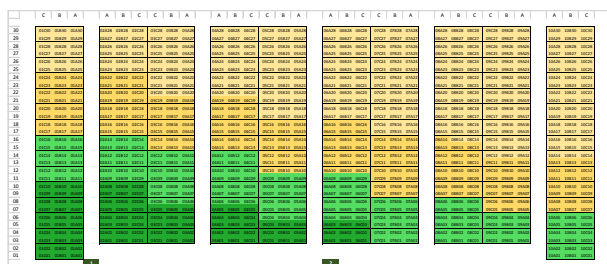
Figure 3: graphical representation of the usage of the locations

Figure 4: random order generator

3.4. Analysis of the TO BE scenarios

Once all possible combinations have been simulated, the results were analysed. A first consideration from the simulation outcomes is that implementing the area batch picking policy without reorganizing the allocation of products in the warehouse would lead to a decrease of performances of 32%. This is caused by picking inefficiencies generated by the random allocation of products combined with the inefficiencies deriving from area batch picking, thus resulting in an increase in timing that would not have been compensated by the elimination of the sorting activity.

Looking at the classes, the performance of the picking system improves with the increase in the number of classes. By observing the deviations from the average of all combinations we can assume that this factor has a significant impact on the final result (see Figure 5). Setting the number of classes at 2 worsens by 12% the average performance of the system; conversely, the configuration with 5 classes improves up to 5% the average solution. We can also appreciate that the improvement decreases as the number of classes increases, becoming almost null if moving from 4 to 5 classes. From a practical point of view, this result suggests to select 4 classes, because adding a further class would make it more difficult to manage the picking system.

As far as the warehouse layout is concerned, the configuration that returns the best results is the shape cross-aisle, which was expected because of the imposed picking route and is consonant with similar findings available in literature. However, we found that this configuration modifies the average system's performance by only 0.4%; hence, the layout criterion does not seem to have a significant impact on the results observed.

Looking at the reference index, it was found that popularity should be preferred over turnover, as this latter worsens the average system's performance by approximately 4.2%. It is reasonable to expect that this result is due to the fact that popularity index, calculated as the probability that each item will be picked at least once per day, is particularly suitable for a batch picking that aggregates all orders of the day (like the one considered in this study).

Finally, as far as the picking policy is concerned, the results obtained with the two alternatives show that in general splitting the picking list by delivery zone (using the area batch picking logic) is the preferred solution. This configuration leads to an average 3.9% saving in time compared to the batch picking & sorting, whose saving compared to the average solution is 1.9%.
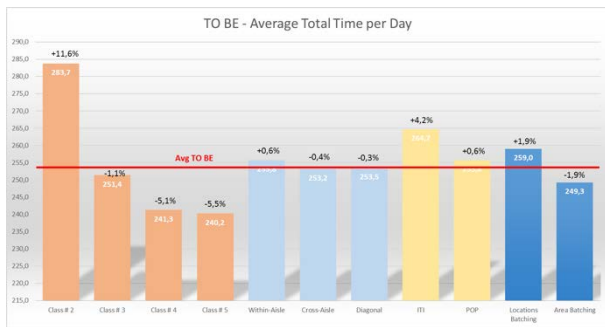
Figure 5: Performance deviation from the average solution of all the considered factors

This first analysis provides an overview of the main outcomes of the study but does not allow to determine the best solution overall, because the performance of each factor was calculated as the average of all the observations. We therefore relied on the analysis of variance (ANOVA) to gain further insights. ANOVA results showed that the variables having a significant effect on the result are the number of classes and the reference index, with the former having the greatest effect. ANOVA also revealed a significance of the combined effect for the Picking policy – Reference Index and Picking policy - Number of classes.

On the basis of this outcome, all the TO BE scenarios were evaluated singly and the saving in time with respect to the AS IS situation was identified for each scenario. It was found that all 48 combinations had a lower total time than the AS IS scenario, proving the effectiveness of the warehouse reorganization. It was also observed that the combination that returned the best result consisted of 5 classes, arranged with Cross-Aisle layout, with SKUs assigned according to the Popularity index and picked according to the area batch picking policy. In addition, the same analysis was carried out evaluating the specific results obtained for each combination on every day of the week, to check whether the average results were similar when evaluating the single weekdays. This hypothesis was confirmed.

4. DISCUSSION

The results proposed in section 3 lead to some considerations on the solution to be adopted for the case study company. As stated earlier, the best configuration obtained from the simulation consists of 5 classes, arranged with Cross-Aisle layout, with SKUs assigned according to the Popularity index and picked according to the area batch picking policy. Nonetheless, another interesting combination could be obtained with 4 classes. In fact, it was also observed that keeping the remaining factors unchanged and choosing 4 classes instead of 5, returns similar results in terms of total logistics time but, at the same time, leads to a combined an easier management of the process, caused by the reduced number of classes. This combination results in an average performance deterioration of 0.87% only compared to the optimal combination and in a deviation of less than 2% looking at the single weekdays.

Compared to the current configuration, the adoption of this configuration would generate an average saving of 223 minutes per day in the company under examination, and of about 615 hours per year; this amount of time could be used for other activities or to allow a shift in the cut-off time of orders, thus enhancing the service level offered to customers.

5. CONCLUSIONS

This paper has proposed an evaluation of the real picking system of a UK company operating in the food wholesale. The current policy adopted by the company is batch picking & sorting. By means of an *ad hoc* simulation model developed in Microsoft Excel^{TM}, several alternative configurations were examined for the picking process, including an alternative picking policy (area batch picking), various storage assignment policies and different product classes. Overall, the number of scenarios examined is 48. Although all these scenarios returned a lower picking time compared to the current configuration, one of them turned out to be particularly interesting for practical implementation. To be more precise, the settings that returned the best result was as follows: 5 product classes, arranged with Cross-Aisle layout, with SKUs assigned according to the Popularity index and taken according to the area batch picking policy. Nonetheless, from a practical point of view, the most promising configuration would have 4 classes, which makes it easier to manage and update the product allocation inside the warehouse.

Practical implications of this work concerns the suggestions that can be elaborated for the company under examination, to improve the current picking process. From a scientific perspective, this work has some main strong points compared to the available literature. First, the analysis carried out takes a different perspective compared to most of the studies concerning picking optimization: the typical approach followed in literature, indeed, is to evaluate only one factor affecting the picking performance at a time, keeping the remaining factors unchanged. Conversely, through the analysis of 48 scenarios, this paper has evaluated the effect of more factors simultaneously and identified also significant two-factor interactions. The Microsoft Excel^{TM} model developed for the analysis is original as well, as to the best of the authors' knowledge, there are no available simulation tools for the analysis of the picking process. A further important point is that the warehouse layout of the company examined is particular, as the picking corridor ends with a blind wall. This does not reflect the typical layout structure assumed in picking studies and obviously needs a tailored evaluation, as most of the models available in literature cannot be applied to such configuration.

Starting from this paper, future research activities could be carried out to apply the Microsoft Excel^{TM} model to additional case studies, with different warehouse configurations, in the attempt to generalize the results obtained in this study or to investigate whether these

results could change depending on the warehouse layout.

REFERENCES

Bottani, E., Cecconi, M., Vignali, G. & Montanari, R. 2012. Optimisation of storage allocation in order picking operations through a genetic algorithm', International Journal of Logistics: Research and Applications, 15(2), 127–146

Bottani, E., Montanari, R., Rinaldi, M., & Vignali, G. 2015. Intelligent Algorithms for Warehouse Management. In C. Kahraman, & S. Çevik Onar, Intelligent Techniques in Engineering Management: Theory and Applications, p.645-667. Switzerland: Springer International Publishing.

Chen, F., Wang, H., Qi, C. & Xie, Y. 2013. An ant colony optimization routing algorithm for two order pickers with congestion consideration. Computers & Industrial Engineering, 66(1), 77–85.

Chen, F., Wang, H., Xie, Y. & Qi, C. 2016. An ACO-based online routing method for multiple order pickers with congestion consideration in warehouse. Journal of Intelligent Manufacturing, 27(2), 389-408

Coyle, J., Bardi, E., & Langley, C. 1996. The management of business logistics. Minneapolis: West Publishing Company.

de Koster, R., Le-Duc, T. & Zaerpour, N. 2012. Determining the number of zones in a pick-and-sort order picking system. International Journal of Production Research, 50(3), 757–771

de Koster, R., Le-Duc, T., & Roodbergen, J. 2007. Design and control of warehouse order picking: a literature review. European Journal of Operational Research, 182(2), 481-501.

De Santis, R., Montanari, R., Vignali, G., & Bottani, E., 2018. An adapted ant colony optimization algorithm for the minimization of the travel distance of pickers in manual warehouses. European Journal of Operational Research, 267, 120-137

Frazelle, E. 2002. World-class Warehousing and Material Handling. New York: McGraw Hill.

Gu, J., Goetschalckx, M., & McGinnis, L. 2007. Research on warehouse operation: A comprehensive review. European Journal of Operational Research, 177, 1-21.

Guerriero, F., Musmanno, R., Pisacane, O., & Rende, F. 2013. A mathematical model for the Multi-Levels Product Allocation Problem in a warehouse with compatibility constraints. Applied Mathematical Modelling 37, 4385–4398

Hall, R. 1993. Distance approximations for routing manual pickers in a warehouse. IIE Transactions, 25(4), 76-87.

Henn, S. 2012. Algorithms for on-line order batching in an order picking warehouse. Computers & Operations Research, 39, 2549–2563

Hong, S., Johnson, A.L. & Peters, B.A. 2012. Batch picking in narrow-aisle order picking systems with consideration for picker blocking. European Journal of Operational Research, 221, 557–570

Jane, C-C. & Laih, Y-W. 2005. A clustering algorithm for item assignment in a synchronized zone order picking system. European Journal of Operational Research, 166, 489–496.

Jarvis, J., & McDowell, E. 1991. Optimal product layout in an order picking warehouse. IIE Transactions, 23(1), 93-102.

Kulak, O., Sahin, Y. & Taner, M. 2012. Joint order batching and picker routing in single and multiple-cross-aisle warehouses using cluster-based tabu search algorithms. Flexible Services and Manufacturing Journal, 24(1), 52–80.

Le-Duc, T. & de Koster, R. 2007. Travel time estimation and order batching in a 2-block warehouse. European Journal of Operational Research, 176(1), 374–388

Mowrey, C.H. & Parikh, P.J. 2014. Mixed-width aisle configurations for order picking in distribution centers. European Journal of Operational Research, 232(1), 87–97

Pan, J.C-H. & Wu, M-H. 2012. Throughput analysis for order picking system with multiple pickers and aisle congestion considerations. Computers & Operations Research, 39(7), 1661–1672

Parikh, P. & Meller, R. 2010. A travel-time model for a person-onboard order picking system. European Journal of Operational Research, 200, 385–394

Petersen, C. 1999. The impact of routing and storage policies on warehouse efficiency. International Journal of Operations & Production Management, 19(10), 1053–1064

Petersen, C. 2002. Considerations in order picking zone configuration. International Journal of Operations & Production Management, 22(7), 793-805.

Petersen, C., & Schmenner, R. 1999. An evaluation of routing and volume-based storage policies in an order picking operation. Decision Science, 30(2), 481-501.

Petersen, C. & Aase, G. 2004. A comparison of picking, storage, and routing policies in manual order picking. International Journal of Production Economics, 92(1), 11–19.

Roodbergen, K. & Vis, I., 2006. A model for warehouse layout. IIE Transactions, 8(10), 799–811

Roodbergen, K., & de Koster, R. 2001. Routing methods for warehouses with multiple cross aisles. International Journal of Production Research, 39(9), 1865-1883.

Rouwenhorst, B., Reuter, B., Stockrahm, V., van Houtum, G., Mantel, R., & Zijm, W. 2000. Warehouse design and control: Framework and literature review. European Journal of Operational Research, 122, 515-533.

Tompkins, J., White, J., Bozer, Y., Frazelle, E., Tanchoco, J., & Trevin, J. (1996). Facilities Planning. New York: Wiley.

Van Nieuwenhuyse, I. & de Koster, R. 2009. Evaluating order throughput time in 2-block warehouses with time window batching. International Journal of Production Economics, 121(2), 654–664

Webster, S., Ruben, R., & Yang, K.-K. 2012. Impact of storage assignment decisions on a bucket brigade order picking line. Production and Operations Management, 21(2), 276-290.

Zhang, G., & Lai, K. 2006. Combining path relinking and genetic algorithms for the multiple-level warehouse layout problem. European Journal of Operational Research, 169(2), 413-425.

AUTHORS BIOGRAPHY

Eleonora BOTTANI is Associate professor in Mechanical Industrial Plants at the Department of Engineering and Architecture of the University of Parma since September 2014. She graduated (with distinction) in Industrial Engineering and Management in 2002 and got her Ph.D. in Industrial Engineering in 2006, both at the University of Parma. Her research activities concern logistics and supply chain management issues. She is author (or co-author) of more than 160 scientific papers (H-index=17), referee for more than 60 international journals, editorial board member of five scientific journals, Associate Editor for one of those journals, and editor-in-chief of a scientific journal.

Andrea PANCIROLI graduated in December 2016 in Industrial engineering and management (master degree) at the University of Parma. During his studies, he spent some months in the UK for the development of the master degree thesis. He currently works as supply chain analyst software in a software development company.

Roberto MONTANARI is Full professor of Mechanical Plants at the University of Parma. He graduated (with distinction) in 1999 in Mechanical Engineering at the University of Parma. His research activities mainly concern equipment maintenance, power plants, food plants, logistics, supply chain management, supply chain modelling and simulation, inventory management. He has published his research in approx. 70 papers, which appear in qualified international journals and conferences. He acts as a referee for several scientific journals, is editorial board member of 2 international scientific journals and editor of a scientific journal.

Andrea VOLPI graduated in July 2003 in Mechanical Engineering at the University of Parma. Since January 2006, he has been working as Ph.D. student in Industrial Engineering Department at the same University, his major activities have been devoted to managing the research projects carried out in RFID Lab, a forefront laboratory in the same department. Since November 2015, he works as Associate Professor at University of Parma, and his research activities are mainly concerned with logistics, supply chain and operation management; thus his skills and competences are mainly related to RFID and logistics topics which are expressed in many papers produced. He acts as a referee for some international scientific journals, such as International Journal of RF Technology: Research and Applications, International Journal of Logistics: Research and Applications.

DIFFERENT TRAFFIC SUBMODELS WITHIN SCALABLE UNITARY HYBRID SIMULATOR RELATED TO RAILWAY SYSTEMS

Radek Novotný[a], Antonín Kavička[b]

[a],[b]Faculty of Electrical Engineering and Informatics, University of Pardubice

[a]radek.novotny3@student.upce.cz, [b]antonin.kavicka@upce.cz

ABSTRACT
The contribution deals with various approaches to modelling of railway traffic, which are part of a coherent methodology of building unitary hybrid simulation models. Those models apply different level of abstraction (granularity) to diverse parts of a simulating system. Special attention is paid to different traffic models, especially in macroscopic elements of hybrid model, i.e. in macro-segments encapsulate different infrastructure submodels. From the viewpoint of the macroscopic traffic submodels is pay attention mainly to selection of traffic models for macro-edges.

Keywords: scalable simulation model, hybrid model, railway traffic, transformations of traffic flows, macroscopic traffic model

1. INTRODUCTION
Modelling a railway infrastructure and a corresponding railway traffic represents an important part of the research focused on railway system optimizations. For such purposes the researchers use the experimental research method of computer simulation in which the level of *granularity* (applied within simulators) plays an important role. It defines the level of details considered within an examined simulating system. The different levels of details required for investigating the railway traffic, can determine various simulation models utilizing different granularity. Thus, simulations can be classified according to their granularities as *microscopic, mesoscopic*, and *macroscopic* (Krivy and Kindler 2003; Burghout 2004).

Traditional approaches apply the same level of details for the entire simulator – i.e. that homogenous approach does not allow to combine microscopic and mesoscopic levels of details within one simulator. There is a strong motivation for designers of traffic simulations to use methodologies for building scalable simulation models of railway traffic. Those models enable to combine and interconnect various submodels of infrastructure built on different levels of details and different traffic submodels reflecting granularities of relevant infrastructural submodels - certainly relevant transformations of traffic flows are supposed to be carried out on the boundary between corresponding

submodels (Hansen and Pachl 2008; Cui, and Martin 2011; Novotny and Kavicka 2016).

2. STATE OF THE ART
There are various approaches of building scalable simulation models focused on railway traffic. Generally, there are variants of simulation models, which enable to change the level of details dynamically during the simulation run computing the traffic within the entire observed railway network. That effect can be achieved if the simulation scene is zoomed in or zoomed out (*scalable simulation model with continuous changeover*). A different approach represents the combination of static areas with different levels of details (*hybrid model*). Those areas are constructed before executing a simulation trial. Multiplatform hybrid models can utilize the combination of several different simulation tools – for example the microscopic tool *RailSys* and the macroscopic tool *NEMO* (Novotny and Kavicka 2016).

3. UNITARY HYBRID SIMULATION MODEL
Our presented methodology is based on a hybrid simulation model implemented within one simulation tool (*unitary hybrid model*). That methodology supports combining submodels exploiting the microscopic and macroscopic levels of details. Microscopic simulation is connected to particular areas, within the frame of which important details about traffic (and infrastructure) are important for the experimenter. On the other hand, macroscopic simulation is utilized within those parts of the simulator for which rough operational/traffic observations are sufficient. Unitary hybrid model enables to adjust the *granularity* of selected parts of a simulator. The mentioned parts are connected to relevant traffic submodels operating over corresponding infrastructure submodels (Novotny and Kavicka 2016).

4. HYBRID INFRASTRUCTURE MODEL
The methodology of building unitary hybrid models focuses primarily on the construction of a track infrastructure submodel (Novotny and Kavicka 2015). From the viewpoint of the implementation of *hybrid submodel/layer of infrastructure* (e.g. built in editing tool *TrackEd*) it is necessary to distinguish between *micro-layer*, which corresponds to the microscopic

submodel applies the highest level of details which can be required for the given part of the railway network, and *hybrid-layer* composed of *micro-segments* and *macro-segments*. *Micro-segments* are represented by sub-graphs directly taken from the micro-layer. *Macro-segments* apply higher degree of granularity (i.e. lower level of details) to relevant disjoint connected sub-graphs from the *micro-layer*. Two types of macro-segments (*macro-nodes* and *macro-edges*) are distinguished within the presented methodology. *Macro-edges* typically encapsulate line sequences of edges from micro-layer. *Macro-nodes* can enclose a

general connected sub-graph from the micro-layer. Constructions of *macro-segments* support creating variant configurations of hybrid submodels of railway infrastructure. It means in fact that different scenarios of simulation experiments can apply various levels of details (micro- or macroscopic) within an infrastructure submodel (Novotny and Kavicka 2016).

LEGEND

φ_c — current intesity of traffic flow

ρ_c — current density of traffic flow

$V(\rho_c)$ — average speed reflecting current density

$t_{(i)}$ — time of entry into the macro-segment

$L_{(i)}$ — length of train

L_S — length of train path in macro-segment

H_S — headway distance between trains in macro-segment
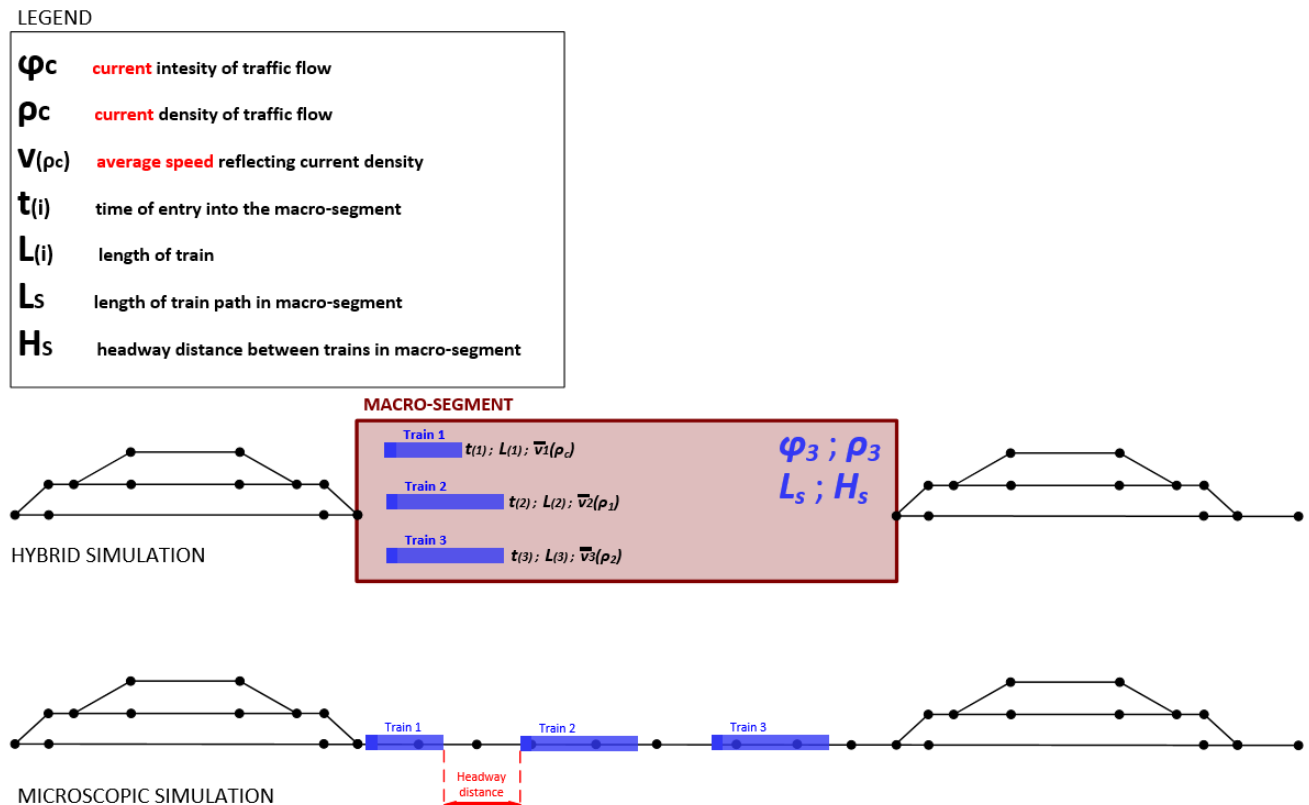
Figure 1 – Hybrid simulation model

5. HYBRID TRAFFIC MODEL

Because of combining macro-segments with areas including microscopic elements within the *hybrid-layer*, it is necessary to apply different traffic models implementing various levels of abstraction, which are connected to different traffic indicators. From the viewpoint of the implementation of the unitary hybrid model it is necessary to distinguish between traffic models applied to microscopic (*microscopic traffic submodels)* and macroscopic (*macroscopic traffic submodel*s) infrastructure segments of hybrid model. Because several different traffic submodels coexist within a hybrid model, it is necessary to solve transformations of traffic flows, i.e. it is necessary to unambiguously define the information about railway traffic on the interface between each microscopic and macroscopic submodel in order to maintain consistency of data.

Regarding the train movement between different traffic submodels (i.e. transformation of traffic flows), it is necessary to distinguish between the transition from the microscopic to the macroscopic submodel, with which there is a loss of detailed information about the individual train, and the transition from the macroscopic submodel back, with which it is necessary to derive back the clearly detailed information, while taking into account the current traffic situation in the relevant surrounding area (Burghout 2004; Burghout 2006; Novotny and Kavicka 2016; Novotny and Kavicka 2017).

6. MICROSCOPIC TRAFFIC SUBMODEL

Microscopic traffic submodel is based on applying realistic calculations connected with the train ride dynamics and train interactions. Train rides computations use detailed information about railway infrastructure (real topology/metric and slope

properties) defined in *micro*-layer of infrastructure model. It is also necessary to include train parameters that are necessary to simulate their real movement along the track (e.g. traction characteristics, resistive, braking and other train parameters). To calculate the dynamics of train running, numerical integration is repeatedly used, according to a defined time step, due to the changing position of the train and the characteristics of the track. In other words, the movement of trains on the infrastructure reflects the real driving characteristics with respect to the train and tracks properties. Regarding the presented microscopic traffic submodel, it is possible even with respect to the used abstraction degree to achieve high quality results of simulation experiments without greatly ruining their corresponding values (Divis and Kavicka 2015; Novotny and Kavicka 2017).

7. MACROSCOPIC TRAFFIC SUBMODEL

From the viewpoint of *macro-edges* (encapsulating open tracks etc.) respectively *macro-nodes* (encapsulating railways station etc.) within *hybrid-layer* of infrastructure, it is necessary to apply different macroscopic models of traffic. Selected concepts of macroscopic traffic models respectively the movement of trains over *macro-segments* can be imagined as i) competion for a shared resource, ii) fluid flow (Novotny and Kavicka 2017).

7.1. The concept of traffic model within macro-nodes

In general, in context of traffic modelling, the *macro-segment* can be understood as a form of shared resource that is only able to accommodate (process) a certain number of trains. The maximum number of trains within this submodel can then be given by one of the attributes defined in the respective *micro-* layer.

This concept is already applied in the case of modelling traffic inside the *macro-nodes* encapsulating the railway station. Particularly because a similar parallel can be seen in real railway traffic, where the number of tracks in the station can be the factor determining the maximum number of trains in the station. Other trains are then not allowed to enter the station and must wait for some of the tracks to be cleared out (Novotny and Kavicka 2017).

The basic idea is that the trains do not influence each other, i.e. do not change the density of traffic flow that would directly affect the average speed assigned to the next incoming train. In other words, if the train can enter the macroscopic submodel (from the rules defined above), the moment of the simulation time, when the train leaves the submodel, is calculated individually based on attributes from the respective microscopic elements forming the train path through the *macro-node*. For braking, or for acceleration that would occur for an area with a microscopic model of traffic, a correct time reserve if the train stops within the *macro-node* is an important factor

With the selected model of traffic for macroscopic submodels in the form of one shared resource, the *macro-node* can be blocked by trains coming from one direction only. This would, of course, lead to an increase in the delay in trains in the opposite direction and an inconsistency of the hybrid simulation model of railway traffic against a purely microscopic approach. If we take a closer look at real traffic in e.g. a railway station, there is always a different set of station tracks designated for each direction. If we disregard the exceptional circumstances of real traffic, when the train uses a station track for any other direction (methodology operated by a dispatcher), a group of station tracks based on their directions can be recorded within each *macro- node*. The station track allocation logic then considers the routing of trains within the *macro- node*. The advantage is that trains coming from different directions will only be affected in cases where the railway station uses common station tracks for these directions (Novotny and Kavicka 2017).

7.2. The concept of traffic model within macro-edges

Similarly, the idea of a macroscopic traffic model operating on the principle of a shared resource can also be used for *macro-edges*. The maximum number of trains determining the maximum capacity of the *macro-edge* must be defined from other attributes of the respective *micro*-layer, contrary to the *macro- node* (encapsulating the railway station). As a result of establishing lower capacity of the *macro-segment* compared to real rail traffic in the submodel, automatic delays which would not actually occur at all and vice versa may be generated. In other words, the correct definition of the maximum number of trains within the *macro-edge* is important for correct simulation of real traffic in relevant encapsulated infrastructure. Assuming that the *macro-edge* serves to encapsulate only a path between adjacent stations (without track intersection), maximum permeability can be determined based on the length of the train path inside, headway distance and the average length of incoming trains, and thus to individually calculate the moment of the simulation time, when the trains leave the submodel, for each train. Similarly to the *macro*-node, the correct time addition is an important factor. This is the consequence of braking a train, for example, before the railway station in which it stops, which would occur if it were an area with a microscopic model of traffic. In other words, it is a situation where the *macro-edge* adjoins directly with the railway station where the train stops and starts to brake on any of the relevant microscopic elements forming the train path through the *macro-edge*.

Different concept to modelling traffic is to utilize the analogy between a flow of a fluid and the movement of trains through the macroscopic submodel, because just as the fluid particles motion is affected by the movement of the surrounding particles, the movement of trains within the *macro-segment* is affected by surrounding trains (Daiheng 2011). The presented methodology of transformation of traffic flows allocates each vehicle entering the macroscopic submodel an average speed determined from the current density of

traffic flow in the *macro-segment*. The density of traffic flow for each *macro-segment* determined from the attributes defined in the relevant *micro*-layer (number of isolated circuits, the average length of the defined train routes, etc.), and the current number of rolling stock inside. From the viewpoint of macroscopic traffic submodel, it is possible to determine the simulation time when given *macro-segment* leaves, based on the density of traffic flow and assigned average speed of the rolling stock entering the *macro-segment*, with respecting the assigned schedule, and thus it is not necessary to individually monitor it during its movement in a macroscopic submodel (Daiheng 2011; Burghout, Koutsopoulos and Andreasson 2006).

Concept can be applied in the case of modelling of traffic inside the *macro-edges* (encapsulating open tracks). Based on knowledge of real railway traffic between adjacent stations it can be, based on information about:

- infrastruture (e.g. length and topology of track section between stations),
- technical and technological rules (e.g. line headway specifying the minimum time span of two consecutive trains) and
- current traffic (actual number of trains in submodel, etc.)

determining the *current density of traffic flow* within *macro-edge* (*Figure 1*).

Regarding both approaches to modelling the traffic within the *macro-edge,* it is necessary to realize that the *macro-edge* always serves to encapsulate only the linkage of the *micro*-layer edges (i.e., it forms a subgraph where each inner node is incident with only two edges). Thus, unlike traffic within the railway station (in the *macro-node*), trains always leave the *macro-edge* in the order in which they enter it. Therefore, the headway distance must always be met between trains (i.e. the minimum time span condition between two consecutive trains must not be violated). This is especially important to keep if it is not possible to leave the *macro-edge* because of blocking traffic in the surrounding area.

7.3. Coexistence of different traffic models
The result of different principles in the macroscopic traffic submodel is their different application in the case of *macro-nodes*, or *macro-edges*. The general assumption is the application of shared resources for *macro-nodes* encapsulating a part or whole railway stations and for *macro-edges* (aggregating open tracks) a traffic model based on fluid flow. To accept this fact, all presented concepts of macroscopic traffic submodel for both types of *macro-segments* must be implemented and a given hybrid model of traffic must be validated and verified by a series of simulation experiments.

Within the introduced unitary hybrid model of railway traffic, we assume different traffic submodels:

- a microscopic traffic submodel based on realistic calculations connected with the train ride dynamics,
- a macroscopic traffic submodel based on a shared resource rivalry in the case of macro-nodes,
- a macroscopic traffic submodel based on an analogy of liquid flow for macro-edges.

8. VERIFICATION AND VALIDATION
Regarding using a unitary hybrid model in practice, it is necessary that the results of the simulation experiments are correct and correspond to reality. Due to the application of different degrees of abstraction on different parts of the simulation system, a validation methodology consisting of several phases was identified:

- deterministic simulation of the microscopic traffic model,
- deterministic simulation of a hybrid traffic model, and
- hybrid traffic simulation with random-time delay (stochastic simulation).

Primarily, it was necessary to validate and verify the implementation of train running dynamics and thereby confirm the correctness of used microscopic traffic model. In order to verify the correctness, the infrastructure of a part of the railway network of the Czech Republic comprised of a prototype station and border stations used for dispatching trains was used and a series of deterministic simulation experiments was carried out according to a real timetable. Basically, it was a comparison of a tachograph compiled from a real environment with a tachograph obtained from simulator results (a series of simulation experiments) and a comprehensive verification with the results from another already validated simulator (Villon), which represents a simulation tool generally accepted by railroad experts (Divis and Kavicka 2015; Novotny and Kavicka 2017).

Subsequently, the prototype station was encapsulated in the *macro-node*, resulting in a variation of the hybrid traffic model, which applied different degrees of *granularity* within the simulator. The verification of the correctness of such constructed hybrid traffic model was focused mainly on deviations in delays of trains passing through the *macro-node* for all presented concepts of macroscopic submodels of traffic. Based on the results of the simulation experiments published in the previous paper (Novotny and Kavicka 2017), the concept of traffic based on the analogy of shared resource rivalry was generally accepted for *macro-nodes*, which, according to the prescribed graphical timetable, showed little deviation in delays to purely microscopic traffic simulation.

9. CASE STUDY

Regarding the validation of the macroscopic traffic submodel within the *macro-edges* only open track between the prototype and the border stations were encapsulated into *macro-edges*. Verification of correctness was, of course, again focused on deviations in delays of trains this time passing through the *macro-edges*. In other words, the conclusion of simulation experiments was based on the assumption that the transformation of traffic flows on the boundary between the microscopic and macroscopic components of the hybrid model must have a minimal effect on the final train delays.

For *macro-edges*, macroscopic traffic model based on the analogy of shared resources was tested in deterministic mode, the maximum number of trains within the *macro-edge* was determined by the length of the path within and the average length of the train. Similarly, the approach based on the analogy of fluid flow when the density of traffic flow changed based on the headway distance, the length of train path and the number of trains within the *macro-edge* was tested. For both implemented concepts there was no negative impact (*Figure 2*) on the delays of trains passing through the *macro-edges*. However, the reason for that may be the lack of sufficient traffic on those parts of the infrastructure that have been encapsulated in the *macro-edges*. As a result, it will be necessary to monitor in future how the deviation of delay of trains leaving the *macro-edges* under the load of railway traffic by random delay will change and to possibly verify the two concepts of macroscopic traffic models more consistently.

The following step is the traffic examination of the hybrid traffic model, which is constructed from both the *macro-node* and the *macro-edges* that are connected to one another from the point of view of the construction of the hybrid model of infrastructure (i.e. the *macro-edge* is directly connected to the *macro-node*). The results of the simulation experiments will then determine the usability of selected macroscopic traffic models with an emphasis on correct traffic flow transformation not only at the boundary of the microscopic and macroscopic elements but also at the boundary of different *macro-segments*
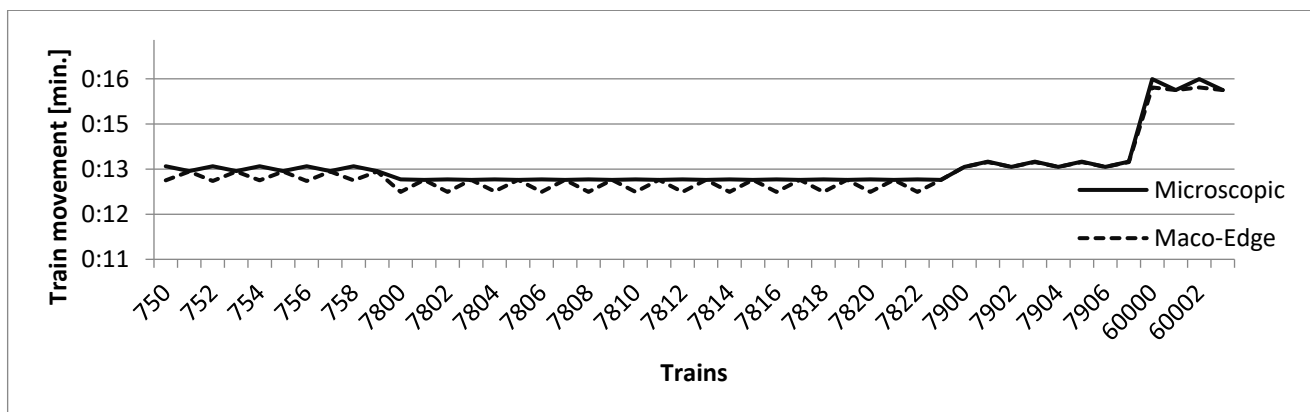
Figure 2 – Comparsion times of train movement through infrastructure

10. PERSPECTIVES OF DEVELOPMENT

Regarding future development, it is intended to carry out a rigorous operational examination of various combinations of microscopic and macroscopic components (applying differently selected traffic submodels) within the hybrid model of infrastructure. On the boundary of these different traffic submodels, it is necessary to verify the correctness of the transformation of traffic flows, mainly due to deviations in train delays. Perspective of further development may be to design a methodology of a general macroscopic model of traffic applicable to any defined *macro-segment*.

Next prospective option could be to build a hybrid infrastructure model without the need to create a microscopic model of the entire railway network. Extensions will allow modelling of some infrastructure submodels with a higher degree of abstraction (macroscopic) and defining only the rough characteristics of the tracks needed for the macroscopic traffic submodel.

11. CONCLUSION

The contribution follows the methodical approach to the construction of the hybrid model of infrastructure and emphasizes the choice of different traffic models for various infrastructure submodels and their mutual coexistence within the hybrid traffic model.

The hybrid traffic model combines areas built with different degrees of granularity and therefore distinguishes between a microscopic traffic submodel (detailed information on individual rolling stock) and a macroscopic traffic submodel (rough operating characteristics only). Hybrid traffic model constructed this way, of course, also brings along the issues of solving the transformation of traffic flows on their boundaries.

Achieving high quality results for the microscopic traffic submodel has led to further phasing of development focused on the selection and evaluation of macroscopic traffic models for different *macro-segments*. Based on a series of simulation experiments, the traffic model based on the analogy of shared

resource rivalry of *macro-nodes* was successfully selected and validated. Similarly, validation took place in cases where a *macro-edge* was created within the hybrid layer of infrastructure. Both presented concepts of macroscopic traffic models (i.e. fluid flow and shared resource) were adopted according to the results obtained for the *macro-edges*. The presented implementation of the hybrid traffic model has been demonstrated in *TrackEd* integrated development environment for a case study on railway traffic of a selected area of the Czech railway network. For future development, it is intended to verify the transformation of traffic flows on the boundary between *macro-nodes* and *macro-edges*.

REFERENCES

Cui Y., and Martin U., 2011. Multi-scale Simulation in Railway Planning and Operation. PROMET Traffic. Available from: http://www.fpz.unizg.hr/traffic/index.php/PROMT T/article/view/186 [Accessed 22 March 2018].

Burghout W., 2004. Hybrid microscopic-mesoscopic traffic simulation. Doctoral Dissertation. Royal Institute of Technology.

Divis R., and Kavicka A., 2015. Design and development of a mesoscopic simulator specialized in investigating capacities of railway nodes. The 27th European Modeling & Simulation Symposium. Bergeggi, Italy.

Novotny R., and Kavicka A., 2015. Model of a railway infrastructure as a part of a mesoscopic traffic simulator. The 27th European Modeling & Simulation Symposium. Bergeggi, Italy.

Novotny R., and Kavicka A., 2016. Scalable simulation models of railway traffic. The 28th European Modeling & Simulation Symposium. Larnaca, Cyprus.

Novotny R., and Kavicka A., 2017. Unitary hybrid model of railway traffic. The 29th European Modeling & Simulation Symposium. Barcelona, Spain.

Krivy I., and Kindler E., 2003. Modeling and simulation I. Ostrava: PrF OU. [in Czech]

Hansen Ingo, Pachl Jorn, 2008. Railway timetable and traffic. Hamburg: Euraipress.

Daiheng Ni, 2011. Multiscale modeling of traffic flow. Mathematica Aeterna, 27-54. University of Massachusetts.

Burghout W., Koutsopoulos H., and Andreasson I., 2006. A discrete-event mesoscopic traffic simulation model for hybrid traffic simulation. To appear in: Intelligent Transportation Systems Conference. Toronto.

Burghout W., Koutsopoulos H., and Andreasson I., 2006. A discrete-event mesoscopic traffic simulation model for hybrid traffic simulation. To appear in: Intelligent Transportation Systems Conference. Toronto.

INCLUDING CO-SIMULATION IN MODELING AND SIMULATION TOOL FOR SUPPORTING RISK MANAGEMENT IN INDUSTRIAL CONTEXT

[a]Simon Gorecki, [b]Youssef Bouanan, [c]Judicael Ribault, [d]Gregory Zacharewicz, [e]Nicolas Perry

[a], [b], [c], [d]Univ. Bordeaux, Lab. IMS, UMR CNRS 5218, 33400, Talence, France
[e]Arts et métiers, ParisTech, ENSAM of Bordeaux, France

[a], [b], [c], [d]{firstname.lastname}@u-bordeaux.fr
[e]nicolas.perry@ensam.eu

ABSTRACT

Due to increasing complexity of engineered system of systems, development of software to design and support them must tend to be more and more concurrent and distributed. To more easily tackle these systems design, global problem is decomposed into several sub-ones where each sub problem is allocated and solved by different contributors. Each participant develops a fragment of the global solution that need after to be integrated with other ones. In this paper we present an extension to the UML/BPMN modeling and simulation tool: Papyrus. This module allows to factor complex tasks during the modelling step and simulation execution process. In detail, we propose to add risk management and other potential interruptions features to BPMN models and Simulation. This is made possible according to Functional Mock-up Interface standard, a co-simulation standard that define how to orchestrate components while simulation execution process.

Keywords: Model Driven Architecture; Co-Simulation; Functional Mockup-Interface; Risk Management.

1. INTRODUCTION

The Modeling & Simulation (M&S) concept is now a required step in any design of complex systems. It allows to early represent its behavior and interaction. The modeling phase describes a process and allows the development of an executable simulation that virtually designs our subject and anticipates its study. As technologies are growing, systems complexity increases, and makes system more difficult to model and simulate. Along with this growing complexity, risks, hazards, and threat must also be considered during the modeling process. Several research has been done about project risk management (Altuhhova, Matulevicius, and Ahmed 2013; Better et al. 2008). In this paper we propose a way to integrate them during the modeling and simulation phases without overloading models.

Modeling are one of the primary and most important steps in a project development process. In our case, we need a modeling language able to represent risk management. For that, the Unified Modeling Language (UML) is a general purpose, widely used for describing the different aspects of software and complex systems. It offers several modeling notations to express not only the structure but the behavior of the modeled system. However, this language is also criticized for his low capacity to give precision to the system description. For this reason, the Object Management Group (OMG) has created the concept of UML profile which allows users to create their own UML specification. This UML specification will allow user to define his own language depending on his semantic subject, and provide it to the community: Systems Modeling Language (SysML), Use Case Diagram, etc.

This language is a viable solution for representing risks in a system description. Models will be designed and executed with Papyrus tool.

Papyrus is an open source UML/SysML/BPMN modeler of the Eclipse foundation that provides to users and developers a powerful tool for modeling UML models. Another interesting part of Papyrus tool is the execution of UML models due to fUML standards (Semantics of a Foundational Subset for Executable UML Models) allows by the MOKA engine (Guermazi et al. 2015).

Our proposition in this paper consist in defining an extension to MOKA engine able to interrupt the simulation execution and do a request to an external simulation component through Functional Mock-up Interface (FMI). FMI Co-Simulation standard will allow us to relocate and factor complex tasks without overloading models.

In the case studied in this paper, an M&S tool is used in a semi-academic, semi-professional context: a French company has launched an innovative project to set up a solar power plant. This project deals with different domains and several simulations tools. All those domains will imply many constraints that must be taken into account during modeling and simulation phases. One of the main aspect we are working on is risk management. Indeed, in the renewable energy domain, many risks and issues must be taken in account by engineer at the modeling phase of the project such as weather issues impact, etc. Our contribution consists in adding a risk management module into an open source modeling and simulation environment: Papyrus.

2. BACKGROUND

In this section, recent contributions in co-simulation approach are briefly discussed first, efforts in risk management in process modeling are explained in 2.2, Papyrus, a UML modeler is described in 2.3, and finally, Functional Mock-up Interface standard is explained in 2.4 section.

2.1. Complex Systems simulation and co-simulation

The emergence of complex engineered systems that integrate both physical, software and network aspects are posing challenges in their design, operation, and maintenance. The current business climate and market pressure are forcing the design of systems to be concurrent, interoperable, distributed and reusable. This is done in order to be divided between different teams and/or external suppliers, each with its own expertise domain and each with its own tools. Here comes the role of Distributed Simulation (DS): one simulation is divided into multiple sub functions (or models) from a large system. Each function is executed on a different computer possibly geographically distributed from others. From a general point of view, this solution divides complex problems into simpler modular sub problems, but also rises interoperability issues.

Modeling and Simulation (M&S) of complex systems requires the simultaneous consideration of several points of view. The system behavior has to be considered at different levels and scales. In addition, the study of these systems involves skills from different scientific, business and technical fields. The challenge is then to reconcile these heterogeneous points of view, and to integrate each domain models and tools (or subsystems) within a unified framework, orchestrated by an M&S process. Two of the most popular efforts going in these directions are FMI (Functional Mock-up Interface) and HLA (High Level Architecture).

HLA is an IEEE standard (IEEE Computer Society 2010) for distributed computer simulation systems (IEEE Computer Society 2003). In the HLA standard, a distributed simulation is called Federation (see Figure 1). A Federation is composed of several HLA simulation entities, called Federate, which can interact among them by using the Run-Time Infrastructure (RTI). The RTI represents a Federation execution backbone and provides a set of services to manage the communication and data exchange among Federates.

FMI (Functional Mock-Up Interface) (Blochwitz et al. 2012) establishes itself as a standard for model exchange and co-simulation of equational models. The FMI functions are used (called) by a simulation environment to create one or more instances of the FMU (Functional Mockup Unit) and to simulate them, typically together with other models. An FMU may either have its own solvers (FMI for Co-Simulation) or require the simulation environment to perform numerical integration (FMI for Model Exchange). It enforces some generic rules and a software interface to manipulate equational models and their numerical solver using a combination of XML-files and compiled C-code. On that interface, any equational component can be embedded into an FMU (Functional Mock-up Unit) helping to solve the interoperability problem for the co-simulation of equational models. Then, the numerical resolution of a system can be performed by defining a set of communication points between the FMUs according to a trade-off between the accuracy of the simulation results and the performances of the co-simulation process (Camus et al. 2016). The FMI standard defines two interfaces: FMI for Model Exchange and FMI for Co-Simulation (Blochwitz et al. 2012). The FMU CS contains its own solver that will be built when generating the tool. The advantage of this model is to combine two or more simulation tools in a co-simulation environment. The exchange of data between the subsystems is limited to "Communication Points". Between two Communication Points, the subsystems are solved independently from each other by their individual solver. Within a master-slave view, slaves simulate sub-problems while the master is responsible for the coordination of the overall simulation and data transfer. Several tools are compatible with the FMI interface at Export/Import for both components FMU, Model-Exchange (ME) and co-simulation (CS). Example: JModelica, Dymola, LMS AMESim, EnergyPlus, CATIA, NI LabVIEW, Ptolemy II, etc.

2.2. Risk management in process modeling

The concept of risk is highly polysemous and supports a large number of definitions.

In the context of risk management, we can introduce a number of concepts revolving around risk and conditioned by the environment and the components of the project. The project risk is related to the occurrence of events, from internal or external origin, which may affect the achievement of the initial target.

The risk qualify the effect of these events on the achievement of project's objectives. The anticipation of these events via the factor's identification, internal or external, which are the cause, the evaluation of their impact on the project progress and the proposal of appropriate treatment actions are the purpose of risk management.

In literature, we observed most recurrent major steps in risk management that we can cite: identification, analysis, evaluation and treatment of risks. These keywords can be used in tools such as brainstorming guidelines in order to anticipate, minimize risks in a project. However, these methods are not much structured, mostly handle qualitative information and are frequently limited to user experience and point of view. In the following, we cite some relevant methods and tools that were proposed in literature to manage risks.

- Information Systems Security Risk Management (ISSRM) methods and standards (according to (Dubois et al. 2010)) mainly consist of process guidelines that help identify vulnerable assets, determine security objectives, and assess risks as well as define and implement security requirements to treat the

risks. By using these methods one reduces the losses that might result from security problems. However, these methods generally offer quite poor modelling support. Instead, they usually resort to informal documentation in natural language and ad hoc diagrams. According to Figure 1, this analysis method allow user to identify and classify risks into three categories: - *asset-related concepts* are used to identify in a systems, or in a company, skills of the organization, and security risks that must be avoid. - *risk-related concepts* identify risk events and threat related to assets defined previously. - *Risk-treatment concepts* are defined depending on risks possibilities. They will represent the decision of how to treat the identified risks. A treatment satisfies a security need, expressed in generic and functional terms, and can lead to security requirements.

- Business Process Modeling Notation Extension for Risk Handling was proposed in (Marcinkowski and Kuciapski 2012). The paper identify three different risk types: - Business-driven risks, strategic in nature aimed at protecting the business and keeping it accessible whenever and whoever in support of continuous business operations. - Data-driven risks, dealing with the availability of data and information in all of its different forms as used by the organization. - Event-driven risks, focusing on actual events that create risk to business continuity and viability. It propose to extend BPMN standard in order to modeling the several risks and handle it in three different ways: reduce it, retain it, avoid it, or transfer it.

2.3. Papyrus

Papyrus is the UML/SysML modeler of the Eclipse foundation. It provide tools for executing and debugging UML models. The execution part is handled by MOKA,

a fUML execution engine. Papyrus is based on Eclipse and is open source. In accordance with its primary goal to implement the complete standard specification of UML2, Papyrus provides an extensive support for UML profiles. It includes hence all the facilities for defining and applying UML profiles in a very rich and efficient manner. But, it also provides powerful tool customization capabilities similar to DSML-like metatools. This way, Papyrus is a tool enabling to gather the advantages of using a general purpose language such as UML2, but also those of DSML-based approaches.

2.4. FMI

The Functional Mock-up Interface (FMI) for Co-Simulation interface is designed both for the coupling of simulation tools (simulator coupling, tool coupling), and coupling with subsystem models, which have been exported by their simulators together with its solvers as runnable code. It is an interface standard for the solution of time dependent coupled systems consisting of subsystems that are continuous in time or time-discrete (Bastian et al. 2011; Blochwitz 2016; Sievert 2016). It provides interfaces between master and slaves and addresses both data exchange and algorithmic issues. FMI for Co-Simulation consists of two parts (Figure 2):

- Co-Simulation Interface: a set of C functions for controlling the slaves and for data exchange of input and output values as well as status information.

- Co-Simulation Description Schema: defines the structure and content of an XML file. This slave specific XML file contains "static" information about the model (input and output variables, parameters …) and the solver/simulator (capabilities …). The capability flags in the XML file characterize the ability of the slave to support advanced master algorithms which use variable communication step sizes, higher order signal extrapolation etc.
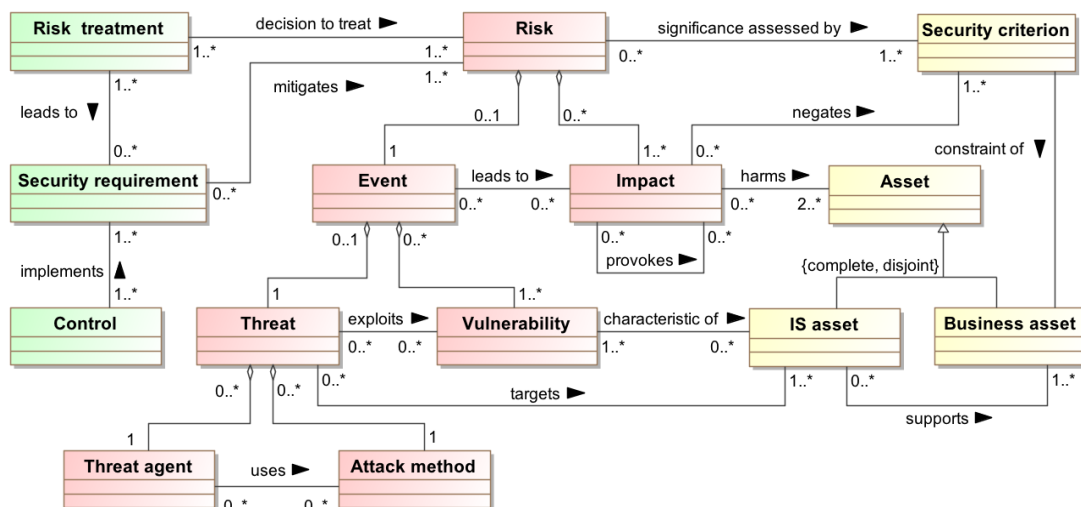

Figure 1: ISSRM Risk Data Model

A component implementing the FMI is called Functional Mock-up Unit (FMU). It consists of one zip file containing the XML description file and the implementation in source or binary form (dynamic library). A master can import an FMU by first reading the model description XML file contained in the zip file. Coupling simulators by FMI for Co-Simulation hides their implementation details and thus can protect intellectual property.
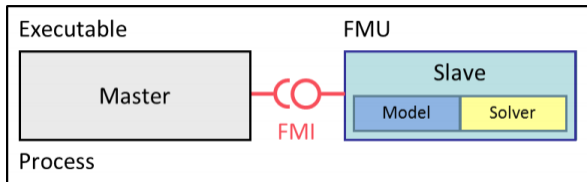

Figure 2: FMU / FMI Concepts

3. CONTRIBUTION

3.1. Integrating risk management in modeling and simulation process

In order to integrate concepts described in section 2.2 one of the first solution was to implement risks treatment directly on models. However, risk management, particularly in renewable energy production domain imply different and complex methodologies and make the modeling too heavy and not systematic for the user.
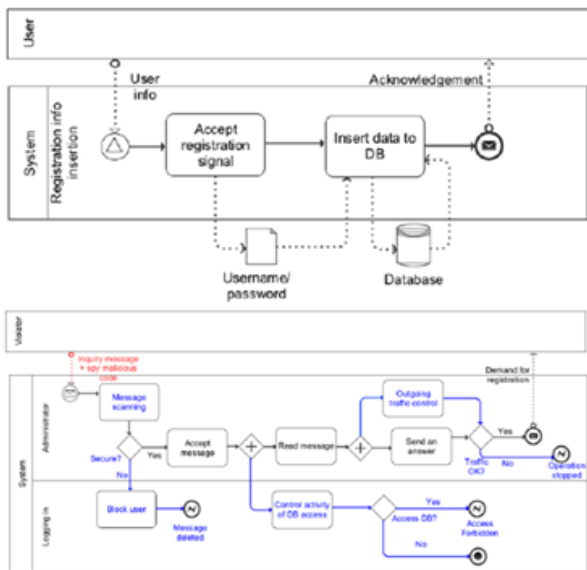

Figure 3: Risks Modeling in BPMN

We can see on the top of the above Figure 3 a BPMN model of a simple database login action between a user and a system. The BPMN diagram at the bottom of Figure 3 represent the same upper model, with risk treatment taken in account: model can be very complex. Modeling and simulation a global solar energy production site with this method of risk management is too complex for user.

According to our subject, we must manage risks depending on several levels:

- A risk can block a task, or it can slow it down (depending on a degree) as described in Figure 4.
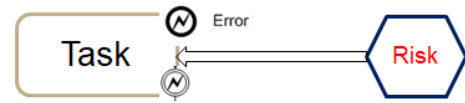
Figure 4. Risk impact on a task

- A risk can influence another one (increase or decrease its impact), it can form a causality chain such as described in Figure 5.

Figure 5. Risk causality chain

- Several risks can be composed to generate or implicate a new hazard as described in Figure 6.
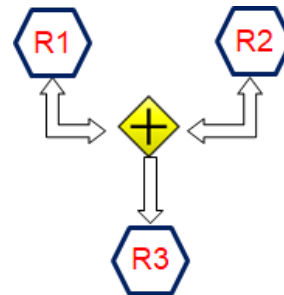
Figure 6: Composed Risk

Those risk management mechanisms appear too complex and heavy for being implemented directly on process model, also the rules can be dependent on the domain studied. It forms the reason why we propose to outsource them from papyrus model designer.

3.2. Proposition

We propose to define an extension to a modeling and simulation tool to include risk treatment separated from the main model. In our case, Papyrus, based on Eclipse, allow user to model UML diagram and, with the mechanism of UML-profiles, enable UML-based diagram modeling like SysML or BPMN. One of the advantages of using Papyrus as a modeling tool is the included MOKA execution engine which make possible to simulate fUML models.

Our goal is to implement an ad-hoc system (Figure 7) to Papyrus in order to manage constraints, risks, and hazards during the simulation execution. This module is able to generate issues in the main system described by the process model. All the potentials issues are generated according to equations defined outside of the process model. This risk management extension is disconnected from the initial model in order to keep it clean (see section 4.1). The global simulation execution will react depending on hazards and constraints generated and referenced by the risk management module (as described in Figure 7).

Figure 7 represents the proposed architecture, we can observe the process model editor and the MOKA execution engine combined into Papyrus, and a connection to an external risk management module. This new module is connected to both Process Modeler and Moka Execution module to interact with them.

The objective of this proposition is to relocate and factorize complex tasks (risk management) during the simulation execution process. This may involve to use a co-simulation standard for insure communication between different external modules. Another way to communicate with the outside is to request web services API. According to this proposition, every type of complex systems can be relocated outside of the model.

Figure 7: Defining and Using Risks in M&S

FMI standard, propose two mechanism: the first is "simulation exchange", the one that we are using in this paper. But the standard propose also "model exchange" mode which could be also implemented in this context. Using FMI as model exchange would means to modeling process into an external FMU and import it in the simulation. However, the MOKA engine could not execute fUML models described in external models.

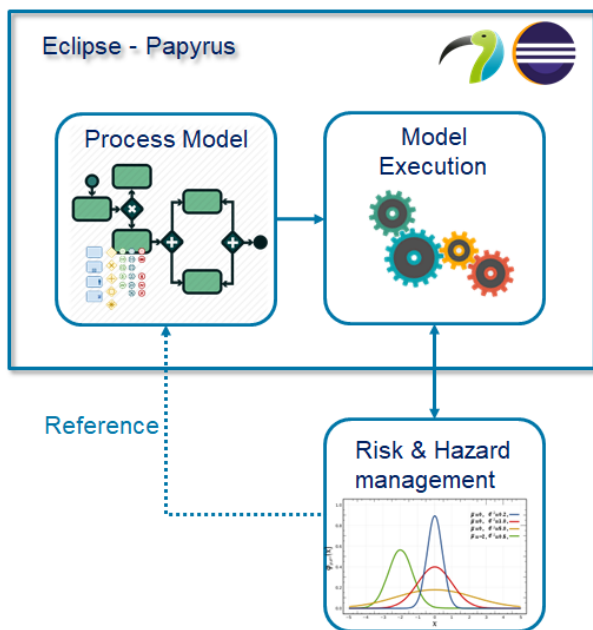## 4. BUSINESS CONTEXT

In our context, a company designing solar power plants has special needs. This project consists in installing solar panels fields to provide electricity and heat in a large area which is not powered so far. However, the transport of solar panels fields is extremely expensive. To reduce this cost/blow, they are designing a mobile factory which will be able to manufacture and assemble the solar panels on site. Rather than transporting finished products, only the mobile plant and raw materials would be carried out. The main challenges of this project are : the factory miniaturization to fit in the least transport containers (around 20) (Benama 2014), risks management (Rodney 2014) caused by low knowledge, and designing resistant

structure depending on the environment of the power plant (Piegay and Breysse 2015), (El Amine 2016).

To guide the project and model the conception process, the company use Papyrus tool. The objective is to create several models for modeling and simulation of all workflow from the deployment of the mobile factory, to the management in real time of the production site. With the implementation of risk management module, the company aim at running simulations for every case possible in order to being able to anticipate and avoid problems.

5. REALISATION

According to (Guermazi et al. 2015), when the MOKA engine execute a fUML model, a mechanism named *visitors* is executed at each steps of the simulation process. This visitor can be surcharged and can execute java code at each steps of the simulation process. This is our entry point to the MOKA engine. During the execution process, at each task parsed by the engine, a visitor is called, we can test the name of the task and have access to his parameters (that is the "Reference" link between "Process Model" and "Risk & Hazard management" in Figure 7). During a global simulation process, the risk management module must know the name of each task of the model for allowing interactions with it.

The entry point of the MOKA engine is a java function. From it, we can integrate a co-simulation environment with Java-FMI. The library allow us to load an FMU file in order to interact with another simulation. In our context, we build a simple FMU which can generate errors in the process model according to a normal law (see Figure 8). In the same time, we are requesting weather information to a web service (OpenWeatherMap). Location is given in input of the API and it return to the visitor weather information. In our context, for a solar system, electricity production yield will be impacted depending on clouds and sunshine.
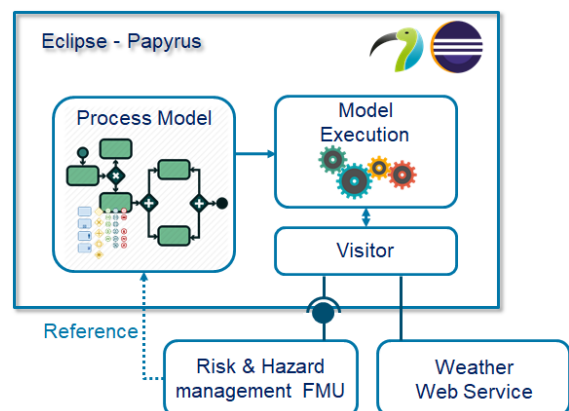

Figure 8: Requesting FMU and Web Service from Papyrus Visitor

Using MOKA engine to execute the models allows us the implementation of preconditions for tasks and resources.

They determine the conditions under which tasks or resources become available for execution in simulation process. Coupling an FMU component with precondition implementation offers a collaborative environment to control the execution of the elements (tasks or resources). For example, limiting elements start only under certain additional conditions calculated by other tools or environment.

As a first step, a new extension of the UML metamodel is created by adding new concepts (classes) and relationships (associations) using profile and stereotype mechanism. In our work we created a specialized object (Failure Element) that suspends the execution of an element (task or resource) based on the mean time between failure indicator and external variables (e.g. weather condition).
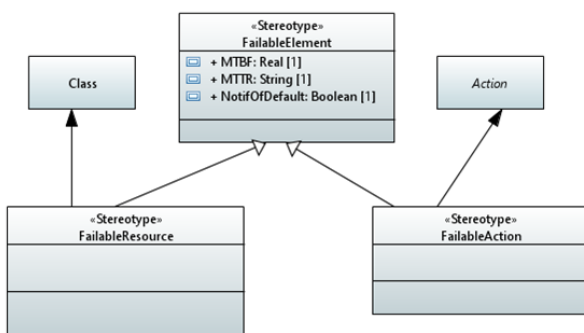

Figure 9: UML Profile describing the new concepts

- FailableAction stereotype: Applied on Tasks (UML actions) with two attributes: (i) Mean Time Between Failure defines the average time (in hours) during an action can be executed before a failure occurs over a specified time period. (ii) Mean Time To Repair represents the average time required to repair a failed action (during this time the task can't be executed). (iii) Notification of Default suspends the execution of the task depending on external variables and indicators.

- FailableResource stereotype: Applied on Resources (UML Class) with three attributes: (i) Mean Time Between Failure defines the average time (in hours) during the resource can be used before a failure occurs over a specified time period. (ii) Mean Time To Repair represents the average time required to repair a failed resource (during this time the resource can't be allowed or used by tasks independently from Availability constraints). (iii) Notification of Default suspends the availability of the resource depending on external variables and indicators.

The second step consists in generating the source code of the profile using the Eclipse Modeling Framework (EMF). The code generator for EMF models can be adjusted and in its default setting. It provides change notification functionality to the model in case of model changes. EMF generates interfaces and a factory to create object.
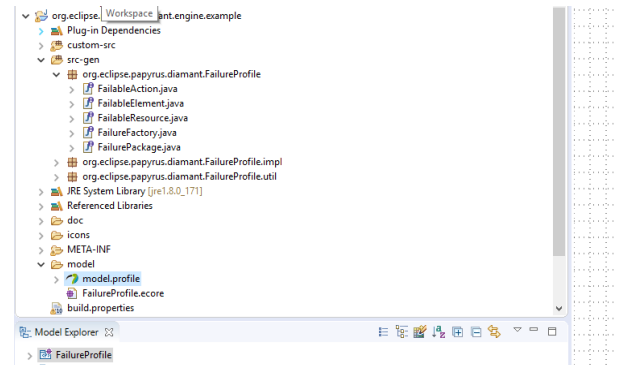
Figure 10: Code generated using EMF

Then, we customize the execution engine by adding the implementation of the new execution engine which associate new Advices to the execution visitors, interacting with a FailureManager. The FailureManager centralized class counting the number of FailableElement executions and activating failures. We also add the implementation of the two advices (advice for FailureResource and advice for FailureAction). The first advice is associated to tasks which use Resources with FailableResource stereotype. It will ask to the failure manager if a task can start or finish and it =will also execute additional start/finish actions for a given task. Concerning the second advice, it is associated to Tasks with the FailableAction stereotype. It verify also on the failure manager if a task can start or finish and is executes additional start/finish actions for a given task. The part that allows to import an FMU and to execute it is implemented within these advices.

6. CONCLUSION

In modeling and simulation domain, many efforts are done to increase reusability and creating bridges between technologies. In this paper we presented a contribution to extend Papyrus execution engine for FMI co-simulation in the context of risk management. The paper demonstrate also the link between BPMN models to risk description. Then these risks characteristics are used at the simulation step.

However, many aspects must be improved for our contest. It is necessary to declare risks and hazards equations linked to our model. Efforts must be done to increase usability of this extension for enable model exchange aspects of FMI.

7. REFERENCES

Altuhhova, Olga, Raimundas Matulevicius, and Naved Ahmed. 2013. "An Extension of BPMN for Security Risk Management." *International Journal of Information System Modeling and Desigh*, January, pp 93-113.

Bastian, Jens, Christoph Clauß, Susann Wolf, and Peter Schneider. 2011. "Master for Co-Simulation Using

FMI." *Proceedings of the 8th International Modelica Conference*, March, 115–20.

Benama, Youssef. 2014. "Supporting Make or Buy Decision for Reconfigurable Manufacturing System, in Multi-Site Context." *Ajaccio, France*, September, 150–58.

Better, Marco, Fred Glover, Garry Kochenberger, and Haibo Wang. 2008. "Simulation Optimization Applications in Risk Management." *International Journal of Information Technology & Decision Making, Vol. 7, No. 4*, 2008, World Scientific Publishing Company edition.

Blochwitz, Torsten. 2016. "Functional Mock-up Interface for Model Exchange and Co-Simulation." https://www.fmi-standard.org/Downloads.

Blochwitz, Torsten, Martin Otter, Johan Åkesson, Martin Arnold, Christoph Clauss, Hilding Elmqvist, Markus Fredrich, et al. 2012. "Functional Mockup Interface 2.0: The Standard for Tool Independent Exchange of Simulation Models." *Proceedings of the 9th International Modelica Conference, Munich, Germany*, January, 173–84.

Camus, Benjamin, Virginie Galtier, Mathieu Caujolle, Vincent Chevrier, Julien Vaubourg, Laurent Ciarletta, and Christine Bourjot. 2016. "Hybrid Co-Simulation of FMUs Using DEV&DESS in MECSYCO." *Symposium on Theory of Modeling & Simulation, Pasadena, USA*, January, 1–8.

Dubois, Eric, Patrick Heumans, Nicolas Mayer, and Raimundas Matulevicius. 2010. "A Systematic Approach to Define the Domain of Information System Security Risk Management, Edit Dubois, Patrick Heymans." *Intentional Perspectives on Information Systems Engineering*, 2010.

El Amine, Mehdi. 2016. "Integration of Concept Maturity in Decision-Making for Engineering Design: An Application to a Solar Collector Development." *Springer-Verlag, London*, October, 235–50.

Guermazi, Sahar, Jérémie Tatibouet, Arnaud Cuccuru, Saadia Dhouib, and Sébastien Gérard. 2015. "Executable Modeling with FUML and Alf in Papyrus: Tooling and Experiments." *EXE MoDELS*, 2015.

IEEE Computer Society. 2003. *IEEE Recommended Practice for Distributed Simulation Engineering and Execution Process*.

IEEE Computer Society. 2010. *IEEE Standard 1516-2010 for M&S - HLA - Framework and Rules*.

http://ieeexplore.ieee.org/stamp/stamp.jsp?arnumber=5553440.

Marcinkowski, Bartosz, and Michal Kuciapski. 2012. "A Business Process Modeling Notation Extension for Risk Handling." *International Conference on Computer Information Systems and Industrial Management*, September, 374–81.

Piegay, Nicolas, and Denys Breysse. 2015. "Multi-Objective Optimization and Decision Aid for Spread Footing Design in Uncertain Environment." *Geotechnical Safety and Risk 5, Rotterdam, the Netherlands*, October, 419–24.

Rodney, Elodie. 2014. "Integrating Risks in Project Management." *16th International Dependency and Structure Modelling, Paris*, June, 419–24.

Sievert, Nicke. 2016. "Modelica Models in a Distributed Environment Using FMI and HLA."

8. AUTHOR BIOGRAPHIES

SIMON GORECKI is Ph.D. Student at University of Bordeaux in IMS Lab. Domain research is about simulating process with distributed simulations and HLA (High Level Architecture). His email address is simon.gorecki@u-bordeaux.fr

YOUSSEF BOUANAN is Postdoctoral researcher at University of Bordeaux. He received his Ph.D. degree in Production Engineering from University of Bordeaux, France. His research interests include M&S Theory, agent-based model and workflow. His email address is youssef.bouanan@u-bordeaux.fr

JUDICAEL RIBAULT is a Ph.D. freelance software architect and associate researcher at University of Bordeaux and IMS Lab. His email address is judicael.ribault@u-bordeaux.fr

GREGORY ZACHAREWICZ is Associate Professor HDR at University of Bordeaux and IMS Lab with both competences in enterprise engineering and M&S. His email address is gregory.zacharewicz@u-bordeaux.fr

NICOLAS PERRY is Full Professor at ParisTech ENSAM of Bordeaux. Domain research is about system engineering, product process integration and green manufacturing. His email address is nicolas.perry@ensam.eu

ON THE GDPR INTRODUCTION IN EU AND ITS IMPACT ON FINANCIAL FRAUD RESEARCH

Edgar Alonso Lopez-Rojas[a], **Dincer Gultemen**[b], and **Erjon Zoto**[c]

[a] ,[b], [c] The Norwegian University of Science and Technology (NTNU)
[a]edgar.lopez@ntnu.no [b]dincer.gultemen@ntnu.no [c]erjon.zoto@ntnu.no

ABSTRACT
With the introduction of GDPR in the European Union (EU) in May 2018, personal data contained within financial records will become even more restricted to researchers due to the strict organisations' internal policies. This is mainly a consequence of the huge fines that will potentially receive the financial institutions that does not comply with GDPR. As a consequence of this, researchers will suffer from getting access to necessary data to develop and implement proper controls and prevention mechanism for fraud in the financial domain.

This paper aims to analyse the impact of GDPR from the financial services perspective regarding the handling of personal data. We argue that the impact for researchers with the introduction of GDPR can be reduced by using simulation of financial transactions as a valid approach that prevent the risk of possessing personal data when doing research with financial data and address, among others, the GDPR article 89(1) on the safeguards for processing or archiving personal data with scientific purposes.

Keywords: GDPR, Synthetic Datasets, Financial Services, Agent Based Simulation, Financial Fraud.

1. INTRODUCTION
The General Data Protection Regulation (GDPR) is a new regulation from the European Union (EU) that replaced the current Directive 95/46/EC with the aim to strength the regulations to protect the EU citizens from privacy and data breaches (The European Parliament and The European Council, 2016). With the introduction of GDPR in Europe, the 25 May 2018, organisations are enforced to follow several rules related with the protection of personal data and the free of movement of personal data. GDPR will cause that personal data contained within financial records become even more restricted to researchers due to the strict organisations' internal policies. This is mainly because of the huge fines that will potentially receive the financial institutions that does not comply with GDPR. As a consequence of this, researchers will suffer from getting access to necessary data to develop and implement proper controls and prevention mechanism for fraud in the fi-

nancial domain.

The main contribution of this paper is in the analysis of the impact of the enforcement of GDPR from the financial services perspective regarding the handling of personal data. Our argumentation explains possible consequences and the impact for researchers with the introduction of GDPR, and we suggest that the negative effect for research can be reduced by using simulation of financial. Simulation of financial data is presented as a valid approach to prevent the risk of possessing personal data when doing research with financial data.

Our suggested approach to deal with GDPR consist in the use of simulation models and tools to generate synthetic datasets to work on fraud detection research within or outside financial organisations. To support our approach we present a compilation of relevant works in the area. Some of the domains covered in this review include mobile money payments, e-payments, retail stores, online bank services and credit card payments.

In this paper we also discuss that there is a need to formalise a method for interaction between organisations and researchers of financial fraud. This method is out of the scope of this paper, but we aim to describe some of the characteristics that such a method should have in order to allow a clean and smooth interaction without any risk of not complying with GDPR.

Outline of the paper The rest of this paper is organised as this: Section 2. introduces the GDPR regulations and relates the topic with financial fraud research. Section 3. summarises previous research in the area of financial fraud research using simulation. We discuss in section 4. the communion of GDPR and simulation tools and finally conclude our work in section 5.

2. GDPR AND FINANCIAL FRAUD RESEARCH
Adopted in April 2016 to come into force in May 2018, and replacing the 1995 Data Protection Directive (DIR95); General Data Protection Regulation (GDPR) regulates the processing and free movement

of personal data (The European Parliament and The European Council, 2016). Accordingly, a data controller (or recipient data processor in case of transfer) of any (research) organisation using personal data is obliged to comply with GDPR.

2.1. GDPR Key changes

The key changes of GDPR in comparison with previous regulations can be summarised in three directions: first, it increases the territorial scope to all companies that handle data from EU residents, regardless of where the company is located; second, it introduces larger penalties (up to 4% of annual global turnover or 20 million euros) for not complying; and third, it extends the conditions on consent of personal data in order to become more clear and distinguishable for the people [1].

Some other important changes regarding the data subjects rights are: breach notifications are now mandatory, all the citizens have the right to access their personal data, they have the right to be forgotten, data portability, privacy by design and finally the incorporation of role of Data Protection Officers (DPO) within the organisations. DPO will play a key role in allowing or blocking research from happening under the GDPR regulations. GDPR includes the basic principles of processing such as consent (Articles 5-11), rights (Articles 12-23) and data transfers (Articles 44-50)

If we only focus in some of the changes of GDPR, such as the risks of larger penalties, the obligation to report data breaches and joint liability (Data Controller-Processor or DCP), the application of GDPR to scientific data has negative impact on researchers-founders willing to provide accessible experimental data and practices such as open interfaces for exchange data repositories, linked data, and meta-data inter-operability. On the other hand, the regulation (Recital 33) has still a room for partial consent to be applied with recognised ethical standards of scientific research, because a complete processing-purpose specification may not be available at the time of collection.

2.2. Pseudoanonymisation and anonymisation

Data-minimisation and pseudoanonymisation based exemptions for scientific-research (Article 89) may still be considered as supportive for open science practices to reduce the cost for repeatable, replicable and reproducible research (Lewis et al., 2017). However, even with this possibility, to make use of scientific research-based justifications we need further evaluation that provides clarification for issues such as pseudoanonymisation and anonymisation. This is important to understand the position of research

---

[1] https://www.eugdpr.org/key-changes.html

ethic committees and transnational collaborative research.

While data processing for pseudoanonymisation aims at personal data non-attributable to a specific data subject, technical organisational measures are also dictated to prevent re-attribution by making use of separately kept additional information (Article 4(5)). By also taking the objective factors (required for a possible identification such as the cost-amount of time and available technology) into consideration; as a safeguard for scientific research, pseudoanonymisation is considered as a measure to prevent direct identification. However, anonymisation remains out of the scope of GDPR by definition of anonymous information as subject non-identifiable data (Recital 26).

In parallel to the decision of Court of Justice of the European Union (CJEU) on IP addresses which are possible to re-attribute with additional information held by Internet Service Providers, the principle of "reasonably likely to be used to identify (by itself or with other information)" may be expected to apply for the sharing of (previously pseudoanonymised) research data, which shall not be counted as personal data. For the cases of "singling out" (Recital 26), causing a person to be regarded as identifiable, such as blockchain use-cases involving encrypted and reference ID based transactions data, financial assets, property registers and smart contracts, the "(reasonably likely) level of identifiability" defined by objective factors will by a large possibility be expected to determine if distributed (previously pseudoanonymised) personal data falls into the scope of GDPR.

In any case, it is clear that the regulatory burden (confidentiality, privacy, criminal offences, data protection) of research will increase dramatically when anonymisation on an individual level may not be possible and while pseudoanonymisation narrows the scope of anonymisation. With the exemption of responding (access-correction-erasure-portability) requests in case that data subjects can not be identifiable, still-personal pseudoanonymised data require privacy impact assessments, the appointment of Data Protection Officer (DPO), processing-records keeping, the demonstration of compliance, and measures against the vulnerability of pseudonymised data against "anonymised information matching" (Mourby et al., 2018).

Thus, from the pseudoanonymisation point of view, the long term protection of personal data may be expected to be never secure enough in the sense that the dynamic level of technology may also cause a dynamic definition for the principle "likely reasonably to be used to identify" and the maintenance of additional information to reverse pseudoanonymisation will impose long-term obligations.

2.3. Internal Regulations

Transaction data are highly useful for social-economic research provided that the negotiation between researchers and data centers on the legal-ethical conditions such as the issues of ownership, intellectual property and personal data is present. While GDPR is providing an exemption for the preservation of transactional data on behalf of public interest, ethical concerns of ethics committees on re-use (and de-identification) of personal data can still impose more stringent requisites than the law requires. Thus, legal-ethical complexity issues can prevent data sharing, even if it is legal.

The cautious approach of data owners can also be partly due to the fact that the size and fragmented nature of transferred data to the researchers are usually not manageable in terms of storage capacity and processing power, thus making the data publicly available fragmented and incomplete (Thomson, 2016). It may then be expected that the data centers will be interested to share the data within a prospective ecosystem where the access to the data will not be easy for individual research.

2.4. Codes of Conduct

For the case of collaborative e-research for transnational cooperation encouraged as a key priority of the European research area, the cross-border exchange of research data and access to data sets should be conducted within the legal framework for the "codes of conduct" introduced by DIR95. While there were no codes of conduct under Article 27 (DIR95), most probably because of lower sanctions for non-compliance, the bio-molecular research initiative 'Code of Conduct on Processing of Personal Data for Purposes of Scientific Research in the Area of Health' (BBMRI-ERIC) is expected to be the first code of conduct under Article 40 of the GDPR.

Purely state-regulated cross-border data transfers requiring jurisdiction-specific compliance tracking, the application of general concepts like such as "public interest, scientific purpose, or appropriate safeguards" may not be effective without self or co-regulation.

Therefore, under GDPR (Article 40) and encouraged by Recital 98, the "codes of conduct" prepared from sector-specific associations can reduce the legal uncertainties such as the scope justification of informed consent during the course of sector-specific research. Otherwise, the excessive emphasis may be expected to decrease the motivation for research dramatically.

A general code of conduct may also be expected to increase the importance of data sharing because a data provider entity needs to ensure the data center collects and processes data in accordance with legal compliance including consent (GDPR Article 7), basic principles (GDPR Article 5), adherence to approved codes of conduct (GDPR Article 24,40), approved certification mechanisms (GDPR Article 42) and the position of DPO in the organisational hierarchy and with respect to research ethics committees (GDPR Article 37).

On the other hand, the data controller of the center also needs to prove the consent and GDPR-compliant processing prior to transfer. Although the preparation and submission of the international codes of conduct by a research specific representing body of controllers could provide a solution for collaborative research, the fragmented research environment organised institutionally by universities, academies, independent research institutions, medical facilities and companies causes an obstacle to represent research discipline to Data Protection Authority (DPA). Also, jurisdictional conflict over scope and applicability are likely over the diverse range of self-regulatory activities (Koščík and Myška, 2018). Despite some initiatives to develop codes of conduct concerning individual research areas, this may create a time gap with negative influence and motivation for prospective research efforts. Besides, the formation of research collaborations may be expected to have members only having organisational maturity in the protection of personal data.

3. SIMULATING FINANCIAL FRAUD FROM REAL WORLD DATASETS

There is a current valid approach in fraud detection which involves the use of simulators to produce enough financial data which contain both the normal behaviour and the fraud behaviour. In a previous survey we found 13 research papers from 19 authors on this field during a period of 5 years, between 2012 and 2016 (Lopez-Rojas and Axelsson, 2016), we also added information about recently interesting research in 2017. Our own previous work represents 7 out of the 13 papers. We intend to show that there are other researchers besides ourselves that are currently working in this area and that are jeopardised by the GDPR law.

The first piece of work in this area is the one presented in the paper (Lopez-Rojas and Axelsson, 2012b). This states the problem of obtaining financial datasets and proposes using synthetic datasets based on simulations. The method used is based on the concept of MABS (Multi Agent Based Simulation). MABS has the benefit that it allows the agents to incorporate similar financial behaviour to the one present in domains such as bank transactions and mobile payments.

Our first implementation of a MABS for financial transaction was a mobile money transactions simulator (Lopez-Rojas and Axelsson, 2012a). This simulator was implemented due to the difficulties to implement a proper fraud detection control on a mobile money system that was under development. This pa-

per was the first to properly present an alternative to the lack of real data problem. The synthetic dataset generated by the simulator was used to test the performance of different machine learning algorithms in finding patterns of money laundering.

The work by (Gaber et al., 2013) presents another similar technique, used to generate synthetic logs for fraud detection. The main difference here was that there were real data available that allowed to calibrate the results and compare their quality. The purpose of this study was to generate testing data that researchers can use to evaluate different approaches.

The fraud in retail stores is a topic related to financial transactions. Our work with the RetSim simulator is presented in several publications that study the implementation of a retail store simulator and several different uses for fraud committed by the staff (Lopez-Rojas et al., 2013; Lopez-Rojas, 2015; Lopez-Rojas and Axelsson, 2015; Lopez-Rojas et al., 2015). The RetSim simulator implements a MABS using the sales database of one of the main shoe retailers in Scandinavia (Lopez-Rojas et al., 2013). In this simulator the agents' behaviour is based not only on a statistical analysis of key performance indicators (like other simulators), but also a social network analysis of the relations between customers and the sales staff of the store. One of the main results of this study is in demonstrating the effectiveness of a simple threshold detection method, which is probably the most popular method for fraud detection (Lopez-Rojas et al., 2015).

The RetSim simulator proved not only to be useful for researchers but also for security officers and managers. The triage process helps security officers to explicitly focus on the fraud that matters, that causes major losses. By using the RetSim simulator, a security officer can implement an experiment with different settings to properly setup a triage model (Lopez-Rojas and Axelsson, 2015). Managers on the other hand are interested in investing in security, but without proper guidance and knowledge about different fraud scenarios it is a guessing game to determine the possible cost of fraud. RetSim was used to generate a variety of diverse fraud scenarios which pictures different forms of fraud in retail store. The scenarios described the different characteristics and the impact on the business allowing a manager to take decisions based on the cost of fraud within the foreseen fraud scenarios (Lopez-Rojas, 2015).

Public databases of financial transactions are almost non existent. We made use of aggregated shared information to build a simulator called BankSim, which implements a MABS of financial payments (Lopez-Rojas and Axelsson, 2014). BankSim is implemented in a similar way as the RetSim simulator using a social network analysis in addition to the statistical one. BankSim is based on the aggregated financial information of payments during

6 months in two main cities in Spain, information provided by a bank in Spain with the purpose of developing applications of different kinds that benefit from this sort of data. This information did not reveal any private customer information because it was aggregated, but was rich enough to build an accurate simulator of financial transactions. The generated synthetic log contained an injected fraud behaviour that was used to test fraud detection methods.

IncidentResponseSim by (Gorton, 2015) is a simulation tool that supports the risk assessment of online banking services. This simulator uses the power of simulation to estimate the economical consequences of current and emerging threats modelled with the aid of an incident response tree in combination with a qualitative model.

The work by (Rieke et al., 2013; Zhdanova et al., 2014) on fraud detection in mobile payments is done in a similar domain as our work and other authors reviewed (Lopez-Rojas and Axelsson, 2012b; Gaber et al., 2013). Rieke et al. uses a tool named Predictive Security Analyzer (PSA) with the purpose of identifying cases of fraud in a stream of events from a mobile money transfer service (Rieke et al., 2013). PSA is based on a dataset of 4.5 million log entries from a mobile money service over a period of 9 months. They use simulation due to the limited number of fraud examples in the period in question, and also their imperfect knowledge of existing fraud in the same period. The main focus on PSA is to detect money laundering cases that are perpetrated by the interaction of several users of the system in an attempt to disguise the fraud among the normal behaviour of the clients. As a result the paper shows that the PSA is able to efficiently detect suspicious cases of money launder with the aim of automatically block the fraudulent transactions.

(Zhdanova et al., 2014) presents a continuation of the work done by (Rieke et al., 2013) and uses the simulator developed by (Gaber et al., 2013) to evaluate the results. Semi-supervised and unsupervised detection methods are applied to a mobile money dataset due to the advantage over supervised methods in this type of data where there is a difficulty in having a training data with known cases of fraud.

(Malekian and Hashemi, 2013) worked on a fraud detection method that handles the concept drift of e-payments. The author used simulation due to lack of real credit card data for testing. This simulator aims to build customers profiles that contain seasonal and weekly patterns. The idea behind is to detect when a customer behaviour differs from the historic pattern. With the introduction of concept drift detection on e-payments the results showed a substantial reduction in the false positives cases.

(Alexandre and Balsa, 2015, 2016) present a method for detecting fraud using intelligent agents that perform the tasks that a security officer does

manually on a limited amount of data. The advantages are that the logic included in the agents allows them to perform well at this tasks. They also used simulated data to evaluate the performance of their methods. The main achievements or this research is that they managed to automatise the otherwise hand labour work of flagging suspicious transactions through a well defined set of autonomous agents.

(Zintgraf et al., 2017) developed MultiMAuS. MultiMAuS is an agent-based simulator for payment transactions, intended for the analysis and development of dynamic on-line fraud detection methods via a multi-modal user authentication system. The multi-modal authentication procedure allows for a flexible number of authentication steps a user has to do before a transaction is processed (or rejected). It can thus adapt to the risk associated with a certain transaction, in the context of a given user. This simulator was based on real-world credit card transaction data that realistically model customer behaviour. The simulator can be used to study short and long term consequences of fraud detection and control algorithms, under different settings.

4. Discussion on GDPR and simulation

Although GDPR seems to apply some positive discrimination towards the scientific research, it may be observed that the provided space can hardly balance the concern caused from the risks of large penalties, the obligation to report data breaches, joint liability, the concerns of ethics committees which usually exceeds legal requirements, the difficulty to obtain anonymised data while pseudonymised data is still personal, and the difficulty in providing the codes of conduct providing a clarified know-how on the use of personal data. Therefore, some innovation may be required for the sake of science itself.

The very basic challenge is to obtain synthetic data that are able to reflect the reality after it is been processed. Although the applications are not mature yet, the use of simulation tools on the replication of real data still deserves to be focused with the motivation to balance the concerns mentioned in section 2..

Assuming that we have the original data, just the processing of the algorithms on personal data has implications. The purpose of limitation restricts the use of collected data for a reason different than the one originally presented. Additional controls must be also incorporated to prevent any data leak (Datatilsynet, 2018).

Many of the previous works in financial simulation presented earlier benefit from not being affected by the GDPR enforcement. The role of the Data Protection Officer (DPO) was not implemented when this happened. Personal data was in most of the cases anonymised but none of the procedures for handling personal data were implemented. This leads us

to think that a method that allows interaction between the organisations and researchers is needed to ensure that none of the GDPR articles are broken.

There is indeed a requirement to define a method that can be suitable to use between financial institutions and researchers. Some of the characteristics of any proposed method can be enumerated here:

- Researchers outside the organisation should not have direct access or store any personal data.

- Clear interfaces that can generate proper inputs for the simulator and a validation of resemblance .

- A proper way to validate the output of the simulator and the resemblance with the original data.

- A way to communicate the methods or techniques researched to be applied on the real data set. .

- Feedback from the impact of the methods of techniques that allow researchers to correct any possible deviation or certify the effectiveness of their methods.

Simulation tools have the benefit to be able to fulfil most of the characteristics presented above. We leave out of the scope of this paper the definition of the mentioned method and encourage the reader to propose a valid approach.

5. CONCLUSIONS

The GDPR introduction in the European Union is not the end of financial fraud research. Although GDPR seems to apply some positive discrimination towards the scientific research, it may be observed that the provided space can hardly balance the concern caused from the risks of large penalties, the obligation to report data breaches, joint liability, the concerns of ethics committees which usually exceeds legal requirements, the difficulty to obtain anonymised data while pseudonymised data is still personal, and the difficulty in providing the codes of conduct providing a clarified know-how on the use of personal data. Therefore, some innovation may be required for the sake of science itself.

The very basic challenge is to obtain synthetic data able to reflect the reality after it is processed. Although the applications are not mature yet, the use of simulation tools on the replication of real data still deserves to be focused with the motivation to balance the concerns mentioned above.

Our suggested approach to deal with GDPR consists in the use of simulation to generate synthetic datasets in order to work on fraud detection research

within or outside financial organisations. To support our approach we present a compilation of relevant works in the area. Some of the domains covered in this review include mobile money payments, e-payments, retail stores, online bank services and credit card payments.

Future work will focus on two main aspects: first, to monitor the impact of GDPR for financial fraud research after the enforcement; and second to develop a method that complies with GDPR and that is comprehensive enough to be understood by the DPO within the organisations and at the same time reliable for research in financial fraud.

References

Claudio Alexandre and Joao Balsa. Integrating client profiling in an anti-money laundering multi-agent based system. In *World Conference on Information Systems and Technologies*, pages 931–941, Recife, Brazil, 2016.

Claudio Reginaldo Alexandre and João Balsa. A multiagent based approach to money laundering detection and prevention. In *International Conference on Agents and Artificial Intelligence*, number April 2016, pages 230–235, 2015. doi: 10.13140/2.1.2227.2327.

The Norwegian Data Protection Authority Datatilsynet. Artificial intelligence and privacy. Technical report, Datatilsynet, The Norwegian Data Protection Authority, 01 2018.

Chrystel Gaber, Baptiste Hemery, Mohammed Achemlal, Marc Pasquet, and Pascal Urien. Synthetic logs generator for fraud detection in mobile transfer services. In *2013 International Conference on Collaboration Technologies and Systems (CTS)*, pages 174–179. IEEE, may 2013. ISBN 978-1-4673-6404-1. doi: 10.1109/CTS.2013.6567225.

Dan Gorton. IncidentResponseSim: An agent-based simulation tool for risk management of online Fraud. In Sonja Buchegger and Mads Dam, editors, *Lecture Notes in Computer Science (including subseries Lecture Notes in Artificial Intelligence and Lecture Notes in Bioinformatics)*,

volume 9417 of *Lecture Notes in Computer Science*, pages 172–187, Cham, 2015. Springer International Publishing. ISBN 978-3-319-26501-8. doi: 10.1007/978-3-319-26502-5.

Michal Koščík and Matěj Myška. Data protection and codes of conduct in collaborative research. *International Review of Law, Computers & Technology*, pages 1–14, 2018.

Dave Lewis, Joss Moorkens, and Kaniz Fatema. Integrating the management of personal data protection and open science with research ethics. In *Proceedings of the First ACL Workshop on Ethics in Natural Language Processing*, pages 60–65, 2017.

Edgar Lopez-Rojas and Stefan Axelsson. Multi agent based simulation (mabs) of financial transactions for anti money laundering (aml). In Audun Josang and Bengt Carlsson, editors, *Nordic Conference on Secure IT Systems*, pages 25–32, Karlskrona, 2012a.

Edgar Lopez-Rojas, Dan Gorton, and Stefan Axelsson. Using the RetSim simulator for fraud detection research. *International Journal of Simulation and Process Modelling*, 10(2):144, 2015.

Edgar Alonso Lopez-Rojas. Extending the RetSim Simulator for Estimating the Cost of fraud in the Retail Store Domain. In *The 27th European Modeling and Simulation Symposium-EMSS, Bergeggi, Italy*, 2015.

Edgar Alonso Lopez-Rojas and Stefan Axelsson. Money Laundering Detection using Synthetic Data. In Julien Karlsson, Lars ; Bidot, editor, *The 27th workshop of (SAIS)*, pages 33–40, Örebro, 2012b. Linköping University Electronic Press.

Edgar Alonso Lopez-Rojas and Stefan Axelsson. Social Simulation of Commercial and Financial Behaviour for Fraud Detection Research. In *Advances in Computational Social Science and Social Simulation*, Barcelona, 2014. ISBN 9789172952782.

Edgar Alonso Lopez-Rojas and Stefan Axelsson. Using the RetSim Fraud Simulation Tool to set Thresholds for Triage of Retail Fraud. In *20th Nordic Conference on Secure IT Systems, NordSec 2015*, pages 156–171, Stockholm, 2015. Springer.

Edgar Alonso Lopez-Rojas and Stefan Axelsson. A Review of Computer Simulation for Fraud Detection Research in Financial Datasets. In *Future Technologies Conference, San Francisco, USA*, 2016.

Edgar Alonso Lopez-Rojas, Stefan Axelsson, and Dan Gorton. RetSim: A Shoe Store Agent-Based

Simulation for Fraud Detection. *The 25th European Modeling and Simulation Symposium*, 2013. (Best Paper Award).

Donia Malekian and Mahmoud Reza Hashemi. An adaptive profile based fraud detection framework for handling concept drift. In *2013 10th International ISC Conference on Information Security and Cryptology (ISCISC)*, pages 1–6. IEEE, aug 2013. ISBN 978-1-4799-1638-2. doi: 10.1109/ISCISC.2013.6767338.

Miranda Mourby, Elaine Mackey, Mark Elliot, Heather Gowans, Susan E Wallace, Jessica Bell, Hannah Smith, Stergios Aidinlis, and Jane Kaye. Are 'pseudonymised'data always personal data? implications of the gdpr for administrative data research in the uk. *Computer Law & Security Review*, 34(2):222–233, 2018.

Roland Rieke, Maria Zhdanova, Jurgen Repp, Romain Giot, and Chrystel Gaber. Fraud Detection in Mobile Payments Utilizing Process Behavior Analysis. In *2013 International Conference on Availability, Reliability and Security*, pages 662–669. IEEE, sep 2013. ISBN 978-0-7695-5008-4. doi: 10.1109/ARES.2013.87.

The European Parliament and The European Council. General Data Protection Regulation. *Official Journal of the European Union*, 2016. ISSN 1098-6596. doi: http://eur-lex.europa.eu/pri/en/oj/dat/2003/l_285/l_28520031101en00330037.pdf.

Sara Day Thomson. Preserving transactional data: Defining the challenges. *International Journal of Digital Curation*, 11(2):126–137, 2016.

Maria Zhdanova, Jurgen Repp, Roland Rieke, Chrystel Gaber, and Baptiste Hemery. No Smurfs: Revealing Fraud Chains in Mobile Money Transfers. In *2014 Ninth International Conference on Availability, Reliability and Security*, pages 11–20. IEEE, sep 2014. ISBN 9781479942237. doi: 10.1109/ARES.2014.10.

Luisa M Zintgraf, Edgar Alonso Lopez-Rojas, Diederik Roijers, and Ann Nowe. Multimaus: A multi-modal authentication simulator for fraud detection research. In *The 29th European Modeling and Simulation Symposium-EMSS, Barcelona, Spain*, 2017.

AUTHORS BIOGRAPHY

Dr. Edgar A. Lopez-Rojas

Edgar Lopez-Rojas is currently a post doctoral researcher at the Digital Forensics group at NTNU in Gjøvik, Norway. Edgar obtained his PhD in Computer Science at Blekinge Institute of Technology and his research area is fraud detection and related interest topics: Multi-Agent Based Simulation, Machine Learning techniques with applied Visualisation in the domain of retail stores, mobile payments and Anti Money Laundering (AML) for financial transactions. Edgar has a Bachelors degree in Computer Science from EAFIT University in Colombia and a Masters degree in Computer Science from Linköping University in Sweden.

Dincer Gultemen

Dincer Gultemen is currently a PhD student at the Digital Forensics group at NTNU in Gjøvik, Norway. He is enrolled as ITN in the ESSENTIAL "Evolving Security SciencE through Networked Technologies, Information policy And Law" project: 722482 funded by the European Research Council.

Dr. Erjon Zoto

Erjon Zoto is currently a post doctoral fellow researcher under the ERCIM 'Alain Bensoussan' Fellowship Programme, hosted by the Information Security and Privacy Management group at NTNU in Gjøvik, Norway. Erjon obtained his PhD in Information Systems at the University of Tirana, Albania, and his current research area is information security economics and related interest topics: Agent-Based Simulation and Modelling, Systems thinking and Adversarial Thinking. Erjon has a Bachelor degree in Economic Informatics from University of Tirana and a joint Masters degree in European Economic Studies from University of Tirana and Bamberg University in Germany.

SIMULATION OF PRODUCTION LINE IMPROVEMENTS IN PANELISED FLOOR MANUFACTURING

Jingwen Wang(a), Xianfei Yin(b), Yichen Tian(c), Xinming Li(d), Mohamed Al-Hussein(e)

(a),(b),(c),(e)Nasseri School of Building Science and Engineering, University of Alberta, Edmonton, Canada
(d)Department of Mechanical Engineering, University of Alberta, Edmonton, Canada

(a)jingwen7@ualberta.ca, (b)xianfei@ualberta.ca, (c)ytian4@ualberta.ca,
(d)xinming.li@ualberta.ca, (e)malhussein@ualberta.ca

ABSTRACT

The prefabricated building process offers undeniable advantages and benefits over conventional building techniques. However, the production process for panelised homes is highly variable and the production time for a single home can vary significantly. This paper presents a case study of an established panelised home manufacturer. In the current state, their floor panel production line is identified as having a lower productivity than the rest of the production line, and thus is an area with potential for improvement. To complement the onsite observation, video recordings are captured of the production area, which allows for the collection of more detailed data. The use of simulation will be investigated in this paper to model a floor panel production line in a panelised home manufacturing facility. After evaluating the current-state performance, several proposed changes will be validated in terms of whether or not they should be implemented in the case study manufacturing facility.

Keywords: production line performance, simulation, panelised construction manufacturing

1. INTRODUCTION

Prefabricated buildings have become a popular construction method for building contractors. The panelised home is one of many prefabricated building methods. Panelised wood-framed homes are well received in North America given the solid material properties and economic efficiency of wood. Within the panelised home manufacturing facility, the various parts of the house are constructed separately, including floor panels, wall panels, and roof panels. They are then transported to the construction site to be assembled into various types of houses.

This paper focuses on the floor-panel production line of the panelised wood-framed home manufacturing process, since the floor panel production line has a lower production rate than other lines in the case study facility. The floor-panel production line presented in Figure 1 is composed of one multi-function bridge (MFB) and two tables that work simultaneously from 7:00 a.m. to 2:30 a.m. every workday. Depending on the time of day, the number of workers may differ. During the day shift, 2 workers work together at each table, which makes the duration of each process shorter than the night shift when there is only one worker at each table. In this manufacturing facility, the floor-panel production process generally follows 6 steps to complete one floor panel, including the layout of the floor frame, gluing with/without the MFB, sheathing, nailing and routering by the MFB, load preparation, and loading process. Quality checking and manual sawing processes are necessary in the production of some floor panels depending on the specific jobs. A single overhead crane is involved in the floor manufacturing process, which conducts material handling, finished floor transferring, and other lifting tasks. Both the MFB and crane are shared resources in this floor panel production process. In this paper, the use of simulation to model a floor panel fabrication line in a panelised home manufacturing facility is investigated to assist management in providing strategies for implementation of the proposed changes for production line improvement. Since the use of the crane in this area has been identified by management as a potential area of improvement, a current-state simulation model is presented as well as the future-state simulation with resource adjustments on the number of cranes.

The research methodology for modelling this production line process is presented in Figure 2. The input data are extracted from the plant observation records, video records and company's production schedule data. Input modelling process is conducted after the data collection, which is to clean the data and fit them into certain distributions. Next, simulation model is developed, and multiple runs are implemented for the comparison purpose. Then, output analysis is conducted to assist in the decision-making process. Last, data validation and verification process is carried out to prove the accuracy of the simulation model.

(a)

(b)

Figure 1: Floor Panel Production Line: (a) North Table; (b) South Table
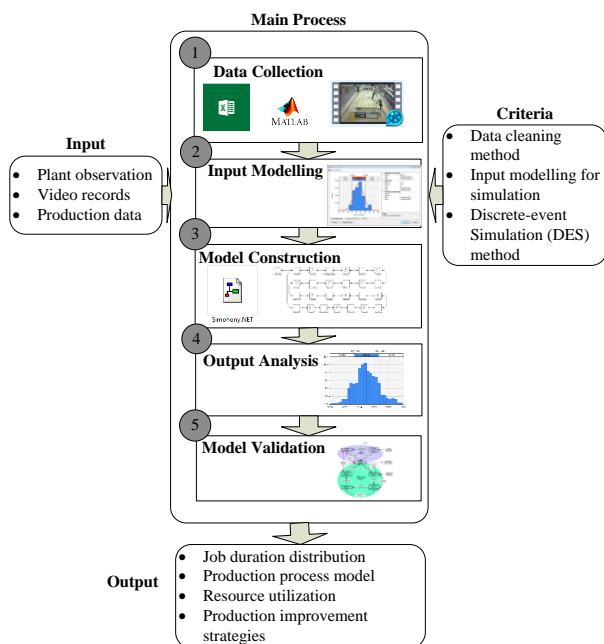

Figure 2: Research Methodology

2. LITERATURE REVIEW

Many studies have focused on various aspects of modular buildings. Retik and Warszawski (1994) attempted to find an effective way to automatically design modular buildings. Neelamkavil (2009) reviewed several automation technologies relevant to modular construction and outlined the technologies that comprise prefab automation. Yu et al. (2013) applied lean production methods in the modular building

process to improve productivity and reduce waste. The results of these studies have bolstered the development of the modular construction industry.

There is a long history of using simulation technology in construction since the emergence of larger and more complex projects, which are difficult for managers or engineers to manage manually. Managers and engineers can use these simulation tools as an effective way to design and analyse the construction process regardless of the complexity and size (AbouRizk 2010). Simulation technology is more applicable in projects that are repetitive and cyclic in nature. It can help managers to gain a better understanding of the interdependencies among various construction projects. An integrated simulation-based optimisation framework was developed within a High Performance Computing (HPC) platform by Salimi et al. (2018) in order to optimise the relationship between cost and time in complex bridge construction projects. The performance of the framework was tested in a bridge construction study.

Substantial researches conducted on the simulation of manufacturing system, in order to optimize the production process and increase the productivity (Negahban & Smith, 2014). A simulation model integrated with dispatching rules and genetic algorithms was developed to facilitate the decision making and problem solving for short period production planning, which turns out to be profitable for the company in Longo's (2013) research. Another research that combines the line balancing and discrete event simulation model to improve the productivity of existing production line by almost 400% (Zupan & Herakovic, 2015). It has been proved that simulation is a flexible and powerful tool in the design and optimization of manufacturing systems (Smith, 2003).

As for modular construction, a study conducted by Altaf et al. (2018) combined radio frequency identification (RFID) technology, data mining, and simulation-based optimisation to build an operation and management system for a panelised wall production line. RFID was used to collect real-time data from the production line, and the data was then cleaned with the data mining method; finally, the processed data was implemented to simulate the production process in Simphony.Net in order to assist management in creating a scientific and effective production schedule. Also, in order to improve the work at a modular construction assembly yard, an integrated model was developed to assist with the time-dependent resource leveling, effective allocation of the yard space, utilisation of scheduling templates for high-level planning, and production of colour-coded layouts and other visual outputs (Taghaddos et al. 2014). Risk management of modular construction in terms of engineering, occupational, cultural, socio-economic, and financial can also be simulated by the computer-based simulation model, which can help stakeholders to identify the primary risks in this particular construction process (Li et al. 2013). Therefore, the benefits of simulation-aided management in the manufacturing

industries motivate this study of implementing simulation in the panelised manufacturing.

3. DATA COLLECTION AND ASSUMPTIONS

3.1. Data collection
For construction manufacturing, the procurement of accurate data for each operation process is a challenge since limited automated data-collection systems applied. Due to the labour-intensive operations in construction manufacturing, a more accurate form of data collection involves the assistance of video recordings, which was previously considered a difficult data-collection method due to the increased amount of data processing that is required using this method, and due to the lack of direct communication with the workers who are being recorded. The detailed steps involved in each task are determined through observation in order to better represent the manufacturing process in the simulation model. As mentioned above, six different tasks are necessary to complete one floor panel at each table, including the layout, gluing with/without MFB, sheathing, MFB process, load preparation, and loading process. A time study was implemented for this panelised floor manufacturing by collecting the detailed tasks processing times using a typical time study template. By observing over 150 working hr of video recordings, the start time and finish time of each task is collected as well as any delay or interruption time between or during those tasks. 137 sets of recorded data detailing the full floor-panel assembly process are implemented as model input data to determine the floor manufacturing method in the case study plant.

3.2. Assumptions
Due to the data collection strategy, various distributions fitted with the observations are used to determine the task durations in constructing the model in Simphony.Net (AbouRizk et al. 2016). The durations of six main tasks as well as two secondary tasks, manually saw process and quality check, are individually stored and imported into Simphony.Net for data distribution fitting process. The method of least squares combined with the lowest score of the Kolmogorov-Smirnov test are implemented to find the best fitting distributions for the following operation processes listed in Table 1. Quantile-Quantile plots also take into account to ensure the accuracy of the fitted distributions. The time distributions for main floor manufacturing process is presented in Table 1. Two types of floor panel sizes, large and small, are considered individually in the simulation. Large floor panel is defined as over 60% of floor panel assembly table covered in this case study based on the observations and the consultation with the experts.

The number of crews in the model is determined based on the observation and crew schedule. Typically, 5 workers are assigned to the floor panel manufacturing line, including 2 workers at each table for the first 4 tasks and 1 worker to control the crane for load preparation, the loading process, and any material lifting tasks. The current labour requirement of each task is presented in Table 2. The model represents a relative ideal situation since the delay time between each task and the interruption time for each activity, such as the discussion between workers and reading the drawings, are not considered in this case. For the future-state model, an additional crane is added without changing other resources or model layout.

Table 1: Time Distributions for Main Manufacturing Process

Processes	Small panels	Large panels
Layout	Beta (1.731, 5.175, 335, 8502)	Beta (1.483, 6.185, 215, 6071)
Gluing (manually)	Beta (1.396, 9.110, 32, 1029)	Gamma (3.618, 57.440)
Gluing (with MFB)	Uniform (120.444, 134.055)	Log Normal (5.325, 0.418)
Sheathing	Gamma (6.316, 82.381)	Weibull (2.389, 767.677, 767.677)
MFB	Log Normal (6.584, 0.284)	Weibull (1.802, 580.679, 580.679)
Saw manually	Uniform (0, 363.541)	Log Normal (4.772, 0.871)
Quality check	Uniform (33.123, 210.652)	Beta (0.544, 1.451, 20, 551)
Load preparation	Log Normal (5.804, 0.482)	Gamma (9.786, 31.105)
Loading	Beta (1.447, 1.499, 118, 489)	Log Normal (5.616, 0.444)

Table 2: Labour Resources Assignment and Shift Schedule
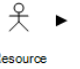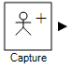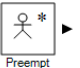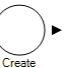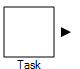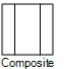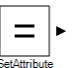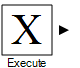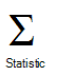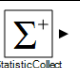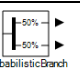
Processes	Day shift	Night shift
Layout	2	1
Gluing	1	1
Sheathing	2	1
Saw manually	1	1
Quality check	1	1
Load preparation	1	1
Loading	1	1

4. MODEL DESCRIPTION
The current-state model represents the relative ideal situation of the panelised floor production line. The future-state model involves the proposed improvements to test the influence on the floor production line. Since the time for each activity is accurate to the second, the time unit for the entire model is measured in seconds. The maximum run time for this model is 20 workdays, which is 1,512,000 seconds. Multiple runs must be conducted since the model is stochastic. In this case, after several experiments such as 100 runs, 200 runs, 300 runs, and 400 runs, have been conducted, 500 runs are finally applied to the model for output analysis due

to simulation time control and results stabilisation. The various elements used in the simulation model are provided in Table 3 (AbouRizk et al. 2016).

Table 3: Clarification of Simulation Elements

Resource	Represents a resource with a specified number of servers
File	A file where entities wait for resources
Capture	Allows an entity to request servers of one or more resources
Release	Allows an entity to release servers of one or more resources
Preempt	Allows an entity to preempt a single server of a resource
Create	Creates entities
Task	Delays entities by a specified amount
Composite	A container for other elements that allows a modelling hierarchy to be created
SetAttribute	Sets one or more attributes to an entity
Execute	Executes a formula when an entity passes through
Counter	Counts the number of entities passing through the elements
Destroy	Destroys entities
Statistic	A statistic that can collect numerical observations
StatisticCollect	Collect observations for a specified statistic
ConditionalBranch	Allows an entity to take one of two paths depending on a specified condition
ProbabilisticBranch	Allows an entity to take one of multiple paths depending on specified probabilities

The resources in the floor production simulation model include north table, south table, crane, MFB, workers for north table, and workers for south table. The number of servers is assigned to each resource based on the actual case. For activities that are resources dependent, the appropriate resources and the number of servers will be assigned to the activity. When entity passes the activity, the corresponding number of resources will be captured by the entity. The captured resources will be released when the activity is finished. If the resource required by the activity is in use, the entity will wait in queue until the resource is available. Figure 3 presents the necessary resources for the proposed model.
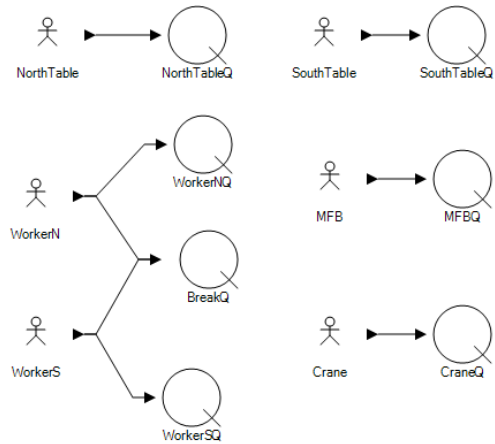
Figure 3: Resources and Queue Files for Floor Production Simulation Model

In the manufacturing process, two tables, which are independent of one another, are used to assemble the floor panels. Therefore, two cycles are developed in this model, namely the north table cycle and south table cycle. 1,000 entities are created during each cycle to ensure there are enough entities to complete the cycle within the maximum simulation time. There are two types of panel sizes, large and small. The size of the panel is assigned using a probability branch (tree diagram), and a local variable is assigned to each panel in order to separate the different panel sizes.

On this floor panel manufacturing line, workers are assigned one of two shifts. During the daytime shift (7:00 a.m. to 5:30 p.m.), two workers work together to assemble one panel at each table. During the night shift (4:00 p.m. to 2:30 a.m.), there is only one worker at each table to assembles each floor panel. The main activities to produce a floor panel include frame layout, gluing (which can be conducted manually or using the MFB), sheathing, the MFB process (which includes cutting and drilling), cleaning the MFB track, quality checking (QC), load preparation, and the loading process. Other activities which may occur occasionally are QC after the panel layout and manual sawing after the MFB process. Also, the panel will occasionally be transferred to a storage area before it is loaded onto the trailer. Activities which only sometimes occur are simulated using a probability branch. Difference distributions for the activity durations function as inputs to the model. The cycle times for both the north table and the south table will be calculated using the statistic element and the number of panels assembled at each table will be counted using the counter element. Figure 4 presents the layout of the floor line simulation model.

(a)

(b)
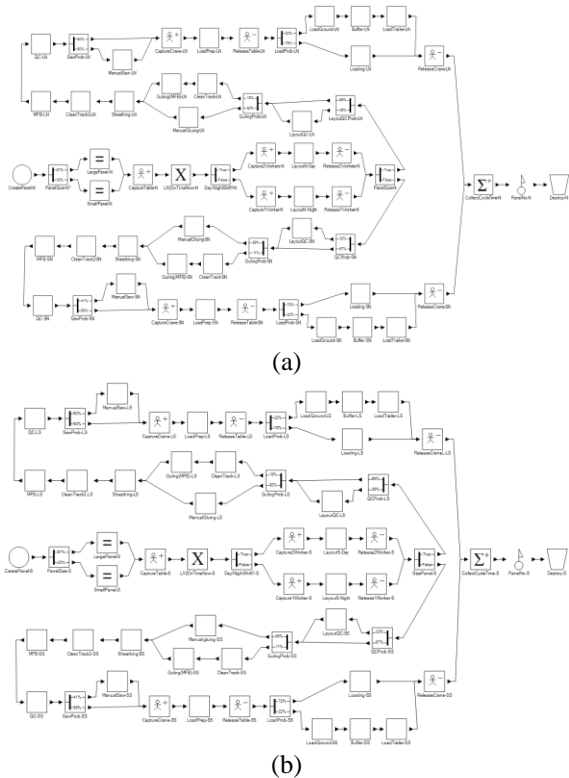
Figure 4: Main Layout of Floor Line Simulation Model:
(a) North Table; (b) South Table

There are three primary crane functions: (1) loading of panels onto the transport trailers, or to the temporary storage area in cases when the trailer is full; (2) transporting other materials within the plant; (3) and adjusting the panel layouts at the assembly tables. The material moving and layout adjusting crane functions are given higher priority than the panel loading function. Therefore, material moving and layout adjusting will be executed first than panel loading if crane is available. Since loading panels is the only crane activity for the north table cycle and south table cycle, a crane cycle is developed for any crane use other than for loading panels. Figure 5 demonstrates the crane cycle.
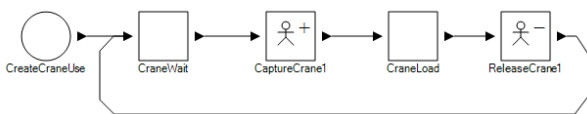
Figure 5: Crane Cycle in Floor Production Simulation Model

The model also includes the shift and break schedule for workers. Separate cycles are created for shifts and breaks, which allows work to be left in progress at break times. Both the day shift and night shift are 10 hours in length with a total of three breaks per shift. Day shift breaks include a 15-minute morning break, a 30-minute lunch break, and a 15-minute afternoon break, and the night shift includes two 15-minute breaks and a 30-minute meal break. The model will capture the resources and halt work during breaks. Figure 6

presents the shift schedule and Figure 7 presents the break schedule.
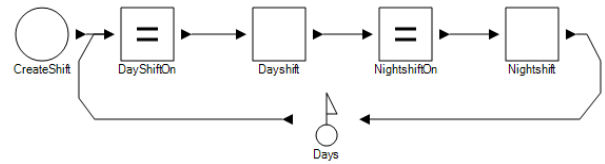
Figure 6: Shift Cycle for Floor Production Simulation Model
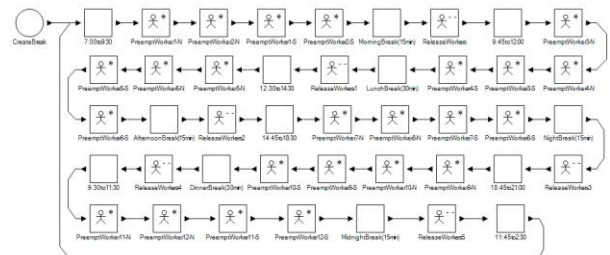
Figure 7: Break Cycle for Floor Production Simulation Model

5. OUTPUT ANALYSIS

The output of the simulation model for the floor production line is summarised by the statistics report in Simphony.Net. The output statistics include the utilisation of each resource, the cycle times for each table, the number of panels assembled at each table. The results of 500 runs of the simulation model are summarised in Tables 4, 5, and 6.

Table 4: Resource Utilisation for Current-state Model

Resources	Average Utilisation	Standard Deviation
Crane	79.00%	1.20%
MFB	31.30%	0.60%
North Table	100.00%	0.00%
South Table	100.00%	0.00%
Worker (North)	50.90%	0.70%
Worker (South)	57.30%	0.70%

Table 5: Cycle Time for North Table and South Table in Base Model

Cycle time	Mean Value (Seconds)	Standard Deviation	Mean Value (Hr)	Standard Deviation
North	7,526.61	163.98	2.09	0.0456
South	7,686.62	168.57	2.14	0.0468

Table 6: Number of Panels Assembled at North Table and South Table in Base Model

Table	Number of Panels (20 days)	Number of Panels (per days)
North	232	11.60
South	237	11.85
Total	469	23.45

In the current-state simulation, only one server is used for the crane resource, and the crane utilisation is 79.0%. The average waiting time for crane queue is 529 seconds. As can be seen in Table 6, in 20 days, 232 panels are assembled on the north table and 237 panels are assembled on the south table. The average cycle time for the north table and the south table are 2.09 hr and 2.14 hr, respectively. Figure 8 and Figure 9 present the relative frequency of cycle time after 500 runs for north table and south table, respectively, both of which reveal a relatively normal distribution.
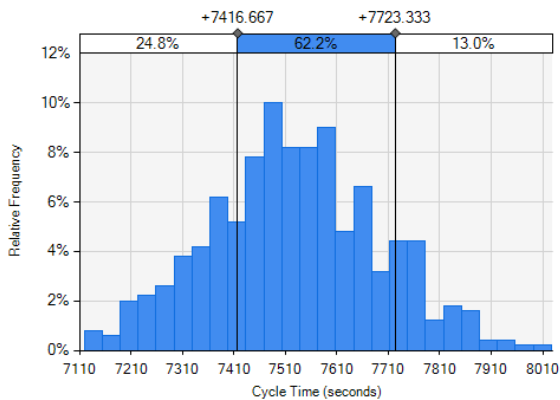
Figure 8: Cycle Time of North Table for Base Model after 500 Runs
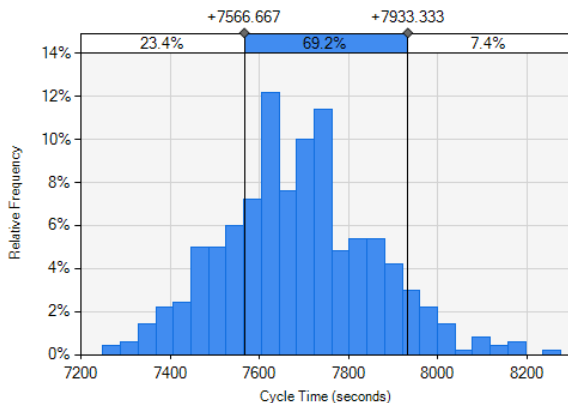
Figure 9: Cycle Time of South Table for Base Model after 500 Runs

In the future-state model, the server of crane resources changes to 2. The statistics presented in Tables 7, 8, and 9 demonstrate the results after 500 runs for an improved model.

Table 7: Resource Utilisation for Improved Model

Resources	Average Utilisation	Standard Deviation
Crane	50.40%	1.20%
MFB	35.20%	0.50%
North Table	100.00%	0.00%
South Table	100.00%	0.00%
Worker (North)	56.00%	0.50%
Worker (South)	51.20%	0.60%

Table 8: Cycle Time for North Table and South Table in Improved Model

Cycle time	Mean Value (Seconds)	Standard Deviation	Mean Value (Hr)	Standard Deviation
North	6,771.00	116.92	1.89	0.0325
South	7,021.36	127.72	1.95	0.0355

Table 9: Number of Panels Assembled at North Table and South Table in Improved Model

Table	Number of Panels (20 days)	Number of Panels (per day)
North	265	13.25
South	257	12.85
Total	522	26.10

In the future-state model, the crane utilisation decreases to 50.4%. The average waiting time is approximately 32 seconds. The average cycle time at the north table is 1.88 hr, which is less than the base model. The same changes are applied to the average cycle time for the south table, and the number of panels assembled in 20 days increases by 50 as compared to the base model. Figure 10 and Figure 11 present the relative frequency for cycle time after 500 runs for the north table and the south table, respectively, both of which show a relatively normal distribution.

Figure 10: Cycle Time of North Table for Improved Model after 500 Runs

Figure 11: Cycle Time of South Table for Improved Model after 500 Runs

6. DATA VALIDATION AND VERIFICATION

The model has been validated and verified by using face validity technique, as was described by Sargent (2013). Experts from the manufacturing industries were consulted for validating and verifying both the logic of the conceptual and the compu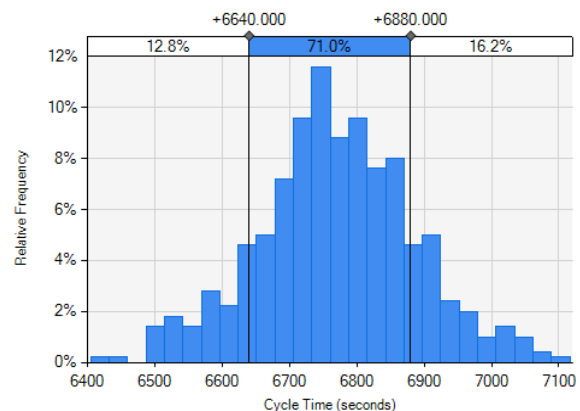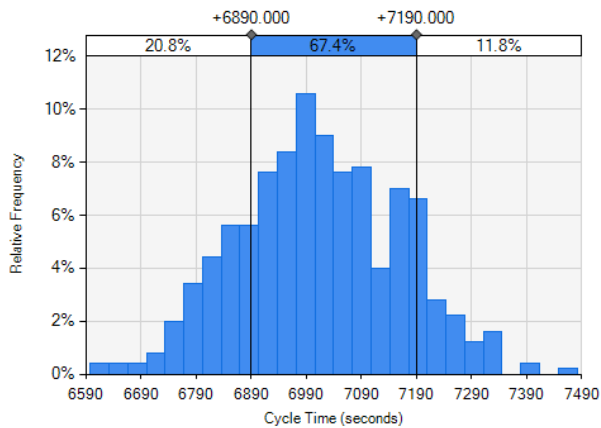terized aspects of the simulation model in this case study. The data from the model was also verified by using the original data obtained by data collection. In the case study floor manufacturing facility, each panel can be completed in approximately 7,200 seconds, which is approximately 2 hr. The actual cycle data obtained already excludes the interruption time from workers such as discussion and drawing checks. The simulated mean cycle time for the base case is approximately 7,600 seconds for both tables. By comparing the actual average cycle time with the simulated cycle time for the current-state case, the times are consistent with one another; however, the constructed model marginally over-simulates the process compared to the observations. This could be due to the limitations of the model (such as statistical error, observational error, and the delay time during or between tasks). Therefore, there is sufficient basis to use the constructed model to simulate the influence of resource changes on the production line.

7. CONCLUSION AND RECOMENDATIONS

This study investigates the use of simulation to model a floor panel fabrication line in a panelised home manufacturing facility to assist management in providing strategies for implementation of the proposed changes for production line improvement. The simulation assists in identifying the floor production line as a potential area of improvement. By comparing the simulation results with current and future states, the production line productivity can be increased by introducing a second crane to the process, thereby increasing the utilisation of all other resources with the exception of the cranes. Therefore, the deployment of a second crane can be considered as an investment in the floor production line in order to implement greater productivity and higher utilisation of resources. Further analysis can then be carried out with more realistic

simulation, which can consider any delay or interruption time between or during each task.

REFERENCES

AbouRizk, S., 2010. Role of Simulation in Construction Engineering and Management. Journal of Construction Engineering and Management, 136(10), 1140–1153.

AbouRizk, S., Hague, S., and Ekyalimpa, R., 2016. Construction Simulation: An Introduction Using Simphony. University of Alberta: Edmonton, Alberta. ISBN: 978-1-55195-357-1.

Altaf, M. S., Bouferguene, A., Liu, H., Al-Hussein, M., and Yu, H., 2018. Integrated production planning and control system for a panelized home prefabrication facility using simulation and RFID. Automation in Construction, Elsevier, 85(November 2017), 369–383.

Li, H. X., Al-Hussein, M., Lei, Z., and Ajweh, Z., 2013. Risk identification and assessment of modular construction utilizing fuzzy analytic hierarchy process (AHP) and simulation. Canadian Journal of Civil Engineering, 40(12), 1184–1195.

Longo, F. (2013). On the short period production planning in industrial plants: a real case study. International Journal of Simulation and Process Modelling, 8(1), 17-28.

Negahban, A., & Smith, J. S. (2014). Simulation for manufacturing system design and operation: Literature review and analysis. *Journal of Manufacturing Systems*, *33*(2), 241–261. https://doi.org/10.1016/J.JMSY.2013.12.007.

Neelamkavil, J., 2009. Automation in the prefab and modular construction industry. International Symposium on Automation and Robotics in Construction ISARC, (Isarc), 24–27.

Retik, A., and Warszawski, A., 1994. Automated design of prefabricated building. Building and Environment, 29(4), 421–436.

Salimi, S., Mawlana, M., and Hammad, A., 2018. Performance analysis of simulation-based optimization of construction projects using High Performance Computing. Automation in Construction, Elsevier, 87(December 2017), 158–172.

Sargent, R. G. (2013). Verification and validation of simulation models. Journal of simulation, 7(1), 12-24.

Smith, J. S. (2003). Survey on the use of simulation for manufacturing system design and operation. *Journal of Manufacturing Systems*, *22*(2), 157–171. https://doi.org/10.1016/S0278-6125(03)90013-6.

Taghaddos, H., Asce, A. M., Hermann, U., Asce, M., Abourizk, S., and Mohamed, Y., 2014.

Simulation-Based Multiagent Approach for Scheduling Modular Construction. Journal of Computing, 28(April), 263–274.

Yu, H., Al-Hussein, M., Al-Jibouri, S., and Telyas, A., 2013. Lean Transformation in a Modular Building Company: A Case for Implementation. Journal of Management in Engineering, 29(1), 103–111.

Zupan, H., & Herakovic, N. (2015). Production line balancing with discrete event simulation: A case study. IFAC-PapersOnLine, 48(3), 2305-2311.

AUTHORS BIOGRAPHY

Jingwen Wang is a PhD student in the Department of Civil and Environmental Engineering at the University of Alberta, Edmonton, Canada. Her research interests include production line improvement, 3D modelling, and ergonomic risk assessment in construction manufacturing.

Xianfei Yin is a PhD student in the Department of Civil and Environmental Engineering at the University of Alberta, Edmonton, Canada. His research interests include modular construction, construction automation and, BIM.

Yichen Tian is an MSc student in the Department of Civil and Environmental Engineering at the University of Alberta, Edmonton, Canada. Her research interests include construction automation, 3D modelling, and the automation of the design process.

Xinming Li is an assistant professor in the Department of Mechanical Engineering at the University of Alberta, Edmonton, Canada. Her research interests include ergonomic risk assessment in construction manufacturing, optimisation of construction operations, project scheduling, and general project management.

Mohamed Al-Hussein is a professor in the Hole School of Construction Engineering and Director of the Nasseri School of Building Science and Engineering at the University of Alberta, and holds an NSERC Industrial Research Chair in the Industrialisation of Building Construction. A highly sought researcher and consultant in the areas of lean manufacturing, construction process improvement, CO_2 emission quantification and reduction, and BIM, Dr. Al-Hussein has successfully applied lean principles to improve work methods and productivity standards for various industries and projects. His research has developed best practices for panelised building systems, lean production, and modular construction, and has been published in approximately 200 peer-reviewed journals and conference proceedings.

USE REDUCED TRACK PROFILE AND DISCRETE SIMULATION TO CALCULATE TRAIN TRAVEL TIME

Jan Fikejz[a], Jan Merta[b]

[a,b] Department of Software Technologies, FEI, University of Pardubice, Pardubice, Czech Republic

[a] Jan.Fikejz@upce.cz ,[b] Jan.Merta@student.upce.cz,

ABSTRACT
This article deals about utilization of reduced track profile for dynamic calculation of train travel time. Attention is firstly aimed on the description of the location of trains in the designed model of railway network. Further attention is aimed on the design of the dynamic calculation of train travel time. This calculation utilization of computer simulation and reduced track profile as a substitute of the real track profile of substitute gradients.

Keywords: Railway infrastructure models, train positioning, train travel time, reduced track profile

1. INTRODUCTION

Precise dynamic calculation of train travel time is not exactly trivial and includes a wide variety of aspects affecting the resulting journey time. Such are both, technical parameters of (i) a train set (e.g. train acceleration or overall train set weight) and (ii) railway infrastructure (character of the line, velocity limits), and (ii) external influences like weather (e.g. temperature, weather conditions, visibility). Train travel time calculation is always dependant on the current train location in the railway network in given time, thus current information about location is an inseparable part of dynamic calculation of delay. In this case, it is not necessary to demand such accuracy as for safety systems to determine location and thus it is possible to use satellite navigation (GNSS – Global Navigation Satellite System) for finding the current location of a train.

2. POSSIBLE TYPES OF LOCALIZATION

Generally, localisation is prone to a wide range of approaches on how to identify the position of trains on a track. Put simply, localisation may be divided into the following three groups:

- Localization without the use of GNSS,
- GNSS using localization,
- GNSS-based, involving further support systems.

2.1. Trains localization without the use of GNSS

This type of trains localization often requires complementing the rail network infrastructure with additional construction elements, which entails higher costs of the actual implementation. On the other hand, this type of localization shows a high accuracy and reliability and is often used in the railway signalling technology. Essentially, it relates to the system of:

- ETCS (Ghazel 2104; Lieskovský and Myslivec 2010),
- Automatic train control (Chudacek and Lochman 1998; Lieskovský 2004),
- Track circuits (Dorazil 2008),
- RFID.

2.2. Trains localization using GNSS

When using GNSS for various application levels, it is necessary to take an indicated position error into consideration. Indicated position error is generally based on the nature of the satellite navigation. If we use systems that operate with the position information on an informative level only, we can tolerate a certain error; however, such inaccuracy is unacceptable in the railway signalling technology. However, various additional systems can be implemented to eliminate the error (completely or at least partially), thus making the position of the tracked object more accurate. The following systems can be listed in this group:

- EGNOS (Senesi 2012),
- Differential GPS (O'Connor 1997).

2.3. GNSS based localization involving additional support systems

As mentioned above, precise localization of trains using GNSS, especially for the needs of signalling technology, is a priori impossible. Nevertheless, the position of a rail vehicle can be determined significantly more precisely with the use of additional systems. This concern especially solutions using inertial systems (Standlmann 2006), but also less known systems such as those based

on GNSS and contactless eddy current measurement (Becker and Poliak 2008).

3. RAILWAY NETWORK MODEL

Undirected graph, as defined graph theory, is a natural candidate for a railway network model. Based on an analysis of data provided by the company SŽDC-TUDC (consisting of service regulations, passports, and codebooks), sets of algorithms were subsequently created, with which it was possible to generate a three-layer model of the rail network (Fikejz and Kavička, 2011). Roughly speaking, the track can be divided into individual so called supertracks, which consist of definition supra-sections (TDNU), where each supra-section contains track definition sections (TUDU) with mileposts (in hectometres). Basic aspects of the description of the rail network are collectively shown in Figure 1.

Mileposts (in hectometres) are shown in Figure with the distance in kilometres and are graphically represented using gray points. TUDU is recorded using a six-digit code (163105, 163106, 16307, 173202) and are graphically represented using solid lines (red, black, orange, brown). Individual supra-sections (CLS 007, CLS008, REG023) are shown in light blue and supertracks (B421021 1 and B421021 1A) are shown in dashed lines. A place significant in terms of transportation (branch line) is symbolized by a green square.
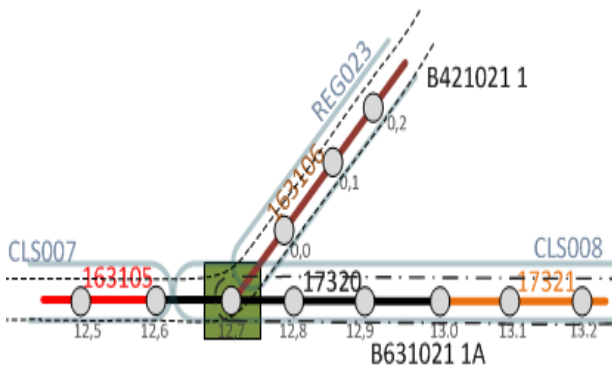
Figure 1: Basic aspects of the description of the rail network

The algorithm of railway network model (Fikejz and Kavička, 2011; Fikejz and Řezanina 2014.) was implemented directly on the database level using PL/SQL language. However, the algorithm had to be adjusted and generalized several times since there are various nonstandard conditions in the data, such as jumps in the mileposts (nonlinear growth of the kilometre succession between the mileposts) or change of an increasing kilometre sequence into a decreasing one and vice versa. The final model includes three data layers:

- **Data-Micro**, consisting of vertices and edges,
- **Data-Mezo**, include mezo-vertices and mezo-edges

- **Data-Macro**, containing super-vertices and super-edges.

Figure 2 presents the overall concept of a complete three-layer railway network model.
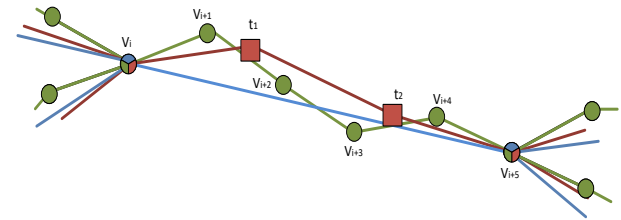
Figure 2: Illustration overall concept of a three-layer module

The data structure non-oriented graph was finally implemented directly in the ORCLE database using the ORACLE Spatial Network Data Model (Kothuri et al. 2007) technology. This technology enables the user to build a various network representation, involving also the object scheme and the communication interface API.

The objects scheme includes metadata and network tables. The interface contains on the server side PL/SQL API (an SDO_NET packet) for the creation, control and analysis of the database network, and a middle layer Java API (on client´s side) for the network analysis. The actual network is then defined by means of two compulsory tables:

- Node table,
- Link table.

For the work with spatial data, ORACLE with Spatial technology defines a special object data type SDO_GEOMETRY, which enables its user to store a number of spatial information and geometric types, such as various points, arcs, linear chains or polygons.

4. LOCALIZATION

The idea of trains localisation access to tracks is based on the correct pairing up of GPS information on position, provided by communication terminals, with the nearest vertex or edge of the graph. The discovered vertex/hectometre post disposes not only of a multi-dimensional key in the form of a GPS coordinate, it is also linked, through definition sections, to further information concerning the railway network infrastructure.

View of the situation that the model of railway infrastructure is stored in the database Oracle we can use the native database functions and operators. The SDO_NN (*nearest neighbor*) operator was selected in view of realising this unique trains localisation approach. The aforementioned operator searches for a geometric object that is closest to the object entered (like a point, for example). In other words, it is possible to find the

nearest vertex, or more precisely edge in a model, from the current position trains, Figure 3.
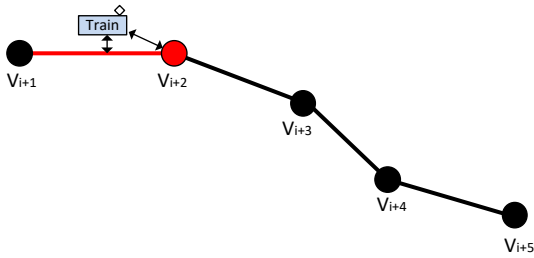
Figure 3: Main concept of localization

The actual detection of the current position of the trains can be divided into the following steps:

1. **Finding the nearest vertex and edge of the graph** – from the current position of the trains given the three-layer railway network model

2. **Assessment of the relevancy of incoming GPS information from the communication terminal** – verification whether the current position is not burdened by a disproportionate error (like, for example, that the distance of the trains from the nearest vertex/edge is a mere few meters or tens of metres, or that the trains is still assigned to the same super-edge, provided that it should still be located on it)

3. **Calculation of the exact position of the trains on the edge of the model** – using perpendicular projection of the point (current trains position) onto the line

The trains position data are collected from the communication terminals. These communication terminals sent position information to the central database every 30 second, Figure 4
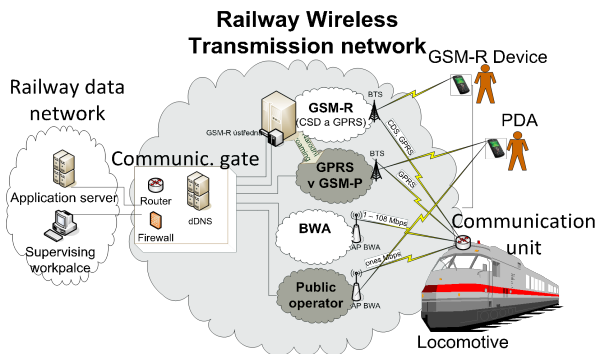
Figure 4 : Communication between the rail vehicle and dispatching centre

5. REDUCED TRACK PROFILE

Railway infrastructure is rather varied and contains many areas affecting the train dynamic (Bandžuch 2006). For common traction calculations, it is possible to substitute the real track profile by a reduced set of substitute gradients, so called line resistance, which includes:

- gradient resistance
- curve resistance
- tunnel resistance

Curve resistance sl_c is substituted by fictive incline, for which the curve radius R<300 m for secondary and regional lines is defined by:

$$sl_c = \frac{500}{R - 30} \ [‰] \tag{1}$$

Reduced incline sl_r is then defined by:

where:

- sl_1 to sl_k -actual gradient in per mille (incline „+", decline „-")
- sl_{c1} to sl_{cm} -fictive gradient, substituting set of curves
- l_1 to l_k -length of gradients s_1 to s_k in meters
- l_{c1} to l_{cm} -curve lengths 1 to m

While condition
$(l_1 + l_2 + \cdots + l_k) \leq 2,5 \ (l_{c1} + l_{c2} + \cdots + l_{cm})$ must be valid

An example of a reduced track profile is illustrated on the following Figure 6, in which arrows show the intended direction of movement of the train. The data in tables then depict:

- **kilometric position** of a change in profile $[km]$
- **the direction** where:
  - „+" expresses change in direction
  - „−" expresses change opposite the direction
- **track resistance** $[‰]$ where:
  - positive value expresses track incline
  - negative value expresses track decline

6. TRAIN ACCELERATION

Train acceleration is influenced mainly by

- technical parameters of a locomotive (acceleration)
- overall weight of the train set

$$sl_r = \frac{sl_1 l_1 + sl_2 l_2 + sl_3 l_3 + \cdots + sl_k l_k + sl_{c1} l_{c1} + \cdots + sl_{cm} l_{cm}}{l_1 + l_2 + \cdots + l_k} \ [‰] \tag{2}$$

Station 1 49,058 **Station 2** 55,683

48,771   49,303   49,529   55,591   55,628   55,711

Position	Direction	Track res.
49,303	+	0,300
49,100	+	1,370
48,771	-	0,030
49,100	-	-0,300

Position	Direction	Track res.
49,529	+	-6,700
49,303	-	6,700

Position	Direction	Track res.
55,591	+	-1,110
55,100	+	-2,530
54,000	+	2,600
53,000	+	-4,620
52,300	+	0,610
50,900	+	1,900
50,100	+	-6,700
49,529	-	6,700
50,100	-	0,600
50,900	-	4,610
52,300	-	10,780
53,000	-	4,580
54,000	-	2,790
55,100	-	2,610

Position	Direction	Track res.
55,711	+	-1,110
55,628	-	2,610

Position	Direction	Track res.
49,529	+	-6,700
49,303	-	6,700

- Station track
- Deviated track
- Line track

Figure 5 : Example of reduced track profile

Using a special software tool for simulation train dynamics developed at University of Pardubice (Diviš and Kavička 2015), a set of measuring simulations focused on acceleration and breaking deceleration of trains was conducted for selected trains for the following track resistances:

- 0.5 %
- 1.0 %
- 1.5 %
- 2.0 %

Assessment of data from individual measurings has shown that data can be approximated by a linear equation for other calculations.

If we consider a train set with the following parameters:

- Acceleration: 0,6497725 m/s^2
- Length: 96 m
- Weight: 234 t

then individual measured values of acceleration can be reflected in a graph on Figure 7.

Train acceleration for ascending gradient

$y = 0,0982x + 0,65$
$R^2 = 0,99996$

Acceleration [m/s^2] vs Slope of track [%]
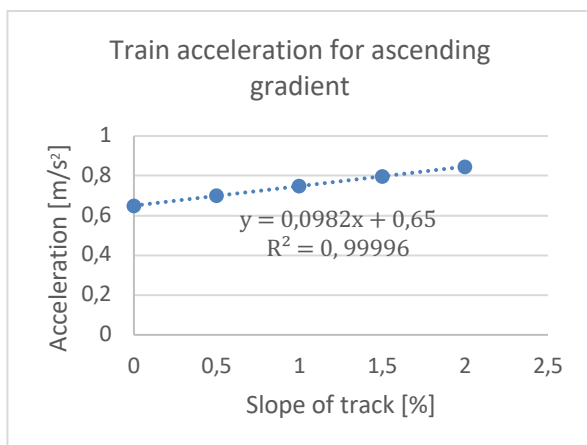
Figure 6: Example of train acceleration

From the graph above, it is clear that measured acceleration for incline can be approximated by a linear equation

$$y = 0,0982x + 0,65 \qquad (3)$$

for reliability $R^2 = 0,99996$.

When data from measured acceleration for a declining track are applied, then through approximation we can achieve linear equation

$$y = -0,1044x + 0,6511 \qquad (4)$$

for reliability $R^2 = 0,99974$.

7. CALCULATING TRAIN TRAVEL TIME

One way of calculating the train travel time to a track point (typically a railway station) is to use static calculations (acceleration times, riding times and braking times) of a given train configuration (Fikejz and Merta, 2017). If this travel time is compared with the timetable, then the train delay can be determined from such data.

To calculate the train travel time from the current position to the selected location, it is possible to use computer simulation, which iteratively calculates the travel times in observed track segments that contain different line speed limits. Each observed track segment is always divided into speed limits v_{max_i}, which are also considered in the dynamic calculation. The last speed segment can then be labelled as $v_{max_{Last}}$. The individual line speed limits are shown in Figure 7.

60 km/h   80 km/h   70 km/h   60 km/h

Station 1   Station 2
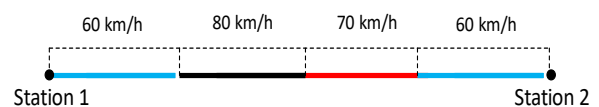
Figure 7: Maximum speeds of track segments

For dynamic calculation of train travel, discrete simulation and infrastructure model of a railway network are used. The infrastructure model is used to determine the current train's position on the track. From the current position on the track the following calculation include:

- current line resistance and corresponding acceleration of the train a
- current maximum speed on a given segment

For each calculation, we use the general formula for constant speed based on:

$$t = \frac{v}{s} \qquad (5)$$

For uniformly accelerated linear motion, we use relations based on:

$$v = v_0 + at \implies t = \frac{v - v_0}{a} \qquad (6)$$

$$s = v_0 t + \frac{1}{2} at^2 \implies v^2 = 2as + v_0{}^2 \qquad (7)$$

7.1.1. Calculation algorithm

The algorithm itself works iteratively with a fixed time step k. In each iteration step, a calculation of the current speed and the distance travelled at time $k+1$ to the current track profile and the maximum permitted speed is always performed. It is then checked whether the required speed has been reached. If the train accelerates or decelerates, Formulae 6 and 7 are used. Actual acceleration is always dependent on the given track resistance corresponding to the current train position. If the train has already reached the maximum speed in the current segment, v_{max_i} then Formula 5 is used.

The actual algorithm is divided into three steps:

1. Reverse train braking simulation from the target point (from zero speed) to the point where the train will have the maximum speed of the last segment $v_{max_{Last}}$.

   a. If the algorithm reaches the maximum segment speed $v_{max_{Last}}$, we get the point $p_{deceleration}$ where the train must start braking to have a zero speed at the target point. Furthermore, we will get:

      i. braking time $t_{deceleration}$

      ii. braking path $s_{deceleration}$.

   b. If before $v_{max_{Last}}$ we reach the current train position, then:

      i. $t_{total} = t_{deceleration}$

      ii. $s_{total} = s_{deceleration}$

and the algorithm of that iteration ends.

2. From the current train position on the track and its current speed, we perform the simulation of the movement (riding) until the breaking point is reached $p_{deceleration}$. This will give us:

   a. train travel time t_{drive}

   b. train path S_{drive}

3. It is then possible to determine the total time t_{total} and s_{total} train path from the current position to the destination according to:

   a. $t_{total} = t_{drive} + t_{deceleration}$

   b. $s_{total} = s_{drive} + s_{deceleration}$

Figure 8 shows a selected situation for iterative calculation where the current train position does not occur in the braking zone.
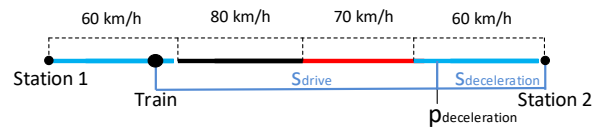
Figure 8: Example of selected train position for iterative calculation

The complete calculations for the dynamic calculation of the train travel were subsequently implemented in the *infraRail* software tool. With discrete simulation, it was then possible to check various variants of options of speed limits and train configuration. These parameters then affected the overall travel time. It was also possible to compare the travel times with the current timetable and to identify possible delays to the train, both based on historical data and based on the data generated. The running application captures the current position of the train on the track with a set of information relating to its position, including the calculation of the current delay on arrival to the next railway station, Figure 9.

CONCLUSION

This article deals primarily with the design of a dynamic calculation of train travel time using a computer simulation. A multilayer model of the rail network and satellite navigation were used for this train travel time calculation. The multi-layered model of the rail network was designed to reflect a non-oriented graph. Furthermore, the algorithm for the identification of the current position on the railway network is described in the article. The article also focuses on the description of reduced track profile and the determination of equations for calculating the acceleration of selected train sets. The reduced profile and acceleration were subsequently used in the design of the algorithm for dynamic calculation of train travel time. Designed algorithms were implemented in *InfraRail* software (developed by authors at University of Pardubice) in which various speed setting
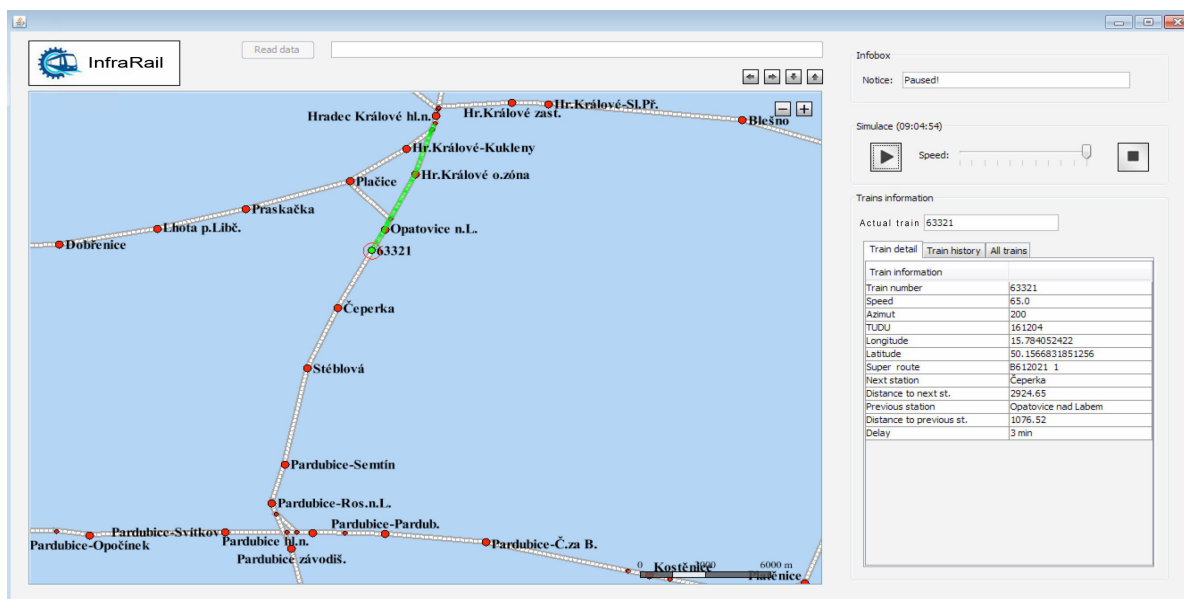
Figure 9: Running application

and train configuration variants could be verified. It was also possible to compare the travel times with the current timetable and to identify possible delays to the train, both based on historical data and based on the data generated.

REFERENCES
Becker, U. and J. Poliak. DemoOrt repositions trains with satellite. In: EURAILmag Business & Technology. 18. BLUE LINE & Bro, France, 2008,s. 216-219.

Chudaček, V. and L. Lochman. Vlakový zabezpečovací systém ERTMS/ETCS. In: Vědeckotechnicky sborník ČD, č. 5/1998

Dorazil, P. Základní vlastnosti kolejových obvodů bez izolovaných styků. Pardubice, 2008. Bachelor thesis. University of Pardubice. Supervisor: Milan Kunhart.

Fikejz, J. and A. Kavička. Modelling and simulation of train positioning within the railway network. In: KLUMPP, Matthias. ESM'2012. The European simulation and modelling conference. Ostende: EUROSIS - ETI, 2012, s. 366 -376. ISBN 978-9077381-73-1.

Fikejz, J. and A. Kavička. Utilisation of computer simulation for testing additional support for dispatching rail traffic. In: European Simulation and Modelling Conference, 2011. Ostende: EUROSIS - ETI, 2011. p. 225-231. ISBN 978-90-77381-66-3.

Fikejz, J. and J. Merta, Utilization of railway network model for dynamic calculation of train delays. In: The 26th European Modeling & Simulation Symposium. Barcelona, Spain, 2017 s. 248-254, ISBN 978-1-5108-4765-1

Fikejz, J. and E. Řezanina, Utilization of computer simulation for detection non-standard situations within the new data layer of railway network model. In: The 26th European Modeling & Simulation Symposium. Bordeaux, 2014 s. 371-377, ISBN 978-88-97999-32-4

Ghazel, M. Formalizing a subset of ERTMS/ETCS specifications for verification purposes. In:Transportation Research Part C: Emerging Technologies. Elsevier Limited, 2014, pp. 60-75 ISSN: 0968-090X

Kothuri, R. et al. Pro Oracle Spatial for Oracle database 11g. New York, NY: Distributed to the book trade worldwideby Springer-Verlag New York, c2007, xxxiv, 787 p. ISBN 15-905-9899-7.

Lieskovský, A. and I. Myslivec. ETCS a AVV - poprvé společně. In: EuroŽel, Žilina, 2010

Lieskovský, A. Automatické vedení vlaků Českých drah. In: Automatizace. Praha: Automatizace, 2004, roč. 10. ISSN 0005-125x.

O'connor, M. L. Carrier-phase differential gps for automatic control of land vehicles, In: Dissertation Abstracts International, Volume: 59-06, Section: B, page: 2876.; 158 p. 1997, Stanford University, ISBN: 9780591909272

Senesi, F. Satellite application for train control systems, In: The Test Site in Sardinia, Journal of Rail Transport Planning and Managemt. Elsevier BV, 2012, s. 73-78, ISSN:2210-9706

Bandžuch, Ľubomír. Modernizácia elektrifikovanej trate v rámci V. koridoru v úseku Košice – Poprad. Žilina, 2006. Diplomová práce. ŽILINSKÁ UNIVERZITA V ŽILINE. Vedoucí práce Doc. Ing. Gabriela Lanáková, PhD.

Diviš, Roman a Antonín Kavička. Design and development of a mesoscopic simulator specialized in investigating capacities of railway nodes. In: The 27th European Modeling and Simulation Symposium (EMSS 2015): 12th International Multidisciplinary Modeling and Simulation Multiconference (I3M 2015). 1. Rende, Italy: CAL-TEK S.r.l, 2015, s. 52-57. ISBN 9781510813762

RESOURCE CONSTRAINED PROJECT SCHEDULING: A REAL-WORLD EXTENSION FOR STEEL INDUSTRY

Viktoria A. Hauder[a][b], Andreas Beham[a][c], Sebastian Raggl[a], Michael Affenzeller[a][c]

[a] Heuristic and Evolutionary Algorithms Laboratory,
University of Applied Sciences Upper Austria, Hagenberg, Austria

[b] Institute for Production and Logistics Management,
Johannes Kepler University Linz, Austria

[c] Institute for Formal Models and Verification,
Johannes Kepler University Linz, Austria

[a]{viktoria.hauder,andreas.beham,sebastian.raggl,michael.affenzeller}@fh-hagenberg.at

Project scheduling is an essential operational optimization task when precedence relations and the access to limited resources are problem inherent. In this work, a real-world production and logistics planning process of a steel manufacturer is modeled. Production activities have to be scheduled in a way such that real-world restrictions and objectives are considered. Therefore, the basis for this model is the well-known resource constrained project scheduling problem. However, for the consideration of all necessary real-world requirements, a new problem model with various extensions concerning project flexibility and the production of multiple lots is developed. Within a first step, the developed model is solved exactly for small instances by using IBM ILOG CPLEX. As a second step, for larger (real-world) instances which are not solvable within a reasonable time for real-world applications, a Constraint Programming model is developed and applied successfully for large real-world problem instances.

Keywords: flexible resource constrained project scheduling, alternative production routes, constraint programming, production optimization

1. INTRODUCTION

Project scheduling is an essential operational task of project management if limited resources and precedence relations are problem inherent. Examples are the management of special projects of a company such as the organization of an extraordinary event or the introduction of a new software (Schnell and Hartl 2016). Another example is a special form of a production and logistics planning process where a number of tasks has to be performed and limited resources have to be shared.

In this work, a real-world production and logistics planning process of a steel industry production site which includes production, warehouse, and transportation tasks is modeled. Tasks have to be scheduled in such a way that real-world inherent restrictions and objectives are considered. As the well-known resource constrained project scheduling problem (RCPSP) is the typical standard problem in the scientific literature for such

project scheduling problems (Bartusch, Möhring, and Radermacher 1988; Blazewicz, Lenstra, and Kan 1983; Hartmann and Briskorn 2010), it builds the base for this steel industry optimization case. However, for the consideration of all necessary real-world requirements, a mixed integer programming (MIP) model with various extensions is developed. On the one hand, the production of multiple lots has to be considered. On the other hand, a flexible project structure has to be taken into account which means that not all tasks have to be scheduled. Alternative routes per lot which include different tasks are incorporated and one out of multiple existing alternatives has to be selected.

Within a first step, the developed model is implemented in the optimization studio IBM ILOG CPLEX (https://www.ibm.com/products/ilog-cplex-optimization-studio) and small test instances are solved to optimality. As a second step, for larger (real-world) instances which are not solvable within a reasonable time for real-world applications, a Constraint Programming solution model is developed.

The article is organized as follows. First, related work concerning the resource constrained project scheduling problem is described in Section 2. Next, the exact model is developed in Section 3. Solution methods and results are presented in Section 4. Finally, Section 5 concludes the work and gives directions for further research.

2. LITERATURE OVERVIEW

The standard problem in the scientific literature for project scheduling problems is the NP-hard resource-constrained project scheduling problem (Bartusch, Möhring, and Radermacher 1988; Blazewicz, Lenstra, and Kan 1983; Hartmann and Briskorn 2010). The RCPSP consists of $j \in \{0, \dots, J + 1\}$ activities where 0 and $J + 1$ are virtual nodes representing the start and end of the project. Activities are not allowed to be preempted and every activity has got a specific duration or processing time p_i. There is a set of renewable resources $k \in \{1, \dots, K\}$ with a constant capacity C_k per period and every activity j has a demand of Q_{jk} units of resource k. Precedence relations of activities are considered by a

defined number of sets of immediate predecessors P_j which show that activity j cannot be started before all of its predecessor activities are completed. Such relations can be represented by an acyclic activity-on-node network. The goal is to find a schedule which integrates all activities and assigns a starting time S_j to every activity. Figure 1 shows an example activity-on-node network for a RCPSP.

The most common objective is the minimization of the makespan of the whole project (Kolisch and Hartmann 2006). However, alternative objectives are amongst others the minimization of lateness or tardiness (Słowiński 1989) or changes in the level of resource usage (Neumann and Zimmermann 2000; Neumann, Schwindt, and Zimmermann 2002).
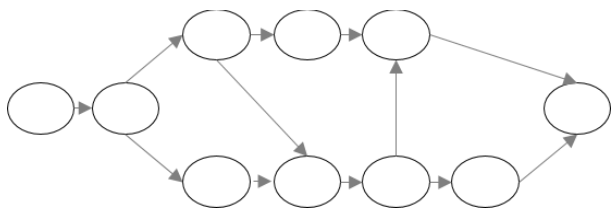

Figure 1: RCPSP activity-on-node network.

As the RCPSP and subsequent presented extensions are characterized by extensive research, a numerous amount of exact and heuristic solution procedures has already been developed. Examples for exact solution approaches are branch-and-bound, branch-and-cut or dynamic programming (Hartmann and Briskorn 2010). Heuristic methods are for example priority rules or genetic algorithms (Hartmann and Briskorn 2010). For a deeper examination of developed solution approaches, the interested reader is referred to Hartmann and Briskorn (2010) and Schwindt and Zimmermann (2015) where further examples can be found.

The RCPSP can be extended by multiple ways (Hartmann and Briskorn 2010). Besides the already introduced renewable resources, two more types, particularly nonrenewable and doubly constrained resources can also be taken into account (Słowinski 1981M; Weglarz 1980). Renewable resources are for example machines or staff. Despite their capacity is limited, they can be used again after the demand of selected activities is satisfied. Taking for example a production machine, after finishing one or multiple activities it is available for production again. An example for a nonrenewable resource is money, which cannot be utilized again after it has been consumed once. For the third extension, the doubly constrained resources, it can for instance be the case that there is a budget limit per period and another one for the whole project. However, this extension can be represented by transforming it into renewable and nonrenewable resources (Hartmann and Briskorn 2010).

One variant of the RCPSP where nonrenewable resources are considered is the so-called multi-mode RCPSP (MRCPSP) (Hartmann and Briskorn 2010; Van Peteghem and Vanhoucke 2014). In the RCPSP, every activity has a specific processing time and a demand. However, within the MRCPSP every activity has to be executed in one out of multiple possible execution modes. For every mode, a processing time and a demand is defined. An example would be the possibility of activity i executing it with a demand for one machine and a related processing time of six time slots (=mode one with one renewable resource) or with a demand for two machines with a related processing time of three time slots, where the second machine is rented and only available for a limited amount of time slots (=mode two with one renewable and one nonrenewable resource). The selected and used mode per activity is part of the decision process of the optimization.

One further extension is called RCPSP with flexible project structures. Pritsker introduced flexible project structures already in 1966 by the presentation of so-called 'And' nodes and 'Or' nodes. In contrary to 'And' nodes which require the selection of all successor nodes, an 'Or' node requires the possibility to select only one out of multiple alternative successor activities. As a result, a RCPSP with a flexible project structure does not request the selection and scheduling of all activities in the network in contrast to the standard RCPSP and many other variants of it where this requirement is mandatory. An exemplarily illustration of precedence relations of an activity-on-node network for a flexible project structure can be found in Figure 2. A more recent work which considers flexibility is for example the one of Kellenbrink and Helber (2015) where a real-world application for the airline industry is solved by the development of a genetic algorithm.

It may be noted that flexible RCPSP are a generalized form of the RCPSP (Kellenbrink and Helber 2015) and also of the MRCPSP. In the multi-mode case, there is the possibility of choosing *between different modes* but not the flexible project inherent possibility of choosing *between different activities* within one project or one mode.
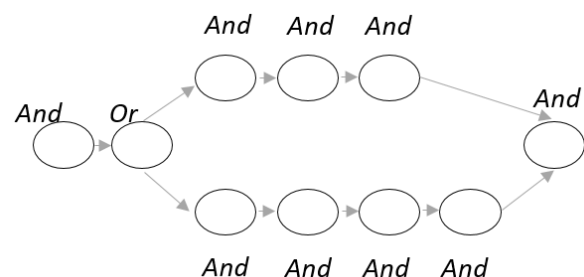

Figure 2: Exemplarily RCPSP activity-on-node network with a flexible project structure.

In the following chapter, a new real-world extension for a flexible project scheduling problem for a steel

application case is presented. Production, warehousing and transport activities of multiple lots are optimized and the selection of one out of multiple possible production routes and thus activities is possible.

3. RCPSP WITH A FLEXIBLE PROJECT STRUCUTRE FOR PRODUCTION PLANNING WITH MULTIPLE LOTS

With the subsequent presented new extension of a flexible RCPSP, the possibility of alternative production ways or routes where one route has to be selected, and the production of multiple lots is modeled. Within the considered steel production plant, there are multiple lots which have to be produced by passing different production stations. An example illustration of this project network can be found in Figure 3.
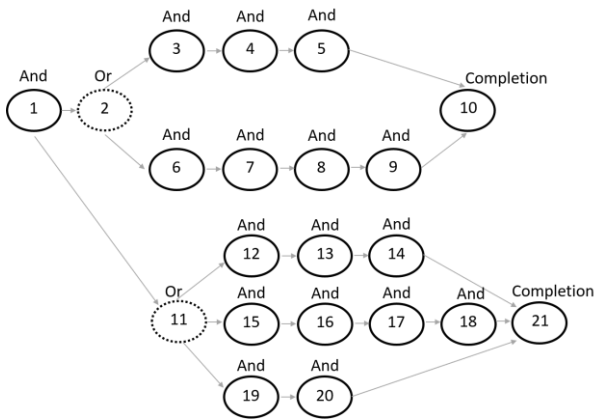

Figure 3: Flexible project scheduling for the production of multiple lots.

The different operations which have to be performed per lot are called activities (or tasks or nodes) and have to be distinguished from the term 'job', which corresponds to a customer order. Every activity $i, j \in \{0, ..., N + 1\}$ where $\{0, N + 1\}$ are virtual start and end nodes has a specific task. For example 'activity 1' could be the mixing of different ingredients, 'activity 2' the transportation of the manufactured product, and 'activity 3' the necessary warehousing of the product for a cooling or heating phase. An adjacency matrix A_{ij} and the flexibility type f_i give information about the connection between activities within the project network. A_{ij} shows if there is a connection ($A_{ij} = 1$) between two activities or not ($A_{ij} = 0$). The flexibility type f_i specifies if an activity is an 'Or' activity, which means that only one successor can be performed ($f_i = 0$) or an 'And' activity, which means that all successor activities have to be performed ($f_i = 1$). The third, newly introduced type is called 'Completion' activity and represents the last activity of one production lot ($f_i = 2$). The introduction of the new 'Completion' activity type and related new restrictions in the subsequent presented mixed integer programming (MIP) model are necessary since there is not only one virtual end node, as in traditional RCPSP models (Hartmann and Briskorn 2010). For every customer, one specific completion activity has to be

defined per lot. With $L \subset N$, the set of completion activities is defined. This extension can also be seen in Figure 3, where the RCPSP project network is enlarged by the third activity type. For every lot which has to be produced, one starting activity ('Or' node), multiple possible routes, and one completion activity ('Completion' node) is defined. For lot 1, activity 2 is the starting activity, followed by two possible routes, and activity 10 is the completion activity. For lot 2, activity 11 is the starting activity, followed by three possible routes, and activity 21 is the completion activity.

Moreover, every activity has a fixed processing time p_i. Activities can use renewable resources $k \in \{1, ..., K\}$ with a demand Q_{ik} per activity and renewable resource. The capacities of resources are given by C_k. With the consideration of a given time horizon $t \in \{1, ..., T\}$, a maximum planning period is defined. Nonrenewable resources are not considered, since they do not exist in this steel industry real-world application.

There are two decision variables y_i and z_{it}. Decision variable $y_i = 1$ if activity i is selected to be performed and 0 otherwise and $z_{it} = 1$ if activity i is selected to be performed and completed at the end of time slot t and 0 otherwise. The minimization of the completion time per lot and thus, the makespan, is the objective. The model can be formulated as follows.

Minimize

$$\sum_{t \in T} \sum_{i \in L} t \cdot z_{it} \tag{1}$$

subject to

$$y_0 = 1 \tag{2}$$

$$\sum_{t \in T} z_{it} = y_i \qquad \forall i \in N, \tag{3}$$

$$\sum_{j \in N} A_{ij} \cdot y_j = y_i \quad \forall i \in N, \quad if \ f_i = 0, \tag{4}$$

$$y_j \geq A_{ij} \cdot y_i \qquad \forall i, j \in N, \quad if \ f_i = 1, \tag{5}$$

$$\sum_{j \in N} A_{ij} \cdot y_j = y_j \quad \forall i \in N, \quad if \ f_j = 2, \tag{6}$$

$$A_{ij}\left(\sum_{t \in T} t \cdot z_{it}\right) + (y_j + y_i - 2) \cdot M \leq \sum_{t \in T} t \cdot z_{jt} - p_j$$
$$\forall i, j \in N, \tag{7}$$

$$\sum_{i \in N} \sum_{\tau = t}^{t + D_i - 1} z_{i\tau} \cdot Q_{ik} \leq C_k \quad \forall k \in K, t \in T, \tag{8}$$

$$y_i, z_{it} \in \{0,1\} \qquad \forall i \in N, t \in T. \tag{9}$$

With objective function (1), the makespan of every single lot is minimized which means that the completion time of the last activity of every lot is minimized. Restriction (2) defines that the production process has to be started and that the starting activity of the first lot is the first activity of the production process. Constraints (3) ensure that every selected activity is finished exactly once. With conditions (4) – (6), selection relations of the three different existing activity types are satisfied. If an activity is an 'Or' activity ($f_i = 0$) only one of its successors must be selected, and if an activity is an 'And' activity ($f_i = 1$) all of its successors must be selected. For the newly defined 'Completion' activity, it is determined that all predecessor activities within one production route of one 'Completion' activity ($f_i = 2$) must be selected. Therefore, it is not allowed to select an additional predecessor activity of another lot or another production route within the same lot. With restrictions (7), it is guaranteed that no activity within one chain can be started before the predecessor activity is finished and that only activities can be selected which are related to each other. Moreover, it is defined that the production process of one lot can be started before the previous lot is completely finished (before all necessary activities for the production of the previous lot are completed). Conditions (8) make sure that capacity restrictions for the existing renewable resources are met. Constraints (9) define both decision variables as Boolean ones.

4. SOLUTION METHOD AND COMPUTATIONAL EXPERIMENTS

For the optimization of the considered production process, the MIP model is implemented in and solved by IBM ILOG CPLEX 12.8.0. However, tests with larger real-world instances show the limits of this exact approach. Not only the number of activities, but even more the time horizon T, or in other words, the discretization of time within the exact model are limiting factors for the possibility of getting exact solutions in a reasonable period of time. Therefore, an alternative solution approach has to be developed. Subsequently, the successfully applied solution method of constraint programming is presented in Section 4.1. Afterwards, results of both optimization methods are provided in Section 4.2.

4.1. Constraint Programming

For this work, a Constraint Programming (CP) (Bockmayr and Hooker 2005) model is developed by using the CP concept of IBM ILOG CPLEX CP Optimizer (https://www.ibm.com/analytics/data-science/prescriptive-analytics/cplex-cp-optimizer). For the CP optimizer, a three-stage method is necessary which consists of a problem description, a problem model, and the solution process. The meta goal of Constraint Programming is the reduction of the search space and thus, the reduction of possible values of decision variables. Besides constraint propagation which removes all values of the search space which cannot take part in any solution, the CP optimizer also uses several

heuristics, such as constructive search strategies and branching strategies (Laborie et al. 2018).

For the developed CP model, different expressions and functions are applied. The introduced decision variable *interval* w_i represents an interval of time (processing time) w for every activity i. Thus, time discretization of the MIP model is substituted.

The *interval* decision variable can be constrained by several expressions. Besides logical expressions, such as `presenceOf`(w_i) which replace Boolean decision variables that were necessary for the development of the MIP model in Section 3, time expressions and alternative expressions are applied. With time expressions such as `endAtStart`(w_i, w_j) or `startOf`(w_i), time positions can be defined for every activity. With so-called alternative expressions, flexibility is realized since thereby one activity can be selected out of a set of multiple alternatives.

Renewable resources can be considered by the CP typical '*cumul*' (abbreviation for 'cumulative') function (Bockmayr and Hooker 2005). Thus, with the introduced *cumul* function $resourceUsage_r$, the cumulative usage over time of a renewable resource r is modeled.

To be able to model alternative activities, a set of meta (artificial or dummy) activities $M \subset N$ and corresponding sets S_i and E_i which define possible start and end alternatives for one activity i are introduced. All further sets and parameters for the developed CP model are the same as presented in Section 3 for the development of the MIP model. Based on the above described available CP functions and expressions and the additional introduced sets, the following CP model is developed for the steel industry problem.

Minimize

$$\sum_{i \in L} (\text{endOf}(w_i)) \qquad (10)$$

subject to

$$\text{startOf}(w_0) = 1, \qquad (11)$$

$$\text{presenceOf}(w_0) = 1, \qquad (12)$$

$$\text{presenceOf}(w_i) = 1 \qquad \forall i \in L, \qquad (13)$$

$$\text{lengthOf}(w_i) = p_i \qquad \forall i \in N, \qquad (14)$$

$$\text{endAtStart}(w_i, w_j) \qquad \forall (i, j) \in A_{ij}, \qquad (15)$$

$$\text{presenceOf}(w_i) = \text{presenceOf}(w_j) \qquad \forall (i, j) \in A_{ij}, \qquad (16)$$

$$\text{alternative}(w_i, \{w_a \in S_i\}) \qquad \forall i \in M, \qquad (17)$$

$$endAtStart(w_i, w_a) \qquad \forall i \in M, a \in E_i, \quad (18)$$

$$resourceUsage_r \leq Q_r, \qquad \forall r \in R. \quad (19)$$

With the objective function (10), the makespan of all to be produced lots is minimized. Constraints (11) and (12) ensure the start of the production process with the first activity of the first lot. With restrictions (13) it is guaranteed that every lot is produced. The processing time of every activity has to be met through constraints (14). Conditions (15) ensure that no time lags between activities are allowed. Precedence relations are satisfied by restrictions (16). With constraints (17), the choice between alternative routes per lot is introduced. Connected to this, constraints (18) make sure that there are no time lags between the production of different lots. Finally, with restrictions (19) capacity limits are satisfied.

4.2. Results
Subsequently, optimization results for the steel manufacturing application case presented in this work are provided. Both models (MIP and CP) are implemented in IBM ILOG CPLEX 12.8.0. All tests are run on a virtual machine Intel(R) Xeon(R) CPU E5-2660 v4, 2.00GHz, with 28 logical processors, Microsoft Windows 10 Education.

The data used for optimization runs is real-world data from the steel manufacturer. For the first iteration of the scheduling optimization and validation process, the wished amount of included lots in the optimization is 15 lots and associated 188 real-world activities which have to be optimized for a planning period of 2.170 time slots. It is agreed to plan with time periods of 30 minutes which means that for a planning horizon of $T = 2.170$ every time slot $t \in \{1, ..., T\}$ corresponds to half an hour.
For the presentation of optimization results in Table 1, the amount of lots (L), the corresponding amount of nodes (N) and the considered planning horizon (T) are displayed. Moreover, the gap to optimality and the run time in seconds are presented.

Table 1. Optimization results of MIP and CP models.

	L	N	T	Result	Gap	Run Time
MIP model results	5	70	1,776	**1,317**	0	156.23
	10	138	2,064	**4,500**	0	4,108.97
	15	188	2,170	-	-	5,400.00
CP model results	5	75	1,776	**1,317**	0	0.04
	10	148	2,064	**4,500**	0	4.33
	15	203	2,170	**6,863**	0	7.86

As it can be seen in Table 1, capacities of the MIP model optimization are limited. The consideration of 15 lots and related 188 activities does not even reveal a heuristic

solution within the predefined maximum run time of one hour (5,400 seconds) of the steel manufacturer. For the sake of completeness, it is mentioned that a test run with unlimited run time shows that the MIP model optimization finds at least a heuristic solution (27,586 with 78,65% gap) after 7,700 seconds. However, as this long run time is a lot higher than the accepted run time of the manufacturer, it is not shown in the results table.
In contrary to the MIP model optimization, the development of the Constraint Programming model seems to be the right decision. The results in Table 1 show that the production scheduling problems are exactly solvable with the developed CP model although the introduction of meta (dummy) activities described in Section 4.1 leads to the consideration of a higher amount of nodes during the optimization process. Besides getting exact solutions with the CP model, especially the very short run time is a main advantage in contrary to the MIP model optimization.

The divergent optimization results of the two solution approaches in Table 1 reveal the question why both solution approaches although implemented in the same solver CPLEX yield such substantially different results especially concerning optimization run time. The answer seems to lie in the different algorithmic methods which are used during the optimization process and in distinct modeling possibilities. The MIP model is solved with standard exact solution procedures provided by IBM ILOG CPLEX (https://www.ibm.com/analytics/cplex-optimizer). Nevertheless, the Constraint Programming optimizer applies very different solution strategies as already described in Section 4.1.
Moreover, as stated in various works on constraint programming, the way of modeling has enormous influence on the optimization results (Bockmayr and Hooker 2005, Laborie et al. 2018). This influence becomes especially visible when the amount of decision variables and constraints of the MIP and the CP model presented in Sections 3 and 4 are compared. If one takes the MIP model with input data of 15 lots, 188 activities and 2,170 time slots, a total number of 15,590 constraints and 409,414 variables have to be considered. In contrary to that, with the CP model (15 lots and 203 activities and 2,170 time slots), the CP optimizer only has to consider 583 constraints and 203 variables for the optimization process.
Connected to the very different number of variables and constraints of the MIP and the CP models, as previously mentioned in Section 4.1, another major reason for the run time reduction is the different consideration of time discretization. In the MIP model, the time index of decision variables and thus, the huge planning horizon requires an enormous amount of decision variables. In contrary to that, the CP model considers the whole planning horizon by the *interval* decision variable. Consequently, no time index t is required any longer.

5. CONCLUSION AND OUTLOOK

In this work, a new flexible project scheduling problem for a steel industry application case has been proposed. With this development, the concurrent scheduling of the production of multiple lots and the related selection of activities of one out of multiple existing alternative production routes per lot is possible. After the development of a mixed integer programming model for the newly introduced extension, a new constraint programming model is successfully applied for the optimization of large real-world instances.

The described results have already been discussed with the steel industry company partner. As the CP approach offers the possibility to solve production planning schedules including hundreds of production activities within seconds to optimality, the steel manufacturer is very interested in further advancements of the developed scheduling optimization. It is planned to consider multiple new, additional data and restrictions of the manufacturer, such as time buffers and tardiness considerations. Balanced resource utilization and balanced processing times are also new topics which will be examined. Furthermore, it is planned to increase the precision of the optimization results by changing time periods from half an hour slots to minute-based slots.

Related to the planned extensions for the steel scheduling optimization case, future challenges will lie in the efficient modeling of the problem and the solution approach. The proficient modeling and implementation of the requirements in an enhanced constraint programming model will play a decisive role concerning the quality of optimization results, since additional considered decision variables and constraints will lead to even more complexity during the solution process for this NP-hard optimization problem.

ACKNOWLEDGMENTS

REFERENCES

Bartusch, M., Möhring, R.H. and Radermacher, F.J., 1988. Scheduling project networks with resource constraints and time windows. Annals of operations Research, 16(1), pp.199-240.

Blazewicz, J., Lenstra, J.K. and Kan, A.R., 1983. Scheduling subject to resource constraints: classification and complexity. Discrete applied mathematics, 5(1), pp.11-24.

Bockmayr, A. and Hooker, J.N., 2005. Constraint programming. Handbooks in Operations Research and Management Science, 12, pp.559-600.

Hartmann, S. and Briskorn, D., 2010. A survey of variants and extensions of the resource-constrained project scheduling problem. European Journal of operational research, 207(1), pp.1-14.

Kolisch, R. and Hartmann, S., 2006. Experimental investigation of heuristics for resource-constrained project scheduling: An update. European journal of operational research, 174(1), pp.23-37.

Kellenbrink, C. and Helber, S., 2015. Scheduling resource-constrained projects with a flexible project structure. European Journal of Operational Research, 246(2), pp.379-391.

Laborie, P., Rogerie, J., Shaw, P. and Vilím, P., 2018. IBM ILOG CP optimizer for scheduling. Constraints, 23(2), pp.210-250.

Neumann, K., Schwindt, C. and Zimmermann, J., 2002. Recent results on resource-constrained project scheduling with time windows: Models, solution methods, and applications. Inst. für Wirtschaftstheorie und Operations-Research.

Neumann, K. and Zimmermann, J., 2000. Procedures for resource leveling and net present value problems in project scheduling with general temporal and resource constraints. European Journal of Operational Research, 127(2), pp.425-443.

Pritsker, A.A.B., 1966. GERT: Graphical evaluation and review technique (p. 138). Santa Monica, CA: Rand Corporation.

Schwindt, C. and Zimmermann, J., 2015. Handbook on Project Management and Scheduling Vol. 1. Cham: Springer International Publishing.

Schnell, A. and Hartl, R.F., 2016. On the efficient modeling and solution of the multi-mode resource-constrained project scheduling problem with generalized precedence relations. OR spectrum, 38(2), pp.283-303.

Słowinski, R., 1981. Multiobjective network scheduling with efficient use of renewable and nonrenewable resources. European Journal of Operational Research, 7(3), pp.265-273.

Słowiński, R., 1989. Multiobjective project scheduling under multiple-category resource constraints. In Advances in project scheduling (pp. 151-167).

Van Peteghem, V. and Vanhoucke, M., 2014. An experimental investigation of metaheuristics for the multi-mode resource-constrained project scheduling problem on new dataset instances. European Journal of Operational Research, 235(1), pp.62-72.

Weglarz, J., 1980. On certain models of resource allocation problems. Kybernetes, 9(1), pp.61-66.

COMPLEX NESTED SIMULATIONS WITHIN SIMULATORS REFLECTING RAILWAY TRAFFIC

Roman Diviš[a], Antonín Kavička[b]

[a],[b]University of Pardubice, Faculty of Electrical Engineering and Informatics

[a]roman.divis@upce.cz, [b]antonin.kavicka@upce.cz

ABSTRACT

Nested simulations present a general method suitable for use in realizing a multi-trajectory simulation or as a decision support in a simulator. The principle of nested simulation (as a decision support) is to find a solution to a problem using other time-limited simulations which verify alternative options. After the nested simulations have finished, the solutions of individual alternatives are assessed and the best solution is applied to the main simulation.

The aim of the article is to extend nested simulation capabilities to support multiple replications (of one scenario) and recursion (solving conflicts in nested simulation). A comparison of results (different parameterizations of nested simulations) will be presented with respect to the quality and computational complexity of the results.

Keywords: nested simulations, decision support, rail transport

1. INTRODUCTION

The stochastic simulator requires implementation of some of the decision support techniques. There are a number of ways to solve conflicting situations - from leaving the solution to the user (interactive mode of simulation) through various complex mathematical models (fuzzy logic, artificial neural networks, ...). Even though there are a number of complex decision support techniques, in practice, one of the easiest methods - priority planning - is often implemented in microscopic railway simulators. This method is used in OpenTrack, Villon and other rail simulators.

Nested or recursive simulations represent another methodology that can be used to support decision making in simulators. The principle of the method consists in suspending the actual main simulation at the moment when the conflict situation occurs and the simulation is then cloned into several variants. Individual clones have modified parameterization to allow testing of different options for resolving the conflict situation. These nested/recursive simulations (basically different outlooks for the future within a limited time horizon) are triggered, and after a certain period of time, it is evaluated which one has the best results. The optimal one is then used as a solution and the main simulation continues only with the chosen variant. Nested simulations are implemented and tested as experimental decision support in the developed MesoRail simulation tool (Diviš and Kavička 2015).

The aim of this article is to generalize the technique of nested simulations on the use of multiple replications of nested simulations combined with the possibility of recursive calculations. These two techniques bring with them a number of new problems, which are described below. In conclusion, the evaluation of a number of different variants of parameterization of nested simulations, their impact on the quality of the results, and the complexity of the calculations is presented.

1.1. Brief overview of the state-of-the-art

It has to be declared that not many authors pay attention to the research of nested/recursive simulations.

The authors Gilmer and Sullivan were focused in several of their articles on the efficiency of higher number of replications in contrast with multi-trajectory simulation (Gilmer and Sullivan, 1999). Their main interest is related to the military simulator Eaglet, which simulates the movement of military units of two armies and their mutual interactions.

Eugen Kindler (as a pioneer of nested simulation in Europe) published many articles with the focus on both, the theoretical description of nested simulations (classification, terminology, etc.) and their applications in practice (Kindler, 2010).

The issue of a planning support system is discussed by Hill, Surdu, Ragsdale, and Schafer (2000). Those authors were engaged in military planning.

Another area of applied nested simulations is connected with scalable simulation models, which allow applying both a macroscopic and a microscopic level of investigation within the frame of one simulator (Bonté, Duboz, Quesnel and Muller, 2009). Another area of exploiting nested simulations is financial a risk management – e.g. Gordy and June (2010).

2. POSSIBLE APPROACHES TO THE USE OF NESTED SIMULATIONS

The method of *nested/recursive simulations* presents a principle of a simulation inside a simulation used to examine the results of multiple alternative scenarios (or developments) of the simulation. One possible use of this method is *decision support in a simulation*. Nested simulations run for a limited time, and after they are

completed, their results are evaluated. Subsequently, the nested simulations are merged back into a single instance and the main simulation can continue in a selected manner. The flow chart of a simulation using decision support with the use of nested simulations is shown in figure 1.
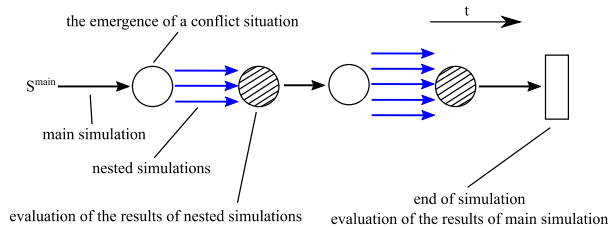

Figure 1: Using nested simulations as simulation decision support technique

Another use of nested simulations can be implemented as a *multi-trajectory simulation* - the simulation experiment is divided into nested simulations at individual points of decision and the simulation is gradually branched more and more and various scenarios are explored. According to the article (Gilmer and Sullivan, 1999), this process can be more effective than using a large number of replications of a single simulation scenario. The flow chart of a simulation using a multi-trajectory simulation is shown in figure 2. In addition, attention will be paid to the first method of use – as a decision support in simulation.
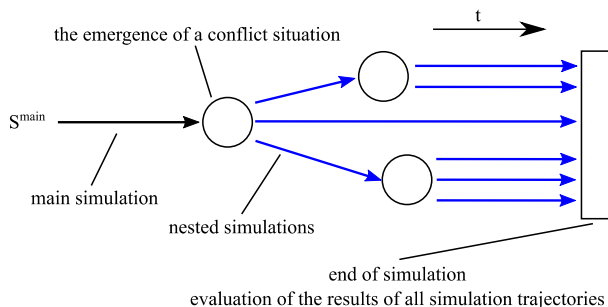

Figure 2: Using nested simulations to implement multi-trajectory simulation

3. NESTED SIMULATION TECHNIQUE

Decision support in the simulator can use the standard simulation engine for both the main simulation and nested simulations. The processing of nested simulation is very different from the usual simulation process of the main simulation. The following procedure formalizes the decision-making process of solving a particular conflict using nested simulations (Diviš and Kavička, 2016):

1. The simulation identifies a conflict state that requires decision support
2. The current instance of one replication of the main simulation (S^m) is paused in time t.
3. For the needs of nested simulation, it is necessary to set their parameters:

(a) the optimality criterion (*CrOpt*), comparative function of the optimality criterion (*CrOptComparer*)
(b) the nested simulation run-length (or more precisely, the stopping condition, *StopCond*),
(c) the (maximum) number of alternative scenarios (*ScnCount*),
(d) the generator of alternative scenarios (*ScnGen*),
(e) the parameters associated with multiple replications of nested simulations,
(f) the parameters associated with recursive calculations of nested simulations.
4. Decision support will create N alternative scenarios of how to continue in the given situation.
5. The main simulation S^m is cloned and *ReplCount* of replications is created for each *i-th* scenario.
6. Individual replications ${}_t S^m S_j^i$ are started (for $I = 1…N, j = 1…ReplCount$).
7. Decision support waits for all replications to complete ${}_t S^m S_j^i$ (for $i = 1…N$, $j = 1…ReplCount$).
8. Decision support evaluates the results of individual scenarios from replications ${}_t S^m S_j^i$ (for $i = 1…N$, $j = 1…ReplCount$) and then selects the scenario that provides the best results according to *CrOpt* and *CrOptComparer*.
9. The simulation S^m continues according to the selected scenario from time t.

It follows from the above procedure (shown in figure 3) that it is necessary to solve several basic questions before the actual realization of the nested simulations about how to actually parameterize and set the nested simulations. A separate issue may also be how to choose alternative scenarios for solving a conflict situation, but this issue depends on the particular application of the method and the type of conflict situation, and may be a non-trivial task in the outcome.

The use of nested simulations in rail transport is limited by possible alternative scenarios. In solving the problems, we are especially limited by the track infrastructure and signalling equipment, which defines the permissible possibilities for the movement of individual trains. Even so, there may emerge many ways to resolve the conflict situations that have arisen.

3.1. Basic parameters of the nested simulations

Before performing the nested simulations, we need to set the parameter group. This set of parameters may vary according to the type of conflict situations to be addressed. Depending on the implementation of decision support using nested simulations, the set of parameters may vary, or some parameters may be implemented differently.
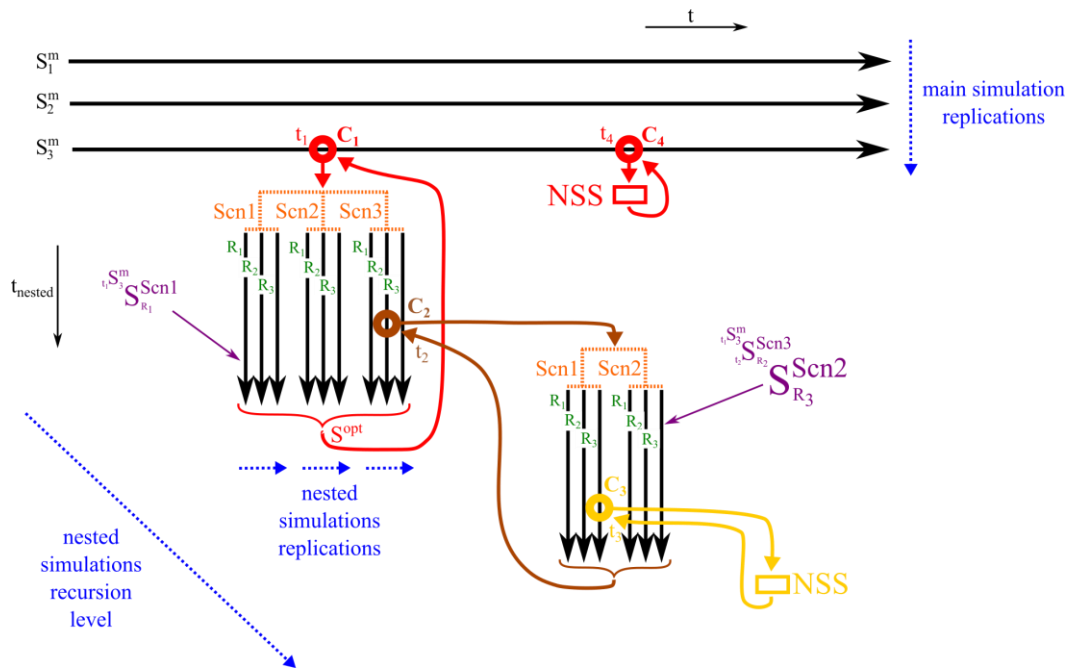
Figure 3: Illustration of occurrence and process of solving one conflict situation in one simulation replication

The first parameter is the number of alternative scenarios (or, more precisely, their minimum and maximum admissible counts), *ScnCount*) indicating how many different alternatives will be examined in the nested simulations. However, this parameter does not tell us how many scenarios in total can be created in a particular situation. The actual preparation of scenarios, which may be a solution to the conflict situation, must be ensured by a component defined by the parameter *ScnGen*. The scenario creation process will vary for different models and may even vary for different conflict situations.

Individual nested simulations must be completed after a certain period of time so that the results can be evaluated. The stopping condition *StopCond* determines the simulation time (or under what particular conditions) after which the nested simulations will be terminated.

After the nested simulations are over, they are evaluated. The next parameter is the optimality criterion (*CrOpt*) - this function evaluates the results of individual scenarios that have been performed as nested simulations. The parameter *CrOptComparer* defines the comparison function for choosing of the best criterium (minimum, maximum). Based on parameters *CrOpt* and *CrOptComparer* the best fitting scenario is then chosen. This scenario then continues the original (main) simulation instance.

4. GENERALIZATION OF NESTED SIMULATIONS

After performing the first attempts with nested simulations, several basic deficiencies have been identified that have led to degradation of the quality of the solution. Nested simulations did not provide as good results as we initially expected.

For these reasons, support for multiple replications of nested simulations and enabling recursive nested simulations (i.e. to solve a conflict occurring within a nested simulation using new process of nested simulations) was created in the interest of further research. The introduction of support, for multiple replication of nested simulations and recursive computations, brings with it many new specific problems to be solved.

4.1. Simulation of multiple replications of nested simulations

Computer simulation as an experimental method is based on the ability to test different variants of system behaviour under different initial conditions. This is accomplished by changing the seed of random number generators (by performing different replications of the simulation). Similarly, in nested simulations, we may require the testing of different evolutions of simulation calculation which respond to the events that may occur in the distant future (which doesn't belong to simulated outlook of nested simulations).

The very process of making multiple copies of the main simulation and modifying them to match different replications is the extension of the original algorithm of nested simulations, and it needs to be further analyzed. When replication of the main simulation is created, the seed for the random number generator is selected. The subsequent random values or seeds for other random number generators are derived the from master generator. If we create an exact copy of the master simulation, each of the nested simulations would exactly match the main simulation behaviour and effectively predict the future for the main simulation.

Creating a copy of the master simulation and changing the seed of the master random number generator may, depending on how the simulator is implemented, begin

to provide alternative values. The nested simulation will provide a different outlook in the future compared to the main simulation. If the simulation uses multiple independent random number generators (initially their seed is derived from the master generator), then it is necessary to modify these generators accordingly.

After making these changes, we will get a different replication of the future behaviour of the main simulation. However, it is still necessary to assume, that in a simulation, there may be a set of values that have been defined by the original replication. These values can be present, for example, in the calendar of the discrete event simulation core. So the near future of the nested simulation can be scheduled according to the original replication.

4.2. Parameters of nested simulations for processing of multiple replications

Following chapters summarize parameters that affect behaviour of the multiple replications of nested simulations.

4.2.1. Number of replications (of one scenario simulation) (*ReplCount*)

The parameter specifies how many replications from each scenario will be simulated. The parameter can be static and immutable for all conflict situations throughout the simulation. Alternatively, it is possible to introduce a different number of replications according to the type of conflict situation. The number of replications could also be determined dynamically, e.g. with respect to the current level of recursive computation of nested simulations.

4.2.2. Preserving of one "main simulation replication" (for each scenario) (*ReplPreserveOriginal*)

Performing replications that will behave differently in the future rather than the current main simulation can be a problem if we want to achieve good results from a decision support system. As an alternative solution, we may preserve the exact copy of the main simulation as one of the replications, and continue the calculation with one copy of the main simulation and a few other different replications.

4.2.3. Results aggregation function (*ReplResultsAggregateFunction*)

Decision support must determine which scenario is best by using the functions defined by the *CrOpt* and *CrOptComparer* parameters. Simulating N replications ends with up to N results for one scenario, and it is necessary to determine how to define the final value of a scenario criterion. Typical representatives for aggregation functions are the average, median, minimum, maximum, or other statistical value pointers.

4.3. Recursive computations of nested simulations

Recursive nested simulations allow you to respond and resolve conflicts within nested simulations. When a conflict occurs inside a nested simulation, the situation is processed as if there was a conflict in the main simulation, and decision support triggers recursive nested simulations.

If the next level of recursive calculations is not allowed, the situation needs to be resolved in a different way. According to the simulation you can use the default solution to the given problem (e.g. do nothing - wait for the track to be released). Another option is to exclude such a simulation from further processing and therefore not to consider the relevant scenario as a usable solution to the conflict situation.

4.4. Parameters of nested simulations for calculating recursive nested simulations

Following chapters summarize parameters that affect behaviour of the recursive nested simulations.

4.4.1. Depth limit of recursion (*RecLimit*)

The parameter specifies how many recursive computation levels can be performed. A value of 0 means that it is possible to create nested simulations from the main simulation, but recursive calculations are not allowed. Each level of recursion additionally increases the algorithm's memory requirements and the computational time required to complete nested simulations.

4.4.2. Stop condition behaviour for recursive nested simulations (*RecStopCondBehaviour*)

The parameter specifies the behaviour of the ending condition (or duration of outlook) within recursive nested simulations. Nested simulations are performed for a limited time (or until a certain condition is met - *StopCond*). If there is a conflict simulation in the middle of a nested simulation, it is a question of how long the outlook is to be, in the second level. Intuitively, three basic types of behaviour can be proposed:

- using standard outlook duration - extending the outlook beyond the end of first level of nested simulations;
- limiting to the outlook of the first level of nested simulations;
- combining the previous two options.

Extending the outlook in recursive simulations will increase computational difficulty while allowing recursive simulations to look into a more distant future. A strict limitation of the outlook may result in a lack of information about the results of recursive nested simulations and thus lead to a suboptimal solution.

4.4.3. Action when reaching limit of recursion (*RecOnLimitAction*)

If a new conflict situation occurs and the current recursion depth limit no longer allows such a situation to be solved using the next level of nested simulations, it is necessary to decide what to do next:

- continue simulation using the default action (*FallbackScenario*);
- continue simulation using other decision support (priority planning, ...);
- stop the simulation prematurely and exclude it from usable results.

If the simulation is terminated prematurely, this nested simulation instance must be discarded from usable results. Other simulations that perform simulations of a longer outlook will show a different character of the results, and the prematurely terminated situation could be incorrectly evaluated as the best solution. Removal of a nested simulation from the conflict solution can lead to the problem of discarding all solutions and thus not finding any solution or finding a suboptimal solution.

Continuing a nested simulation using the default action (or using alternative decision support) allows completion of the simulation and correct evaluation of the result.

4.5. The problem of early decision

The case study focuses on the simulation of a railway station. Decision support is used to determine the replacement station track for the train that arrives at the station and its originally planned track is occupied. A conflicting situation (the occupancy of the default station track) is detected when the incoming train requests the allocation of the last section of its path associated with the station track. This can cause detection of the conflict, even when the station track will be released before the next train physically arrives.

The first experiments using nested simulations selected alternate station tracks that were useable (the track was not occupied, and the train had the possibility of using this track) as possible scenarios for solving conflict. Based on their results, the train was redirected to another track. The implications of this implementation have been revealed during simulation experiments, which in many cases resulted in worse results than in simulations, when no nested simulations were applied, and trains only waited for the release of the originally planned track. Forcing the use of an alternative station track may also lead to the occurrence of secondary conflicts as a result of a previous change in the train track (see figure 4).
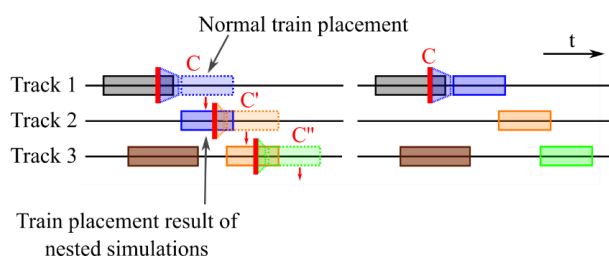
Figure 4: Results of train placement and subsequent conflicts (left - without usage of fallback scenario, right - with usage of fallback scenario)

Based on this behaviour, it was necessary to introduce a default scenario (*FallbackScenario*) into nested simulations. The *FallbackScenario* did not redirect the train to an alternative track, but only caused it's waiting on the rails for release of the originally planned track. During the simulation of such a scenario, the same conflict situation occurs in virtually every simulation calculation step (the train moves along the original route to the occupied station track). This will cause an insoluble exponential increase in computations of nested simulations. This situation is illustrated in figure 5 where during t_{start} to t_{end}, the simulator is repeatedly detecting the same conflict and resolving it with the fallback scenario.
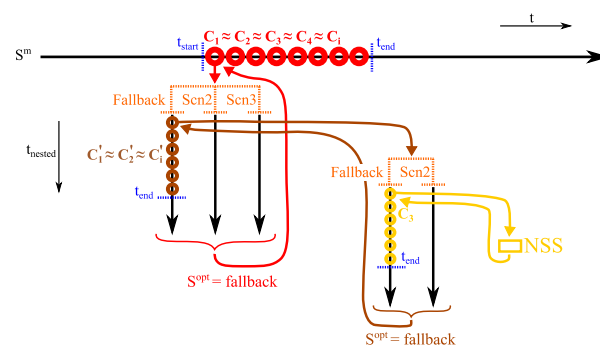
Figure 5: Exponential overflow of fallback scenario

In order to effectively simulate the *FallbackScenario*, it is necessary to limit the possibility of such unlimited execution of nested simulations. A new parameter (*FallbackScenarioConflictLimiter*) has been introduced into the simulation, which blocks the creation of new nested simulations for a given entity (train) for a specified time period.

5. TEST SCENARIO

For the purpose of conducting the initial case study (Diviš and Kavička, 2017), the infrastructure of a smaller scale prototype railway station with several adjacent track sections (ending with simplified railway station models) was created. In particular, the operation of passenger services and a smaller range of freight transport are expected to take place at the station. In the case study, the behaviour of the station was tested at the arrival of delayed trains. For each train, alternative train paths were defined that use alternate station tracks.
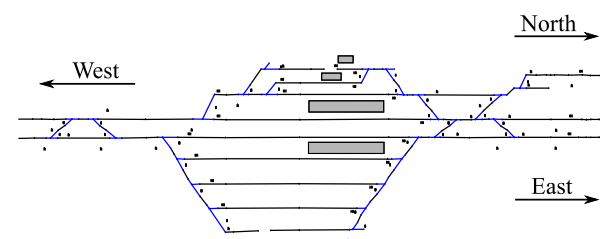
Figure 6: Schematic representation of central station and adjacent tracks

Table 1: Parameterization of trains in the simulation model

Train type	Locomotive / vagons	Course	Interval between trains [h:mm:ss]	Total train count	Delay prob.	Delay mean time (exponential distribution) [s]
Express	1 / 7	West → Central → East	30:00	5	50 %	420
Express	1 / 7	East → Central → West	30:00	5	50 %	420
Passenger	2 / 4	West → Central → East	10:00	12	33 %	270
Passenger	2 / 4	East → Central → West	10:00	12	33 %	270
Passenger	1 / 2	West → Central → North	30:00	4	33 %	270
Passenger	1 / 2	North → Central → West	30:00	4	33 %	270
Cargo	1 / 22	West → East	1:00:00	2	50 %	1800
Cargo	1 / 22	East → West	1:00:00	2	50 %	1800
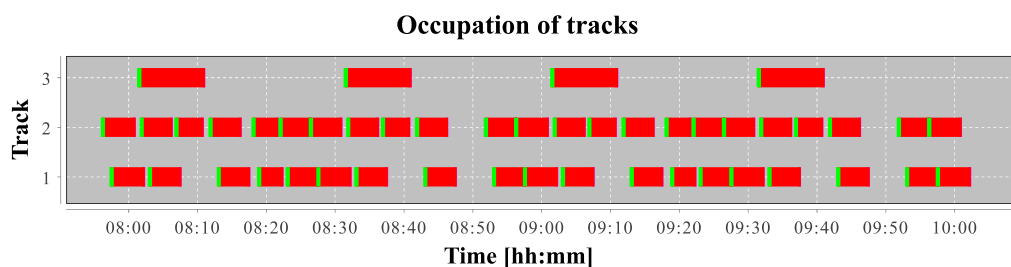
Figure 7: Occupation of station tracks during deterministic simulation

The representation of the main (central) station and the adjacent lines is shown in figure 6. There are two double-track lines (to the stations *West* and *East*) and one single-track line (to the station *North*) leading from the central station. The total distance between the eastern and western stations is about 20 km. The infrastructure is not completely fictional; it is inspired by several railway tracks and stations in the Czech Republic. The track profile contains sections with significant slope and arc ratios.

The simulation study focuses on the station traffic in a two-hour peak period. Passenger and freight trains are included, with the emphasis placed on passenger transport. Passenger transport is divided into two groups: (a) long distance transport - express trains; (b) regional transport - passenger trains. The traffic overview is shown in table 1. Figure 7 shows the occupation of station tracks in the central station under the conditions of deterministic simulation.

In the case study nested simulations are used as decision support. Its task is to select a replacement track for delayed train, for which originally planned track is occupied.

In the case study, various parameterizations of nested simulations were tested and obtained results were compared. Basic parameterization of nested simulations:

- *CrOpt* – average weighted increment of train delays
  - weight is defined by a type (priority) of the train,
    - delay increment – the value is defined as the nonnegative portion of the train delay difference when leaving the simulation model minus train's input delay
- *CrOptComparer* – minimum function,
- *ScnCount* – without restriction,
- *ScnGen* – according to the available train paths,
- *ReplPreserveOriginal* – yes,
- *ReplResultsAggregateFunction* – average function,
- *RecStopCondBehaviour* – extension of the simulation time,
- *RecOnLimitAction* – usage of *FallbackScenario*,
- *FallbackScenarioConflictLimiter* – 15 s.

Varied parameters according to configuration:

- *StopCond* – 1, 15, 30, 45, 60, 75, 90 minutes,
- *ReplCount* – 1, 3 replications
- *RecLimit* – 0, 1, 3 levels of recursion,
- *FallbackScenario* – enabled (1) / disabled (0).

For each test configuration was calculated 200 replications of main simulation.

6. SIMULATION RESULTS

Before performing simulations using nested simulations, a series of simulations was performed

Table 2: Results and computational difficulty of different configurations of nested simulations

Parameter		Average delay [s]			Computation time [s]		
		Worst	Average	Best	Worst	Average	Best
FallbackScenario [-]	**0**	56.18	54.27	51.72	15 970	4 555	240
	1	55.35	50.07	45.86	7 618	2 311	237
RecLimit [-]	**0**	56.18	52.73	48.61	2 199	1 098	246
	1	55.97	51.25	45.86	15 970	6 047	237
	3	55.94	55.42	54.90	1 472	923	375
ReplCount [-]	**1**	56.18	51.52	45.86	15 970	3 820	237
	3	56.16	53.99	49.36	12 867	2 503	295
StopCond [min]	**1**	56.18	55.55	54.90	1 472	427	237
	15	54.15	51.69	48.83	12 867	3 300	573
	30	54.49	51.11	47.98	4 884	2 392	846
	45	54.76	50.55	47.10	9 105	3 949	1 095
	60	54.81	50.61	46.25	13 146	5 510	1 267
	75	54.91	50.48	45.86	14 847	6 267	1 427
	90	54.90	50.62	46.26	15 970	6 826	1 518

without the use of decision support to measure the reference delay of trains in the individual replications. The results without decision support are: weighted average delay – 59.81 s, express trains – 62.01 s, passenger trains – 59.56 s and cargo trains – 41.30 s.

Weighted average of delay with usage of nested simulations are in range 45.86 s – 56.18 s. Half width of 95 % confidence interval doesn't exceed value 8.23 s. The delay of individual train types ranges from:

- express trains 48.21 – 58.61 s,
- passenger trains 45.52 – 55.89 s,
- cargo trains 24.57 – 37.36 s.

The best results were achieved with *FallbackScn* 1, *StopCond* 75 min, *ReplCount* 1, *RecLimit* 1 – 45.86 s (express trains 48.21 s, passenger trains 45.88 s, cargo trains 24.57 s). A summary of the results is given in table 2.

6.1. Discussion
From the measured results it is possible to determine several assumptions for further use and research of the nested simulations.

The quality of the result is significantly affected by the *StopCond* parameter. The optimization of station traffic was better with longer outlook of the nested simulations. However, the disproportionate extension of the outlook period did not lead to further improvement of the results (saturation occurred at 45 mins, respectively 75 mins, according to other parameters).

Enabling recursive nested simulations (*RecLimit*) leads to a significant improvement in the quality of the result. It also leads to a significant increase in computational complexity. In the case study, variants involving 3

recursion levels and a longer outlook period were not tested for their computational (time) difficulty.

Enabling *FallbackScenario* (ie. the option to postpone applying of the solution at a later stage of simulation) greatly improves the results achieved.

Increasing the number of replications of nested simulations (*ReplCount*) has not yet lead to improving of the results. Because of the high computation difficulty scenarios with longer outlook period and more replications were not thoroughly tested.

From figure 8 (d) it can be determined that certain configurations achieve worse results and their computational demands are higher than other better parameterized simulations. E.g. in scenarios where the use of *FallbackScenario* is not allowed, the best result of 51.72 seconds has been achieved with a computational time of 4 110 s. In the scenarios where the *FallbackScenario* was enabled, the result of 48.73 seconds was achieved with a computational time of 1 057 s. Thus, a better result was achieved with roughly four times smaller computational demands.

7. CONCLUSION
The experiments show that the parameterization of the nested simulations significantly influences the achieved results and the computational demands of the whole process. Based on the results obtained, we can find basic recommendations for parameterization of nested simulations.

The usage of *FallbackScenario* (ability to postpone solving of conflict at a later time) has a great positive impact on achieved results. This parameter has increased the computational time twice, but has significantly improved the value of the resulting criterion.

(a) StopCond parameter

(b) RecLimit parameter

(c) ReplCount parameter

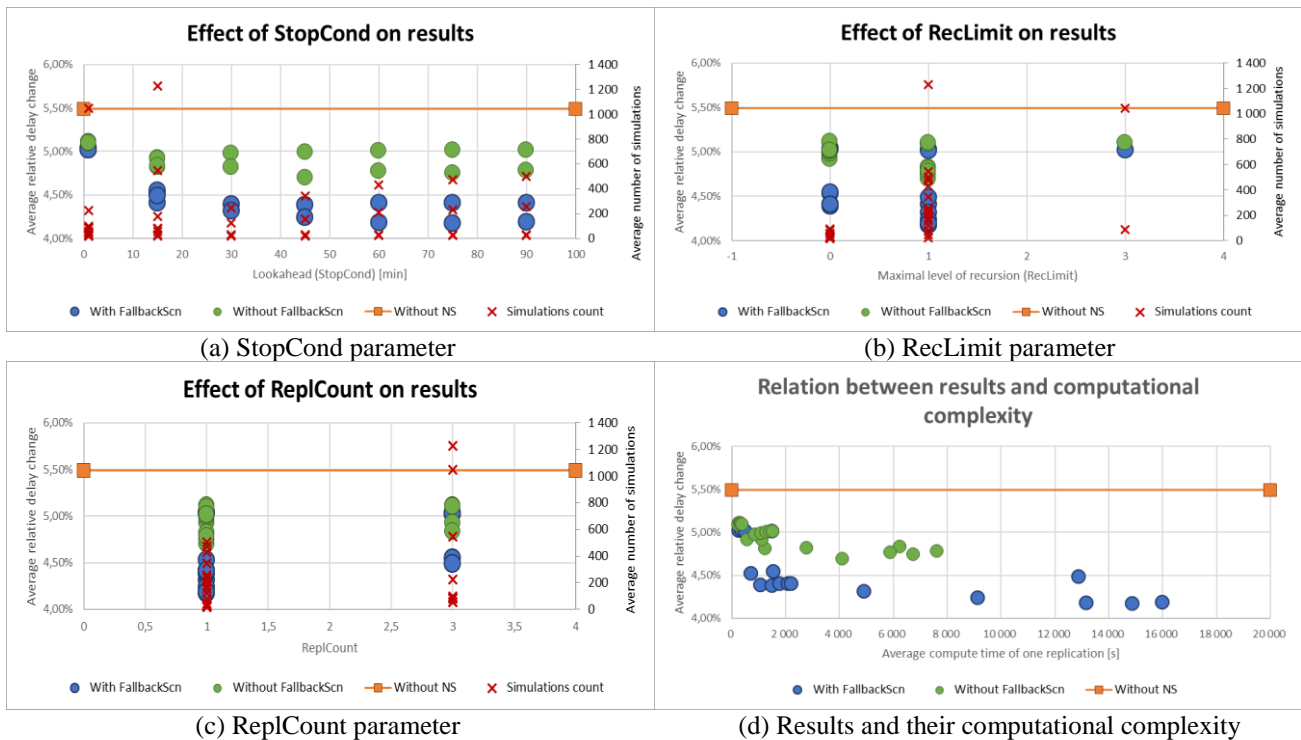(d) Results and their computational complexity

Figure 8: Influence of individual parameters on achieved results

Another important parameter is *RecLimit* and allowing at least one level of recursion. As a drawback, a significant increase in the calculation time can be noted. In experiments conducted with enabled recursion, the computation time was extended up to 7 times.

The *StopCond* parameter greatly influences both the quality of the result and the computational difficulty. His choice should be based on rigorous statistical evaluation of the results.

The *ReplCount* parameter in the experiments that we have done so far has not led to a significant improvement in the results, and we cannot provide suitable recommendations for setting this parameter at this time.

These experiments show different levels of benefit of individual parameters and also the issue that it is not possible to see the individual parameters completely separately. Their interactions further influence the achieved values of the results and the computational demands of the individual experiments Examining these interactions will continue to take place in the future.

REFERENCES

Bonté B., Duboz R., Quesnel G., Muller J. P., 2009. Recursive simulation and experimental frame for multiscale simulation. In: Proceedings of the 2009 Summer Computer Simulation Conference, 164-172. July 13-16, Istanbul, Turkey.

Diviš R., Kavička A, 2015. Design and development of a mesoscopic simulator specialized in investigating capacities of railway nodes. Proceedings of the European Modeling and Simulation Symposium, 52-57. September 21-23, Bergeggi, Italy.

Diviš R., Kavička A, 2016. The method of nested simulations supporting decision-making process within a mesoscopic railway simulator. Proceedings of the European Modeling and Simulation Symposium, 100-106. September 26-28, Larnaca, Cyprus.

Gilmer J. B., Sullivan F. J., 1999. Multitrajectory simulation performance for varying scenario sizes [combat simulation]. In: WSC'99. 1999 Winter Simulation Conference Proceedings. 'Simulation - A Bridge to the Future' (Cat. No.99CH37038), 1137-1146. December 5-8, Phoenix, AZ, USA.

Gordy M. B., Juneja S., 2010. Nested Simulation in Protfolio Risk Measurement. Management Science 56:1833-1848.

Hill J. M. D., Surdu J. R., Ragsdale D. J., Schafer J. H., 2000. Anticipatory planning in information operations. In: SMC 2000 Conference Proceedings. 2000 IEEE International Conference on Systems, Man and Cybernetics. 'Cybernetics Evolving to Systems, Humans, Organizations, and their Complex Interactions' (Cat. No.00CH37166),

2350-2355. October 8-11, Nashville, Tennessee, USA.

Kindler E., 2010. Nested Models Implemented in Nested Theories. In: Proceedings of the 12th WSEAS International Conference on Automatic Control, Modelling & Simulation, 150-159. May 29-31, Catania, Sicily, Italy.

ANALYSIS OF RESOURCE MANAGEMENT METHODOLOGIES FOR THE DEVELOPMENT OF DISCRETE EVENT SIMULATION MODELS REPRESENTATIVE OF THE WORKS DEVELOPED IN SHIPYARDS

Adolfo Lamas-Rodríguez[a], David Chas-Álvarez[b], José Antonio Muiña-Dono[c]

[a] Universidade da Coruña, Navantia, UMI Navantia-UDC
[b] UMI Navantia-UDC
[c] Universidade da Coruña

[a]alamas@udc.es
[a]david.chas@udc.es
[a]jose.mdono@udc.es

ABSTRACT

Nowadays it is very common for certain types of workshops to organize their work based on predefined milestones from the beginning of the project. In shipbuilding, it is common for the primary manufacturing workshops to work according to the milestones established by the final assembly. Similarly, offshore wind projects that are currently being developed in different shipyards work in the same way. In addition, it is common in these manufacturing projects apply high penalties in case of non-compliance with established delivery milestones.

Likewise, the usual work done in the shipyards have a high dependence on labor, so it seems interesting to study different resource allocation methodologies in order to develop the simulation models that represented the manufacturing processes developed in a shipyard.

Keywords: resource management, jacket, dispatch rules, discrete events simulation.

1. INTRODUCTION

Scheduling is a common problem in the currently industry and thus, any industrial process must be perfectly programmed and defined. Normally with the aim of assigning a series of resources, normally limited, to a task and in a certain period of time. With the implementation of a methodology for allocating these resources, it is intended to reach an optimum point of one or several objectives designated by the company and that normally lead to reduce production time and costs.

As shown in (Henrique, Pinheiro, Santos, and Venâncio 2014) the authors remark that the scheduling problem has been posing since the 1950s, in search of ever better solutions. With approximately 200 works of some importance about hybrid metaheuristic methods using different techniques to solve problems associated with scheduling have been published between 2003 and 2013. Likewise, it is important to highlight the importance of dispatch rules in the problems associated with production scheduling. Although, normally dispatch rules are simply based on time-related criteria, however, other criteria should be taken into account. For example, the profit margins offered by each product, or the importance of one client over another, when assigning priorities (Scudder and Hoffmann 1986).

In turn, in certain scheduling problems, the added difficulty of having one limited resource more, the operator, must be taken into account. Which is known as DRC (Dual Resource Constrained) problems.

In (Treleven 1985) the author studies the behavior of the rules of dispatch in a problem where the limited resources are machines and operators. In this case, the author plans an operator-machine relationship of 50% or 66.67%. Because he suggested that they are the most general. Therefore, in the analyzed case of a workshop of 18 machines, 9 or 12 employees will be used respectively.

In (Park 1990) is studied the impact of the rule of allocation of workers to the workshop, in a workshop with limited number of operators and machines, as well as how the workers allocation rule affect at the different rules of dispatch used.

In (Cappadonna, Costa, and Fichera 2013) the influence of workers when planning production is studied in a workshop with the number of employees and parallel machines are limited. To study the influence of the operators and the number of machines, different workshop conditions are evaluated, varying the number of jobs, machines and operators, taking into account setup times.

In (Scholz-reiter, Heger, and Hildebrandt 2009) the importance of having a series of resources that present a critical behavior, which will be machines, operators, or a mixture of both, is studied. Emphasizing that this last case has been one of the least studied due to its complexity, but nevertheless it stands out as a problem of real application, and it can be complicated to solve in a real situation.

With these precedents, it is expected that the number of workers is a key factor in the productive system of the company, and their work in plant should be designed to offer the maximum performance of the workshop.

On the other hand, the offshore wind market is in a stage of expansion heading towards jacket structures or floating structures, because offshore wind farms are increasingly built with generators of greater capacity and farther from the coast (Musial, Walter et al. 2016)

The manufacture of this type of structure is generally carried out in shipyards, particularly in shipyards that have the capacity to act as a logistics port. As staged by (Lantz, Hand, and Wiser 2012), the future of wind power will depend on the industry´s ability to continue achieving reductions in the cost of energy. In turn, the work required to manufacture this type of structures requires a large amount of labor, so that the programming of the production must be subject to the human resources available in the shipyard.

Due to the complexity of programming the production for these projects, the simulation is postulated as an appropriate method, since it allows to perform very complex problems and see the behavior of the simulated system in different situations.

Since the 50s and 60s, with the increase of computers it is possible to represent the structure of the workshop, as well as its activities, work and other limitations in detail, with which, with the appropriate input data, it can be predicted by simulation programming at a future time at a low cost.

Another important aspect to deal with the problem of production programming, is knowing what type of problem is being studied, whether a static or dynamic case, since its characteristics are very different, as well as how to solve it.

Static problems are characterized because at a certain moment a series of works will arrive at the workshop, and until these are completely finished, no new works will arrive. Therefore, we know from the beginning the priorities to be assigned to a job, without taking into account that its attributes will vary over time.

The dynamic case problems are characterized by the continual arrival of different works to the workshop, which will cause us to continually modify our work plan to adapt it to the new needs that have arisen.

Although in the static case is possible use a series of algorithms in order to solve the problem (where usually do not take into account or change times, or flexibility of routes or the operator as a limited resource), in dynamic cases we will mainly opt for simulation techniques, which allow complex real problems to be addressed, without the need to apply as much simplification as with other methods, giving us the system's response to a series of situations

On the other hand, one of the greatest advantages of simulation is the simplification of complexity and the ability to analyze different environments, offering great results.

As for simulation software, there is a wide variety of programs that can be used, but in this case the use of ExtendSim has been chosen. This software is developed and created by Imagine That Inc., currently one of the best 2D simulation programs and optimization offered by the market, allowing to simulate: continuous and discrete elements, as well as discrete rates and optimization systems.

2. TYPES OF RESOURCE MANAGEMENT METHODOLOGIES USED

This work focuses on manufacturing processes dependent on delivery milestones, which can be milestones marked by subsequent stages of manufacture or milestones of final delivery of the product.

The reason for focusing the study on this type of manufacturing projects is, in large part, because most of the projects carried out in the shipyards involve manufacturing dependent on delivery milestones. For example, in naval manufacturing, the process can be simplified to the creation of blocks and its subsequent assembly stage. With this simplified is evident that the delivery of the blocks will depend on the milestones marked by the assembly strategy used. At the same time, if the blocks are break down into sub-blocks, as in the previous case, the delivery of the sub-blocks will be marked by the milestones of the formation of the block, which, as mentioned above, have the delivery milestone set according to the final assembly strategy used.

The same situation in terms of manufacturing strategy is found in offshore wind projects, such as the manufacture of jackets (Figure 1), or the manufacture of Spar type structures (Figure 2).

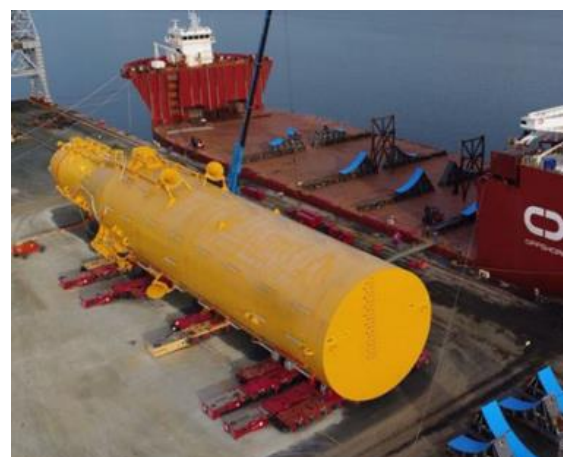Figure 1: Jacket manufacturing

Figure 2: Spar structure manufacture

Focusing the study on the manufacture of jackets, and simplifying the construction process we have the flow chart of the (Figure 3).
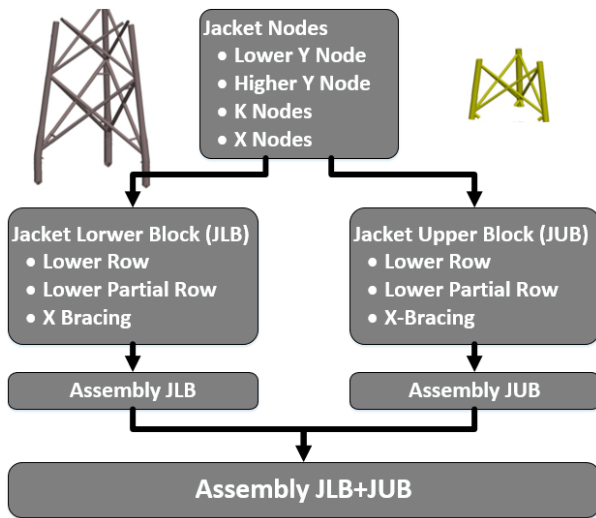

Figure 3: Jackets manufacture flow chart

On it can be seen that the first stage is the manufacture of the nodes, in a second stage from the nodes and the steel pipes the X-Bracings, Rows and Partial Rows, of the jacket lower block (JLB) and the jacket upper block (JUB) are formed. Third stage the JLB and the JUB are assembled, and finally in the fourth stage the assembly of the JUB and JLB is done.

Likewise, as a general rule, in offshore wind projects it is very likely to have intermediate delivery milestones. Among other things because, due to the dimensions of the jackets, (approximately 30 meters of footprint and 80 meters of height) it is very complicated to transport more than 4 jackets in each shipment. In addition, when the jackets are installed in the sea, it is impossible to store them near the offshore wind farm.

In this way, the delivery milestones to the client can be considered as main milestones of an offshore manufacturing projects. But if these milestones are extended upstream in the manufacture of the jackets, adjusting the fabrication to the available resources of the shipyard, it is possible to mark intermediate milestones for each manufacture stage.

On the other hand, as it is a manufacturing strategy with great dependence on intermediate delivery milestones, it has been considered to use mainly two dispatch rules. First, the rule first in first out (FIFO) are proposed. Because the manufacture of jackets is a mass production and it does not make sense to manufacture jacket number 2 before number 1. Secondly, the critical ratio (RC) rule is used, due to between the different components of the same jacket there is a big difference in the manufacturing times. For this reason, it can be considered interesting in certain workshops to manufacture components of the jacket number 2 before finishing with the components of jacket number 1.

3. THEORETICAL SIMULATION MODEL

In order to illustrate the problem that is developed in this work, a theoretical simulation model has been proposed. The theoretical simulation model, which is represented in an aggregate form in Figure 4, has been developed with the discrete event simulation software ExtenSim. For the design of the model, libraries of items and values have been used, which come pre-defined in the software used.

Figure 4: Theoretical simulation model

As is possible to see in the previous image, the model has two clearly differentiated parts, the left part of process analysis through discrete events, and the right part of representation of results. Also, in each of the blocks represented in the left part of Figure 4, a block structure similar to that represented in Figure 5 has been designed, which represents the theoretical manufacturing process that is studied in this work.
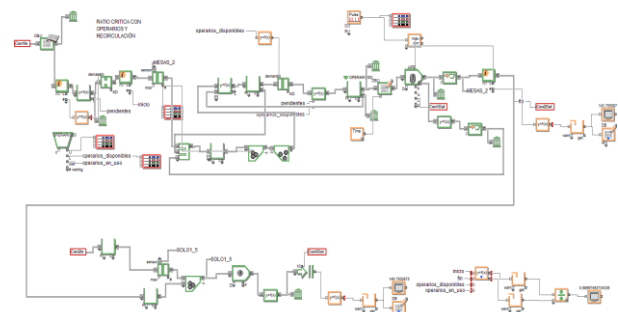
Figure 5: Model blocks design

This theoretical simulation model developed represents an item processing workshop with capacity for three items in parallel prior to an assembly area. And in which, each item that enters the processing workshop can have between 1 and 4 workers at the same time.

Finally, the simulation model is based on the following hypotheses to perform the comparative study among resource allocation methodologies:

- Each product will have a different delivery milestone.
- Operator downtimes will not be assumed.
- The use of extra shifts is not possible.
- Processing time is a function of the number of operators assigned.

- A total of 6 workers will be available per work shift.
- The results achieved are calculated within a 95% confidence interval

3.1. Resources assessment methodology and experiments description

The simulation model developed represents the processing of 100 items that must be assembled in a final stage with capacity for a single assembly in parallel. In terms of resource management, the simulation model proposes the comparison of five resource management strategies based on the dispatch rules FIFO and RC:

- Dispatch rule FIFO to the entry the items at the processing workshop and with static operator assignment for each item (Strategy 1).
- Dispatch rule RC to the entry the items at the processing workshop and with static operator assignment for each item (Strategy 2).
- Dispatch rule FIFO to the entry the items at the processing workshop and with dynamic operator assignment for each labor turn. Being possible to assign between 1 and 4 operators for each item (Strategy 3).
- Dispatch rule RC to the entry the items at the processing workshop and with dynamic operator assignment for each item that entry in the processing workshop. Being possible to assign between 1 and 4 operators for each item (Strategy 4).
- Dispatch rule RC to the entry the items at the processing workshop and with dynamic operator assignment for each labor turn. Being possible to assign between 1 and 4 operators for each item (Strategy 5).

These five rules of resource allocation are differentiated mainly because they are FIFO or RC strategies. In addition, these rules are intended to study the impact on the results provided by the simulation models based on the frequency with which resources are assigned to each task.

Because, at the time of designing the models of simulation it is of common to use the assignment of resources in a static way at the beginning of a process, and then this resource will be occupied until the end of the process.

For this reason, with the rules for allocation of resources studied, it is intended to see the impact on the results of the simulation models of allocating resources in a different way to assignment by task. Choosing in this case to make assignments per work shift as represented in the flow diagram of Figure 6.
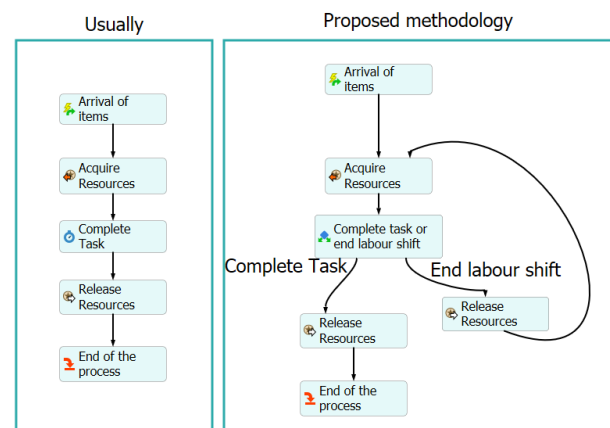
Figure 6: Process flow of resources management methodology

With the objective of obtaining quantitative results of the proposed resource allocation methodologies, three different experiments have been considered as a function of the time of processing of the items. The process time for each item in this model, will be represented by the minimum unit of the work shift. Because, as has been observed during the data collection for this study, most of the works, which can be represented in a planning, last longer than one work shift.

1. First experiment, each item has a duration represented by a LogNormal distribution of mean 1 work shift, with a standard deviation of 0.5 labor turns.
2. In the second case each item has a duration represented by a LogNormal distribution of mean 10 working shifts, with a standard deviation of 3 shifts.
3. Finally, in the third experiment each item has a duration represented by a LogNormal distribution of mean 100 work shift, with a standard deviation of 20 shifts and shifted 30 shifts to the left side.

Finally, in this theoretical model, delivery milestones have been established for each experiment based on the sum of the average process times in each scenario, the number of workstations available in the processing workshop, and the sum of the average process times of the assembly stage in each scenario (1)

$$H(j) = \left(\sum_{i=1}^{j} \frac{T_p(i)}{N^o_{workshops}} \right) + \left(\sum_{i=1}^{100} \frac{T_p(i)}{N^o_{workshops}} - \sum_{i=1}^{100} T_e(i) \right) \quad (1)$$

Where:
- H (j): It is the delivery milestone for the item j
- Tp: It is the average time of process
- Te: It is the average assembly time

3.2. Results of the theoretical simulation model

With the theoretical model developed, results have been obtained in a first instance that allow to see the differences between modeling the resource methodology in one way or another. The results evidence that, although the completion time of the items processing is similar for all cases, the time of non-fulfillment of milestones and the number of milestones unfulfilled varies considerably among the different methodologies studied.

The results obtained with the theoretical simulation model are represented in Table 1 for the first scenario, Table 2 for the second, and Table 3 for the last scenario. For complete the results tables average values have been taken after having made 100 repetitions for each experiment.

Table 1: Results to scenario 1

Scenario 1			
Strategy	Unfulfilled milestones	Cumulative delay [turns]	Final time [turns]
Strategy1	6,70	8,45	34,64
Strategy2	10,11	10,18	34,64
Strategy3	6,05	8,00	34,51
Strategy4	11,70	29,76	35,71
Strategy5	8,12	8,05	34,51

In the first experiment, with work times represented by a LogNormal distribution of mean 1 shift and deviation 0.5 turns. The results shown that the best way to represent the resources in the simulation model to this type of projects is through the resource management strategy3. Improving by around 6% in terms of accumulated lag times and around 10% in terms of the number of milestones that have not been met with respect to strategy1. Then, the second best strategy is between the strategy1 and strategy5. Because the first has smaller number of unfulfilled milestones, but a higher average of cumulative delays than the strategy5. Finally, the worst strategy to this scenario is the strategy4. Because it has the higher number of unfulfilled milestones and the higher cumulative delays.

Table 2: Results to scenario2

Scenario 2			
Strategy	Unfulfilled milestones	Cumulative delay [turns]	Final time [turns]
Strategy1	3,61	22,38	343,25
Strategy2	4,73	24,99	342,70
Strategy3	3,23	13,96	341,99
Strategy4	5,00	64,46	347,36
Strategy5	3,66	14,66	342,00

Second scenario, raises the same strategy of manufacture, but with process times represented by a LogNormal distribution of mean 10 turns and deviation 3 turns. As in the previous scenario, the best result is

obtained with the resource management strategy3. Obtained an improvement of 38% in terms of accumulated delay times and around 10% in terms of the number of broken milestones with respect to strategy1. Again, the second best strategy is between the strategy1 and strategy5. And also, the worst strategy is the strategy4.

Table 3: Results to scenario 3

Scenario 3			
Strategy	Unfulfilled milestones	Cumulative delay [turns]	Final time [turns]
Strategy1	5,92	372,81	2374,73
Strategy2	8,24	456,95	2371,05
Strategy3	5,85	285,89	2358,56
Strategy4	8,24	763,74	2411,92
Strategy5	7,26	325,17	2358,13

Finally, third scenario has process times represented by a LogNormal distribution of mean 100 work shift and standard deviation of 20 turns, displaced to the left 30 turns. In this last scenario, the resource management strategy3 improves by 24% in terms of accumulated lag times and around 1% in terms of the number of milestones that have not been met with respect to strategy1.

As summary of the three scenarios, it can be highlighted that, for the three experiments performed with the theoretical simulation model, the resource management strategy that offers the best results is the strategy3. Among the others strategies, the second that works best is between strategy1 and strategy5. Finally, the worst strategy in all scenarios is to strategy4.

4. PARTICULARIZATION OF THE MODEL FOR THE MANUFACTURE OF JACKETS

In order to verify the results obtained with the theoretical simulation model developed, a simulation model based on a real jackets manufacturing process for offshore wind was made.

The simulation model encompasses all jackets manufacturing process, from the nodes manufacturing to the final assembly in the order shown in the flow diagram of the (Figure 3).

In order to simplify the analysis of the results, the model has been focused on the manufacturing of the nodes. For the nodes manufacturing, the demand milestones are marked by the need of nodes in the assembly stages of X-Bracings, Rows and Partial Rows.

For the jackets manufacturing project modeled, four types of nodes are differentiated in the design of the jacket (Figure 7).
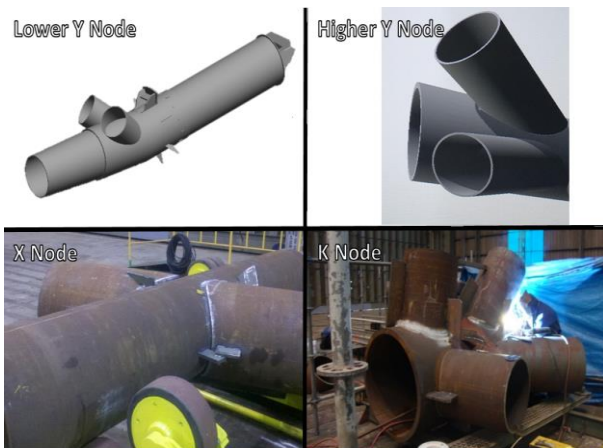
Figure 7: Nodes types

Table 4 shows the average process times, as well as the work stations in parallel and the maximum and minimum personnel that can work in parallel in the same type of node. At this point it is important to emphasize that the normal thing in these projects is that the workers work in pairs, due to the regulation of prevention of occupational risks.

Table 4: Information about nodes manufacturing

Description	Average process time [turns]	Workshops in parallel	Max and Min operators number
Lower Y node	6	3	2-6
Upper Y node	3	2	2-4
K node	2	2	2-4
X node	2	3	2-4

In order to represent the times of nodes fabrication in the simulation model a LogNormal distribution was used. The LogNormal distribution used as mean the average process time for each node type and deviation 0.25 turns. At the same time, for the manufacture of these nodes there is a group of 20 workers, who can work indifferently in any of the node manufacturing stations.

The real manufacturing project studied in this work consists of the manufacture of 20 jackets, with 3 legs each one, as represented in the Figure 1.

With these project characteristics, is necessary to manufacture 60 lower Y nodes, higher Y nodes, 120 K nodes, and 180 X nodes. Because the jacket has three levels with X nodes, two level with K nodes and the lower an upper level with Y nodes.

Applying the same five resource management strategies that have been applied in the theoretical simulation model. Table 5 represents the results for this representative model of nodes manufacturing for a real manufacturing project of 20 jackets.

Table 5: Results to the nodes manufacturing model

Nodes manufacturing model			
Strategy	Unfulfilled milestones	Cumulative delay [turns]	Final time [turns]
Strategy1	15,18	18,10	115,20
Strategy2	12,72	12,18	114,84
Strategy3	6,42	8,56	114,21
Strategy4	20,18	35,18	121,73
Strategy5	3,39	4,80	114,20

The results obtained in Table 5, have been obtained from the average values after executing the simulation model until obtaining a confidence interval of the relative error regarding to final time of 95%.

According to the results obtained, the best strategy for modeling resource management is Strategy5. On the contrary that the theoretical model, where the best strategy had been the Strategy3. The difference between the theoretical model and the model representative of the manufacture of jackets, and for which, the strategy of resource management is different, lies in the need for the items with respect to their creation in the model. In the theoretical model the items entry the assembly stage in the same order that they were created in the model. But in the representative model of the actual process of manufacturing jackets, the nodes are required in the assembly stages in different order to the creation in the simulation model.

Finally, it is interesting to note that in both models, the best results are obtained with strategies that include the calculation of resources dynamically and periodically. Reducing in all the analyzed scenarios the number of milestones broken and the accumulated time of delay.

5. CONCLUSIONS

In general, this work has demonstrated the importance of efficiently modeling resource management in projects with intermediate delivery milestones. On the other hand, it is important to highlight that resource management plays a very important role in projects such as those studied, where labor represents most of the work carried out in the project.

Likewise, it has been found that to make efficient management of resources is necessary to recalculate their allocation periodically. Because, if the resources allocation is done for a time equivalent to the task processing time, the simulation model gets erroneous data, and that also do not correspond to the actual process. Usually, in projects with large labor needs, and in which the work stations are not fixed, the rotation of operators from one station to another depending on the needs of the project is evidence.

Finally, this work aims to show the importance of modeling the intermediate milestones of product delivery to reliably represent the real manufacturing process. Because, as a general rule, intermediate delivery milestones are associated with contract terms that

influence both manufacturing processes as in economic terms.

ACKNOWLEDGMENTS

REFERENCES

Cappadonna, F. a., Costa, a., & Fichera, S. (2013). Makespan minimization of unrelated parallel machines with limited human resources. Procedia CIRP, 12, 450–455. doi:10.1016/j.procir.2013.09.077

Henrique, T., Pinheiro, G., Santos, A., & Venâncio, C. R. (2014). A hybrid Lagrangean metaheuristic for single machine scheduling problem with sequence-dependent setup times and due dates.

Musial, Walter et al. 2016. "2016 Offshore Wind Technologies Market Report, U.S. Depart-ment of Energy.": 131. http:/www.osti.gov/scitech.

Lantz, E., Hand, M., and Wiser, R. 2012. "The Past and Future Cost of Wind Energy." World Renewables Energy Forum 2012 (August): 1–10.

Park, P. (1990). A study of labor assignment rules with bottlenecks. Omega, 18(3), 247–257. doi:10.1016/0305-0483(90)90039-C

Scholz-reiter, B., Heger, J., & Hildebrandt, T. (2009). Analysis And Comparison Of Dispatching Rule-Based Scheduling In Dual-Resource Constrained Shop-Floor Scenarios, II.

Scudder, G., Hoffmann, T. (1986). The Use of Value-Based Rules to Avoid Shop Disruption. Omega, 14, 259-264. doi:10.1016/0305-0483(8690046-0)

Treleven, M. (1985). An investigation of labor assignment rules in a dual-constrained job shop. Journal of Operations Management, 6(1), 51–68. doi: 10.1016/0272-6963(85)90035-X

AUTHORS BIOGRAPHY

ADOLFO LAMAS RODRÍGUEZ graduated from the University of Vigo in 1998. He holds an MSc and a PhD in Industrial Engineering. He combines his research activities in the researching group Grupo Integrado de Ingeniería and his position as a senior engineer and Project Manager in the Spanish leading shipbuilding company Navantia. He is also Associate Professor in the University of A Coruna since 2004 teaching in subjects related to manufacturing, simulation and Lean Manufacturing techniques He is the coordinator of one of the researching lines in the joint venture Navantia-University of Coruña (UMI) related to simulation and optimization models of industrial processes.

DAVID CHAS ÁLVAREZ holds an MSc in Industrial Engineering since 2015 and PhD student since 2016. He works as research engineer in the joint venture Navantia-University of Coruña (UMI) and he is mainly involved in the development of simulation and optimization models of industrial processes, especially in models of manufacture wind turbines foundations.

JOSÉ ANTONIO MUIÑA DONO holds a university degree in Industrial Technology since 2015. He holds an MSc in Industrial Engineering since 2017 from the University of Coruña, and PhD student since 2017. He works as research engineer in the joint venture Navantia-University of Coruña (UMI) and focusing his activity on the M&S of industrial processes.

BSE: A MINIMAL SIMULATION OF A LIMIT-ORDER-BOOK STOCK EXCHANGE

Dave Cliff

Department of Computer Science
University of Bristol
Bristol BS8 1UB, U.K.

csdtc@bristol.ac.uk

ABSTRACT

This paper describes the design, implementation, and successful use of the *Bristol Stock Exchange* (BSE) a novel minimal simulation of a centralized financial market, based on a Limit Order Book (LOB) such as is commonly in major stock exchanges. Construction of BSE was motivated by the fact that most of the world's major financial markets have automated, with trading activity that previously was the responsibility of human traders now being performed by high-speed autonomous automated trading systems. Research aimed at understanding the dynamics of this new style of financial market is hampered by the fact that no operational real-world financial exchange is ever likely to allow experimental probing of that market while it is open and running live, forcing researchers to work primarily from time-series of past trading data. Similarly, university-level education of the engineers who can create next-generation automated-trading systems requires that they have hands-on learning experiences in a sufficiently realistic teaching environment. BSE as described here addresses both needs: it has been successfully used for teaching and research in a leading UK university since 2012, and the BSE program code is freely available as open-source on *GitHub*.

Keywords: simulation for education, financial markets, automated trading.

1. INTRODUCTION

This paper reports on the design, implementation, and successful use of a simulated financial exchange, for use in university teaching and research. The simulated exchange implements the same central dynamic data structure (the *Limit Order Book,* or LOB) as is found in major national financial exchanges such as NYSE or NASDAQ in the USA, and LSE in the UK. Having been developed at the University of Bristol, the exchange simulator is named the *Bristol Stock Exchange* (BSE). BSE was deliberately written to be easy to use by, and to understand for, novice programmers; and it does not require powerful hardware to run (it happily executes, slowly, on the popular *Raspberry Pi* low-cost single-board computer). BSE is written in *Python* (v.2.7) and the full source-code has been made freely available as open-source on the *GitHub* repository.

The crucial difference between BSE and traditional financial-market simulators that operate by regurgitating a time-series database of historical transaction prices is that the traders in BSE can directly affect the prices at which transactions take place, pushing prices up when demand exceeds supply and driving prices down when supply exceeds demand. In BSE, the price at time $t + 1$ is not simply whatever price is recorded on the historical time series but is instead directly dependent on the actions and interactions of the traders active in the market at time t. This is explained and explored in more detail later in this paper.

The creation of BSE was motivated primarily by the observation that many of the world's major financial markets now have very high levels of automation, with human traders having been replaced by autonomous *algorithmic trading* systems, known colloquially as "robot traders" or simply as "algos". Early automated trading systems were often introduced to perform simple routine trading activities that it was not worth asking a highly-paid human trader to do, but over time the capabilities of robot traders, particularly the amount of data that they could assimilate and act upon, and/or the sheer speed at which they could respond to changes in the market, meant that the robot traders could outperform human traders, at lower cost. At that point, simple considerations of economic efficiency meant that robots traders proliferated in many markets, and the number of trades that involved human counterparties negotiating at the point of execution fell sharply. The change to automated trading has altered the dynamics of major financial markets and has created a demand for people with university-level education in the design and construction of automated trading systems, and in the analysis and management of automated markets. BSE is a simple minimal abstraction of an automated market, and includes reference implementations of a number of well-known robot trader algorithms. Section 2 of this paper gives background information on auctions, financial markets, and the LOB. Section 3 then describes BSE's LOB, its array of robot traders, and how the robot traders can be used to populate a market and interact via

the LOB. After that, Section 4 talks about experiences of using BSE and its array of robot traders in teaching and research at the University of Bristol.

2. BACKGROUND

In very many human societies, for hundreds or thousands of years, buyers and sellers have met at marketplaces and haggled. When haggling, the seller states the offer-price that he or she wants to sell at, the buyer typically responds with a bid-price that is lower than the offer. The seller might drop the offer a little; the buyer might increase the bid a little; and they repeat these price revisions until they have struck a deal or one side walks away.

In the language of economics, the word "auction" is used to refer to the means by which buyers and sellers come together to agree a transaction price, exchanging money for goods or services. Haggling is a form of auction. There are lots of other different types of auction, here we will briefly review only five, but our review ends with the most economically significant style of auction, as is used in most of the world's major financial markets.

One well-known type of auction is the *English Auction*, where the seller stays silent and the buyers announce increasing bid-prices until only one buyer remains, who then gets the deal. This is a popular way of selling fine art, and livestock too. A more technical name for the English auction is a *first-price ascending-bid auction* because the first (highest) price becomes the transaction price. In contrast, if you've ever bought anything on eBay, you'll know that a lot of the auctions there are ascending-bid, but run as *second-price:* that is, you win the deal by bidding highest, but the price you pay is the bid-price of the second-highest bidder. And, when you're in a shopping mall, you're in an auction too. It's what economists refer to as a *Posted Offer Auction*: the sellers name (or "post") their offer-prices, and the buyers simply take it or leave it at that price.

However, if you go to Amsterdam or Rotterdam and try to buy tulip or daffodil bulbs (a big business in the Netherlands) you'll see almost exactly the opposite process in action. In the *Dutch Flower Auction*, the buyers stay silent while the seller starts with an initial high offer-price and then gradually drops the offer price until a buyer jumps in to take the deal. This is a *descending-offer* auction.

In many of the world's major financial markets, the style of auction used is a very close relative of the basic haggling process. This is much like having an ascending-bid and a descending-offer auction going on in the one market simultaneously. It is known as the *Continuous Double Auction*, or *CDA*. In the CDA, a buyer can announce a bid at any time and a seller can announce an offer at any time. We'll refer to bids and offers here collectively as *quotes*. While this is happening, any seller can accept any buyer's bid at any time; and any buyer can accept any seller's offer at any time. When a quote is accepted by a counterparty, the deal goes through and the quote's price becomes the transaction price for that deal. The CDA is a continuous asynchronous process, and it

needs no centralized auctioneer, but it does need some way of recording the bids and offers that have been made and not yet transacted: this is the *limit order book* (LOB) that we will look at in some detail in this paper. In market terminology, a "limit order" is a quote that will only be executed when a counterparty is found who is willing to transact at the quote's pre-specified *limit price*: this distinguishes it from other types of order that execute immediately, at whatever price the market will bear at the moment the order is submitted.

The CDA interests economists because, even with a very small number of traders, the transaction prices rapidly approach the theoretical market equilibrium price. The equilibrium price is the price that best matches the quantity demanded to the quantity supplied by the market, and in that sense it is the most efficient price for the market. The CDA is also of pragmatic interest because of the trillions of dollars that flow through national and international CDA-based markets in commodities, equities (stocks and shares), foreign exchange, fixed income (tradable debt contracts such as government bonds, known in the UK as *gilts* and in the USA as *treasury bills*), and derivatives contracts. Although there are still some exchanges where human traders physically meet in a central trading pit and shout out verbal bids and offers, in very many major markets the traders engage with one another remotely, via a screen-based electronic market, interacting by placing quotes for specific quantities at specific prices on the LOB.

The LOB displays data that summarizes all the outstanding bids and offers, i.e. the "live" quotes that have not yet cancelled by the traders that originated them. In market terminology, offers are also referred to as *asks*, and the LOB has is typically described as having two sides: the *bid side* and the *ask side*. The bid side shows the prices of outstanding bid orders, and the quantity available at each of those prices, in descending order, so that the best (highest) bid is at the top of the book. The ask side shows the prices of outstanding asks, and the quantity available at each of those prices, in ascending order, so that the best (lowest) ask is at the top of the book.

So, for example, if there are two traders each seeking to buy 30 shares in company XYZ for no more than $1.50 per share, and one trader hoping to buy 10 for a price of $1.52; and at the same time if there was one trader offering 20 shares at $1.55 and another trader offering 50 shares at $1.62, then the LOB for XYZ would look like the one illustrated in Figure 1: traders would speak of XYZ being priced at "152-55", and the bid-offer *spread* is $0.03.

The information shown on a LOB is referred to as "Level 2" or "market depth" data. In contrast, "Level 1" market data shows only the price and size (quantity) for the best bid and ask, along with the price and size of the last recorded transaction, of the instrument being traded. Some people like to try their hand at "day trading" on their home PCs and they often operate with even more restricted data, such as the time-series of whatever price

the instrument was last traded at, or the mid-price, the point between the current best bid and the best ask (so in this example, the mid-price of XYZ would be $1.535). The richer the data, the more expensive it is to purchase from a commercial provider of financial data. Full Level 2 data is routinely used by professional traders in investment banks and hedge funds, but research and development engineers in those institutions are famously much better resourced than meagerly-funded university academics. Buying access to records of Level 2 data in the quantities needed for teaching or research is typically prohibitively expensive for routine academic use.

XYZ			
Bid		Ask	
10	152	155	20
60	150	162	50

Figure 1: Illustrative Limit Order Book (LOB): how the LOB for a fictional stock with ticker-symbol XYZ might be displayed on a trader's screen. Left-hand (pale-text) columns show the bid-side of the book, quantity then price, ordered in descending order of price; right-hand (dark text) columns show the ask-side, price then quantity, in ascending order of price. See text for further discussion.

However, even if such historical data was available for free, it does not allow us to study what is known as *market impact*, where the actions of a particular trader or group of traders moves the price of a tradeable instrument. For example, if a trader sells a very large amount of IBM shares, the increased supply will depress the subsequent price of IBM stock (assuming that all other things, especially the level of demand for IBM stock, remain the same). In a teaching or research context, a database of historical price time-series cannot exhibit market impact: if a trader decides, on the basis of the price of IBM stock at time *t*, to sell 100 million IBM shares, the price at time *t+1*, i.e. the next price in temporal sequence available from the historical database, will be unaffected by that sudden massive increase in supply of IBM stock; that is, there will be no market impact effect. And yet we want to explore understand market impact from a research perspective, and we want our students to experience their systems dealing with market impact too.

For these reasons, and on the basis of earlier experiences with having supervised PhD students and postdoctoral researchers constructing more sophisticated and complex simulations of financial markets for use in research and in teaching (see e.g.: Stotter *et al.*, 2013, 2014; De Luca, 2016), I designed and implemented a simple minimal simulation of a LOB-based financial market. Because I work at the University of Bristol, I gave this simulator the name *Bristol Stock Exchange*, or BSE.

3. BSE: THE BRISTOL STOCK EXCHANGE

BSE has been successfully used as a research tool, most recently in experimental studies of applying deep learning neural networks (DLNN) machine learning methods to create robot traders that adapt to changing market circumstances and which learn from their experience of the market, discussed further in Section 4. In such contexts it is sensible to talk about the user of BSE as an *experimenter* or *researcher*. BSE was originally developed as, and was successfully used as, a resource in teaching on a masters-degree course at the University of Bristol: see Cliff (2018) for further discussion of use of BSE in teaching. In teaching contexts, the user of BSE is more appropriately referred to as an *educator* (someone setting up BSE to be used in teaching, to achieve learning outcomes in students) or as a *student* (i.e., someone using BSE to expand their learning and understanding of contemporary financial market systems). In the text that follows, *user* will be used as a generic term for experimenter, researcher, teacher, and student, all working with BSE.

BSE has the following features:

- While real financial exchanges will typically simultaneously maintain LOBs for tens, hundreds, or thousands of types of tradeable item (i.e., different stocks, or different commodities), BSE has just one LOB, for recording limit orders in a single anonymous type of tradeable item.

- BSE allows for the user to control the specification of any of a wide range of dynamics of supply and demand in the BSE market.

- BSE includes a number of pre-coded robot trading algorithms drawn from the literature on automated trading over the past 30 years. This allows the user to explore the dynamics of LOB-based CDA markets without having to write their own robot-trading algorithms.

- BSE is deliberately written as a simple, intelligible, single-threaded minimal simulation, in the widely used programming language *Python* 2.7, so that students with only elementary programming experience can readily experiment with altering aspects of the existing system, or extending it by adding their own robot trading algorithms. The BSE souce-code has been available as open-source from the *Github* code repository since October 2012 and has been downloaded many times, with a number of individuals contributing uploads of their edits and extensions of the system.

In Section 3.1 the BSE LOB is described in more detail; Section 3.2 then gives a brief overview of the array of robot traders currently available in BSE; Section 3.3 then talks about how a market session can be organized, with some number of robot traders interacting in BSE via the LOB; Section 3.4 gives details of how the market's supply and demand are specified, by defining the flow of customer orders into the market.

3.1. The BSE Limit Order Book (LOB)

BSE is a minimal simulation of a financial exchange running a limit order book (LOB) in a single tradable security. It abstracts away or simply ignores very many complexities that can be found in a real financial exchange. In particular, a trader can at any time issue a new order, which immediately replaces any previous order that the trader had on the LOB: that is, any one trader can have at most one order on a LOB at any one time. Furthermore, as currently configured, BSE assumes zero latency in communications between the traders and the exchange, and also conveniently assumes that after any one trader issues an order that alters the LOB, then any transaction triggered by the update is immediately resolved and the updated LOB is distributed to all traders before any other trader can issue another order: that is, all LOB updates are assumed to take place at zero latency. In the days when all traders were humans, the speed at which computerized updates to the LOB could be executed were so much faster than human reaction times that transmission latencies along conventional wired or wireless telecoms links could safely be assumed to be zero, as in BSE. However now that many traders active on major markets are no longer humans but instead are high-speed automated systems, transmission latencies can matter a great deal. This is just one respect in which BSE is a major simplification of the real-world situation. Real-world exchanges and markets are really *much* more complicated than BSE. Nevertheless, the abstractions embodied within BSE render it a genuinely useful platform for leading-edge research.

BSE is written in *Python v.2.7* as a single-threaded process intended to be run in batch-mode, writing data to files for subsequent analysis, rather than single-stepping with dynamic updating of displays via an interactive graphical user interface (GUI). A GUI-based version is in development, but even that would require the user to switch into batch-mode to generate statistically reliable data from many hundreds or thousands of repeated market simulation experiments, as is discussed further in Section 3.3.

For ease of distribution, and to help people who are new to *Python*, currently all of BSE fits in a single source-code file: BSE.py, the latest major release of which is available for download from the popular GitHub open-source repository (BSE, 2012). BSE.py has been written to be easy to understand; it is certainly not going to win any prizes for efficiency; probably not for elegance either. It's roughly 1000 lines of code.

The output data-files created by BSE.py are all ASCII comma-separated values (i.e., files of type .csv) because that format can easily be imported by all popular spreadsheet programs (such Microsoft *Excel*) and can also be readily imported by more sophisticated statistical analysis systems such as those offered by *Matlab* or *R*.

Examining the BSE code you can see that the Exchange has to keep internal records of exactly which trader submitted which order, so that the book-keeping can be done when two traders enter into a transaction, but that the LOB it "publishes" to the traders deliberately discards a lot of that data, to anonymize the identity of the traders. This is exactly what real-world LOB-based exchanges do. The Exchange class's `publish` method uses values from the exchange's internal data structures to build the market's LOB data as a *Python* dictionary structure containing the time, the bid side of the LOB and the ask side of the LOB, referred to as the Bid LOB and the Ask LOB, respectively. The Bid and Ask LOBs are both also dictionary structures. Each LOB shows: the current best price; the worst possible price (i.e. the lowest-allowable bid-price, or the highest-allowable offer price: these values can be of use to trader algorithms, i.e. for making "stub quotes": an example is given later in this document); the number of orders on the LOB; and then the anonymized LOB itself.

The anonymized LOB is a list structure, with the bids and asks each sorted in price order. Each item in the list is a pair of items: a price, and the number of shares bid or offered at that price. Prices for which there are currently no bids or asks are not shown on the LOB.

Quotes that are issued by a trader have a trader-identification (TID) code, a quote type (bid or ask), price, quantity, and a timestamp. In the current version of BSE, for extra simplicity, the quantity is always 1. In this document we'll show the quote as a list: [TID, type, price, quantity, time], hence if trader T22 bids $1.55 for one share at time t=10 seconds after the market opens, we'd write the quote as: `[T22,bid,155,1,0010]`. Figure 2 shows an example in which the LOB is initially empty and on successive lines the LOB is shown after it is updated in response to the quote shown on that line.

Note that in Figure 2 the order issued at t=21 comes from trader T11, and hence replaces T11's previous order issued at t=2, which is why the bid at $0.22 is deleted from the bid LOB at t=21. At this stage, the *bid-ask spread* (i.e., the difference between the best bid and the best ask) is $0.32.

```
                        bid:[]              ask:[]
[T11, bid, 022, 1, 0002]  bid:[(22,1)]        ask:[]
[T02, bid, 027, 1, 0006]  bid:[(22,1),(27,1)] ask:[]
[T08, ask, 077, 1, 0007]  bid:[(22,1),(27,1)] ask:[(77,1)]
[T01, bid, 027, 1, 0010]  bid:[(22,1),(27,2)] ask:[(77,1)]
[T03, ask, 062, 1, 0018]  bid:[(22,1),(27,2)] ask:[(62,1),(77,1)]
[T11, bid, 030, 1, 0021]  bid:[(27,2),(30,1)] ask:[(62,1),(77,1)]
```

Figure 2: Changes in the LOB Data Structure in Response to a Succession of Orders. The top line shows the initially empty LOB, as the bid-side list (center column) and the ask-side list (right-hand column). Successive lines show a sequence of orders arriving (left-hand column) and the resultant state of the LOB after it is updated to represent each order: see text for further discussion.

In financial-market terminology, if a trader wants to sell at the current best bid price, that's referred to as "hitting the bid"; if a trader wants to buy at the current best ask-price, that's referred to as "lifting the ask". Both are instances of "crossing the spread". So, to continue our example, let's say that trader T02 decides to lift the ask.

In BSE, this is signalled by the trader issuing an order that crosses the spread, i.e. issuing a bid priced at more than the current best ask, and the transaction then goes through at whatever the best price was on the LOB as the crossing order was issued. So, continuing the sequence of events in Figure 2, if at *t*=25s Trader 02 lifts the ask by bidding $0.67, the updated LOB would be as illustrated in Figure 3.

```
[T02, bid, 067, 1, 0025]  bid:[(27, 1),(30, 1)] ask:[(77, 1)]
```

Figure 3: Illustration of changes in the LOB in response to a quote issued at t=25s, one that crosses the spread, thereby lifting the best ask.

Note that, as shown in Figure 2, T02 already had an earlier bid on the LOB, one of the two priced at 27, so when T02's new bid of 67 was received at *t*=25s by BSE, it first deleted the earlier bid (i.e., the new order replaced the old one), and then the exchange system detected that the bid crossed the best ask (which was priced at 62, from the order sent at *t*=18s by trader T03) and so the exchange deleted that ask from the LOB too. Immediately afterwards, the exchange and the traders do some book-keeping: the exchange records the transaction price and time on its "tape" (the time-series record of orders on the exchange); and the two counterparties to the trade, traders T02 and T03, each update their "blotters" (their local record of trades they have entered into): these uses of the words "tape" and "blotter" are common terminology among financial-market traders.

3.2 BSE Robot Traders

BSE includes a sample of various simple automated trading algorithms, or "robot traders". These are all automated execution systems: that is, they automate the process of executing an order that has originated elsewhere. In investment banking, the human workers that do this job are known as "sales traders": a human sales trader waits for an order to arrive from a customer, and then works that order in the market: that is, the sales trader just executes the order without giving any advice or comment on the customer's decision to buy or sell. At its simplest, a customer order will state what instrument (e.g., which stocks or shares) the customer wants to deal in, whether she wants to buy or sell, how many, and what price she wants. If the customer is keen to complete the transaction as soon as possible, she should instead specify a *market order*, i.e. just do the deal at whatever is the best price in the market right (i.e., on the LOB) now. But if the customer is happy to wait, then she can specify a *limit order*, a maximum price for a purchase or a minimum price for a sale, and then the sales trader's job is to wait until the conditions are right for the deal to be done. The execution of limit orders is where the sales trader can make some money. Say for example that the customer has sent an order stating that she wants to sell one share of company XYZ for no less than $10.00, at a time when XYZ is trading at $9.90 but where the price

has been rising steadily: if the sales trader waits a while and executes the order when XYZ has risen to $10.50, the trader can return the $10.00 to the customer and take the extra $0.50, a margin of 5%, as a fee on the transaction; but if the trader instead executes this order at the precise moment that the price of XYZ hits $10.00, then the customer's order has been satisfied but there is no extra money, no margin on the deal, for the trader to take a share of. Similarly for a customer order to buy at a limit price of than $15.00, if the trader can instead execute the order by buying at $13.00 then there is $2.00 "profit" to keep or share, a margin of 13%.

So, the simple robot traders in BSE can all be thought of as computerized sales-traders: they take customer limit orders, and do their best to execute the order in the market at a price that is better than the limit-price provided by the customer (this is the price below which they should not sell, or above which they should not buy). Customer orders are issued to traders in BSE and then the traders issue their own quotes as bids or asks into the market, trying to get a better price than the limit-price specified by the customer.

BSE is written as object-oriented *Python*. There is a generic Trader class that specifies stub implementations of core methods that any robot needs to implement such as how the robot calculates the price of its next quote that it will send as an order to the LOB (getorder()), how to update any learning variables in response to market events (respond()), or the book-keeping and record-updating that needs to be done when an order is executed (bookkeep()). The definitions of each specific type of robot trader in BSE then inherit these generic methods and extend them as required.

For brevity in the BSE code each type of robot trader has an identifier of up to four characters, similar to a stock-ticker symbol. The robot trader algorithms currently available in BSE are:

- **Giveaway (GVWY):** a totally dumb robot that issues a quote-price that is identical to its limit price, thereby maximising its chances of finding another trader to transact with, but guaranteeing to make no profit should a trade result from its quote. The GVWY trader makes no use of any LOB data.
- **Zero-Intelligence Constrained (ZIC):** an implementation of Gode & Sunder's ZIC traders, as introduced in their seminal 1993 paper which demonstrated that, when evaluated via a common measure of the efficiency of market mechanisms, markets populated by ZIC traders are just as efficient as comparable markets populated by human traders.
- **Shaver (SHVR):** this is a minimally simple trader that, unlike GVWY, does actually use LOB data. If it is working a sell order, the SHVR algorithm simply looks at the best ask on the LOB and undercuts it by quoting one penny less (i.e., 0.01: the smallest unit of currency in BSE) so long as this does not go below the sell order's limit price. Similarly if working a buy order, SHVR quotes a bid-price that is one penny more than the current

best bid, so long as that price is not more than the buy-order's limit price.

- **Sniper (SNPR):** in a famous early public contest in automated trading on experimental markets, organized at the Santa Fe Institute, Todd Kaplan submitted a trader-robot spent most of its time doing nothing, "lurking in the background" and then, if the market was about to close or if the bid-ask spread had narrowed to a sufficiently small value, Kaplan's strategy came in to the market to "steal the deal". This strategy, now known as *Kaplan's Sniper*, won the contest: see Rust *et al.* (1992) for further details. In BSE the code for SHVR is extended to include elementary sniping capability: the BSE SNPR robot reads a system-wide global variable that indicates the percentage of time remaining in the market session, lurks for a while, and then rapidly increases the amount it shaves off the best price as time runs out.

- **Zero-Intelligence Plus (ZIP):** the ZIP trading algorithm (Cliff, 1997) was devised to address shortcomings in ZIC traders. A ZIP trader uses simple machine learning and a shallow heuristic decision tree to dynamically alter the margin that it aims to achieve on the order it is currently working. In 2001, Das *et al.* at IBM reported on experiments in which they demonstrated that ZIP, and also IBM's own "MGD" algorithm modified from an algorithm first reported by Gjerstad & Dikhaut (1998), could outperform human traders in controlled laboratory experiments.

- **Adaptive-Aggressive (AA):** for his PhD research, Vytelingum (2006) made significant extensions to the ZIP algorithm, adding an *aggressiveness* variable that determines how quickly the trader alters its margin, and this variable is itself adaptively altered over time in response to events in the market. AA has been shown to dominate prior trading algorithms such as ZIP and MGD (Vytelingum, Cliff, & Jennings, 2008). In later work (De Luca & Cliff, 2011) AA was demonstrated to dominate not only all other algorithmic trading strategies, but also human traders.

The *Python* source-code for each of these robot traders is available on the BSE GitHub repository (BSE, 2012).

3.3 Using the LOB with Robot Traders

The core of a market session in BSE is a while loop that repeats once per time-step until a pre-specified time-limit is reached. In each loop-cycle, the following happens:

- There is a check to see if any new customer orders need to be distributed to any of the traders, via a call to the BSE customer_orders() method. The call to that method includes a parameter, order_schedule, which specifies various aspects of how customer orders are generated, such as whether new orders arrive randomly or regularly in time, what the balance is between sell orders and

buy orders, and how the price of each order is generated. Prices can be constant, or generated according to a deterministic function of time, or generated at random from a stochastic function: conditionally heteroscedastic price-generating functions can easily be constructed.

- An individual trader is chosen at random to issue its current response by invoking the trader's getorder() method: this will either return the value None, signalling that the trader is not issuing a quote at the current time, or it will return a quote, i.e. a fresh order to be added to the LOB; if that is the case then BSE processes the order via a method called process_order().

- The updated LOB is then made available to all traders via a call to BSE's publish_lob() method.

- If processing the order resulted in a trade, the traders involved do the necessary book-keeping, updating their blotters, via a call to bookkeep().

- Each trader is given the chance to update its internal values that affect its trading behavior, via a call to the trader's respond() method.

Before any of that happens, the market needs to be populated by an invocation of the populate_market() method, which is where the number of traders and the type of each trader is determined. Thus the core loop of the BSE simulator resembles the code shown in Figure 4. To make a proper rigorous evaluation, comparing different trading robots across a realistic variety of market conditions, it is necessary to run multiple sequences of statistically independent sessions, and then calculate appropriate summary statistics from, and/or perform appropriate tests of statistical significance on, the results. This is easily done in BSE. Nevertheless, establishing which robot trader performs best across a number of different supply and demand schedules, and with differing numbers and ratios of robot types, can require very large number of trials, of individual market sessions. In a teaching context, this is an advantage: BSE's ability to routinely generate very large data-sets can be used to motive students to learn "big data" tools and techniques for managing, visualizing, and analyzing large data-sets.

3.4. Altering supply and demand schedules in BSE

De Luca *et al.* (2011) and Cartlidge & Cliff (2012) discuss the need to explore trading agents in simulated markets that are more realistic than those used in prior experimental studies of robot traders interacting with one another and/or with human traders. The current version of BSE can be configured to run "traditional" economics experiments switching between static-equilibrium supply/demand schedules and with periodic simultaneous replenishment of orders, but it can also be configured to have continuous "drip-feed" replenishment, along with fine-grained dynamic variations in the supply and demand schedules, and hence also in the market equilibrium.

BSE allows the customer orders to arrive in a continuous random stream, rather than periodically having every

single trader being given a new customer order, all at the same instant. Such full periodic replenishment of customer orders is something that was introduced in Vernon Smith's seminal (and subsequently Nobel Prize winning) experiments reported in (Smith, 1962), which very many experimenters have used since, but there are good reasons for wanting to explore simulation experiments where instead the replenishment is continuous: in very many real-world markets, for much of the time, the flow of orders is a continuous random feed of orders into the market. For more discussion of this, see Cliff & Preist (2001), De Luca *et al.* (2011).

```python
# initialise population of traders to empty
traders = {}
# set clock to zero
time = 0

# create a population of traders
populate_market(n_traders, traders)

while time < endtime:

    # how much time left, as a percentage?
    duration = float(endtime-starttime)
    time_left = (endtime – time) / duration

    # distribute any new customer orders to the traders
    customer_orders(time, traders, order_schedule)

    # get an order (or None) from a randomly chosen trader
    # tid is Trader Identifier
    tid = random_tid(traders)
    lob = exchange.publish_lob(time)

    order = traders[tid].getorder(time,time_left,lob)

    if order != None:

        # send order to exchange
        trade = exchange.process_order(time, order)

        lob = exchange.publish_lob(time)

        if trade != None:
            # trade occurred,
            # counterparties update order-lists & records
            traders[trade['party1']].bookkeep(trade, order)
            traders[trade['party2']].bookkeep(trade, order)
            # update exchange records/stats for later viz/analysis
            trade_stats(expid, traders, tdump, time, lob)

    # traders respond to whatever happened
    lob = exchange.publish_lob(time)
    for t in traders:
            traders[t].respond(time, trade, lob)

time = time + timestep
```

Figure 4: Main loop of a market session in BSE. See text for further explanation.

4. BSE IN USE

BSE was created in 2012 to meet a need in our teaching of a unit/module currently known *as Internet Economics and Financial Technology*, available to masters-level students at the University of Bristol. In the six years since then approximately 250 masters students have used BSE in coursework assignments, typically requiring the students to develop and test their own robot trader. In some years the assignment required students to create a sales-trader robot (as described above) and in other years a *proprietary-trader* robot, which starts with a sum of money and then buys and sells on its own account, attempting to make a profit by selling each thing it buys

for more than the price at which it was purchased. Student feedback on using BSE was generally highly positive, and several graduates of the module have gone on to permanent employment with major investment banks and hedge funds. For more detailed discussion of the use of BSE in teaching see (Cliff, 2018).
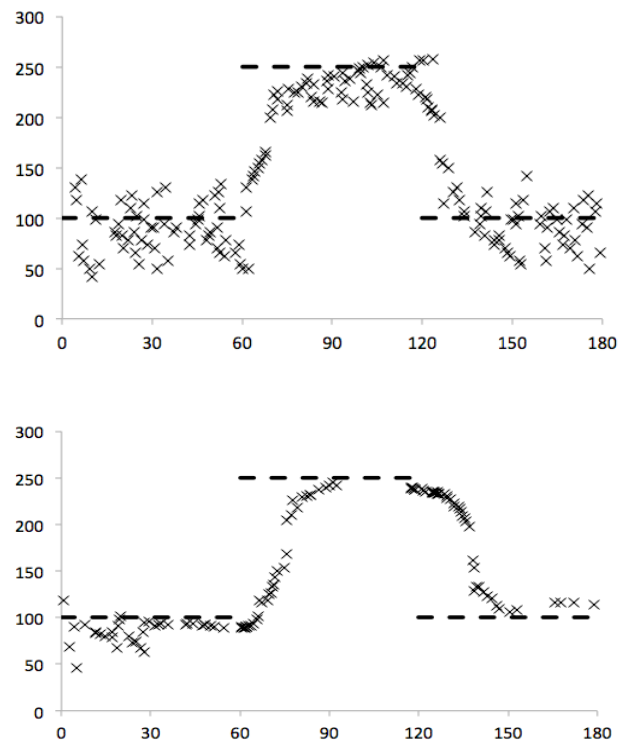

Figure 5: Sample transaction-price time-series from BSE markets with shock-changes in supply and demand. altering the market's equilibrium price. Horizontal axis is time in seconds; vertical axis is price. Data-points are individual transactions. The equilibrium price P_0 is indicated by the horizontal dashed line: in the first minute $P_0=\$1.00$, then at $t=60$ there is a shock change to $P_0=\$2.50$, and then after a further minute the equilibrium price undergoes another shock change at $t=120$ back to $P_0=\$1.00$. In each time-series, the traders' response to the step-change in the equilibrium price as it shifts up at $t=60$ and back down at $t=120$ is clear. In each market there are 40 buyers and 40 sellers: upper graph shows results from a market of GVWY traders; lower graph shows results from a market of ZIP traders.

Latterly BSE has been used as the basis for research work, most recently described in (le Calvez & Cliff 2018), exploring the use of deep learning neural networks (DLNNs: see e.g. Krizhevsky *et al.*, 2012) to replicate the behavior of adaptive traders in a CDA markets. DLNNs are a contemporary machine learning technique that have been successfully demonstrated to

perform surprisingly well in a wide range of highly challenging application areas, but which typically only perform well when trained on data-sets that are extremely large by traditional standards. BSE can readily generate data in the volumes required for DLNN training, as was first demonstrated by Tibrewal (2017) who showed successful results from training a DLNN network to replicate the trading activity of a specific ZIP robot-trader in BSE, thereby establishing a proof-of-concept that DLNNs could learn to trade in LOB-based CDA markets; le Calvez (2018) recently replicated Tibrewal's work and extended it by demonstrating a DLNN-trained robot trader operating successfully, trading live in BSE, and at times outperforming the trader from which the training data was generated: see le Calvez & Cliff (2018) for further details.

To illustrate this, Figure 6 shows the top-level *Python* code required to launch a sequence of 22,750 successive independent experiments in BSE, each lasting 5 minutes of simulated time, with varying proportions of ZIP, ZIC, GVWY, and SHVR robots, keeping the total number of traders in the market fixed at 32 (16 working buy orders and 16 working sell orders), recording 50 separate experiments for every possible permutation ranging from homogenous markets where all 32 traders are the same type, through to the case where there are 8 traders running each of the four robot strategies. To specify this takes less than 40 lines of code: students interested in studying market dynamics, or evaluating the performance of their own self-0designed robot trading algorithm can operate at the level of code shown in Figure 6: they do not need to understand implementation details of the BSE LOB or the array of robot traders already coded in; all those details are abstracted away and the students need only understand how to interact with the BSE LOB's interface, and the interfaces of the generic `Trader` object class.

5. DISCUSSION AND FURTHER WORK

A quick trawl of the Web reveals a variety of stock-market simulators, many of them aimed at day-traders wanting to evaluate an automated strategy. Such simulators almost always are designed to work with historical data of stock prices: by back-testing on historical data, it is possible to estimate how much money an automated trading strategy would have made (or lost) if it had been running live.

Clearly, BSE is quite different to such trading simulators, but there are good reasons for that. Very few trading simulators work with Level 2 data (i.e. with the full LOB, changing order-by-order), and the cost of obtaining such data is often very high. More fundamentally, trading simulators based on historical market data typically cannot model *market impact*, where buying or selling large amounts of an instrument shifts the demand and/or

supply curves in such a way that the equilibrium price of the instrument then alters. In that sense, conventional trading simulators require the trader (human or automated) to act solely as a *price-taker*, trading at time *t* at whatever price is on the screen, whatever price the historical data says the instrument was trading at, at time *t*. Whether they sell 1 share or 10 million shares at time *t*, the price immediately after the sale will still be whatever the historical data says it was at time *t*+1. Yet a sale of 10 million shares would in reality almost definitely move the price down, in a way that selling a single share simply wouldn't. Unlike trading robots dealing with historical data, trading robots in BSE can be *price-makers*: their activity can shift the supply and demand, and they can generate, and have to deal with, market impact. In that sense, the scenario in BSE is more like a modern-day "dark pool", a private online exchange where a relatively small number of traders meet to conduct big transactions: participants in dark pools are typically traders working for major banks or fund-management companies, dealing large blocks of tradable instruments.

Nevertheless, in comparison to real markets, the lack of any latency in the system is the probably the biggest issue. It would be relatively easy to introduce simulated latency at the exchange (so the LOB data that is received by the traders at time *t* actually reflects the state of the LOB a little earlier, at time *t*–*Δt*) and we could also introduce "communications latency" so that when a trader issues an order at time *t* it does not arrive at the exchange until a little later at some time *t*+*Δt*, but in a single-threaded simulation it would require quite a lot more work to accurately model processing latency in each trader. That is, in the current version of BSE, each trader gets as long as it wants to process its `respond()` method, whereas in a reality a lot of effort goes into making the response-time of automated trading systems as low as possible while still being capable of generating profitable behaviors. To better model real market systems, we would need to switch to a multi-threaded implementation, and/or to configuring BSE as a distributed client-server architecture over multiple virtual or physical machines. That remains one next step for further work.

```python
start_time = 0
start_time = 240

n_trader_types = 4
equal_ratio_n = 4
n_trials_per_ratio = 50
n_traders = n_trader_types * equal_ratio_n

fname = 'balances_%03d.csv' % equal_ratio_n

tdump=open(fname,'w')

min_n = 1

trialnumber = 1
trdr_1_n = min_n
while trdr_1_n <= n_traders:
        trdr_2_n = min_n
        while trdr_2_n <= n_traders - trdr_1_n:
                trdr_3_n = min_n
                while trdr_3_n <= n_traders - (trdr_1_n + trdr_2_n):
                        trdr_4_n = n_traders - (trdr_1_n + trdr_2_n + trdr_3_n)
                        if trdr_4_n >= min_n:
                                buyers_spec = [('GVWY', trdr_1_n),
                                               ('SHVR', trdr_2_n),
                                               ('ZIC',  trdr_3_n),
                                               ('ZIP',  trdr_4_n)]
                                sellers_spec = buyers_spec
                                traders_spec = {'sellers':sellers_spec,
                                                'buyers':buyers_spec}
                                print buyers_spec
                                trial = 1
                                while trial <= n_trials_per_ratio:
                                        trial_id = 'trial%07d' % trialnumber
                                        market_session(trial_id,
                                                       start_time, end_time,
                                                       traders_spec, order_sched,
                                                       tdump, False)
                                        tdump.flush()
                                        trial = trial + 1
                                        trialnumber = trialnumber + 1
                        trdr_3_n += 1
                trdr_2_n += 1
        trdr_1_n += 1
tdump.close()

print trialnumber-1
```

Figure 6: Top-level *Python* code for running an experiment with 32 traders (16 buyers and 16 sellers) of types GVWY, SHVR, ZIC, and ZIP; with the ratio of the four types of traders being systematically varied across all possible nonzero values, and performing 50 independent trials for each specific ratio. The main BSE loop illustrated in Figure 5 is her wrapped into a single method invoked as market_session(). The nested loops here cause a total of 22,750 trials to be performed, and on a single CPU would take several hours of continuous computation. As each trial is independent, this task is *embarrassingly parallelizable*: in principle, 22,750 separate machines (e.g., that number of virtual machines/instances rented on a pay-by-the hour basis from a cloud service provider) could perform the necessary computation in parallel, taking only a few seconds.

REFERENCES

BSE, 2012. GitHub open-source code repository at http://github.com/davecliff/BristolStockExchange/

Cartlidge, J. & Cliff, D., 2012. Exploring the 'robot phase transition' in experimental human-algorithmic markets. UK Government Office for Science, *Foresight Project: Future of Computer Trading in the Financial Markets, Driver Review DR 25.* https://bit.ly/2llHjbh.

Cliff, D., 1997. Minimal-Intelligence Agents for Bargaining Behaviors in Market-Based Environments. HP Labs Tech Report HPL-97-91. www.hpl.hp.com/techreports/97/HPL-97-91.pdf

Cliff, D. & Preist C., 2001. Days without end: on the stability of experimental single-period CDA markets. HP Labs Tech. Report HPL-2001-325. www.hpl.hp.com/techreports/2001/HPL-2001-325.pdf

Cliff, D., 2018. A Free Open-Source Limit-Order-Book Simulator for Teaching and Research. Submitted to *Computational Intelligence in Financial Engineering (CIFEr)* track at IEEE Symposium Series on Computational Intelligence, Bengaluru, India, November 2018.

Das, R., Hanson, J., Kephart, J., & Tesauro, G., 2001. Agent-Human Interactions in the Continuous Double Auction. *Proceedings International Joint Conference on Artificial Intelligence* (IJCAI'01).

le Calvez, A., 2018. *Learning to be a Financial Trader: An Exploration of Neural Networks in a Continuous Double Auction.* Masters Thesis, Department of Computer Science, University of Bristol.

le Calvez, A. & Cliff, D., 2018. Deep Learning can Replicate Adaptive Traders in a Limit-Order-Book Financial Market. Submitted to *Computational Intelligence in Financial Engineering (CIFEr)* track at IEEE Symposium Series on Computational Intelligence, Bengaluru, India, November 2018.

De Luca, M., & Cliff, D., 2011. Human-Agent Auction Interactions Adaptive-Aggressive Agents Dominate. *Proceedings International Joint Conference on Artificial Intelligence* (IJCAI-2011).

De Luca, M., Cartlidge, J., Szostek, C., & Cliff, D., 2012. Studies of interactions between human traders and algorithmic trading systems. UK Government Office for Science, *Foresight Project: Future of Computer Trading in Financial Markets, Driver Review DR13.* https://bit.ly/2llv52c.

De Luca, M., 2016. *Adaptive Algorithmic Trading Systems.* PhD thesis, Department of Computer Science, University of Bristol.

Gjerstad, S. & Dickhaut, J., 1998. Price Formation in Double Auctions. *Games & Economic Behavior,* 22(1):1-29.

Gode, D. & Sunder, S., 1993. Allocative efficiency of markets with zero-intelligence traders: Market as a partial substitute for individual rationality. *Journal of Political Economy*, 101(1):119-137.

Krizhevsky, A., Sutskever, I, & Hinton, G., 2012. ImageNet classification with deep convolutional neural networks. In *Proc. 25th International Conf. on Neural Information Processing Systems, Vol.1 (NIPS'12)*, F. Pereira, *et al.* (eds), pp.1097-1105.

Rust, J., Miller, J., & Palmer, R., 1992. Behaviour of trading automata in a computerized double auction market. in D. Friedman & J. Rust (eds) *The Double Auction Market: Institutions, Theories, & Evidence.* Addison Wesley, pp.155-198.

Smith, V., 1962. An experimental study of competitive market behavior. *J. Polit. Economy*, 70(2):111-137.

Stotter, S., Cartlidge, J., & Cliff, D., 2013. Exploring assignment-adaptive (ASAD) trading agents in financial market experiments, in *Proceedings of the 5th International Conference on Agents and Artificial Intelligence,* (ICAART). J. Filipe & A. Fred, (eds). Barcelona: SciTePress, Vol.1.pp.77-88.

Stotter, S., Cartlidge, J., & Cliff, D., 2014. Behavioural investigations of financial trading agents using Exchange Portal (ExPo). In: N. Nguyen, *et al.* (eds) *Transactions on Computational Collective Intelligence XVII.* Springer, pp. 22-45

Tibrewal, K., 2017. *Can Neural Networks be Traders? Explorations of Machine Learning Using the Bristol Stock Exchange.* MEng Thesis, Department of Computer Science, University of Bristol.

Vytelingum, P., 2006, *The Structure and Behaviour of the Continuous Double Auction.* PhD Thesis, School of Electronics and Computer Science, University of Southampton.

Vytelingum, P., Cliff, D., & Jennings, N. 2008. "Strategic Bidding in Continuous Double Auctions". *Artificial Intelligence*, 172(**14**):1700-1729.

AUTHOR'S BIOGRAPHY

Dave Cliff is a full Professor of Computer Science at the University of Bristol, UK, a post he has held for the past 11 years. Previously he has held professorial posts at the University of Southampton, UK, and at the MIT Artificial Intelligence Lab in Cambridge, USA. He also spent seven years working in industrial technology R&D at Hewlett-Packard Laboratories and as a Director & Trader in the Foreign Exchange Complex Risk Group at Deutsche Bank in the City of London. He has a BSc in Computer Science (Leeds, 1987) and MA and PhD degrees in Cognitive Science (Sussex, 1988 & 1992). For the past 22 years Cliff's research has focused on applications of artificial intelligence and machine learning in financial markets, and on issues in systemic risk and stability in networked financial systems. Cliff has recently served as a lead expert advisor to the UK Government Office for Science in its two-year "Foresight" investigation *The Future of Computer Trading in Financial Markets*, for its *Blackett Review* of the UK FinTech Industry, and is a founder member the Academic Advisory Council on Data Analytics for the UK Financial Conduct Authority, the main regulator of financial-market activity in the UK. He is a Fellow of the British Computer Society and a Fellow of the Royal Society of Arts.

RAPID 3D SHAPE FORMING COMPUTATION WITH PIECEWISE HEATING LINES USING A FIFTH ORDER SPLINE FORMULATION

Henri Champliaud[a], Valentin Vieillot[b], David Provencher[b], Ngan Van Lê[d]

[a],[b],[c],[d]Department of Mechanical Engineering
École de technologie supérieure
Montreal, QC, Canada

[a]henri.champliaud@etsmtl.ca, [b]valentin.vieillot.1@ens.etsmtl.ca, [c]David.provencher.1@ens.etsmtl.ca ,
[d]vanngan.le@etsmtl.ca

ABSTRACT
An originally developed fifth order piecewise spline formulation is used to compute how a flat plate will be progressively deformed to a specific shape by a set of sequentially applied linear heating lines. In order to reproduce the complex trajectories realized for example by skilled workers in shipbuilding to achieve a 3D curved hull one should be able to impose continuous non-linear or piecewise heating lines over a workpiece. In this paper curved heating lines are decomposed in a series of straight line segments to allow the application of the methodology developed for linear heating lines. The deforming effect of each segment is computed and added to the previous achieved geometry. Results show the potential of the approach that would eventually lead to an optimized shaping procedure for dieless forming.

Keywords: piecewise heating line, 5th order spline interpolation, dieless metal forming

1. INTRODUCTION
Skilled workers in shipyards have demonstrated their ability to apply heating lines with a torch on a plate for progressively forming it until it reaches the desired geometry of a boat hull body shell (Doo Jang and Choon Moon 1998; Chu, Lin and Chen 2016; Vega, Rashed and Murakawa 2015; Park, Kim, Mun, Kwon, Lee and Hee Ko 2016; Gao, Sheikoleislami, Dearden and Edwardson 2017). In the hydroelectricity industry, since the turbines are different from one site to another, small batch is the norm for producing the blades (Feng, Champliaud, Sabourin and Morin 2013). A dieless procedure will then save the costs of the dies and even though the blades would have been formed by a punch and die pressing process, there is still an opportunity with a line heating procedure to get back in the design dimensions a blade pressed out of tolerances. Experiments with heating lines applied on pressed blades, in the workshop of a turbine manufacturer, have shown this possibility. The objective of this paper is to present the methodology used to deformed an originally flat plate with a piecewise heating

line, since workers don't necessarily follow a straight pass over the workpiece to reach the desired geometry. A fifth order spline interpolation model is applied to compute the new shape of the plate by imposing at each point of the area affected by a heating line the changes in slopes and curvatures that would occurred following the structural distortion observed when the plate gets back to room temperature (Reutzel, Zhang and Michaleris 2006; Reutzel E.W. 2007; Champliaud, Feng, Lê and Gholipour 2015; Champliaud, Feng, Gholipour, Provencher and Tousignant 2016). Slopes and gradients occurring at the outer surface of a workpiece are extracted from finite element models or from experiments (Provencher 2017) and then can be repeatedly applied at different locations all over the workpiece to generate the intended geometry. Following the presentation of the methodology, different applications from one to multiple line heating procedure demonstrate the ability of the process to compute the displacements and the new shape of the initially flat plate. Finally the results of the dieless line heating procedure using a piecewise heating line is compared to a thermal-structural finite element (FE) simulation.

2. FIFTH ORDER SPLINE PROCEDURE
A piecewise fifth order spline model (Champliaud, Feng, Lê and Gholipour 2015; Champliaud, Feng, Gholipour, Provencher and Tousignant 2016) is used for imposing slopes and curvatures along the area of the heating line trajectory. The key element here is that the C3 model is solved with the 3rd order derivative, i.e. the gradient of the curvature, equal at each shared point in between 5th order splines.

2.1. 5th spline order formulation
A 5th order parametric spline model is fitted on the local mesh, allowing the computation of the displacements occurring on the local grid following the imposition of a map of slopes and curvatures all over it. As mentioned in the previous section, slopes and curvatures are known from experiments or a FE model.
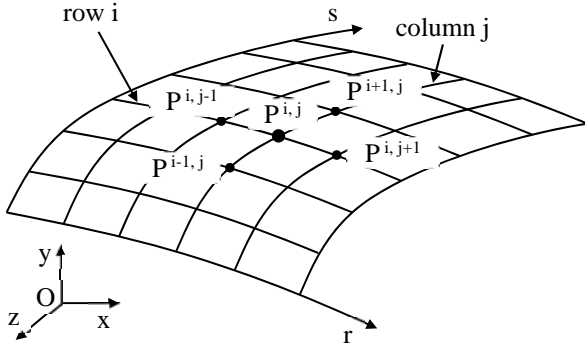
Figure 1: Parametric surface (adapted from Champliaud, Feng, Gholipour, Provencher and Tousignant 2016)

Fifth order parametric polynomials are given below for coordinate x (Eq. 1 and 2), with r and s normalized parameters and a_{ri} and a_{si} constants determined from end conditions and P points. Similar expressions represent y and z coordinates.

$$x(r) = a_{r0} + a_{r1}r + a_{r2}r^2 + a_{r3}r^3 + a_{r4}r^4 + a_{r5}r^5 \qquad (1)$$

$$x(s) = a_{s0} + a_{s1}s + a_{s2}s^2 + a_{s3}s^3 + a_{s4}s^4 + a_{s5}s^5 \qquad (2)$$

Solving with the C3 continuity condition (equaling the gradient of curvature of both sides at any point) lead to the following system:

$$\begin{bmatrix} 20 & -40 & 20 \end{bmatrix} \begin{bmatrix} \alpha^{i,j-1} \\ \alpha^{i,j} \\ \alpha^{i,j+1} \end{bmatrix} = \begin{bmatrix} -1 & 6 & -1 \end{bmatrix} \begin{bmatrix} \alpha^{i,j-1}_{,\beta\beta} \\ \alpha^{i,j}_{,\beta\beta} \\ \alpha^{i,j+1}_{,\beta\beta} \end{bmatrix} + \begin{bmatrix} -8 & 0 & 8 \end{bmatrix} \begin{bmatrix} \alpha^{i,j-1}_{,\beta} \\ \alpha^{i,j}_{,\beta} \\ \alpha^{i,j+1}_{,\beta} \end{bmatrix} \qquad (3)$$

where α represents any Cartesian coordinate x, y or z, β stands for the parametric coordinate r or s, $\alpha^{i,j}$ is a coordinate of a point P located at the intersection of a row i and a column j, and $\alpha_{,\beta} = \partial\alpha / \partial\beta$, $\alpha_{,\beta\beta} = \partial^2\alpha / \partial\beta^2$ are first and second order derivatives of the variable α with regards to the parametric variable β.

2.2. One line heating procedure

Based on the 5th order spline formulation briefly described above, four main steps need to be followed to apply the heating line effects on a specific geometry:

1 - Define a heating line trajectory. Fig 2 illustrates a straight heating line crossing the width of a flat plate (red line) and its area (in between blue lines) that will be affected by the thermal gradient i.e. where the gradient of the displacements (slopes) and the gradient of the slopes (curvature) are modified by heating and then cooling.

2 - Overlay a local mesh on the heating line area defined at step 1 (Fig 3). The new first and second order derivatives will be first applied to this local grid avoiding the need of a mask (Champliaud, Feng, Gholipour, Provencher and Tousignant 2016) encompassing the

entire plate. The local mesh will allow to transfer accurately the hinge effect i.e. the local bending in the heated area, to the workpiece.
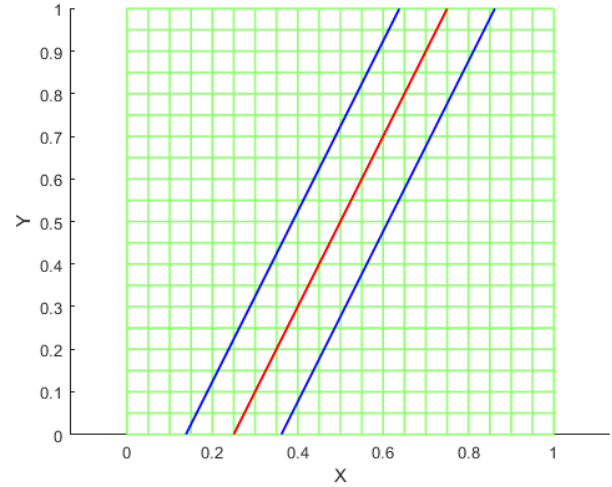

Figure 2: Initial plate mesh with the heating line trajectory (red line) and area of influence (blue lines)
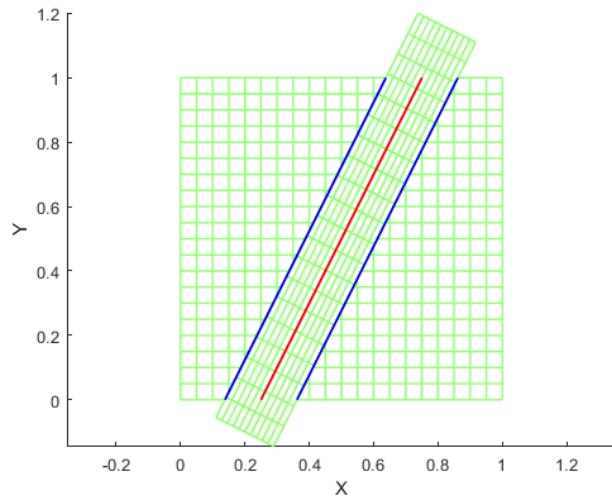

Figure 3: Local mesh fitted with the heating line zone

3 - The piecewise fifth order spline model is solved over the heating line area. The resulting displacements occurring all over the deformed local mesh are shown on Fig 4.
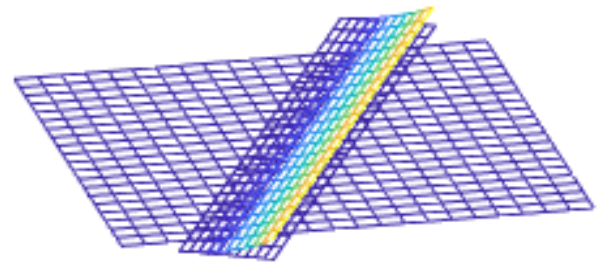

Figure 4: Computed displacements on the local mesh

4- Interpolate the coordinates of the local mesh for transferring the new coordinates of the mesh of the plate (Fig. 5). The slopes at the edges of the local mesh are used to compute the orientations of the remaining part outside of the heat affected zone. Figure 6 illustrates the final result of the interpolation from the local mesh to the plate.
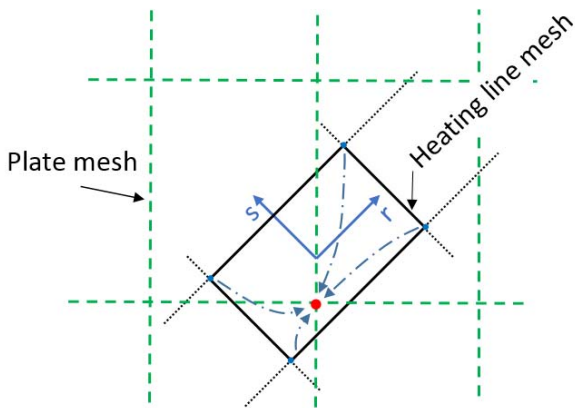

Figure 5 : Transfer local nodes information (blue dots) i.e. displacements, slopes and curvatures, using a 4-point interpolation procedure, of the deformed grid to the plate nodes (red dot).
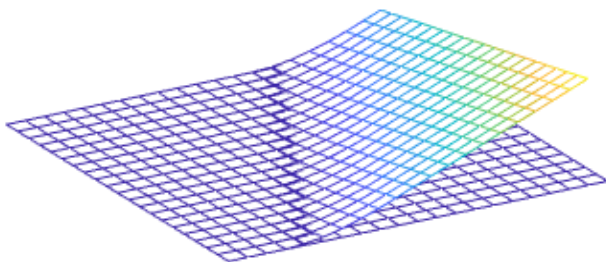

Figure 6: Deformed plate following one heating line

3. MULTIPLE HEATING LINES

As shown in Figure 7, three heating lines were applied, one at a time, across an initially flat plate. The procedure described in section 2 was then applied three times, with the data computed on the local grid transferred to the evolving geometry i.e. obtained from the computed displacements of the preceding heating line. Slopes and curvatures are also transferred to the new geometry. This is particularly important to preserve the data transferred, especially in the case of crossing lines.

Figure 8 gives the shape obtained after having sequentially applied the three heating lines. The bottom view (Fig. 7b) reveals the heating line trajectories and how they are clearly related with the "hinge" effect of each heat input energy lines.
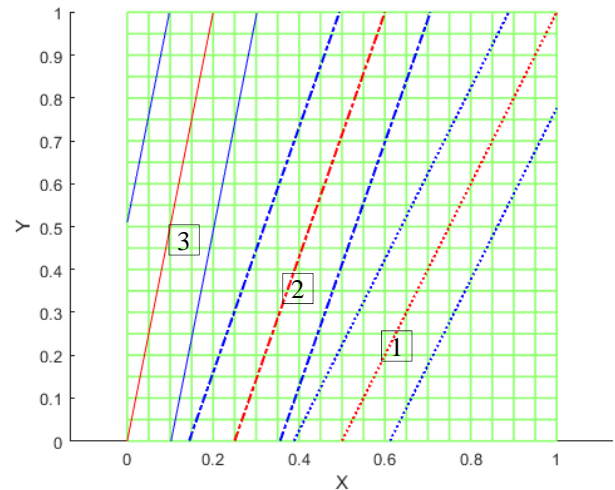
Figure 7: Heating line pattern sequentially applied from 1 to 3

a)

b)

Figure 8: Plate shape obtained after applying three heating line passes: a) isometric view, b) bottom view

4. PIECEWISE HEATING LINE
In order to test the ability of the heating line procedure to predict the change of geometry of a plate following the energy input by a piecewise heating line. The heating is formed of two straight segments, each of them with different length. See in Fig. 9 the heat input source area

moving at a speed V along the piecewise heating line trajectory. A finite element model has been built for applying the energy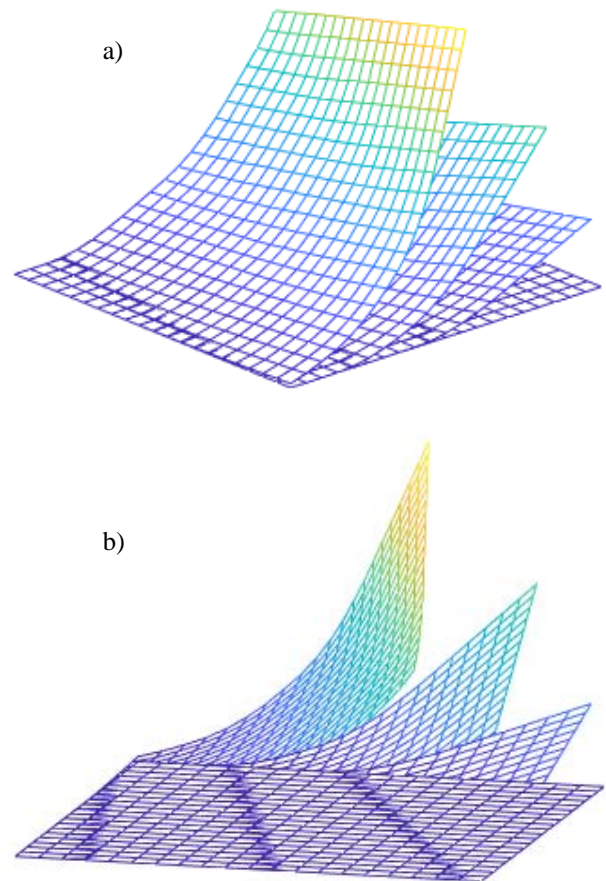 input and a decoupled thermal-structural simulation was performed to get the detailed results of this virtual experiment.
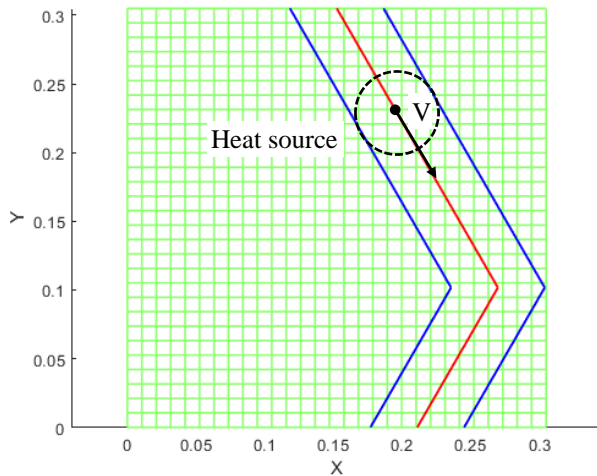

Figure 9: Plate mesh with the piecewise heating line trajectory and the input area of the heat source

4.1. Finite element model

The heat source model was calibrated with experiments (Provencher 2017). It was found that a power of 1850 W for a torch speed V of 2.7 mm/s was transferred in the workpiece through the Goldak's ellipsoid (Goldak 1984; Morin 2006; Provencher 2017). The heat input is propagated by conduction through the workpiece and is assumed to be dissipated from the plate to the atmosphere mainly by convection with a heat transfer coefficient h and a film temperature T_f of 22°C. The temperature dependent physical properties (T temperature, k coefficient of conduction, C specific heat, h convection coefficient, E Young's modulus, E_T tangent modulus and S_Y elastic limit) of the 305 mm x 305 mm x 12.7 mm steel plate are given in Table 1. The transient FE thermal simulation was performed in Ansys 18.2 version using the linear 8-node SOLID278 brick element type. The model is meshed with 48 015 nodes and 36 864 elements.

Table 1: Physical properties for the FE model

T	k	C	h	E	S_Y	E_T
°C	W/m/°C	J/kg/°C	W/m/°C	GPa	MPa	MPa
20	15.0	442	1.0	200	230.0	2800.0
200	17.5	515	12.4	185	157.8	2490.5
400	20.0	563	26.1	170	132.0	2380.0
600	22.5	581	48.7	153	104.7	1618.7
800	25.5	609	82.4	130	77.3	857.3
1000	28.3	631	129.8	96	50.0	96.0
1200	31.1	654	193.0	50	10.0	50.0
1400	33.1	675	274.3	10	10.0	10.0

At each time step, elements beneath the heat source area are receiving an amount of energy that is dependent of their centroid distance to the heat source center following the Goldak's distribution equation of energy. The heat source trajectory and the temperature distribution, with the peak temperature occurring at the center of the heat source is shown in Figure 10 a) to c).
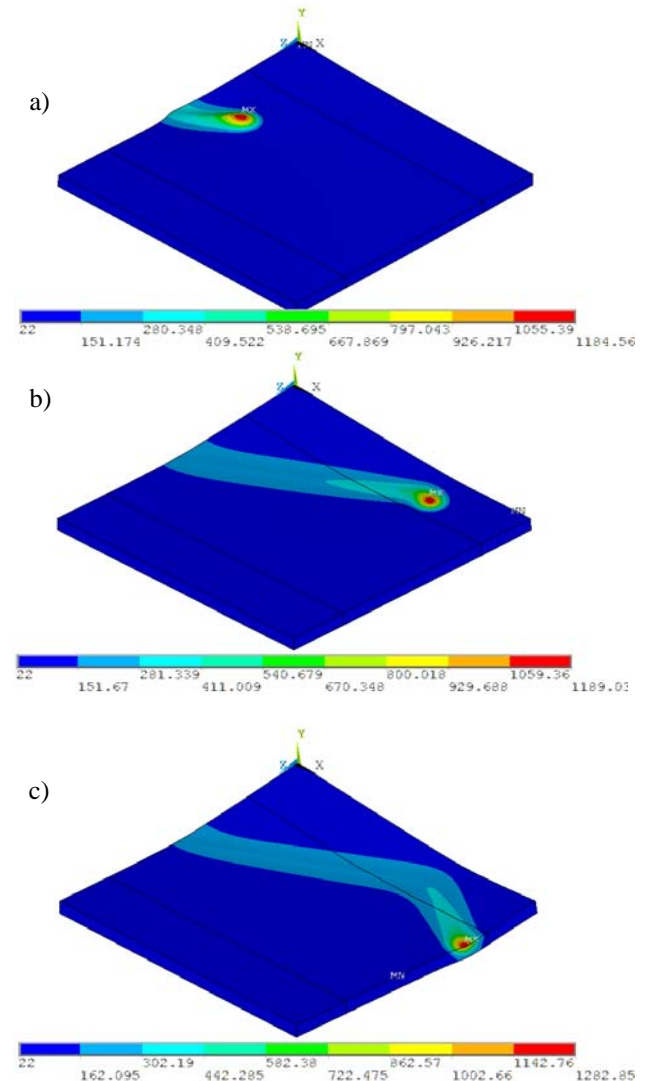
Figure 10: Thermal FE simulation results - Evolution of the temperature distribution for different times and locations a), b) and c) of the heat source along the heating line trajectory

The structural behavior of the material was assumed to behave as a temperature dependent bi-linear kinematic hardening model defined by the Young's modulus E, the elastic limit S_Y and the tangent modulus E_T (See Table 1 for the temperature dependent values of the material parameters). For the structural analysis, the thermal SOLID278 element type is replaced by the structural SOLID185 8-node element type. The same mesh is kept which has a 4-element mesh density through the thickness to better capture the bending effect caused by the heat input. The plate is simply supported at three of

its bottom vertices and rigid body movements are prevented without over constraining the model. The following figures illustrate the displacement observed on the plate (Fig. 11), the equivalent plastic strain (Fig. 12) and the von Mises residual state of stress (Fig. 13) when the plate has completely cooled down to the room temperature.
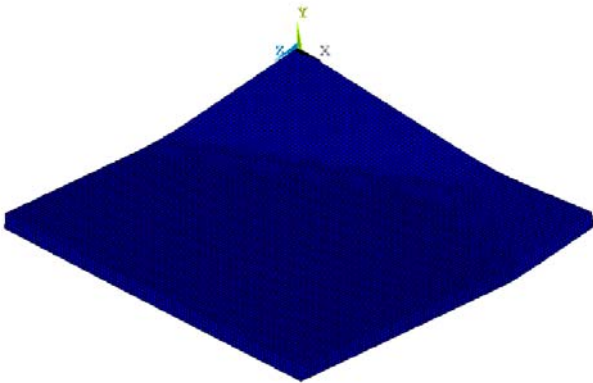

Figure 11: Structural FE simulation results - deformed plate after cooling down

In Figure 12, the extremely localized plastic strain occurring along the heat source trajectory illustrates clearly where the bending occurs (and where was applied the heating line) and how the "hinge effect" could be controlled by the heat input energy. Too much heat input would create more plastic strain but not much "hinge effect" and too few energy input wouldn't create any plastic strain. It has been observed that the maximum bending effects are obtained when the plastic strains occur on the outer surface of the plate and at a shallow depth.
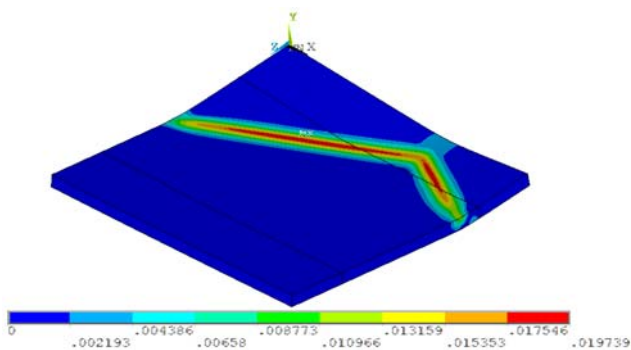

Figure 12: Structural FE simulation results - Plastic equivalent strain

Figure 13 displays the von Mises stress distribution across the deformed plate. One can notice that the maximum residual stresses occurred naturally in the bent areas, where the heat source was imposed along the piecewise heating line trajectory. Note also that the maximum residual stresses are located where the plastic strains get their higher values and especially in the plate kinked area at the heating line elbow.
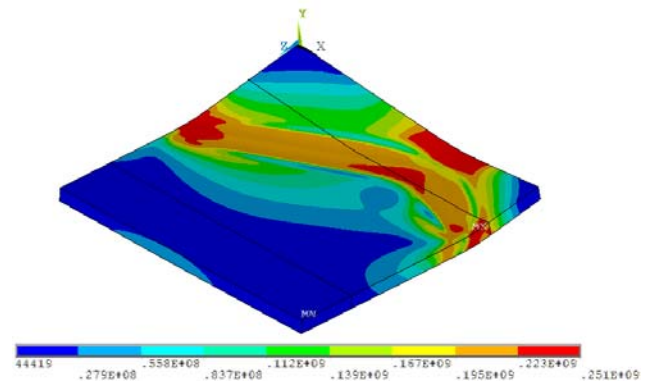
Figure 13: Structural FE simulation results - von Mises stress distribution at room temperature

4.2. Piecewise heating results

A piecewise heating line, as shown in Fig. 9 was applied on an initially flat plat plate. The heating line was divided in two parts, one for each of its straight segments. Local meshes were then applied to cover the heated areas and the displacements were computed. Figure 14 shows the local meshes and the local resulting shape.
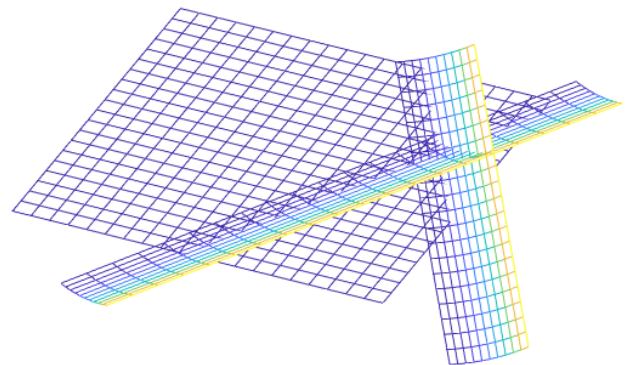
Figure 14: Local meshes adjusted to the heated areas

The distorted grid computed with the 5th order spline methodology is presented in Figure 15. The new geometry is closely similar to the one computed with the FE model (Fig. 11).

Figure 15: Piecewise heating line resulting shape

4.3. Results comparison

Next plot (Fig.16) illustrates how nearly a perfect match is achieved between the FE model results and the line heating procedure with the nodes (blue dots) laying on the red grid of the shape computed with the 5th order spline methodology. Note that the computational time for the FE model is over 4 hours versus less than one minute for the fifth order spline formulation programmed in MatLab (MatLab 2017) using, for simplification, the computed mean value of the radius of curvature obtained from the FE simulation.
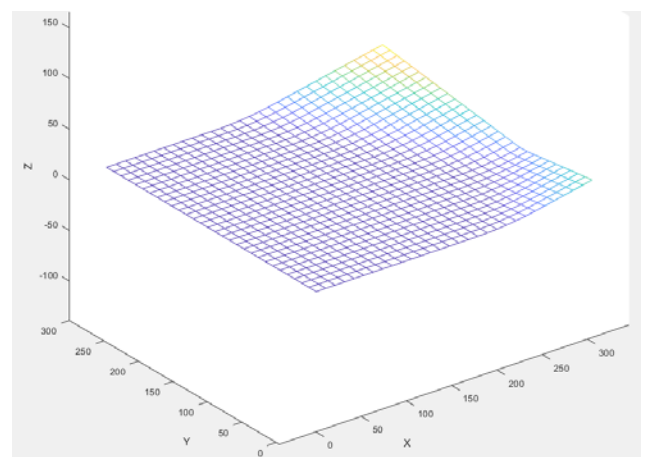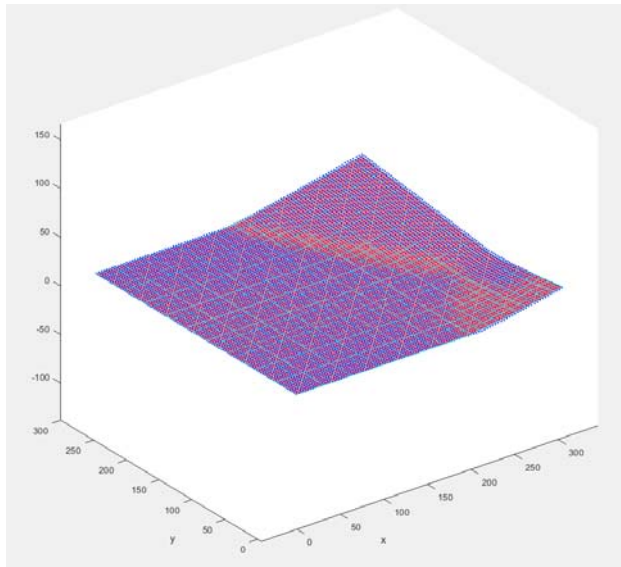

Figure 16: Results comparison: heating line computation (red mesh), thermal-structural FE simulation (blue dots)

CONCLUSIONS

A fifth order piecewise spline formulation was used to compute the displacements caused by the bending effect of a heating line across a flat plate. The methodology presented proves its ability to recreate the evolution of the geometry following a sequence of heating lines. The displacements computed on a local mesh fitted with the heating line trajectory are transferred by interpolation to the evolving geometry of the plate. An application with a piecewise heating line compared to a finite element model shows the potential of the methodology to reproduce the effects of complex trajectories performed by skilled workers. This opens the possibility of optimizing the process since, even with an imposed constant radius of curvature, results are very close to time consuming FE simulations and obtained in a glimpse of time in comparison. Future developments will include a variable parameter approach for curvatures.

AKNOWLEDGEMENTS

REFERENCES

Adan Vega, Sherif Rashed, Hidekazu Murakawa 2015. Analysis of cross effect on inherent deformation during the line heating process Part 1 Single crossed heating lines. Marine Structures, 40, 92-103.

Champliaud H., Feng Z., Gholipour J., Provencher D., Tousignant D. 2016. Piecewise fifth order spline interpolation for line heating forming process. Proceedings of the IMECE conference, Phoenix, AZ, USA, 11-17 November.

Champliaud H., Feng Z., Lê, V.N., Gholipour J. (2015). Line Heating Forming: Methodology and Application Using Kriging and Fifth Order Spline Formulations, International Journal of Mechanical, Aerospace, Industrial, Mechatronic and Manufacturing Engineering, 9 (9), 1461-1466.

Chu G., Lin Y., Chen G. 2016. A green line heating forming technology for ultra-thick plate. International journal advanced manufacturing technology, DOI 10.1007/s00170-016-8574-8

Doo Jang C., Choon Moon S. 1998. An Algorithm to Determine Heating Lines for Plate Forming by Line Heating Method. Journal of Ship Production, 14 (4), 238-245.

Feng Z., Champliaud H., Sabourin M., Morin S. 2013. Optimal blank design based on FE method for blades of large Francis turbines. Simulation Modelling Practice and Theory, 36, 11-21.

Gao H., Sheikoleislami G., Dearden G., Edwardson P., 2017. Reverse analysis of scan strategies for controlled 3D laser forming of sheet metal. Procedia Engineering 183, 369-374.

Goldak J. 1984. A New Finite Element Model for Welding Heat Sources. Metallurgical Transaction, 15B, 299-305.

MATLAB R2017b (9.3.0.713579), Natick, Massachusetts : The MathWorks Inc., 2017.

Morin O. 2006. Calcul des contraintes résiduelles dues au soudage par la méthode des éléments finis. Thesis (Master). École de Technologie Supérieure, University of Quebec.

Park J., Kim D., Mun S.H., Kwon K., Lee J., Hee K.K. 2016. Automated thermal forming of curved plates in shipbuilding: system development and validation, International Journal of Computer Integrated Manufacturing, http://dx.doi.org/10.1080/0951192X.2016.1145800.

Provencher D. 2017. Étude du procédé de mise en forme par application de lignes de chauffe effectuées sur plaques d'acier inoxydable AISI 304L. Thesis (Master). École de technologie supérieure, University of Quebec.

Reutzel E.W., Zhang L., Michaleris P. 2006. A differential geometry approach to analysis of thermal forming. International Journal of Mechanical Sciences 48, 1046-1062.

Reutzel E.W. 2007. Deformations analysis and path planning for thermal forming of complex shape. Thesis (PhD), The Pennsyvalnia State University.

OPENCAL SIMULATION OF THE 1992 TESSINA LANDSLIDE

Donato D'Ambrosio[a], Alessio De Rango[b], Rocco Rongo[c]

[a],[b],[c]Department of Mathematics and Computer Science, University of Calabria, Rende, Italy

[a]donato.dambrosio@unical.it, [b]alessio.derango@mat.unical.it, [c]rocco.rongo@unical.it

ABSTRACT
OpenCAL is a scientific software library developed for the simulation of 2D/3D complex dynamical systems on multi/many-core systems. A MPI preliminary extension also allows for the execution on cluster of many-core devices. The library provides the Extended Cellular Automata paradigm as a Domain-Specific Language for modeling complex systems on structured grids. Here we briefly describe the software library and show a first application regarding the implementation of a simple but effective landslide simulation model, namely the *SciddicaT* extended cellular automaton. The application to a real case of study, namely the 1992 Tessina landslide (Italy), is also shown. Computational results achieved on an Intel Xeon E5-2650 socket, a Nvidia Tesla K40 compute dedicated many-core device and a Nvidia GeForce GTX 980 GPU are reported.

Keywords: Extended Cellular Automata, Parallel Software Library, 2D/3D Structured Grids, GPGPU, Landslide Simulation

1. INTRODUCTION

Due to current technological limitations, increasing the number of transistor on silicon can not be pushed beyond a certain limit, making necessary the adoption of parallel computing solutions in order to improve performances (Kumar 2002). Parallel computing machines are nowadays equipped with multi-core CPUs and many-core devices like GPUs, and their use has recently been more and more applied in Scientific Computing (Golub and Ortega 2014). Different software systems have been proposed aiming simplifying the programming of such systems. Among them, well-known examples are OP2 (Giles *et al.* 2013), and OPS (Reguly *et al.* 2014), Domain-Specific Languages (DSLs) for unstructured and structured grid applications, respectively, able to run on clusters of CPUs and GPUs. Other valid software systems able to hide the complexity of the underlying parallel hardware are ArrayFire (Malcolm *et al.* 2012), a mathematical library for linear algebra and Fast Fourier transform, clSpMV (Su and Keutzer 2012; Zhang *et al.* 2016), a sparse matrix vector multiplication library, and SYCL-BLAS (Aliaga *et al.* 2018), an OpenCL parallelization of the Blas linear algebra library.

In this context, the OpenCAL (Open Computing Abstraction Layer) software library was recently released (as LGPL version 3 software, freely available at GitHub) for modeling 2D/3D discrete dynamical systems based on structured grids of cells, allowing for their execution on multi-core CPUs and many-core devices like GPUs (D'Ambrosio *et al.* 2018). Low-level programming details can be ignored and different efficient serial, multi-core, single-GPU, and multi-GPU applications straightforwardly obtained. A preliminary component also allows to exploit clusters of many-core devices (cf. De Rango *et al.* accepted). A first application of OpenCAL to the simulation of a 3D particle system was already shown in De Rango *et al.* (2018). At the highest level, OpenCAL provides a Domain-Specific Language based on the Extended Cellular Automata formalism (XCA) (Di Gregorio and Serra 1999). XCA represent a computationally equivalent extension of Cellular Automata (CA), which is particularly suitable for the modeling of macroscopic phenomena like fluid-flows (Avolio *et al.* 2006; Avolio *et al.* 2013; D'Ambrosio *et al.* 2013; Spataro *et al.* 2013; Machado *et al.* 2015), besides others.

2. OVERVIEW OF OPENCAL

A model suitable to be implemented in OpenCAL is formally defined as a XCA. Informally, XCA are a *structures grid* parallel computational paradigm, whose dynamics is mainly ruled by local rules (i.e., they are function of the states of a - generally small - set of *neighboring cells*), which define the cell's *transition function*. With respect to classic definition of CA, XCA split the transition function in *elementary processes*, as well as the cell state in *substates*. Global parameters can also be defined (e.g. viscosity or temperature of solidification of lava). Eventually, *external influences* and *global operation* can be considered: the first are used to provide some input to the system during its evolution (e.g., lava feeding in lava flow simulations); the seconds allow to perform reductions operations over the domain.
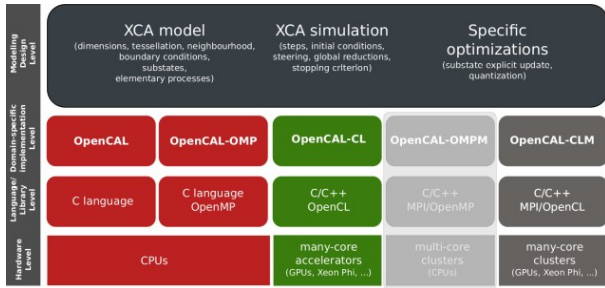
Figure 1: OpenCAL architecture. The computational model, together with the simulation process and possible optimizations, is designed at the higher level of abstraction. The OpenCAL components can be found at the implementation abstraction layer level, each one specifically designed on top of lower level parallel APIs for the execution on multi-core CPUs, many-core devices and clusters of many-core accelerators. The OpenCAL component for cluster of multi-core CPUs is planned as a future development of the project.

Regarding the implementation, OpenCAL was written in C for maximum efficiency and is made by four components, each one for a different device/system: OpenCAL-S is the serial version, OpenCAL-OMP the OpenMP implementation for CPU-based shared memory systems, OpenCAL-CL the OpenCL implementation of the library for single/multi-GPU devices, and OpenCAL-CL/MPI (currently supporting 2D grids only) the MPI-based extension of OpenCAL-CL, which permits to exploit clusters of GPU-equipped nodes (Figure 1).

OpenCAL adopts the *Structure of Array* paradigm. Accordingly, a *substate object* is actually implemented either as a double (*double-layer substate*) or single (*single-layer substate*) buffer (this latter currently not available in OpenCAL-CL), with buffer element defining a sub-information of the state of the corresponding domain cell. A classic, seamless, data parallel decomposition was considered for the multi-core implementation, with computational domain decomposed in chunks, while a one-thread/one-cell execution policy was considered for the many-core component. Note that, chunks sizes are implicitly defined in OpenCAL-OMP by the scheduling adopted (e.g., static scheduling is based on a uniform partition of the computational domain), while it must be set explicitly in the case of OpenCAL-CL/MPI to deal with possible unbalance among cluster nodes.

Eventually, the *active cells* optimization was implemented in OpenCAL, permitting to restrict the computation to the set of non-stationary cells, where a stationary cell is defined as a cell that can not change state to the next computational step. This kind of optimization can give a great advantage in the simulation of topologically connected phenomena (D'Ambrosio et *al*. 2018). The optimization adopts two arrays: a Boolean array of flags, *F*, of the same dimension of the computational domain (*true* meaning

that the cell is active), and an array of active cells, *A*, containing the coordinates of non-stationary cells. At step *t*=0 and subsequently during the computation, cells can be marked to be added/removed to/from *A* by means of specific API functions, which update the flags in *F*. At the end of each elementary process with add/remove calls, a stream compaction algorithm is applied to *F* in order to update *A*. In the case of OpenCAL-S/OpenCAL-OMP, a new instance of *A* is created (to match the new number of active cells) and then a loop checks *F*, by saving active cells coordinates in *A*. Instead, the strategy proposed by Filippone et *al*. (2015), based on the parallel prefix sum algorithm, was considered in OpenCAL-CL.

3. THE SCIDDICA-T XCA

SciddicaT was considered as a first application for assessing OpenCAL performances and correctness because, despite its simplicity, it demonstrated to be able to simulate the dynamics of real *non-inertial* landslides on complex topographic surfaces (Avolio et al. 2000). Two formal definitions of *SciddicaT* were here considered, namely $SciddicaT_{naive}$ and $SciddicaT_{ac}$, the first adopting a *naive* optimization, the second the active cells one. Both of them are formally described in the following, and an OpenCAL-S implementation shown for the second one.

3.1. The $SciddicaT_{naive}$ model
The $SciddicaT_{naive}$ XCA model is formally defined as:

$$SciddicaT_{naive} = <R, X, Q, P, \sigma>$$

where R is the two-dimensional computational domain, subdivided in square cells of uniform size, while X is the von Neumann cell's neighborhood, composed by adjacent neighbors located to North, East, West, and South.
$Q = Q_z \times Q_h \times Q_o^4$ is the set of states of the cell, split in the following substates:

- Q_z represents topographic altitudes a.s.l.
- Q_h represents landslide thickness.
- Q_o^4 represent outflows from the central cell to the four neighbors.

$P = \{p_\epsilon, p_r\}$ is the set of parameters ruling the model dynamics: p_ϵ specifies the minimum thickness below which the fluid cannot outflow the cell due to the effect of adherence; p_r is the relaxation rate parameter, representing an outflow damping factor.
$\sigma : Q^5 \to Q$ is the deterministic cell transition function. It is composed by three elementary processes, listed below in the same order they are applied:

- $\sigma_{o0} : Q_o^4 \to Q_o^4$ sets the outflows from the central cell towards its four neighbors to zero.

- $\sigma_o : (Q_z \times Q_h)^5 \times p_\epsilon \times p_r \to Q_o^4$ computes the outflows from the central cell towards its four neighbors. The condition $h(0) \le p_\epsilon$ is preliminarily evaluated, being $h(0)$ the debris thickness in the central cell. If it is true, the outflow computation is skipped (*naive optimization*). In the other case, the *minimization algorithm of the differences* (Di Gregorio and Serra 1999) is applied to evaluate *minimizing* outflows $f(0, m)$ $(m = 0, \ldots, 3)$, i.e. that outflows that, if actually distributed, would lead the local system composed by central cell and its neighbors to the hydrostatic equilibrium. For this purpose, by neglecting kinetic head (slow-moving flows with no run up effects are here considered), hydraulic heads $z(m) + h(m)$ $(m = 0, \ldots, 3)$ are provided as input to the minimization algorithm. Actual outflows are then computed as $q_o(0, m) = f(0, m) \cdot p_r$ $(m = 0, \ldots, 3)$, where $p_r \in \,]0, 1]$ is a damping factor introduced to smooth the local convergence process.

- $\sigma_h : Q_h \times (Q_o^4)^5 \to Q_h$ determines debris thickness inside the central cell due to mass exchange within the cells belonging to the neighborhood:

$$h^{t+1}(0) = h^t(0) + \sum_{m=0}^{3} (q_o(0, m) - q_o(m, 0))$$

Here, $h^t(0)$ and $h^{t+1}(0)$ are the mass thickness inside the cell at the t and $t + 1$ computational steps, respectively, while $q_o(m, 0)$ represents the inflow from the mth neighboring cell.

About the implementation details, thanks to the cell's state decomposition and the elementary processes considered, only single-layer substates were adopted in the OpenCAL-S and OpenCAL-OMP versions od *SciddicaT_naive*, while double-layer substates were not considered in the implementation based on OpenCAL-CL since this latter currently does not support single-layer substate oblects. The adoption of single-layer substate was possible in this case since elementary processes either update a single substate of the central cell as a function of substates of the same cell (i.e., the elementary process is an *internal transformation*), or as a function of different substates of its neighbors (i.e., that does not depend on the substate which is going to be updated).

The initial condition of the system is defined by the Digital Elevation Model (DEM) of the surface over which the mass will flow down, and by a map of the mass thickness in each cell of the landslide source, also provided as a raster map. This information is used to set up the $q_z \in Q_z$ and $q_h \in Q_h$ substates for each domain cell. The dynamical evolution of the system is therefore obtained by applying, to each cell of the cellular space, the elementary processes in the order they are defined, and then by updating substates.

3.2. The *SciddicaT_ac* model

SciddicaT_ac exploits the active cells optimization briefly outlined in Section 2. The set of active cells, A, is initialized with coordinates of source cells (i.e., of cells belonging to the landslide source). Then, a cell is added to A if an outflow is computed towards it, while is removed from A if its debris thickness drops below the p_ϵ threshold. *SciddicaT_ac* is formally defined as:

$$SciddicaT_{ac} = < R, A, X, Q, P, \sigma >$$

where $A \subseteq R$ is the set of active cells, while the other components are defined as in the formal definition of *SciddicaT_naive*. The transition function is now defined as $\sigma_{|A} : Q^5 \to Q$, denoting that it is applied only to the cells in A and that it can add/remove cells to/from A. The $\sigma_{o|A}$ elementary process was modified, since it can now determine the activation of new cells. Moreover, a new elementary process, $\sigma_{A|A}$, was considered, in order to remove cells whose debris thickness becomes lower than or equal to the p_ϵ threshold as a result of the application of the $\sigma_{o|A}$ elementary process. The new sequence of elementary processes is listed below, in the same order in which they are applied.

- $\sigma_{o0|A} : Q_o^4 \to Q_o^4$ sets the outflows from the central cell towards its four neighbors to zero.
- $\sigma_{o|A} : (Q_z \times Q_h)^5 \times p_\epsilon \times p_r \to Q_o^4$ determines the outflows from the central cell to its four neighbors. Neighbors toward which non-null flows are evaluated are added to the set of active cells.
- $\sigma_{h|A} : Q_h \times (Q_o^4)^5 \to Q_h$ determines mass balance within the cell. This elementary process does not differ from that defined in *SciddicaT_naive*.
- $\sigma_{A|A} : Q_h \times p_\epsilon \to A$ removes a cell from A if its debris thickness is lower than or equal to p_ϵ.

Even for *SciddicaT_ac*, single-layer substates were adopted in the OpenCAL-S and OpenCAL-OMP implementations.

3.2.1. OpenCAL implementation of *SciddicaT_ac*

Given the simplicity of the model, we report the OpenCAL-S implementation of *SciddicaT_ac* below. The OpenCAL-OMP implementation of the of the same model only differs for the included header files.

```
1  #include <OpenCAL/cal2D.h>
2  #include <OpenCAL/cal2DRun.h>
3  ...
4
5  #define P_R 0.5
6  #define P_EPSILON 0.001
7  #define STEPS 4000
8  ...
```

```
9
10  struct sciddicaTSubstates {
11    struct CALSubstate2Dr *z;
12    struct CALSubstate2Dr *h;
13    struct CALSubstate2Dr *f[NUMBER_OF_OUTFLOWS];
14  } Q;
15
16  struct sciddicaTParameters {
17    CALParameterr epsilon;
18    CALParameterr r;
19  } P;
```

Figure 2: OpenCAL-S *SciddicaT_{ac}* header, substates and parameters definitions

Listing shown in Figure 2 includes OpenCAL's header files, besides defining model's substates and parameters (lines 10-19), while Figure 3 shows the implementation of model's elementary processes. The XCA model object is defined in the main function, shown in Figure 4, by means of the `calCADef2D()` API function, which receives domain dimensions, type of neighborhood, boundary conditions and the optional optimization to be used as parameters (lines 94-98). The simulation object is then defined thanks to the `calRunDef2D()` function. This latter requires a XCA model to be run, initial and final computational steps, and the substate update policy to be used (lines 99-101). Implicit update means that OpenCAL transparently performs the operation. In this case, however, substates do not need to be updated, being only single-layer objects adopted (cf below). Elementary processes are therefore registered to the model object thanks to `calAddElementaryProcess2D()` as callback functions for seamless application (lines 103-106). Even substates are registered to the model object by means of the `calAddSingleLayerSubstate2Dr()` API function (lines 108-113). The alternative API function `calAddSubstate2Dr()` can is used to register double-layer substates. The call to `CalRun2D()` eventually enters the simulation loop (line 117). In this case, the simulation process is completely performed by the library. Nevertheless, the main computational loop can be made explicit for finer control over the simulation. Finallly, the `calRunFinalize2D()` and `calFinalize2D()` API functions release previously (implicitly) allocated memory resources (lines 53-54).

```
21  void sigma_o0(struct CALModel2D* xca_obj,int i,int j) {
22    calSetCurrent2Dr(xca_obj,Q.f[0],i,j,0.0);
23    calSetCurrent2Dr(xca_obj,Q.f[1],i,j,0.0);
24    calSetCurrent2Dr(xca_obj,Q.f[2],i,j,0.0);
25    calSetCurrent2Dr(xca_obj,Q.f[3],i,j,0.0);
26  }
27
28  void sigma_o(struct CALModel2D* xca_obj, int i, int j) {
29    CALbyte eliminated_cells[5]={CAL_FALSE,...,CAL_FALSE};
30    CALbyte again;
31    CALint cells_count, n;
32    CALreal z, h, f, m, u[5], average;
33
34    m = calGet2Dr(xca_obj,Q.h,i,j)-P.epsilon;
35    u[0] = calGet2Dr(xca_obj,Q.z,i,j)+P.epsilon;
36    for (n=1; n<xca_obj->sizeof_X; n++) {
37        z = calGetX2Dr(xca_obj,Q.z,i,j,n);
38        h = calGetX2Dr(xca_obj,Q.h,i,j,n);
```

```
39        u[n] = z+h;
40      }
41
42    //computes outflows and updates debris thickness
43    do {
44      again = CAL_FALSE;
45      average = m;
46      cells_count = 0;
47
48      for (n=0; n<xca_obj->sizeof_X; n++)
49        if (!eliminated_cells[n]){
50          average += u[n];
51          cells_count++;
52        }
53
54      if (cells_count != 0)
55        average /= cells_count;
56
57      for (n=0; n<xca_obj->sizeof_X; n++)
58       if( (average<=u[n]) && (!eliminated_cells[n])
){
59          eliminated_cells[n]=CAL_TRUE;
60          again=CAL_TRUE;
61        }
62
63    }while (again);
64
65    for (n=1; n<xca_obj->sizeof_X; n++)
66      if (eliminated_cells[n])
67        calSetCurrent2Dr(xca_obj,Q.f[n-1],i,j,0.0);
68      else {
69  calSetCurrent2Dr(xca_obj,Q.f[n-1],i,j,(average-u[n])*P.r);
70        calAddActiveCellX2D(xca_obj, i, j, n);
71      }
72  }
73
74  void sigma_h(struct CALModel2D* xca_obj,int i,int j) {
75    CALreal h_next;
76    CALint n;
77
78    h_next = calGet2Dr(xca_obj, Q.h, i, j);
79    for(n=1; n<xca_obj->sizeof_X; n++)
80      h_next+=calGetX2Dr(xca_obj,Q.f[NUMBER_OF_OUTFLOWS-n],
81                i,j,n)-calGet2Dr(xca_obj,Q.f[n-1],i,j);
82
83    calSetCurrent2Dr(xca_obj, Q.h, i, j, h_next);
84  }
85
86  // The sigma_3 elementary process
87  void sigma_A(struct CALModel2D* xca_obj,int i,int j) {
88    if (calGet2Dr(xca_obj, Q.h, i, j) <= P.epsilon)
89      calRemoveActiveCell2D(xca_obj,i,j);
90  }
```

Figure 3: OpenCAL-S *SciddicaT_{ac}* elementary processes

The `sigma_o0` callback function, shown in Figure 3, resets the outflows from the central cell to the four neigbors by means of the `calSetCurrent2Dr()` function (the alternative `calSet2Dr()` function is used to update double-layer substates) (lines 21-26).
The subsequent `sigma_o` function implements the $\sigma_{o|_A}$ elementary process (lines 28-72). It applies the minimization algorithm of the differences in order to evaluate outflows. Cells whose hydrostatic condition does not permit to receive mass are preliminary eliminated (lines 43-61). Outflows are then evaluated for non eliminated cells and saved into the corresponding substates for subsequent mass balance by means of the `calSetCurrent2Dr()` function. The functions `calGet2Dr()` and `calGetX2Dr()` are here used to retrieve substate values for central and neighboring cells, respectively (lines 65-71).

Contextually to mass balance, cells receiving outflows are marked to be added to the set of active cells, *A*, by the `calAddActiveCellX2D()` function (line 70). Note that, however, *A* is actually updated by OpenCAL transparently to the user at the and of the elementary process application.

The next `sigma_o` callback function implements the $\sigma_{h|A}$ elementary process (lines 74-84). It simply computes mass balance by subtracting outgoing flows from the central cell and by adding inflows to it.

Eventually, the `sigma_A` function implements the $\sigma_{A|A}$ elementary process, which marks cells to be removed from the set *A* of active cells by means of the `calRemoveActiveCell2D()` function. Even in this case, *A* is actually updated by OpenCAL transparently to the user at the and of the elementary process application.

```
92   int main(int argc, char** argv)
93   {
94     struct CALModel2D* xca_obj=calCADef2D(rows,
95              cols,
96              CAL_VON_NEUMANN_NEIGHBORHOOD_2D,
97              CAL_SPACE_TOROIDAL,
98              CAL_OPT_ACTIVE_CELLS);
99     struct CALRun2D* sim_obj = calRunDef2D(xca_obj,
100             1, STEPS,
101             CAL_UPDATE_IMPLICIT);
102
103    calAddElementaryProcess2D(xca_obj, sigma_o0);
104    calAddElementaryProcess2D(xca_obj, sigma_o);
105    calAddElementaryProcess2D(xca_obj, sigma_h);
106    calAddElementaryProcess2D(xca_obj, sigma_A);
107
108    Q.z   = calAddSingleLayerSubstate2Dr(xca_obj);
109    Q.h   = calAddSingleLayerSubstate2Dr(xca_obj);
110    Q.f[0] = calAddSingleLayerSubstate2Dr(xca_obj);
111    Q.f[1] = calAddSingleLayerSubstate2Dr(xca_obj);
112    Q.f[2] = calAddSingleLayerSubstate2Dr(xca_obj);
113    Q.f[3] = calAddSingleLayerSubstate2Dr(xca_obj);
114
115    calLoadSubstate2Dr(xca_obj,Q.z,argv[DEM_PATH_ID]);
116    calLoadSubstate2Dr(xca_obj,Q.h,argv[SOURCE_PATH_ID]);
117    calRun2D(sim_obj);
118    calSaveSubstate2Dr(xca_obj, Q.h, argv[OUTPUT_PATH_ID]);
119
120    calRunFinalize2D(sim_obj);
121    calFinalize2D(xca_obj);
122
123    return 0;
124  }
```

Figure 4: OpenCAL-S *SciddicaT$_{ac}$* main function

As it can be seen, OpenCAL makes straightforward the implementation of a computational model formally defined by the XCA general formalism and, in this respect, it represents a Domain-Specific Language for this computational paradigm. Moreover, it permits to relieve the user of many low-level issues, allowing to considerably reduce the development effort. As a matter of fact, *SciddicaT$_{ac}$* was implemented in little more than 120 lines of code, making the application elegant, readable, and easy to be maintained and, in case of need, updated.

4. SIMULATION OF THE 1992 TESSINA LANDSLIDE

For each version of the *ScidicaT* XCA landslide model defined in the previous Section, we developed an OpenCAL-S, OpenCAL-OMP, and OpenCAL-CL-based implementation, resulting in six different applications. Each of them was considered for the simulation of a real case of study, namely the 1992 Tessina Landslide, and execution times registered to evaluate computational performances, as described in the next Sections.

4.1. Simulation of the Tessina Landslide

The 1992 Tessina (Italy) landslide occurred between 1,220 m and 625 m a.s.l., with an extension of nearly 3 km and a maximum width of about 500 m.

The topographic surface was discretized as a DEM (Digital Elevation Model) of 410 rows per 294 columns, with square cells of 10 m side, for a total of 102,540 cells. The landslide source, specifying the location and thickness of the detachment area, was also described by means of a raster map of the same dimensions.

According to Avolio et al. (2000), model parameters p_ϵ and p_r were set to 0.001 and 0.5, respectively, and a total of 4000 steps were considered. The Tessina landslide, as simulated by the two versions of *SciddicaT* here considered, is shown in Figure 5.

Both versions resulted numerically correct. Indeed, we evaluated the `md5sum` signature of the outcome of each serial and parallel simulation, by obtaining a perfect match. In addition, simulation outcome matched that obtained by Avolio et al. (2000), proving the agreement of the models here developed with the original one on the simulation of the considered real case of study.
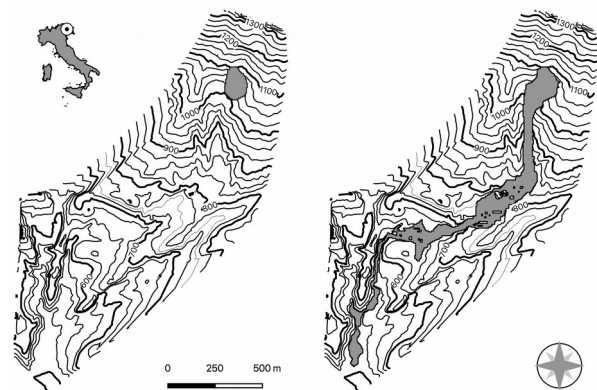

Figure 5: *SciddicaT* simulation of the 1992 Tessina (Italy) landslide. Landslide source on the left, path of the simulated landslide on the right. According to Avolio et al. (2000), model parameters were set to the values 0.001 and 0.5, respectively, and 4000 simulation steps were considered.

4.2. Performances Achieved

A total of four simulations were performed for each implementation of *SciddicaT* by considering three different computational devices, namely an Intel Xeon E5-2650 2.0GHz (16 thread, 8 core) socket, and Nvidia Tesla K40 many-core compute dedicated device and a GeForce GTX 980 GPU. Regarding OpenCAL-OMP implementations, the default (static) OpenMP scheduling was considered during the experiments. Minimum execution times were registered and speed-up evaluated with respect to the execution time of the serial version of *SciddicaT_{naive}* on the Xeon socket (reference simulation). Specifically, the reference simulation required a total of 56.50 seconds to simulate the case of study.
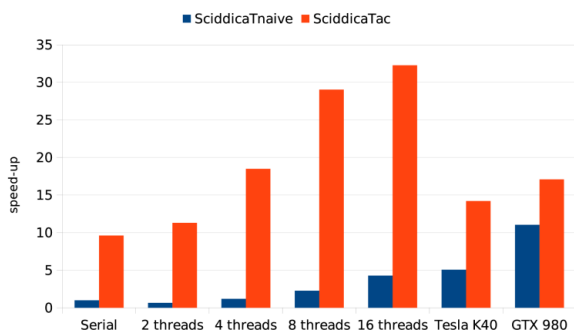

Figure 6: Computational performances achieved by different versions of *SciddicaT* on the simulation of the the Tessina (Italy) landslide on different computational devices. The "Serial" label on the refers to the execution of the serial implementations on a single core of the Xeon 2.0GHz E5-2650 socket, while the "*n* threads" ones (*n*=2,4,8,16) to multi-thread executions on the same socket. Eventually, last two labels refer the speed-up achieved on the Tesla K40 and GTX 980 many-core devices.

Table 1: Execution times registered on the execution of the Tessina Landslide case of study.

ScddicaT execution times (in seconds)		
	ScddicaT_{naive}	*ScddicaT_{ac}*
Serial	56.50	5.88
2 threads	85.62	4.99
4 threads	47.38	3.06
8 threads	24.90	1.95
16 threads	13.21	1.75
Tesla k40	11.15	3.98
GTX 980	5.12	3.31

Table 1 and Figure 6 report execution times and chart of speed-up achieved on the considered computational devices, respectively.

Here is evident how the active cells were effective already in the case of serial implementations, with

SciddicaT_{ac} running almost 9.6 times faster than the reference simulation.

Concerning the executions of the OpenCAL-OMP implementations of the two versions of *SciddicaT* considered, an increasing speed-up was observed according to the number of threads adopted, with the best performance achieved by *SciddicaT_{ac}* on 16 threads. This latter ran about 32.27 times faster than the reference simulation.

Eventually, also the OpenCAL-CL implementations evidenced an increasing speed-up according to the adopted optimization. However, performances achieved were relatively below expectations, with *SciddicaT_{ac}* running about 11.05 times faster on the Tesla K40 and 17.08 times faster on the GTX 980 than the reference simulation. Indeed, even if the above results could be considered good in absolute terms, the OpenCAL-OMP implementation of *SciddicaT_{ac}* resulted faster when executed on the Xeon socket. Probably, the greater number of memory accesses in the OpenCAL-CL based implementations, due to the lack of single-layer substates in the OpenCAL component, penalized the overall GPU performances. Another OpenCAL-CL implementation issue that could have penalized performances is the management of substates in the device memory. Indeed, while each substate is a single object, independent from each other, in OpenCAL-S and OpenCAL-OMP, substates are grouped together in OpenCAL-CL based of their type (i.e., one single long buffer is used for all the double precision substates, one for integer substates, and so on). In the *SciddicaT* versions here considered, only double precision substates were considered. As a consequence, they were grouped together (transparently to the user) in a single, extended buffer on the device memory. A similar choice forced to update the buffer containing all the model's substates even in the case just one of them was changed, with a waste of computational and bandwidth resources. For instance, even if the $\sigma_{h|A}$ elementary process only affects the substate Q_h, the subsequent update of the wall buffer of substates (made by six double precision double-layer objects) is necessary. A similar waste of resources also occurs after the applications of the other *SciddicaT* elementary processes, resulting in an unavoidable degradation of performances.

Nevertheless, better results were achieved in the case of the *SciddicaT_{naive}* simulations of the Tessina landslide, with GPUs always performing better than the Xeon CPU. In this case, the greater amount of computation (due to the fact that the simulation loop actually processed the whole computational domain, not only the subset of active cells) balanced the greater number of memory accesses.

Eventually, it is worth to note that the GeForce GPU performed better than the Tesla many-core device in all cases, even if this latter belongs to the compute dedicated Nvidia solutions. Probably, the GTX 980 GPU, which is based on a more recent (thus efficient)

architecture, took advantage of the low computational request of the algorithms by the relatively small dimensions of the computational domain. Indeed, being a Computer Graphics dedicated solution, the GTX 980 GPU was designed to be efficient in fetching data from device memory and then performing a limited amount of computation, which is a common situation, for instance, in OpenGL applications. At the contrary, the Tesla device was designed to be more effective on more computational intense tasks and extended domains.

5. CONCLUSIONS

In this paper we briefly described OpenCAL, a new software library providing a Domain-Specific Language for Extended Cellular Automata.

The *SciddicaT* XCA landslide model was considered to test the library in terms of correctness and computational performances. For this purpose, the Tessina (Italy) landslide, occurred in 1992, was considered as reference case of study.

Two versions of *SciddicaT* were considered, the first exploiting a *naive* optimization, consisting in processing the whole computational domain by skipping those cells with negligible amount of debris, the second exploiting the active cells optimization embedded in OpenCAL, which permitted to restrict the computation process to the limited subset of non-stationary cells.

Serial, multi and many core implementations of both versions of *SciddicaT* were implemented by means of the OpenCAL-S, OpenCAL-OMP and OpenCAL-CL components, respectively. Six implementations were thus obtained. Each of them was tested on three different computational devices, namely an Intel Xeon socket, used for evaluating serial and OpenMP based implementations, and two Nvidia GPUs, namely a Tesla K40 and a GTX 980, adopted for evaluating the OpenCL based versions of *SciddicaT*.

GPUs resulted the best solution for the *SciddicaT* version adopting the naive optimization, while the Xeon socket performed better in the case the active cells optimization was exploited. This apparently surprising result can be explained by considering that the serial and OpenCAL-OMP based implementations of *SciddicaT* could exploit single-layer substates, resulting in a significant reduction of memory accesses. In addition, it is worth to note that the OpenCAL-CL based implementations were further penalized by the fact that this component groups substate objects in a unique contiguous buffer on the GPU memory, forcing to update the whole block even in the case a single substate is affected (this is the case, for instance, of the $\sigma_{h|A}$ elementary process that only updates Q_h).

According to the results achieved, CPUs resulted more suitable for low computationally demanding simulations (i.e., those performed by *SciddicaT$_{ac}$*), while GPUs in the other cases. Moreover, among the considered many-core solutions, the GeForce GPU performed better than the Tesla on the considered case of study, probably due to the greater amount of memory accesses required by the OpenCAL-CL implementations, which give an advantage to the game-oriented solution.

Among future development of the project, besides improving the above discussed issues, e.g. in the OpenCAL-CL memory management of substates, OpenCAL-CL/MPI support to three-dimensional models will be introduced, other benchmarks implemented (e.g. Clover Leaf could be a good candidate), performances tested on more performing hardware (multi-node systems included), and a comparison with other software, like OPS, performed.

REFERENCES

Kumar V., 2002. Introduction to Parallel Computing, 2nd Edition. Addison-Wesley Longman Publishing Co., Inc., Boston, MA, USA.

Golub G.H., Ortega J.M., 2014. Scientific computing: an introduction with parallel computing. Academic Press, London, UK.

Giles M., Mudalige G., Spencer B., Bertolli C., Reguly I., 2013. Designing OP2 for GPU architectures. Journal of Parallel and Distributed Computing, 73 (11), 1451–1460.

Reguly I., Mudalige G., Giles M., Curran D., McIntosh-Smith S., 2014. The OPS domain specific abstraction for multi-block structured grid computations. Proceedings of WOLFHPC 2014: 4th International Workshop on Domain-Specific Languages and High-Level Frameworks for High Performance Computing - Held in Conjunction with SC 2014: The International Conference for High Performance Computing, Networking, Storage and Analysis, pp. 58–67. November 17, New Orleans (Louisiana, USA).

Malcolm, J., Yalamanchili, P., McClanahan, C., Venugopalakrishnan, V., Patel, K., Melonakos, J., 2012. ArrayFire: A GPU acceleration platform. Proceedings of SPIE - The International Society for Optical Engineering, 8403, art. no. 84030A.

Su, B.-Y., Keutzer, K., 2012. clSpMV: A cross-platform OpenCL SpMV framework on GPUs. Proceedings of ICS 2012: 26th ACM international conference on Supercomputing, 2012, pp. 353–364.

Zhang, Y., Li, S., Yan, S., Zhou, H., 2016. A cross-platform SpMV framework on many-core architectures. ACM Transactions on Architecture and Code Optimization, 13 (4), 33.

Aliaga, J.I., Reyes, R., Goli, M., 2018. SYCL-BLAS: Combining Expression Trees and Kernel Fusion on Heterogeneous Systems. Advances in Parallel Computing, 32, 349–358.

D'Ambrosio D., De Rango A., Oliverio M., Spataro D., Spataro W., Rongo R., Mendicino G., Senatore A., 2018. The Open Computing Abstraction Layer for Parallel Complex Systems Modeling on Many-Core Systems. Journal of Parallel and Distributed Computing, doi: 10.1016/j.jpdc.2018.07.005

De Rango A., Spataro D., Spataro W., D'Ambrosio D., accepted. A First Multi-GPU/Multi-Node Implementation of the Open Computing Abstraction Layer. Journal of Computational Science.

De Rango A., De Napoli P., D'Ambrosio D., Spataro W., Di Renzo A., Di Maio F., 2018. Structured Grid-Based Parallel Simulation of a Simple DEM Model on Heterogeneous Systems. Proceedings of The 26th Euromicro International Conference on Parallel, Distributed, and Network-Based Processing, pp. 588-595. March, 21-23, Cambridge (UK).

Di Gregorio S., Serra R., 1999. An empirical method for modelling and simulating some complex macroscopic phenomena by cellular automata. Future Generation Computer Systems, 16, 259–271.

Avolio M.V., Crisci G.M., Di Gregorio S., Rongo R., Spataro W., D' Ambrosio, D., 2006. Pyroclastic flows modelling using cellular automata. Computers and Geosciences, 7 (32), 897–911.

Avolio M.V., Di Gregorio S., Lupiano V., Mazzanti P., 2013. Sciddica-SS3: A new version of cellular automata model for simulating fast moving landslides. The Journal of Supercomputing, 65 (2), 682–696.

D'Ambrosio D., Filippone F., Marocco D., Rongo R., Spataro W., 2013. Efficient application of GPGPU for lava flow hazard mapping. The Journal of Supercomputing, 65 (2) 630–644.

Spataro D., D'Ambrosio D., Filippone G., Rongo R., Spataro W., Marocco D., 2013. The new SCIARA-fv3 numerical model and acceleration by GPGPU strategies. International Journal of High Performance Computing Applications, 31 (2), 163–176.

Machado G., Lupiano V., Avolio M.V., Gullace, F., Di Gregorio, S. 2015. A cellular model for secondary lahars and simulation of cases in the Vascún Valley, Ecuador. Journal of Computational Science, 11, 289–299.

Filippone G., Spataro W., D'Ambrosio D., Spataro D., Marocco D., Trunfio G., 2015. Cuda dynamic active thread list strategy to accelerate debris flow simulations. Proceedings of The 23rd Euromicro International Conference on Parallel, Distributed, and Network-Based Processing, pp. 316–320. March 4-6, Turku (Finland).

Avolio MV, Di Gregorio S., Mantovani F, Pasuto A, Rongo R, Silvano S., Spataro W., 2000. Simulation of the 1992 Tessina landslide by a cellular automata model and future hazard scenarios. International Journal of Applied Earth Observation and Geoinformation, 1(2), 41–50.

AUTHORS BIOGRAPHY

Donato D'Ambrosio was born in Cosenza (Italy) on 23 January 1973. He graduated *summa cum laude* in Mathematics in 1999 and earned a PhD in Artificial Intelligence in 2004 at UniCal (University of Calabria, Italy). He has been member of the UniCal HPCC (High Performance Computing Centre) since 2002 and Research Fellow at the Department of Mathematics and Computer Science since 2004. Since November 2006, he is Assistant Professor in Computer Science. His research interests regard Parallel Computing, Complex Systems Modeling and Evolutionary Algorithms. He has taken part in many research projects and is the author of more than 60 peer-reviewed scientific publications. He is also member of the Scientific Committee of PDP, PDPTA and CSC conferences. His teaching activity started in 2000 and he currently teaches Computer Graphics and GPGPU programming on the MS Computer Science Course and C++ programming on the Chemistry Course of the University of Calabria. He is the chief designer of OpenCAL and the head of the OpenCAL Team.

Alessio De Rango was born in Cosenza (Italy) on 19 October 1990. He holds a MS in Computer Science *summa cum laude*, during which he conducted researches regarding high-performance lava modeling and risk mitigation using evolutionary techniques. Currently, he is a PhD student in Mathematics and Computer Science at University of Calabria (Italy). His research interests mainly regard High Performance Computing for Scientific Applications, by means of Parallel Computing Paradigms, like GPGPU Computing on CUDA and OpenCL, OpenMP, and MPI. His interests include also Modeling and Simulation by Cellular Automata and Finite Differences Methods, and Evolutionary Computation by Genetic Algorithms. He is one of the major contributor of OpenCAL and recently has become developer of the OPS/OP2 Domain Specific Languages for structured/unstructured grids high-performance modeling.

Rongo Rocco was born in Naples (Italy) on 8 August 1965. He is Assistant Professor in Computer Science at the University of Calabria (Italy). His scientific activity is mainly focused on the modeling and simulation of Complex Systems by Cellular Automata and Genetics Algorithms using Parallel Computing, Statistical and Spatial Analysis by GIS. He currently teaches Computer Science fundamentals and GIS analysis techniques at the Earth Science Department. He is the author of several papers regarding Cellular Automata methods, Genetic Algorithms and Parallel Computing published in international journals and conferences.

EXPLOITATION OF HPC INFRASTRUCTURE SERVICES FOR REAL-TIME CRITICAL SMALL REQUESTS

Jiří Ševčík[a], Martin Golasowski[b], Jan Martinovič[c], David Vojtek[d], Jan Faltýnek[e]

[a],[b],[c],[d],[e]IT4Innovations, VŠB - Technical University of Ostrava,
17. listopadu 15/2172, 708 33 Ostrava, Czech Republic

[a]jiri.sevcik@vsb.cz, [b]martin.golasowski@vsb.cz, [c]jan.martinovic@vsb.cz ,[d]david.vojtek@vsb.cz
[e]jan.faltynek@vsb.cz

ABSTRACT

Modern smart devices are often supported by innovative online services which bring new challenges for cloud and high-performance computing industry. These services have to be designed to handle a dynamic load from various sources while maintaining efficient operation in a given computing environment. Operation of such services has to conform to a multi-criteria service level agreement which can include availability, response time, energy efficiency and other factors. In the field of high-performance computing, this is accomplished by using specialized mechanisms and tools for efficient scheduling and resource allocation. This paper proposes a system which can be used to implement such service on a high-performance computing infrastructure. We demonstrate our approach on an experimental server-side traffic navigation service. The solution is applicable both for high-performance and cloud computing.

Keywords: high-performance, cloud, quality of service, routing navigation, service level agreement.

1. INTRODUCTION

A number of smart devices integrated into our daily lives increases every day. There is a lot of effort supported by public and private entities often focused on increasing the quality of everyday life while consuming less energy. Such activities often span multiple disciplines and involve topics like optimization of public and personal transport, fine control over heating and cooling systems in commercial buildings, weather nowcasting, waste management logistics and others. These activities often make use of the so-called edge computing which is a combination of small embedded computing devices (IoT) and a central data storage accompanied by powerful computing resources like high-performance computing (HPC) clusters.

Edge computing offers a degree of autonomy for the individual devices such that the sensor itself can directly affect another device (switch, actuator) without the need to contact the central unit. This is especially useful in situations with little power available and limited network connectivity in remote locations.

The device can contact the central unit only in case there are interesting data available. The central unit stores the received data and executes further processing and aggregation of data. A result of the processing can be further used to perform simulations and projections. The processing pipeline can consist of several steps which can involve heavy computations like training of a deep neural network, filtering or clustering. The same pipeline can be used either to receive a continuous stream of data in an online mode or to process a set of historical data in a batch mode.

In this paper, we propose a system which can be used to execute a single pipeline of tasks on the HPC cluster in above mentioned modes. The system consists of a master process which handles the incoming data sets and a set of worker processes which communicate with the management process. The master process manages the distribution of the work to the workers using a custom message passing protocol.

In the online mode, the master process of the system resides outside of the cluster and handles deployment of the individual workers by submitting jobs to the cluster scheduler. The system is also prepared to handle dynamic loads by using external tools for autotuning (Gadioli, Palermo and Silvano 2015, Silvano 2017) which provides a number of resources for individual stages of the pipeline to handle variations in the request load while maintaining efficient operation of the service.

In the batch mode, the master and worker processes run together in a single job and process a predefined set of data. The workers can be run as a native Linux application directly on a compute node which introduces a possibility to use a massive parallel code and highly optimized math and data processing libraries. In both mentioned modes the defined pipeline remains the same, the only difference is in location of the master process. In this way, we focus on improving the usability of the HPC platform.

HPC infrastructure provides a vast amount of computational resources. Current clusters usually consist of multiple types of devices, including CPUs, GPUs or other types of specialized accelerators, connected by high bandwidth network with redundant

topology. In order to exploit the power efficiently, the applications have to run with as little overhead as possible. This is achieved by using specialized parallel programming models like MPI, OpenMP or CUDA.

On the other side, cloud services provide vastly easier access to a large number of computing resources through simple APIs. This abstraction is usually at the cost of overhead introduced by virtualisation or similar technology. Also, high bandwidth network typical for HPC installations is less common in the cloud environment. The central unit of such a smart system can be a combination of multiple types of resources.

There are similar tools which can be used to implement such a system. The streaming interface of Apache Kafka (Dunning and Friedman 2016) can serve as a message broker using the consumer-producer pattern and can be used by clients from different programming languages via its own binary protocol. However, it does not offer integration with HPC cluster scheduler and due to its robustness and vast array of features is unsuitable for lightweight job batch processing of data.

There is also a number of systems coming mainly from the biochemistry field which allows specification of data processing pipelines by using the Common Workflow Language (CWL). One example of such system is Toil (Vivian, et al. 2017), which supports specification of such workflows, allows integration with many common Cloud and HPC environments. It is suitable for launching extensive workflows with many stages. It does not offer a possibility for running an online service and integration of the autotuning interface. There are also other systems which main aim is to utilize workflows mainly in a specialized case (Al-Ali, et al. 2016) or offering a system for executing pipelines independently of their types (Cima, et al. 2018).

We demonstrate the functionality of the proposed system on an experimental server-side traffic navigation service deployed on an HPC cluster.

This paper is organized as follows: Section 2 describes the architecture, its components and main features. Next section is dedicated to the description of communication between the system parts. Extensibility of the system is also introduced. Section 5 provides an overview of Quality of Service requirements. Description of usage of external data is also provided. In Section 7, navigation use case for proposed architecture is presented. Testing methodology and its results are provided in Section 8. In the end, we mention the possibility of future work.

2. SOLUTION ARCHITECTURE OVERVIEW

Our proposed solution is a specialized architecture which is divided into two main parts - a management system part and a computation part. This paper is focused mainly on the second part, but the first part will be briefly described as well.

2.1. Management system

The management system part facilitates communication with service clients and routing workers. It is divided into two services – proxy and management service. Both are designed to run completely independently on different machines and communication between them is secured by TCP/Linux sockets. Both parts use multiple threads and because of this fact, computation resources could be exploited very efficiently. For the best performance in the area of network communication, it is recommended to run both parts of the system on the same machine using Linux-based sockets because an amount of transmitted data could be very high (Stevensson, Fenner and Rudoff 2004).

The proxy service is responsible for direct communication with clients. After accepting the connection, the request is parsed and sent to the management service. Computed result is then returned, and proxy service sends it to the client, so no additional computation or modification is done. The proposed solution of that part allows separation of the pre-processing of the request and the computation. This separation is useful not only in case of the scattering load on different machines, but it is also a security feature because clients do not have a direct access to part of the system part responsible for computation. Protocol for this client-server communication is based on HTTP REST protocol but it is possible to develop and use a different form for the communication, for example, binary based streaming or permanent connection between client and server side.

The management service communicates with the proxy service and with the part of the system which is responsible for the computation. Scheduling and allocation of the computing resources will be done at this part. An important part of work is also transformation of the data which are used as an input or output for the computation part. Transformation after receiving and before sending the data is necessary for two main reasons which are based on a communication protocol and also on the data transfer performance. The protocol is described in Section 3 of this article. For the data transfer performance, only relevant data, which are really necessary for the next computation are sent to the next computing part.

To obtain statistics, it is possible to enable optional logging to an external database. This could be done in both of parts of the system.

Because of the separation of the management system and the part responsible for the computation, both parts could be replaced by different modules which implement the same communication protocol. This can be useful for example in the case when there is a need for a different type of work scheduler.

2.2. Computation worker

As it was stated, our solution separates communication and scheduling from computation. This part is marked as a computation worker and its architecture is designed to exploit all available computing resources in an

efficient way. This separation allows the system to be efficient and to provide high request throughput.

The worker communicates only with the management service so every request for computation has to be passed through it. Thus, every information or statistics from the computation in the worker has to be sent into that part of the system.

The worker internal architecture allows multi-threading. This allows to exploit all available resources effectively and also it is possible to process many requests concurrently. The system was also designed with emphasis on usage of usage locks to ensure efficient concurrent communication and memory access. Amount of threads can be configured dynamically which is an advantage for example in the case where resources are limited and there is a need to run multiple types of workers on a single device.

Architecture of the worker is separated into two parts to ensure efficient implementation of various types of tasks. The first is a core, which is responsible for communication with the management system which also includes service messages which are part of the service communication protocol. Actual computation is performed in the second part of the worker which uses the provided worker

2.2.1. Worker mode

The purpose of modes is fact that the whole architecture can be used for resolving tasks which could contain a lot of different computations. Internally, the modes represent the states of a deterministic finite automaton. The messages exchanged between the different parts of the system represent transitions between the different states of the request

The mode at the beginning receives a message which contains input information which is necessary for a performing the computation. After performed computation, mode creates a message with results and this message is passed to the core part of the worker and then transmitted to the management system. As it is described below, messages could contain various types of values. Thanks to this fact, the mode itself could execute a lot of different types of computation and messages with result could also vary as well.

For a better scalability, every instance can run only one mode at a time, but modes can be changed dynamically during the worker life cycle. This fact corresponds with the proposed approach for a high scalability.

3. COMMUNICATION

There are three different types of communication in the system:

- communication with external sources - client with the proxy service,
- internal communication between the proxy and the management part,
- internal communication between the management and workers.

The first type of communication is based on HTTP REST and the second type is based on binary based object passing. For the third, the most crucial part, the specialized internal protocol is implemented. It is based on binary data format which ensures better throughput in comparison with the text-based HTTP protocol used by web services. The protocol uses only signed and unsigned numbers. Combination of both is allowed. For a special occasion, the string could be also used.

3.1. Communication workflow

The communication design uses two separate threads. Both of these threads use input and output message queue which is shared with all other threads. Communication with the management service is currently based on sockets and could be both TCP or UNIX based.

Input thread waiting for an incoming message and after successful read and base validation is that message pushed to the input queue. On the other hand, the output thread is waiting for new messages in the output queue and without any further validation send these messages into the management server.

Each computation thread operates in a loop. At the beginning of the loop, a message from the input queue is removed and then processed. Result of that computation processing is returned as an output message and pushed into the output queue.

With this design, there are no delays or possible deadlock which can occur in case of sharing communication socket.

3.2. Protocol

The protocol is divided into two parts – input and output messages. For a possible extensibility, both parts have mandatory and optional parameters and contain a header. The header is the same for both types and includes values which are used for validation and identification:

1. ID – unique value for each message during a whole run of the service. Value is generated in management service.

2. Origin – original source of the message.

3. Type – type of the message. An important value for a next processing of the message.

4. Worker type – used mostly for control that request will be handled by according worker.

After receiving the request, validation is carried out and the message is pushed for a next processing.
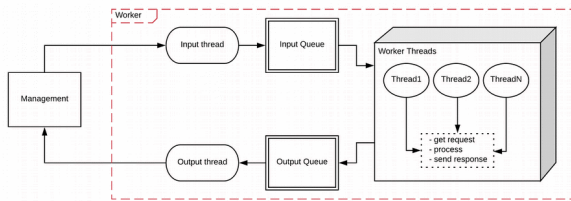
Figure 1: Flow of communication

3.2.1. Input messages

Processing of that message depends on value of the Type field. For example, in case of stopping or reloading the worker, no additional parameters in the message are used. But in the case of route request, other message parameters are parsed, and computation is done with these parameters.

3.2.2. Output messages

In that message type, various values can be used. Their type depends on requested computation. The header has the same structure as described above but Type is changed according to the type of the result.

3.3. Special messages

Currently, we integrated some specialized message types which are not directly used for the computation. These messages are handled directly in the input thread.

- reload – reload routing graph. It is possible to reload only selected parts,

- change type of worker – due to adaptivity, the worker could easily change its computation purpose just-in-time without the need of restarting and subsequent initialization,

- kill – stop the worker,

- ping – similar to network ping utility.

4. EXTENSIBILITY

The system can be extended with more functionality. In the case of adding a new type of worker, changes have to be added in both of management service and worker. In management, new protocol parameters has to be specified and also its passing into the worker. On the worker side, there are base rules on how to add new functionality. First of all, the new Worker type has to be added into enumeration with available types, and optionally, a new Type of message can be added. Next, the handler for the new type of the message must be created and integrated into input thread. It is also possible to exploit inheritance and extend existing message structures and handlers.

It is necessary, in the case of creating new message types, to keep the structure of the base header which was described in Section 3. Any additional parameters have to be processed by the newly created handler. The system itself contains a lot of utilities for parsing messages, decoding from/to binary form, so no additional work in that area is necessary.

There is a possibility to replace communication system with management service for use on a different architecture (current implementation uses Linux-based sockets). Moreover usage of different communication styles e.g. pipes or shared memory is possible to implement.

Due to a logical separation of handlers and messaging system, these improvements require changes only at one place of the code so other parts will not be affected. It is possible to change the whole communication protocol if necessary entirely, but that change will require a bigger modification of the worker core.

As we can see, adding a new handler is simple so a current system can be extended easily which is useful if there is a demand for high flexibility. After this step, new pipelines can be specified.

Because of fact, that the system has to be to modifiable and easily extensible, all of the parts of its architecture are designed to do these possible changes.

5. QUALITY OF SERVICE REQUIREMENTS

There are multiple points of view on the Quality of Service (QoS) and Service level agreement (SLA) (Chu 2014) requirements. The most important criteria is the response time which means, that the system has to be able to process a certain amount of requests in the selected time. This requirement can be further refined into two tasks. The first is dealing with SLA which is chosen for single computation e.g. all requests have to be computed in this time. The second is focused on time which is required for the computation of the whole demanded requests.

These requirements could be achieved thanks to the dynamical ability of allocation of additional computation resources on-demand. As it is shown in a section with experiments, the system is able to determine a minimal amount of resources for fulfilling demanded SLA.

6. USAGE OF EXTERNAL DATA

The system is designed to be autonomous without the need for other external data sources e.g. databases or other services running outside HPC environment. Main reason is coming from the fact that computation is carried out on dynamically allocated resources (nodes) which are inside HPC network and access to the externally running systems or sources is not allowed on the network layer.

In cases, where access to the database is necessary, the management system offers functionality for communication with this source. But for enabling it, it has to be an ad-hoc solution considering necessity of its usage and also the network has to be configured which could be a problem in some cases. The next important fact is a security of the computation and a whole HPC environment (Nowak, et al. 2013).

7. SERVER-SIDE TRAFFIC NAVIGATION USE CASE

Our case of the architecture was to implement a system which is responsible for a computation of routes for vehicles navigation. This scenario uses all of the three parts of the architecture – the management, the proxy and also worker modes. Each part extended the system functionality for parts which are necessary for the routing navigation server-side. Also specialized algorithms for a route computation are used as well.

The service also offers a system for communication with external services. In our case, this system is used for receiving notification about the actual traffic situation which is represented as changes in a routing graph. Next usage is for communication with a system responsible for autotuning.
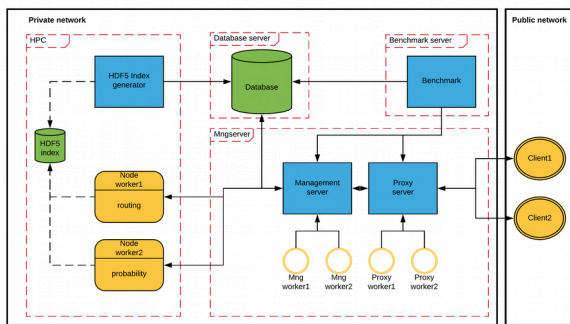

Figure 2: Base architecture scheme

7.1. Used worker modes

Currently, there are four worker modes:

1. One to one routing (Simple) - computes single path – Dijkstra and A* algorithm.
2. Alternative routing (Alternatives) - k-shortest paths based on the plateau algorithm.
3. Probabilistic Time-Dependent Routing (PTDR) (Golasowski, Tomis, Martinovič, Slaninová, and Rapant 2016) - estimates the distribution of the path travel time.
4. GPS translate (GPS to Internal) - translates GPS coordinates to routing graph nodes identifier.

7.2. Request handling

With current functionality, the system can handle client requests for computing routes based on origin/destination (O/D) parameters. For internal usage, an identifier is used as O/D, but for an external client requests, GPS coordinates are demanded as an input. In a basic case, the client wants only one route (the first mode - Simple) or demand alternatives routes (the second mode - Alternatives).

In some cases, for client request it is necessary to perform more than one computation with the use of different modes. This is, in the current state of work, a case, in which alternative routes has to be computed and based on a result of this computation, PTDR algorithm is carried out. To achieve this, two workers with different modes have to be available. There is also another case in which is the necessary usage of the fourth mode. This can occur in a case when the first or second mode does not use functionality for GPS to Internal, so separate workers with that functionality have to be available.

As it was mentioned before, single worker instance can be run just only in one mode and then is available for computing only one kind for the request. For solving cases with a request containing multiple computation steps, a specialized request pipelining is used.

7.3. Request pipelining

For the description of pipelining functionality, the case with the computation of Alternatives with integrated functionality of GPS to Internal and following usage of PTDR will be used as an example.

After passing the request into the management service, the internal system finds out which parts have to be computed for the given request. In our example, the system creates an info structure in which it is saved information that Alternatives and PTDR computation have to be carried out. This information is stored during a whole lifetime of the request. The system next work in these steps:

1. Send data for computation into worker running in the Alternative mode.
2. Receive resulted data from the worker and store them in the info structure.
3. Prepare data for the form suitable as an input into the PTDR mode.
4. Send data to worker running in PTDR mode.
5. Receive data from the worker, transform them into a form suitable for the proxy service and send them into this service.
6. Remove info structure belonging to the current request.

Transformation after receiving and before sending the data is necessary for two main reasons which are based on a communication protocol and also on the data transfer performance. The protocol is described below in this article. For the data transfer performance, only relevant data, which are necessary for the next computation, are sent to the workers. In this example case, step 2 return computed routes in GPS coordinates and also in internal identifiers which are used as an input for the step 3. Identifiers have a smaller size and therefore performance and communication are faster because they are used as an input for the next step.

After getting results from step 5, route result obtained in step 2 are re-ordered based on these results and finally sent back to the client through the proxy service. This example could be extended by two additional steps in case of usage of worker running in GPS to Internal mode. In that case, one step will be added before step 1 (translation from GPS to internal identifiers) and the next one will be added between step 2 and 3 (obtained

routes will be translated from internal identifiers into GPS format).

Described pipelining is adaptable for various schemes, but appropriate methods for data transformation and preparation have to be developed for its proper usage.

7.4. Data sources

The data used by workers can be obtained from various sources, such as traffic monitoring or weather prediction. Because of a high amount of stored data, an HDF5 file format was chosen as the main type for storage. This standardized format enables a solid compression for storing data and also offers a mechanism for fast access to the required part of data. Thanks to this characteristic, dealing with HDF5-based sources is fast and efficient in terms of input/output. As others data sources, SQLite with its SpatiaLite superstructure is used as well.

These sources are processed to a form suitable for the individual workers and stored in appropriate formats:

- Routing index (routing graph) - contains a graph representation of a road network used for route computation. The graph is stored in a structured HDF5 file.
- Routing index changes – particular speed changes in a road network.
- Spatial data structure based on SpatiaLite (Marchesini, Neteler, Frigeri, Casagrande, Cavallini and Furieri 2014) which provides GPS to internal IDs which are necessary for routing computations.
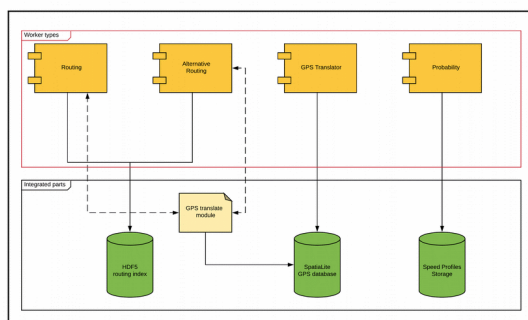- Probabilistic speed profiles - used by the PTDR worker, stored in an HDF5 file.

Figure 3: Worker modes with data sources

7.4.1. Data acquisition

Open Street Map dataset (OSM) (Ptošek and Slaninová 2018) is a main data source for the routing index but only OSM line data with tag value highways. The result of our processing is a road network. Transformation of a spatial and non-spatial attribute of OSM highways lines is performed so the resulted road network meets basic needs for usage in server-side routing. These criteria are:

- The road cannot self-intersect or self-overlaps.
- One road cannot overlap another one.
- The roads can intersect only when it is logically correct (e.g. roads intersection or change of non-spatial attribute of road).
- Each road and its direction has own spatial representation.

Next step in processing is a derivation of nodes from basic road network. Each node has a flag, so roads intersection, dead-end, border node, one-way dead-end and pseudo-node can be distinguished. In the following step, aggregation of the road network features into segments to eliminate all pseudo-nodes is carried out. Loops and multiple edges for the segment network are allowed. Partition of roads, nodes and segments according to geographic areas into smaller sets is also allowed. As a result, SQL HDF5 set, in SQL OpenLR set (OpenLR 2012), benchmark set and other product from the nodes and the segment network is created. In the last step SpatiaLite database for each partition, with basic network analysis capabilities is produced as well.

The routing index is based on data obtained in this processes. For a creating of the routing index file is used a special process which is adapted for an effective loading of the file in the routing worker. This index is loaded at the start of the worker and data are read-only for its computation threads.

For achieving reliable routes, the system has to be able deal with an actual data which can vary with the base data. Thus, the system has to be able to work and integrate new information. This is done through a next HDF5-based file. The file with changes represents an actual speed on the road network. The changes contain information about actual traffic jams, weather conditions, etc. External processes generate the file and every running worker is notified about this new data changes. For saving storage space, only changes from the previous state are stored. Changes in the graph could be done only through the main thread and just after a notification from the management service.

8. EXPERIMENTS

Two types of experiments were carried out according to the topic of this article. Both are focused on how many resources are needed for handling all requests in a given time which is differently specified for each experiment. Types of these tests are focused on previously mentioned QoS and SLA for the current system.

8.1. Experiments dataset

The points have been selected from geographical areas defined by Local Administrative Units (LAU1) corresponding to the three biggest cities in the Czech Republic (Praha, Brno and Ostrava). The dataset is then created as a cartesian product of the entire set to create pairs of origin and destination location. The used probabilistic speed profiles emulate the behaviour of the real world traffic using a custom Markov chain model. The whole dataset contains 25,560 pairs from which the

first 2,000, 500 and 250 were chosen for experiment cases.

8.2. Quality of Service for a single request

In this scenario, tests are focused on detecting how many resources are needed for resolving every incoming routing request in a given time. Because the current workers can run in different modes, two types of measurement for different modes were performed. In the first, 2,000 parallel request for single route response (worker mode 1) was created and in the second one, 500 parallel requests with 10 alternatives (worker mode2). In every iteration, one computation worker (node) were added. Results of these tests are shown in Figures 4. and 5.

For the first test, SLA time for resolving every request was chosen to be 1 second. As the results show, for achieving this time, at least 6 workers (nodes) are necessary. For the second test, SLA was 5 seconds and so 7 workers are necessary for fulfilling this SLA.
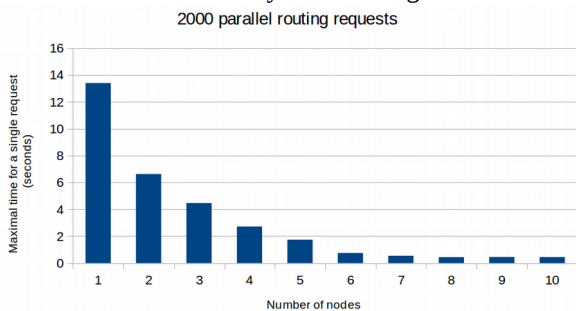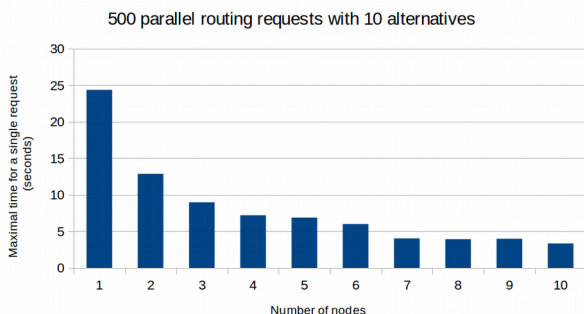

Figure 4: Single request test – 2,000 requests

Figure 5: Single request test – 500 requests with 10 alternatives

8.3. Quality of Service for all requests

This test is based on fact that there are cases in which is it not necessary to resolve every routing request in such time as in the previous scenario. For this case, the test is finding how many resources are necessary for resolving all routing requests in a given time. Two different types of the worker mode are used in that scenario.

Configuration for this test case was chosen as one constant Alternative worker and an increasing amount of PTDR workers (worker mode 2 and 3). As the PTDR

configuration, sample count was set 100 and departure usual Monday at 6 AM.

200 requests with 5 alternatives routes and PTDR were executed and SLA time for completing all request was 30 seconds. As is it shows in Figure 6, 8 nodes are necessary for the chosen time.
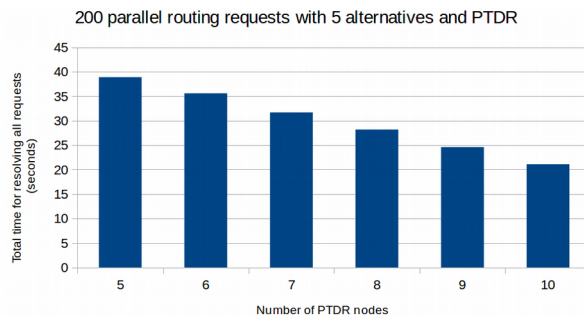

Figure 6: All requests test – 200 requests with 5 alternatives and PTDR.

8.4. Tests evaluation

As the results proved, the system is able to achieve demanded SLA times with a proper amount of resources. Tests also confirm a scalability with a growing amount of computation resources.

9. CONCLUSION AND FUTURE WORK

We proposed and created a highly scalable system for usage on HPC architecture which offers efficient resource allocation and scheduling as well. Thanks to its design, this solution could be applied in different areas of computation and extensibility could be done easily. This allows the creation of advanced pipelining with a big amount of different worker modes.

As the experiments on our use case proved, the system is able to fulfil different demands in the area QoS and SLA. Also, the scalability in case of usage of increasing number of computation resources was confirmed.

Future work will be done mainly in the area of automatic resources allocation and integration of external tools used for autotuning. Another goal is an improvement in scalability.

REFERENCES

Silvano, Cristina, et al., 2017 The ANTAREX tool flow for monitoring and autotuning energy efficient HPC systems. SAMOS 2017 - International Conference on Embedded Computer Systems: Architecture, Modeling and Simulation. 2017.

Gadioli D., Palermo G. and Silvano C., 2015. Application autotuning to support runtime adaptivity in multicore architectures. SAMOS 2015 - International Conference on Embedded Computer Systems: Architecture, Modeling and Simulation, 2015 International Conference, IEEE, pp. 173-180.

Chu W.C.C., et al., 2014. An Approach of Quality of Service Assurance for Enterprise Cloud Computing (QoSAECC). International Conference on Trustworthy Systems and their Applications - Taichung, pp. 7-13.

Marchesini I., Neteler M., Frigeri A., Casagrande L., Cavallini P. and Furieri A., 2014. GIS Open Source: GRASS GIS, Quantum GIS and SpatiaLite [Kindle Edition]. Dario Flaccovio Editore.

Cima V., Böhm S., Martinovič J., Dvorský J., Ashby T.J. and Chupakhin V., 2018. HyperLoom Possibilities for Executing Scientific Workflows on the Cloud. Barolli L., Terzo O. (eds) Complex, Intelligent, and Software Intensive Systems - CISIS 2017. Advances in Intelligent Systems and Computing, vol 611. Springer, Cham.

Ptošek, V. and Slaninová K., 2018, Multinode Approach for Map Data Processing, 5th International Doctoral Symposium on Applied Computation and Security Systems (ACSS)

OpenLR™ White Paper, 2012. Available from: http://www.openlr.org/data/docs/OpenLR-Whitepaper_v1.5.pdf [accessed 23 July 2018]

Golasowski M., Tomis R., Martinovič J., Slaninová K. and Rapant L., 2016. Performance evaluation of probabilistic time-dependent travel time computation. IFIP International Conference on Computer Information Systems and Industrial Management, Springer, pp. 377-388.

Nowak M., Frankowski G., Meyer N., Yilmaz E., Erdogan O., Nominé J.P. and Robin F., 2013. Security in HPC Centres. Available from: http://www.prace-ri.eu/IMG/pdf/wp79.pdf [accessed 10 June 2018]

Dunning T. and Friedman E., 2016. Streaming architecture: new designs using Apache Kafka and MapR streams. O'Reilly Media, Inc..

Vivian J., Rao A.A., Nothaft F.A., Ketchum C., Armstrong J., Novak A. and Schmidt H., 2017. Toil enables reproducible, open source, big biomedical data analyses. Nature biotechnology 35, pp. 314-316.

Stevenson W.R., Fenner B., Rudoff A.M., 2004. UNIX Network Programming. Addison-Wesley Professional.

Al-Ali R., Kathiresan N., El Anbari M., Schendel E. and Abu Zaid T., 2016. Workflow optimization of performance and quality of service for bioinformatics application in high performance computing. Journal of Computational Science – Volume 15, pp. 3-10.

PERFORMANCE OF INDUSTRIAL SENSOR DATA PERSISTENCE IN DATA VAULT

Florian Bachinger[(a)], Jan Zenisek[(b)], Lukas Kammerer[(c)], Martin Stimpfl[(d)], Gabriel Kronberger[(e)]

[(a),(c),(e)] Josef Ressel Centre for Symbolic Regression, School of Informatics, Communications and Media, University of Applied Sciences Upper Austria, Hagenberg
[(b)] Heuristic and Evolutionary Algorithms Laboratory, University of Applied Sciences Upper Austria, Hagenberg
[(d)] Miba AG, Dr. Mitterbauer Str. 3, Postfach 3, A-4663 Laakirchen, Austria

[(a)] florian.bachinger@fh-hagenberg.at, [(b)] jan.zenisek@fh-hagenberg.at, [(c)] lukas.kammerer@fh-hagenberg.at,
[(d)] martin.stimpfl@miba.com, [(e)] gabriel.kronberger@fh-hagenberg.at

ABSTRACT

Today manufacturing companies are facing important challenges from the market in terms of flexibility, ever growing product mixes, small lot sizes, high competition, etc. To meet these market conditions, digitalization and the use of data are offering a viable toolset considering the advances in the field throughout the last couple of years.

The increasing use of sensor technology and the need for interconnecting data from different departments in smart production leads to a surge of recorded data. Persistence and integration of heterogeneous data, generated in a variety of software systems, is a key factor to gain value from data and its analysis. High flexibility in regards to the model is required to accommodate the data. Hence, application of the data vault modelling approach is a fitting candidate to design a data warehouse model. In this paper we present a data vault model for factory sensor data. We analyze the performance of the data warehouse in regards to bulk load of data and common analytic queries.

Keywords: industrial data warehouse, data vault, sensor data persistence, performance analysis

1. INTRODUCTION

Industry 4.0 and the Internet of Things (IoT) accelerate Digitalization of today's production plants. Modern production machines are now equipped with a variety of sensors measuring operational data of the machine and the product. In combination with data from material acquisition or quality assurance departments industrial companies aim to identify key input factors of the production process in a smart factory (Bauernhansl, ten Hompel, 2014). Persisting and connecting this data enables optimization of the process parameters and lays the foundation for applying new strategies such as Predictive Maintenance (PdM).

With the increasing volume and diversity of data, new challenges in data storage arise. Data is required to be stored in a structured and performant manner connected in a centralized data warehouse (DWH). The DWH enables the integration of various data sources and serves as data source for reporting, knowledge bases or PdM systems (Inmon, 2002). The data-model contained by the database management system (DBMS) must be able to handle insertion of data at a high bandwidth, while still providing fast analytic query-results based on the existing data.

Additionally, the model has to be flexible in order to easily incorporate changes in the structure of the operational data and it must stay well-defined to support query languages. The data vault modelling approach by Linstedt (2002) describes a system well suited for this scenario. Hultgren (2012) defines key indicators for determining if the application of the data vault modelling approach is a good fit.

1. Integration of multiple heterogeneous data sources
2. Accurate and complete time-slice history including audit information for full replicability
3. Frequent addition of new sources or change of existing ones
4. Commitment of the organization to incorporate an Enterprise Data Warehouse (EDW)

With all these indicators applicable, the data vault modelling approach fits the scenario at hand. In this paper, we investigate how the data vault model designed for this scenario scales and how reoccurring operations (bulk load, analytic queries) perform over increasing data volume. This should provide insight if the data vault modelling approach is a good fit for persisting sensor data of today's smart factories.

Related work in this area includes van der Veen et al., (2012) who compared sensor data storage performance of relational SQL databases with NoSQL DBMS systems in physical and virtualized environments. Collins and Shibley (2014) investigated applicability of high quality data modelling (HQDM), which define desirable properties of a DWH. They showed that the application of HQDM principles, as defined by West (2011), is well supported by the DV modelling approach.

This paper differs from previous work in that it focuses on applying the data vault modelling approach for sensor data storage and investigates the model's performance behavior over a growing data volume.
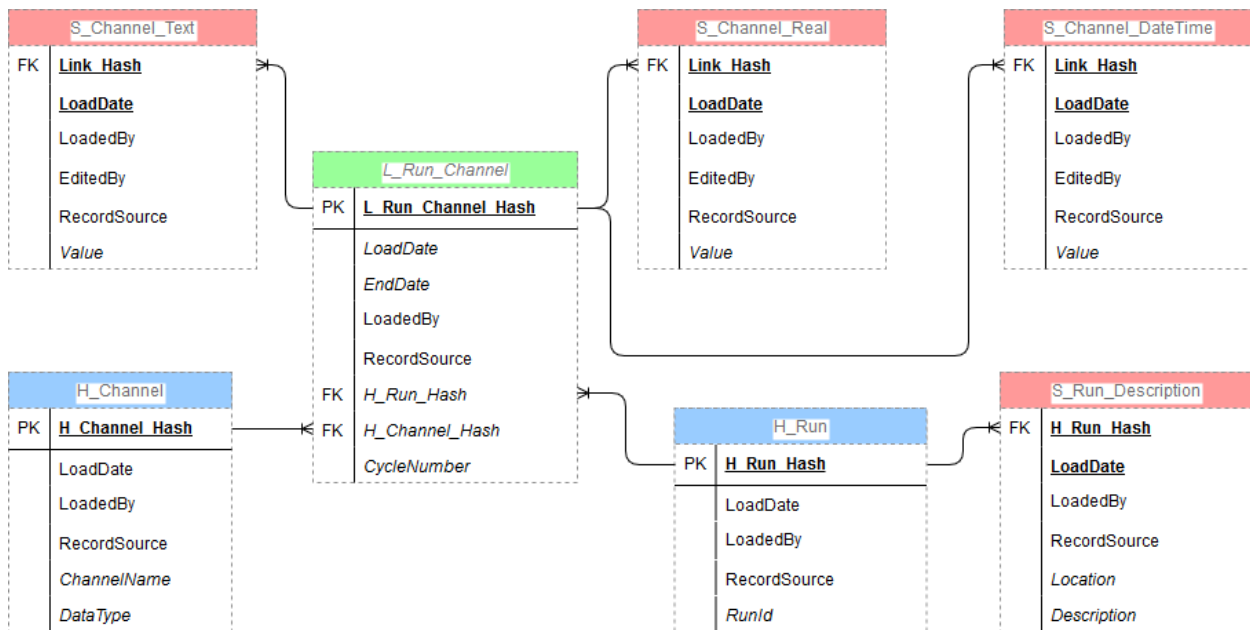
Figure 1: The devised data vault model for channel oriented storage of production machine sensor data

This paper is organized as follows. First, the data vault modelling approach is described in Section 2. Next, the data vault model used for the experiments and the kind of data to be stored in the DWH is defined in Section 3, with focus on how the data in this scenario differs from simple high resolution sensor data. Section 4 describes the performance-test setup and the results. Finally, Section 5 will draw conclusions and describe future work in this area.

2. DATA VAULT

The data vault (DV) modelling approach was defined by Linstedt (2002) and was since then further evolved into data vault 2.0 (Inmon & Linstedt, 2014; Linstedt & Olschimke, 2015). DV supports the requirements of next generation data warehouses (DWH 2.0), as defined by Inmon et al. (2010). DV differs significantly from 3rd Normal Form (3NF) model first defined by Codd (1970), which is the widest spread modelling approach. However DV is still compliant with the technical restrictions of a relational database management system (RDBMS) consisting of tables and their relationships only.

2.1. Table types

Each RDBMS table represents either a hub (H), link (L) or satellite (S) entity, which are used to store and model business concepts and their relationships. These three core components of DV are covered briefly in the next subsections. The description is based on the model depicted in Figure 1 where the different table types are also marked in different colors and with the type abbreviation as prefix.

2.1.1. Hub

Each logical business concept modelled by DV is represented by a hub entity. Besides the audit attributes (covered in Section 2.2), a hub only stores the business

key used to uniquely identify a single instance of the business concept.

Sensor channels (as stored in the table *H_Channel*) for instance are identified by their channel-name and the type of data they store (e.g. the combination of name *'surface temperature'* and data type *'real-number'* identifies a specific channel). Only on first occurrence of this key-combination a new *H_Channel* hub entry is created, no duplicated hub entries are allowed. As this example illustrates, the business key can also be a composite key. Per definition of data vault 2.0 the business key is combined and subsequently reduced by a hash function like MD5 to a single identifier (128 bit sized, in the case of MD5). This calculated hash is stored as the primary key of the hub entity alongside the business key. The business key can still be used for searching by queries but for references only the calculated hash may be used.

2.1.2. Link

Link entities represent relationships between business concepts and logically connect an arbitrary number of hubs or other link entities. The link entity therefore stores the primary hash keys of all connected hub instances. This allows representation of n:m cardinality for any business relationship in data vault, effectively providing important flexibility to incorporate cardinality change in the logical model. A link's business key consists of the sum of all foreign key hash references which are subsequently combined and hashed to create the link's primary key.

Each link entry and its foreign key values represent an existing relationship between logical business concepts. To represent invalid relationships, the link entity stores an end-date to mark from when on the relationship is no longer existent. This is necessary since deletion of data, in any table type, is not permitted.

As depicted in Figure 1 for instance an entry in *L_Run_Channel* represents the assignment of a sensor channel value to a specific run instance. The run and channel hashed business keys are stored as foreign keys.

2.1.3. Satellite
Whereas hubs store only the key of a business concept, the connected satellites store all associated descriptive attributes. In the case of a sensor installed in a smart factory plant, the sensor satellite might store the location and a description. Each satellite stores the foreign key reference to the hub or link instance and the specific date and time when the current state of attributes was loaded, making up the primary key of a satellite. Consequently, each entry of a satellite is a time slice representing the states of the business concept stored in the hub and its connected satellites, with the latest entry representing the current state. Following the DV modelling approach the entire attributes associated with a hub entity are not necessarily stored in one single satellite table. Hultgren (2012) encourages to separate satellites by:

1. Subject Area / Data Context
2. Rate of Change
3. Source System
4. Type of Data

This means that new satellites are created to store additional attributes that are defined for a business entity instead of adding new columns to existing tables. Separating satellites by the above criteria reduces the amount of sparse values and duplicated data on insertion of a new time slice and therefore reduce the total memory space.
In the case of the depicted model of Figure 1, the satellites storing the sensor values are separated according to the last 3 separation indicators.

2.2. Historical data and auditing
Generally speaking the DV allows only additive changes to the model/schema and the data, to provide historically correct and complete data views, with the only exception to that rule being the link's *EndDate* column which is updated once a relationship is no longer valid. Each change in the source data is persisted by insertion of a new satellite data slice.
Apart from the business data the DV entities store audit fields. The attributes *LoadedBy, RecordSource* and *LoadDate* provide information about the data source system and the import service. Whereas *EditedBy* and the *LoadDate* provide information about the user, who conducted the data change.

2.3. Unique features of the data vault approach
The utilization of hashed business keys as primary key holds two main benefits in this scenario. First, it improves join performance of analytical queries. Key comparison is faster for a single primary key of fixed data type and consistent length when compared to the join performance of longer natural keys or utilization of

composite keys (Linstedt, 2014). Second, the hash value of the business key can be calculated at load time of the data. This improves performance of bulk inserts, since hubs and satellites can be loaded parallel after foreign key constraints are deactivated for the load process or not present at all. In contrast, utilization of a *bigint* with auto increment also creates keys of equal lengths, but the hub entry has to be created beforehand in order to load the satellites.

3. MODEL AND DATA QUANTITY
This section aims to provide a clearer picture of the kind of data to be stored in the DV model. We describe a more complex scenario where the data differs from a simple log of recorded sensor data. A description of the origin of the data will highlight the need for storing audit information. Subsequently we describe why we chose to model the data as shown in Figure 1 and how we improved the performance of the model.

3.1. Data origin
Typically, a sensor records data in high frequency, resulting in a high volume of, mostly monotonous, data. This kind of raw sensor data is best stored as a compressed binary file or in a database table without the additional overhead of audit attributes, in order to handle the huge volume of data. However, in the scenario described in this paper, the high resolution sensor data is at first analyzed by domain experts and subsequently filtered and aggregated into lower resolution. Figure 2 illustrates this well-established process. The aggregated and filtered sensor data is read from the file share and imported in the DWH. Data analysts might even create several iterations of analyzed data by applying different thresholds and aggregation functions to the raw source data, thus requiring a DWH to store audit information for each data slice. In addition to the sensor data recorded at each run of the machine (e.g. actual oven temperature) the DWH also stores the production parameters set by the operator (e.g. target oven temperature) to provide a full representation of the production process.
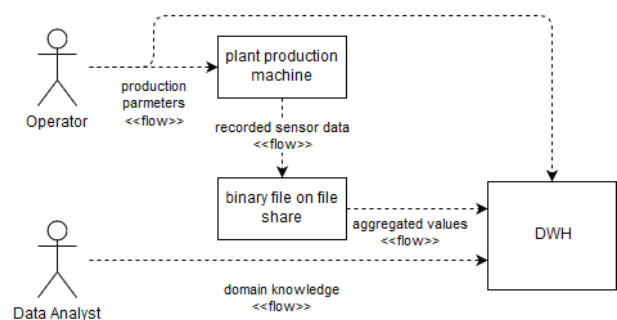

Figure 2: Schematic representation of scenario data flow

By combining parameters and recorded sensor values the DWH is able to provide a full picture of all relevant production data. The data therefore serves as a comprehensive source for analytical queries or PdM systems.

3.2. Data volume analysis

The performance of the devised model will be analyzed in regards to the data volume expected after up to 5 years of usage. As Figure 2 shows, each production machine creates a binary file that is stored on a file share. One file is created for each single run of the production machine. For analysis however only the average state (sensor values) of the machine at specific time slots is relevant. The machine runs can vary in duration but consist of up to 3,700 individual time slots at maximum run duration. Exactly one value for each installed sensor is assigned to the individual time slot. With up to 24 different sensors per machine, this results in 88,800 individual values per run. It is expected that the operator configures one daily run per machine, which would result in up to 780 per year, since this feature will be rolled out to 3 machines of the same type.

For the analysis we investigate the performance of key operations for every 500 runs, up to a total of 4000 runs saved in the DWH.

3.3. Description of the DV model

To accommodate the heterogeneous data described in Section 3.1 the devised DV model has to be generic and flexible. Sensor values are therefore not persisted in column orientation, with one table column storing a sensor value at any given point of time (as illustrated in Figure 3), but are instead stored in a channel-oriented manner. This allows easy addition, relocation or upgrade of sensors to the production machines without the need to change the DWH model or the importer process.

3.3.1. Column-oriented storage of sensor data

In column-oriented storage, each sensor channel corresponds to a single column in the data table. This storage variant of sensor data would be more efficient than the devised model, if the attributes of the table, respectively the different applied sensors themselves, are well known and change little over time. The frequent addition of new sensor channels or the removal / relocation of existing ones leads to fragmentation of the table and consequently to weaker performance and higher storage consumption in this model approach. Additionally, the importing tool would need frequent updates in order to accommodate the change in model structure.
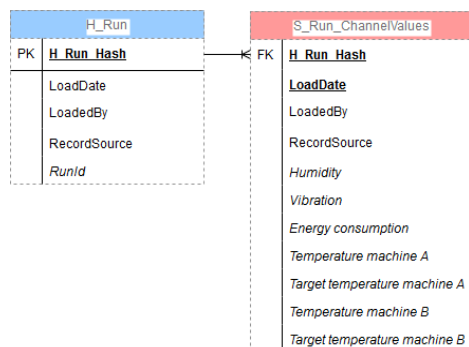

Figure 3: Alternative column-oriented storage of channel values

3.3.2. The devised channel-oriented model

Instead, a channel-oriented model approach was used, as depicted in Figure 1, wherein each run is assigned a number of different sensor channels. A single channel is identified by its name (e.g. 'Temperature Machine A') and the type of data stored in this channel (numeric, text or datetime values). Sensor channel values are assigned to a run by creating an entry in the link entity. The time slot dependent order of the sensor values is maintained by the 'CycleNumber' attribute of each link entry. Each cycle represents a point of time defined by the data analysts (see Figure 2). All values assigned to a specific cycle represent the aggregated values, recorded in different frequencies by the sensor, of one pre-defined time interval. To provide type safe access and to reduce storage space each datatype (text, numeric, and timestamp) is stored in a separate satellite respectively, as opposed to one large binary column.

The data stored in this generic storage schema is subsequently transformed periodically into the, easily humanly interpretable, column-oriented storage form for on-line analytical processing (OLAP). Transformed data is stored as data mart, which form a subset of total data persisted (Chaudhuri & Dayal, 1997). The transformation operation is defined in Section 4 as one of the analyzed DBMS queries.

3.4. Applied performance improvements to the model

The performance improvements discussed in this section are in many cases specific to the software used in the experiments and production environment. Some improvements to ETL and Query performance however are generally applicable to any RDBMS. E.g., relationships between the hubs, links, and satellites were not enforced by foreign keys, reducing load time of the RDBMS. Instead, the importer tool is expected to take care of these restrictions. Besides enforcing the foreign key references, the importer tool caches the primary keys of entries. This increases error resilience of the importer tool for already seen values, since the unique constraints enforced by the DWH are not violated.
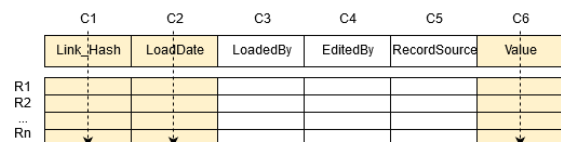
Figure 4: With columnar storage only the relevant columns have to be retrieved at query time (compare to Kamal & Gupta (2015))

3.4.1. MSSQL-Server specific improvements

In order to keep the disk size of the database manageable a clustered columnar store index was applied to the DV tables. This feature was introduced with MSSQL server 2012 Enterprise. Instead of a traditional row storage, the values are stored in a columnar storage (see Figure 4 and Figure 5).

Figure 5: With standard row storage the complete row has to be retrieved (compare to Kamal & Gupta (2015))
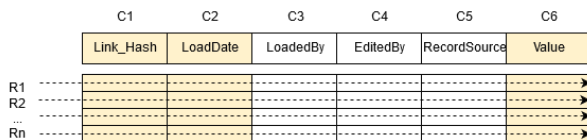
Column storage allows compression of stored values. In their paper Kamal & Gupta (2015) showed that columnar storage not only reduced the page sizes of the DB but also improved performance in an OLAP environment.

Besides the clustered column store, the unique indices for primary keys were also compressed, which significantly reduced the database size.

3.4.2. ETL tool improvements

As it is typical for DWH data integration, the data is first *Extracted* then *Transformed* and subsequently *Loaded* (ETL) into the DWH. All three steps of this process are performed by a custom importer implemented in C# and running on the .NET Core Framework. A custom parser reads the proprietary binary format containing the preprocessed sensor data. The parsed data is then transformed to fit the DWH schema and loaded into the DB using entity framework (EF).

Memory consumption of the importer tool was reduced significantly by creating a new EF DbContext for every single imported binary file. This allowed the .NET garbage collector to remove the inserted entities and the EF object graph.

A first version of the importer tool kept a set of all hash keys to enforce the unique constraint during ETL, which quickly exceeded memory limits for larger data volumes. To reduce memory consumption of the tool, only hashes associated with the current binary source file were kept in memory.

4. PERFORMANCE ANALYSIS

Typically, a simple high frequency sensor data store must support regular small writes and occasional large read bursts, as described by van der Veen et al. (2012), whereas in this scenario both reads and writes are only occasional and in large volume.

For this performance analysis though the source data was not read from a binary file but was instead generated to simulate the estimated data volume the next 1-5 years of production usage. Existing sensor data was analyzed beforehand, to ensure that the generator samples from an equally distributed value range, which holds representative values for each individual sensors. For each of the 5 years the following performance analysis was made:

a) Average time elapsed on a single ETL file import.
b) Time elapsed for total index rebuild.
c) Execution time of transformation query for the single imported run.
d) Execution time of transformation queries for total data volume for data-mart creation.

e) Sum of used storage space for the DV data.
f) Sum of storage size for compressed indices in the DWH.
g) Total size of the DB.

The time measured for (a) of a single ETL file import task is comprised of time spent on generating values (comparable to time spent reading the binary file) and the transactional write to the DWH. In the best case, this metric changes little over increasing DWH size. This would indicate that the DWH is able to handle bulk inserts in short time over all years. Due to increasing index size however the import duration will increase over total DWH volume.

After successful execution of the ETL process the fragmentation of indices was checked. Following recommendations by Microsoft documentation, if critical fragmentation is reached (Microsoft, 2017), a stored procedure executes statements as listed in Algorithm 1 for every table affected by the ETL process. The index is rebuilt with data compression to reduce DB size needed for indices to a minimum. The elapsed time for execution is represented by measure (b).

Algorithm 1: snippet for rebuild of compressed index

```
ALTER INDEX dv_L_Run_Channel_unique_hash
      ON dv.L_Run_Channel
   REBUILD PARTITION = ALL WITH (DATA_COMPRESSION = PAGE)
```

Measure (c) shows the elapsed execution time of pivot transformation of the data of the single imported run. The data is transformed from full historical channel oriented storage of sensor data (as described in Section 3.3.2) to column-oriented storage for OLAP, showing only latest state of values. The transformed values are then added to the transformed data mart table *(dm.RunData)*. The transformation query, as part of listing Algorithm 2, is prepared as a view and queried after every finished ETL process (to improve readability of the code snippet the view is included as the actual select query). In order to calculate the measure (c) the view is filtered by *RunId*. If however the structure of the data mart table has to change, the complete script of Algorithm 2 is executed. The elapsed time of this script is indicated by measure (d).

Algorithm 2: rebuild and pivot transformation of channel oriented data into table oriented representation of data mart

```
BEGIN
 DROP TABLE dm.RunData

 SELECT * INTO dm.RunData
 FROM (SELECT c.[Name] AS ChannelName
     , p.RunNr
     , l.CycleNumber
     , d.[value] AS DataValue
   FROM dv.L_Run_Channel l
 JOIN dv.H_Channel c
  ON l.H_Channel_Hash = c.H_Channel_Hash
 JOIN dv.H_Run p
  ON l.H_Run_Hash = p.H_Run_Hash
 LEFT JOIN dv.S_Channel_Double d
  ON d.L_Run_Channel_Hash = l.L_Run_Channel_Hash
  AND c.DataType = 'Double'
  AND d.LoadDate = (SELECT MAX(LoadDate)
```

```
        FROM dv.S_Channel_Double sub
        WHERE sub.L_Run_Channel_Hash =
           l.L_Run_Channel_Hash)) p
   PIVOT
   (
    MIN(DataValue)
      FOR ChannelName IN (
           <comma separated list of relevant channel names>
           )
   ) AS PivotTable;
 CREATE NONCLUSTERED INDEX dm_RunNR ON dm.RunData(RunNr)
END
```

Measures (e) and (f) where calculated by executing the '`exec sp_spaceused`' command, which provides those exact measures, whereas (g) is simply the sum of (e) and (f).

4.1. Test Setup

The model was implemented on a Microsoft SQL Server 2017 running on a Windows 10 machine with an Intel i5 7300U @ 2,6GHz, 32GB RAM and a 512GB SSD. Both the DB and the importer tool ran on the same computer simultaneously. To measure the time elapsed during DB operations or queries the MSSQL statistics time was turned on. Queries were executed using the MSSQL server management tool.

4.2. Test Results and Discussion

The main goal of the conducted experiments was to investigate if the presented model for sensor storage is able to handle the load of several years in production usage. To investigate the behavior both elapsed time of regular operations and storage consumption was observed.
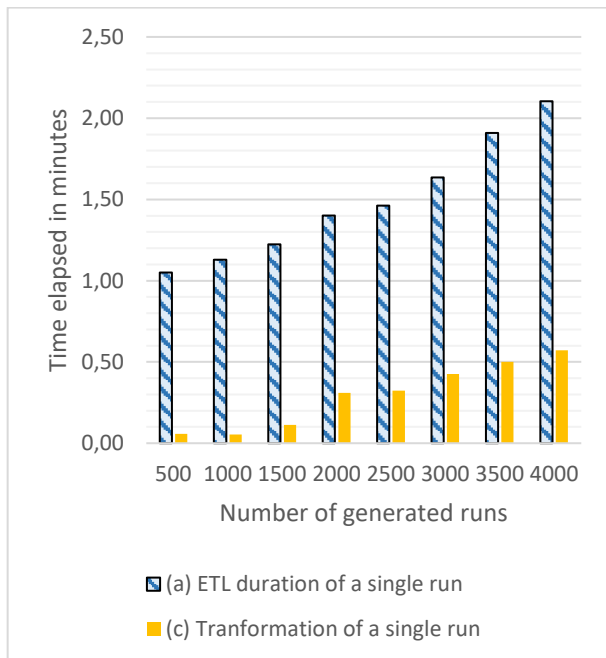

Figure 6: comparison of operation timings of regular measures (a) and (c) over number of runs

Measures (a) and (c) indicate the timings of regular operations of the DWH. A single experiment is expected to be inserted every day, and subsequently has to be transformed into the data mart table. The timings as

depicted in Figure **6** show that these regular operations can be performed in reasonable time, with less than 3 minutes elapsed after the maximum of 4000 imported runs. The import of a new run into the DV and the addition of transformed run data into the data mart causes fragmentation of the applied indices. In production environment, indices will be monitored and if the fragmentation exceeds 30% the indices will be rebuild.
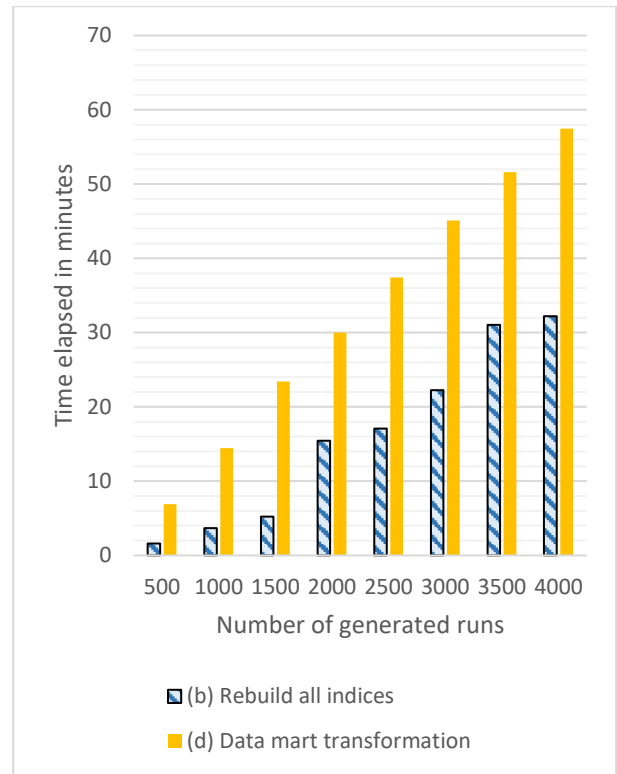

Figure 7: comparison of operation timings of irregular measures (b) and (d) over number of runs

In Figure 7 the timings of measures (b) and (d) are presented. These measures represent DWH operations which occur only irregularly, but require longer runtimes. For high amounts of data (355.320.000 single values in value satellites and the link table, at 4000 runs stored in the DB) the operations are still manageable from the perspective of elapsed time. Especially, since the experiments were conducted on standard, off the shelf, hardware. Index rebuild (b) and data mart transformation (d), executed on all data stored, were both observed to have spiked CPU usage and RAM consumption to 100% for the total duration of the operation. As observed during the experiments, a total rebuild of indices (b) after reaching >30% fragmentation of the unique indices will be needed after roughly every ten imported runs.

As Figure **8** shows, the DB size scales linearly with the number of stored runs. It also shows very nicely the effect of column store compression from 500 to 1.000 where the index size increased but data itself could be compressed more efficiently. With 53.58GB of total DB size at 4.000 imported runs, the DB remains manageable.
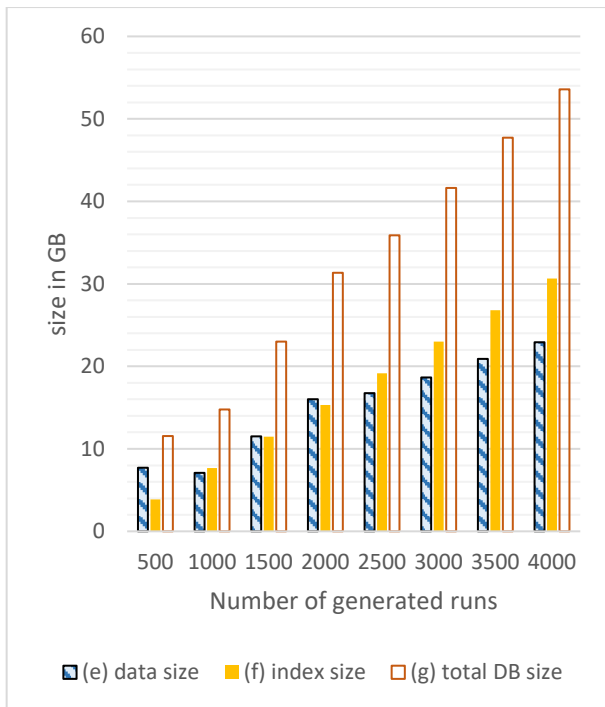
Figure 8: comparison of data size (e), index size (f) and total DB size (g) over number of runs

Besides the total DB size, the positive effects of the applied compression techniques can be very nicely observed in Figure 9. Where the disk space required for storage of one singe run is shown to decline to as low as 13.71MB, whereas the proprietary binary format used to store preprocessed runs on the file share, as discussed in Section 3.1, requires roughly 34MB of storage. These files however store only the actual sensor values and no overhead in form of additional audit or info attributes.
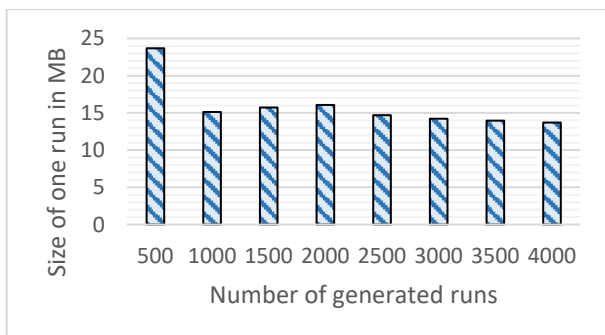

Figure 9: DB size needed for data of one single run

5. CONCLUSIONS

The DV modelling approach provides a high degree of flexibility in regards to the schema. One first has to get accustomed to the concept of hubs, links and satellites though. The inherit flexibility of this concept proved to be beneficial during the development of the schema and the development of the importer tool. Additional attributes in need of persistence were easily added as new satellites.

Moreover, the utilization of calculated hash values for primary keys instead of DB generated sequence IDs proved very helpful for ETL, manual correction of the data and also for tuning queries (e.g. calculating hash value of a RunId on client side frontend instead of using the business key in the query). Especially when the business keys consist of strings of variable length the hash values even provide performance improvements. This technique is not limited to the DV modelling approach and can only be endorsed.

The proposed channel oriented model provides a generic storage for industrial sensor values, resulting in low to no maintenance effort needed when additional sensor channels get introduced in the source files. The model was observed to be able to handle the expected load of 5 years of production usage.

However, the amount of single rows in the value satellites and the link table *L_Run_Channel* might present a performance bottleneck in the future. One possible enhancement is to scale the DWH horizontally by separating the stored runs of the three different machines onto three different DWH instances.

Another solution to counter the potential performance bottleneck of the value satellites would be extract all types of sensors shared by the different machines into a separate satellite (e.g. all machines measure energy consumption, temperature). Effectively storing all common channels and their values in a column-oriented way but keeping the uncommon channels stored in the devised generic model.

REFERENCES
Chaudhuri, S., & Dayal, U. (1997). An overview of data warehousing and OLAP technology. ACM SIGMOD Record, 26(1), 65–74. https://doi.org/10.1145/248603.248616

Codd, E. F. (1970). A Relational Model of Data for Large Shared Data Banks. Communications of the ACM, 13(6), 377–387. https://doi.org/10.1145/362384.362685

Collins, G., & Shibley, M. (2014). Data Vault and HQDM Principles. SAIS 2014 Proceedings.

Hultgren, H. (2012). Modeling the agile data warehouse with data vault. New Hamilton.

Inmon, W. H. (2002). Building the data warehouse. John

Wiley & Sons, Inc.

Inmon, W. H., & Linstedt, D. (2014). Data Architecture: A Primer for the Data Scientist: Big Data, Data Warehouse and Data Vault. Morgan Kaufmann.

Inmon, W. H., Strauss, D., & Neushloss, G. (2010). DW 2.0: The Architecture for the Next Generation of Data Warehousing. Morgan Kaufmann.

Kamal, A., & Gupta, S. C. (2015). Query based performance analysis of row and column storage data warehouse. 9th International Conference on Industrial and Information Systems, ICIIS 2014. https://doi.org/10.1109/ICIINFS.2014.7036537

Linstedt, D. (2002). Data Vault Series 1 – Data Vault Overview. Retrieved July 10, 2018, from http://tdan.com/data-vault-series-1-data-vault-overview/5054

Linstedt, D. (2014). datavault 2.0 hashes versus natural keys. Retrieved May 7, 2018, from http://danlinstedt.com/allposts/datavaultcat/datavault-2-0-hashes-versus-natural-keys/

Linstedt, D., & Olschimke, M. (2015). Building a Scalable Data Warehouse with Data Vault 2.0. Morgan Kaufmann. https://doi.org/10.1016/C2014-0-02486-0

Microsoft. (2017). Reorganize and Rebuild Indexes. Retrieved July 10, 2018, from https://docs.microsoft.com/en-us/sql/relational-databases/indexes/reorganize-and-rebuild-indexes?view=sql-server-2017

Thomas Bauernhansl, Michael ten Hompel, B. V.-H. (2014). Industrie 4.0 in Produktion, Automatisierung und Logistik. (T. Bauernhansl, M. ten Hompel, & B. Vogel-Heuser, Eds.). Wiesbaden: Springer Fachmedien Wiesbaden. https://doi.org/10.1007/978-3-658-04682-8

van der Veen, J. S., van der Waaij, B., & Meijer, R. J. (2012). Sensor Data Storage Performance: SQL or NoSQL, Physical or Virtual. 2012 IEEE Fifth International Conference on Cloud Computing, 431–438. https://doi.org/10.1109/CLOUD.2012.18

West, M. (2011). Developing High Quality Data Models. Morgan Kaufmann.

AN EFFICIENT GLOBAL SENSITIVITY ANALYSIS METHOD BASED ON SEQUENTIAL LATIN HYPERCUBE SAMPLING

Lingyun Lu[a], Wei Li[b], Ping Ma[c], Ming Yang[d]

Control and Simulation Center, Harbin Institute of Technology, Harbin 150080, P.R. China

[a]jyzluhit@gmail.com, [b]frank@hit.edu.cn, [c]pingma@hit.edu.cn, [d]myang@hit.edu.cn

ABSTRACT
Many simulation models involve inputs and parameters, which are not precisely known. Global sensitivity analysis aims to identify these inputs and parameters whose uncertainty has the largest impact on the variability of model output. In this paper, an efficient global sensitivity analysis method based on sequential Latin hypercube sampling is proposed. Firstly, the basic theory of Sobol' method is formulized and a generalized estimator of first order sensitivity analysis indices is proposed. Then, a sequential sampling strategy based on extended optimal Latin hypercube sampling is adopted to improve the sampling efficiency of sensitivity analysis. Finally, the proposed method is verified by the test function.

Keywords: global sensitivity analysis, Sobol indices, sequential sampling

1. INTRODUCTION
Global sensitivity analysis is a technique for investigating how the variability of the output of a model can be apportioned to a set of inputs. Unlike global sensitivity analysis, local sensitivity analysis only reflects the effect of input on the model output at one given point. It is a useful tool in the building, use and understanding of complex simulation models. Over the past few decades, many types of global sensitivity analysis methods have been developed by researchers, such as regression based methods, variance-based methods, moment-independent methods, and so on (Borgonovo 2016).

Variance-based methods assess the importance of model inputs which influence the model output. The theory basis is variance decomposition, and the results of variance decomposition are accordance with the form of high dimensional model representation. As a kind of variance-based methods, Sobol indices have received much attention since they can provide more accurate information for most of models (Burnaev 2017). The Sobol indices can be computed by two kinds of methods, including sampling-based and metamodel-based (Burnaev 2017, Cheng 2017). The sampling-based methods require many simulation runs to obtain more accurate Sobol indices. In order to improve the efficiency of sampling-based methods, several kinds of estimators and sampling strategies have been proposed

(Jansen 1999, Sobol' 2007, Saltelli 2010, Janon 2014). In this paper, the way to estimate Sobol indices is investigated. The remainder of the paper is organized as follows. In Section 2, the basic theory of Sobol' method is formulized and the generalized estimator of first order sensitivity indices is proposed. To measure the quality of the proposed estimator, unbiasedness and efficiency are demonstrated. In Section 3, a sequential sampling strategy based on extended optimal Latin hypercube sampling (OLHS) is proposed to improve the sampling efficiency. In Section 4, the proposed method is illustrated and verified by two test functions. Finally, the paper is concluded in Section 5.

2. A GENERALIZED SOBOL INDICES ESTIMATOR

2.1. The Sobol' Method
Given a model $Y = f(X) = f(X_1, X_2, \mathsf{K}, X_d)$, where X is a $n \times d$ matrix of input factors, n is the sample size, d is the number of factors. The variance of X_i can be written as

$$V_i = V_{X_i}\left(E_{X_{-i}}(Y \mid X_i)\right) \tag{1}$$

where $X_{\sim i}$ denotes the matrix of all factors except X_i, $E(\cdot)$ and $V(\cdot)$ indicate the mean and variance respectively.

Then the first order sensitivity indices of X_i is

$$S_i = \frac{V_i}{V(Y)} = \frac{V_{X_i}\left(E_{X_{-i}}(Y \mid X_i)\right)}{V(Y)} \tag{2}$$

Due to

$$V_{X_i}\left(E_{X_{-i}}(Y \mid X_i)\right) + E_{X_i}\left(V_{X_{-i}}(Y \mid X_i)\right) = V(Y) \tag{3}$$

So, the total effect index is

$$S_{Ti} = \frac{E_{X_{-i}}\left(V_X(Y \mid X_{-i})\right)}{V(Y)} = 1 - \frac{V_{X_{-i}}\left(E_{X_i}(Y \mid X_{-i})\right)}{V(Y)} \tag{4}$$

Furthermore, assume that the inputs space of the model considered above is $\Omega = (X \mid 0 \leq x_i \leq 1, i = 1, 2, \ldots, d)$

and uniformly distributed in $[0,1]$. Then the model can be decomposed as follows

$$f = f_0 + \sum_i f_i + \sum_i \sum_{j>i} f_{ij} + L + f_{12K\,d} \tag{5}$$

where $f_i = f_i(X_i)$, $f_{ij} = f_{ij}(X_i, X_j)$, all items are square integrable over Ω.

To ensure the Equation (5) is unique, it should be satisfied with the following condition

$$\int_0^1 f_{i_1,i_2,\ldots,i_s}(x_{i_1}, x_{i_2}, \ldots, x_{i_s})dx_{i_w} = 0 \tag{6}$$

where $1 \le i_1 < i_2 < L < i_s \le i_d$, $i_w = \{i_1, i_2, \ldots, i_s\}$. The functions f_0, f_i, f_{ij} are obtained from

$$\begin{cases} f_0 = E(Y) \\ f_i = E_{X_{-i}}(Y \mid X_i) - E(Y) \\ f_{ij} = E_{X_{-ij}}(Y \mid X_i, X_j) - f_i - f_j - E(Y) \end{cases} \tag{7}$$

and similarly for high orders.

Correspondingly, the partial variance of functions f_i and f_{ij} are

$$\begin{cases} V_i = V(f_i(X_i)) = V_{X_i}\left(E_{X_{-i}}(Y \mid X_i)\right) \\ V_{ij} = V(f_{ij}(X_i, X_j)) \\ \quad = V_{X_i X_j}\left(E_{X_{-ij}}(Y \mid X_i, X_j)\right) - V_{X_i}\left(E_{X_{-i}}(Y \mid X_i)\right) \\ \quad\quad - V_{X_j}\left(E_{X_{-j}}(Y \mid X_j)\right) \end{cases} \tag{8}$$

and similarly for high orders.
Then

$$V(Y) = \sum_i V_i + \sum_i \sum_{j>i} V_{ij} + L + V_{12\ldots d} \tag{9}$$

The Equation (9) can be written as the follows

$$\sum_i S_i + \sum_i \sum_{j>i} S_{ij} + L + S_{12\ldots d} = 1 \tag{10}$$

where S_{ij} is the second order sensitivity indices.

To compute the sensitivity indices of S_i and S_{Ti}, sampling method can be used to estimate their values. Two independent sampling matrices A and B. Assume that matrix $A_B^{(i)}$ ($B_A^{(i)}$) is A (B) which the i-th column is replaced by the i-th column of B (A). Then S_i and S_{Ti} can be written as

$$\begin{cases} S_i = \left(\dfrac{1}{n}\sum_{j=1}^n f(A)_j f(B_A^{(i)})_j - f_0^2\right)\Big/ V(Y) \\ S_{Ti} = \dfrac{1}{2n}\sum_{j=1}^n \left(f(A)_j - f(A_B^{(i)})_j\right)^2 \Big/ V(Y) \end{cases} \tag{11}$$

Assume that the output variables of A and $B_A^{(i)}$ are Y and Y^X respectively. Then the estimation of S_i can be written as follows

$$\$_o = \frac{\dfrac{1}{n}\sum_{j=1}^n Y_j Y_j^X - \left(\dfrac{1}{n}\sum_{j=1}^n Y_j\right)^2}{\dfrac{1}{n}\sum_{j=1}^n Y_j^2 - \left(\dfrac{1}{n}\sum_{j=1}^n Y_j\right)^2} \tag{12}$$

However, the estimation of S_i considered by Janon (2014) is

$$\$_S = \frac{\dfrac{1}{n}\sum_{j=1}^n Y_j Y_j^X - \left(\dfrac{1}{n}\sum_{j=1}^n Y_j\right)\left(\dfrac{1}{n}\sum_{j=1}^n Y_j^X\right)}{\dfrac{1}{n}\sum_{j=1}^n Y_j^2 - \left(\dfrac{1}{n}\sum_{j=1}^n Y_j\right)^2} \tag{13}$$

and the variance of $\$_S$ is

$$\sigma_S^2 = \frac{V\left((Y - E(Y))(Y^X - E(Y)) - S_X(Y - E(Y))\right)}{(V(Y))^2} \tag{14}$$

2.2. A Generalized Estimator of First Order Sensitivity Indices

To improve the efficiency of sensitivity analysis, a generalized Sobol indices estimator for calculating the first order sensitivity indices is proposed as follows:

$$\$_X = \frac{\dfrac{1}{n}\sum_{j=1}^n Y_j Y_j^X - \left(\dfrac{1}{n}\sum_{j=1}^n \left(wY_j + (1-w)Y_j^X\right)\right)^2}{\dfrac{1}{n}\sum_{j=1}^n \left(wY_j^2 + (1-w)(Y_j^X)^2\right) - \left(\dfrac{1}{n}\sum_{j=1}^n \left(wY_j + (1-w)Y_j^X\right)\right)^2} \tag{15}$$

where $w \in [0,1]$.

In order to measure the quality of $\$_X$, the unbiasedness and efficiency are analyzed as follows.
(1) Unbiasedness
Theorem 2.1 Assume that

$$\lim_{n\to\infty} E(\$_X) = S_X \tag{16}$$

Then $\$_X$ is the asymptotic unbiased estimation of S_X.

Proof. Let $\$_X = \dfrac{\$_a}{\$_b}$, where

$$\begin{cases} \$_a = \dfrac{1}{n}\sum_{j=1}^n Y_j Y_j^X - \left(\dfrac{1}{n}\sum_{j=1}^n \left(wY_j + (1-w)Y_j^X\right)\right)^2 \\ \$_b = \dfrac{1}{n}\sum_{j=1}^n \left(wY_j^2 + (1-w)(Y_j^X)^2\right) \\ \quad\quad - \left(\dfrac{1}{n}\sum_{j=1}^n \left(wY_j + (1-w)Y_j^X\right)\right)^2 \end{cases} \tag{17}$$

Then

$$\lim_{n\to\infty} \$_a = \lim_{n\to\infty} \frac{1}{n}\sum_{j=1}^{n} Y_j Y_j^X$$
$$-\lim_{n\to\infty}\left(\frac{1}{n}\sum_{j=1}^{n}\left(wY_j + (1-w)Y_j^X\right)\right)^2 \tag{18}$$

According to the law of large numbers,

$$E(Y) = E(Y^X) = E\left(wY + (1-w)Y^X\right) \tag{19}$$

Then

$$\lim_{n\to\infty}\$_a = \lim_{n\to\infty} E(YY^X) - \lim_{n\to\infty}\left(E\left(wY + (1-w)Y^X\right)\right)^2$$
$$= \lim_{n\to\infty}\left(E(YY^X) - E(Y)E(Y^X)\right) \tag{20}$$

Similarly,

$$\lim_{n\to\infty}\$_b = \lim_{n\to\infty}\left(E(Y^2) - (E(Y))^2\right) \tag{21}$$

Finally,

$$\lim_{n\to\infty} E(\$_X) = E\left(\lim_{n\to\infty}\frac{\$_a}{\$_b}\right)$$
$$= E\left(\frac{\lim_{n\to\infty}\left(E(YY^X) - E(Y)E(Y^X)\right)}{\lim_{n\to\infty}\left(E(Y^2) - (E(Y))^2\right)}\right) \tag{22}$$
$$= E\left(\frac{Cov(Y,Y^X)}{V(Y)}\right) = S_X$$

Based on above all, it can be easily concluded that $\$_X$ is the asymptotic unbiased estimation of S_X.

(2) Efficiency

Theorem 2.2 Assume that

$$\sigma_X^2 \le \sigma_S^2 \tag{23}$$

Then σ_X^2 is more effective than σ_S^2. Where σ_X^2 is the variance of $\$_X$.

Proof. Firstly, the equation of σ_X^2 should be obtained. The derivation of σ_X^2 is described as follows:

Let $\boldsymbol{U} = [U_1, U_2, U_3]^T$, where

$$\begin{cases} U_1 = (Y - E(Y))(Y^X - E(Y)) \\ U_2 = w(Y - E(Y)) + (1-w)(Y^X - E(Y)) \\ U_3 = w(Y - E(Y))^2 + (1-w)(Y^X - E(Y))^2 \end{cases} \tag{24}$$

Assume that $\psi(\boldsymbol{U}) = \psi(U_1, U_2, U_3) = \dfrac{U_1 - U_2^2}{U_3 - U_2^2}$, then

$$\$_X = \psi(\bar{u}_1, \bar{u}_2, \bar{u}_3) \tag{25}$$

According to the central limit theorem,

$$\frac{1}{\sqrt{n}}(\boldsymbol{U} - E(\boldsymbol{U})) \xrightarrow{n\to\infty} N(0, \Gamma) \tag{26}$$

where

$$\begin{cases} E(\boldsymbol{U}) = E[U_1, U_2, U_3]^T = \left[Cov(Y,Y^X), 0, V(Y)\right]^T \\ \Gamma = Cov(\boldsymbol{U}, \boldsymbol{U}^T) = E\left((\boldsymbol{U} - E(\boldsymbol{U}))(\boldsymbol{U}^T - E(\boldsymbol{U}^T))\right) \end{cases} \tag{27}$$

By the Delta method (Hoef 2012)

$$\frac{1}{\sqrt{n}}(\$_X - S_X) \xrightarrow{n\to\infty} N(0, \sigma_X^2) \tag{28}$$

where $\sigma_X^2 = \boldsymbol{g}^T \Gamma \boldsymbol{g}\big|_{\boldsymbol{U}=E(\boldsymbol{U})}$, $\boldsymbol{g}$ denotes the gradient of $\psi(\boldsymbol{U})$.

$$\boldsymbol{g} = \nabla\psi(\boldsymbol{U})$$
$$= \left[\frac{1}{U_3 - U_2^2}, \frac{2U_2(U_1 - U_3)}{(U_3 - U_2^2)^2}, -\frac{U_1 - U_2^2}{(U_3 - U_2^2)^2}\right]^T \tag{29}$$

When $\boldsymbol{U} = E(\boldsymbol{U})$,

$$\boldsymbol{g}\big|_{\boldsymbol{U}=E(\boldsymbol{U})} = \left[\frac{1}{V(Y)}, 0, -\frac{Cov(Y,Y^X)}{(V(Y))^2}\right]^T \tag{30}$$

Then

$$\sigma_X^2 = \boldsymbol{g}^T \Gamma \boldsymbol{g}\big|_{\boldsymbol{U}=E(\boldsymbol{U})}$$
$$= V\left((Y - E(Y))(Y^X - E(Y)) - S_X\left(w(Y - E(Y))^2\right.\right. \tag{31}$$
$$\left.\left.+ (1-w)(Y^X - E(Y))^2\right)\right)\Big/(V(Y))^2$$

Furthermore, to analyze the influence of σ_X^2 with different w:

Let

$$T(w) = V\left((Y - E(Y))(Y^X - E(Y))\right.$$
$$\left. - S_X\left(w(Y - E(Y))^2 + (1-w)(Y^X - E(Y))^2\right)\right) \tag{32}$$

Without loss of generality, let $E(Y) = 0$, then

$$T(w) = V\left(YY^X - S_X\left(wY^2 + (1-w)(Y^X)^2\right)\right)$$
$$= V(YY^X) + S_X^2 w V(Y^2) + S_X^2(1-w)^2 V\left((Y^X)^2\right)$$
$$- 2S_X w Cov(YY^X, Y^2)$$
$$- 2S_X(1-w)Cov\left(YY^X, (Y^X)^2\right)$$
$$+ 2S_X^2 w(1-w)Cov\left(Y^2, (Y^X)^2\right)$$

Let $\dfrac{\partial T(w)}{\partial w} = 0$, then

$$0 = wS_X V(Y^2) - S_X(1-w)V\left((Y^X)^2\right) - Cov(YY^X, Y^2)$$
$$+ Cov\left(YY^X, (Y^X)^2\right) + (1-2w)S_X Cov\left(Y^2, (Y^X)^2\right)$$

From the equations above, σ_X^2 will get minimum value when $w = 1/2$. And the estimation of first order sensitivity indices can be written as

$$\hat{S}_x = \frac{\frac{1}{n}\sum_{j=1}^{n} Y_j Y_j^X - \left(\frac{1}{n}\sum_{j=1}^{n}\left(\frac{Y_j + Y_j^X}{2}\right)\right)^2}{\frac{1}{n}\sum_{j=1}^{n}\left(\frac{Y_j^2 + (Y_j^X)^2}{2}\right) - \left(\frac{1}{n}\sum_{j=1}^{n}\left(\frac{Y_j + Y_j^X}{2}\right)\right)^2} \quad (33)$$

Finally, for Equation (30), when $w = 1/2$, let $EY = 0$, then

$$\left(V(Y)\right)^2 (\sigma_S^2 - \sigma_X^2) = \frac{(S^X)^2}{2}\left(V(Y^2) - Cov\left(Y^2, (Y^X)^2\right)\right) \quad (34)$$

By Cauchy-Schwarz inequality

$$Cov\left(Y^2, (Y^X)^2\right) \leq \sqrt{V(Y^2)V\left((Y^X)^2\right)} = V(Y^2) \quad (35)$$

it can be easily concluded that $\sigma_X^2 \leq \sigma_S^2$.

3. SEQUENTIAL SAMPLING STRATEGY BASED ON EXTENDED OLHS

To avoid the oversampling problem, sequential sampling is an effective strategy and has attracted much attention in recent years. In this paper, a sequential sampling strategy using extended OLHS is adopted, where the ESE algorithm (Jin 2005) is used to optimize space-filling property of LHS sample points. It allows to add n sample points each time which satisfies stratified structure of LHS. The procedure of the sequential sampling strategy is described as follows:

Sequential sampling strategy
1: Generate two independent midpoint-LHS sample $A_{n\times d}$ and $B_{n\times d}$
2: Let $X_{n\times 2d} = [A_{n\times d}\ B_{n\times d}]$ to be the initial sample
3: Obtain $(X_{n\times 2d})^*$ by optimizing $X_{n\times 2d}$ based on the algorithm of $ML_2 - ESE$
4: Set $r = 2$
5: **do**
6: Generate new sample matrix $X_{n\times 2d}^{(r)}$ by the extending rule (Li 2017)
7: Obtain $(X_{n\times 2d}^{(r)})^*$ by optimizing $X_{n\times 2d}^{(r)}$ based on the algorithm of $ML_2 - ESE$
8: Get $A_{n\times d}^{(r)}$ and $B_{n\times d}^{(r)}$ according to $(X_{n\times 2d}^{(r)})^*$
9: Obtain $A_B^{(i)}$ and $B_A^{(i)}$ where $i \in \{1, 2, \ldots, d\}$
10: Generate the output by running simulation model
11: Compute sensitivity indices S_i and S_{Ti}
12: $r = r + 1$
13: **until** $r > k$ or $S_i(r) - S_i(r - t) < \varepsilon \Delta S_i^t$

where r is the multiple of the current extension, k is the maximum multiple of the extension, $S_i(r)$ is the value of S_i when the multiple of the extension is r. $\Delta S_i^t = S_i(t+1) - S_i(1)$, ε is the acceptable threshold.

4. NUMERICAL ILLUSTRATION

In this section, two classic test functions are used to demonstrate the effectiveness of the proposed method.
1) Ishigami function (Sudret 2008)

$$y = \sin(x_1) + a\sin(x_2)^2 + bx_3^4\sin(x_1) \quad (36)$$

where $x_i : \mathsf{U}(-\pi, \pi)$, $a = 7$, $b = 0.1$.
2) Borehole function (Burnaev 2017)

$$y = \frac{2\pi x_3(x_4 - x_6)}{\ln(x_2/x_1)\left[1 + \frac{2x_7 x_3}{\ln(x_2/x_1)x_1^2 x_8} + \frac{x_3}{x_5}\right]} \quad (37)$$

where $x_1 : \mathsf{U}(0.05, 0.15)$, $x_2 : \mathsf{U}(100, 50000)$, $x_3 : \mathsf{U}(63070, 115600)$, $x_4 : \mathsf{U}(990, 1110)$, $x_5 : \mathsf{U}(63.1, 116)$, $x_6 : \mathsf{U}(700, 820)$, $x_7 : \mathsf{U}(1120, 1680)$, $x_8 : \mathsf{U}(9855, 12045)$.

To measure the efficiency of sampling strategies, the absolute error

$$AE_i = | S_i - \hat{S}_i | \quad (38)$$

and the mean squared error

$$MSE = \frac{1}{n_r}\sqrt{\sum_{i=1}^{d}(S_i - \hat{S}_i)^2} \quad (39)$$

can be used, where AE_i indicates the accuracy of estimation for each factor and MSE indicates the accuracy of estimation for all factors, $\hat{S}_i$ is the estimation of S_i, n_r is the number of repetitions.

For Equation (36), $\hat{S}_i$ is computed analytically. For Equation (37), $\hat{S}_i$ is computed by the Equation (11) with the sample size $n = 10000$ and $n_r = 100$, where the sampling method is midpoint-LHS. The reference values of each function are shown in Table 1.

Table 1: Reference Values of Fisrt Order Sensitivity Indices

Estimators	Reference Values	
	Ishigami Function	Borehole Function
$\hat{S}_1$	0.3138	0.8297
$\hat{S}_2$	0.4424	0
$\hat{S}_3$	0	0
$\hat{S}_4$	/	0.0429
$\hat{S}_5$	/	0
$\hat{S}_6$	/	0.0420

$\hat{S}_7$	/	0.0388
$\hat{S}_8$	/	0.0092

To account for the efficiency and convergence of the proposed estimator $\hat{S}_X$, two estimators are compared, including $\hat{S}_O$ and $\hat{S}_S$. Simple random sampling (SRS) is used to generate sampling matrices, where $n_r = 100$ and the sample size is increased from $n = 50$ to $n = 5000$. The results of first order sensitivity indices' error for two test functions are shown in Figure 1 and Figure 2, respectively. It can be concluded from these figures that with the sample size increases, three estimators tend to be convergence. Furthermore, Figure 1(d) and Figure 2(b) show that $\hat{S}_X$ and $\hat{S}_S$ are clearly superior than $\hat{S}_O$ on the whole, where $\hat{S}_X$ is the best.

To illustrate the efficiency and convergence of the proposed method, SRS and random LHS are compared, where $\hat{S}_X$ ($w = 1/2$) is used to estimate first order sensitivity indices. As shown in Figure 3, the sample size increases from $n = 100$ to $n = 700$ and $n_r = 30$. It can be easily concluded that three sampling methods appear to be convergence. Moreover, the proposed method is superior than the other two sampling methods on the whole.

5. CONCLUSIONS

Sensitivity analysis plays an important role in the development of metamodeling, optimization and so on, which allows one to do further studies on the relative important factors. As a kind of global sensitivity analysis method, Sobol' method has been studied in this paper. The generalized Sobol indices estimator has been proposed. It has been proved that the estimator is the most effective when $w = 1/2$. To improve the sampling efficiency of sensitivity analysis, a sequential sampling strategy using extended OLHS is adopted. It is demonstrated from the numerical example that the proposed method appears to perform well in both efficiency and convergence. As a future work, some other sequential sampling strategies will be studied to improve the efficiency of sensitivity analysis.
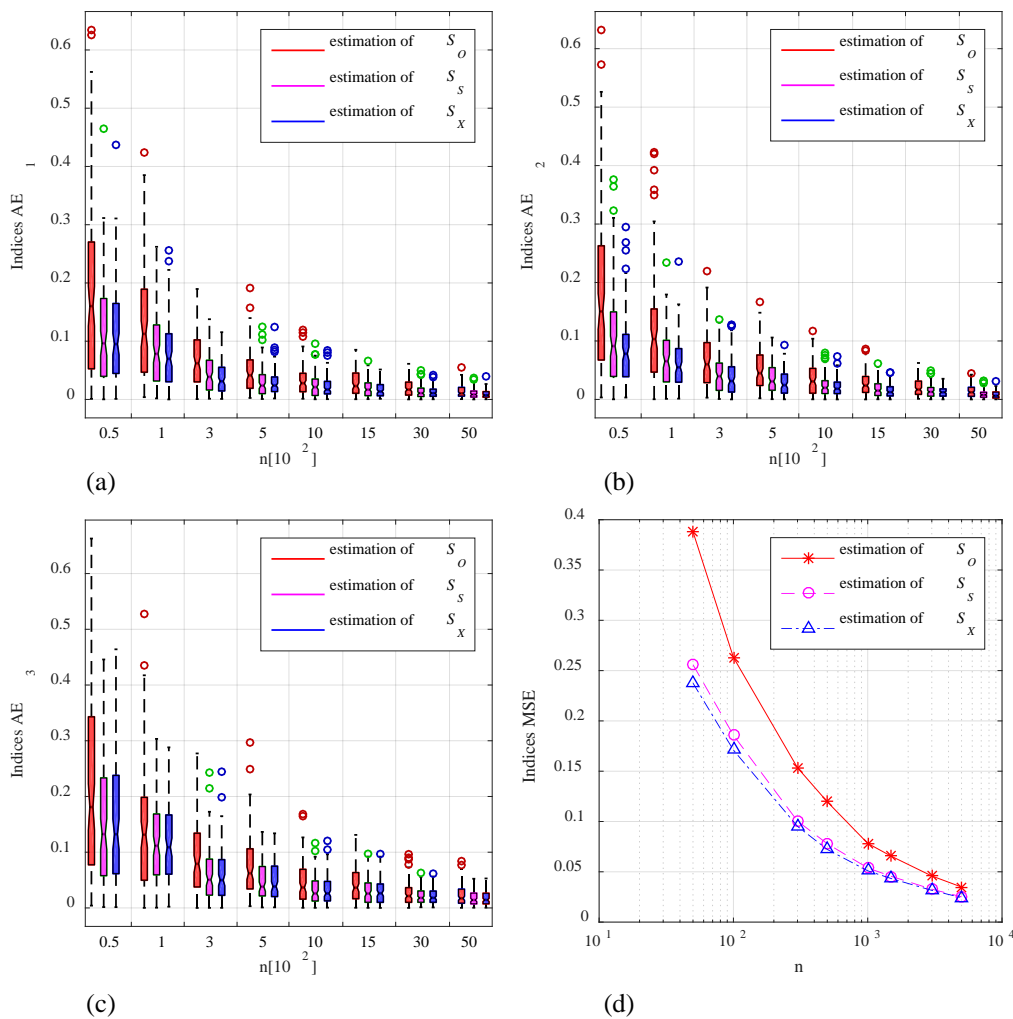

Figure 1: Comparison of First Order Sensitivity Indices' Error for Ishigami Function with Different Estimators
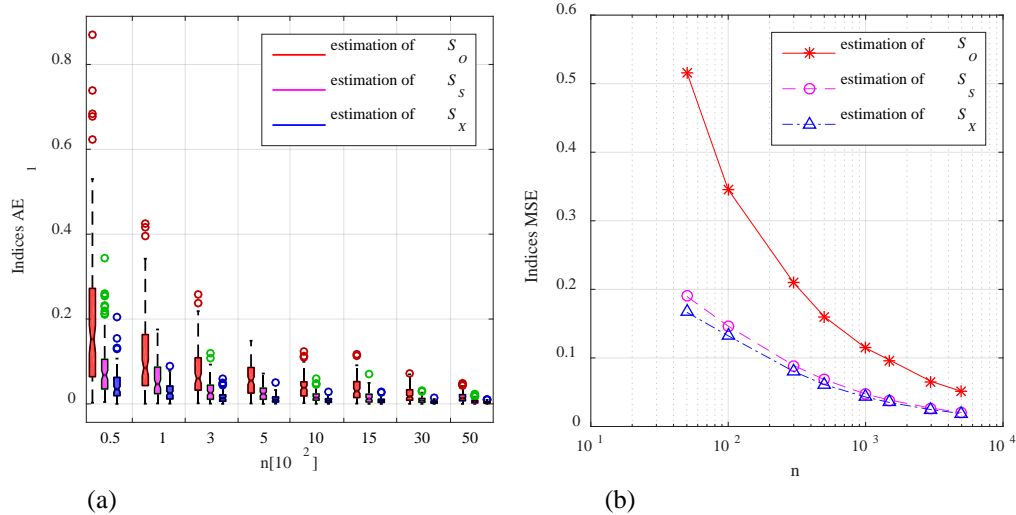
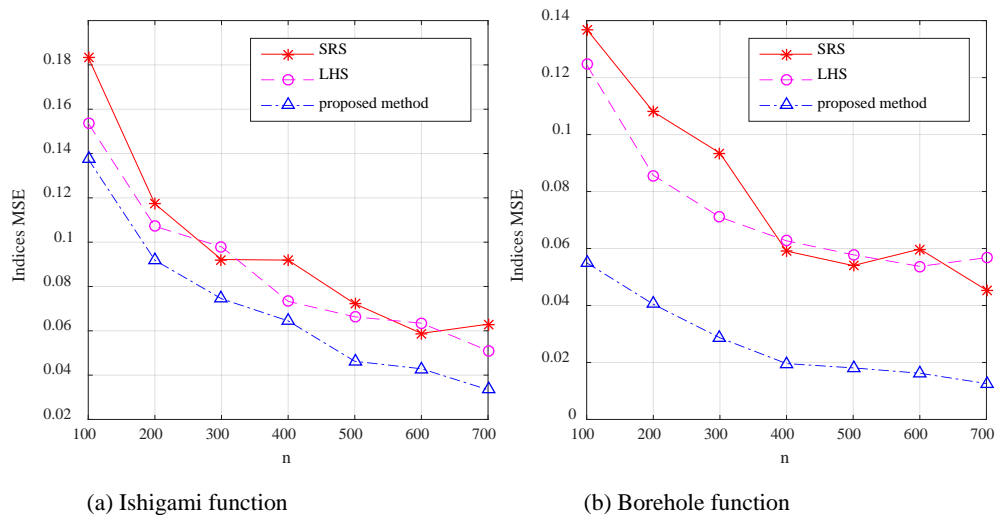Figure 2: Comparison of First Order Sensitivity Indices' Error for Borehole Function with Different Estimators

(a) Ishigami function

(b) Borehole function

Figure 3: Comparison of First Order Sensitivity Indices' Error with Different Sampling Methods

REFERENCES

Borgonovo E., Plischke E., 2016. Sensitivity analysis: A review of recent advances. European Journal of Operational Research, 248, 869–887.

Burnaev E., Panin I., Sudret B., 2017. Efficient design of experiments for sensitivity analysis based on polynomial chaos expansions. Annals of Mathematics and Artificial Intelligence, 81(1-2), 187–207.

Cheng K., Lu Z.Z., Zhou Y.C., 2017. Global sensitivity analysis using support vector regression. Applied Mathematical Modelling, 49, 587–598.

Jansen M.J.W., 1999. Analysis of variance designs for model output. Computer Physics Communications, 117, 35–43.

Sobol' I.M., 2007. Global sensitivity analysis indices for the investigation of nonlinear mathematical models. Matematicheskoe Modelirovanie, 19(11), 23–24.

Saltelli A., Annoni P., Azzini I., et al., 2010. Variance based sensitivity analysis of model output. Design and estimator for the total sensitivity index. Computer Physics Communications, 181, 259–270.

Janon A., Klein T., Lagnoux A., et al., 2014. Asymptotic normality and efficiency of two Sobol index estimators. ESAIM: Probability and Statistics, 18, 342–364.

Hoef J.M.V., 2012. Who invented the Delta method?. American Statistician, 66(2): 124–127.

Li W., Lu L.Y., Xie X.T., et al., 2017. A novel extension algorithm for optimized Latin hypercube sampling. Journal of Statistical Computation and Simulation, 87(13), 2549–2559.

Jin R., Chen W., Sudjianto A., 2005. An efficient algorithm for constructing optimal design of computer experiments. Journal of Statistical Planning and Inference, 134(1), 268–287.

Sudret B., 2008. Global sensitivity analysis using polynomial chaos expansion. Reliability Engineering and System Safety, 93(7), 964–979.

AUTHORS BIOGRAPHY

LINGYUN LU is a Ph.D. candidate at Harbin Institute of Technology (HIT), and received the M.E. from HIT in 2013. His research interest covers simulation experiment design and analysis. His email is jyzluhit@gmail.com.

WEI LI is an associate professor at HIT, and received the B.S., M.E. and Ph.D. from HIT in 2003, 2006 and 2009 respectively. His research interest covers simulation evaluation, simulation experiment design and analysis, and distributed simulation. His email is frank@hit.edu.cn.

PING MA is the corresponding author. She is a professor at HIT, and received Ph.D. from HIT in 2003. Her research interest covers complex system modeling and simulation, distributed simulation and VV&A. Her email is pingma@hit.edu.cn.

MING YANG is a professor and the director of control and simulation center at HIT. Also he is the vice editor-in-chief for Journal of System Simulation and editor for International Journal of Modeling Simulation and Science Computing. His research interest covers vehicle guidance and control, complex system simulation theory and method. His email is myang@hit.edu.cn.

PROCESSABILITY ANALYSIS OF AN INJECTED PART IN VIRGIN OR RECYCLED POLYPROPYLENE

José Galve[a], Daniel Elduque[b], Carmelo Pina[c], Isabel Clavería[d], Carlos Javierre[e]

[a],[c]BSH Electrodomésticos España, S.A. Avda. de la Industria, 49, Zaragoza (Spain)
[b],[d],[e]i+aitiip, University of Zaragoza, C/ María de Luna 3, Zaragoza (Spain)

[a]jose.galve@bshg.com, [b]delduque@unizar.es, [c]carmelo.pina@bshg.com,
[d] iclaver@unizar.es, [e]carlos.javierre@unizar.es

ABSTRACT

Nowadays in the industry, exists the trend to use more ecologic materials to decrease the environmental impact of their products. One way to produce components with lower environmental impact is using recycled materials obtained from post-industrial wastes. In this article, the processability of an injected moulded part of an induction hob is going to be studied for both virgin and recycled polypropylene. One of the limitations of injection is that each material requires a mold specifically designed for the properties of the selected plastic material such as viscosity or melting point. Changing the mold can be very expensive. To cope with this problem, it is possible to simulate the injection of both materials in the same mold to observe the differences between the injection of these two materials and improve the operation conditions to get a component that can replace the original.

Keywords: injection molding, Cadmould, recycled plastic, simulation

1. INTRODUCTION

Plastic injection molding is one of the most used processes in industry, and used to obtain different parts in diverse fields like automotive or home appliances. In this process raw material is forced into the cavity of a mold to obtain the defined shape (Kamal, Isayev and Liu 2009; Javierre, Fernández, Clavería, and Elduque 2014; Elduque, Javierre, Elduque, and Fernández 2015). This mold is usually designed to produce a part with a specific material because each plastic has its peculiarities like density or viscosity and therefore it has optimized process conditions such as temperature, filling time and compaction pressure.

Nowadays, the use of plastics is increasing every year. This can be due to the increase in production and consumption after the economic crisis (Elduque, Elduque, Javierre, Fernández, and Santolaria 2015).

As the consumption has grown, the price of the plastics has increased during these years. At that point, plastic manufacturers investigated for new ways to reduce costs. A remarkable option is using recycled materials. Big plastic parts producers have also lots of plastics cuts and defective parts that can be recycled. In addition, if the industries do not recycle theses wastes, there is a lot of plastic that will be sent to landfilling or incineration. Besides the costs lose on reworking, scrap and processing, not paying attention to these industrial cuts leads to another problem not only economic but also environmental. Incineration and specially the landfilling have a great impact to the environment. One way to analyze the effect of these different end of life is Life Cycle Assessment methodology (Martínez, Blanco, Jiménez, Saenz-Díez, and Sanz 2015; Fraile-Garcia, Ferreiro-Cabello, Martinez-Camara, and Jimenez-Macias 2016).

There are different end of life treatments for plastics and each one of them has a different impact on the environment. Due to the high environmental impact of incinerating and landfilling plastics (Hottle, Bilec, and Landis 2017; Galve, Elduque, Pina, and Javierre 2016; Camañes, Elduque, Javierre, and Fernández 2014), the European Union has developed specific legislation devoted to stimulate the use of recycled plastic.

The possibility of changing the injection material to a recycled one can be of interest for industrial companies. Nowadays, one of the causes to use recycled plastic is to reduce the environmental impact, as previous researches have established that using recycled plastics instead virgin reduce the environmental impact of a product. (Simões, Costa Pinto, and Bernardo 2013; Rajendran, Scelsi, Hodzic, Soutis, and Al-Maadeed 2012; Noda, Komatsu, Sumi, and Kasakura 2001; Gu, Guo, Zhang, Summers, and Hall 2017).

Changing the injection material for another type of plastic already in production results in different obstacles. As the mold and the operation conditions are designed for a specific material, changing the material can cause different problems like insufficient filling, air entrapment due to non-existence of air vents or excessive deformation caused by using non adequate operation conditions. This is caused by the different properties of the plastics.

There are several types of recycling techniques like the chemical or the mechanical (Hamad, Kaseem, and Deri 2013). The chemical one uses many organic solvents which can be dangerous to the environment (Achilias,

Roupakias, Megalokonomos, Lappas, and Antonakou 2007). The mechanical route grinds the used plastic to obtain a new raw material to use in injection or extrusion. This way produces changes in the properties of the polymer because by cutting it, the molecular chains of the polymer break, altering the structure of the molecules (Kozdeka, Rose, Koci, Caillaud, and Bahlouli 2016).

These environmental benefits, which allow reducing the environmental impact, contrast with properties changes of the recycled plastics. These alterations depend on the type of recycling technique and on the polymer used to produce the new material. Differences in the rheological properties cause a modification in the operation conditions for the virgin and recycled material. Using the same process variables would translate in inadequate dimensions.

As the cost of manufacturing a new mold for the new material is high, it is suggested the possibility of using the same mold by optimizing the operation conditions to obtain a part that meets dimensional requirements.

Knowing the differences between the properties of virgin and recycled material and having the optimized operation conditions for the virgin plastic, this material change can be supported on a software simulation, which allows obtaining ideal results of an injection introducing concrete mold and operation conditions.

Starting from a 3D model, simulation software obtains illustrative results such as filling time or clamp force (Fernández, Muniesa, and Javierre 2014). These outcomes cannot be directly transferred to real process because the software simplifies the geometry and also doesn´t take into account different parameters that may affect the real process.

This study focuses on a specific part of an induction cooktop. In this case, two polypropylenes have been used, one virgin and one recycled.

2. METHODOLOGY

For the study of these two materials and their processability as example, an induction hob part is used to simulate this process.

2.1. Used materials

This article focuses on the changes given in an injection using the same mold and conditions but different plastics. In this case, two different polypropylenes are going to be simulated on the software.

Figure 1: Instron Ceast sr20 Capillary Rheometer

To see the differences between the properties of these two materials, a rheological analysis of viscosity has been made. The capillary rheometer used has been the Instron Ceast sr20 (Figure 1).

The results obtained in this analysis are shown in figure 2. As it can be seen, these two plastics do not have the exact same viscosity properties but can be considered similar.
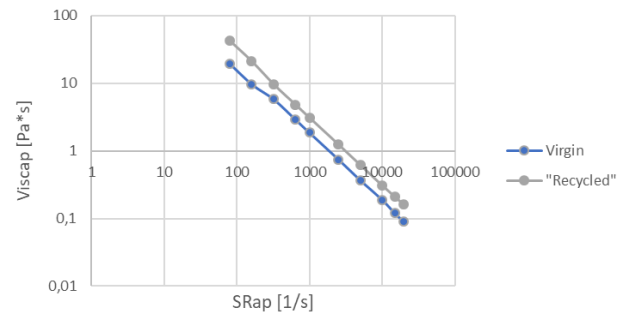

Figure 2: Viscosity Analysis for Virgin and Recycled Material

The mechanical technique grinds the used plastic to obtain a new raw material to use in injection or extrusion. This method produces changes in the properties of the polymer because by cutting it, they break the molecular chains altering the structure of the molecules.

The recycled polymer used in these simulations is a plastic produced by the mechanical method. This plastic was obtained from a mixture of different polypropylenes which have similar properties to the virgin plastic. The origin of these materials has been tracked to ensure that only pure polypropylene has been used and that there will not be any impurity that can spoil the recycled material.

Apart from this, the way of producing this recycled plastic is not by simply grinding parts and introducing them in the injection machine. This polypropylene is obtained by melting recycled materials, treating them and adding additives to improve and stabilize their properties.

This is why instead of just being called recycled material, it should be called material made from recycled materials.

After this process, the obtained plastic made from waste has similar properties than the virgin one.

2.2. Simulated part

The part that is going to be simulated is an internal component of an induction hob (Pina, Elduque, Javierre, Martínez, and Jiménez 2015), so it is not necessary that this part has careful aesthetics (Figure 3). However, it has to meet several dimensional requirements to fit with other parts of the induction hob. In addition, this part is located below different heavy components. This condition forces deformations to be minimized as the parts of the induction hob must fit properly.
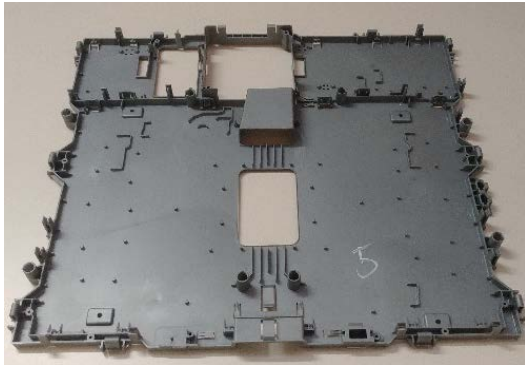
Figure 3: Reference Component of an Induction Hob

This part has a dimension of approximately 534x472mm and is currently produced with virgin polypropylene. This is why there is no chance to change the mold. The mold is an expensive part and as the part that is going to be produced with the recycled plastic must be the same, it was decided to maintain the mold although the materials have some different properties. To counteract these differences in the material properties and using the same mold, operating conditions have to be refined to obtain similar parts.

2.3. Simulation

It has been decided to make the comparative of the two materials on a simulation software in order to save plastic material, time and energy because the process only runs in a computer (Jiménez, Ruiz, Blanco, and Pérez 2009). Software used for simulation has been Cadmould 3D-F (patented technology EP1 385 5103), which allows to analyze filling stages of the injection molding, as well as cooling and warping effects on the part.

This software allows introducing 3D models and mold to obtain a part by injection. Mesh model generation is based on a special 3D-framework (3D-F) crosslinking method with at least twenty-five sampling points across the thickness as described in (Filz, Webelhaus, 2006). This method generates a final mesh model from a standard STL geometrical model, ready to carry out the finite elements analysis (Figure 4).
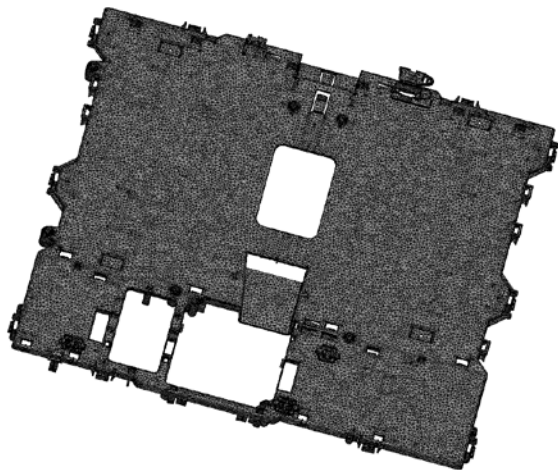

Figure 4: Mesh Example for the Part.

Once the mesh is obtained, it is necessary to introduce the injection points through which the material enters in the mold. These injection points can be directly in contact with the mold or can be placed with feeding runners for a better control of the material injection pressure.

In this case, the injection points are placed directly in the component, as shown in Figure 5.

Figure 5: Injection Points on Cadmould

Materials are selected from the software database. With the mesh, injection points and fixed operation conditions, the software runs the simulation and shows different results like filling time or commutation pressure.

2.4. Process

This study is based on specific operation condition and a specific mold designed for the virgin plastic. This study is going to be named case 0 and will be the reference to optimize the injection of the recycled material. Seeing the differences between the results of these two cases, operation condition can be modified to improve the filling with recycled material.

The first step of this process is simulate the case 0 on Cadmould.

The case 0 consist on a mold and a refrigeration system through which water circulates to cool down the injected material in a uniform manner. This refrigeration system is extracted from the current mold used for production series (Figure 6).
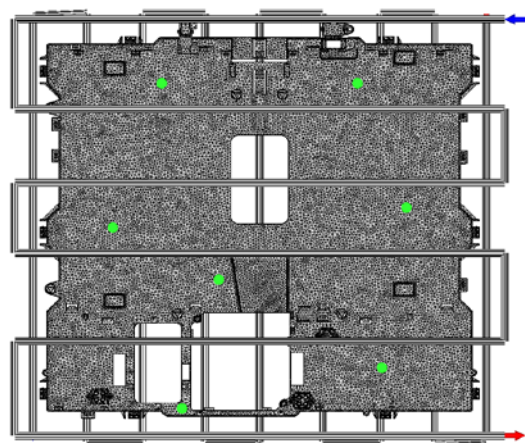

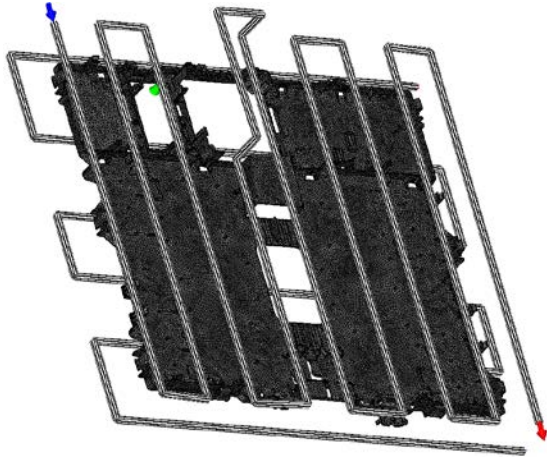Figure 6: Top Refrigeration System Model

Figure 7: Lower Refrigeration System Model

This system, described on figures 6 and 7, is composed of upper and lower circuit of 10 mm diameter channels, with independent water inputs and outputs. Both systems are fed with a flow of 10 l/min at a temperature of 15 ºC. The refrigeration will run during 35 seconds.

After configuring the refrigeration, operation conditions must be set. As it´s based on an optimized process, injection time will be 2.5 seconds and compaction profile will use 40 MPa during 12 seconds with 250 ºC of mass temperature.

Once the simulation is complete, the outcomes are taken as reference. After this, another simulation will run, but this time, with the recycled polymer and the conditions of case 0. Since these two materials have different properties, the results will not be the same and filling time in the recycled material is expected to be different and insufficient. Although the conditions were not valid, these outcomes are taken as reference to improve the operation conditions of the recycled plastic using the same tool.

2.5. Differences in the injection process

The recycled plastic used in these simulations is not exactly the same than the virgin. To elaborate this polymer, different sources of polypropylene are used because as it was commented before, when PP is grinded loses properties. Therefore, the plastics used for recycling have different injection properties and are mixed in the adequate proportion, looking for a resulting polymer with similar behavior to the virgin one.

Although this material is as similar as possible to the virgin material, there will be differences in the injection and this may change properties in the produced component.

3.   RESULTS

3.1. Virgin polypropylene and optimized operation conditions

One of the most representative outcomes is the filling time, which is going to indicate the total time and how the part fills.
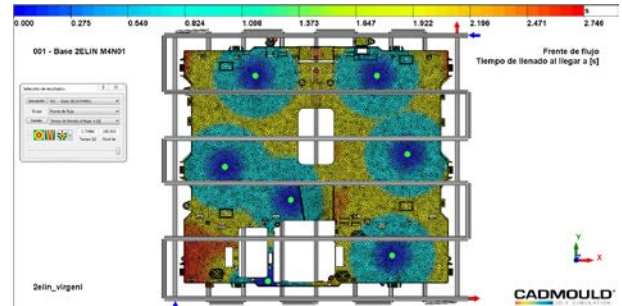
Figure 8: Fill Distribution for Virgin Material

As presented, the part fills up completely. Filling time introduced in the software was 2.5 seconds and the result has been 2.75 seconds.

The following result is the pressure at the shift between speed and pressure control. When the 99% of the part is filled, this process is going to be compacted under a pressure of 40 MPa.
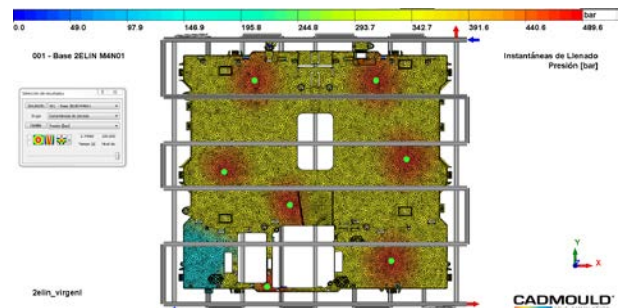
Figure 9: Commutation Pressure V/P for the Virgin Material

As it can be seen, there is an area in the lower left corner that will be filled by pressure.

If material temperature is not high enough, the polymer could solidify before filling all the details present in the design. However, in this case, the temperature is adequate and the filling process is enough.
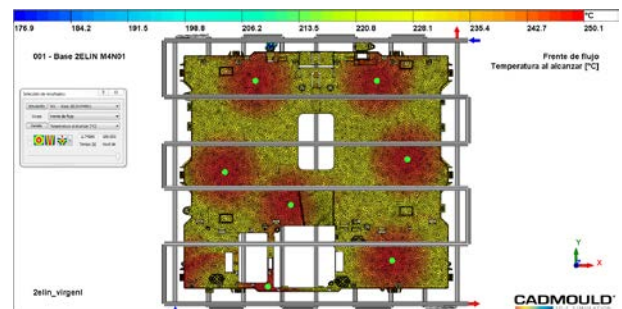
Figure 10: Distribution Temperature for the Virgin Material

Nevertheless, as the injection speed is enough and the temperature is higher than the melting point, the part fills completely. After the filling time is necessary to control the pressure during the compactation. If this compactation pressure is not high enough there is the possibility not to fill completely the remaining percentage.

In contrast, extremely high pressure cause excessive deformations. The next figure shows the injection pressure.
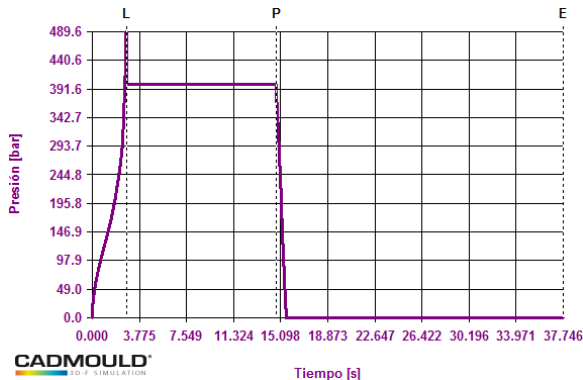
Figure 11: Pressure at Injection Point for the Virgin Material

The maximum injection pressure obtained for the virgin polymer is 489.6 bar

In addition, another important parameter is the clamping force. This force keeps the mold closed during the injection. An excessive clamping force might damage the part. In this case, the clamping force isn´t excessive. The value of this outcome is 8328 kN.
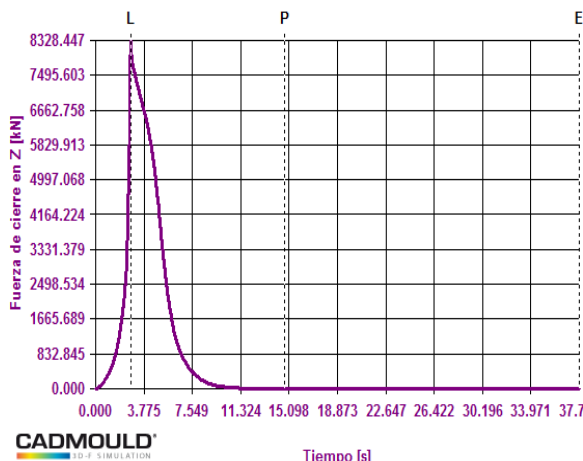
Figure 121: Clamp Force for the Virgin Material

3.2. Recycled polypropylene with same conditions of case 0

The next step simulates the injection process using the recycled material. The mold, injection points and the operation conditions are the same than the previous case.

Although this polypropylene is a recycled material, it is produced using only industrial wastes from factories that use virgin polypropylene. This ensures that this raw material has only been reprocessed once after the original polymer.

As has been mentioned before, changing the material within modifying any parameter, can cause several problems in the process. First of all, the first problem is the fill. Recycled polypropylene has a higher viscosity

than the virgin and this difference cause that it flows slower, cooling faster and hence, solidifying.
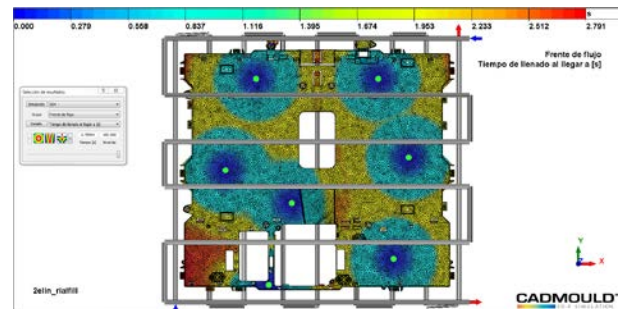
Figure 2: Fill Distribution for the Recycled Material

Although recycled polymers have different properties than virgin ones, Figure 13 shows that this specific plastic does not have problems during the injection process and the part fills completely.

Filling time of virgin polymer was 2.75 seconds and in this case is 2.79. This indicates that filling time is not seriously affected by the change of the material.
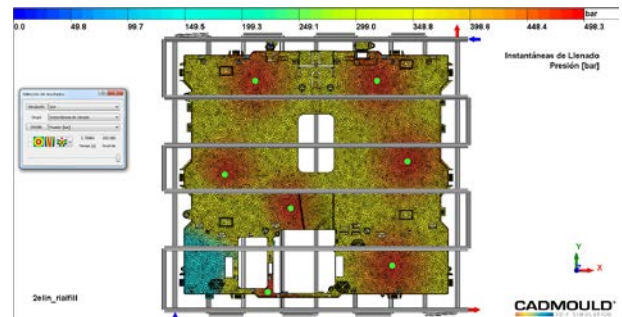
Figure 3: Commutation Pressure V/P in the Injection of the Recycled Material

On top of that, pressure loss is neither severely affected. This can be seen in Figure 14. In virgin material is 489.6 bar and in recycled 498.3 bar.
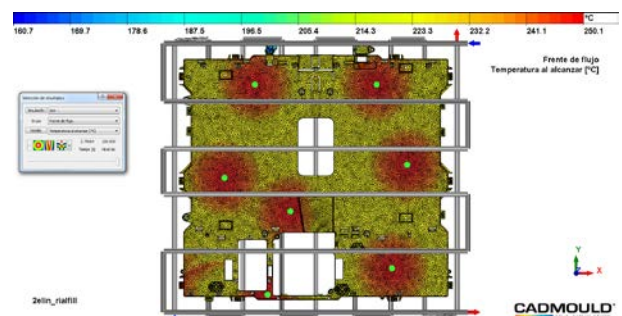
Figure 154: Distribution Temperature for the Recycled Material

As can be observed in Figure 15, the filling temperature is enough to keep the material liquid during the injection. This allows to fill the part without solidification problems in the injection. The maximum temperature reached in the injection is 250.1 ºC.

Another important outcome is the injection pressure.
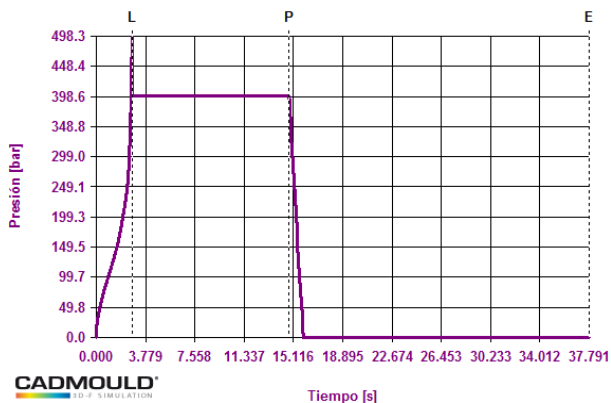
Figure 5: Pressure at Injection Point for the Recycled Material

In this case, the injection pressure isn´t excessive to produce deformations in the part. The maximum obtained value is 498.3 bar which is similar to the result of the virgin polymer.

Finally, the last important result for the recycled material is the clamping force.
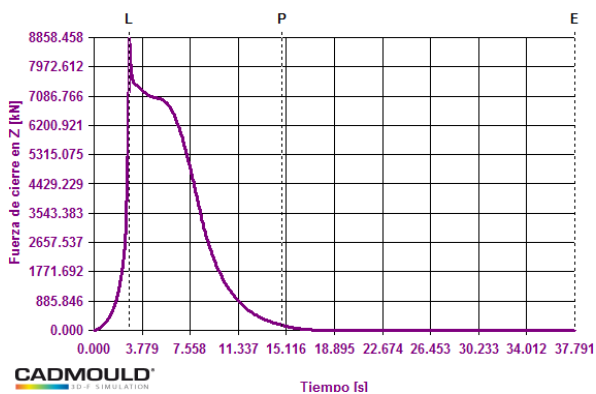
Figure 6: Clamp Force for the Recycled Material

The maximum value obtained is 8858 kN, similar to the result of the virgin one.

4. CONCLUSIONS

After performing both simulations, the following conclusions have been obtained:

- Although the raw materials of this recycled plastic have different origins and later have been treated with additives, the obtained material produced from recycled has similar properties to the virgin.
- The rheological analysis is similar for the two compared materials although properties as viscosity are slightly higher in the recycled material.
- Filling distribution is practically the same in both cases despite the existence of different thicknesses in the part. Pressure is similar, a little higher in the recycled one due to the viscosity in accordance with rheological analyzes. This difference in pressure values is also caused by the cooling of the material as

the second one cools faster. Clamp force is higher in the recycled plastic due to the pressure and the viscosity.
- From the point of view of processability, these two materials are similar.

REFERENCES
Achilias D, Roupakias C, Megalokomos P, Lappas A, Antonakou E, 2007. Chemical recycling of plastic wastes made from polyethylene (LDPE and HDPE) and polypropylene (PP). Journal of Hazardous Materials 149:536-542

Camañes V, Elduque D, Javierre C, Fernández A, 2014. The Influence of Different Recycling Scenarios on the Mechanical Design of an LED Weatherproof Light Fitting. Materials 7:5769-5788

Elduque A, Elduque D, Javierre C, Fernández A, Santolaria J, 2015. Environmental impact analysis of the injection molding process: analysis of the processing of high-density polyethylene parts. Journal of Cleaner Production 108:80-89

Elduque A, Javierre C, Elduque D, Fernández A, 2015. LCI Databases Sensitivity Analysis of the Environmental Impact of the Injection Molding Process. Sustainability 7:3792-3800

Fernández A, Muniesa M, Javierre C, 2014. In-line rheological testing of thermoplastics and a monitored device for an injection moulding machine: Application to a raw and recycled polypropylene. Polymer Testing 33: 107-115

Filz P.F., Webelhaus F.K., 2006. Technical Explanation of the CadmouldR 3D-F Technology in CADMOULD 3D F Fill User Manual 2006: 202-206.

Fraile-Garcia E, Ferreiro-Cabello J, Martinez-Camara E, Jimenez-Macias E, 2016. Optimization based on life cycle analysis for reinforced concrete structures with one-way slabs. Engineering Structures 109:126-138

Galve J, Elduque D, Pina C, Javierre C, 2016. Sustainable Supply Chain Management: The Influence of Disposal Scenarios on the Environmental Impact of a 2400 L Waste Container. Sustainability 8:564

Gu F, Guo J, Zhang W, Summers P, Hall P, 2017. From waste plastics to industrial raw materials: A life cycle assessment of mechanical plastic recycling practice based on a real-world case study. Science of the Total Environment 601-602:1192-1207

Hamad K, Kaseem M, Deri F, 2013. Recycling of waste from polymer materials: An overview of the recent

works. Polymer Degradation and Stability 98: 2801-2812

Hottle T, Bilec M, Landis A, 2017. Biopolymer production and end of life comparisons using life cycle assessment. Resources, Conservation and Recycling 122:295-306

Javierre C, Fernández A, Clavería I, Elduque D, 2014. Textile injection process characterisation by means of a spiral mould. Measurement 47:200-109

Jiménez, E., Ruiz, I., Blanco, J., Pérez, M. (2009). Design and simulation of production of injection pieces in automobile industry. International Journal of Simulation: Systems, Science and Technology, 10(3), 23-30.

Kamal M, Isayev A, Liu S, 2009. Injection moulding, Technology and Fundamentals. Cincinnati: Hanser Publications, Inc.

Kozderka M, Rose B, Koci V, Caillaud E, Bahlouli N, 2016. High impact polypropylene (HIPP) recycling – Mechanical resistance and Lifecycle Assessment (LCA) case study with improved efficiency by preliminary sensitivity analysis. Journal of Cleaner Production 137: 1004-1017

Martínez E, Blanco J, Jiménez E, Saenz-Díez J.C, Sanz F, 2015. Comparative evaluation of life cycle impact assessment software tools through a wind turbine case study. Renewable Energy 74:237-246

Noda R, Komatsu M, Sumi E, Kasakura R, 2001. Evaluation of material recycling for plastics: environmental aspects. Journal of Material Cycles and Waste Management 3:118-125

Pina C, Elduque D, Javierre C, Martínez E, Jiménez E, 2015. Influence of mechanical design on the evolution of the environmental impact of an induction hob. The International Journal of Life Cycle Assessment 20:937-946

Rajendran S, Scelsi L, Hodzic A, Soutis C, Al-Maadeed, M, 2012. Environmental impact assessment of composites containing recycled plastics. Resources, Conservation and Recycling 60:131-139

Simões C, Costa Pinto L, Bernardo C, 2013. Environmental and economic assessment of a road safety product made with virgin and recycled HDPE: A comparative study. Journal of Environmental Management 2013:209-215

AUTHORS BIOGRAPHY

José Galve finished his degree in Industrial engineering in 2012. He works as mechanical development for BSH Home Appliances Group – Spain. He works also as a part time teacher of the CAD software NX. He is a Mechanical Engineering PhD candidate since September 2014 in the University of Zaragoza. In his work he researches the environmental impact of the thermoplastic recycling process.

Carmelo Pina is a part-time professor at the University of Zaragoza in the Department of Design and Manufacturing and PhD Co-Director of José Galve. He works, as well, at BSH Home Appliances Group – Spain and is the Head of Mechanical Platform Development of Induction Cooktops. He received his PhD in 2015. His main research interests include mechanical engineering, life cycle assessment and environmental impact.

Daniel Elduque is an Assistant Professor at the University of Zaragoza in the Mechanical Engineering Department and PhD Co-Director of José Galve. He is part of the I+ research group. He received his PhD in 2014. His main research interests include mechanical engineering, life cycle assessment and environmental impact. Some of his latest publications are the analysis of the environmental impact of the injection moulding process, and the study of the influence of the composition on the environmental impact of SMD transistors and aluminium casting alloys.

Isabel Clavería is Senior Lecturer at University of Zaragoza in Mechanical Engineering Department since 2007. She belongs to I+ research group. His main research interests include mechanical engineering and industrial design of plastic parts. Some of her latest publications are a new extrusion head with integrated ultrasonic device and online process parameters measurements system and textile injection process characterization by means of a spiral mould.

Carlos Javierre is a Professor at the University of Zaragoza in the Mechanical Engineering Department. He is part of the I+ research group. His main research interests include mechanical engineering, life cycle assessment and environmental impact. Some of his latest publications are the study of the influence of environmental conditions on the dimensional stability of components injected with PA6 and PA66; or the analysis of the environmental impact of the injection moulding process of high-density polyethylene parts by carrying out a life cycle assessment.

AGENT-BASED MODEL FOR TUMOR-ANALYSIS
USING PYTHON+MESA

Ghazal Tashakor [(a)], Remo Suppi [(a)]

(a) Universitat Autònoma de Barcelona, Department Computer Architecture & Operating Systems, School of Engineering, Campus Bellaterra,
Cerdanyola del Vallès, Barcelona, 08193, Spain

[(a)] Ghazal.Tashakor@caos.uab.cat [(a)] Remo.Suppi@uab.cat

ABSTRACT
The potential power provided and possibilities presented by computation graphs has steered most of the available modeling techniques to re-implementing, utilization and including the complex nature of System Biology (SB). To model the dynamics of cellular population, we need to study a plethora of scenarios ranging from cell differentiation to tumor growth and etcetera.
Test and verification of a model in research means running the model multiple times with different or in some cases identical parameters, to see how the model interacts and if some of the outputs would change regarding different parameters.
In this paper, we will describe the development and implementation of a new agent-based model using Python. The model can be executed using a development environment (based on Mesa, and extremely simplified for convenience) with different parameters. The result is collecting large sets of data, which will allow an in-depth analysis in the microenvironment of the tumor by the means of network analysis.

Keywords: Agent-based models, Python, System Biology, Graph, Simulation modeling

1. INTRODUCTION
At the cellular level, Systems Biology (SB) is mainly a complex natural phenomenon that today has become important for research in certain areas such as drug development and biotechnological productions and applications.
Mathematical models of cellular level are built in bio repeated cycles at a portion of time to arrive at a decision. The primary idea behind the bio iterative cycles is to develop systems by allowing software developers to redesign and translate the cellular metabolism. The objective is bringing the desired decision or result closer to discovery in each iteration; these experiments on multi-scale iterative cycle of computational modeling - besides experimental validation and data analysis- would produce incremental samples for the high-throughput technologies.
Also the behavior of the cell emerges at the network-level and requires much integrative analysis. Moreover, due to the size and complexity of intercellular biological networks, computational model should be a considerate part of the production or application.
In the following whole simulation challenges, SB would not be needless of developing integrated frameworks for analysis and data management. Alongside the intercellular level, many researches in SB also address the issue of cellular population.
In evolutionary versions of these scenarios, modeling the interactions of these type of models across large multi-scale would need agent-based modeling. Each agent has a Boolean network for its own expression, much like a gene. So a proper production or application for SB must support not only a compatible simulation method but also suitable methods for model parameter estimations which represent the experimental data (D.2011; An2008).
Therefore, ABMs start with rules and mechanisms to reconstruct through the mathematical or computational form and observe the pattern of data. Processing the heterogeneous behavior of individual agent within a dynamic population of agents -which cannot be controlled by an overall controller- needs a higher-level system parallelism which ABMs supports.
Biological systems include random behaviors and ABMs accommodate this via generation of population agents in the agent's rules.
ABMs have a level of abstraction to create new cellular states or environmental variables without changing core aspects of the simulation. To aggregate the paradoxical nature of emergent behavior which could be observed from any agent in contrast to a conceptual rules of the model, ABMs reproduce emergent behavior. Emergent behavior has a range of stochasticity similar to real world Systems Biology (Bonabeau2002).
Finding software platforms for scientific agent-based models require comparing certain software design parameters such as emulating parallelism, and developing schedulers for multiple iterations, which manage ABM run.
Many references reviewed and compared different agent-based modeling toolkits. However, from the perspective of biotechnological application and biotechnologists, most of them share a key weakness. It is using complex languages which are not Python. Perhaps re-implementing ABMs in Python would be a wiser technical strategy since it is becoming the language of

scientific computing, facilitating the web servers for direct visualization of every model step, debugging and developing an intuition of the dynamics that emerge from the model, also allowing users to create agent-based models using built-in core components such as agent schedulers and spatial grids (Villadsen and Jensen 2013).

2. BACKGROUND

Spontaneous tumor, which progresses from the initial lesion to highly metastatic forms are generally profiled by molecular parameters such as prognosis response, morphology and pathohistological characteristics. Tumors can induce angiogenesis and lymph-angiogenesis, which plays an important role in promoting cancer spread. Previous studies have shown that the cancer stem cell (CSC) theory could become a hypothesis for tumor development and progression.

These CSCs have the capability of both self-renewal and differentiation into diverse cancer cells, so one small subset of cancer cells has characteristics of stem cells as their parents. Hereditary characteristics play a certain role in malignant proliferation, invasion, metastasis, and tumor recurrence.

In recent researches the possible relationship between cancer stem cells, angiogenesis, lymph-angiogenesis, and tumor metastasis is becoming a challenge. Due to many evidences and reviews such as (Li 2014; Weis and Cheresh 2011; Carmeliet, P., & Jain, R. K. 2000), metastasis is defined as the spread of cancer cells from the site of an original malignant primary tumor to one or more other places in the body. More than 90% of cancer sufferings and death is associated with metastatic spread. In 1971, Folkman proposed that tumor growth and metastasis are angiogenesis-dependent, and hence, blocking angiogenesis could be a strategy to intercept tumor growth.

His hypothesis later confirmed by genetic approaches. Angiogenesis occurs by migration and proliferation of endothelial cells from original blood vessels (Weis and Cheresh 2011).

Accordingly, translational cancer research has contributed to the understanding of the molecular and cellular mechanisms occurring in the tumor and in its microenvironment which causes metastasis and this could present a model relatively similar to physiology of human or at least has the capability of going through genetic manipulations that bring them closer to humans. Hence tumor modeling with a high spatiotemporal resolution combined with parametric opportunities has been rapidly applied in technology (Granger and Senchenkova 2010).

2.1. Agent-based Models in Systems Biology

A primary tumor model addressing the avascular growth state depends on differential equations. They are classified as "lumped models" to predict the temporal evolution of overall tumor size. Since lumped models just provide a quantitative prediction of tumor size over time with only a few parameters and very low computational results, they would not be enough for an explicit investigation of many other events such as spatiotemporal dynamics of oxygen and nutrients or cell to cell interactions; also, stromal cells which play a major role in cancer growth and progression in the interaction with tumor cells. The result is disregarding the mutations in the tumor microenvironment and metastasis.

These shortcomings lead us to In Silico models of tumor microenvironment. In Silico (Edelman, Eddy & Price 2010) refers to computational models of biology and it has many applications. It is an expression performed on a computer simulation. In Silico models are divided to three main categories (Thorne, Bailey, & Peirce 2007; Soleimani et al., 2018):

1. Continuum based models which solve the spatiotemporal evolution problems of density and concentration of cellular population in the tumor microenvironment.
2. Discrete or agent based on a set of rules which change the cells' states and manage the cells' interactions within the tumor microenvironment.
3. Adaptive Hybrid models which integrate the above solutions.

Mathematical and computational models of the tumor should cover different aspects of tumor interactions in its microenvironment. Most of the avascular tumor models address the tumor growth dynamics not taking into account the angiogenesis setting; but computational models have started research on tumor-induced angiogenesis since the beginning of cancer research.

Therefore, the angiogenesis models have a very strong background in experimental observations. The most established researches have explicitly focused on the stromal cells to achieve a close computational model of angiogenesis.

For example, according to Monte Carlo simulations and energy minimization, cellular models are expanded and elaborated on cellular automata to allocate more than one lattice site to each cell and describe cell to cell and tumor stroma interactions. Nevertheless, building a bulky model over a range of matrix densities -which covers numerous factors for a large domain size and 3D simulations- is restricted by computational and application costs.

Based on a paper written by Soleimani et al. (2018), a minimal coupling of a vascular tumor dynamics to tumor angiogenic factors through agent-based modeling has progressed the experimental studies in the recent years. They have mentioned in both reviews that it is challenging to mathematically simulate all the process of a complex system such as tumor growth, metastasis and tumor response treatments, because mathematical modeling is still a simplification of the system biology and the results requires validation.

Also, building a predictive experimental plus theoretical application without clinical data requires parametrizing and validating again. The best improvement which is expected would be predictive modeling in both

preclinical and clinical states (Thorne, Bailey, & Peirce 2007).

2.2. Complex Networks in Biological Models
Another interesting approach is the network models. Networks follow patterns and rules and have a specific topology, which allows scientists to go through with a deeper investigation towards biology information extraction.

Within the fields of biology and medicine, Protein-protein interaction (PPI) networks, biochemical networks, transcriptional regulation networks, signal transduction or metabolic networks are the highlighted network categories in systems biology which could detect early diagnosis.

All these networks need compatible data to be produced experimentally or retrieved from various databases for each type of network; but besides analyzing data structures for computational analysis, several topological models have been built to describe the global structure of a network (Girvan, Newman 2002; 2004).

3. MODELING AND SIMULATION
Our approach to the generation of an ABM model considered different temporal and spatial scales, focusing first on mitosis as the main axis of tumor growth. This model and its analysis developed in Netlogo (section 3.1). Then large number of environment limitations were detected with a high number of agents and difficulties to analyze the microenvironment of emergent growth. The second approximation is presented in this paper (section 3.2) used dynamic networks based on a large number of interactive agents. This model makes it possible to help researchers in carrying out more detailed research on intercellular network interactions and metastasis in a multiple scale model (Grimm2005).

3.1. Netlogo Model and Experimental Results
Our ABM NetLogo model is designed as a self-organized model that illustrates the growth of a tumor and how it resists chemical treatment.

This model in NetLogo (based on Wilensky's tumor model (Wilensky 1999)) permits us to change the parameters that affect tumor progression, immune system response, and vascularization. Outputs included the number of living tumor cells and the strength of the immune system which control cells. In this model the tumor has two kinds of cells: stem cells and transitory cells. In the model, tumor cells are allowed to breed, move, or die.

The simulation presented cells' control with different and constant immune responses through killing transitory cells, moving stem cells and original cells.

Figure 1 shows the steady state of a tumor metastasis visualization with 6 stem cells and the grow-factor =1.75, replication-factor=high, and apoptosis=low.

As it could be seen, the growth of metastasis is more aggressive and through reducing apoptosis, there is a greater number of cells that do not die, amounting to near 200,000 cells (agents) (Tashakor, Luque & Suppi, 2017).

The main problem with this implementation was the limitations of the execution environment (Java memory limitations) and loss of performance with a high number of metastasis cells. In addition, this model did not allow capturing in detail the interactions between the different parameters at the microenvironment level.
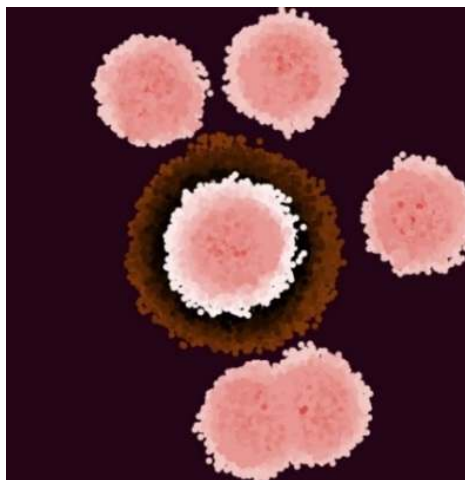
Figure 1: stem cells evolution and metastasis visualization with grow-factor=1.75, apoptosis=low and replication-factor=high (near 200,000 cells in steady state).

3.2. Python Model and Experimental Results
To solve the aforementioned problems, we started a new development using Python +Mesa. Mesa is the agent-based Python project, which has started recently and it has rapidly found its place among the researchers. Mesa is modular and its modeling, analysis and visualization components are integrated and simple to use.

This feature convinced us to re-implement our tumor model with Mesa network structure. Furthermore, it supports multi-agent and multi-scale simulations, which is suitable for creating dynamic agent-based models. This paper documents our work with the Python +Mesa to design an agent model based on the tumor model scenario.

At the beginning, Mesa was just a library for agent-based modeling in Python but now it is a new open-source, Apache 2.0 licensed package meant to fill the gap in the modeling complex of dynamical systems.

In Mesa, the Model class to define the space where the agents evolve handles the environment of an agent-based model. The environment defines a scheduler which manages the agents at every step.

For studying the behavior of model under different conditions, we needed to collect the relevant data of the model while it was running; Data Collector class was defined for this task. The adapting modules of Mesa allow us to make changes in the existing ABMs for the purpose of conforming with the requirements of our future framework.

Also, monitoring the data management issues when processing actions happen in parallel seems facile in Mesa, since each module has a Python part which runs on the server and turns a model state into JSON data (Masad & Kazil, 2015). The advantage of Mesa is its browser for visualization which allows the user to see the model while running in the browser.

Tumor progression is a complex multistage process and the tumor cells have to acquire several distinct properties either sequentially or in parallel.

The first problem using NetLogo framework for simulation was using behavioral space which supports multithreading. In this way, performance is limited to the number of cores at the local infrastructure.

To solve the local processing problem, we utilized the parametric simulations using a HPC cluster in order to reduce the necessary time to explore a determinate model data space.

Since we needed to distribute our model through the distributed architecture to explore the model states in the microenvironment scale, it was revealed that NetLogo also has scalability issues in designing graph networks.

Although there are available extensions for scaling up the model in the form of graph, it still depends on the size of the tumor and it could be a very slow process, taking days to finish experiment considering the checkpoints and performance bottlenecks while using a HPC cluster.

We had to translate and move our model to a new framework such as the style and structure of Mesa to facilitate our distributed executions.

The newest changes in the ground of the old scenario is increasing the population of agents, obtaining graph-based representation of biological network and consideration of multi-state and multi-scale components (An2008).

The initial design aspect of the multi-scale architecture of out tumor growth model in Python comes from the acute inflammation based on the key factors such as angiogenesis. Tumor angiogenesis is critical for tumor growth and maintenance (Kaur et al., 2005).

Our new model strategy begins with an initial identification of a minor population of cells with the characteristics of "tumor-initiating" cancer stem cells and these cancer stem cells in the assumed tumor reside in close proximity to the blood vessels. Therefore, we chose an angiogenetic switch for our model which have to balance this dynamic. We had angiogenetic and anti-angiogenetic factors.

In the case of anti-angiogenetic, we will have the probability of quiescent tumor. In this agent-based model, tumor cells are affected, inflamed and turn quiescent.

Table 1 shows the range of parameters we implemented to control the factors.

Based on these factors, we can achieve a simulation evolution of metastasis and measure the tumor volume ratio along with the dynamics of the tumor under the influence of the factors.

Table 1: different control factors of tumor growth

Factors			
	Low	Medium	High
Angiogenesis	0.0	0.4	1
Recovery	0.1	0.3	1
Quiescent	0.1	0.5	1

To select a network topology for tumor model, we selected a random graph. Barabasi-Albert model is a scale-free network and it is one of the most basic models since it describes most of the biological networks - especially in evolutionary models; but since there is a need to manage the cell interactions and stromal cells behavior within the tumor microenvironment and due to the time-dependency of the connections, we developed our Python agent-based model on Erdös-Rényi topology. The visualization of the model is a network of nodes (using the Mesa architecture) that shows the distribution of agents and their links. Considering the architecture of Mesa, the creation of agents occurs based on the assignment of nodes to a graph. A scheduler (time module) activates agents and stores their locations and updates the network.

The total operation time is directly related to the number of steps necessary to deploy all the agents. Since each agent changes in three states, the process goes on until the tumor agent's volume appears as metastasis.

Thus, for P as a Probability and for edge creation in n number of nodes, if ($Ps > log (n)/n)$) almost all vertices are connected and this function returns a directed graph as we described in Algorithm 1.

Erdös-Rényi model takes a number of vertices *N* and connecting nodes by selecting edges from the (*N (N-1)/2*) possible edges randomly. The pseudo-code generating a random network is described in Algorithm 1:

```
Algorithm 1
Input: (n,p, p* )
Output: (True, False)
Begin Algorithm
   For n in enumerate(nodes):
      For p in enumerate(Ps):
         If  p > p* then
            p_connected(n, p) = 1
         Else
            return 0
         Endif
      Endfor
   Endfor
End Algorithm
```

The interactive visualization in Mesa helps us to identify insights and generate value from connected data. Considering the data analysis for life sciences such as tumor which is almost about connections and dependencies, the large amount of data makes it difficult for researchers to identify insights.

Graph visualization makes large amounts of data more accessible and easier to read, as it has been illustrated in Figure 2.
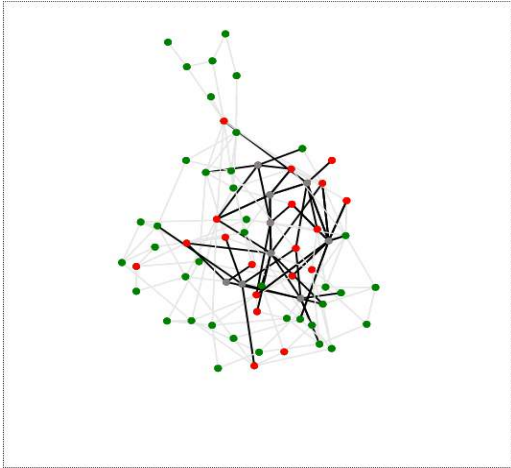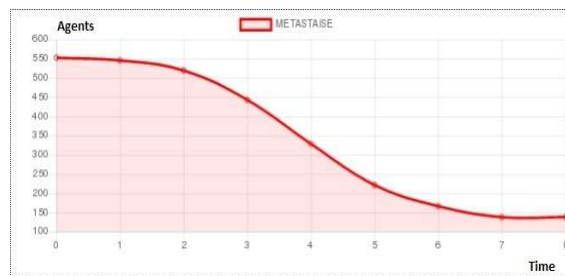

Figure 2: Graph visualization for three states (normal, dead and metastatic) shown in three colors

Tumor Volume Ratio: 2.02

Figure 3: Tumor stabilization challenges for cancer stem cells (CSC) with control factors more than medium

Figure 3 shows the reduction of cancer stem cells in 550 initial stem cells which are affected by control factors in the time it took, which was about 8 minutes for this simulation.

Tumor growth curves are used for derivation of the Tumor Control Index (TCI), such as tumor progression, rejection and stabilization. We tried to combine both rejection and stabilization challenges to show the potential of Python agent-based modeling with different control factors.

According to (Peskin 2009), we need a statistical method that leads to volume ratio measurements of tumor, as it could be seen in figure 3. To calculate tumor volume using (Monga.s 2000) we needed tumor width (W) and tumor length (L) which is presented in formula 1:

$$Tumor\ Volume = W^2 \times \frac{L}{2} \qquad (1)$$

This calculation which works pretty well for clinical issues, was made based upon the assumption that solid tumors are more or less spherical like the version we had before in Netlogo Wilensky's tumor model, but not proper for the metastatic diseases, which due to the phase

transition and spreading dynamics will be defined by graph presentations in the future.

According to Rai (2017), the model which have the same size and number of connections as of a given network could maintain the degree sequence of the given network. By generating a random network with a given average degree (K) and initial size of tumor (N), we could construct degree sequence (*m*) and it is presented in formula 2:

$$m = \frac{1}{2}\sum_{i=1}^{N} Ki$$
$$N = \binom{n}{2}, K=\{3,4,5,6,7,8\} \qquad (2)$$

For volume calculation, we start by assuming that every cell inside the tumor has three states (normal, dead and metastatic) which corresponds to tumor by edges. With the given K degree from three to eight and N initial nodes, we constructed an ER (Erdös-Rényi) network, whose degree sequence of (*m*) could lead us to the tumor volume ratio.

The pseudo-code using the dynamic of degree sequence under the influence of above factors producing tumor volume in graph network is described in Algorithm 2:

Algorithm 2
Input: (N,K=3)
Output: (Tumor Volume)
Begin Algorithm
While p_connected= 1
For N in nodes(G)
If P $\binom{N}{K}$ < Factor then
Return m/n
Endif
Endfor
End Algorithm

In Figure 4, we executed the model with different angiogenesis control factor in (0.1 to 0.9) for 60, 360, 650, 100 and 1200 cancer stem cells (CSCs) to produce the tumor volume analysis based on the density distribution of the graph.
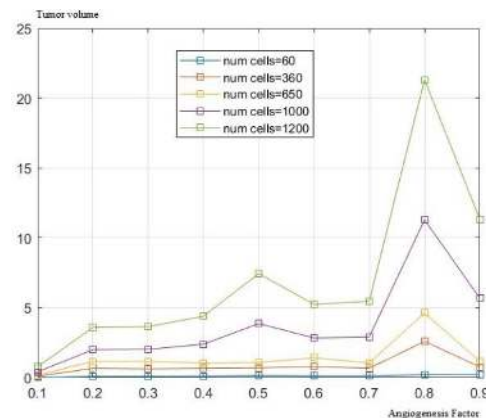

Figure 3: Tumor Angiogenesis volume ratio for 60 to 1200 cancer stem cell (CSC)

4. CONCLUSION

In summary, agent-based modeling in Python with Mesa project represents a valuable and time-saving simulation technique, which allowed us to re-implement our tumor model across a network based space.

Mesa enable a modeler to quickly write down the code and quickly explore the results. Mesa also collect the results easily and help us in data integration which is very important in the case of phase transition and pattern-oriented modeling.

We migrated successfully from Netlogo to Python-Mesa, which will allow us to reintegrate our system quicker and reiterate simulations taken on previous system with more data in considerably less time.

In the future, we will extend the model to run on cloud infrastructure in parallel. This could be an impressive achievement for fast analysis purposes in clinics, both on the predictive diagnostic and therapeutic side.

As advantages of this contribution, we have a scalable model that together with Python can be distributed over an HPC architecture eliminating the limitations of other environments (e.g. Netlogo due to memory limitations of the JVM).

When Python + Mesa can be deployed over an HPC architecture, there will be a notable increase in scalability and performance since, in this type of environment, the simulation will not be limited by memory.

One of the most important disadvantages is the model visualization and animation for oncologists. Netlogo has a cells visualization and animation that can be useful to medical environments. Mesa only has the visualization of the network of agents and their interconnections, so graphic functions must be developed to see the evolution of the cells and the degree of metastasis/apoptosis and other relevant parameters for the medical analyst.

Another important aspect that must be addressed will be the functional validation of the whole model since at this moment only a verification and partial validation of the behavior of the affected cells has been carried out.

REFERENCES
Wilensky, U., 1998. NetLogo Tumor model. Center for Connected Learning and Computer-Based Modeling, Northwestern University, Evanston, IL. Project Integrated Simulation & Model Environment. National Science Foundation REC-9814682 and REC-0126227

Li, S., & Li, S., 2014. Cancer stem cells and tumor metastasis (Review). International Journal of Oncology, 44, 1806-1812.

Weis, S. M., & Cheresh, D. A., 2011. Tumor angiogenesis: Molecular pathways and therapeutic targets. Nature Medicine.

Carmeliet, P., & Jain, R. K., 2000. Angiogenesis in cancer and other diseases. Nature.

Thorne, B. C., Bailey, A. M., & Peirce, S. M., 2007. Combining experiments with multi-cell agent-based modeling to study biological tissue patterning. Briefings in Bioinformatics.

Edelman, L. B., Eddy, J. A., & Price, N. D., 2010. In silico models of cancer. Wiley Interdisciplinary Reviews: Systems Biology and Medicine.

Soleimani, S., Shamsi, M., Ghazani, M. A., Modarres, H. P., Valente, K. P., Saghafian, M., Sanati-Nezhad, A., 2018. Translational models of tumor angiogenesis: A nexus of in silico and in vitro models. Biotechnology Advances.

Tashakor, G., Luque, E., & Suppi, R., 2017. High Performance Computing for Tumor Propagation Agent-based Model.

Granger, D. N., & Senchenkova, E, 2010. Inflammation and the Microcirculation. Colloquium Series on Integrated Systems Physiology: From Molecule to Function, 2(1), 1–87.

Girvan, M., & Newman, M. E. J., 2002. Community structure in social and biological networks. Proc. Natl. Acad. Sci. USA, 99(12), 7821–7826.

Tashakor, G., Suppi, R., 2017. HpcNetlogo. Frontend for the concurrent execution of Netlogo experiments using SGE HPC cluster.

Cho, D.-Y., Kim, Y.-A., & Przytycka, T. M., 2012. Chapter 5: Network Biology Approach to Complex Diseases. PLoS Computational Biology, 8(12), e1002820.

Masad, D., & Kazil, J., 2015. MESA: An Agent-Based Modeling Framework. Proceedings of the 14th Python in Science Conference.53–60.

Xing, F., Eisele, J., Bastian, P., & Heermann, D. W., 2015. Computational complexity of agent-based multi-scale cancer modeling. Simulation Series, 47(10), 351–358.

Villadsen, J., Jensen, A. S., Ettienne, M. B., Vester, S., Andersen, K. B., & Frøsig, A., 2013. Reimplementing a multi-agent system in python. In Lecture Notes in Computer Science (including subseries Lecture Notes in Artificial Intelligence and Lecture Notes in Bioinformatics) (Vol. 7837 LNAI, pp. 205–216).

An, G. 2008. Introduction of an agent-based multi-scale modular architecture for dynamic knowledge representation of acute inflammation. Theoretical Biology and Medical Modelling.

Railsback, S. F., Lytinen, S. L., & Jackson, S. K., 2006. Agent-based Simulation Platforms: Review and Development Recommendations. Simulation, 82(9), 609–623.

Bonabeau, E., 2002. Agent-based modeling: methods and techniques for simulating human systems. Proceedings of the National Academy of Sciences, 99(suppl. 3), 7280–7287.

Norton, K.-A., McCabe Pryor, M. M., & Popel, A. S., 2015. Multiscale Modeling of Cancer. bioRxiv, 33977.

D., M., R.S., C., M., R., E.C., F., B., T., & I., R., 2011. Modeling formalisms in systems biology. AMB Express, 1(1), 1–14.

Grimm, V., Revilla, E., Berger, U., Jeltsch, F., Mooij, W. M., Railsback, S. F, DeAngelis, D. L. (2005). Pattern-oriented modeling of agent-based complex systems: Lessons from ecology. Science.

ALITALO, K., TAMMELA, T. and PETROVA, T.V. 2005. Lymphangiogenesis in development and human disease. Nature 438: 946-953.

Kerbel, Robert S., (2008). Tumor angiogenesis. New England Journal of Medicine 358.19 2039-2049.

Peskin, A., Kafadar, K., Santos, A., & Haemer, G. 2009. Robust Volume Calculations of Tumors of Various Sizes.

Monga, S. P. S., Wadleigh, R., Sharma, A., Adib, H., Strader, D., Singh, G. Mishra, L. 2000. Intratumoral therapy of cisplatin/epinephrine injectable gel for palliation in patients with obstructive esophageal cancer. *American Journal of Clinical Oncology: Cancer Clinical Trials*, *23*(4), 386-392

Rai, A., Pradhan, P., Nagraj, J., Lohitesh, K., Chowdhury, R., & Jalan, S. 2017. Understanding cancer complexome using networks, spectral graph theory and multilayer framework. Scientific Reports, 7.

AUTHORS BIOGRAPHY

GHAZAL TASHAKOR is Research Fellow and PhD Candidate for trainee research staff position (PIF) at the Computer Architecture & Operating Systems Department (CAOS) of the University Autònoma de Barcelona. Her research interests include high performance simulation, agent-based modelling and their applications, service systems, integration, resource consumption, and execution time. Her e-mail address is: ghazal.tashakor@caos.uab.cat

REMO SUPPI received his diploma in Electronic Engineering from the Universidad Nacional de La Plata (Argentina), and the PhD degree in Computer Science from the Universitat Autonoma de Barcelona (UAB) in 1996. At UAB, he spent more than 20 years researching on topics including computer simulation, distributed systems, high performance and distributed simulation applied to ABM or individual-oriented models. He has published several scientific papers on the topics above and has been the associate professor at UAB since 1997, also a member of the High Performance Computing for Efficient Applications and Simulation Research Group (HPC4EAS) at UAB. His email address is: remo.suppi@uab.cat.

AN AGENT BASED MODELLING APPROACH FOR THE OFFICE SPACE ALLOCATION PROBLEM

Alexandra Dediu[(a)], Dario Landa Silva[(b)], Peer-Olaf Siebers[(c)]

[(a),(b)]ASAP Research Group, School of Computer Science, University of Nottingham, UK
[(c)]IMA Research Group, School of Computer Science, University of Nottingham, UK

[(a)]alexandra.dediu@nottingham.ac.uk, [(b)]dario.landasilva@nottingham.ac.uk
[(c)]peer-olaf.siebers@nottingham.ac.uk

ABSTRACT
This paper describes an agent based simulation model to create solutions for the office space allocation (OSA) problem. OSA is a combinatorial optimization problem concerned with the allocation of available office space to a set of entities such as people. The objective function in the OSA problem involves the minimization of space misuse and the minimization of soft constraints violations. Several exact and heuristic algorithms have been proposed to tackle this problem. This paper proposes a rather different approach by decomposing the problem into smaller goals, which are delegated to individual agents each representing an entity in the problem. Agents have an internal decision making process which guides them throughout their search process for a better allocation (room). That is, agents seek to satisfy their individual requirements in terms of room space and constraints. Computational experiments show that the agent based model exhibits competitive performance in terms of solution quality and diversity when compared to neighborhood search heuristics.

Keywords: agent based modelling, office space allocation, problem decomposition, distributed optimization

1. INTRODUCTION
Office Space Allocation is a combinatorial optimization problem concerned with the planning and distribution of the available physical space (e.g. rooms) to a set of entities such as people. When planning the distribution of office space in buildings, administrators or managers have to consider the practical issues involved in the allocation process, such as the spatial needs, proximity relations, facilities infrastructure, as well as occupancy costs and effectiveness of the working environment. The aim of OSA is to find an allocation (entities assigned to rooms) such that the misuse of space is minimized, and the satisfaction of constraints is maximized. The OSA problem is faced by many organizations, both academic institutions and businesses, where entities need to be distributed over an often limited amount of room space. Examples of such scenarios where OSA has been investigated as an optimization problem are the NASA Langley Research Center (Kincaid et al. 2007), the

European Space Research and Technology Center (Lopes and Girimonte 2010), and dormitories in an academic institution (Trung, Tuan and Anh 2009). So far, this problem has been tackled using various heuristic algorithms, such as asynchronous cooperative local search (Landa-Silva and Burke 2007), nature-inspired algorithms such as harmony search (Awadallah et al. 2012), evolutionary algorithms (Adewumi and Ali 2010; Ülker and Landa-Silva 2012), as well as mathematical programming (Ülker and Landa-Silva 2010). More recent works include greedy algorithms with tabu search (Castillo, Riff and Montero 2016) and artificial bee colony algorithms (Bolaji, Michael and Shola 2017), that reported competitive results with the integer programming model from Ülker and Landa-Silva (2010). The heuristic algorithms developed until now for OSA tackle the problem as whole, and do not incorporate problem decomposition mechanisms. Consequently, the preferences of office occupants are not treated individually, but rather globally by aggregating them into the overall objective function of the problem.

Rather than developing more sophisticated heuristic algorithms, this study proposes a novel approach to solve the OSA problem by using the support of Agent Based Modelling (ABM). This allows the consideration of behavioral aspects and individual preferences of the office occupants. The remainder of the paper provides details about this approach to tackle the OSA problem and evaluates its performance by means of computational experiments on a set of benchmark instances from the literature.

2. BACKGROUND
2.1. Agent Based Modelling (ABM)
Modelling and simulation can be used to reproduce a real world environment with its features, forecast and explore different scenarios, experiment with possible alternative decisions, and set different values for decision variables. In ABM, a system is modelled as a collection of autonomous decision-making entities called agents (Pourdehnad, Maani and Sedehi 2002). Each agent individually assesses its situation and makes decisions on the basis of a set of rules. Individual agents interact with each other and their environment to produce complex collective behavior patterns. ABM is well suited to

modelling systems with heterogeneous, autonomous and proactive actors, such as human-centered systems (Siebers et al. 2007).

ABM has a variety of applications from modelling the behavior of stock market and supply chains to predicting the spread of epidemics and understanding factors that may be responsible for the fall of ancient civilizations. All these make it possible to analyze the effects of changes in a specific system or environment, without affecting the real world during this process (Macal and North 2010).

Within the operations research discipline, agent based approaches have been used to solve problems like: scheduling (Sabar, Montreuil and Frayret 2011), knapsack (Polyakovskiy and M'Hallah 2007), transportation and supply chain planning (Persson et al. 2005). It has been reported that the agent based approaches proved to be competitive with heuristic optimization techniques, one advantage being that the problem can be divided into sub problems, and the work delegated to agents. Thus, when the size of the problem is large and the timescale is short, the decomposition nature of ABM can help to reduce the computational time needed to produce competitive solutions to the problem in hand (Barbati, Bruno and Genovese 2012). However, if the communication between agents has a high cost and if the high quality of solutions is a priority, then classical optimization techniques are preferred. According to Persson et al. (2005), who applied both ABM and classical optimization techniques to a production and transportation supply chain problem, a hybrid approach proved to be beneficial. They added optimization to agents during the decision making process, and obtained better results than having each method applied by its own. The performance of a hybrid system was also reported as highly satisfactory in a study by Daniels and Parsons (2006). They used agents to improve the population of candidate solutions in a genetic algorithm used to solve the zone-deck allocation of space in a preliminary ship general arrangements design.

According to Polyakovskiy and M'Hallah (2007), the agent based model developed for a knapsack problem, allows the investigation of a larger part of the solution space, leading to high quality solutions. They propose an agent based framework where the agent is characterized by its fitness, behavioral rules and parameters. The framework is then used in the decision making process to assess the potential of each possible action, and choose the one which optimizes the reward.

An interesting case of ABM is the Schelling Segregation Model (Schelling 1971), where, based on a simple rule of neighborhood satisfaction, people/entities of two types are moving on a grid and in time they start to segregate. Each entity is represented by an agent with an attached happiness value. If the percentage of agents of the same type among one's neighbors is lower than a certain threshold value, that agent changes the state to unhappy and moves to a randomly chosen new location. If the state remains happy, then the agent does not move. So, following a rule for changing the state of an agent, after

several state changes, the agents exhibit patterns, order and structure in their behavior.

Starting from the principles of the Schelling Segregation Model and other examples of ABM for combinatorial optimization problems, this paper proposes an ABM approach for solving the OSA problem, where agents have an internal decision making process based on heuristics.

2.1.1. The Office Space Allocation Problem

The office space allocation problem used in this study was defined initially by Landa-Silva (2003) and updated later by Ülker (2013). This is a minimization combinatorial optimization problem that is highly constrained. In this problem there is a set of rooms – representing the space available for the allocation process, and a set of entities – representing people or resources that must be allocated to the rooms. Each room has a given size and each entity requires a given amount of space. There is also a set of constraints, which represent the requirements that should be met when creating an allocation. The constraints establish hard or soft restrictions on proximity and spatial relations among the entities and rooms. There are 9 types of such constraints: allocation, non-allocation, capacity, same-room, not-same-room, not-sharing, adjacency, nearby, away-from. The full definition and the penalty weights associated to each in the case of non-satisfaction are given in (Ülker 2013). A solution to the problem requires that each entity is allocated to a room. The quality of a solution is evaluated in terms of space misuse penalty (SMP in equation 1) and soft constraints penalty (SCP in equation 2). The aim is to minimize the total penalty (F in equation 3) associated with a solution. The usage of each room is calculated according to the entities allocated to the room. Overuse of space is less desirable hence penalized twice compared to underuse of space, as shown in equation 1. The violation of each constraint contributes with the associated weight towards the overall penalty for that solution.

$$SMP = \sum_{i=1}^{|R|} \max(cap(r_i) - usg(r_i), 2 \times (usg(r_i) - cap(r_i))) \quad (1)$$

$$SCP = \sum_{i=1}^{|C|} (w(c_i) \times v(c_i)) \quad (2)$$

$$F = SMP + SCP \quad (3)$$

In equations (1)-(3), $cap(r_i)$ is the capacity of room r_i, $usg(r_i)$ is the actual usage of room r_i, $v(c_i)$ is 1 if the constraint c_i is violated and 0 if it is satisfied, $w(c_i)$ is the weight of the soft constraint c_i, $|R|$ is the number of rooms in the problem, and $|C|$ is the number of constraints in the problem.

The data sets used in this paper were proposed by Ülker and Landa-Silva (2011). These problem instances vary on two dimensions: the number of constraints, and the space misused expected, all having a constant number of entities and rooms. One data set corresponds to a problem instance and it contains a list of entities (with id, group and space required), a list of rooms (with id, floor, and a

set of neighbors of the room) and a list of constraints (with id, type, subject and target – defined depending on the type of the constraint). These data sets are called SVe150 and PNe150 and were generated based on four parameters: S, V, P and N. For the parameters S, P and N, variations are made to adjust the size of the rooms as follows. S represents the slack space rate expected (general misuse of space), P represents a positive slack amount expected (underuse) and N represents a negative slack amount expected (overuse). The V parameter expresses the violation rate expected in regards to the constraints. The data sets selected for conducting experiments in this paper are: s000v000 - low space misuse and low constraint violation, s100v000 - high space misuse and low constraint violation, s000v100 - low space misuse and high constraint violation, s100v100 - high space misuse and high constraints violation, p025n000 - expect high underuse, p000n025 - expect high overuse.

3. METHODOLOGY
3.1. ABM for OSA
The agent based model developed here for OSA is a synchronous simulation model, and has the following components: entities, rooms, constraints and the environment. The *environment* is the space where all the agents are located and takes care of their coordination. It also keeps track of the global objective value for the current solution to the problem, using the information received from the rooms (about space misused) and from the constraints (about their violation). However, the environment does not have a mechanism to minimize this global objective, but rather it monitors the objective value and the solution, making the calculations available for agents on request. The responsibility for minimizing the objective function value is distributed to the agents of the system. The rooms and the constraints are represented as passive agents (objects). Entities (people) are represented as active agents (entities from OSA problem definition). From this point onwards in this paper, active agents are referred to as *agents* and passive agents as *objects*.

Being a synchronous model, all agents move simultaneously, evaluating possible rooms for themselves. The system then gathers all the individual allocations of agents to rooms and builds the overall solution for the problem. Because of these mechanisms, this approach can be seen as distributed optimization. The overall evaluation function is split based on constraints. Then, some components of that evaluation function are delegated to each individual agent.

Figure 1 presents the conceptual model of the system, showing the interaction between the different components. Agents, through their behavior, search and build a solution for the problem. They have two possible states, *satisfied* and *not satisfied* and they move between them based on an internal evaluation process. This will be detailed in the next subsection. During their internal evaluation process, the agents request information from the rooms and from the constraints. From the constraints,

the agents get a list of those directly involving them and in turn affect their satisfaction score. From the rooms, the agents get information about occupancy of the rooms and the neighborhood relationships between rooms defined by the problem instance.
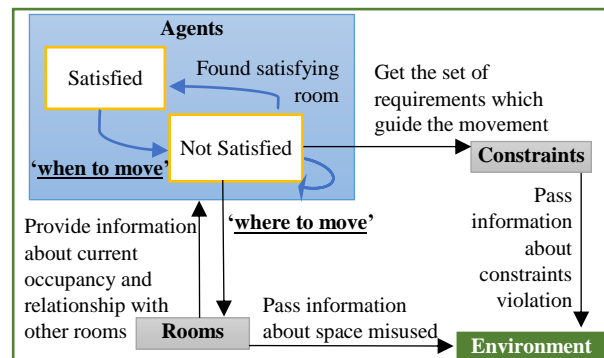

Figure 1: Agent Based Model for the Office Space Allocation Problem.

3.2. Agents Structure
As mentioned in the previous section, the agents proposed in this model represent the entities in an instance of the OSA problem. During their search process, agents move between rooms and analyze their own satisfaction state, choosing 'when' and 'where' to change their allocation. The state of an agent can be either *satisfied* or *not satisfied*. Four strategies are proposed for agents to decide 'when to move':

- Percentage Based (PB): The agent has a current penalty given by the constraints which are associated with it and are violated in the current position (calculations of this penalty are detailed in Algorithm 1). If this penalty is more than 30% of the total possible penalty, then the agent moves. The total possible penalty is calculated as a pessimistic scenario, when all the constraints associated with the agent are violated, thus is the maximum penalty that the agent can have.

- Always Move (AM): All the agents are moving at every step of the simulation.

- Highest Penalised (HP): The agent with a current penalty larger than the average penalty for all agents in that particular moment, are moving to a different location. This implies that every step approximately half of the agents are moving to a different room.

- Random Chance (RC): Each agent has a chance of 1 in 6 to move to a different location. This chance is based on the 'dice rolling' probability.

Depending on the outcome of the strategy applied, an agent makes the first decision from its internal 'thinking process', namely it defines its satisfaction state. If this process results in being *not satisfied* and therefore having to move to a different room, the agent goes to the second stage, and it analyses 'where to move'. This means that the agent searches for a room which will fulfil its

requirements and get back to a *satisfied* state. If a room is not found, or it does not improve its current position, then the agent stays in the current room returning to a *not satisfied* state.

Algorithm 1 Penalty calculation for an agent

agent.penalty = 0
for (constraint c : agent.associatedConstraints)
    switch (c.type)
        if(c is violated) //defined based on c.type
            agent.penalty += c.weight
        end if
agent.penalty += agent.room.misusedPenalty /
                 room.noOfAgentsInRoom
return agents.penalty

There are four strategies proposed for the 'where to move' decision. These are heuristic based approaches, and vary from random to greedier ones:

- Rnd: The choice of the new room for the agent is picked at random.

- BestPotential: The agent evaluates the potential of each available room and selects the one which returns the smallest penalty in the scenario of moving there. The potential of a penalty is relative to other agents moving in the same time, thus the evaluation may not be the same before and after the move is done.

- AllConstr: The agent is trying to find a room which will not violate its associated constraints. Instead of analysing all the rooms and calculating a penalty, this approach is narrowing down the list of rooms based on the constraints. If there is no room satisfying all constraints, the agent goes back and tries to satisfy most of the constraints.

- OneByOne: At every simulation step, the agent picks at random currently violated constraint and finds a room which will satisfy it in the scenario of moving there.

The simulation based ABM executes the search process in steps. At each step, all the agents act simultaneously. Before the step, agents calculate their satisfaction, based on one of the four strategies mentioned. Then, they choose the room where to move, again using one of the strategies mentioned. On the actual step, the agents are essentially executing the move, so they change their allocation to a new room. The entire process is represented in Algorithm 2.

Algorithm 2 ABM simulation process

On start-up:
    initialize the agents from external database
    build the neighborhood links between rooms
    assign the constraints to the agents (entities)
On before step:
    agents.satisfied = agents.decide('when to move')

---

    if (agents.satisfied = false)
        newRoom = agents.choose('where to move')
On step:
    if (agents.satisfied = false)
        agents.room = newRoom
On after step:
    rooms.misusedPenalty -> update (with new occupancy)
    agents.totalPenalty -> update (in the new allocation)
    environment.fitnessFunction ->update (from agents)

The ABM for OSA described above is relatively simple but is it designed to serve as a baseline methodology to investigate the suitability of tackling OSA through a distributed optimization paradigm instead of a typical centralized optimization or heuristic approach. This investigation will hopefully inform the development of more elaborate behavior in the agents and conditions in the environment.

4. EXPERIMENTAL RESULTS

There are 16 behaviors which can be exhibited by an agent, combining the two decision mechanisms of 'when' and 'where' to move. This resulted in 16 different neighborhood exploration strategies that are evaluated. The simulation was run with each algorithm for 5000 steps, and 50 replications on each data set. The number of steps was set to 5000, because preliminary experiments showed that after this point all the agents' strategies did not continue to improve the overall solution for the problem. The results presented in Table 1 correspond to the s000v000 problem instance. The same rankings of the algorithms was also observed in the other problem instances mentioned in section 2.1.1 above. For this reason, details of the experimental results for those other instances are omitted here but are available for further analysis.

Table 1: Neighbourhood exploration strategies built in the ABM for OSA on the s000v000 problem instance

ABM Strategy	Diversity	Min	Mean	Max
PB-Rnd	50.08	2878.00	3181.68	3553.50
PB-BestPotential	0	3971.50	3971.50	3971.50
PB-AllConstr	30.96	1969.00	2432.36	2808.00
PB-OneByOne	33.36	1691.50	2247.53	2710.00
AM-Rnd	70.78	2890.00	3591.48	4076.00
AM-BestPotential	0	8238.50	8238.50	8238.50
AM-AllConstr	34.69	1853.50	2602.69	3150.00
AM-OneByOne	32.94	1835.00	2499.79	3083.50
HP-Rnd	52.25	2942.50	3444.55	3871.50
HP-BestPotential	0	4210.00	4210.00	4210.00
HP-AllConstr	27.33	1889.50	2465.24	2991.00
HP-OneByOne	31.24	1751.00	2279.42	2761.50
RC-Rnd	66.31	2347.50	2599.97	2952.50
RC-BestPotential	41.54	3053.00	3502.37	4265.50
RC-AllConstr	21.29	1536.00	1899.82	2318.00
RC-OneByOne	21.40	1346.00	1751.50	2069.00

Table 1 contains the min (best), mean and max (worst) evaluation function values for the best solutions produced by each combination of agents' strategies. The diversity value represents the degree of difference in the actual structure of best solutions produced. A detailed description of how the diversity is calculated can be found in the next section.
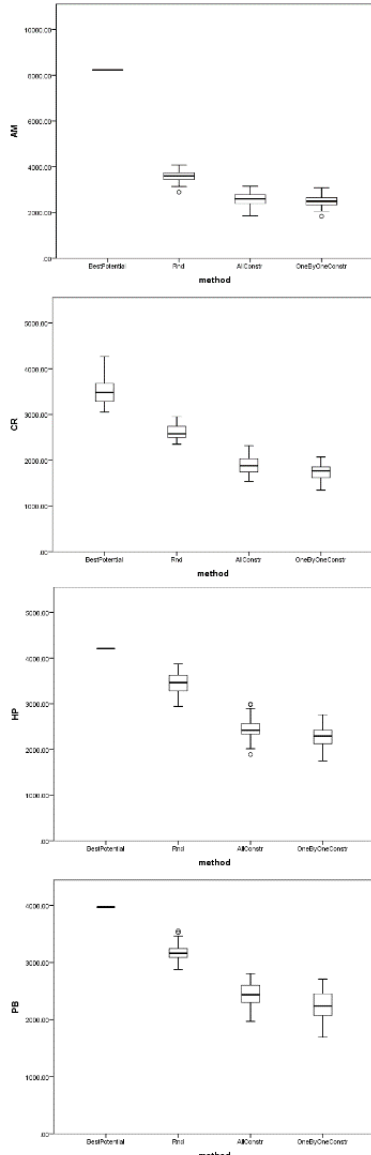

Figure 2: Boxplots of 'where to move' strategies in all the 'when to move' cases.

The results presented in Table 1 show that, in general, the RC strategy performs best amongst 'when to move' strategies, and OneByOne approach performs best amongst 'where to move' strategies. This can also be seen in the boxplots from Figure 2. The rankings of the 'where to move' strategies are maintained throughout all the 4 'when to move' cases. From best to worse, the ranking of the algorithms is: OneByOne, AllConstr, Rnd and BestPotential. Contrary to what it name suggests, the BestPotential approach performs very poor, because it is heavily relying on the penalty evaluation done 'on before step', which does not correspond with the actual penalty

seen 'on after step'. RC, although being of a random nature, it is the 'when to move' strategy that makes the least amount of agents to move simultaneously, thus the least disruption in the environment from one step to another. Therefore, RC is the best performing strategy because the penalty evaluations made by an agent are less likely to change from 'on before step' to 'on after step'.

4.1. Diversity in the solutions
The diversity in the solutions produced by one algorithm is represented in this paper as the degree of differences in the structure of the best solutions returned throughout all the repetitions of the experiments. This is calculated using equation (4) taken from (Landa-Silva 2003). The diversity ranges from 0 to 100, 0 meaning that all the solutions compared are exactly the same and 100 meaning that all the solutions compared do not have any one element in common. A solution of the office space allocation problem is represented as an array, where the index represents the entity (agent) id and the value in the array represents the room id to which that agent is allocated (see Figure 3). Having 50 such arrays (solutions), from the 50 replications of an experiment, the diversity is represented by the agent being allocated to different rooms in those solutions. So, if the value in the solution array corresponding to and agent is different from the value in the same position in another solution array, then the two solutions have a difference between them in that position. $D(j)$ is the number of unique values in the jth position of the solution, p is the number of solutions compared, and n is the length of the solution. Figure 4 illustrates the use of this equation for $p = 5$ solutions and $n = 7$ agents.

$$V(p) = \frac{\sum_{j=1}^{n} \frac{D(j)-1}{p-1}}{n} \times 100 \qquad (4)$$

e_1	e_2	e_3	e_4	e_5	e_6	e_7	e_8	...	$e_{|E|}$
r_5	r_7	r_1	r_9	r_2	r_5	r_3	r_8	...	r_6

Figure 3: Representation of a solution for OSA.

A	A	A	A	A	A	A
A	A	B	B	A	B	B
A	B	B	C	B	C	C
A	B	B	C	B	D	D
A	B	B	C	C	D	E
$D(j)$	1	2	2	3	3	4	5
$(D(j)-1)/(p-1)$	0	0.25	0.25	0.50	0.50	0.75	1

$V(p) = (3.25 / 7) \times 100 = 46.42 \%$

Figure 4: Example of calculation of the diversity in solutions.

Looking at the diversity column in the results presented in the previous section, it can be observed that the Rnd strategy scores the highest. It is expected to have a higher diversity in the solutions, when rooms are chosen at random, and therefore the agents explore more. On the other hand, BestPotential strategy, being a greedy one, almost in all cases chooses the exact same rooms, and

therefore producing the same solutions regardless of the number of the experimental repetitions. In general, the RC strategy also scores lower in terms of diversity, because a smaller number of agents move at a time, thus creating a smaller disturbance in the solutions.

5. COMPARISON
5.1. Heuristics for Neighborhood Exploration
For comparison purposes, the ABM strategies for neighborhood exploration are evaluated against known heuristic algorithms used for neighborhood exploration on the OSA problem. They were originally proposed by Landa-Silva (2003) and applied to the OSA data sets from three UK universities. This paper presents a replication of those heuristics and two additional ones, implemented for this study, all tested on the new generated data sets by Ülker and Landa-Silva (2013). These heuristics are based on the main idea of the relocation of an entity to a different room. The methods of selecting the entity to relocate vary from completely random to greedier ones:

- RelocateRndRnd: Selects an entity at random and relocates it to another random room;
- RelocateRndBestRnd: Selects an entity at random and relocates it to the best room, in terms of evaluation function value, out of a randomly selected subset of rooms;
- RelocateRndBestAll: Selects an entity at random and relocates it to the best room out of all the available rooms;
- RelocatePntyBestRnd: Selects the entity with the highest current penalty associated with it and relocates it to the best room out of a randomly selected subset of rooms;
- RelocatePntyBestAll: Selects the entity with the highest current penalty and relocates it to the best room out of all the available rooms.

These heuristics are tested separately using an 'only improving' local search algorithm (see Algorithm 3). The reason for applying each neighborhood exploration strategy separately, and using a simple algorithm, is to analyze the individual behavior and identify the strengths and weaknesses, without having external influencing factors.

Algorithm 3 Local search

generate initial solution X
repeat
    apply neighborhood heuristic (select entity and room
     for the move)
    apply the relocation move to X to produce X'
    perform acceptance test of X'
    if (X' is better than X)
        X = X'
until termination criteria

Each neighborhood exploration heuristic was run until no improvement was found for a number of iterations. Each experiment was replicated 50 times as it was the case for the ABM simulation. The results are included in Table 2.

Table 2: Heuristic neighborhood exploration algorithms for OSA on the s000v000 problem instance

Heuristic	Diversity	Min	Mean	Max
RndRnd	52.34	1558.00	1983.27	2439.00
RndBestRnd	52.67	1446.00	1930.56	2361.00
RndBestAll	50.89	1364.50	1861.27	2383.00
PntyBestRnd	51.77	1785.50	2348.92	2818.00
PntyBestAll	52.60	1493.00	2304.80	2800.50

The differences between the heuristic neighborhood exploration algorithms seen in the boxplots (Figure 5) are not major. However, they do show that RndRnd, RndBestRnd and RndBestAll are overall better than the PntyBestRnd and PntyBestAll. Performing ANOVA statistical analysis confirmed that the RndBestAll is the best performing algorithm when compared with the rest of the heuristics, having a significance difference p value of less than 0.005.
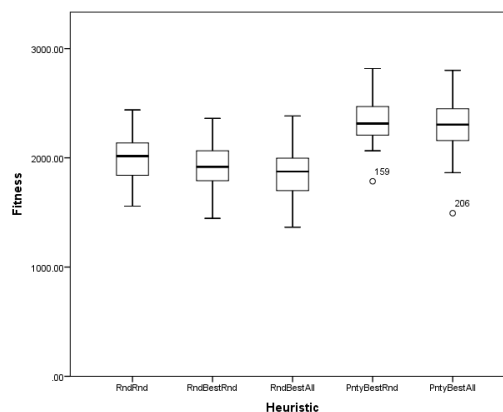

Figure 5: Boxplots for all the heuristic neighborhood exploration algorithms on s000v000.

5.2. Comparison of the results
The two winning neighborhood exploration strategies, namely the heuristic RndBestAll and the ABM CR-OneByOne, are compared with each other on all the 6 problem instances selected: s000v000, s000,v100, s100v000, s100v100, p025n000, and p000n025. The results are included in Table 3. For all the instances except p025n000, there is statistical significance between the two methods. CR-OneByOne is the one which produces better results for almost all the instances in terms of evaluation function value of a solution for OSA. The exceptions are for the s100v100 and p025n000 instances. For p025n000 the statistical analysis does not show significant difference between the two algorithms. However, for s100v100 the difference is statistically significant, RndBestAll being the better one. The s100v100 problem instance is expected to have high space misuse and high constraints violation. This might

suggest that the current ABM simulation for OSA is not coping well with high expected penalty, both from constraints and from space misused. However, this cannot be generalized by looking at only one instance of this type for the problem. Further analysis has to be made in order to confirm this conclusion.

In terms of the diversity of the solutions produced by the two algorithms, RndBestAll has a higher score (50-55%), while CR-OneByOne has a lower one (20-30%). The ABM CR-OneByOne produces less diversity in the solutions because the agents have the option of not moving if they do not find a promising better room than the one they already are allocated to, hence not exploring more rooms.

Table 3: Comparison of RndBestAll and CR-OneByOne algorithms for OSA on the s000v000, s000_v100, s100v000, s100v100, p025n000 and p000n025 problem instances

Algorithm	Diversity	Min	Mean	Max
p000n025				
CR-OneByOne	21.43	1541.80	1901.66	2291.20
RndBestAll	52.15	1698.00	2107.18	2662.20
p025n000				
CR-OneByOne	23.95	1496.00	1938.04	2359.10
RndBestAll	51.54	1418.60	1889.23	2339.30
s000v000				
CR-OneByOne	21.40	1346.00	1751.50	2069.00
RndBestAll	50.89	1364.50	1861.27	2383.00
s000v100				
CR-OneByOne	25.42	1539.00	2035.58	2522.50
RndBestAll	51.21	1723.50	2103.48	2503.00
s100v000				
CR-OneByOne	17.61	1536.80	1913.06	2314.60
RndBestAll	54.32	1560.90	2023.64	2498.20
s100v100				
CR-OneByOne	27.31	1810.70	2282.53	2564.40
RndBestAll	54.11	1653.10	2162.81	2606.90

The performance of the neighborhood exploration strategies is given by the overall value of the objective function. However, for a better understanding of the strengths and weaknesses of the approaches used to solve the OSA problem, the objective function values obtained were split by constraints and space misuse penalty. As it can be seen in Figure 6 and Figure 7, the ABM CR-OneByOne strategy is optimizing better the satisfaction of constraints, having less violation than the RndBestAll heuristic. On the other hand, the RndBestAll strategy is coping better with the space misuse, reporting lower values for this component of the objective function. The agents built in the simulation model do not have mechanisms to cope with space misuse, so there is potential for improvement in this direction.
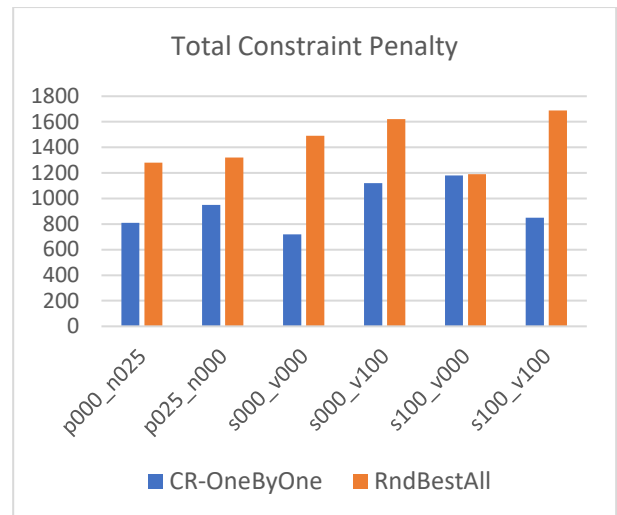

Figure 6: Constraints penalty obtained by the ABM and heuristic neighbourhood strategies for all the instances.
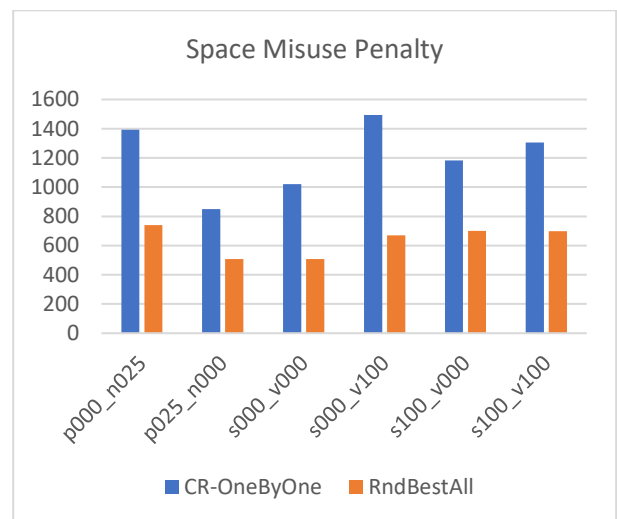
Figure 7: Space misuse penalty obtained by the ABM and heuristic neighbourhood strategies for all the instances.

Going further and splitting the total constraint penalty by each of the individual constraints, it is observed that CR-OneByOne get the highest penalty from 'nearby', 'not sharing' and 'same room' constraints (see Figure 8). The heuristic for neighbourhood exploration, RndBestAll, gets the highest penalty from 'nearby', 'allocation' and 'same room' (see Figure 9).

From the analysis, the overall performance of the strategies compared in this paper does not seem to depend much on the problem instance. The constraint penalty (total or split by individual constraints) and space misuse penalty keep their proportions across all the instances.

Figure 8: Individual constraint penalty obtained by CR-OneByOne for all the instances.

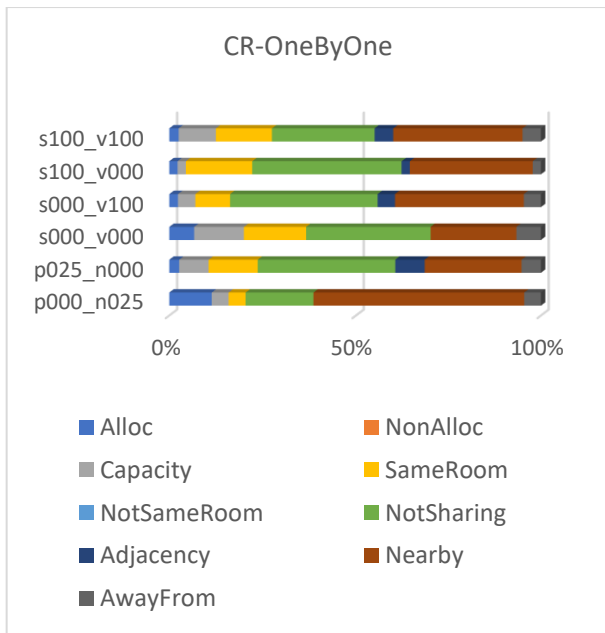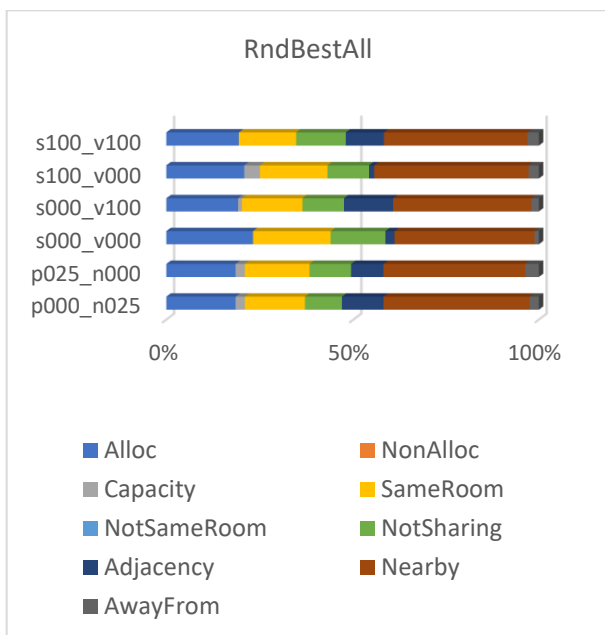Figure 9: Individual constraint penalty obtained by RndBestAll for all the instances.

6. CONCLUSION
6.1. Discussion

A key factor which influences the performance of the behaviors in the proposed ABM is the fact that the model is implemented synchronously. This means that agents move in steps, and at the same time with others, as described in this paper. So the environment constantly changes, and the calculations that an agent does when deciding 'where to move', might be completely wrong, because they depend on other agents and their locations too. Thus, when one moves, it can negatively influence the decisions which were already taken by another agent.

The BestPotential strategy is the most appropriate example in this case, when the synchronous nature of the system influences a moving strategy to the point where it makes it become the worst performing strategy. OneByOne mechanism is the least affected by the synchronous nature of the system, and in consequence is the best performing algorithm from ABM.

From the 'when to move' strategies, the RC performs better because it is less influenced by the fact that the environment changes. On the other and, the AM strategy is among the worst in terms of performance, because the calculation of potential penalty does not match the actual penalty once the move is made.

A solution to this problem would be to create an asynchronous system or to include communication mechanisms between agents. This way agents can still follow their individual goal, but also collaborate with each other in taking decisions and coordinate their movement when they are involved in the same constraints. The results in the previous section about the individual contribution of the different types of constraints to the overall penalty from the objective function, indicate that the ABM can be further improved to better cope with the 'nearby', 'not sharing' and 'same room' constraints. This is a promising direction to further develop the ABM in the future.

Regarding the heuristics, it was seen that PntyBestRnd and PntyBestAll are not performing better than the rest of the methods, although they are always trying to move the highest penalized entity and find a better allocation for it. This is because these heuristics do not explore too much the search space and get very easily trapped in a local optima. The heuristics considered here move from a solution to another by changing only one entity from a current allocation to another, limiting the neighborhood exploration, which also influences the performance of the algorithms.

A future direction for this study is to analyze all the other available instances for the problem, and see if the performance of the agent based model is still comparable to the neighborhood search heuristics. A couple of improvements to the existing agent based model can also be made. For example, adding a learning mechanism to the agents, and including communication between agents as mentioned previously. Although the agents in this model are working and following an individual goal, they have the potential of improving their movement strategies by collaborating with each other. The constraints, due to their nature, usually involve more than one entity (agent) in their formulation. Therefore, negotiation mechanisms between the agents involved in the same constraint will make them work towards the same goal, and possibly improving on the results presented in this paper.

6.2. Summary

This paper presented an agent based simulation model (ABM) for the OSA problem that overall performs better than or as good as the heuristics used as neighborhood exploration in the literature. The model is based on the

individual agents' behavior and strategies, which aim to improve their current position. This approach allowed for problem decomposition to be achieved, which is also the first time this was done for the OSA problem.

There is room for improvement in the model presented, and the fact that it already produces results comparable with existing methods, suggests that it is a promising direction for future research in this problem.

OSA can be associated with a general assignment problem, it has similarities with bin packing, container loading and general resource allocation. It has many more types of constraints than these well-known problems, which is making it more difficult to solve. However, the model used for solving OSA can be also applied to these other similar assignment problems.

ABM simulation proves to be a good methodology for solving the office space allocation problem, thus making this a valuable contribution to the field, because the same principles are easy to adapt to other real world assignment problems.

REFERENCES

Adewumi, A. O., and Ali, M. M., 2010. A multi-level genetic algorithm for a multi-stage space allocation problem. Mathematical and Computer Modelling, 51(1-2), 109-126.

Awadallah, M. A., Khader, A. T., Al-Betar, M. A., and Woon, P. C., 2012. Office-space-allocation problem using harmony search algorithm. In International Conference on Neural Information Processing (pp. 365-374). Springer, Berlin, Heidelberg.

Barbati, M., Bruno, G., and Genovese, A., 2012. Applications of agent-based models for optimization problems: A literature review. Expert Systems with Applications, 39(5), 6020-6028.

Bolaji, A. L. A., Michael, I., and Shola, P. B., 2017. Optimization of Office-Space Allocation Problem Using Artificial Bee Colony Algorithm. In International Conference in Swarm Intelligence (pp. 337-346). Springer, Cham.

Castillo, F., Riff, M. C., and Montero, E., 2016. New Bounds for Office Space Allocation using Tabu Search. In Proceedings of the 2016 on Genetic and Evolutionary Computation Conference (pp. 869-876). ACM.

Daniels, A., and Parsons, M. G., 2006. An agent based approach to space allocation in general arrangements. Proceedings of the 9th IMDC, Ann Arbor, MI.

Kincaid, R., Gates, R., and Gage, R., 2007. Space allocation optimization at nasa langley research center. In Proceedings of the Seventh Metaheuristics International Conference, Montreal, Canada.

Landa Silva, J. D., 2003. Metaheuristic and multiobjective approaches for space allocation. Thesis (PhD). The University of Nottingham.

Landa-Silva, D., and Burke, E. K., 2007. Asynchronous cooperative local search for the office-space-allocation problem. INFORMS Journal on Computing, 19(4), 575-587.

Lopes, R., and Girimonte, D., 2010. The office-space-allocation problem in strongly hierarchized organizations. In European Conference on Evolutionary Computation in Combinatorial Optimization (pp. 143-153). Springer, Berlin, Heidelberg.

Macal, C. M., and North, M. J., 2010. Tutorial on agent-based modelling and simulation. Journal of simulation, 4(3), 151-162.

Persson, J. A., Davidsson, P., Johansson, S. J., and Wernstedt, F., 2005. Combining agent-based approaches and classical optimization techniques. In Third European Workshop on Multi-Agent Systems.

Polyakovsky, S., and M'Hallah, R., 2007. An agent-based approach to knapsack optimization problems. In International Conference on Industrial, Engineering and Other Applications of Applied Intelligent Systems (pp. 1098-1107). Springer, Berlin, Heidelberg.

Pourdehnad, J., Maani, K. and Sedehi, H., 2002. System dynamics and intelligent agent-based simulation: where is the synergy. In Proceedings of the 20 International Conference of the System Dynamics Society.

Sabar, M., Montreuil, B., & Frayret, J. M., 2009. A multi-agent-based approach for personnel scheduling in assembly centers. Engineering Applications of Artificial Intelligence, 22(7), 1080-1088.

Schelling, T. C., 1971. Dynamic models of segregation. Journal of mathematical sociology, 1(2), 143-186.

Siebers PO, Aickelin U, Celia H and and Clegg C, 2007. A Multi-Agent Simulation of Retail Management Practices. In: Proceedings of the 2007 Summer Computer Simulation Conference (pp. 959-966), San Diego, CA, USA.

Trung, N. T., Tuan, T. N., and Anh, D. T., 2009. Informed simulated annealing for optimizing dorm room assignments. In Intelligent Information and Database Systems, 2009. ACIIDS 2009. First Asian Conference on (pp. 265-270). IEEE.

Ülker, Ö., and Landa-Silva, D., 2010. A 0/1 integer programming model for the office space allocation problem. Electronic Notes in Discrete Mathematics, 36, 575-582.

Ülker, Ö., and Landa-Silva, D., 2011. Designing difficult office space allocation problem instances with mathematical programming. In International Symposium on Experimental Algorithms (pp. 280-291). Springer, Berlin, Heidelberg.

Ülker, Ö., and Landa-Silva, D., 2012. Evolutionary local search for solving the office space allocation problem. In Evolutionary Computation (CEC), 2012 IEEE Congress on (pp. 1-8). IEEE.

Ülker, Ö., 2013. Office space allocation by using mathematical programming and meta-heuristics. Thesis (PhD). The University of Nottingham.

AUTHORS BIOGRAPHY

Alexandra Cristina Dediu is a PhD student from the Automated Research Optimization and Planning (ASAP) Research Group, in the School of Computer Science, University of Nottingham, UK. Her main research interests are in the optimization of problems related to resource allocation, especially when solutions can improve the businesses processes and facilitate management operations.

Dr Dario Landa-Silva is an Associate Professor in the School of Computer Science at the University of Nottingham in the UK. His research interests are in the interface between computer science, operations research and artificial intelligence for the application of modeling, search and optimization techniques to underpin the development of intelligent decision support systems across a range of real-world applications, particularly in logistic and operational scenarios. More recently, he is also conducting research on the interplay between optimization and other methodologies such as machine learning, computer simulation, data science and human computation. He has over 95 scientific publications in refereed journals, edited books, and proceedings of international conferences and workshops.

Dr Peer-Olaf Siebers is an Assistant Professor at the School of Computer Science, University of Nottingham, UK. His main research interest is the application of computer simulation to study human-centric complex adaptive systems. He is a strong advocate of Object Oriented Agent-Based Social Simulation. This is a novel and highly interdisciplinary research field, involving disciplines like Social Science, Economics, Psychology, Operations Research, Geography, and Computer Science. His current research focusses on Urban Sustainability and he is a co-investigator in several related projects and a member of the university's "Sustainable and Resilient Cities" Research Priority Area management team.

ULTRA-WIDEBAND RADIO-BEAM DIRECTION FINDER BASED ON MICROWAVE PHOTONICS AND ALL-OPTICAL PROCESSING

M.E. Belkin, T.N. Bakhvalova, I.V. Gladyshev, and A.S. Sigov

MIREA - Russian Technological University, Scientific and Technological Center "Integrated Microwave Photonics", Moscow, Russian Federation

belkin@mirea.ru

ABSTRACT

We propose an upgrading design approach to an ultra-wideband radio-beam direction finder based on microwave photonics and all-optical processing. The validity and accuracy of its operation principle are analyzed in detail and optimized by the simulation using a special photonic computer-aided design tool VPIphotonics Design Suite. As a result of the calculations it was obtained that the dynamic range of the measurement can exceed 10 dB even at a comparatively low power of the laser emitter and that accuracy at the level of units of degrees is provided without problems using the simplest method of determining the direction of arrival by scanning the delay in the optical path.

Keywords: microwave photonics, radio-beam direction finder, computer-aided design

1. INTRODUCTION

One of the most important scientific and technological breakthroughs that occurred in the current decade in the fields of applied physics, microelectronics and radio engineering is the widespread intervention of microwave photonics technology (Capmany, Li, and Lim 2013). The key industry areas for its implementation are telecommunications (Waterhouse and Novak 2015), radar and electronic-warfare means (Ng 2015), and metrology (Zou, Lu, and Pan 2016; Pan and Yao 2017). For instance, in the latter area, superior photonics-based methods and approaches related to the traditional measuring techniques in microwave (MW) band are currently demonstrated possessing accuracy, resolution and size, weight and power (SWAP) characteristics that may not be achievable even using state-of-the-art electronics. In general, photonics-based MW measurements are able to share within two groups including the measurements of the inherent parameters of a MW waveform such as power, phase, phase noise, instantaneous frequency, and spectrum, or functionality of some active object, for example its position, travel speed, as well as time-difference-of-arrival (TDOA) and angle-of-arrival (AOA) or direction-of-arrival (DOA) of its MW beaming. Accurate knowledge of the beam arrival parameters allows one to increase significantly the input signal-to-interference ratio that leads to improved quality and processing speed, which is of particular importance in advanced ultra-wideband telecom systems and electronic-warfare means. In traditional radio devices of a similar purpose, DOA evaluation is usually performed using digital signal processor that at the current level of technology results in limiting operation frequency range and instantaneous bandwidth. The disadvantage can be easily overcome by implementing MWP technology. Following this, to date a number of optical approaches to design of the direction finder have been proposed (Biernacki, Ward, and Nichols 1998; Tonda-Goldstein, Dolfi, and Monsterleet 2006), but they are characterized by a complex schematic with processing in the range of intermediate frequencies, which also limits the possibilities for processing broadband MW signals.

Some years ago, a simple ultra-wideband technique to determine simultaneously TDOA and AOA using all-optical processing, was presented and verified by the theory and proof-of-concept experiment (Zou, Li, and Pan 2012). The proposed approach is feasible in far-field scenario when the distance between the MW source and measurement system is far enough to support the same AOA for the both antennas. In the scheme, two connected in series electro-optic modulators (EOM) manage the intensity of the optical carrier from continuous-wave (CW) laser by the incoming MW signals, which can be continuous or pulsed. The both EOMs are based on Mach-Zehnder interferometric architecture, are biased at so-called minimum transmission point to suppress the optical carrier, and receive a MW signal with a certain phase shift. In this configuration, after elimination of sideband components through the narrow-band optical filter, the total power at the output will be a function of the phase shift between incident waves of MW band. Thus, by measuring the power at the optical carrier wavelength, the phase shift can be reviewed, leading to the measurement of the TDOA and the AOA. Despite the merits of the concept described in (Zou, Li, and Pan 2012) that was published in physics-grade journal, the layout has been proposed cannot be applied in a realistic project, since it does not contain a clear description of the operation mode of each incoming circuit element, its optimization, and there is no analysis of the measurement error and the sensitivity of the characteristics to the deviation of the key parameters. In addition, the narrow-bandwidth optical

filter used in the scheme will lead to a significant deterioration in the economic characteristics of the device and in the quality of its operation under real conditions. To remedy the above shortcomings, in this paper we propose an upgrading layout of the device whose operation principle is analyzed in detail and optimized by the simulation using a widespread off-the-shelf photonic computer-aided design (CAD) tool VPIphotonics Design Suite (VPIphotonics™).

2. THE LAYOUT AND COMPUTER MODEL OF ALL-OPTICAL-PROCESSING-BASED DIRECTION FINDER

Figure 1 depicts the proposed upgrade of the all-optical-processing-based radio-beam direction finder (AODF) layout. As seen, there are the same optical chain as in (Zou, Li, and Pan 2012) including CW laser, biased at minimum transmission point EOM1 and EOM2, and the tunable delay line located between them. However, instead of an optical bandpass filter, the optical circuit terminates with a narrow-bandwidth photodetector (NBW PD) as optical-electrical converter. As the result, the optical sidebands are automatically removed and the DC electrical voltage through the load of the NBW PD is digitized by the analog-to-digital converter (ADC).
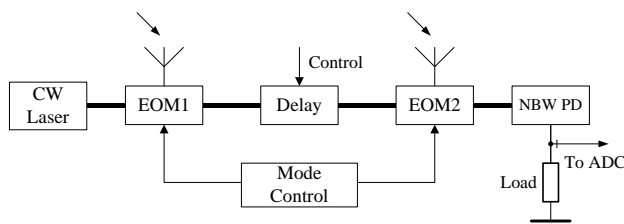

Figure 1. All-optical-processing-based Radio-beam Direction Finder (Thick line means optical connection, thin line means RF connection)

The operation principle of the proposed AODF can be explained with the aid of the phase equation:

$$\frac{\Omega L n}{c} - \frac{\Omega d \sin \theta}{c} = \Delta \phi + 2\pi k \qquad (1)$$

where Ω is the angular frequency of MW signal ($2\pi F$), L is the length of the optical line between output of EOM1 and input of EOM2, n is the group index of the optical line, c is the light velocity in vacuum, d is the distance between two receiving aerials, θ is the AOA of MW beam relative to the antenna's principal axis, $\Delta\phi$ is the phase shift at the output of EAM2, k is the integer that can be clear from the physical parameters of the device under research. From (1) for known F, L, d, and $\Delta\phi$, the AOA as well as the TDOA (τ) at the antenna inputs can be defined:

$$\tau = \frac{d \sin \theta}{c} \qquad (2)$$

The standard analysis taking into account the operations of the EOMs biased in the minimum transmission mode and ideal pin-photodetector (Urick, McKinney, and Williams 2015) allows us to derive the following connection between the photo-voltage V_{PD} at the output of the NBW PD and the phase shift of the MW signal:

$$V_{PD} \propto 2 S_I R_L \left[J_1 \; \beta_1 \; J_1 \; \beta_2 \; \right]^2 \times \left[1 + \cos \; 2\Delta\phi \right] \qquad (3)$$

where S_I is the photodetector's current responsivity (A/W), R_L is the load resistance, $J_1(.)$ is the first-order Bessel function of the first kind, β_1 and β_2 are the modulation indices of EOM1 and EOM2, correspondingly. As it is clear from (3), the value of photo-voltage at the output of NBW PD is a function of the phase shift between two input MW signals.
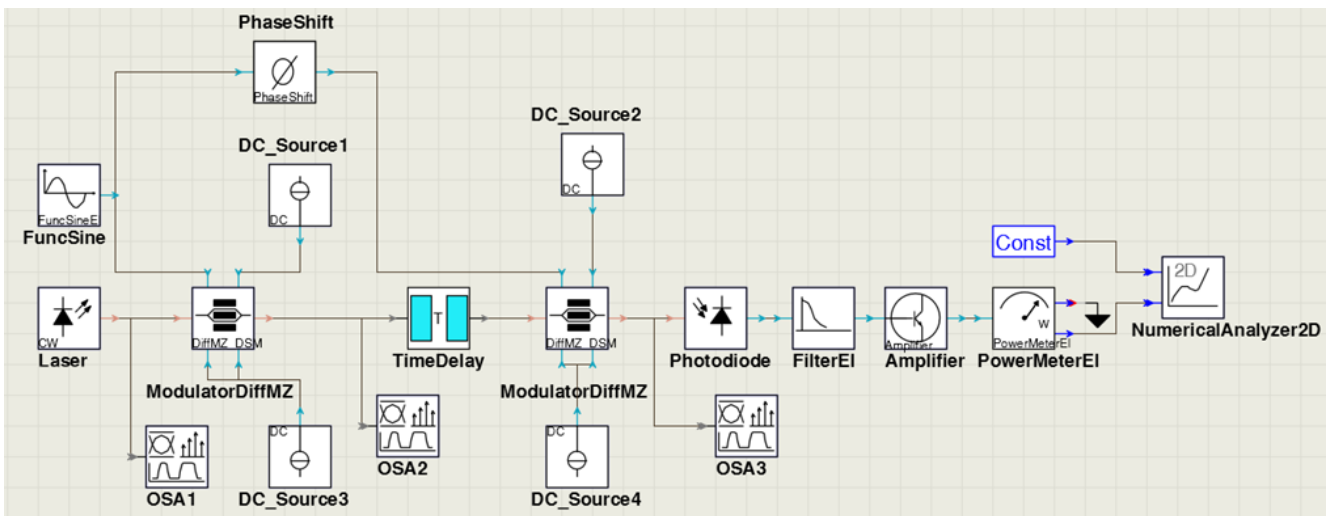

Figure 2. VPIphotonics Design Suite's Testbed for the Following Simulation Experiments

Figure 2 shows VPIphotonics Design Suite's testbed for the simulation experiments that according to Figure 1 consist of the library model of CW laser, two similar models DiffMZ_DSM of EOM with the model of time delay element T between them, the model of a photodiode followed by the electrical low passband filter model FilterEl and amplifier model. Besides, there are some library models to bias, control, and measure the AODF model under research including the models of DC Sources 1-to-4 for biasing the modulators into the minimum transmission point, the model of AC source FuncSine that generates electrical sine waveform for emulating incident MW signal, the Hilbert transform-based model of electrical phase shifter providing with phase difference between the electrical inputs of EOMs. In addition, two kinds of measuring means are included into Figure 2, such as the model of versatile Signal Analyzer SA to display and analyze optical and electrical signals, the model of Electrical Power Meter calculating the power of DC component, and the model of Numerical Analyzer 2D for two-dimensional graphical representation of the data from the Power Meter.

3. SIMULATION EXPERIMENTS

Figure 3 depicts the simulation results of optical spectra at the output of the laser (green) and the first (black) and second (blue) EOMs controlled by MW signals of 5 GHz with electrical phase shifts 0° (Fig. 3a) and 90° (Fig. 3b) respectively.

(a) MW Phase Shift 0°
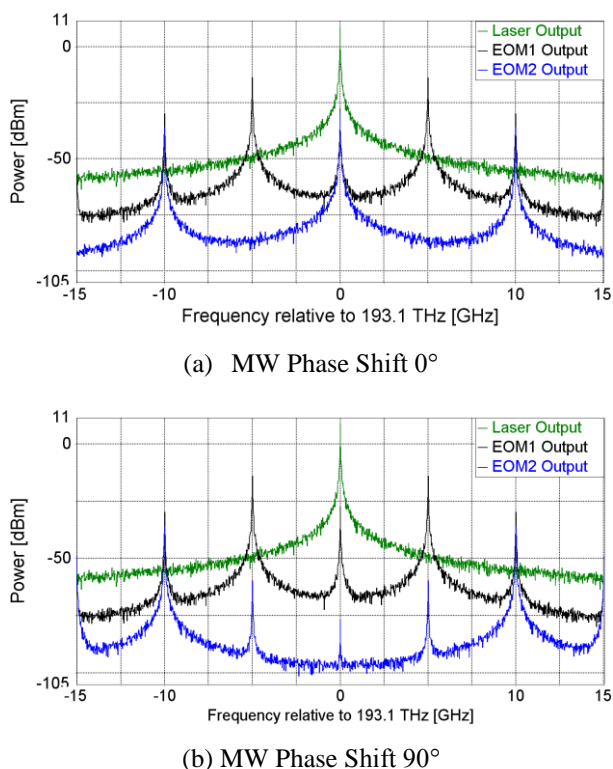

(b) MW Phase Shift 90°

Figure 3. Simulation of Optical Spectra

As one can see from the Figure, thanks to the biasing the modulators to the minimum transmission point, the

optical carrier is successively suppressed by 35 and 45 dB when the phase difference of the input MW signals is 0°, corresponding to the maximum of the output photo-voltage V_{PD} (see Eq. (3)), and by 35 and 90 dB with the phase shift of 90° corresponding to its minimum. This result confirms the dependence of the DC power on the phase difference between two input MW signals predicted in (3). Moreover, more than 100-GHz instantaneous bandwidth of modern EOMs used in the scheme of Figure 1 for all-optical processing validates the ultra-broadbandness of the device that implements the given operation principle.

It follows from Fig. 1, the most acceptable operating principle of the realistic AODF is to determine the DOA and TDOA of the MW beam by adjusting the length (delay time) of the optical delay line between the output of the first EOM and the input of the second one. Figure 4 demonstrates the results of calculating the NBW PD output DC power dependence on the differential time delay (DTD) in the range of 0-100 ps. The following parameters are selected for the simulation: the frequencies of the input MW signal are 5 GHz (a) and 10 GHz (b) that is equal to octave-frequency band; the versions of AOA are 0 (circles), 15 (squares), -30 (triangles), and +30 (stars) degrees; the distance between two receiving aerials d=1.5 cm. The value of the last parameter coincides with half the wavelength at the upper frequency of the range under investigation.
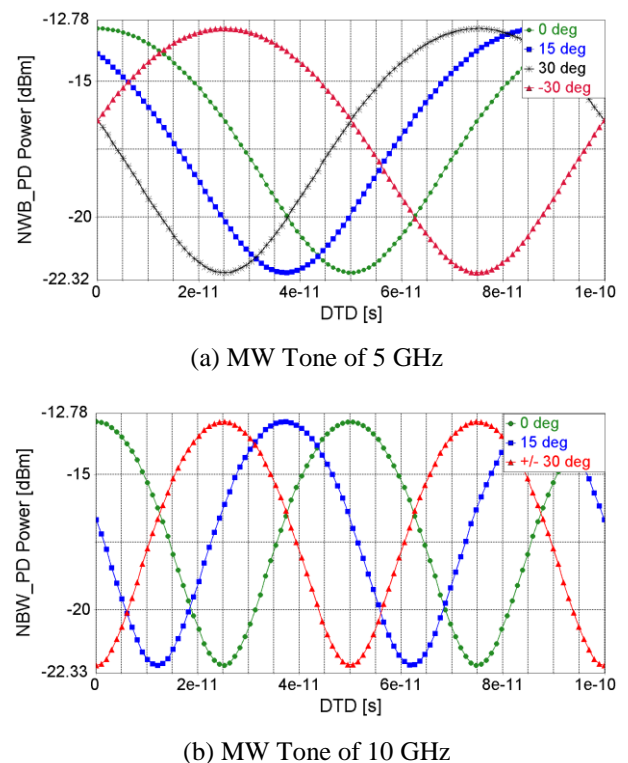

(a) MW Tone of 5 GHz

(b) MW Tone of 10 GHz

Figure 4. Simulation of Time Retarding Characteristics

There are three valued outcomes from Figure 4. The first one is that the adjustment of the time delay significantly affects the position of the maxima and minima in the output power of the photodetector. In particular, when

irradiated with signals of frequency 5 and 10 GHz, the power minima are displaced exactly by 25 ps, regardless of the angle of arrival, which indicates a high accuracy of the device built on the basis of the proposed scheme. The second one is that the maximum and minimum power positions retain their identity even with a twofold change in the frequency of the MW signal, which confirms the above conclusion referred to the ultra-broadbandness of the device under investigation. The third one is that the dynamic range of the measurement can exceed 10 dB even at a comparatively low power of the laser emitter (10 dBm during the simulations) and will expand as it increases.

4. CONCLUSION

We proposed and described an upgrading design approach to ultra-wideband radio-beam direction finder based on microwave photonics and all-optical processing, which is characterized by a very simple implementation scheme, ultra-broadbandness, and high accuracy in determining the direction of arrival of the microwave beam. The validity and accuracy of its operation principle are analyzed in detail and optimized by the simulation using a widespread off-the-shelf photonic computer-aided design tool VPIphotonics Design Suite. As a result of the calculations it was obtained that the dynamic range of the measurement can exceed 10 dB even at a comparatively low power of the laser emitter and that accuracy at the level of units of degrees is provided without problems using the simplest method of determining the direction of arrival by scanning the delay in the optical path. Besides, the shift of maximum and minimum power positions retain their identity even with a twofold change in the frequency of the MW signal, which confirms ultra-broadbandness of the device under investigation. Further work on this topic will be aimed to optimizing the parameters, experimental confirmation of the simulation results and then on the development of the device in the form of a photonic integrated circuit.

REFERENCES

Biernacki P. D., Ward A., Nichols L. T., and Esman R. D., 1998. Microwave phase detection for angle of arrival detection using a 4-channel optical downconverter. Proceedings of International Topical Meeting on Microwave Photonics, pp. 137–140. October 12-14, Princeton (New Jersey, USA).

Capmany J., Li G., Lim C., and Yao J., 2013. Microwave Photonics: Current challenges towards widespread application. Optics Express, 21 (19): 22862-22867.

Ng W., 2015. Photonics for microwave systems and ultra-wideband signal processing. Optics Communications, 373: 1-13.

Pan S. and Yao J., 2017. Photonics-Based Broadband Microwave Measurement. IEEE Journal of Lightwave Technology, 35 (16): 3498-3513.

Tonda-Goldstein S., Dolfi D., Monsterleet A., Formont S., Chazelas J., and Huignard J. P., 2006. Optical signal processing in radar systems. IEEE Transactions on Microwave Theory and Techniques, 54 (2): 847–853.

Urick V.J., McKinney J.D., Williams K.J., 2015. Fundamentals of Microwave Photonics. Hoboken (New Jersey, USA): John Wiley & Sons.

VPIphotonics™. Available from: http://www.vpiphotonics.com/index.php

Waterhouse R. and Novak D., 2015. Realizing 5G. IEEE Microwave Magazine, 16 (8): 84-92.

Zou X., Li W., Pan W., Luo B., Yan L., and Yao J., 2012. Photonic approach to the measurement of time-difference-of-arrival and angle-of-arrival of a microwave signal. Optics Letters, 37 (4): 755-757.

Zou X., Lu B., Pan W., Yan L., Stohr A., and Yao J., 2016. Photonics for microwave measuring. Laser Photonics Review, 10 (5): 711-734.

MODELING MULTI-CORE FIBER-OPTIC WAVEGUIDE

M.E. Belkin[a], V. Golovin[b], Y. Tyschuk[b], and A.S. Sigov[a]

[a] MIREA - Russian Technological University, Scientific and Technological Center "Integrated Microwave Photonics",
Moscow, Russian Federation
[b] Sevastopol State University (SevSU), Sevastopol, Russian Federation

belkin@mirea.ru

ABSTRACT

We propose and demonstrate an equivalent-circuit model of multicore optical fiber waveguide. This model takes into account all the parameters of the single-core fiber-optic model described early with the addition of crosstalk parameter, which is the main issue in the practical application of modern multicore optical fiber. Validity of the proposed model is highlighted by two simulation experiments connected with the transmission of high-speed digital signals in a fiber-optic telecom system and the delay of super-bandwidth microwave-band signals in optical fiber delay line photonic processor. As the result of both experiments, it was found that the critical impact of the crosstalk between the cores occurs at its level over -40 dB, which coincides with the known calculated and experimental data described in the papers of other authors.

Keywords: fiber-optics telecom system, fiber-based delay line photonic processor, multicore optical fiber, computer-aided design

1. INTRODUCTION

It is well known that a throughput feature of the information and communication system (ICS) principally determines its profitability, especially in broadband access networks (Lee and Kang 1996). For today, in the most widely used class of ICS: fiber optic telecom systems (FOTS), two methods of increasing it, called time and wavelength division multiplexing (TDM and WDM, correspondingly) have been implemented. However, the record speeds of commercial digital FOTS up to 400 Gbit/s (Lavigne and Bertran-Pardo 2016) achieved on the basis of a combination of TDM/WDM, do not already satisfy modern social demands (Effenberger 2016). An intriguing candidate for overcoming the throughput limit of a current FOTS is, so called space division multiplexing (SDM) technique using multicore optical fiber (MCOF) (Saitoh and Matsuo 2016). As another promising application, a long-term fiber-based delay-line photonic processor of radio frequency (RF) and microwave signals is considered, which will significantly reduce its form factor (Belkin 2016; Egorova and Belkin 2017).

Recently, we proposed and verified by the simulation experiments using NI AWRDE off-the-shelf software tool a behavior model of single-mode optical fiber feasible for various operating regimes of realistic FOTS (Belkin and Golovin 2018) that is taken into account the key limiting factors of fiber-optic waveguide, for example chromatic dispersion, time retarding, insertion loss, operating temperature dependence. Developing the approach in this paper, we propose and demonstrate an equivalent-circuit model of MCOF waveguide. This model takes into account all the parameters of the single-core one described above with the addition of crosstalk parameter, which is the main issue in the practical application of MCOF (Egorova and Belkin 2017; Fini and Zhu 2011). Validity of the proposed model is highlighted by two simulation experiments connected with the transmission of high-speed digital signals and the delay of super-bandwidth microwave-band signals.

2. MULTICORE FIBER-OPTIC WAVEGUIDE MODEL

Although at present, in the result of MCOF development, the number of cores inside single-mode fiber has already reached 19 (Sakaguchi and Puttnam 2013), to improve perception, the studies below are conducted on the basis of MCOF with moderate number of cores. Fig. 1 shows the cross-section of a 5-core optical waveguide, which we will investigate in this paper. There are one central single-mode core (numbered "0") and four peripheral single-mode cores (numbered "1-to-4") inside the cladding with a standard diameter of 125 μm.
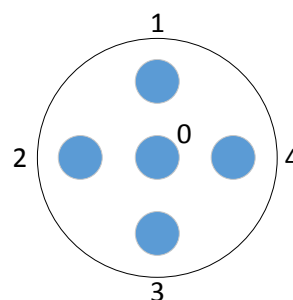

Figure 1: The Cross-Section of a 5-core Fiber-optic Waveguide

In this construction, simple geometric considerations allow us to realize that the distance between the peripheral cores is almost 1.5 times greater than between each of them and the central core. Consequently, it will be a negligible error to assume that the crosstalk power will be distributed uniformly between the central core and each peripheral one and lack even between the adjacent peripheral cores.

Figure 2 depicts a general equivalent-circuit model of 5-core single-mode MCOF feasible for various operating regimes of realistic fiber-optic link developed on the basis of this assumption, as well as on the previously presented AWRDE model of single-core optical fiber (Belkin and Golovin 2018) in the form of sub-circuit SUBCKT "Fiber". In according to Figure 1 there are five optical channels consisting of one central port ("0") and four peripheral ports ("1-to-4") where the crosstalk is simulated using the models of 2-tap and 5-tap splitters SPLIT with a given coupling factors.
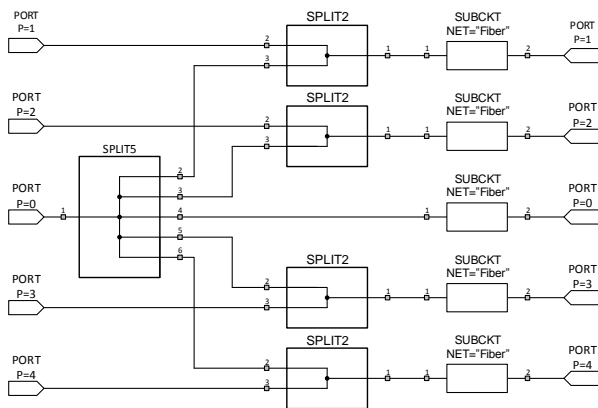

Figure 2: A General Model of 5-core Single-mode Optical Fiber

3. SIMULATION EXPERIMENTS

Figure 3 shown the testbed for the AWRDE software tool's simulation experiments using equivalent circuit model of 5-core MCOF and measurement ports. Differences from Fig. 2 are due to the fact that there is no library model of the splitter with more than 3 taps and with an unequal coupling coefficient between the input port and each of the taps in this program environment. In addition, to remove the reflections through these non-direction couplers that distort the quasi-optical (QO) signals being propagated, the library isolator models ISOL8R with the isolation level of 100 dB are inserted. Using this testbed below, the results of two simulation experiments to assess the impact of inter-channel crosstalk (XT) are highlighted.

First, the impact of XT is checked under the transmission of high-speed digital signals. Figure 4 demonstrate the simplified AWRDE testbed for the simulation experiment referred to the transmission of digital pseudo-random sequence of 2.5 Gbit/s on sub-carrier 40 GHz over 5-core optical fiber of 10 km length. This simplification is justified by the earlier assumption of the same level of XT between the central core (see sub-circuit LIN_S NET="Optic_m_0") and each peripheral one (see sub-circuit LIN_S NET="Optic_m_1").

Besides, there are some library models to generate digital pseudo-random ('RND_D'), microwave sub-carrier ('TONE RF'), QO ('TONE OPTIC'), and noise ('AWGN') signals, to process ('DAC', 'AM_MOD', 'MIXER_B') them and measure ('TP') the output MW carrier-to-noise ratio (CNR).

Figure 5 shows the spectrum of digitally modulated RF signal at the output of the modulator model 'AM_MOD' including MW sub-carrier of 40 GHz and many sideband responses at the levels near -20 dB, which indicates a sufficient value of the modulation index for conducting noise studies.
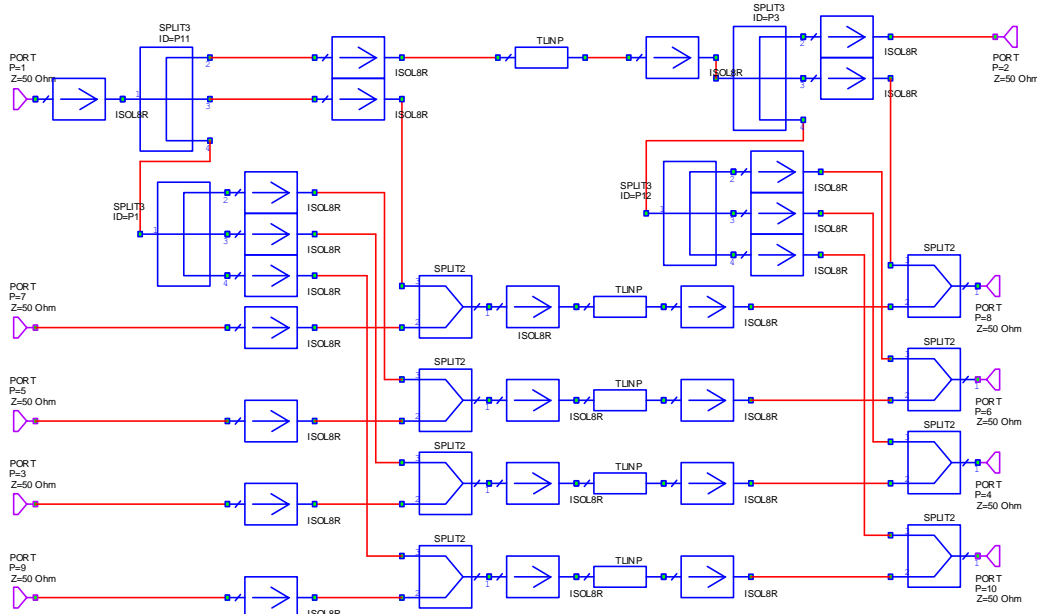

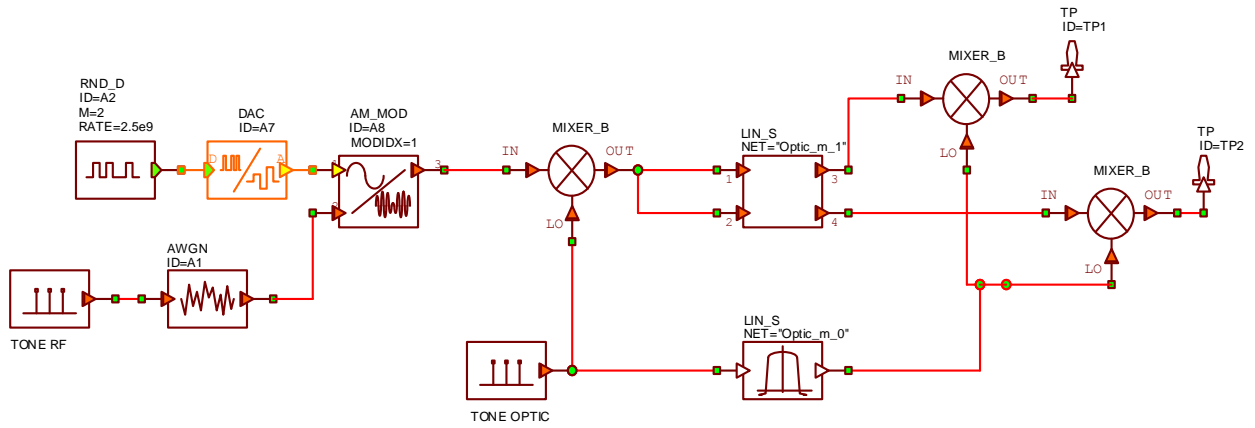Figure 3: Testbed for the AWRDE Software Tool's Simulation Experiments

Figure 4: Simplified AWRDE Testbed for the Simulation Experiment Referred to the Transmission of Digital Pseudo-random Sequence
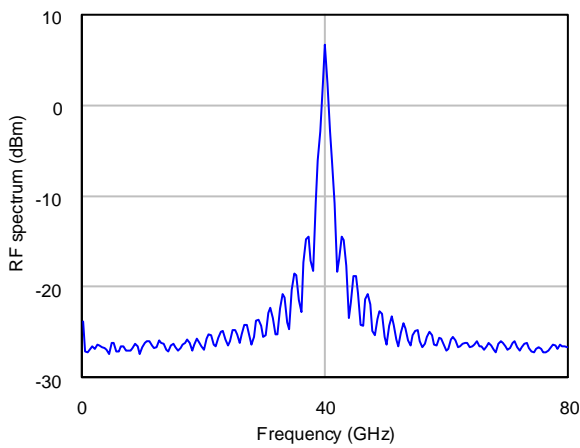
Figure 5: The Spectrum of Digitally Modulated RF Signal
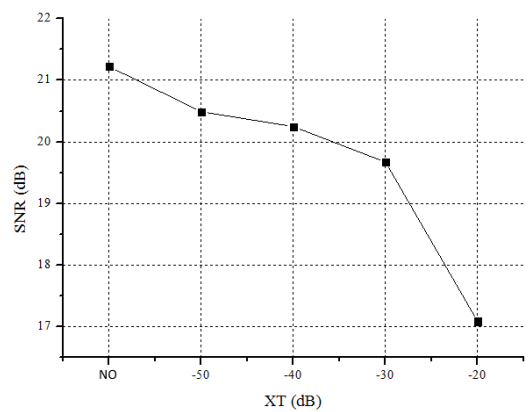
Figure 6: The Results of MCOF's CNR Calculation at the Typical Crosstalk Levels NO Indicates the Lack of Crosstalk

Figure 6 exemplifies the results of CNR calculation at XT levels in the range of -50…-20 dB, which corresponds to typical values of average crosstalk in long multi-core optical fibers (Koshiba and Saitoh 2012). As seen, up to a level of -40 dB, the XT has a weak effect on the CNR, but when it exceeds -40 dB their influence becomes remarkable, which corresponds to known experimental data (Luis and Puttnam 2016).

Second, the impact of XT is checked on the delay of super-bandwidth microwave-band signals. Figure 7 demonstrate the AWRDE testbed for the simulation experiment referred to the retarding effect for 5-core optical fiber of 3 m length with serially connected cores (or the ports in Fig. 2) during transmission of a quasi-optical carrier modulated with a MW signal in the one-octave-wide band (from 5 to 10 GHz). The
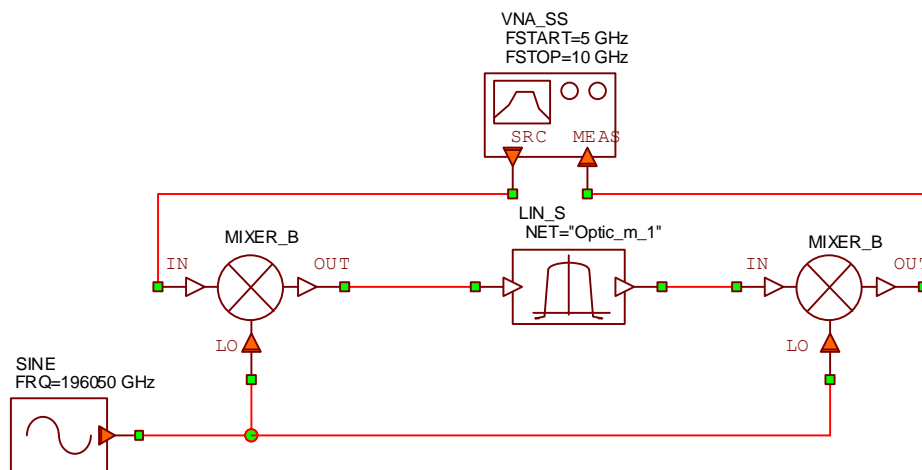
Figure 7: AWRDE Testbed for the Simulation Experiment Referred to the Retarding Effect of 5-core Optical Fiber

measurement is carried out by a standard technique using the library model of the Vector Network Analyzer ('VNA_SS'), the source of the quasi-optical signal is formed on the basis of a library generator model ('SINE'), modulation and demodulation are realized by means of an ideal mixer model ('MIXER_B').

Figure 8 exemplifies the results of the Group Time Delay (GTD) calculation in 5-core MCOF at XT levels in the range of -60…-30 dB. For comparison, the graphs also show the results of calculating the GTD in a standard single-core single-mode fiber (SMF) of the same length.
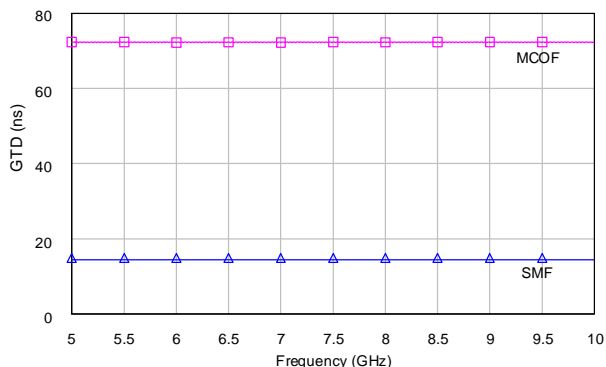
(a) XT=-60 dB
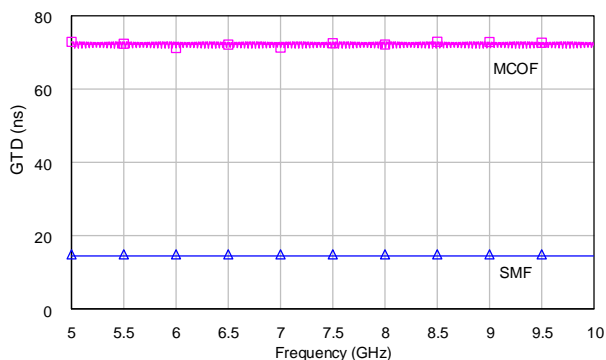
(b) XT=-40 dB
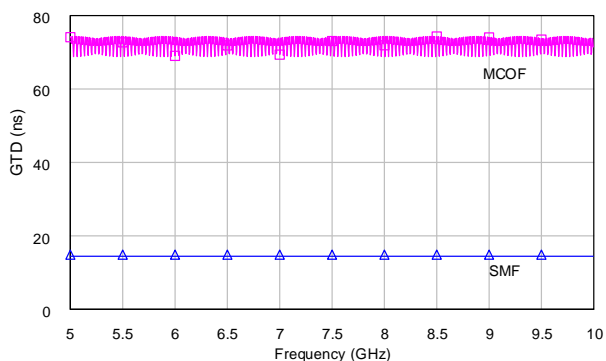
(c) XT=-30 dB

Figure 8: Impact of Crosstalk on Variance of Group Time Delay in 5-core Optical Fiber

The following outcomes can be drawn from the Figure. For identical fiber lengths, the time delay value of 5-core fiber is five times the delay of a single-core fiber, which can significantly reduce the form factor of a fiber-optic delay line photonic processor. Despite the 5-fold length of the optical path in the 5-core MCOF, the direct proportionality between the phase shift and the frequency change of the transmitted radio signal remains even in the octave band, as evidenced by the uniform characteristic of GTD. An increase in average crosstalk above -40 dB results in noise on the GTD characteristic, which greatly increases the error in determining the delay. Note that the critical level of crosstalk coincided with the beginning of a steep SNR decrease registered in the course of the previous simulation experiment (see Figure 6).

4. CONCLUSION

Above, an equivalent-circuit model of multicore optical fiber waveguide is proposed using NI AWRDE off-the-shelf software tool. The model is feasible for various operating regimes of realistic fiber-optic telecom systems taking into account the key limiting factors of fiber-optic waveguide, such as chromatic dispersion, time retarding, insertion loss, operating temperature dependence with an addition of the crosstalk parameter, which is the main issue in the practical application of a multicore optical fiber. Two simulation experiments validate the proposed model referred to the transmission of digital pseudo-random sequence of 2.5 Gbit/s on radio-frequency sub-carrier 40 GHz over 5-core optical fiber of 10 km length and to the retarding effect for 5-core optical fiber of 3 m length with serially connected cores during transmission of an optical carrier modulated with a MW signal in the one-octave-wide band. The both conclude that a growth in average crosstalk above -40 dB results in steep degrading the total carrier-to-noise ratio and in increasing noise on the group time delay characteristic, which greatly enlarges the error of time delay detection.

REFERENCES

Belkin M.E., Golovin V., Tyschuk Y., Vasil'ev M., and Sigov A.S., 2018. Computer-Aided Design of Microwave-Photonics-based RF Circuits and Systems. In: Xi Sung Loo, ed. RF Systems, Circuits and Components,. IntechOpen Publisher (in print).

Belkin M.E., 2016. Design principles of long-term analog RF memory based on fiber-optics and microwave photonics approaches. Proceedings of IEEE Avionics and Vehicle Fiber-Optics and Photonics Conference (AVFOP 2016), pp. 21-22. July 31 − November 3, Long Beach (California, USA).

Effenberger F., 2016. Future Broadband Access Networks. Proceedings of the IEEE, 104 (11): pp. 2078-2081.

Egorova O. N., Belkin M. E., Klushnik D. A., Zhuravlev S. G., Astapovich M. S., and Semojnov S. L., 2017. Microwave Signal Delay Line Based on Multicore Optical Fiber. Physics of Wave Phenomena, 25 (4): pp. 289–292.

Fini J. M., Zhu B., Taunay T. F., Yan M. F., and Abedin K. S., 2011. Crosstalk in multicore optical fibers. Proceedings of 37th European Conference and Exhibition on Optical Communication, pp. 1-3. November 3, Geneva (Switzerland).

Koshiba M., Saitoh K., Takenaga K., and Matsuo S., 2012. Analytical expression of average power-coupling coefficients for estimating intercore crosstalk in multicore fibers. IEEE Photonics Journal, 4 (5): pp. 1987–1995.

Lavigne B., Bertran-Pardo O., Bresson C., 2016. 400 Gb/s Real-Time Trials on Commercial Systems for Next Generation Networks. IEEE Journal of Lightwave Technology, 34 (2): pp. 477-483.

Lee B. G., M. Kang, Lee J., 1996. Broadband Telecommunication Technology. Norwood, (MA, USA): Artech House.

Luis R.S., Puttnam B.J., Cartaxo A.V.T., Werner K., Mendinueta J.M.D., Awaji Y., Wada N., Nakanishi T., Hayashi T., and Sasaki T., 2016. Time and Modulation Frequency Dependence of Crosstalk in Homogeneous Multi-Core Fibers. Lightwave Technology, 34 (2): pp. 441–447.

Saitoh K. and Matsuo S., 2016. Multicore Fiber Technology. Lightwave Technology, 34 (1): pp. 55-66.

Sakaguchi J., Puttnam B. J., Klaus W., Awaji Y., Wada N., Kanno A., Kawanishi T., Imamura K., Inaba H., Mukasa K., Sugizaki R., Kobayashi T., and Watanabe M., 2013. 305-Tb/s space division multiplexed transmission using homogeneous 19-core fiber. Lightwave Technology, 31 (4): pp. 554–562.

REAL TIME TRAFFIC SIMULATOR FOR SELF-ADAPTIVE NAVIGATION SYSTEM VALIDATION

Vít Ptošek[a], Jiří Ševčík[b], Jan Martinovič[c], Kateřina Slaninová[d], Lukáš Rapant[e], Radim Cmar[f]

[a],[b],[c],[d],[e]IT4Innovations, VŠB - Technical University of Ostrava,
17. listopadu 15/2172, 708 33 Ostrava, Czech Republic
[f]Sygic

[a]vit.ptosek@vsb.cz, [b]jiri.sevcik@vsb.cz, [c]jan.martinovic@vsb.cz, [d]katerina.slaninova@vsb.cz,
[e]lukas.rapant@vsb.cz, [f]rcmar@sygic.com

ABSTRACT

We have developed an enhanced real time traffic simulator running on High Performance Computing infrastructure for testing an efficiency and usability of a self-adaptive navigation system which implements a traffic flow optimization service coordinated with external client-side navigation applications and heterogeneous traffic data sources collected and fused in an intelligent way. Building blocks of the simulator include a server-side navigation system, Virtual Smart City World, benchmark settings, and a test bed containing industrial Sygic client-side navigation and a simplified simulation of vehicles. The important feature of the simulator is the ability to evaluate the traffic flow control strategy in the Smart City world, both with and without enabled Global View calculation of a traffic network for a given percentage of vehicles connected to the server-side service. The integration of the Sygic navigation to the large-scale traffic simulator allows performing compliance test of real navigation applications to the developed central navigation system.

Keywords: traffic simulator, dynamic routing, HPC, smart city, navigation optimization

1. INTRODUCTION

One of the most significant challenges in a field of dynamic routing algorithms development and testing is to create a stable environment with data sets which it is possible to perform reliable and repeatable experiments on. Client-side navigation implemented as a mobile application by Sygic provides us with floating car data (FCD) which can be well used for our self-adaptive navigation system running on a central and knowledgeable server along with other data sources. This data is crucial for dynamic routing enhancement and the bigger the data is the better and more improved service of higher quality we can offer. However, to validate such dynamic routing, we need to ensure the correctness of the data in the first place. Simulating traffic from a macroscopic perspective turned out to be a convenient way how to repeatedly achieve a controlled traffic situation without massive amounts of data required by microscopic models. Nevertheless, our developed approach is also borrowing some ideas from the microscopic traffic simulation because the basic unit of the simulation is an individual vehicle driving along the chosen route. These vehicles then generate physical quantities like traffic flow or speed for the road network. In general, we consider this mixed approach to be a macroscopic model because these vehicles do not directly interact, and purpose of the model is to monitor the behavior of physical quantities describing the traffic and not behavior of individual vehicles. Our proposals are supported by article written by Harri, Filali and Bonnet (2009). By combining both macro and microscopic approaches we can have the model which does not require much data and is as easily manageable and adaptable as a microscopic simulation.

The traffic simulator represents a move of an imaginary world vehicles based on a real world routing system. The whole simulator and its parts are meant to exploit High Performance Computing (HPC) infrastructure as the process itself is computationally demanding as described by Zehe, Knoll, Cai and Aydt (2015) and in need of many computational resources to work properly in time.

The aim is to reflect current and future traffic situation and not only to find the shortest path while still on the road but also the most efficient one changing accordingly to traffic conditions. Thanks to above mentioned process we are able to give such a result with respect to data, benchmark and visualization. Our another goal was to keep a response time limit for every navigation request irrespective of the number of concurrent requests at all times. We consider 500 ms to be a reasonable threshold.

There are many kinds of existing macroscopic traffic models and simulators. For instance, Abadi, Rajabioun and Ioannou (2015) utilize macroscopic simulation to predict the traffic flow. However, their simulation is closer to the classical macroscopic model because while they simulate individual routes, they utilize only information about traffic flow in conjunction with link-to-link dividing ratio to simulate its changes. The article from Batista, Leclercq and Geroliminis (2017) utilizes the combination of macroscopic and microscopic models to simulate and describe the behaviour of the traffic network. Behaviour of their model is, though, more
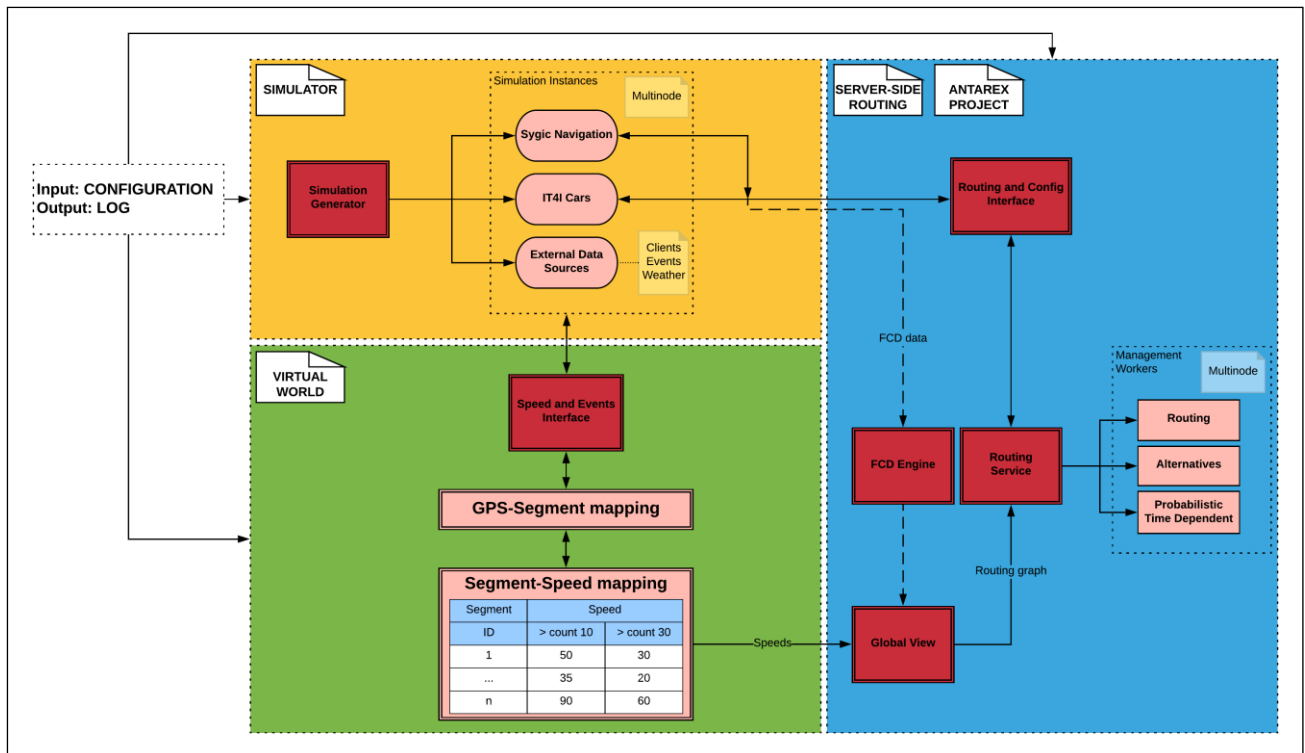
Figure 1: Simulation design

influenced by the macroscopic part of the simulation than the behaviour of individual vehicles influenced by changing the traffic conditions during the simulation. Zhang, Wolshon and Dixit (2015) try to integrate two macroscopic models (Cell Transmission Model (CTM) with the Macroscopic Fundamental Diagram (MFD)) for urban networks in their article. While CTM is a very useful tool for macroscopic modelling, its data requirements are approaching the microscopic model.

There is also a number of both free and paid traffic simulators like VISSIM (Fellendorf and Vortisch, 2010), SUMO (Behrisch, Bieker, Erdmann and Krajzewicz, 2011), TRANSIMS (Smith, Beckman, Anson, Nagel and Williams, 1995) or Matsim (Horni, Nagel and Axhausen, 2016). Generally, these products usually require much more data for their proper functioning because they are mainly based on microscopic approaches. Also, their potential application on an HPC infrastructure is questionable because of their existing implementation limits. Therefore, for our application, creating our own traffic simulator is more preferable.

2. TRAFFIC SIMULATOR STRUCTURE

The traffic simulator consists of several mutually cooperating parts that can be imagined as modules. The proposed design of the simulation model is divided into three main groups pictured and coloured in Figure 1:

1. Simulator – yellow,

2. Virtual World – green,

3. Server-side Routing – blue.

These groups use interfaces to communicate together and those are further explained in Section 3. They also have in common a general configuration file as an input used across all the parts (described in Section 4.1) and a united logging environment for the entire output.

2.1. Simulator

The Simulator part is responsible for initializing and running simulation modules that contribute to the Virtual World and thus affect the Global View. The initialization strongly depends on simulation inputs that can be generated prior to the simulation optionally. Every simulation module subsists up to hundreds of simulated instances running in threads and to exploit HPC infrastructure better, every module can simultaneously run on numerous cluster computing nodes in parallel. Simulation instances are also able to directly obtain itineraries from the Routing service and actual road speed from the Virtual World.

Every simulation experiment we launch must be accompanied by its description. This helps us to reproduce experiments, tell them apart knowing immediately what the aim of the experiment was supposed to be, and mainly to keep them deterministic. Because simulation consists of different modules, each one of them has its own setting file representing simulation instances. Each entry of a concrete setting file then represents a single instance of a given simulation module giving us total number of simulation instances per module.

In the case of vehicle module description, we distinguish between Sygic and IT4I cars and especially keep the

track of their individual travelling intensions. These are recognized by origins and destinations, start times, frequency of logging, requests for a current segment speed from the Virtual Smart City World (Section 2.2), and routing request to the Server-side Navigation System (Section 2.3).

Even if we do not touch the vehicle setting, we can still adjust another simulation results seriously by changing the initial state of the Virtual World describing road network conditions and a traffic status. Every single segment is defined by a set of thresholds representing number of concurrent vehicles and their matching speeds. That way we are able to decide how many vehicles on the same way would imply a traffic jam, or when they should slow down or speed up.

2.1.1. Generator
As we need to modify the whole simulation run for various experiments repeatedly, we often need to adjust specified simulation settings. This task can be done manually by a user or automatically by a setting generator which creates setting files if those do not exist. The generator uses the general configuration file and runs in two modes – lightweight one for testing purposes or another one considering simulation aspects.

With both modes, the segment setting resolves how the initial state of the Virtual World would be generated and the vehicle setting determines the initial state of every single instance of a vehicle.

For example, if we choose generating vehicle setting for the testing mode, we need to declare origin-destination positions and those will be used for all the vehicles, basically creating desired number of vehicle instance copies. On the other hand, if we want simulated vehicles to vary, we can use our ordered routing graph to generate a different route for each vehicle in a deterministic manner as the ordering by a unique identifier stays the same. It is also possible to postpone start time of a vehicle and its round trip individually. Vehicles may use the Global View more or less often or not at all depending on the configuration file.

We can also set a length of a vehicle, which will take effect in generating more realistic routing segment speed relations. Due to the fact that each routing segment has its known length, we can calculate how many vehicles would fit on such segment. This gives us an idea of concurrent vehicle thresholds. Connecting this information with the known maximal allowed speed of a specific segment extracted from OpenStreetMap (Ptošek and Slaninová, 2018) road classification (highway, motorway, tertiary, etc.) we are able to set corresponding speeds for these thresholds. We are aware of a model like this being considerably simplified, but sufficient enough for our deterministic testing purposes.

In even more simplified testing case, we have omitted any of this information and let the speed table to be generated with the same thresholds and speed values for all the segments.

2.1.2. Sygic Navigation System
To enhance the Global View's data from the Virtual World by results coming from the real world, it is possible to use data from the Sygic mobile application as an additional input for FCD Engine producing an output.

2.1.3. IT4I Cars Simulation
The IT4I car (also producing FCD) is a basis of the simulation as every instance can interact with the Virtual World and the FCD Engine, both contributing to the Global View. HPC environment enables us to launch thousands of virtual cars simultaneously. This is very important as it allows us to get better and faster results in the case of urgent need of alternative routes to avoid the creation of higher traffic load on some roads.

The logic behind the simulation of a moving IT4I car is explained in Section 4.2.

2.1.4. External Data Sources
External Data Sources (EDS) are a part of simulation instances and speak for any (third party) modules, such as clients for weather, traffic events, or yet another navigations, which are able to use our exposed interfaces (Section 3). We generally expect fewer EDS in comparison with instances of simulated moving vehicles. Unlike vehicles, EDS do not need to directly interact via routing interfaces.

2.2. Virtual Smart City World
As our simulation experiments rely mainly on dynamic routing, it is crucial to keep track of actual road network situation once it is generated (explained in Section 2.1.1) and initialized. The update of the Virtual World is based on many requests of running simulation instances that can indirectly (via interfaces) start to modify number of concurrent vehicles on segments and even segment speeds alone in the case of traffic events. How often is the Virtual World updated depends on individual setting of every simulation instance.

In return, all vehicles are moving along their itinerary according to the speed they retrieve from the Virtual World. In response to the updated Virtual World, they can actually get a different itinerary, because the Virtual World plays a part in the Server-side routing graph update as it is more or less reflected in the Global View.

Although the Virtual World can be updated in milliseconds, the update period of the Global View is set from the configuration. After that period, a snapshot of actual Virtual World changes is transformed into HDF5 (Folk, Heber, Koziol, Pourmal and Robinson, 2011) format and stored in a real time. This means that vehicle's speed on a certain segment can change immediately, but its itinerary would change no sooner than after the Global View update even though the vehicle is forced to request new route more often.

Updating the routing graph for speed weight of segments gives us a testing and validation tool for our dynamic routing environment as shown in Sections 5.1 and 5.2.

2.2.1. GPS-Segment Mapping

Simulation instances can use GPS coordinates to determine their positions, however our routing graph is derived from geometries representing edges (segments in our Virtual World). We have decided to use library called SpatiaLite (Casagrande, Cavallini, Frigeri, Furieri, Marchesini and Neteler, 2014) that extends SQLite for spatial queries and helps us with translation between segments and coordinates.

2.2.2. Segment-Speed Mapping

To update our Virtual World correctly, we need to know a current position in the case of an event (Section 3.2.2) and both previous and current position of every moving instance, like vehicle (Section 2.1.3). After mapping these positions to segments (if there is a need), it is possible to change speed value based on thresholds (shown in Table 1).

The following simplified pseudocode describes obtaining speed value based on an instance of a vehicle and its visited segments. If the vehicle moves between two segments, the counts of concurrent vehicles on a given segments should change. Actual speed value of a current segment is returned even if the segment has not changed from the previous one, because meanwhile another vehicles could have entered or left from this segment and therefore affected thresholds. In spite of the multimode and multithread simulation process, it is inevitable to use locks.

Structure segmentSpeedTable = InitializeSpeedTable();

UpdateVirtualWorld(previousSegment, currentSegment){
Speed speed;

Lock(segmentSpeedTable);

If(previousSegment <> currentSegment){
    segmentSpeedTable[previousSegment]-=1;//decrease
    segmentSpeedTable[currentSegment]+=1;//increase
}

//get count of concurrent vehicles for actual segment
var count = segmentSpeedTable[currentSegment];
//get speed matching actual segment's threshold
speed = segmentSpeedTable[currentSegment][count];

Unlock(segmentSpeedTable);

Return speed;
}
Algorithm 1: Virtual World Update Pseudocode

Because a behavior of every simulated vehicle at a certain point of a time is highly dependent on its actual segment and speed, we came up with a bound system based on a relation of the two.

Let speed value (sv) expressed in km h^{-1} for a segment (S) with ID (n) be set to number (v) in the case of count of concurrent vehicles (ccv) being greater or equal to number (k). The expression can be written in the following form

$$S_n = \begin{cases} ccv \geq k_1, & sv = v_1 \\ ccv \geq k_2, & sv = v_2 \\ ccv \geq k_3, & sv = v_3 \end{cases}$$

The examples of a segment-speed relations based on thresholds (bounds) are explained in Table 1 and expressed as

$S_n=<ccv\_min_n, ccv\_max_n):sv_n$ and therefore for ID 1
$S_1=<0, 3):90; <3, 10):50; <10, +\infty):1$ and therefore
$S_1=0:90, 3:50, 10:1$ to only use inclusive bounds

Table 1: Segment Speeds

Segment ID	Speed for Bounded Intervals of Concurrent Vehicles		
	Threshold 1	Threshold 2	Threshold 3
1	<0,3):90	<3,10):50	<10, +∞):1
2	<0,3):50	<3,10):30	<10, +∞):1
3	<0,10):130	<10,30):90	<30, +∞):1

The default threshold count is three (as used for a demonstration), but can be changed dynamically. The only rule is that regardless the number of bounds, they should always cover the interval of $<0, +\infty)$. Then we are able to check the actual speed for the currently highest applicable bound. In the case of nine vehicles, that would be 50 km h^{-1} from the second threshold on S_1, but 30 km h^{-1} for the same number of vehicles and threshold on S_2, and 130 km h^{-1} on S_3 from the first threshold. This is applied and shown in the Algorithm 1 where *segmentSpeedTable[S_n][ccv]* is referring to a formally expressed $sv_{n,bound}=S_n:ccv$ giving the actual speed for the specific segment bound in respect of a current number of vehicles on the specific segment, therefore $S_1:9=50_{1,2}$ and analogically $S_2:9=30_{2,2}$ and $S_3:9=130_{3,1}$.

The more vehicles, the higher bound and the lesser speed. It is important to mention, that the highest bound tends to be set at least to 1 km h^{-1} to prevent vehicles belonging to affected segment to get stuck there forever as they would be unable to leave with a zero speed. But as vehicles are slowly leaving a segment with speed of 1 km h^{-1}, the segment can eventually get to lower bound and thus higher speed. In the case of S_1, the speed would increase back to 50 km h^{-1} and 90 km h^{-1} afterwards.

2.3. Server-side Navigation System

The server-side routing optimized by ANTAREX tools – project use case II, Silvano, C. et al. (2016) is the core of the Smart City navigation that is designed to handle a significant number of routing requests and processes them in parallel within low-level computing workers running on a heterogeneous HPC cluster. This self-adaptive navigation system is largely used within

simulation instances and covers every part related to the routing. It can be enriched by the Global View of the traffic network.

2.3.1. Routing Service
The service is based on a management system providing scheduling and allocation of computing resources for routing workers as well as their communication with service clients. These workers can run in multinode mode in order to reach sufficient request throughput.

At this moment the routing service supports several routing algorithms on a custom-generated routing graph. The routing algorithm option is part of a simulation configuration. By default, to find the shortest path our implementation of Dijkstra routing algorithm is used. We have chosen this algorithm for all of our simulation testing experiments to omit any need of a heuristic function which served our performance purposes well.

2.3.2. Global View
As every routing algorithm needs a network to find a path between nodes, we advance our routing graph edges with additional information and metrics to balance it accordingly. Changing weights of edges (costs) gives us an opportunity of the dynamic routing. The Global View can be calculated on the basis of the Virtual World data and the FCD Engine output.

2.3.3. FCD Engine
If we wanted to connect the Virtual World with the real one, we could connect another module into the scheme. Our FCD Engine manages to process data from Sygic navigations outside the simulation and offers a real time traffic monitoring that could serve for the initial Global View state instead of generated Virtual World.

Processing FCD from Sygic navigation inside the simulation could help us comprehend what minimal percentage of FCD coverage (in comparison with IT4I cars) is needed to reliably monitor the traffic situation in the case of collaborative routing usage.

3. TRAFFIC SIMULATION INTERFACES
Interfaces serve to connect component modules described in Section 2 together as well as they help external parts to communicate with the server-side navigation services. They are based on HTTP and TCP protocols and are meant to serve two fundamental roles – simulation run and validations of aforehand mentioned services.

3.1. Server-side Navigation Interface
This interface is crucial for all the simulations, but has zero dependency on the simulation itself, because routing services can be used for a real world real-time navigations outside the simulation process as well.

3.2. Simulation Interface
The following interfaces were specially built for the simulation purposes and are highly dependent on the simulation itself.

3.2.1. Configuration
Since we can generate configurations for EDS instances described in Section 2.1.4, this interface can be used to deliver particular configurations before the simulation starts. For example, if Sygic navigation application wanted to use our pre-generated scenarios, they could ask for every single instance's setting from the application. This guarantees simulation consistency as we are in charge of their origin and destination positions, number of instances, request limits and many more. This approach takes the advantage of avoiding hard-coded simulation scenarios and being able to change them relatively easily and quickly.

3.2.2. Events
By events we generally mean road closures, accidents or lane restrictions formed by their geozones and optional speeds that affect the Global View directly. Events can
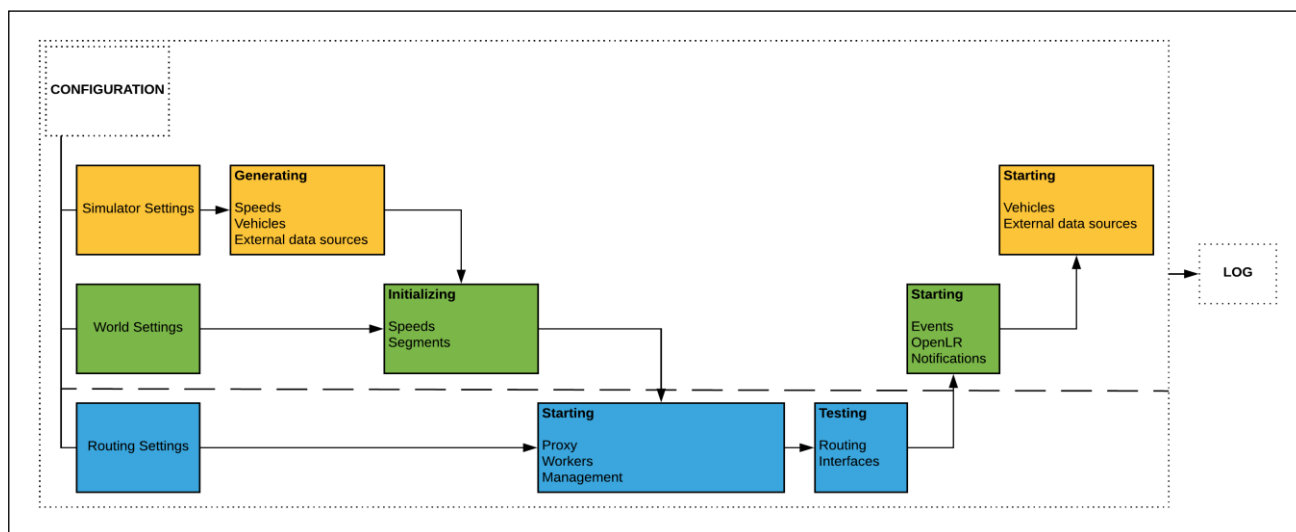

Figure 2: Simulation run

be raised interactively from within a map as shown in Figure 10 or by planned event instances based on a simulation setting.

3.2.3. Speed

Because our objective is not to develop a multi-agent system where simulation instances interact with each other, this interface was introduced to map position of a vehicle onto our routing graph returning a segment speed relation in response to the Virtual World. This way, each vehicle is assured to know how fast it can move without knowing about other vehicles it shares the road with and vice versa. It also delegates a vehicle's understanding of our routing road network topology and corresponding threshold speed limits to centralized Virtual World.

Speed interface works both ways, it returns value based on a current road type and number of concurrent vehicles and updates the Global View metrics at the same time to avoid cumulating, as can be seen in Figure 11.

4. TRAFFIC SIMULATION PROCESS

The whole simulation process is based on a communication between the connected modules described in Section 2. After preparing essential environment (endpoints, datasets, services, notifications, etc.) and generating simulation settings, simulation instances are initialized, and vehicles start to move. The simulation runs until the last vehicle reaches its destination.

Figure 2 shows the model described in Figure 1 from the runtime execution perspective.

4.1. Execution

The execution is done automatically and completely in the HPC environment and is handled by one main script. This master script is linked to all the modules' initial settings, configurations and auxiliary scripts as well as their separate process runtime logging. With this design we can easily launch self-contained experiments repeatedly to reproduce the results or to see how they change in time with different properties.

4.2. Vehicle moving behaviour

The moving strategy of a vehicle object is based on its itinerary and a speed determined by the road network condition at the time, e.g., free flow speed, heavy traffic, traffic jam or even a closure-causing obstacle. The itinerary may vary as the Global View keeps updating during a simulation. The speed may differ from the same reason, but based on the Virtual World.

The vehicle (repeatedly) obtains its route itinerary from the server-side navigation system as seen in Figure 3, and its (in this case constant) speed from the Virtual World. The blue line represents a current itinerary and the purple line stands for already visited segments from either current or past itineraries (they can differ based on the Global View). The most recent position of the vehicle is

represented by the blue dot, whereas the purple dots express tracks of history positions of the same vehicle.

Figure 3: Vehicle route start

Unlike the speed from the Virtual World, the itinerary is a subject to change with the Global View enabled only (described in Section 2.3.2). It is important to always be aware of the current road segment the vehicle is on because its travelled distance depends on the actual speed of the current segment for a given vehicle count. Since there is only one vehicle situated on the segment, as pictured, the speed does not change and neither do the distances between its positions.

The vehicle does not leave its current segment till the total distance travelled by the vehicle is shorter than the distance from the start of the route to the end of a current segment as pictured in Figures 4 and 5.
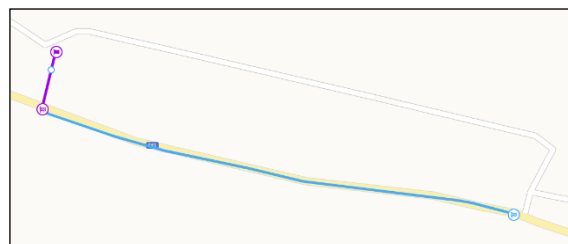
Figure 4: Vehicle route move on a segment
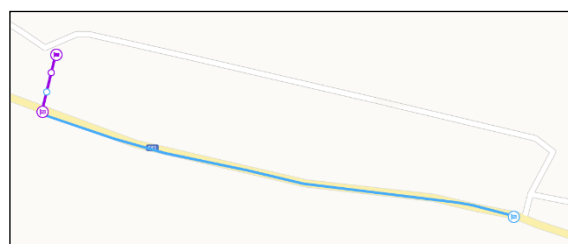
Figure 5: Vehicle route move on the same segment

While the vehicle is travelling along the road segment, its speed may be affected by a volume of concurrent vehicles on the same segment at the same time. As the vehicle instance continues, it may move onto a following road segment (as seen in Figure 6) from its (updated) itinerary (that can vary from the previous one) or not – regarding the actual segment speed and remaining segment distance.

This motion process continues until a vehicle reaches its destination regardless an alternative route (no following segment – graph edge exists) as is depicted in Figure 7.
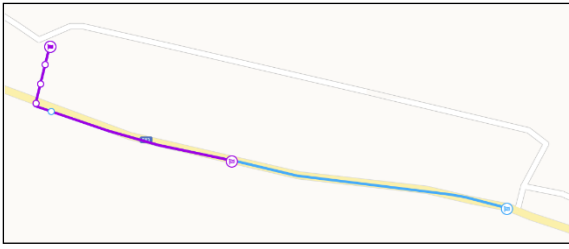
Figure 6: Vehicle route extended by following segment
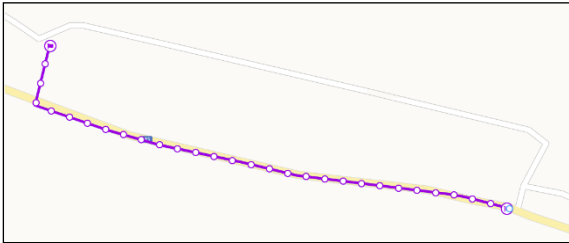
Figure 7: Vehicle route finished

Moving a certain instance of a vehicle on segments of a routing graph is relied upon an invariant that can be described in do-while block by the pseudocode in Algorithm 2.

```
Time time = GetTimeNow();
Position actualPosition = GetGpsFromSettings();

MOVE:
do {
    WaitForNextMove(waitingPeriod);

    Route route = GetRoute(vehicleId); //Figure 3
    Speed speed = GetSpeed (vehicleId, actualPosition);
    Distance distance = speed * (GetTimeNow() - lastTime);

    vehicleDistance += distance;
    while (vehicleDistance >= routeDistance) {
        If (routeItineraryNotEmpty) {
            segment = DequeueItinerary();
            routeDistance += segmentLength; //Figure 6
        } else {
            Finished = true; //Figure 7
            break;
        }
    }

    //get ratio value between 0 (start) and 1 (end) inclusive
    segmentRatio =
    1 – (routeDistance – vehicleDistance) / segmentLength;

    actualPosition = GetGpsFromSegmentRatio(); //Figure 4
    Log(route, speed, distance,  actualPosition);

    lastTime = GetTimeNow();
} while (NotFinished);

If(RoundTrip){
    Finished = false;
    vehicleDistance = routeDistance = 0;
    Swap(GetGpsFromSettings(), actualPosition);
    GoTo MOVE;
}
```

Algorithm 2: Real time Position Change Pseudocode

4.3. Routing adaptation

The adaptation is based on a cost of a given route and a chosen routing algorithm which calculates a total cost. The total cost of the route is a summary of costs of all the segments belonging to a given route – itinerary cost. This means that few segments of a route can outweigh the rest and vice versa. When the cost changes significantly, it may happen that from the point of the Global View, another route becomes more convenient than the existing one (as is illustrated in Figures 8, 9 and 10).

The weight of an edge of a routing graph between two nodes can be in our case:

1. Static – distance, which is not subject to change,

2. Dynamic – transition time based on a speed being calculated just-in-time from the Global View according to a current traffic situation.
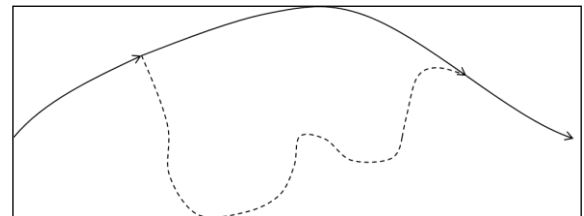
Figure 8: Original route based on distance
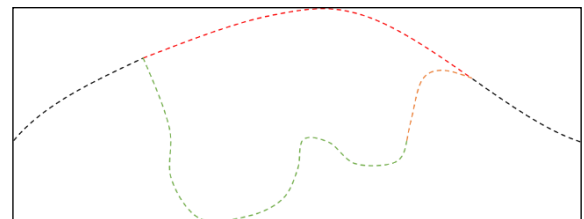
Figure 9: Segment speed evaluation
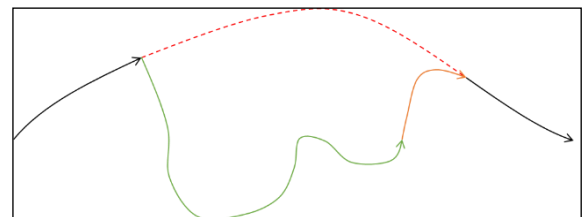
Figure 10: Alternative route

5. SIMULATION SCENARIOS

The strategy and use cases of a simulation are created by an initial setting. It is also possible to use a map visualization to interact with the still running simulation itself. We have picked two use cases for a demonstration – roadblocks in Vienna, Austria city centre and a wilful cumulative traffic jam in Ostrava city, Czech Republic.

5.1. Forcing optimization with blockages

Figure 11 represents a scenario where we generated multiple vehicle instances and assigned them unique pair of nodes belonging to a routing graph, such that the nodes meet a criterion of having at least one crucial edge

between them. In a real world, the nodes represent origin and destination points and a set of edges creates a routing path. From a traffic experience, bridges are examples of critical edges, so we aimed at destinations across a river. The bridge areas being a part of their way were then flagged as traffic jams gradually in such manner so that their way was no longer considered as the optimal one. Affecting an actual road situation with the accidents shows vehicles rerouting eventually to avoid a rush.
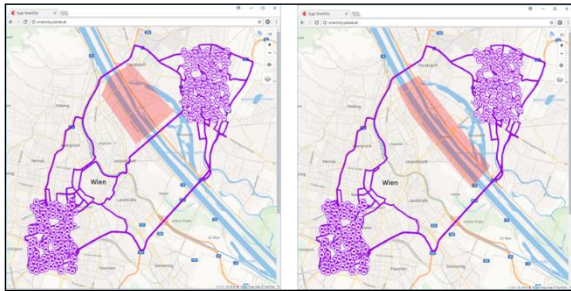
Figure 11: Static traffic jam

5.2. Forcing optimization with Global View

Our aim is to be able to dynamically cope with traffic jams accordingly – in our case to change the route of a vehicle based on a community contributing to the traffic situation as a whole. This means the final route is both individually the most beneficial as well as efficient from a global point of view.

Figure 12 demonstrates numerous vehicle instances driving from and to the very same start and end points. In contrast with Figure 11 we decided not to influence the road network with any blockages and had vehicles to form the traffic jam themselves as they are moving.

The route optimal for a single vehicle is shown on the left side and was used for all the vehicles, which leads to an overall slowdown caused by a traffic jam. To mitigate the slow-down and compare our results, we also run the same simulation, but with the Global View enabled at this time. As can be seen on the right side, there are several routes pictured apart from the original one. Distributing the vehicles into diverse routes helped the road network to balance and the last vehicle to arrive significantly sooner via the more fluent way as described in Section 6.
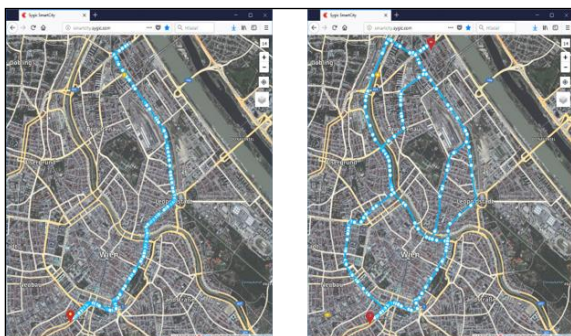
Figure 12: Dynamic traffic jam handling

6. RESULTS

We have chosen three different origin locations and a common destination (route lengths 11.5, 6.5 and 5.9 kilometres) such that they share final parts of their routes as captured in Figure 13 that represents every route without applying updates from the Global View. In this case, only one route exists for every origin-destination.
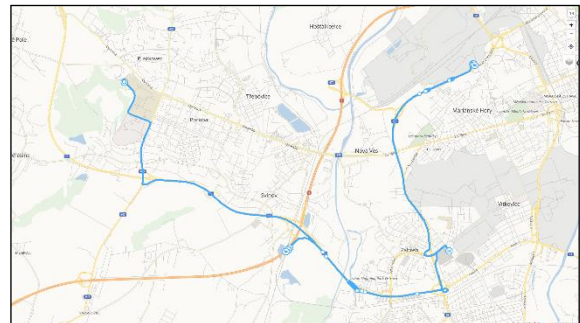
Figure 13: Static routes during a simulation

We have applied lightweight mode for generating testing Virtual World (described in Sections 2.1.1 and 2.2) and launched 200 vehicles for each starting position, 600 in total. Then, we have run the simulation with both Global View disabled and enabled several times to verify that our results match our settings repeatedly in both cases. Figures 14 and 15 show an obvious navigation adaptation where, unlike in Figure 13, vehicles started using by degrees more than three original routes obtained for three origin-destination pairs depending on another vehicle instances already sharing the same route at the time.
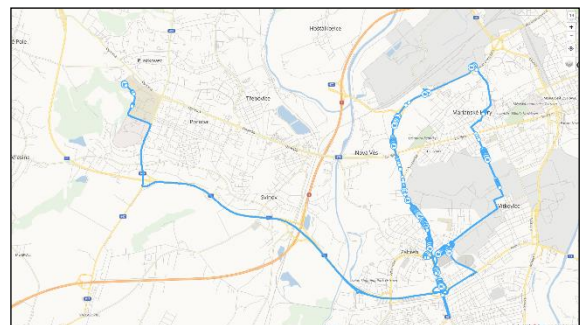
Figure 14: Alternative routes during a simulation
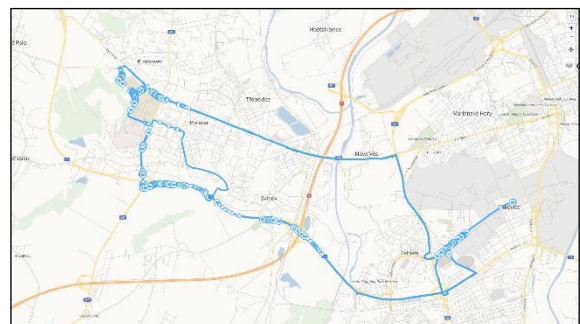
Figure 15: Alternative routes during a simulation II

Our first step was to prove our model to be deterministic in the meaning that the same simulation gives us very similar results regularly with little to no deviation caused by occasional request/response delays. When this has been achieved, we started with measuring the impact of the Global View usage being assured that the difference would not come from nondeterministic behaviour. These results based on the Global View only are showed below in Table 2, the better values are highlighted in green.

Table 2: Driving Times in minutes and seconds

Global View	600 Vehicles (3x200)			
	Average	Median	Minimum	Maximum
Off	17:26	14:28	04:36	39:49
On	14:13	14:28	04:27	30:52

We were able to observe ≈22.5% speed-up in the case of the maximal duration of a vehicle run with the Global View enabled. In our testing simulation scenario, this duration represents the very last car arriving to its destination.

Our final results helped us to prove that from a globally collaborative perspective, utilization of the Global View based self-adaptive routing was timewise more efficient than in the event of a static one causing traffic jams.

7. CONCLUSION AND FUTURE WORK

We have presented the real time traffic simulator developed for running on HPC infrastructure for testing an efficiency and usability of the self-adaptive navigation system. Our first proposal was to meet a response time limit for every navigation request under 500 ms, which we are able to achieve at the moment. During our development and after the testing phase, we have discovered that the proposal can be different for our simulation case.

We came up with the fact that during a simulation, a vehicle does not need to receive a response for an updated route in a strictly short time requiring more computing resources, especially when its amount for the simulation with thousands of cars could be very highly computationally demanding and not necessary for our case. Also, as mentioned in Section 2.2, the routing graph changes much less often than the Virtual World that vehicles contribute to; therefore, routing services give the same results during a short interval. And lastly, we have learnt that a vehicle is able to drive even without an updated route for some time as there is usually no need to obtain a completely new route every half a minute.

Thus, our proposal has changed to satisfy a condition where every vehicle gets a response with a service-level agreement (SLA) much higher than the previous request limit time. As pictured in Graph 1, for the selected SLA 60 seconds and for 5,000 simultaneous vehicles, we need to allocate approximately 43 cores, which corresponds to 3 compute nodes from the Anselm cluster (2x8 Intel Sandy Bridge cores @2.4 GHz, 64 GB RAM per node) to reach that SLA.

From the self-adaptive routing system perspective, we have achieved promising navigation time improvement in the form of global traveling time speed-up.
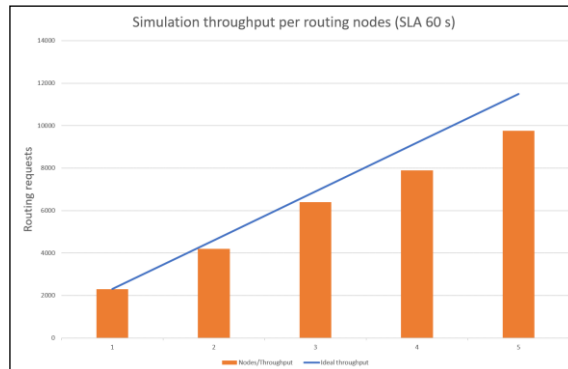
Graph 1: Simulation throughput – SLA 60 s

Because our simulation process is data-driven, we plan to scale up our simulations and extend various models with EDS, better speed profiles and a related data fusion.

In the future, we would like to continue our work with the second proposal and experiment with SLA levels sufficiency. Another goal is to examine the minimal percentage coverage of the external navigation (Figure 16) vehicles needed for reliable traffic monitoring in respect of simulated vehicle instances yet managed.

Figure 16: ANTAREX mobile navigation by Sygic

REFERENCES

Harri, J., Filali, F. and C. Bonnet, 2009, Mobility models for vehicular ad hoc networks: a survey and taxonomy, Communications Surveys & Tutorials, Volume 11, Part 4, Pages 19-41

Zehe, D., Knoll, A., Cai, W. and Aydt H., 2015, Simulation Modelling Practice and Theory, Volume 58, Part 2, Pages 157-171

Abadi, A., Rajabioun, T. and Ioannou P. A., 2015, Traffic Flow Prediction for Road Transportation Networks with Limited Traffic Data, Transactions on Intelligent Transportation Systems, Volume 16, Part 2, Pages 653-662

Batista, S., Leclercq, L. and Geroliminis N., 2017, Trip lengths and the macroscopic traffic simulation: an interface between the microscopic and macroscopic networks. hEART2017 - 6th symposium of the European Association for Research in Transportation, HAIFA, France. hEART2016 - 6th symposium arranged by European Association for Research in Transportation, Page 5

Zhang, Z., Wolshon, B. and Dixit V.V., 2015, Integration of a cell transmission model and macroscopic fundamental diagram: Network aggregation for dynamic traffic models, Transportation Research Part C: Emerging Technologies, Volume 55, Pages 298-309

Fellendorf, M. and Vortisch P., 2010, Microscopic Traffic Flow Simulator VISSIM, Fundamentals of Traffic Simulation. International Series in Operations Research & Management Science, vol 145. Springer, New York

Behrisch, M., Bieker, L., Erdmann, J. and Krajzewicz, D., 2011, SUMO – Simulation of Urban MObility An Overview, SIMUL 2011, The Third International Conference on Advances in System Simulation, pp. 63-68

Smith, L., Beckman, R., Anson, D., Nagel, K. and Williams, M., 1995, TRANSIMS: TRansportation ANalysis and SIMulation System, 5. National transportation planning methods applications conference

Horni, A., Nagel, K. and Axhausen, K.W., 2016, Introducing MATSim, The Multi-Agent Transport Simulation MATSim, Ubiquity Press

Ptošek, V. and Slaninová K., 2018, Multinode Approach for Map Data Processing, 5th International Doctoral Symposium on Applied Computation and Security Systems (ACSS)

Folk, M., Heber, G., Koziol, Q., Pourmal, E. and Robinson, D., 2011, An overview of the HDF5 technology suite and its applications, Proceedings of the EDBT/ICDT 2011 Workshop on Array Databases, p.36-47, March 25-25, Uppsala, Sweden

Casagrande, L., Cavallini, P., Frigeri, A., Furieri, A., Marchesini, I. and Neteler, M. G., 2014, GIS Open Source: GRASS GIS, Quantum GIS and SpatiaLite

Silvano, C. et al., 2016, Autotuning and adaptivity approach for energy efficient Exascale HPC systems: The ANTAREX approach, 2016, Design, Automation & Test in Europe Conference & Exhibition (DATE), Dresden, pp. 708-713

MODELING OF WAVEGUIDE MODES EXCITAION IN THIN-FILM MULTILAYER STRUCTURES BY TM-POLARIZED GAUSSIAN LIGHT BEAM

Viktor I. Sokolov[(a)], Alexander S. Akhmanov[(b)], Ivan O. Goriachuk[(c)]

[(a),(b),(c)]Institute on Photonic Technologies, Federal Research Center "Crystallography and Photonics", Russian Academy of Sciences
[(a),(b)]Federal Research Center "Scientific Research Institute for System Analysis", Russian Academy of Sciences

[(a)]visokol@rambler.ru, [(b)]asakhmanov@mail.ru, [(c)]io.gorjachuk@physics.msu.ru,

ABSTRACT

The prism coupling technique is widely used for measuring optical parameters of thin light-guiding films. In this technique the probe laser beam scans the interface between the measuring prism of high refractive index and the film from the side of the prism, which leads to the excitation of guided modes in the film at certain resonant angles θ_i. The values of resonant angles θ_i correspond to sharp dips in the angular reflection spectrum (so called m-lines) and are used to calculate the refractive index and thickness of the film. Recently we have shown that using prism coupling technique one can determine not only the refractive index and thickness, but also the extinction coefficient of the films from the angular width of m-lines. In this paper we propose the modified mathematical algorithm and reveal that by taking into consideration the angular divergence of the probe laser beam one can improve the accuracy of extinction coefficient measurement. The problem of guided modes excitation in the multilayer thin-film structures by TM-polarized Gaussian light beam in the prism coupling geometry is considered theoretically. By using spectral approach the analytical formulas for the reflected TM Gaussian beam are derived. The developed fitting algorithm is used to calculate optical parameters of the four-layer metal-dielectric structure. It is shown that the algorithm is effective and permits to calculate optical parameters of multilayer structures in the high-coupling limit in the broad angular range.

Keywords: thin films, multilayer metal-dielectric structures, Gaussian beams, prism-coupling technique, measurement of optical parameters of films, fitting algorithms.

1. INTRODUCTION

The prism coupling technique is widely used for measuring refractive index and thickness of thin dielectric films (Ulrich, Torge 1973; Chiang, Cheng, Liu 2007; Dawson, Cairns, O'Prey 2000; Sotsky, Chudakovskii, Steingart, Jackson, Sotskaya 2013; Khomchenko, Sotsky, Romanenko, Glazunov, Kostyuchenko 2002; Pasmooij, Mandersloot, Smit 1989). In this technique the probe laser beam scans the interface between the measuring prism and the film

from the side of the prism in the broad range of angles θ, which leads to the excitation of guided modes in the film at certain resonant angles θ_i. The values of θ_i correspond to sharp dips in the angular reflection spectrum $R(\theta)$ (m-lines) and are then used to calculate the refractive index n and thickness H of the film. Recently we have shown that one can determine not only n and H, but also the extinction coefficient m of the film from the angular width of m-lines (Sokolov, Marusin, Panchenko, Savelyev, Seminogov, Khaidukov 2013; Sokolov, Glebov, Malyutin, Molchanova, Khaydukov, Panchenko 2015). In this paper we propose the modified mathematical algorithm and reveal that by taking into consideration the angular divergence of the probe Gaussian laser beam one can improve the accuracy of extinction coefficient measurement. The developed algorithm is valid both in the low and high coupling limits and can be used in the very broad angular range.

2. THE MODEL OF TM POLARIZED GAUSSIAN LIGHT BEAM AND IT'S REFLECTION FROM THE THIN-FILM STRUCTURE VIA PRISM COUPLING

Consider TM polarized Gaussian light beam of wavelength λ, which is incident at angle θ_0 upon the interface between the base of the measuring prism and thin-film metal – dielectric structure, Figure 1. The prism I of high refractive index N_p is separated from the multilayer structure by the gap layer II (immersion liquid or air), the thickness of the gap being $H_i = 10 - 150$ nm. The structure consists of the substrate VI, isolating layer V of thickness H_{f2}, light-guiding film IV of thickness H_{f1}, and cap layer III of thickness H_m. The dielectric permittivities of the substrate, thin-film layers V, IV, III and the gap are:

$$\varepsilon_s = (n_s + im_s)^2, \quad \varepsilon_{f2} = (n_{f2} + im_{f2})^2, \quad \varepsilon_{f1} = (n_{f1} + im_{f1})^2,$$
$$\varepsilon_m = (n_m + im_m)^2, \quad \varepsilon_i = (n_i + im_i)^2,$$

where n and m are refractive indexes and extinction coefficients of the pertinent mediums. In what follows we suppose that mediums VI – III are made of copper (Cu), sapphire (Al$_2$O$_3$), polymer PMMA with embedded

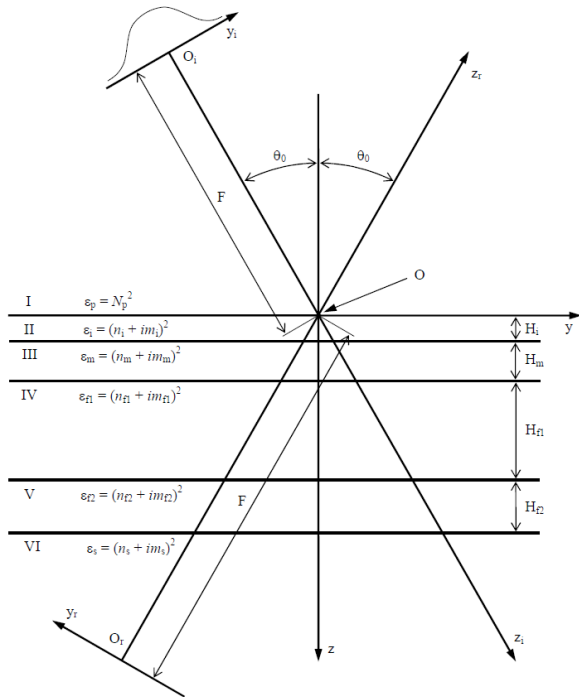chromophore DR13 and Cu correspondingly, medium II is air.

Figure 1. Reflection of the Gaussian light beam from the multilayer thin – film structure in prism coupling geometry. ε_p, ε_i, ε_{f1}, ε_{f2} and ε_s are dielectric permittivities of the measuring prism I, gap II, semitransparent copper film III, polymer light-guiding layer IV, isolating Al_2O_3 layer V and copper substrate VI. H_i is thickness of the gap between the prism and the structure, θ_0 is angle of incidence.

In the coordinate system (y_i, z_i), which is connected with the incident light beam, the magnetic field of TM polarized two-dimensional Gaussian beam has the form

$$\vec{h}_i(y_i, z_i, t) = \vec{h}_i(y_i, z_i)\exp(-i\omega t) + c.\,c.$$

$$\vec{h}_i(y_i, z_i) = \vec{x}_i \frac{w_0}{2\sqrt{\pi}} \int_{-\infty}^{+\infty} \exp\left(-\frac{k_{iy}^2 w_0^2}{4} + ik_{iy}y_i + ik_{iz}z_i\right)dk_{iy} \qquad (1)$$

In Equation (1) $2w_0$ is diameter of the Gaussian beam at the waist, $k_{iz} = \sqrt{k^2\varepsilon_p - k_{iy}^2}$, $k = 2\pi/\lambda$. It is easy to show that in the coordinate system (y_r, z_r), which is connected with the reflected beam, the magnetic field of the beam reads

$$\vec{h}_r(y_r, z_r) = \vec{x}_r \frac{w_0}{2\sqrt{\pi}} \int_{-\infty}^{+\infty} R_a^p(k_{iy})\exp\left(-\frac{k_{iy}^2 w_0^2}{4} - ik_{iy}y_r + ik_{iz}z_r\right)dk_{iy} \qquad (2)$$

The expressions for the amplitude reflectivity $R_a^p(k_{iy})$ are presented in the Appendix. Similar expressions in the case of TE polarized Gaussian beam can be found in the literature (Sokolov, Marusin, Molchanova, Savelyev, Khaydukov, Panchenko 2014). Equation (2) holds for arbitrary coupling strength, i.e. for arbitrary

correlation between the beam diameter $2w_0$ and propagation length l of TM modes in the light-guiding layer IV (see Figure 1).

3. FABRICATION OF MULTILAYER THIN FILM STRUCTURE AND MEASURING REFLECTIVITY USING PRISM COUPLING TECHNIQUE

The thin-film structure under investigation contained four layers on the silica plate. First, ≈ 1 µm thick copper layer was deposited on the SiO2 plate using magnetron sputtering technique. Since the thickness of the copper layer exceeds the skin layer considerably it will be considered as the substrate in what follows. Then, Al_2O_3 isolating film with the thickness 0.3 – 0.4 µm was fabricated on the Cu substrate. The light-guiding layer made of PMMA polymer with embedded DR13 electro-optical chromophore (guest – host structure) was spin-coated on the Al_2O_3 film using SPIN-1200T spinner (Midas System Co., Ltd.). The thickness of the light-guiding layer was estimated to be $\approx 8 - 9$ µm. Finally, thin semi-transparent conducting copper film was deposited on the PMMA/DR13 layer by magnetron sputtering.

Reflection coefficients for TE and TM polarized probe laser beam were measured using prism coupler Metricon2010/M (Metricon Inc.). The device was equipped with He-Ne laser ($\lambda = 632.8$ nm), having the diameter of the beam at the waist 0.65 mm and the angular divergence $\Delta\theta = 0.07$ grad. The experimental scheme realized in Metricon2010/M is shown in Figure 2.
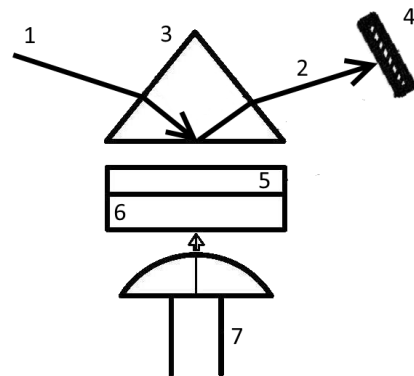
Figure 2. Scheme of the experiment setup for measuring the reflectivity of thin film structures using prism coupling technique. 1, 2 – incident and reflected laser light beams, 3 - measuring prism of high refractive index, 4 – photodetector, 5 – thin film structure to be measured, 6 - substrate, 7 - pneumatically-operated coupling head.

The laser beam 1, 2 enters the measuring prism of high refractive index 3, strikes the base side of the prism and is reflected onto photodetector 4. The thin film structure 5 on the substrate 6 is brought into close optical contact with the base side of the prism by means of the pneumatically-operated coupling head 7 so that the air

gap (typically 10 – 100 nm) separates the film and the prism. The angle of incidence θ of the laser beam is varied by means of the rotary table so the broad angular range (typically 30 – 60 deg) is covered. At certain values of the incident angles θ, which are called mode angles, the total internal reflection criteria is violated and photons from the laser beam can tunnel across the air gap into the film and enter into optical propagation modes. The resonant excitation of the waveguide mode in the thin film structure causes a sharp drop in the intensity of reflected laser light striking the photodetector.

Figure 3 shows the measured reflection coefficients $R_{TE}(\theta)$, $R_{TM}(\theta)$ for TE and TM polarized incident laser beams. One can see from Figure 3 that the angular width of resonances for TE and TM m-lines equals $\delta\theta = 0.06$ and 0.15 grad correspondingly, which is comparable to angular divergence $\Delta\theta = 0.07$ grad of the probe He-Ne laser beam used in Metricon2010/M prism coupler. It means that the influence of incident beam divergence upon the measured width of m-lines can be considerable and should be taken into consideration.
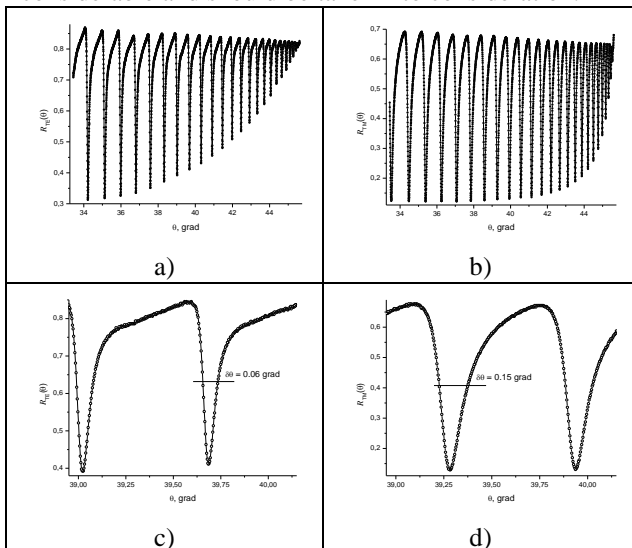
Figure 3: Reflection coefficients $R_{TE}(\theta)$ (a), (c) for TE- and $R_{TM}(\theta)$ (b), (d) for TM-polarized Gaussian light beam ($\lambda = 632.8$ nm) measured with Metricon2010/M prism coupler.

4. CALCULATION OF OPTICAL PARAMERS OF THIN FILMS USING PLANE WAVE AND GAUSSIAN BEAM MODELS

The standard approach in the prism coupling technique used to calculate optical parameters of thin films from the measured reflectivity coefficient $R(\theta)$ is based on the analysis of positions of resonance angles θ_i (Ulrich, Torge 1973; Chiang, Cheng, Liu 2007). This approach is valid only in the small coupling limit and only for single dielectric films on the substrate. Moreover it is used to calculate refractive index and thickness, but not the extinction coefficient of the film.

In contrast to the standard approach we propose to analyze not only the positions of resonant angles θ_i (m-lines), but also the amplitude and shape of reflection

coefficients $R(\theta)$ for TE and TM polarized light beams in the broad angular range. The curves $R(\theta)$ contains much more information about the multilayer structure than θ_i. For example, the angular width of the m-lines characterizes the extinction coefficient of the light-guiding film (Sokolov, Marusin, Panchenko, Savelyev, Seminogov, Khaidukov 2013; Sokolov, Glebov, Malyutin, Molchanova, Khaydukov, Panchenko 2015), whereas the amplitude of reflectivity dips gives the information about the thickness of the gap between the measuring prism and the structure. We propose also to take into consideration the angular divergence of the probe laser beam. It permits to improve the accuracy of measuring film parameters, especially for highly transparent films, which have very narrow m-line resonances.

The mathematical algorithm we propose is based on the fitting approach. First, the reflectivity of TE and TM polarized Gaussian laser beam from the multilayer thin-film structure is measured with high accuracy by prism coupling technique. The theoretical curves $R(\theta)$ are then calculated for both polarizations and the mean-square difference D_{abs} between the measured and calculated reflectivities is determined. By variating the parameters of the structure (refractive index, extinction coefficient and thickness of films as well as the thickness of the gap between the prism and the sample) and using the special highly-effective computation algorithm, the minimal value of D_{abs} is determined. The parameters which provide the smallest D_{abs} value are believed to be the real parameters of the structure.

In Figure 4 the result of fitting is presented, when the angular divergence of the incident beam is neglected ($\Delta\theta = 0$, Plane Wave (PW) model). The calculated parameters of the layers are given in the caption to Figure 4. One can see that in PW case the mean-square difference between the measured and calculated reflectivities equals $D_{abs} = 2.28$.

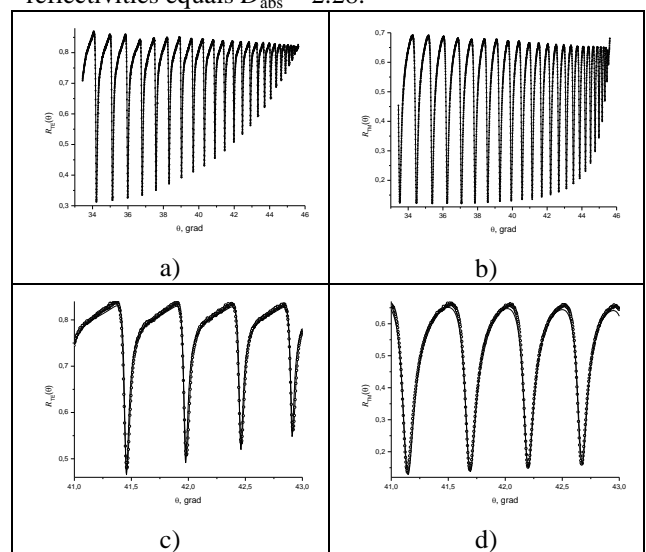Figure 4: Measured (dots) and calculated (solid lines) reflection coefficients $R_{TE}(\theta)$ (a), (c) and $R_{TM}(\theta)$ (b), (d) for TE and TM polarized light correspondingly. The fitting procedure was done using plane wave model,

D_{abs} = 2.28. Calculated parameters of the air gap and thin films in the structure: H_i = 10.32 nm, n_m = 0.4245, m_m = 3.0403, H_m = 38.92 nm, n_{f1} = 1.5339, m_{f1} = 0.0003262, H_{f1} = 8265.07 nm, n_{f2} = 1.6045, m_{f2} = 0, H_{f2} = 330.51 nm, n_s = 0.5796, m_s = 3.2271.

Figure 5 shows the result of fitting, when the angular divergence of the probe Gaussian light beam $\Delta\theta$ = 0.07 is taken into consideration (Gaussian Beam (GB) model). One can see that for GB model D_{abs} = 2.18 which is smaller than D_{abs} = 2.28 for PW model. Thus, the fitting is better when the divergence of the probe Gaussian laser beam is taken into account.
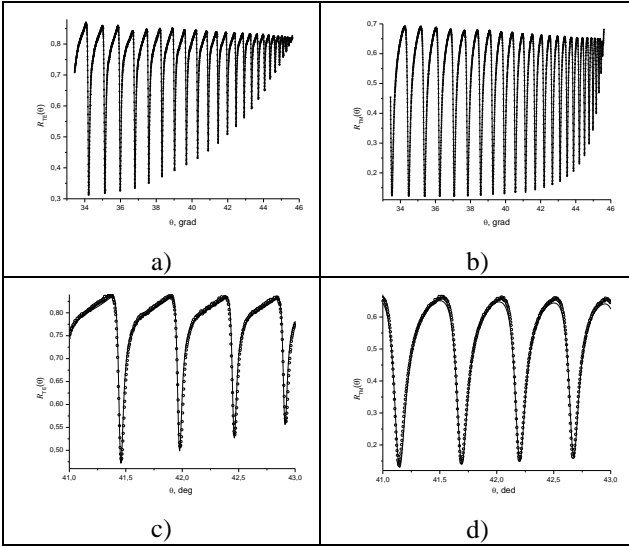

Figure 5: Measured (dots) and calculated (solid lines) reflection coefficients $R_{TE}(\theta)$ (a), (c), $R_{TM}(\theta)$ (b), (d) for TE and TM polarized light. The fitting procedure was done using Gaussian beam model, D_{abs} = 2.18. Calculated parameters of the air gap and thin films in the structure: H_i = 10.42 nm, n_m = 0.4263, m_m = 3.0258, H_m = 39.21 nm, n_{f1} = 1.5333, m_{f1} = 0.0002529, H_{f1} = 8240.56 nm, n_{f2} = 1.6022, m_{f2} = 0, H_{f2} = 337.77 nm, n_s = 0.6242, m_s = 3.2845.

The calculated thickness of the air gap H_i = 10.42 nm (see caption to Figure 5) indicates that the high coupling limit was realized in the experiment. Nevertheless, the agreement between the measured and calculated curves $R_{TE}(\theta)$, $R_{TM}(\theta)$ in Figure 5 is very good. Thus, the developed algorithm can be used in the very broad coupling range in contrast to standard approach which is valid only in the low coupling limit. Table 1 summarizes the results of fitting in the case of PW and GB models.

Table 1. Optical parameters of the light-guiding layer IV (see Figure 1) calculated using Plane Wave (PW) and Gaussian Beam (GB) models of the probe beam.

	n_{f1}	m_{f1}	H_{f1}, nm
PW model	1.5339	3.262×10^{-4}	8265.07
GB model	1.5333	2.529×10^{-4}	8240.51

It can be seen from Table 1 that the used models of the incident probe beam give similar values for refractive index n_{f1} and thickness H_{f1} of the light-guiding film, but different values of extinction coefficient m_{f1}. The Gaussian beam model gives a factor 1.3 lower value of m_{f1} than the Plane Wave model. For highly transparent films the difference in calculated values of m_{f1} of the light-guiding film can be even higher.

The proposed algorithm can also be used for measuring electro-optical coefficients r_{33} and r_{13} of thin films.

CONSLUSIONS

The problem of guided modes excitation in thin-film structures by TM-polarized Gaussian light beam using prism coupling technique is considered. It is shown that by taking into consideration the angular divergence of the probe laser beam one can improve the accuracy of measuring optical parameters of multilayer metal – dielectric structures, including the accuracy of extinction coefficient measurement. Also we have developed the effective mathematical algorithm, which permits to calculate optical parameters of multilayer thin film structures using TE and TM polarized laser beams. The algorithm is valid both in the low and high coupling limits in the broad angular range.

ACKNOWLEDGMENTS

APPENDIX

The amplitude reflectivity $R_a^p(k_{iy})$ in Equation (2) reads

$$R_a^p(k_{iy}) = \frac{\varepsilon_i k_z - i\gamma^{II}\varepsilon_p}{\varepsilon_i k_z + i\gamma^{II}\varepsilon_p}\left[1 + \frac{4\varepsilon_i k_z i\gamma^{II}\varepsilon_p}{(\varepsilon_i k_z)^2 + (\varepsilon_p\gamma^{II})^2}\times\frac{e^{-2\gamma^{II}H_i}}{\frac{1}{A_p} + \frac{\varepsilon_i k_z - i\gamma^{II}\varepsilon_p}{\varepsilon_i k_z + i\gamma^{II}\varepsilon_p}e^{-2\gamma^{II}H_i}}\right]$$

where

$$A_p = \frac{\varepsilon_m\gamma^{II} - \varepsilon_i\gamma^{III}}{\varepsilon_m\gamma^{II} + \varepsilon_i\gamma^{III}}\left[1 + \frac{4\varepsilon_m\gamma^{II}\varepsilon_i\gamma^{III}}{(\varepsilon_m\gamma^{II})^2 - (\varepsilon_i\gamma^{III})^2}\times\frac{e^{-2\gamma^{III}H_m}}{\frac{1}{B_p} + \frac{\varepsilon_m\gamma^{II} - \varepsilon_i\gamma^{III}}{\varepsilon_m\gamma^{II} + \varepsilon_i\gamma^{III}}e^{-2\gamma^{III}H_m}}\right]$$

$$B_p = \frac{\varepsilon_{f1}\gamma^{III} - \varepsilon_m\gamma^{IV}}{\varepsilon_{f1}\gamma^{III} + \varepsilon_m\gamma^{IV}}\left[1 + \frac{4\varepsilon_{fi}\gamma^{III}\varepsilon_m\gamma^{IV}}{(\varepsilon_{f1}\gamma^{III})^2 - (\varepsilon_m\gamma^{IV})^2}\times\frac{e^{-2\gamma^{IV}H_{f1}}}{\frac{1}{C_p} + \frac{\varepsilon_{f1}\gamma^{III} - \varepsilon_m\gamma^{IV}}{\varepsilon_{f1}\gamma^{III} + \varepsilon_m\gamma^{IV}}e^{-2\gamma^{IV}H_{f1}}}\right]$$

$$C_p = \frac{\varepsilon_{f2}\gamma^{IV} + \varepsilon_{f1}\gamma^{V}}{\varepsilon_{f2}\gamma^{IV} - \varepsilon_{f1}\gamma^{V}}\left(\frac{\varepsilon_{f2}\gamma^{IV} - \varepsilon_{f1}\gamma^{V}}{\varepsilon_{f2}\gamma^{IV} + \varepsilon_{f1}\gamma^{V}}e^{\gamma^{V}H_{f2}} + \frac{\varepsilon_s\gamma^{V} - \varepsilon_{f2}\gamma^{VI}}{\varepsilon_s\gamma^{V} + \varepsilon_{f2}\gamma^{VI}}e^{-\gamma^{V}H_{f2}}\right)/$$

$$\left(\frac{\varepsilon_{f2}\gamma^{IV} + \varepsilon_{f1}\gamma^{V}}{\varepsilon_{f2}\gamma^{IV} - \varepsilon_{f1}\gamma^{V}}e^{\gamma^{V}H_{f2}} + \frac{\varepsilon_s\gamma^{V} - \varepsilon_{f2}\gamma^{VI}}{\varepsilon_s\gamma^{V} + \varepsilon_{f2}\gamma^{VI}}e^{-\gamma^{V}H_{f2}}\right)$$

Here

$$\gamma^{II} = \left(k_y^2 - k^2\varepsilon_i\right)^{1/2}, \operatorname{Re}\gamma^{II} \geq 0, \operatorname{Im}\gamma^{II} \leq 0; \gamma^{III} = \left(k_y^2 - k^2\varepsilon_m\right)^{1/2}, \operatorname{Re}\gamma^{III} \geq 0, \operatorname{Im}\gamma^{III} \leq 0;$$

$$\gamma^{IV} = \left(k_y^2 - k^2\varepsilon_{f1}\right)^{1/2}, \operatorname{Re}\gamma^{IV} \geq 0, \operatorname{Im}\gamma^{IV} \leq 0; \gamma^{V} = \left(k_y^2 - k^2\varepsilon_{f2}\right)^{1/2}, \operatorname{Re}\gamma^{V} \geq 0, \operatorname{Im}\gamma^{V} \leq 0;$$

$$\gamma^{VI} = \left(k_y^2 - k^2\varepsilon_s\right)^{1/2}, \operatorname{Re}\gamma^{VI} \geq 0, \operatorname{Im}\gamma^{VI} \leq 0.$$

REFERENCES

Chiang K.S., Cheng S.Y., Liu Q., 2007. Characterization of ultrathin dielectric films with the prism-coupler method. J. of Lightwave Technology 25 (5) 1206-1211.

Dawson P., Cairns G.F., O'Prey S.M., 2000. Prism coupler with variable coupling gap. Review of Scientific Instruments 71 (11) 4208-4212.

Khomchenko A.V., Sotsky A.B., Romanenko A.A., Glazunov E.V., Kostyuchenko D.N., 2002. Determining thin film parameters by prism coupling technique. Technical Physics Letters 28 (6) 467-470.

Pasmooij W.A., Mandersloot P.A., Smit M.K., 1989. Prism coupling of light into narrow planar optical waveguides. Journal of Lightwave technology (7) (1) 175 - 180.

Sokolov V.I., Marusin N.V., Panchenko V.Ya., Savelyev A.G., Seminogov V.N., Khaidukov E.V., 2013. Determination of refractive index, extinction coefficient and thickness of thin films by the method of waveguide mode excitation. Quantum Electronics 43 1149–1153.

Sokolov V.I., Marusin N.V., Molchanova S.I., Savelyev A.G., Khaydukov E.V., Panchenko V.Ya., 2014. Reflection of a TE-polarised Gaussian beam from a layered structure under conditions of resonance excitation of waveguide modes. Quantum Electronics 44 1048–1054.

Sokolov V.I., Glebov V.N., Malyutin A.M., Molchanova S.I., Khaydukov E.V., Panchenko V.Ya., 2015. Investigation of optical properties of multilayer dielectric structures using prism-coupling technique. Quantum Electronics 45 868–872.

Sotsky A.B., Chudakovskii P.Y., Steingart L.M., Jackson J.H., Sotskaya L.I., 2013. Prism excitation of leaky modes of thin films. Technical Physics. The Russian Journal of Applied Physics 58 (11) 1651-1660.

Ulrich R., Torge R., 1973. Measurement of thin film parameters with a prism coupler. Applied Optics 12 (12), 2901-2908.

AUTHORS BIOGRAPHY

Viktor I. Sokolov. Department of Physical and Quantum Electronics of Moscow Institute of Physics and Technology (State University), 1980. Fields of scientific interests: integrated optics, high-speed data- and telecommunications, interaction of laser radiation with multilayer thin-film structures, prism coupling technique, high-speed electro-optic modulators, waveguide optical amplifiers. Currently, he is director of the Institute on Photonic Technologies, Federal Research Center "Crystallography and Photonics" of the Russian Academy of Sciences, Moscow, Russia. (www.kif.ras.ru).

Alexander S. Akhmanov. Department of Physics of Moscow State University, 1978. Fields of scientific interests: light interaction with thin-film structures, high-speed data communications. Currently, he works in the Institute on Photonic Technologies, Federal Research Center "Crystallography and Photonics" of the Russian Academy of Sciences, Moscow, Russia. (www.kif.ras.ru).

Ivan O. Goriachuk. Department of Physics of Moscow State University, 2017. Fields of scientific interests: interaction of laser radiation with multilayer thin-film structures, polymer waveguides, optical chromophores, prism coupling technique, high-speed electro-optic modulators. Currently, he works in the Institute on Photonic Technologies, Federal Research Center "Crystallography and Photonics" of the Russian Academy of Sciences, Moscow, Russia. (www.kif.ras.ru).

ANALYSIS OF MULTILAYER METAL-DIELECTRIC THIN-FILM STRUCTURES USING PRISM COUPLING TECHNIQUE

Ivan O. Goriachuk[(a)], Vladislav N. Glebov[(b)], Andrey M. Maliutin[(c)], Viktor I. Sokolov[(d)]

[(a),(d)]Institute on Photonic Technologies, Federal Research Center "Crystallography and Photonics", Russian Academy of Sciences
[(b),(c)]Institute on Laser and Information Technologies, Federal Research Center "Crystallography and Photonics", Russian Academy of Sciences
[(d)]Federal Research Center "Scientific Research Institute for System Analysis", Russian Academy of Sciences
[(a)]io.gorjachuk@physics.msu.ru, [(b),(c)]ammaliutin@rambler.ru, [(d)]visokol@rambler.ru

ABSTRACT

The mathematical algorithm and fitting method for measuring optical parameters (refractive index, extinction coefficient as well as thickness of layers) of multilayer thin-film structures using prism coupling technique is proposed. The algorithm works well both in the low and high coupling limits. It is valid for dielectric and metallic films and takes into account the variation of refractive index and extinction coefficient of the film in the direction normal to the film plane. The efficiency of the algorithm is demonstrated by measuring optical parameters of the metal-dielectric structure, which includes copper film on quartz substrate, isolating sapphire film, light-guiding polymer film with embedded electro-optical chromophores and semitransparent conducting Cu cap layer. The proposed algorithm and fitting method can be used for measuring electro-optical coefficients in thin films.

Keywords: measuring multilayer thin-film structures, prism-coupling technique, surface plasmons, fitting method.

1. INTRODUCTION

The prism coupling technique based on resonant excitation of guided modes in thin films is an effective and convenient method for measuring refractive index and thickness of optical layer (Ulrich, Torge 1973; Chiang, Cheng, Liu 2007; Dawson, Cairns, O'Prey 2000; Ay, Kocabas, Cocabas, Aydinli, Agan 2004). However the standard algorithms for calculating thin film parameters, which are realized in commercially available prism couplers (see, for example, www.metricon.com), have a number of significant drawbacks. First, they can determine only the refractive index and thickness of the film. This is because the standard algorithms analyze only the angular positions of m – lines, but not the whole reflectivity spectrum $R(\theta)$. The $R(\theta)$ involves much more information about the film under investigation than m - lines positions. For example, the width and depth of m - lines depend upon the extinction coefficient of the film and can be used for determining this important parameter of the film

(Sokolov, Marusin, Panchenko, et al 2013). Second, the standard algorithms are valid only in the low coupling limit when the thickness of the gap between the film and the measuring prism exceeds 100 – 150 nm. Third, they do not take into consideration the variation of refractive index and extinction coefficient of the film in the direction normal to the film plane.

Finally the standard algorithms cannot work with complex multilayer structures. The necessity of studying structures with a large number of layers frequently arises in practice, e.g. in fabricating multilayer interference mirrors (Sokolov, Glebov, Malyutin, et al 2015) and high-speed electro-optic polymer modulators (Nazarov, Glebov, Goriachuk, et al 2018). Therefore the effective algorithms which can be used for analyzing such structures are highly desirable.

In this paper we propose the effective algorithm and fitting method, which permit to calculate optical parameters of metal and dielectric thin-film structures from the angular reflection spectra $R(\theta)$, when the number of layers in the structure exceeds two. The mathematical model, which describes excitation of guided modes and surface plasmons in the multilayer structure by TE and TM polarized light is developed. The model is valid both in the low and high coupling limits and takes into account the variation of refractive index and extinction coefficient in the film. The developed algorithm was used to calculate the optical parameters of the three-layer metal-dielectric structure, which includes the copper layer on quartz substrate, isolating Al_2O_3 film, light-guiding PMMA polymer film with embedded electro-optical chromophores DR13 and semitransparent conducting Cu cap layer. This layered structure can be used for measuring electro-optical coefficients r_{33} and r_{13} in the films and for fabricating high-speed polymer electro-optical modulators.

2. FABRICATION OF MULTILAYER THIN-FILM METAL-DIELECTRIC STRUCTURE

The three-layer light-guiding structure was fabricated on the polished quartz substrate. First, the copper layer (down electrode) with the thickness $\approx 1~\mu m$ was deposited on the quartz substrate using magnetron

sputtering technique. Then ≈ 300 nm amorphous Al_2O_3 isolating film was fabricated on the copper layer by electron beam evaporation method. The PMMA polymer film with embedded DR13 chromophore was spin coated on the Al_2O_3 layer and had the thickness 7 – 9 μm. The PMMA/DR13 electro-optical film was annealed in the inert atmosphere during 2 hours. Finally, the semitransparent conducting Cu film with the thickness 30 – 40 nm (top electrode) was fabricated on the polymer film by magnetron sputtering. The sketch of the fabricated structure, which is in contact with the measuring prism of high refractive index N_p, is shown in Figure 1. ε_p, ε_i, ε_m, ε_{f1}, ε_{f2} and ε_s is dielectric permittivity of the medium I, II, III, IV, V and VI correspondingly. H_i denotes the thickness of the gap between the prism and the structure, H_m, H_{f1} and H_{f2} denote the thicknesses of the layers, n and m with proper subscript are refractive indices and extinction coefficients of films in the structure.
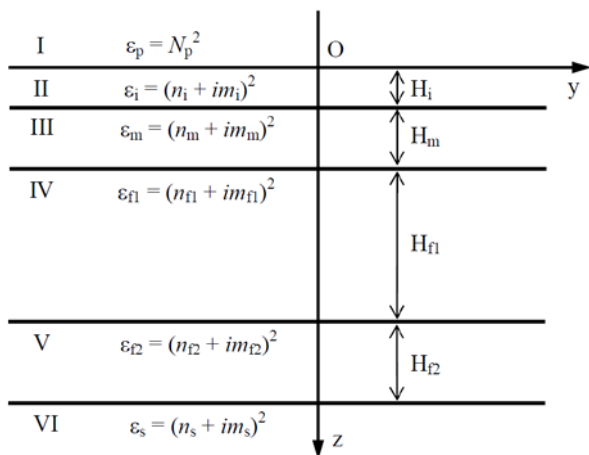

Figure 1: Sketch of the Multilayer Thin-film Structure and the Measuring Prism. I – Measuring Prism, II – Gap Between the Prism and the Structure, III – Semitransparent Copper Layer (Top Electrode), IV – Light-Guiding Polymer Film With Embedded Electro-optic Chromophores, V - Al_2O_3 Isolating Layer, VI – Copper Film on Quartz Substrate (Down Electrode).

3. MEASURING REFLECTIVITIES $R_{TE}(\theta)$, $R_{TM}(\theta)$ OF TE- AND TM-POLARIZED LIGHT WAVES FROM METAL-DIELECTRIC STRUCTURE

In the prism coupling technique the sample (a film on a substrate) is set in optical contact with the base of a measuring prism, the thickness of the gap between the prism and the sample being H_i = 10 – 150 nm. TE- or TM-polarized laser beam is incident on the interface between the prism and the sample and then is reflected from the interface back into the prism. The reflection coefficient R as a function of the incidence angle θ is measured in the broad angular range, both at θ < θ_{crit} and θ > θ_{crit}, where θ_{crit} is the critical angle of total internal reflection on the prism - sample interface. The graph $R(\theta)$ shows the dips (characteristic resonances or m - lines), which correspond to the excitation of guided

TE- or TM modes in the light-guiding structure. In Figure 2 one can see $R_{TE}(\theta)$ and $R_{TE}(\theta)$ spectrums for TE and TM light waves reflected from the three-layer metal-dielectric structure presented in Figure 1. The spectrums $R_{TE}(\theta)$, $R_{TE}(\theta)$ were measured using Metricon2010/M prism coupler at wavelength λ = 632.8 nm (red He-Ne laser).
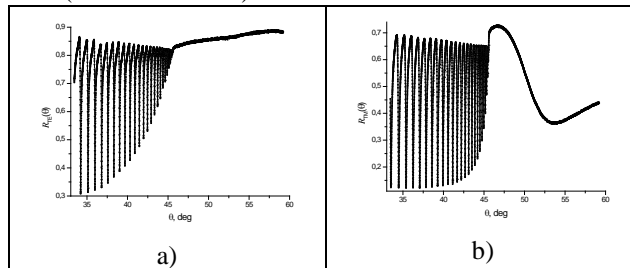
Figure 2: Reflectivity $R_{TE}(\theta)$ for TE (a) and $R_{TM}(\theta)$ for TM (b) Waves of Wavelength λ = 632.8 nm Measured with Metricon2010/M Prism Coupler.

The sharp m – lines at θ < 45.5 deg in Figure 2a and Figure 2b are stipulated by resonant excitation of TE and TM modes in the light-guiding PMMA/DR13 film, whereas the broad dip at θ ≈ 53.8 deg in Figure 2b is due to the excitation of the surface plasmon in the semitransparent top copper film III (see Figure 1) by incident TM wave.

4. ANALYSIS OF REFLECTION COEFFICIENTS

Consider first the simple model of the structure, which implies that permittivities ε_m, ε_{f1}, ε_{f2} and ε_s do not vary along z – axis (see Figure 1). In this case, the reflectivity $R(\theta)$ can be calculated analytically as a function of structure parameters (Nazarov, Glebov, et al 2018). By variating the parameters of the structure we fit the calculated reflectivity to the measured one thus minimizing the mean-squared difference D_{abs} between the measured and calculated $R(\theta)$. In this way the parameters of the structure, which correspond to the minimal value of D_{abs}, are found. Because of the big number of parameters of the structure to be analyzed the computations are rather time-consuming. To reduce the time of the computations we have developed the mathematical algorithm and effective fitting method. The algorithm is based on the gradient descent approach and permits to reduce the computation time considerably.

The reflectivity $R_{TE}(\theta)$, $R_{TM}(\theta)$ for TE and TM polarized light waves, calculated using the simple model are presented in Figure 3. One can see from Figure 3 that the model fits well the positions of m - lines, but does not permit to fit the angular position of the surface plasmon. The fitting parameter D_{abs} equals 5.04.

a)

b)

Figure 3: Reflectivity $R_{TE}(\theta)$ for TE (a) and $R_{TM}(\theta)$ for TM (b) Waves of λ = 632.8 nm Incident Upon the Multilayer Structure. Dots - Experiment, Solid Line - Theory (Fitting Curve). The Model Used Suggests the Dielectric Permittivities of All Mediums are Constant. The Calculated Parameters of the Structure are: H_i = 13.12 nm, n_m = 0.3442, m_m = 2.822, H_m = 36.15 nm, n_{f1} = 1.5338, m_{f1} = 0.000667, H_{f1} =8254.20 nm, n_{f2} = 1.6092, m_{f2} = 0, H_{f2} = 342.27, n_s = 0.047, m_s = 3.6474.

Then we have developed the more sophisticated mathematical model for determining the optical parameters (refractive index n and extinction coefficient m) as well as thickness of films in the multilayer structure. The model takes into account the modulation of n and m in the cap metal layer III in the direction normal to the film plane. The detailed description of this model and exact expressions for reflectivities $R_{TE}(\theta)$ and $R_{TM}(\theta)$ are presented in the Appendix. Figure 4 shows the calculated reflectivity in this case. The fitting between experimental and theoretical curves is much better in comparison to the case of homogeneous metal layer and D_{abs} = 3.09. One can see also that the calculated angular position and the depth of the surface plasmon fit well the measured ones.
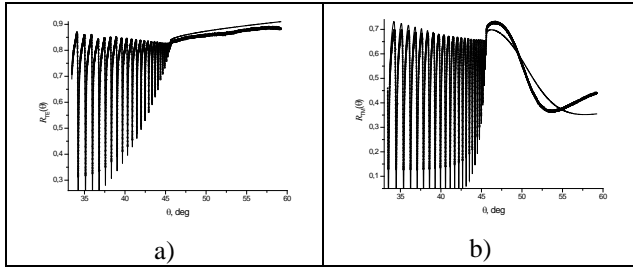

a)

b)
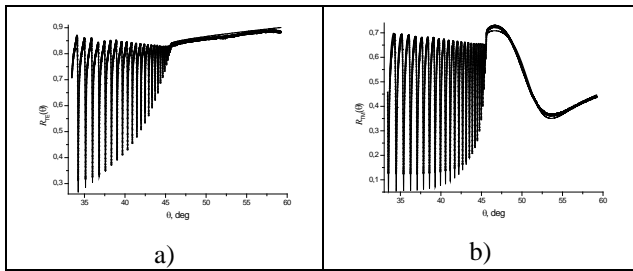
Figure 4: Reflectivity $R_{TE}(\theta)$ for TE (a) and $R_{TM}(\theta)$ for TM (b) Waves of λ = 632.8 nm Incident Upon the Multilayer Structure. Dots - Experiment, Solid Line - Theory (Fitting Curve). The Model Used Suggests the Dielectric Permittivity of the Cap Copper Layer Varies vs z – Coordinate. Dielectric Permittivities of Other Mediums are Constant. The Calculated Parameters of the Structure are: H_i = 8.49 nm, H_m = 36.54 nm, n_{f1} = 1.5337, m_{f1} = 0.000667, H_{f1} =8258.11 nm, n_{f2} = 1.6092, m_{f2} = 0, H_{f2} = 342.47, n_s = 0.468, m_s = 3.164.

The distribution of refractive index n_m and extinction coefficient m_m in the cap copper layer are shown in Figure 5.

a)

b)
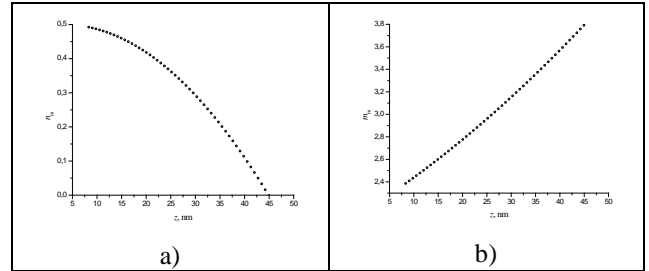
Figure 5: Calculated Distribution of Refractive Index n (a) and Extinction Coefficient m (b) in the Cap Copper Layer.

CONSLUSIONS
We have developed the mathematical model and effective algorithm for analyzing multilayer thin-film structures using prism coupling technique. The algorithm is valid for dielectric and metallic films both in the low and high coupling limits and takes into consideration the variation of refractive index and extinction coefficient of the film in the direction normal to the film plane. The efficiency of the algorithm is demonstrated by measuring optical parameters of the metal-dielectric structure, which includes copper film on quartz substrate, isolating sapphire film, light-guiding polymer film with embedded electro-optical chromophores and semitransparent conducting Cu cap layer. The proposed algorithm and fitting method can be used for measuring electro-optical coefficients r_{33} and r_{13} in thin films. The new technique may find applications in developing of high-speed polymer electro-optic modulator for radio photonics.

APPENDIX
When complex dielectric permittivity varies with the thickness of semitransparent metal layer (medium III), a mathematical model of the light reflection from multilayer thin film structure is constructed in the self-consistent field regime as follows. Firstly, the solutions of Maxwell equations

$$rot\vec{E}(y,z) = ik\vec{H}(y,z),$$
$$rot\vec{H}(y,z) = -ik\varepsilon(z)\vec{E}(y,z),$$
(1)

(where $k = 2\pi / \lambda$) for complex amplitudes $\vec{E}, \vec{H}$ of monochromatic light fields are found in every medium. In homogeneous media I, II, IV, V, VI these solutions are described by plane waves, proportional to

$\exp\left(ik_y y \pm \gamma z\right)$ (see Eqs. (7) and (8)). TE polarization corresponds the case when the electric field strength vector is directed along the x axis, while for TM waves it lies in the incidence plane Oyz (see Figure 1) and the magnetic field strength vector is orthogonal to it. Secondly, the field sawing conditions on the boundaries of layers are imposed. Then amplitudes of down-going and up-going waves become interrelated, permitting to find the intensity of reflected light with the given intensity of incident radiation.

The value of complex reflection coefficient R_{aTE} for TE (or s) polarized plane wave is given by the following expressions:

$$R_{aTE} = \frac{\dfrac{k_z - i\gamma^{II}}{k_z + i\gamma^{II}} + A_s e^{-2\gamma^{II} H_i}}{1 + \dfrac{k_z - i\gamma^{II}}{k_z + i\gamma^{II}} A_s e^{-2\gamma^{II} H_i}}, \qquad (2)$$

$$A_s = \frac{\left(e^{\downarrow} + \dfrac{1}{\gamma^{II}}\dfrac{de^{\downarrow}}{dz}\right) - B_s\left(e^{\uparrow} + \dfrac{1}{\gamma^{II}}\dfrac{de^{\uparrow}}{dz}\right)}{\left(e^{\downarrow} - \dfrac{1}{\gamma^{II}}\dfrac{de^{\downarrow}}{dz}\right) - B_s\left(e^{\uparrow} - \dfrac{1}{\gamma^{II}}\dfrac{de^{\uparrow}}{dz}\right)}\Bigg|_{H_i}, \qquad (3)$$

$$B_s = \frac{\left(e^{\downarrow} + \dfrac{1}{\gamma^{IV}}\dfrac{de^{\downarrow}}{dz}\right) - C_s\left(e^{\downarrow} - \dfrac{1}{\gamma^{IV}}\dfrac{de^{\downarrow}}{dz}\right)e^{-2\gamma^{IV} H_{f1}}}{\left(e^{\uparrow} + \dfrac{1}{\gamma^{IV}}\dfrac{de^{\uparrow}}{dz}\right) - C_s\left(e^{\uparrow} - \dfrac{1}{\gamma^{IV}}\dfrac{de^{\uparrow}}{dz}\right)e^{-2\gamma^{IV} H_{f1}}}\Bigg|_{H_i + H_m}, \qquad (4)$$

$$C_s = \frac{\dfrac{\gamma^{IV} - \gamma^{V}}{\gamma^{IV} + \gamma^{V}} + \dfrac{\gamma^{V} - \gamma^{VI}}{\gamma^{V} + \gamma^{VI}}e^{-2\gamma^{V} H_{f2}}}{1 + \dfrac{\gamma^{IV} - \gamma^{V}}{\gamma^{IV} + \gamma^{V}} \cdot \dfrac{\gamma^{V} - \gamma^{VI}}{\gamma^{V} + \gamma^{VI}}e^{-2\gamma^{V} H_{f2}}}, \qquad (5)$$

where functions $e^{\downarrow}(z)$ and $e^{\uparrow}(z)$ are arbitrary linearly independent solutions of

$$\frac{d^2 e(z)}{dz^2} + \left(k^2 \varepsilon_m(z) - k_y^2\right)e(z) = 0. \qquad (6)$$

This differential equation has to be solved numerically for each incidence angle and every specific set of structure parameters, i.e. for every type of behavior of semitransparent metal layer refractive index $n_m(z)$ and the extinction coefficient $m_m(z)$ of the layer. These functions are fitted using polynomial template of the 4th order.

In the expressions above for each homogeneous layer we introduced the value γ, which is related to the complex dielectric permittivity and the wave number k in the following way:

$$\gamma^2 = k_y^2 - k^2\varepsilon, \text{Re}(\gamma) \geq 0, \text{Im}(\gamma) \leq 0, \qquad (7)$$

while the projections of the wave vector are related with the incidence angle θ:

$$\begin{aligned} k_y &= kN_p\sin(\theta) \\ k_z &= kN_p\cos(\theta) \end{aligned}. \qquad (8)$$

For TM polarization analogous formulae read as follows:

$$R_{aTM} = \frac{\dfrac{\varepsilon_i k_z - \varepsilon_p i\gamma^{II}}{\varepsilon_i k_z + \varepsilon_p i\gamma^{II}} + A_p e^{-2\gamma^{II} H_i}}{1 + \dfrac{\varepsilon_i k_z - \varepsilon_p i\gamma^{II}}{\varepsilon_i k_z + \varepsilon_p i\gamma^{II}} A_p e^{-2\gamma^{II} H_i}}, \qquad (9)$$

$$A_p = \frac{\left(\varepsilon_m h^{\downarrow} + \dfrac{\varepsilon_i}{\gamma^{II}}\dfrac{dh^{\downarrow}}{dz}\right) - B_p\left(\varepsilon_m h^{\uparrow} + \dfrac{\varepsilon_i}{\gamma^{II}}\dfrac{dh^{\uparrow}}{dz}\right)}{\left(\varepsilon_m h^{\downarrow} - \dfrac{\varepsilon_i}{\gamma^{II}}\dfrac{dh^{\downarrow}}{dz}\right) - B_p\left(\varepsilon_m h^{\uparrow} - \dfrac{\varepsilon_i}{\gamma^{II}}\dfrac{dh^{\uparrow}}{dz}\right)}\Bigg|_{H_i}, (10)$$

$$B_p = \frac{\left(\varepsilon_m h^{\downarrow} + \dfrac{\varepsilon_{f1}}{\gamma^{IV}}\dfrac{dh^{\downarrow}}{dz}\right) - C_p\left(\varepsilon_m h^{\downarrow} - \dfrac{\varepsilon_{f1}}{\gamma^{IV}}\dfrac{dh^{\downarrow}}{dz}\right)e^{-2\gamma^{IV} H_{f1}}}{\left(\varepsilon_m h^{\uparrow} + \dfrac{\varepsilon_{f1}}{\gamma^{IV}}\dfrac{dh^{\uparrow}}{dz}\right) - C_p\left(\varepsilon_m h^{\uparrow} - \dfrac{\varepsilon_{f1}}{\gamma^{IV}}\dfrac{dh^{\uparrow}}{dz}\right)e^{-2\gamma^{IV} H_{f1}}}\Bigg|_{H_i + H_m}, $$
$$(11)$$

$$C_p = \frac{\dfrac{\varepsilon_{f2}\gamma^{IV} - \varepsilon_{f1}\gamma^{V}}{\varepsilon_{f2}\gamma^{IV} + \varepsilon_{f1}\gamma^{V}} + \dfrac{\varepsilon_s\gamma^{V} - \varepsilon_{f2}\gamma^{VI}}{\varepsilon_s\gamma^{V} + \varepsilon_{f2}\gamma^{VI}}e^{-2\gamma^{V} H_{f2}}}{1 + \dfrac{\varepsilon_{f2}\gamma^{IV} - \varepsilon_{f1}\gamma^{V}}{\varepsilon_{f2}\gamma^{IV} + \varepsilon_{f1}\gamma^{V}} \cdot \dfrac{\varepsilon_s\gamma^{V} - \varepsilon_{f2}\gamma^{VI}}{\varepsilon_s\gamma^{V} + \varepsilon_{f2}\gamma^{VI}}e^{-2\gamma^{V} H_{f2}}}, \qquad (12)$$

while the equation for arbitrary linearly independent functions $h^{\downarrow}(z)$ and $h^{\uparrow}(z)$ is

$$\frac{d}{dz}\left(\frac{1}{\varepsilon_m(z)}\frac{dh(z)}{dz}\right) + \left(k^2 - \frac{k_y^2}{\varepsilon_m(z)}\right)h(z) = 0. \qquad (13)$$

REFERENCES

Ay F., Kocabas A., Cocabas C., Aydinli A., Agan S., 2004. Prism coupling technique investigation of

elasto-optical properties of thin polymer films. Journal of Applied Physics, 96 (12), 7147-7153.

Chiang K.S., Cheng S.Y., Liu Q., 2007. Characterization of ultrathin dielectric films with the prism-coupler method. Journal of Lightwave Technology 25 (5), 1206 - 1211.

Dawson P., Cairns G.F., O'Prey S.M., 2000. Prism coupler with variable coupling gap. Review of Scientific Instruments, 71 (11), 4208 - 4212.

Nazarov M.M., Glebov V.N., Goriachuk I.O., Dubrova G.A., Malyutin A.M., Sokolov V. I., 2018. A Method for Measuring the Electro-optical Response of Chromofore-embedded Polymer Films Using a Prism Coupler. Instruments and Experimental Techniques, 61:106

Sokolov V.I., Glebov V.N., Malyutin A.M., Molchanova S.I., Khaydukov E.V., Panchenko V.Ya., 2015. Investigation of optical properties of multilayer dielectric structures using prism-coupling technique. Quantum Electronics 45 (9), 868–872

Sokolov V.I., Marusin N.V., Panchenko V.Ya., Savelyev A.G., Seminogov V.N., Khaidukov E.V, 2013. Determination of refractive index, extinction coefficient and thickness of thin films by the method of waveguide mode excitation. Quantum Electronics 43 (12), 1149–1153.

Ulrich R., Torge R., 1973. Measurement of thin film parameters with a prism coupler. Applied Optics 12 (12), 2901-2908.

AUTHORS BIOGRAPHY

Ivan O. Goriachuk. Department of Physics of Moscow State University, 2017. Fields of scientific interests: interaction of laser radiation with multilayer thin-film structures, polymer waveguides, optical chromophores, prism coupling technique, high-speed electro-optic modulators. Currently, he works in the Institute on Photonic Technologies, Federal Research Center "Crystallography and Photonics" of the Russian Academy of Sciences, Moscow, Russia. (www.kif.ras.ru)

Viktor I. Sokolov. Department of Physical and Quantum Electronics of Moscow Institute of Physics and Technology (State University), 1980. Fields of scientific interests: interaction of laser radiation with multilayer thin-film structures, prism coupling technique, integrated optics, high-speed electro-optic modulators, waveguide optical amplifiers. Currently, he is director of the Institute on Photonic Technologies, Federal Research Center "Crystallography and Photonics" of the Russian Academy of Sciences, Moscow, Russia. (www.kif.ras.ru).

Vladislav N. Glebov. Kazan National Research Technical University, 1966. Fields of scientific interests: physics and technology of thin-film structures. Currently, he is head of the laboratory in the Institute on Laser and Information Technologies, Federal Research Center "Crystallography and Photonics" of the Russian Academy of Sciences, Shatura, Moscow region, Russia. (www.kif.ras.ru).

Andrey M. Maliutin. ITMO University in St. Petersburg, 1988. Fields of scientific interests: physics and technology of thin-film structures. Currently, he works in the Institute on Laser and Information Technologies, Federal Research Center "Crystallography and Photonics" of the Russian Academy of Sciences, Shatura, Moscow region, Russia. (www.kif.ras.ru).

SIMULATION OF AN AUTOMOTIVE SUPPLY CHAIN IN SIMIO: DATA MODEL VALIDATION

António AC Vieira[a], Luís MS Dias[a], Maribel Y Santos[b], Guilherme AB Pereira[a] and José A Oliveira[a]

[a]Department of Production and Systems, ALGORITMI Research centre, University of Minho
[b]Department of Information Systems, ALGORITMI Research centre, University of Minho

[a]{antonio.vieira, lsd, gui, zan}@dps.uminho.pt
[b]maribel@dsi.uminho.pt

ABSTRACT

This paper presents a simulation model of the supply chain of a company of the automotive industry. The purpose of this paper is to use the presented model to validate the considered set of variables that we think are relevant to the problem. This approach was important as it allowed to consider a set of variables that could have been ignored if a different approach had been followed. It should be stressed that, due to privacy concerns, real data was not used, but rather random distributions assigned by the modeler. Notwithstanding, by recognizing that, for the data used, the outputs are in accordance to what happens in the real system, the authors concluded that the set of variables can be considered as validated. Yet, it is still necessary to further complement the model with additional available variables that were not included at this stage, due to its complexity, e.g., customer demand variability, uncertainty associated to suppliers' and impact of external events, such as transportation delays.

Keywords: Big Data (BD), real-time, discrete-event simulation, logistics, supply chain, industry 4.0.

1 INTRODUCTION

As defined by Levi et al. (2003), Supply Chains (SC) are complex and dynamic networks, comprised by entities, such as suppliers and customers, wherein material and information exchanges occur, driven by demand and supply interactions between these entities. Several activities take place in SC, e.g., manufacture products, transport of raw materials from supplier to manufacturers, etc. Ultimately, the goal of each entity in these networks may be seen as the ability to fulfil their customers' orders, at a minimum cost, whilst improving their competitiveness. In other words, to efficiently manage raw materials receipt and timely schedule deliveries at the right time, place and quantities.

In light of this, companies need to carefully manage their role in the SC. To ensure this, Supply Chain Management (SCM) plays a relevant role. According to Levi e al. (2003), some relevant factors to efficiently manage the role of a company in a SC include the need to deliver products according to customer's requirements and reducing total costs with inventory and transportation costs associated with the delivery of goods. On the other hand, their dynamic nature also contributes to the increasing complexity of such networks, since the relationships between involved entities and other aspects such as customer demand, supplier capacity and others may abruptly change. Furthermore, risks are inherent to SC, since uncertain events and variability may lead to SC disruptions, affecting all involved entities' performance.

Usually, uncertain events that affect the performance of a SC can be started from either the customer or the supplier end. For instance, customers' demand variability may originate situations in which production is insufficient, leading to orders unfulfillment, or overstock situations. Another example is given by products that are in end-of-series phase, because they may need to be scrapped, leading to further unnecessary costs. Lastly, unpredictable and rare external events, such as transportation delays, accidents, or even natural disasters (e.g., earthquakes, floods, etc.) may jeopardize the performance of the SC.

In fact, a proper assessment of consequences of certain events in a global SC is not easy to determine, due to the complexity associated to these networks. Thus, rather than being preemptive, involved agents are left with reactive responses, due to the lack of such tools.

These slow actions can, in their turn, lead to further negative impacts to a company and to other companies with relationships with the affected company. Such an example could be witnessed in the infamous earthquake that occurred in March 2011, which damaged the Tohoku Pacific Coastline, causing severe damage factories in that zone of the globe, also affecting other companies around the globe, including zones not affected by the earthquake (Matsuo 2015, Park et al. 2013).

It is in this context that the need to properly assess the performance of a company inserted in a SC of the automotive industry sector emerged. The purpose is to develop a real-time simulation model capable of assessing relevant metrics, while being fed with real data from a Big Data Warehouse (BDW). The goal is to use the simulator as a tool capable of extracting additional knowledge from the BDW, apart from traditional Big Data Analytics (BDA) approaches. This way, managers are capable of using these tools to properly assess the performance of their SC and even to test different scenarios, in real-time, among many other advantages, arising from the combined benefits of these two techniques: Simulation and Big Data.

In light of this, the purpose of the present paper is to document the work conducted to develop a discrete-event simulation model, representing the SC of the company at hand. The simulation model is not yet finished. Thus, this paper presents a version of the model that was developed to validate the data model necessary for this project, i.e., the variables that are more relevant to address this problem. The current version of the simulation model was developed in Simio (Vieira et al. 2014, Dias et al. 2016, Vieira et al. 2015).

In light of the exposed, next section of this paper contributes with a literature review of related past works existing in literature. Section 3 describes some of the main variables that were included in the model, as well as the mechanics associated to the problem. Thereafter, section 4 focuses on describing how this simulation model was developed in Simio. In its turn, section 5 discusses some of the results analysis that is possible to do at this phase. Lastly, the conclusions section finishes by presenting the main contributions of work conducted until this phase, while also highlighting some future work directions for the next phases of this project.

2 LITERATURE REVIEW

Assessing risks associated to SC is a recent and boiling research topic, which is dedicated to developing proactive mechanisms to mitigate risks throughout the entire SC (Ponis and Ntalla 2016). To thoroughly address this problem, companies should extract knowledge from their stored data, through BDA techniques (Hofmann 2017), which are aligned with the industry 4.0 movement. However, Kache et al. (2017) consider that, despite the advantages of BDA, it is still in its early steps, regarding its application in SC management.

In light of the above, Tiwari et al. (2018) characterized the available BDA techniques and provided a comprehensive review of BDA applications in SC contexts, between the years 2010 and 2016. Sanders (2016) examined how leading companies use BDA to extract knowledge and improve the performance of their SCs. The author also proposed a framework for the use of BDA, based on lessons learned from experience. In their turn, Zhong et al. (2016) summarized some of the most successful implementing cases of Big Data solutions, by analyzing several cases throughout the world. The authors also analyzed the possible impacts of BDA on the decision-making process in the performance of SC. Chen et al. (2015) examined how the use of BDA can contribute to the added-value in a SC. Lastly, Zhong et al. (2016) reviewed currently used BDA technologies, while also identifying some challenges, opportunities and future perspectives for BDA. More recently, Santos et al. (2017) presented a BDA architecture, under an industry 4.0 perspective, in a company of the Bosch Group. The presented architecture collects, analyzes and visualizes data related to quality complains and internal defect costs.

Despite the reviewed studies, to the best of the author's knowledge, less attention has been paid to BDA techniques focused in logistics problems related to the automotive industry. A fortiori, there is also a lack of proposed BDW with the same scope and of simulation models that use data provided by these systems to properly assess the performance of a SC. In fact, from the examples found in literature, few are oriented towards SC management and no solution oriented towards SC problems of the automotive industry was found. This idea is also corroborated by Ivanov (2017). In fact, even discrete-event simulation models of SC problems are rarely approached, as suggested by Kagermann et al. (2013), which identity this as one of the most important fields requiring the use of simulation approaches, allowing companies to comply with the industry 4.0 agenda. According to the authors, due to the high levels of uncertainty and variability of SC, simulation is one of the most effective technique to address these problems.

3 SIMULATION MODEL

The first subsection of this section focuses on describing the main relevant variables associated to the problem in analysis. In its turn, the last subsection

focuses on explaining how the described system was modelled in Simio.

3.1 Relevant Variables

Car manufacturers must comply with very strict security norms for their products, while still providing high levels of product customization, required by their customers (Simchi-Levi et al. 2015, Masoud and Mason 2016). On the other hand, a single car is comprised by roughly 5 000 parts, thus factories coexisting in these SC need to cooperate, in order not to jeopardize the entire chain (Kırılmaz and Erol 2017). Due to this, companies in these SC tend to apply Just in Time philosophies which consist in scheduling the materials' arrival to when they will be required and avoiding as much as possible stocking them, otherwise the costs with stock would be unbearable. Thus, safety stock, or safety time is used, which consists in buffers of materials to be used in production.

Typically, one of the main characteristics of automotive SCs is that materials are supplied by a single supplier, exposing manufacturers to the possibility of materials' disruption (Thun and Hoenig 2011). Furthermore, most first-tier suppliers purchase the same materials from the same suppliers. Because of this, when these non-first-tier suppliers fail to fulfill orders, several other plants are affected. This problem is prolonged in time, since usually suppliers take too much time to recover from these failures (Matsuo 2015).

To efficiently manage the entire SC, companies must cooperate. One of the ways of doing this is by forecasting sales and sharing information between them. This allows companies to schedule long-term orders.

When customers' orders arrive, the bill of materials explodes the needs associated to the required finished goods and the respective orders are sent to the suppliers of these materials. In their turn, suppliers must repeat these steps, in order to collect their raw materials from their suppliers. Depending on the situation, when the final customer changes its orders, it may be possible for companies to contact their suppliers and change their orders. It should also be noted that the quantity to be shipped from a supplier to the plant must be negotiated and, in some cases, there are constrains, e.g. minimum order quantity. Along with the quantity of the required material, a delivery time may also be associated, indicating when the material needs to arrive to the plant, in order not to arrive too late, neither too soon, which could cause additional unnecessary stock costs.

When materials are ready to be sent, a regular transporter is assigned. Yet, if by some reason, the regular transport cannot deliver the materials in the scheduled time, a special transport, or freight, must be assigned. Yet, these special freights have considerable costs. When materials arrive to the plant, they are stocked for a brief period of time, since everything was planned so that their production could start after their arrival.

To give a small perspective on the scale of values in analysis, on the company in question, just in 2017, more than 5 000 different raw materials were supplied by 400 different suppliers, spread across the globe. Most of these suppliers are located in Asia, thus, many times, the sea transport is used, which considerably increases the transport duration. Their activity resulted in more than 200 000 material receipts, comprised by different materials and quantities.

The description of the problem at hand, provided in this subsection, contributed with an overall overview and also with some variables that must be considered by the simulation model. The next subsection describes how this model was developed.

3.2 Modeling

The main steps conducted to develop the current simulation model is here addressed. The model was developed in Simio, a recent object-oriented tool. The first step consisted in developing the main object of the model, which is the factory of the company in question. The Simio standard objects used to achieve this can be seen in Figure 1.
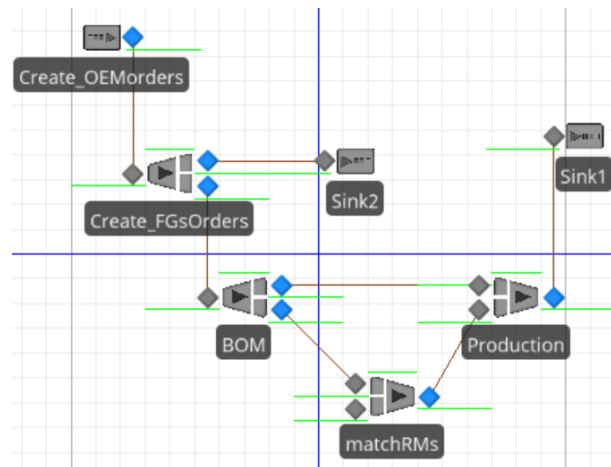
Figure 1: Simio standard objects used to model the behavior of the system.

The flow of entities in this simulation model starts at the "Create_OEMorders", which is responsible for creating customers' orders, which can be comprised of several finished goods. Because of this, the next object creates a new entity for each finished good ordered, representing this information. Thereafter, for each finished good order, it is necessary to explode its BOM (Bill Of Materials), in order to create orders for the respective raw materials. For each exploded raw

material, a new entity is created which is sent to the "matchRMs", in order to wait for the arrival of the ordered material. At the same time, an additional entity is created, which represents the raw materials. These are transferred to the suppliers' location and are kept there until the correct time to send the orders arrives. It should be noted that this transfer of material between the suppliers and the plant is modeled as Free Space, which is a Simio feature which allows users to model entity flows without the need to use any type of connector between different objects (see Figure 4). When the raw materials are ready to be sent to the plant, they can either be sent via normal transport, or via special freight, in case it is determined that the material will not arrive in time to initiate production at the scheduled time, therefore jeopardizing the fulfillment of a customer's order. Lastly, the materials arrive at the plant via the "matchRMs" (see Figure 1). When they enter this object they execute a process, as is illustrated in Figure 2. The process is depicted in Figure 3.
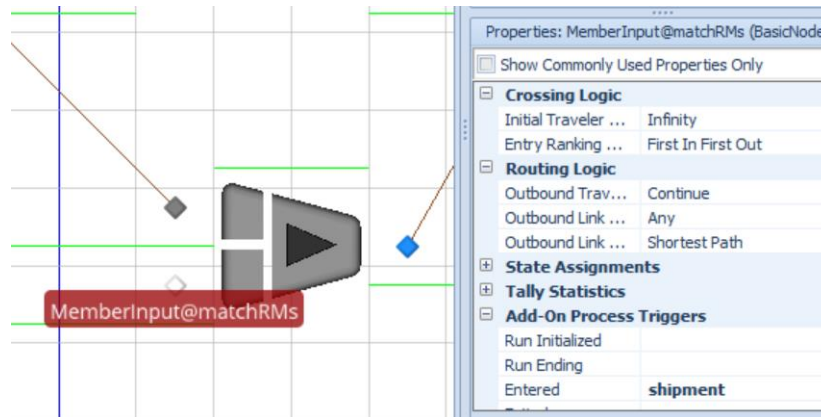
Figure 2: Properties of one of the standard Simio objects used in the simulation model.

It should be stressed that this is just an example of a process used in this model. Simio allows users to create several processes and execute them at any physical location of the model, as shown in Figure 2. This gives the user increasing model flexibility since it allows to mix different simulation modelling approaches, objects and processes, in this case.
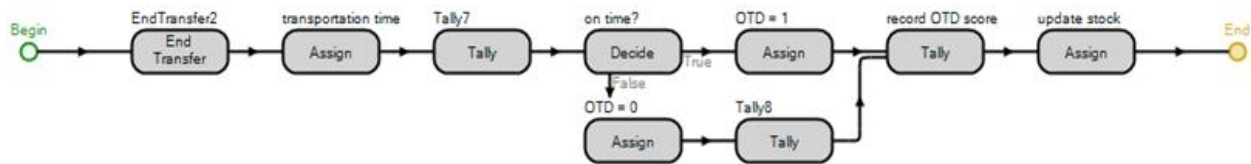
Figure 3: Process used to model the arrival of raw materials to the plant.

The process represented in the above figure starts by communicating to another process in execution that the entity executing this process has been transferred from Free Space to the input node of the "matchRMs" object (see Figure 2). Thereafter, the process saves the transportation time of this order and assesses if the part arrived according with the planned schedule, or if it was a delay. Lastly, the process finishes by updating the stock levels with this arrival.

After the arrival of the materials, these are matched with the entities that represent these orders and they are afterwards stored until the time for them to initiate the production arrives. At this point, the entities can proceed to the "Production" object, in order to produce the corresponding finished good and deliver it to the customers.

Figure 4 shows a 3D view of the model in execution. In the figure, it is possible to see, at the center, an object which represents the plant in question. The yellow triangles spread across the model represent orders that were already sent to the corresponding suppliers' location, but that were still not sent to the plant, since they are still in production. On the other hand, several small truck objects can be seen throughout the model, which represent orders that have already been shipped to the plant. Furthermore, these represent normal transports. In its turn, in the figure, special freights are represented with the symbol of an airplane. In the figure, it is possible to see two special freights arriving to the plant.
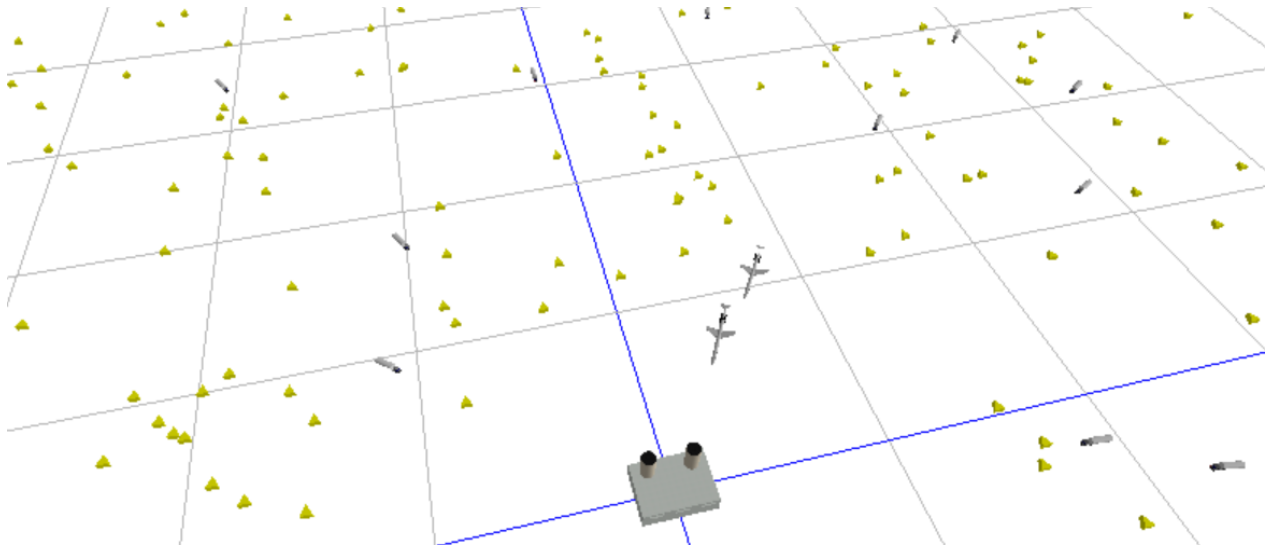
Figure 4: 3D view of the simulation model while running.

4 PRELIMINARY RESULTS

This section presents some preliminary results analysis that is already possible to perform with the developed simulation model. Whilst the model is not completely finished, while developing such model, it was possible to identify the need for certain variables, which is important, especially when tackling such complex problems, such as the dynamics of an automotive SC. Therefore, this approach allowed validating the data model used until this phase by conducting simulation experiments and assessing their adequacy to the problem at hand.

The first thing that should be noted is that the results presented in this section are not real, since, for security reasons, it was not possible to show the obtained results. Thus, the authors assigned random distribution values for the considered variables. Therefore, the purpose of this section is not to analyze the specific obtained results, but rather to analyze if the results make sense for the tested scenarios and thus validate the applied data model.

Several performance indicators and properties were implemented in the simulation model in order to assess the impact of the later on the former by running different simulation experiments. In this sense, the following Key Performance Indicators (KPI) were considered:

- Stock levels
- Percentage of suppliers' on-time deliveries
- Percentage of special freights
- Percentage of delayed orders

Furthermore, 4 different scenarios were tested. The results obtained for these 4 scenarios are presented in

Table 1. For these scenarios, 6 months of simulation time was used, with 15 days of warm-up period and 5 replications.

Table 1: Simulation results obtained for the 4 considered scenarios.

	Stock	On-time deliveries	Freights	Delayed deliveries
Scenario 1	85%	97%	0%	0%
Scenario 2	92%	98%	0%	0%
Scenario 3	85%	100%	52%	0%
Scenario 4	88%	100%	58%	0,2%

In the first 2 scenarios, special freights were not considered, as the corresponding KPI indicates (0% of transports were special freights). This resulted in a percentage of suppliers' on-time deliveries of 97%. The 3% of orders that did not arrive on the scheduled date can be explained by the variability on the supplier side of the SC, e.g., a transportation delay occurred, or some disruption on the second-tier suppliers. On this light and to further increase the percentage of on-time deliveries, in scenario 2 suppliers send their orders up to 3 days

before the scheduled date. Yet, as the results indicate, the percentage of on-time deliveries only increased 1%, whilst the stock levels increased 7%, from 85% to 92%, thus, the solution seems to be to include special freights, which is considered by scenarios 3 and 4.

In Scenario 3 orders are sent on the scheduled date and special freights are considered. As the results indicate, the simulated plant achieved a percentage of on-time deliveries of 100%, whilst maintaining the stock levels in 85%. This indicates that the simulation model mimics the real systems, since in this type of SC, managers must carefully ponder between storage costs and costs with special freights. In scenario 4 the number of customers' orders was increased, in order to assess its impact on the established KPI. By analyzing the results of this scenario, it is possible to see that the stock levels increased as expected, as well as the percentage of special freights. Apart from these, some delayed orders were registered (0.2%), as result of increasing the customers' orders intensity.

5 CONCLUSIONS

The efficiently managing of complex Supply Chain (SC) networks is a very complex task. Modelling such systems with simulation can be very useful in order to test different scenarios, quantify different performance measures, thus contributing to a more preemptive approach, rather than a reactive one. In fact, addressing SC problems is one of the purposes of the industry 4.0 movement. Moreover, also aligned with this new movement, Big Data Analytics (BDA) allows managers to extract knowledge from their stored Big Data (BD) sets. It is in the light of this that this project is being conducted in a company of the automotive industry. The work consists in developing a discrete-event simulation model supported by a Big Data Warehouse (BDW) system that stores the available data, oriented towards specific logistic problems. Thereafter, the BDW can support the developed simulation model with data, which, in its turn, is able to provide extra knowledge, aiding in the decision-making process.

In this regard, this paper presented a version of the developed simulation model, which was developed in Simio. For privacy reasons, it was not possible to show real data from the case study company. Rather, random distributions values assigned by the modeler were used, in order to validate the variables used in this model. As the results presented in section 4 suggest, the response of the output results, for the tested scenarios, are in accordance with what is expected and with what happens in the real system in analysis. Due to this, the authors concluded that the set of variables used in this model is validated. It should be noted that the authors were not interested in the concrete values, but rather, in the response of outputs to the different tested scenarios.

This approach was important because it allowed to consider variables that otherwise could not have been included, or forgotten. The obtained results indicate that, despite still being incomplete, it was possible to model the most important processes associated to the problem at hand with the considered variables.

For the next development steps regarding the development of the simulation model, it is important to include other variables that were identified but not yet implemented, such as: production capacities; customer demand variability; suppliers' constraints, such as minimum and maximum order quantity; impact of external events, for instance, transportation delays or natural disasters; costs associated with production line stoppages; costs with overstock; materials' shelf life; consider different storage units; consider measures and volume occupation on the warehouse; customers' orders forecast; consider customer order change and, based on this possibility, react by changing orders with suppliers, if possible, in order not to incur in unnecessary order costs; and consider secondary suppliers for a given material, despite these being rarely used in these type of SC.

REFERENCES

Chen, D. Q., Preston, D. S. & Swink, M. 2015. How the use of big data analytics affects value creation in supply chain management. Journal of Management Information Systems, 32, 4-39.

Dias, L. M. S., Vieira, A. A. C., Pereira, G. A. B. & Oliveira, J. A. 2016. Discrete Simulation Software Ranking – a Top list of the Worldwide most Popular and Used Tools. Proceedings of the 2016 Winter Simulation Conference.

Hofmann, E. 2017. Big data and supply chain decisions: the impact of volume, variety and velocity properties on the bullwhip effect. International Journal of Production Research, 55, 5108-5126.

Ivanov, D. 2017. Simulation-based single vs. dual sourcing analysis in the supply chain with consideration of capacity disruptions, big data and

demand patterns. International Journal of Integrated Supply Management, 11, 24-43.

Kache, F. & Seuring, S. 2017. Challenges and opportunities of digital information at the intersection of Big Data Analytics and supply chain management. International Journal of Operations & Production Management, 37, 10-36.

Kagermann, H., Helbig, J., Hellinger, A. & Wahlster, W. 2013. Recommendations for implementing the strategic initiative INDUSTRIE 4.0: securing the future of German manufacturing industry; final report of the Industrie 4.0 working group, Forschungsunion.

Kirilmaz, O. & Erol, S. 2017. A Proactive approach to supply chain risk management: Shifting orders among suppliers to mitigate the supply side risks. Journal of Purchasing and Supply Management, 23, 54-65.

Levi, D. S., Kaminsky, P. & Levi, E. S. 2003. Designing and managing the supply chain: Concepts, strategies, and case studies, McGraw-Hill.

Masoud, S. A. & Mason, S. J. 2016. Integrated cost optimization in a two-stage, automotive supply chain. Computers & Operations Research, 67, 1-11.

Matsuo, H. 2015. Implications of the Tohoku earthquake for Toyota′s coordination mechanism: Supply chain disruption of automotive semiconductors. International Journal of Production Economics, 161, 217-227.

Park, Y., Hong, P. & Roh, J. J. 2013. Supply chain lessons from the catastrophic natural disaster in Japan. Business Horizons, 56, 75-85.

Ponis, S. T. & Ntalla, A. C. 2016. Supply chain risk management frameworks and models: a review. International Journal of Supply Chain Management, 5, 1-11.

Sanders, N. R. 2016. How to use big data to drive your supply chain. California Management Review, 58, 26-48.

Santos, M. Y., E Sá, J. O., Andrade, C., Lima, F. V., Costa, E., Costa, C., Martinho, B. & Galvão, J. 2017. A Big Data system supporting Bosch Braga Industry 4.0 strategy. International Journal of Information Management, 37, 750-760.

Simchi-Levi, D., Schmidt, W., Wei, Y., Zhang, P. Y., Combs, K., Ge, Y., Gusikhin, O., Sanders, M. & Zhang, D. 2015. Identifying risks and mitigating disruptions in the automotive supply chain. Interfaces, 45, 375-390.

Thun, J.-H. & Hoenig, D. 2011. An empirical analysis of supply chain risk management in the German automotive industry. International journal of production economics, 131, 242-249.

Tiwari, S., Wee, H. & Daryanto, Y. 2018. Big data analytics in supply chain management between 2010 and 2016: Insights to industries. Computers & Industrial Engineering, 115, 319-330.

Vieira, A., Dias, L., Pereira, G. & Oliveira, J. 2014. Comparison of Simio and Arena simulation tools. ISC. University of Skovde, Skovde, Sweden.

Vieira, A., Dias, L. S., Pereira, G. A. B., Oliveira, J. A., Carvalho, M. S. & P., M. 2015. Using Simio to Automatically Create 3D Warehouses and Compare Different Storage Strategies. Faculty of Mechanical Engineering Transactions, 43, 335-343.

Zhong, R. Y., Newman, S. T., Huang, G. Q. & Lan, S. 2016. Big Data for supply chain management in the service and manufacturing sectors: Challenges, opportunities, and future perspectives. Computers & Industrial Engineering, 101, 572-591.

AUTHOR BIOGRAPHIES

ANTÓNIO A C VIEIRA was born in 1989 in Vila Nova de Famalicão, Portugal. He graduated in Informatics Engineering in the University of Minho. He holds a MSc degree in Systems Engineering at the University of Minho. He is making his doctoral studies in Advanced Engineering Systems for Industry at the University of Minho, in partnership with Bosch Car Multimedia Braga. His main research interests are Modelling and Simulation, Programming Languages and Big Data Analysis. He is Invited Assistant Professor at the University of Minho. His email address is antonio.vieira@dps.uminho.pt.

LUÍS M S DIAS was born in 1970 in Vila Nova de Foz Côa, Portugal. He graduated in Computer Science and Systems Engineering in the University of Minho, Portugal. He holds an MSc degree in Informatics Engineering and a PhD degree in Production and Systems Engineering from the University of Minho, Portugal. His main research interests are Simulation, Systems Performance, Operational Research and Systems Visual Modeling. He is Auxiliar Professor at the University of Minho. His email address is lsd@dps.uminho.pt.

MARIBEL Y SANTOS

Maribel Yasmina Santos is an Associate Professor at the Department of Information Systems and Researcher of the ALGORITMI Research Centre, University of Minho (UMinho), in Portugal. She received the Aggregated title (Habilitation) in Information Systems and Technologies (IST) from UMinho in 2012 and a PhD in Information Systems and Technologies from UMinho in 2001. She was Secretary-General of the Association of Geographic Information Laboratories for Europe (AGILE) from May 2013 to June 2015. Her research interests include Business Intelligence and Analytics, Big Data and (Big) Data Warehousing.

GUILHERME A B PEREIRA was born in 1961 in Porto, Portugal. He graduated in Industrial Engineering and Management in the University of Minho, Portugal. He holds an MSc degree in Operational Research and a PhD degree in Manufacturing and Mechanical Engineering from the University of Birmingham, UK. His main research interests are Operational Research and Simulation. Currently he is Pro-Rector of the University of Minho. He is Associate Professor at the University of Minho. His email address is gui@dps.uminho.pt.

JOSÉ A OLIVEIRA was born 1966 in Matosinhos, Portugal. He studied Mechanical Engineering at the University of Porto, Portugal. He graduated with a Ph.D. in Production and Systems Engineering at University of Minho, Portugal. His main research interests are Optimization with Heuristic Methods in Systems Engineering. He is Auxiliar Professor at the University of Minho. His email address is zan@dps.uminho.pt.

ASSESSING THE PERFORMANCE OF A RESTAURANT THROUGH DISCRETE SIMULATION IN SIMIO

António A. C. Vieira[a], Luís M. S. Dias[b], Guilherme A. B. Pereira[c] and José A. Oliveira [d]

[a],[b],[c], [d] University of Minho, Campus Gualtar, 4710-057, Braga, Portugal

[a], [b], [c], [d]{antonio.vieira, lsd, gui, zan}@dps.uminho.pt

ABSTRACT

For the purpose of evaluating the level of service of a Portuguese self-service restaurant, a simulation model was developed in Simio. The purpose of such model was to quantify specific performance indicators. In this sense, data was gathered by conducting observations of the field, which allowed the authors to find relevant problems in the system. The simulation model was validated and, afterwards, simulation experiments were conducted, which suggested some changes that could be implemented, without reducing the performance of the restaurant and reduce the utilization of workers, who become available for other tasks with more added-value, such as supplying critical items (e.g., main dishes and soap). Moreover, the potential impact of the introduction of an information device used to warn workers responsible to supply items was assessed through simulation, indicating that it would lead to benefits both for customers and workers.

Keywords: Discrete-Event Simulation, Simio, Object Modelling, Performance indicators.

1. INTRODUCTION

Today's competitive market companies make efforts to improve their service level, thus aiming to eliminate waste and pursue continuous improvement, which is in accordance to lean philosophy (Womack J.P., Jones D.T., Roos D. 1990). Lean philosophy is a production organizational model with focus on overall client's satisfaction and continuous improvement, through waste elimination. It should be noted that this philosophy can also be applied in other non-production systems. In this regard, one of the ways to achieve this customer satisfaction, waste elimination and continuous improvement is through the assessment of the efficiency of processes, according to performance indicators, such as queue size and customer waiting time (Gross 2008).

This study originated from the need the assess the performance of a restaurant in Portugal. Therefore, the purpose of this paper is to document the work conducted in this project, namely to:

Identify possible bottlenecks in the system and propose improvements. More specifically, reasons for the waiting time per client, the queue size and the work in process (WIP) should be found.

Improve the utilization rate of workers. This can be done by identifying flaws in the workflow, changing work locations, task allocations, etc.

Simulation is oftentimes considered as the best choice to tackle this kind of problems, due to its capability of addressing stochastic systems and the possibility of dealing with uncertainty. Moreover, simulation can also be used to test alternative scenarios that would lead to considerable costs if they were experimented on the ground. Thus, a simulation model was developed in Simio, an object-oriented simulation tool. Thus, it is possible to model the behaviour of clients in the restaurant and the workflow of workers, to test alternative scenarios.

The next section focuses on reviewing literature related to the topics of this study. The third section described the case study in question and the data gathering process, as well as the main problems that were identified in the restaurant. The main steps to model the system in question are described in the fourth section and the fifth describes the main simulation experiments conducted and discusses the results. Lastly, conclusions are discussed in the last section.

2. LITERATURE REVIEW

The literature on modelling and simulation is vast (Longo F. 2011, Jiménez E., Martínez E., Blanco J., Pérez, M., Graciano C., 2014, Mangina E., Vlachos I. P., 2005). When searching literature for papers trying to improve the service level of restaurants using simulation, it is possible to notice a lack of such studies.

Ju and Wang (2010) specifically used simulation to a similar problem. The authors used WITNESS to simulate the behaviour of a restaurant, to try to identify bottlenecks and propose improvements, with the goal of improving the level of service. Zhao X., Lau R.S.M. and Lam K. (2002) used ProModel to simulate a similar problem. The authors of both studies agree on the benefits of simulation to this kind of problems.

As can be seen, there is a lack of such studies using discrete-event simulation models in these kind of problems, even though simulation is considered the most appropriate tool for these problems.

There is a great number of simulation tool options, thus tool comparison becomes a very important task. However, most of scientific works related to this subject

analyse a small set of tools and evaluate several parameters individually, avoiding to make a final judgement, due to the subjective nature of that task (Dias L.M.S, Pereira G.A.B. and Rodrigues G. 2007, Dias L.M.S, Pereira G.A.B., Vik P. and Oliveira J.A., 2011, Dias L.M.S, Vieira A.A.C., Pereira G.A.B. and Oliveira J.A. 2016).

Hlupic V. and Paul R. (1999) compared a set of simulation tools, distinguishing between users of software for educational purpose and users in industry. In his turn, Hlupic V. (2000) developed a survey on the use of simulation software of academic and industrial users, which was conducted to discover how the users were satisfied with the simulation software they used and in which ways could the software be improved.

In their turn, Dias and Pereira et al. (2007, 2011, 2016) compared a set of tools based on popularity on the internet, scientific publications, WSC (Winter Simulation Conference), social networks and other sources. According to the authors, popularity should not be used as the only criteria, otherwise new tools, better than existing ones would never get their market share. However, a positive correlation may exist between popularity and quality, since the best tools have a greater chance of being more popular. According to their study, the most popular tool is Arena, however, the good classification of Simio is also noteworthy. Based on these results, Vieira A.A.C., Dias L.M.S., Pereira, G.A.B. and Oliveira J.A. (2014) and Oueida S., Char P.A., Kadry S. and Ionescu S. (2016) compared both tools, considering several factors. WITNESS, the tool used in the study of Ju and Wang (2010) finished in 5th place in this ranking, in a very close classification to the 2nd, 3rd and 4th ranked tools. In its turn, the tool used in Zhao X., Lau R.S.M. and Lam K. (2002) – ProModel – finished in 2nd place in this ranking.

Simio was created in 2007 from the same developers of Arena and is based on intelligent objects (Sturrock and Pegden 2010, Pegden 2007, Pegden and Sturrock 2008). Unlike other object-oriented tools, in Simio there is no need to write programing code, since the process of creating objects is completely graphic (Pegden and Sturrock 2008, Pegden 2007, Sturrock and Pegden 2010). The activity of building an object in Simio is identical to the activity of building a model. In fact, there is no difference between an object and a model (Pegden 2013). A vehicle, a costumer or any other agent are examples of possible objects and, combining several of these, one can represent the components of the system in analysis. In other words, the user can use realistic representations of the objects that compose the real system being modelled and, thereafter, at a lower level, define additional logic to the model, through the development of processes for instance. This way, Simio complements the main object paradigm with other paradigms such as events and processes.

A Simio model looks like the real system, which can be useful when presenting the results to non-familiars with simulation concepts. In Simio the model logic and animation are built in a single step (Pegden and Sturrock 2008, Pegden 2007), which makes the modelling process very intuitive. In addition to the usual 2D animation, Simio also supports 3D animation as a natural part of the modelling process. Moreover, Simio provides a direct link to Google Warehouse, a library of graphic symbols for animating 3D objects (Oueida S. Char P.A., Kadry S. and Ionescu S. 2016).

3. CASE STUDY

The case study of this problem is discussed in this section. The first subsection focuses in describing the system to be analysed. In its turn, next subsection describes the data gathering process. The last subsection discusses the main problems that were identified.

3.1. System Description

The system at hand can be divided in 2 main areas. The first consists in the kitchen, wherein workers prepare the food to supply the second area, where costumers pick intended items, such as trays, food and cutlery. Figure 1 shows a 3D view over the simulation model, with some labels of the layout of the restaurant.

As the figure depicts, when costumers arrive to the restaurant, they enter through a common entrance. At this point, they can choose from 2 available access ramps: access ramp 1 (AR1) or access ramp 2 (AD2). Furthermore, at the beginning of AR2 the path forks into AR1_1 and AR2_2.

The observations conducted on the ground allowed the authors to verify that, usually, customers decide on which ramp to take by evaluating the size of the queues. Yet, even if the queue of AR2 is higher than the one of AR1, costumers may still opt for this former, since it has forks into two ramps, and thus dispatches customers faster; this choice is rather subjective. After choosing an access ramp, customers collect intended items (e.g. trays, cutlery, food, etc.), in different sequences, depending on the access ramp.

The restaurant's kitchen, as Figure 1 illustrates, is located at the centre of the plant, in order for workers to be able to equally supply items to both ramps. The existing workers are divided by tasks, which can go from preparing food, supplying it to the ramps and serving it to customers on the queues. There are other tasks involved, however these are the main ones which are critical for the system in analysis, as was observed by the authors when conducting in loco observations on the field. It should be noted that some workers can do more than one of these tasks and, depending on the task, workers can even help each other, comprising interesting situations to model in Simio
.

Figure 1: 3D view of the restaurant

3.2. Data Gathered

To develop a simulation model representative of the real system at hand, data related to the self-service restaurant was gathered through field observations. These observations allowed the authors to observe that cutlery and trays are only supplied before the opening of the restaurant, thus in the simulation model these resources were not considered.

Table 1 shows some of the data that were gathered.

Table 1: Sample of data collected on the field

Item	Time to collect (seconds)	Customers that want an item	Quantity at the restaurant opening			Number of supplies		
			AR2_1	AR2_2	AR1	AR2_1	AR2_2	AR1
Tray	1 to 3	100%	-		-	-	-	-
Bread	2 to 5	60%	100		100	5		3
Cutlery	1 to 3	100%	-	-	-	-	-	-
Dessert	2 to 5	60%	120	120	120	-	-	-
Soap	2 to 6	80%	60		60	12		7
Cup	4 to 6	85%	150	150	100	-	-	-
Main dish	3 to 9	100%	50	50	50	7	6	11
Juice						4	7	6

When picking items, customers can either take a cup with a drink, or take an empty cup, if there are no filled cups. If there are no cups with water or juice, there is a proper places to fill cups– 15% of the clients fills the cup with water. Yet, on some ramps workers do not fill cups, thus customers have to fill their own, which takes them about 4 to 6 seconds.

Apart from the indicators presented in
Table 1, the number of meals served per day were also recorded, which in average, was roughly1500. Additionally, it was also found that the average time for a customer to pick the items and exit the ramps to the eating room is around 20 minutes. Moreover, at the entrance of the restaurant, it was also found that roughly 40% of the customers chose the AR1 access ramp, whilst the remaining take AR2 ramp. From these, 60% chose AR2_2 and the remaining chose the AR2_1. Lastly, it should be noted that the gathered values were introduced in the simulation model by conducting proper distribution fitting.

3.3. Problems Identified

In the light of the exposed, the authors identified two critical workers, which perform several activities and whose delay can severely affect the overall performance of the system. In this regard, the following is the list of such workers along with the tasks they perform and the

name which will be used throughout the remaining of this document to refer to those workers:

- worker A - responsible for supplying dessert, juice and bread to both AR2_1 and AR2_2 access ramps;
- worker B - responsible for supplying the main dish at both AR2_1 and AR2_2 access ramps, supplying soap in all ramps and juice, bread and dessert at the AR1 ramp. Since this worker supplies critical item, such as soup and main dish, he is also responsible for constantly monitoring these, in order to supply them when needed.

In its turn, the following were the main problems identified in the restaurant, while conducting in loco observations:

1. Worker A is responsible for preparing and supplying juice containers in both AR access ramps. Yet, this worker travels a long distance to perform this task. There are other closer and available places, which could be used for this task, thus it should be assessed if it would lead to benefits to the system;
2. As stated in the previous subsection, in AR2_1 and AR1 no worker fills cups with juice and this did not seem to affect the performance of the system. Therefore, it should be assessed if stopping worker A from filling cups with juice in the remaining ramp would affect the system;
3. It was found that the monitoring performed by worker B was not efficient, since it could take him much time to notice lacking items, since he also had to do other tasks. To overcome this situation, the authors would like to test the impact of implementing an information device to warn the workers that an item needs to be supplied.

4. MODEL DEVELOPMENT

To enhance the animation of the model, 3D objects of persons, food and others were downloaded from Google Warehouse. The restaurant opens during specific times of the day, for customers to have lunch and dinner. In this regard, during the time the restaurant is open, the income flow of clients changes throughout the time. In this regard, different interarrival time rates of customers were defined in Simio, in accordance to the data gathered on the field. Thus, Figure 2 shows how to define these different interarrival time of customers in Simio.

When customers arrive at the restaurant, they pick items in different orders, depending on the access ramp they take. When a customer tries to collect an item, he executes a process to verify if the item in question is available. To this end, a different process is executed for each item in question. The process represented in Figure 3 illustrates the process executed to verify if the item bread is available, when a given customer executes this process.

From (hour:minute)	To (hour:minute)	Average arrival rate per hour
12:00	12:05	1373
12:05	12:10	1280
12:10	12:15	739
12:15	12:20	634
12:20	12:25	620
12:25	12:30	1404
12:30	12:35	768
12:35	12:40	624
12:40	12:45	972
12:45	12:50	1392
12:50	12:55	1560
12:55	13:00	888
13:00	13:05	1080
13:05	13:10	468
13:10	13:15	1656
13:15	13:20	672
13:20	13:25	708
13:25	13:30	288
13:30	13:35	120
13:35	13:40	216
13:40	13:45	300
13:45	13:50	144
13:50	13:55	156
13:55	14:00	24
14:00	14:05	120
14:05	14:10	120
14:10	14:15	96
14:15	14:20	0
14:20	14:25	0
14:25	14:30	0

Figure 2: Interarrival time rates used

When this process is executed, customers check the value of a state variable in Simio, which stores the quantity available of a certain item. If the value is not 0, the state variable in question is updated, indicating a reduction in the number of available items, i.e., the item is picked. On the other hand, if the item is not available, the customer waits a certain time to check again, until the item is available. When a customer waits for an item, other customers behind him, are not allowed to proceed, forming a waiting queue. Figure 7 shows the developed simulation model during run time in 3D.

The process of modelling workers in Simio is very simple, which is not true to all discrete-event simulation tools (Vieira A.A.C., Dias L.M.S., Pereira G.A.B. and Oliveira J.A. 2014). Yet, in some situations, modelling complex behaviour of workers in Simio can also become a complex task. These more complex situations to model will now be described:

I. *Set the processing time of a task depending on the number of workers*

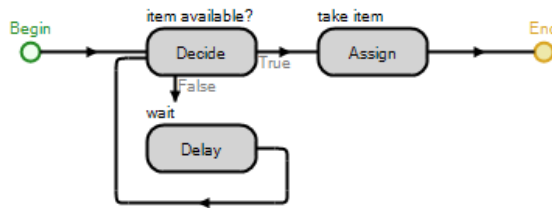To model workers who help other workers, and thus the respective task is done at a faster pace, the process represented in Figure 4 and Figure 5 is executed.
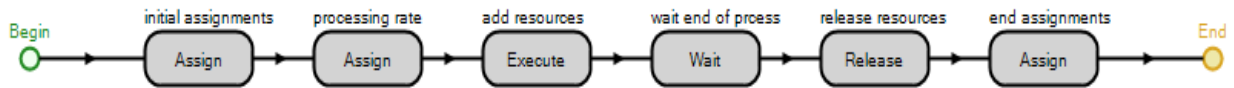
Figure 3: Process executed by customers to take bread

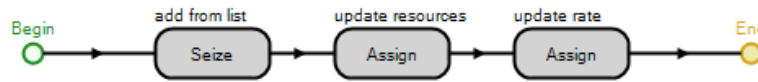Figure 4: Process executed to dynamically assign the processing time of a task

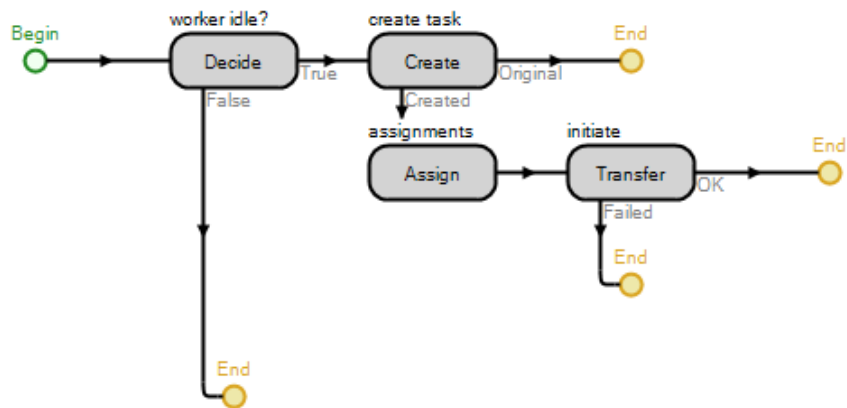Figure 5: Process executed to seize additional workers

Figure 6: Process executed by worker on idle

Figure 7: Simulation model during run time

In this process, the first three steps are responsible for assigning the processing time of the task in question as proportional to the number of workers seized to perform the given task. Thereafter, the process represented in Figure 5 is executed. In this process, a new worker is assigned to the same task and the processing time of the task is updated according to the number of resources. After executing this process, the previous one continues (Figure 5). Thus, when the task finishes, the seized resources are released.

II. Worker performs a given task on idle status

To make a worker perform a specific action when he is on idle, i.e., when there are no tasks assigned to this worker, the process represented in Figure 6 was created. The workers who execute this process start by executing a step which checks if the worker in question is on idle. In this case, if the worker is on idle, the process will make him refill cups with juice. Thus, in this case, an entity is created which seizes the worker to perform the task in question. This way, a new task is assigned to the worker on idle.

4.1. Model Validation

In order for the developed simulation model to correspond to the self-service restaurant in analysis, the validation is an important step. Thus, this subsection briefly addresses the steps conducted in this process, by showing the obtained results for some indicators that can be compared to the data gathered on the ground. In this regard, Table 2 presents some of the obtained simulation results. By conducting this validation process, it is expected that the confidence level in the developed model is increased.

Table 2: Sample of data used to validate

Item	Number of supplies		
	AR2_1	AR2_2	AR1
Bread		5	3.1
Soap		12	7.7
Main dish	7.2	6.2	12.3
Juice	3.5	7.1	6.7

Regarding the average crossing time per customer, a value of 20,19 minutes was obtained, which is a similar value to the obtained and discussed in last section. As can be seen, the comparison of these values with the ones presented throughout the previous section allows to consider that the model has been properly validated.

5. SIMULATION EXPERIMENTS

One of the major benefits of using Simio is the possibility of conducting experiments to assess the performance of the simulated system. A simulation experiment is a set of scenarios, each one executing the model with different values on the properties of the model, which produces results in the identified Key Performance Indicators (KPI). Thus, to properly assess the performance of the system, the authors identified the following KPI of the restaurant system:

- total time required for a customer to go to the eating room;
- time customers are stopped on the queue;
- utilization rate of workers A and B.

To use simulation experiments, it is necessary to define the properties of the model that produce changes on the performance of the system (in Simio these are called responses). In this sense, the properties of the model consist on a possible solution to each of the problems identified in section 3.3, i.e., 3 different solutions were addressed:

- scenario 1: current scenario;
- scenario 2: worker A prepares the juice in a closer place;
- scenario 3: worker A does not fill cups with juice in AR2_2;
- scenario 4: model the system with an information device that helps workers notice the need to supply lacking items;
- scenario 5: scenarios 2 to 4 together;

The experiments were run with 10 replications with a simulation time of 2.5 hours.
Table 3 summarizes the obtained simulation experiments results

Table 3: Simulation results

	Customer centric KPI		Worker centric KPI	
Scenario	Total time (minutes)	Waiting time (minutes)	Utilization of Worker A	Utilization of Worker B
1	18.3	9.3	71.7 %	81.5 %
2	18.2	9.2	74.6 %	85.1 %
3	18.8	9.8	59.6 %	81.2 %
4	16.1	7.1	74.9 %	19.9 %
5	14.8	5.8	60.7 %	19.2 %

The considered KPI were divided in two groups: customer and worker centric, since the total time spent on the system and the waiting time are KPI which are mostly felt by customers, whilst the utilization rates are felt by workers. It is true that, globally, the two groups

affect the system, but if one considers the view-point of customers and workers, then these two groups can be set. By analysing scenario 2, it is possible to see that the results do not present significative changes, for both groups, when comparing to scenario 1. This suggests that the place where the worker prepares the juice is not

relevant for the performance of the system. Therefore, other metrics should be assessed. In its turn, it can be noted that the proposed scenario 3 also achieved a performance similar to scenario 2, regarding the customers KPI. On the other hand, on the workers KPI, it can be noted that the utilization of worker A decreased around 12%, which indicates that this solution could be used in the restaurant. Therefore, it is verified worker A may perform tasks other than filling cups, being available for more added-value tasks, which could culminate in improving the customers' KPI.

By analysing the results concerned with scenario 4, it can be seen that a reduction of more than **2.5 minutes** of average waiting time and average total time per customer, is obtained. Even so, the greatest gain comes from the reduction of the percentage usage of workers B, which was responsible for monitoring lacking items – a reduction of more than **60%** could be verified. Therefore, it can be concluded that the worker in cause could be used for several other activities.

Regarding the last scenario, it can be seen that the results are similar to scenarios 3 and 4, with further improvements in the KPI of customers, leading to a reduction of **3.5 minutes** of waiting time and total time spent on the system.

6. CONCLUSIONS

This paper documented the work conducted to assess the performance of a restaurant in Portugal. In this sense, a simulation model was developed to evaluate the performance of the system, by quantifying several performance indicators concerned with the service provided to the customers and the utilization of the involved workers. In addition, the model was also used to test alternatives scenarios.

The data used in the simulation model was collected through field observations, which also allowed to identify problems in the system in analysis. The developed model was validated by comparing the results obtained with the ones observed during the data collection process, thus contributing to increase the confidence level in the simulation model.

The experiments suggested that, from the previously hypothesized scenarios that could improve the performance of the system (see section 3.3 and the list of the 5 considered scenarios), only scenario 3 and 4 lead to significant improvements on the system, with scenario 2 indicating that the location where worker A performed a particular task did not impact the performance of the system.

Regarding the KPI considered for costumers, it was found that their waiting times could be reduced from 2.5 to 3.5 minutes if one of two solutions, which impacted different workers, was adopted: have customers fill cups with juice, freeing worker A for other tasks, or implement an information device to warn worker B of lacking items, thereby fastening the replenish of lacking items and also freeing this worker for other tasks, which could further improve the performance of the system.

This paper presented findings from a real case study consisting of Portuguese restaurant. The findings were reported to the management staff and are currently being pondered. Moreover, this paper also aims to contribute to the simulation community, more specifically the users of the Simio tool with some complex modelling situations that were faced during this project.

REFERENCES

Dias L.M.S., Pereira G.A.B. and Rodrigues G., 2007. A Shortlist of the Most Popular Discrete Simulation Tools. Simulation News Europe, 17, 33-36.

Dias L.M.S., Pereira G.A.B., Vik P. and Oliveira J.A., 2011. Discrete simulation tools ranking: a commercial software packages comparison based on popularity. Industrial Simulation Conference. Venice, Italy, 6-8 June: Eurosis.

Dias L.M.S., Vieira A.A.C., Pereira G.A.B. and Oliveira J.A., 2016. Discrete Simulation Software Ranking – a Top list of the Worldwide most Popular and Used Tools. Proceedings of the 2016 Winter Simulation Conference.

Gross D., 2008. Fundamentals of queueing theory, John Wiley & Sons.

Hlupic V., 2000. Simulation software: an Operational Research Society survey of academic and industrial users. Proceedings of the 32nd Winter Simulation Conference (pp. 1676-1683 vol. 2). Society for Computer Simulation International.

Hlupic V. and Paul R., 1999. Guidelines for selection of manufacturing simulation software. IIE Transactions, 31, 21-29.

Jiménez E., Martínez E., Blanco J., Pérez M., Graciano C., 2014. Methodological approach towards sustainability by integration of environmental impact in production system models through life cycle analysis: Application to the Rioja wine sector. Simulation, Volume 90, Issue 2, February 2014, Pages 143-161

Ju X. and Wang Y., 2010. Simulation and Improvement of Multiple Queue Multiple Serve System Based on Witness. International Conference on Multimedia Technology (ICMT), IEEE, 1-4.

Longo F., (2011). Advances of modeling and simulation in supply chain and industry. SIMULATION, 87(8), pp. 651-656.

Mangina E., Vlachos I. P., 2005. The changing role of information technology in food and beverage logistics management: Beverage network optimisation using intelligent agent technology. Journal of Food Engineering, Volume 70, Issue 3, October 2005, Pages 403-420

Oueida S., Char P.A., Kadry S. and Ionescu S., 2016. Simulation Models for Enhancing the Health Care Systems. FAIMA Business & Management Journal, 4, 5.

Pegden C.D., 2007. Simio: A new simulation system based on intelligent objects. Proceedings of the 39th Winter Simulation Conference: 40 years! The best is yet to come, pp. 2293-2300, IEEE Press.

Pegden C.D., 2013. Intelligent objects: the future of simulation. Simio. White paper. Available online at: http://www.simio.com/resources/white-papers/Intelligen-objects/Intelligent-Objects-The-Future-of-Simulation-Page-1.htm.

Pegden C.D. and Sturrock D.T., 2008. Introduction to Simio. 2008 Winter Simulation Conference, pp 29-38, IEEE.

Sturrock D.T. and Pegden C.D., 2010. Recent innovations in Simio. Proceedings - Winter Simulation Conference, pp. 52-62. Proceedings - Winter Simulation Conference, pp. 52-62.

Vieira A.A.C., Dias L.M.S., Pereira G.A.B. and Oliveira J.A., 2014. Comparison of Simio and Arena simulation tools. ISC. University of Skovde, Skovde, Sweden.

Womack J.P., Jones D.T. and Roos D., 1990. The machine that changes the world. Rawson Associates, NY

Zhao X., Lau R. and Lam K., 2002. Optimizing the service configuration with the least total cost approach. International Journal of Service Industry Management, 13, 348-361.

BIOGRAPHY

António A C Vieira was born in 1989 in Vila Nova de Famalicão, Portugal. He graduated in Informatics Engineering in the University of Minho. He holds a MSc degree in Systems Engineering at the University of Minho. He is making his doctoral studies in Advanced Engineering Systems for Industry at the University of Minho. His main research interests are Simulation and Big Data.

Luís M S Dias was born in 1970 in Vila Nova de Foz Côa, Portugal. He graduated in Computer Science and Systems Engineering in the University of Minho, Portugal. He holds an MSc degree in Informatics Engineering and a PhD degree in Production and Systems Engineering from the University of Minho, Portugal. His main research interests are Simulation, Systems Performance, Operational Research and Systems Visual Modeling.

Guilherme A B Pereira was born in 1961 in Porto, Portugal. He graduated in Industrial Engineering and Management in the University of Minho, Portugal. He holds an MSc degree in Operational Research and a PhD degree in Manufacturing and Mechanical Engineering from the University of Birmingham, UK. His main research interests are Operational Research and Simulation.

José A Oliveira was born 1966 in Matosinhos, Portugal. He studied Mechanical Engineering at the University of Porto, Portugal. He graduated with a Ph.D. in Production and Systems Engineering at University of Minho, Portugal. His main research interests are Optimization with Heuristic Methods in Systems Engineering.

DATA MODELLING APPROACH FOR PHYSICAL SYSTEMS

S. Winkler[a], A. Körner[b], F. Breitenecker[c]

[a],[b],[c]Institute for Analysis and Scientific Computing, TU Wien

[a]stefanie.winkler@tuwien.ac.at, [b]andreas.koerner@tuwien.ac.at, [c]felix.breitenecker@tuwien.ac.at

ABSTRACT
This contribution deals with the possible applications of neural networks for hybrid models. After a basic introduction to neural networks and hybrid modelling some applications are discussed. On the one hand, the substitutability of hybrid models is up for debate. On the other hand, the possibility of combining neural networks with physical models, e.g. for determining individual parameters, are focused. In the end the discussed approaches are applied and compared using a fundamental example.

Keywords: modelling and simulation, dynamic hybrid systems, neural networks, benchmark

1. INTRODUCTION
Data modelling is one of the leading research areas. Nowadays, it is very reasonable that neural networks are one of the techniques in modelling and simulation. The fact that neural networks focus on imitating processes in human brains might be part of the explanation. Furthermore the accumulation of data in various applications, platforms and software enforces researchers to look for powerful alternatives to process big data structures.

In several research fields it is nonsense to describe certain system behaviour without using physical foundation and mathematical formulations, respectively. In some cases first principle models are available, but neural networks are used to parameterise certain variables of the model. This combination of neural networks and first principle models can be found in Psichogios and Ungar (1992) and is referred to as hybrid neural networks.

Sometimes the usage of one physical model is not sufficient. Complex structures often require a combination of different methods and models. These combinations mostly consist of a mixture of discrete and continuous processes and therefore are called hybrid models. Assuming that the system contains at least one continuous part these models are named hybrid dynamical model.

Considering a model containing discrete and continuous processes with partly undefined parameters, a neuronal network can be used to determine these parameters in advance or even within the simulation. For example in optimisation and automotive industry this combination was already tested for a combination of different LTI systems, see Lu et al. (2016).

In the following we will present the basic structure of hybrid models and neural networks and the possibilities to combine these approaches. A basic example will be used to demonstrate the different approaches and model structures.

2. MODEL STRUCTURE
For a better understanding of the model structure mentioned above a short introduction to both approaches pointing out their properties and peculiarities will be given in the following subsections.

2.1. Hybrid Models
Hybrid is an often used term with many different meanings. In the automotive industry hybrid defines the combination of a petrol and an electrical engine. In modelling and simulation this term simply describes a certain collection of modelling approaches, which are necessary to describe a certain (complex) system. This model behaviour can be described by a hybrid dynamical system, see Figure 1 left. In order to realize this behaviour it has to be modelled. A hybrid automaton is an often used illustration of such complex behaviours.
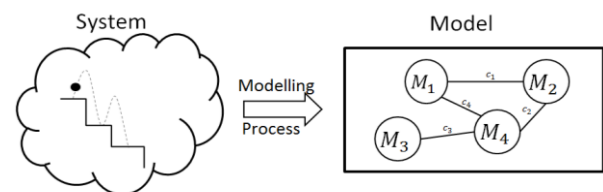
Figure 1: This illustration depicts the model process coming from a system and developing the according hybrid model description.

An extension of this illustration enables also modelling hybrid dynamical systems using an automaton like in Figure 1 right. These automaton are no unique description in terms of layout. In general an automaton consists of different nodes symbolising different states of the system. Speaking of a hybrid dynamical system the nodes do not just symbolize a certain fixed state but characterise the discrete or continuous system behaviour. The lines connecting these nodes are only valid if certain conditions are fulfilled. Therefore an automaton can also

be compared to a graph. This characterisation of hybrid dynamical systems focuses on the modelling approach.

A well-known formalism for such combinations of discrete time event systems is also known as DEVS (Discrete Event System Specification) which is an formalism invented by Zeigler and Praehofer (2000). Since its first introduction the formalism has been extended to meet the growing requirement including not only combinations of discrete but also continuous model descriptions.

Despite of this definition various other formulations as mentioned in Körner et al. (2016) and Mehlhase (2014) focussing either on the mathematical or the computer science point of view. In general hybrid dynamical systems can contain various different sub models with certain transitional regulations. Every sub model can either be described by ODEs (ordinary differential equations), DAEs (differential algebraic equations), DES (Discrete event systems) or ABM (Agent Based Modelling) and anything else which describes discrete or continuous system behaviour.

So called guard regions G and jump relations J control the behaviour change of the system by defining the transitions. If the state vector x enters the guard region, in other words $x \in G$, a transition occurs. There are two possible definitions for a guard region. Either the guard region is a set of all values x which lead to a system change. Or the border of this guard region is formulated by using an event function $h(x)$. If the condition $h(x) = 0$ is fulfilled the jump occurs. Therefore the event localisation transforms into a zero-crossing or root-finding problem. Then the jump relation J defines the changes of the system parameters and function after the transition. Two different types of events can be distinguished:

- time event,
- state event.

If the event occurs at a certain point in time it is called time event. An event depending on the current state of the system is called state event. In case of a time event the transition location is quite easy. If the time variable reaches the value where the event occurs the system change is executed. On the contrary conditions to characterize state events have to be defined. If the condition for the event is fulfilled the correct point in time has to be determined. The jump itself represents a discrete part of the model. Depending on the complexity and number of sub models the level of implementation can vary highly.

2.2. Neural Network

In general, a neural network consists of 3 different components. Two of them are defined inherently by the regarded system. Depending on all possible inputs and the desired output parameter the initial structure of input and output layer are specified. Every input value generates a so called node as illustrated in Figure 2

with $x_i, i \in \{1,2,3\}$. In this example the output layer on the right hand side consists only of one node labelled y. The number of these values regulates the structure of the input and output layer. The number and structure of hidden layers can diversify. The illustration in Figure 2 consists of two hidden layers with the nodes b_{11}, b_{12}, b_{21}.
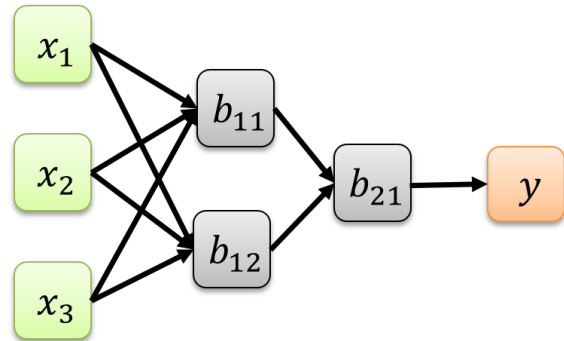
Figure 2: The basic structure of a neural network with a two hidden layer in grey b_{11}, b_{12}, b_{22}. There are three input values x_1, x_2, x_3 and one output value y.

The structure of these hidden layers defines the type of neural net. All the grey nodes of the hidden layers are called neurons. The connections between all the nodes and neurons are annotated with weights which either accelerate or damp the incoming signal. Additionally, there is an activation function embedded in the neurons, which is applied to the signal after multiplying it with the weight. There are different common activation functions, varying from linear via logistic functions through to the nonlinear sigmoid functions. Applying the linear activation function the output signal $O(b_{11})$ of neuron b_{11} would be as follows:

$$O(b_{11}) = x_1 w_1 + x_2 w_2 + b_{11}$$

Whereas $w_i, i \in \{1,2\}$ donates the weights from node x_i to b_{1i}.

The complexity of the system influences the choice of the activation function. If the system is quite simple the linear function might be as sufficient as a more complex choice of activation function.

The weights of all the connections, often referred to as edges, are determined by using datasets containing the desired input and output data relation of the regarded system. The data sets have to be big enough to enable a solid training and good performance. For training neural networks, different algorithms are known. An often used method is the backpropagation. For this algorithm the weights are set to random variables in the beginning. After the neural network is once executed with the chosen training input data the resulting error of the output signal and the provided data in the training set is used to adapt the values of the weights. Layer by layer the errors are calculated back from the output to modify the weights accordingly in order to achieve the best results. Different algorithms can be used to determine the modification, for example gradient descent, newton method and Levenberg Markquart.

3. BASIC APPLICATION EXAMPLE FOR HYBRID SYSTEMS

3.1. Problem Definition

In the following we will use the model of the bouncing ball as an example for a hybrid system. Whenever the ball hits the ground, due to the bounce and gravity, the velocity decreases and the direction of the ball changes. Due to this change this model is categorised as hybrid model and can be illustrated by one node with changing parameters. In this node the model is described using a differential equation. Only the parameter value changes, which can be depicted using an arrow going in and out into the same node. The differential equation (1) together with the given initial conditions describe the system behaviour whereas $h(t)$ defines the height of the bouncing ball with respect to time as shown in Figure 3.

$$\ddot{h}(t) = -g$$
$$h(0) = h_0, \dot{h}(0) = v_0 \tag{1}$$

This equation can be reformulated so that the system behaviour can be given as state space description whereas g defines the gravity.

$$\dot{x}(t) = \begin{pmatrix} 0 & 1 \\ 0 & 0 \end{pmatrix} x(t) + \begin{pmatrix} 0 \\ -g \end{pmatrix} \tag{2}$$

The vector $x(t)$ stands for the height in the first and the velocity of the ball in the second component.

As mentioned before the actual bounce defines the event of the hybrid model. This event can be formulated using a guard region, as mentioned in section 2.1. The first line of (3) defines the guard region for the bouncing ball. It can be verified to determine if a system change, therefore a new initialization of the parameter, occurs. This equations in the guard region set can also be formulated as event function. It states two conditions for height and velocity of the ball. The second line in (3) defines the jump relation. $\tag{3}$

$$G = \left\{ \left(h(t), \dot{h}(t) \right) : h(t) = 0 \wedge \dot{h}(t) = v(t) \le 0 \right\}$$

$$J\left(v(t_e) \right) = -\lambda v(t_e), \lambda \in (0,1)$$
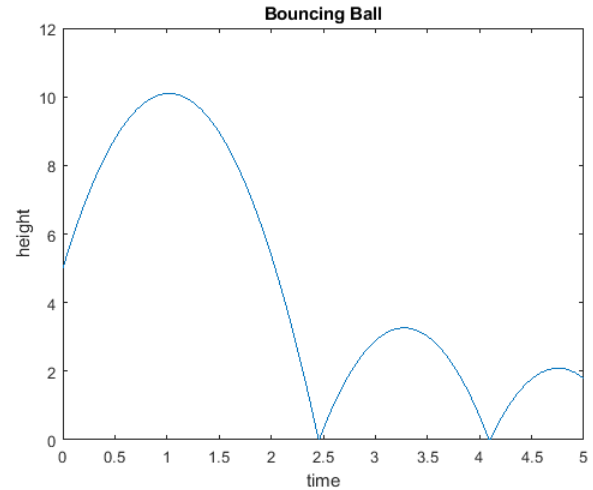
Figure 3: This plot shows the analytical solution of the bouncing ball model.

Neglecting the system changes at the bounce, an analytical solution of the model can be given, see equation (4).

$$\begin{pmatrix} x_1 \\ x_2 \end{pmatrix} = \begin{pmatrix} -\dfrac{g}{2} t^2 + c_2 t + c_1 \\ -g\, t + c_2 \end{pmatrix} \tag{4}$$

3.2. Implementations using the ODE

The bouncing ball model can be implemented in different ways. In the following MATLAB® is used to realise different approaches. Due to the fact that the system is described by a parametrised ordinary differential equation, ODE solvers can be used to simulate the system. Another possibility is the usage of the MATLAB® embedded event function. Additionally to these two implementations different realisation in Simulink® are done. On the one hand the differential equation is implemented block oriented including an if-condition to realise the guard region. The second Simulink structure include of a memory block to realise this hybrid transition.

The results of these implementations show almost no differences to the analytical solution, see Figure 4. The Simulink model is very accurate. Only after some bounces small discrepancy occurs due to numerical calculation errors.
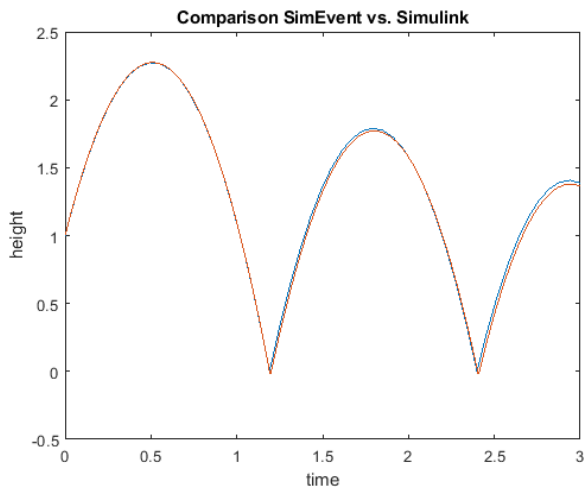
Figure 4: The graphic shows a comparison of the results of the MATLAB implementation using an event function (red) and the SIMULINK model containing the memory block (blue).

3.3. Implementation of the Neural Network

The analytical solution of the model is not only used comparison but also to create input and output values for training the neural network. There are different software solutions supporting creating a neural network which only require a set of input and output data. In this case the MATLAB toolbox for neural network is used. In order to create such data sets one has to define the input for the regarded model description and useful output values to analysis the results.

In case of the bouncing ball example one possibility is to use initial values, the parameter of the differential equation and also a discretisation of the time axis for this data set. Therefore the desired output would then be the height of the ball at any point in time. This data set would present the input output relation of the model as the ODE implementations do. Depending on the resolution this can lead to an unnecessary overflow of data points, nodes, neurons and of course weights to determine.

Therefore it is important to decide which results are necessary to characterise the model outcome sufficiently.

In the following implementations the input is defined as initial values and parameter of the model. The output data are the extrema of the flying phase of the ball and the point of the following event. As mentioned before the generation of the necessary datasets to train the neural network are generated by using the analytical solution of the model. Therefore an arbitrary size of data sets with varying initial conditions was created. With this data the input and output layer of the neural network are defined. The only missing piece is now the structure of hidden layers. Due to the fact that the number of input nodes equals the number of output nodes the hidden layers also have to consist of 3 neurons. Due to the easy structure of the analytical solution only one hidden layer was implemented. For the activation function of the neurons, explained in section 2.2, different approaches were implemented. First of all the more or less linear approach

was taken. This means that in the neural network the incoming signal was multiplied by the weights determined using the training algorithm and then added to a constant, which was also defined during training.

In the second approach the MATLAB implemented tool box *nnstart* was used to generate automatically the neural network applying the commonly used nonlinear sigmoid function.
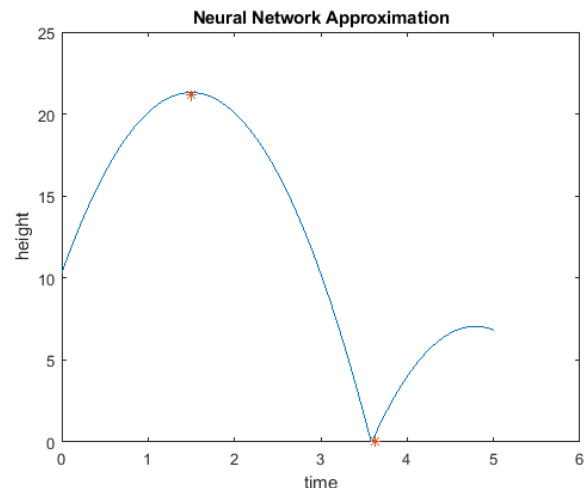
Figure 5: The red stars are marking the prediction from the neural network of the extrema and the next event.

The results of this implementation can be seen in Figure 5. The analytical solution (blue line) and the prediction from the neural network (red stars) are fitting quite well.

4. COMPARISON OF THE MODEL APPROACHES

In the following section we compare and discuss the properties, similarities, advantages and disadvantages of the different approaches.

4.1. Zeno Effect

Hybrid models have the ability to show very special system behaviour. The so called zeno effect describes the situation of a hybrid system where infinite switches happen in a finite time span. For the bouncing ball example this effect means that an infinite number of bounces happens in a quite short time interval. The mathematical model of the bouncing ball of course respects this rare incident. Realising such behaviour in a simulation model is of course not possible like that.

The analytical solution gives an idea how such cases might look like. The results of this simulation run are depict in Figure 6. Of course due to numerical issues and small calculation errors the zeno effect is not absolutely reproducible in this implementations. Or and Teel (2010) were using a different approach to create the zeno effect, a so called set-valued bouncing ball definition.

Regarding the implementation in Simulink an error occurs stating that the maximum number of zero crossings is exceeded. Concerning the neural network this approximated effect has to be embedded in the training data. Therefore it is impossible for the neural net

to generate such output. For the current choice of data set this effect is not considered. The output only suggests the next event, and therefore not provides a sufficient setting. Future implementations will focus on this zeno effect in detail.

Figure 6: This plot shows the analytical with an almost zeno effect between second eight and nine.

4.2. Advantages and Disadvantages
Compared to the numerical implementations of the differential equation the number of resulting data points might be an issue for further usage. In the implementation explained in section 3.2 the choice of input and limits the number of output nodes. In the current setting the results of the neural network can be used to predict the next event of the hybrid system. Additionally the peak of the current bounce is calculated. Dep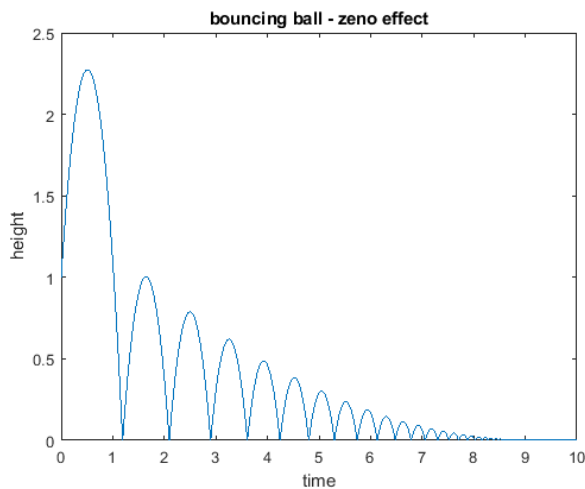ending on the usage of the model this information could be too less. Compared to the numerical simulation in MATLAB, where the behaviour of the system for every point in time is returned, the enabled analysis for the neural network is limited.

Regarding the limit data points another application could be predicting only the height of the ball for the next two time steps. This could be useful if such neural network would be embedded in a bigger real time system to calculate the approximation for the next time steps which would determine the setting of a connected machine.

4.3. Comparison of Results
K. Hornik (1989) claims that feedforward networks are capable of arbitrarily accurate approximation to any real-valued continuous function over a compact set. Therefore it is not surprising that the error of the neural network compared to the analytical solution is small, as shown in Figure 5. Additionally the usage of the analytical solution for generating the training data also leads to solid results.

The error of the numerical model, depicted in Figure 4, is quite low. Also the results of the neural network in Figure 5 encourage the usage of neural networks for simulation models describing the behaviour of hybrid models. Figure 7 shows the error compared to the best possible value (dotted line). There were 39 iterations and

the best values was reached after the 33th itteration. The here defined values for the weights were used to generate the results in Figure 5.
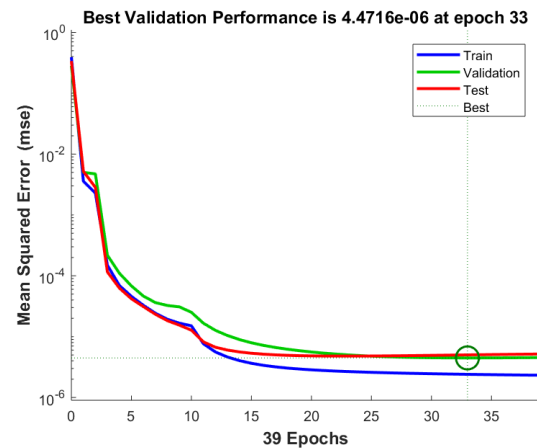
Figure 7: This shows the results of training and validation of the neural network using the MATLAB Toolbox.

Of course the numerical and the network models are hard to compare. On the one side you have the height for every point in time which means you can apply different mathematical algorithms to compare the different numerical implementations with each other because the type of result is always the same. The neural network on the other hand returns three values, which are not even only concerning the height of the ball at a certain point in time but also the resulting points regrading moment in time. Therefore the error values of this approaches cannot be set in relation directly.

Due to the fact that the example was particularly chosen the complexity of the implementation of both approaches is comparable. The time to establish the model as well as the accuracy of the models are similar.

5. DISCUSSION
The bouncing ball might not be the best practice example to show the usefulness of such combinations. Psichogios et. Al (1992) and Lu (2016) present applications where the neural network is used to determine a certain parameter of the simulated system on the one hand in a model approach and on the other hand in a real time simulation. This shows the trend of using neural networks not only for pattern recognition in image processing or social networks but also for engineering applications. Depending on the application of the neural network, if embedded in a bigger system or standing alone, the usability can vary.

The biggest disadvantage of using neural networks in the engineering field of course represents the availability of data. The possibility of using an analytical solution or similar information about the system behaviour is of course not given in most practical application. If available, the purpose of a neural network as well as a numerical approximation would be senseless. Therefore, if thinking about including a neural network in a

modelling system the possibility to gather enough data for the learning process is critical.

Due to the fact that in the last years the gathering of data, not only in social media but also in the modern industry increased exponentially mathematical modelling and simulation tools should include this data at some level. Neural network are a possible method which can use this data and be combined with first principle approaches to possibly improve existing processes. One very recent example of new approaches combining this strategies can be found in Martinus and Lambert (2016). In this article the structure of neural networks are used to create a equation based model formulation to not only interpolate but extrapolate the behaviour of a system. With this method it then should be possible to let machines not only learn from mistakes, as it is done with ordinary neural network, but also predict future mistakes in order to avoid them without trying and failing first.

6. OUTLOOK

This work was just a first step. There are many more steps which have to follow in order to answer the questions if neural networks and hybrid modelling can be combined practically.

Firstly, the next implementations will focus on the evaluation of the zeno effect in different implementation. This scenario is interesting for the neural network approach but also for numerical models. Reproducing this effect with neural networks represent the greater challenge of course. For an ordinary neural network, structured, as defined in section 2, this effect must be included in the training data. The approach of Martinus and Lambert (2016) could be useful to cope this challenge in a different way.

Secondly the currently used structure of neural network will be modified regarding the desired output data. In order to explore the possibility to predict the system behaviour for the next time steps, the training data has to be defined differently. It will be important to investigate how much the data set influences the results. Therefore the case study will include cases where the test data will not be related only little to the training data to verify applicability.

Last but perhaps most important, after finishing both tasks explained before, this gathered knowledge should be applied on a more sophisticated and realistic example. Although this example would have a more complex structure in the sense of the hybrid model definition the availability of data is still important. Providing the necessary data for training and validation guarantee a solid analysis of the system and provide possible answers to some of the following questions:

- What model structures can be replaced by neural networks?
- Which type of hybrid models benefit from embedded neural networks?
- What are the limits of this approach in hybrid modelling?

The last question can never be fully answered but it is important to look for new enhancements and combinations of existing model approaches to keep pace with development and technology.

REFERENCES

Hornik K., 1989. Multilayer Feedforward Networks are Universal Approximators. In: Neural Networks, vol 2, pp.359-366.

Körner A., Winkler S., Breitenecker F., 2016. Possibilities in State Event Modelling of Hybrid Systems. In: Proceedings of 9th EUROSIM Congress on Modelling and Simulation, pp. 542-543.

Lu W., Pingping Z.,Ferrari S., 2016. A Hybrid-Adaptive Dynamic Programming Approach for the Model-Free Control of Nonlinear Switched Systems. In: IEEE Transactions on automatic control, vol 61, No. 10, pp.3203-3208.

Martinus G., Lampert C.H., 2016. Extrapolation and learning equations. 2016. arXiv preprint https://arxiv.org/abs/1610.02995.

Mehlhase A., 2014. A Python framework to create and simulate models with variable structure in common simulation environments.In: Mathematical and Computer Modelling of Dynamical Systems 20 (6), pp. 566-583

Or Y., Teel A. R., 2010. Using the Set-Values Bounding Ball for Bounding Zeno Solution of Lagrangian Hybrid Systems. In Proceedings: 8th IFAC Symposium on Nonlinear Control Systems, pp 801-806.

Psichogios D.C., Ungar L.H., 1992. A Hybrid Neural Network-First Principles Approach to Process Modeling. In: AIChE Journal vol. 38, No. 10, pp. 1499-1511.

Ziegler B. P., Praehofer H., Kim T.G., 2000 Theory of Moedling and Simulation, 2nd Edition. Academic Press.

AUTHORS BIOGRAPHY

Stefanie Winkler passed her bachelor study in technical mathematics in 2012 and her master study as well in technical mathematics in 2014. Both theses covered applications of mathematical modelling and simulation. The master thesis in particular covers a comparison of different approaches to simulate groundwater pollution.

Her fields of activity include numerical aspects of simulation, comparison and evaluation, simulation of partial differential equations as well as applied mathematics in engineering. Since 2014 she is project assistant in the research group of Mathematical Modelling and Simulation at the Institute for Analysis and Scientific Computing at Vienna University of Technology. She is currently working on finishing her PhD in mathematics.

A COMPARISON OF VARIOUS BIOMECHANICAL MODELLING APPROACHES FOR ANATOMIC JOINTS INCLUDED IN A CLOSED SIMULATION LOOP

Ruth Leskovar[a], Andreas Körner[b], Felix Breitenecker[c]

[a],[b],[c] TU Wien, Institute for Analysis and Scientific Computing, Wiedner Hauptstraße 8-10, 1040 Vienna, Austria

[a]ruth.leskovar@tuwien.ac.at, [b]andreas.koerner@tuwien.ac.at, [c]felix.breitenecker@tuwien.ac.at

ABSTRACT

This contribution develops a design of a closed system simulation loop for various modelling approaches in biomechanics. Two different modelling approaches are widely used describing anatomical joints which are based on different mathematical descriptions. Some basic insights to multibody models, based on ordinary differential equations and models based on partial differential equations are given. The fundamental distinctions between these two modelling approaches require different restrictions respectively reformulations. This work deals with finding requirements for both modelling approaches to achieve the incorporation into a closed feedback loop. The possibilities in the design of a closed feedback loop depend on the simulation environments. The aim of this work is to establish a loop where as well the biomechanical model as the control tools are embedded in a powerful environment.

Keywords: biomechanical models, feedback simulation loop, multibody modelling, pde modelling

1. INTRODUCTION

Biomechanical models are used analysing the interactions taking place in the human body and are an indispensable tool in medical research, as e.g. in the development of implants or even prostheses. The development of a closed simulation loop for biomechanical models using different modelling approaches is the aim of this work.

This enables the application of the achieved system-based modelling approach in the field of prostheses due to its flexible adaptation to different scenarios in the daily use of prostheses.

The use of biomechanical models in the research of prostheses is indispensable. Their applications are widely distributed. For example, new technologies or new materials used in prostheses can be validated easily and economically with mathematical models of the human body.

Depending on the miscellaneous demands on the simulation, different modelling approaches are used. For biomechanical models, two approaches are mainly considered:

- Modelling with partial differential equations,
- Multibody modelling.

Using models described by PDEs requires a more complex structure than multibody models on the one hand, but on the other hand, finite element solutions have higher accuracy and furthermore even small interactions can be analysed. Therefore, PDEs are widely used for analysing adaptions in biological tissue resulting from daily loads. Multibody models are used in biomechanics analysing gross motions and interactions taking place between two or more bodies in daily movements. The usage of different biomechanical modelling approaches can be found in Machado et al. (2010).

First, basic principles of both modelling approaches will be discussed and some insights to their applications are given. This illustrates the differences between the modelling approaches. The distinct properties of the modelling approaches have impact on their incorporation to a closed feedback loop which will be discussed.

Finally, an already established multibody model is included in a closed simulation loop using Simulink. First results are presented for a basic control circle.

The issues and the possibilities regarding the incorporation of a model described by PDEs to a closed feedback loop are discussed.

2. DISTRIBUTED PARAMETER MODEL

Models described by partial differential equations are widely used in the field of biomechanics. The finite element method is a powerful tool analysing structural alterations and it gives deep insights about biomechanical interactions.

2.1. Modelling aspects of PDE approach

Since, accurate and specific results are obtained using this method, detailed knowledge of the underlying system is required in advance. Due to the complex model structure it is common to formulate the model only for small body parts in order to facilitate the model development.

In biomechanics, PDE models are used to calculate resulting strains and stresses in biological tissues under loads and strains exposed during movements. Here, no kinematic interactions between multiple body parts are analysed.

Since models described by PDEs depend not only on time but also on spatial variables, they are models with distributed parameters.
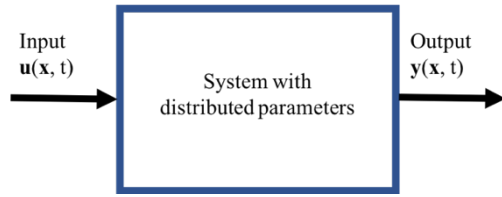
Figure 1: System with distributed parameters.

This description underlies an infinite state space description. Figure 1 illustrates a system with distributed parameters with the vectorial input $\boldsymbol{u}$ and the vectorial output $\boldsymbol{y}$, both dependent on time t and space coordinates merged in the vector $\boldsymbol{x}$.

PDE models have a wide field of applications, as e.g. solutions for electromagnetic, thermodynamic or even structural mechanic problems can be calculated. This contribution deals with structural mechanic problems only, where stresses are calculated. For small displacements u_x of a body in the direction x, the resulting stresses σ_x and shear stresses τ_{yx}, τ_{zx} under an applied force F_x can be calculated with the equation of motion

$$\frac{\partial \sigma_x}{\partial x} + \frac{\partial \tau_{yx}}{\partial y} + \frac{\partial \tau_{zx}}{\partial z} = \rho \frac{\partial^2 u_x}{\partial t^2} - F_x, \tag{1}$$

whereby ρ denotes the density of the material. This can be found in detail in Slaughter (2002).

Two examples of PDE models demonstrate the variety of usage and their importance in research.

2.2. Analysis of soft tissue interaction

As biomechanical models using the finite element method is suitable for small structures, it is a common used tool investigating strains and stresses in soft tissues. Due to the complex structure of the knee, composed of various materials as bone, cartilage and ligaments, the biomechanics in the joint cover various aspects. In order to analyse the interaction between menisci and ligaments, Peña et al. (2006) established a detailed 3D model of the healthy human knee joint. The detailed geometry of the elements is derived by MR and CT images. The ligaments are modelled as hyperelastic material, i.e. soft tissue. The resulting total stress σ in the ligaments, is calculated by

$$\sigma = \frac{2}{J} F_r \left(\frac{\sigma_0}{2} + \frac{\partial \Psi_{\Omega_0}(C)}{C} \right) F_r^T, \tag{2}$$

whereby F_r denotes the deformation gradient by applying loads to the initial configuration Ω_0 with its initial stress σ_0 in the reference state, Ψ_{Ω_0} the strain-energy function dependent on the Cauchy-Green strain measure C.

After definition and validation of the model, three different load cases were applied to study the load propagation in the ligaments and their dependence of the menisci. This knowledge is essential figuring out the stability in the human knee.

2.3. Development of biomaterials used in implants

As PDE models are widely used calculating strain and stresses in biomaterials, they are as well used in the development of new materials incorporated in implants. Bone is a biomaterial where adaptions take place throughout life due to the applied loads. Biomaterials with similar properties reduce the risk of loosening implants and raise the incorporation in the present structure. In the work established by Bahraminasab et al. (2014), the finite element analysis is used to develop a new biomaterial included in knee implants. The investigated biomaterial consists of various components, a functionally graded material The parameters determing the composition were calculated with finite element solutions of a model for the knee implant.

3. MULTIBODY MODELLING

Multibody models are used in biomechanics for the analysis of the kinematics in a system undergoing movements and their resulting loads.

3.1. Modelling aspects of multibody models

Multibody modelling is a non-causal modelling approach which implies that the implementation does not start with mathematical formulas but considering only the physical interactions taking place in the investigated system. For example, the development for a multibody model of an anatomical joint starts by declaring all involved body parts and in which way they are connected.

A multibody model contains rigid and flexible bodies which are connected to each other by joints. There exist various types of joints, which differ by the degree of freedom and the different type of movement they offer, e.g. spherical and revolute joints. A more detailed explanation of multibody modelling can be seen in Rill and Schaeffer (2010).
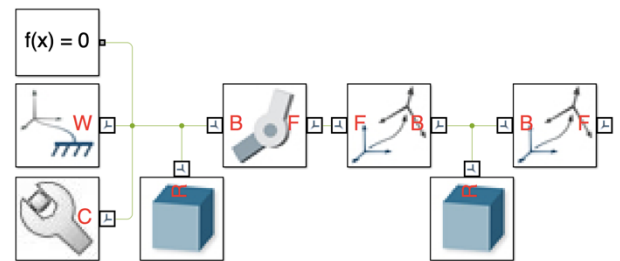
Figure 2: Multibody model of the mathematical double pendulum, implemented in Simscape.

A simple multibody model, implemented in Simulink, is depicted in figure 2, representing the mathematical double pendulum. Two solids are connected by each other with one revolute joint. The properties of the bodies and the connection via the joint define the system of second order differential equations describing the pendulum.

Each multibody model is described by ordinary differential equations. Since, mechanical systems are investigated, the motion of rigid bodies is derived by the Newton-Euler equation and the Lagrange formalism, which leads to the equation

$$M\ddot{x} + J_x^T \lambda = F. \tag{3}$$

The various variables describe parameters of the system, M is the mass matrix of the system, the vector x contains the coordinates w.r.t. the states, J_x represents the Jacobian of the coordinates and λ holds the Lagrange multipliers. The acting force exposed on the system is denoted as F.

This description leads to a time-dependent structure of the state variables. As opposed to models with distributed parameters, multibody models are lumped systems which depend on finite numbers of parameters.

3.2. Multibody modelling used for gait analysis

A widely used application of multibody models is gait analysis, i.e. the analysis of resulting interactions and strains in the human body under loads during walking. Multibody models are used hereby because they are useful analysing body parts under gross movements. Here, not only the legs or even only one bone but the whole body can be investigated. This allows to study the biomechanical performance taking place in the human body during walking, running or even climbing.

In the multibody model for the human knee joint, developed by Xu et al. (2014), not only the bones but the ligaments and the patellar tendon are considered. This allows a more specific and detailed analysis of the biomechanical interactions taking place during walking.

Since, the variety of human movements are wider than only walking, multibody models are used for various movement analysis. For example, multibody models are used to investigate the reactions of the human body under falling scenarios as it is done by Welke et al. (2013). These results are used in further analysis of injuries and therapy.

3.3. Multibody models used for knee replacements

As mentioned above, biomechanical models are necessary improving knee implants, multibody models are used as well in this technology. Piazza and Delp (2001) presented a multibody model for the analysis of climbing stairs. This model is further used for the investigation of different full knee replacements. The investigation of contact mechanics in the knee joint with an implant is analysed within motion. This allows an improved insertion of a full knee implant and gives more insight to the wearing losses of knee implants.

Insights derived from multibody models are intrinsic in the development of leg prostheses to improve their functionality and wear comfort.

4. MULTIBODY MODEL OF THE HUMAN KNEE JOINT

In order to design a closed simulation loop, first a validated and well defined model of an anatomical joint is needed. Since, this work focuses on the feedback loop and not on the biomechanical definition of a joint model, an already implemented model is used. The platform SimTK, found on https://simtk.org, offers a wide variety of various biomechanical models that are provided by the

researchers itself. This assembly does not cover only mathematical models of human joints but it comprises as well geometries in order to facilitate the implementation of own biomechanical models. The models provided cover multibody models as well as model descriptions by PDEs in various simulation environments.

The model used in this work is developed by Guess et al. in multiple works and is explained in more detail in the following. It deals with the development of subject specific multibody models of human knee joint. In the following, a multibody model for the right knee of a 77 year old man is considered. The model is implemented in the software Adams (MSC Software Coorporation).

The multibody model consists of the three main bones of the human knee joint, the femur, the tibia and the patella. The articular cartilage is included in the geometry of the bones. Additionally, the patellar tendon which is responsible for propagating the force acting from the quadriceps as well as the cruciate and the collateral ligaments are embedded in the model structure.
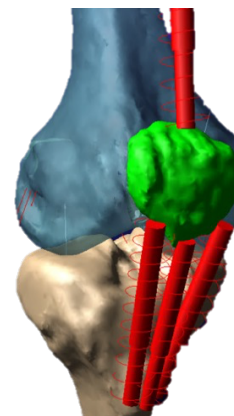
Figure 3: Multibody model of a human knee joint developed by Guess et al. (2013).

In figure 3, the multibody model, developd by Guess et al. (2013) in the software Adams is depicted with the three bones and the patellar tendon, modelled as linear spring. The force acting on the joint is propagating over the tendon.

The development of the model comprised three phases. First, the research focused on the modelling for the cartilage on the femur and tibia interacting with the menisci. As it can be read in detail in Guess et al. (2010), PDE models are used for the calibration of the multibody models in order to calculate contact parameters between cartilage and meniscus.

In a further step, the contact parameters between cartilage and the bones were derived as it is written in detail in Guess et al. (2013). The parameters were calculated using three different methods. Again, finite element analysis was used to determine parameters, the Hertzian contact theory was used for calculation and last, the elastic foundation contact theory was applied. The evaluation of the parameters was done using a knee simulator for the developed multibody model and after compared to measured data in vitro kinematics.

The contact force F between bone and cartilage is finally

defined by the Hertz contact law

$$F = k\delta^n + B\dot{\delta},\qquad(4)$$

with the interpenetration δ of the geometries, $\dot{\delta}$ the velocity of interpenetation, the damping coefficient B and a spring coefficient k.

The ligaments in this model are implemented as bundles of one-dimensional non-linear spring damper elements. Bloemker et al. (2012) discovered that the parameter defining the zero-load length is highly sensitive, which requires a valid and quick method to find it. The parameter defining the zero-load length is the length of the ligament when it first becomes taut. Since ligaments are elastic and their biomechanical behaviour changes under stress, the modelling of these bundles is complex. Ligaments have a non-linear toe region, i.e. the fibers are crimped first under stress. When all fibers become taut, the ligament behaves as a linear spring with the spring parameter k.

Calculating the force f, resulting from the ligaments is calculated by a subroutine following the equation

$$f(\varepsilon) = \begin{cases} \dfrac{\varepsilon^2}{4\varepsilon_l}k, & 0 \le \varepsilon \le 2\varepsilon_l, \\ k(\varepsilon - \varepsilon_l), & \varepsilon > 2\varepsilon_l, \\ 0, & \varepsilon > 0. \end{cases} \qquad(5)$$

The strain, respectively the displacement, of the ligament is calculated by

$$\varepsilon = \frac{l - l_0}{l_0},\qquad(6)$$

whereby l defines the length of the ligament and l_0 the zero-load length.

The work of Guess et al. includes two multibody models in Adams, one applying the force during normal gait cycle, resulting in knee flexion and the second one applies static load to the joint.

5. EMBEDMENT OF A BIOMECHANICAL MODEL IN A CLOSED SIMULATION LOOP

Embedding biomechanical models in a closed feedback loop gives the opportunity to extend the variety of applications of biomechanical models. For example, acting forces on human joints can be adjusted in a more easy and effective way using control theory.
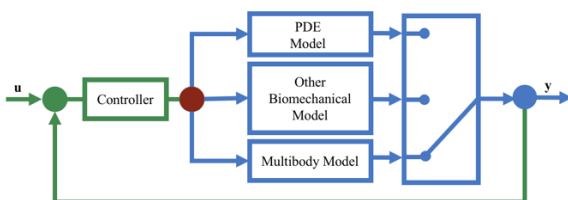
Figure 4: Block diagram of embedding biomechanical models to a feedback loop.

Figure 4 represents a block diagram of the inclusion of biomechanical models in a closed simulation loop and

further displays the possibility to consider some other biomechanical models.

5.1. Requirements on the biomechanical models

For the formulation of the biomechanical model in a closed simulation loop, some prerequisites have to be fulfilled. The biomechanical models must fulfil the requirements for a dynamic systems.
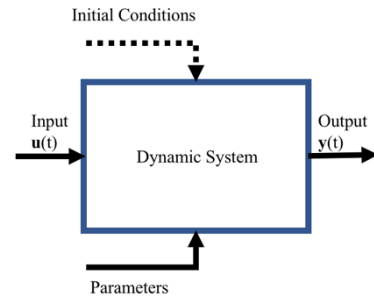
Figure 5: Block diagram of a dynamical system.

Dynamic systems are sets of interacting components forming an integrated whole. A block diagram of a dynamic system is depicted in figure 5.

The change of the state variables defining the dynamic system over time depends on the input, the output, initial values and acting parameters. This can be summarised in the following first order differential equation

$$\dot{y} = f(t, u(t), y(t), p),\qquad(7)$$

where y represents output and u the input. Both depend on time t and p depicts the acting parameters on the system. It is important to notice, that the dependence is not direct proportional but the system changes its behaviour on its own dynamic.

In this contribution, the input for the investigated biomechanical models is considered as the acting force on the bones resulting from walking. The extension of the biomechanical model to a closed simulation loop allows a simulation of different scenarios, e.g. the adaptation of various walking respectively running scenarios.

The output of the multibody models is the angle in the human knee joint respectively the strains and stresses in the bones for the models with distributed parameters.

This definition of the output allows an adaptation of the acting force on the knee joint which illustrates a changed walking scenario.

5.2. Multibody models included in a closed feedback loop

Multibody models give the opportunity to include them easily in the desired loop. Hence, the motion is described by a second order ordinary differential equation, the desired description is easy to derive.

Having the multibody model implemented by Guess et al. (2013) in Adams, gives the possibility to export it as plant and use it as subsystem in Simulink. Adams allows to define system variables which act as input and output variables. As mentioned above, the input for the plant is

the force acting on the patellar tendon, which is normally driven from the quadriceps. The function *Algebraic Variable Value* is able to evaluate extern variables. For the output, the angle between patella and tibia is chosen. The angle can be calculated directly in Adams using the implemented function *angle about x* between two defined markers at the bodies.

After defining the in- and output of the model and exporting the plant as a subsystem to MATLAB, this gives the opportunity to include it directly in a closed control circle using Simulink. The block diagram for the Adams subsystem is depicted in figure 6. A valid connection to the software Adams must be available in order to achieve the simulation.
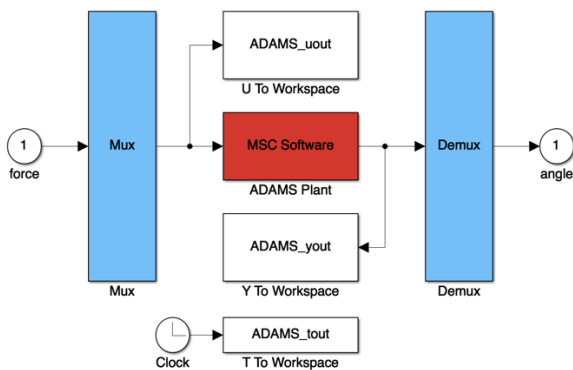

Figure 6: Subsystem of the Adams model in Simulink.

In the first approach, a simple PID controller is used for the closed simulation loop. The reference signal for the angle is a sine wave with an amplitude of 1. The proportional and integrator parameter of the PID controller are set to 1, the differentiator to 0.1.

Since, the PID controller is linear, but the multibody model is a non-linear system, the results are not satisfying. In figure 7, the output angle is plotted with a low amplitude. At least, the behaviour of the sine wave is fitting.
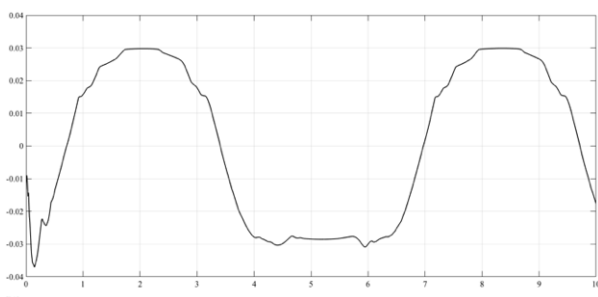

Figure 7: Angle between tibia and patella controlled with PID control.

5.3. PDE Models included in a feedback loop

Models described by PDEs need more effort in order to include them in a closed simulation loop due to their more complex structure and their dependence on more parameters.

Since, a comparison of including both biomechanical modelling approaches in the same feedback loop, a software for finite element analysis with an easy link to

MATLAB is required. This is the reason why COMSOL was chosen, although ABAQUS is a widely used software for biomechanical models. The approach to implement a feedback loop with finite element analysis calculated in ABAQUS and using the control tools of Simulink was established by Orszulik and Gabbert (2016). Another work establishing a feedback loop for a model with distributed parameters is done by Bertagne et al. (2014), using again a model with ABAQUS but implementing the controller in Python.

In the first attempt of this contribution, a model studying the solid mechanic behaviour of the tibia reacting on the load during walking was established. The same geometry and parameters of the tibia were used as implemented in the multibody model. In figure 8, the model in COMSOL, calculating the von Mises stress in the tibia, is depicted.
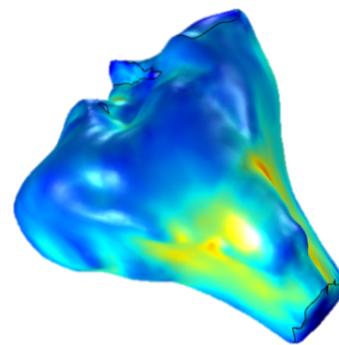
Figure 8: COMSOL model of the tibia.

COMSOL gives the opportunity to link directly the simulation environment to MATLAB, where more control possibilities are available and the connection to Simulink is present.

In previous versions of MATLAB, there exists a similar possibility as in Adams to export the COMSOL model as subsystem directly to Simulink. Hulko et al. developed the Distributed Parameter Systems Blockset for MATLAB and Simulink. The connection to COMSOL and the derivation of the Simulink block is found in Hulkó et al. (2009) and in Belavý et al. (2014). This Third Party Product is available in MATLAB Versions R12-R14 and 2009a. It relies on the assumption that in control theory, models with distributed parameters are considered as lumped input and distributed parameter output systems. This implies a finite input of the system and an output which depends on time and space again. Finally, the output $Y(x, s)$ of the system can be described in the s-domain by the equation

$$Y(\boldsymbol{x}, s) = \sum_{i=1}^{n} S_i(\boldsymbol{x}, s) U_i(s), \qquad (8)$$

where the vector $\boldsymbol{x}$ contains the coordinates of the position, $S_i(\boldsymbol{x}, s)$ are transfer functions and $U_i(s)$ are lumped input quantities. Using the developed Blockset and the co-simulation for COMSOL Multiphysics and MATLAB allows the design of control feedback loops for models with distributed parameters.

In the actual versions of COMSOL and MATLAB two more options exist using finite element method in a closed feedback loop.

COMSOL has the possibility to calculate the corresponding state space matrices as it is done in the contribution of van Schijndel (2018). Depending on the complexity of the system, this is a useful option. For the knee model investigated in this work, no state space description could be found.

The most adjustable way to include the COMSOL model in MATLAB is the co-simulation by using S-Function in SIMULINK as it is established in van Schijndel (2014).

6. CONCLUSION AND OUTLOOK

This contribution presents a system simulation loop for multibody models simulating anatomical joints. The human knee joint is modelled in the software Adams which is widely used in biomechanics. Including this model as control plant to a closed feedback loop in MATLAB allows to use powerful control tools available in Simulink and all possibilities of multibody modelling in Adams.

Further work focuses on the implementation of the feedback loop for a model using finite element analysis. The incorporation of a COMSOL model in MATLAB is possible but requires more effort due to the complexity of the model structure.

Additionally, the results of the feedback loops are compared in order to analyse the behaviour of different modelling approaches used in biomechanics. Various designs of feedback loops will be considered in future work in order to detect best fitting parameters and approaches for both biomechanical models.

The results will give insights about biomechanical modelling and enhance the usage and applications of models for anatomical joints.

REFERENCES

Bahraminasab M., Sahari B. B., Edwards K. L., Farahmand F.,Hong T. S., Arumugam M., Jahan, Ali, 2014. Multi-objective design optimization of functionally graded material for the femoral component of a total knee replacement. Materials and Design 53: 159-173.

Belavý C., Hulkó G., Lipár S., Barbolyas B., 2014. Control of Real Distributed Parameter Systems Modeled by COMSOL Multiphysics. Proceedings of the COMSOL Conference, 2014, Cambridge.

Bertagne C., Malak R., Moghadas P., Hartl D., 2014. Feedback Control Applied to Finite Element Models of Morphing Structures. Proceedings oft he ASME 2014 Conference on Smart Materials, Adaptive Structures and Intelligent Systems, Volume 1: Development and Characterization of Multifunctional Materials; Modeling, Simulation and Control of Adaptive Systems; Structural Health Monitoring; Keynote Presentation.

Bloemker K.H., Guess T.M., Maletsky L., Dodd K., 2012. Computational Knee Ligament Modeling Using Experimentally Determined Zero-Load Lengths. The Open Biomedical Engineering Journal, 6: 33-41.

Guess T.M., Liu H., Bhashyam S., Thiagarajan G., 2013. A multibody knee model with discrete cartilage prediction of tibio-femoral contact mechanics. Computer Methods in Biomechanics and Biomedical Engineering, 3: 256-270.

Guess T.M., Thiagarajan G., Mohammed K., Meenakshi M., 2010. A subject specific multibody model of the knee with menisci. Medical Engineering and Physics, 32: 505-515.

Hulkó G., Belavý C., Bucek P., Ondrejkovic K., Zajicek P., 2009. Control of Systems Modeled by COMSOL Multiphysics as Distributed Parameter Systems. Proceedings of the COMSOL Conference, 2009, Milan.

Machado, M., Flores, P., Claro, J. C. P., Ambrósio, J., Silva, M., Completo, A., Lankarani, H. M., 2010. Development of a planar multibody model of the human knee joint. Nonlinear Dynamics, 60(3): 459–478.

Orszulik R.R., Gabbert U., 2016. An Interface Between Abaqus and Simulink for High-Fidelity Simulations of Smart Structures. IEEE/ASME Transactions on Mechatronics, 21(2): 879-887.

Piazza S.J., Delp S.L., 2001. Three-Dimensional Dynamic Simulation of Total Knee Replacement Motion During a Step-Up Task. Journal of Biomechanical Engineering, 123: 599-606.

Peña E., Calvo B., Martínez M. A., Doblaré M., 2006. A three-dimensional finite element analysis of the combined behavior of ligaments and menisci in the healthy human knee joint. Journal of Biomechanics 39: 1686-1701.

Rill G., Schaeffer T., 2010. Grundlagen und Methodik der Mehrkörpersimulation. 3rd ed. Wiesbaden: Springer Vieweg.

van Schijndel A.W.M., 2014. Implementation of COMSOL Multiphysics in Simulink S-Functions, Revisited. Proceedings of the COMSOL Conference, 2014, Cambridge.

van Schijndel A.W.M., 2017. Getting state-space models from FEM simulations. Proceedings of European COMSOL Conference, 18-20 October 2017, Rotterdam, The Netherlands.

Slaughter W.S., 2002. The Linearized Theory of Elasticity. Birkhäuser Boston.

Welke B., Schwarze M., Hurschler C., Calliess T., Seehaus F., 2013. Multi-body simulation of various falling scenarios for determining resulting loads at the prosthesis interface of transfemoral amputees with osseointegrated fixation. Journal of Orthopaedic Research 31: 1123-1129.

Xu H., Bloswick D., Merryweather A., 2015. An improved OpenSim gait model with multiple degrees of freedom knee joint and knee ligaments. Computer Methods in Biomechanics and Biomedical Engineering, 18:11, 1217-1224.

SENSOR-BASED MODELING OF RADIAL FANS

Florian Holzinger[(a)], Michael Kommenda[(b)], Erik Strumpf[(c)], Josef Langer[(d)], Jan Zenisek[(e),] Michael Affenzeller[(f)]

[(a),(b),(e),(f)] Heuristic and Evolutionary Algorithms Laboratory, University of Applied Sciences Upper Austria, School of Informatics, Communications and Media, Softwarepark 11, 4232 Hagenberg, Austria
[(c)] Scheuch GmbH, Weierfing 68, 4971 Aurolzmünster, Austria
[(d)] Research Group Embedded Systems, University of Applied Sciences Upper Austria, School of Informatics, Communications and Media, Softwarepark 11, 4232 Hagenberg, Austria

[(a)]Florian.Holzinger@fh-hagenberg.at, [(b)]Michael.Kommenda@fh-hagenberg.at, [(c)]E.Strumpf@scheuch.com, [(d)]Josef.Langer@fh-hagenberg.at, [(e)]Jan.Zenisek@fh-hagenberg.at, [(f)]Michael.Affenzeller@fh-hagenberg.at

ABSTRACT

Predictive maintenance poses a new way to minimize costs and downtime of machinery. The combination of sensor data, intelligent algorithms and computing power allows this new approach to monitor the current health-state of machinery and detect possible failures early on or even in advance. Previous work in this field regarding radial fans focused on aspects such as vibration and noise, whereas this paper concentrates on the influence of multiple sensor data when modeling radial fans. In a case study multiple sensors are mounted on a radial fan and the importance of their signals on damage prediction is presented. The correlation between them is analyzed and the variable impact of sensor signals for approximating the rotational speed of a healthy and a damaged radial fan is identified.

Keywords: Condition Monitoring, Radial Fans, Predictive Maintenance

1. INTRODUCTION

Industry 4.0 and Internet of Things (IoT) are two trending topics in the field of computer science and production. With the increasing amounts of computational power, data transfer rates and cheap sensors, many use cases that were unthinkable ten years ago can nowadays be realized. One manifestation of these trends is a slow shift from preventive to predictive maintenance (Swanson 2001). This approach is especially promising for high-cost machinery or machinery with high safety regards, where an unforeseen failure resulting in downtime is disastrous. Radial fans are an integral part of a wide variety of industrial facilities and therefore one candidate application. They are mainly used as the core component of a ventilation system. Their application varies between simple air conditioning for buildings up to the ventilation of critical systems in chemical plants, where dangerous gases may build up over time with insufficient ventilation. Other examples are cement plants, wood processing plants and generally industry with dusty air.

In contrast to axial fans, radial fans are designed to create higher pressure and perform more energy efficient, whereas axial fans are able to transport more volume and can be manufactured in a more compact way (Chung and Goetzler 2015).

Radial fans have a limited useful lifetime that can be prolonged with a detailed maintenance schedule. To delay the wearing of radial fans and lower the risk of premature, unforeseen failure, a maintenance interval is specified. Insight into the casing to inspect the impeller during operation is nearly, if not at all, impossible. Due to the nature of the high rotational speed of a radial fan, it has to be shut down before a service technician can begin the inspection. Additionally, as a safety measure, vibration sensors can be mounted on the bearings. As soon as the vibration exceeds a predefined threshold, the fan must be stopped and the cause of the increased vibration has to be detected, which further increases the downtime and respectively the costs, but prevents a possible failure. The downtime of radial fans without a backup results in a stoppage of the whole ventilation system. To complement the current preventive maintenance approach, additional methods to determine the overall health status of a radial fan should be elicited. The eventual goals of predictive maintenance are to approximate the remaining useful lifetime, detect the optimal time for maintenance and identify which parts have to be replaced next. The first step towards these goals and focus of this paper is to examine the influence of multiple sensor data on modeling radial fans.

This work is structured as follows. Section 2 contains a summary of the related work in the field of radial fans with a strong focus on the selected sensors. Section 3 describes the experimental setup, which has been chosen for the generation of data and the installed sensors and introduces the extensible sensor platform used to connect most of the sensors. In Section 4, the methodical approach is defined. Section 5 contains the results, followed by a brief conclusion in Section 6 and outlook in Section 7.

2. RELATED WORK

Renwick and Babson (1985) monitored the vibrations of a finish mill, cooler vent fan and gear reducer and they were able to detect specific problems of the machineries. They relied on their technical knowledge about the system and applied *Fast Fourier Transformations* (Bracewell 1986) on the vibration signals.

Garcia, Sanz-Bobi, and del Pico (2006) focused on a windturbine gearbox and designed a complete system named "Intelligent System for Predictive Maintenance" (SIMAP). They used a combination of artificial neural networks, fuzzy logic and an expert system with the possibility to generate a complete maintenance schedule and did not rely on a single model. They were able to give a prediction of the time remaining till failure, which is synonymous with the before mentioned remaining useful lifetime.

Jung, Zhang, and Winslett (2017) generated data with sensors mounted on vacuum pumps. They also tackled the prediction of the remaining useful lifetime with a more general framework based on vibration analysis.

Velarde-Suárez et al. (2006) focused on a predictive maintenance methodology, specifically for radial fans. In addition to vibration, they also used accoustic pressure signals and observed the deviation between a signal and a reference value for defined frequencies.

Rusiński et al. (2014) tried to find if the current operation of a radial fan creates resonance, which means the configuration of the fan needs to be adapted to prevent faster degradation of the fan.

Datong et al. (2009) followed another approach. They measured the efficiency and noise emmitted from different radial fans and compared them to sucessfully find suitable modifications of the fan to reduce the emitted noise and increase the efficiency. This indicates the correlation between efficiency and noise. Their experiments required a hemi-anechoic chamber to reduce noise and create comparble results. Khelladi et al. (2008) gave theoretical background on how to calculate the emitted noise of radial fans. Abid et al. (2012) focused solely on tonal noise emitted by an axial fan and created a model to identify healthy and damaged axial fans.

Summarizing, one common approach is to monitor vibration, which is applicable for different rotational machinery. Vibration signals provide additional information, as some authors applied fast fourier transformations to check the harmonic frequencies. The second most common way to predict the health of machinery is to analyze the noise emitted during operation. All these previously mentioned papers either focus on few signals to predict the health of machinery or proposed a holistic framework for predictive maintenance such as SIMAP. However, none of the reviewed related literature examined the influence of different kinds of sensor data and their combination to model the state of radial fans. The goal of this paper is to analyze the impact of different sensor signals for health prediction of radial fans.

3. EXPERIMENTAL SETUP

In our experiments we investigate the behavior of a radial fan driven by a two-pole electric motor with a power of 37 kW (see Figure 1). The motor speed is adjustably by an electric frequency converter up to a rotational speed of 2960 rpm and pressure loss of the system can be modified by a control flap, which results in a large flexibility of operating states that can be investigated. An impeller with a weight of 38 kg, 12 impeller blades and a diameter of 625 mm is used as reference. Another set of impellers is modified in a specific way to simulate long term abrasive stress on a short time scale. The engine shaft is connected to the engine by a coupling (see Figure 2). This setup is common for many industrial applications and therefore is chosen for the experimental campaigns.

Figure 1: New Radial Fan.
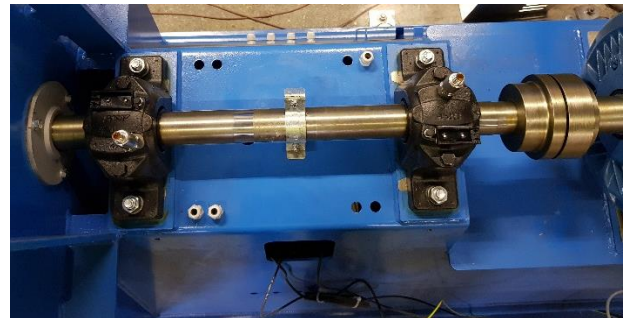
Figure 2: Engine Shaft, Spherical Roller Bearings, Coupling and Vibration Sensors without Protective Cover.

3.1. Sensor Types

The first step to model the health state of radial fans is to identify appropriate sensors for the modeling later on, where some restrictions need to be addressed. Considering the possibly predominating high gas flow rates, high pressures, heat or abrasive media inside the case of radial fans, the range of compatible/possible sensors, which can be mounted inside the case, is limited. Another restriction is sensor cost. Ultimately, every sensor has to be sold to the customer, which means that the least expensive sensors should be used to achieve the

required accuracy and to draw conclusions about the current health state of the fan. Furthermore, such sensors should be durable, maintenance-free and non-calibratable. Every intrusive measurement system has an impact on the process itself, therefore we focus on non-intrusive methods.

The backbone of every prediction model, agnostic of the methodical approach, are the chosen sensors and the quality of the signals. Most failures are forecasted by subtle physical manifestations in the system. Some possibilities are an increase in temperature (friction) and accelerated wear of mechanical components (vibrancy).

3.1.1. Vibrations and Temperature

In industry applications, monitoring vibrations of the bearings and temperature is state of the art. This allows determining a vast variety of machinery fails. In most cases, amplitudes, frequencies and envelopes of vibration signals are processed to pinpoint the exact cause of failure, e.g. imbalances, cracks, bearing damage or lack of lubricant.

3.1.2. Noise

As mentioned in Section 2, the emitted noise might indicate the current health state. Although some of the literature focuses on the emitted noise in an experimental setup, in real world scenarios this idea poses difficulties. Often the environment is polluted by noise emitted by other machinery or will not allow any additional external acoustic sensor due to space restrictions. In contrast to Datong et al. (2009), who experimented in a hemi-anechoic chamber, fans installed in production plants most likely are not deployed in such a controlled environment and the noise emitted by radial fans is disturbed by other sources of inference. Because of this, we do not use microphones in our experimental setup.

3.1.3. Moisture

The degree of moisture can influence mass- and energy balances of the system and therefore such sensors are part of the measurement campaign.

3.1.4. System Efficiency and Power Consumption

As a first characteristic to determine the health of a fan, the system efficiency is considered in such way that energy consumption is correlated with gas flow rate and temperature rise of the gas after passing the fan. To calculate the efficiency we determine gas flow rates by measuring gas temperatures and differential pressures at a Venturi-tube, as well as electrical power consumption.

3.1.5. Abrasion and Caking

The detection of these parameters is accomplished by optical examination during standstill, as it is common in industry. Different methods to quantify the damages and to determine the remaining useful lifetime are currently under investigation.

3.2. Sensor Setup

The measurement of process parameters is accomplished twofold.

3.2.1. Self-build Setup

We use a self-developed data acquisition and data processing system (see Figure 3) that contains a certain set of sensors. Two temperature sensors (MAX31855K) measure gas temperatures at inlet and outlet of the fan, two gyroscopes (BMX055) determine accelerations and rotations at the bearings in all 3 dimensions, a hygrometer (HDC1000) measures the surrounding moisture, an ampere meter (WAGO 857-550) the electrical power consumption and a rotation speed control counter (GS100102) the revolution. Sensors are connected to sensor hubs that send data to a computer for further procession. Sensors are attached to specific positions by using special 3D-printed mounts.
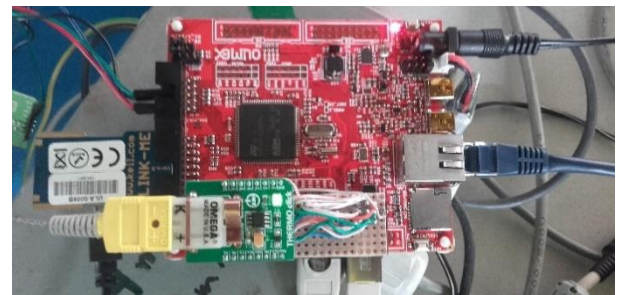
Figure 3: The Prototype Platform (built on STM32F407 from STMicroelectronics).

3.2.2. Commercial Sensors

As a reference, additional commercial senors are applied to measure gas temperatures (JUMO PT100), bearing temperatures (JUMO 902050/40), pressures (KSE DMU2), revolutions (IFM DI602A) and vibrations (IFM VTV122) of the system. Data acquisition is completed by a commercial datalogger (Graphtec GL820 and HBM QuantumX MX840B, respectively) and data is post processed afterwards.

The data acquisition rates of both systems can be adjusted to find an optimum between accuracy and data traffic. Currently we experiment with sampling rates between 50 Hz and 300 Hz.

3.3. Custom Sensor Platform

The number and type of sensors needed to predict maintenance intervals depends on the particular application. Therefore, the sensor platform has been designed to be modularly expandable using the same hardware and firmware.

3.3.1. Hardware System Concept Sensor Platform

Figure 4 shows the system concept of the sensor platform. In the picture on the left (shown in blue) is the gateway to collect data, which allows a connection to the internet. This gateway can also store the data locally in a

CSV file. Through the system bus (shown in green), the gateway communicates with the sensor nodes, which are the heart of the sensor platform. The data communication is based on TCP / IP and uses 100 Mbit/s Ethernet. At least one sensor node is necessary for the measurement, significantly more sensor nodes can be connected to the gateway. The limiting feature is the data rate of 100 Mbit/s, which cannot be exceeded. The net payload data rate is significantly lower (about 50 Mbit / s), since the packet sizes differs depending on the sensor type from 50 to a few 100 bytes and the overhead of TCP / IP (40 bytes per packet) must be taken into account.

In our example, we used the STM32-E407 development board from Olimex for the sensor platform, which provides both Ethernet and the necessary connections for the sensors. Via I2C, SPI, UART and analog and digital inputs, the sensor data are read in. The sensor platform contains a real-time clock that precisely documents the time of the measurement on a millisecond basis.
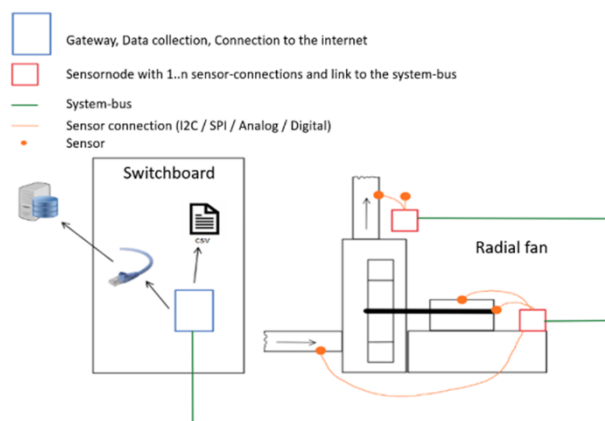

Figure 4: System Concept Sensor Platform, taken and adapted from Grasböck and Schmidt (2017).

3.3.2. Firmware Architecture Sensornode

The firmware is designed to read the sensors on a millisecond base or a multiple of milliseconds. Then data is transmitted to the gateway via Ethernet / TCP-IP.

Each sensor uses one task to process its data. For the transmission of the sensor data to the gateway, a separate task is used. Thus, new sensors can be added simply by adding tasks without changing the software of existing sensor tasks.

The operating system is FreeRTOS, which is an open source embedded real time system. STM's board support package has been enhanced for our application so that the different sensors are easy to be read. The CMSIS library of ARM was used unchanged, for the HAL (hardware abstraction layer) the software was adapted.

4. METHODICAL APPROACH

As mentioned in Section 3, every sensor mounted on a fan increases its costs and sensors cannot be placed on the impeller itself. The first step towards modeling the health state of a radial fan is to gather as much data from as many sensors as possible. Because the radial fan is placed in an experimental setup, we can measure the

efficiency accurately and generate a characteristic curve of this specific, brand-new fan. Afterwards we will model the efficiency with the sensors, available in real world scenarios. This test run will be repeated several times. Between each test run, highly abrasive air will be used to wear off the impeller. After each cycle a technician will sight check the impeller for a subjective impression of the state of wearing and caking. As soon as the predefined vibration-threshold is reached and safety-issues may occur, the impeller will be changed and the experiment starts again with the first iteration. The highly abrasive air poses a possible health-hazard, therefore an additional filter system will be attached, preventing the highly abrasive air from contaminating the surrounding area. The construction of this filter system has not been finished yet. As an interim stage, several pre-damaged impellers, which show common deterioration patterns in different stages are prepared and will be used to sample sensor data. With all this data available, several machine learning algorithms for modeling the current state of the radial fan are applicable. To select suitable sensors, several considerations are necessary. If the signal of a specific sensor has an influence on the prediction of the health state of a radial fan, a deviation of this signal between the same operational conditions of a healthy and faulty/worn fan should be noticeable. Another indication for the impact of sensor data is a changing correlation between different signals.

The data used for the scope of this paper was generated by the following configuration of the experimental setup. Two different impellers, one brand new and one pre-damaged (see Figure 5), were mounted to generate two different datasets, one with good running conditions and one with a known damage. The rotational speed was incremented stepwise from 0 rpm to 2960 rpm in 370 rpm-steps, each with a recording period of 15 minutes to gather data from different running conditions, resulting in a total observation period of 4 hours.

Figure 5: Manually Pre-Damaged Impeller.

5. RESULTS

In this section, the results of the analysis of the experimental runs are presented. The relation between the different sensor types and the rotational speed is the modeling goal, because it is the only manually adjustable and monitored parameter of the experimental setup at the

given moment. The efficiency, which will be used for the advanced modeling goals and prediction of the remaining useful lifetime, will be available once the experimental setup is complemented by the filter system mentioned in the previous section.

5.1. Preliminary Experiments

The preliminary experimental setup used before the pre-damaged impeller was available, generated data from two vibration and one rotational speed sensor, using a new impeller. A first analysis shows a reoccurring pattern of vibration signals during an increase and decrease of the rotational speed (see Figure 6). If each signal is compared with itself during ascents (see Figure 6, Subsection 1 and 3), the signal is correlated with a Spearman's Rank of 0.798 (Vibration Sensor 1) and 0.874 (Vibration Sensor 2) and a Pearson's R of 0.748 and 0.888. During the descents (see Figure 6, Subsection 2 and 4), the signals correlate with a Spearman's Rank of 0.879 and 0.912 and a Pearson's R of 0.897 and 0.936. These correlations confirm the importance of previous works that monitored vibration signals and underline their usefulness for health state modeling of radial fans. Especially a change in a reoccurring pattern under similar running conditions may be an additional, more subtle indication of a damage.
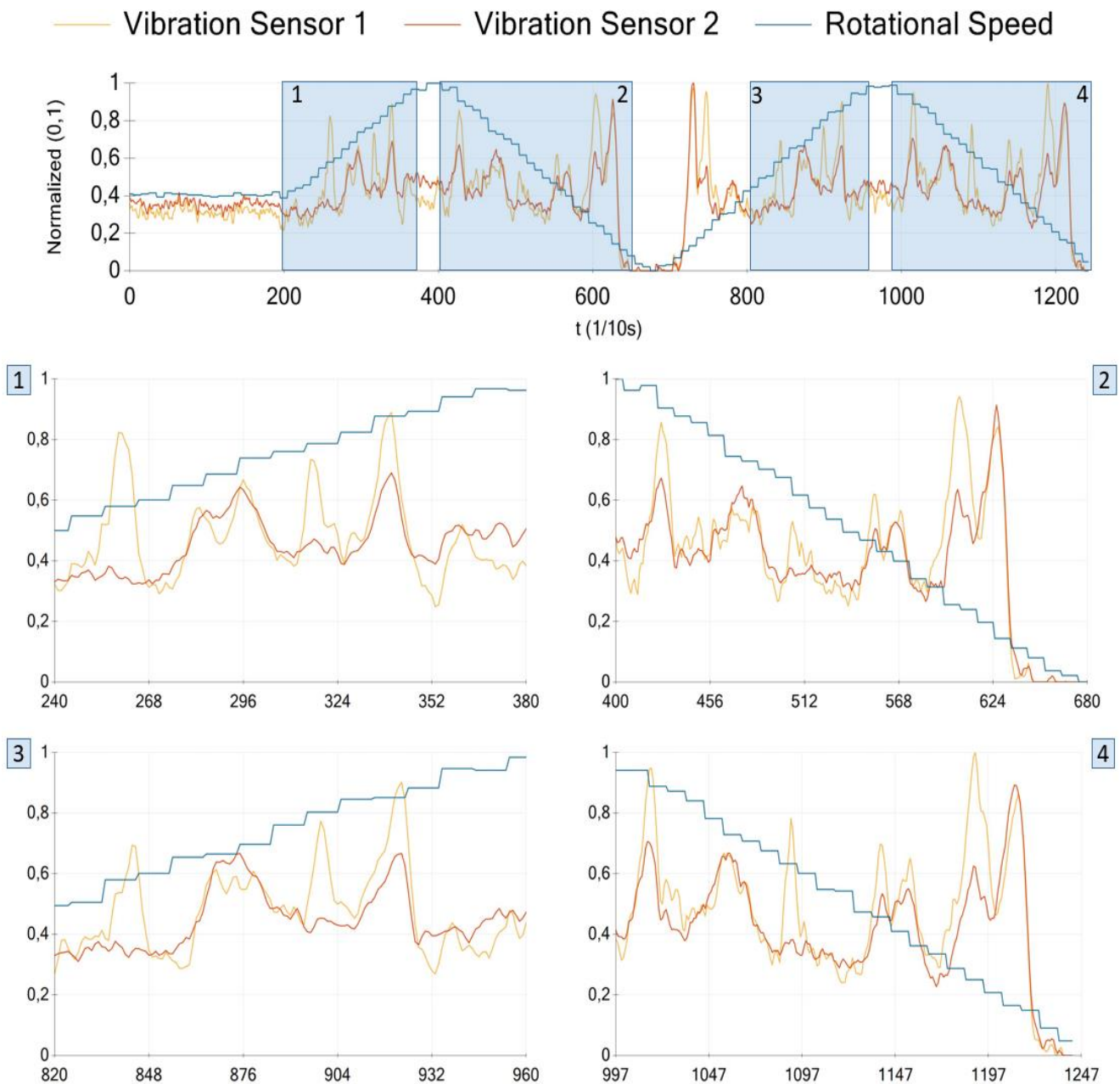

Figure 6: Correlation of Vibration during Increase/Decrease of Rotational Speed (Scales Normalized between 0 and 1).

5.2. Pressure Signals

The pressure signals at the inlet, aperture and the differential pressure (measured, not calculated) show a strong correlation with each other and the rotational speed (see Table 1). Both impeller have similar characteristics, the correlations do not change significantly. An error cannot be detected by examining the correlation alone.

Table 1: Pearson's R² of the Healthy Impeller (top line) and the Damaged Impeller (bottom line) for the Pressure Difference, Rotational Speed, Pressure at Aperture and Pressure at Inlet.

	Press (Diff)	Rotational Speed	Press (Aper)	Press (Inlet)
Press (Diff)	1.000	0.951	0.993	0.995
	1.000	0.956	0.999	0.999
Rotational Speed	0.9505	1.000	0.951	0.953
	0.9564	1.000	0.949	0.951
Press (Aper)	0.993	0.951	1.000	0.999
	0.999	0.949	1.000	1.000
Press (Inlet)	0.995	0.953	0.999	1.000
	0.999	0.951	1.000	1.000

As the high correlation indicates, a function to approximate an arbitrary pressure signal by a different one can be found. An example is as follows, calculated with Genetic Programming solving a Symbolic Regression Problem (Affenzeller et al. 2009) using the HeuristicLab Framework (Wagner et al. 2012).

$$P_{Inlet} = c_0 \cdot P_{Aperture} + \frac{c_1 \cdot P_{Aperture} + c_2}{c_3 \cdot P_{Aperture} + c_4} + c_5$$

$$
\begin{aligned}
c_0 &= 1.1664 \\
c_1 &= 1.1387 \\
c_2 &= -94.699 \\
c_3 &= 0.0066872 \\
c_4 &= -61.742 \\
c_5 &= 3.2566
\end{aligned}
\tag{1}
$$

Equation 1 approximates the pressure at the inlet with the pressure of the aperture and five constants, achieving an R² of 0.99992 and a mean absolute error of 4.14. This illustrates the interchangeability between these two pressure signals. Due to the high correlation, any of these three pressure signals can be approximated by the others. This is illustrated by Equation 1. Equation 2 shows the relation between the rotational speed and the pressure signals, whereas the pressure at the inlet was not necessary, which seems plausible, considering the strong correlation.

$$RotationalSpeed = c_0 \cdot P_{Difference} + \frac{1}{c_2 \cdot P_{Aperture} + c_3} + \frac{c_4 \cdot P_{Aperture}}{c_5 \cdot P_{Aperture} + c_6} + c_7$$

$$
\begin{aligned}
c_0 &= 1.4035 \\
c_2 &= -4.4875E - 05 \\
c_3 &= -0.0019993 \\
c_4 &= -425.69 \\
c_5 &= -0.22457 \\
c_6 &= -319.32 \\
c_7 &= 520.95
\end{aligned}
\tag{2}
$$

5.3. Temperature Signals

We monitored the temperature at the inlet and the outlet of the radial fan and the ambient temperature. The basic idea is that a damaged impeller may create more friction and therefore a raise in temperature occurs. Figure 7 shows the three monitored temperature signals and the rotational speed during the test run, normalized between zero and one.
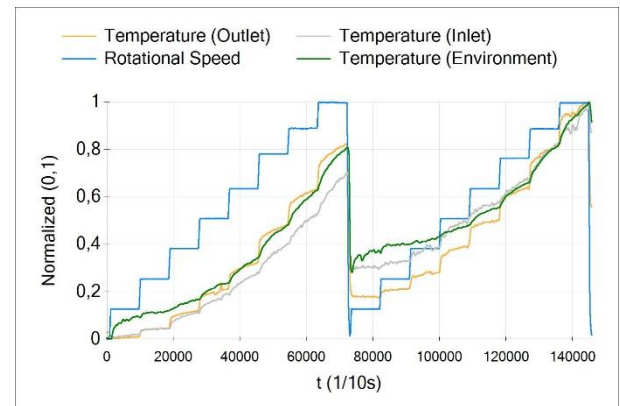
Figure 7: Temperature Signals and Rotational Speed of the Test Run, Normalized between 0 and 1.

Further on, the Pearson's R² and Spearman's Rank of the different sensor data were calculated, as shown in Table 2 for the healthy impeller and Table 3 for the damaged impeller. They indicate a strong correlation of these four signals.

Table 2: Pearson's R² (top line) and Spearman's Rank (bottom line) for the Temperatures and Rotational Speed of the Healthy Impeller.

	Temp (Outlet)	Rotational Speed	Temp (Inlet)	Temp (Env)
Temp (Outlet)	1.000	0.913	0.988	0.982
	1.000	0.976	0.997	0.996
Rotational Speed	0.913	1.000	0.868	0.855
	0.976	1.000	0.967	0.967
Temp (Inlet)	0.988	0.868	1.000	0.996
	0.997	0.967	1.000	0.999
Temp (Env)	0.982	0.855	0.996	1.000
	0.996	0.967	0.999	1.000

Table 3: Pearson's R² (top line) and Spearman's Rank (bottom line) for the Temperatures and Rotational Speed of the Damaged Impeller.

	Temp (Outlet)	Rotational Speed	Temp (Inlet)	Temp (Env)
Temp (Outlet)	1.000 1.000	0.900 0.962	0.977 0.994	0.948 0.988
Rotational Speed	0.900 0.962	1.000 1.000	0.827 0.936	0.748 0.931
Temp (Inlet)	0.977 0.994	0.827 0.936	1.000 1.000	0.973 0.995
Temp (Env)	0.948 0.988	0.748 0.931	0.973 0.995	1.000 1.000

5.4. Signal Smoothing

A necessary preprocessing step to utilize the signals from the gyroscopes, acceleration and vibration sensors was to smooth the signal. As shown in Figure 8 and Figure 9, a moving average filter was applied. The smoothed signal indicates the changes in rotational speed. All gyroscope and acceleration signals show similar margins of noise, which suggests the presence of electromagnetic interference or another source of disturbance influencing the sensor signals.

All gyroscope and acceleration sensors provide data in x, y and z dimension. Each sensor is identified by an ID as multiple sensors of the same type could be attached on a fan. As an example: *Acceleration 3 – Y* means the signal of acceleration sensor with ID 3 in y direction. This ID does not imply that at least three acceleration sensors are mounted on the radial fan.
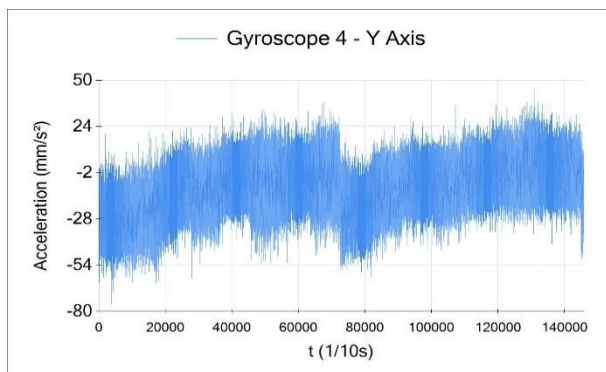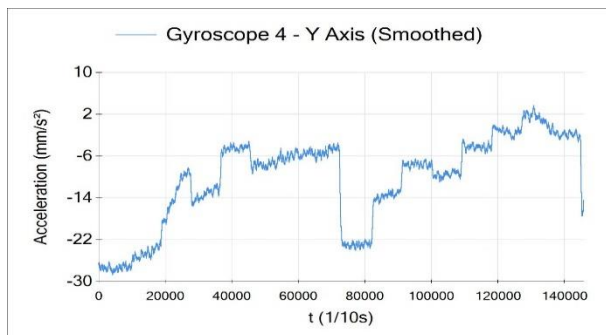

Figure 8: Gyroscope Signal (raw).

Figure 9: Gyroscope Signal smoothed by a Moving Average Filter (sliding window size 401, type central).

5.5. Combination of Gyroscope, Acceleration and Vibration Signals

We applied a linear regression (Draper, Smith, and Pownell 1966) and a random forest modeling approach (Breiman 2001), calculating the variable impacts for the healthy and damaged impeller by approximating the rotational speed. The top five influencing variables, calculated by using a linear regression model and a random forest model are presented in Table 4 and Table 5 (healthy impeller), and Table 6 and Table 7 (damaged impeller). For the calculation of the variable impacts, each sensor data was shuffled individually and the resulting worsening of the models are quantitatively described by the variable impact. The linear regression solution for the healthy impeller achieved a Pearson's R² of 0.989 and a mean absolute error of 71.68, the random forest solution a Person's R² of 0.999 and a mean absolute error of 0.22. For the damaged impeller the linear regression solution attained a Pearson's R² of 0.995 and a mean absolute error of 46.62, the random forest solution a Pearson's R² of 0.999 and a mean absolute error of 0.18.

Table 4: Overview of the Top Five Variable Impacts calculated from a Linear Regression Model using a Healthy Impeller.

Sensor Type	Impact
Acceleration 3-Y	0.519
Gyroscope 4-X	0.273
Acceleration 1-Y	0.069
Acceleration 9-Z	0.036
Gyroscope 8-Y	0.029

Table 5: Overview of the Top Five Variable Impacts calculated from a Random Forest Model using a Healthy Impeller.

Sensor Type	Impact
Acceleration 9-Z	0.147
Gyroscope 4-X	0.044
Acceleration 7-Z	0.024
Acceleration 9-Y	0.020
Gyroscope 4-Y	0.014

Table 6: Overview of the Top Five Variable Impacts calculated from a Linear Regression Model using a Damaged Impeller.

Sensor Type	Impact
Vibration 21	0.721
Acceleration 9-Z	0.374
Gyroscope 4-Y	0.086
Vibration 22	0.081
Acceleration 9-Y	0.040

Table 7: Overview of the Top Five Variable Impacts calculated from a Random Forest Model using a Damaged Impeller.

Sensor Type	Impact
Vibration 21	0.155
Vibration 22	0.031
Acceleration 9-Z	0.025
Gyroscope 4-Y	0.023
Acceleration 1-Y	0.012

These results show a clear divergence of variable impact between a healthy and a damaged impeller. Vibration had a major influence on modeling a damaged state, but was negligible for a healthy impeller. The signal from the acceleration 9 sensor in z-dimension had a relevant impact on all four models, but was more important for the healthy impeller. The gyroscope 4 signal in x dimension only had a noteworthy impact on modeling healthy fans.

6. SUMMARY AND DISCUSSION

The pressure signals alone can give a good approximation of the rotational speed, but the intentional and prevalent error of the current experimental setup could not be indicated by the pressure signals alone. A possible leak in the tube may have an influence on the relation between the pressure signals. Therefore, it is advised to keep all three pressure signals and discourage the usage of one pressure signal as a substitute alone, which is possible as shown in Section 5.2.

The data from the temperature sensors also correlate with the rotational speed, but the correlation alone could be misleading. As the experimental setup defines two runs, each with eight increments of the rotational speed, the power consumption of the radial fan increases, more work is done and more heat is dispersed. Therefore, both the rotational speed and the temperature will be monotonically increasing. The second run was executed after the first run later the same day. The offset temperature was still elevated from either the first run or the weather conditions. More experimental runs with different changes in rotational speed are necessary to rule out a spurious correlation.

As for the gyroscope, acceleration and vibration sensor data, a preceding smoothing was necessary, eliminating most of the noise. Another approach may be a reduction of the sampling rates. A complementary spectrogram should be created to further investigate the signal before reducing the sampling rates, preventing a possible loss of information.

The calculated linear regression solutions and random forest solutions suggest a disparity of variable impacts between a healthy and a damaged impeller. The vibration signal had very little impact on the experimental run with the healthy impeller, in opposition to the run with the damaged one. The data from the acceleration sensor 9 in z-dimension had a noticeable impact on each model. This may be useful for the approximation of the rotational speed, but is a weak indication of a damage, whereas the data from gyroscope 4 in x-dimension only had an impact on the modeling of the fan with the healthy impeller. A desired outcome from the variable impact calculation for error modeling would be a great disparity between a healthy and damaged impeller. If a signal has a high or low impact on both impeller it is probably negligible for error modeling.

Further on, not only the absolute value of a signal should be investigated, also a change of a reoccurring pattern could be interesting (see Section 5.1), although this approach requires more research and insight than a simple threshold-analysis.

7. OUTLOOK/FURTHER STEPS

As soon as the experimental setup is completed (insofar as the filter system is integrated), the same methodology currently used to approximate the rotational speed, will be applied on the efficiency of healthy and gradually damaged impellers, mounted on a radial fan. The characteristics curve and a spectrogram will be created. With this data available, the influence of the sensors on health modeling will be explored by applying the concept of variable interaction networks (Winkler et al. 2012).

A possible direction for future work may be guided by the work of Saxena et al. (2008) and related publications to predict the remaining useful lifetime.

REFERENCES

Abid M. et al., 2012. Tonal prediction of a faulty axial fan. Applied Acoustics, 73(10), 1022–1028.

Affenzeller M. et al., 2009. Genetic Algorithms and Genetic Programming. Chapman and Hall / CRC Press

Bracewell R. N., 1986. The Fourier transform and its applications (Vol. 31999). McGraw-Hill New York.

Breiman L., 2001. Random forests. Machine Learning, 45(1), 5–32.

Chung G. and Goetzler W., 2015. Pump and Fan Technology Characterization and R & D Assessment, (October 2015).

Datong Q. et al., 2009. Experimental study on the noise reduction of an industrial forward-curved blades centrifugal fan. Applied Acoustics, 70(8), 1041–1050.

Draper N. R. and Smith H. and Pownell E., 1966. Applied regression analysis (Vol. 3). Wiley New York.

Garcia M. C. and Sanz-Bobi M. A. and del Pico J., 2006. SIMAP: Intelligent System for Predictive Maintenance. Application to the health condition monitoring of a windturbine gearbox. Computers in Industry, 57(6), 552–568.

Grasböck J. and Schmidt B., 2017. DigiVent Hardware Prototyp, Pflichtenheft. Internal Document.

Jung D. and Zhang Z. and Winslett M., 2017. Vibration analysis for iot enabled predictive maintenance. Proceedings - International Conference on Data Engineering, 1271–1282.

Khelladi S. et al., 2008. Predicting tonal noise from a high rotational speed centrifugal fan. Journal of Sound and Vibration, 313(1–2), 113–133.

Renwick J. T. and Babson P. E., 1985. Vibration Analysis—A Proven Technique as a Predictive Maintenance Tool. IEEE Transactions on Industry Applications, IA-21(2), 324–332.

Rusiński E. et al., 2014. Investigation of vibrations of a main centrifugal fan used in mine ventilation. Archives of Civil and Mechanical Engineering, 14(4), 569–579.

Saxena A. et al., 2008. Damage Propagation Modeling for Aircraft Engine Prognostics. Proceedings of IEEE International Conference on Prognostics and Health Management, 1–9.

Swanson L., 2001. Linking maintenance strategies to performance. Int. J. Production Economics, 70, 237–244.

Velarde-Suárez S. et al., 2006. A predictive maintenance procedure using pressure and acceleration signals from a centrifugal fan. Applied Acoustics, 67(1), 49–61.

Wagner S. et al., 2012. Architecture and Design of the {HeuristicLab} Optimization Environment. First Australian Conference on the Applications of Systems Engineering, ACASE, 6, 197–261.

Winkler S. M. et al., 2012. Variable interaction networks in medical data. 24th European Modeling and Simulation Symposium, EMSS 2012, (c), 265–270.

MODELING AND ENVIRONMENTAL ASSESSMENT OF STRUCTURAL SOLUTIONS FOR A SINGLE-FAMILY HOME

E. Fraile-Garcia [(1*)], J. Ferreiro-Cabello [(1)], Mª del Mar Villamil, E. Jimenez Macias [(2)]

[(1)] University of La Rioja (Spain), Department of Mechanical Engineering, ScoDIP Group
[(2)] University of La Rioja (Spain), Department of Electrical Engineering, Modeling and Simulation in Science and Engineering Group

[(1)] esteban.fraile@unirioja.es , [(1)] javier.ferreiro@unirioja.es , [(2)] emilio.jimenez@unirioja.es

ABSTRACT

This article analyzes the impact of different structural solutions for single-family homes on the environment. following a Life Cycle Analysis (LCA) methodology for different construction elements in its early stages, the product and construction phase. We have divided the construction stage into transportation and installation, according to UNE-EN 115804: 2012. The analysis was carried out using two indicators of environmental impact, the energy incorporated in MJ and the equivalent CO2 emissions. For the case study, a single-family detached house has been proposed.

The study is focused on three representative items: foundation, structure and floors. Two cases have been made combining different construction elements. As a modeling tool, CYPECAD and CYPE 3D have been used together with databases that provide unit costs and environmental indicators for materials. A reflection is made on two models with structural alternatives, justifying the need to delve into multicriteria methods as an aid to decision making.

Keywords: modeling, environmental assessment, structural solutions, simulation, single-family home

1. INTRODUCTION

The residential building has multiple types and structural alternatives (wooden structures, metal, prefabricated concrete, concrete "In situ" ...). Each type has strengths and weaknesses, this situation is the reason why none is clearly imposed by benefits or appreciable advantages. This lack of leadership, in the concrete structures "In situ", can be seen in the different alternatives: solid slabs (Armed, Post-tensioned), reticular forgings (lost box, recoverable box), unidirectional slabs (Armed, Prestressed, "In situ").

The residential sector uses traditional construction processes. The reasons are localized in the success of the traditional techniques and the reserve or distrust of the technicians to the employment of different typologies. This sector is very traditional and is usually reluctant to change. Despite this, the evolution of the different regulations requires a greater dynamism of the sector. The structural regulations incorporate environmental aspects in the shadow of, new concepts such as, sustainable construction. Following the guidelines of sustainable construction, the economic, social and environmental impacts must be evaluated.

For the economic valuation, there are databases with prices for the construction sector. Social assessment is incorporated with the fulfillment of basic comfort, acoustic, thermal and fire resistance. To quantify the environmental impacts, the use of Life Cycle Analysis (LCA) tools is proposed. A typical indicator is the Carbon Footprint. The Carbon Footprint consists in quantifying the totality of Greenhouse Gases (GHG) emitted by direct or indirect effect of a product / service or an organization as a whole (eg CO2, methane, HFCs, sulfur hexafluoride, etc.). The determination of the carbon footprint does not stop being a study of Life Cycle Analysis (LCA) in which only a single category of environmental impact is calculated and considered, the Global Warming, whose units of measure are kg of CO2 equivalent.

This article analyzes the impact of different structural solutions for single-family homes on the environment. The importance of environmental conditions in the development of projects is growing, both for society and for the different administrations; this is reflected in the European guidelines and their incorporation to the norms of each country. This highlights the importance of the impact of buildings on the environment and the need to focus projects under the prism of sustainable construction.

The analysis was carried out following a Life Cycle Analysis (LCA) methodology for different construction elements in its early stages, the product and construction phase. We have divided the construction stage into transportation and installation, according to the UNE-EN 115804: 2012. The analysis was carried out using two indicators of environmental impact, the energy incorporated in MJ and the equivalent CO2 emissions. For the case study, a single-family detached house of a 100 m2 plant has been proposed.

We have focused the study on three representative items: the foundation, the structure and the floors. Two cases have been made combining different construction elements to perform the analysis. As a modeling tool, CYPECAD and CYPE 3D have been used together with databases that provide unit costs and environmental indicators for materials. The research makes a reflection on two models with structural alternatives, justifying

the need to delve into multicriteria methods as an aid to decision making.

The structure in residential construction is composed of primary elements and secondary elements. The primary element object of our investigation, the configuration of beams and pillars, is solved with two usual structural materials: reinforced concrete and laminated steel. The case study focuses on a single-family house of 100 square meters of useful area. The secondary element, the floor, is an element that must satisfy: functionality, safety, economy and aesthetics. Obviously, the relative importance of each one of the criteria in play depends very much on the type of structure in question. In this case for the house two types of floor are analyzed. The one carried out on the ground floor that corresponds to a forged "in situ" and that of the forged support of the roof made by a system of reinforced beam and concrete vault.

Global warming is a category of environmental impact that has gained great importance in recent years. This study identifies and locates the production sources of the impact on equivalent CO_2 emissions to obtain the primary structure. This information is complementary and useful for the correct decision making.

2. METHODOLOGY

The research focuses on the modeling of a single-family home with different primary structural solutions, namely a laminated steel structure and a reinforced concrete structure. In both cases, the environmental impacts generated are analyzed and evaluated.

To do this, we apply the proposed methodology to a case study with the following characteristics: Isolated building with a square floor of 10x10 m, will be composed of a single floor. The pillars will be placed every 5 meters as indicated in figure 1.
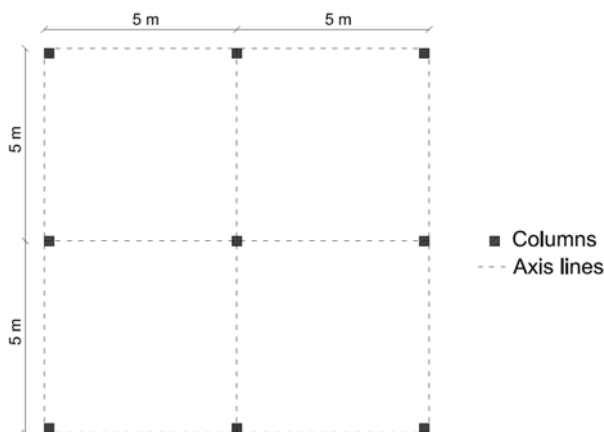
Figure 1: Distribution of pillars for the case studies.

The items to which the study is subject are: the foundation, pillars, beams and slabs. In regard to the foundation, centered shoes and tie beams are analyzed in the perimeter of the house, as shown in figure 2.
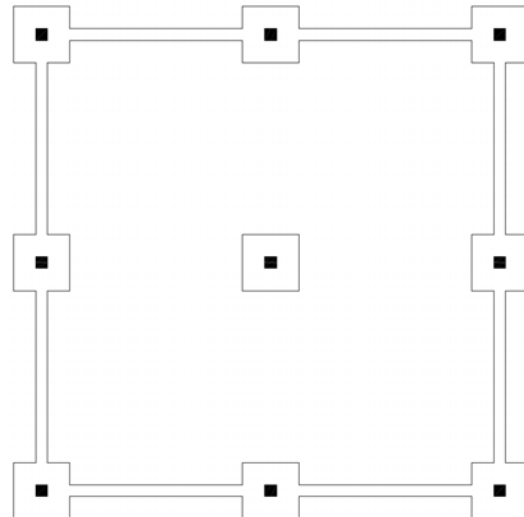
Figure 2: Types of foundations to study. A) centered shoes. B) Off-center shoes.

The configuration of the primary structural elements, pillars and beams, is made using different materials: reinforced concrete and rolled steel (figure 3). Therefore we will have two cases of study called H FU is the reinforced concrete and the so-called A FU for the case of laminated steel structure.
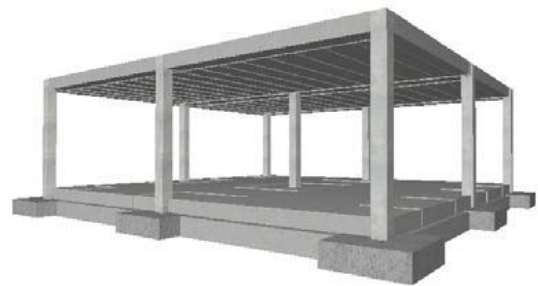
(a)

(b)

Figure 3: Scheme of structures. a) reinforced concrete. b) steel.

In both cases, the foundation, structure and slabs are evaluated, but they have different items in the case of reinforced concrete, the forging is included in the beams, since they are executed at the same time, on the

other hand in the case of steel, the steel beams with the pillars in the structure heading.

For the secondary structural elements, two types of slab are modeled. The sanitary forging formed by a system of lost formwork with monoblocks of recycled polypropylene assembled together and the slab that sustains the roof by means of a system of reinforced joist and concrete vault.

The geometry of the house has a floor area of 100m2. The pillars for the cases of concrete and steel have a height of 3.35 m, since it is considered a sanitary floor of 0.35 m and a height between plants of 3 m. The materials used for reinforced concrete are HA-25 / B / 20 / IIa corrugated steel B500S. In the case of rolled steel S275JR.

In the modeling has taken into account the Spanish regulations Technical Building Code (CTE) specifically DB SE Structural safety, DB SE AE: Actions in the building, DB SE C: Foundations and NSCE-02 (resistant construction rule). In this way the own weight of the structure, 2 kN / m2 are taken as permanent loads and 2 kN / m2 as housing overload for housing and 1 kN / m2 as cover. For wind loads we will take in the case of study the wind area B and degree of roughness IV, with a basic wind speed of 27 m / s it is considered that it is not in a seismic zone.

The modeling of structural materials incorporates the Structural Concrete Instruction EHE-08 and the EAE Structural Steel Instruction. The structural analysis, at a resistant level, through the final limit states is complemented by service limitations. Taking into account the regulations, the following arrow limitations are considered: for the active arrow FAct = L / 500 or FAct = L / 1000 + 0.5 and for the arrow with infinite term: FPlazo Inf = L / 500 + 1 or L / 250

The structural analysis is carried out by matrix methods using the CYPE software version 2016g, considering the elements that define the structure: footings, foundation beams, pillars, beams and slabs. The compatibility of displacements in all the nodes is established, considering six degrees of freedom and the hypothesis of indeformability in the plane for each continuous slab, preventing the relative displacements between nodes. In order to obtain the different structural responses (stresses, displacements, tensions, etc.) a linear behavior of the materials is assumed.

The modeling of the structure determines the quantities of the materials and in this way the concrete measurements of each of the items. Through the database, specific to the construction sector, which incorporates the CYPE tool, we obtain the unit values in environmental cost and impacts for each item. The cost is evaluated in euros and the environmental impacts by means of two indicators: the incorporated energy (MJ) and the CO_2 equivalent emissions (kg). Following the guidelines of the UNE-EN 15804: 2012 + A1: 2014 standard, the environmental impact is divided into the product sections (A1-A2-A3) and construction (A4-A5). Based on this database you can graph the results as reflected in the following section.

3. RESULTS

Once the two case studies were modeled and the structural calculation was carried out, we obtained the amounts of materials used as well as the costs of each of the structures studied, as shown in Table 1.

	Foundation	Structure	Forged	Total
H FU	2547.54	1019.77	16208.84	19776.15
A FU	2705.73	7482.63	15174.66	25363.02

Table 1: Costs in the two case studies.

As we can see in the table, the cost in the case of study with metal structure is 28.25% greater than the case of reinforced concrete. We can see that the most relevant item is that of slabs corresponding to 81.96% in the case of concrete and in 59.83% in the case of steel. Another important fact that we can observe is that the structure represents 5.16% in the concrete and 29.50% in the steel. This oscillation is due to the consideration of the primary beams, of the reinforced concrete slab, included in the chapter of slabs. With regard to the foundation, the cost of the steel option is slightly higher.

To represent the environmental impacts, the results are shown by graphs. The representation reproduces on the vertical axis the value of the energy imbibed for the graph on the left and the equivalent emissions of CO_2 in kg for the one on the right. The horizontal axis shows the case study. The legend indicates the execution item in which the impact occurs.
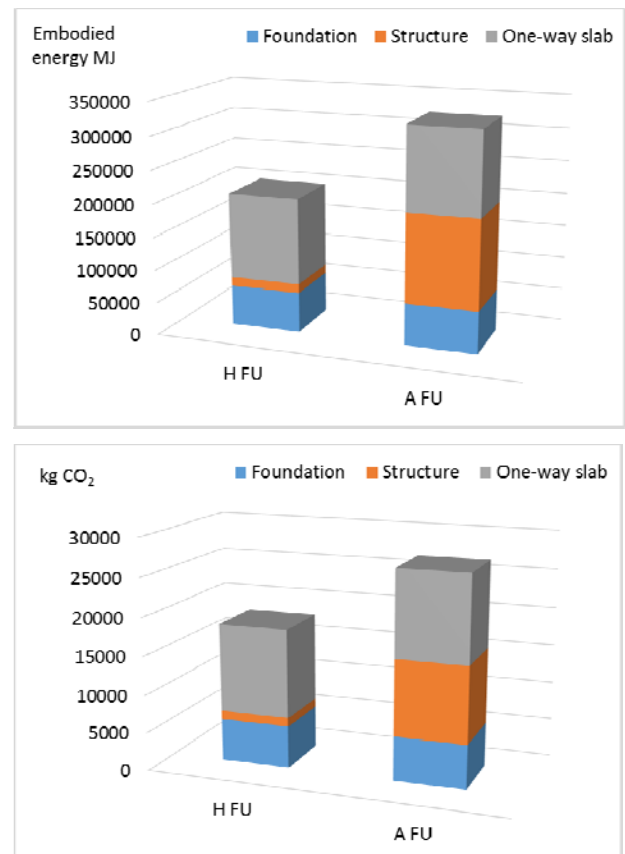

Figure 4: Environmental impacts by execution phases.

In the graphs it can be seen that the AFU study case has greater environmental impacts, more specifically 59.02% in embedded energy and 47.77% in kg CO_2. It can be seen that the greatest impact for the case of the HFU study occurs in the slabs heading 63.58% followed by the foundation with 29.93% and finally the structure 6.49% in relation to embedded energy. On the other hand, in the case of the AFU study, the greatest impact occurs in the structure item 41.51% followed by the floors with 38.83% and finally the foundations 19.65% in relation to embedded energy. Regarding the environmental impact in kg of CO_2, we can see that the percentages vary, being for the case of AFU study 21.44% in foundation, 36.78% in structure and 41.78% in floors. For the HFU case, the foundations are a higher percentage of 30.29%, 6.16% in structure and 63.58% in floors. The total sum of kg of CO_2 in the case of HFU amounts to 18204.47 while for the case AFU the value is of 26900.42 $kgCO_2$.

If we focus on the phases, the product phase (A1-A2-A3) is in all cases 98% of the impact, leaving the production phase at values that are around 2%.

4. CONCLUSIONS

The present investigation makes a reflection on two models with different structural alternatives, justifying the need to go deeper into multicriteria methods as an aid to decision making. The current modeling and simulation means allow to incorporate metadata in the project phases.

The influence of the different materials according to the stages and the departures vary according to the cases. After the analysis of the incorporated energy and the CO_2 emissions eq in summary we have:

• In stages A1-A2-A3: the concrete in the foundation part and the floor slabs with the concrete structure are of great importance. In the case of the steel structure, it is the steel of the heading structure that has the most weight.

• In stage A4: concrete is the main element in the construction of the slabs of steel and concrete structures that were modeled with unidirectional slab.

• In stage A5: the greatest impact is generated by diesel in the machinery in all the items studied.

If we analyze the costs of the different chapters studied and their totals we would have that the items with a greater weight in the costs would be the forged ones and in total values the cases of rolled steel as a structural system. The foundation is presented as a game with little difference between the different cases.

REFERENCES

Agutter A.J., 1995. The linguistic significance of current British slang. Thesis (PhD). Edinburgh University.

Adeli, H., Sarma, K.C. (2006) "Cost optimization of structures. Fuzzy, Genetic Algorithms and Parallel Computing", ED. WILEY-VCH.

Amir, O. (2013) "A topology optimization procedure for reinforced concrete structures", Computers & Structures, Vol. 114, Pag. 46-58.

Armengou J., Aguado A., Ormazábal G. (2012) "Sistema integrado para toma de decisiones en el diseño de estructuras de hormigón". Informes de la construcción, ISSN 0020-0883, Vol. 64, Nº. 527, págs. 391-400.

BEDEC (2013) "Banco Estructurado de Datos de Elementos Constructivos". Instituto de Tecnología de la Construcción de Cataluña (ITeC).

CTE "Código Técnico de la Edificación". Real Decreto 314/2006, de 17 de marzo, del Ministerio de Vivienda (España).

CYPECAD (2012) "CYPE Ingenieros Software para Arquitectura, Ingeniería y Construcción". CYPE Ingenieros S.A.

Danatzko, J.M., Sezen, H., Chen, Q. (2013)" Sustainable design and energy consumption analysis for structural components" Journal of Green Building 8 (1), pp. 120-135.

EHE-08 "Instrucción de Hormigón Estructural", Real Decreto 1247/2008, de 18 de julio, del Ministerio de Fomento (España).

Fernandez-Ceniceros, J., Fernandez-Martinez, R., Fraile-Garcia, E., Martinez-De-Pison, F.J. (2013)."Decision support model for one-way floor slab design: A sustainable approach" Automation in Construction 35 PP. 460 – 470.

Ferreiro-Cabello, J., Fraile-Garcia, E., Martinez-Camara, E., Perez-de-la-Parte, M. (2017) Sensitivity analysis of Life Cycle Assessment to select reinforced concrete structures with one-way slabs. Engineering Structures 132, pp. 586-596

Ferreiro-Cabello, J., Fraile-Garcia, E., Martinez de Pison Ascacibar, E., Martinez de Pison Ascacibar, F.J. (2016) Minimizing greenhouse gas emissions and costs for structures with flat slabs. Journal of Cleaner Production, 137, pp. 922-930

Ferreiro Cabello J, Fraile Garcia E, Martinez de Pison E, Jimenez Macias E. (2017) Metodologia para seleccion de alternativas estructurales en edificacion residencial empleando forjados unidireccionales. DYNA Ing e Ind. 2015;90(3):491–502.

Fraile-Garcia E, Ferreiro-Cabello J, Martinez-Camara E, Jimenez-Macias E. Optimization based on life cycle analysis for reinforced concrete structures with one-way slabs. Engineering Structures. 2016;109:126–38.

Fraile-Garcia, E., Ferreiro-Cabello, J., Martinez-Camara, E., Jimenez-Macias, E. Document Repercussion the use phase in the life cycle assessment of structures in residential buildings using one-way slabs. Journal of Cleaner Production 143, pp. 191-199

Fraile-García E, Ferreiro-Cabello J, Sodupe-Ortega E, Sanz-Garcia A. Evaluación combinada de los impactos ambientales, económicos y sociales de soluciones estructurales para la construcción de

viviendas. Informes de la Construcción 2015;67(539):e101.

Fraile-Garcia E, Ferreiro-Cabello J, Martinez-Camara E, Jimenez-Macias E. Adaptation of methodology to select structural alternatives of one-way slab in residential building to the guidelines of the European Committee for Standardization (CEN/TC 350). Environmental Impact Assessment. 2015;55:144–55.

Huedo Dorda P., López Mesa B. (2013) "Revisión de herramientas de asistencia en la selección de soluciones constructivas sostenibles de edificación". Informes de la construcción, ISSN 0020-0883, Vol. 65, Nº. 529, págs. 77-88.

Kaveh, A., Abadi, A.S.M. (2010) "Cost optimization of a composite floor system using an improved harmony search algorithm", Journal of Constructional Steel Research, Vol. 66, Num. 5, Pag. 664-669.

Kaveh, A., Ahangaran, M. (2012) "Discrete cost optimization of composite floor system using social harmony search model", Applied Soft Computing, Vol. 12, Num. 1, Pag. 372-381.

Klansek, U., Kravanja, S. (2006) "Cost estimation, optimization and competitiveness of different composite floor systems - Part 1: Self-manufacturing cost estimation of composite and steel structures", Journal of Constructional Steel Research, Vol. 62, Num. 5, Pag. 434-448.

Kravanja, S., Klansek, U. (2008) "Cost optimization of composite floors", High Performance Structures and Materials IV, Book Series: Wit Transactions on the Built Environment Vol. 97 Pag. 109-118.

Martín Gil, D. González Valle, E. (2010) "La deformabilidad de las estructuras de hormigón en la edificación: su evolución". Hormigón y acero, ISSN 0439-5689, Nº 256, págs. 61-69.

Martinez-Martin, F.J., Gonzalez-Vidosa, F., Hospitaler, A., Yepes, V. (2012) "Multi-objective optimization design of bridge piers with hybrid heuristic algorithms", Journal of Zhejiang University-Science A, Vol. 13, Num. 6, Pag. 420-432.

Payá, I., Yepes, V., Clemente, J.J., González, F. (2006) "Optimización heurística de pórticos de edificación de hormigón armado", Métodos numéricos para cálculo y diseño en ingeniería: Revista Internacional, Vol. 22, Num. 3, Pag. 241-260.

Sahab, M.G., Ashour, A.F., Toropov, V. (2005) "Cost optimisation of reinforced concrete flat slab buildings " Engineering Structures, Vol. 27, Num. 3, Pag. 313-322.

Senouci, A.B., Al-Ansari, M.S. (2009). "Cost optimization of composite beams using genetic algorithms", Advances in Engineering Software, Vol. 40, Pag. 1112-1118.

Sharafi, P., Hadi, M.N.S., Teh, L.H. (2012) "Heuristic Approach for Optimum Cost and Layout Design of 3D Reinforced Concrete Frames", Journal of Structural Engineering-ASCE, Vol. 138, Num. 7, Pag. 853-863.

UNE-EN ISO 14040 (2006) "Gestión ambiental. Análisis de ciclo de vida. Principios y marco de referencia" (ISO 14040:2006).

UNE-EN ISO 14044 (2006) "Gestión ambiental. Análisis de ciclo de vida. Requisitos y directrices" (ISO 14044:2006).

UNE-EN 15804 (2012) "Sostenibilidad en la construcción. Declaraciones ambientales de producto. Reglas de categoría de productos básicas para productos de construcción"

UNCERTAINTY IN TWO-STAGE MEASUREMENT: EXPLANATION USING SIMULATION STUDIES

Jaroslav Marek[a], Marie Nedvědová[b]

[a],[b]University of Pardubice, Faculty of Electrical Engineering and Informatics

[a]jaroslav.marek@upce.cz, [b]marie.nedvedova@student.upce.cz

ABSTRACT

In geodesy we often estimate coordinates of a two-dimensional point in a model of two-stage measurements. The points from the national trigonometric network have different accuracy, and independence is not met. We encounter situations where we cannot get quality results even by repeating measurements. The dependency among old points and their accuracy may have a considerable impact on the estimated coordinates of new points. To examine the impact, this paper presents simulation methods describing the uncertainty of estimated points. The main goal of this paper is to study the uncertainty of Least Squares Estimators in one surveying problem. This is a situation where an object should be very precisely connected to the government network. We draw attention to the fact that the Least Squares Method can give non-admissible geometric representation of an object's estimated coordinates. The main objective is to compare outputs from the two-stage regression model and from simulation studies.

Keywords: two stage regression model, model of connecting measurement, uncertainty of measurement in geodesy, B-type uncertainty, A-type uncertainty, simulation of measurement

1. INTRODUCTION

In geodesy, unknown coordinates of new points are generally determined with the use of indirect measurement models. For estimates of point coordinates are using measured values of angles in triangles, where one vertex is a new point and another vertex of triangle is a point of existing geodetic network. Direct distance measurement is not frequent approach, as angle measuring devices enable more accurate results. Mathematical models used in surveying are studied in the book (Anderson, 2013), (Kubáček, 1995), (Kubáček, 2013) and (Uren, 2010).

Even if geodetic networks were created and are heretofore designed with maximal possible precision, then precision of geodetic points is determined by the degree of knowledge or technical and instrumental apparatus of its period. Advancement of practical and theoretical knowledge, as well as development of measuring, instrumental perfection, and PC techniques,

lead to a difference between the possibilities of existing networks and their state.

In many geodetic situations, available coordinate are estimators of points of an existing network from the first stage of measurement.

In geodetic model of measurement a new measurement is combined with the existing geodetic networks data.

The coordinates of new points (objects) are determined, based on measurements of distances and angles. In this case we connect the network by measuring in the second stage (connecting network) to the existing one (connected network).

First stage measurement errors are called B type uncertainties. Measurement errors in the second stage are referred to as type A uncertainties.

It should be remembered that in such a situation new calculations work with several decades old measurements. The influence of the B-type uncertainties of the original points has a detrimental effect on the accuracy of the newly determined points. By repeating the second stage measurement, we can of course increase the accuracy of the measurement and reduce the uncertainty of the type A measurement. When n replication is used, the variance is reduced $1/n$ times. However, we do not reduce the impact of type B uncertainties by replication of second stage measurements.

The aim in geodetic statistical models is to determine an estimator of the unknown parameters on the basis of the observation vector. One possible approach is using the Least Squares method. When processing geodetic data sets it is necessary to consider the uncertainty of national geodetic points and the uncertainty of new measurements. According to literature, a two-stage regression model is considered as the most appropriate model for many surveying situations. From state documentation, coordinate estimates of first stage points and knowledge of precision of new angles and distance measurements, allows the estimation of coordinates and a covariance matrix of new points. Two stage regression model are studied in (Kubáček, 1993), (Kubáček, 2005), (Marek, 2014).

Because we would like to investigate how the various uncertainty of connected structure influences the accuracy of new points (object) estimates, we proposed a larger numerical study with measurement simulations.

The main goal of the paper is to explore the possibilities of maintaining the inner geometry of a new object, by reducing the influence of metrological uncertainty of the connected stage by increasing the number of measurements in the connecting stage.

The inner geometry of an object can be better preserved if we use a new custom coordinate system. We will measures the object in our coordinate system and then we transform the coordinates of the object into the state system. Coordinate recalculation uses Helmert's transformation. For detail see (Marek, 2015), (Neitzel, 2010).
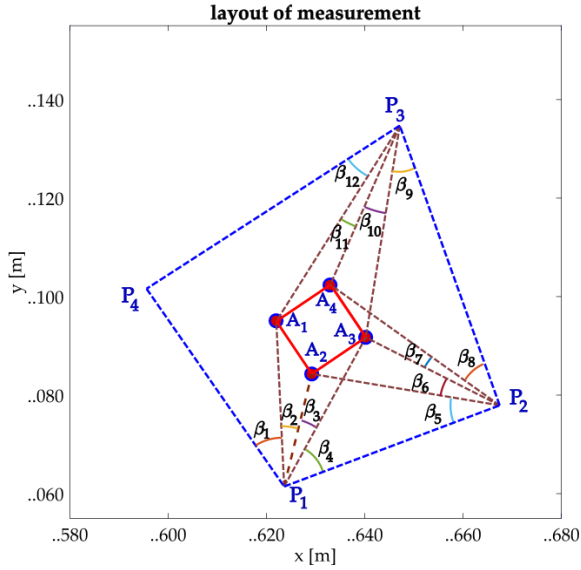

Figure 1: Layout of measurement

In our example, coordinates of a new object (exactly defined rectangular object with sizes 12.90 m and 13.25 m) will be computed using the measurement of angles from four existing points in three different regression models, with an increasing number of measured parameters. In the first case, we will work with 12 measured angles. The second problem will consider 28 measured angles. In the third case, the 4 sides of the rectangle will be measured in addition to measuring 28 angles.

We use theta parameter to indicate the actual coordinates of the points of the national network. Actual values of angles and distances from the second measurement stage are marked with $\boldsymbol{\beta}$, their measurement is marked with $\mathbf{Y}$.

There are constraints between the first stage points and the second phase measurement, in which the unknown points of the new points appear.

Measured angles (constraints g_1 to g_{28}) and distances (constraints g_{29} to g_{32}) are given by points P and A coordinates as follows:

$$g_1 = \operatorname{atan}\left(\frac{\theta_{1,1} - \theta_{4,1}}{-\theta_{1,2} + \theta_{4,2}}\right) - \operatorname{atan}\left(\frac{\theta_{1,1} - A_{1,1}}{-\theta_{1,2} + A_{1,2}}\right),$$

$$g_2 = \operatorname{atan}\left(\frac{\theta_{1,1} - A_{1,1}}{-\theta_{1,2} + A_{1,2}}\right) - \operatorname{atan}\left(\frac{\theta_{1,1} - A_{2,1}}{A_{2,2} - \theta_{1,2}}\right),$$

$$g_3 = \operatorname{atan}\left(\frac{\theta_{1,1} - A_{1,1}}{-\theta_{1,2} + A_{1,2}}\right) - \operatorname{atan}\left(\frac{\theta_{1,1} - A_{2,1}}{A_{2,2} - \theta_{1,2}}\right),$$

$$g_4 = \operatorname{atan}\left(\frac{A_{3,2} - \theta_{1,2}}{A_{3,1} - \theta_{1,1}}\right) - \operatorname{atan}\left(\frac{\theta_{2,2} - \theta_{1,2}}{\theta_{2,1} - \theta_{1,1}}\right),$$

$$g_5 = \pi + \operatorname{atan}\left(\frac{\theta_{2,1} - A_{2,1}}{\theta_{2,2} - A_{2,2}}\right) - \operatorname{atan}\left(\frac{\theta_{2,1} - \theta_{1,1}}{\theta_{2,2} - \theta_{1,2}}\right),$$

$$g_6 = \operatorname{atan}\left(\frac{\theta_{2,1} - A_{2,1}}{A_{2,2} - \theta_{2,2}}\right) - \operatorname{atan}\left(\frac{\theta_{2,1} - A_{3,1}}{A_{3,2} - \theta_{2,2}}\right),$$

$$g_7 = \operatorname{atan}\left(\frac{\theta_{2,1} - A_{3,1}}{A_{3,2} - \theta_{2,2}}\right) - \operatorname{atan}\left(\frac{\theta_{2,1} - A_{4,1}}{A_{4,2} - \theta_{2,2}}\right),$$

$$g_8 = \operatorname{atan}\left(\frac{\theta_{2,1} - A_{4,1}}{A_{4,2} - \theta_{2,2}}\right) - \operatorname{atan}\left(\frac{\theta_{2,1} - \theta_{3,1}}{\theta_{3,2} - \theta_{2,2}}\right),$$

$$g_9 = \pi - \operatorname{atan}\left(\frac{\theta_{3,2} - \theta_{2,2}}{\theta_{2,1} - \theta_{3,1}}\right) - \operatorname{atan}\left(\frac{-A_{3,2} + \theta_{3,2}}{-A_{3,1} + \theta_{3,1}}\right),$$

$$g_{10} = \operatorname{atan}\left(\frac{\theta_{3,1} - A_{4,1}}{\theta_{3,2} - A_{4,2}}\right) - \operatorname{atan}\left(\frac{-A_{3,1} + \theta_{3,1}}{-A_{3,2} + \theta_{3,2}}\right),$$

$$g_{11} = \operatorname{atan}\left(\frac{\theta_{3,1} - A_{1,1}}{\theta_{3,2} - A_{1,2}}\right) - \operatorname{atan}\left(\frac{\theta_{3,1} - A_{4,1}}{\theta_{3,2} - A_{4,2}}\right),$$

$$g_{12} = \operatorname{atan}\left(\frac{\theta_{3,1} - A_{4,1}}{\theta_{3,2} - A_{4,2}}\right) - \operatorname{atan}\left(\frac{\theta_{3,1} - A_{1,1}}{\theta_{3,2} - A_{1,2}}\right),$$

$$g_{13} = \operatorname{atan}\left(\frac{\theta_{3,2} - \theta_{4,2}}{\theta_{3,1} - \theta_{4,1}}\right) - \operatorname{atan}\left(\frac{A_{4,2} - \theta_{4,2}}{A_{4,1} - \theta_{4,1}}\right),$$

$$g_{14} = \operatorname{atan}\left(\frac{A_{4,2} - \theta_{4,2}}{A_{4,1} - \theta_{4,1}}\right) - \operatorname{atan}\left(\frac{A_{1,2} - \theta_{4,2}}{A_{1,1} - \theta_{4,1}}\right),$$

$$g_{15} = -\operatorname{atan}\left(\frac{A_{2,1} - \theta_{4,1}}{\theta_{4,2} - A_{2,2}}\right) + \operatorname{atan}\left(\frac{A_{1,1} - \theta_{4,1}}{\theta_{4,2} - A_{1,2}}\right),$$

$$g_{16} = -\operatorname{atan}\left(\frac{\theta_{1,1} - \theta_{4,1}}{-\theta_{1,2} + \theta_{4,2}}\right) + \operatorname{atan}\left(\frac{A_{2,1} - \theta_{4,1}}{\theta_{4,2} - A_{2,2}}\right),$$

$$g_{17} = \operatorname{atan}\left(\frac{\theta_{1,1} - \theta_{4,1}}{-\theta_{1,2} + \theta_{4,2}}\right) - \operatorname{atan}\left(\frac{\theta_{1,1} - A_{3,1}}{A_{3,2} - \theta_{1,2}}\right),$$

$$g_{18} = \pi + \operatorname{atan}\left(\frac{\theta_{2,1} - A_{4,1}}{\theta_{2,2} - A_{4,2}}\right) - \operatorname{atan}\left(\frac{\theta_{2,1} - \theta_{1,1}}{\theta_{2,2} - \theta_{1,2}}\right),$$

$$g_{19} = \pi - \operatorname{atan}\left(\frac{\theta_{3,2} - \theta_{2,2}}{\theta_{2,1} - \theta_{3,1}}\right) - \operatorname{atan}\left(\frac{\theta_{3,2} - A_{1,2}}{\theta_{3,1} - A_{1,1}}\right),$$

$$g_{20} = \pi + \operatorname{atan}\left(\frac{A_{2,1} - \theta_{4,1}}{A_{2,2} - \theta_{4,2}}\right) - \operatorname{atan}\left(\frac{A_{2,1} - \theta_{1,1}}{A_{2,2} - \theta_{1,2}}\right),$$

$$g_{21} = \pi - \operatorname{atan}\left(\frac{A_{2,2} - \theta_{2,2}}{\theta_{2,1} - A_{2,1}}\right) - \operatorname{atan}\left(\frac{A_{2,2} - \theta_{1,2}}{A_{2,1} - \theta_{1,1}}\right),$$

$$g_{22} = -\operatorname{atan}\left(\frac{\theta_{2,1} - A_{3,1}}{\theta_{2,2} + A_{3,2}}\right) + \operatorname{atan}\left(\frac{\theta_{1,1} - A_{3,1}}{\theta_{1,2} - A_{3,2}}\right),$$

$$g_{23} = \operatorname{atan}\left(\frac{-A_{3,2} + \theta_{3,2}}{-A_{3,1} + \theta_{3,1}}\right) - \operatorname{atan}\left(\frac{\theta_{2,2} - A_{3,2}}{\theta_{2,1} - A_{3,1}}\right),$$

$$g_{24} = \operatorname{atan}\left(\frac{\theta_{3,2} - A_{4,2}}{\theta_{3,1} - A_{4,1}}\right) - \operatorname{atan}\left(\frac{\theta_{2,2} - A_{4,2}}{\theta_{2,1} - A_{4,1}}\right),$$

$$g_{25} = \pi + \operatorname{atan}\left(\frac{A_{4,1} - \theta_{3,1}}{A_{4,2} - \theta_{3,2}}\right) - \operatorname{atan}\left(\frac{A_{4,1} - \theta_{4,1}}{A_{4,2} - \theta_{4,2}}\right),$$

$$g_{26} = \operatorname{atan}\left(\frac{\theta_{3,2} - \theta_{4,2}}{\theta_{3,1} - \theta_{4,1}}\right) - \operatorname{atan}\left(\frac{A_{2,2} - \theta_{4,2}}{A_{2,1} - \theta_{4,1}}\right),$$

$$g_{27} = -\operatorname{atan}\left(\frac{\theta_{4,2} - A_{1,2}}{A_{1,1} - \theta_{4,1}}\right) + \operatorname{atan}\left(\frac{-\theta_{1,2} + \theta_{4,2}}{\theta_{1,1} - \theta_{4,1}}\right),$$

$$g_{28} = \pi - \operatorname{atan}\left(\frac{A_{4,2} - \theta_{2,2}}{\theta_{2,1} - A_{4,1}}\right) - \operatorname{atan}\left(\frac{A_{4,2} - \theta_{4,2}}{A_{4,1} - \theta_{4,1}}\right),$$

$$g_{29} = \sqrt{\left(A_{2,1} - A_{1,1}\right)^2 + \left(A_{2,2} - A_{1,2}\right)^2}.$$

$$g_{30} = \sqrt{\left(A_{3,1} - A_{2,1}\right)^2 + \left(A_{3,2} - A_{2,2}\right)^2},$$

$$g_{31} = \sqrt{\left(A_{4,1} - A_{3,1}\right)^2 + \left(A_{4,2} - A_{3,2}\right)^2},$$

$$g_{32} = \sqrt{\left(A_{1,1} - A_{4,1}\right)^2 + \left(A_{1,2} - A_{4,2}\right)^2}.$$

These constraints are non-linear, so the constraints must be linearized.

For example derivative of g_1 by $\theta_{1,1}$, $\theta_{1,2}$ and derivative of g_{29} by $A_{1,1}$, $A_{1,2}$ are:

$$\frac{\partial g_1}{\partial \theta_{1,1}} = \left\{(\theta_{4,2} - \theta_{1,2})\left[\frac{(\theta_{1,1} - \theta_{4,1})^2}{(\theta_{4,2} - \theta_{1,2})^2} + 1\right]\right\}^{-1} -$$

$$- \left\{(A_{1,2} - \theta_{1,2})\left[\frac{(\theta_{1,1} - A_{1,1})^2}{(A_{1,2} - \theta_{1,2})^2} + 1\right]\right\}^{-1},$$

$$\frac{\partial g_1}{\partial \theta_{1,2}} = \frac{\theta_{1,1} - \theta_{4,1}}{(\theta_{4,2} - \theta_{1,2})^2\left[\frac{(\theta_{1,1} - \theta_{4,1})^2}{(\theta_{4,2} - \theta_{1,2})^2} + 1\right]} -$$

$$- \frac{\theta_{1,1} - A_{1,1}}{(\theta_{4,2} - \theta_{1,2})^2\left[\frac{(\theta_{1,1} - A_{1,1})^2}{(A_{1,2} - \theta_{1,2})^2} + 1\right]},$$

$$\frac{\partial g_{29}}{\partial A_{1,1}} = -\frac{A_{2,1} - A_{1,1}}{\sqrt{\left(A_{2,2} - A_{1,2}\right)^2 + \left(A_{2,1} - A_{1,1}\right)^2}},$$

$$\frac{\partial g_{29}}{\partial A_{1,2}} = -\frac{A_{2,2} - A_{1,2}}{\sqrt{\left(A_{2,2} - A_{1,2}\right)^2 + \left(A_{2,1} - A_{1,1}\right)^2}}.$$

Here, we can see that the use of the atan function is more appropriate than the use of other cyclometric functions where derivatives would be more complex.

The simulation study in the model of connecting measurement can help geodetic engineering, when forecasting not only precision of new points referred to in the first stage point uncertainty but also the ability to maintain the internal geometry of the new object.

2. MATHEMATICAL FORMULATION

2.1. Two stage-regression model
Base type of model, which is a point of research, is a "two stage model of indirect measurement with constraints of type I and II".

For understanding of terms as are constraints of type I and II see (Kubáček, 2005).
Mathematically it is possible this model express as follows:

$$\begin{pmatrix} \mathbf{Y_1} \\ \mathbf{Y_2} \end{pmatrix} \approx \left[\begin{pmatrix} \mathbf{X_1} & \mathbf{0} \\ \mathbf{D} & \mathbf{X_2} \end{pmatrix}\begin{pmatrix} \mathbf{\Theta} \\ \mathbf{\beta} \end{pmatrix}, \begin{pmatrix} \mathbf{\Sigma_1} & \mathbf{0} \\ \mathbf{0} & \mathbf{\Sigma_2} \end{pmatrix}\right], \quad (1)$$

where

$\mathbf{Y}$ is random vector of model of connecting measurement expressed as $\mathbf{Y} = (\mathbf{Y_1}, \mathbf{Y_2})'$,
$\mathbf{X_1}$ is known matrix of type $n_1 \times k_1$ (design matrix in the first stage),
$\mathbf{X_2}$ is known matrix of type $n_2 \times k_2$ (design matrix in the second stage),
$\mathbf{D}$ is known matrix of type $n_2 \times k_1$, which realises interconnection between the first and second stage,
n_1 is number of measured quantities in the first stage,
n_2 is number of measured quantities in the second stage,
k_1 is number of unknown quantities in the first stage,
k_2 is number of unknown quantities in the second stage,
$\mathbf{\Theta}$ is unknown k_1-dimensional parameter, which is estimated on a base of vector $\mathbf{Y_1}$ in the first stage,
$\mathbf{\beta}$ is unknown k_2-dimensional parameter, which is estimated on a base of vectors $(\mathbf{Y_2} - \mathbf{D\Theta})$ and $\mathbf{\Theta}$,
$\mathbf{\Sigma_1}$ is covariance matrix of the first stage,
$\mathbf{\Sigma_2}$ is covariance matrix of the second stage.
For constraints of type I, $\mathbf{a} + \mathbf{C\widehat{\Theta}} + \mathbf{B\widetilde{\beta}} = \mathbf{0}$ has to be fulfilled, where
$\mathbf{B}$ is the matrix of partial derivations of function formulas of constraints for parameter $\mathbf{\beta}$,
$\mathbf{C}$ is the matrix of partial derivations of function formulas of constraints for parameter $\mathbf{\Theta}$,
$\mathbf{a}$ is vector of constraints,
$\mathbf{\widetilde{\beta}}$ is estimator from the second stage,
$\mathbf{\Theta}$ is estimator from the first stage.

Formulas for estimation in a model with constraint of type I as well as complete mathematical formulations of above mentioned notes are described in (Kubáček, 1993), (Kubáček, 2005), (Kubáček, 2013), and (Korbašová, 2004).

$$\widehat{\boldsymbol{\beta}} = (\mathbf{X'_2\Sigma_2^{-1}X_2})^{-1}\mathbf{X'_2\Sigma_2^{-1}}(\mathbf{Y_2} - \mathbf{D\widehat{\Theta}}) -$$

$$- (\mathbf{X'_2\Sigma_2^{-1}X_2})^{-1}\mathbf{B'}[\mathbf{B}(\mathbf{X'_2\Sigma_2^{-1}X_2})^{-1}\mathbf{B'}]^{-1} \times$$

$$\times \{\mathbf{a} + \mathbf{C\widehat{\Theta}} + \mathbf{B}(\mathbf{X'_2\Sigma_2^{-1}X_2})^{-1}\mathbf{X'_2\Sigma_2^{-1}}(\mathbf{Y_2} - \mathbf{D\widehat{\Theta}})\},$$

$$(2)$$

$$Var(\widehat{\boldsymbol{\beta}}) = Var_A(\widehat{\boldsymbol{\beta}}) +$$

$$\left\{\left[\mathbf{I} - (\mathbf{X'_2\Sigma_2^{-1}X_2})^{-1}\mathbf{B'}\left(\mathbf{B}(\mathbf{X'_2\Sigma_2^{-1}X_2})^{-1}\mathbf{B'}\right)^{-1}\mathbf{B}\right] \times\right.$$

$$\times \, (X'_2 \Sigma_2^{-1} X_2)^{-1} X'_2 \Sigma_2^{-1} D - (X'_2 \Sigma_2^{-1} X_2)^{-1} \times$$
$$\times \, B'[B(X'_2 \Sigma_2^{-1} X_2)^{-1} B']^{-1} C \, \} \times Var(\widehat{\Theta}) \times$$
$$\left\{ \left[I - \left(X'_2 \Sigma_2^{-1} X_2 \right)^{-1} B' \left(B\left(X'_2 \Sigma_2^{-1} X_2 \right)^{-1} B' \right)^{-1} B \right] \times \right.$$
$$\times \, (X'_2 \Sigma_2^{-1} X_2)^{-1} X'_2 \Sigma_2^{-1} D - (X'_2 \Sigma_2^{-1} X_2)^{-1} \times$$
$$\left. \times \, B'[B(X'_2 \Sigma_2^{-1} X_2)^{-1} B']^{-1} C \, \right\},$$

$$(3)$$

where uncertainty of type A is

$$Var_A(\widehat{\beta}) = \left(X'_2 \Sigma_2^{-1} X_2 \right)^{-1} -$$
$$- \left(X'_2 \Sigma_2^{-1} X_2 \right)^{-1} B' \left(B\left(X'_2 \Sigma_2^{-1} X_2 \right)^{-1} B' \right)^{-1}$$
$$\cdot B\left(X'_2 \Sigma_2^{-1} X_2 \right)^{-1}$$

2.2. Confidence domain

The confidence domain (see (Kubáčková, 1996) and Alexandersson, 2004)) for the parameter $\boldsymbol{\beta}$ is a set in parametric space of $\boldsymbol{\beta}$, which covers the true value of $\boldsymbol{\beta}$ with a given probability 1-α.

Formula for (1-α)% -confidence domain is given by

$$\varepsilon_{1-\alpha}(\boldsymbol{\beta}) = \left\{ \boldsymbol{u} : \boldsymbol{u} \in \Theta_\beta, (\boldsymbol{u} - \widehat{\boldsymbol{\beta}}) [\text{var} \, \widehat{\boldsymbol{\beta}}]^{-1} (\boldsymbol{u} - \widehat{\boldsymbol{\beta}})' \right.$$
$$\left. \leq \chi_k^2 (1 - \alpha) \right\}.$$

$$(4)$$

The symbol $\chi_k^2(1 - \alpha)$ denotes the $(1 - \alpha)$-quantile of a χ^2 distribution with k degrees of freedom.

3 EXPERIMENT - EXAMPLE

At our disposal are government coordinates of points P_1, P_2, P_3 and P_4. See Fig. 1. We will use the symbol $\boldsymbol{\Theta}$ for coordinates of the existing network $P_1 = \boldsymbol{\Theta}_1'$, $P_2 = \boldsymbol{\Theta}_2'$, $P_3 = \boldsymbol{\Theta}_3'$, $P_4 = \boldsymbol{\Theta}_4'$.

The aim is to find estimators of coordinates of new points A_1, A_2, A_3 and A_4. Suppose the measuring $\mathbf{Y}$ of angles and distances
$\beta_1 = \angle P_4, P_1, A_1, \beta_2 = \angle A_1, P_1, A_2, \beta_3 = \angle A_2, P_1, A_3,$
$\beta_4 = \angle A_3, P_1, P_2, \beta_5 = \angle P_1, P_2, A_2, \beta_6 = \angle A_2, P_2, A_3,$
$\beta_7 = \angle A_3, P_2, A_4, \beta_8 = \angle A_4, P_2, P_3, \beta_9 = \angle A_3, P_3, P_2,$
$\beta_{10} = \angle A_4, P_3, A_3, \beta_{11} = \angle A_1, P_3, A_4, \beta_{12} = \angle P_4, P_3, A_1,$
$\beta_{13} = \angle P_3, P_4, A_4, \beta_{14} = \angle A_4, P_4, A_1, \beta_{15} = \angle A_1, P_4, A_2,$
$\beta_{16} = \angle A_2, P_4, P_1, \beta_{17} = \angle P_4, P_1, A_3, \beta_{18} = \angle P_1, P_2, A_4,$
$\beta_{19} = \angle P_2, P_3, A_1, \beta_{20} = \angle P_1, A_2, P_4, \beta_{21} = \angle P_1, A_2, P_4,$
$\beta_{22} = \angle P_1, A_2, P_2, \beta_{23} = \angle P_1, A_3, P_2, \beta_{24} = \angle P_2, A_3, P_3,$
$\beta_{25} = \angle P_2, A_4, P_3, \beta_{26} = \angle P_3, A_4, P_4, \beta_{27} = \angle A_2, P_4, P_3,$
$\beta_{28} = \angle P_4, P_4, A_1, \beta_{29} = |A_1 \, A_2|, \beta_{30} = |A_2 \, A_3|,$
$\beta_{31} = |A_3 \, A_4|, \beta_{32} = |A_4 \, A_1|$ is given at our disposal.

We prepare the simulation of the measurements so that we can observe the influence of the uncertainties of the first stage measurement and the uncertainties of the second stage measurement on the resulting estimates of the coordinates of the points of the new object

In the calculations we will gradually increase the number of measurements of directly observable

parameters β_i. Increasing the number of measurement parameters of the second stage will allow us to monitor the decrease of the influence of the uncertainty of the first stage measurement on the resulting estimates.

In the simplest model, we will only consider measuring β_1 to β_{12}, in the second simplest model, we will consider measuring β_1 to β_{13}. The most complex model will include measurement of β_1 to β_{32}.

We will use the following markings when presenting some results: Y^A vector of first 12 measurements, Y^B vector of first 27 measurements, Y^C vector of all 32 measurements.

Measurement simulations will be performed for different variation matrices Σ_1^i. These matrices indicate how accurate the original points P_1 to P_4 in the first stage were measured.

In our calculation, we will use the covariance matrix. $W = (W_a, W_b)$ that was calculated in one particular geodetic measurement, cf. (Korbašová, 2004):

$$W_a = \begin{pmatrix} 0.007100 & 0.000063 & 0.000046 & 0.000093 \\ 0.000063 & 0.009300 & 0.000093 & 0.000071 \\ 0.000046 & 0.000093 & 0.006400 & 0.000085 \\ 0.000093 & 0.000071 & 0.000085 & 0.014100 \\ 0.000047 & 0.000071 & 0.000043 & 0.000027 \\ 0.000052 & 0.000082 & 0.000049 & 0.000043 \\ 0.000031 & 0.000039 & 0.000038 & 0.000037 \\ 0.000042 & 0.000068 & 0.000061 & 0.000049 \end{pmatrix},$$

$$W_b = \begin{pmatrix} 0.000047 & 0.000052 & 0.000031 & 0.000042 \\ 0.000071 & 0.000082 & 0.000039 & 0.000068 \\ 0.000043 & 0.000049 & 0.000038 & 0.000061 \\ 0.000027 & 0.000043 & 0.000037 & 0.000049 \\ 0.006100 & 0.000058 & 0.000029 & 0.000097 \\ 0.000065 & 0.010000 & 0.000083 & 0.000067 \\ 0.000058 & 0.000093 & 0.005600 & 0.000085 \\ 0.000087 & 0.000086 & 0.000107 & 0.138000 \end{pmatrix}.$$

In total, the simulation includes 10 variance matrices, which are obtained by multiplying the matrix Σ_1^1 by Renard numbers. An inverted sequence was used.
$R_{10} =$
[8.00, 6.30, 5.00, 4.00, 3.15, 2.50, 2.00, 1.60, 1.25, 1.00].
Thus, for our needs, matrices Σ_1^1 to Σ_1^{10} were created. Such a modification ensures that the accuracy ratio between any two consecutive matrices will always be constant.

For the first matrix Σ_1^1, the original points have the least accuracy. For the last (tenth) matrix Σ_1^{10}, the original points have the highest accuracy.

When simulating measurements we proceeded as follows: we first determined the exact coordinates of the rectangle shape object with vertices [0, 0], [12.90, 0], [12.90, 13.25], [0, 13.25], which was rotated by an angle of 56 degrees counterclockwise and moved by

[536622, 1118095] meters. Then we calculated the exact values of angles and distances β_1 to β_{32}.

To these accurate β_i values, we have added a measurement error that had a normal distribution with zero mean value and variance σ_a^2 when measuring angles and variance σ_d^2 when measuring the sides.

$$\sigma_a^2 = (30^{cc})^2 = \left(30 \cdot \frac{\pi}{20000}\right)^2 [rad^2],$$
$$\left(1^{cc} = \frac{grad}{100}, 100 \, grad = \frac{\pi}{2}\right).$$
$$\sigma_d^2 = 0.01 \text{ m}^2.$$

The simulations were performed sequentially for all ten variance matrices Σ_1^i. For each i-th variance matrix, 10 replications of measurement were simulated. For each generated measurement, the resulting angles and lengths of the sides of the measured object were then calculated.

Furthermore, we present the results in tables and figures in order to allow the reader to monitor the accuracy of the results on the input error in the first and second measurement stage. Figures 3a and 3b show the dependence of the size of the calculated angle and the length of the side of the object on the number of used measurements, in the tenth replication, for two variants of the matrix $\Sigma_1 : \Sigma_1^1$ with the worst accuracy and Σ_1^{10} with the best accuracy of the original points.

Figures 4a and 4b show the dependence of the size of the calculated angle and the length of the side of the object on inaccuracies in the first stage of measurement for 12 (solid line), 28 (dash line) and 31 (dash-dot line) initial parameters.

For example in situation with Σ_1^{10}, the measurement in first experiment (given in degrees)

$Y^C = (32.1551, 16.5232, 14.9404, 40.6641, 30.0851,$
$\quad 17.3736, 8.5467, 34.9119, 28.8278, 14.4851, 8.6820,$
$\quad 24.9544, 31.4951, 15.2764, 13.1901, 27.8890,$
$\quad\quad 63.6187, 56.0054, 51.9949, 103.4327, 94.3104,$
$\quad\quad 91.8772, 107.7136, 101.7752, 114.8685, 59.9616,$
$\quad\quad 41.0791, 12.9000, 13.2500, 12.9000, 13.2500 \,)'$

is at our disposal.

Estimates obtained by formula (2) are shown in Tab. 1. Covariance matrices are presented in Tab. 2.

Table 1: Estimates obtained by formula (3)

$\widetilde{\boldsymbol{\beta}}^A$	$\widetilde{\boldsymbol{\beta}}^B$	$\widetilde{\boldsymbol{\beta}}^C$
..622.0268	..622.0405	..622.0293
..094.7213	..095.0161	..094.9742
..629.2002	..629.1725	..629.1773
..084.3719	..084.2211	..084.2382
..640.2033	..640.2033	..640.1394
..091.7063	..091.6413	..091.6908
..632.9944	..632.9458	..632.9699
..102.4710	..102.4836	..102.4309

Table 2: Covarinace matrix of new points obtained by formula (4): first stage uncertainty Σ_1^{10}

var(A_1)	Σ_1^1	var(A_1)	Σ_1^{10}
0.00672	0.00665	0.00181	0.00176
0.00665	0.00956	0.00176	0.00152
var(A_2)	Σ_1^1	var(A_2)	Σ_1^{10}
0.00607	0.00646	0.00108	0.00005
0.00646	0.00966	0.00005	0.00168
var(A_3)	Σ_1^1	var(A_3)	Σ_1^{10}
0.00607	0.00644	0.00124	0.00004
0.00667	0.00940	0.00004	0.00135
var(A_4)	Σ_1^1	var(A_4)	Σ_1^{10}
0.00634	0.00681	0.00157	0.00033
0.00681	0.00968	0.00033	0.00159

Point coordinates in Tab. 1 have an unusual format that contains two dots at the beginning of the number. In the Czech SJTSK geodetic system, for example, the coordinates of point A_1 are 536622.0268 and 1118094.7213.

The main objective of the whole geodetic calculation is to obtain the most accurate estimator of the unknown parameter $\boldsymbol{\beta}$. To find the most effective approach, it is useful to apply the theory of optimal design of experiments. Cf. (Pázman, 1986), (Kubáček, 1998), (Kubáček, 2013). Carefully chosen design for the measurement allow us to get better estimators of the parameters.

In a specific local geodetic problem, only numbers in the order of hundreds of meters are changed. Therefore, two dots indicate a part of the number that does not change.

A comparison of estimates of object characteristics is given in Tab. 3.

Table 3: Sizes of the object and the following angles for the estimates $\widetilde{\boldsymbol{\beta}}^A$, $\widetilde{\boldsymbol{\beta}}^B$ and $\widetilde{\boldsymbol{\beta}}^C$ (simulation No. 10 with matrix Σ_1^{10})

	variant A	variant B	variant C
$d(A_1, A_2)$	12.9882	12.9433	12.9045
$d(A_2, A_3)$	13.2881	13.2927	13.2368
$d(A_3, A_4)$	12.8694	12.8609	12.9139
$d(A_1, A_4)$	13.3094	13.3121	13.2471
$\angle A_1, A_2, A_3$	90.0974°	90.0624°	90.0431°
$\angle A_2, A_3, A_4$	89.9419°	89.9650°	89.9538°
$\angle A_3, A_4, A_1$	90.0504°	90.0279°	90.0416°
$\angle A_4, A_1, A_2$	89.9083°	89.9436°	89.9605°

In Tab. 3, it can be seen that in variant C the estimates are very close to real values 12.90 m, 13.25 m, and 90°.

Figure 2a,b,c,d depicts confidential ellipses for the matrix Σ_1^1 (dash line) and for the matrix Σ_1^{10} (solid line).
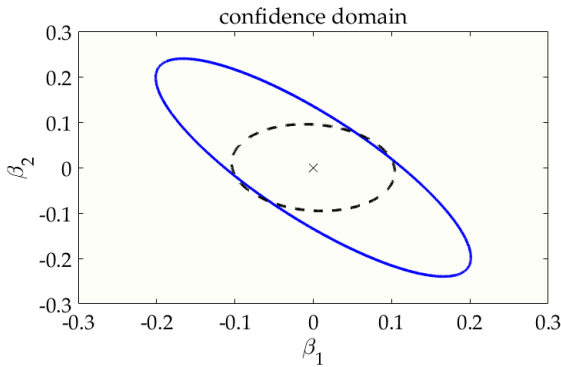
Figure 2a: Confidence domain – point A_1.
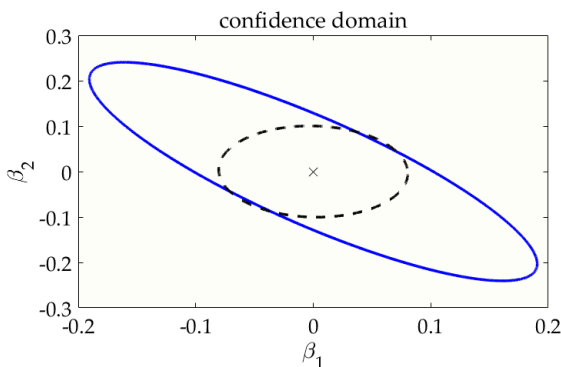
Figure 2b: Confidence domain – point A_2.
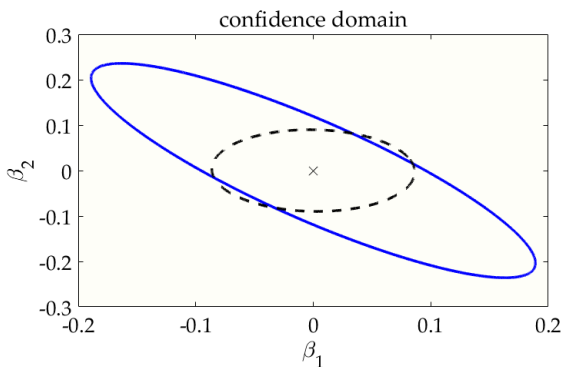
Figure 2c: Confidence domain – point A_3.
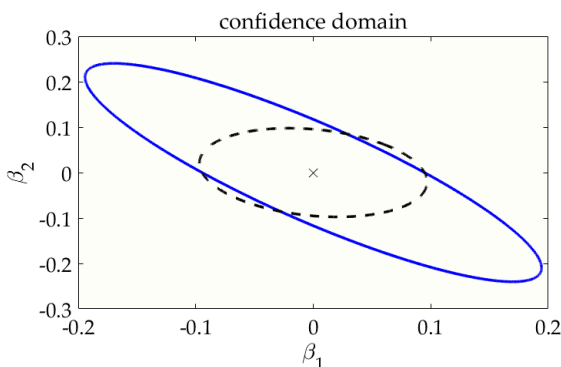
Figure 2d: Confidence domain – point A_4.

Figure 3a, b presents results for the estimates of object characteristics using a two-stage regression model described above, for different numbers of measured parameters.

The confidence ellipse sets domain outside which the true coordinates lie with a probability smaller than 5 %.

As expected, the estimates of characteristics becomes better as the number of second stage parameters increases. Unfortunately, a larger number of connected measurements does not guarantee unbiased estimates of object characteristics.
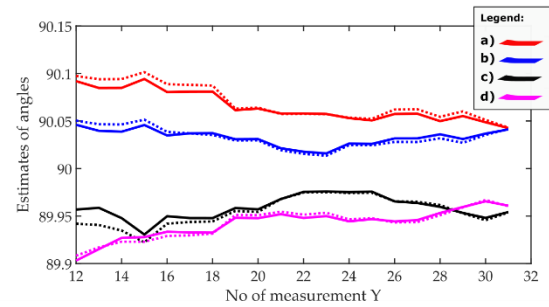
Figure 3a: Dependency of angle estimates on second stage uncertainty.
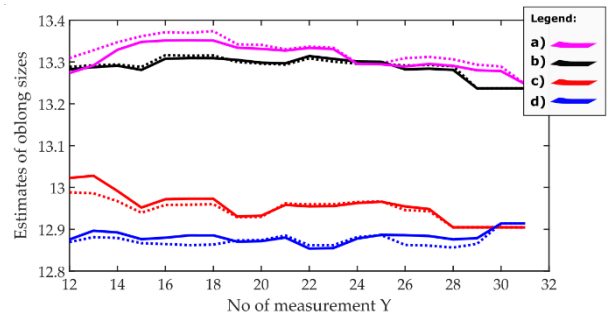
Figure 3b: Dependency of size estimates on second stage uncertainty.
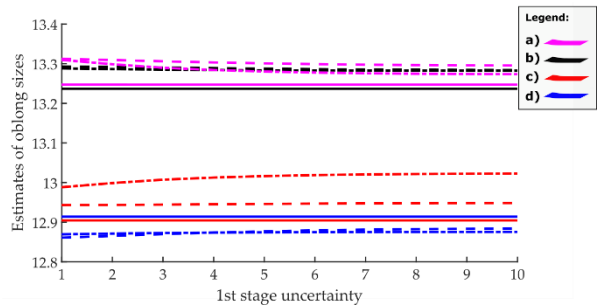
Figure 4a: Dependency of angles estimates on first stage uncertainty.

Figure 4b: Dependency of sizes estimates on first stage uncertainty.

When the increasing second stage parameters are used, the estimates of object sizes and angles are shown in Fig. 3a and 3b.

Statistical analysis for the estimates of sizes and angles of an object yields the 3D graph in Fig. 5a,b. The trend toward an oblong object with sizes 12.95 m and 13.10 m is evident.

Figure 5a: 1st angle dependency of estimates on No of experiment and No of measurement.

Figure 5b: 1st size dependency of estimates on No of experiment and No of measurement.
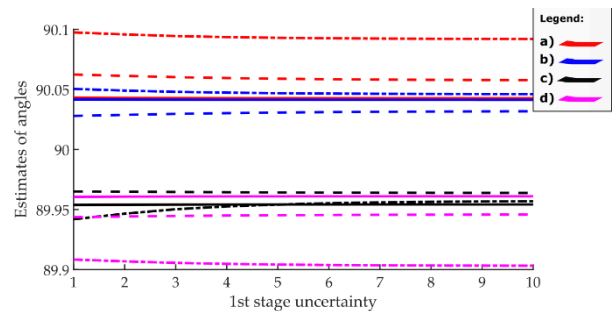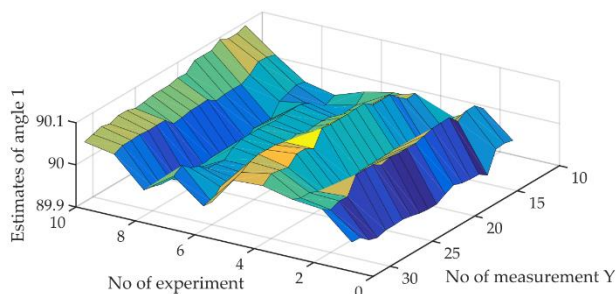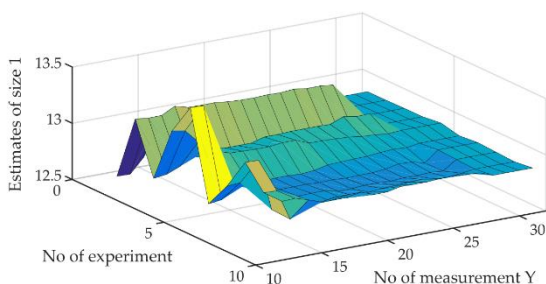
Results obtained from the studied model does not provide a constraint on inner geometry of a new object. In (Marek, 2015) is given another solution that respects such constraints based on rotation.

3. CONCLUSION

Numerical studies show how metrological uncertainty of government points and the increasing number of measured angles, change the inner geometry of a rectangular object. Results demonstrate that standard estimators can make non-admissible changes in the geometry of a new object. If the accuracy of coordinates of the existing network, which we connect to, is higher or equal to the accuracy of measurement of angles being connected, then the ordinary squares method is appropriate.

If uncertainty of existing networks is smaller, then the method can give bad estimators.

REFERENCES

Alexandersson A., 2004. Graphical confidence ellipses: An update of ellip for Stata 8. The Stata Journal 4 (3), 242-256.

Anderson J., 2013. Surveying: Theory and Practice. McGraw-Hill, New York. ISBN: 978-1259025648 ISBN: 978-1259025648.

Kubáček L., 1993. Two stage regression models with constraints. Math. Slovaca 43, 643-658.

Kubáček L., Kubáčková, L., Tesaříková, E., Marek, J., 1998. How the design of an experiment influences the nonsensitiveness regions in models with variance components. Applications of Mathematics 43 (6), 439-460.

Kubáček L., Kubáčková L., Volaufová J., 1995. Statistical models with linear structures. Veda, Bratislava.

Kubáček L., Marek J., 2005. Partial optimum estimator in two stage regression model with constraints and a problem of equivalence. Mathematica Slovaca 55 (4), 477–494.

Kubáček L., 2013. Statistical theory of geodetical networks. Academia, Praha. ISBN: 978-80-85881-31-8.

Kubáčková L., 1996. Joint confidence and threshold ellipsoids in regression models. Tatra Mountains 7, 157-160.

Korbašová J., Marek J., 2004. Connecting measurements in surveying and its problems. Proceedings of INGEO 2004 and FIG Regional Central and Eastern European Conference on Engineering Surveying, November 11-13, Bratislava (Slovakia).

Marek, J., Heckenbergerová, J., 2014. Heuristics and H-optimum Estimators in a Model with Type-I Constraints. In: Kromer, Pavel, Abraham, Ajith, Snášel, Václav (eds.). Proceedings of the Fifth International Conference on Innovations in Bio-Inspired Computing and Applications IBICA 2014. New York: Springer, 33-42. ISBN 978-3-319-08155-7.

Marek J., Kubáček L., 2015. Transformation problem with different uncertainty of measured data. Journal of applied geodesy 9 (4), 207–212.

Neitzel F., 2010. Generalization of total least-squares on example of unweighted and weighted 2D similarity transformation, J Geod 84,751–762.

Uren J., Price W. F., 2010. Surveying for Engineers. Palgrave, London. ISBN: 978–0–230–22157–4.

FUZZY ADAPTATION OF INTELLIGENT CONTROL FOR SOLAR THERMAL POWER PLANTS

Esko K. Juuso

Control Engineering, Faculty of Technology, FI-90014 University of
Oulu, Finland

Email esko.juuso@oulu.fi

ABSTRACT

Solar power plants can collect efficiently thermal energy in varying operating conditions by using linguistic equation (LE) controllers which extend the operation to varying cloudy and even heavy cloudy conditions and handle efficiently disturbances in energy demand in a wide operating range. The new solution includes advanced temperature control, working point based supervisory control and new fuzzy adaptation systems. The smooth operation in the allowed temperature range, including difficult situations, is extended to situations where the oscillation risks are so low that the working point area can be extended to use higher temperatures to optimize the energy collection. This has already been tested at the collector field in short periods in special cases where the working point was changed manually. Temporal reasoning is used for detecting early the changes of operating conditions. The new fuzzy approach introduces an additional level where also the working point is automatically constrained.

Keywords: solar energy, fuzzy logic, intelligent control, nonlinear systems, adaptation, linguistic equations.

1. INTRODUCTION

Solar power energy in a usable form at the desired temperature range in spite of changes in atmospheric conditions, e.g. cloud cover, humidity, and air transparency. The irradiation depends strongly on seasonal and daily cyclic variations. Fast and reliable operation in varying conditions is important (Camacho, Berenguel and Rubio 1997; Juuso 1999; Camacho Berenguel, Rubio and Martinez 2012).

Advanced control techniques and accurate mathematical models are needed to improve the overall solar plant efficiency. Gallego, Yebra, Camancho and Sánchez (2016) present the mathematical modeling of the new TCP-100 parabolic trough collector (PTC) research facility at the Plataforma Solar de Almería (PSA). The first commercial trough plants were commissioned between 1985 and 1990 in California. Several plants have been commissioned in Spain and Arizona (Camacho and Gallego 2013).

One of the first experimental solar trough plants was the solar field Acurex at the PSA. This plant has been operating from 1980 to 2013. Various methodologies, including basic feedforward and PID schemes extended with adaptive control, model-based predictive control, frequency domain and robust optimal control and fuzzy logic control, have been tested for solar thermal collector fields (Johansen and Storaa 2002; Cirre, Berenguel, Valenzuela and Camacho 2007; Limon, Alvarado, Alamo, Ruix and Camacho 2008; Roca, Guzman, Normey-Rico, Berenguel and Yebra 2011; Ayala, Roca, Guzman, Normey-Rico, Berenguel and Yebra 2011) The operating area is extended by model-based approaches, including feedforward approaches based on the energy balance and measurements of solar irradiation and inlet temperature (Camacho, Rubio and Hughes 1992). The sun position, the field geometry, the mirror reflectivity, the solar irradiation and the inlet oil temperature are used lumped parameter models presented in (Camacho, Berenguel and Rubio 1997). Feedback controllers are needed to remove the offset of the feedforward controllers (Valenzuela and Balsa 1998) and varying time delay conditions can be handled by the classical internal model control (IMC) (Farkas and Vajk 2002). Bonilla, Yebra, Dormido and Zarza (2012) used genetic algorithms for multiobjective tuning.

Dynamical mathematical models for the parabolic trough systems have been developed during past years (Carmona 1985; Yilmaz and Soylemez 2014). More precise and complex models trough plants with direct vapor generation are described in (Bonilla, Yebra, and Dormido 2011; Bonilla, Yebra, Dormido and Zarza 2012; Bonilla 2013).

Linguistic equation (LE) controllers are compact solutions which use intelligent analysers together with model-based adaptation and feedforward features. The controller presented in (Juuso and Valenzuela 2003) already used these to define the actual setpoints of the temperature. The manual adjustment of the working point limit improved the operation considerably. Parameters of the LE controllers can be tuned with neural networks and genetic algorithms. Genetic algorithms combined with model-based predictive control have further reduced temperature differences between collector loops (Juuso 2006). The data-driven scaling approach based on generalised norms (Juuso and Lahdelma 2010) suits for a recursive analysis (Juuso 2011).

In practical applications, the smart adaptation requires the detection of the operating conditions. The fluctuation indicator introduced by Juuso (2012) detects cloudy conditions and other oscillatory situations by analyzing fluctuations of irradiation, temperature and oil flow. The smart LE control includes advanced model-based LE control (Juuso and Yebra 2013a) and intelligent analyzers (Juuso and Yebra 2013b). The working point is highly important in varying operating (Juuso 2017) and the temporal analysis provides additional tools for the early detection of changes in the operating conditions (Juuso 2018).

The parabolic trough collectors track the sun, and the corrected irradiation and the solar hour are calculated by using the standard meridian for the local time and the longitude of the location in degrees (Osterholm and Palsson, 2014; Blanco and Santigosa, 2017).

This paper presents fuzzy solutions for adapting the LE controller in changing operating conditions at the Acurex Solar Collectors Field of the PSA in Spain. Operating conditions are summarized in Section 2. Section 3 focuses on the possibilities of the fuzzy adaptation in the decision making. Section 4 summarizes the overall system. Conclusions and future research are presented in Section 5.

2. OPERATING CONDITIONS
The fuzzy solution is tested in different operating conditions collected from the results of the six-day test campaign at the Acurex collector field (Figure 1). The energy collection is modified by adjusting the oil flow in changing irradiation conditions defined by the irradiation (Figure 2).

2.1. Irradiation
The corrected irradiation is every day increasing in the morning until the solar noon and decreases after that (Figure 1(a)). There are daily differences because of atmospheric conditions and disturbances are introduced by cloudiness. This period of six days covers several typical situations. The irradiation levels are rather low when compared with the clearest days at PSA. Therefore, the period is very suitable for adapting the solutions to seasonal and local variations.

2.2. Working point
The normal behaviour of the solar collector field corresponds to $wp = 0$, where the irradiation I_{eff} and the temperature difference, T_{diff}, are on the same level. The operation is smooth throughout the day if there are no difficult cloudy conditions, e.g. during the first two days, the setpoints are limited by this working point value $wp = 0$ with very slight modifications caused small oscillations (Figure 1(b)), i.e. T_{diff} can be lower if a lower setpoint is selected manually. The oil flow becomes very high if the setpoint is very low in the high irradiation conditions. The flows around above 8 l/s are not optimal (Figure 1(c)).

A high working point (wp > 0) means low T_{diff} compared with the irradiation level I_{diff}. Oscillatory

periods can be stopped by setting e.g. ($wp_{min} = 1$). A fluctuation indicator is used to modify the working point to avoid heavy oscillations in cloudy conditions. In Figure 1(a), there are four such periods, where the working point is increased, even close to Level 2 in some cases. This means that the allowable range of wp is very narrow and hardly any temperature increase is achieved at the field (Figure 1(d)), e.g. in the afternoon of Day 4, the field is kept ready to start operation if the situation improves.

The normal operation defines the default lower limit, i.e. $wp = 0$. However, even lower working points are possible: $wp < 0$ means that T_{diff} is high compared with the irradiation level I_{diff}. Negative wp values can be used in good operating conditions when there are not any severe oscillatory behaviour in the irradiation or load disturbances. During the test campaign, this was tested during last two days (Figure 1(b)). The temperature levels were quite similar to the levels on the first two days where the irradiation was on slightly higher levels. In this case, the high temperatures were achieved by using the lower oil flow allowed by the wp.

These wp values are used as lower limits of the allowable range. The upper limit always +2 and higher wp levels can be used simply by using lower setpoints of T_{out}. The lower wp limit can activate any time and reduce the setpoint if needed.
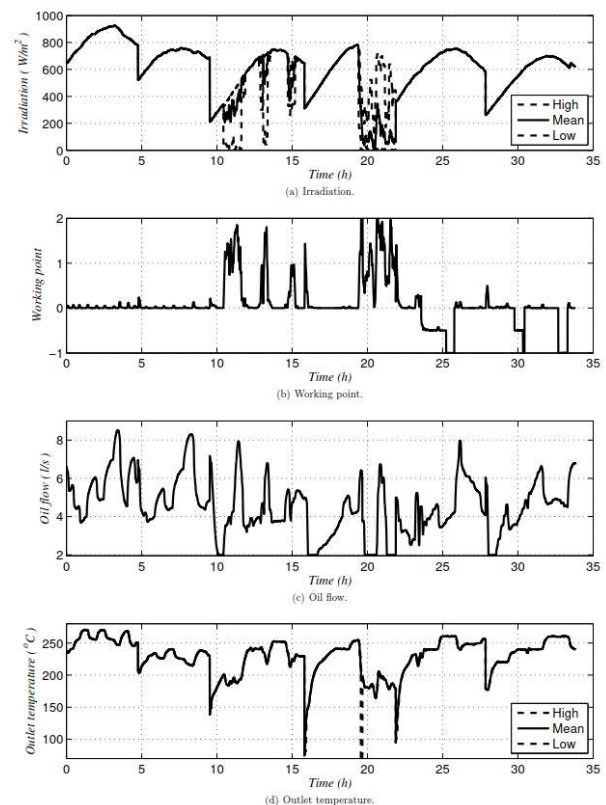

Figure 1: Results of the LE controller on a six-day test campaign, combined from (Juuso and Yebra 2014)

2.3. Temporal analysis

The nonlinear scaling makes the temporal analysis available to all measurements and features: trend indices are calculated by comparing the averages of the scaled values in the long and short time windows, a weighted sum of the trend index and its derivative is used in detecting the trend episodes and severity of the trend is estimated by including also the variable level in the sum. The trend index, trend episodes and especially, the deviation index reveal evolving changes in the operating conditions, including cloudiness and load disturbances. All variables, features and indices are transformed to the range [-2, 2] and represented in natural language which is important in integrating data-driven solutions with domain expertise. (Juuso, 2018)

The fluctuations are evaluated as the difference of the high and the low values as a difference of two moving generalized norms:

$$\Delta x_j^F(k) = \left\| {}^{K_s\tau} M_j^{p_H} \right\|_{p_H} - \left\| {}^{K_s\tau} M_j^{p_L} \right\|_{p_L}, \qquad (1)$$

where the orders p_H and p_L are large positive and negative real numbers, respectively. The norms are calculated from the latest $K_S + 1$ values, and an average of several latest values of   is used as the feature of fluctuation (Juuso 2012). The method is easy to calculate and more robust than the difference between the actual maximum and minimum. The fluctuation indices are calculated from features (1) by the nonlinear scaling.

For any variable x_j, a trend index $I_j^T(k)$ is calculated from the scaled values with

$$I_j^T(k) = w_j \left[\frac{1}{(n_S)_j + 1} \sum_{i=k-(n_S)_j}^{k} X_j(k) - \frac{1}{(n_L)_j + 1} \sum_{i=k-(n_L)_j}^{k} X_j(k) \right], \qquad (2)$$

which is based on the means obtained for a short and a long time period, defined by delays $(n_S)_j$ and $(n_L)_j$, respectively. The weight w_j is variable specific.

Severity of the situation can be evaluated by a deviation index $I_D(k)$ which combines three indices: the scaled value, trend index and the change of the trend index (Juuso, 2018).

2.4. Power collection

In the collector field, the outlet temperature increases with the irradiation, which is the highest close to the solar noon (Figure 2). The outlet temperature has a safety limit 295 ℃ and the temperature difference is limited to 100 ℃ to keep the collector field in good conditions. These constraints cut operating area which is realized by limiting the working point wp.

As the inlet temperature often increases slightly during the day, there is a possibility to use even higher outlet temperatures. The temperatures increase with decreasing oil flow, which can be controlled smoothly in a wide range, $2 - 10$ l/s. However, the power collection starts to decrease if the oil flow is too low (Figure 2). The maximum collected power is achieved when the oil flow is close to 6 l/s.

A trade-off of the temperature and the flow is needed to achieve a good level for the collected power. The allowed power levels depend on the irradiation. The power surface is highly nonlinear because of the properties of the oil (Figure 2).
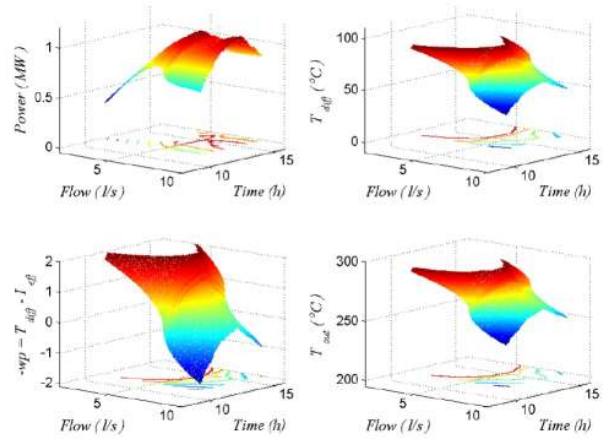
Figure 2: Operating area of the field on a clear day: (a) *power*, (b) T_{diff}, (c) *wp*, (d) T_{out} (Juuso, 2017)

3. FUZZY DECISION MAKING

The present multilevel LE control operates well in varying operating conditions: the risky situations are avoided well. The fuzzy system modifies this by using levels of irradiation, flow, temperature and the energy demand. The fuzzy adaptation is only needed to decide preferable temperatures or power. The optimization can allow wide ranges for all variables (Figure 2).

3.1. Temperature control

The oil flow is the manipulated variable whose value is kept within the range 4 . . . 8 l/s in the normal operation (Figure 1). Lower flows are needed in the startup and heavy cloudy conditions. The first two days, which were aimed at the setpoint tracking, have both low and high flows which are seen as increasing and decreasing outlet temperatures, correspondingly. In this system, the flow can be changed by changing the setpoint of T_{out} or the working point limit which limits the available range of the setpoint.

3.2. Supervisory control

The setpoint of the outlet temperature is limited by choosing the working point limit *wp*. The operation range is controlled by changing the working point (Figure 1(b)): the normal range is [0, 2]. The low working points result oscillations if the changes of control are too large compared with the level of oil flow. This situation, which is typical during the startup, can be avoided by keeping *wp* positive. The normal limit *wp = 0* operates well in the startup as can be seen in Figure 3. The disturbance of the inlet temperature is compensated fast. Startup is needed every day as can be seen in Figure 1.

The fluctuations indicator is highly important for cloudy conditions and other oscillatory situations. The working point changes reduce the reference value T_{ref}. The operation returns to the normal when recovering from the cloudiness (Figure 4). *Day 4* had a long cloudy period (Figure 1). The periods of improvement were very short and not sufficient for higher reference values.
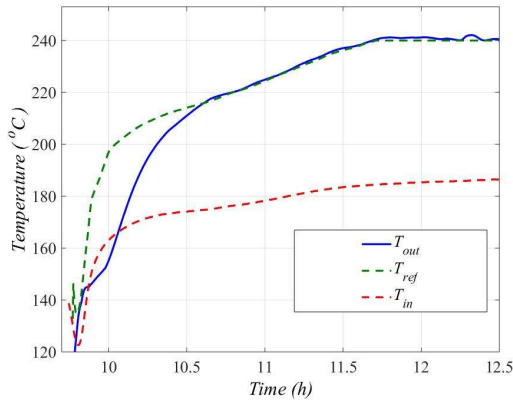

Figure 3: Outlet temperature in the startup of *Day 4*.

3.3. Fuzzy adaptation

Fuzzy corrections of the working point are aimed for getting the oil flow close to 6 *l/s* by increasing or decreasing the working point limit *wp*. In this way, the disturbances to the operation are minimized since the adaptation and detection of harmful situations are kept in operation.
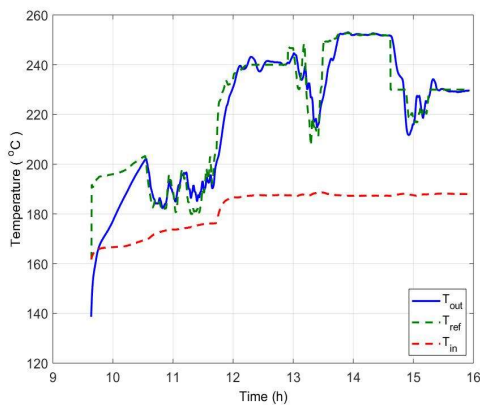

Figure 4: Outlet temperature on cloudy conditions (Juuso and Yebra, 2013b).

The recovering from cloudy conditions results high oil flows when the controller prevents high increases of T_{out} when the irradiation fluctuations are heavy, e.g. the oil flow goes up to 8 *l/s* at the end of the first cloudy period in *Day 3* (Figure 1(c)). The same effect is seen during two shorter periods on the same day.

The increase in the irradiation, oil flow and temperature are easily detected with the trend analysis (Juuso, 2018). In the trend analysis of the fluctuation index, the recovery of the irradiation is detected faster in

the deviation index $I_D (k)$ than in the fluctuation index $X(k)$ (Figure 5).

The improvements of the irradiation conditions would permit the fuzzy system to allow lower working point values, i.e. *wp* goes closer to zero. This would result a faster increase of the temperature. The fluctuation indicator is all the time used for detecting if the heavy irradiation disturbances continue, e.g. the increase stops and the oil flow went to minimum on *Day 4* when the cloudiness continued.
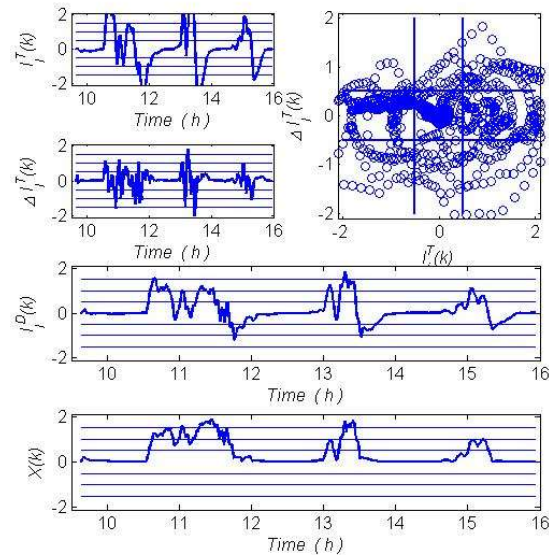
Figure 5: Trend analysis of total fluctuations in cloudy operating conditions, *Day 3* (Juuso, 2018)

The default working point limit, *wp =0*, operated well for the startup on every test day, also during the early startups on *Days 4* and *5*. Around the solar noon on *Days 1* and *2*, the high flows (Figure 1(c)) resulted when the temperature was kept lower than the working point requires (Figure 1(d)). The same situation was on *Day 4* (Figure 3).

For high irradiation, the negative values of the working point help to reach and keep high temperatures, e.g. on *Days 5* and *6*, the outlet temperature on *Days 5* and *6* are close to the levels seen on *Day 1* (Figure 1(d)) although the irradiation is lower (Figure 1(a)). On *Day 4*, the increase was stopped by the cloudy period. The oil flow in the feasible range. On *Day 5*, the outlet temperature increased 20 degrees but by reducing the oil flow by 1 *l/s*.

In the afternoons, the irradiation decrease results a decreasing temperature if the working point is kept constant. The outlet temperature can be kept high longer by using negative *wp*s although the irradiation is lower and decreases further as can be seen on *Days 5* and *6* (Figure 1). Moving back to *wp = 0* introduced a high peak for the oil flow.

On *Day 5*, a considerable load disturbance of the inlet temperature introduced oscillations for the outlet. Effects were reduced by using slight changes in the working point limit (Figure 6). The operation continued

with a constant reference value. Smooth operation was achieved after moving to $wp = -\frac{1}{2}$. Reference values 235 ^oC was too low, a higher level 250 ^oC was achieved and finally, even higher temperatures were achieved when the working point limit was lowered to -1.

Predictive negative wp values were reduced efficiently the oscillations on *Day 6*. The set point tracking was done highly accurately for all the reference values defined either manually or by the working point limit.

Figure 6: Outlet temperature close to the solar noon.

4. DISCUSSIONS

During the test campaign, the working point limits were defined manually. The tests confirmed that the negative working point limits can be used on clear periods.

For the fuzzy system, there are two alternative goals: (1) maximal energy collection and (2) maximal outlet temperature. The fuzzy system is aimed for h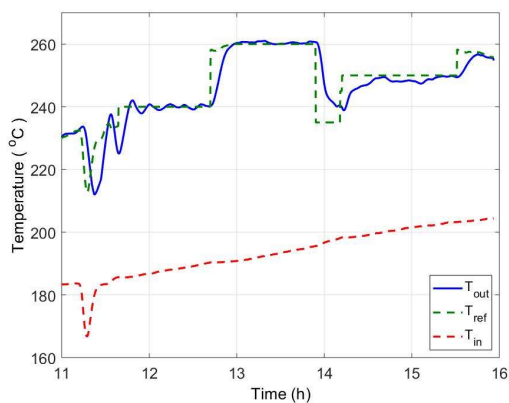andling the part which is in the current system done manually. The negative working point values can be taken into use only if the field is operating smoothly, i.e. fast increasing or decreasing is stopped and there are no severe fluctuations.

The recovering from cloudy conditions is accepted on the basis of the temporal analysis. The fluctuation indicator is highly important in these cases.

The Acurex field is not any more available. The development continues with the simulation models and the implementation of the extended LE control system is planned for the new TCP-100 parabolic trough collector (PTC) research facility.

5. CONCLUSIONS

The fuzzy adaptation solution opens additional possibilities to the decision making by extending the smart working point control. The operation is kept smooth by limiting the allowed temperature range in difficult situations. The new fuzzy extension moves the collector system to more efficient operation and finds the situations where the oscillation risks are so low that the working point area can be extended to use higher temperatures to optimize the energy collection. The short period tests at the collector field support these new developments. The new fuzzy approach introduces an additional level to automatically constrain the working

point. The research continues with simulation models and implementation for the new collector field.

REFERENCES

Ayala C.O., Roca L., Guzman J.L., Normey-Rico J.E., Berenguel M., and Yebra L., 2011. Local model predictive controller in a solar desalination plant collector field. Renewable Energy, 36, 3001–3012. doi:10.1016/j.renene.2011.03.037.

Blanco M.J. and Santigosa L.R., 2017. Advances in concentrating solar thermal research and Technology. Elselvier. doi:978-0-08-100517-0.

Bonilla J., 2013. Modeling of Two-phase Flow Evaporators for Parabolic-Trough Solar Thermal Power Plants. PhD thesis, University of Almería, 2013.

Bonilla J., Yebra L.J., and Dormido S., 2011. A heuristic method to minimise the chattering problem in dynamic mathematical two-phase flow models. Mathematical and Computer Modelling, 54(5-6), 1549–1560.

Bonilla J., Yebra L.J., Dormido S., and Zarza E., 2012. Parabolic-trough solar thermal power plant simulation scheme, multi-objective genetic algorithm calibration and validation. Solar Energy, 86, 531–540. doi: 10.1016/j.solener.2011.10.025.

Camacho E., Berenguel M., and Rubio F.R., 1997. Adaptive Control of Solar Plants. Springer, London.

Camacho E.F., Berenguel M., Rubio F.R., and Martinez D., 2012. Control of Solar Energy Systems. Advances in Industrial Control. Springer, London.

Camacho E.F. and A. J. Gallego A.J., 2013. Optimal operation in solar trough plants: a case study. Solar Energy, 95, 106–117.

Camacho E., Rubio F., and Hughes F., 1992. Self-tuning control of a solar power plant with a distributed collector field. IEEE System Control Magazine, 12(2), 72–78.

Carmona R., 1985. Análisis, Modelado y control de un campo de colectores solares distribuidos con sistema de seguimiento en un eje. PhD thesis, Universidad de Sevilla.

Cirre C.M., Berenguel M., Valenzuela L., and Camacho E., 2007. Feedback linearization control for a distributed solar collector field. Control engineering Practice, 15, 1533–1544.
doi: 10.1016/j.conengprac.2007.03.002.

Farkas I. and Vajk I., 2002. Internal model-based controller for a solar plant. Proceedings of the 15th Triennial World Congress, pp. 49-54, Barcelona, Spain, July 21-26, IFAC. http://www.ifac-papersonline.net/.

Gallego A.J., Yebra L.J., Camancho E.F., and Sánchez A.J., 2018. Mathematical Modeling of the Parabolic

Trough Collector Field of the TCP-100 Research Plant. Proceedings of 9th EUROSIM Congress on Modelling and Simulation (EUROSIM 2016) and 57th SIMS Conferenceon Simulation and Modelling (SIMS 2016), pp. 912-918. Linköping Electronic Conference Proceedings, No. 142.

Johansen T.A. and Storaa C., 2002. Energy-based control of a distributed solar collector field. Automatica, 38, 1191–1199.

Juuso E. and Lahdelma S., 2010. Intelligent scaling of features in fault diagnosis. In 7th International Conference on Condition Monitoring and Machinery Failure Prevention Technologies, CM 2010 - MFPT 2010, pp. 1358–1372, 22-24 June, Stratford-upon-Avon, UK, volume 2. URL www.scopus.com.

Juuso E.K., 1999. Fuzzy control in process industry: The linguistic equation approach. In H.B. Verbruggen, H.J. Zimmermann, and R. Babuška (eds.), Fuzzy Algorithms for Control, International Series in Intelligent Technologies, volume 14 of International Series in Intelligent Technologies, 243–300. Kluwer, Boston. doi: 10.1007/978-94-011-4405-6 10.

Juuso E.K., 2006. Modelling and simulation in development and tuning of intelligent controllers. Proceedings of 5th Vienna Symposium on Mathematical Modelling, February 8-10, 2006, Vienna, Austria, Argesim Report 30, 6–1 – 10. Argesin Verlag, Vienna. ISBN 3-901608-30-3.

Juuso E.K., 2011. Recursive tuning of intelligent controllers of solar collector fields in changing operating conditions. Proceedings of the 18th World Congress The International Federation of Automatic Control, pp. 12282–12288. August 28 - September 2, Milano (Italy), IFAC. doi:10.3182/20110828-6-IT-1002.03621.

Juuso E.K., 2012. Model-based adaptation of intelligent controllers of solar collector fields. Proceedings of 7th Vienna Symposium on Mathematical Modelling, Part 1, volume 7, pp. 979–984. February 14-17, Vienna, Austria, IFAC. doi:10.3182/20120215-3-AT-3016.00173.

Juuso E.K., 2017. Intelligent control of a solar thermal power plant-adaption in varying conditions. Journal of Automation and Control Engineering, 5, 26–30. doi: 10.18178/joace.5.1.26-30.

Juuso E.K., 2018. Intelligent trend analysis for a solar thermal energy collector field. IOP Conference Series: Earth and Environmental Science, 136(1), 012007. doi: 10.1088/1755-1315/136/1/012007.

Juuso E.K. and Valenzuela L., 2003. Adaptive intelligent control of a solar collector field. In Proceedings of Eunite 2003 - European Symposium on Intelligent Technologies, Hybrid Systems and their implementation on Smart Adaptive Systems, pp. 26–35. July 10-11, Oulu, Finland. Wissenschaftsverlag Mainz, Aachen.

Juuso E.K. and Yebra L.J., 2013a. Model-based intelligent control of a solar energy collector field.

Proceedings - 8th EUROSIM Congress on Modelling and Simulation, EUROSIM 2013, pp. 513–518. 10-13 September, Cardiff, UK,. doi:10.1109/EUROSIM.2013.92.

Juuso E.K. and Yebra L.J., 2013b. Optimisation of solar energy collection with smart adaptive control. IECON Proceedings, pp. 7938–7943 (Industrial Electronics Conference). 10-14 November, Vienna, Austria. doi:10.1109/IECON.2013.6700459.

Juuso E.K. and Yebra L.J., 2014. Smart adaptive control of a solar collector field. IFAC-PapersOnline, 19, 2564–2569.

Limon D., Alvarado I., Alamo T., Ruiz M., and Camacho E.F., 2008. Robust control of the distributed solar collector field ACUREX using MPC for tracking. Proceedings of 17th IFAC World Congress, Seoul, Korea, July 6-11, 2008, volume 17, 958–963. IFAC. http://www.ifac-papersonline.net/.

Osterholm R. and Palsson J., 2014. Dynamic modelling of a parabolic trough solar power plant. Proceedings of the 10th International Modelica Conference. March 10-12, Lund, Sweden.

Roca L., Guzman J.L., Normey-Rico J.E., Berenguel M., and Yebra L., 2011. Filtered smith predictor with feedback linearization and constraints handling applied to a solar collector field. Solar Energy, 85, 1056–1067. doi: 10.1016/j.solener.2011.02.026.

Valenzuela L. and Balsa P., 1998. Series and parallel feedforward control schemes to regulate the operation of a solar collector field. Proceedings of the 2nd User Workshop Training and Mobility of Researchers Programme at Plataforma Solar de Almeria, pp. 19-24. November 10-11. Ciemat.

Yilmaz I.H. and Soylemez M.S., 2014. Thermo-mathematical modeling of parabolic trough collector. Energy Conversion and Management, 88, 768–784.

AUTHORS BIOGRAPHY

Esko Juuso has D.Sc.Tech. on Control and Systems Engineering at the University of Oulu and M.Sc. in Technical Physics at the same university. He has earlier worked as research engineer and process computer analyst in metal industry. Currently, he is a team leader and a project manager of several research projects on intelligent systems applications. The fields of industry include energy, water, bioprocesses, pharmaceuticals, pulp and paper, steel and mining. Dr. Juuso has developed the linguistic equation (LE) approach and the nonlinear scaling methodology, which is currently used in various applications. His research interests are in the modelling and control of industrial processes with a special emphasis on combining intelligent control, fault diagnosis and performance monitoring into smart adaptive systems. Dr. Juuso has been the President of EUROSIM 2013-2016 and he is currently the member of the Executive Board of EUROSIM, ISCM Fellow and the Management Board of ISCM.

WEB-BASED OPTIMIZATION WITH JAVASCRIPT FRAMEWORKS AND A GRAPHQL-API-INTERFACE

Yu Xingyue [a], Thomas Wiedemann [b], Wilfried Krug [c]

[a],[b] University of applied Science Dresden (Germany)
and [a] Zhejiang University of Science and Technology Hangzhou (China)
[c] Dualis IT Solution GmbH (Germany)

[a]YuXingyue@outlook.com, [b]wiedem@informatik.htw-dresden.de, [c]WKrug@dualis-it.de

ABSTRACT

There is a quiet revolution in the IT-area. Nearly all new web sites are realized as so called single page web apps with a desktop-like user interaction. The server side is also changing: instead of using hundreds of traditional web-servers in expansive server farms, only one powerful server based on NodeJS is used. The secret behind this global development is the powerful JavaScript engine called V8 by Google. It improves the JavaScript performance and allows up to 1 Million parallel running requests on the same machine.

This paper analyses the options for using this multitasking power for building web based optimizations. The first realized option is a complete client side optimization environment especially for testing and teaching purposes. The second option is a distributed client-server web environment with the new GraphQL interface for a very flexible and powerful optimization API for any simulation or universal application. The optimization methods are based on the well-known ISSOP (Intelligent System for Simulation and Optimization) desktop optimizer with about 7 different, parallel running optimization strategies.
Keywords: optimization, JavaScript, GraphQL

1. INTRODUCTION

The web community is seeing a dramatic change: nearly all web companies focus on the new JavaScript (JS) options in the browser and on the server, and develop new JS-frameworks for all needs like visualization, data handling and 3D-design. The first time in web history there is no programming break between the browser client and the server. By using the JS-framework NodeJS JavaScript-code is implemented both on the browser and the client (NodeJs 2016). So there is just one code base for both sides.
We also see big advantages for using this general JavaScript-based approach for simulation and optimization. A first paper published in 2016 already showed the usage of NodeJS for simulation (Wiedemann 2016). This paper will now show the implementation of two different system architectures for optimization with only one piece of code for the central optimization module.

2. INTRODUCTION IN OPTIMIZATION WITH HEURISTIC METHODS

In general, common mathematical approaches are not often applicable for practical optimization tasks – the restrictions are too complex and the search takes too long for all the value combinations. As a result, some specialized optimization methods have been developed over the last 4 decades (Krug 2002). They are also applicable for simulations based optimizations, where no mathematical function exists, but only a large amount of result points from simulation experiments. The following list of optimization methods is ranked in order of usage frequency in practical optimizations.

2.1 Genetic algorithm

A genetic Algorithm is a computational model that simulates the natural selection and genetic mechanism of Darwin's Theory of Evolution. It is a method of searching for optimal solutions by simulating natural evolutionary processes.
Genetic algorithms are implemented by relying on bio-inspired operators such as selection, crossover and mutation. First, an initial population will be generated, after the generation of the initial population, according to the principle of survival of the fittest, the selection will be performed on the base of the fitness of the individuals in the problem domain. Then, repeating the crossovers and mutations, new populations are generated and better and better solutions will be found in each evolution process. The algorithm terminates when no better significant improvement can be found.

2.2 Gradient method

The gradient method is a deterministic method which finds the optimal solution by iteration. The iteration starts with a random point in the search area. Around this starting point a set of neighboring points with a given search step is generated. For each new point the difference in the goal function value, compared to the starting point is, calculated and the point with the minimum is selected as new starting point.

The method continues this procedure until no significant improvement can be found. It must be remarked that this methods will stop on local optimums, so multiple starts with randomly generated starting points are recommended.

2.3 Monte Carlo

The Monte Carlo method is a stochastic search method which continuously generates a number of random points within a predefined search area, in which a certain percent of points will be selected by the value of the goal function. Then a new, narrower search area is defined by the selected points and the methods repeats, until no significant improvement can be found.

2.4 Common optimization scenarios

The speed and quality of the optimizations depend heavily on the type of the (n+1–dimensional) surface, defined by the n-input parameters and the goal function as the n+1. dimension. It is well known that all types of gradient-like methods will work very fast and efficient on (soft) convex surfaces, but they will fail on concave surfaces by stopping on the first sub-optimum. All methods with integrated stochastic components, like Monte Carlo with a pure random approach or the Genetic method with a more "intelligent" approach of randomness, can find a global optimum also on multiple concave surfaces, but of course, there is no guarantee. . Because the type of the search space is not known in advance in practical applications, it is a very good idea from Krug (Krug 2002) to start all available methods (in the case of the ISSOP – optimization system there are 7 methods, but this number is not limited) and to compare the results and to give more time to successful methods. Supported by an advanced analysis framework (in (Krug 2002) defined as learning approach) the speed and quality of optimizations can be improved significantly. It is one goal of this paper to migrate this approach to the new JavaScript world.

3. THE SYSTEM ARCHITECTURE OF THE BROWSER OPTIMIZATION APPLICATION

The first example of a JavaScript (JS) based optimization app is a complete client side optimization environment, especially for testing and teaching purposes. The main architecture is simple: it consists of an optimization calculation kernel and a user interface (GUI) (see fig. 1), both programmed with JavaScript.

In order to ensure an efficient management of the two applications architectures (single browser vs. distributed client-server (see chapter 7) the program is divided in a user interface and the code for optimization itself. Both modules communicate by calling normal JavaScript functions.
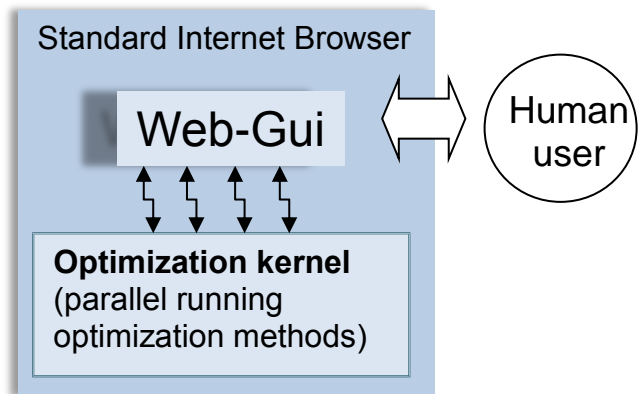
Figure 1: Client side optimization app architecture

The main goal of this first JS-based optimization app is to teach and demonstrate heuristic optimization. Because all methods are running inside a standard web-browser - no installation is necessary – it is an "open link and use" application.

One disadvantage of this approach is the full visibility of all the JS-code. So far, there is no way to secure parts of JS-Code inside a browser against reading and modifying (there is some option like obfuscation (see (Obfuscator 2018) for details), but this is only an attempt to change the syntax of the code – the algorithm itself stays visible and an experienced JS-programmer can rebuild the original code. In the case of the optimization-Web-GUI this problem of visible JS-code is not relevant. Students and other users are encouraged to analyze and possibly improve the code on their own if they are interested.

The actual version of the optimization app is programmed for an n-dimensional search space, where n is not limited to some value. In contrast to the unlimited number of search dimensions, the GUI is actually limited to 5 dimensions, because for each dimension some parameter fields and buttons are necessary and the GUI is of course limited in screen size. But it is very easy to extend the actual GUI to n=>10 or more if necessary, but for testing and teaching purposes n=5 seems enough.
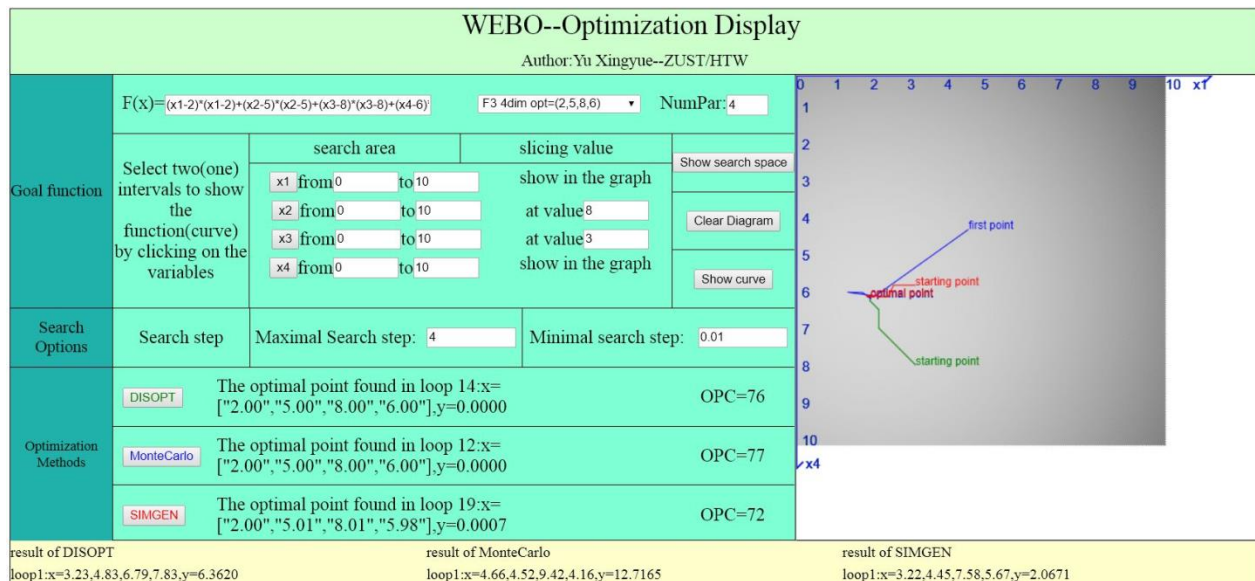
Figure 2: The user interface of the browser-based optimizing system

The user interface is realized with well-known JavaScript frameworks like JQuery. The page is divided into four main areas:

1. Located in the first part are the goal function definition area and some special options for analyzing the goal function characteristics (see chapter 5).
2. The search space and the search options are defined in the second part.
3. Part three offers the optimization methods and some summaries about the result.
4. The fourth, lower part shows the results details for each method.

4. IMPLEMENTATION DETAILS

The already shown Graphical User Interface (GUI) is designed using HTML5 and jQuery. The three optimization methods are implemented in JavaScript and are located in one separate JS file – the optimization kernel. The specific implementations of the optimization algorithms are described in the following sub chapters.

4.1 Genetic algorithms

The algorithm starts with a set of random points, the so-called population. The function *initpopulation()* will generate the **initial population** with 60 points.
Selection and crossover are performed together, the function *cross ()* selects half of the points randomly and lets the selected points **crossover randomly** and replace the previously selected amount of points of the population.

After implementing the selection and crossover process to the population, the function *mutation ()* will be performed under a small value of probability, then the function *checkfeasible ()* will check if the point generated after the mutation is still in the search area. If yes, the new point will replace the original point, else it will not, the original point stays in the population.

Criterion of termination: Having finished the process above, a new population is generated, the function *getbestfitness ()* will get the best point in the current population, and the current best point will be compared to the points found in the last iteration. The algorithm terminates if the difference of the fitness value of these two points is less than GA_ENDCOND_MinDIFF over a longer period of generations (GA_ENDCOND_ GENCOUNT), else the algorithms continues with the new population.

4.2 Gradient method

Starting point: The algorithm starts with one random point generated in the search area. A function *getSurroundingPoint(x)* will generate the surrounding points around the starting point in each dimension. During this process, in an n-dimensional search space, n^3-1 surrounding points will be generated.
In order to improve the efficiency of the algorithm, from the second iteration, all the surrounding points will be compared to the surrounding points generated in the last iteration, to see if there are same points appeared already in the last iteration. If so, such points will be deleted, and the rest of the points are the real surrounding points.

The real surrounding points will also be checked to see if they are still in the search area after the getSurroundingPoint(x) process. The function getNextPoint () will be performed to get the best point in the current surrounding points, according to the goal value of the points. This current best point will be used as the starting point for the next iteration.

Change of the search step: To improve the efficiency of the algorithm, the search step stays the same until the difference of the goal value between the current starting point and the last starting point is less than GRA_Eps_Max (=1…5), else it will decrease by half. In order to improve the convergence speed, the search step would not go down unrestricted, if the search step becomes smaller than GRA_Eps_Max (e.g. = 0.2). When started with an inappropriate search step, there wouldn't be a new best point selected from the current surrounding points, since all the goal values of the surrounding points could be greater than the goal value of the starting point. In this case, the search step will reduce to a quarter of the original search step to keep finding the next best point. To improve the accuracy of the result, when the starting point gets very close to the globe optimal, the search step will be set to 0.01 to keep finding more accurate results.

Criterion of termination: The best point found in each iteration will be compared to the best point found in the last iteration. The algorithm terminates when the difference of the goal value of the two best points is less than GRA_Endcond_Eps (set to 0.001 in general, but depends from the tasks), else it will continue.

4.3 Monte Carlo

The algorithm starts with a set of random points, the function getpoint () will generate 50 random points in the search area.

Get the new search area: The function *Sort ()* will sort the points according to the goal values, and to get the best point. Then the function *getnextsearcharea ()* will be performed to get the new search area. First, ten points will be selected according to goal values which are the ten points with the smallest goal values. Second, these ten points will be sorted again in each dimension, and the new lower bound and upper bound of the search area in each dimension will be reset according to the values of each dimension of these ten points.

Criterion of termination: The algorithm continues with the new and smaller search area, and finds one best point in each iteration. The algorithm terminates when the difference of the goal value of the two best points is less than MC_Endcond_Eps, else it continues.

This set of optimization methods will be extended in the future by many more methods such as threshold accepting, cuboid strategy, evolution strategy and coordinate strategy, as this was already shown by the ISSOP – optimization system (Krug 2002).

5. THE OPC -EVALUATION

For determining and comparing the quality and performance of optimization methods, we discussed some options. Actually, we calculate a new, empirically defined "Optimization Performance coefficient (OPC)" by formula (1), where we combine the quality of the achieved goal function value by the number of iterations needed for this result.

$$\text{OPC} = \frac{100}{d_k^{dp} * \sqrt[np]{n_k}} \tag{1}$$

where $d_k = (R_k - R_{best}) * 2 + 1$ (2)

and where

- R_k - best result found by method k
- R_{best} - best result from all methods
- n_k - iterations needed for the terminal result$_k$
- dp - power coefficient of d_k (set to 20)
- np - power coefficient of n_k (set to 10)

It's impressive that in many cases of testing, the Monte Carlo method seems to be the most efficient one of the 3 methods, even though it is a non-intelligent randomness method without memory, compared to the much more complex Generic algorithms (see OPC values in fig. 2).

In the future, we will use the OPC coefficient for scheduling the methods in parallel: the higher the OPC was in older experiments of the same type of goal function (not only the same), the more time will be given to each method!

6. GOAL FUNCTION VISUALIZATION IN THE SEARCH SPACE

For teaching applications and for getting a first idea of an unknown goal function the web app supports two visualizations methods: a gray-shaded mapping of the goal function (see fig. 3) and a slicing of the N-dimensional search space to a 2-dimensional subset and showing slicing curves (see fig. 4).

The gray shaded background gives an impression of the goal function in the selected 2-dimensional subset. In the shown example there is a goal function with an included sinus()-component, which generates some slight fluctuations in the search space.

Of course, this visualization can also help to define the best region for searching the optimum without spending a lot of calculation time in "bad" regions.
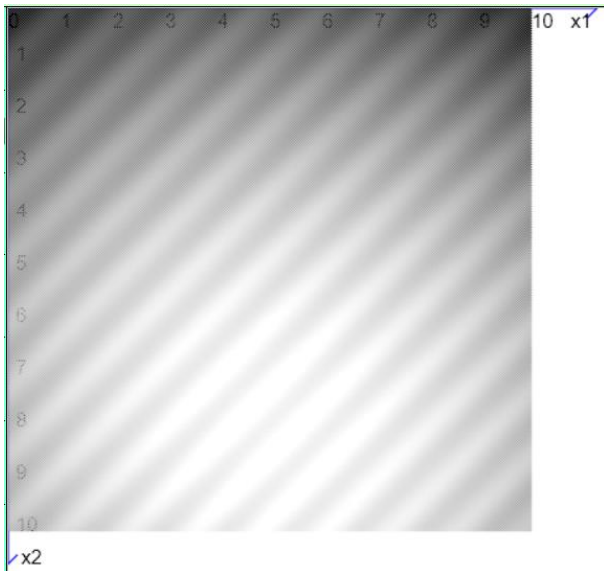
Figure 3: The gray shaped goal function area

The gray shaping is good for understanding the whole search space, but it is difficult to determine the point of the optimum by using the fine colors changes.

For this purpose, there is a second method of slicing the search space and of generating slicing curves. From this curve it is easy to graphically determine the optimum (see right side of fig. 5). This is mainly intended for getting an impression of the optimization situation in teaching situations.

In an n-dimensional case with n>3, a 2-dimensional surface is selected from the n-dimensional hyperspace by fixing n-2 dimensions by a specific value. On this extracted surface a curve can be shown, where n-1 parameters are fixed and only one parameter is changing. Because this paper is also only a 2D-approach and our world is 3D, the general approach is graphically explained in figure 4.

Of course this approach is good for understanding the situation, but as a result of fixing n-2 parameters, there are an endless number of possible curves and results, so the optimization methods are still needed for getting the global optimum with some significance.

In the GUI, the users need to select only two variables of interest and click on the "show curve" button in the Goal Function part, in order to get a visualization of the slicing curves,. The other (n-2) variables stay at the defined values and fix the dimension. Users are allowed to change the values of all variables, which could result in a set of curves. (see right part of Fig. 5).
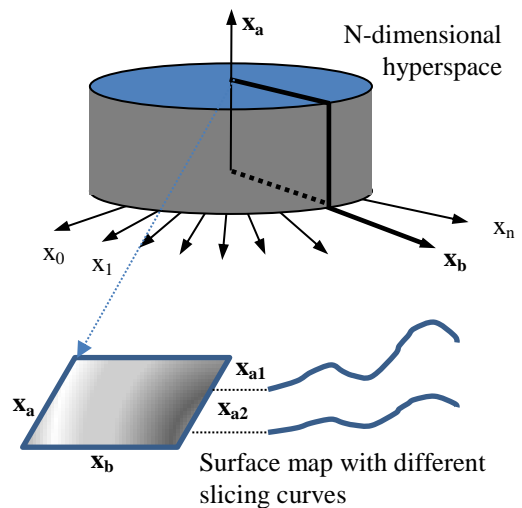
Figure 4: The N-dimensional slicing approach
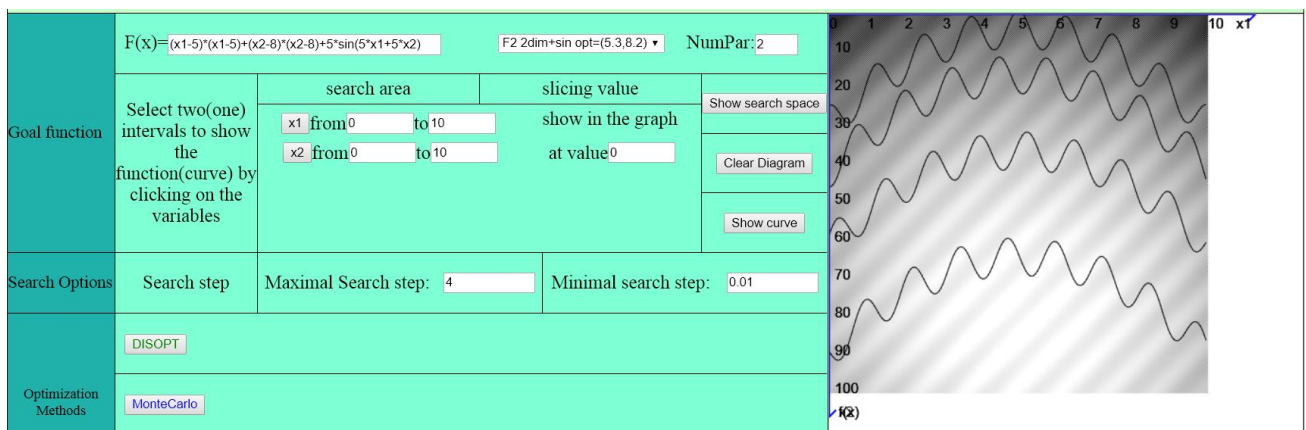
Figure 5: The slicing add-on for analyzing the goal function in the search space
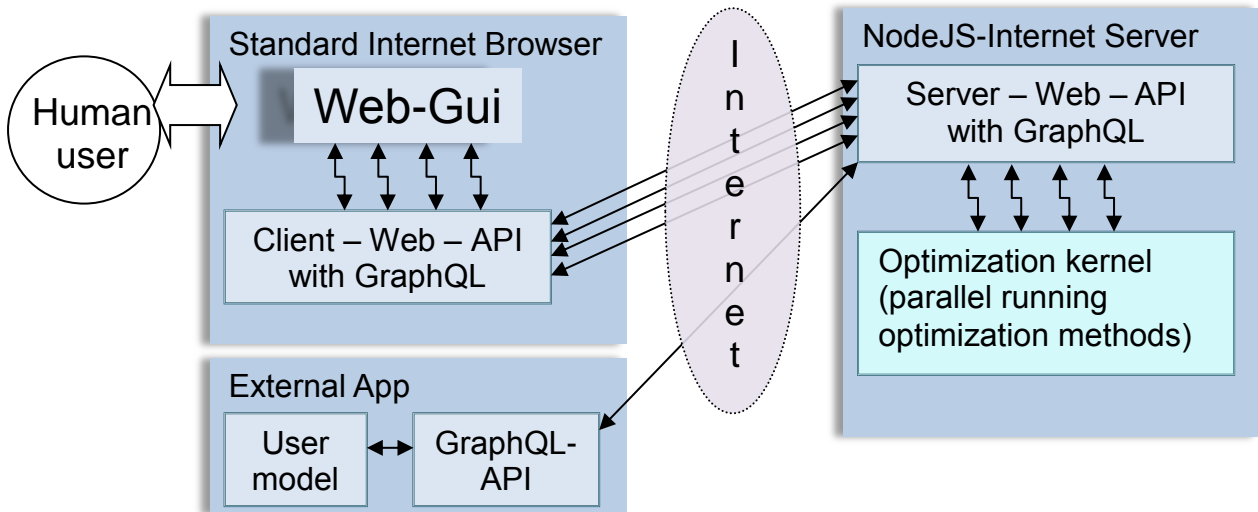
Figure 6: The client server architecture of the optimizing environment

7. THE CLIENT-SERVER OPTIMIMIZATION SYSTEM

As has been mentioned in the introduction, the actual support of JavaScript both in the browser and on the server side now allows the usage of the same code base, without the need to write new server versions of PHP or Java code.

So it was very easy to move the optimization kernel to the server without any changes. To connect the server and clients, the new GraphQL interface is used.

GraphQL was defined by Facebook for flexible interfacing of different application modules (GraphQL 2018) (GraphQL specification 2016).

GraphQL is a query language for APIs and a runtime interface for fulfilling those queries with the existing data. GraphQL provides a complete and understandable description of the data in the API. With an interface based on GraphQL, users can get their required online data much more efficiently - exactly what they need and nothing more.

GraphQL can be seen as a new option instead of traditional Web services or REST-services, where for each new idea of getting some data from a server, a new service implementation must be done.

When running the optimization with a GraphQL interface, the optimization code will run under node.js. Users are allowed to enter the necessary data such as the goal function for optimization on the left side of the GraphQL interface, and the GraphQL will pass the data to the node.js server. After the calculation is finished, it will send the results back to the GraphQL which will display the results users require on the right side, see figure 6.

Of course the main application of the GraphQL interface is not mainly intended for interaction with humans, but for connecting external applications to the optimization server. The GraphQL supports nearly all existing data formats (JSON, XML) and languages, so the flexibility is very high.

Figure 7: An example view for the developer into the running GraphQL-interface

8. CONCLUSION AND OUTLOOK

In the two different optimization applications – the simple web-browser based and the client-server-based – the same code base was used for the optimization kernel. This shows the practical power of the actual JavaScript Version ECMAScript6. JavaScript now becomes a real programming language and this opens up a lot of options: each time the developer can ask for the best place for each part of the code or he can use the same code on the client and server.

The GraphQL API is very flexible and can be used by the external developer to more easily understand the interface and then for connecting external applications to the optimization server without human interaction.

REFERENCES

Clifford, Daniel 2012. Breaking the JavaScript Speed limit with V8   http://v8-io12.appspot.com/#2 2012

GraphQL Specification 2016
    http://facebook.github.io/graphql/October2016/#sec-Enum

GraphQL 2018 http://graphql.org/

Krug, W, 2002. Modelling, Simulation and Optimisation for Manufacturing, Organizational and Logistical Processes, SCS European Publishing House: Delft

NodeJs 2016.   https://nodejs.org/en/

Obfuscator 2018   https://javascriptobfuscator.com/

Wiedemann, T. 2016. Using the JavaScript engine NodeJS for discrete simulation in a web-based environment. Proceedings of the I3M conference, 2016, Larnaca Cyprus

AUTHORS BIOGRAPHY

THOMAS WIEDEMANN is a professor at the Department of Computer Science at the University of Applied Science Dresden (HTWD). He completed his studies at the TU Sofia and holds a Ph.D. degree from the HU Berlin. His research interests include simulation methodology, tools and environments in distributed simulation and manufacturing processes, intranet solutions and database applications.

YU XINGYUE is a student from Zhejiang University of Science and Technology (ZUST) in Hangzhou and currently studies at the Department of Computer Science at the University of Applied Science Dresden (HTWD) in the area of mathematics and computer science.

WILFRIED KRUG is the founder of DUALIS IT SOLUTUIONS Company in Dresden (Germany) with a very successful long term activity in practical simulation and optimization. In 1990, he invented the ISSOP optimization system with 7 parallel running optimization methods.

AUTOMATIC DETECTION OF SENTIMENTS IN TOURIST REVIEWS BY USING LONG SHORT-TERM MEMORY RECURRENT NEURAL NETWORKS

C.A. Martín[a], R.M. Aguilar[b], J.M. Torres[c], S. Díaz[d]

[a],[b],[c],[d]Department of Computer and Systems Engineering, University of La Laguna,
38200 La Laguna (Tenerife), Spain.

[a]carlos.martin.galan@iac.es, [b]raguilar@ull.edu.es, [c]jmtorres@ull.edu.es, [d]sdiazgon@ull.edu.es

ABSTRACT

This paper describes an algorithm for automatically identifying the sentiments expressed by tourists on electronic Word of Mouth platforms. Based on reviews published by tourists after staying in hotels, a classifier is trained using a Long Short-Term Memory neural network supervised learning algorithm. We present a use case for this method involving a group of hotels located on the island of Tenerife (Canary Islands).

Keywords: sentiment analysis, social media, machine learning, long short-term memory, tourism

1. INTRODUCTION

The widespread use of social media and its role in modern society has repercussions on how various business models are evolving. The interconnection between active users creates a discussion space that is able to motivate and involve people, uniting people with common goals and facilitating diversity in discussions on various factors. This gives rise to what is called "online individualism": instead of relying on a single community for reference, thanks to social media it is possible to access more people and resources, which are often diverse.

The revolution in social media makes it possible to talk about our emotions and opinions with everyone in a globalized world. In this context, sentiment analysis aims to make obvious what people think by providing representations and algorithms capable of converting "simple, unstructured text" into "A complex vision of what users feel". These models make it easier for companies and organizations to innovate processes, products and services, and thereby to become more competitive.

If we focus on the tourism industry, we find that tourism has no other goal than to "stir emotions in tourists". Emotion is defined as "A strong feeling deriving from one's circumstances, mood, or relationships with others" [Oxford]. It is emotions that create all the business that underlies the entertainment industry. The emotions of guests, for example, determine whether they leave a tip, which hotel they choose or simply why they publicly share their mood while enjoying their holiday. Hence the importance placed on customer satisfaction by tourism operators. This level of satisfaction is directly related to the emotions that the tourists feel during their stay. It is also related to the insistence on wanting to gauge these emotions, to be able to grade the service provided in order to verify a job well done, or to improve it if necessary.

The idea is to ascertain what types of comforts trigger emotions and to be able to identify them. But to do this, we must first be able to measure these emotions. It is said that that which you cannot measure cannot be controlled, and therefore cannot be improved.

The above statement is not that simple to understand. We are talking about measuring emotions, which is never an easy task; for example, how we register that feeling of smelling freshly-brewed coffee while answering the first call of the day. That type of feeling happens every day, but we do not tend to register it as such, and yet it triggers an emotion. That emotion, later on, is what accompanies the memories we store in our mind. And that is how we give shape to the experience.

We know that a tourism product, by virtue of consisting of services, is characterized by, among other things, its expiration date. In other words, a tourism product cannot be saved for later. It is consumed at the scheduled time or it is lost. Once consumed, the wrapper, which is all that remains of it, is that memory containing the emotions recorded during the stay. And that memory is one of the components of the reputation that a tourism company earns. The set of emotions felt by the client during her stay is what will help create the image of the chain. And these emotions, in turn, later converted into memories, are what will compel the tourist to share her experience with those around her, which nowadays means on social media. We must not forget that emotions are the most viral concept in the world of social media. Tourists have to be made to feel in order for them to speak well of the chain voluntarily.

To measure these emotions on social media, in this paper we propose the use of deep learning to automatically extract the sentiments expressed by tourists during their visit to hotels on Tenerife (Canary Islands). Section 2 of this paper describes the architecture used for automatic detection of sentiments. In the next section, the tourism review dataset for training and test is presented. Section 4 shows the recurrent neural network utilized to determine the sentiments in the comments: long short-term memory neural network (LSTM). Section 5 presents the results of the implementation of this algorithm, and we end with some conclusions.

2. METHODS

The classification of text involves a general class of problems, such as predicting the sentiment in tourist reviews on social media or classifying an email as spam or not. Deep learning methods are proving to be good for this type of classification (Gichang, 2018). In this section we describe the LSTM deep-learning algorithm for classifying text.

The modus operandi for classifying text entails the use of word embedding to represent words and a classifier to learn to discriminate documents. In his introduction to deep learning for processing natural language, Y. Goldberg-2016 states that neural networks in general perform better than classical linear classifiers, especially when used with word embeddings.

In this paper we want to demonstrate that LSTM recurrent neural networks are effective for classifying documents, specifically because they are able to select salient features (such as tokens or sequences of tokens) regardless of their position within the input sequence.

The architecture therefore consists of three key pieces:

- Word Embedding: A distributed representation of words where different words that have a similar meaning (based on their usage) also have a similar representation (Maas, 2011).
- LSTM Model: A feature extraction model that learns to extract salient features from documents represented using a word embedding.
- Fully Connected Model Net: The interpretation of extracted features in terms of a predictive output.

The combination of these three elements yields good results for classifying the sentiments in tourist reviews for distinguish between *good* and *bad*

3. TOURISM REVIEW DATASET

The text data were prepared differently for each problem. The preparation begins with simple steps, like loading data, but quickly becomes difficult with the clean-up tasks, which are very specific to the data in question.

For the case of automatically monitoring the sentiments of tourists in Tenerife, we extracted samples of reviews with their ratings for tourists at hotels in Arona, Costa Adeje and Puerto de la Cruz. The goal was to build a classifier that indicates the sentiment reflected in each comment. To build the classifier, a sample of already classified text must be used to serve as a training set. To carry out this training, we obtained 1500 samples of positive reviews and 1500 samples of negative reviews.

The first phase consisted in the preparation of the data set for the application of deep learning models. Each comment that is used of the training set is submitted to a preprocessing before it can be used. The treatments carried out on the comments consisted of: separating them into words, eliminating punctuation marks and those terms that were not alphabetic and, finally, eliminating the words identified as stopwords. These words do not provide information when determining whether a comment is positive or negative.

The algorithms used require as input a vector of fixed dimension, in which each component is a number. In the technique of coding of texts to numerical vectors known as Bag of Words (BoW), a dictionary will be created with the most frequent words in all training comments. Each comment will then be coded into a fixed dimension vector that corresponds to the number of words in the created dictionary. In

BoW a comment is encoded in a vector in which each component is an apparition counter for each word in the dictionary throughout the comment. We discard this form of coding because even if the frequency of words in the comment is represented, the information regarding the order in which they are contained within it is lost.

The Word Embedding technique is currently one of the techniques that produce better results to represent texts as numerical vectors. It is a learned representation in which words with similar meaning will have a similar representation. A vector will represent each word of the vocabulary, and its representation is learned according to the use that has been given in the training comments, so that words that have been used in a similar way will have a similar representation. The learning process for the embedding is done in the framework of this work by adding a layer to the front of the neural network.

The output of the embedding layer is a 582x32 matrix in which each comment is transformed into a vector of 582 components, and each of the components (representing a word) was encoded in a vector of dimension 32.

Finally, the architecture of the whole automatic learning algorithm is designed as the one described in Figure 3

4. LONG SHORT-TERM MEMORY FOR CLASSIFICATION

Long Short-Term Memory is a type of recurrent neural network that has proven useful in complex problems in various application domains, such as language translation, automated captioning of images and text generation.

LSTM are very different from other deep-learning techniques, like multi-layer perceptron (MLP) and convolutional neural networks (CNN), as they are designed specifically for sequence prediction problems.

Like any neural network, an LSTM network consists of layers of neurons. The input data propagate through the network to make a prediction. As with RNN (recurrent neural networks), LSTM have recurrent connections such that the state of the network in the previous instant is used to formulate the output of the current instant. But unlike other RNN, an LSTM has a unique formulation that allows it to avoid problems with training and scaling the network (Jason Brownlee, 2017).

The main problem with RNN is finding a training algorithm that avoids degrading the

gradient, which makes the weights of the connections become so small that they prevent convergence (Glorot, 2010). The key historical challenge facing RNN is how to train them effectively. LSTM overcome this handicap by design.

An LSTM layer consists of a set of recurrently connected blocks known as memory blocks (Figure 1). Each cell has three inputs (previous state of the cell, previous output and current input) and two outputs (current output and state).
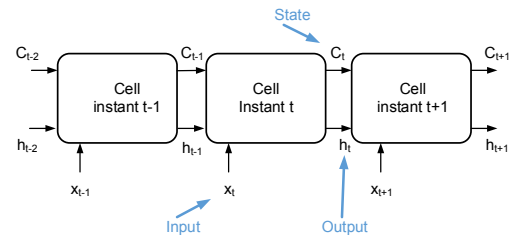
Figure 1 – Inputs and outputs of an LSTM.

The network can only interact with other cells through the gates, which are weighted functions that define the operation of the network (Figure 2). There are three gates:

- Reset gate (f1): decides what information to reject from the cell.

- Input Gate (f2): decides what input values will update the state of the memory.

- Output Gate (f3): decides what output to generate based on the cell's input and memory.
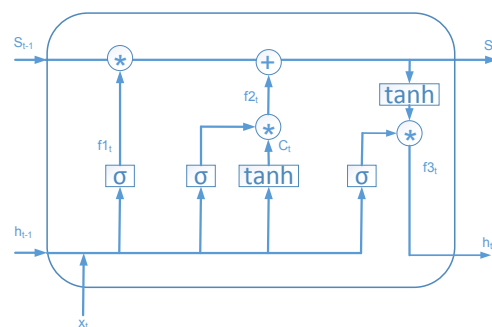
Figure 2 – Gates of an LSTM

5. RESULTS

The goal of this work is to create an automatic classifier that can determine the sentiment that tourists who visit the island of Tenerife have regarding the hotels where they stayed. This sentiment is taken from the comments left on eWOM platforms like booking.com and tripadvisor.com. (García-Pablos, 2016).
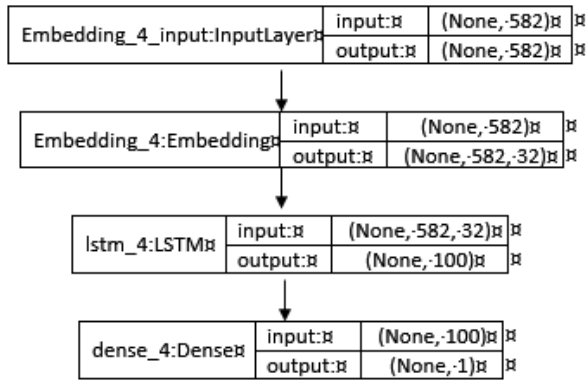
Figure 3 – Structure of sentiment classifying algorithm.

The architecture described in Figure 3 was implemented in Python, consisting of one embedding layer where each word in the review being input (maximum of 582 words) is coded into a vector with 32 values.

The LSTM was defined using 100 cells, whose input is the review (582 words coded using 32 values), which creates one output per cell.

Finally, the perceptron multi-layer, consisting of one 100-neuron input layer and a 1-neuron output layer, determines if the review is positive or negative.

The results of the training process are shown in Figures 4 and 5 over 10 epochs, the error is 0.05 and the accuracy is 0.98.
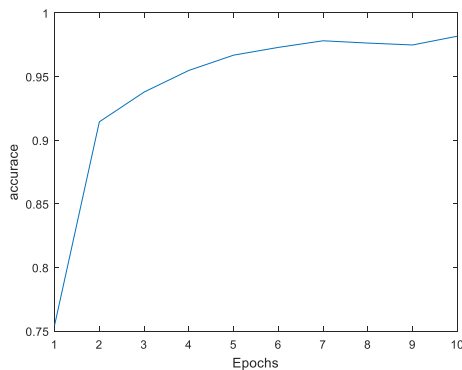
Figure 4 – Performance of the training process for good sentiments and bad sentiments.
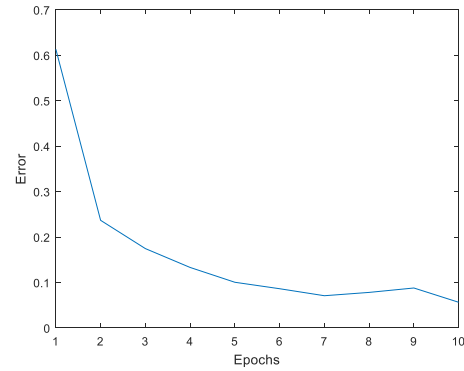
Figure 5 – Error of the training process for good sentiments and bad sentiments.

The confusion matrix shows that the total number of faulty predictions was 295, with 2490 correct predictions, yielding an error percentage of 10.59%. The bias produced in the classifier makes for more false negatives than false positives.

		Predicted value	
		Positive	Negative
Real value	Positive	1216	192
	Negative	103	1274

Table 1 – Confusion matrix for the training results

6. CONCLUSIONS

In this paper, we propose a classification model with LSTM neural network, which is a sentiment classification model with word embedding. The results shows that is a good approach in order to determine the sentiments in short texts. In the case of tourism, the main driver of the economy in the Canary Islands, it is a useful tool. In this area, in which there are millions of users, finding information on their perceptions of the service received is a cumbersome task. Moreover, the use of questionnaires does not provide accurate information on how customers feel about the service they received. As a result, in this paper we propose using a LSTM neural network to automation the sentiment's detection on eWOM platforms like tripadvisor.com and booking.com.

In order to identify the sentiment of a review, we used an LSTM training algorithm that,

according to the bibliography, exhibits very good efficiency indices with classification problems.

In future work we plan to create a classifier that can identify what tourists are discussing so that we can determine what aspects they like and thus what to promote, as well as what elements are associated with negative comments so that they can be improved.

ACKNOWLEDGMENTS

REFERENCES

Yoav Goldberg, "A Primer on Neural Network Models for Natural Language Processing", Journal of Artificial Intelligence Research 57 (2016), pp. 345-420

García-Pablos A., Lo Duca A., Cuadros M., Linaza M.T., and Marchetti A. 2016, "Correlating Languages and Sentiment Analysis on the Basis of Text-based Reviews," in Information and Communication Technologies in Tourism 2016, pp. 565–577.

Maas, Andrew L and Daly, Raymond E and Pham, Peter T and Huang, Dan and Ng, Andrew Y and Potts, Christophe, "Learning Word Vectors for Sentiment Analysis", Proceedings of the 49th Annual Meeting of the Association for Computational Linguistics: Human Language Technologies - Volume 1, 42-150, 2011.

Glorot, Xavier and Bengio, Yoshua, "Understanding the difficulty of training deep feedforward neural networks", Proceedings of the International Conference on Artificial Intelligence and Statistics (AISTATS'10). Society for Artificial Intelligence and Statistics, 2010

Jason Brownlee, Long Short-Term Memory Networks With Python, 2017

Gichang Lee, Jaeyun Jeong, Seungwan Seo, CzangYeob Kim, Pilsung Kang, Sentiment classification with word localization based on weakly supervised learning with a convolutional neural network, Knowledge-Based Systems, Volume 152, 2018, Pages 70-82, ISSN 0950-7051

HOW DO TRAVELLERS DECIDE: A STOCHASTIC MODELLING APPROACH TO DETERMINE DECISION FACTOR SIGNIFICANCE

Faboya T. Olusola[(a)], Peer-Olaf Siebers[(b)], Brendan Ryan[(c)], Grazziela P. Figueredo[(d)]

[(a), (b),(d)]School of Computer Science, University of Nottingham, Nottingham, United Kingdom
[(c)]Faculty of Engineering, University of Nottingham, Nottingham, United Kingdom

[(a)]itxotfa, [(b)]pszps, [(c)]epzbr [(d)]pmzgf@nottingham.ac.uk

ABSTRACT

Many factors are involved in travellers' mode choice decision processes. Such factors include individuals' physical, cognitive, and emotional abilities, which play a significant role in travellers' attitude and mode usage patterns. Understanding how important each of these factors is to individuals, as well as understanding their impact on travellers' behaviour in general, will assist policymakers to provide appropriate interventions when necessary. To gain this understanding, we propose to use a stochastic modelling, supported by a fuzzy inference system. In this paper, we describe our approach and demonstrate it with the help of a case study, looking at cyclists and car users in the context of travelling to and from a university. The aim is to understand which of the travel requirements (physical, cognitive, and affective) is considered most when people are planning for their journey, and to understand the level of efforts regarding the three factors required to make use of their mode. The results show that both sets of travellers engage more with their cognitive aspect during journey planning, but cyclists have a higher cognitive share as a result of optimising safe routes to the university.

Keywords: stochastic modelling, fuzzy-intelligence, abstraction hierarchy, mode choice, travel requirements

1. INTRODUCTION

Research on travel mode choice has been ongoing since the 1960s (Möller, 2014). However, the concerns on the need for transport mode shift only started receiving attention in recent times. The current attention is due to persistent challenges of the sociotechnical transport system as well as substantial socioeconomic benefits that a shift in the mode usage pattern can bring. Consequently, in addition to existing approaches to mitigate challenges due to the transport system, behavioural change in passengers' mode choice has been suggested as a short-term solution with reduced costs (Roberts et al., 2017). Nevertheless, the transport system organisational structures, policies and designs often impose constraints on actors' activities within the system. The constraints, which could be physical, cognitive and affective (Wardman et al., 2001) are the requirements that need to be satisfied in order to make a journey and are the factors that shaped travellers behaviour in mode choice. The constraints can manifest from individuals psychological (Gardner & Abraham, 2008), symbolic and affective (Steg et al., 2001) traits, as

well as travel mode's instrumental attributes (Derek Halden Consultancy, 2003). Due to heterogeneity in human nature, the travel requirements, i.e. physical, cognitive and affective constraints, have varying impact on individuals mode choice decisions; and gaining insight into such impacts is essential to the provision of the right interventions to stimulate travellers' behaviour (Faboya et al., 2017).

Furthermore, our review of the literature indicates that factors that determine travellers' mode choice are not linear and with no apparent boundaries. Besides, individual travellers make a subjective judgment under uncertainty due to information deficiency or the fuzziness of the decision variables boundaries. There are existing studies on mode choice, but models that look at mode shift through behavioural change are scarce. We believe the first step to achieving mode shift is to understand the decision variables (Faboya et al., 2018). To the best of knowledge, however, there is no in-depth study providing the techniques to identify the significance of the decision factors and their impacts on travellers' mode choice decision, bearing in mind the uncertainties surrounding the process.

Therefore, in this paper, we introduce a fuzzy-decision technique that analyses a transport system environment with the Human Factors' Cognitive Work Analysis (CWA), and models the perception and attitude of a set of travellers, using a stochastic modelling approach. We demonstrate the application of this technique by looking at a case study, where we focus on cyclists and car users in the context of travelling to and from a university. The case study aims to investigate:

1) which of the travel requirements, namely physical, cognitive or affective consideration, is paramount to travellers' mode choice decision.
2) the physical, cognitive and affective efforts demanded from the travellers to make use of their usual travel mode as a result of constraints imposed by the transport system's environment.

The outcome will provide a detailed understanding and insights into the aspects of the transport system's objects, resources or processes that need improvement. In addition, it will assist to identify (i) elements within the system's environment that need interventions; and (ii) the factors (ergonomics and non-ergonomics) that may require attention in order to achieve a shift in mode usage pattern.

The remainder of the paper is organised as follows: Section 2 discusses the background information,

including decision factors in mode choice and their relationships, modelling uncertainty in decision-making, Human Factors' cognitive work analysis, and Monte Carlo methods. Section 3 presents data collection and analysis. Details about model development, verification and validation are given in Section 4, while experimentation and results are presented in Section 5. Finally, Section 6 and 7 provide the discussion of the results and conclusions, respectively.

2. BACKGROUND

2.1. Travel Demands Consideration

Behaviour change in passengers' mode choice has been suggested to be a possible way to mitigate environmental, social, economic, and health challenges due to the transport system (Roberts et al., 2017). Nevertheless, the challenges lie in the many interdependent factors that determine traveller decision in the travel mode choice process. The considerations include the traveller's attributes such as personality, privacy etc., (Steg et al., 2001; Gardner & Abraham, 2008; Steg, 2007), social interactions; motives for mode usage and behavioural controls which include individual mental and physical ability (Wardman et al., 2001). Other considerations are the travel mode characteristics (Derek Halden Consultancy, 2003); and the system's environment (Rasmussen, 1986; Wickens et al., 2004). Mann and Abraham (2006) state that certain considerations are paramount to individual travellers in making mode choice. These considerations influence the motives for mode usage (Steg, 2005). To an individual, the motive might be instrumental such as travel time concerns (e.g. get to work on time), while others may consider symbolic-affective factors such as autonomy, personal status etc. However, Steg (2005) and Mann and Abraham (2006) observe that the majority of the existing models of mode choice have been based on cognitive antecedents of behaviour, but treat "affect" as an undifferentiated aspect of attitude formation. The researchers' assertions are due to the overlap and the fuzziness in the boundaries and interrelated nature of the mode choice decision factors. Consequently, our findings from the literature about the considerations for mode choice decisions are represented in a Venn relationship diagram in Figure 1. Our diagram explains the relationship between the mode choice decision (the centre) and its various influencing factors. The considerations in the diagram include the travel mode attributes (e.g. speed, cost); traveller attributes (e.g. status); the motives for mode use (e.g. get to work on time); and the possible behavioural influence on the mode choice decision (physical fitness). The *mode choice decision* at the centre of the relationship diagram is influenced by trip-makers' motives for using a mode which can be instrumental, symbolic-affective, or both. The decision often manifest along the considerations that the decision maker thought of being paramount.
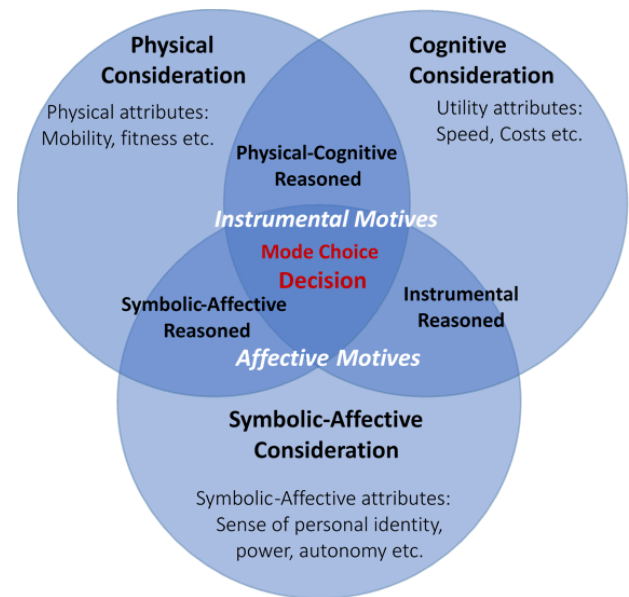
Figure 1: Travel Demands Relationship Diagram

The *cognitive consideration* is primarily driven by the utility and functional attributes of the travel mode such as travel time and speed. It also has influences from other considerations such as physical (e.g. personal mobility) and symbolic-affective (e.g. autonomy). The cognitive consideration often results in instrumental-reasoned and motives (e.g. get to work on time) (Steg, 2005). The *symbolic-affective consideration* is more psychologically related. It includes travellers' attributes such as status, superiority, personal identity etc. Mann & Abraham (2006) argue that psychological analysis of affective functions always reveals affective motives of mode use among which are autonomy, the feeling of control, etc. In addition, context (e.g. worries not to be late to an appointment) and environmental conditions (e.g. bad weather) are other forms of affective sources that influence decision-making. Lastly, *Physical consideration* is related to personal mobility, fitness, environment (e.g. platform or interchange design). Each of the factors has its degree of impact on the mode choice decision. To address the overlap and boundary issues in decision factors, a computational intelligence technique Fuzzy Logic system is discussed in Section 2.2.

2.2. Imprecise Information and Fuzziness of Decision Factors

Human beings make subjective judgements under uncertainty in decision-making processes. Two categories of uncertainty are bound to arise from the conceptual relationship diagram presented in Figure 1:

1. Uncertainty due to imprecise boundaries of the factors considered in the decision process.
2. Uncertainty due to fragmentary or vagueness of natural language as a result of imprecision of the words used in the measuring instrument, as words mean different things to different people.

When there is the possibility of uncertainty in perceptions, Zadeh (1996) suggests the Computing with

Words (CW) methodology. The exploitation of the tolerance of imprecision is an issue of central importance in CW where words are used in place of numbers for computing and reasoning. Fuzzy logic (FL) plays a pivotal role in CW and vice versa (Zadeh, 1996). The FL idea is similar to the human being's feeling and inference process of providing vague answers to responses. For instance, to answer questions such as how satisfied are you with your travel mode today, one could answer with 'Quite Satisfied'. Quite satisfied is both fuzzy and ambiguous because it fails to indicate exactly to what degree is the satisfaction. Computers as discrete number based machines can only be used on vague responses with the help of computational intelligence techniques such as FL and fuzzy inference systems. The implementation of FL techniques to a real application involves three major steps (Bai & Wang, 2006) as depicted in the fuzzy inference system (FIS) diagram shown in Figure 2 below:
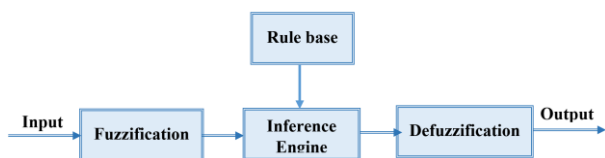

Figure 2: Fuzzy Inference System Block Diagram

o   Fuzzification: the process of converting the classical or crips data into fuzzy data or membership functions.
o   The Inference Engine: combines membership functions with the control rules to derive a fuzzy output.
o   Defuzzification: the use of different methods such as centrifugation to calculate each associated output and put them into a lookup table. The final output is picked up from the lookup table based on the current input during application.

The fourth box (the rule base) contains the linguistic rules that can be derived from survey data or provided by experts, which form the bases upon which the inference engine maps the input fuzzy sets into the output fuzzy sets.

In addition to being able to represent uncertainty in the system, travellers' emotions is a key component of the mode choice decision-making process. Hence, the following section discusses the approach to measuring emotional perception in this study.

2.3. Measuring Traveller's Affective Response
Some of the mode choice decision factors can be obtained using common survey method such as questionnaire only, but the requirements for capturing emotional perception require additional techniques beyond such data gathering tools. A literature review in the field of Psychology unearthed that the most common method for measuring human emotion in Psychology is the "circumplex model of affect" (Russell, 1980). It is a well-established framework, which proposes that all affective states arise from cognitive interpretation of core neural sensations. The sensations are the product of two independent neurophysiological systems (Posner et al., 2005), namely affective valence (also termed pleasure-displeasure) and perceived activation (also termed arousal) (Ekkekakis & Petruzzello, 2002). The two independent systems give rise to about 48 different levels of emotion, which are represented in a circular fashion of a two-dimensional space of the model. Although some emotions are similar, they are measurably different from each other. The circumplex model has been successfully implemented in areas like social behaviour (Carney & Colvin, 2010); medicine (Posner et al., 2005; Tseng et al., 2014) and e-commerce (Jascanu et al., 2010). The framework could be of great help in measuring travellers' emotional perception; however, the dynamics in travellers' activities during the journey may pose questions regarding its adequacy. Capturing traveller's perception at various stages of a journey with respect to objects and resources within the transport system's environment as the journey progresses could be complicated. Human Factors' CWA (Rasmussen et al., 1994; Vicente, 1999) discussed in Section 2.4 provides a useful investigative approach.

2.4. Overview of Cognitive Work Analysis
The CWA is a five-phase analytical framework for the evaluation of complex sociotechnical systems (Jenkins et al., 2009). Each phase of CWA models a different constraint set within the system. The overview of the five phases is detailed in Cornelissen et al. (2013), but our focus is on the first two phases. First is the Work Domain Analysis (WDA) that models the system constraints by describing what the system is trying to achieve, and how it tries to achieve it. The WDA uses the Abstraction Hierarchy (AH) to simultaneously describe constraints on the performance of actors enacted by system's characteristics (Cornelissen et al. 2013), as well as the environment in which the activity is performed. The AH represents the means-ends relationships with the system environment (Baker et al., 2008). Elements at one level of abstraction are the means to achieving elements at the next higher level, and the ends achieved by elements below. The links are made following a 'how-what-why' triad (Rasmussen & Pejtersen, 1990). It follows the process that when a node is taken as the 'what' (at any level in the hierarchy), nodes linked in the hierarchical level above the node indicate why the chosen node is necessary within the system. Any connected nodes on the level immediately below that node can be taken to answer the question of 'how' that function is to be achieved or fulfilled (Vicente, 1999).

Starting from the top level of the AH, *the functional purpose* of the existence of the entire transport system to the University in the case of this study is to ensure efficient, comfortable and safe trip. The second level from the top has the *values and priority measures* nodes which are the criteria used to judge whether the system

is achieving its purpose. The middle-level of the AH is the *purpose-related functions* which identify how the travel modes actually achieve the aim of providing efficient, comfortable and safe transport to the university. The *object-related processes* are processes that make use of transport system's objects to achieve the desired result. The physical objects and resources that are needed by travellers to make a pleasant journey. The second phase is the Control Task Analysis that produces a Contextual Activity Template for each purpose-related function in the AH by modelling the situational constraints and decision-making requirements. Details of an illustrative example of the AH application is given in Section 3.3.

2.5. Monte Carlo Approach

The complexity of social systems in which travellers operate (Wickens *et al.*, 2004), and their multivariate, as well as interrelated attributes, explains nonlinearity in their decision-making processes. Understanding the impact of variables that present certain levels of uncertainty, ambiguity and variability in decision process required mathematical models such as Stochastic process (Lewerenz, 2002). Stochastic modelling allows access to a range of possible outcomes of decisions and the probability that they will occur for any choice of action (Field Jr., 2008). The features make the stochastic process an ideal method to analyse the impact of variables and allow better decision making under uncertainty.

3. DATA COLLECTION AND ANALYSIS

This section presents the data collection and survey data analysis processes undertaken in this study.

3.1. Questionnaire Design

A questionnaire tagged "Passenger's Mode Shift Survey" was developed from the discussions emanated from two focus group meetings. The focus group involved a private car user, a cyclist, two pedestrians and three public transport users. The participants' views on various factors they put into consideration while planning a trip to the university were discussed. The discussions in the first meeting formed the contents of the draft questionnaire. The contents and the nature of the questions were reviewed in the second meeting. To ensure that the questionnaires measure what is expected, experts were consulted for a further review of the questions. The final version of the questionnaire was provided in online and paper-based versions to enable wide circulation.

There are two sections in the questionnaire, one focusing on demographics and one focusing on travel mode perception. The travel mode perception section consists of several Likert scale and open-ended questions. Items in the questionnaire are on the following transport system specific areas: *information provision, mode timeliness,*

reliability, frequency, speed, security, safety, autonomy and privacy, control over journey and protection from bad weather. The questions are on the following focus items: ease of accessing information, reliability of available information, ease of getting to destination on time, ease of getting on and off the mode, parking space concern, delays, security en-route the university, safety en-route the university, availability of road signs, attitude of other road users and protection from weather. All the questions were intuitively asked and tailored towards mode-related scenarios so that neutrality in affect and utility measures would emerge (Steg, 2005). Each Likert scale question requires two responses, one answers *"how satisfied"*, and the other answers *"how important"* is the item under consideration to the respondent.

3.2. Questionnaire Execution

The participants were:

- 82 cyclists, comprised of 37 females and 45 males, aged between 20 and 56 years
- 81 personal vehicle users comprise 46 female and 34 male aged between 18 and 63 years.

The choice of the two travel modes was due to our interest in investigating the levels of physical, cognitive and affective efforts demanded from the travellers by the transport system, and the view to knowing which of the factors is paramount to their decisions to choose a mode.

3.3. Abstraction Hierarchy Development

Our focus items (i.e. the transport system's attributes mentioned in the questionnaire and listed in Section 3.1), together with related physical objects and resources within the university's transport system are used to construct the AH in Figure 3. Each of the *functional purposes* and *values and priority measures* nodes is shaded with unscaled two or three different colours. The colours are used to indicate that each box has its potion of affective, cognitive and/or physical involvement that contributed to mode choice decision.

To illustrate how AH was constructed using the *'how-what-why'* triads. Trace through and focus on the highlighted nodes and means-ends links. For instance, if *Convenience* node is taken as the '*what*' at the *values and priority measures level*, the means-end links connecting this node up to the higher levels of abstraction show that it can support the *comfortable, functional purpose* of the system. That is, it can be seen that C*onvenience (what)* occurs to ensure that *Comfortable (i.e. the 'why')* is provided in the system. To show how the *convenience* node ('*what*') has been derived. The boxes below the *convenience* indicate that it is supported by the *travel mode protection, passenger protection, cater for biological needs desires, cater for task needs and mode real time (i.e. the 'how')*. The same process was used to form the links on the AH from the participants responses in the survey data.
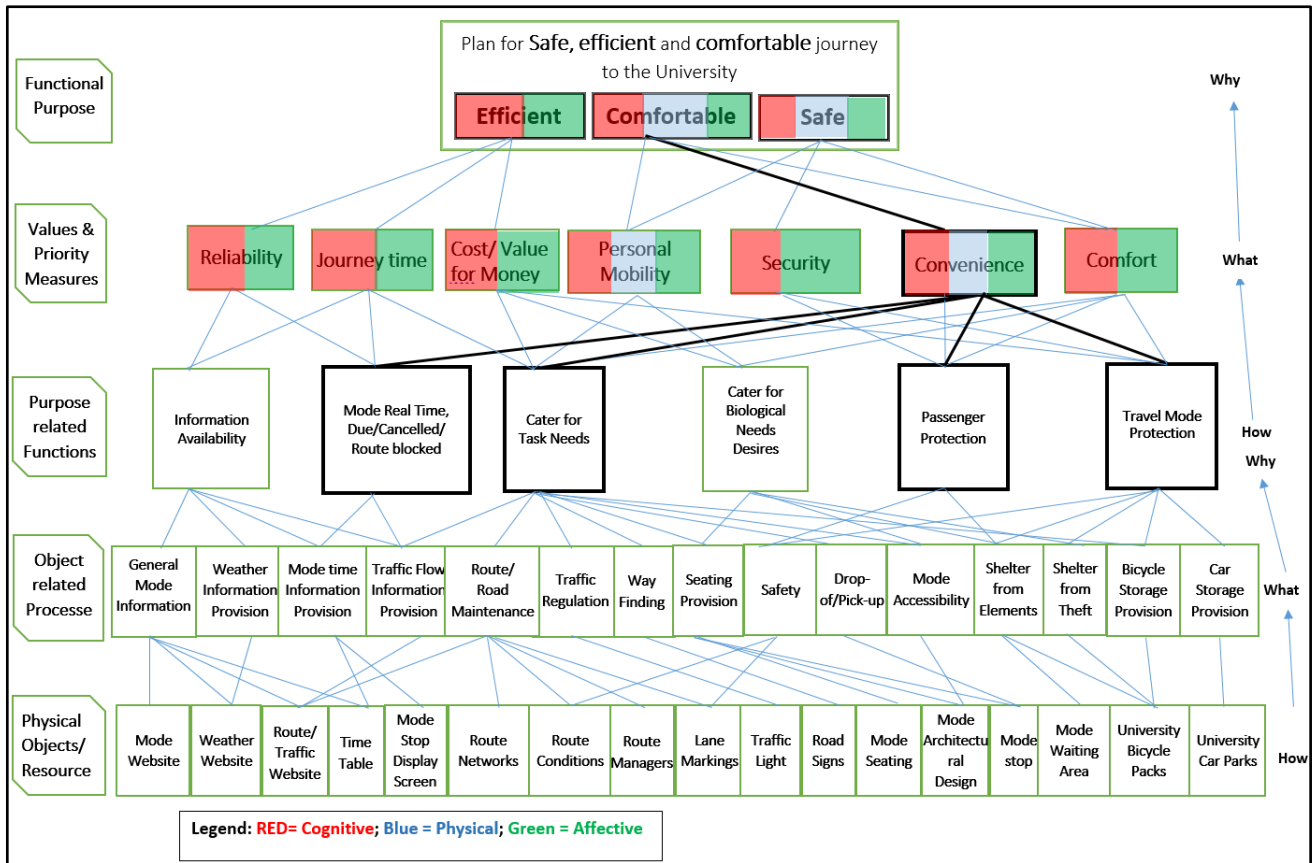
Figure 3: The Abstraction Hierarchy (inspired by Stanton, et al. (2013)

3.4. Data Analysis

3.4.1. Deriving Affective Value from the Survey Data

The affective perception for each participant is derived from the survey data as follows. A two-column table is formed for the analysis. The first column contains the perception of the *importance* of the item to the decision maker, and the second has the perception of the *satisfaction*. However, in situations where more than one item is related to one travel mode attribute, the mean of responses to all questions that related to the attribute is calculated for each participant (see Algorithm 1).

The data distributions for the importance and satisfaction entries follow a normal distribution bell shape. Thus, the Gaussian membership function was used for the affective generator fuzzy system.

Algorithm 1 Affective component from survey data

Create a two-column table for *importance* and *satisfaction* attributes

1: **for** each participant **do**
2:   **for** each x **do**   where ▷ x is the *focus items.*
3:     Find the mean $\bar{\imath}$ and $\bar{\jmath}$ $\forall$ questions related to x.
      where ▷ i = importance, j = satisfaction
4:     $x_i = \bar{\imath}$ and $x_j = \bar{\jmath}$
5:   **end for**
6:   **for** each x **do** where ▷ x is the *focus items*
8:     Generate affective values from x_i and x_j
9:     Return affective value
10:   **end for**
11: **end for**

The two entries (i.e. importance and satisfaction) form the two dimensions of the input into the affective fuzzy inference system. The rule base for the system follows the fuzzy mapping rule provided in Table 1.

Table 1: Affective Generator Input Mapping

Pleasantness \ Arousal	Arouse	Somewhat-Arouse	Neither-Arouse-Nor-Unaroused	Somewhat-Unaroused	Unaroused
Pleasant	Excited	Enthusiastic	Pleased	Contented	Relaxed
Somewhat-Pleasant	Stimulated	Elated	Happy	Comfortable	Calm
Neither-Pleasant-Nor-Unpleasant	Afraid	Anxious	Neutral	Bored	Fatigued
Somewhat-Unpleasant	Angry	Frustrated	Dissatisfied	Uncomfortable	Bored
Unpleasant	Disgusted	Discontent	Disappointed	Sad	Dejected

Table 1 describes the relationship between the two inputs (i.e. arousal (importance) and pleasantness (satisfaction), and the output (affective). The interception of a row and a column represents an emotional point (affective perception). Furthermore, each participant's perceptions and his or her corresponding affective value for all mode's attributes are recorded. A correlation analysis is performed on the travellers' perception values and the corresponding affective values to identify highly correlated attributes so as to reduce to a manageable size the number of attributes to be considered in the determination of the travellers' stereotypes.

3.4.2. Deriving Physical and Cognitive Values from the Survey Data

The travellers' physical and the cognitive aspect of the general perceptions are derived from the survey data as follows: each of the focus items is examined to determine whether it answers the question that relates to physical (mobility), cognitive (mental) or both activities. For instance, the question "*How satisfied are you with the ease of accessing information about your main mode?*", is more related to satisfaction regarding the cognitive effort to access information than the physical effort. Following this process, all focus items related to a mode attributes are classified accordingly as physical or cognitive perception. Where more than one focus item relates to a mode attribute, the average value is taken. With the derivation of the physical and cognitive perceptions from the survey data, all travel requirements (i.e. physical, cognitive and affective) values which form the input into the focus item's fuzzy decision system are in place.

3.4.3. Groups within the Population

K-Medoids clustering also known as Partitioning Around Medoids (PAM) algorithm (Agrawal et al., 2016) was used to learn the stereotypes present in the dataset. Four and three stereotypes were identified within cyclists and car users' populations respectively. Each stereotype has a range of minimum and maximum values for physical, cognitive, affective aspect as well as the perceived overall satisfaction within which they are grouped. The percentage of each stereotype within their respective population together with their minimum and maximum values are used for model calibration at implementation stage.

4. MODEL DEVELOPMENT

4.1. Model Conceptualisation

The study conceptual model depicted in Figure 4 shows the inputs into the system; the decision system, and the expected outputs from the system. The model development follows the conceptual design. The passenger perceives the quality of mode attributes and makes a subjective judgement on each of the focus items bearing in mind the physical, cognitive and affective efforts associated with the items being considered. Each focus item has values for importance and pleasantness as inputs from which the affective value is produced. The affective value is after that combined with the physical and cognitive perceptions values of the same focus item to form a set of input into the focus item decision system. The evaluation of each of the system's metrics (i.e. *value and priority measures* of the AH in Figure 3) is based on relevant and related focus items. The outputs from the focus item fuzzy system are the general perception of the focus item and the physical, cognitive and affective strengths that made up the general perception.

The following assumptions were made in the model design process:

1) the number of car user and cyclist participants considered in the simulation will provide information regarding their behaviours in response to the journey requirements
2) the travellers already have previous experiences of travelling to the university

A simplification that we made in the model design is that the travellers' usual mode choice behaviours are not influenced by their interactions with other traveller's behaviour.
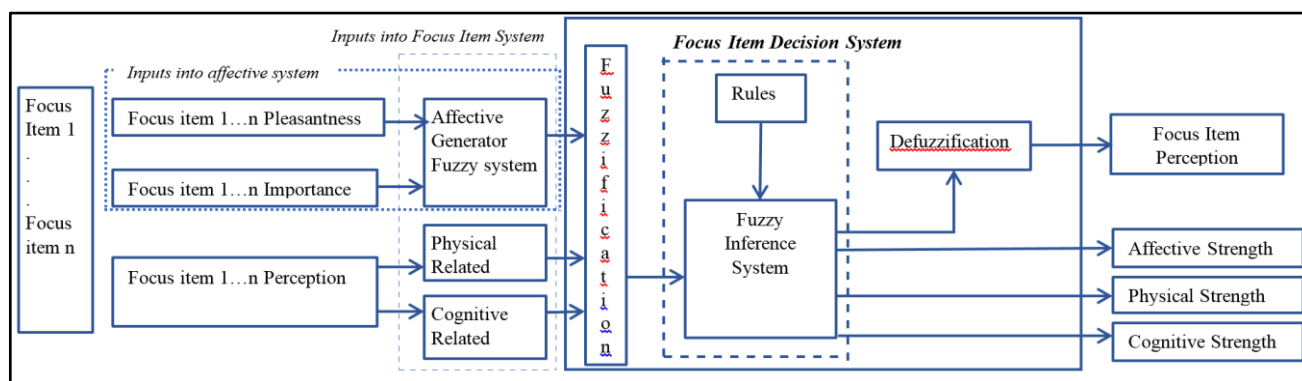
Figure 4:The Study Conceptual Model

4.2. Model Implementation

The model was implemented in REPAST, a Java-based simulation toolkit for ABM (https://repast.github.io). There are two classes of active objects in the model: The Passenger and Mode agents. The Passenger agents are the cyclist and the car users; the Mode agents are the cycle and the personal vehicle. The model calibration was based on the stereotypes information. A population of 163 passengers consisting of 81 car users and 82 cyclists was created; the uncertainty tolerance and aspiration level parameters were randomly generated.

A fuzzy implementation of the perception process was also on a Java-based fuzzy logic toolkit called Juzzy (Wagner, 2013). The toolkit Type-1 fuzzy inference system was extended to fit the needs of this study. A section of the extension is listed in Algorithm 2. The Algorithm was executed on each of the focus items having the physical, cognitive and affective variables as input. A triangle membership function was used because of its flexibility and suitability to model distributions derived from natural phenomena, also its ability to automatically adjust its centre point to capture

uncertainty/variation in the survey data. The system's rule-base consist of 27 rules derived from the relationships that exist among the survey data sets of the three input variables and the perceived overall satisfaction. The outputs from the system are: (i) the name of the input variable that contributes to the final travellers' perception. (ii) the linguistic labels (*Pleasant, Unpleasant etc.*) in the membership functions which correspond to the inputs and their respective firing strengths (i.e. the strength that the linguistic label contributed to the final perception) and (iii) the travellers' actual perception of the focus item being considered (i.e. the defuzzified value).

Algorithm 2 Identifying travel requirements that contribute to perception and their strengths

There are 3 inputs: physical, cognitive and affective each with 3 linguistic labels: Pleasant, Unpleasant and NeitherPleasantNorUnpleasant into the fuzzy system

1: Declare a Vector v to return multiple values
2: set the input i ▷ $i_1 =$ physical, $i_2 =$ cognitive, $i_3 =$ affective
3: get rule r.size ▷ r size is the total number of rules in the fuzzy system rule base
4: **for** each r **do**
5:   **for** each x **do** ▷ x = the linguistic labels
6:     get the variable x . name ▷ = name
7:     get the variable x . Input ▷ = crisp input
8:     get the variable x. Firing Strength ▷ = strength
9:     **if** (strength >=0)
10:       Map.put (name, strength)
11:   **end for**
12: **end for**
13: $v.add(Map)$
14: $v.add(Perception)$
15: end.

4.3. Model Verification and Validation
The credibility of our model was ensured by using various techniques. Firstly, we used verification to ensure that the model is programmed correctly, and the algorithms have been implemented appropriately. Secondly, we used expert validation (with experts from the simulation and transportation domains) to ensure that the model represents the real world with sufficient accuracy for our purpose In addition, as part of the validation process, a highly correlated result of the generated affective and the corresponding travelers' perception values was obtained from the survey data. The results point to the accuracy of the expert knowledge (i.e. circumplex model) used in the affective fuzzy inference system. Furthermore, the assumptions made and input parameters reflect the reality from the survey data.

5. EXPERIMENTATION
5.1. Experimental Setup
The experimentation looked into the following purposes:

1) the significance of the three travel requirements to the travellers' perception of their travel mode to the university, by observing the numbers of times physical, cognitive or affective factor is considered in their travel experiences.
2) The level of effort demanded regarding the most considered travel requirement.

The model was executed 100 times for the population of 163 passengers consisting of 81 car users and 82 cyclists. The number of times that a travel requirement contributed to travellers' perception on each of the focus items was generated as model output. In addition, the values of individuals perceived overall mode satisfaction, perceived mode's comfortability, efficiency, and safety was also returned as outputs. The results are presented in Section 5.2

5.2. Results
5.2.1. The Significance of Travel Requirements
The significance of the three travel requirements to the travellers' modes' perception in their journey planning processes is presented in Figure 5. Each histogram represents the average number of times that a travel requirement occurs in travellers' planning process for 100 runs. The vertical axis of the histogram represents the average number of times a requirement is considered; the horizontal axis shows mode counts. The diagrams on the left side of Figure 5 represent the histograms of overall travellers' *physical*, *cognitive* and *affective* considerations, respectively. The top left diagram shows the overall average physical considerations for car users as 307.32 and 140.00 for the cyclists, respectively. The middle left diagram indicates that the average cognitive consideration has the highest number of occurrences for both modes with an average of 1101.09 for car users and 1181.00 occurrences for cyclists. The bottom left diagram presents the average affective considerations with car users having an average of 125.22 and cyclists having an average of 184.00 occurrences. The output shows that both sets of users involved more in mental thinking in their planning than physical and affective considerations.

However, due to high values recorded in cognitive consideration, further investigation into the breakdown of its linguistics labels' (i.e. pleasant, unpleasant, etc.) distributions counts is depicted in the diagrams on the right side of Figures 5. The "pleasant cognitive considerations" histogram (top right diagram) indicates that the car users achieved average of 602.27 occurrences of pleasant cognition (i.e. satisfactory) while cyclists have an average of 552.00 pleasant cognition occurrences. The right middle diagram shows the "neither pleasant nor unpleasant considerations" histogram, an average of 375.54 occurrences of neutrality is recorded with the car users' and an average of 384.00 for cyclists, respectively. The bottom right diagram shows an average of 73.22 occurrences of "unpleasant cognitive considerations" for car users, and 202.00 occurrences occur for cyclists.
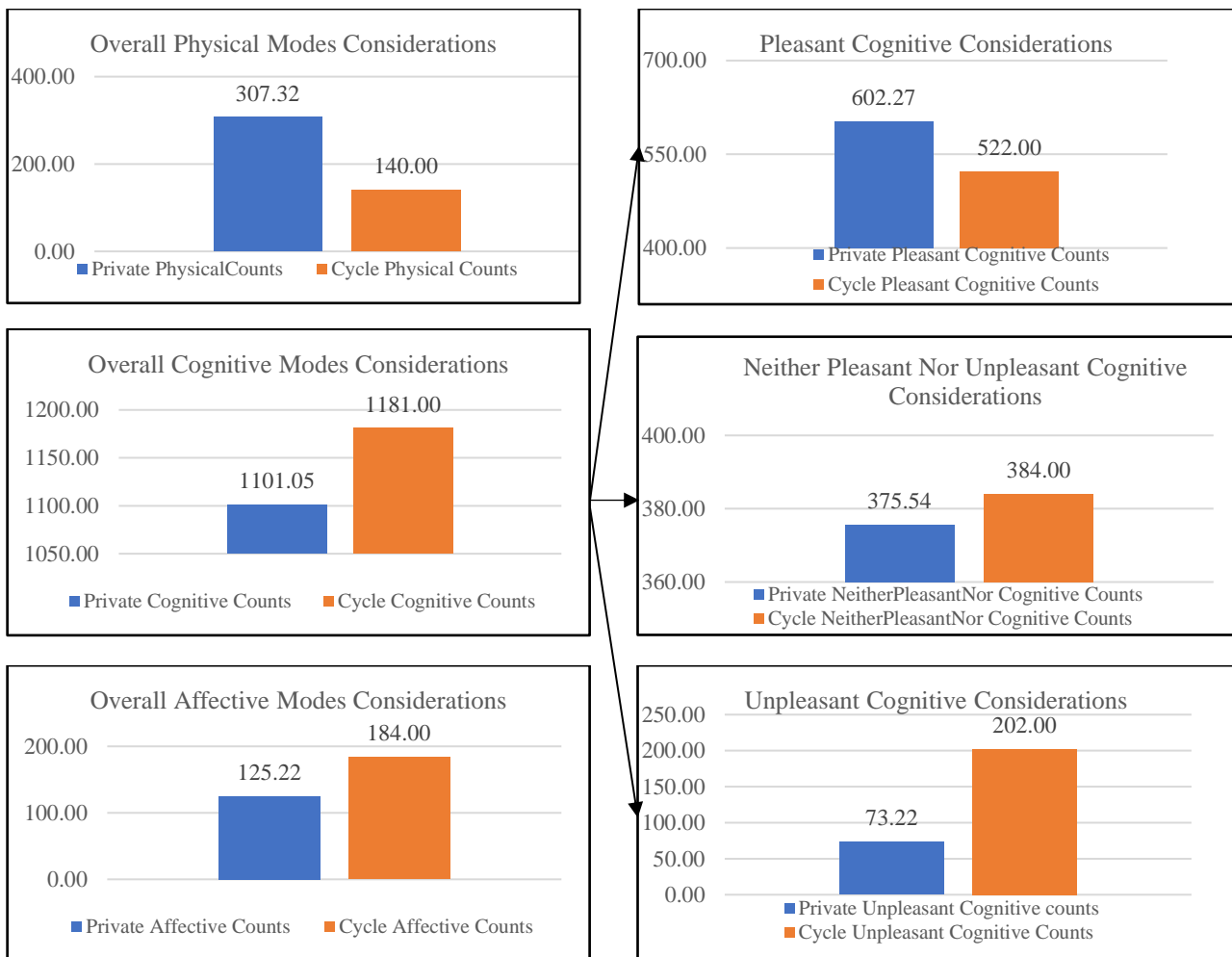
Figure 5: Overall Physical, Cognitive and Affective Travel Requirements Considerations

5.2.2. Effort Demanded by the Travel Requirements

This result focus on the perceived efforts regarding cognition put into the use of the modes. The cognitive demand is investigated further due to its number of occurrences in both modes' perception. The representations of each of the cognitive requirements are observed within the modes *functional purposes* (i.e. mode *efficiency, comfortability* and *safety*) that form the travellers' perceived satisfaction. Jaccard's distance measures that gives statistical dissimilarity between two sets was used to determine the level of variation between the travellers' perceived satisfaction and cognitive involvement in each of the modes' functional purpose. Jaccard's measure explains that the closer the distance to zero the lower the level of dissimilarity. Figure 6 shows the cyclist perceived satisfaction level (blue points) and the *safe, efficient* and *comfortable* purpose cognitive demand. The satisfaction-safety set has 0.0714 distance of dissimilarity; satisfaction-comfortability set has a negative value of -3.4629, and satisfaction-efficiency set has another negative value of -7.0894. The values show that cyclists perceived cognitive efforts on safety have a close relationship to their perceived satisfaction, but the cognitive efforts put into comfort and efficiency are at variance to the perceived satisfaction, which indicates that they are not
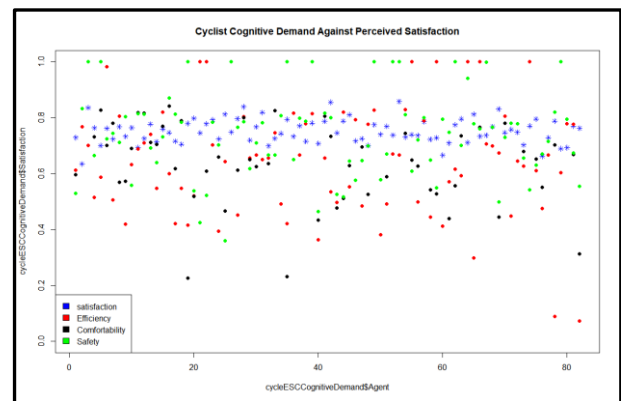
Figure 6: Cyclist Perceived Satisfaction and Cognitive Demand Relationships

important determinants of cyclists' satisfaction. Furthermore, the negative values can be attributed to the travellers' perceptions on the metrics as well as the focus items from which efficiency and comfortability were developed (see Figure 3). For instance, mode *reliability, journey time and cost/value for money* are the metrics that form the *efficiency (functional purpose)*. Thus, it shows that cyclists do not put much emphasis on these metrics as much as they put to the safety while planning for their journey to the university.

Figure 7 shows the car users perceived satisfaction level (blue points) and the *safe, efficient* and *comfortable* purpose cognitive demand. The Jaccard's distance measures indicate that the satisfaction-safety set has 0.4548 dissimilarity distance, the satisfaction-comfortability set has dissimilarity of 0.2773, and satisfaction-efficiency set has 0.5888 of dissimilarity. The values show that car users' perceived cognitive efforts on comfortability is least dissimilar to satisfaction compared to safety and efficiency.
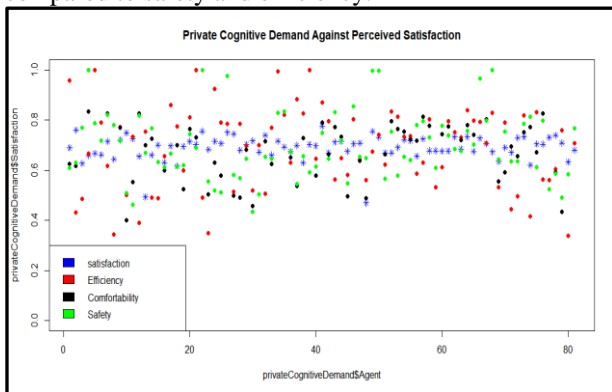
Figure 7: Car users' Perceived Satisfaction and Cognitive Demand Relationships

Although all the Jaccard distance values are positive, the high dissimilarity in efficiency can be attributed to reliability, journey time and costs metrics which are the factors that determine the mode efficiency (see Figure 3). From the questionnaire transcripts, most car users expressed displeasure about the high cost of parking fee within the university. Also,some mentioned peak hour delays as part of the reasons to plan around the time to set out or the routes with less traffic. However, the low dissimilarity value in satisfaction-comfortability set reflects the common knowledge that personal vehicles have better comfortability experience than other modes in terms of protection against bad weather, ease of visiting secondary places etc.

6. DISCUSSION

It was observed in the experiment that cognitive considerations in planning for a journey to the university have the highest number of occurrences for both cyclists and car users. The survey provides the reasons for high cognitive considerations. The survey transcripts recorded that factors such as concern over journey time to avoid traffic delays, as well as parking space when arrived the university at a particular period contributed to car users' high cognitive considerations. The cyclists, on the other hand, are more concerned about their safety, therefore, plans for safe and direct routes with fewer obstructions or with less mounting/dismounting during the journey. Moreover, in Figure 5 the top right and right middle diagram indicate that both modes have fairly the same number of occurrences of pleasant and neutral cognitive experiences, but the bottom right diagram shows that cyclists have more number of occurrences of unpleasant cognitive experiences compared to the car users. The

experience can be attributed to factors such as the attitude of other road users, which always contribute to their planning to use less busy and direct cycle routes to the university. More importantly, the need for planning around available information regarding the journey (e.g. road closure) and daily weather condition is an essential part of cyclists' daily experience.

Regarding the level of effort demanded by the travel requirements, Figure 6 shows that cyclists level of exerted cognition to achieve safety almost correspond to the perceived satisfaction when compared to cycling efficiency and comfortability. This can be attributed to factors such as attitude of road users, as earlier mentioned. The car users comfortability reflects the general perception about the car comfort. However, the insight from the results points to the fact that policymakers need to encourage more pleasant travel experience for the university-bound cyclists, by focussing on improving items that contribute to safety, such as general route network management, and lane markings (see Figure 3). In addition, attitudes such as obstructing the cycle routes should be discouraged, and public awareness on the need to respect the right of cyclists is essential. With the measures in place, car users to the university may be encouraged to shift mode to cycle. Moreover, for car users, as the university does not have a responsibility to improve traffic flow, more parking space around the offices at a reduced price will likely improve their experience.

The results of the experiments show that the technique is capable of providing insight into the level of importance placed upon each of the travel requirements, and how these influence travellers' overall mode perceptions. The information provided will help to identify the area of concern of individual travellers and assist in providing necessary interventions. However, this is just a means to an end in order to further develop our Modal Shift (MOSH) framework (Faboya et al., 2017), where we look into how travellers' interactions with other travellers and their environment influence their mode choice decisions. The MOSH framework employs a more complex agent-based modelling approach. It will allow studying the impact of interventions on travellers' behaviour.

7. CONCLUSIONS

Travellers' mode usage is guided by many factors, among which are travel requirements namely physical, cognitive and affective consideration. Detail insight into the importance and the impact of each requirement on individuals' mode usage experience is essential for the provision of interventions for the enjoyable daily journey and stimulation of travellers' mode choice behaviour. In this paper, we have used a Monte Carlo stochastic approach with fuzzy-decision techniques to model travel mode perception of a set of cyclists and private cars users to a university. The survey focused on the constraints imposed on the travellers by the transport system environment. The data collected were analysed with the Human Factors' abstraction hierarchy to determine the

relationships among the transport system's objects, the constraints that the objects imposed on the travellers. The results of the model revealed that both sets of users engaged in more cognitive process than the physical and affective aspect while palnning for journey, and the reasons for their considerations were explained

It is believed that the method presented in this paper will be helpful in providing insight into the level of considerations given to travel requirements by travellers, and how the requirements influences travellers' overall mode perceptions. The study will also help transport managers by providing reliable indicators to aspects of travellers' experience that needs improvement. However, limitations are found in the use of Likert scale questionnaire for data collection, because some responses might not be adequately captured. In the future, we intend to make a further test of the affective generator's expert knowledge (i.e. circumplex model) with relevant statistical tool against more real-life data to establish its reliability. In addition, we intend to investigate travellers' social interaction and emergent behaviour. We believe agent-based modelling and simulation will enable us to understand further how the travellers respond to behavioural stimulation when exposed to different interventions.

References

Agrawal, U. et al. (2016): Cancer subtype identification pipeline: A classifussion approach. In IEEE *Congress on Evolutionary Computation*.

Bai, Y., & Wang, D. (2006). *Fundamentals of Fuzzy Logic Control – Fuzzy Sets, Fuzzy Rules and Defuzzifications*. *Adv Fuzzy Logic Tech in Industrial Applications*. Berlin: Springer.

Baker, C., Naikar, N., & Neerincx, M. (2008). Engineering planetary exploration systems: integrating novel technologies and the human element using work domain analysis. *International Astronautical Congress*.

Carney, D. R., & Colvin, C. R. (2010). The Circumplex Structure of Affective Social Behavior. *Social Psychological and Personality Science*, *1*(1), 73–80.

Cornelissen, M., Salmon, P. M., McClure, R., & Stanton, N. (2013). Using cognitive work analysis and the strategies analysis diagram to understand variability in road user behaviour at intersections. *Ergs*, *56*, 764–80.

Derek Halden Consultancy. (2003). *Barrier to Modal Shift*. Retrieved from http://www.gov.scot/Resource/Doc/47176/0026887.pdf

Ekkekakis, P., & Petruzzello, S. J. (2002). Analysis of the affect measurement conundrum in exercise psychology: IV. A conceptual case for the affect circumplex. *Psychology of Sport and Exercise*, *3*, 35–63.

Faboya, O. T. et al. (2018). Position Paper: The Usefulness of Data-Driven, Intelligent Agent-Based Modelling for Transport Infrastructure Management. In *IEEE Intl Conf on Intelligent Transportation Systems*. Hawaii, USA.

Faboya, O. T. et al. (2017). A Novel Modal Shift Modelling Framework for Transport Systems. In *Proc. of the 13th Annual Conf. of Social Simulation*. Dublin.

Field Jr., R. V. (2008). *Stochastic Models: Theory And Simulation. Sandia, Report SAND2008-1365*.

Gardner, B., & Abraham, C. (2008). Psychological correlates of car use: A meta-analysis. *Transportation Research Part F*, *11*, 300–311.

Jascanu, N., Jascanu, V., & Bumbaru, S. (2010). Toward Emotional E-Commerce. *Agent and Multi-agent Technology for Internet and Enterprise Systems* (Studies in, Vol. 289, p. 345). Berlin Heidelberg: Springer.

Jenkins, Daniel P, et al (2009). *Cognitive Work Analysis: Coping with Complexity*. Abingdon, GB:

Lewerenz, M. (2002). Monte Carlo methods: Overview and basics. *NIC Series*, *10*, 1–24.

Mann, E., & Abraham, C. (2006). The role of affect in UK commuters' travel mode choices: An interpretative phenomenological analysis. *B J of Psy*, *97*(2), 155–176.

Möller, D. P. F. (2014). *Introduction to Transportation Analysis, Modeling and Simulation*.

Posner, J., Russel, J. A., & Peterson, B. S. (2005). The circumplex model of affect: An integrative approach to affective neuroscience, cognitive development, and psychopathology. *Dev and Psychopathol*,*17*(03).

Rasmussen, J. (1986). *Information Processing and Human-Machine Interaction: An Approach to Cognitive Engineering*. Elsevier Science Ltd.

Rasmussen, J., & Pejtersen, A. M. (1990). *Taxonomy for Cognitive Work Analysis*. *Analysis* (Vol. 157).

Rasmussen, J., Pejtersen, A. M., & Goodstein, L. P. (1994). *Cognitive systems engineering*. Wiley.

Roberts, J., Popli, G., & Harris, R. J. (2017). Do environmental concerns affect commuting choices?: Hybrid choice modelling with household survey data. *J of the Royal Stat Soc. Series A: Statistics in Society*.

Russell, J. A. (1980). A Circumplex Model of Affect. *J of Personality and Soc. Pscychology*, *39*(6), 1161–1178.

Stanton,N.A. et al. (2013). Following the CWA train of thought:Exploring the constraints acting on modal shift to rail transport. *Ergonomics*, 56(3), 522-540.

Steg, L. (2005). Car use:Lust and must. Instrumental, symbolic and affective motives for car use. *Transp Res Part A: Policy and Practice*, *39*, 147–162.

Steg, L. (2007). Sustainable Transportation. *IATSS Research*, *31*(2), 58–66.

Steg, L. et al. (2001). Instrumental-reasoned and symbolic-affective motives for using a motor car. *Transp Res Part F: Traffic Psy and Behaviour*, *4*(3), 151–169.

Tseng, A., et al. (2014). Using the circumplex model of affect to study valence and arousal ratings of emotional faces by children and adults with autism spectrum disorders. *J of Aut and Dev Disorders*, *44*(6), 1332–1346.

Vicente, K. J. (1999). *Cognitive Work Analysis Toward Safe , Productive , and Healthy*.

Wagner, C. (2013). A Java based Toolkit for Type-2 Fuzzy Logic. In *Proc IEEE Symp on Comp Int*.

Wardman, M., Hine, J., & Stradling, S. (2001). Interchange and Travel Choice Volume 1.

Wickens, D. C. et al. (2004). *An Introduction to Human Factors Engineering* (2nd ed.).

Zadeh, L. A. (1996). Fuzzy Logic = Computing with Words. *IEEE Trans ON Fuzzy Systems*, *4*(2).

A SIMULATION APPROACH FOR HUMAN RELIABILITY ANALYSIS IN AN ORTHOPAEDIC OPERATING ROOM

Di Pasquale V.[a], Iannone R.[b], Maffulli N. [c], Miranda S.[d], Riemma S.[e]

[a], [b], [d], [e] Department of Industrial Engineering (DIIN), University of Salerno
[c] Department of Musculoskeletal Disorders, University of Salerno School of Medicine, Surgery and Dentistry

[a]vdipasquale@unisa.it, [b] riannone@unisa.it, [d] smiranda@unisa.it, [e]riemma@unisa.it
[c] nmaffulli@unisa.it

ABSTRACT

Surgical context is characterized by a strong human component with low probability of human error occurrence but high consequences. A human operator can make a mistake that has both a social implication, from the point of view of patient's safety, and economic, from the point of view of the costs incurred. For these reason, the last few years have seen growing interest in a wider range of human reliability techniques used in other industries applied in healthcare environments. In this study, the Simulator for Human Error Probability Analysis (SHERPA) has been applied for modelling and simulating the activities performed by a surgical team during the reconstruction of the Achilles tendon following rupture. The proposed simulation approach provides for the evaluation of the human reliability on the result of an orthopaedic procedure, in terms of errors committed and time taken to perform it. This simulation approach has been verified and validated through a statistical analysis, which showed its applicability to real scenarios for the improvement of the orthopaedic operating team's performance.

Keywords: Human error, Human Reliability Analysis, Orthopaedic Procedure, Simulation.

1. INTRODUCTION

Surgical context is a risky environment with low probability of human error occurrence but high consequences. The consequence of an error is of crucial importance, and the spectrum varies from no consequence to serious and fatal. Some errors are intrinsically more important than others, although their effects or consequences vary with extraneous circumstances (Cuschieri 2000). For example, in endoscopic surgery, a surgeon may exert too much tenting force during use of an electrosurgical knife with inevitable follow-through of the hook knife once the tissue is cut. It is a matter of luck, where the hook knife stops without consequences, or damages a bowel or large vessel with serious consequence (Cuschieri 2000). Therefore, it is essential to use human error estimation techniques as a tool for risk analysis and decision support in surgical environments, to intervene by improving the

reliability of the operating team through, for example, the optimal management of work shifts, breaks and workloads assigned to each operator.

The methodologies for Human Reliability Analysis (HRA) identify the errors and weaknesses in the system focusing on those who work in the system and they have evolved into a discipline that encompasses theoretical and analytic tools needed for understanding how human actions and decisions are influenced by the system's complexity and dynamics. HRA approaches have been developed in industrial contexts, such as the nuclear power plants or aviation industry, where the consequences of errors are catastrophic. Such a retrospective approach is considered unacceptable (Di Pasquale et al. 2013).

In the last few years, there has been growing interest in these safety and human reliability techniques used in other industries for application in healthcare environment. In particular, an important characteristic of the HRA approaches, which fits well with the need to improve patient's safety in healthcare, investigates the HRA anticipatory pattern rather than retrospective one (Onofrio, Trucco, and Torchio 2015). The human error probability (HEP) estimation allows providing ex ante analysis before incidents or adverse events occur, and identify appropriate corrective measures that can be implemented before inadequacies of system can occur. Cox, Dolan and Macewen (2008) describe the application of HRA as a tool to quantify errors that occur during small incision cataract surgery, whereas Malik, White and Macewen (2003) describe the nature of active skill-based errors occurring in endoscopic dacrocystorhinostomy surgery.

Lyons et al. (2004) performed a full literature review of HRA techniques in healthcare, producing a brief list of fourteen primary HRA techniques, which have either had practical application in healthcare or which were well-established elsewhere and had potential application. Most of these techniques are based on an initial task analysis and a task simulation to identify a list of the potential errors that could occur associated with this task. Quantification is usually based on either fault trees or event trees, which provide the basis for quantification. Some identified methodologies take into account also the

influencing factors, that are individual, situational, contextual or environmental factors that may affect surgeons' performance.

Onofrio, Trucco and Torchio (2015) developed an ad hoc taxonomy of ten Influencing Factors for surgery (Table 1), extracted from the literature and classified according to the SHELL model (Software, Hardware, Environment, and Liveware). This model defines the interaction between procedures (software), equipment (hardware), environment and plants present in the working context, and the operator (liveware), taking into account the possibility of interaction of the operator with other operators or supervisors (liveware) (Trucco and Leva 2007).

The breadth of HRA techniques applications suggests that the potential application of these techniques is very wide, encompassing design of surgical instruments, equipment and procedures; decisions about the labelling of dangerous drugs; design of a system of double checks for drug administration; organization of work processes such as booking appointments or patient flow in accident and emergency; identification of the factors that lead to high stress and liability to error in clinicians; and the analysis of the range of factors involved in a serious incident and in the subsequent implementation of safety solutions across a clinical department or healthcare system.

Table 1: Influencing Factors in Surgery Applications (Onofrio, Trucco and Torchio 2015).

Influencing factors	Valence
Noise & back-ground talk not related to the task	+/-
Safety Culture and Safety Climate	+/-
Standardization	+/-
Equipment, HMI and space design	+/-
Communication and team-work	+/-
Experience and Team Training	+
Fatigue	-
Leadership	+/-
Staffing and team member familiarity	+/-
Workload	-

There is a growing interest on HRA methodologies and techniques in healthcare and in particular in surgery. Some authors also recognise in the inherent complexity of healthcare operations the main barrier against the diffusion of Human Reliability Analysis (HRA) techniques in the same domain.

An opportunity to overcome this limitation is related to human performance simulation, which reveals important new data sources and possibilities for exploring human reliability. Many efforts have been recently directed towards simulation, in order to assess human behaviour and calculate the reliability for the performed activity in HRA field. For example, Azadeh et al. (2015) described

a simulation optimization of an emergency department in a general hospital in Iran by modelling human error.

For these reasons, this paper proposes a simulation approach for human reliability analysis in an orthopaedic operating room. The main purpose is to provide an approach that can evaluate and quantify HEP of the operating team in order to intervene in the error reduction through the management of shifts and break scheduling. To achieve this goal it is necessary a simulator that reproduces human behaviour, characterized by high variability and randomness and which cannot easily be reproduced in a deterministic manner.

In this regard, this paper applied the Simulator for Human Error Probability Analysis (SHERPA) (Di Pasquale et al. 2015a,b) for modelling and simulating the activities performed by a surgical team during the reconstruction of the Achilles tendon following rupture, for the evaluation of the human reliability effects on the result of an orthopaedic surgery, both in terms of errors committed and in terms of the time taken to perform it.

Starting from the shortcomings of the existing HRA approaches, SHERPA model has been developed for predicting the probability of human error for a given scenario in every type of industrial system or other type of working contexts (Di Pasquale et al., 2015a, 2017). It is designed for HRA, and unlike many existing HRA methods that are deeply qualitative and include excessive levels of detail for many assessments, SHERPA focuses on the quantitative aspect to obtain a significant numerical result in terms of HEP. The knowledge of the HEP distribution allows to intervene from the perspective of reducing errors with re-design tasks or other interventions such as the management of the worker's psychophysical recovery through appropriate break configurations. SHERPA is, in fact, addressed to the break scheduling problems through the hypothesis that breaks allow the mental and physical recovery and lead to improvements of human reliability. The simulation model includes the occurrence of human errors and the processes of error consequences. The main strength of this approach is to combine the break scheduling management with HEP quantification, allowing to:

- Assess the impact of the environment on human reliability.
- Simulate large numbers of rest configurations.
- Determine optimal breaks scheduling, identifying for each case: the number, the position in the shift and the optimal break time.

To the authors' knowledge this is the first application of SHERPA simulator for assessing human errors in operating rooms, and in particular an orthopaedic operating room, to enhance the patient safety and quality of care in operating rooms. The results of the proposed approach help decision makers to enhance team performance by considering human error through the appropriate setting of break scheduling and the workloads.

2. PROBLEM STATEMENT

The operating room is the set of premises, structures, and resources necessary for the execution of surgical operations. It is the nerve centre of hospital activity and its efficiency is a fundamental objective to guarantee adequate levels of production, management of resources and necessary levels of safety for patients and operators. Its organization also directly affects the proper management of many hospital departments and support services.

Surgical team performance affect in most cases the surgery results, as previously underlined. Human performance, in fact, depends on individual factors (such as age, experience, physical and mental stress, medical status), contextual factors (microclimate, lightning, noise, equipment and space design) or organizational factors (communication and team-work, safety culture). Furthermore, the management and scheduling of sequential surgeries may impact on the physical and mental fatigue, increasing human error probability, if operators cannot recovery with appropriate scheduling. Therefore, the surgical team resources, involved in a surgery, have particular characteristics which are challenging to model and simulate. The surgical team, in fact, differs from production or assembly working team as surgical task cannot be simply compared to other working tasks, for which existing HRA methods were developed and applied to a wide range of case studies.

The main challenge in this context is therefore the application of traditional and existing approach to assess the human reliability of surgical team considering the specific features of operators, environments, performed tasks and error consequences. The modelling and simulation of surgical team performance, using the HRA approach, could support the prevention or reduction of the human error occurrence, through proper key interventions to improve patient safety and quality of care.

3. CASE STUDY

The study was carried out in orthopaedic surgery: the reconstruction of the Achilles tendon following rupture, conducted in an operating room of Department of Orthopaedics and Traumatology of the University Hospital San Giovanni di Dio-Ruggi d'Aragona of Salerno. This surgery was carried out using an innovative technique developed by Maffulli, Longo, Gougoulias, and Denaro (2008). Task analysis was performed to determine the chronological steps involved, as reported in Table 2.

4. SOLUTION APPROACH

The previous problem statement was addressed through the simulation of the whole surgical process, using the Simulator for Human Error Probability Analysis (SHERPA) model (Di Pasquale et al. 2015a, 2015b, 2016, 2017) to evaluate human performance, using the Anylogic simulation package.

Table 2: Operating activities.

TASK	DESCRIPTION	RESOURCES
Anaesthesia room	The identity of the patient and of the site to be operated is verified. The anaesthetist administers the anaesthesia and waits until the patient is anesthetized.	Nurse Anaesthetist
Pre-intervention in the operating room	A nurse and a theatre nurse proceed with the preparation of the material and equipment used during the operation.	Nurse Theatre nurse
Patient positioning	The patient is moved to the operating bed and he/she is positioned prone with a thigh tourniquet.	Nurse
Operating field preparation	Skin preparation is performed, and sterile drapes are applied.	Surgeon Nurse Anaesthetist
Operating activity 1	Pre-operative anatomical markings include the palpable tendon defect and both malleoli.	Surgeon
Operating activity 2	Two skin incision are made. The first incision is a 5 cm longitudinal incision, made 2 cm proximal and just medial to the palpable end of the residual tendon.	Surgeon
Operating activity 3	The second incision is 3 cm long and it is also longitudinal but is 2 cm distal and in the midline over the distal end of the tendon rupture. The proximal and distal AT stump are mobilised, freeing them of all the peritendinous adhesions.	Surgeon
Operating activity 4	The tendon of the semitendinosus is harvested through a vertical, 2.5–3 cm longitudinal incision over the pes anserinus	Surgeon
Operating activity 5	An osteotomy of the postero-superior angle of the calcaneus is performed.	Surgeon
Operating activity 6	The calcaneus is pierced and reamed in order to obtain a bone tunnel to pass the semitendinosus to be transplanted.	Surgeon
Operating activity 7	The semitendinosus tendon is passed through an incision of the proximal stump and secured to the entry and exit points of the incision.	Surgeon
Operating activity 8	The tendin of the semitendinosus is passed through the bone tunnel made in the calcaneus stretched with the foot put in complete plantar flexion. The tendin fixed with an interface screw in the calcaneus and sutured to the distal stump of the Achilles tendon.	Surgeon
Operating activity 9	The incisions are sutured, and the limb is put in a plaster cast.	Surgeon

The HRA approach was set for the surgical team resources, considering their professional features. In this way, the orthopaedic surgery was reproduced in a simulation model, that is able to represent and predict the team performance in every hypothesized scenario.

4.1. Modelling of surgical activities

As initial assumption, it was decided to study the process that includes the activities performed in the operating room starting from the patient entry time to the anaesthesia room to the ends of surgery. Moreover, it was hypothesized (even considering the surgery that was chosen to simulate) that the operating team is composed of two nurses, a theatre nurse, an anaesthetist and two surgeons.

The flow of patients in surgery is shown in Fig. 1, where the surgical team (nurses, anaesthetist and surgeons) are engaged in two distinct environments: the anaesthesia room in orange and operating room (green). Each resource performs one or more activities following the sequential steps reported in Table 2. These activities are performed both simultaneously and in parallel. This orthopaedic surgery may involve possible errors and hazards related to the procedure, that were identified followed Maffulli et al. (2008):

- Inadequate exposure and traction of the proximal stump of the Achilles tendon (operating activity 3). → Solution - Complete the exposure.
- Incorrect positioning, breaking, loss or loosening of the screw (operating activity 8) → Solution - Remove the screw.
- Inadequate tendon tension (operating activity 8) → Solution - Repetition of the intervention.
- Calcaneus fracture (operating activities 5 and 6) → Solution - Fracture reduction and internal fixation.
- Damage to the sural nerve.
- Prevent infection → Solution - Antibiotics.
- Reduced mobility → Solution - Physiotherapy.
- New rupture → Solution - New reconstruction procedure.

As indicated by this list, the error consequences involve both post-intervention complications and lengthening of the average surgery time. The possible errors related to the operating activities that may lead to possible post-intervention complications are mainly found in the operating activity 8, while the others can be easily recovered, leading to a lengthening of the times of the operation itself.

Such errors depend on the reliability level of each surgical team member. For these reasons, HR levels need to be modelled and simulated to prevent or reduce the human error occurrences, improving human performance through proper key interventions to improve patient safety and quality of care.

4.1.1. Human performance modelling

The SHERPA (Di Pasquale et al. 2015a, 2015b, 2016, 2017) model was chosen as HRA approach to model the human resources involved in the surgery and to quantify their human error probability during the surgical steps. SHERPA is a new HRA model that exploits the advantages of the simulation tools and the traditional HRA methods to predict the likelihood of operator error, for a given scenario, in every kind of industrial system or other type of working environment (Di Pasquale et al. 2015a, 2015b, 2016, 2017).

SHERPA can be used in the preventive phase, as an analysis of the possible situations that may occur and for the evaluation of the percentage of non-compliant performed tasks arising human error and in post-production to understand the nature of the factors that influence human performance in order to reduce errors.

The theoretical framework is described in Figure 2. The four sub-activities (entities entry, HR quantification, process simulation, entities exit) are supported by the operating logic shown in Figure 3.
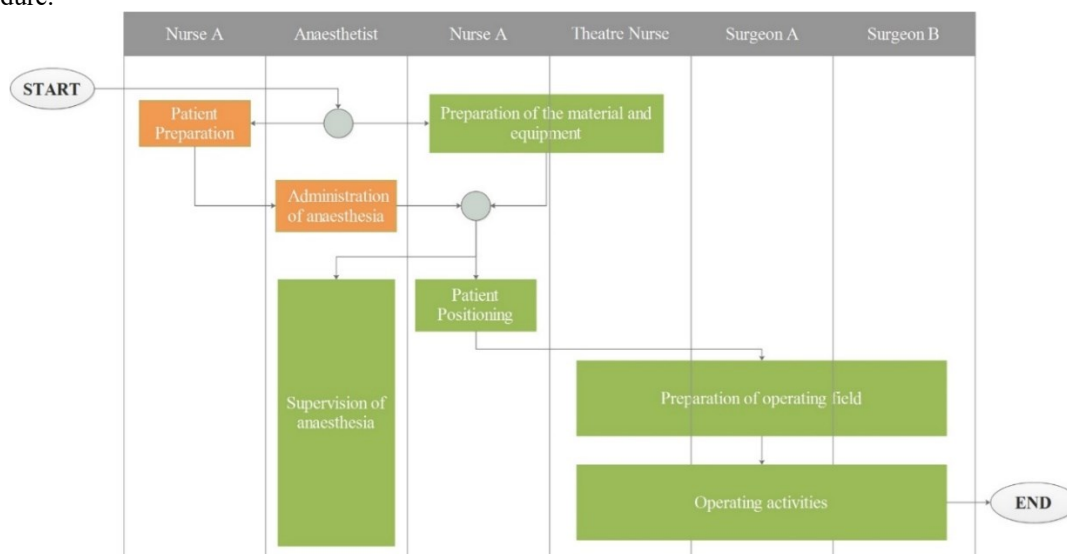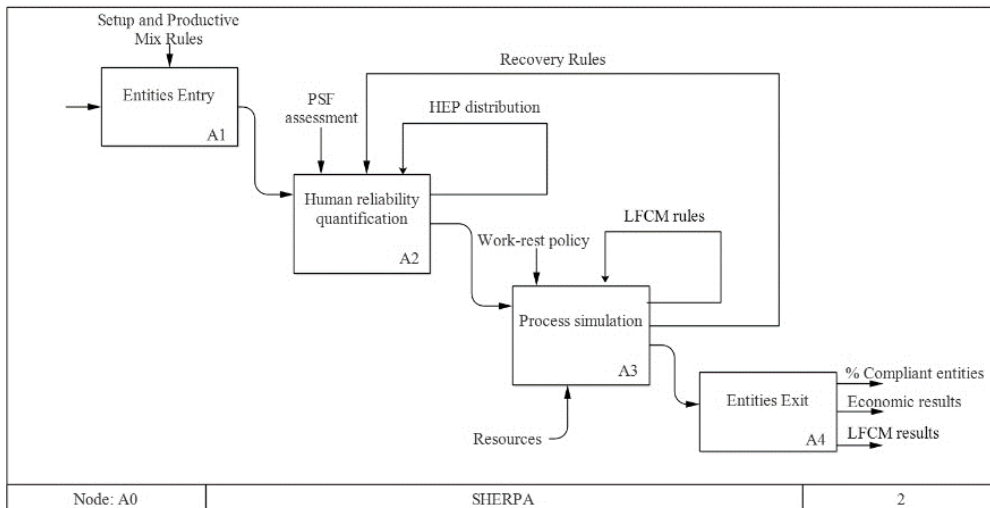

Figure 1: Operating activities.
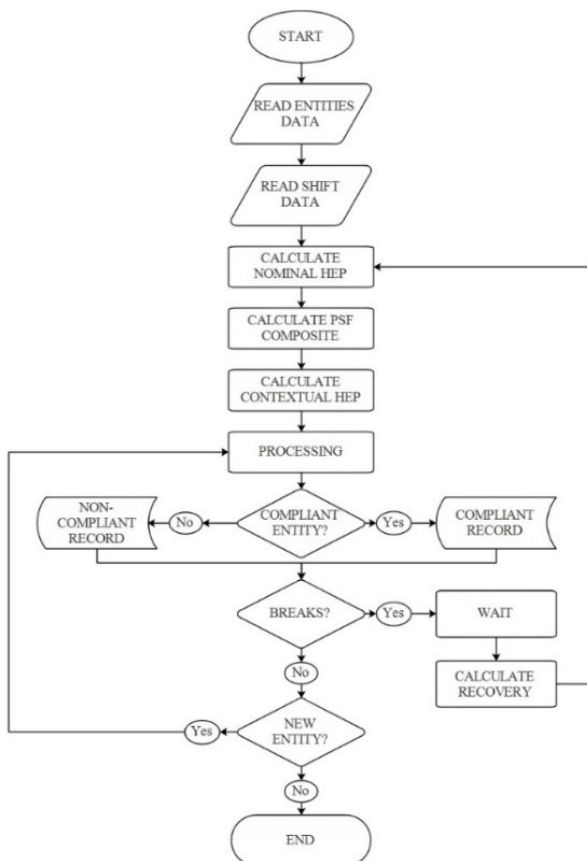
Figure 2: Overview of SHERPA.

Figure 3: Logical architecture of SHERPA model (Di Pasquale et al. 2017)

The model reproduces the employee's work during a whole shift, quantifying the reliability and error probability that moved on the outputs of the system. The starting analytical basis for the assessment of human errors in SHERPA is the determination of HEP, followed by quantification of Performance Shaping Factors (PSF) influences on the initial value of HEP Human reliability is estimated as a function of the performed task, influencing factors, and time worked, with the purpose of considering how reliability depends on the task and working context as well as on the time that the workers have already spent at their work. In the HRA methods, conditions that influence human performance are often referred by term performance shaping factor (PSF). These contextual factors are determined by the individual characteristics of the human being, the environment, the organization or the activity that enhances or decreases human performance and increases or decreases the likelihood of human error (Di Pasquale et al. 2015a).

The nominal HEP is a Weibull probability distribution as follows:

$$\begin{cases} HEP_{nominal}(t) = 1 - k \cdot e^{-\alpha \cdot (1-t)^{\beta}} \ \forall \ t \in [0; \tau] \\ HEP_{nominal}(t) = 1 - k \cdot e^{-\alpha \cdot (t-1)^{\beta}} \ \forall \ t \in]\tau; \infty[\end{cases} \quad (1)$$

where t is the time worked by an employee; k, β, and α change the scale and shape of the curve for the six generic tasks used in the model; and τ is the length of the transitional phase of human adaption. The working context and employee state are taken into account through the PSFs of the SPAR-H method. Nominal HEP is therefore modified by these eight PSFs using the following adjustment factors:

$$HEP_{contextual}(t) = \frac{HEP_{nominal}(t) \cdot PSF_{composite}}{HEP_{nominal}(t) \cdot (PSF_{composite} - 1) + 1} \quad (2)$$

where $PSF_{composite}$ is calculated as

$$PSF_{composite} = PSF_1 \times \dots \times PSF_x \times \dots \times PSF_8 \quad (3)$$

where PSf_x is the assigned multiplier for each PSF.

The strength of SPAR-H is in providing a guide for assigning numerical weights for the PSFs; the multiplier values for every PSF are reported in Table 3. These PSFs can easily set for every kind of work environment or workforce, in order to reproduce the given scenario.

Knowing the HR distribution allows to intervene from the perspective of reducing errors with re-design tasks or other interventions such as the management of the worker's psychophysical recovery through appropriate break configurations. Moreover, the tool provides the possibility of determining the optimal configuration of

breaks considering the operator's psychophysical recovery that involve the increase of human reliability.

Table 3: PSF multipliers for action and diagnosis (Gertman et al. 2004).

SPAR-H PSFs	PSF Levels	Multipliers Action	Multipliers Diagnosis
Available Time	Inadequate Time	P(failure)=1	P(failure)=1
	Time available = time required	10	10
	Nominal time	1	1
	Time available > 5 x time required	0.1	0.1
	Time available > 50 x time required	0.01	0.01
	Insufficient information	Nominal	Nominal
Stress/ Stressors	Extreme	5	5
	High	2	2
	Nominal	1	1
	Insufficient information	Nominal	Nominal
Complexity	Highly complex	5	5
	Moderately complex	2	2
	Nominal	1	1
	Obvious diagnosis	-	0.1
	Insufficient information	Nominal	Nominal
Experience/ Training	Low	3	10
	Nominal	1	1
	High	0.5	0.5
	Insufficient information	Nominal	Nominal
Procedures	Not available	50	50
	Incomplete	20	20
	Available, but poor	5	5
	Nominal	1	1
	Diagnostic/symptom oriented	-	0.5
	Insufficient information	Nominal	Nominal
Cognitive Ergonomics	Missing/Misleading	50	50
	Poor	10	10
	Nominal	1	1
	Good	0.5	0.5
	Insufficient information	Nominal	Nominal
Fitness for Duty	Unfit	P=1	P=1
	Degraded Fitness	5	5
	Nominal	1	1
	Insufficient information	Nominal	Nominal
	Poor	5	2
Work Processes	Nominal	1	1
	Good	0.5	0.8
	Insufficient information	Nominal	Nominal

The third SHERPA sub model, in fact, represents the process modelling, and allows to simulate the execution of human working activities, taking into account the features of the process, the HEP, and the assigned breaks scheduling. The selection of the input variables such as performed task, level of contextual factors, or physical and mental employee condition, allows to model the specific system considering all the working context and worker features. SHERPA can manage three different rest breaks policies:

- no break in the shift (continuous working);
- fixed breaks (several timing and length);
- automatic break scheduling management.

The absence of breaks corresponds to the mere reproduction of the process. The fixed break or automatic sections involve the break scheduling management through the hypothesis that breaks allow the mental and physical recovery and lead to improvements of human reliability. The worker's recovery is modelled as a function of the break length and of the type of activity carried out. This function can be used to evaluate the best break scheduling to assign during a work shift.

Finally, SHERPA usually determines as outputs the number of compliant, non-compliant, and rework entities as function of quantified human error probability. In the context under investigation, the errors were modelled as post-intervention complications and lengthening of the average surgery time. The available outputs allow a clear and direct assessment of how the system reacts to change in the given break scheduling, as well as to change in environmental and psychophysical conditions.

4.2. Surgery simulation

The conceptual model was implemented in the simulation model as graphically shown in Figure 4.

The arrival of a single patient determines the beginning of the whole surgical process. The surgical team marks the succession of tasks to be performed and it determines the progress of the operation within the simulation model. In particular, the *State Chart* in Figure 4 manages all the operating activities as reported in Table 2. The number, type and duration of each activity are regulated by *Statechart* which has a double utility: it manages the sequence of actions performed by the agents and it allows interaction between the various resources involved. Once the operating activity is performed, the *Statechart* moves on to the next activity until the surgery is complete, when it returns to its initial state, waiting to be activated again. A SHERPA template (*hRAblock*) was assigned to each resource. The SHERPA template allows the collection of reliability level of resources and the relative performance, in terms of errors committed and times taken to complete the activities, as described in the next sub-section.

The activities performed in the pre-operative anaesthesia room, and operating theatre by each resource was modelled in detail. For example, the activities performed by Nurse were modelled as shown in Figure 5, where the *hRAblock* allows the implementation of SHERPA model to quantify HEP. The *State chart* allows managing and processing all the activities performed by the individual

operator in the sequence reported in Table 2, and calculating in real time the operator's performance and the possible errors committed with the relative consequences. For each resources, it has been assumed that the so-called "passive" actions (for example the activity of control of vital parameters by the anaesthesiologist in the operating room) are not subject to reliability analysis, therefore they have not been modelled.

At the end of the operation, the patient operated leaves the model, which is ready to receive another one.
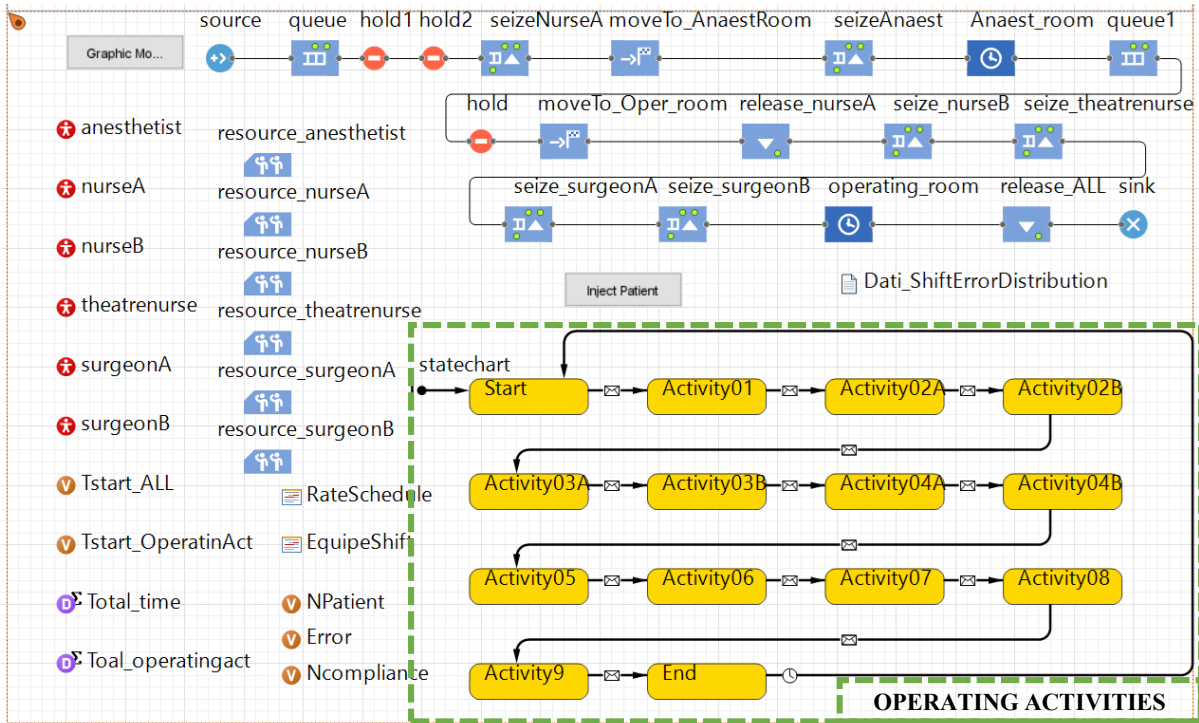
Figure 4: Operating room model.
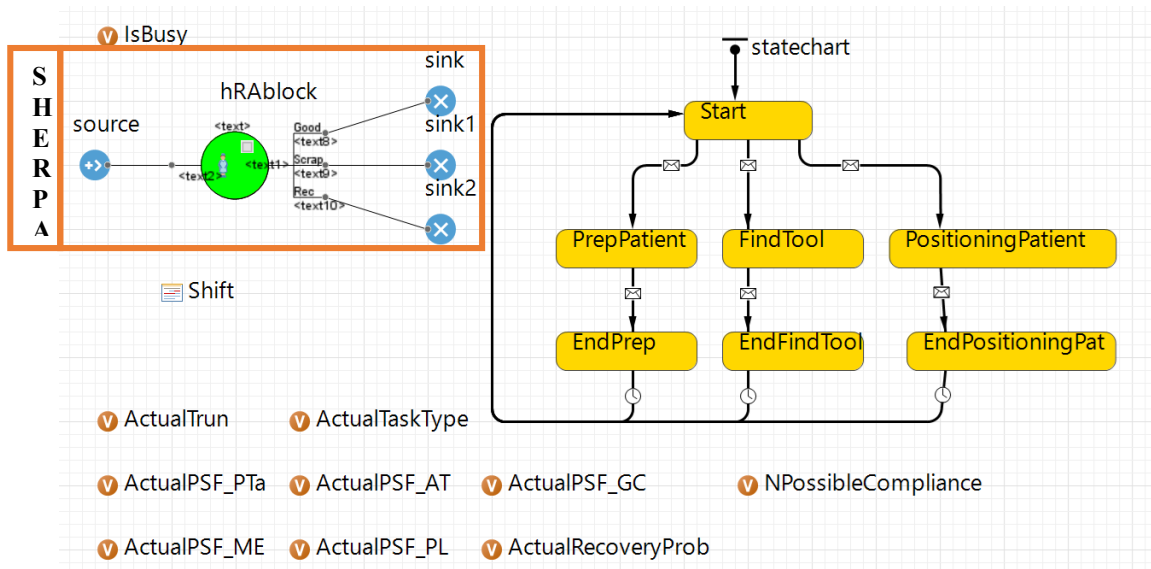
Figure 5: Nurse Agent.

4.2.1. Simulation human performance

Each resource (nurse, anaesthetist, theatre nurse and surgeon) corresponds to an SHERPA agent, and it was modelled from relevant field data. The PSF levels were defined considering the specific features of the operating room and surgical team, as for example the microclimatic and lighting levels, defined according to the law, or the excellent integration into the team and high level of experience. Furthermore, available time, general complexity, mental efforts, parallel tasks and precision level were assigned with dynamic values, that can change during the surgery execution and as function of possible error occurrences. The SHERPA blocks, one for each

resource involved, allow the collection of reliability level of resources and the relative performance, in terms of errors committed and times taken to complete the activities. In this case, the SHERPA simulates the completion of an elementary operation: each processed entity represents an activity that can end with a success, a rework or an error, as function of the error probability curves that characterize the resource who performs the task. In particular, the rework entails an increase of the operating activity time. Human errors are, therefore defined as combination of errors committed by surgical teams.

4.2.2. Surgery time

Table 4 shows the times of the performed surgical activities. These times were obtained through a direct comparison with the personnel taking part in the surgery on the basis of their internal database, and these data were re-elaborated to be implemented in the simulator (Table 5a and 5b).

Table 4: Time of operating activities.

Activity	Minimum time	Modal time	Maximum time
Anaesthesia room	15 min	20 min	30 min
Pre-intervention in the operating room	5 min	10 min	15 min
Patient positioning	—	—	2 min
Operative field preparation	5 min	7-8 min	10 min
Operating activity 1	—	—	1 min
Operating activity 2	1 min	2 min	3 min
Operating activity 3	—	—	1 min
Operating activity 4	—	—	1 min
Operating activity 5	—	—	2 min
Operating activity 6	—	—	2 min
Operating activity 7	3 min	4 min	5 min
Operating activity 8	—	—	1 min
Operating activity 9	5 min	7-8 min	10 min

Table 5a: Distribution used in the model.

Activity	State	Agent Resource	Distribution (min)
Anaesthesia room	PrepPatient	NurseA	Uniform (0.5, 2)
Anaesthesia room	Anaesthesia	Anaesthetist	Triangular (15,30,20)
Pre-intervention in the operating room	FindTool	NurseB	Triangular (0.15, 1.50, 0.25)
Pre-intervention in the operating room	Positioning Tool	Theatre nurse	Uniform (0, 0.15)
Patient positioning	PositioningPatient	NurseB	Uniform (0.25, 2)

Table 5b: Distribution used in the model.

Activity	State	Agent Resource	Distribution (min)
Operative field preparation	PrepSkin	Theatre nurse	Triangular (3, 6, 4.5)
Operative field preparation	PrepDrapes	SurgeonB	Triangular (2, 4, 3)
Operating activity	TakeTool	Theatre nurse	Uniform (0.05, 0.15)
Operating activity 1	Activity01	SurgeonA	Uniform (0.25, 1)
Operating activity 2	Activity02A	SurgeonA	Uniform (0.15, 0.25)
Operating activity 2	Activity02B	SurgeonA	Triangular (1, 3, 2)
Operating activity 2	Activity02B	SurgeonB	Uniform (0.25, 0.5)
Operating activity 3	Activity03A	SurgeonA	Uniform (0.15, 0.25)
Operating activity 3	Activity03B	SurgeonA	Uniform (0.50, 1)
Operating activity 4	Activity04A	SurgeonA	Uniform (0.15, 0.25)
Operating activity 4	Activity04B	SurgeonA	Uniform (0.50, 1)
Operating activity 4	Activity04B	SurgeonB	Uniform (0.25, 0.5)
Operating activity 5	Activity05	SurgeonA	Triangular (1, 2, 1.5)
Operating activity 6	Activity06	SurgeonA	Triangular (1, 2, 1.5)
Operating activity 6	Activity06	SurgeonB	Uniform (0.25, 0.5)
Operating activity 7	Activity07	SurgeonA	Triangular (3, 5, 4)
Operating activity 8	Activity08	SurgeonA	Uniform (0.50, 1)
Operating activity 9	Activity09	SurgeonA	Triangular (5, 10, 7.5)

For each entity entering SHERPA, the attribute corresponding to the activity time is assigned. If all the values were known, a triangular distribution was defined, in the other cases, without enough information available, it was decided to use a uniform distribution. Some activities were divided because they are composed of more sub-activities that require the use of different tools (for example the operating activities 2, 3 and 4) or the collaboration among more team resources (if there is a request for an instrument or a request for assistance). In Table 5a and Table 5b, there is a collection of all the distributions used to the surgical resource involved.

4.2.3. Simulation approach validation

Verification and validation of simulation model is usually part of the model development process. In order to enhance the assurance of the results and evaluate the accuracy of models, it is necessary to verify and validate the simulation model. The model validation is defined as proving that the conceptual model is an accurate representation of real system which deals with forming the correct model.

The model presented was validated and verified by statistical test considering the total time of the intervention (from the beginning of the administration of the anaesthesia to the end of the operating activities), and then the time of the operating activity with data collected within the operating registry from November 2015 to October 2016 and shown in Table 6.

Table 6: Historical data from operating registry.

Patient	Date	Room Entry	Start of anaesthesia	Start of Surgery	End of Surgery	End anaesthesia	Room Exit
01	26/01/2016	14:30	14:30	14:50	15:10	—	15.20
02	15/03/2016	8:50	9:00	9:10	9:25	9:30	10:00
03	17/03/2016	8:00	8:00	8:30	9:40	—	9:45
04	29/03/2016	13:00	13:00	13:20	14:00	—	14:10
05	05/04/2016	10:50	11:00	11:30	12:10	12:20	12:30
06	28/04/2016	12:00	12:00	12:15	12:40	—	12:45
07	16/06/2016	8:15	8:30	9:00	9:40	—	9:50
08	23/06/2016	8:00	8:00	8:45	9:15	—	9:20
09	14/07/2016	8:00	8:30	9:00	9:15	—	9:30
10	26/07/2016	8:00	8:10	9:00	9:50	—	10:00
11	06/09/2016	8:00	8:25	9:00	9:30	—	9:40

Real time were subjected to a boxplot analysis that led to the exclusion of the real patient number three. Table 7 contains the durations obtained by running a model run on the simulator. The tests necessary for the validation of the model were applied both for the total duration of the intervention and for the individual operating activities that allowed to consider the model as validated. In this way the lengthening of the average surgery time in presence of human error was validated. Future studies are ongoing, instead, to validate the post-intervention complications, that are more complex to identify and measure in this environment.

5. CONCLUSIONS

The application of HRA in healthcare environments is not widespread, even though the human component affects the results of each medical process. The human error assessment in these contexts it is fundamental for the social implication that mistakes could have if they were committed. In this paper, a simulation approach using SHERPA model for human reliability analysis in an orthopaedic operating room was proposed. A real case study was used to validated the model.

Table 7: Data derived from real system and simulator.

Real system			Model to the simulator		
Patient	Total activity duration (min)	Duration of surgery (min)	Patient	Total activity duration (min)	Duration of surgery (min)
1	40	20	1	59.131	23.076
2	25	15	2	70.701	24.547
3	100	70	3	70.879	21.539
4	60	40	4	53.956	22.036
5	70	40	5	51.302	22.165
6	40	25	6	51.991	21.867
7	70	40	7	57.687	21.323
8	75	30	8	60.466	26.046
9	45	15	9	53.025	23.362
10	100	50	10	71.152	24.565
11	65	30	11	54.003	22.692
			12	60.909	23.279
			13	59.987	28.120
			14	51.008	22.323
			15	60.146	26.596

This simulation approach is able to reproduce alternative scenarios with the change of the PSF levels or break scheduling, to evaluate the impact of individual, contextual and organizational factors as well as identify the best break configuration. It is a decision support system to take into account the human performance in healthcare environment. Furthermore, the proposed simulation approach has general validity and it can be extended and applied to any surgery changing the *StateChart* related to the operating activities for each resource.

Future steps include the application for scenario analysis according to the characteristics of the operating team and the assigned break configurations, to assess their impact on human reliability and on the results of surgical interventions. These studies will allow identifying the optimal conditions for the reduction of errors, intervening in particular on work shifts, workloads and break configuration. Future studies involve, also, the validation of post-complications from human error and in depth analysis of key performance shaping factors impact on surgical team performance.

REFERENCES

Azadeh A., Ahvazi M. P., Haghighii S. M. and Keramati A., 2015. Simulation Optimization of an Emergency Department by Modeling Human Errors. Simulation Modelling Practice and Theory 67: 117–36.

Cox A., Dolan L., and Macewen C. J., 2008. Human Reliability Analysis: A New Method to Quantify Errors in Cataract Surgery. Eye (London, England) 22(3): 394–97.

Cuschieri A., 2000. Human Reliability Assessment in Surgery - a New Approach for Improving Surgical Performance and Clinical Outcome. The Royal College of Surgeons of England 82: 83–87.

Di Pasquale V., Miranda S., Iannone R., and Riemma S., 2013. An overview of human reliability analysis techniques in manufacturing operations. In Operations management. InTech.

Di Pasquale V., Miranda S., Iannone R., and Riemma S., 2015a. A simulator for human error probability analysis (SHERPA). Reliability Engineering & System Safety, 139, 17-32.

Di Pasquale V., Miranda S., Iannone R., and Riemma S., 2015b. An HRA-based simulation model for the optimization of the rest breaks configurations in human-intensive working activities. IFAC-PapersOnLine, 48(3), 332-337.

Di Pasquale V., Franciosi C., Lambiase A.and Miranda, S., 2016, December. Methodology for the analysis and quantification of human error probability in manufacturing systems. In Research and Development (SCOReD), 2016 IEEE Student Conference on (pp. 1-5). IEEE.

Di Pasquale V., Fruggiero F., Iannone R. and Miranda S., 2017. A Model for Break Scheduling Assessment in Manufacturing Systems. Computers and Industrial Engineering 111: 563–80.

Gertman D. et al., 2004. The SPAR H Human Reliability Analysis Method. In American Nuclear Society 4th International Topical Meeting on Nuclear Plant Instrumentation, Control and Human Machine Interface Technology, Columbus, OH, United states, 17–24.

Lyons M., Adams S., Woloshynowych M. and Vincent C., 2004. Human Reliability Analysis in Healthcare: A Review of Techniques. International Journal of Risk and Safety in Medicine 16(4): 223–37.

Maffulli N., Umile G. L., Gougoulias N. and Denaro V., 2008. Ipsilateral Free Semitendinosus Tendon Graft Transfer for Reconstruction of Chronic Tears of the Achilles Tendon. BMC musculoskeletal disorders 9(1): 100.

Malik R., White P. S. and Macewen C. J., 2003. Using Human Reliability Analysis to Detect Surgical Error in Endoscopic DCR Surgery. Clinical Otolaryngology and Allied Sciences 28(5): 456–60.

Onofrio R., Trucco P. and Torchio A., 2015. Towards a Taxonomy of Influencing Factors for Human Reliability Analysis (HRA) Applications in Surgery. Procedia Manufacturing 3: 144–51.

Trucco P., and Leva M. C., 2007. A probabilistic cognitive simulator for HRA studies (PROCOS). Reliability Engineering & System Safety, 92(8), 1117-1130.

LONGWALL TECHNOLOGY SIMULATION

Victor V. Okolnishnikov[a], Alexander A. Ordin[b], Sergey V. Rudometov[c]

[a],[b],[c] Institute of Computational Technologies SB RAS
Novosibirsk, Russia

[a]okoln@mail.ru, [b] ordin@misd.ru, [c] rsw@inbox.ru

ABSTRACT

A simulation model of the performance of the longwall in underground coal mine is presented. The simulation model is developed with the help of our own simulation system MTSS, which contains a specialized library of mining equipment models and a coal seam model. The main goal of the simulation for coal mining technological processes in stoping face is the evaluation of productivity of a cutter-loader depending on different factors. Such factors are: technical parameters of a cutter-loader, size of a longwall face, conditions and constrains of technological processes in stoping face, geophysical state of a coal seam.

Keywords: coal mining, simulation system, visual interactive simulation, longwall mining system

1. INTRODUCTION

At present, many coal mines have problems in making decisions to increase productivity, to improve coal production planning, to use new mining equipment and new perspective technologies for coal mining. The most suitable way to solve these problems is simulation.

A large number of publications on the use of simulation to support decision making on the design, the development and the optimization of coal mines testifies the importance of these problems (Cai 2012, Fioroni 2014, Gospodarczyk 2016, Greberg 2011, Kara 2016, Kizil 2011, Meng 2013, Michalakopoulos 2014, Salama 2014).

To solve these problems the simulation system MTSS (Okolnishnikov 2014) was developed.

In the frames of simulation system MTSS a new specialized library of simulating models of mining equipment and a coal seam model were developed. Using the specialized library of simulating models of technological mining equipment an integrated model for technological processes of underground coal mining in stoping face was developed.

In this article the specialized library of models of mining equipment in the stoping face, the coal seam model, and the integrated model for technological processes of underground coal mining in stoping face are considered.

The second section gives the review of capabilities of the simulation system MTSS. The third section provides a mathematical model of the technological process of coal mining in the stoping face. The fourth section describes the simulation model of the technological process of coal mining in the stoping face developed using the new specialized library of models and the results of its implementation.

2. THE SIMULATION SYSTEM MTSS

At present there are a large number of simulation systems and libraries used for simulation of technological systems. But most important is that all these systems can be used just by specialists in simulation. Computer-based simulation is complex. Only specialists in simulation able to make a decomposition of original problem, create simulation experiments, validate and verify models, and most important to make a backward decomposition and analysis of simulation results to final users (subject matter experts).

Therefore, it is required is to reduce or to exclude the participation of specialists in simulation in the process of the simulation model construction.

The simulation system MTSS (Manufacturing and Transportation Simulation System) is a visual interactive and process-oriented discrete event simulation system intended to develop and execute the technological processes models. A distinguishing feature of the simulation system is its orientation toward the users who are the experts in a particular subject area (process engineers, mining engineers) not having experience in usage of universal simulation systems. The fast development of models is carried out owing to the visual-interactive interface and specialized libraries of models of technological equipment for specific subject areas.

The key point in MTSS is an Equipment Model (EM). EM is a simulation model of technological equipment in a technological system. It consists of the following parts:

- two-dimensional and three-dimensional graphic images;
- input and output parameters;
- functionality algorithm describing dependence between parameters;

- states which EM can reach during the simulation process;
- control commands defining switching process between EM states;
- some service function.

MTSS is also a tool for simulating complex models. Statistics are also available as a short overview when model runs, and more statistics are available after model completion.

This simulation system is effective in providing an easy-to-use tool for the rapid creation of simulation models by mining engineers. Usually field engineers do not have enough expertise in software simulation but they are capable to connect correctly EMs to create the required topology.

The simulation system MTSS provides the user with the following options: visually interactive model construction with a graphical editor, setting model parameters, various modes of model execution, 2D and 3D model visualization.

To simulate the technological processes in coal mines in MTSS simulation system the specialized libraries of EMs for such coal mine subsystems as an underground conveyor network, a pumping subsystem, and a power supply subsystem were developed. With the use of the specialized libraries a number of models of these subsystems for underground coal mines in Kuznetsk Coal Basin (Russia, Western Siberia) were created (Okolnishnikov 2016).

3. THE MATHEMATICAL MODEL OF PERFORMANCE OF THE CUTTER-LOADER

The theoretical advance speed of a cutter-loader is (Ordin 2013, Ordin 2015):

$$V = \frac{30N\eta n_1 K_1}{fP\cos\alpha \pm P\sin\alpha + SDn_2 K_2 K_3 K_4 K_5 K_6}, \quad (1)$$

where
V — the speed of the cutter-loader;
N — the power of the effector motor;
η — the efficiency of the effector reduction gearing;
n_1 — the cutting tools in the cutting line;
K_1 — the coefficient of the horsepower input to cutter-loader travel;
f — the cutter-loader and transporter friction coefficient;
P — the cutter-loader weight;
α — the angle of inclination of the cutter-loader;
"plus" and "minus" in front of the cutter-loader weight specify the cutter-loader movement up and down the longwall, respectively;
S — the weighted average of the coal cutting resistance;
D — the diameter of the augers;
n_2 — the cutting tools that synchronously cut the face;

K_2 — the coefficient of squeeze which takes into account the cutting force decrease due to the ground pressure;
K_3, K_4, K_5, K_6 — the coefficients for the cutting angle, the cutting tool width, the cutting tool dulling and the cutting tool shape, respectively.

Among the above mentioned parameters the coal cutting resistance S influences on the motion rate the most. The coal cutting resistance is considered to be invariable in a certain vast area and is defined by data obtained while drilling the geological prospecting well with (2)

$$S_1 = \frac{k(m_c f_c + m_r f_r)}{m_c + m_r}, \quad (2)$$

where
m_c, m_r — the coal mass and the rock mass respectively;
f_c, f_r — the coal hardness and the interbed rock hardness respectively;
k — a certain coefficient.

In the case of several geological prospecting wells S is calculated with the Inverse Distance Weighting method according to (3).

$$S(X,Y) = \begin{cases} \dfrac{\sum\limits_{i=1}^{n} d_i^{-2} S_i}{\sum\limits_{i=1}^{n} d_i^{-2}}, & if \ d_i \neq 0 \\ S_i, & if \ d_i = 0 \end{cases}. \quad (3)$$

where
n — the number of wells nearest to stoping face that are taken into account while calculating;
S_i — the coal cutting resistance in ith well calculated with formula (2);
d_i — the distance between the ith well and the mining face with current position (X, Y), calculated with (4)

$$d_i = \sqrt{(X - x_i)^2 + (Y - y_i)^2}, \quad (4)$$

where (x_i, y_i) — the coordinates of the ith well.
While one-way operating of the cutter-loader the time of one way is:

$$T_{one\,way} = T_1 + T_{scr} + T_{end\,one\,cut} = \frac{L}{V_1} + \frac{L}{V_{scr}} + T_{end\,one\,cut} \quad (5)$$

where
L — the length of the longwall face;
V_1 — the speed of the cutter-loader movement up the longwall determined by (1);
V_{scr} — the speed of the cutter-loader movement when scraping operation is performing;
$T_{end\,one\,cut}$ — the time of the cutter-loader at the end of the longwall face by one-way operating.

While shuttle operating of the cutter-loader the time of one cycle is:

$$T_{shuttle} = T_1 + T_2 + 2T_{end} = \frac{L}{V_1} + \frac{L}{V_2} + 2T_{end} , \qquad (6)$$

where
L — the length of the longwall face;
V_1, V_2 — the speeds of the cutter-loader movement up and down the longwall determined by (1), respectively;
T_{end} — the time of the cutter-loader at the end of the longwall face by shuttle operating.
While one-way operating of the cutter-loader the productivity of the cutter-loader per time T_{work} is :

$$A_{one\ way} = \frac{\gamma mrLT_{work}}{T_{one\ way}} , \qquad (7)$$

where
γ — the average mean density of the rock mass;
m — the working-bed height;
r — the cutter–loader cut width.
Substituting V_1 from (1) into (5) and $T_{one\ way}$ from (5) into (7) we get:

$$A_{one\ way} = \frac{\gamma mrT_{work}}{\dfrac{fP\cos\alpha + P\sin\alpha + SDn_2 K_2 K_3 K_4 K_5 K_6}{30N\eta n_1 K_1} + \dfrac{1}{V_{scr}} + \dfrac{T_{end\ one\ cut}}{L}}$$

$$\qquad (8)$$

While shuttle operating of the cutter-loader the productivity of the cutter-loader per time Twork is:

$$A_{shuttle} = \frac{2\gamma mrLT_{work}}{T_{shuttle}} \qquad (9)$$

Substituting V1, V2 from (1) into (6) and T$_{shuttle}$ from (6) into (9) we get:

$$A_{shuttle} = \frac{\gamma mrT_{work}}{\dfrac{fP\cos\alpha + SDn_2 K_2 K_3 K_4 K_5 K_6}{30N\eta n_1 K_1} + \dfrac{T_{end}}{L}} \qquad (10)$$

4. INTEGRATED SIMULATING MODEL OF STOPING FACE OPERATIONS

In the frames of simulation system MTSS a specialized library of simulating models of mining equipment (a conveyor, a cutter-loader, a self-moving roof support etc.) that are used while coal mining in stoping face was implemented. Using the specialized library of simulating models of mining equipment an integrated model for technological processes of underground coal mining in stoping face was developed. The integrated model involves the following interactive models:

- a coal seam model;
- a cutter-loader model moving up and down the longwall face;
- a model of a self-moving roof support;
- a model of a flight conveyor.

The parameters of the coal seam model are:

- the length of the longwall face;
- the weighted average of the coal cutting resistance;
- the average mean density of the rock mass:
- the coefficient of squeeze which takes into account the cutting force decrease due to the ground pressure etc.

The parameters of the cutter-loader model are:

- the power of the effector motor;
- the efficiency of the effector reduction gearing;
- the cutting tools in the cutting line;
- the coefficient of the horsepower input to cutter-loader travel;
- the cutter-loader and transporter friction coefficient;
- the cutter-loader weight;
- the diameter of the augers;
- the cutting tools that synchronously cut the face;
- the coefficients for the cutting angle, the cutting tool width, the cutting tool dulling and the cutting tool shape etc.

All parameters of the mine equipment models correlate with the parameters of the actual mine equipment operating at one of the coal mine in in Kuznetsk Coal Basin. The goals of the simulation for coal mining technological processes in stoping face are:

- the evaluation of productivity of a cutter-loader depending on different factors including the variety of geophysical conditions of the coal seam;
- the input data acquisition (input coal stream) for operating of the belt conveyor network model of the coal mine.

Generally, in the stoping face the following factors influence the productivity of the cutter-loader:

- the geophysical state of the coal seam;
- the advance speed of the cutter-loader;
- the technical characteristics of the cutter-loader;
- the delays at the end of the longwall face;
- the delays associated with the movement of the roof support;
- the delays associated with the flight conveyor;

- the delays associated with the belt conveyor;
- the delays associated with the increase of methane release;
- the delays associated with equipment failures;
- regulations conditions and maintenance etc.

In this paper the influence of the first six factors on the cutter-loader productivity was studied. Since the main factor influencing on the cutter-loader productivity is the state of the coal seam (the coal cutting resistance) that restricts the advance speed of the cutter-loader, the subject of the research is the detailed simulating of one-way operating and shuttle operating of the cutter-loader together with roof supports movement depending on geophysical state of coal seam. Under these conditions the top speed and the cutter-loader productivity were calculated with (1) and (7) of the mathematical model.

Figure 1 shows the coal seam model with two geological prospecting wells.
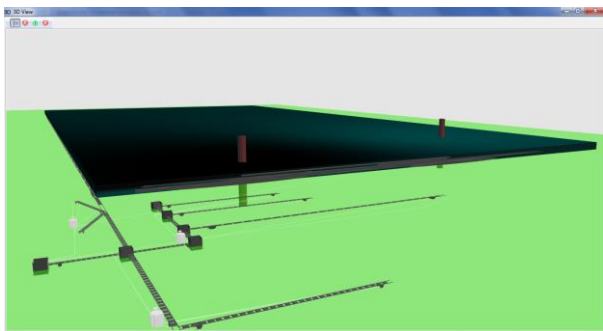

Figure 1: The 3D Coal Seam Model with Two Geological Prospecting Wells

Figure 2 shows the integrated model of underground coal mining technological processes in stoping face carried out with simulation system MTSS. In Figure 2 the coal seam with two geological prospecting wells is painted over. The areas with reduced resistance are painted in a lighter tone. The belt conveyor and power lines are designated in the main window.

The equipment parameters and operation modes can be set interactively in the parameters window. The control buttons are entered in the main window: to start the cutter-loader; to stop the cutter-loader.

With the developed simulation model of the technological process of underground coal mining in the stoping face a series of experiments was performed. For one-way and shuttle operations the average productivity of the cutter-loader was calculated, depending on the length of the longwall face. All experiments were carried out under the equal conditions of the passage of the cutter-loader for a certain depth into the coal seam.

The obtained results are presented in the form of graphs in Figure 3. The obtained results allow us to conclude the following:

- the shuttle operation of coal mining in the stoping face is more productive in comparison with the one-way operation;
- increasing the length of the longwall face, beginning from a certain value, does not significantly affect the increase in the productivity of the cutter-loader.
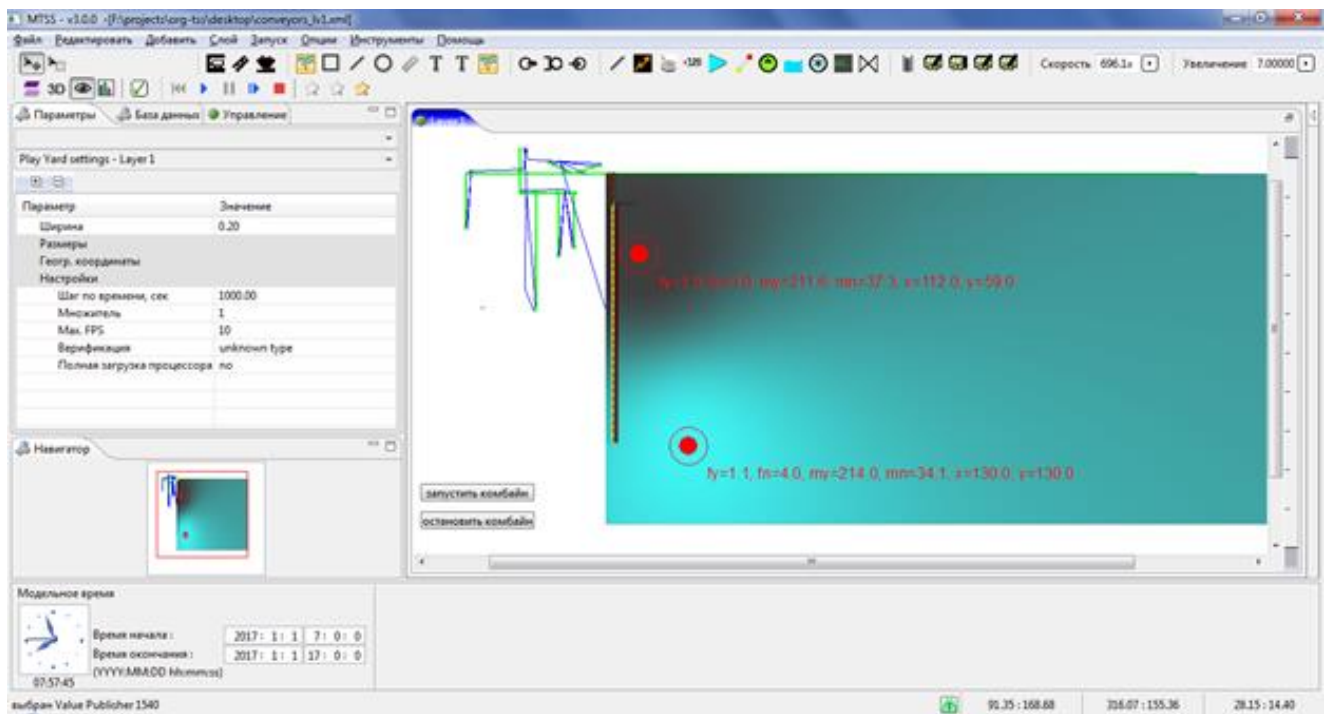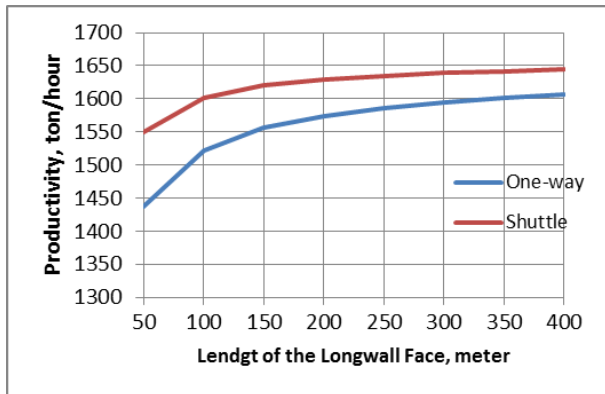

Figure 2: The Main Window of the Stoping Face Model

Figure 3: The Dependence of the Productivity of the Cutter-Loader on the Length of Longwall Face

5. CONCLUSION

The extension of the considered simulation model of the stoping face operation is assumed to be carried out in the future.

Models of aerogasdynamics of methane-air flow in a long stope and models of a belt conveyors subsystem, a ventilating subsystem, and a power supply subsystem of a coal mine will be additionally included into the integrated model of the stoping face operation.

The MTSS simulation system can be used not only for simulation of the existing coal mining technologies, but also for simulation of perspective robotized technologies and manless coal mining technologies.

ACKNOWLEDGMENTS

REFERENCES

Cai D., Baafi E., Porter I., 2012. Modelling a Longwall Production System Using Flexsim 3D Simulation Software. Proceedings of the 21th International Symposium on Mine Planning and Equipment Selection, 107–114. New Delhi, India.

Fioroni M., Santos L., Franzese L., Santana I., Telles G., Seixas J., Penna B., Alkmim G., 2014. Logistic Evaluation of an Underground mine Using Simulation. Proceedings of Winter Simulation Conference, 1855–1865. Savannah, USA.

Gospodarczyk P., 2016. Modeling and Simulation of Coal Loading by Cutting Drum in Flat Seams. Archives of Mining Sciences, 61(2), 385–379.

Greberg J., Sundqvist F., 2011. Simulation as a Tool for Mine Planning. Proceedings of the 2th International Future Mining Conference, 273–278. Sydney, New South Wales.

Kara T., Savaş M.C., 2016. Design and Simulation of a Decentralized Railway Traffic Control System. Engineering, Technology & Applied Science Research, 6(2), 945–951.

Kizil M.S., McAllister A., Pascoe R., 2011. Simulation of Development in Longwall Coal Mines. Proceedings of the 11th Underground Coal Operators' Conference, 91–98. University of Wollongong & the Australasian Institute of Mining and Metallurgy.

Meng C., Nageshwaraniyer S.S., Maghsoudi A., Son Y., Dessureault S., 2013. Data-driven Modeling and Simulation Framework for Material Handling Systems in Coal Mines. Computers & Industrial Engineering, 64(3), 766–779.

Michalakopoulos T.N., Roumpos C.P., Galetakis M.J., Panagiotou G.N., 2014. Discrete-Event Simulation of Continuous Mining Systems in Multi-layer Lignite Deposits. Lecture Notes in Production Engineering, Proceedings of the 12th International Symposium Continuous Surface Mining, 225-239. Aachen, Germany.

Okolnishnikov V.V., Rudometov S.V., 2014. A System for Computer Simulation of Technological Processes. St. Petersburg State Polytechnic University Journal. Computer Science. Telecommunications and Control Systems, 181(1), 62–68.

Okolnishnikov V., Rudometov S., Zhuravlev S., 2016. Simulating the Various Subsystems of a Coal Mine. Engineering, Technology & Applied Science Research, 6(3), 993–999.

Ordin A.A., Metel'kov A.A., 2013. Optimization of the fully-mechanized stoping face length and efficiency in a coal mine. Journal of Mining Science, 49(2), 254–264.

Ordin A.A., Metel'kov A.A., 2015. Analysis of longwall face output in screw-type cutter–loader-and-scraper conveyor system in underground mining of flat-lying coal beds. Journal of Mining Science, 51(6), 1173–1179.

Salama A., Greberg J., Schunnesson H., 2014. The Use of Discrete Event Simulation for Underground Haulage Mining Equipment Selection. International Journal of Mining and Mineral Engineering, 5(3), 256–271.

A MULTIVARIATE MODEL VALIDATION METHOD BASED ON KERNEL PRINCIPAL COMPONENTS ANALYSIS

Yuchen Zhou(a), Ke Fang(b), Ping Ma(c), Ming Yang(d)

(a),(b),(c),(d) Control and Simulation Center, Harbin Institute of Technology

(a) zhouyuchen-01@163.com, (b) hitsim@163.com, (c) pingma@hit.edu.cn, (d) myang@hit.edu.cn

ABSTRACT

Aimed at the similarity measure problem of multi-output simulation with nonlinear correlation between different output variables, a model validation method based on kernel principal component analysis (KPCA) is proposed in this paper. KPCA is utilized to depict the relations among the multiple responses of observed data and simulation data respectively. A new similarity analysis formula is designed to measure the nonlinear relations. The numerical experiment results reflect the effectiveness and reasonableness of the proposed validation method.

Keywords: model validation, kernel principal components analysis, multiple responses, similarity analysis

1. INTRODUCTION

Since simulation is characterized by the economical, repeatable and nondestructive, simulation models play increasingly important roles in the design and development of engineering systems. Model validation is defined as the process of determining the degree to which a model is an accurate representation of the real world system from the perspective of the intended use of the model (Sargent 2013, Roy 2011, Zhou 2018). To guarantee the creditability and usability of computational models, a comprehensive model validation should be conducted.

For complex simulation models, there are many responses which should be considered in the validation (Fang 2017). The multivariate output may be the responses that produced at different space locations or time (Mullins 2016). In literature, several similarity measure methods have been proposed for the validation of multivariate output of computational models. Rebba and Mahadevan (2006) explained the importance of aggregate validation of multiple correlated responses. Compared to individual or univariate validation, aggregate validation provides a more accurate and comprehensive validation result by considering the correlations among the data in the similarity analysis. Based on the univariate validation metrics, the authors provided some multivariate validation metrics, including classical hypothesis testing and Bayesian hypothesis testing. Li (2014) proposed multivariate PIT area metric and t-pooling metric by using multivariate probability integral transformations.

Current researches focus on the statistical validation metrics of model responses with uncertainty. Actually, majority of model outputs are multivariate time series. The dynamic characteristic of time series completely depicts the behavior of numerical models. Thus, the similarity measure of multivariate time series is significant for the validation of multiple correlated model responses.

Karamitopoulos (2008) used principal component analysis (PCA) to transform a set of linearly correlated variables into that of linearly uncorrelated composition variables, then used Frobenius norm or extended Frobenius norm to measure the similarity between two sets of composition variables. However, PCA is unable to describe nonlinear correlations between different variables. Guan (2009) proposed a similarity measure for multivariate time series based on point distribution. They regarded multivariate time series as a hypersurface, then constructed a similarity measure merely aiming at local extreme points of multivariate time series. Those ignored points also contain important trend information, which means this similarity measure may unreliable.

As a nonlinear extension of PCA, KPCA is able to extract nonlinear correlations among different variables using kernel trick. Thus, we use the KPCA to depict the nonlinear relations among the responses and propose a method to measure the similarity of these relations. This paper is organized as follows. In section 2, the basic theory of KPCA is formulated. In section 3, a model validation method combined KPCA and a novel similarity measure criterion is proposed. In section 4, the provided model validation method is tested by a numerical example. Finally, section 5 presents conclusion about the model validation method for multiple correlated responses.

2. KERNEL PRINCIPAL COMPONENTS ANALYSIS

PCA is a linear method for dimensionality reduction which suffers from the linearly non-separable. Scholkopf (1998) proposed a nonlinear component analysis method named kernel principal components analysis. Compared to the linear PCA, KPCA computes the principal eigenvectors of the kernel matrix in feature space, rather than those of the covariance matrix. In this section, we introduce the basic theory of PCA and explain the procedure of KPCA.

PCA attempts to find a linear map $\mathbb{M}$ that maximizes the variances. Suppose $X = \left[x_1, x_2, \cdots, x_n \right], x_i \in \mathbb{R}^m$ are sample points in m-dimensional input space. For the first principal component (PC), it satisfied

$$v = \arg\max_{v} \text{var}\left(v^T X \right) \quad s.t. \ v^T v = 1 . \tag{1}$$

If $E(X) = 0$, then $\text{var}\left(v^T X \right) = v^T \Sigma v$ where Σ is the covariance matrix of X. Use the technique of Lagrange multipliers to transform (1) to the following optimization problem

$$v = \arg\max_{v} \left(v^T \Sigma v - \lambda \left(v^T v - 1 \right) \right) . \tag{2}$$

Perform differentiation with respect to v

$$\lambda v = \Sigma v . \tag{3}$$

Obviously, λ is an eigenvalue of Σ and v is the corresponding eigenvector. Furthermore, the first PC v is the eigenvector corresponding to the largest eigenvalue. It is proved that the i th PC of X is $v_i^T X$ and v_i is the eigenvector corresponding to the i th largest eigenvalue (Jolliffe 2002).

The principle of KPCA is to use a kernel to map the input space nonlinearly into a feature space. A function $K : \mathcal{X} \times \mathcal{X} \to \mathbb{R}$ is called a kernel (Debruyne 2010) on $\mathcal{X}$ if there exists a $\mathbb{R}$-Hilbert space $\mathcal{H}$ and a map $\Phi : \mathcal{X} \to \mathcal{H}$ such that for all $x, y \in \mathcal{X}$ we have

$$k(x, y) = \left\langle \phi(x), \phi(y) \right\rangle . \tag{4}$$

Then ϕ is a kernel or feature map and $\mathcal{H}$ is a feature space of K. Map ϕ is usually nonlinear, so feature space $\mathbb{F}$ produced by ϕ is possibly high-dimensional or even infinite-dimensional. Using kernel function, we can translate the inner product operation in input space into the kernel operation in feature space. Thus, the use of kernel can achieve better feature extraction performance with lower computational complexity, and we needn't consider the concrete form of ϕ.

With nonlinear map ϕ, the sample points $X = \left[x_1, x_2, \cdots, x_n \right]$ are mapped into $\phi(x_1)$, $\phi(x_2)$,..., and $\phi(x_n)$ in feature space, then the covariance matrix is defined as

$$C = \frac{1}{n} \sum_{i=1}^{n} \left(\phi(x_i) - \bar{\phi} \right) \left(\phi(x_i) - \bar{\phi} \right)^{\mathrm{T}} , \tag{5}$$

where $\bar{\phi} = \frac{1}{n} \sum_{i=1}^{n} \phi(n_i)$.

When performing PCA, we need to calculate eigenvalues and eigenvectors of the covariance matrix C. ϕ is expressed implicitly by kernel, however, so we can't calculate eigenvalues and eigenvectors directly. There is a method for indirect calculation.

According to the above analysis, the KPCA procedure consists of the following five steps:

Step 1 Choose a suitable kernel k;

Step 2 For a given sample set $\left(x_1, x_2, \cdots, x_n \right)$ in input space, calculate kernel matrix $K = \left(k\left(x_i, x_j \right) \right)_{n \times n}$;

Step 3 Centralize the kernel matrix K, we get matrix K' as follow

$$K' = K - \frac{1}{l} AK - \frac{1}{l} KA + \frac{1}{l^2} AKA , \tag{6}$$

where A is a $n \times n$ matrix in which all elements are 1;

Step 4 Calculate the eigenvalues and eigenvectors of K', and choose partial eigenvalues λ_i and corresponding eigenvectors ξ^i, where $i = 1, 2, \cdots, u, u < n$;

Step 5 Extract a feature vector from sample x_i, and the extraction result is $y_i = \sum_{z=1}^{n} \xi_z^i K'_{iz}$.

Kernel principal component analysis is a nonlinear extension of PCA. Compared to PCA, KPCA is able to extract nonlinear features.

3. A MODEL VALIDATION METHOD BASED ON KPCA

In this paper, consider m correlated responses $\left(p_1, p_2, \cdots, p_m \right)$ and each response p_k is a time series $\left[p_k(t_1), p_k(t_2), \cdots p_k(t_n) \right]^T, k = 1, 2, \cdots, m$. The multiple outputs may be expressed as the following matrix

$$P = \left(p(t_1) \ p(t_2) \cdots p(t_n) \right)$$

$$= \begin{pmatrix} p_1(t_1) & p_1(t_2) & \cdots & p_1(t_n) \\ p_2(t_1) & p_2(t_2) & \cdots & p_2(t_n) \\ \vdots & \vdots & \ddots & \vdots \\ p_m(t_1) & p_m(t_2) & \cdots & p_m(t_n) \end{pmatrix}. \qquad (7)$$

Suppose $\boldsymbol{P}_{sim}$ denotes the simulation data generated by the simulation model and $\boldsymbol{P}_{obs}$ denotes the observed data collected from the corresponding real-world system.

3.1. A Novel Similarity Measure of Multiple Correlated Responses

Since the performance of KPCA is significantly affected by kernel, a suitable kernel should be carefully selected when applying KPCA to similarity measure of multiple outputs. At present the commonly used kernels for KPCA include Gaussian kernel, polynomial kernel, sigmoid kernel, *et al*. Scholkopf (2002) proposed that Gaussian kernel is the first choice for data set that lack a priori knowledge, because the performance of Gaussian kernel resembles those of other kernels when Gaussian kernel chooses σ from a specific range.
Gaussian kernel is defined as

$$k\big(\boldsymbol{p}(t_i), \boldsymbol{p}(t_j)\big) = \exp\Big(-\big\|\boldsymbol{p}(t_i) - \boldsymbol{p}(t_j)\big\|_2^2 \Big/ 2\sigma^2\Big), \qquad (8)$$

where $\big\|\boldsymbol{p}(t_i) - \boldsymbol{p}(t_j)\big\|_2 = \sqrt{\sum_{z=1}^{m}\big(p_z(t_i) - p_z(t_j)\big)^2}$, σ is

the kernel bandwidth.

By optimizing the parameter of Gaussian kernel, most of the total variance will concentrate on the first principal component. In this paper, we use genetic algorithm to obtain the optimized kernel bandwidth σ^* by maximizing the variance concentration radio of first principal component.

$$\sigma^* = \arg\max_{\sigma \in \mathbb{R}^+} \Bigg[\min\Bigg(\lambda_1\big(\boldsymbol{P}_{obs}, \sigma\big) \Big/ \sum_{i=1}^{n} \lambda_i\big(\boldsymbol{P}_{obs}, \sigma\big), \\ \lambda_1\big(\boldsymbol{P}_{sim}, \sigma\big) \Big/ \sum_{i=1}^{n} \lambda_i\big(\boldsymbol{P}_{sim}, \sigma\big) \Bigg) \Bigg], \qquad (9)$$

where $\lambda_i(\boldsymbol{P}, \sigma)$ is the eigenvalues of datasets $\boldsymbol{P}$ when Gaussian kernel bandwidth is σ and $\lambda_1(\boldsymbol{P}, \sigma)$ is the eigenvalue corresponding the first principal component. Figure 1 reveals the KPCA of responses, including simulation data from numerical models and observed data from real-world systems. It is difficult to depict the nonlinear relations of multiple correlated responses in low dimension space (input space). KPCA provides an effective way to quantify the nonlinear relations. $\phi(\boldsymbol{x})$ maps the responses to feature space with high dimension and linear PCA is conducted on the transformed data and reduces the data to KPCA feature space with lower dimension (compared to feature space). The above process is the primary idea of KPCA based relations quantification of multiple correlated responses.
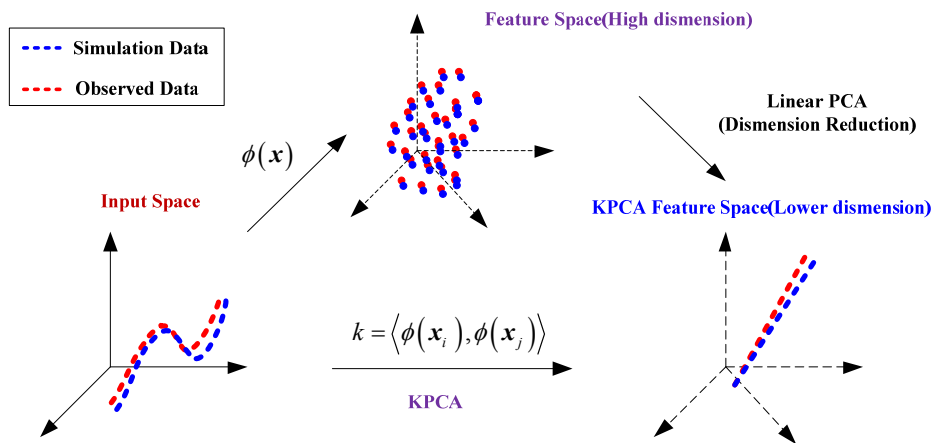

Figure 1: KPCA of responses

From the above quantification process, we obtain the eigenvectors of all the components of simulation data and observed data respectively. The eigenvectors include the transform information from the feature space to KPCA feature space. Through the similarity analysis of the eigenvectors and eigenvalues, we obtain the credibility of the multiple correlated responses. A novel similarity measure of multiple correlated responses between $\boldsymbol{P}_{sim}$ and $\boldsymbol{P}_{obs}$ is defined as

$$Cr_{\text{multi}}\big(\boldsymbol{P}_{sim}, \boldsymbol{P}_{obs}\big) = \sum_{i=1}^{n} \Bigg(\frac{\lambda_i\big(\boldsymbol{P}_{sim}, \sigma^*\big) + \lambda_i\big(\boldsymbol{P}_{obs}, \sigma^*\big)}{\sum_{j=1}^{n}\big(\lambda_j\big(\boldsymbol{P}_{sim}, \sigma^*\big) + \lambda_j\big(\boldsymbol{P}_{obs}, \sigma^*\big)\big)} \cdot \\ \frac{\big\langle \xi_i\big(\boldsymbol{P}_{sim}, \sigma^*\big), \xi_i\big(\boldsymbol{P}_{obs}, \sigma^*\big)\big\rangle}{\big\|\xi_i\big(\boldsymbol{P}_{sim}, \sigma^*\big)\big\|_2 \big\|\xi_i\big(\boldsymbol{P}_{obs}, \sigma^*\big)\big\|_2} \Bigg) \qquad (10)$$

where $Cr_{\text{multi}}\left(\boldsymbol{P}_{sim},\boldsymbol{P}_{obs}\right)$ denotes the credibility of multiple responses(similarity); σ^* denotes the optimized Gaussian kernel bandwidth; $\lambda_i\left(\boldsymbol{P}_{sim},\sigma^*\right)$ and $\lambda_i\left(\boldsymbol{P}_{obs},\sigma^*\right)$ denote the eigenvalues of simulation data $\boldsymbol{P}_{sim}$ and observed data $\boldsymbol{P}_{obs}$ respectively; $\xi_i\left(\boldsymbol{P}_{sim},\sigma^*\right)$ and $\xi_i\left(\boldsymbol{P}_{obs},\sigma^*\right)$ denote the eigenvectors corresponding to the eigenvalue $\lambda_i\left(\boldsymbol{P}_{sim},\sigma^*\right)$ and eigenvalue $\lambda_i\left(\boldsymbol{P}_{obs},\sigma^*\right)$.

3.2. Process of Model Validation Based on KPCA for Multiple Correlated Output

Figure 2 reveals the process of model validation based on KPCA for multiple correlated output. The detailed process is as follows.
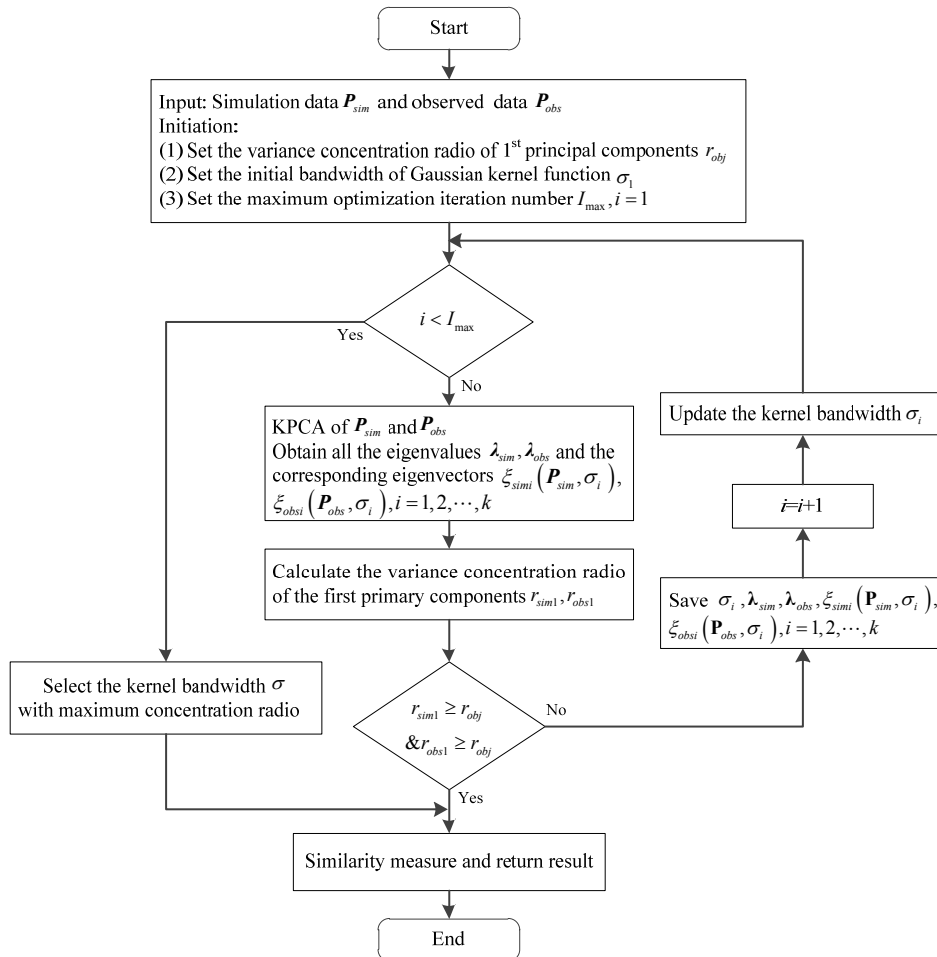

Figure 2: Process of the model validation based on KPCA

Step 1 Initialization. The input is simulation data $\boldsymbol{P}_{sim}$ and observed data $\boldsymbol{P}_{obs}$ of multiple correlated responses. Initialize the optimization parameters: (1) the objective variance concentration radio of 1st principal components r_{obj}, (2) the initial bandwidth of Gaussian kernel function σ_1, (3) the maximum optimization iteration number $I_{\max}, i = 1$.

Step 2 KPCA of simulation data $\boldsymbol{P}_{sim}$ and observed data $\boldsymbol{P}_{obs}$. Using the KPCA procedure formulated in Section 2 to calculate the eigenvalue vector $\lambda_{sim} = \left(\lambda_{sim1},\lambda_{sim2},\cdots,\lambda_{simk}\right)$, $\lambda_{obs} = \left(\lambda_{obs1},\lambda_{obs2},\cdots,\lambda_{obsk}\right)$,

and the corresponding eigenvectors $\xi_{simi}\left(\boldsymbol{P}_{sim},\sigma_i\right)$, $\xi_{obsi}\left(\boldsymbol{P}_{obs},\sigma_i\right)$, $i = 1,2,\cdots,k$.

Step 3 Calculate the variance concentration radio of the first primary components

$$r_{sim1} = \left(100\lambda_{sim1}\bigg/\sum_{i=1}^{n}\lambda_{simi}\right)\% \tag{11}$$

$$r_{obs1} = \left(100\lambda_{obs1}\bigg/\sum_{i=1}^{n}\lambda_{obsi}\right)\% \tag{12}$$

where λ_{sim1} and λ_{obs1} denote the maximum eigenvalues of kernel matrix of simulation data and observed data respectively.

Step 4 Judgment of terminating condition. If both variance concentration radios are equal or greater than objective value r_{obj} ($r_{sim1} \geq r_{obj}$ & $r_{obs1} \geq r_{obj}$), then the optimization process will terminated. Otherwise, update the σ_i and go to the next iteration (repeat Step 2~ Step 4 until the maximum iteration number achieved). If the variance concentration radios not satisfied the terminating condition until reaching maximum iteration number, the eigenvalues and eigenvectors with maximum variance concentration radios will be taken as the results of this step.

Step 5 Similarity analysis of multiple correlated responses. Using the proposed similarity measure (Equation (10)) to calculate the credibility of multiple correlated responses.

4.   CASE STUDY

The coupling Henon map function (Wang 2006, Casas 2012), a discrete-time dynamical system, is defined as

$$x : \begin{cases} x_{n+1} = 1 - 1.4 x_n^2 + 0.3 u_n \\ u_{n+1} = x_n \end{cases},$$

$$y : \begin{cases} y_{n+1} = 1 - 1.4 \left[\delta x_n + (1 - \delta) y_n \right] y_n + 0.3 v_n \\ v_{n+1} = y_n \end{cases} \quad (13)$$

where $\delta \in [0,1]$ is coupling coefficient. Relations between x and y is depending on the coupling coefficient δ; along with coupling coefficient δ increase, the relations are enhanced.

(1) Data generation

Since (x_k, y_k) is sensitive to the initial values, fixed initial values (x_0, y_0) are selected and different coupling coefficient are chosen to generate analysis data. All the initial values of datasets are defined as $x_0 = u_0 = 0$, $y_0 = v_0 = 1$; 3 groups of samples are generated as simulation data with coupling coefficient $\delta_{sim} = \{0.70, 0.72, 0.74\}$; meanwhile, 3 groups of samples are generated as observed data with coupling coefficient $\delta_{obs} = \{0.66, 0.68, 0.70\}$. The simulation data and observed data are listed in table 1.

Table 1: Simulation data and observed data of Henon map function

No.	x_{obs}, x_{sim}	$y_{sim}^{\delta=0.70}, y_{obs}^{\delta=0.7}$	$y_{sim}^{\delta=0.72}$	$y_{sim}^{\delta=0.74}$	$y_{obs}^{\delta=0.66}$	$y_{obs}^{\delta=0.68}$
31	0.9521	0.9411	0.9593	0.9663	0.8752	0.9106
32	-0.1385	-0.1161	-0.1531	-0.1668	0.0183	-0.0540
33	1.2588	1.2609	1.2572	1.2558	1.2647	1.2648
34	-1.2599	-1.2580	-1.2608	-1.2618	-1.2269	-1.2485
35	-0.8446	-0.8398	-0.8472	-0.8498	-0.7654	-0.8163
...	...	...	...	...	...	...
46	0.5866	0.5699	0.5942	0.6002	0.3037	0.4796
47	0.7048	0.7253	0.6956	0.6884	1.0180	0.8327
48	0.4805	0.4491	0.4944	0.5048	-0.0651	0.2745
49	0.8882	0.9214	0.8733	0.8624	1.3323	1.0905
50	0.0397	-0.0238	0.0674	0.0871	-0.9578	-0.3724
...	...	...	...	...	...	...
56	0.1431	0.1936	0.1286	0.1218	0.2546	0.4405
57	1.2018	1.1661	1.2132	1.2193	1.1863	0.9691
58	-0.9791	-0.8863	-1.0080	-1.0228	-0.9108	-0.3973
59	0.0185	0.1695	-0.0292	-0.0524	0.1371	0.8497
60	0.7058	0.7190	0.6978	0.6932	0.7155	0.5424

A group of simulation data and a group of observed data constitute a pair of validation data to test the KPCA-based model validation method. There are two reasons for generating datasets with same x through setting same initial value. On the one hand, the model validation based on KPCA focus on the similarity measure of relations among different variables. Through generating data with same initial value, the influence of input error can be eliminated, which is beneficial for the examination of the proposed method. On the other side, the data visualization with same x will show the correlations between x and y more intuitively.

Figure 3 shows an example of simulation data $(x_{sim}, y_{sim}^{\delta=0.72})$ and observed data $(x_{obs}, y_{obs}^{\delta=0.68})$. Obviously, x_{sim} and y_{sim} are approximately linear related when $\delta = 0.72$. However, x_{obs} and y_{obs} are

nonlinearly coupled when $\delta = 0.68$. We want to quantify the relation difference ($\left|\delta_{sim} - \delta_{obs}\right|$) between simulation data and observed data using the proposed model validation method for multiple correlated responses.
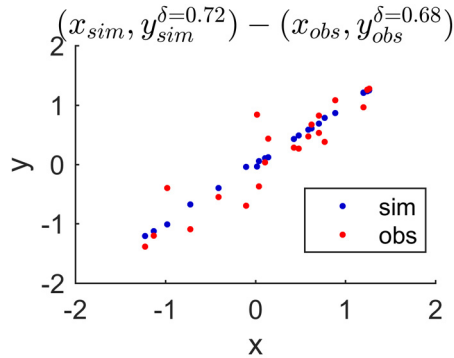

Figure 3: An example of simulation data $\left(x_{sim}, y_{sim}^{\delta=0.72}\right)$ and observed data $\left(x_{obs}, y_{obs}^{\delta=0.72}\right)$

(2) KPCA based model validation
For each set of data, Gaussian kernel is used to map the data to feature space. The object variance radio is set as 0.95. Through the optimization, we obtain the eigenvalues $\lambda_{sim} = \left(\lambda_{sim1}, \lambda_{sim2}, \cdots, \lambda_{sim30}\right)$,

$\lambda_{obs} = \left(\lambda_{obs1}, \lambda_{obs2}, \cdots, \lambda_{obs30}\right)$ and eigenvectors $\xi_{obsi}\left(P_{obs}, \sigma^*\right)$, $\xi_{simi}\left(P_{sim}, \sigma^*\right)$, $i = 1, 2, \cdots, 30$. For instance, the eigenvalues of $y_{sim}^{\delta=0.72}$ and $y_{obs}^{\delta=0.68}$ are $\lambda_{sim}^{\delta=0.72} = [0.09222, 0.00019, 0.00002, 0, \cdots, 0]$ and $\lambda_{obs}^{\delta=0.66} = [0.08953, 0.00274, 0.00018, 0, 0, 0, \cdots, 0]$ respectively. Each eigenvectors $\xi_{sim}\left(P_{sim}, \sigma^*\right)$ or $\xi_{obs}\left(P_{obs}, \sigma^*\right)$ is 30-dimensional, so we don't list them in this paper.

(3) Result
Figure 4 reveals all the data comparison and similarity analysis results of 9 pairs of validation data sets. The similarity between simulation data and observed data decreases from left to right in each row and increase from bottom to top in each column. The trends are related to coupling coefficients δ_{sim} and δ_{obs}. In each row or column, the similarity is increasing along with the decreasing of differences between δ_{sim} and δ_{obs}. For instance, the similarity decrease from 0.9732 to 0.9654 in the second row along with the $\left|\delta_{sim} - \delta_{obs}\right|$ increase from 0.02 to 0.06.
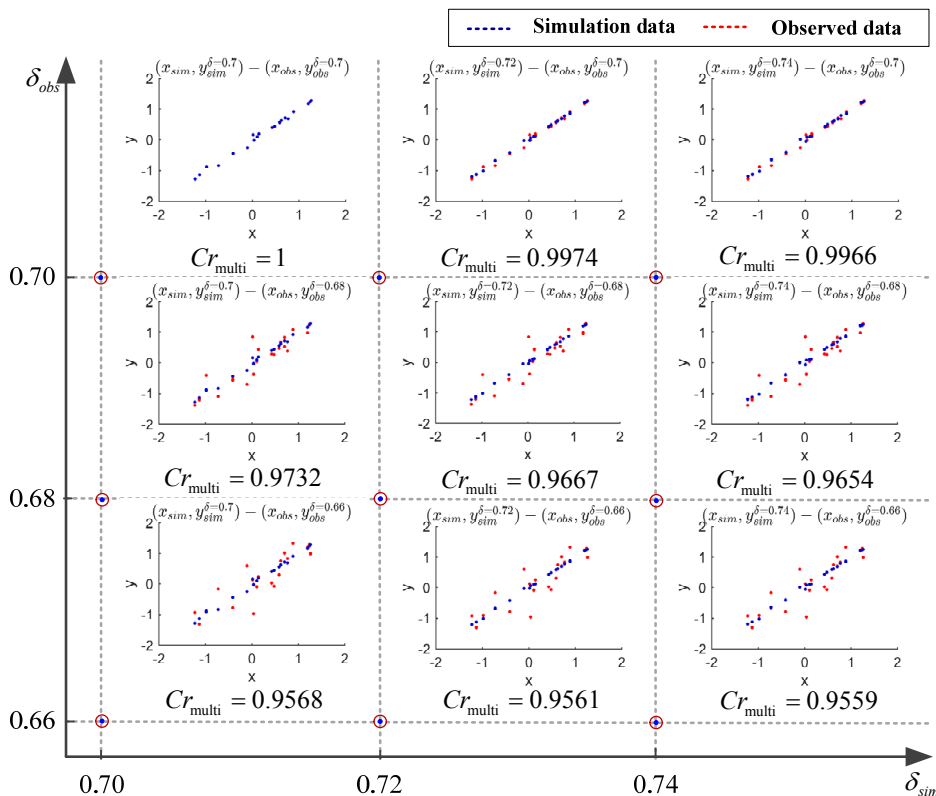

Figure 4: Data comparison and similarity analysis results of Henon map function. The similarity between simulation data and observed data decrease from left to right and increase from bottom to top. The trends are related to coupling coefficients δ_{sim} and δ_{obs}.

It is worth noting that the similarity measure between simulation data and observed data is not a linear function of $\left| \delta_{sim} - \delta_{obs} \right|$. When $\delta_{obs} = 0.70$, $\delta_{sim} = 0.66$, $Cr_{\text{multi}} = 0.9568$; whereas when $\delta_{obs} = 0.72$, $\delta_{sim} = 0.68$, $Cr_{\text{multi}} = 0.9667$. There are various reasons may account for this phenomenon. Firstly, the Henon map function is nonlinear and the degree of nonlinearity is not a linear function of coupling coefficient δ. Secondly, the similarity measure formula is not a linear measure of relations among multiple responses. Thirdly, Gaussian kernel bandwidth among different pair of validation datasets is not equal. Furthermore, although all the similarity analysis results are above 0.95, it does not mean the similarity is pretty well. Actually, the proposed similarity formula is a relative measure of relations. To decide whether the simulation responses are credible, reasonable acceptability criteria (Giannoulis 2013) should be defined. For instance, when $\delta_{obs} = 0.70$, if the acceptable error of $\left| \delta_{sim} - \delta_{obs} \right|$ is lower than 0.02, then the acceptability range of the similarity may be formulated as

$$Cr_{ac-\text{multi}} \in \begin{cases} [0.9974,1], \delta_{sim} \geq \delta_{obs} \\ [0.9732,1], \delta_{sim} < \delta_{obs} \end{cases} \qquad (14)$$

That means if $\delta_{sim} \geq \delta_{obs}$, acceptable credibility of multiple responses is in the interval of $[0.9974,1]$; if $\delta_{sim} < \delta_{obs}$, the acceptable credibility of multiple responses is in the interval of $[0.9732,1]$.

(4) Discussion
In case study, Henon map function is utilized to generate 2-dismension data with different coupling coefficients. According to the similarity analysis results, the proposed model validation method can measure the coupling coefficients difference between simulation data and observed data.

From the numerical experiments and analysis, we may draw the following conclusions. Firstly, compared to univariate output validation, multivariate output validation is more complicated because it is difficult to quantify the relations among multiple responses. Secondly, KPCA is effective to quantify and reduce the nonlinear relations among multiple outputs and the kernel parameters should be carefully selected. Finally, the proposed similarity analysis method is a relative measure of the multivariate output rather than an absolute measure. Thus, the acceptance criterion should be seriously defined.

5. CONCLUSION

Structure-complex simulation models usually have many output variables which have different nonlinear correlations. In this paper, a multivariate model validation method combining kernel principal analysis and a novel similarity measure formula is proposed. KPCA is utilized to extract the relations among multiple outputs of simulation data and observed data respectively. The similarity measure formula is applied to quantify the relations. Furthermore, a comprehensive process of the proposed model validation method for multiple correlated responses is formulated. The numerical experiment reveals that the proposed method can effectively solve the multivariate similarity measure problem.

REFERENCES
Casas G.A., Rech P.C., 2012. Multistability annihilation in the Henon map through parameters modulation. Communication on Nonlinear Science and Numerical Simulation, 17 (6), 2570–2578.

Debruyne M., Verdonck T., 2010. Robust kernel principal component analysis and classification. Advances in Data Analysis and Classification, 4(2), 151–167.

Fang K., Zhou Y.C., Zhao E.J., 2017. Discussion on the factor space of simulation model validation. Systems Engineering and Electronics, 39 (11), 2592–2602.

Giannoulis C., Joakim J., Stromback P., Hellmans R., Heden H., 2013. Exercising GM-VV: verification and validation of a missile model. Proceedings of Fall Simulation Interoperability Workshop, pp. 27–35. September 16–20, Orlando (USA).

Guan H.S., Jiang Q.S., Wang S.R, 2009. Pattern matching method based on point distribution for multivariate time series. Journal of Software, 20(1), 67–79.

Jolliffe I.T., 2002. Principal Component Analysis, 2nd ed. New York: Springer.

Karamitopoulos L., Evangelidis G., Dervos D.A., 2008. Multivariate time series data mining: PCA-based measures for similarity search. Proceedings of the 4th International Conference on Data Mining, pp. 253–259. July 14–17, Las Vegas (USA).

Li W, Chen W., Jiang Z., Lu Z.Z., Liu Y., 2014. New validation metrics for models with multiple correlated responses. Reliability Engineering & System Safety, 127, 1–11.

Mullins J., Ling Y., Mahadevan S., Sun L., Strachan A., 2016. Separation of aleatory and epistemic uncertainty in probabilistic model validation. Reliability Engineering & System Safety, 147, 49–59.

Rebba R., Mahadevan S., 2006. Validation of models with multivariate output. Reliability Engineering & System Safety, 91 (8), 861–871.

Roy C. J., Oberkampf W. L., 2011. A comprehensive framework for verification, validation, and uncertainty quantification in scientific computing.

Computer Methods in Applied Mechanics and Engineering, 200(25), 2131–2144.

Sargent R.G. 2013. Verification and validation of simulation models. Journal of Simulation, 7 (1), 12–24.

Scholkopf B., Smola A., 2002. Learning with Kernels: Support Vector Machines, Regularization, Optimization, and Beyond. Cambridge: MIT Press.

Scholkopf B., Smola A., Muller K., 1998. Nonlinear component analysis as a kernel eigenvalue problem. Neural Computation, 10 (5), 1299–1319.

Wang H.Y, Lu S., 2006. Nonlinear Time Series Analysis and Its Application. Beijing: Science Press.

Zhou Y.C., Fang K., Ma P., Yang M., 2018. Complex simulation model validation method based on ensemble learning. Systems Engineering and Electronics, 40, 1–9.

AUTHORS BIOGRAPHY

YUCHEN ZHOU is a Ph.D. student major in control science and engineering at Harbin Institute of Technology (HIT), Harbin, China. He received the M.S. degree in control science and engineering from HIT in 2014. His research interests include the complex system simulation, model validation, and experiment design. His e-mail address is zhouyuchen-01@163.com.

KE FANG is an associate professor with the Control and Simulation Center, HIT. He received the Ph.D. degree in control science and engineering from HIT, in 2007. He was at Arizona State University as a visiting scholar from 2014 to 2015. His research interests include complex system simulation, verification, validation & accreditation (VV&A) and credibility evaluation of complex simulation system. His e-mail address is hitsim@163.com.

PING MA is a full professor with the Control and Simulation Center, HIT. She received the Ph.D. degree in control science and engineering from HIT, in 2003. Moreover, she serves as the standing director of China Simulation Federation (CSF). Her research interests include the complex system modeling & simulation, VV&A. Her e-mail address is pingma@hit.edu.cn.

MING YANG is a full professor with the Control and Simulation Center, HIT. He received the Ph.D. degree in control science and engineering from HIT, in 1997. Moreover, he serves as vice president of China Simulation Federation. His research interests include the complex system simulation theory and advanced distributed simulation technology & application. His e-mail address is myang@hit.edu.cn.

A COLLABORATION AND ASSET SHARING PLATFORM IN PERISHABLE PRODUCT SUPPLY CHAIN

Francesco Longo[a], Antonio Padovano[b], Letizia Nicoletti[c] Jessica L. Frangella[d], Marina Massei[e]

[a] [d] DIMEG, University of Calabria, Italy
[b] Juno S.r.l.s., Rende (CS), Italy
[c]CAL-TEK srl
(e)DIME, University of Genoa, Italy

[a]francesco.longo@unical.it, [b]a.padovano@juno-srl.com, [c]l.nicoletti@cal-tek.eu, [d]jessica.frangella@unical.it
[e]massei@itim.unige.it

ABSTRACT

Perishable product last-mile transportation is less-than-truckload as relatively small goods are shipped in small batches that can be bundled with each other to increase the filling rate of the trucks' capacity. However, the large number and frequency of trips entails low profitability and environmental sustainability of the companies operating perishable product supply chains. This is mainly due to the fact that the trucks are partially loaded or empty during their trips. The present paper provides a preliminary analysis of the main issues in the perishable product supply chains and propose collaboration and asset sharing as key approaches that can provide operational and economic benefits to all the stakeholders (shippers, carriers, customers) of a regional distribution network. A prototype of new technological multi-sided system has been designed. It consists of two subsystems: (i) carriers can use a multi-product daily assignment and routing system that provide input data to a simulation-based distribution scenario analysis tool for complex transportation scenario analysis and optimization; (ii) customers and producers are provided with an online asset sharing tool (experienced by web platform and mobile application) based on a transportation estimate management tool and a real-time marketplace. Potential advantages of collaboration and asset sharing by using the proposed system in perishable product supply chains are investigated.

Keywords: perishable products, freight transportation, less-than truckload, asset sharing, collaboration

1. INTRODUCTION

Perishable products are defined as items that have a short shelf life time or that easily deteriorate (Karaesmen et al., 2011). Traditional examples are fresh agricultural products, dairy products and pharmaceuticals. Following this definition, items such as newspapers and magazines can be also considered perishable products because their contents become quickly outdated, making those goods invaluable after a short interval of time. Perishable product transportation is less-than-truckload (LTL) as they are usually relatively small goods shipped in the last-mile by third-party transportation providers operating local but dense distribution networks or by specialized carriers that need to ensure specific transportation conditions (e.g. temperature-controlled trucks) in small batches that can be bundled with each other to increase the filling rate of the trucks' capacity.

Since these products are indispensable (e.g. food, pharmaceuticals, newspapers), perishable product carriers are generally supposed to distribute them frequently (e.g. daily) even in remote or rural areas. The large number and frequency of trips entails low profitability and environmental sustainability of the trips. This is mainly due to the fact that the trucks are partially loaded or empty and the economic return for the carriers is very low. Furthermore, partially loaded or empty trips affect negatively their environmental footprint (higher amount of emitted CO_2 per item delivered).

Even lower business performance is observed in logistics providers operating predominantly the LTL distribution of products that are experiencing a sharp drop in sales and production – such as products of the publishing industry, e.g. newspapers, magazines. Hence, operators (shippers, producers, carriers, retailers) in the perishable product supply chains are today asked to reinvent their business in the view of an increased market competition, of the trend of the specific industry they operate (e.g. food industry, publishing industry), and of the today's higher expectations of the consumers in terms of service level and quality of the products.

1.1. Study aims and contribution
This article first explores the main research questions and emerging trends within the LTL transportation of perishable products and provides a background for thinking about how collaboration and new asset sharing management models could challenge existing business

models. Asset sharing among perishable product vendors/producers, carriers and final consumers and dynamic consolidation of LTL orders are proposed as the key for greater efficiency of the perishable products distribution processes. As a proof of concept, the potential of this approach is analyzed in the context of the publishing and agri-food industries, which represent the perfect test-bed for investigating how perishable product supply chains can be enhanced in operational and environmental terms. This study is supported by the Zero-Kilometer Items Routing System (Zerok-IRS) study (CUP J98C17000180006) that has been co-financed by the European Union, the Italian Government and Calabria Region under the POR CALABRIA FESR-FSE 2014/2020, Asse I, Obiettivo specifico 1.2, Azione 1.2.2, whose main aim was to design and develop a new multi-sided platform for a more efficient asset sharing and collaboration among the shippers in perishable product supply chains and for supporting diversification strategies via multi-product assignment to existing distribution routes based on simulation technologies and what-if scenario analysis.

2. LITERATURE REVIEW

According to a recent literature review provided by Lusiantoro et al. (2018), the role of perishable product characteristics and perishable product supply chain performance has been largely ignored in existing research. This study confirms the findings of Chen (2010), which affirms that most of the literature is quite recent when perishable or time sensitive products are considered. This research stream differs from the others because the product has a limited lifetime, the total demand must be satisfied within a planning horizon and multiple trucks are used (Devapriya et al., 2017) to serve a dense network of retailers or customers. To date, a considerable amount of research has been dedicated to tackling challenges in perishable inventory management problems aimed at determining appropriate levels of stock to meet demand under different regimes (Panda et al., 2008) or at analyzing how the stability of certain parameters (e.g. temperature) during the transportation affects the value added and quality of the items delivered (Bogataj et al., 2005). Most of the papers in the LTL transportation literature are therefore based on the vehicle routing problem with time windows and propose models for the operational level of the supply chain to reduce empty miles and decide the most efficient routes for a carrier's vehicles (Tütüncü, 2010). Indeed, despite the distribution of these products by specialized carriers ensures high value added and quality, the current scenario for perishable product involves individual truckload (TL) shipments that are heavily uneconomical because of frequent trips (e.g. every day), destinations in remote areas or low-emission zones and high variability in the returns collection and management. Moreover, several industries are more and more concerned about the environmental impact of their supply chain operations (Mumtaz et al., 2018a, Mumtaz et al., 2018b).

However, besides planning and routing inefficiencies, there are different reasons for empty running of vehicles, including lack of cooperation across the supply chain partners (McKinnon, 2010). Despite the barriers that potentially undermine collaboration among companies within many industries globally, collaboration is becoming more of a necessity than an option. While there are several studies and models for carrier collaboration (Liu et al., 2010; Caballini et al., 2015), there are only a few works focused on the shipper collaboration problem (Ergun et al., 2007; Yilmaz & Savasaneril, 2012) and the potential benefits of collaboration in the perishable product supply chains remain largely untapped. In fact, shippers are exposed to shorter and shorter customers' lead time and have to send less quantities of product more often. In this context of LTL transportation, they can collaborate with other shippers to propose common shipments to a carrier to minimize their transportation costs. Van de Klundert & Otten (2011) explored various models to increase the utilization of already scheduled road transportation activities by accepting extra loads, thus reducing costs for the shippers, increasing revenue for the carrier, and reducing road congestion and pollution for the society at large. Increasing the filling rate of the trucks is a very effective sustainability improvement, as it creates both environmental (Danloup et al., 2015b) and economic benefits (Sarkar & Mohapatra, 2008). Such collaboration could be in form of sharing trucks by retailers, in order to increase filling rate of the vehicles and to reduce their empty running (Danloup et al., 2015a). Recently, Li et al. (2016) also analyzed how time sensitive and perishable product retailers should cooperate in sharing a transportation facility in order to have better economic performance and offer high-quality products at lower costs to their customers.

Furthermore, the specific nature of perishable products (high uncertainty and variability of demand, shelf life and deterioration rates) makes reverse logistics planning and management more complex and challenging than usual reverse logistics processes (Vijayan et al., 2014). Collecting and recycling these products after their "expiration" or "best-by" date could help carriers involved in this supply chain to increase the profitability and sustainability of their trips (Rahimi et al., 2016), but higher degree of on-line planning and coordination is needed among the retailers. A number of start-up companies have emerged to create platforms that connect customers with producers and are able to track demand and send trucks to pick up new jobs on the return trip. However, there is still a big gap in incorporating the backward flows into the planning of forward flows.

Besides the opportunities in collaborative planning, D'Amours & Rönnqvist (2010) also discuss the main issues in the selection of information and decision technologies that are needed for the design and management of supply chain activities. As recently noted by the Wall Street Journal, "there is an Uber for everything now" (Fowler, 2015). Vendors and shippers

are able to provide higher service level and customers can save money. The sharing economy and Internet of Things (IoT) are changing the supply chain ecosystems in unprecedented ways. As suggested by Belk (2007), the sharing economy approach entails 'the act and process of distributing what is ours to others for their use and/or the act and process of receiving or taking something from others for our use'. Yan (2017) shows how IoT is the key enabler of increased profitability of perishable product supply chains. However, it concludes by saying that the application of IoT to efficiently optimize a perishable product supply chain is only applicable for large enterprises, while small enterprises are not supposed to introduce IoT due to its high cost.

2.1. Research questions

Given the results of Yan (2017), the present article aims at discussing whether and how small distribution companies that operate local distribution networks in the context of perishable product supply chains can get improved economic performance. In particular, this research article poses the following questions:

- Perishable product carriers are asked to travel several kilometers every day to deliver indispensable products to every point of sale of a regional distribution network; as a consequence, trucks travel several empty kilometers. Is a diversification strategy convenient and sustainable for the perishable product carriers?

- The fact that collaboration and asset sharing necessarily lead to increased performance of transportation companies operating perishable products supply chains is not a straightforward conclusion. Therefore, how can complex distribution and routing scenarios be evaluated in an "online" and automatic way to allow frequent assessment of different routes configurations?

- Small enterprises cannot sustain the high economic costs of an IoT system or a technological upgrade to implement asset sharing in their daily business. Is it possible to design a new technological platform that enables them to harness the potential benefit of increased technology-driven collaboration and asset sharing at low costs?

This research focuses on the potential collaboration between the publishing industry and the fresh agri-food industry. These two sectors present indeed important trends, which asks researchers and companies to find new business opportunities and ways to enhance their economic performance. The publishing industry is experiencing a sharp decline due to the lower value of information and print copies of newspapers and magazines in the digital era, therefore companies operating the last-mile distribution of these products are also experiencing a profound crisis. Given the fact that

their trucks travel every day several kilometers to reach every single point of sale of a regional distribution network, there are potential business diversification opportunities for them. The fresh agri-food industry is proposed to investigate how trucks and distribution routes of the publishing industry can be used to deliver fresh agri-food products. Benefits for small enterprises (vendors, producers, carriers) and independent operators (farmers, retailers) of the supply chain can be achieved via greater technology-enabled coordination. However, specific technologies have to be combined to link the physical requests of products with the system in an automatic way and to provide efficient routing solutions for the carriers operating perishable product supply chains.

3. COLLABORATION AND ASSET SHARING: THE ZEROK-IRS PILOT STUDY

In the hyper-connected logistics, the operators of a logistics network are part of a hyper-connected ecosystem characterized by real-time connections and communications with the customers, high-automation of the business processes. New collaborative opportunities may emerge from technology-enabled coordination for regional perishable product distribution.

Zerok-IRS is a pilot research project that aims at investigating how companies operating perishable product supply chains can redefine their strategies and business models based on the asset sharing concept and on an innovative knowledge navigation. The concepts above mentioned can be embedded into a multi-sided web platform considered as the point of contact among shippers, carriers and customers. Digitization and asset sharing will be the key elements of the two macro systems that constitute the platform (see Figure 1):

- an *operations management system and decision support system* for the carrier;
- an *online asset sharing system* to implement shipper collaboration.
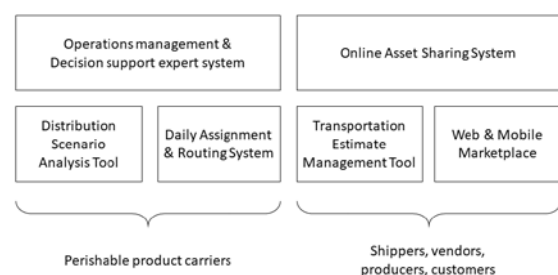

Figure 1. Zerok-IRS main modules

3.1. The ODSS

The Operations Management and Decision Support System is a tool designed to support the carrier's activities. It consists of two subsystems:

- a Distribution Scenario Analysis tool, and
- a Daily Multi-product Assignment and Routing system.

The Distribution Scenario Analysis tool enables the carrier to investigate the performance of different distribution scenarios in terms of mileage indicators, time indicators used for deliveries, customer satisfaction indicators, impact indicators environmental indicators, economic indicators, etc., thus conducting "what-if" analysis. This subsystem is based on a simulation-based tool developed by the authors in the context of a previous research project (called Smart Distr). It is a flexible and configurable decision support system (DSS) that embeds the traditional uncertainty of every supply chain and network logistics and leverages on the MSaaS concept (Modeling & Simulation as a Service) proposed in research works, such as Bruzzone et al. (2017). Screenshots of the system are provided in Figure 2 and 3.

Figure 2. Configuration of the Distribution Scenario Analysis tool
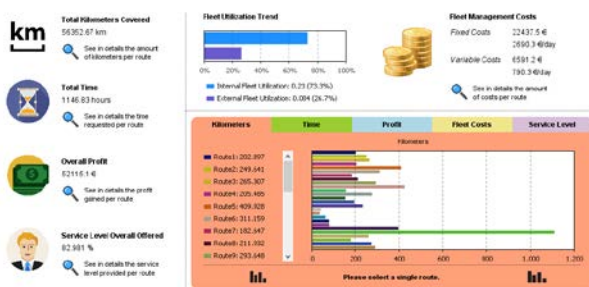
Figure 3. Key performance indicators of the Distribution Scenario Analysis tool

Ad-hoc scenarios for the design of the logistics and distribution network can be explored and evaluated using a dashboard of T-shaped performance measurements, i.e. large in number and deep in detail, thus giving life to a multi-objective decision-making process.

The Distribution Scenario Analysis tool is integrated with a Daily Multi-product Assignment and Routing system, which allows to plan the shipments in a way to convey perishable products towards those vehicles operating a distribution route with partial load capacity. This system will allow the carrier to manage real-time and in an automatic way the dynamic mechanism of delivery/picking. Delivery and picking activities are dynamic since the requests by consumers and producers could come at any time of day and will typically have a cycle of short life (a consumer will require that a product be delivered to him as soon as possible from the date of ordering - probably within a day). The carrier will be able to use a tool with updated information about routing (i.e. the sequence of points to be visited along the route before returning to the center of initial distribution). Pick-up and delivery points will be newsstands or points of sale already served by the operator transport or any additional geographical points to be reached (automatically calculated by the system without making detours or with a small deviation from the optimal route and close to the place of production of the goods themselves, for example the farm in question) in order to obtain a sub-optimal routing solution in terms of mileage but better in economic terms since the vehicles will move at greater load compared to before. The transport will be therefore "zero carbon balance" as the products will move along an already existing distribution network.

The daily assignment and routing system retrieves real-time geographic and routing information in order to provide reliable results and shows the trucks on a user-friendly graphical user interface (see Figure 4).
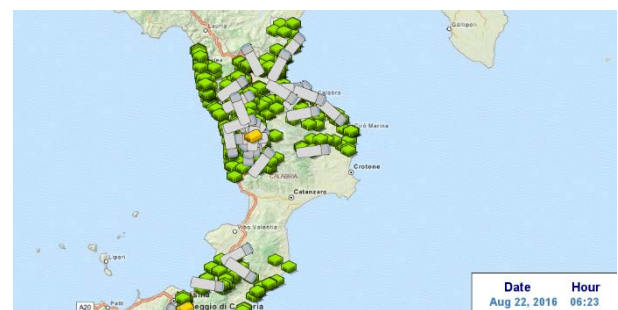

Figure 1. Real-time Daily Multi-product Assignment and Routing system

3.2. The OASS

The Online Asset Sharing System (OASS) is intended as a virtual marketplace that will give the users the opportunity to order and receive perishable products. The Zerok-IRS platform, in fact, will include a virtual marketplace (in the form of an online web portal and an Android and/or iOS mobile application) where the demand and offer of products can meet. The main three operators (producers, carriers, consumers or retailers) will interact with each other according to the framework depicted in Figure 5. In our pilot study, producers of the agri-food industry can access the virtual marketplace and place a product offer. On the other side, customers or retailers can request a product from a producer based on available offers. Here, the collaboration and asset sharing come into play. Based on the availability of the product, on the geographical location of the producer and on the real-time location of the trucks, the carrier will be informed about the product pick-up and delivery locations that will be sent to a truck. The choice of the truck may depend on routing optimization methods and on the current and expected capacity of the truck based on already planned on-route delivery/pick-up tasks. However, also the price and the service level are important. Feedback and recommendation mechanisms will be used to increase the reliability of a specific carrier or producer compared to others, thus increasing the overall service level of the platform. The confirmed

product requests will be managed through the Transportation Estimate Management tool, through which the carriers may also place specific quotations for the distribution service.

The result of the Transportation Estimate Management tool is the carrier that will be used for the transportation. Once the carrier is confirmed, the id of the carrier can be sent for the automatic online design of dynamic routes for vehicles. New delivery/pick-up points along the route may be added. In this new framework for the design of efficient and sustainable urban and extra-urban transport and logistics systems, newsstands or retailers become urban distribution centers (City Distribution Center, CDC).
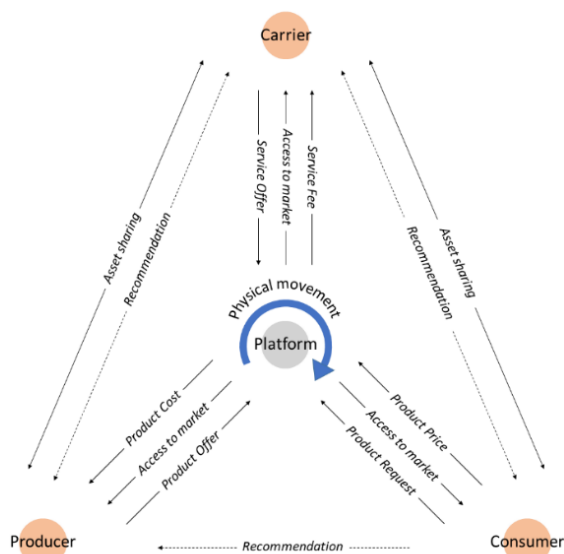
Figure 2. A framework for shipper collaboration

4. CONCLUSIONS

The growth of the online sales is expected to grow in the next years. Although this is encouraging for all the new marketplaces and online platforms that are rising, this also entails greater complexity in the last-mile distribution. This growth could be potentially beneficial in the perishable product supply chains, which are extremely complex due to the short shelf life.

The present article discusses different research and practical questions related to the perishable product supply chain (that by extension can be applied to every kind of product) and propose a collaboration and asset sharing strategy to limit the decline in the business performance of several small enterprises operating the perishable product supply chain (especially in the publishing and agri-food supply chain).

Interesting advantages may be achieved when a web platform for collaboration and asset sharing is used by all the operators of this supply chain, even small enterprises.

The scarce profitability of the empty trips and "rural deliveries" can be limited by leveraging on shared distribution asset and an online multi-product assignment to a distribution route. Carriers can therefore

benefit of increased economic performance. Secondly, customers can explore and navigate a vast set of perishable products. Trust will be the result of a collaborative process of assigning a score to products sold by a specific manufacturer that will determine the overall quality score of the producer (like the classic feedback mechanisms on online portals). The price of these products will be also very competitive. Indeed, these products will have a high-quality as the distribution is very quick and is at "zero cost" of transport because it leverages on already existing distributions routes.

ACKNOWLEDGMENTS

REFERENCES

Belk, R. (2007). Why not share rather than own?. The Annals of the American Academy of Political and Social Science, 611(1), 126-140.

Bogataj, M., Bogataj, L., & Vodopivec, R., 2005. Stability of perishable goods in cold logistic chains. *International Journal of Production Economics*, 93, 345-356.

Bruzzone A.G., Massei M., Agresta M., Sinelshchikov, K., Di Matteo, R., 2017. Agile solutions & data analitics for logistics providers based on simulation. In: Proceedings of the 19th International Conference on Harbor, Maritime and Multimodal Logistics Modeling and Simulation, HMS 2017, held at the International Multidisciplinary Modeling and Simulation Multiconference, I3M 2017, pp. 164-171.

Caballini, C., Rebecchi, I., & Sacone, S. (2015). Combining multiple trips in a port environment for empty movements minimization. *Transportation Research Procedia*, 10, 694-703.

Chen, Z. L. (2010). Integrated production and outbound distribution scheduling: review and extensions. Operations research, 58(1), 130-148.

Choe T., Rosenberger S. A., Garza M., Woolfolk J., 2017. The future of freight - How new technology and new thinking can transform how goods are moved. Deloitte University Press. Available from: https://www2.deloitte.com/content/dam/insights/us/articles/3556_FoM_Future-of-freight/DUP_FoM_the-future-of-freight.pdf [Accessed on May 18th, 2018].

D'Amours, S. and Rönnqvist, M., 2010. Issues in collaborative logistics. In: Bjørndal, M., Bjørndal, E., Pardalos, P. and Rönnqvist, M. (Eds), Energy, Natural Resources and Environmental Economics, Energy System, Springer–Verlag, Berlin Heidelberg, pp. 395-409.

Danloup, N., Allaoui, H., & Goncalves, G. (2015a, May). Green collaborative transport planning model with time windows: A case study in food retailing. In Advanced Logistics and Transport (ICALT), 2015 4th International Conference on (pp. 240-245). IEEE.

Danloup, N., Mirzabeiki, V., Allaoui, H., Goncalves, G., Julien, D., & Mena, C., 2015b. Reducing transportation greenhouse gas emissions with collaborative distribution. *Management Research Review*, 38(10), 1049–1067.

Devapriya, P., Ferrell, W., & Geismar, N. (2017). Integrated production and distribution scheduling with a perishable product. European Journal of Operational Research, 259(3), 906-916.

Ergun, O., Kuyzu, G. and Savelsbergh, M., 2007. Shipper collaboration. Computers and Operations Research, Vol. 34 No. 6, pp. 1551-1560.

Fowler, G.A. (2015). There's an Uber for Everything Now. The Wall Street Journal. Available from: https://www.wsj.com/articles/theres-an-uber-for-everything-now-1430845789.

Karaesmen, I.Z., Scheller-Wolf, A. and Deniz, B. (2011), "Managing perishable and aging inventories: review and future research directions", in Kempf, K.G., Keskinocak, P. and Uzsoy, R. (Eds), Planning Production and Inventories in the Extended Enterprise, Springer, New York, NY, pp. 393-436.

Li, J., Cai, X., & Zeng, Y., 2016. Cost allocation for less-than-truckload collaboration among perishable product retailers. *OR spectrum*, 38(1), 81-117.

Liu, R., Jiang, Z., Fung, R.Y.K., Chen, F. and Liu, X., 2010. Two-phase heuristic algorithms for full truckloads multi-depot capacitated vehicle routing problem in carrier collaboration. Computers & Operations Research, Vol. 37 No. 5, pp. 950-959.

Lusiantoro, L., Yates, N., Mena, C., & Varga, L. (2018). A refined framework of information sharing in perishable product supply chains. International Journal of Physical Distribution & Logistics Management, 48(3), 254-283.

McKinnon, A.C., 2010. Optimising the road freight transport system, in Waters, D. (Ed.), Global Logistics, 5th ed., Kogan Page, London

Mumtaz, U., Ali, Y., Petrillo, A., De Felice, F., 2018-a. Identifying the critical factors of green supply chain management: Environmental benefits in Pakistan. *Science of the Total Environment*, 640-641, pp. 144-152.

Mumtaz, U., Ali, Y., Petrillo, A., 2018-b. A linear regression approach to evaluate the green supply chain management impact on industrial organizational performance. Science of the Total Environment 624, pp. 162-169

Panda, S., Saha, S., & Basu, M., 2008. A note on EPQ model for seasonal perishable products with stock dependent demand. *Asia-Pacific Journal of Operational Research*, 25(03), 301-315.

Rahimi, M., Baboli, A., & Rekik, Y. (2016). Sustainable inventory routing problem for perishable products by considering reverse logistic. IFAC-PapersOnLine, 49(12), 949-954.

Sarkar, A. and Mohapatra, P.K.J., 2008. Maximum utilization of vehicle capacity: a case of MRO items. *Computers & Industrial Engineering*, Vol. 54 No. 2, pp. 185-201.

Tütüncü, G. Y., 2010. An interactive GRAMPS algorithm for the heterogeneous fixed fleet vehicle routing problem with and without backhauls. *European Journal of Operational Research*, 201(2), 593-600.

Van de Klundert, J. and Otten, B., 2011. Improving LTL truck load utilization on line. *European Journal of Operational Research*, Vol. 210 No. 2, pp. 336-343.

Vijayan, G., Kamarulzaman, N. H., Mohamed, Z. A., & Abdullah, A. M. (2014). Sustainability in food retail industry through reverse logistics. International Journal of Supply Chain Management, 3(2).

Yan, R. (2017). Optimization approach for increasing revenue of perishable product supply chain with the Internet of Things. Industrial Management & Data Systems, 117(4), 729–741. doi:10.1108/imds-07-2016-0297

Yilmaz, O. and Savasaneril, S., 2012. Collaboration among small shippers in a transportation market. European Journal of Operational Research, Vol. 218 No. 2, pp. 408-415.

AUTHORS BIOGRAPHY

Francesco Longo is Director of the Modeling & Simulation Center – Laboratory of Enterprise Solutions (MSC-LES), a laboratory operating at University of Calabria. He has published more than 200 scientific papers in international conferences and journals, and has participated as speaker and chairman in a broad range of international conferences. His research activities focus on innovative ways to use simulation paradigms and serious games to achieve new scientific advances in various application areas including Industry, Logistics, Defense and Cultural Heritage.

Antonio Padovano is currently conducting research in the area Human Behavior Modeling for Disasters Management in Industrial Plants at MSC-LES University of Calabria in collaboration with MIT and Harvard Medical School where he spent several periods as visiting researcher. He is also conducting researches on sustainability with specific applications in marine ports in collaboration with Rutgers University. He is expert in discrete event simulation and in developing

simulation solutions as a service. He has been supporting the organization of the I3M Multiconference since 2014.

Letizia Nicoletti was CEO of Cal-tek Srl from 2012 to 2014 where she is currently Senior Manager. She obtained her Master Degree in Management Engineering, Summa cum Laude as well as her PhD in Mechanical Engineering from University of Calabria, Italy. She has followed as Scientific Responsible many research projects in different areas including logistics and distribution, Defense and Cultural Heritage. She was also the main Responsible for all the services provided by CAL-TEK to NATO STO CMRE.

Jessica L. Frangella is currently Research Fellow at the Department of Mechanical, Energy and Management Engineering (DIMEG) of the University of Calabria, Italy. She earned her Master's Degree in Cooperation and Development Sciences, summa cum laude, at University of Calabria, in 2017. She is conducting research activities in the field of wearable augmented reality for employee safety in manufacturing systems and in the last-mile logistics of zero-km agri-food products for the development and business diversification of regional-level logistics companies.

Marina Massei completed her thesis in Genoa University, Humanistic Area on File Structures & Data Warehousing. She had attended Postgraduate Courses in Project Management, Modelling & Simulation, Operational Management, Total Quality Management, Logistics. She operates with the team of Prof. Bruzzone, DIME University of Genoa as project controller. She participated in the organization of SIREN Courses as well as she is serving in the organization committee of the most important simulation conferences. She also serve as General Chair of the International Conference on Modeling & Applied Simulation (MAS)..

POPULATION BEHAVIOR, SOCIAL NETWORKS, TRANSPORTATIONS, INFRASTRUCTURES, INDUSTRIAL AND URBAN SIMULATION

Agostino G. Bruzzone[(a)], **Marina Massei**[(b)], **Kirill Sinelshchikov**[(c)], **Riccardo di Matteo**[(d)]

[(a), (b), (c)] Simulation Team, DIME University of Genoa,
[(d)] SIM4Future
[(a), (b), (c)] {agostino.bruzzone, marina.massei, kirill}@simulationteam.com
[(d)] riccardo.dimatteo@sim4future.com
[(a), (b) , (c)] www.itim.unige.it   -   [(c)] www.sim4future.com

ABSTRACT
Crisis prevention and management are critical tasks for a public administration. In facts, a complex system such as a city could be difficult to keep under control, even in regular conditions, while respect emergencies it is very hard to finalize good preventive and operational plans. In order to succeed in such tasks, it is necessary to have proper support tools, capable to evaluate alternatives and predict effect of decisions in different conditions. To address such issues, the authors developed PONTUS (Population Behavior, social Networks, Transportations, Infrastructures and Industrial & Urban Simulation) which combines ability to model natural disasters with advanced human behaviors of the population.

Keywords: City Simulation, Decision Support Tool

1   INTRODUCTION
A modern city is a very complex System of Systems (SoS) which contains numerous types of infrastructure (e.g. transport network, water and power supply, healthcare) organizations and single individuals (Bruzzone, et al. 2017c). Hence, in order to achieve optimal efficiency, a public administration has to consider interests of numerous public and private subjects, while maintaining consensus with the inhabitants. In fact, even an optimal decision could lead to a protest in case of conflict of interests or simple miscommunications. However, the situation becomes much more complex in case of emergency; for instance, each natural disasters impact in different ways (e.g. flooding, earthquake, fires, hurricanes) and could destroy infrastructures, houses or even entire cities. Another important aspect is related to industrial areas that could ingenerate potential additional environmental damages and heavy impacts on population based on contamination and domino effect. In any case, parts of the city's infrastructures become temporary, or permanently, unavailable, while the lives of inhabitants are in danger and heavily affected by these events (Longo 2010; Longo et al.2012). In order to be ready for such situations, it is common, especially for medium and large cities, to have an emergency plan, which includes sequence of optimal actions in different crisis scenarios. Another important component of city crisis management plan is related to the analysis of high risk events, in order to prevent them or at least to reduce damages and/or probability of occurrence. For instance, this could include even simple actions such as cleaning

river beds, making firebreaks in forests or enforcing earthquake resistant construction. However, it is critical to compare costs and times of preventive measures with possible damages. The present paper focuses on an urban crisis dealing with flooding, however also other disasters could be simulated by proposed simulator.

2   SIMULATION SOLUTIONS
In order to increase awareness regarding possible outcomes of different crisis as well as to improve preparation, it is necessary to have reliable models able to estimate quantitatively impact of events (Bruzzone, 2013). In facts, in the past years, a special interest was on development of solutions capable to recreate a situation in a virtual world and to provide quite precise results, for instance, related to flooded areas after heavy rains (Jasper et al.2002; Chen et al. 2009, Kia et al.2012). Obviously, such systems allow estimating damages of natural disasters and comparing scenarios with different boundary conditions; for instance, it is possible to simulate impact of intense rainfall, using previous weather data, respect potential actions on the stream bed, city storm drains and sewerage. Obviously, such data allows to estimate possible damages and even to decide if worth to perform certain interventions to reduce losses. However, usually such models are not devoted to study population behavior, neither to predict number of involved persons, which is critical considering the fact that depending on timing, day, meteorological conditions, as well as other factors, this number could differs by several orders of magnitude; this aspect is clear considering malls, which are crowded for instance on Saturday while almost empty during the night as well as for schools (Bruzzone et al. 2017a). Furthermore, it is critical to consider also the "status" of the involved persons, especially in term of age and physical conditions; by the way proper behavior introduce also counter flows during crises due to the fact that people is looking for friends and relatives.

In facts, it is much more dangerous to have an emergency situation in proximity of some critical infrastructures, such as hospitals or schools, industrial plants or logistic hubs dealing with explosion, fire, contamination risks or security issues. The literature review reveals how researchers are currently dealing with both theoretical frameworks and practical applications for different types of critical infrastructures (Perrow, 2011; Longo 2012, Hsu et al., 2012). Considering these elements, it is clear the importance to

have a reliable data regarding population distribution during a specific crisis.

Table 1: Virtual World Characteristics Table

Characteristic	Data Example
Transport network	Roads, highways and railways transport graph with corresponding capacities and speed limits
Points of interest	Schools, hospitals, cinemas, trade centers with coordinates, capacity
Physical map	Terrain types and orography
Water flows	Rivers, channels and sewerage, with depth, width and the bed's roughness
Scenario population	Fertility rate, medium income, religions, educational level by country
City population	Urban units, population and income distribution, number of workplaces in different zones

In order to provide such information to PONTUS simulator, it was decided to recreate a population up to the level of individuals, considering age, sex and nationality distributions, medium income in different zones of the city, religion. Such detailed representation of the population is achieved by using data from various sources, such as open data provided by public administration, average rental prices and various statistical data related to different countries.

Furthermore, every generated virtual person has a list of preferences and opinions based on attributes, such as age, which allows to recreate daily behavior with higher accuracy. However, basic individual behaviors differs also based social networks and interactions, such as family, friends and colleagues. In fact, the simulator generates not only single persons, but statistically correct families, creating at the same time also a graph of social interactions considering possible friendship between individuals based on their own attributes, such as workplace, age, sex, income, nationality, religion and education level. Such approach allows to reproduce behaviors of different social groups: for example, during the simulation, a specific procedure proposes exchange of possible leisure activities; in fact, during the free time, agent driven virtual people plan collective actions as virtual persons such as going to the cinema or visiting a park. Obviously, in order to reproduce a city's life cycle correctly, it is necessary also to consider various characteristics of the scenario, as proposed by the examples of table 1.

However, it is almost impossible to collect all required information in consistent way and with a sufficient accuracy. For this reason, the simulator takes care of missing data, creating statistically proper data consistent for generating the objects and the virtual people. For example, in case of missing infrastructures, such as schools or malls, PONTUS generates them based on available data about population density as well as on other critical parameters. Furthermore, the simulator

analyzes terrain types and orography in order to add missing parts of storm drain.
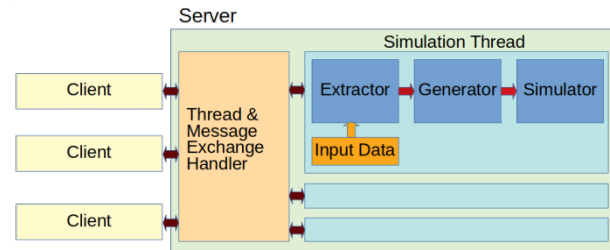

Figure 1: PONTUS Architecture

3 MODELING & SIMULATION AS A SERVICE

Due to big advances in cloud computing along last decade, a lot of solutions once performed locally, are now available to be addressed by solutions based on concept Software-as-a-Service (Bruzzone, 2007; Van Steen & Tanenbaum 2017). In fact, such approach allows to outsource local infrastructure to cloud providers, making the final system easier and cheaper to maintain. Obviously, same considerations are true also in the field of M&S (Modeling and Simulation), especially considering that many models require a significant computational power which would be difficult and expensive to provide. So this is an option to be evaluated and compared with traditional approach. In facts it is important to consider Modeling & Simulation as a Service (MSaaS) as well as Modeling, Interoperable Simulation and Serious Games (MS2G), a new paradigms, adopted for models devoted to multiple applications (Liu et al.2012; Bruzzone et al.2014, 2017b).

3 SYSTEM ARCHITECTURE

One of main benefits derived from Simulation is the ability to run scenarios multiple times in order to acquire enough statistical data to predict the situation and find optimal solutions. Furthermore in decision support tool for public authorities, it is necessary to consider potential limitations imposed by available hardware, which in most cases is not suitable for high computational workload. Based on these consideration, the authors decided to develop a web-based client-server solution, which allows to place the model in a high performance server, while leaving a relatively lightweight graphic user interface to the client. In fact, in this case, the simulator during, at start, launches a web socket server and goes in idle mode; each time a client connects, the program wakes up and starts a dedicated thread of the simulator, which extracts info from available data sources and subsequently generates the virtual world, as illustrated in the figure 1. An interesting fact is that the PONTUS architecture allows not only to perform parallel simulation, but to do it with different data sets. For instance, it is possible to launch scenarios with different transport graphs, meteorological situations and even distinct cities.

One of main advantages of such architecture is related to the implementation of the MSaaS paradigm, which

imposes constraints only on the server's hardware, leaving to all clients the possibility to focus on study of scenarios of interest.
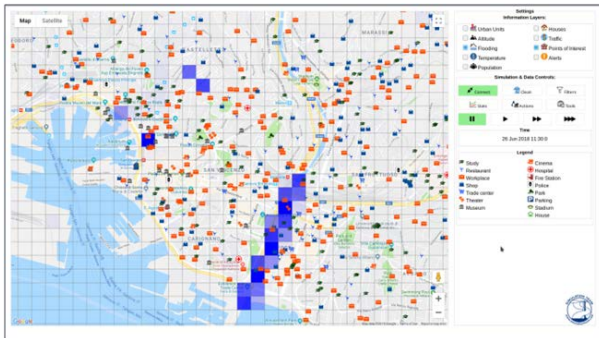

Figure 2: GUI: Points of interest (icons) and the flooded area (blue squares) on the map

As aforementioned, the graphic user interface (GUI), shown in figure 2, is created as web application, which makes it suitable for utilization in any device with sufficient screen size. The main window contains an interactive map based on Google's solution and a control panel to switch between different visualization modes as well to interact with the simulator. PONTUS is an interoperable Simulator using IA-CGF able to interact with other models by using HLA Evolved Standard (Bruzzone 2013). PONTUS allows to select different layers, such as urban units, population density distribution, points of interest, traffic intensity and weather conditions etc. Furthermore, it is possible to filter some data to be visualized: for instance, select only persons of a specific quarter, nationality or age and/or to visualize specific statistical data related to transportations, etc. While the mentioned settings are acting only on a visual part, the GUI allows also to interact with the simulator in order to modify various conditions of the generated scenario. For instance, it is possible to initiate predefined interventions, such as dike construction in a critical sections of rivers, or change 'on the fly' the road network. In order to achieve a compromise between the program's performance and required development time, the authors decided to implement PONTUS in Java. In fact, it allowed integration of various modules maintaining high simulator overall performance. The GUI is developed as a web application, it is an HTML page with formatting declared using CSS and active elements implemented in JavaScript. The proposed solution is quite lightweight and allows to integrate easily different 3rd party and auxiliary modules and extensions, such as Google map, as well as to connect it to the server using Web Socket.

4 CASE STUDY SCENARIO & RESULTS
PONTUS help to optimize many activities related to a city management. For instance, it is possible to estimate impact on traffic caused by road block or by construction of a new mall, or predict people presence in points of interest. However, the main scope is emergency management, with special focus on flooding.

For instance in past, heavy rains caused huge damages and casualties in Genoa (Lanza 2003). For this reason, the authors tested the simulator on this context; in facts weather module of PONTUS is capable to generate rainfalls in a zone based on historical data obtained from different weather stations. In order to elaborate water transfer on the given terrain, the model create a regular mesh, with every cell characterized by multiple parameters, such as size, elevation, terrain type, its capacity to absorb water and initial saturation (Duley & Kellu 1939). During the run, the simulator calculates water flows among neighbor cells based on a average inclination and water speed on a different terrain types. At the next step, based on environmental conditions, some amount of water is evaporated and absorbed by the terrain. However, such model would not be capable to provide an acceptable precision by itself in case of the city simulation. In facts, underground rivers and channels as well as sewerage network transport a lot of water and could not be excluded from the model; for instance, in Genoa one of two big rivers goes underground for about 1 km just before the sea, which in case of utilization of only a terrain model would lead to constant flooding in such zone while in the real world this situation is very rare. Furthermore, in some cases the accessible orography is not precise enough, otherwise only a DEM (Digital Elevation Model) instead of DTM (Digital Terrain Model) is available.

In such cases provided data contains an elevation of artificial constructions, for example, buildings and bridges, instead of a "pure" terrain below them, which leads to flow calculation errors. In order to overcome these problems, the model utilizes special manually created graph which contains all major rivers, underwater channels and sewerage in the zone of interest, representing such infrastructure as nodes and links, with transfer model is based on a Manning's equation (Chanson, 2004). Such combinations of the rain, water transfer and water channel models allow to reproduce major rains of the past as well as to evaluate impact of future ones. In facts, to validate the model it is possible to compare simulated water flows in rivers as well as water levels respect the ones observed in the similar conditions in the past by using results of rain measurements, water flows, precipitations over different city areas and flooded zones. Furthermore, thanks to the human behavior model it is possible to estimate risks related to people being trapped in buildings by water, which is especially important in cases of critical infrastructures, schools and big entertainment locations. Example of this situation is presented in the figure 2, which contains overlaying layers of infrastructure and the one generated by the flooding model. In addition to this aspects the model consider objects related to industrial elements such as plants and tanks that in case are damaged by the other accidents could deal with release, in air or water, of hazardous material and create contaminated areas; obviously it could be possible also to generate explosions and fires and the simulator enables the possibility to consider domino effect

affecting progressively, along time, multiple industrial elements. This approach extends the validity of the model and allows to consider effectiveness of safety engineering solutions. In general to provide decision makers with explicit data about zones of interest, the simulator operates in a special mode to create the scenario once, and then performs multiple runs with different boundary conditions: normal, crisis and crisis after intervention. In this case the scenario is restored to the initial one after each launch using Memento pattern, which is implemented for each and every variable object. Indeed, PONTUS saves in special log files the most important data, for instance, the one related to human presence in points of interest, making it possible to perform comparison and obtain quantitative results after the finish.

CONCLUSIONS

The proposed approach is an effective solution, capable to support decision makers in different aspects, from traffic management to emergency situation forecasting. Furthermore, the platform is open to extensions and to possibility to add further components; indeed special auxiliary tools, developed by authors, allow to define easily the scenario to run the simulator on different locations around the world. Of course, it is possible to argue that some components of this simulator is already available in other software tools, in particular the open-source ones; however PONTUS allows to combine them with population behavior and it is open to interoperate with them through HLA. Hence, it is important to highlight some of the main characteristics of PONTUS that include: capability to integrate different components in order to provide more trustworthy overall results, ability to generate secondary data in consistent way and to reduce quantity of the necessary a priori information, user-friendly interface, an effective system's architecture which implement MSaaS paradigm and it is open to HLA. Indeed these aspects support possibility to extend and keep open the simulator while the MS2G approach improve usability.

Such characteristics allow the PONTUS to be some kind of "Swiss Army Knife" in the field of M&S for urban crisis management support, hence, its comparison with more specialized tools is not yet completed and will be object of future researches. The preliminary verification of the model was performed by implementing unit tests on critical methods, as well as by using static code analysis, integration and beta tests. As anticipated, currently, the simulator development is in a validation phase, which is quite complex considering number of included components, however, preliminary results are quite promising.

REFERENCES

Bruzzone A.G., Bocca E., Longo F., Massei M., 2007. Training and recruitment in logistics node design by using web-based simulation. International Journal of Internet Manufacturing and Services, vol. 1, no. 1, pp. 32-50.

Bruzzone, A.G., Agresta, M., Sinelshchikov, K. (2017a). Simulation as decision support system for disaster prevention. SESDE 2017, Barcelona, Sept.

Bruzzone, A.G., Massei, M., Agresta, M., Sinelshchikov, K., Di Matteo, R. (2017b). Agile solutions & data analitics for logistics providers based on simulation. HMS 2017, Barcelona, Spain.

Bruzzone, A.G., Massei, M., Maglione, G.L., Sinelshchikov, K., Di Matteo, R. (2017c). A strategic serious game addressing system of systems engineering. MAS 2017, Barcelona, Spain.

Bruzzone A.G., Massei M., Agresta M., Poggi S., Camponeschi F. & M. (2014) "Addressing strategic challenges on mega cities through MS2G", Proc. of MAS2014, Bordeaux, September

Bruzzone, A. G. (2013). Intelligent agent-based simulation for supporting operational planning in country reconstruction. Int.Journal of Simulation and Process Modelling, 8(2-3), 145-159.

Chanson, H. (2004). Hydraulics of open channel flow. Elsevier.

Chen, J., Hill, A. A., & Urbano, L. D. (2009). A GIS-based model for urban flood inundation. Journal of Hydrology, 373(1-2), 184-192.

Duley, F. L., & Kelly, L. L. (1939). Effect of soil type, slope, and surface conditions on intake of water.

Hsu W., Tseng C., Chiang W., Chen C., 2012. Risk and uncertainty analysis in the planning stages of a risk decision-making process. Natural Hazards, vol. 61, no. 3, pp. 1355-1365.

Jasper, K., Gurtz, J., & Lang, H. (2002). Advanced flood forecasting in Alpine watersheds by coupling meteorological observations and forecasts with a distributed hydrological model. Journal of hydrology, 267(1-2), 40-52.

Kia, M. B., Pirasteh, S., Pradhan, B., Mahmud, A. R., Sulaiman, W. N. A., & Moradi, A. (2012). An artificial neural network model for flood simulation using GIS: Johor River Basin, Malaysia. Environmental Earth Sciences, 67(1), 251-264.

Lanza, S. G. (2003). Flood hazard threat on cultural heritage in the town of Genoa (Italy). Journal of Cultural Heritage, 4(3), 159-167.

Liu, X., Qiu, X., Chen, B., & Huang, K. (2012, July). Cloud-based simulation: The state-of-the-art computer simulation paradigm. In Principles of Advanced and Distributed Simulation (PADS), 2012 ACM/IEEE/SCS 26th Workshop on (pp. 71-74). IEEE.

Longo F., 2012. Supply chain security: An integrated framework for container terminal facilities. International Journal of Simulation and Process Modelling, vol. 7, no. 3, pp. 159-167.

Perrow C., 2011. The next catastrophe: Reducing our vulnerabilities to natural, industrial, and terrorist disasters. In The Next Catastrophe: Reducing Our Vulnerabilities to Natural, Industrial, and Terrorist Disasters, pp. 1-377.

Van Steen, M. & Tanenbaum, A. S. (2017). Distributed systems: principles and paradigms. Prentice-Hall.

MS2G AS PILLAR FOR DEVELOPING STRATEGIC ENGINEERING AS A NEW DISCIPLINE FOR COMPLEX PROBLEM SOLVING

Agostino G. Bruzzone

Simulation Team, DIME University of Genoa,

agostino@itim.unige.it

www.itim.unige.it

ABSTRACT

Simulation science is a strategic resource to address most challenging problems; in this paper, it is provided an overview about how new simulation capabilities, such as that ones based on MS2G (Modeling, interoperable Simulation and Serious Games), could enable to address complex systems and to support decision making; in addition, the new Strategic Engineering Discipline is proposed as framework where to combine all these new approaches for Problem Solving and Strategic Planning nowadays; several real examples are proposed as case studies to confirm the validity of these innovative concepts.

Keywords: Modelling & Simulation, Interoperability, Decision Support, Strategic Engineering, Serious Games

1 INTRODUCTION

Today very important changes in geo political situations generate a very dynamic evolution: large humans' migrations, climate change affecting nations economies, religious and ethnical conflicts, new emerging powers and their actions devoted to promote power projection.

These situations are related to many factors and affect many different layers: politics, economies, market, homeland security, etc. Along last decades, technology has changed several aspects in human life due to many factors including: interconnectivity, mobile technologies, computational power, data science and machine learning, micro sensors, biomedical devices, etc. These elements are providing us new challenges as well as opportunities that slightly change the potential in analyzing and addressing the strategic issues.

In facts, the term Strategy comes from Greek, combining *stratos* (army) and *agein* (leading) so it is pretty clear that it deals with leading resources. In facts, it has been said that "Strategy is the art of good direction" ("La Stratégie est l'art de bien diriger", Jomini, Prècis de l'Art de la Guerre, 1838), therefore also the necessity to have dynamic solutions for strategic planning was clearly stated by Von Clausewitz, published by his wife while almost 200 years ago (Vom Kriege, 1832): "we need a *philosophy of strategy* that contains the seeds of its constant *rejuvenation*, a way to chart *strategy in an unstable environment*". So this good directions rely today on new supports, simulators and models integrated with other system and devoted to be successful and competitive. In facts to support strategic planning we need *engineering methodologies* able to deal with current complexity of the world and to use the available enabling technologies; in this sense simulation is a crucial science to support these activities and in fact the MS2G (Modeling, interoperable Simulation and Serious Games) paradigm is one of the most promising approach to be used in this context; this paper proposes an overview on how to use new simulation models with other techniques to support strategic decision making and outline the importance to shape new discipline integrating all these capabilities within a framework such as Strategic Engineering.

2 TODAY vs. YESTERDAY

Today it turns possible to identify how to solve a problem by using the high density information available and smart algorithms; it is also possible to test them on models able to simulate reality; in this way the simulators could predict complex system behaviors, on different time horizons, and could analyze a wide spectrum of alternatives that lead to develop dynamic solutions able to self adapt to changes in boundary conditions and eventually to competitor strategies.

This, obviously, have a great impact on problem solving and decision making related to strategic issues. However, somebody might object that this is not new, that these considerations were in place since computer technology was available and that even in the past this process was applied by using M&S; obviously this is partially true (Longo, 2011). In facts a perfect example, to understand this point and related changes, is proposed by Mission Earth initiative and the GENI (Global Energy Network Institute) global simulation; these activities have been inspired by the first report of *Club of Rome*, established in 1968 at *Accademia dei Lincei* in Italy by an international community of individuals including former head of state, diplomats, scientists, economists, business leaders, etc (Meadows et al., 1972). On the early fifties, the founder of *Society for Computer Simulation International*, John McLeod, established the "Simulation in Service of the Society" and later on with another simulation titan, Ben Clymer, activated Mission Earth initiative (McLeod 1968, 1986; McLeod John & Suzette, 1974; Clymer 1969, 1980, 1994; House & McLeod 1977). Mission Earth initiative focused on the creation of new simulators to address in new way the concepts behind World Simulation Game proposed on 60's as well as to support development of new strategies (Fuller 1969). For instance, in this framework, GENI project was devoted to study how to

distribute power around the globe to promote cooperation, to solve major issues and, even, to support Earth Development and Peace (McLeod 1999; Clymer A. 1993; Clymer M. & Mechoso 1997). These are examples about very innovative global models addressing world problems, developed by major experts of simulation, along three decades, many year ago; so it is clear that the idea to use M&S for Strategies has always been there; so what changed? The answer is in the example itself, by analyzing the problems experienced in relation to these initiatives: most of them were based on few extraordinary volunteers with limited visibility on media; in addition the models were pretty complex and the results difficult to understand for a broader audience with no scientific background considering multidisciplinary elements; last, but not least, setting up these scenarios and acquiring reliable data was a major issue (e.g. just the collection of GDP data of all countries over a decade was not "just one click" in 70's or 80's). These considerations make it clear what changed: today we have possibility to cooperate among a wide community of scientists with web technologies, to discuss and share models; we have technologies to integrate models and to let them interoperate over the web; we can access huge amount of pretty reliable data that could *easily* used in simulators; we have much more computational power and even the possibility to distribute these models on smartphone among people and let them play the "Global Energy Distribution Network Game". These are just few examples, but they make it easy to answer the question "what changed?": the change is that today we have technologies, data, resources and capabilities to turn the dreams of our "simulationist fathers" into reality. This means that visionary new projects could be developed and the old ones could be completed providing a real "Service to the Society" by using Modeling and Simulation (M&S).

3 TODAY AND TOMORROW

It is possible to consider a new question "so why we don't do all this marvelous use of simulation if it is possible?". Also in this case, it is easy to reconsider the characteristics of technological enablers that we used to confirm, in previous paragraph, the great current capabilities. For instance, combining different models is obviously a major necessity if we need to address complex strategic problems (Bruzzone et al. 2014); in the proposed case of power distribution and generation over wide regions: there is necessity to combine models related to economy, quality of life, diplomacy, politics, etc. In this case, even if interoperable simulation standards are consolidated since 20 years, it is evident that we are still far away from being able to easily integrate two different simulators (Kuhl et al.2000; Bruzzone & Massei 2017). This is due to currently available standards and developments: they are mostly addressing technological interoperability while conceptual interoperability is an open issue (Bruzzone et al. 2017a); in additions there are programming

aspects that need to be improved in terms of reliability by M&S Research and Developments (R&D) for being able to interconnect such systems (Bruzzone 2017). Human factors represent another crucial element, very hard to be addressed and expected to keep a significant role in future sophisticated models due to its stochastic nature despite the big potential in developing simulators facing these elements (Bruzzone et al. 2015). Another major aspect is related to the quantity of data, including actual ones and collected in quasi real time from the field: it is something pretty new and requires new solutions to be developed for filtering them as well as to extrapolate trends and symptoms that before were impossible to detect due to the low frequency (or not availability) of available samples (McAfee et al.,2012). Similar problems are related to data farming and capability to check and validate output (Sanchez 2014). Another very important factor potential of available algorithms, often based on AI (Artificial Intelligence), that allow to correlated the data and extrapolate behaviors: these need further developments and improvements (Wu et al., 2014;Najafabadi et al., 2015). Some other critical aspects are related to simulators distributed over mobile solutions and smart phones operated by people: also in this case technology is available, but a lot of R&D is required to improve reliability, immersive capability, interactivity, to reinforce and consolidate concepts such as MSaaS (Modeling and Simulation as a Service) or cloud services (Li et al.,2010; Cayirci 2013). So, what is the consequence of this Maieutic analysis? The point is that we have a potential capability, but Simulation Community, as well as other scientists, need to work hard on R&D to turn the potential in reality and to let evolve techniques and methodologies to be reliable and usable. MS2G moves exactly in this direction because it emphasizes not only the technological aspect, but also the necessity to create models that engage and immerse the users, enabling them to understand the simulation framework respect the reality and how to interact with it. In facts, one major future challenge will be also related to the necessity to increase people and decision makers' level of knowledge to properly operate these systems; this requires different kind of cultural developments such as capability to have transdisciplinary teams, to understand big data and complex correlations, to develop skills for interacting with new Simulation Systems (Elfrey 2006; Bruzzone et al.2014b, 2017b). In facts, MS2G deals to develop new features in simulators to facility people, but it is evident that is also fundamental to update Educational Programs and Initiatives to support the evolution of potential users' community.

4 TOMORROW CHALLENGES & THREATS

Tomorrow challenges are always infinite as human imagination; MS2G can be combined (with a great potential) with other sciences & Technologies as very recent researches show in different domains and applications areas, e.g. Data Science (Irani et al., 2018),

AI & Machine Learning (Longo et al. 2017), Internet of Everything (Naranjio et al., 2018) among the others; so it is expected to create a real innovative context where decisions are taken based on deep knowledge, valid models, extensive alternative comparison, multi-criteria analysis and dynamic evaluation of feedbacks.

This sounds as the philosopher's stone, therefore this approach should provide even simple aids; for instance thinking back to the 90's, GPS and driving systems were already there as well as technologies to know traffic density, while Intelligent Transportation Systems were collecting and processing such data; however the available information were much more limited and the driving systems were performing just search on routes, with pretty limited capability to consider traffic situations. (Varaiya 1993; Bart et al. 1996). Today, we have ultra light smart phones with large screens that show us the map including many details (e.g. info on shopping, parking, attractions) while the length of traffic queues estimated with 100m precision (Kim 2017; Wan et al., 2016). This means that in near future MS2G could lead to address not only the "world energy program for United Nations", but also the "recycling process optimization for a town in North Italy", saving few million Euros and improving quality of life of hundred thousand people. In addition MS2G could be used even for more radical changes, such as improving mutual trustiness between Institutions and Populations, by sharing these models and cooperating in developing solutions trough crowd sourcing (Bruzzone et al.2014b). In facts, we might imagine a future where people could run the simulators and analyze proposal from political leaders to check and validate them; at the same time an emerging issue could be addressed by the people that are experiencing it and their proposals could be tested on the model and, if applicable, incorporated in solution to be adopted by authorities. This could lead to have very dynamic decisions and plans, capable to react and adapt to mutating boundary conditions.

In this sense, just in these days, the author is working in using previously developed models to manage the crisis generated by the collapse of "Morandi Bridge" in Genoa (Harding 2018). In this case, a specific model was adapted to study Genoa respect Strategic Urban Planning for preventing and mitigating Flooding as part of "Decision Theater" project framed in Smart City Initiatives, closed just last December (Bruzzone et al.2017b). This means that in August XIV, 2018, when the crisis emerged, the Population and City Models were already available and tuned, so it is currently possible to use them to analyze different solutions.

However, as always, all these capabilities could be sensitive to improper uses and it is recommended to adopt ethical code in developing solutions based on Simulation Science (Oren et al., 2002). It worth to mention some of the major threats: one for all, a misleading Models Validation and Verification (Balci 1997); indeed not validated models or, even worst, simulators deliberately mistuned to provide desired output, could lead to wrong decisions. Therefore there

are more sophisticated threats that are hidden in the folds of the future: a major one is in *the eye of the beholder*. In facts, if the simulation users and decision makers don't know what are the questions or what is the proper perspective to address a problem, even new paradigms cannot provide valid solutions. Considering the above mentioned case of the recycling process applied to a small town: if the Authorities would focus on path optimization in garbage collection service, they might miss the point that population consumption modes could be more sensitive factors to reduce waste: e.g. paying back for empty cans or bottles as happens in some countries (Huang et al., 2005; Duma & Nemeslaki 2013). This reveals a need to educate and train people in strategic view and this is one of the major goals of the new initiatives such as STRATEGOS the new MSc in Strategic Engineering recently activated at the Genoa University (*www.itim.unige.it/strategos*).

Indeed STRATEGOS is devoted to promote quantitative modeling to support decisions by developing a new generation of Engineers able to deal with Strategic Thinking and to support Decision Makers by mastering advance modeling, simulation as well as other enabling technological and scientific areas.

There are many other potential shortfalls, but it is important to outline a major threat related to simulation that in future could turn even more hard to face. A famous quote by Mahatma Gandhi states "*freedom is not worth having if it does not include the freedom to make mistakes*". The new generation solutions, combining science along with all new technologies, could provide very efficient models to predict behaviors, with invasive control of communications, biodata, etc. It could turn possible to control each individual or group and to predict their action influence by violating privacy as it happen usually nowadays. Obviously human factors will be present anyway, but by adopting some kind of sci-fi vision, it could be possible to imagine models able to predict society and group evolution, and to develop plan to influence them it as happen with psychohistory (Asimov 1951). It is important to highlight that this could be an issue for the whole mankind considering that it could reduce *free will* based on a "wide computational intelligence supported by science". In such sense we can figure out a variety of possible future scenarios, not necessarily for the good of the humanity: from the *good shepherds* driving the decisions based on a comprehensive view that overpass individual capability, to *conspiracies* using these technologies passing through a super Artificial Intelligence "*equipped*" of friendly or hostile behavior. Scientific literature considers some of these elements and for sure new predictive and reactive capabilities should be addressed in some way without losing a pragmatic point of view (Duderstadt 2005; Blackmore 2006, Barrat 2013). The Solution to these pitfalls is not easy and unknown, yet. Nevertheless human being is able to be responsible, to behave ethically, to be noble, to lead for equality and freedom, to discern good and evil and to be brave enough to make right decisions

despite consequences; these properties of human beings are unique and probably the basis to find prospective answer based on author point of view. In any case, the scientists should identify as early as possible these potential risks and to work together to find viable solutions; it is evident that the future will require to lead these technologies along with people education while obscurantism might be not a solution.

5 NEW SIMULATION PARADIGMS FOR DECISION MAKING

The MS2G (Modeling, interoperable Simulation and Serious Games) is an innovative paradigm devoted to support development of new solutions able to benefit from the different characteristics of these specific methodologies and to enhance fundamental aspects of Simulation Science such as usability, engagement, fidelity and modularity. In facts, the basic concept is to develop an approach that combines Interoperable Simulation with engagement and immersive capabilities provided by Serious Game approach.

In facts, the MS2G is a pillar for new capabilities development in many applications sectors with particular attention to complex problems affected by uncertainty where the users are decision makers with time and resource constraints. In this case there is often a necessity to have different models interoperating while considering stochastic factors and at the same time to maintain control over results fidelity while the time to configure, use and analyze the results is short and need to be intuitive for the user and able to guaranteeing its trustiness.

6 STRATEGIC ENGINEERING AS EMERGING DISCIPLINE

Strategic Engineering is a new Discipline that could be one of the possible solutions to create skilled experts for developing the new generation of simulators. In facts, the main aim is to prepare experts and develop a framework where to amalgamate different domains and strong scientific foundations that could lead to prepare new models highly interoperable and strongly interconnected with other systems and data. It is evident that Strategic Engineering strongly relies of the capabilities of simulation advances such as MS2G paradigm. Therefore the Strategic Engineering is devoted to develop Strategies in Industry, Business, National and International Activities, Defense and Homeland Security. Indeed the Strategic Engineering considers to address the complexity related to these sectors by creating a combined approach based on Modeling & Simulation, Data Science, Artificial Intelligence and Operational Research combined with enabling technologies, such as IoT (Internet of Things), Cloud Services, etc. Obviously MS2G is an ideal paradigm to support this activity that could be effectively used by Decision Makers dealing with Complex Problem Solving. These activities are eligible to be used into development of new Strategies for a wide spectrum of sectors where transdisciplinary

elements are fundamentals (e.g. economy, operations, politics, social aspects) to succeed (Elfrey 2006).
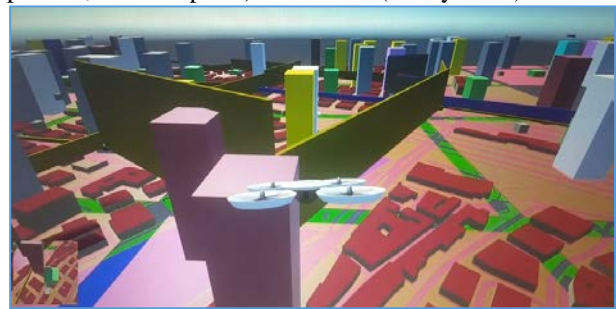

Figure 1 – Flying over Town Dynamics with Big Data

In this sense there is a necessity to develop capabilities and even skills for Strategic Engineering and also the opportunity to create new educational path for engineers and scientists mastering these techniques as well as training programs for Decision Makers and Strategists to learn how to use these innovative approaches. The synergy MS2G and Strategic Engineering could lead to develop new solutions for actual applications.

7 CASE STUDIES AND EXAMPLES

The Strategic Engineering proposes several case for new MS2G Solutions applications; indeed these elements are pretty interesting while addressing problems currently popular, where the number of variables and output data is so large that intuitive and immersive frameworks connected to interoperable simulation are crucial. In this sense, several applications have been developed along last years by authors as summarized by following cases:

ARPIA: MS2G in Urban Strategic Planning

ARPIA (Augmented & virtual Reality for Population modeling based on Intelligent Agents) is a Simulation Environment able to integrates in HLA (High Level Architecture) different Simulation Models and IA-CGF to reproduce City Dynamic Evolution as well as People Consensus and Population Behaviors over Regular conditions as well as during a Crisis or a Disaster.(www.itim.unige.it/projects/arpias.html).

T-REX: MS2G in Homeland Security

T-REX (Threat network simulation for REactive eXperience) is an example of MS2G dedicated to consider different kind of mission environments such as Homeland Security and Hybrid Warfare; indeed T-REX supports HLA Simulation and enable the possibility to be federated federation with other elements to evaluate different aspects and their interactions (e.g. economics, finance, politics) even through interoperability among models (www.liophant.org/projects/t-rex.html).

JESSI: MS2G for Defense & Cyber Warfare

SO2UCI (Simulation for Off-Shore, On-Shore & Underwater Critical Infrastructure) is a Simulation for Vulnerability Reduction in Critical Infrastructures considering direct/indirect impacts & multiple domains (www.itim.unige.it/projects/so2uci.html)

8 STRATEGOS

It worth to mention how critical is promote and develop these concepts, also to activate new initiatives in terms of education and training such as STRATEGOS.

Strategic Thinking and Strategy Development have been always key Competitive Factors, given the Complexity of Reality and Human Goals. Strategy means ability to deal with a variety of variables, taking into account uncertainty, scalability, extensibility, dependability. One statement, among millions, confirms the importance of Strategic Engineering: "If you want to grow, find a good opportunity.

Today, if you want to be a great company, think about what Social Problem you could solve." (Ma Yun, alias Jack Ma, co-founder and executive chairman of Alibaba, in 2018: Personal Net Worth 42.2 GUSD; Alibaba 462th World Raking, 23.8GUSD Revenues, 6.2GUSD Profits, 56% Growth in Net Revenues, Stocks +15% within a single month based on *Fortune Global*). Obviously, Strategy is nowadays strongly related to Complex Systems involving Quantitative Data and Digital Information. However, to the best of our knowledge, there are few Master Programs, worldwide, specifically dedicated to Strategy Development with solid M&S, Engineering Foundations, strong integration in Innovative Enabling Technologies and Information and Communication Technologies (ICT). Indeed, Engineering is not just about designing new Technological Systems and Products, but even to support Identification and Definition of New Strategies devoted to direct Future Developments. These aspects deal with developing New Processes, Solutions and Organizations devoted to achieve the Success respect Strategic Goals. In facts the Operational Lifecycle of Innovative Systems are usually quite long, rich of Uncertainties and strongly affected by many Variables as well as by different potential Scenarios; so a proper approach in Modeling and Analyzing Quantitatively these Elements is fundamental for the Final Success. Up to now, these Strategic Aspects are frequently roughly addressed by traditional approaches and educational practices: often just qualitative approaches or simplified static analysis methodologies are proposed as investigation aid, while, vice versa, today modern M&S, Machine Learning, Big Data, Innovative ICT solutions are potentially more effective in dynamically addressing these Issues. The main goal of this initiative is to set up a new International Engineering Master Program which relies on M&S and ICT education and it is able to address Strategic Modeling and Decision Support, providing the Deep Scientific Knowledge as well as the Technical Engineering Skills needed for developing, tailoring and using methodologies for Strategy Definition, Innovative Solution Development and Capability Assessment. The profile that will result as outcome of this Master Program is expected to operate in a variety of application domains (ranging from Manufacturing to Engineering, from Military Sector to Business, from Politics to Personal and Societal Development), being able not only to apply Strategies using the most appropriate Models, but also to gain Requirements for new Methods and to design new Methodologies, Techniques and Instruments for Strategic Planning and Management.

CONCLUSIONS

This paper proposes a view on emerging innovative concepts and paradigms that could lead simulation to be the strategic resource for future developments; criticalities, opportunities, shortfalls and threats are outlined as well as the requirements to prepare future generations in successfully developing these concepts and mastering these disciplines.

REFERENCES

Asimov (1951) "Foundation", Gnome Press, NYC

Blackmore, S. (2006). Conversations on consciousness. Oxford University Press, UK

Balci, O. (1997, December). Verification validation and accreditation of simulation models. In Proceedings of the 29th conference on Winter simulation (pp. 135-141). IEEE Computer Society.

Barrat, J. (2013). Our final invention: Artificial intelligence and the end of the human era. Thomas Dunne Book, Macmillam, NYC

Bruzzone A.G., Massei M., Longo F., Maglione G.L., Di Matteo R., Di Bella P., Milano V. (2017) "Verification and Validation Applied To an Interoperable Simulation for Strategic Decision Making Involving Human Factors", Proc.of WAMS, Florence, September

Bruzzone A.G., (2017) "Smart Simulation: Intelligent Agents, Simulation and Serious Games as enablers for Creating New Solutions in Engineering, Industry and Service of the Society. Keynote Speech at International Top-level Forum on Engineering Science and Technology Development Strategy- Artificial intelligence and simulation, Hangzhou, China

Bruzzone A.G., Agresta M., Sinelshchikov K. (2017a) "Simulation as Decision Support System for Disaster Prevention", Proc. of SESDE, Barcelona

Bruzzone A.G., Massei, M. (2017b) "Simulation-Based Military Training", in Guide to Simulation-Based Disciplines, Springer, pp. 315-361

Bruzzone A.G., M. Massei, F. Longo, L, Nicoletti, R. Di Matteo, G.L.Maglione, M. Agresta (2015) "Intelligent Agents & Interoperable Simulation for Strategic Decision Making On Multicoalition Joint Operations". Proc. of DHSS, Bergeggi, Italy

Bruzzone A.G., Massei M., Agresta M., Poggi S., Camponeschi F. & M. (2014) "Addressing strategic challenges on mega cities through MS2G", Proc. of MAS2014, Bordeaux, September

Bruzzone A.G., Massei, M., Tremori, A., Poggi, S., Nicoletti, L., & Baisini, C. (2014a) "Simulation as enabling technologies for agile thinking: training and education aids for decision makers"

International Journal of Simulation and Process Modelling 9, 9(1-2), 113-127

Bruzzone A.G., Massei M., Tremori A., Longo F., Nicoletti L., Poggi S., Bartolucci C., Picco E., Poggio G. (2014b) "MS2G: simulation as a service for data mining and crowd sourcing in vulnerability reduction", Proc. of WAMS, Istanbul, September

Cayirci, E. (2013, December). Modeling and simulation as a cloud service: a survey. In Proceedings of the 2013 Winter Simulation Conference: Simulation: Making Decisions in a Complex World (pp. 389-400). IEEE Press.

Barth, M., Johnston, E., & Tadi, R. (1996). Using GPS technology to relate macroscopic and microscopic traffic parameters. Transportation Research Record: Journal of the Transportation Research Board, 1520, 89-96.

Duderstadt, J.J. (2005). A roadmap to Michigan's future: Meeting the challenge of a global knowledge-driven economy, National Academy Press, Washington, D.C.

Clymer, A.B. (1993, December). Applications of discrete and combined modeling to global simulation. In Proceedings of the 25th conference on Winter simulation (pp. 1135-1137). ACM.

Clymer, A.B. & Mcleod, J. (1993) "Mission Earth Symposium", Summer Computer-Simulation Conference, San Diego, July 18-20

Clymer, A.B. (1994). " Mission Earth Symposium: World Simulation for Education", Proc. of the National Educational Computing Conference, Boston, June 13-15

Clymer A.B. (1980). Simulation for training and decision-making in large-scale control systems: Part 1: Types of training simulators. Simulation, 35(2), 39-41.

Clymer, A. Ben (1969, April). The Modeling and Simulation of Big Systems. In Proceedings of the Pittsburgh Simulation and Modeling Conference.

Clymer, M.G., & Mechoso, C. R. (1997) "Mission Earth: Modeling and Simulation for a Sustainable Global System", Proc. of the Western Simulation Multi Conference, SCS, Phoenix, January 12-15

Duma L., Nemeslaki A. (2013) "Of Aluminium, Recycling and the Homeless: A case study of technology driven social inclusion", Proc. of EGPA Annual Conference, Edinburgh, September

Elfrey P. (2006) "Moving out the Planet", Invited Speech at Summer Sim, Calgary, Canada, July

Fuller, R. B. (1969). The World Game. Ekistics, 286-292

Harding J. (2018)"CCTV shows Genoa bridge collapse", BBC News, August 21

House, P. W., McLeod, J (1977). Large-scale models for policy evaluation. John Wiley & Sons, NYC

Huang, G. H., Linton, J. D., Yeomans, J. S., & Yoogalingam, R. (2005). Policy planning under uncertainty: efficient starting populations for simulation-optimization methods applied to

municipal solid waste management. Journal of Environmental Management, 77(1), 22-34.

Irani Z., Sharif A.M., Lee H., Aktas E., Topaloğlu Z., van't Wout T., Huda S., 2018. Managing food security through food waste and loss: Small data to big data. Computers and Operations Research, vol. 98, pp. 367-383.

Kim, J. H. (2013) "Universal GPS traffic monitoring system", U.S. Patent No. 8,386,157, U.S. Patent and Trademark Office, Washington, DC:

Kuhl, F., Dahmann, J., & Weatherly, R. (2000). Creating computer simulation systems: an introduction to the high level architecture. Upper Saddle River: Prentice Hall PTR

Li, B. H., Zhang, L., Wang, S. L., Tao, F., Cao, J. W., Jiang, X. D., ... & Chai, X. D. (2010). Cloud manufacturing: a new service-oriented networked manufacturing model. Computer integrated manufacturing systems, 16(1), 1-7.

Longo F., 2011. Advances of modeling and simulation in supply chain and industry. Simulation, vol. 87, no. 8, pp. 651-656.

Longo F., Nicoletti L., Padovano A., 2017. Smart operators in industry 4.0: A human-centered approach to enhance operators' capabilities and competencies within the new smart factory context. Computers and Industrial Engineering, vol. 113, pp. 144-159.

McAfee, A., Brynjolfsson, E., Davenport, T. H., Patil, D. J., & Barton, D. (2012). Big data: the management revolution. Harvard business review, 90(10), 60-68.

McLeod, J. (1999). Simulation as a Possible Tool for Peace. Simulation, 72(5), 348-352.

McLeod, J., & McLeod, S. (1995) "Mission Earth And The Big Bird From The Ashes", Simulation, SCS, vol.64, n.1, June 1

McLeod, J. (1986). Computer modeling and simulation: The changing challenge. Simulation, 46(3), 114-118.

McLeod, J. (1968). Simulation: the dynamic modeling of ideas and systems with computers. McGraw-Hill.

McLeod, John & McLeod Suzette (1974) "Simulation in The Service of Society: World Simulation Organization", Simulation, SCS/SAGE, April 1st, doi.org/10.1177/003754977402200412

Meadows, D. H., Meadows, D. H., Randers, J., & Behrens III, W. W. (1972). The limits to growth: a report to the club of Rome (1972). Google Scholar

Najafabadi, M. M., Villanustre, F., Khoshgoftaar, T. M., Seliya, N., Wald, R., & Muharemagic, E. (2015). Deep learning applications and challenges in big data analytics. Journal of Big Data, 2(1), 1.

Naranjo P.G.V., Pooranian Z., Shojafar M., Conti, M., Buyya R., 2018. FOCAN: A Fog-supported smart city network architecture for management of applications in the Internet of Everything environments. Journal of Parallel and Distributed Computing (in press).

Oren, T. I., Elzas, M. S., Smit, I., & Birta, L. G. (2002, July). Code of professional ethics for simulationists. In Summer Computer Simulation Conference (pp. 434-435). Society for Computer Simulation International; 1998.

Sanchez, S. M. (2014, December). Simulation experiments: better data, not just big data. In Proceedings of the 2014 Winter Simulation Conference (pp. 805-816). IEEE Press.

Varaiya, P. (1993). Smart cars on smart roads: problems of control. IEEE Transactions on automatic control, 38(2), 195-207

Wan, J., Liu, J., Shao, Z., Vasilakos, A. V., Imran, M., & Zhou, K. (2016). Mobile crowd sensing for traffic prediction in internet of vehicles. Sensors, 16(1), 88

Wu, X., Zhu, X., Wu, G. Q., & Ding, W. (2014). Data mining with big data. IEEE transactions on knowledge and data engineering, 26(1), 97-107

Author's index